Copy No. ___

DEFENCE DÉFENSE

ABSTRACTS and SUMMARIES

of

9TH CF/DRDC MEETING on NAVAL APPLICATIONS of MATERIALS TECHNOLOGY

compiled by
J.R.Matthews

Defence R&D Canada

DEFENCE RESEARCH ESTABLISHMENT ATLANTIC

Special Report
DREA SR 2001-094
October 2001

National Defence Défense nationale

Canada

Abstract

This was the ninth naval materials CF/DRDC (Canadian Forces/Defence Research and Development Canada) meeting. These meetings have been held every two years since 1985. The first four meetings were devoted to fabrication and inspection of submarine pressure hulls with sessions on welding, inspection and fracture. The last five have expanded to include all aspects of naval materials.

The purpose of these meetings has been to bring together industrial research contractors, university contractors, defence scientists, and NDHQ (National Defence Headquarters) design authorities from the naval materials technology area and invited scientists and engineers from other countries to share advances in naval materials technology in a conference like setting.

The program includes Welding and Laser Surface Modification, Environmental Research, Corrosion and Coatings, Vibroacoustic Materials, Ship Fracture, Fatigue, Firesafe Materials, Non-Destructive Evaluation, Metallurgy and Failure Analysis, Organic Materials (Polymers), Fuels and Lubricants and Naval Consulting.

Résumé

Le RDDC/FC (Recherche et développement pour la défense Canada/Forces armées canadienne) a tenu sa neuvième réunion sur les applications de la technologie des matériaux au domaine naval. Ces réunions ont lieu tous les deux ans depuis 1985. Les quatre premières rencontres ont porté sur la fabrication et l'inspection des coques épaisses de sous-marins. Elles comprenaient des ateliers sur la soudure, l'inspection et la rupture. Les thèmes des cinq plus récentes réunions couvraient tous les aspects des matériaux appliqués au domaine naval.

Ces réunions ont pour objet de rassembler des entrepreneurs spécialisés en recherche industrielle ou provenant du secteur universitaire, des scientifiques de la défense représentants du QGDN responsable de projets de conception dans le domaine de la technologie des matériaux appliqués au secteur naval ainsi que des scientifiques et des ingénieurs invités venus de l'étranger afin de leur permettre de partager leur savoir sur les progrès de la technologie des matériaux dans le cadre de rencontres de type conférence.

Les thèmes abordés au cours de la réunion portaient entre autres sur la soudure et la modification d'une surface au laser, la recherche en environnement, la corrosion et les revêtements, les matériaux vibro-acoustiques, la rupture de navires, la fatigue, les matériaux ignifuge, l'évaluation non-destructifs, la métallurgie et analyse des défaillances, les matériaux organiques (polymères), les carburants et lubrifiants et la consultation navale.

9th CF/DRDC MEETING
on
NAVAL APPLICATIONS OF MATERIALS TECHNOLOGY

The Park Place
Ramada Plaza Hotel
Dartmouth N.S.
5th, 6th and 7th June 2001

AGENDA
Tuesday June5 th

Registration: 8:00 am page

Welcome/Opening Remarks: 1

Capt(N) JSR Payne
Commanding Officer, Fleet Maintenance Facility Cape Scott

SESSION I: Park Centre
Chairman: Dr. R. Morchat

1. "Development of a Lithium Ion SuperPolymer Battery", by Sankar Das Gupta, James K. Jacobs, Rakesh Bhola, Electrofuel Inc., Toronto, Ontario, Canada 10

2. "Hydrogen Storage", Richard Jones, DERA, UK 24

3. "Technologies for Corrosion and Wear Control for Naval Applications" Vinod S. Agarwala, Naval Air Systems Command, Patuxent River, MD, U.S.A. 49

4. "Microstructural Characterization of the Corroded Surface of Laser Clad Nickel Aluminum Bronze Following Long-Term Sea-water Exposure", by J.A. Gianetto and G. A. Botton, Materials Technology Laboratory, CANMET, Ottawa, Canada, and C.V. Hyatt, Defence Research Establishment Atlantic 66

SESSION II: Park Room A
Chairman: Dr John Hiltz

5. "A Different Approach to Test Specimen Design and Component Testing", by V. G. DeGiorgi, Naval Research Laboratory and S. A. Wimmer, Nova Research, Inc. 83

6. "Titanium Alloy Ti-5111 for U.S. Naval Applications", by Michael E. Wells and Ernest J. Czyryca, Naval Surface Warfare Center, West Bethesda, Maryland, USA 99

7. "Experiences with T.I.M.E. Welding: Ontario Research, Techno Scientific, Hyundai, European Investigation, Aichi Sangyo, and subsequent experiences in DND: 1980s to present." J. Church, Weld Process International, and J.R. Matthews, DREA 115

8. "Molecular Magnets - Addressing Defence Signature Needs in 2010" by Sandra M. Nevill (DREA) and Vincent J. Castelli (NSWC Carderock Division). 145

9. "Essential testing in Submarine Pressure Hull Weld Acceptance: Victoria Class Subs", J.R. Matthews and John Porter, DREA 154

51. "Advanced Materials Solutions to the Aging Aircraft Problem", by K.I. McRae, Air Vehicles Research Section, Defence and Civil Institute of Environmental Medicine, Ottawa, Ontario, Canada 165

SESSION III: Park Room B
Chairman: Dr Calvin Hyatt

10. "Transmission Electron Microscopy of Martensite in Laser Welded Nickel Aluminum Bronze Alloys", JC Bennett, Acadia University, and CV Hyatt, DREA 183

11. "A New Fracture Criterion For Piezoelectric Solids", S. Xu and N. Rajapakse, Univ of Manitoba 200

12. "Advances in Hydrogen Management for High Strength Steel", by Yeong-Do Park, Chad Lensing, Iman Maroef and D.L. Olson, Center for Welding, Joining, and Coatings Research (CWJCR), Colorado School of Mines, and Zamir Gavra, Nuclear Research Center, Beer-Sheva, Israel 215

13. "Failure analysis of nickel aluminium bronze hydraulic couplings", by D.P. Edwards, S.P. Lynch, J.L. Davidson and R.B Nethercott, Aeronautical and Maritime Research Laboratory, Australia 232

14. "Review of R and D on Cupronickels and Ni-Al Bronzes at the Materials Technology Laboratory, Canmet", by Mahi Sahoo, CANMET, Ottawa, Ontario 245

54. "Copper based alloy fastener materials-stress corrosion studies", by J C Galsworthy,DERA, MoD, UK and K J A Mawella, STGMT, DPA, MoD, UK 273

Tuesday Evening, 5th June
RECEPTION and BANQUET
Roccos Italian Restaurant

Wednesday 6th June

SESSION IV: Park Room B
Chairman: Mr Dwight Veinot

15. "Canadian Navy Pollution Abatement Overview", by LCdr Peter Hartley, NDHQ, DMSS 4-8 281

16. "Impact Of Operational Parameters On A Membrane Based Bilge Water Treatment System", by M. Nottegar, Naval Engineering Test Establishment, LaSalle, Quebec, Canada 295

17. "Studies on Micro and Ultrafiltration in Oily Wastewater Purification", by A.Y. Tremblay and T.H. Li, University of Ottawa, and D.E. Veinot, DREA 309

18. "The Influence of Colloids and Fine Particles on Membrane Performance", by A.Y. Tremblay, M. Nottegar and H. Peng, University of Ottawa, and D.E. Veinot, DREA 317

19. "CPF Biofouling Investigations", B.M. Zwicker, G.R. Pelletier and J.F. Porter, DREA 333

SESSION V: Park Room A
Chairman: Drs Calvin Hyatt/ Mahi Sahoo

20. "The Manufacture of Submarine Valves from Wrought Steel using the Electron Beam Welding Process", Alan Aitchison, Principal Welding Engineer, BAE SYSTEMS Marine, UK and Chris Punshon, Electron Beam Applications Section Manager, TWI, UK. 380

21. "Studies on the effect of impurity elements on the mechanical properties and weldability of alloy C95800", M. Sadayappan, M. Letts, R. Zavadil and M. Sahoo Materials Technology Laboratory (CANMET) Ottawa 401

22. "Low Heat Input Welding and Cladding of Nickel Aluminum Bronze and Related Alloys", Calvin Hyatt, DREA 414

23. "Synthesis and Characterization of Magnetic Shape Memory Materials", by M.A. Gharghouri, Dept. of Mining and Metallurgical Engineering, Dalhousie University and C. Hyatt, DREA 431

24. "Application of Advanced Laser Consolidation Process for Manufacturing Complex FSP Shells', by L. Xue, A. Theriault and M. U. Islam, Integrated Manufacturing Technologies Institute, NRC, and C. J. Purcell, DREA 442

SESSION VI: Park Room B
Chairman: Mr John Porter

25. "The Effects of Decaying Organic Matter on the Corrosion of Copper-Nickel Alloys in Sea Water", by D. R. Lenard and R. R. Welland, EDRD 454

26. "An Overview of the DREA Program for Modelling Impressed Current Cathodic Protection Systems", by K.J. KarisAllen, FACTS Engineering, D. Brennen and K.D. Mackay, Martec and J.F. Porter, DREA 472

27. "Fatigue Crack Growth in 350WT Steel Subjected to Intermittent Tensile Overloads & Compressive Underloads", by P.A.Rushton, Martec Limited, Halifax, F. Taheri, Civil Engineering Department, Dalhousie, and D.C. Stredulinsky, Structural Acoustics & Strength Group, DREA 493

28. "Minor Corrosion - Major Mechanical Failure", by J.C. Thornley, RPC, Fredericton, New Brunswick, Canada 510

29. "Diesel Dilemmas", by Dan Morehouse, John Porter, and John Hiltz, DREA 535

SESSION VII: Park Room A
Chairman: Dr Terry Foster

30. "Ultrasonic Weld Testing and Imaging Using Portable Automated Non-Destructive Arm", A. Chahbaz, A. Cyr, R. Sicard, A. Pelletier and M. Brassard, Tektrend International, and J.R. Matthews, DREA 543

31. "Reference Temperatures for 350WT and A517 Plate and Welds", J. Morrison, DREA DL(P), X. Wu, Bombardier Aerospace, Montreal, and D.A. Hull, Engineering Material Research, Downsview, ON 554

32. "Master Curve Description of the Crack Arrest Toughness of 350WT Steel", by Jack Morrison, DREA DL(Pacific), L. N. Pussegoda, Fleet Technology, R. B. Nethercott, Aeronautical and Maritime Research Laboratory, Melbourne, Australia, and J.D. Sumpter, DERA Rosyth, UK 570

33. "Assessment of Meta-Lax on ASTM A517 and HY80 Weldments", by G.R. Pelletier, DalTech, J.F. Porter, DREA, and G.M.C. Lee, DalTech 586

34. "Toughness Envelope Definition of Pulsed Gas Metal Arc Welds in HY80 Steel", by D.S. Begg, Fleet Technology Limited and J.R. Matthews, DREA 616

Wednesday 6th June
Historic Properties/ Mar II Harbour Cruise
Host: Dwight Veinot

Thursday 7th June

SESSION VIII: Park Centre A
Chairman: Mr Dwight Veinot

35. "Composite Material Durability for Naval Structures", by Françoise Dubois-Artiga, DCN, Indret, France, J. Dalzel-Job, DERA Rosyth, Dunfermline UK, J. Mawella, DPA, Bristol UK, and F. Decobert, DGA, Paris, France 630

36. "Affect of Time in Service on the Oxidative Induction Time of Shell Rimula X Diesel Lubricating Oil", by John A. Hiltz, Irvin A. Keough, and Randall D. Haggett, DREA 644

37. "Synthesis and Characterization of a Series of Thermoplastic Polyurethanes", J.P. Szabo, D. Cook, J. Hackett, and I.A. Keough, DREA 664

38. "Polymer Actuators Based on Maxwell Forces", J.P. Szabo, DREA, Brian White and J. Leidner, Bodycote Ortech 676

39. "CPF Heated Window Failures", by Dwight Veinot, et.al., DREA 687

SESSION IX: Park Centre B
Chairman: Dr Calvin Hyatt

40. "Probabilistic Service Life Assessment of Missile Structures", by U. O. Akpan and F. Wong, Martec 701

41. "Delayed Cracking in Simulated Submarine Repair Welds", N. Pussegoda, A. Dinovitzer, and Bo Xu, FTL, Kanata, ON, Canada, B.A Graville, Graville Associates, Georgetown, ON, Canada 721

42. "Crevice Corrosion Susceptibility of Mixtures of Monel and HY-80 Steel", R.D. Klassen and P.R. Roberge, RMC, and C.V. Hyatt, DREA 733

43. "Crack-tip Blunting and Fracture Resistance of a Ship Plate Steel), by G. Shen and S. Xu, MTL/CANMET, J. Morrison, DND, Dockyard Laboratory, Esquimalt and W.R. Tyson, MTL/CANMET, Ottawa, Canada 752

44. "Investigation of Plastic Zone Development In Dynamic Tear Test Specimens", by T.S. Koko and B.K. Gallant, Martec, and J.R. Matthews, DREA 760

SESSION X: Park Centre B
Chairman: Dr Jeff Szabo

45. "Production and Maintenance of Nickel Aluminum Bronze Submarine Seawater System Castings", by John Bird, former Head of Materials Technology, MoD, UK 775

46. "Probabilistic Risk Assessment of Aging Ship Structures", by U. O. Akpan, T. S. Koko, B. Ayyub and T. Dunbar, Martec 795

47. "A Neural Network Analysis of HSLA Steels", E. A. Metzbower, U. S. Naval Research Laboratory, E. J. Czyryca, Naval Surface Warfare Center, Carderock Division, and H.K.D.H. Bhadeshia, University of Cambridge 813

SESSION XI: Park Centre A
Chairman: Mr John Porter

49. "Non-Magnetic Stainless Steel Hulls: Past, Present and Future" A. John Sedriks, Office of Naval Research, Arlington, Virginia, USA and Philip J. Dudt Naval Surface Warfare Center, Carderock, Maryland, USA 830

50. "An Evaluation of Microbiologically Influenced Corrosion in Double-Hull Ships", by Brenda Little and Richard Ray, Naval Research Laboratory, Stennis Space Center, MS and Joanne Jones-Meehan, Naval Research Laboratory, Washington, D.C 850

48. "An Efficient Fuzzy Finite Element Methodology for Structural Systems", by U. O. Akpan, T. S. Koko and B. K. Gallant 866

52. "Publishing with Web Tools", by P.R. Roberge, Royal Military College of Canada 882

53. " Lessons Learned From Operational CPF Trials", by John F. Porter, DREA, Colin Smith, NETE, and LCdr. Chris Hargreaves, Directorate of Maritime Ship Support, Hull, Quebec 894

55. "Application of Modern S690 Materials for the Hull of Minesweeper Drones", by Cees van Sevenhoven, Royal Dutch Navy 907

List of Attendees 922

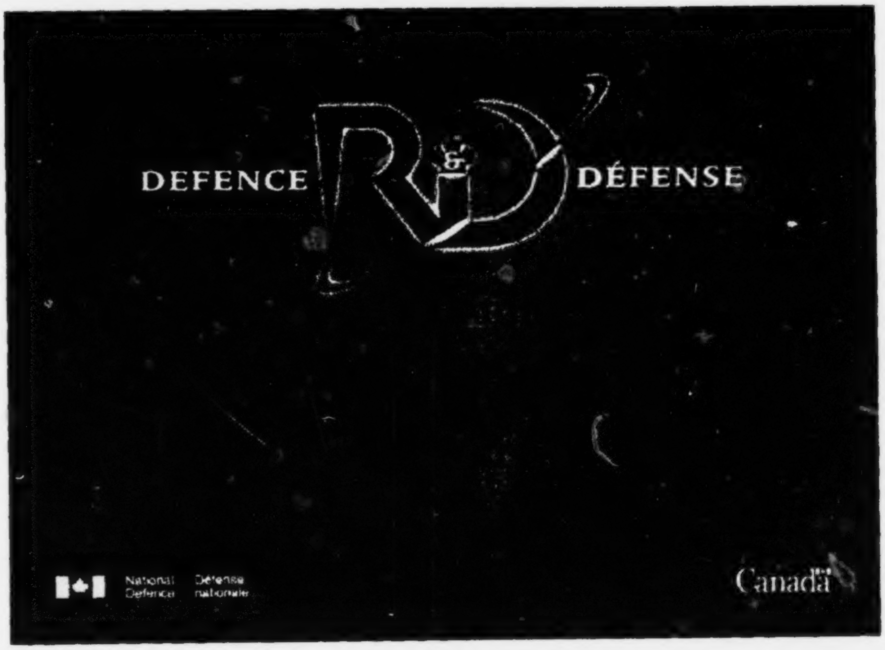

DEFENCE R&D DÉFENSE

National Defence Défense nationale

Canada

Good morning. I am Captain Rick Payne, the Assistant Chief of Staff Naval Engineering and Maintenance, and the Commanding Officer of our Navy's east coast fleet maintenance facility, FMF Cape Scott.

It is my distinct pleasure to make the opening comments for your 9th Canadian Forces/Defence Research and Development Canada Meeting on the Naval Applications of Materials Technology.

Welcome to

NOVA SCOTIA

CANADA

DEFENCE R&D DEFENSE

Defence Research Establishment Atlantic (DREA)

I understand that there are guests from ministries of defence and defence contractors from New Zealand, Australia, France, US, The Netherlands and the UK here today, and we have Canadian guests from virtually every province in Canada. Let me start by welcoming all of you to Canada, to Nova Scotia, to Halifax and to Canada's East Coast Navy .

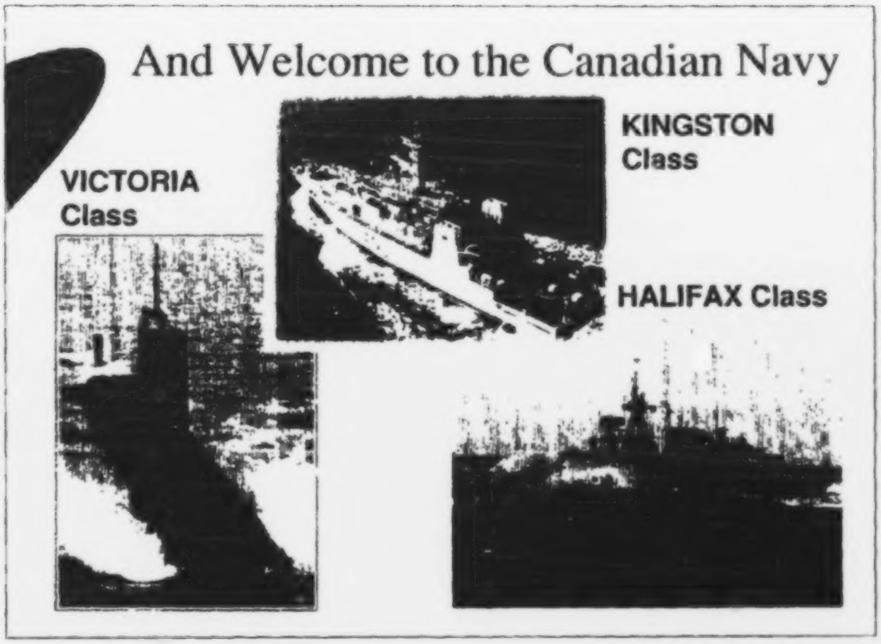

And Welcome to the Canadian Navy

Adm MacLean, the commander of our East Coast fleet, also extends his welcome. I don't know how familiar you are with our Navy, but we feel very fortunate having recently bought from the UK the four UPHOLDER submarines, which will re-enter service here in Canada's Navy as the Victoria Class. We have also built twelve KINGSTON Class Maritime Coastal Defence Vessels, and twelve HALIFAX Class patrol frigates, all in the last decade. In addition, the government has given us the go ahead to start the procurement process for new Maritime Helicopters. All of our new Naval platforms have brought with them new and challenging materials problems and as the Commanding Officer of the Fleet Maintenance Facility in Halifax, I see the results of these problems on our ships and the importance of their resolution almost on a daily basis.

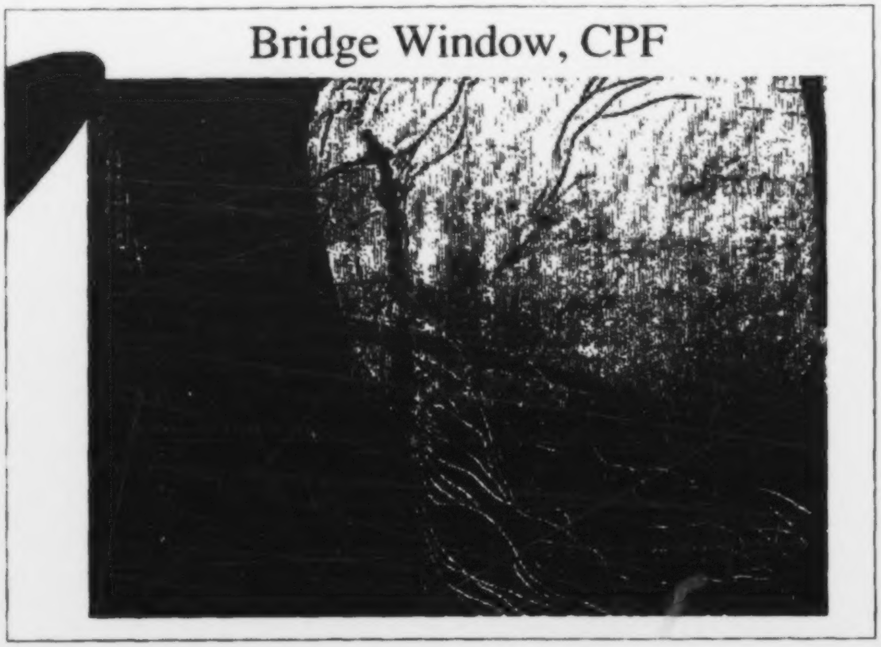

Bridge Window, CPF

Here's but one example, and a very interesting one. The heated windows on all of our Canadian Patrol Frigates have been overheating and cracking. Replacing these specially designed windows is both expensive and resource intensive. We asked our Dockyard Labs for help. They applied their theoretical understanding of the materials in these windows to not only identify the cause of the cracking but to recommend a cost effective solution. Our Dockyard Labs, DND engineering organizations, universities and Canadian industry have been invaluable to the solving of a multitude of materials related problems, for example, proving that the catastrophic failures of the diesel engines in our HALIFAX Class ships were the result of a design deficiency, thus causing the prime contractor to repair all of the diesel engines under warrantee, and, in another requirement, devising welding techniques for welding on the pressure hulls of our new submarines.

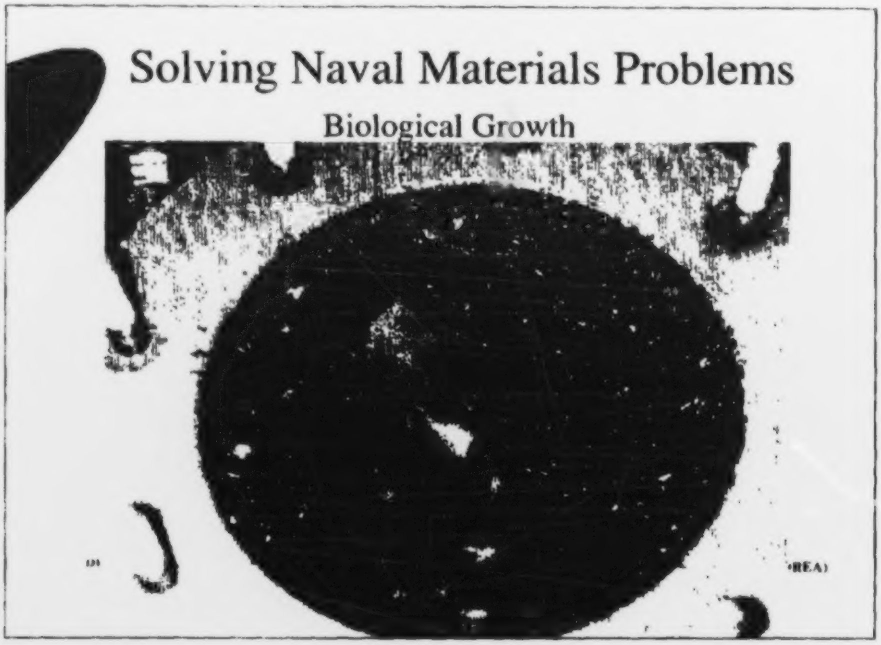

Solving Naval Materials Problems

Biological Growth

Another pressing problem being addressed is the eliminating of biological growth in our HALIFAX Class sea water lines. Pictured here is blue mussel fouling.

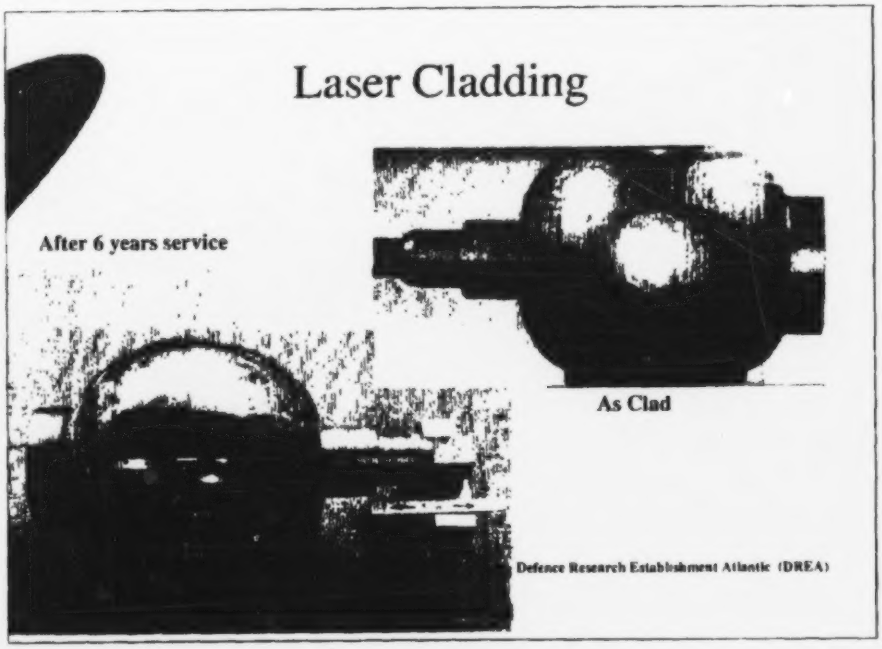

Laser Cladding

After 6 years service

As Clad

Defence Research Establishment Atlantic (DREA)

Another success story concerns the refurbishment of submarine valves through a novel laser cladding process developed at DREA. The valve shown is still useable after more that six years of service in an Oberon Submarine, which is a significant improvement over the unclad component.

It would not be possible to solve problems such as these without laboratories, defence engineering and research organizations and companies in Canada and in your countries applying state of the art knowledge and understanding of modern materials to help the Canadian Navy and your Navies to solve these problems. I know that the progress made in any one area is often the result of sharing of new ideas between the technology leaders, such as yourselves. And that of course, is the reason why meetings such as this one are so important to the Canadian Navy and navies throughout the world.

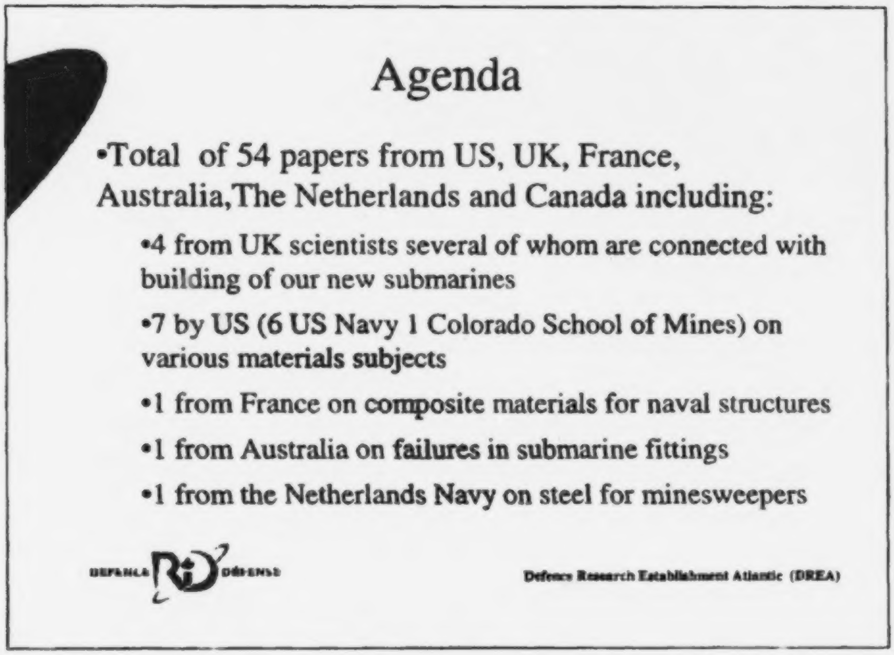

Agenda

- Total of 54 papers from US, UK, France, Australia, The Netherlands and Canada including:
  - 4 from UK scientists several of whom are connected with building of our new submarines
  - 7 by US (6 US Navy 1 Colorado School of Mines) on various materials subjects
  - 1 from France on composite materials for naval structures
  - 1 from Australia on failures in submarine fittings
  - 1 from the Netherlands Navy on steel for minesweepers

Defence Research Establishment Atlantic (DREA)

In addition to being responsible for seeking solutions to the materials related problems in our Navy, I am, by profession, a Marine Systems Engineer, and therefore have a professional interest in materials technology. I must say that I look forward to attending this 9th conference on Naval Applications of Materials Technology, and learning from you where the state of the art in Naval materials is today.

I won't go over the agenda in any detail, but I am pleased to note that there are papers being presented from five other countries in addition to those from Canada. All of the 54 papers address important materials technology issues, and cover a wide range of interests.

- I am pleased to note that we have four papers from UK scientists and engineers several of whom are connected with the building of our new Victoria Class submarines. Also;
- 7 papers by the US (6 US Navy and one Colorado School of Mines) including several by some very senior people and strong supporters of DREA
- Une presentation importante par la France sur les materiaux composes de structures navales
- A presentation from Australia on failures in fittings
- A presentation from The Netherlands on steel for minesweepers

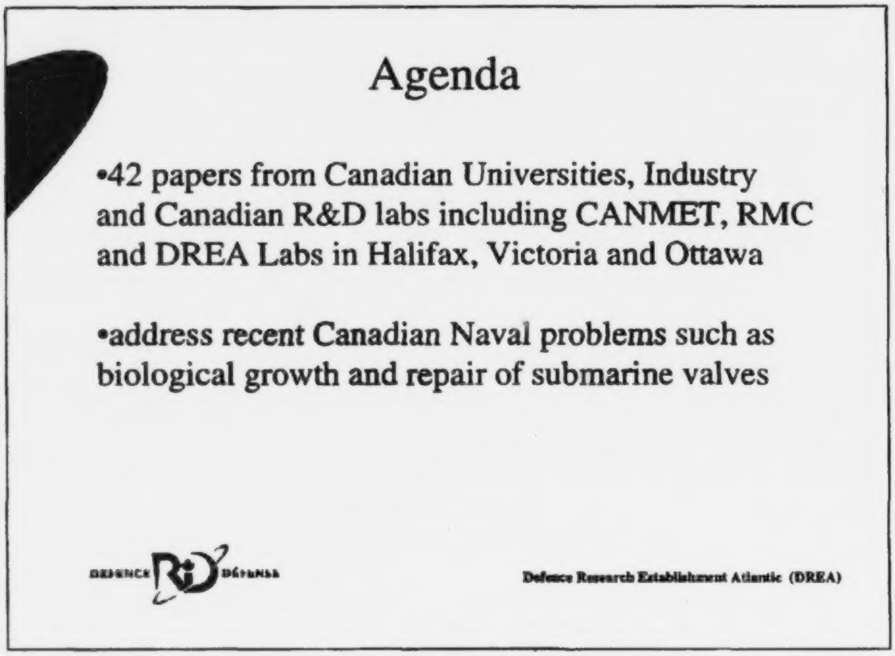

Agenda

- •42 papers from Canadian Universities, Industry and Canadian R&D labs including CANMET, RMC and DREA Labs in Halifax, Victoria and Ottawa
- •address recent Canadian Naval problems such as biological growth and repair of submarine valves

Defence Research Establishment Atlantic (DREA)

I note that among the Canadian papers are ones on retarding biological growth and laser cladding, which has potential for use in cost effective repair of submarine valves. As I mentioned earlier, these address two serious problems faced by our Navy today.

•9 papers from DREA Halifax and 3 from DREA Victoria
•Several presentations where Canada is breaking new ground, including ...SuperPolymer batteries, T.I.M.E. welding, computer aided ultrasonics and others
•and many presentations from diverse organisations including RMC, NDHQ, NRC, AND Canadian Universities, Industry and R&D labs

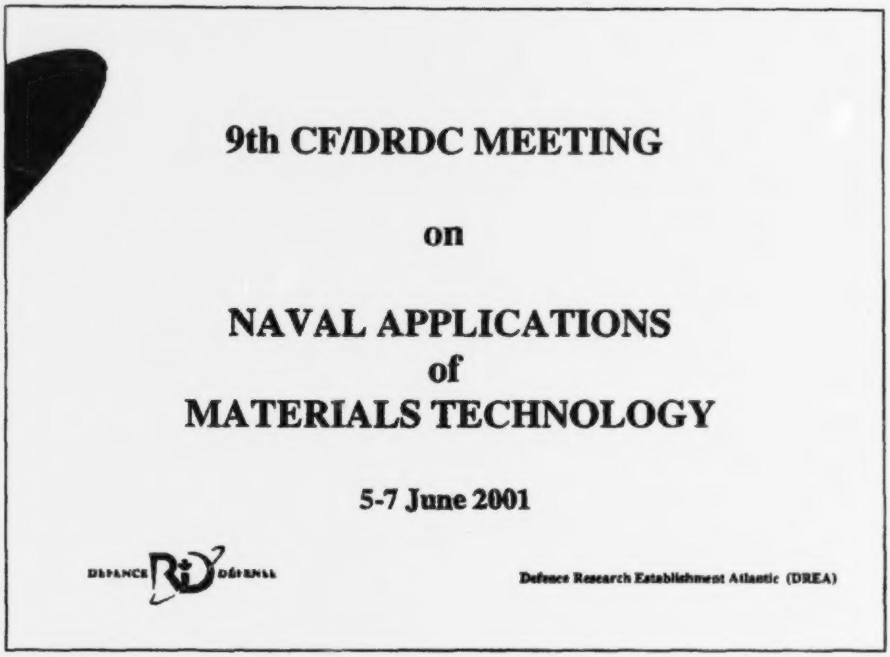

9th CF/DRDC MEETING

on

NAVAL APPLICATIONS
of
MATERIALS TECHNOLOGY

5-7 June 2001

Defence Research Establishment Atlantic (DREA)

I encourage you to enjoy the famous Nova Scotia hospitality while you are here. I know that Jim Matthews and Dwight Veinot have some fine dining planned as well as a historic cruise on the MAR II around the Halifax Harbour.

This is a very important conference for the navy and our materials experts in Canada. I wish you a very successful and rewarding conference and we hope that you'll all be back in 2003 for our 10th anniversary meeting on Naval Applications of Materials Technology. Thank you !!

Development of a Lithium Ion SuperPolymer Battery

by

Sankar Das Gupta, James K. Jacobs, Rakesh Bhola

Electrofuel Inc.
Toronto, Ontario, Canada

Abstract

Electrofuel has developed and commercialized the patented rechargeable Lithium Ion SuperPolymer Battery, which has the highest energy density in the world. The energy density of the battery is 435 Watt hour per litre and 175 Watt hour per kilogram, a significantly higher energy density than any other rechargeable battery technology currently in commercial production.

The Lithium Ion SuperPolymer Battery has initially been launched for powering portable computers and the PowerPad 160 has delivered up to 16 hours of computer run time. Electrofuel's battery technology has potential applications in many sectors including telecommunications, defence, aerospace, medical, transportation among others. A program for investigating its application in electric vehicles is underway. The paper will discuss the aspects of materials science involved with the development program and other related matters.

RECENT ADVANCES IN LITHIUM ION POLYMER BATTERIES

ELECTROFUEL INC.

SANKAR DAS GUPTA

"Portable Power will be the Critical Technology of the 21st Century"

Japanese Think-Tank
(CRIEPI)

electrofuel

DILBERT
CAROL, ORDER AN EXTRA BATTERY FOR MY MOBILE TECHNOLOGY PLATFORM
www.dilbert.com
DO YOU WANT THE ONE THAT STRAPS TO YOUR BACK OR THE ONE WITH ITS OWN WHEELBARROW?
© 2001 United Feature Syndicate Inc
I THINK I JUST LOST A LUNG

Globe & Mail . [illegible] 2001

Batteries: Critical Component of almost All Naval Systems

- Weapons: torpedoes, mines, missiles
- Powering Counter Measures: buoys, communication equipment, surveillance etc
- Submersibles & submarines: diesel-electric, unmanned etc.

Submarine Batteries
Pb acid

- New SEAWOLF battery:

  126 cells at 60"x16"x16"

  total weight: 95 tons, 6525 Ah
- TRIDENT: Battery weight 130 tons
- DSRV's and DSV's:

Li Polymer at 17% of the weight and volume, hermetically sealed and no exhaust requirement for Hydrogen is worth some investigation

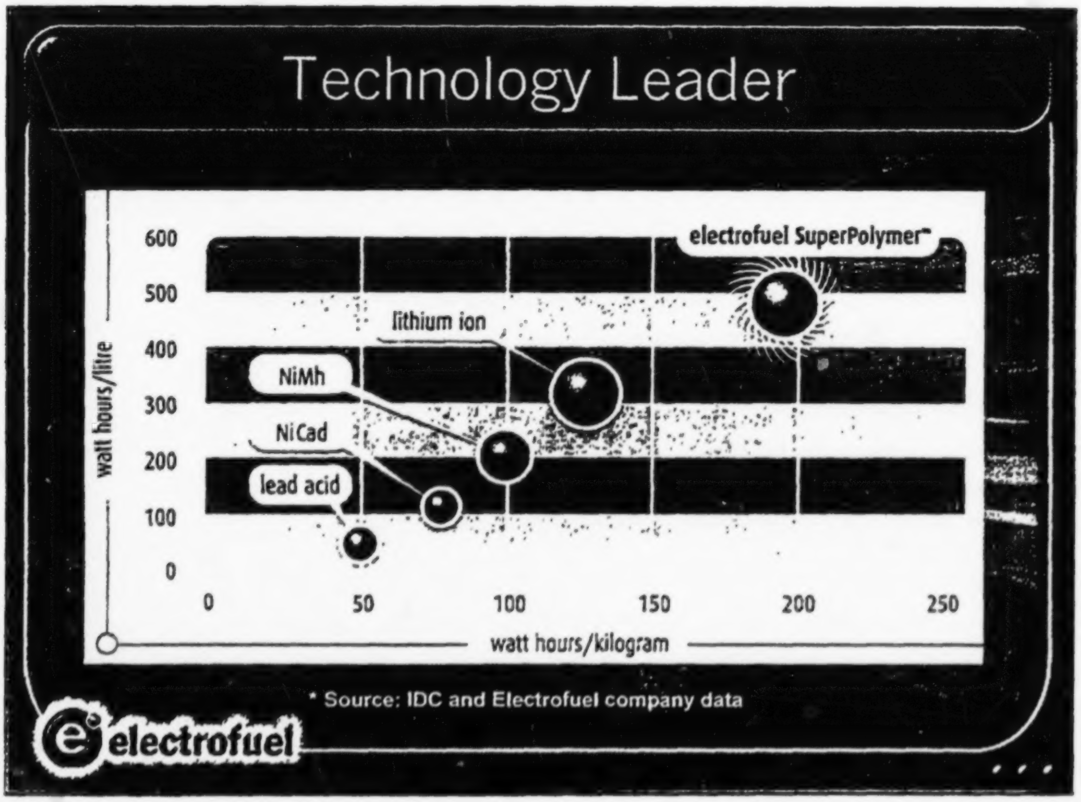

Technology Leader

* Source: IDC and Electrofuel company data

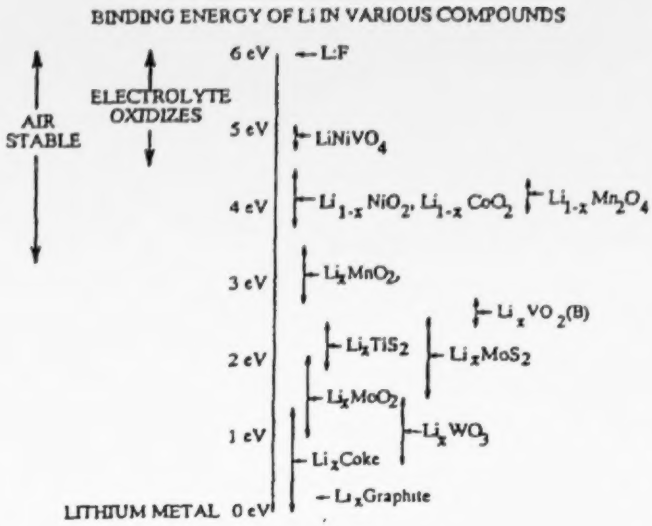
BINDING ENERGY OF Li IN VARIOUS COMPOUNDS
AIR STABLE
ELECTROLYTE OXIDIZES
6 eV
5 eV
4 eV
3 eV
2 eV
1 eV
LITHIUM METAL 0 eV
LiF
$LiNiVO_4$
$Li_{1-x}NiO_2$, $Li_{1-x}CoO_2$
$Li_{1-x}Mn_2O_4$
Li_xMnO_2
$Li_xVO_2(B)$
Li_xTiS_2
Li_xMoS_2
Li_xMoO_2
Li_xWO_3
Li_xCoke
$Li_xGraphite$

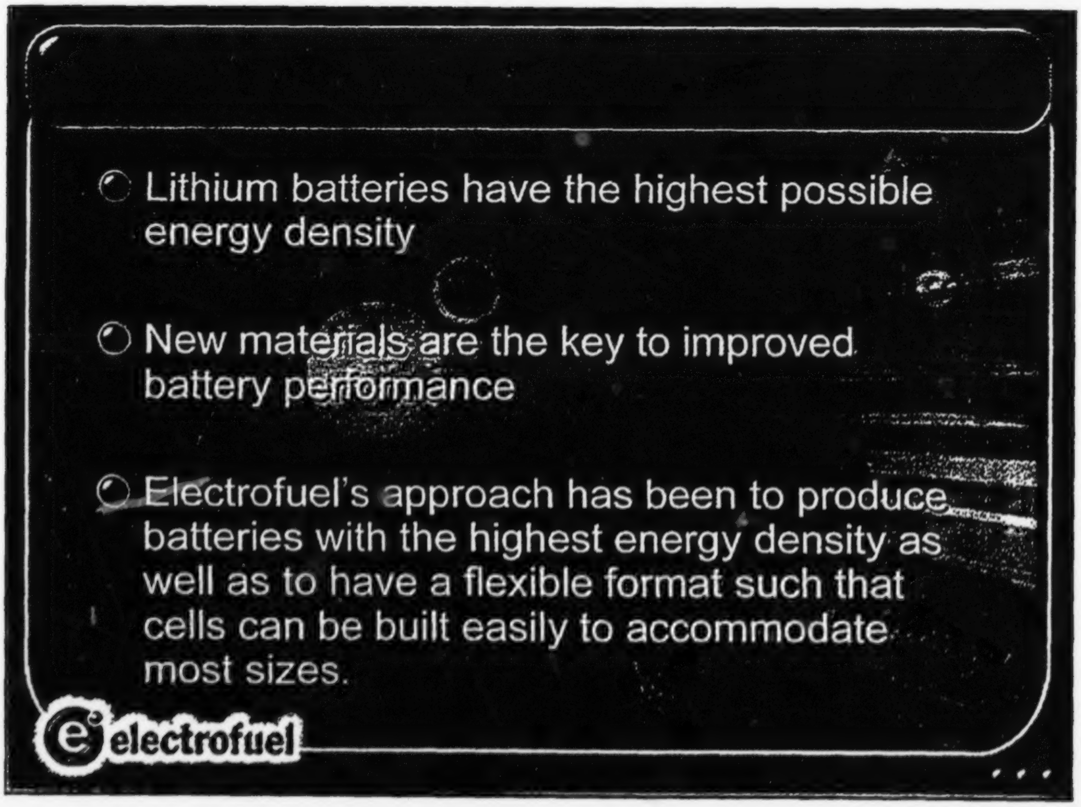

- Lithium batteries have the highest possible energy density
- New materials are the key to improved battery performance
- Electrofuel's approach has been to produce batteries with the highest energy density as well as to have a flexible format such that cells can be built easily to accommodate most sizes.

electrofuel

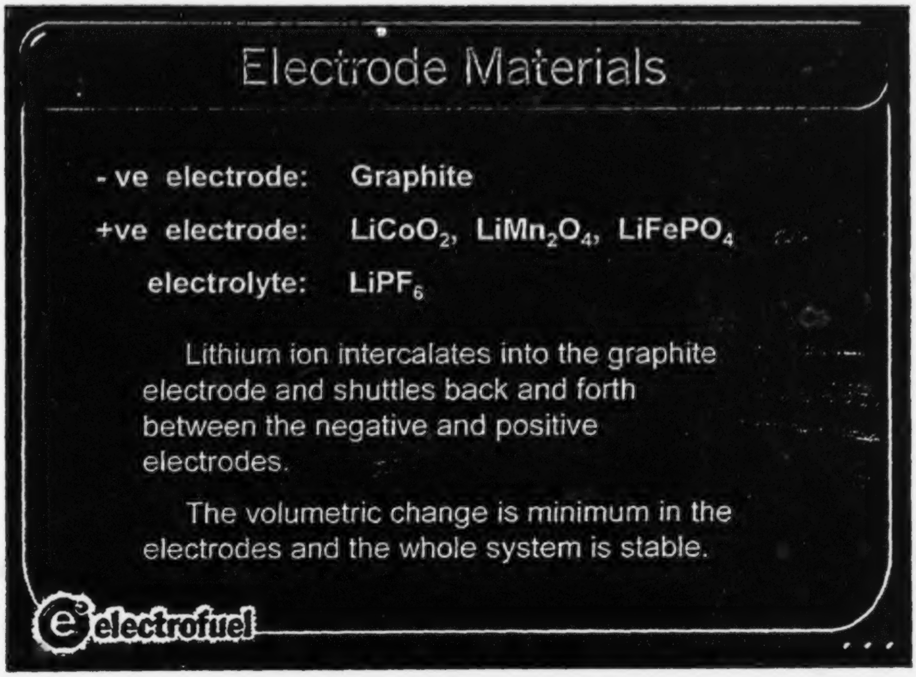

Electrode Materials

- ve electrode: **Graphite**

+ve electrode: **$LiCoO_2$, $LiMn_2O_4$, $LiFePO_4$**

electrolyte: **$LiPF_6$**

Lithium ion intercalates into the graphite electrode and shuttles back and forth between the negative and positive electrodes.

The volumetric change is minimum in the electrodes and the whole system is stable.

electrofuel

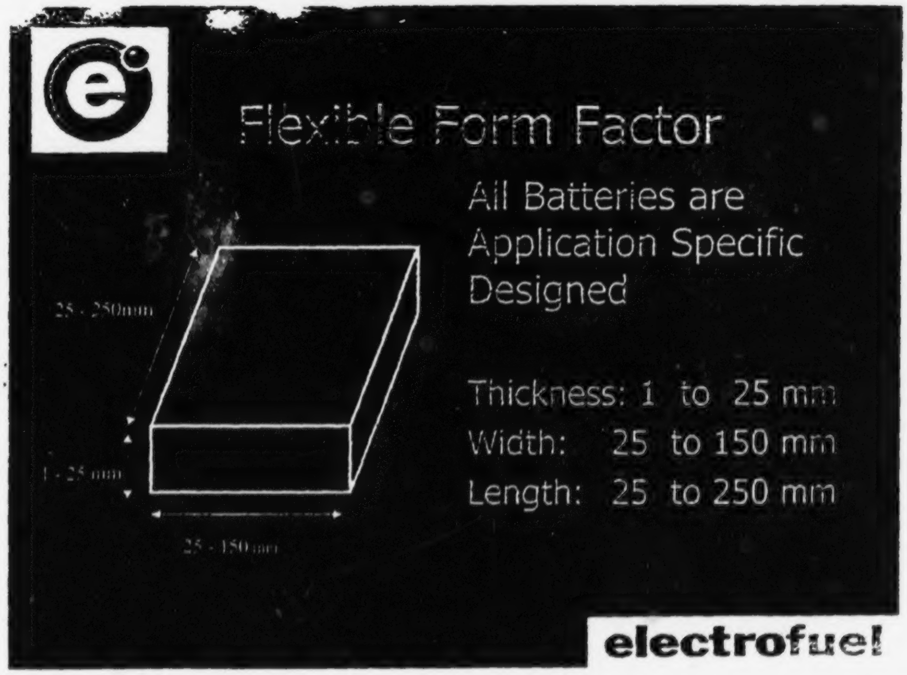

Flexible Form Factor

All Batteries are Application Specific Designed

Thickness: 1 to 25 mm
Width: 25 to 150 mm
Length: 25 to 250 mm

electrofuel

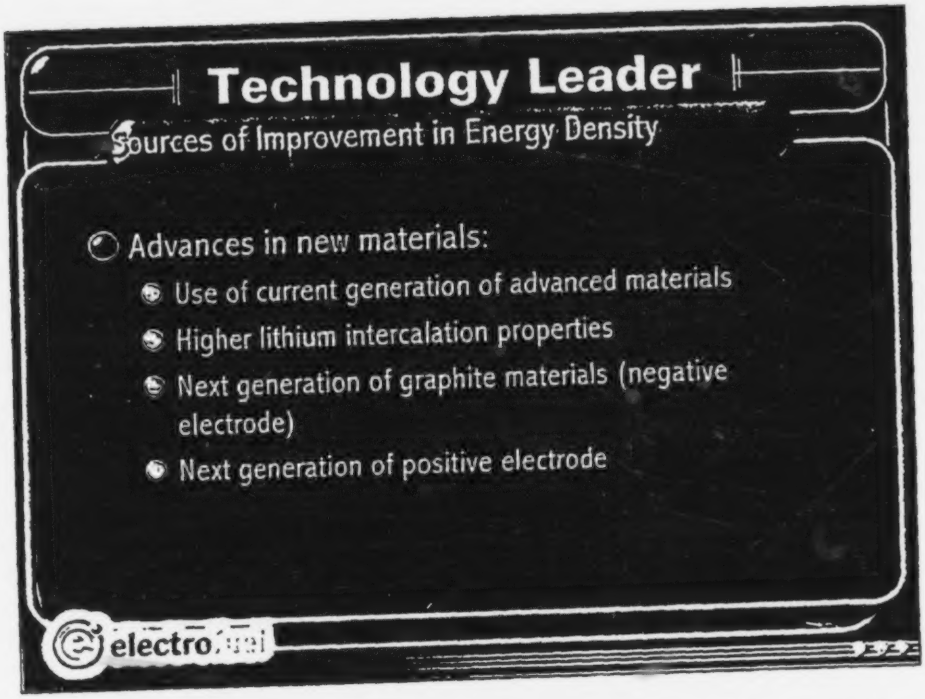

Technology Leader

Sources of Improvement in Energy Density

- Advances in new materials:
  - Use of current generation of advanced materials
  - Higher lithium intercalation properties
  - Next generation of graphite materials (negative electrode)
  - Next generation of positive electrode

electrofuel

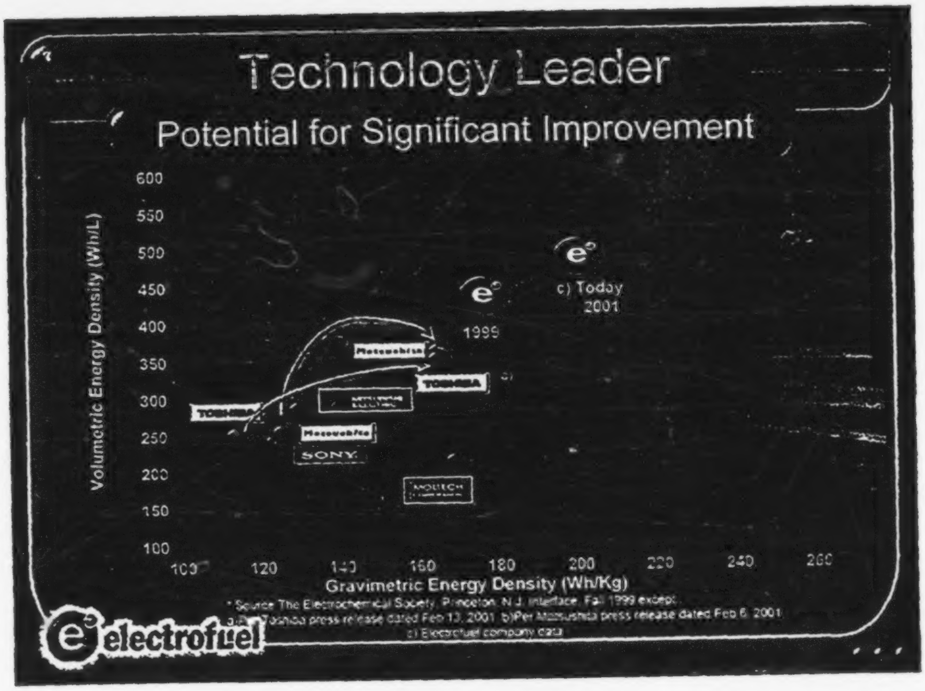

Technology Leader

Potential for Significant Improvement

* Source The Electrochemical Society, Princeton, N.J. Interface, Fall 1999 except: a)Per Toshiba press release dated Feb 13, 2001 b)Per Matsushita press release dated Feb 6, 2001 c) Electrofuel company data

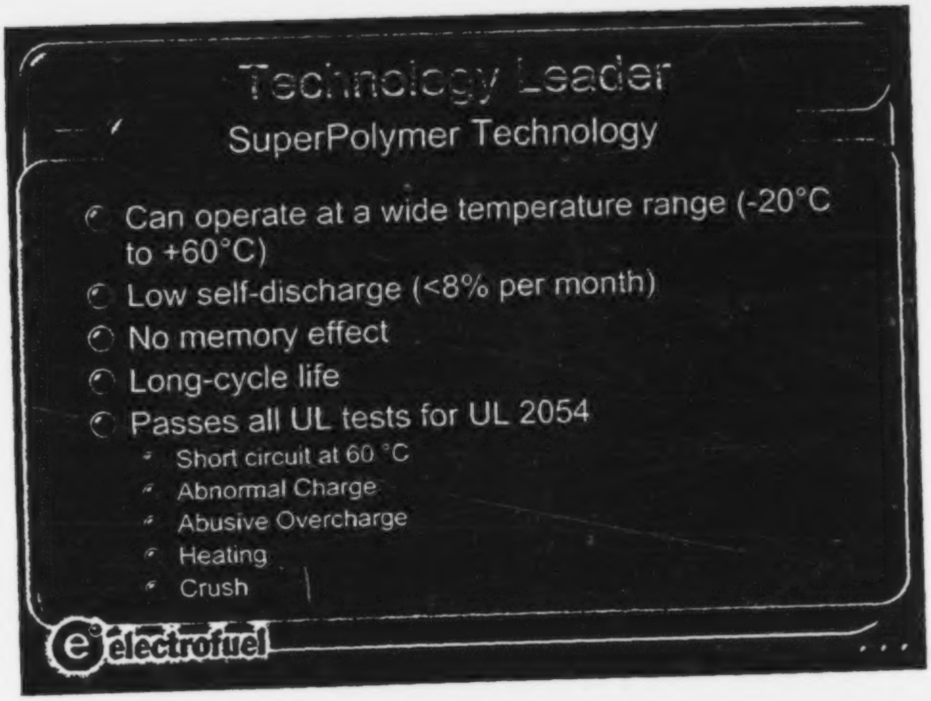

Technology Leader

SuperPolymer Technology

- Can operate at a wide temperature range (-20°C to +60°C)
- Low self-discharge (<8% per month)
- No memory effect
- Long-cycle life
- Passes all UL tests for UL 2054
  - Short circuit at 60 °C
  - Abnormal Charge
  - Abusive Overcharge
  - Heating
  - Crush

electrofuel

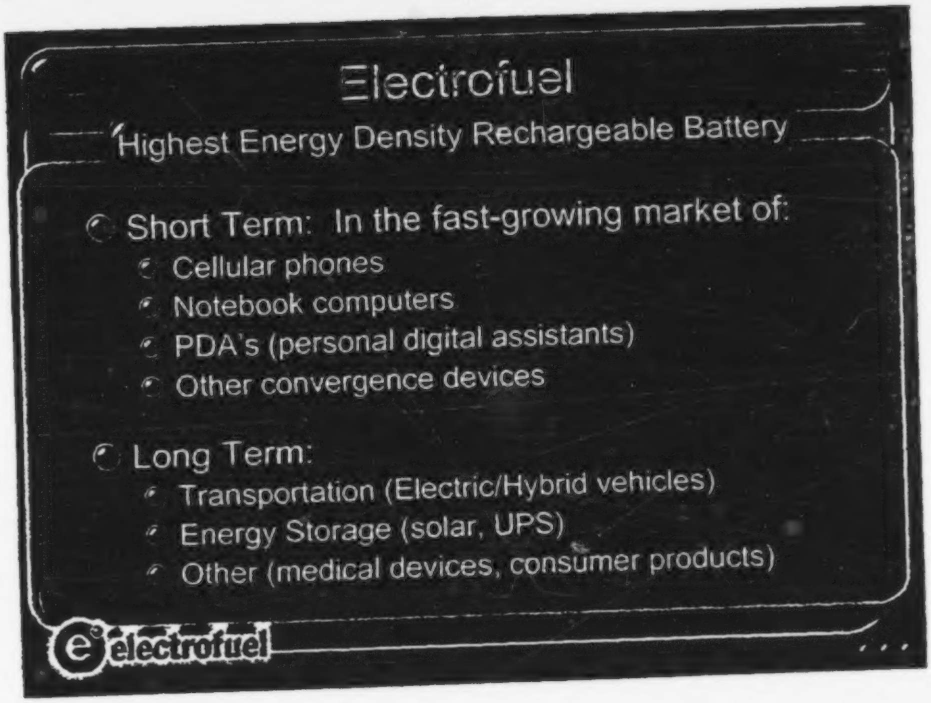

Electrofuel

Highest Energy Density Rechargeable Battery

- Short Term: In the fast-growing market of:
  - Cellular phones
  - Notebook computers
  - PDA's (personal digital assistants)
  - Other convergence devices
- Long Term:
  - Transportation (Electric/Hybrid vehicles)
  - Energy Storage (solar, UPS)
  - Other (medical devices, consumer products)

electrofuel

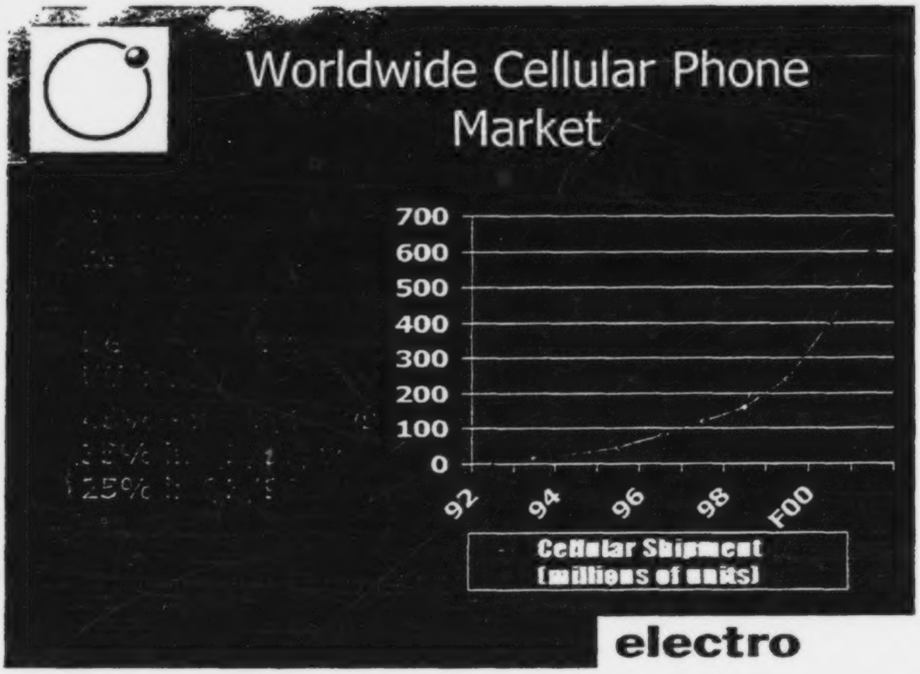

Worldwide Cellular Phone Market

[illegible]

25% [illegible]

electro

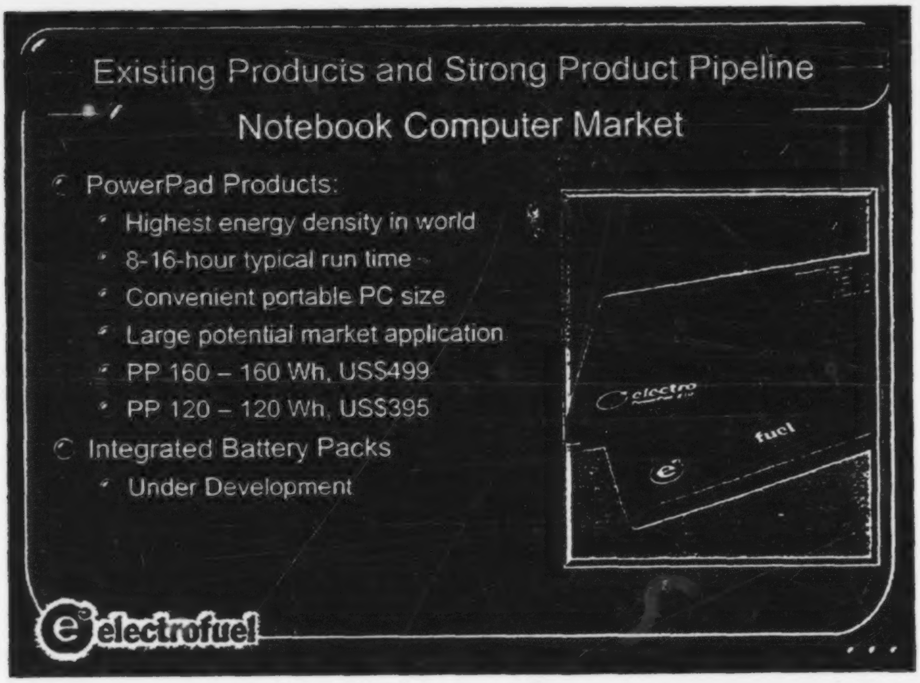

Existing Products and Strong Product Pipeline

Notebook Computer Market

- PowerPad Products:
  - Highest energy density in world
  - 8-16-hour typical run time
  - Convenient portable PC size
  - Large potential market application
  - PP 160 – 160 Wh, US$499
  - PP 120 – 120 Wh, US$395
- Integrated Battery Packs
  - Under Development

electro
fuel

electrofuel

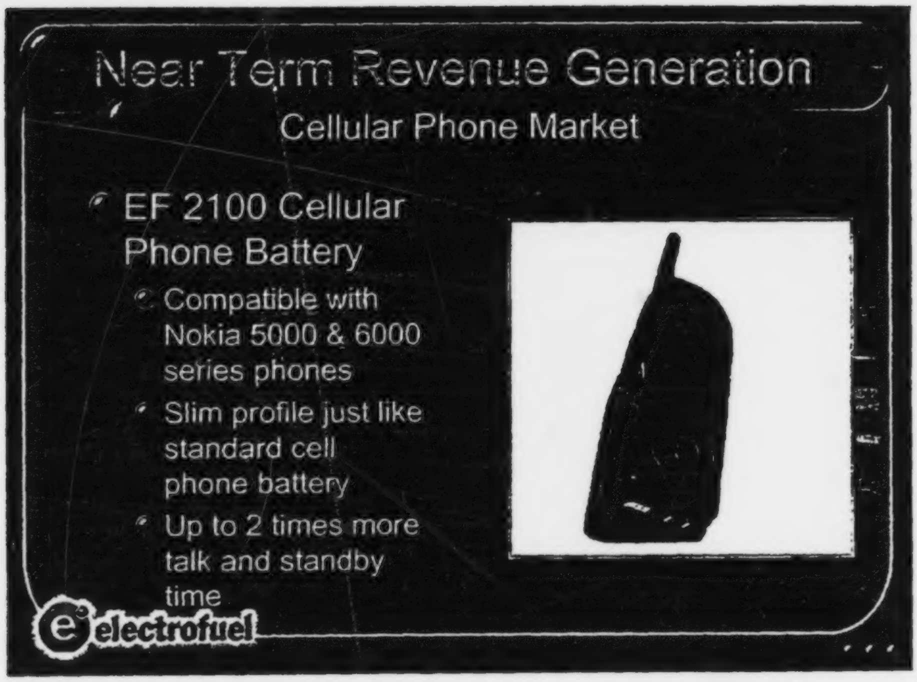

Near Term Revenue Generation

Cellular Phone Market

- EF 2100 Cellular Phone Battery
  - Compatible with Nokia 5000 & 6000 series phones
  - Slim profile just like standard cell phone battery
  - Up to 2 times more talk and standby time

electrofuel

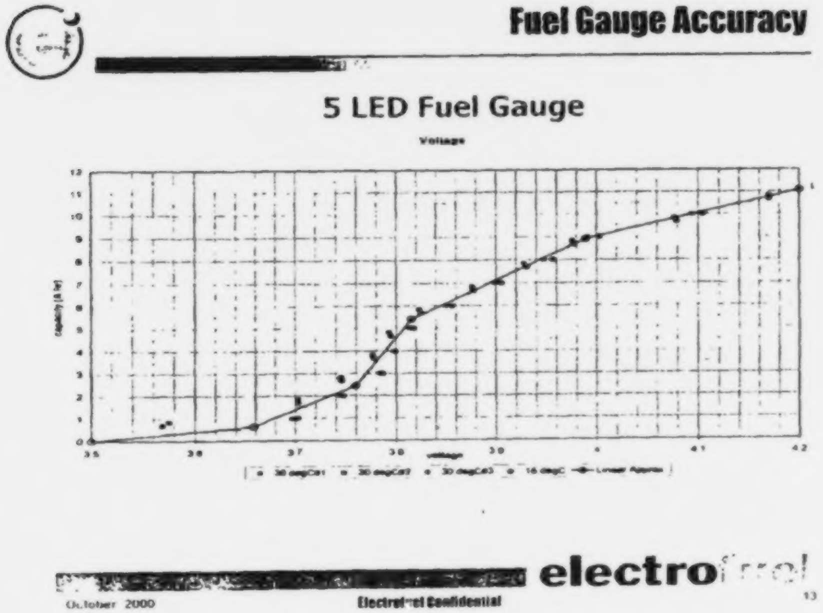

Fuel Gauge Accuracy

5 LED Fuel Gauge

electrofuel

October 2000

Electrofuel Confidential

13

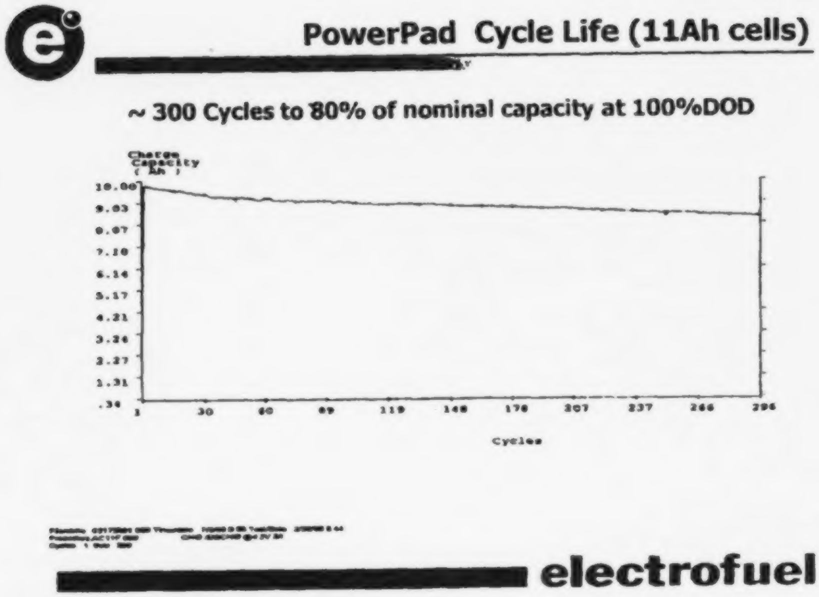

PowerPad Cycle Life (11Ah cells)

~ 300 Cycles to 80% of nominal capacity at 100%DOD

electrofuel

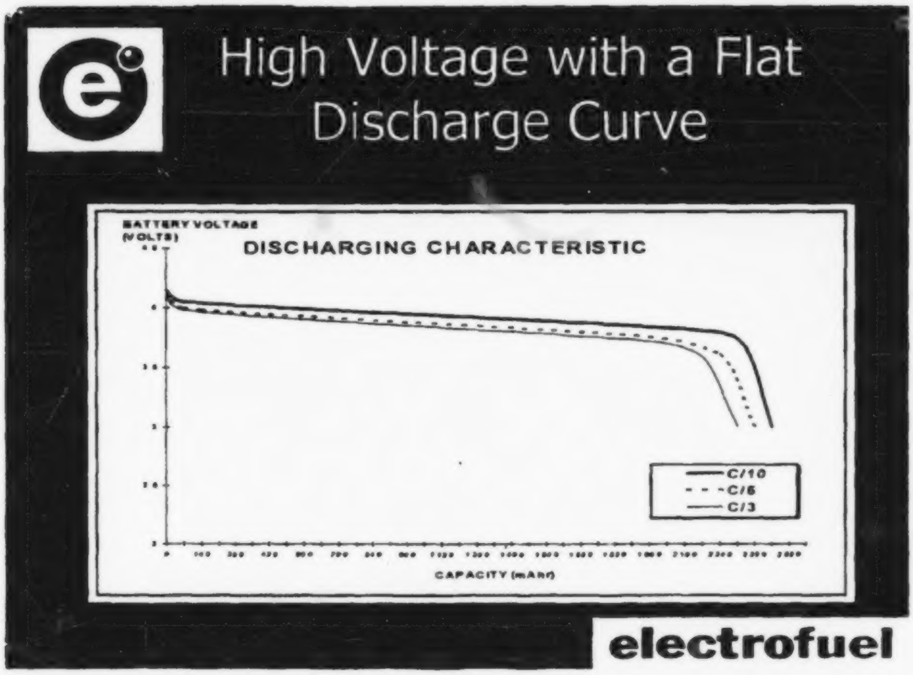

High Voltage with a Flat Discharge Curve

electrofuel

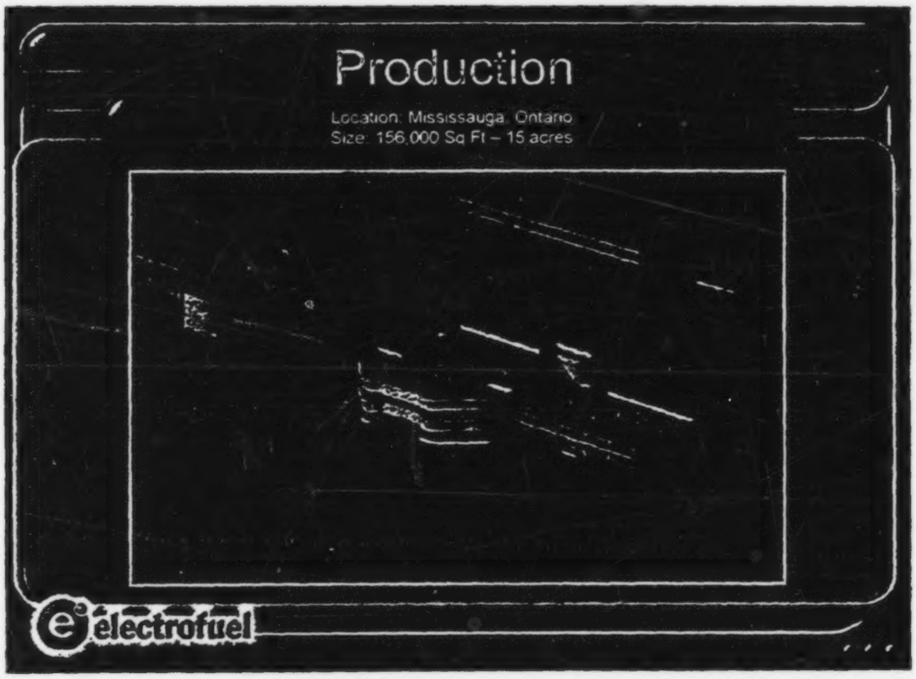

Production

Location: Mississauga, Ontario
Size: 156,000 Sq Ft – 15 acres

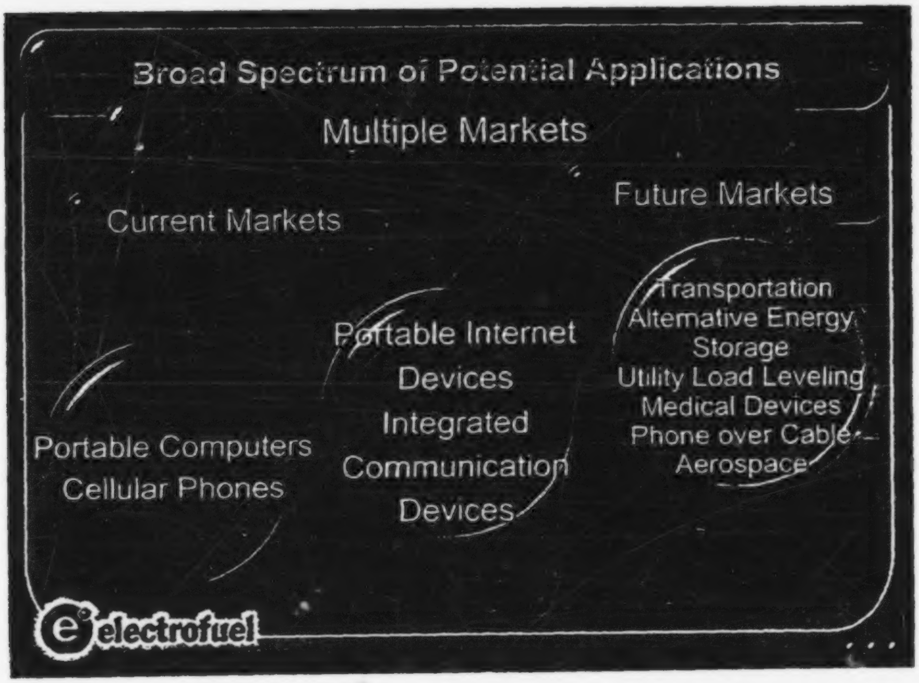

Broad Spectrum of Potential Applications

Multiple Markets

Current Markets

Portable Computers
Cellular Phones

Portable Internet
Devices
Integrated
Communication
Devices

Future Markets

Transportation
Alternative Energy
Storage
Utility Load Leveling
Medical Devices
Phone over Cable
Aerospace

electrofuel

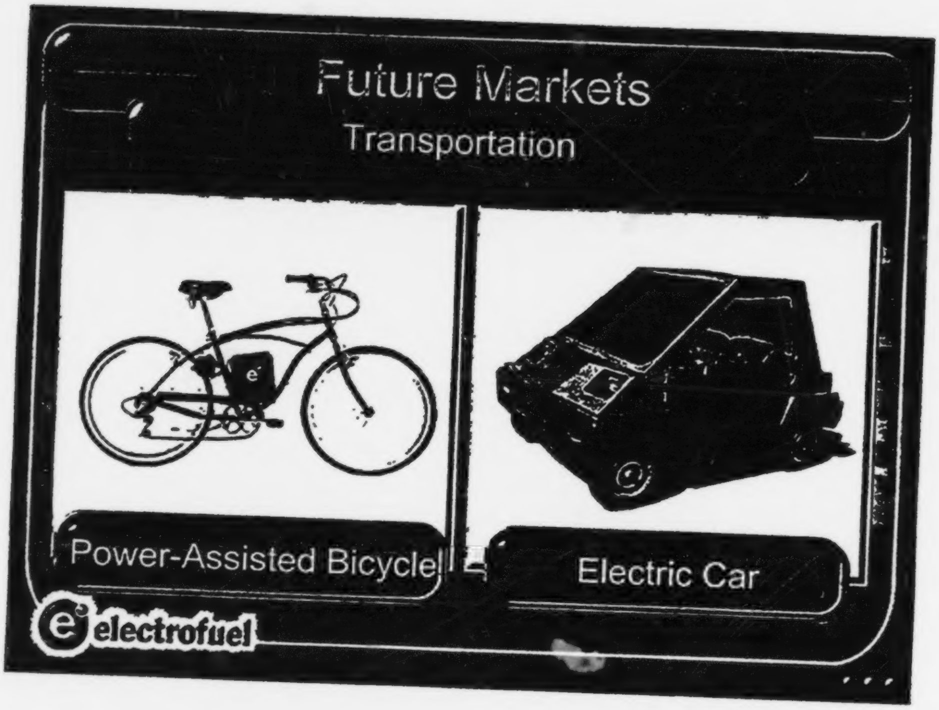

Future Markets

Transportation

Power-Assisted Bicycle

Electric Car

electrofuel

Environmental Benefits

- Switching ICVs for EVs can create a reduction of emissions in urban areas of:
  - 99% carbon monoxide
  - 98% hydrocarbons
  - 92% nitrogen oxides

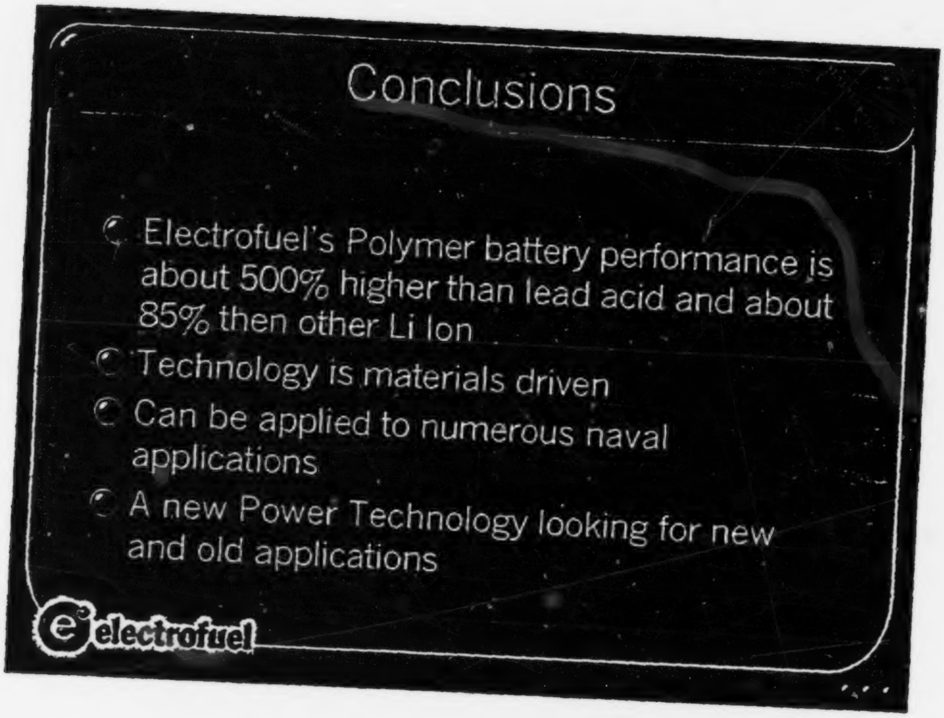

Conclusions

- Electrofuel's Polymer battery performance is about 500% higher than lead acid and about 85% then other Li Ion
- Technology is materials driven
- Can be applied to numerous naval applications
- A new Power Technology looking for new and old applications

electrofuel

Hydrogen Storage

Prof Richard Jones

DERA

Power Sources Research

- Battery Technology
  - Primary & secondary lithium batteries
  - Thermal reserve batteries
- Alternative power sources
  - Thermoelectrics, piezoelectrics, photovoltaics
- Fuel Cells
  - PEM; stack design, new plates, novel geometry's, hybrids
  - Direct methanol fuel cells
  - High temperature proton conducting ceramic fuel cells
- Hydrogen sources
  - Storage
  - Generation
  - Reformation

DERA

Research on Hydrogen at DERA

- Primary Hydrogen Storage
  - Cylinders
  - Reversible metal hydrides
  - Carbon nanofibres/nanotubes
- Secondary Hydrogen Storage
  - Hydrolysis
  - Thermolysis
- Liquid fuel processing
  - Methanol
  - Diesel

DERA

HYDROGEN

- Hydrogen ideal fuel for fuel cells
- Simple, clean reaction
- $H_2 + \frac{1}{2} O_2 \longrightarrow H_2O$ (1.23 V)
- High energy per unit weight (26.6 Ah/g)
- Wide range of technologies for storage/generation of H_2
- 1 wt % = 186 Wh/kg (0.7 V)
- c.f. Li ion cells 130-150 Wh/kg

- Storage of hydrogen difficult

DERA

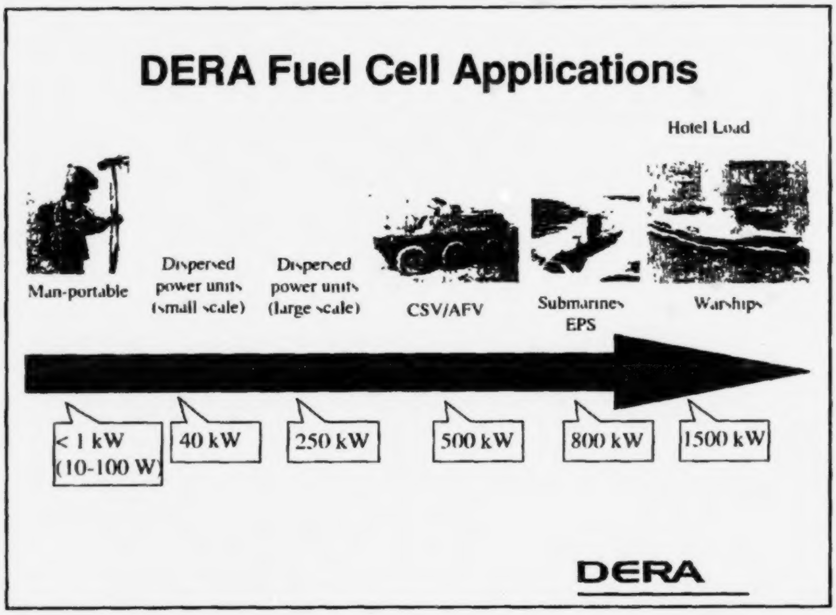

DERA Fuel Cell Applications

Hotel Load
Man-portable
Dispersed power units (small scale)
Dispersed power units (large scale)
CSV/AFV
Submarines EPS
Warships
< 1 kW (10-100 W)
40 kW
250 kW
500 kW
800 kW
1500 kW
DERA

Physical storage

- Compressed gas
- Cryogenic liquid
- Reversible intermetallic metal hydrides
- Carbon nano-adsorbents
- Glass micro-spheres
- Hydrogenation

DERA

Compressed gas

- Traditional steel cylinders
  - heavy, typically <1 wt % (186 Wh/kg)
- Composite cylinders
  - carbon fiber wrapped over an inner Al or thermoplastic liner
  - much lighter than steel cylinders, ca. 3 wt % (560 Wh/kg)
  - Ultra high pressure composite cylinders, ca. 10 wt% (1860 Wh/kg)
- Bulky storage method
- User resistance to high pressure cylinders

DERA

Cryogenic hydrogen storage

- Liquid hydrogen is an efficient method of storing hydrogen on a weight basis
  - 20 wt % hydrogen storage (3800 Wh/kg) (For a 120 litre cylinder)
  - Less efficient for smaller systems
- Boiling point of liquid H_2 at 1 atm is 20 K
- Special, very well insulated containers are needed
- Bulky method of storage
- Lose 1.5 % per day from natural boil off

DERA

Reversible metal hydrides

$$M + xH_2 \rightleftharpoons MH_{2x}$$

- Good volumetric performance
  - theoretical 100 g/L,1860 Wh/L
- Poorer gravimetric performance
  - theoretical 1-2 wt %, 186-370 Wh/kg
- Desorption endothermic
  - requires heat
- H_2 stored at constant P
  - safe storage

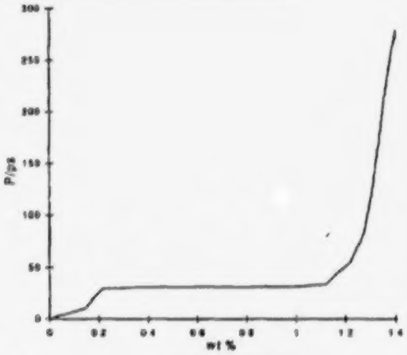

DERA

Rechargeable metal hydrides

$$M + xH_2 \rightleftharpoons MH_{2x}$$

- Hydrogen is Stored as a Chemically Bound Species
- A Range of Temperatures is Available from Different Compounds
- Desorption of Hydrogen is Endothermic
- Some Alloys Commercially Available

Alloy	Temp	%wt
FeTi	293 K	1.8
$CaNi_5$	340 K	1.4
Mg_2Ni	523 K	3.8

DERA

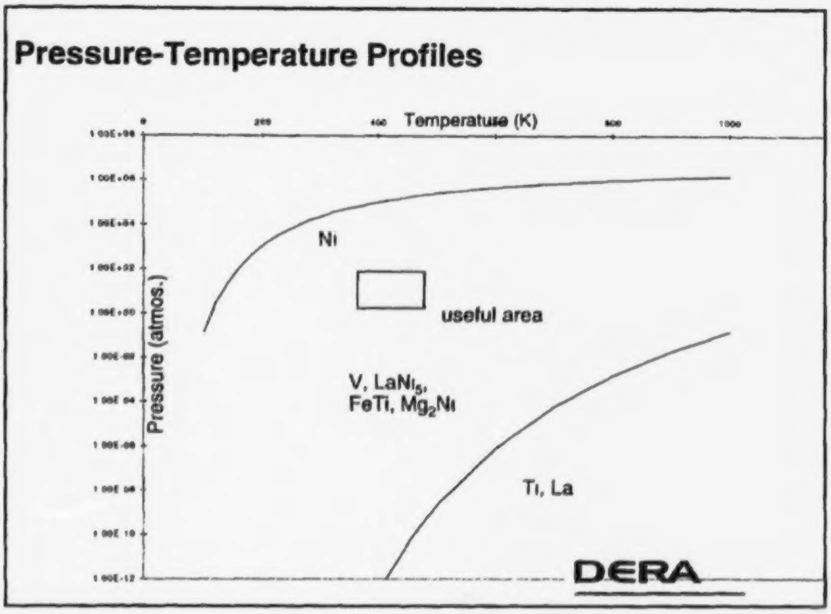

Pressure-Temperature Profiles

Composite alloys

- Novel synthesis routes
  - Physical vapour deposition (PVD)
  - Mechanical Alloying (MA)
- Magnesium based alloys
  - Mg-x wt % FeTi
  - x = 30-80 %

DERA

Structure of Vapour Deposited Titanium

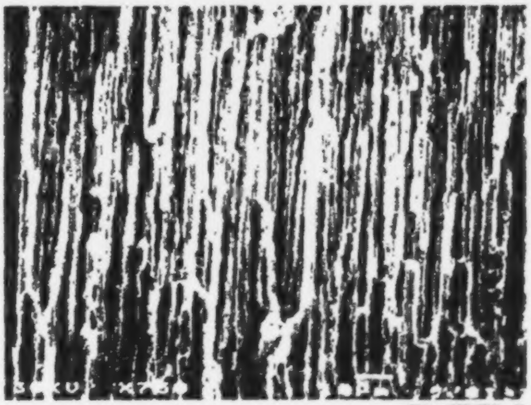

DERA

Mechanically alloyed Mg-x% FeTi

- Temperatures > 250°C required for uptake
- 3.2 wt % reversible capacity @ ~300°C
- Single plateau
- No activation

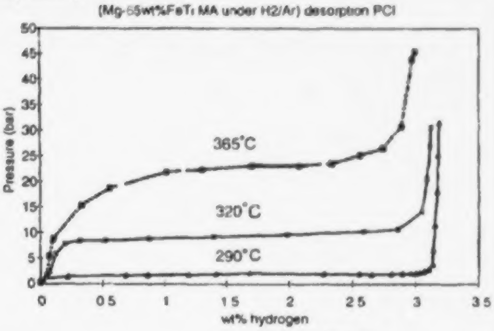

DERA

Preliminary Conclusions & Future Work on Metallic Hydrides

- Both PVD and MA improved the hydrogen take-up of FeTi
- Mg-Fe-Ti alloys showed increased storage capacity but the absorption/desorption temperatures were much higher
- Modeling is being used to refine the alloy compositions.
- Work is continuing using inert processing of PVD material to improve activation.

DERA

Carbon nanofibres

- Developed by Northeastern University
- Consist of stacked graphite plates
- Thin fibres of 5 - 100 nm diameter and 5 - 100 μm length
- Spacing between planes (0.34 nm) perfect for H_2 (H_2 Ø 0.29 nm)
- Potentially store over 50 wt % H_2 (9300 Wh/kg)
- Room temperature storage
- High pressure required

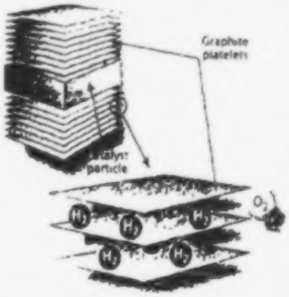

DERA

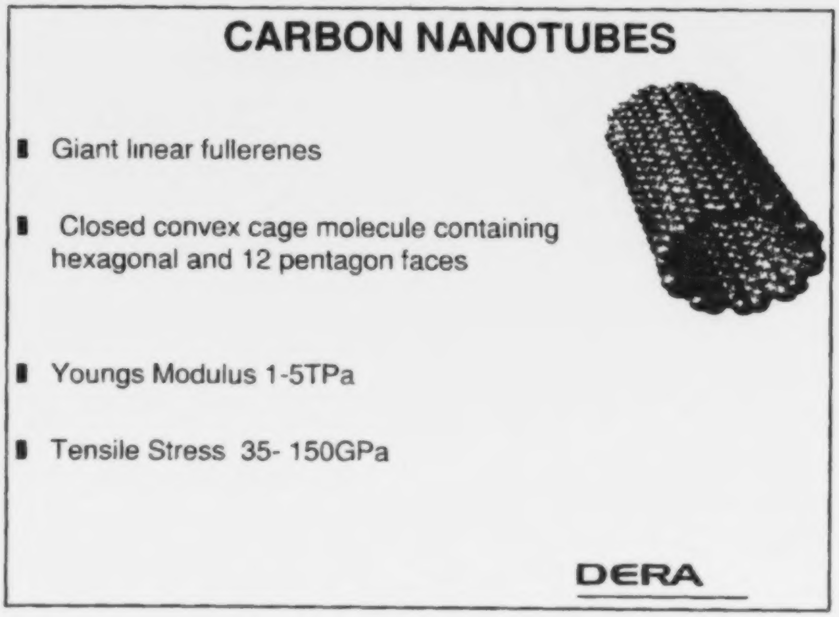

CARBON NANOTUBES

- Giant linear fullerenes
- Closed convex cage molecule containing hexagonal and 12 pentagon faces
- Youngs Modulus 1-5TPa
- Tensile Stress 35- 150GPa

DERA

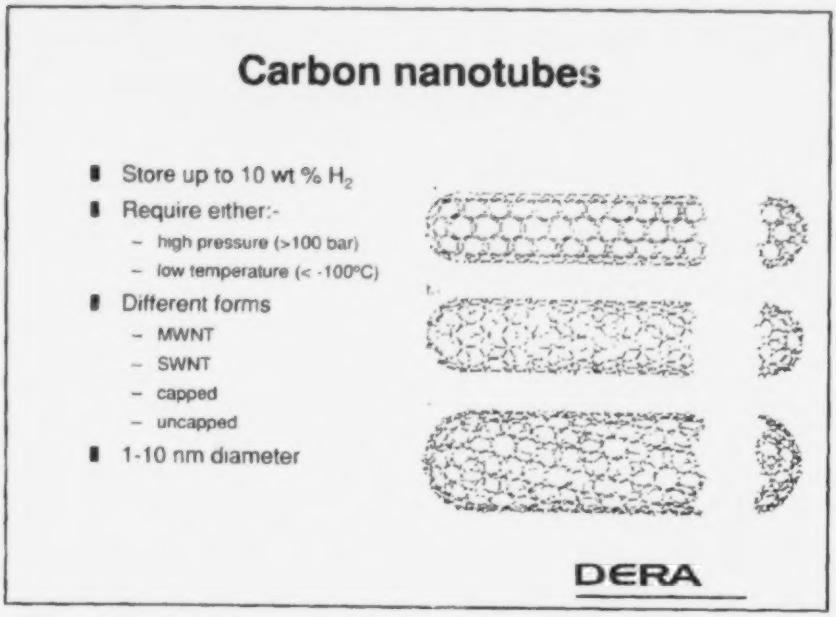

Carbon nanotubes

- Store up to 10 wt % H_2
- Require either:-
  - high pressure (>100 bar)
  - low temperature (< -100°C)
- Different forms
  - MWNT
  - SWNT
  - capped
  - uncapped
- 1-10 nm diameter

DERA

Hydrogen Storage in Graphite Nanostacks

- Currently hydrogen can be stored as a liquid, as compressed gas or as metal hydrides. All suffer from efficiency, weight, bulk or safety problems
- Research suggests that hydrogen can be stored in a special form of graphite, i.e. nanostacks, at very high concentrations
- For example
  - a pressure vessel of 70 litres at 230 atm will hold 16,100 litres of hydrogen
  - a 70 litre container of graphite nanostacks would hold 650,000 litres of hydrogen

- Diesel CH2 =14% Hydrogen, density 0 8g/cc =effective hydrogen density of 0.112g/cc

- Liquid Hydrogen density 0.07g/cc

- Hydrogen in graphite CH12, assumed density 1g/cc =effective hydrogen density 0.5g/cc

DERA

Hydrogen storage methods

Excluding ancillaries

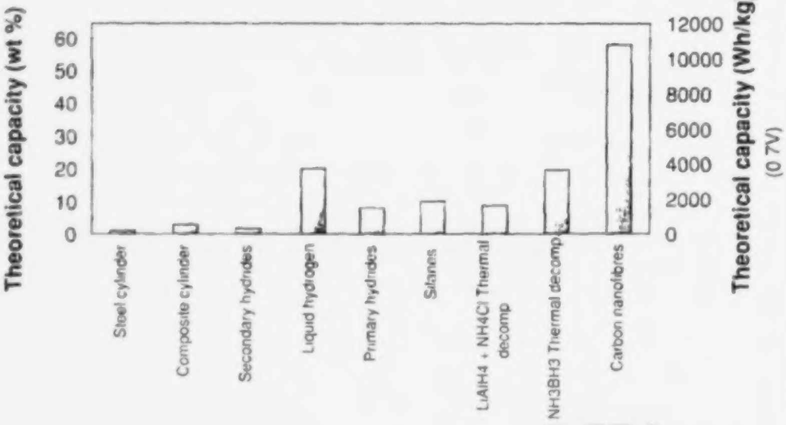

DERA

Modelling

- Physisortion limited to single layer and hence 5%
- H-H interatomic distance at claimed packing density is 0.126 metallic form of hydrogen with delocalised electrons most likely structure.
- However, pressure to form metallic hydrogen at room temperature is 500kbar
- Adsorption in carbon reported at pressures of 140bar

DERA

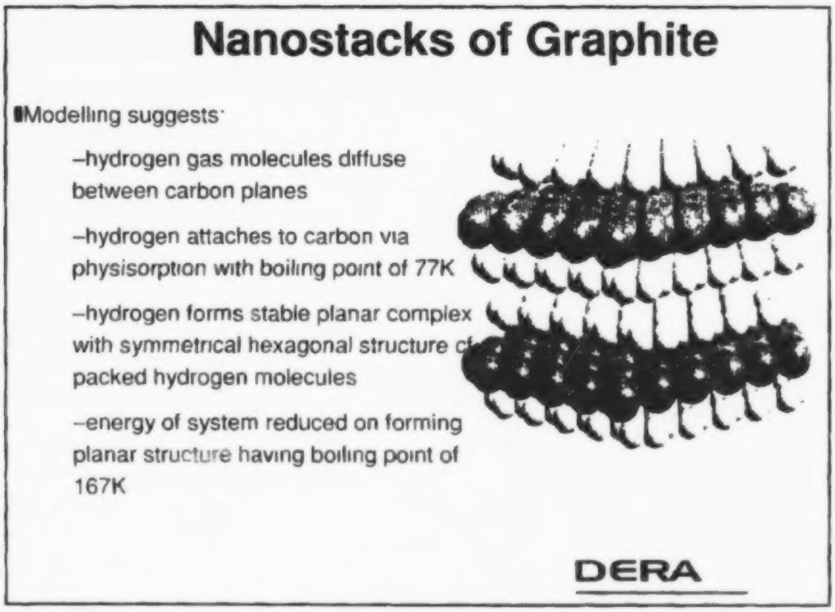

Nanostacks of Graphite

- Modelling suggests:
  - –hydrogen gas molecules diffuse between carbon planes
  - –hydrogen attaches to carbon via physisorption with boiling point of 77K
  - –hydrogen forms stable planar complex with symmetrical hexagonal structure of packed hydrogen molecules
  - –energy of system reduced on forming planar structure having boiling point of 167K

DERA

Measurement of Hydrogen Absorption

- Very prone to error
- Most claims can be explained by measurement errors
- The differential pressure method was chosen as the preferred method for preliminary analysis
  - quick, simple, easy to understand
- An analysis of the errors demonstrates that errors are manageable

DERA

H_2 adsorption

- Used a differential pressure adsorption apparatus
  - increased sensitivity
  - reduces temperature errors
- As synthesised samples
  - max 3 wt % adsorption
- Treated @ 1000°C / Ar
  - max 6.5 wt % adsorption
  - difficult to repeat
  - should improve as purity of fibres increase

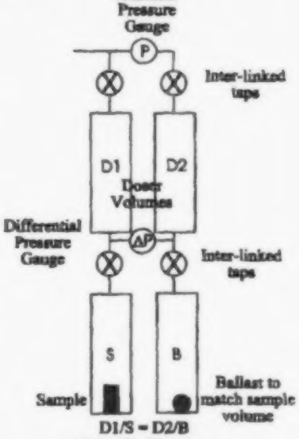
Absolute Pressure Gauge
P
Inter-linked taps
D1
D2
Doser Volumes
Differential Pressure Gauge
ΔP
Inter-linked taps
S
B
Sample
Ballast to match sample volume
D1/S = D2/B

DERA

Analysis of differential absorption system

- The equation used is:-

$$\frac{PV}{RT} = nZ\,(p,T)$$

- where:- P = Pressu
- V = Volume (m^3)
- R = Gas constant (8.314 JK^{-1}mol^{-1})
- T = Temperature (K)
- n = number of moles of gas
- Z = molar compressibility

Molar compressibility for hydrogen has been very accurately measured for a wide range of temperatures and pressures. Using molar compressibility overcomes problem of modelling the effects of pressure and temperature on hydrogen.

DERA

Differential Pressure

$$P_1 = \frac{P_0 D_1 Z(P)}{TZ(P_0)} \left\{ \frac{1}{{D_1}/{T_1} + {D_3}/{T_3}} \right\} - \frac{xRZ(P)}{{D_1}/{T_1} + {D_3}/{T_3}}$$

$$P_2 = \frac{P_0 D_2 Z(P)}{TZ(P_0)} \left\{ \frac{1}{{D_2}/{T_2} + {D_4}/{T_4}} \right\}$$

DERA

Pressure variations calculated for imbalances in temperatures, volumes and absorption efficiencies

Input parameters								
P_0/bar	200	200	200	200	200	200	200	200
T/K	300	300	300	300	300	300	300	300
Doser vol (D_2)/cm^3	300	300	300	300	300	300	300	300
(D_2-D_1)/cm^3	0	0	0	-1	0	0	0	0
blank vol (D4)/cm^3	100	100	100	100	100	100	100	100
(D_4-D_3)/cm^3	0	0	-1	0	0	0	0	0
sample mass (m)/g	0.3	0.3	0.3	0.3	0.3	0.3	0.3	0.3
C density (ρ_0)/(gcm^{-3})	2.2	2.2	2.2	2.2	2.2	2.2	2.2	2.2
massH$_2$absorbed/(massH$_2$+massC) (α)	0.060	0.060	0.060	0.060	0.030	0.010	0.120	0.120
density decrease function (δ)	0.1	0.1	0.1	0.1	0.1	0.1	0.1	1
(T_1-T)/K	0	0	0	0	0	0	0	0
(T_2-T)/K	0	0	0	0	0	0	0	0
(T_3-T)/K	0	1	0	0	0	0	0	0
(T_4-T)/K	0	0	0	0	0	0	0	0
Output		Temp imbalance	Volume imbalance		Variation in amount absorbed			Increased Carbon expansion
ΔP/mbar	**649.3**	**528.7**	**285.8**	**284.6**	**314.6**	**102.8**	**1387.2**	**1380.2**
vol of C before absorption/cm^3	0.136	0.136	0.136	0.136	0.136	0.136	0.136	0.136
vol of C after absorption/cm^3	0.146	0.146	0.146	0.146	0.141	0.138	0.157	0.176

DERA

Example

P_0 = 200 bar ,T = 300 K

Reservoir volumes	= 300 ml
Sample/blank chamber volumes	= 100 ml
Sample mass	= 0.3 g
Carbon density	= 2.2 g/cu.cm
Assumed H mass storage	= 6 %

then:

ΔP = 649.3 mbar

DERA

Errors

- in pressure measurement
- in measurement of volumes
- control of temperature
- due to density change during absorption
- due to contamination of hydrogen
- due to contamination of carbon samples

DERA

Errors in pressure measurement

- Measurement of pressure difference enables use of more sensitive gauge
- Apparatus design must protect gauge from overpressure

DERA

Errors in reservoir volumes

P_0 = 200 bar T = 300 K

Reservoir volumes = 300 ml

Sample/blank chamber volumes = 100 ml

Sample mass = 0.3 g

Error between reservoir volumes = 1 ml

Then: ΔP = 284.6 (c.f. 649.3)

Conclusion - volume errors very important - but controllable by careful manufacture

DERA

Errors in sample volumes

P_0 = 200 bar T = 300 K

Reservoir volumes = 300 ml

Sample/blank chamber volumes = 100 ml

Sample mass = 0.3 g

Error between sample volumes = 1 ml

Then: ΔP = 285.8 (c.f. 649.3)

Conclusion - volume errors very important - but controllable by careful manufacture

DERA

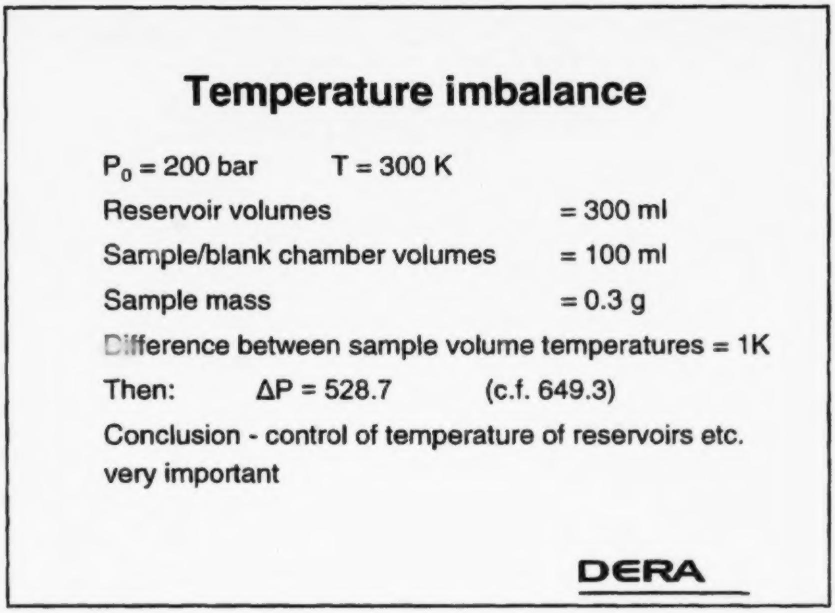

Temperature imbalance

$P_0 = 200$ bar T = 300 K

Reservoir volumes = 300 ml

Sample/blank chamber volumes = 100 ml

Sample mass = 0.3 g

Difference between sample volume temperatures = 1K

Then: $\Delta P = 528.7$ (c.f. 649.3)

Conclusion - control of temperature of reservoirs etc. very important

DERA

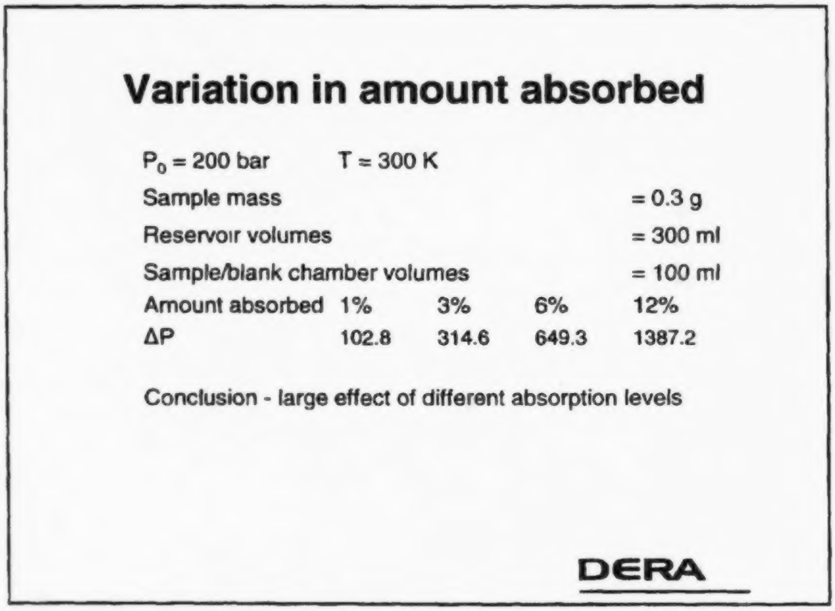

Variation in amount absorbed

$P_0 = 200$ bar T = 300 K

Sample mass = 0.3 g

Reservoir volumes = 300 ml

Sample/blank chamber volumes = 100 ml

Amount absorbed	1%	3%	6%	12%
ΔP	102.8	314.6	649.3	1387.2

Conclusion - large effect of different absorption levels

DERA

Errors in estimate of carbon volume change on absorption of hydrogen

P_0 = 200 bar T = 300 K

Reservoir volumes	= 300 ml	
Sample/blank chamber volumes	= 100 ml	
Amount absorbed	12%	
Assumed volume of C before absorption	0.136 ml	
Assumed volume of C after absorption	0.157 ml	ΔP = 1387.2
Assumed volume of C after absorption	0.176 ml	ΔP = 1380.2

Conclusion - very small effect - probably can be ignored

DERA

Errors due to contamination of hydrogen

- Contamination of the measurement gas with water vapour or air will have a major effect on perceived absorption due to the very high molecular weight of these gases.

DERA

Errors due to contamination of carbon

Other materials can absorb hydrogen.

e.g.

- Catalyst particles associated with carbon nanofibre production
- Other elements incorporated in the fibres as deliberate additions or as contaminants - e.g. Li
- Contaminants derived from equipment - e.g. mechanical attrition

DERA

Carbon production

- Do we need SWNT's, MWNT's or nano fibres
- Catalysts for nanofibres
- Nanofibres - need to be more graphitic

DERA

Synthesis

- Internal work and collaboration with Loughborough and Cambridge University to synthesise and test fibres
- Vapour grown from hydrocarbon gas over metal catalyst
- Tried range of bi and tri metallic metal catalysts
  - Fe, Ni and Cu found to be best

DERA

Bulk analysis of 85Fe:10Ni:5Cu

Technique	Result		
	Fe	Ni	Cu
SEM/EDX	89.4	6.3	3.7
XRF	87.2	9.2	3.5
ICP-AES	89.4	7.8	3.6
Average	88.7	7.8	3.6

DERA

Particle analysis 85Fe:10Ni:5Cu

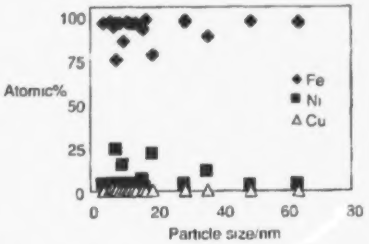

- No Cu
- Mainly Fe

DERA

Catalyst composition

- Agrees with the phase diagram
- Fe-Ni-Cu ternary at 400 deg C shows 3 phases
  - α-Fe, γ-(Cu, Ni), γ-(Fe,Ni)
- Catalyst segregates during reduction from oxide form
- Splits along grain boundaries
  - H_2 embrittlement could help.
- Ni and Cu miscible in all proportions

DERA

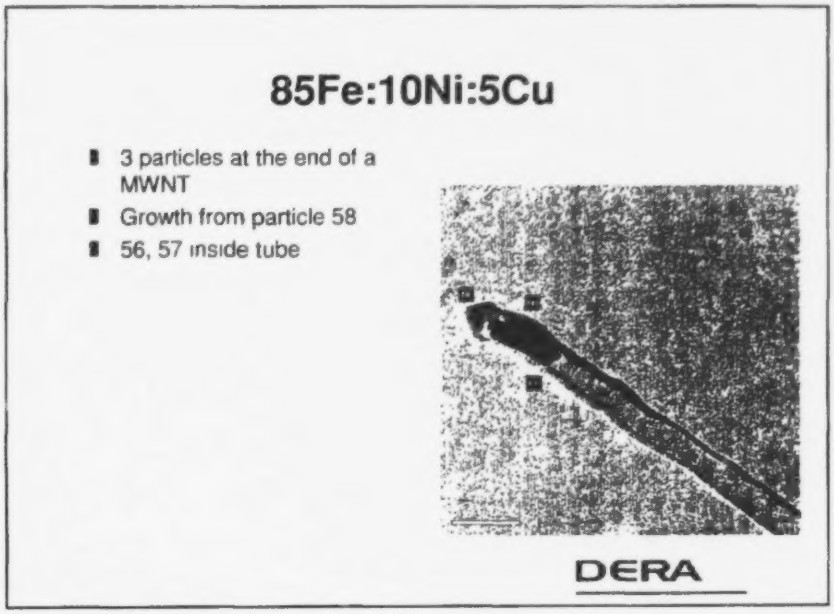

85Fe:10Ni:5Cu

- 3 particles at the end of a MWNT
- Growth from particle 58
- 56, 57 inside tube

DERA

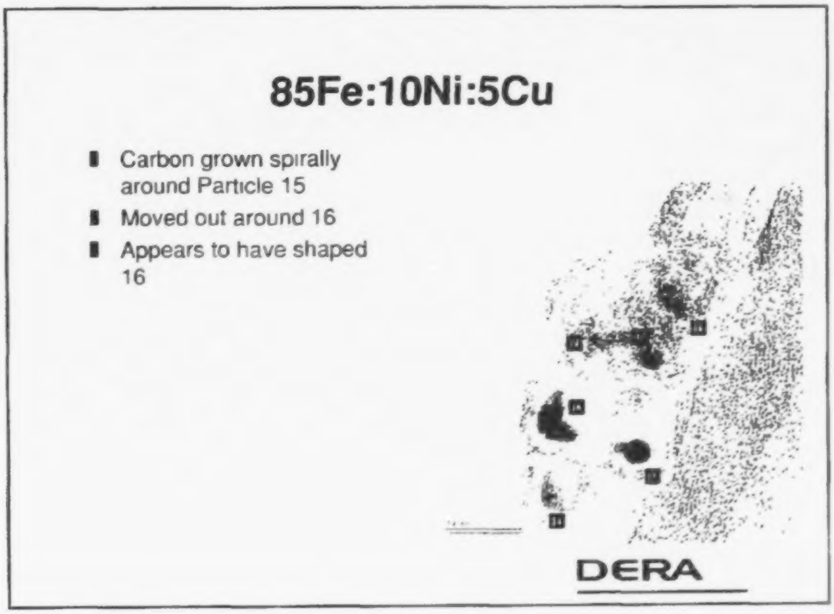

85Fe:10Ni:5Cu

- Carbon grown spirally around Particle 15
- Moved out around 16
- Appears to have shaped 16

DERA

85Fe:10Ni:5Cu

- Catalyst particles inside MWNTs
- Shapes of particles determined by MWNTs
- Most likely rapid solid state diffusion Typical temperatures 500 -700°C
- Would segregate Ni from Cu
  - C soluble in Ni, Fe, not Cu

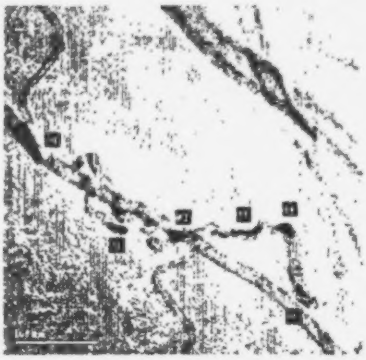

DERA

Reactor orientation effects

- Gas flow and natural convection assist heat transfer from catalyst in vertical reactor
- Heat transfer likely to be less efficient in horizontal reactor
- Odd effects seen in horizontal system at Loughborough
- Implies reactions are rapid and exothermic
  - Carbon yields suggest that all carbon arriving in gas stream is converted in most samples.

DERA

Types of carbon produced

- MWNTs if catalyst particle is <50nm
- CNFs if catalyst particle is >100nm
- Catalyst composition of secondary importance
- Graphitic content of these samples was low
  - Need higher temperature
  - Lower rate of arrival of reactants

DERA

Conclusions

- Catalyst composition is of secondary importance
  - Ni, Fe or Co can all produce the various carbon nanostructures
  - Reactants and temperature more important
- Carbon production can be quite rapid and exothermic
  - Difference between horizontal and vertical reactors probably associated with solid - gas heat transfer
- Could be implication for scale up of a process
  - Maybe supporting catalyst in insulators like silica or alumina is not a good idea.
- Need to Model reaction and heat transfer
- Instrument reactor and obtain more information

DERA

Future Work

Work in FY 01/02 will concentrate on:

- Developing a reliable hydrogen measurement technique
- Using a very limited range of catalysts, prepare C-nanofibres under different reactor conditions
- Explore a number of post treatments
- Determine hydrogen absorption/desorption

DERA

Key Issues

- Importance of structure / degree of graphitisation of nanofibres
- Importance of post-treatments
- Accuracy of hydrogen measurement

Other issues

- Impurity effects
- Storage in SWNT's and MWNT's
- Large diameter SWNT's >~6 and <10 nm diameter

DERA

#516413 ③

Technologies For Corrosion And Wear Control For Naval Applications

by

Vinod S. Agarwala

Naval air Systems Command
Research & Engineering Group
48110 Shaw Road
Patuxent River, MD 20670-1906, U.S.A.

Abstract

Naval aircraft perform in most corrosive and demanding environments. Thus, maintenance and readiness issues impact extremely in both system integrity and costs. Corrosion and corrosion related wear problems are major concerns and if not taken care as soon as possible they exacerbate to a point where depot-level maintenance becomes necessary. This paper describes a number of technologies for both monitoring corrosion and wear as they occur and providing solutions to control them. The subject will include: (1) early warning methods of detection and monitoring degradation of both structural and functional materials; (2) provide products and processes for control; and (3) alternatives or replacement technologies for environmentally hazardous materials and processes such as non-toxic conversion coatings for aluminum alloys, photochemical stripping of paints/coatings and smart self-healing/repair coating systems. The objective of this briefing is to provide concepts for reducing total ownership costs (TOC) in acquisition, operation and maintenance support of aircraft systems by incorporating new technologies which can find damage early and provide methods and products to correct them in an affordable manner or make small repairs. The paper will also discuss how a strategy of condition based maintenance (CBM) can be employed to address aging aircraft problems.

RESEARCH & ENGINEERING

TECHNOLOGIES FOR CORROSION AND WEAR CONTROL FOR NAVAL APPLICATIONS

Dr. Vinod S. Agarwala
Aerospace Materials Division
Naval Air Systems Command
Patuxent River, MD 20670

9TH CF/DRDC Meeting 5-7 June 2001
Dartmouth N.S. Canada

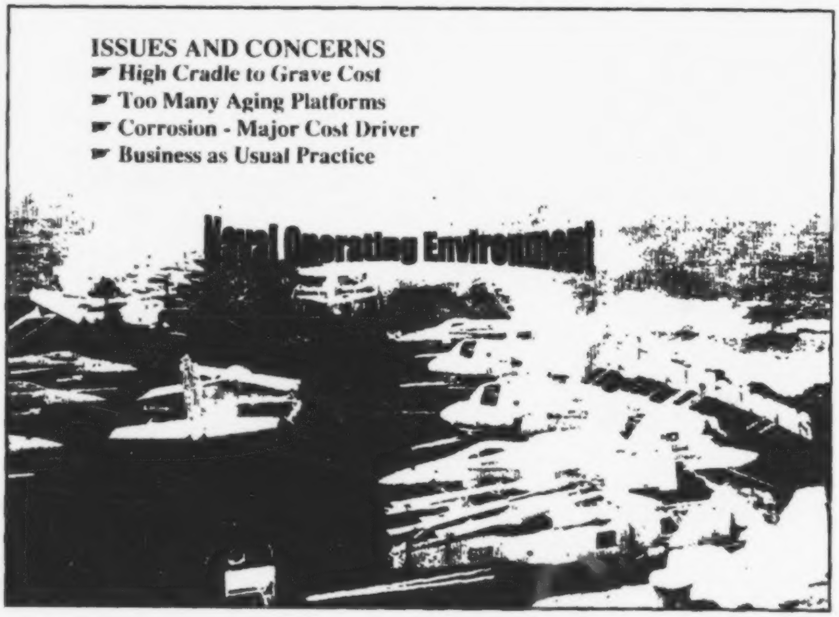

ISSUES AND CONCERNS

- High Cradle to Grave Cost
- Too Many Aging Platforms
- Corrosion - Major Cost Driver
- Business as Usual Practice

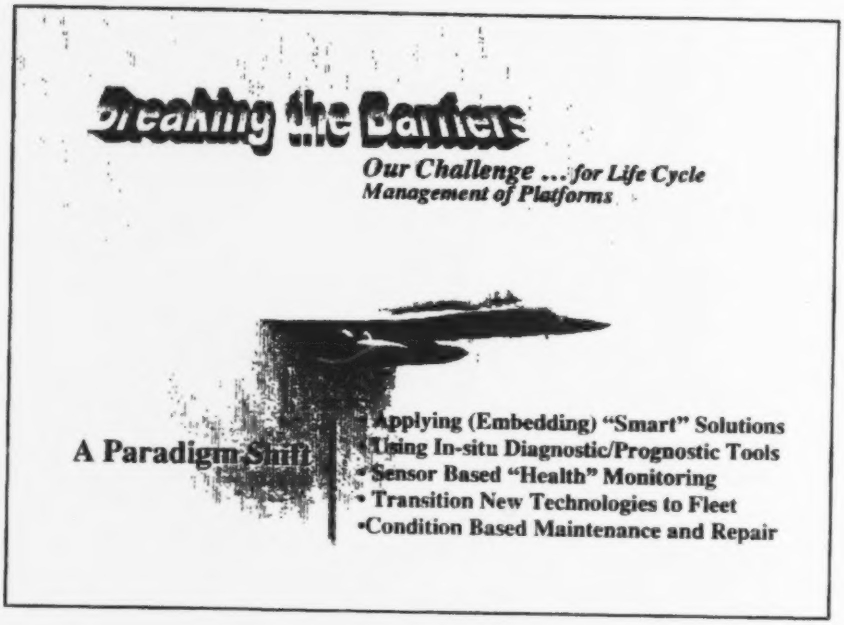

Breaking the Barriers

Our Challenge ... for Life Cycle Management of Platforms

A Paradigm Shift

- **Applying (Embedding) "Smart" Solutions**
- **Using In-situ Diagnostic/Prognostic Tools**
- **Sensor Based "Health" Monitoring**
- **Transition New Technologies to Fleet**
- **Condition Based Maintenance and Repair**

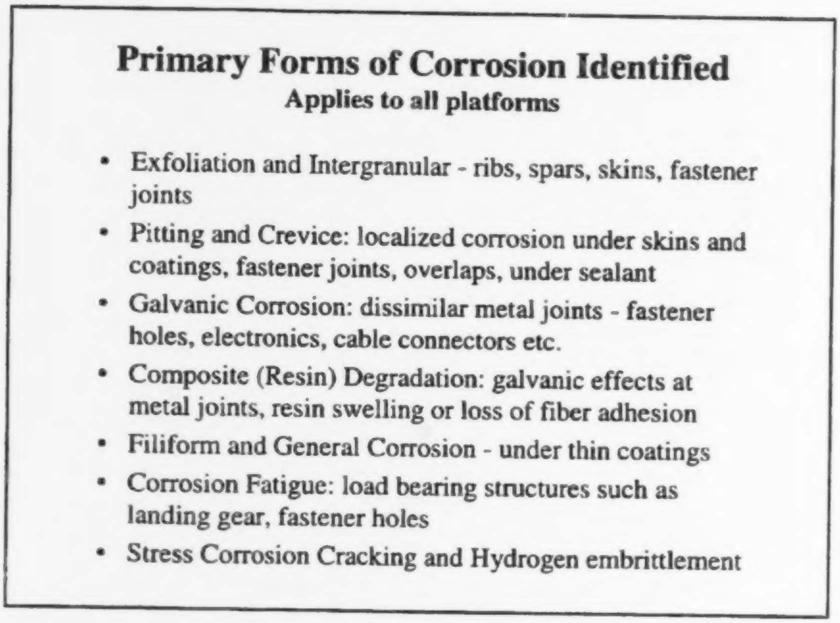

Primary Forms of Corrosion Identified

Applies to all platforms

- Exfoliation and Intergranular - ribs, spars, skins, fastener joints
- Pitting and Crevice: localized corrosion under skins and coatings, fastener joints, overlaps, under sealant
- Galvanic Corrosion: dissimilar metal joints - fastener holes, electronics, cable connectors etc.
- Composite (Resin) Degradation: galvanic effects at metal joints, resin swelling or loss of fiber adhesion
- Filiform and General Corrosion - under thin coatings
- Corrosion Fatigue: load bearing structures such as landing gear, fastener holes
- Stress Corrosion Cracking and Hydrogen embrittlement

P-3 Orion

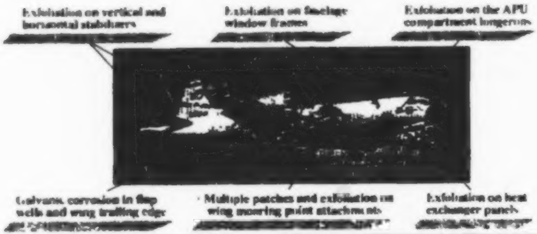

Exfoliation on vertical and horizontal stabilizers

Exfoliation on fuselage window frames

Exfoliation on the APU compartment longerons

Galvanic corrosion in flap wells and wing trailing edge

Multiple patches and exfoliation on wing mooring point attachments

Exfoliation on heat exchanger panels

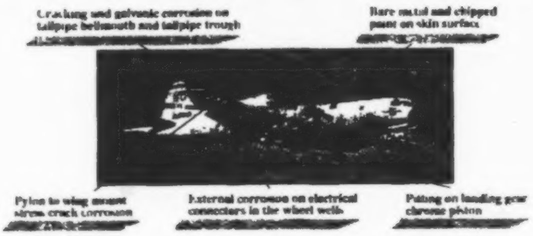

Cracking and galvanic corrosion on tailpipe bellmouth and tailpipe trough

Bare metal and chipped paint on skin surface

Pylon to wing mount stress crack corrosion

External corrosion on electrical connectors in the wheel wells

Pitting on landing gear chrome piston

CORROSION AND WEAR CONTROL TECHNOLOGIES

- **Inspection Techniques**
  - **Conventional methods**
  - **New NDI methods**
  - **On-the-horizon technologies**
- **Detection and Monitoring (Early Warning Devices)**
  - **Environmental corrosivity sensors**
  - **In-place corrosion monitoring sensors**
  - **Hidden corrosion detectors**
  - **Corrosion sensing coating**
- **Products and Processes for Control**
  - **CPCs, adhesives and sealant**
  - **Coatings and Appliques**
  - **H.T. lubricants (hydraulic fluids, oils and greases)**
  - **Inorganic films, surface pre-treatments**

Green Technologies (Non-toxic Substitutes)
  - **Cleaners and strippers**
  - **Conversion coatings**
  - **Primers and paints**

Corrosion Monitoring Requirements

what is monitored or detected?

- *Corrosion causing elements* - **operational or system environment, atmospheric parameters like humidity, temperature, pressure, radiation, air speed**
- *Microstructural or preferential corrosion* - **Pitting, crevice and exfoliation corrosion, galvanic corrosion - dissimilar metal joints**
- *Crack and crack growth* - **corrosion fatigue, stress corrosion cracking, hydrogen embrittlement**
- *General corrosion* - **thickness (mass) loss, hidden damage**
- *Interior/Exterior surface corrosion* - **pillowing, paint lifting**
- *Coating and sealant failure* - **disbonding, moisture pick-up**
- *Corrosion in joints and overlaps* -
- *Degradation of resins and composites*

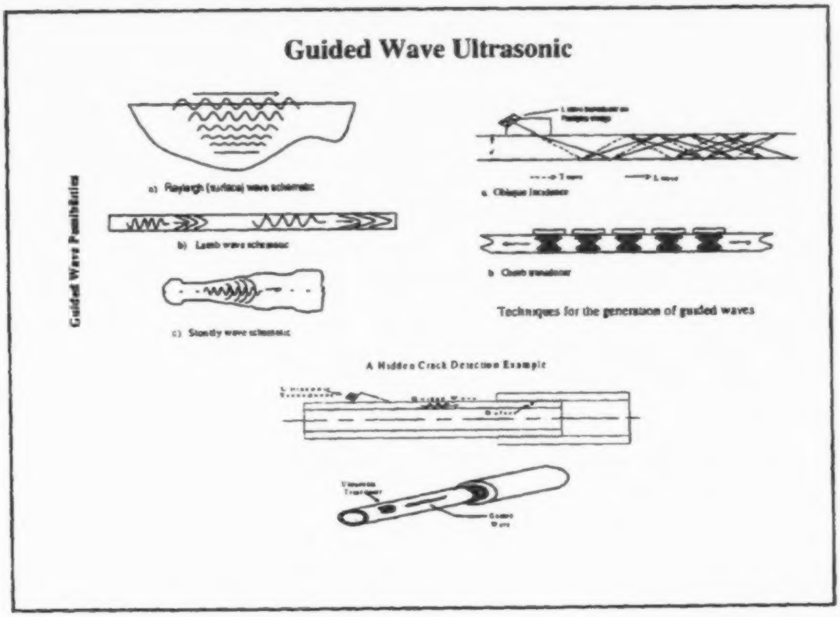

Guided Wave Ultrasonic

Guided Wave Possibilities

a) Rayleigh (surface) wave schematic

b) Lamb wave schematic

c) Stoneley wave schematic

a. Oblique Incidence

b. Comb transducer

Techniques for the generation of guided waves

A Hidden Crack Detection Example

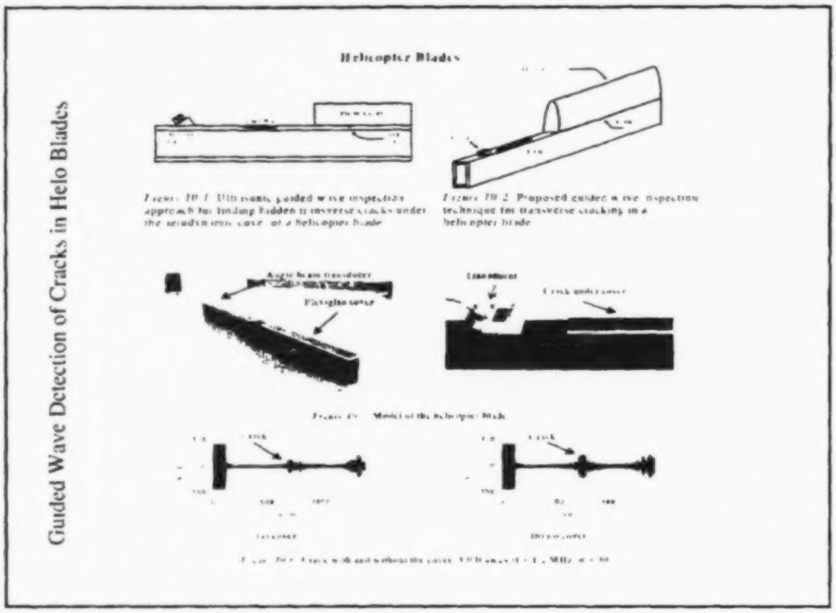

Guided Wave Detection of Cracks in Helo Blades

Helicopter Blades

Figure 10.1 Ultrasonic guided wave inspection approach for finding hidden transverse cracks under the aerodynamic cover of a helicopter blade

Figure 10.2 Proposed guided wave inspection technique for transverse cracking in a helicopter blade

Angle beam transducer
Plexiglass cover
Transducer
Crack under cover

Figure [illegible] Model of the helicopter blade

Crack
Crack

Figure [illegible] Crack with and without the cover [illegible]

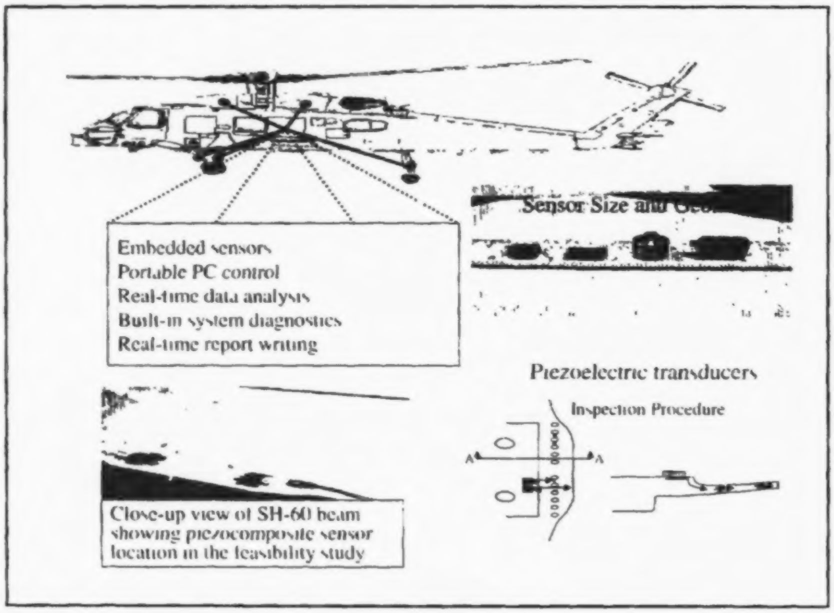

Embedded sensors
Portable PC control
Real-time data analysis
Built-in system diagnostics
Real-time report writing

Sensor Size and Geo
Piezoelectric transducers
Inspection Procedure
A
A

Close-up view of SH-60 beam showing piezocomposite sensor location in the feasibility study

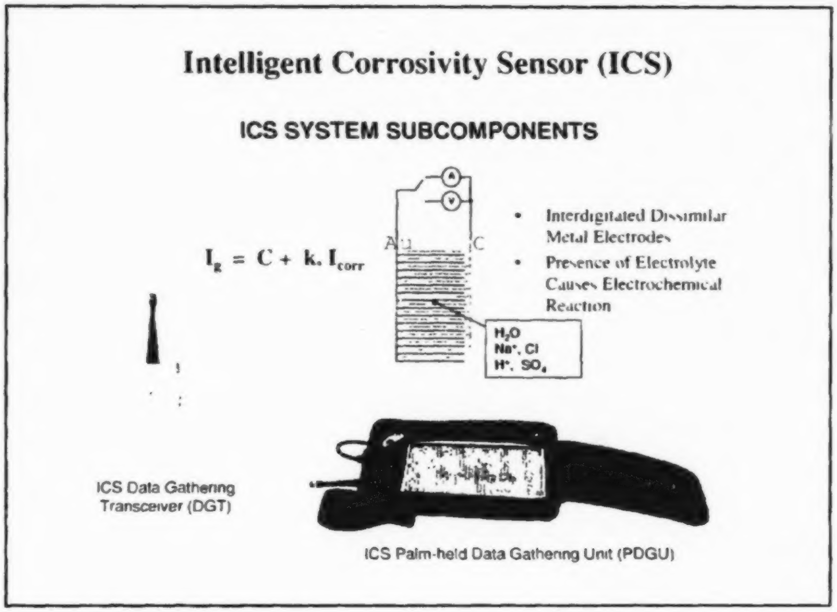

Intelligent Corrosivity Sensor (ICS)

ICS SYSTEM SUBCOMPONENTS

$I_g = C + k. I_{corr}$

- Interdigitated Dissimilar Metal Electrodes
- Presence of Electrolyte Causes Electrochemical Reaction

A
C
A
V
H_2O
Na^+, Cl
H^+, SO_4

ICS Data Gathering Transceiver (DGT)

ICS Palm-held Data Gathering Unit (PDGU)

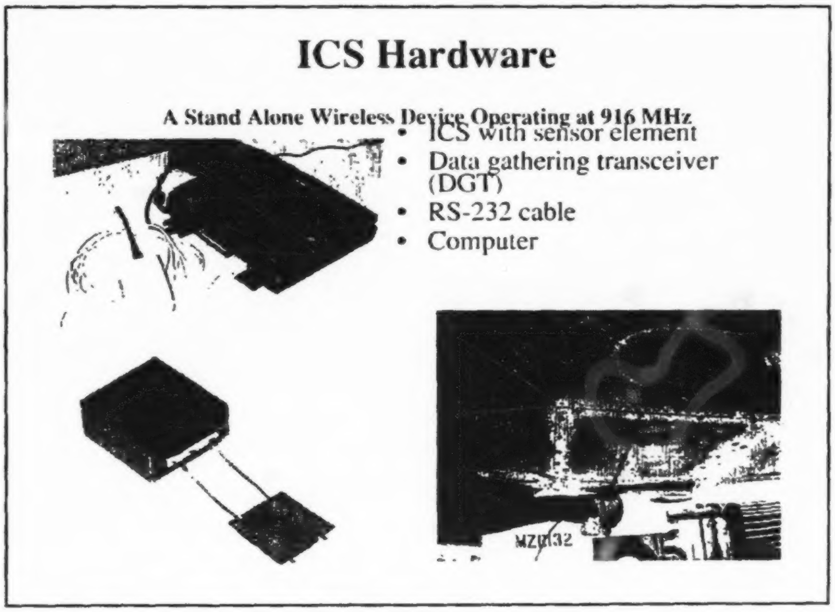

ICS Hardware

A Stand Alone Wireless Device Operating at 916 MHz

- ICS with sensor element
- Data gathering transceiver (DGT)
- RS-232 cable
- Computer

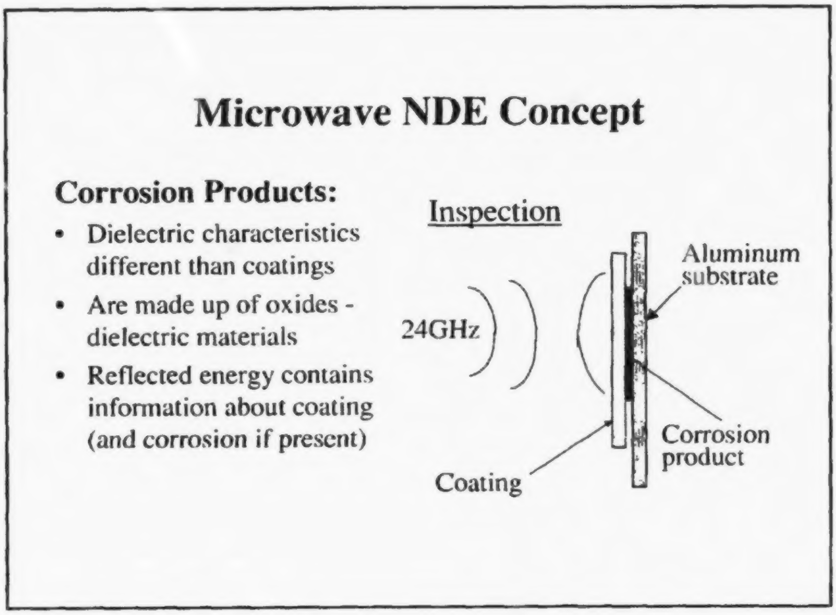

Microwave NDE Concept

Corrosion Products:

- Dielectric characteristics different than coatings
- Are made up of oxides - dielectric materials
- Reflected energy contains information about coating (and corrosion if present)

Inspection
24GHz
Aluminum substrate
Corrosion product
Coating

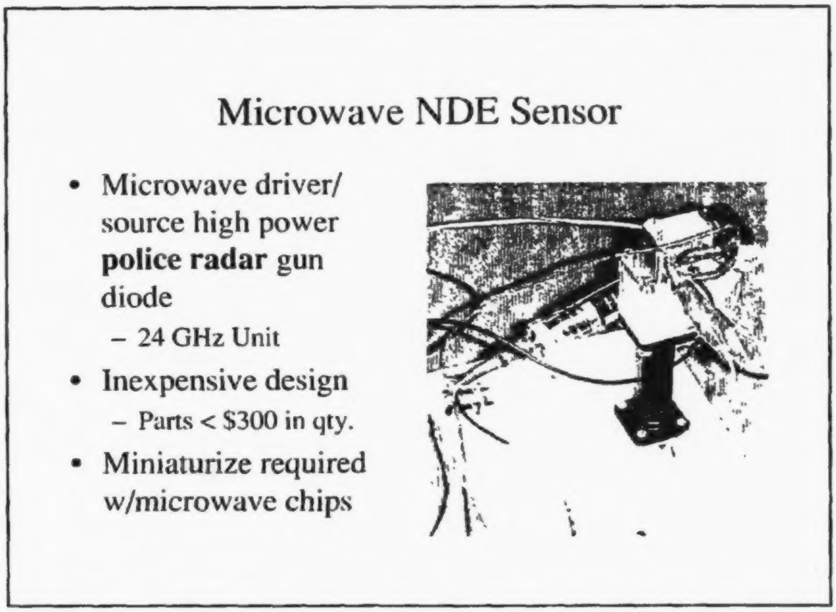

Microwave NDE Sensor

- Microwave driver/ source high power **police radar** gun diode
  - 24 GHz Unit
- Inexpensive design
  - Parts < $300 in qty.
- Miniaturize required w/microwave chips

Microwave Detector on Appliques Film

FP 1500 Appliques

- Panel with Appliques`
- Scratched 7075 T6 w/ Anti-Corrosion Sub-Coat
- Note: increase in sensor output shows system is reliably detecting early of corrosion

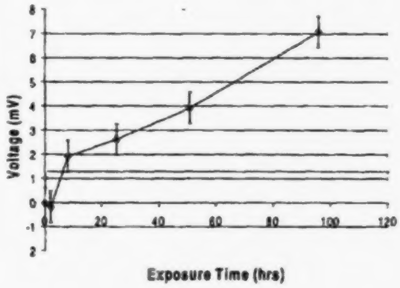

FLUORESCENCE IMAGING
CORROSION SENSING 'SMART' COATING

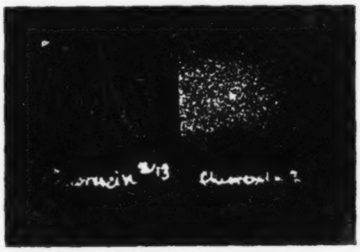

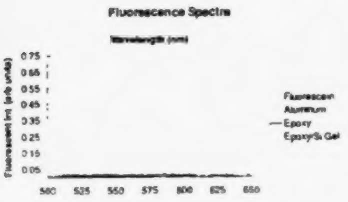

FLUORESCENT MATERIALS

Monitoring Optical Response From Chemical Change By Reaction With Corrosion Product Or Corrosive Specie

- Detection of Corrosion Product - Metal Oxides
- Detection of REDOX Reactions
- Detection of Cations - M^{+n}, H^{+}
- Detection of Anions - OH^{-}

Dyes: Fluorescien, Morin, 8- Hydroxyquinoline, Schiff bases, Coumarin etc.

Fluorescent Indicator
Oxine in Silica Under Epoxy

Comparison of oxine in silica under cured epoxy in 7075 and 7075ccc plates

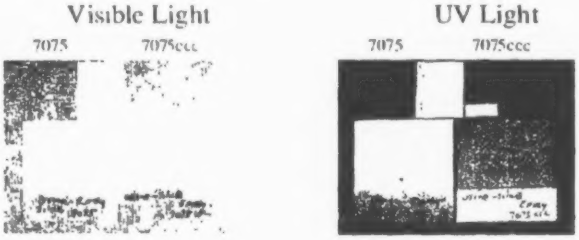

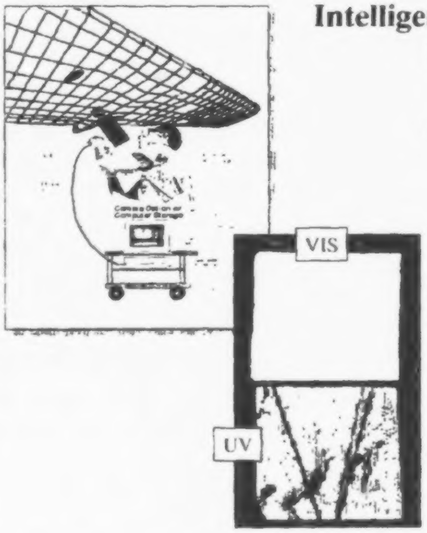

Intelligent Corrosion Indicator
SBIR N97-056

DESCRIPTION

- Embedded indicator normally fluorescent in applied coating
- Products from anodic sites in corrosion pits quench pH sensitive indicator
- Pits disclosed by dark spots in fluorescence

NAVAL AVIATION IMPACT

- Faster, easier corrosion inspections
- High resolution shows <1 mm pits
- Indication before visible damage

OTHER IMPLICATIONS

- Immense commercial market
- Net savings to industry, nation, public

Corrosion Prevention and Control

Products and Processes

Corrosion Preventives
Surface Pretreatments
Coatings
Sealant Materials
Corrosion Inhibitors
Paint Strippers
Lubricants
Self-Lubricating Bearing Materials

Aircraft	Special CPCs	Stripper	Sensors	Applique	HVOF	Skyflex	Zn/Ni Plating	TCC Coating	
AV-8B	⬅			⬅	⬅	⬅		⬆	
C-130	⬅	⬅		⬅	⬅				
F-4			⬆						
H-1	⬅				⬅	⬆	⬅		
H-3	⬅				⬅		⬅		
H-46	⬆		⬆		⬅	⬆			
H-53	⬆								
H-60/H-2	⬆	⬅	⬅			⬆			
V-22	⬅					⬅			
P-3	⬆		⬅	⬅	⬆	⬆		⬆	
EA-6B	⬅				⬆	⬆			
F-14									
T-45						⬅			
E-6					⬆				
S-3	⬆			⬆	⬅	⬆		⬆	
F-18				⬆	⬅	⬆			

⬆ *Implemented on one or more aircraft* ⬅ *Under consideration*

CPC's CURRENTLY USED FOR NAVAL AIRCRAFT

SPECIFICATION	DESCRIPTION	APPLICATION
MIL-C-81309 Type II	Water- displacing, short term protection, soft thin film (0.5 mils) with some lubrication	Temporary protection of hinges, bomb racks, sliding parts
MIL-C-81309 Type III	Water-displacing, short term protection, soft very thin film (0.2 mils) with some lubrication	Avionics equipment, connector plugs
MIL-C-16173 Grade 1	Non-displacing, heavy-duty, thick, hard film (4mils)	Long term protection of metal equipment during outdoor storage
MIL-C-16173 Grade 2	Non-displacing, soft, thick, (2mils)	Protection of metal equipment during indoor and outdoor storage
MIL-C-16173 Grade 4	Non-displacing, soft but tack free, thick film (2mils)	Protection of metal equipment during indoor and outdoor storage; protection of control cables
MIL-C-85054	Water-displacing, dry, colorless, thin film (1mil)	Protection of equipment not requiring lubrication where paint has been damaged and which will be washed during routine maintenance
MIL-L-63460	Water-displacing, oily, thin film	Cleaning, lubricating and preservation of small and large weapons

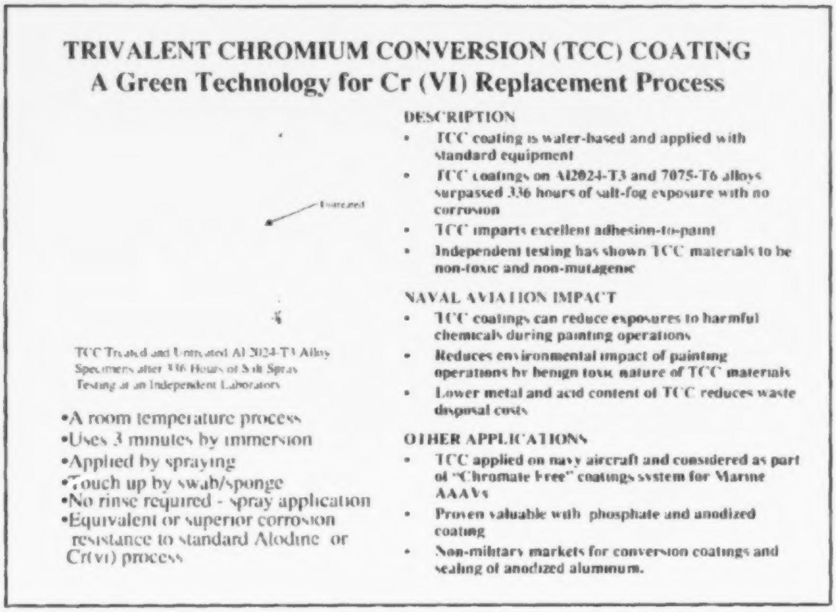

TRIVALENT CHROMIUM CONVERSION (TCC) COATING
A Green Technology for Cr (VI) Replacement Process

TCC Treated and Untreated Al 2024-T3 Alloy Specimens after 336 Hours of Salt Spray Testing at an Independent Laboratory

- •A room temperature process
- •Uses 3 minutes by immersion
- •Applied by spraying
- •Touch up by swab/sponge
- •No rinse required - spray application
- •Equivalent or superior corrosion resistance to standard Alodine or Cr(vi) process

DESCRIPTION

- **TCC coating is water-based and applied with standard equipment**
- **TCC coatings on Al2024-T3 and 7075-T6 alloys surpassed 336 hours of salt-fog exposure with no corrosion**
- **TCC imparts excellent adhesion-to-paint**
- **Independent testing has shown TCC materials to be non-toxic and non-mutagenic**

NAVAL AVIATION IMPACT

- **TCC coatings can reduce exposures to harmful chemicals during painting operations**
- **Reduces environmental impact of painting operations by benign toxic nature of TCC materials**
- **Lower metal and acid content of TCC reduces waste disposal costs**

OTHER APPLICATIONS

- **TCC applied on navy aircraft and considered as part of "Chromate Free" coatings system for Marine AAAVs**
- **Proven valuable with phosphate and anodized coating**
- **Non-military markets for conversion coatings and sealing of anodized aluminum.**

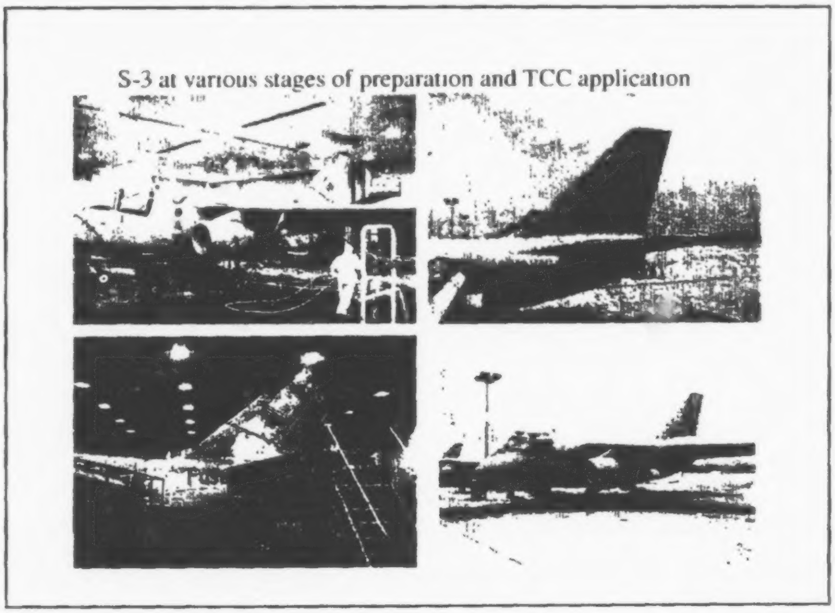

S-3 at various stages of preparation and TCC application

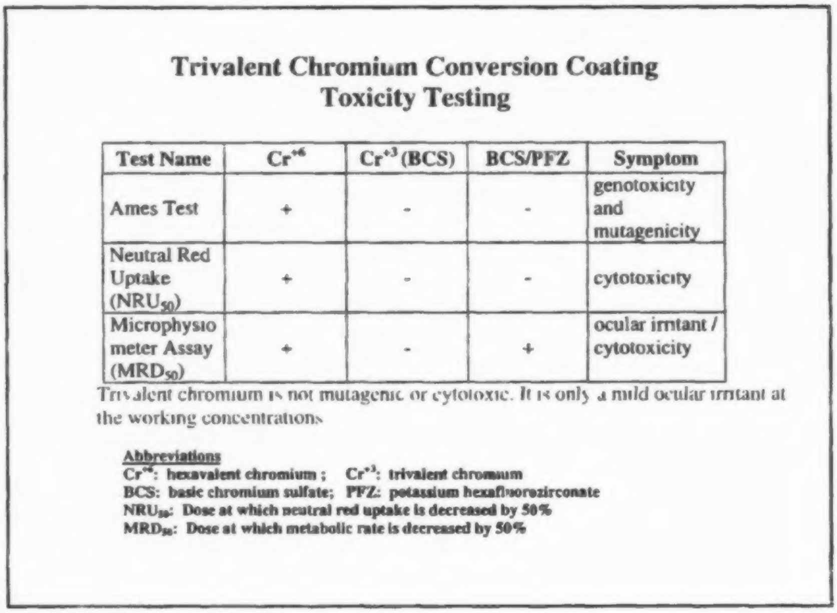

Trivalent Chromium Conversion Coating Toxicity Testing

Test Name	Cr^{+6}	Cr^{+3} (BCS)	BCS/PFZ	Symptom
Ames Test	+	-	-	genotoxicity and mutagenicity
Neutral Red Uptake (NRU_{50})	+	-	-	cytotoxicity
Microphysiometer Assay (MRD_{50})	+	-	+	ocular irritant / cytotoxicity

Trivalent chromium is not mutagenic or cytotoxic. It is only a mild ocular irritant at the working concentrations

Abbreviations

Cr^{+6}: hexavalent chromium ; Cr^{+3}: trivalent chromium
BCS: basic chromium sulfate; PFZ: potassium hexafluorozirconate
NRU_{50}: Dose at which neutral red uptake is decreased by 50%
MRD_{50}: Dose at which metabolic rate is decreased by 50%

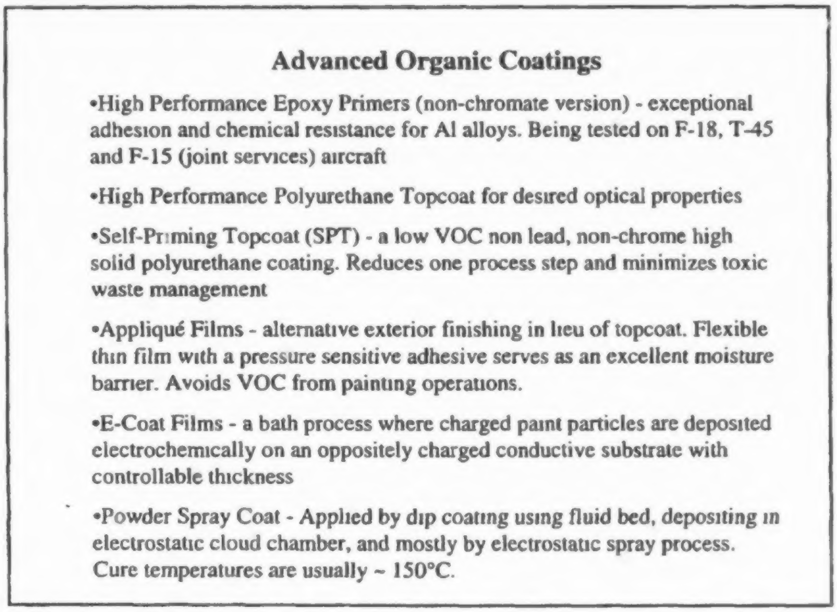

Advanced Organic Coatings

- •High Performance Epoxy Primers (non-chromate version) - exceptional adhesion and chemical resistance for Al alloys. Being tested on F-18, T-45 and F-15 (joint services) aircraft
- •High Performance Polyurethane Topcoat for desired optical properties
- •Self-Priming Topcoat (SPT) - a low VOC non lead, non-chrome high solid polyurethane coating. Reduces one process step and minimizes toxic waste management
- •Appliqué Films - alternative exterior finishing in lieu of topcoat. Flexible thin film with a pressure sensitive adhesive serves as an excellent moisture barrier. Avoids VOC from painting operations.
- •E-Coat Films - a bath process where charged paint particles are deposited electrochemically on an oppositely charged conductive substrate with controllable thickness
- •Powder Spray Coat - Applied by dip coating using fluid bed, depositing in electrostatic cloud chamber, and mostly by electrostatic spray process. Cure temperatures are usually ~ 150°C.

Skyflex Sealant

- An expanded polytetrafluoroethylene (ePTFE) sealant/gasket material
- Excellent environmental seal, hydrophobic and removable/reusable
- Reduces need for frequent reapplication (typical for current sealants)
- Requires no mixing, masking or lengthy cure times
- Replaces toxic polysulfide, which contains chromates and HAP solvents
- Current Navy efforts include access panels of P-3, S-3, H-1, E-6 and H-60
- Approved for sealing floorboards for the P-3, H-60 and H-53 platforms

Hard Chrome Replacement

Hard chromium is used for fatigue, wear and corrosion resistance for high strength steel (4340, 300M and Aermet 100) components
Environmental regulations restrict use of chromium

- High Velocity Oxygen Fuel (HVOF) metal spray coating
- A line-of-sight thermal spray process to replace Cr
- Deposited coating alloy is 83% WC and 17% Co
- WC-Co coating is tested form landing gears, hydraulic parts, rotary components and propeller hubs
- Naval Aviation Depots (NADEPs) at Jacksonville, Cherry Point have operational systems

Coating Removal

During life-cycle of military aircraft paint stripping and re-coating is required periodically for inspection, maintenance and repair

Traditional Paint Strippers

➤Chemical: use methylene chloride, phenol and benzyl alcohol based solvents

➤Mechanical: hand scrubbing using sanders

➤Media blasting: PMB, starch, bicarbonate, sand, polymer beads etc.

New Non-HAP Technologies

➤N-methyl pyrrolidone (NMP) and peroxide based removers (at 160 to 180° F)

➤Flashjet® Process - Xe flashlamp-induced coating volatilization followed by low pressure CO_2 particle sweep to remove soot etc. using robotic gantry system

➤Photostrip Process - Non-VOC/non-HAP water based chemical spray treatment followed by UV exposure for up to 6 hours. Strips of coating peels off for disposal as solid waste.

PHOTOSTRIP - PHOTOCHEMICAL STRIPPING OF AIRCRAFT COATINGS

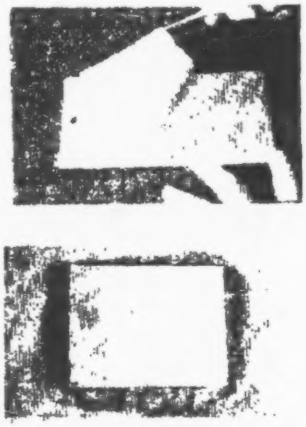

PROCESS HIGHLIGHTS:

- Photochemical process using UV light and inorganic chemicals to delaminate paint from painted surfaces.
- Process duration is less than 8 hours.
- Paint can be stripped from a variety of different substrates, such as, aluminum, stainless steel, composites, fiberglass, wood, and radome material.
- Process can be automated for each application.
- Minimal waste generated. No toxic waste contributed by the process and the chemicals used.

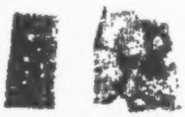

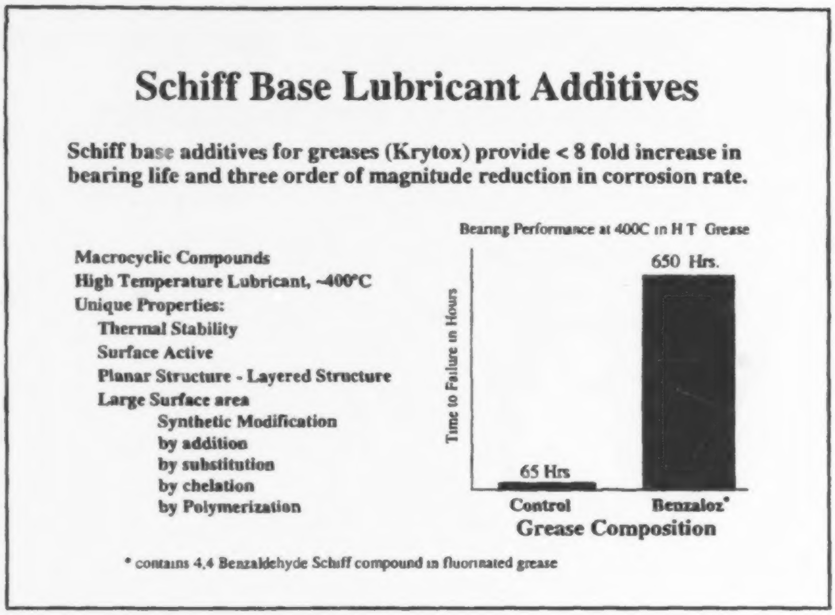

Schiff Base Lubricant Additives

Schiff base additives for greases (Krytox) provide < 8 fold increase in bearing life and three order of magnitude reduction in corrosion rate.

Macrocyclic Compounds
High Temperature Lubricant, ~400°C
Unique Properties:
- **Thermal Stability**
- **Surface Active**
- **Planar Structure - Layered Structure**
- **Large Surface area**
  - **Synthetic Modification**
  - **by addition**
  - **by substitution**
  - **by chelation**
  - **by Polymerization**

Bearing Performance at 400C in H T Grease
650 Hrs.
Time to Failure in Hours
65 Hrs
Control
Benzaloz*
Grease Composition

* contains 4,4 Benzaldehyde Schiff compound in fluorinated grease

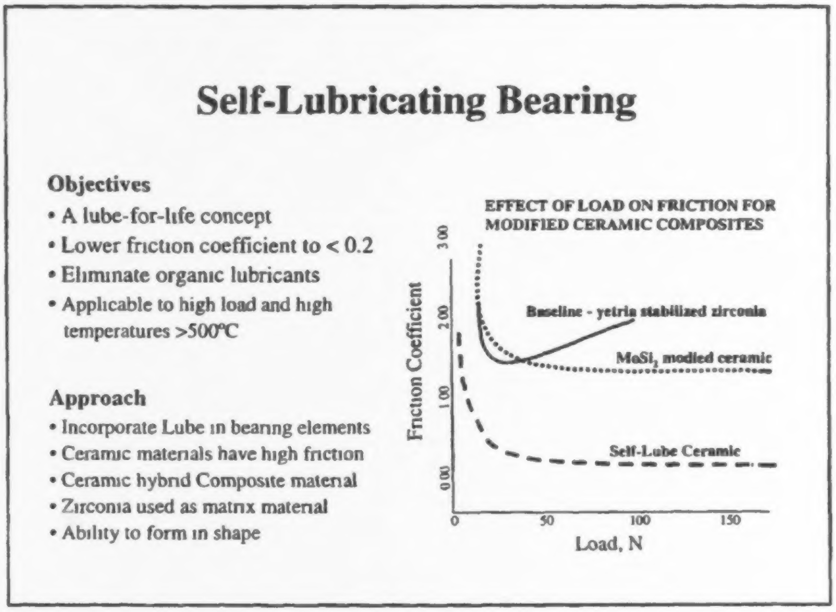

Self-Lubricating Bearing

Objectives
- A lube-for-life concept
- Lower friction coefficient to < 0.2
- Eliminate organic lubricants
- Applicable to high load and high temperatures >500°C

Approach
- Incorporate Lube in bearing elements
- Ceramic materials have high friction
- Ceramic hybrid Composite material
- Zirconia used as matrix material
- Ability to form in shape

Microstructural Characterization of the Corroded Surface of Laser Clad Nickel Aluminum Bronze following Long-Term Sea-water Exposure

by

J.A. Gianetto[1], G. A. Botton[1] and C.V. Hyatt[2]

[1] Materials Technology Laboratory, CANMET, Ottawa, Canada
[2] Defence Research Establishment Atlantic, P.O. Box 1012, Dartmouth, Nova Scotia, Canada, B2Y 3Z7

Abstract

The long-term corrosion performance of surface ship and submarine components that are made of nickel-aluminum bronze (NAB) continues to be of interest to the Canadian Navy. Collaborative research between the Defence Research Establishment Atlantic and CANMET's Materials Technology Laboratory has focused on ways of improving the surface sensitive properties of NAB components utilizing laser weld cladding procedures. In the study described in this presentation laser clad weld specimens exposed to stagnent polluted seawater for several years were characterized using optical and scanning electron microscopy, as well as focused ion beam (FIB) techniques to prepare samples for detailed transmission electron microscopy (TEM). This new FIB/TEM approach characterizing the microstructural features associated with corrosion offers new insights about the detailed microstructure of the corrosion films. Data on corrosion film structure and composition as assessed by high-resolution elemental mapping, energy loss spectroscopy for chemical state analysis, and electron diffraction will be described in this presentation.

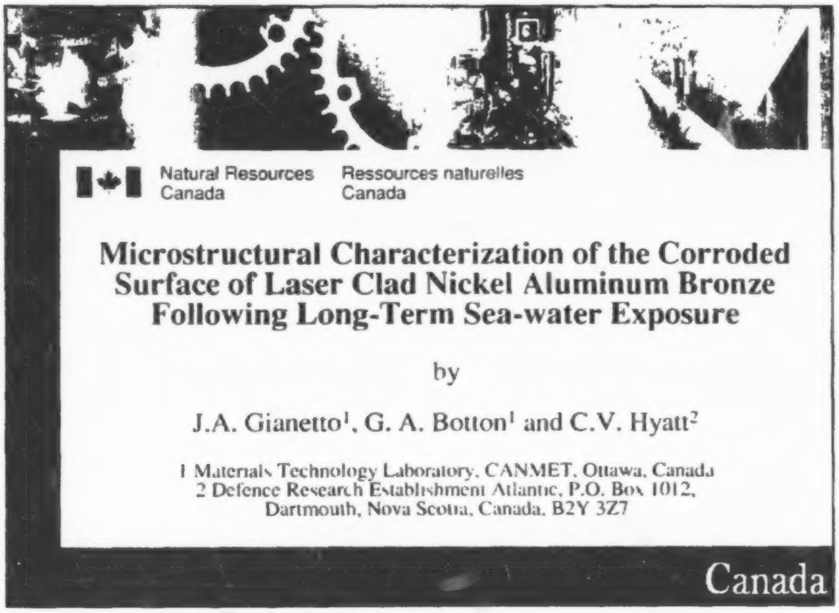

Natural Resources Canada Ressources naturelles Canada

Microstructural Characterization of the Corroded Surface of Laser Clad Nickel Aluminum Bronze Following Long-Term Sea-water Exposure

by

J.A. Gianetto[1], G. A. Botton[1] and C.V. Hyatt[2]

1 Materials Technology Laboratory, CANMET, Ottawa, Canada
2 Defence Research Establishment Atlantic, P.O. Box 1012,
Dartmouth, Nova Scotia, Canada, B2Y 3Z7

Canada

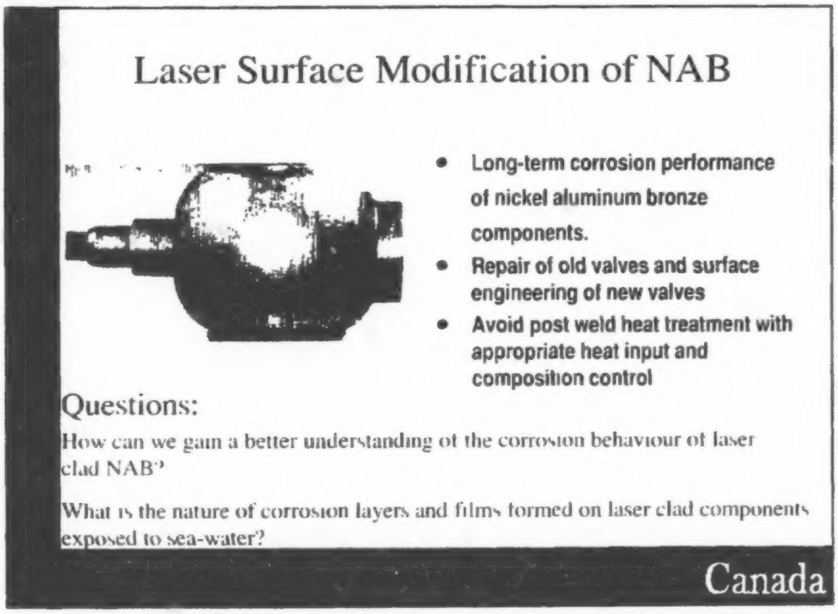

Laser Surface Modification of NAB

- **Long-term corrosion performance of nickel aluminum bronze components.**
- **Repair of old valves and surface engineering of new valves**
- **Avoid post weld heat treatment with appropriate heat input and composition control**

Questions:

How can we gain a better understanding of the corrosion behaviour of laser clad NAB?

What is the nature of corrosion layers and films formed on laser clad components exposed to sea-water?

Canada

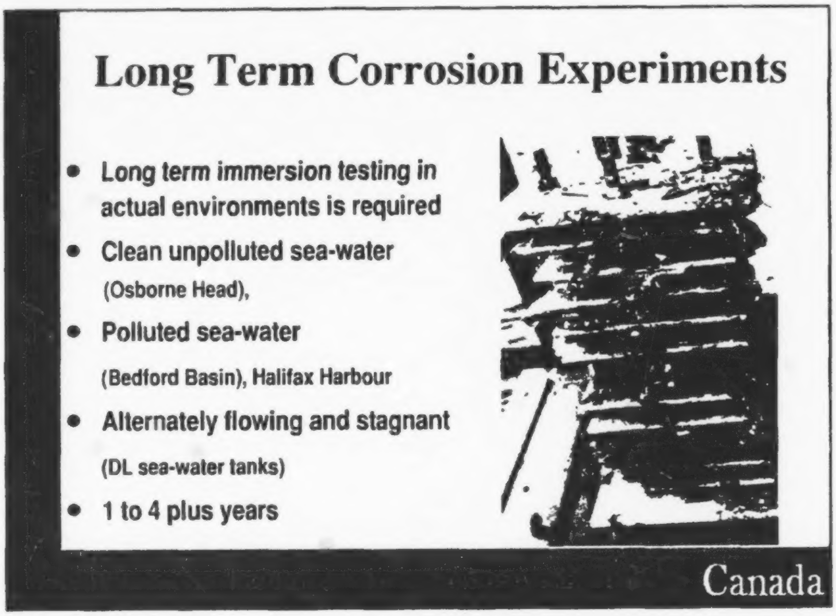

Long Term Corrosion Experiments

- Long term immersion testing in actual environments is required
- Clean unpolluted sea-water (Osborne Head),
- Polluted sea-water (Bedford Basin), Halifax Harbour
- Alternately flowing and stagnant (DL sea-water tanks)
- 1 to 4 plus years

Canada

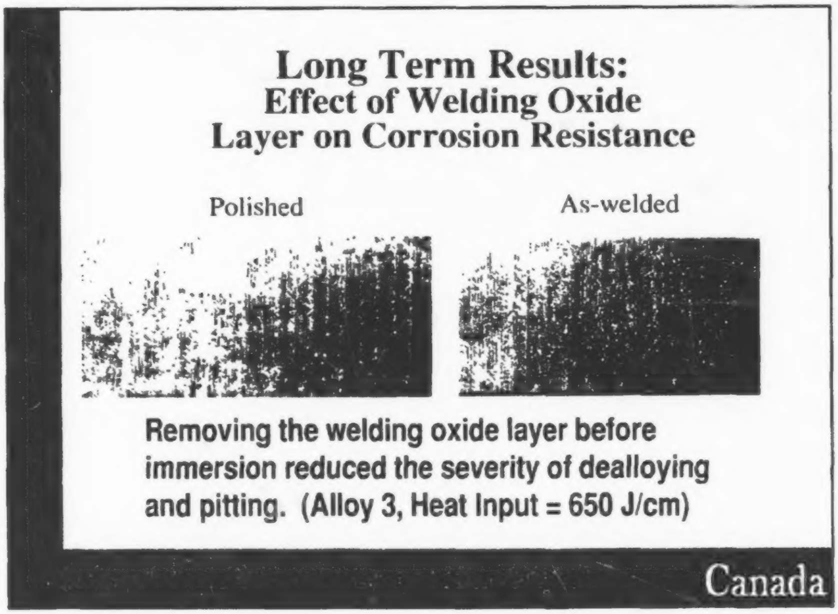

Long Term Results: Effect of Welding Oxide Layer on Corrosion Resistance

Polished

As-welded

Removing the welding oxide layer before immersion reduced the severity of dealloying and pitting. (Alloy 3, Heat Input = 650 J/cm)

Canada

Objective

- To characterize the microstructural and chemical nature of corrosion products, including surface layers and oxide films for a laser clad Cr modified NAB weld after long term sea-water exposure.

Canada

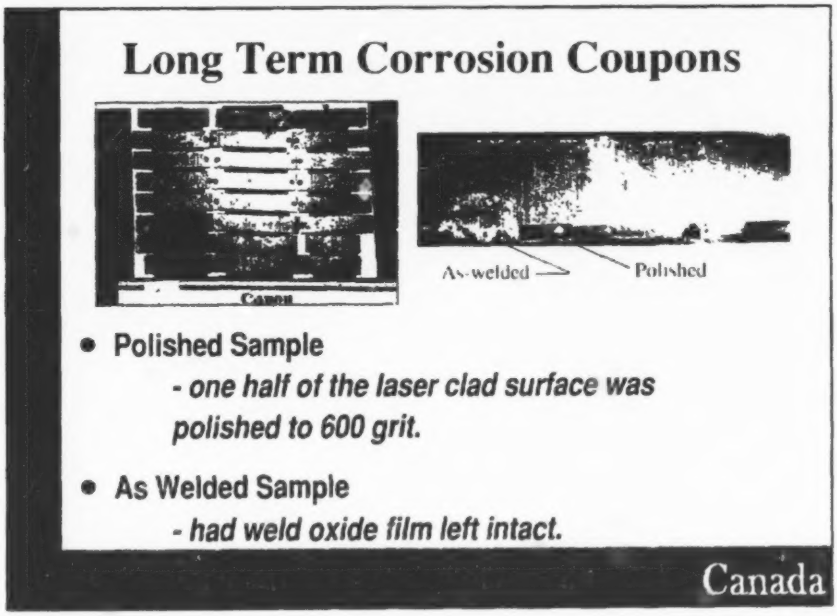

Long Term Corrosion Coupons

- **Polished Sample**
  - *one half of the laser clad surface was polished to 600 grit.*
- **As Welded Sample**
  - *had weld oxide film left intact.*

Canada

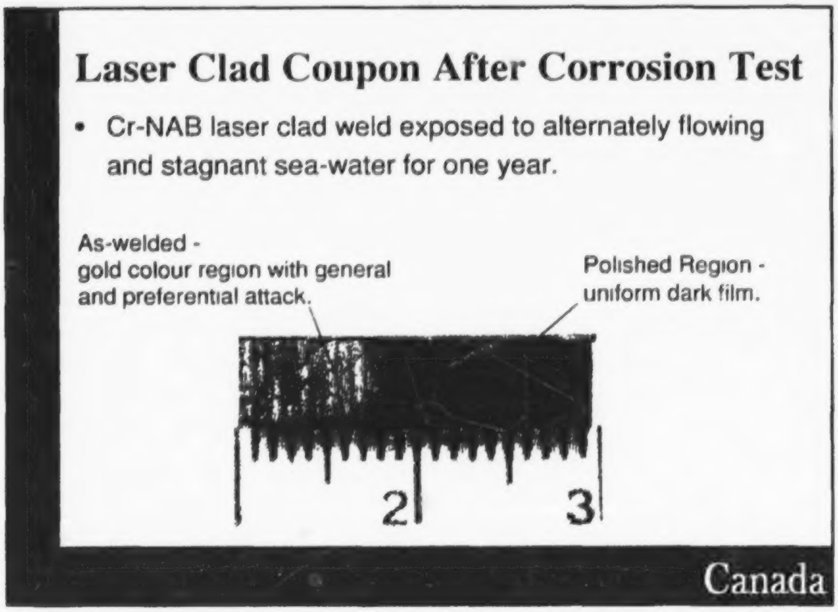

Laser Clad Coupon After Corrosion Test

- Cr-NAB laser clad weld exposed to alternately flowing and stagnant sea-water for one year.

As-welded -
gold colour region with general
and preferential attack.

Polished Region -
uniform dark film.

Canada

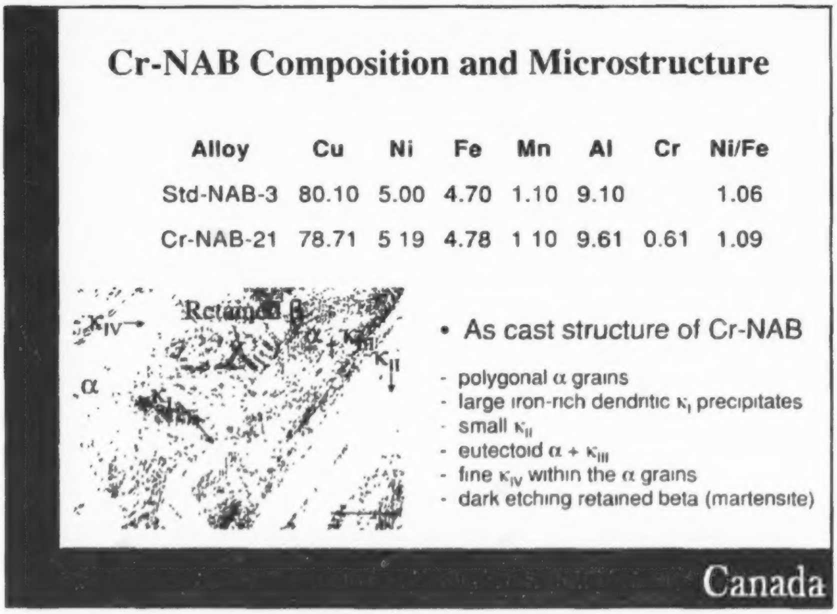

Cr-NAB Composition and Microstructure

Alloy	Cu	Ni	Fe	Mn	Al	Cr	Ni/Fe
Std-NAB-3	80.10	5.00	4.70	1.10	9.10		1.06
Cr-NAB-21	78.71	5.19	4.78	1.10	9.61	0.61	1.09

κ_{IV}
Retained β
α
κ_{III}
κ_{II}
α
κ_I

- As cast structure of Cr-NAB
  - polygonal α grains
  - large iron-rich dendritic κ_I precipitates
  - small κ_{II}
  - eutectoid $\alpha + \kappa_{III}$
  - fine κ_{IV} within the α grains
  - dark etching retained beta (martensite)

Canada

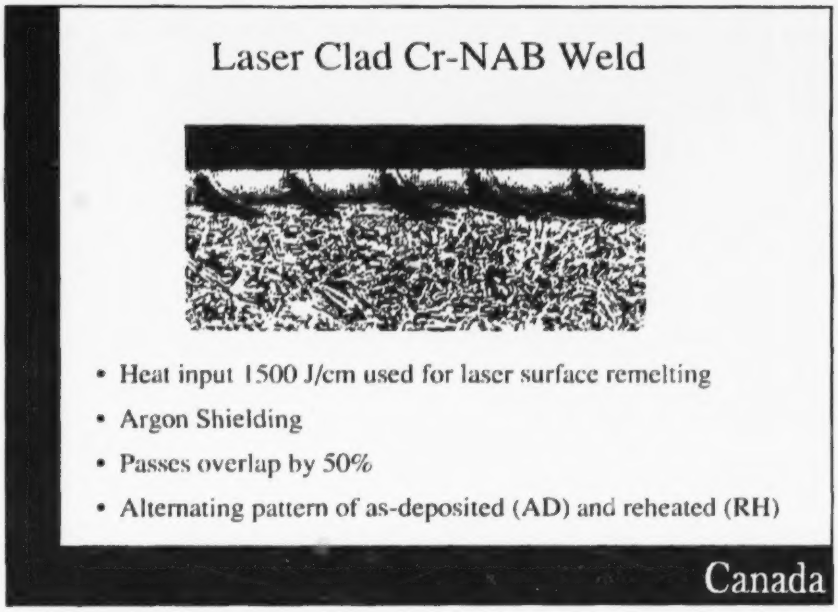

Laser Clad Cr-NAB Weld

- Heat input 1500 J/cm used for laser surface remelting
- Argon Shielding
- Passes overlap by 50%
- Alternating pattern of as-deposited (AD) and reheated (RH)

Canada

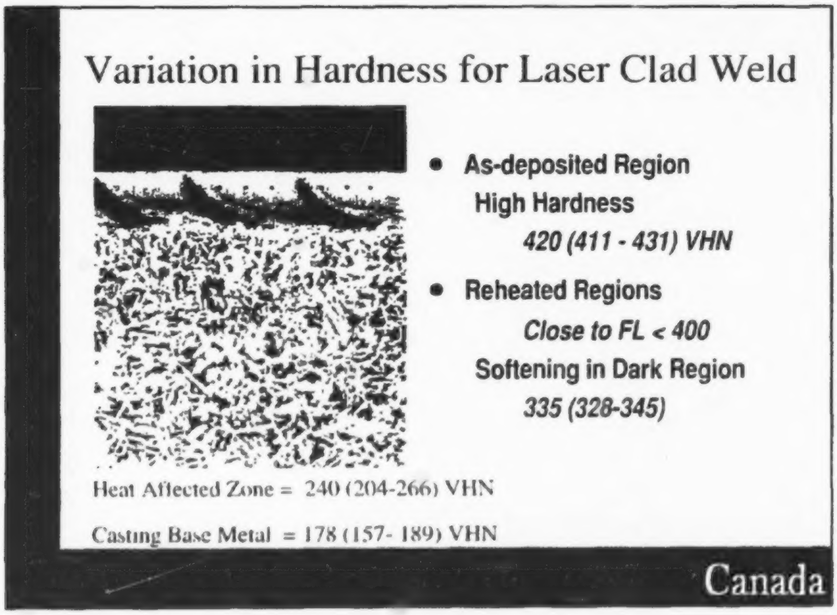

Variation in Hardness for Laser Clad Weld

- **As-deposited Region**
  High Hardness
  420 (411 - 431) VHN
- **Reheated Regions**
  Close to FL < 400
  Softening in Dark Region
  335 (328-345)

Heat Affected Zone = 240 (204-266) VHN

Casting Base Metal = 178 (157- 189) VHN

Canada

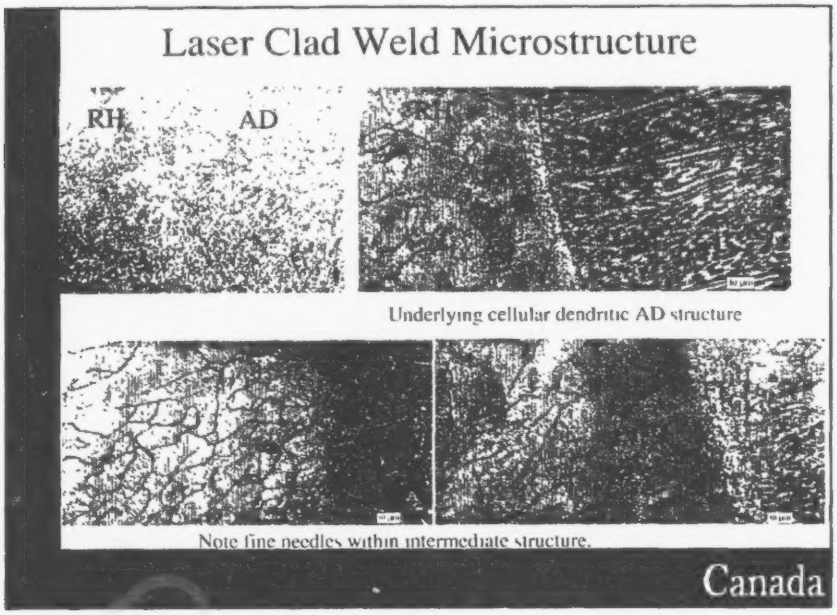

Laser Clad Weld Microstructure

Underlying cellular dendritic AD structure

Note fine needles within intermediate structure.

Canada

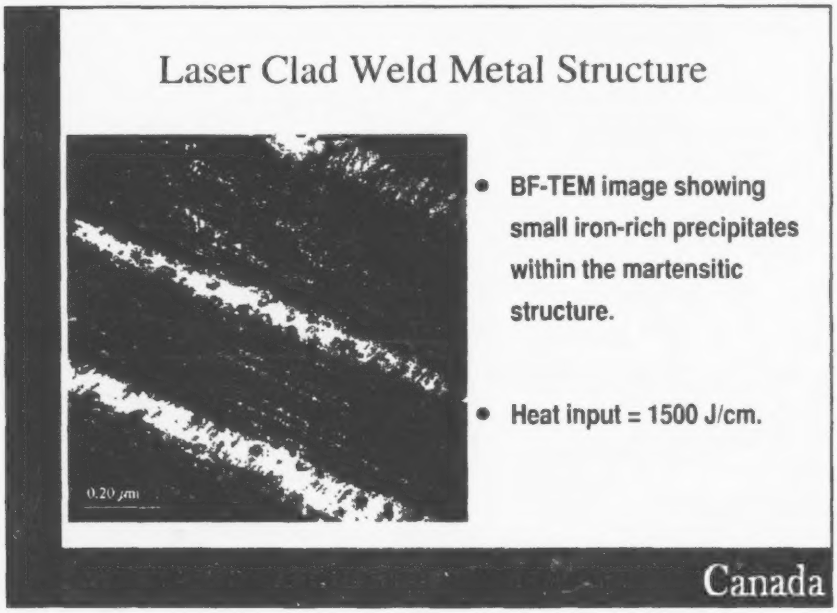

Laser Clad Weld Metal Structure

- **BF-TEM image showing small iron-rich precipitates within the martensitic structure.**
- **Heat input = 1500 J/cm.**

Canada

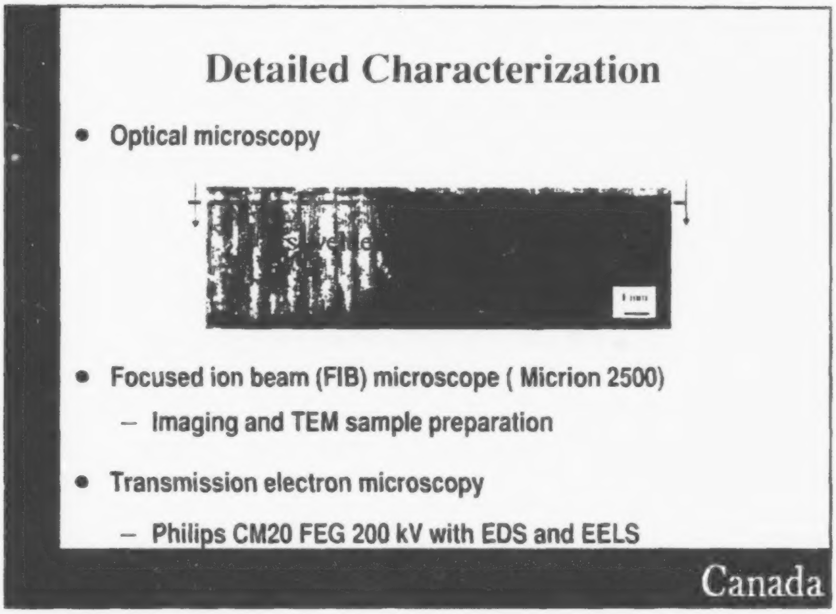
Stellite
1 mm

Detailed Characterization

- Optical microscopy
- Focused ion beam (FIB) microscope (Micrion 2500)
  - Imaging and TEM sample preparation
- Transmission electron microscopy
  - Philips CM20 FEG 200 kV with EDS and EELS

Canada

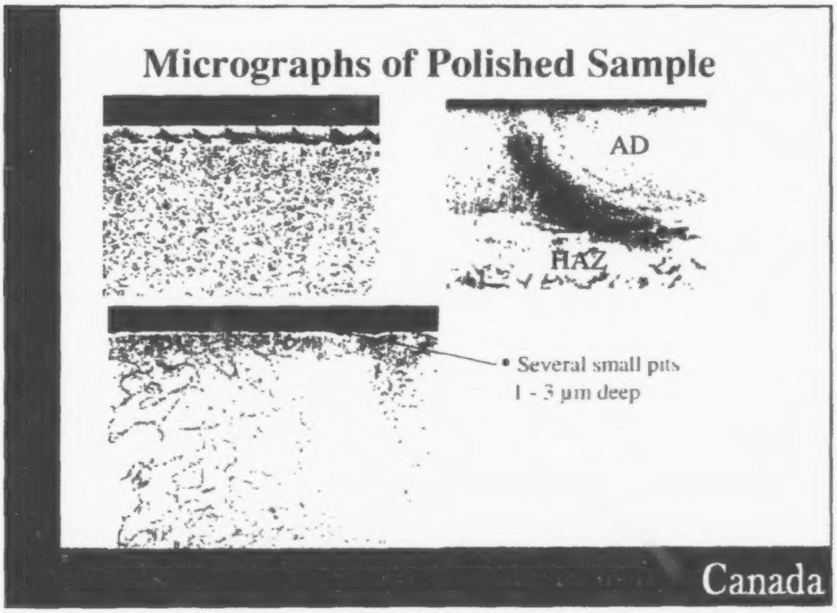

Micrographs of Polished Sample

- Several small pits 1 - 3 μm deep

Canada

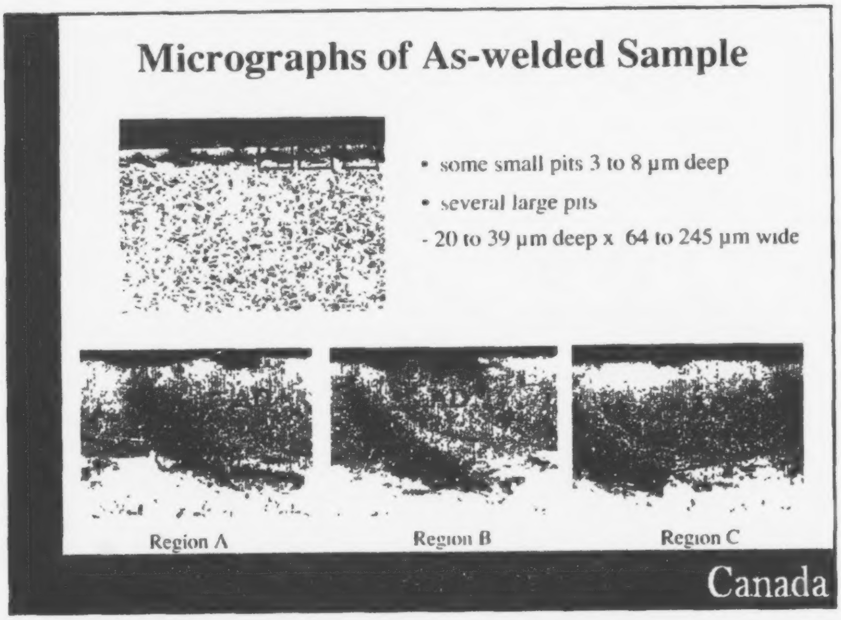

Micrographs of As-welded Sample

- some small pits 3 to 8 μm deep
- several large pits
  - 20 to 39 μm deep x 64 to 245 μm wide

Region A

Region B

Region C

Canada

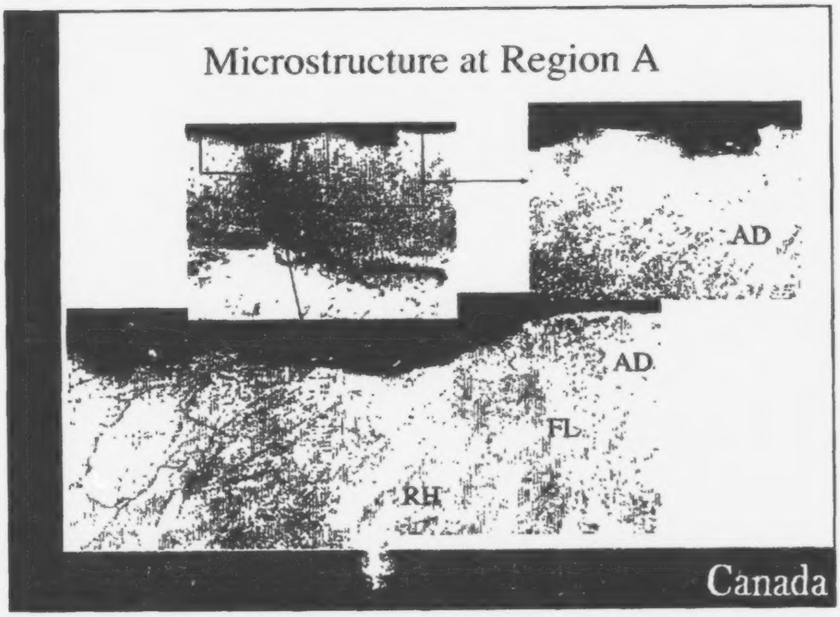

Microstructure at Region A

Canada

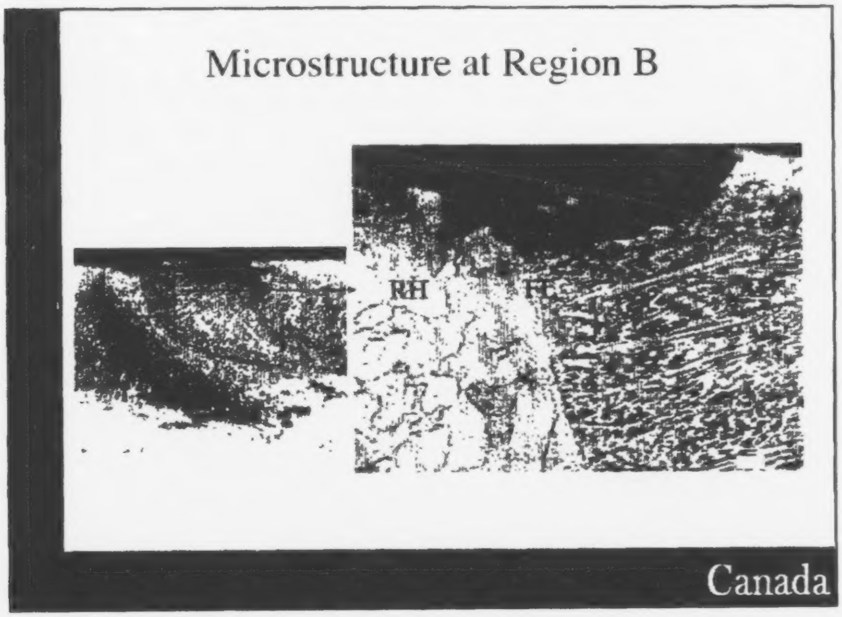

Microstructure at Region B

Canada

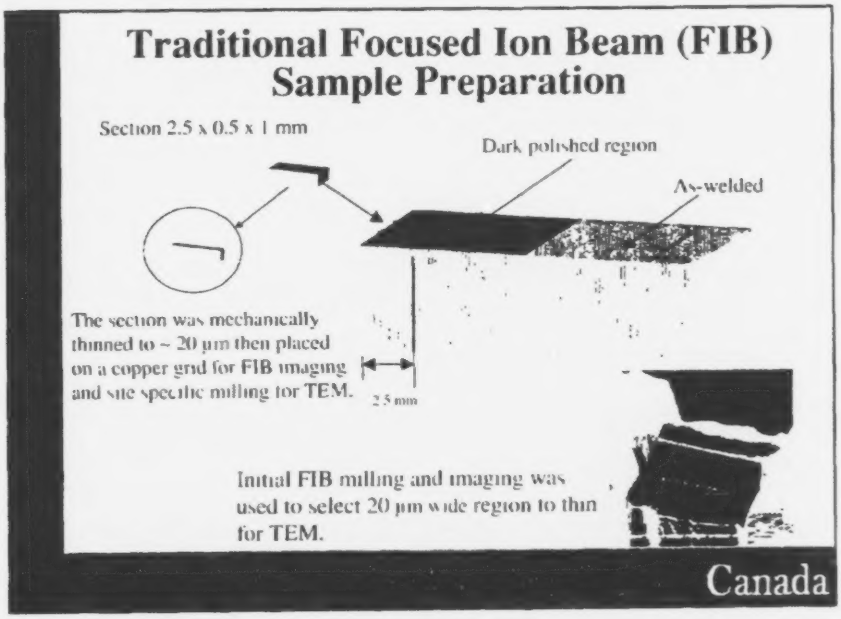

Traditional Focused Ion Beam (FIB) Sample Preparation

Section 2.5 x 0.5 x 1 mm

Dark polished region

As-welded

The section was mechanically thinned to ~ 20 μm then placed on a copper grid for FIB imaging and site specific milling for TEM.

Initial FIB milling and imaging was used to select 20 μm wide region to thin for TEM.

Canada

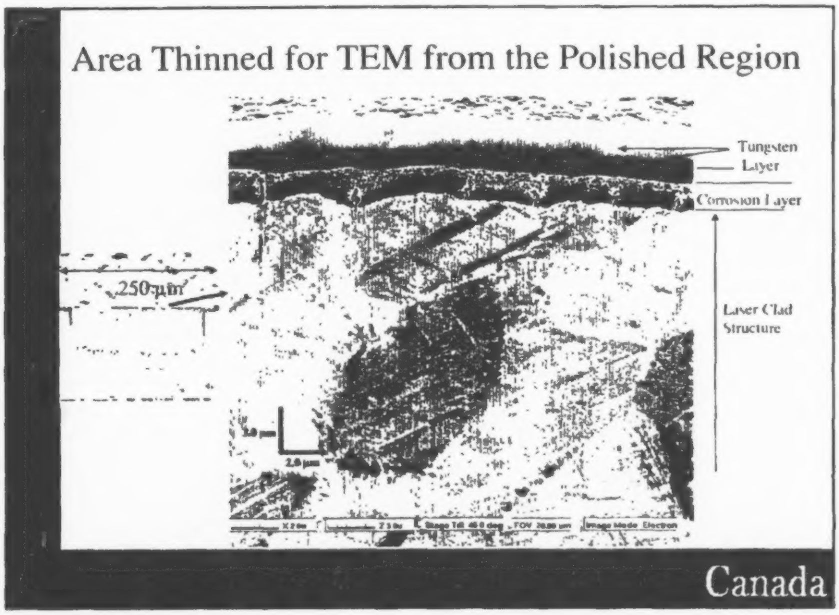

Area Thinned for TEM from the Polished Region

Tungsten
Layer
Corrosion Layer
Laser Clad
Structure
250 µm
2.0 µm
2.0 µm
Stage Tilt 45.0 deg
FOV 20.00 µm
Image Mode Electron

Canada

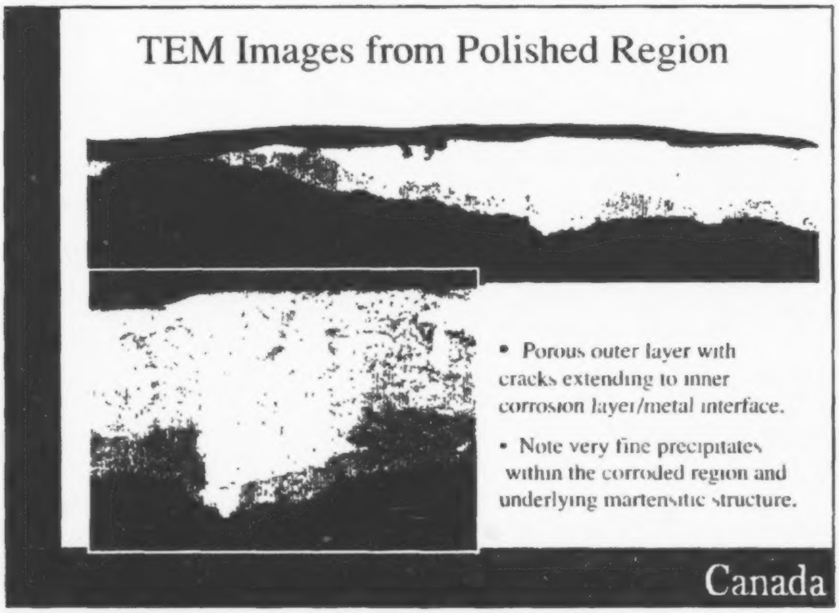

TEM Images from Polished Region

- Porous outer layer with cracks extending to inner corrosion layer/metal interface.
- Note very fine precipitates within the corroded region and underlying martensitic structure.

Canada

High Resolution STEM Images
Polished Region

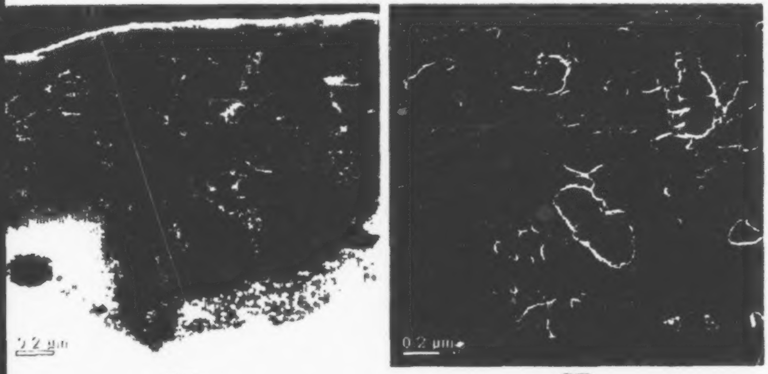

DF SE

Porous outer layer with cracks (channels) extending through to metal interface.

Canada

Elemental Maps from Polished Sample

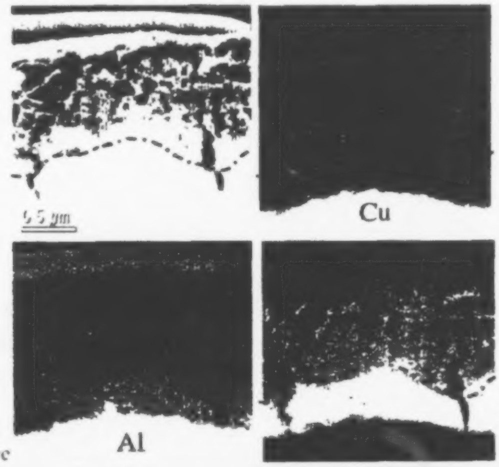

STEM-DF

Al-rich film at the interface

Oxygen rich inner layer

Canada

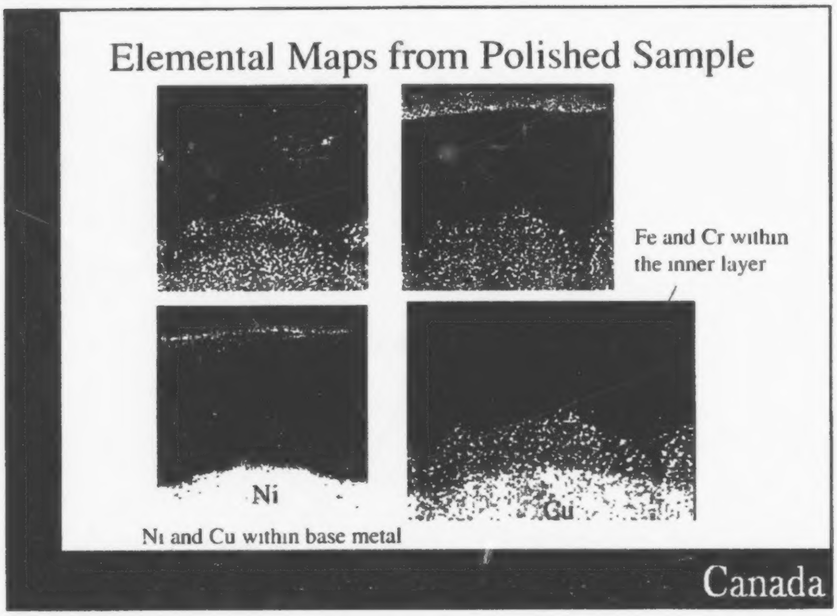

Elemental Maps from Polished Sample

Fe and Cr within the inner layer

Ni and Cu within base metal

Canada

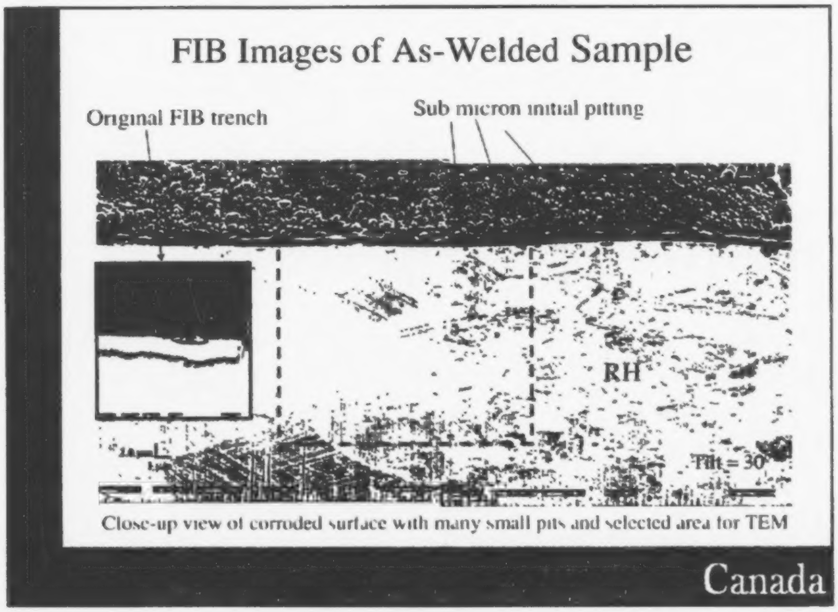

FIB Images of As-Welded Sample

Original FIB trench

Sub micron initial pitting

Close-up view of corroded surface with many small pits and selected area for TEM

Canada

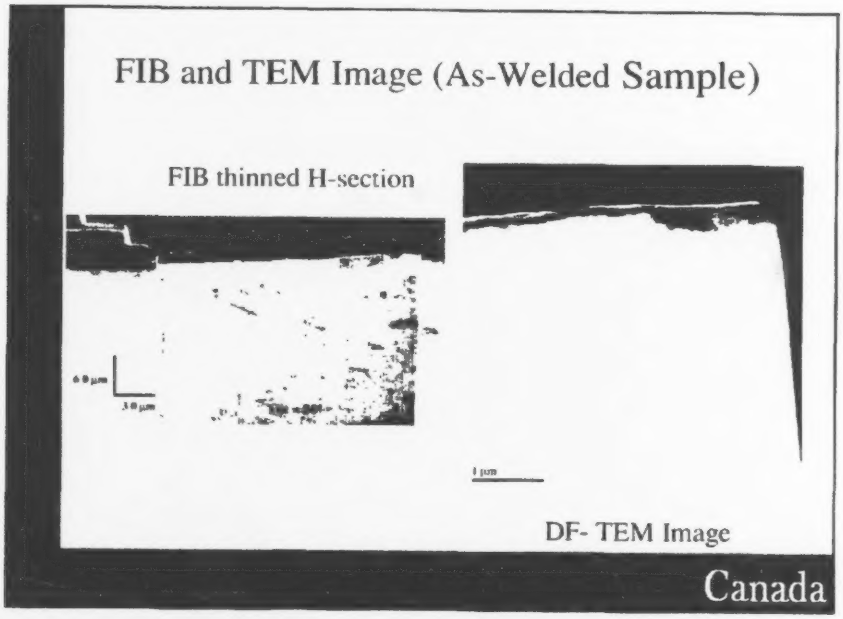

FIB and TEM Image (As-Welded Sample)

FIB thinned H-section

6.0 µm
3.0 µm
1 µm

DF- TEM Image

Canada

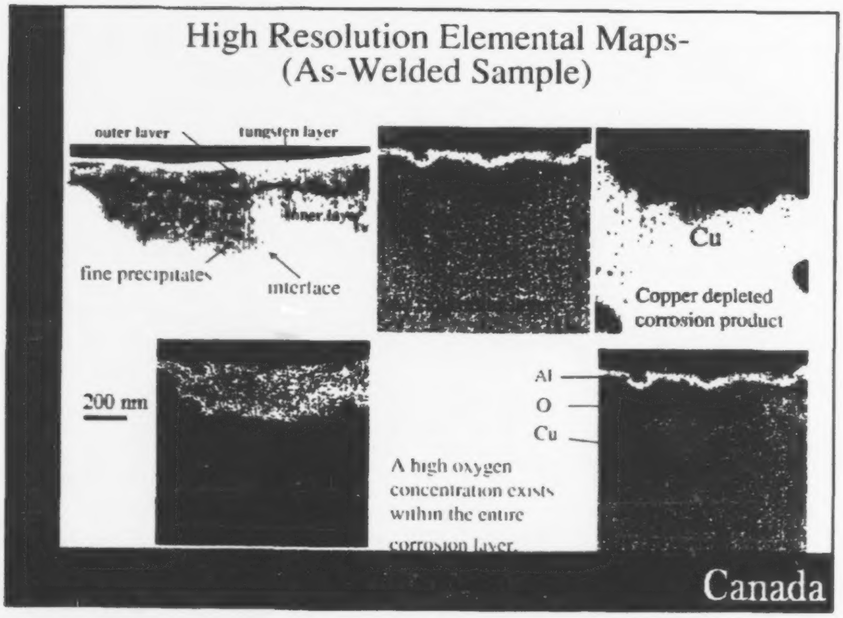

High Resolution Elemental Maps-(As-Welded Sample)

outer layer
tungsten layer
inner layer
fine precipitates
interface
Cu
200 nm
Al
O
Cu

Copper depleted corrosion product

A high oxygen concentration exists within the entire corrosion layer.

Canada

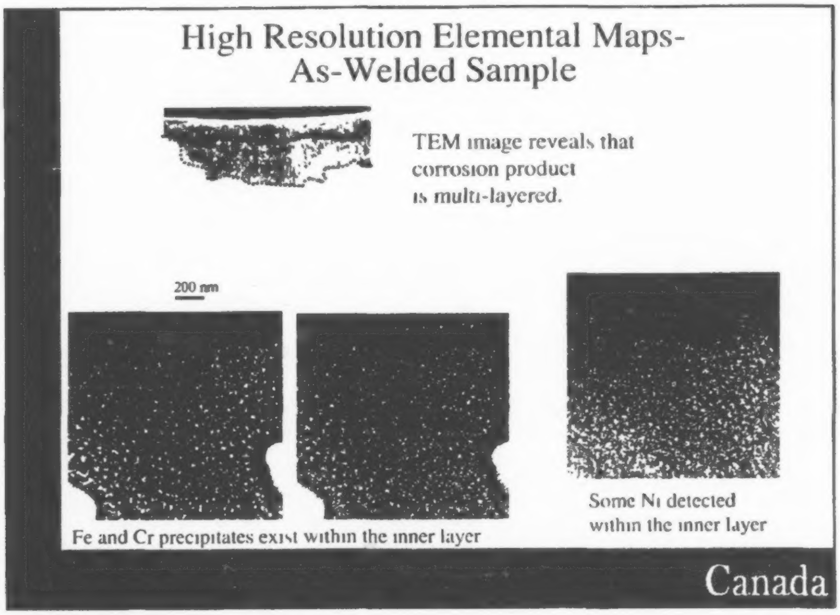

High Resolution Elemental Maps-
As-Welded Sample

TEM image reveals that corrosion product is multi-layered.

Fe and Cr precipitates exist within the inner layer

Some Ni detected within the inner layer

Canada

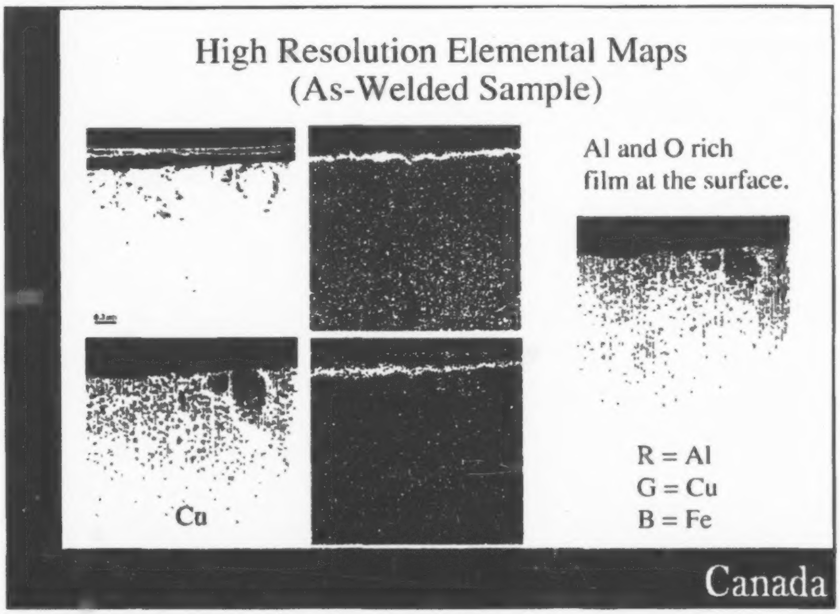

High Resolution Elemental Maps
(As-Welded Sample)

Al and O rich film at the surface.

R = Al
G = Cu
B = Fe

Canada

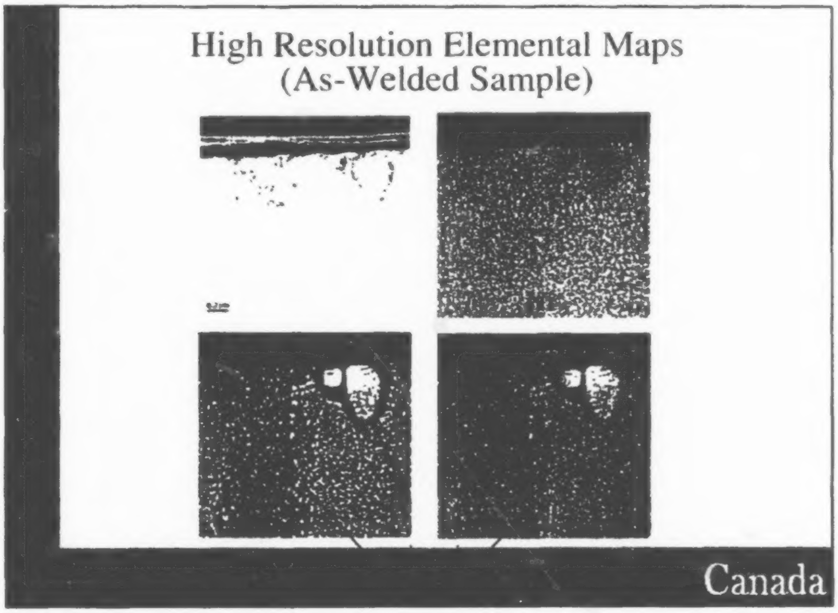

High Resolution Elemental Maps (As-Welded Sample)

Canada

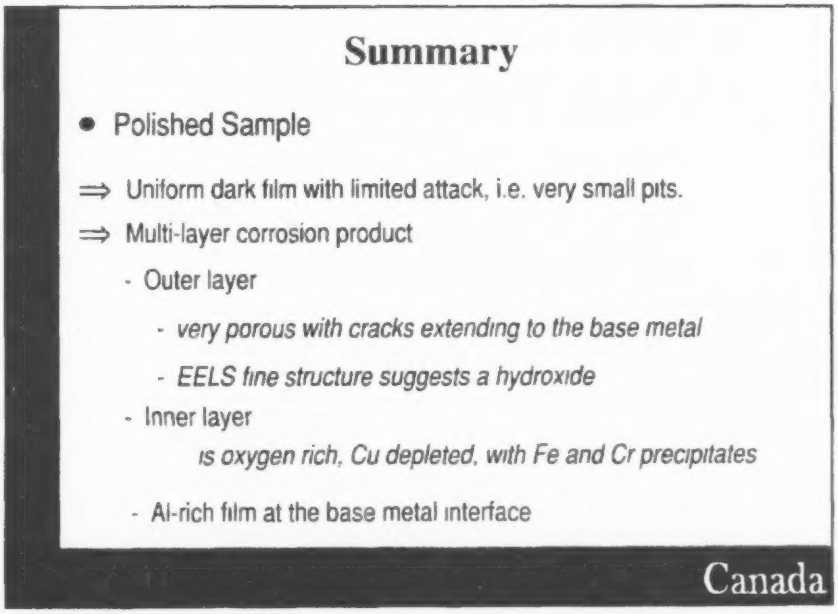

Summary

- Polished Sample

⇒ Uniform dark film with limited attack, i.e. very small pits.

⇒ Multi-layer corrosion product

- Outer layer
  - *very porous with cracks extending to the base metal*
  - *EELS fine structure suggests a hydroxide*
- Inner layer
  - *is oxygen rich, Cu depleted, with Fe and Cr precipitates*
- Al-rich film at the base metal interface

Canada

Summary

- As-Welded Sample

⇒ Much more pitting

- *with several large pits up to 40 μm deep and 250 μm wide.*

⇒ At shallow pitted region

- Multi-layer corrosion product that is oxygen rich
  - *Outer layer has the Al oxide film (welding oxide*)*
  - *Inner layer contains oxygen, is Cu depleted, with Fe and Cr precipitates*

⇒ At the region that shows limited corrosion attack

- *there is an Al oxide film (welding oxide*)*

* Characterization and comparison with an unexposed weld oxide film is planned

Canada

Concluding Remarks

- Focused ion beam (FIB) microscope allows
  - Preparation of cross-sectional samples with
    - ⇒ *imaging capability*
    - ⇒ *site specific TEM sample preparation*
    - ⇒ *excellent means of preserving delicate surface films and corrosion layers*
- The FIB/TEM combination offers a novel characterization technique for high resolution imaging and elemental mapping of complex layers and structures.

Canada

#516415

A Different Approach to Test Specimen Design and Component Testing

V. G. DeGiorgi[*] and S. A. Wimmer[**]

**[*]System Design and Integration Section, Naval Research Laboratory,
Washington, DC 20375-5000
[**]Nova Research, Inc. 1900 Elkin St., Suite 230, Alexandria, VA 22308**

ABSTRACT

Test specimens have been traditionally designed to duplicate relatively simple stress or strain states. For instance the primary goal in a standard test specimen design (such as the ASTM E8 specimen) is to achieve a stress state as near as possible to uniaxial tension. This single stress state design produces limited test data per specimen. Material property response determined from these simplified stress state tests are then used in computational and analytical evaluations of structures that typically do not have simple stress states. If multiaxial material response data is desired a series of test specimens of similar geometries, such as used in torsion tests or bulge tests, are required.

A new concept of test specimen customization is presented [1,2]. Rather than design so that a simplified stress state is maintained through out the loading sequence, the specimen is designed to match the complex stress state found in the structure. The structure of interest is initially examined and computational techniques are used to determine the complex stress state that occurs in a component due to an applied loading. Computational techniques are then applied to a basic test specimen design to add geometric features that duplicate the complex stress state of interest. The final test specimen is a combination of simple geometric features (flat plate) and stress concentration factors (through thickness holes or partial thickness indentations) and is designed so that testing is performed in standard laboratory loading frames. Examples of the approach are presented for several geometries including those that would be of interest in pressure vessel and piping components.

INTRODUCTION

One of the reoccurring themes in material characterization is the determination of geometry independent material properties. A fundamental issue that must be addressed when characterizing a material is how to isolate basic material characteristics from geometry effects. The need for high quality material characterization data has intensified in recent years. Today state of the art computational capabilities (hardware and software) allows for detailed modeling of complex geometries subjected to complex applied loads and boundary conditions. More detailed modeling implies that some simplifying assumptions have been eliminated and the results are expected to be more accurate. The more accurate the input material characterization, the more accurate the calculated results. Reduction in section thickness due to use of high strength materials, evaluations to approve extended service life, fitness for service evaluations and move to design by analysis rather than design by rule are some of the factors that have increased the need for and expectations of accuracy from detailed computational evaluations. While the need for highly accurate material characterization information is not new, it is becoming more important so that full advantage can be taken of advances in computational methods.

There are two basic approaches that can be adapted to the development of the high quality material characterization data needed for advanced computational simulations. One can develop techniques to determine geometry independent constitutive response from experimental data. An example of this is work by Matic et al that used a combination experimental and computational approach to eliminate geometry effects from stress-strain curves determined from uniaxial tension test data [3]. The second approach focuses on the development of stress-strain curves that are appropriate for a given set of geometries. The approach is based on the observation that different geometric configurations and loading conditions result in similar constraint conditions. Rather than eliminating geometric effects, these are matched between component of interest and test specimen used to generate the material characterization.

The custom test specimen design approach extensive uses computational results. A computational analysis of the component of interest is completed. This may be performed as part of the design cycle. The goal of the custom design test specimen is to provide improved material information for a more accurate evaluation. The custom test specimen is then used to determine a more accurate material response [4]. A second computational evaluation of the component of interest is completed with the improved material characteristics. In some cases the second evaluation using the newly determined material information derived from the custom test specimen design may be after significant environment exposure that has changed material characteristics. This approach does require more computational work than tradition design cycle but results in more accurate computational results. This additional effort may not be appropriate for all structures but would be for critical components.

In this work we look in detail at the geometry defined constraint space developed in a test specimens. A key feature of the custom test specimen design approach is the matching of component and test specimen constraint conditions. This work examines the constraint conditions generated by simple thin and thick wall cylinder components, previously defined custom test specimen designs and selected standardized test specimens. Custom test specimen design does not arbitrarily eliminate the use of standard test specimens. It simply means that test specimens should be chosen based on generated constraint conditions. Standard test specimens examined are ASTM E8 tension bar [5] and ASTM E399 fracture specimens [6]. Computational work presented uses the commercial finite element (FE) code ABAQUS [7]. All finite element models are built using MSC Patran [8]. Post processing is done using ABAQUS/Post [9] to examine standard contour plots and using AVS [10]. All analyses use HY-100 material properties [3].

CUSTOM TEST SPECIMEN DESIGN

Traditional test specimen design focuses on the development of geometry and loading condition combination that results in one stress state; for example uniaxial tension in a round bar tensile test specimen. As a result, many test specimens and individual experiments are necessary for determination of the material's constitutive response. Multiple experiments can become expensive in terms of both time and money. There are also situations where material is not readily available such as when material comes from failed components, components removed because of questionable service or coupons exposed for a set period of time to the operating environment. In these cases, the amount of material available for testing can be very limited.

Material may not be available for the multiple conventional test specimens required for full characterization of the material so an analysis of the complex stress state found in the component can be performed.

The custom test specimen design process is described in detail in DeGiorgi et al [1]. Specimens are designed so that testing can be done on conventional tension test machines. The specimen is a combination of primary, secondary and tertiary geometric features. The primary geometry is a flat plate. Stress concentration factors (SCFs) are added as in Matic et al [11]. The flat plate produces a primary tension field that is nominally uniform. The key to increasing the data yield from the specimen is the ability to create multiple stress concentration sites away from the specimen boundary. The secondary geometry or SCF added to the specimen is a through-thickness hole, one quarter of the specimen's width, positioned at the center. This results in a wide range of stress states around the hole when the specimen is subjected to tensile loading. Along the edge of the hole, the traction free surface yields uniaxial stress states. The maximum stress concentrations are produced at the edge of the hole, on the diameter perpendicular to the tension axis. Fracture will normally occur at these points. Tertiary SCFs can be included to further increase the stress states. The tertiary SCFs are areas of reduced thickness, generated using a spherical ball mill, to produce a spherical profile on each side. Figure 1 shows a typical specimen design. The deformation at each point in the specimen is due to the coupled interaction between the primary deformation due to tension, the secondary deformation due to the hole, and the tertiary deformation due to the reduced thickness areas. This is not a simple superposition, so identifying the stress or strain states within the specimen is determined by computational methods. While circular holes and indents are used in conjunction with a flat plate, any combination of basic geometry and features that induce SCFs can be used to create a custom test specimen design. Computational evaluation is required to determine the resulting constraint conditions.

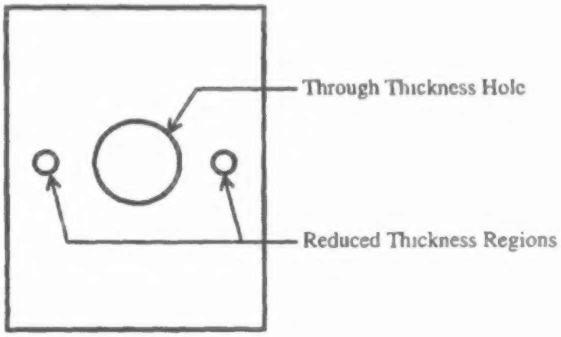

Figure 1 – *Geometry for a custom designed test specimen with one secondary and one tertiary geometry.*

STRESS STATE POINT PLOTS

In conventional test specimen design geometry and loading path are defined to maintain a single stress or deformation state. In custom test specimen design geometry and loading path are defined to maintain a defined stress state. Measuring the constraint condition requires a metric different that what is normally used in computational simulations. A single parameter metric could not adequately define the multiple stress states that will be present in a custom test specimen. Commonly used methods for visualization of computational results such as contour plots may contain the required information but not in an easily understood form. Therefore a different method for examining and visualizing stress state has been developed. Stress state point plots, representations of the principal stress or strain values, are used to visualize the various stress states in a component or test specimen.

Stress state plots are a mapping of each material point to a stress or strain state coordinate. The coordinate is defined as the principal stress ratio. For finite element (FE) generated data, each integration point is mapped. Stress or strain state point plots identify which stress or strain states are generated anywhere in the component and compare the frequency of their appearance throughout the component. Details of stress state plot calculations are found in Geltmacher et al [12].

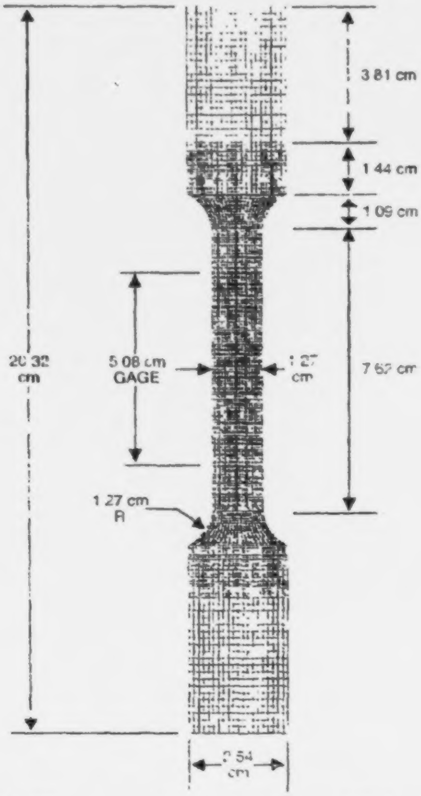

Figure 2 – *ASTM E8 test specimen, courtesy of Geltmacher et al. [12].*

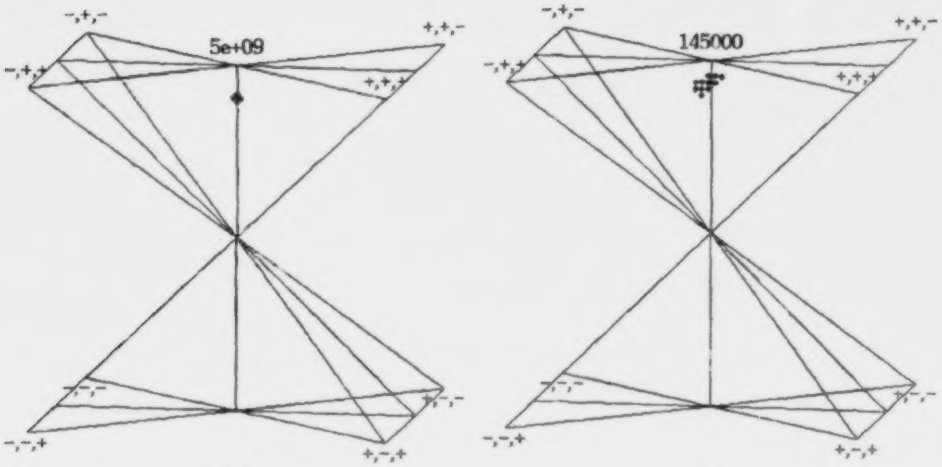

(a) (b)

Figure 3 – *Stress state point plots for (a) flat plate and (b) ASTM E8 specimen under uniaxial tension.*

As an example stress state plots for an ASTM E8 tension specimen (Figure 2) and a flat plate specimen are shown in Figure 3. Using two planes of symmetry, a FE simulation of one quarter a flat plate was done using 7803 hex elements. Figure 3 shows stress state point plots in N/m^2 for the flat plate (0.101 x 0.0508 x 0.0016 m) and for an ASTM E8 specimen gage area. Both were subjected to tensile loading. For the flat plate, all the stress state points (Figure 3a) fall at the same point on the vertical axis, showing a pure uniaxial state. In Figure 3b, the ASTM E8 specimen shows that some stress states are off axis and the stress state generated within the gage area is not purely uniaxial. Using a finer or coarser finite element mesh will not change the position of the points, but may alter the density of the points.

The stress state point plots for the custom test specimen designs developed in Ref. [2] are shown in Figure 4. A through-thickness hole, with a radius of 0.00635m, is inserted in the middle of a flat plate. This is the secondary SCF geometry. One quarter of the specimen is model using 3400 hex elements. The resulting stress state point plot is shown in Figure 4a. Most of the stress states lie on a 2-D plane, however some (+, +, +) and (+, +, −) stress states are exhibited. When tertiary SCF geometries of reduced thickness sections are added; a broader range of stress states is encountered. The reduced thickness section was generated on both sides to model a truncated spherical profile generated by a spherical ball mill. The thickness was reduced to 0.33 times the plate thickness. The truncated sphere had a radius of 0.0118m (1.75 times that of the through-thickness hole), resulting in a free surface radius of 0.001588m. The reduced section was placed at the 0.04 equivalent strain contour along the x-axis. The final geometry of the custom test specimen design is shown schematically in Figure 1. The finite element mesh consisted of 38,268 hex elements with 4 elements through the thickness. As seen in Figure 4b, the test specimen experiences stress states of (+, +, +), (+, +, −), (−, +, +), (−, +, −), and (+,−, 0).

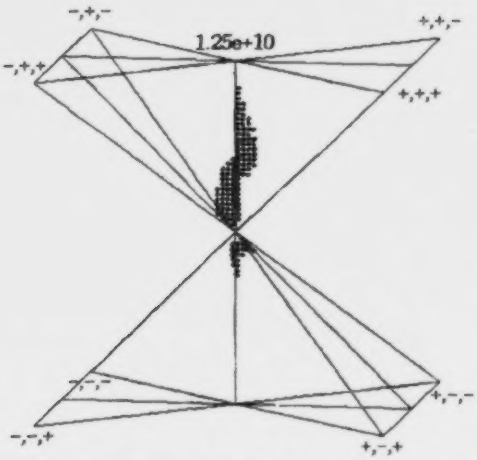

Figure 4a – *Stress state point plot for a custom designed test specimen with a secondary geometry of a through-thickness hole.*

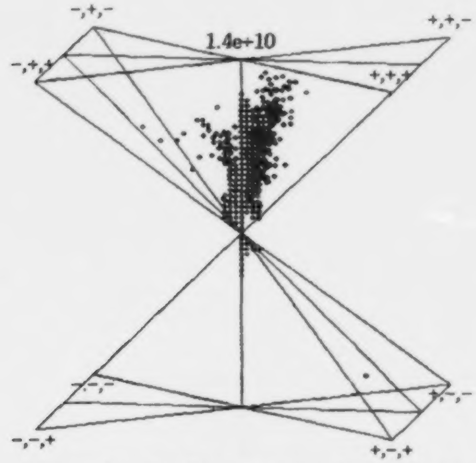

Figure 4b – *Stress state point plot for a custom designed test specimen with one secondary and one tertiary geometry (Figure 1).*

COMPONENT ANALYSIS

Key to the custom test specimen design is the computational evaluation of the component of interest. In many cases this is already done as part of the component design process. The stress states associated with the component and service conditions can be readily determined from computational results. In order to demonstrate the variations in stress state than can occur in relatively simple geometries a thick wall and thin wall cylinder were evaluated in terms of stress state plots. Damage was simulated in the case of the thick wall cylinder to show what changes can occur in the design stress state conditions.

Thin Wall Cylinder

The stress state plot was generated for a pressurized thin wall cylinder. Dimensions were chosen arbitrarily. It is the intent that this geometry would be representative of a pressure vessel rather than piping. A cylinder measuring 1.829m with an outer radius of 0.6096m was subjected to an internal pressure of 2000 N/m^2. The wall thickness was one tenth of the outer diameter. The FE mesh consisted of 15,616 hex elements, with two layers of elements through the thickness.

The stress state is uniform with compressive radial (σ_1), tensile hoop (σ_3) and tensile axial (σ_2) stresses. A contour plot of the hoop principal stress is shown in Figure 5. Contours of the radial and axial principal stresses show the same shading, just with different magnitudes. The resulting stress state point plot is shown in Figure 6. All the stress state points fall in the (+, +, –) quadrant. Due to the geometry used, the hoop stress is greater than the axial stress which is greater than the absolute value of the radial stress at all material points, $|\sigma_3| > |\sigma_2| > |\sigma_1|$.

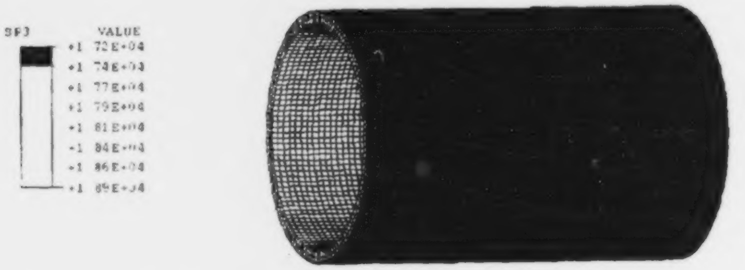

Figure 5 – *Contour plot of hoop principal stress for a thin wall pressurized cylinder.*

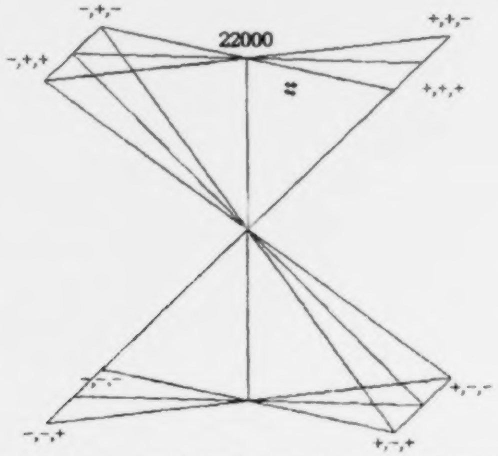

Figure 6 – *Stress state point plot for a thin wall pressurized cylinder.*

Thick Wall Cylinder

When the wall of the cylinder is thickened, the absolute value of the radial stress component becomes greater than the hoop stress. A second geometry of a small diameter, thick wall pipe was modeled to demonstrate this affect. The smaller dimension pipe was is representative of tubing that may be found in heat exchangers. A thick wall pipe of length 0.05m with an outer radius of 0.01032m and an inner radius of 0.00556m is modeled by 16,250 hex elements, with five layers of elements through the thickness. A contour plot of σ_3 is shown in Figure 7.

The resulting stress state point plot is shown in Figure 8. In addition to the points in the (+, +, −) quadrant seen by the thin wall cylinder, points in the (−, +, +) quadrant are seen. However, like the thin wall section, the thick wall pipe has no stress state points lying in the (+, −, +) quadrant.

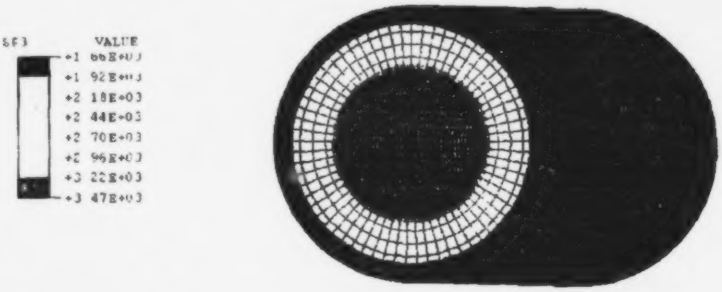

Figure 7 – *Contour plot of σ_3 for a thick wall pressurized pipe.*

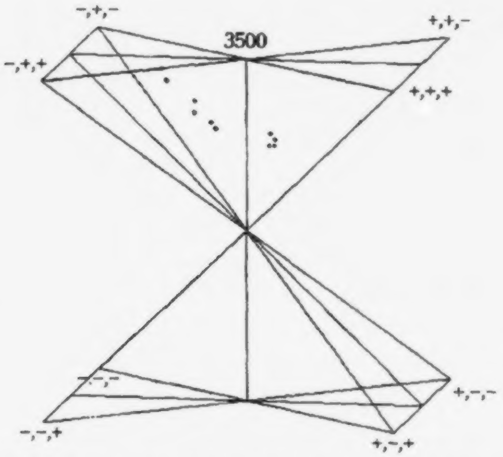

Figure 8 – *Stress state point plot for a thick wall pressurized pipe.*

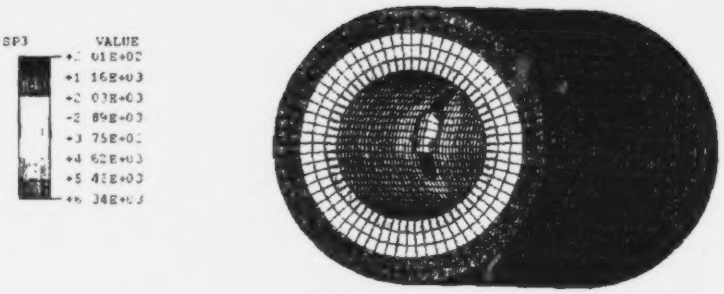

Figure 9 – *Contour plot of σ_3 for a thick wall pressurized pipe with damage on the inner surface.*

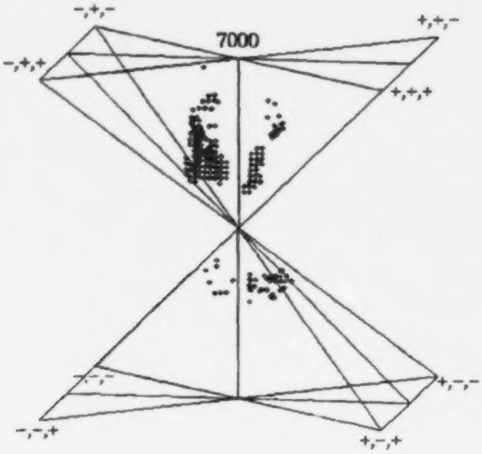

Figure 10– *Stress state point plot for a thick wall pressurized pipe with damage on the inner surface.*

To represent damage to the interior of the thick wall pipe, a 6x6 block of elements one layer thick was removed from the inner surface. In the finite element simulation, pressure was exerted against all internal free surfaces. A contour plot of σ_3 is shown in Figure 9. The resulting stress state point plot shows values in all the quadrants except (+, +, +), (–,–,–) and (+,–, +), see Figure 10.

Damage to the outer wall was simulated by removal of a 4x4 block of elements one layer thick from the outer surface. A contour plot of σ_3 is shown in Figure 11. The resulting stress state point plot shows values in the quadrants (+, +, –) and (–, +, +), see Figure 12.

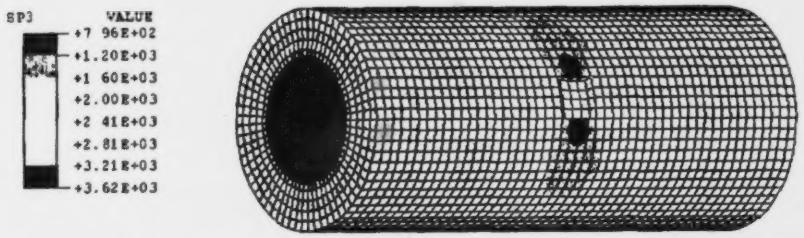

Figure 11 – *Contour plot of* σ_3 *for a thick wall pressurized pipe with damage on the outer surface.*

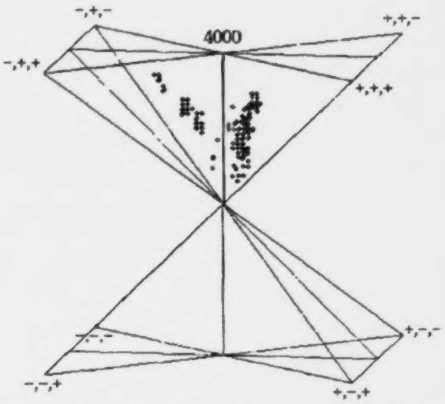

Figure 12 – *Stress state point plot for a thick wall pressurized pipe with damage on the outer surface.*

The stress states shown in Figures 8 and 10 are more similar to those of the custom test specimen (Figures 4) than the ASTM E8 specimen (Figure 2b). Therefore the custom test specimen would be a better candidate for material characterization for these components.

STANDARD TEST SPECIMEN DESIGN

The custom test specimen design concept does not prevent or limit the use of standardized test specimen design. Rather, it provides a means to assist in the selection of test specimen geometry. There are many reasons to maintain the use of standard test specimen designs. There is a great wealth of existing data that has been generated using these specimens. Standard test specimen designs would be evaluated in the same way as a customized design. The component of interest is computational evaluated and the stress state plot generated. Stress state plots for standard test specimen designs would then be evaluated to determine the most appropriate specimen.

In this section stress state plots are determined for a series of ASTM E399 defined fracture specimens. Four specimens defined in the standard are evaluated: bend specimen SE(B), Compact specimen C(T), arc shaped tension A(T) and disk shaped compact specimen

DC(T). Specimens were defined as fabricated from HY-100 steel. The high strength characteristics of HY-100 made specimens than met plane strain conditions impractical. This is not an uncommon phenomenon in testing HY-100. The specimens were given a reasonable thickness representative of typical plate applications. Specimen dimensions are provided in the detailed description of results.

Bend Specimen SE(B)

Critical specimen dimensions are width (W) of 50.8 mm and thickness (B) of 22.9 mm. Dimension definitions are according to ASTM E399. No crack was included in the FE model. A 3-D FE mesh of the entire specimen was created. The FE mesh consisted of 9792 hex elements, with 8 layers of elements through the thickness. Principal stress contours and stress state point plot for the entire specimen are shown in Figure 13. The stress state plot for the region in the vicinity of the notch tip is shown in Figure 14.

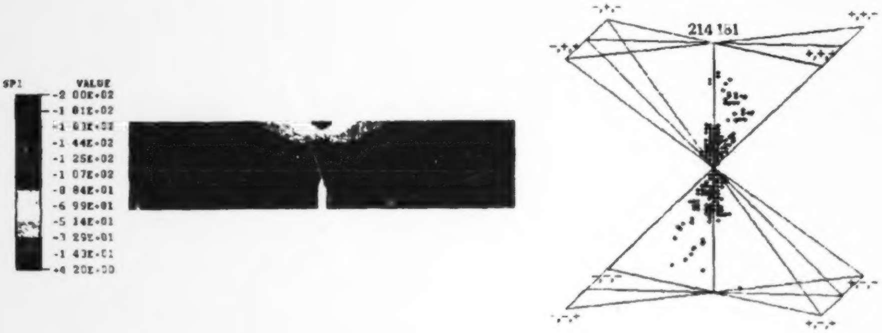

(a) (b)

Figure 13 – (a) Contour plot of σ_1 and (b) *stress state point plot for the bend specimen SE(B).*

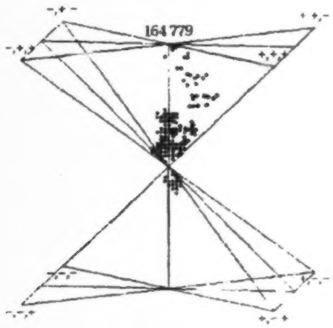

Figure 14 – *Stress state point plot in the vicinity of the notch tip area for the bend specimen SE(B).*

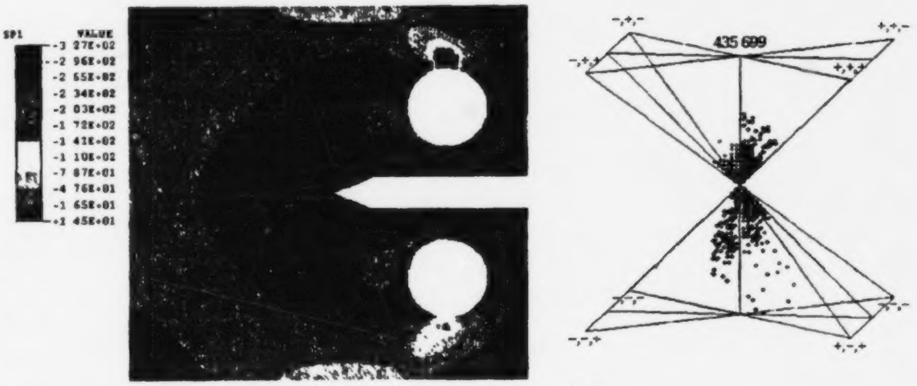

(a) (b)

Figure 15 – (a) Contour plot of σ_1 and (b) *stress state point plot for the compact C(T).*

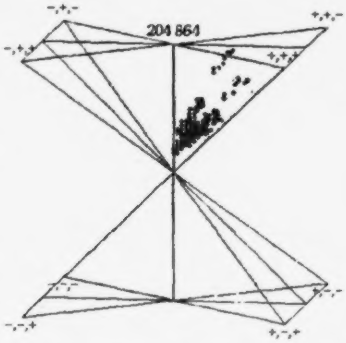

Figure 16 – *Stress state point plot in the vicinity of the notch tip area for the compact C(T).*

Compact C(T)

Critical specimen dimensions are width (W) of 50.8 mm and thickness (B) of 22.9 mm. Dimension definitions are according to ASTM E399. No crack was included in the FE model. A 3-D FE mesh of the entire specimen was created. The FE mesh consisted of hex 13,040 elements, with 10 layers of elements through the thickness. Principal stress contours and stress state point plot for the entire specimen are shown in Figure 15. The stress state plot for the region in the vicinity of the notch tip are shown in Figure 16.

Arc Shaped Tension A(T)

Critical specimen dimensions are width (W) of 50.8 mm and thickness (B) of 22.9 mm. The specimen has an inside radius (r_1) of 50.8 mm and an outside radius (r_2) of 101.6 mm. Dimension definitions are according to ASTM E399. No crack was included in the FE model. A 3-D FE mesh of the entire specimen was created. The FE mesh consisted of 9216 hex elements, with 6 layers of elements through the thickness. Principal stress contours and stress state point plot for the entire specimen are shown in Figure 17. The stress state plot for the region in the vicinity of the notch tip are shown in Figure 18.

Disk Shaped Compact DC(T)

Critical specimen dimensions are width (W) of 50.8 mm and thickness (B) of 22.9 mm. Dimension definitions are according to ASTM E399. No crack was included in the FE model. A 3-D FE mesh of the entire specimen was created. The FE mesh consisted of 7088 hex elements, with 8 layers of elements through the thickness. Principal stress contours and stress state point plot for the entire specimen are shown in Figure 19. The stress state plot for the region in the vicinity of the notch tip are shown in Figure 20.

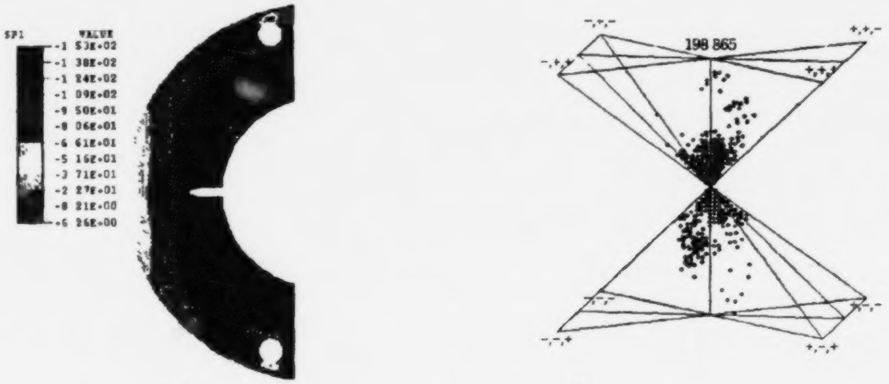

(a) (b)

Figure 17 – (a) Contour plot of σ_1 and (b) *stress state point plot for arc shaped tension A(T).*

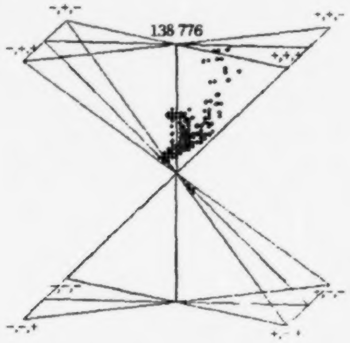

Figure 18 – *Stress state point plot in the vicinity of the notch tip area for the arc shaped tension A(T)*

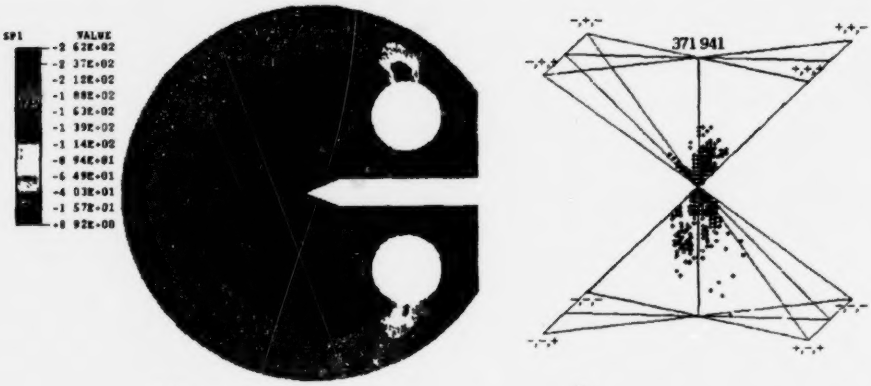

(a) (b)

Figure 19 – (a) Contour plot of σ_1 and (b) *stress state point plot for disk shaped compact DC(T).*

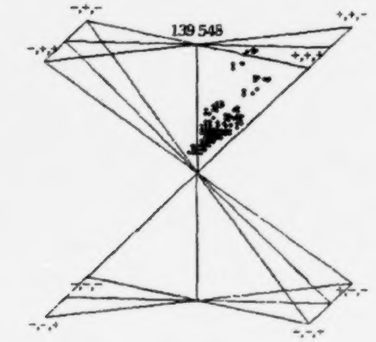

Figure 20 – *Stress state point plot in the vicinity of the notch tip area for the disk shaped compact DC(T).*

A review of the stress state plots indicates that the constraint state, as represented by the stress state, is not identical for this series of fracture specimens. This is true for both the entire specimen and notch tip region stress state plots. It is not the intent of this analysis to select 'better' specimens but to simply provide additional information to assist in the selection of specimen geometry. Variations in stress state may provide insight into differences in fracture parameters determined from each of these test specimens.

SUMMARY

In the ideal world test specimen designs would be customized to capture the constraint conditions associated with the component of interest. The concept of custom test specimen design takes advantage of computational capabilities to evaluate the stress and strain states in the component of interest and design a specimen with similar conditions. This specimen is then used to determine the high quality material constitutive response required for detailed evaluation of the component and similar components. The current goal is to create specimen designs that can provide multiaxial stress state data when tested using standard tension test machines. In many ways this approach is similar to the use of standard test specimen. Standardized test specimen designs do not eliminate geometric effects but use of a standardized design offer a means to eliminate differences in geometry effects. Standard test specimens match states between specimens. Custom specimen design takes this one step further and adds geometric features to match states between specimen and component.

The metric presented to evaluate the state of a specimen under load, either test specimen or component, is the stress state plot. Stress state plots of standard test specimen designs provide additional information for the selection of test specimens. While not the ideal situation where a specimen is custom designed, specimen selection based on stress state plots allows for matching of constraint conditions. In addition, evaluation of standard specimen designs in this method allows for additional insight into the observed performance and measured material characteristics obtained from these specimens.

ACKNOWLEDGEMENTS

The work was supported in part by a grant of High Performance Computing time from the DoD HPC Center at the Naval Research Laboratory, Washington, DC.

REFERENCES

1. DeGiorgi, V. G., Geltmacher, A. B., Matic, P. and Everett, R. K., "Test Specimen Design Incorporating Multiple Fracture Sites and Multiple Strain Material Fractures", U S Patent 5, 905,204, 18 May 1999.
2. Wimmer, S. A. and DeGiorgi, V. G., "Component Based Test Specimen Design", ASTM STP 1418, 2001 (In Review).
3. Matic, P., Kirby, G. C. and Jolles, M. I., "The relation of tensile specimen size and geometry effects to unique constitutive parameters for ductile materials", Proc. *Royal Soc.*, A4176, 309-333, 1988.
4. Matic, P., Geltmacher, A. B., and Gombert, G., "Material Fracture Characterization Using Novel Specimen Geometries and Finite Element Analysis", *ABAQUS User's Conference Proceedings*, Hibbitt, Karlsson and Sorensen, Inc., Pawtucket, RI, 1996.
5. *Standard Test Methods for Tension Testing of Metallic Materials*, Standard E8-96a, ASTM, West Conshohocken, PA 1997.
6. *Standard Test Method for Plane-Strain Fracture Toughness of Metallic Materials*, Standard E399-90 (Re-approved 1997), ASTM, West Conshohocken, PA, 1997.
7. *ABAQUS/Standard User's Manual: Version 5.8*, Hibbitt, Karlsson and Sorensen, Inc., Pawtucket, RI, 1998.
8. *MSC Patran: Version 2000*, MSC Software Corporation, Los Angeles, CA, 2000.
9. *ABAQUS/Post Manual: Version 5.8*, Hibbitt, Karlsson and Sorensen, Inc., Pawtucket, RI, 1998.
10. *AVS Developer's Guide: Release 5.3*, Advanced Visual Systems, Inc., Waltham, MA, 1995.
11. Geltmacher, A. B., Matic, P., and Everett, R. K., "Integrated Experimental-Computational Characterization of TIMETAL 21S", *Materials Science & Engineering A272*, 99-113, 1999.

12. Matic, P., and Geltmacher, A. B. (1998) "Visualization of Material Performance in a Component: Stress and Strain State Frequency Distribution Plots from ABAQUS Data Files", *ABAQUS User's Conference Proceedings,* Hibbitt, Karlsson and Sorensen, Inc., Pawtucket, RI, 1998.

#516418 ⑥

Titanium Alloy Ti-5111 for U.S. Naval Applications

by Michael E. Wells
and
Ernest J. Czyryca

Naval Surface Warfare Center
West Bethesda, Maryland, USA

ABSTRACT

Titanium and its alloys are finding increasing applications on U.S. Naval surface ships and submarines. The physical, mechanical and corrosion properties of titanium favorably impact current U.S. Navy ship design requirements for increased reliability with reduced maintenance and weight. Based on the excellent erosion-corrosion properties of titanium, commercially pure grades are used extensively for seawater pumps, cooling and piping applications on surface ships and for a number of seawater cooling components on nuclear submarines. For high-strength critical applications, the US Navy developed and certified the Ti-6Al-2Cb-1Ta-0.8Mo (Ti-100) alloy. While this alloy was used for pressure hulls on Navy deep submersibles, the high cost of alloying additions and low product yields limited the use of this material. The Naval Surface Warfare Center, in cooperation with Titanium Metals Corporation, developed the Ti-5Al-1Sn-1Zr-1V-0.8Mo (Ti-5111) alloy as a lower cost, more producible alternative alloy. This presentation will describe the result of studies to characterize the strength, fracture toughness, weldability, and seawater corrosion/stress corrosion resistance properties of this alloy, including the results of fracture testing under dynamic (UNDEX) conditions using the recently developed hull toughness element test. In addition, the presentation will describe current and candidate applications of this alloy for surface ships and submarines.

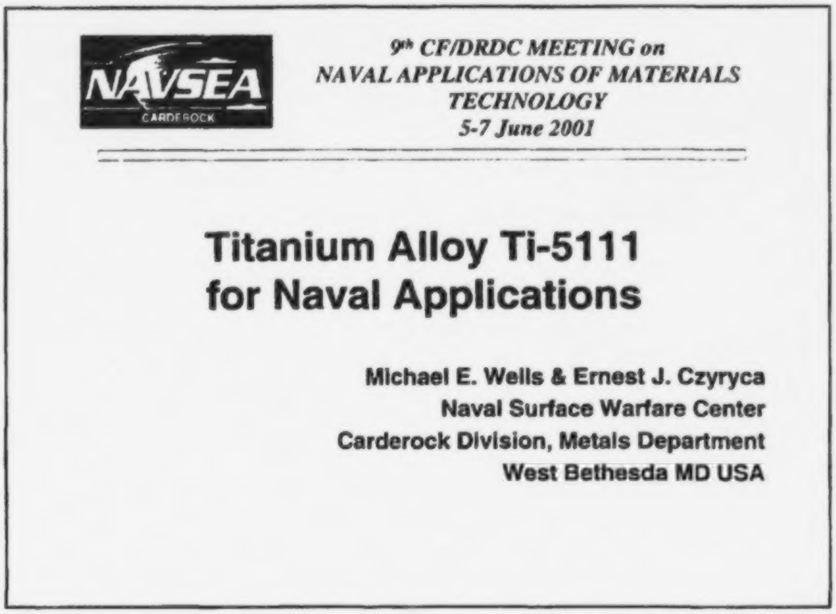

9th CF/DRDC MEETING on
NAVAL APPLICATIONS OF MATERIALS
TECHNOLOGY
5-7 June 2001

Titanium Alloy Ti-5111 for Naval Applications

Michael E. Wells & Ernest J. Czyryca
Naval Surface Warfare Center
Carderock Division, Metals Department
West Bethesda MD USA

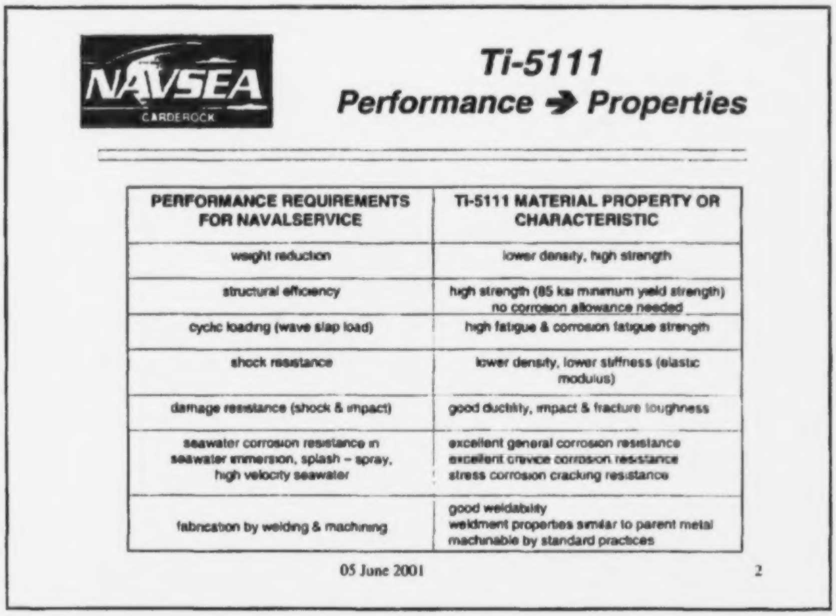

Ti-5111
Performance ➔ Properties

PERFORMANCE REQUIREMENTS FOR NAVALSERVICE	TI-5111 MATERIAL PROPERTY OR CHARACTERISTIC
weight reduction	lower density, high strength
structural efficiency	high strength (85 ksi minimum yield strength) no corrosion allowance needed
cyclic loading (wave slap load)	high fatigue & corrosion fatigue strength
shock resistance	lower density, lower stiffness (elastic modulus)
damage resistance (shock & impact)	good ductility, impact & fracture toughness
seawater corrosion resistance in seawater immersion, splash – spray, high velocity seawater	excellent general corrosion resistance excellent crevice corrosion resistance stress corrosion cracking resistance
fabrication by welding & machining	good weldability weldment properties similar to parent metal machinable by standard practices

05 June 2001

2

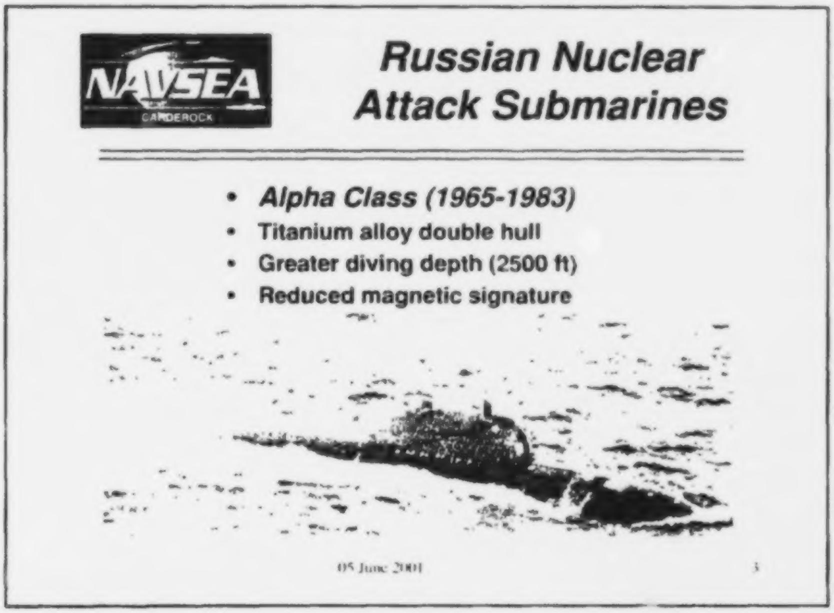

Russian Nuclear Attack Submarines

- *Alpha Class (1965-1983)*
- Titanium alloy double hull
- Greater diving depth (2500 ft)
- Reduced magnetic signature

05 June 2001 3

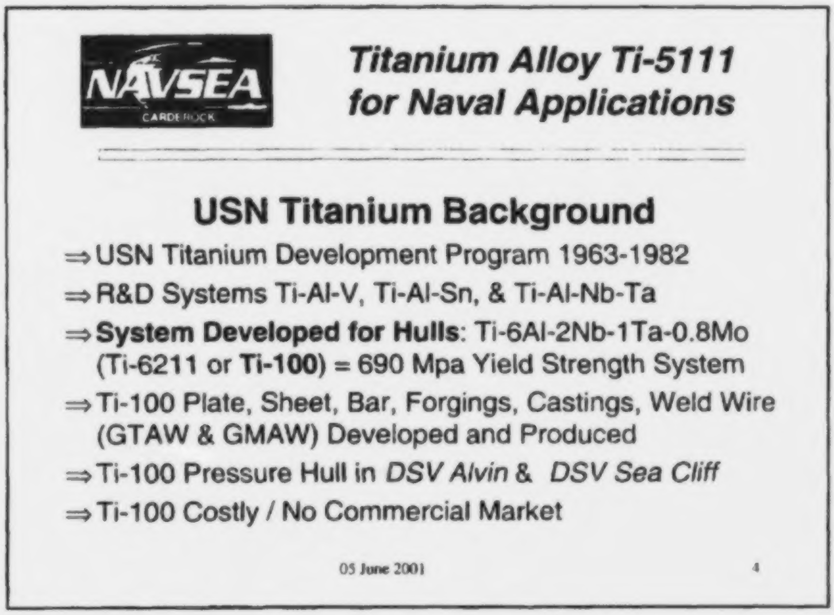

Titanium Alloy Ti-5111 for Naval Applications

USN Titanium Background

⇒ USN Titanium Development Program 1963-1982

⇒ R&D Systems Ti-Al-V, Ti-Al-Sn, & Ti-Al-Nb-Ta

⇒ **System Developed for Hulls**: Ti-6Al-2Nb-1Ta-0.8Mo (Ti-6211 or **Ti-100**) = 690 Mpa Yield Strength System

⇒ Ti-100 Plate, Sheet, Bar, Forgings, Castings, Weld Wire (GTAW & GMAW) Developed and Produced

⇒ Ti-100 Pressure Hull in *DSV Alvin* & *DSV Sea Cliff*

⇒ Ti-100 Costly / No Commercial Market

05 June 2001 4

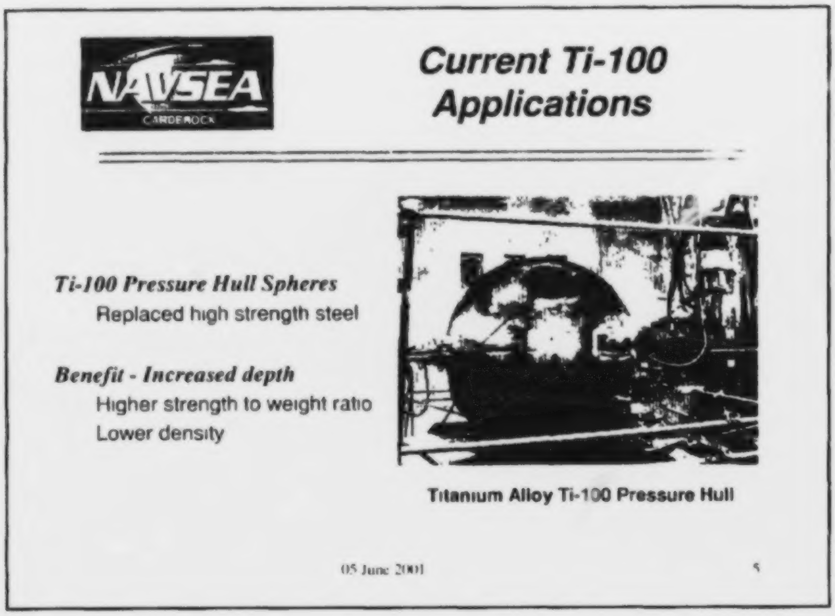

Current Ti-100 Applications

Ti-100 Pressure Hull Spheres

Replaced high strength steel

Benefit - Increased depth

Higher strength to weight ratio

Lower density

Titanium Alloy Ti-100 Pressure Hull

05 June 2001

5

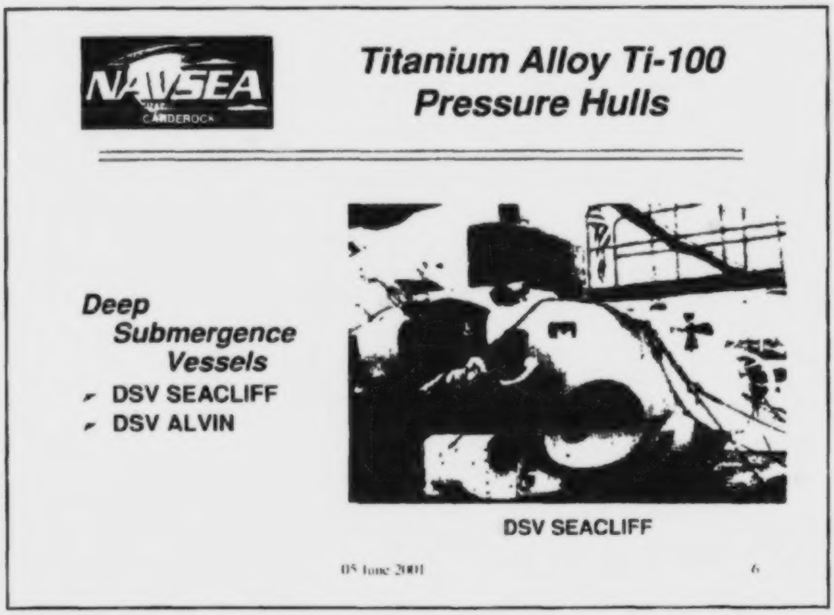

Titanium Alloy Ti-100 Pressure Hulls

Deep Submergence Vessels

- **DSV SEACLIFF**
- **DSV ALVIN**

DSV SEACLIFF

05 June 2001

6

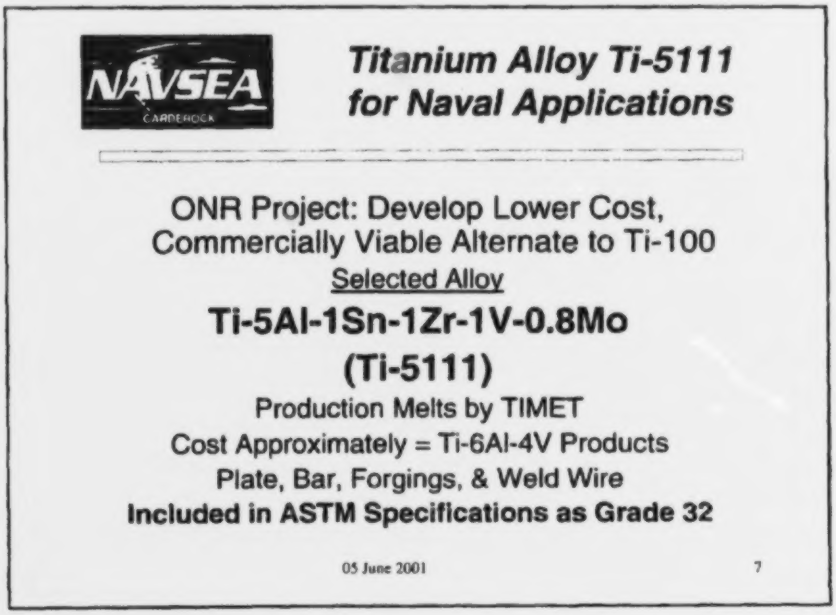

Titanium Alloy Ti-5111 for Naval Applications

ONR Project: Develop Lower Cost, Commercially Viable Alternate to Ti-100

Selected Alloy

Ti-5Al-1Sn-1Zr-1V-0.8Mo

(Ti-5111)

Production Melts by TIMET

Cost Approximately = Ti-6Al-4V Products

Plate, Bar, Forgings, & Weld Wire

Included in ASTM Specifications as Grade 32

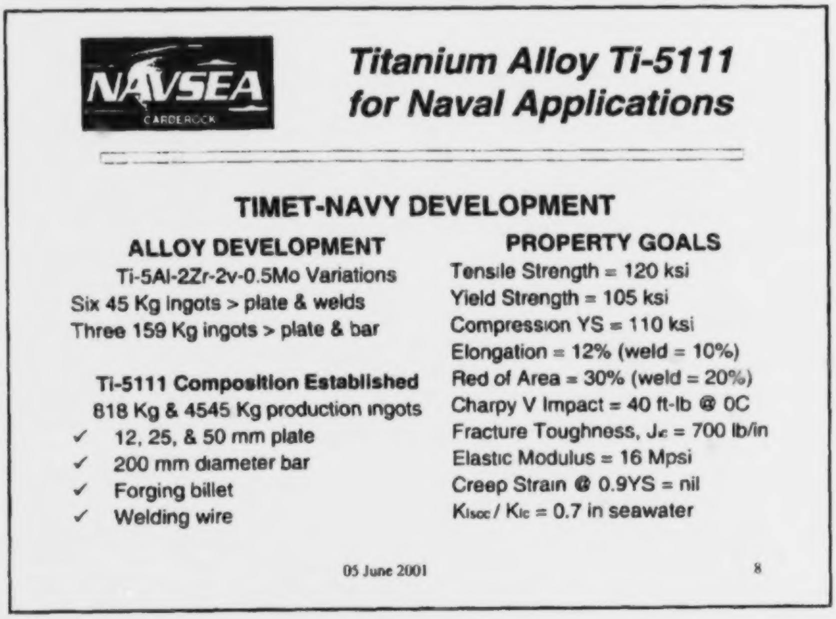

Titanium Alloy Ti-5111 for Naval Applications

TIMET-NAVY DEVELOPMENT

ALLOY DEVELOPMENT

Ti-5Al-2Zr-2v-0.5Mo Variations

Six 45 Kg ingots > plate & welds

Three 159 Kg ingots > plate & bar

Ti-5111 Composition Established

818 Kg & 4545 Kg production ingots

- ✓ 12, 25, & 50 mm plate
- ✓ 200 mm diameter bar
- ✓ Forging billet
- ✓ Welding wire

PROPERTY GOALS

Tensile Strength = 120 ksi

Yield Strength = 105 ksi

Compression YS = 110 ksi

Elongation = 12% (weld = 10%)

Red of Area = 30% (weld = 20%)

Charpy V Impact = 40 ft-lb @ 0C

Fracture Toughness, J_{Ic} = 700 lb/in

Elastic Modulus = 16 Mpsi

Creep Strain @ 0.9YS = nil

K_{Iscc} / K_{Ic} = 0.7 in seawater

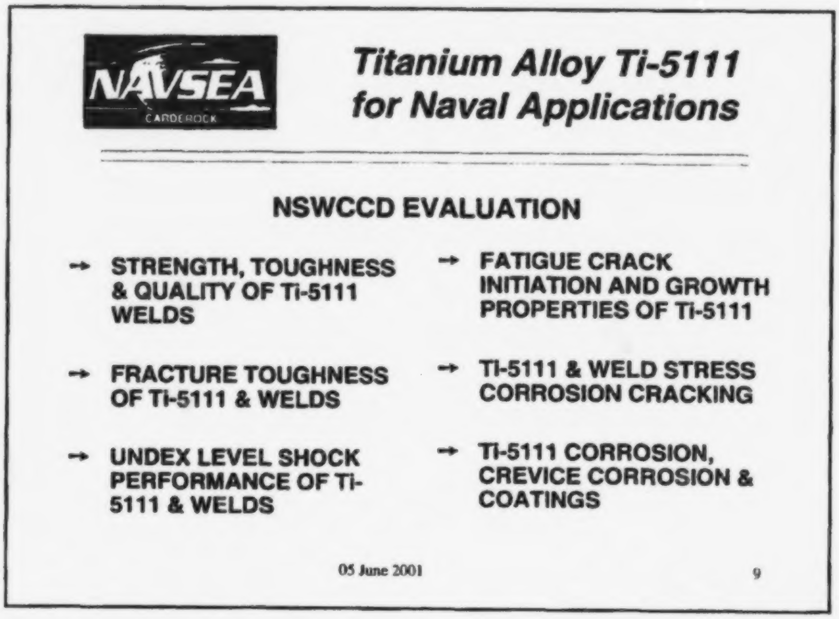

NAVSEA
CARDEROCK

Titanium Alloy Ti-5111 for Naval Applications

NSWCCD EVALUATION

- → **STRENGTH, TOUGHNESS & QUALITY OF Ti-5111 WELDS**
- → **FRACTURE TOUGHNESS OF Ti-5111 & WELDS**
- → **UNDEX LEVEL SHOCK PERFORMANCE OF Ti-5111 & WELDS**
- → **FATIGUE CRACK INITIATION AND GROWTH PROPERTIES OF Ti-5111**
- → **Ti-5111 & WELD STRESS CORROSION CRACKING**
- → **Ti-5111 CORROSION, CREVICE CORROSION & COATINGS**

05 June 2001

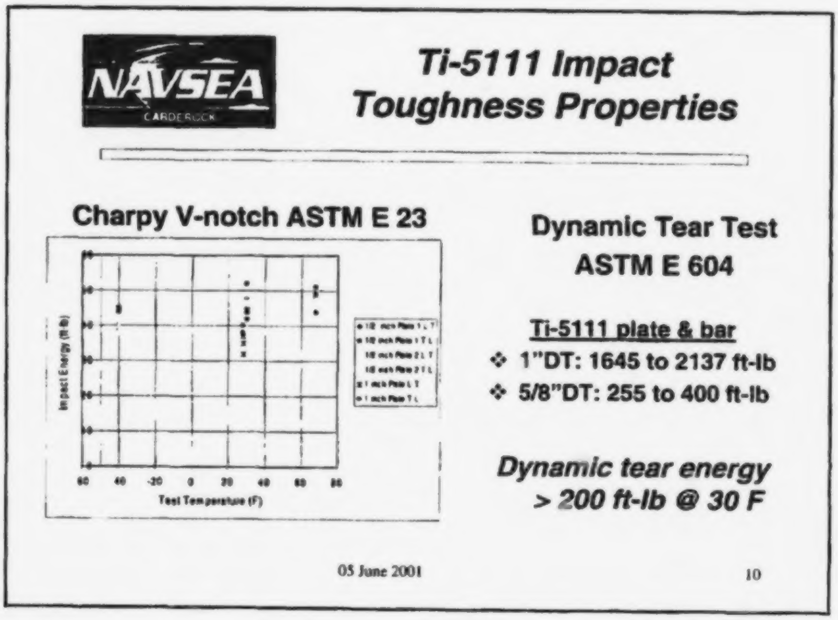

NAVSEA
CARDEROCK

Ti-5111 Impact Toughness Properties

Charpy V-notch ASTM E 23

Dynamic Tear Test ASTM E 604

Ti-5111 plate & bar

- ❖ **1"DT: 1645 to 2137 ft-lb**
- ❖ **5/8"DT: 255 to 400 ft-lb**

Dynamic tear energy > 200 ft-lb @ 30 F

05 June 2001

Ti-5111 Fracture Toughness Properties

Fracture Toughness for Ductile Metals
J-Tests (ASTM E 1820)

- ✓ Quasi-Static, Intermediate, & High rate (UNDEX rate) tests of Ti-5111 plate conducted
- ✓ Demonstrate increased initiation toughness with strain rate @ -40C; all ductile fracture
- ✓ J_{Ic} = 500 to 690 lb/in, J_{Id} = 660 to 820 lb/in
- ✓ K_{MAT}/ YS ≈ 1 (flaw tolerance threshold)
- ✓ T ≤ 10 (marginal by FTRP)

Ti-5111 Hull Toughness Element (HTE) Test

HTE Test

Large (50mm t X 200mm w X 600mm l) structural element

Surface flaw, UNDEX load @ 28 °F (-1 C)

Ti-5111 & Ti-100 HTE machined, fatigue pre-cracked, instrumented

Ti-100 HTE v. Ti-5111 HTE tests to 2% and 3% peak strain completed – no crack extension

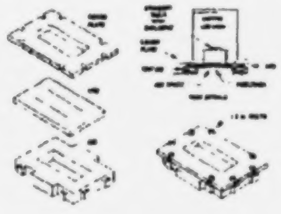

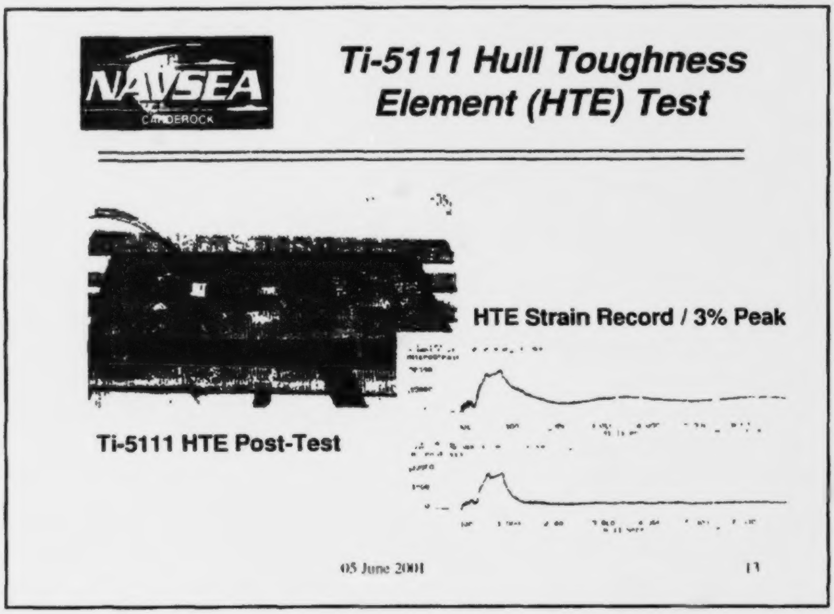

Ti-5111 Hull Toughness Element (HTE) Test

HTE Strain Record / 3% Peak

Ti-5111 HTE Post-Test

05 June 2001

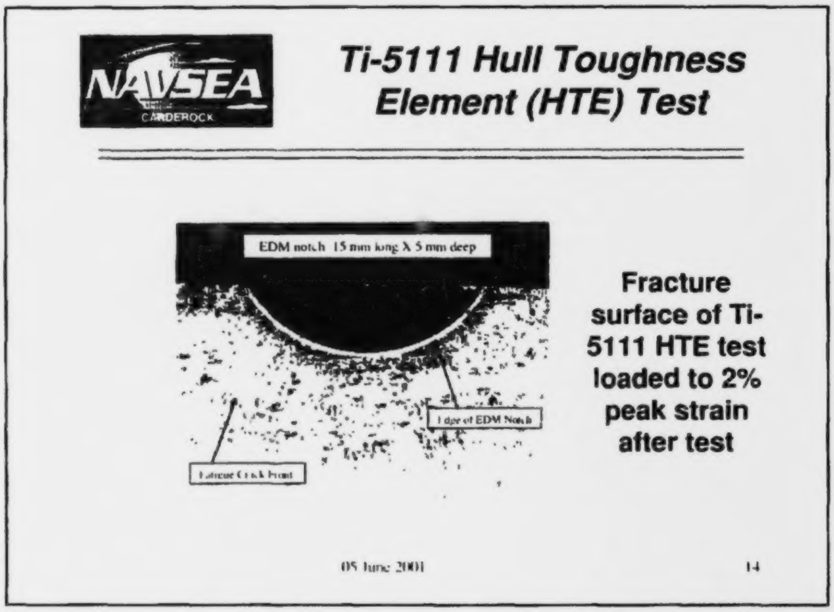

Ti-5111 Hull Toughness Element (HTE) Test

EDM notch 15 mm long X 5 mm deep
Edge of EDM Notch
Fatigue Crack Front

Fracture surface of Ti-5111 HTE test loaded to 2% peak strain after test

05 June 2001

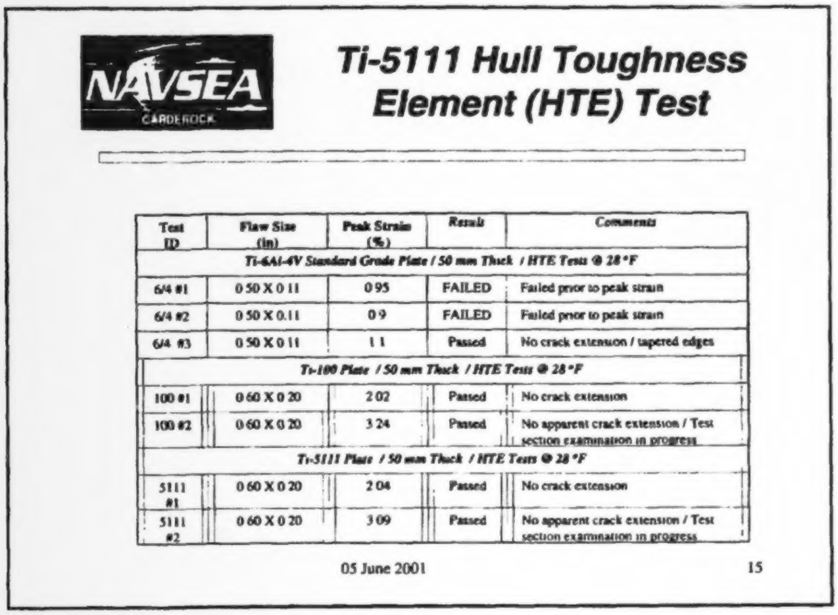

Ti-5111 Hull Toughness Element (HTE) Test

Test ID	Flaw Size (in)	Peak Strain (%)	*Result*	*Comments*
Ti-6Al-4V Standard Grade Plate / 50 mm Thick / HTE Tests @ 28 °F				
6/4 #1	0 50 X 0 11	0 95	FAILED	Failed prior to peak strain
6/4 #2	0 50 X 0.11	0 9	FAILED	Failed prior to peak strain
6/4 #3	0 50 X 0 11	1 1	Passed	No crack extension / tapered edges
Ti-100 Plate / 50 mm Thick / HTE Tests @ 28 °F				
100 #1	0 60 X 0 20	2 02	Passed	No crack extension
100 #2	0 60 X 0 20	3 24	Passed	No apparent crack extension / Test section examination in progress
Ti-5111 Plate / 50 mm Thick / HTE Tests @ 28 °F				
5111 #1	0 60 X 0 20	2 04	Passed	No crack extension
5111 #2	0 60 X 0 20	3 09	Passed	No apparent crack extension / Test section examination in progress

05 June 2001

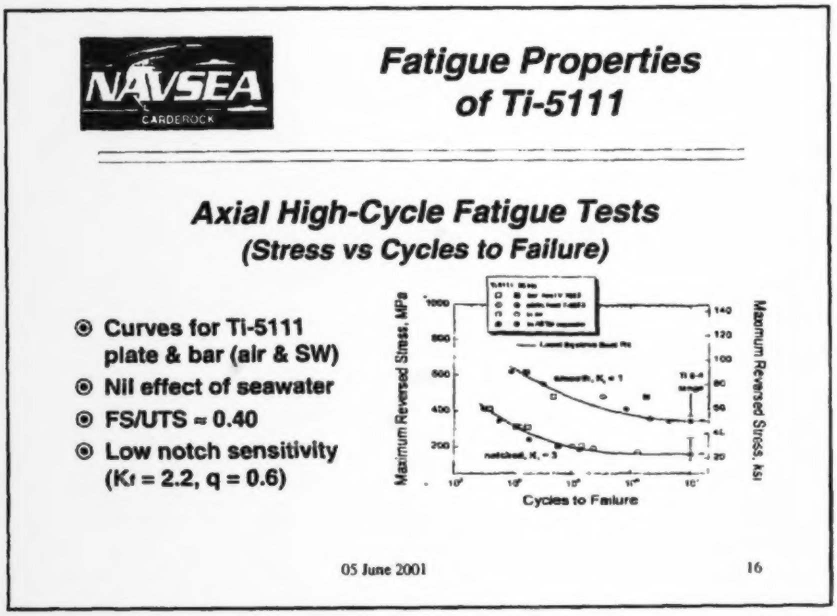

Fatigue Properties of Ti-5111

Axial High-Cycle Fatigue Tests
(Stress vs Cycles to Failure)

- **Curves for Ti-5111 plate & bar (air & SW)**
- **Nil effect of seawater**
- **FS/UTS ≈ 0.40**
- **Low notch sensitivity (K_t = 2.2, q = 0.6)**

05 June 2001

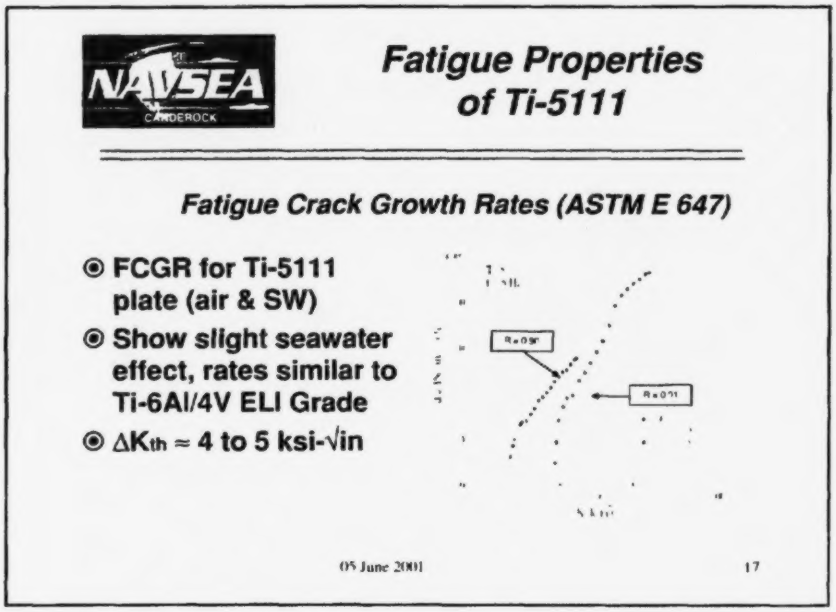

Fatigue Properties of Ti-5111

Fatigue Crack Growth Rates (ASTM E 647)

- FCGR for Ti-5111 plate (air & SW)
- Show slight seawater effect, rates similar to Ti-6Al/4V ELI Grade
- $\Delta K_{th} \approx 4$ to 5 ksi-$\sqrt{in}$

05 June 2001

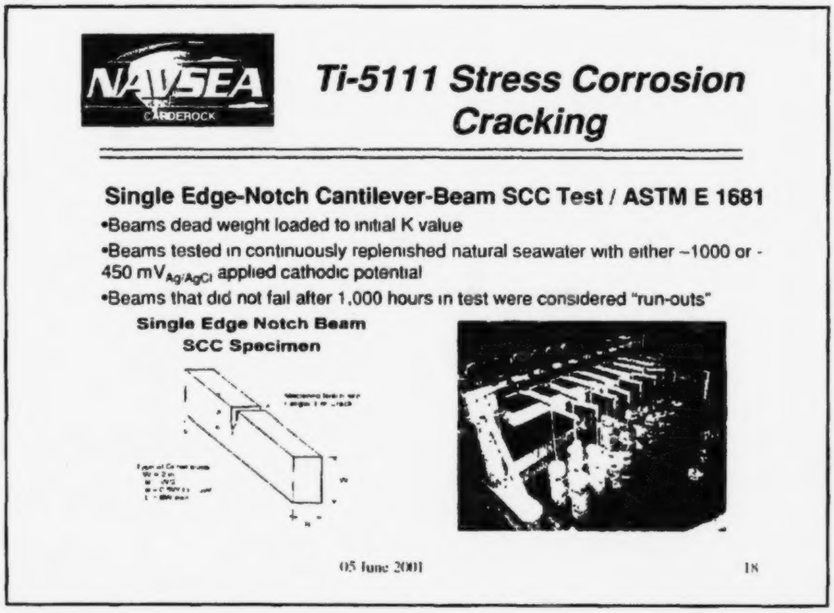

Ti-5111 Stress Corrosion Cracking

Single Edge-Notch Cantilever-Beam SCC Test / ASTM E 1681

- Beams dead weight loaded to initial K value
- Beams tested in continuously replenished natural seawater with either −1000 or -450 $mV_{Ag/AgCl}$ applied cathodic potential
- Beams that did not fail after 1,000 hours in test were considered "run-outs"

Single Edge Notch Beam SCC Specimen

05 June 2001

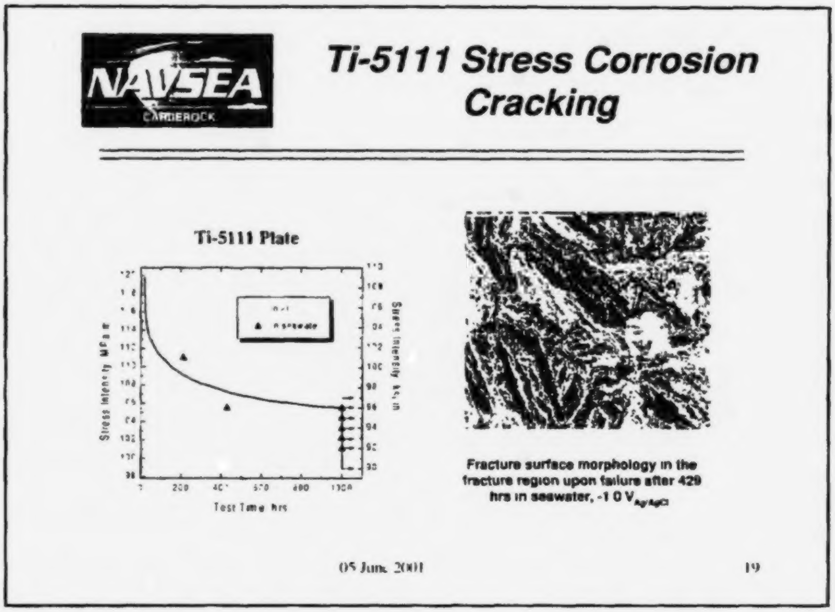

Ti-5111 Stress Corrosion Cracking

Ti-5111 Plate

Stress Intensity MPa√m
Stress Intensity ksi√in
Test Time hrs
200
1000

Fracture surface morphology in the fracture region upon failure after 429 hrs in seawater, -1.0 $V_{Ag/AgCl}$

05 June 2001

19

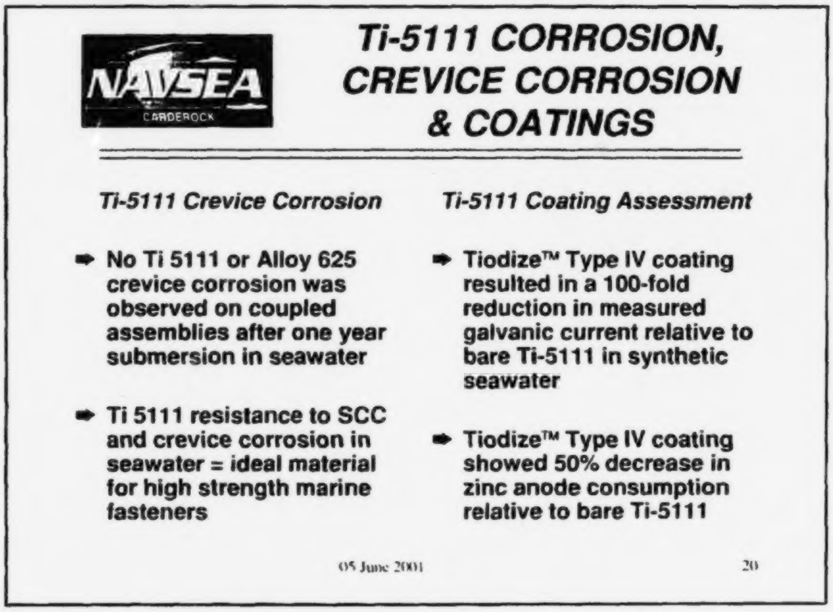

Ti-5111 CORROSION, CREVICE CORROSION & COATINGS

Ti-5111 Crevice Corrosion

- **No Ti 5111 or Alloy 625 crevice corrosion was observed on coupled assemblies after one year submersion in seawater**
- **Ti 5111 resistance to SCC and crevice corrosion in seawater = ideal material for high strength marine fasteners**

Ti-5111 Coating Assessment

- **Tiodize™ Type IV coating resulted in a 100-fold reduction in measured galvanic current relative to bare Ti-5111 in synthetic seawater**
- **Tiodize™ Type IV coating showed 50% decrease in zinc anode consumption relative to bare Ti-5111**

05 June 2001

20

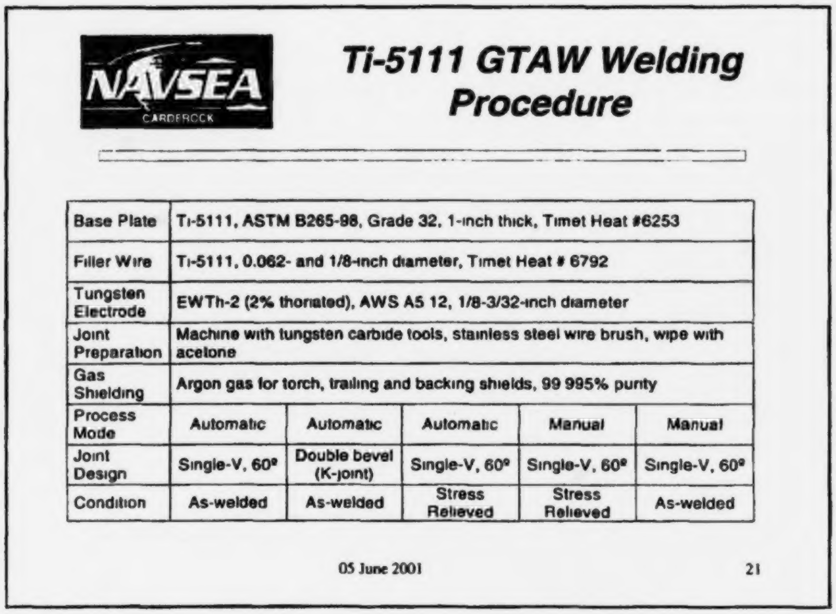

NAVSEA CARDEROCK

Ti-5111 GTAW Welding Procedure

Base Plate	Ti-5111, ASTM B265-98, Grade 32, 1-inch thick, Timet Heat #6253				
Filler Wire	Ti-5111, 0.062- and 1/8-inch diameter, Timet Heat # 6792				
Tungsten Electrode	EWTh-2 (2% thoriated), AWS A5.12, 1/8-3/32-inch diameter				
Joint Preparation	Machine with tungsten carbide tools, stainless steel wire brush, wipe with acetone				
Gas Shielding	Argon gas for torch, trailing and backing shields, 99.995% purity				
Process Mode	Automatic	Automatic	Automatic	Manual	Manual
Joint Design	Single-V, 60°	Double bevel (K-joint)	Single-V, 60°	Single-V, 60°	Single-V, 60°
Condition	As-welded	As-welded	Stress Relieved	Stress Relieved	As-welded

05 June 2001

21

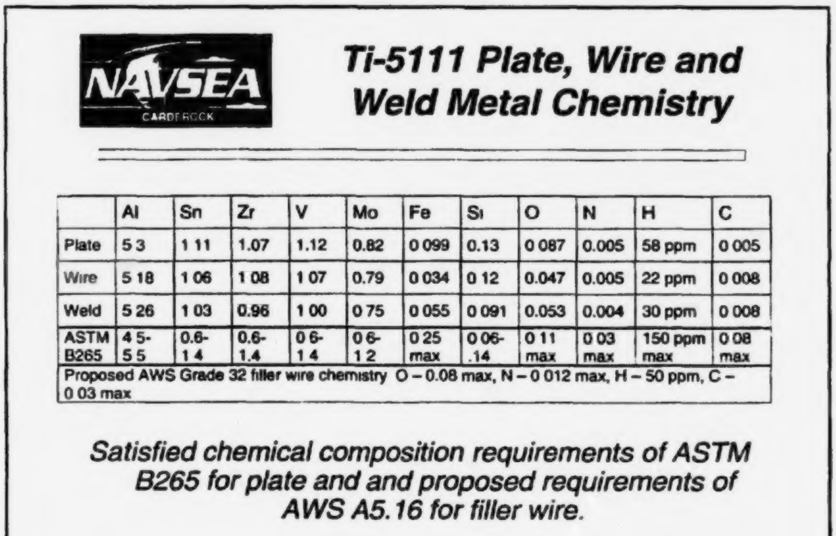

NAVSEA CARDEROCK

Ti-5111 Plate, Wire and Weld Metal Chemistry

	Al	Sn	Zr	V	Mo	Fe	Si	O	N	H	C
Plate	5.3	1.11	1.07	1.12	0.82	0.099	0.13	0.087	0.005	58 ppm	0.005
Wire	5.18	1.06	1.08	1.07	0.79	0.034	0.12	0.047	0.005	22 ppm	0.008
Weld	5.26	1.03	0.96	1.00	0.75	0.055	0.091	0.053	0.004	30 ppm	0.008
ASTM B265	4.5-5.5	0.6-1.4	0.6-1.4	0.6-1.4	0.6-1.2	0.25 max	0.06-.14	0.11 max	0.03 max	150 ppm max	0.08 max
Proposed AWS Grade 32 filler wire chemistry O – 0.08 max, N – 0.012 max, H – 50 ppm, C – 0.03 max											

Satisfied chemical composition requirements of ASTM B265 for plate and and proposed requirements of AWS A5.16 for filler wire.

05 June 2001

22

Ti-5111 Macrosection and Hardness Profiles

- **Bright, silver weld deposits indicative of proper shielding**
- **Sound welds with no indications of porosity or other defects**
- **Rockwell C hardness scans indicated uniform hardness**

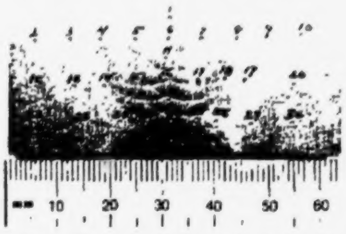

R^c - Plate: 27 to 30, HAZ: 30-31, Weld: 28-31

Ti-5111 Weld Tensile Properties

Process Mode	Type	UTS, ksi	0.2% YS, ksi	El, %
Automatic Stress Relieved	AWM	128.0, 129 8	120.2, 118.7	13, 18
	Transverse	127.7, 127.8	98.5, 105 9	
Manual Stress Relieved	AWM	131 9, 131.6	122.5, 123 4	11, 11
	Transverse	133.9, 131.8	100.2, 105.9	
Manual As Welded	AWM	119.5, 116.5	105.8, 99.6	13, 16
	Transverse	127.0, 126.7	112 3, 114.0	

Exceeded minimum requirements for ultimate strength (100 ksi), yield strength(85 ksi) and elongation(10%)

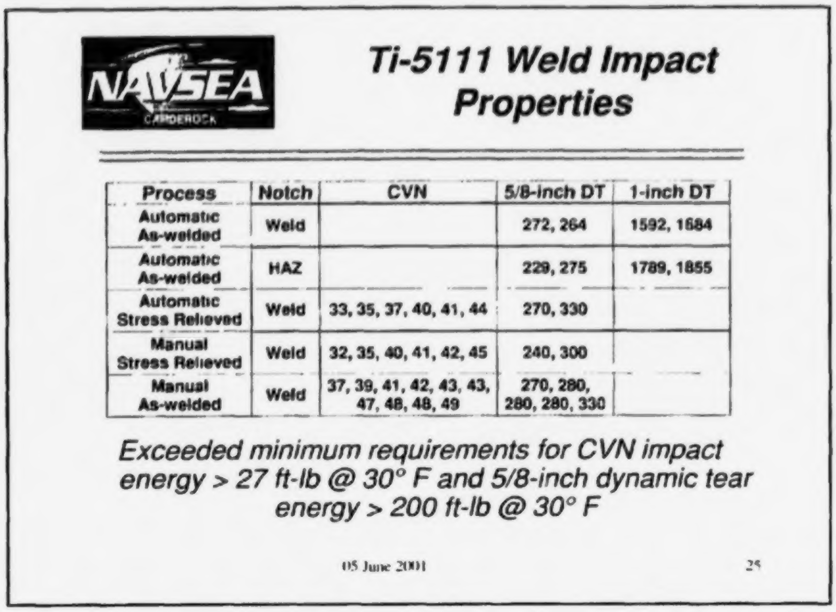

Ti-5111 Weld Impact Properties

Process	Notch	CVN	5/8-inch DT	1-inch DT
Automatic As-welded	Weld		272, 264	1592, 1684
Automatic As-welded	HAZ		229, 275	1789, 1855
Automatic Stress Relieved	Weld	33, 35, 37, 40, 41, 44	270, 330	
Manual Stress Relieved	Weld	32, 35, 40, 41, 42, 45	240, 300	
Manual As-welded	Weld	37, 39, 41, 42, 43, 43, 47, 48, 48, 49	270, 280, 280, 280, 330	

Exceeded minimum requirements for CVN impact energy > 27 ft-lb @ 30° F and 5/8-inch dynamic tear energy > 200 ft-lb @ 30° F

05 June 2001

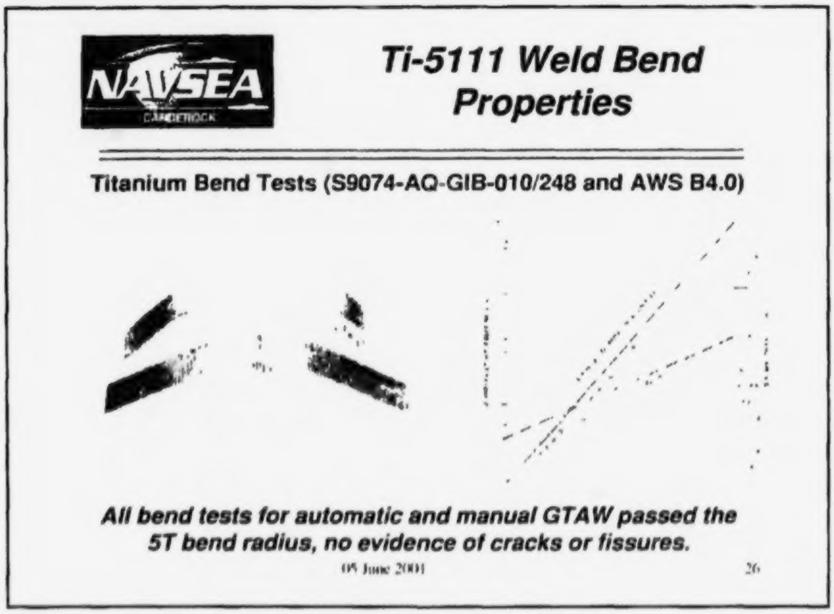

Ti-5111 Weld Bend Properties

Titanium Bend Tests (S9074-AQ-GIB-010/248 and AWS B4.0)

All bend tests for automatic and manual GTAW passed the 5T bend radius, no evidence of cracks or fissures.

05 June 2001

Ti-5111 Weld Metal Stress Corrosion Cracking

- **Cantilever beam specimens notched in weld (V-groove) and HAZ (K-joint).**
- **Tested in continuously replenished natural seawater with either –1000 or -450 mV$_{Ag/AgCl}$ applied cathodic potential.**

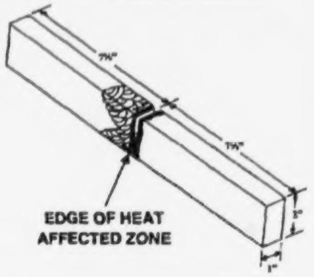

***Weld Metal*: K$_{ISCC}$ > 90 ksi-√in [@ -1000mV & @ -450 mV], no failures**

***Heat Affected Zone (HAZ):* K$_{ISCC}$ > 85 ksi-√in [@ -1000mV & @ -450 mV]**

Titanium Alloy Ti-5111 for Naval Applications
SUMMARY

All material property tests to date show that Ti-5111 is well suited for Navy applications

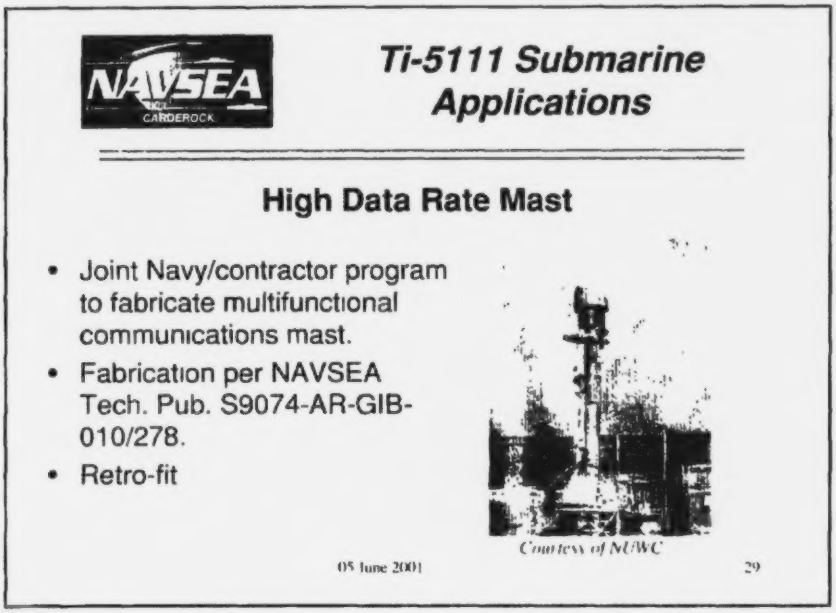

Ti-5111 Submarine Applications

High Data Rate Mast

- Joint Navy/contractor program to fabricate multifunctional communications mast.
- Fabrication per NAVSEA Tech. Pub. S9074-AR-GIB-010/278.
- Retro-fit

Courtesy of NUWC

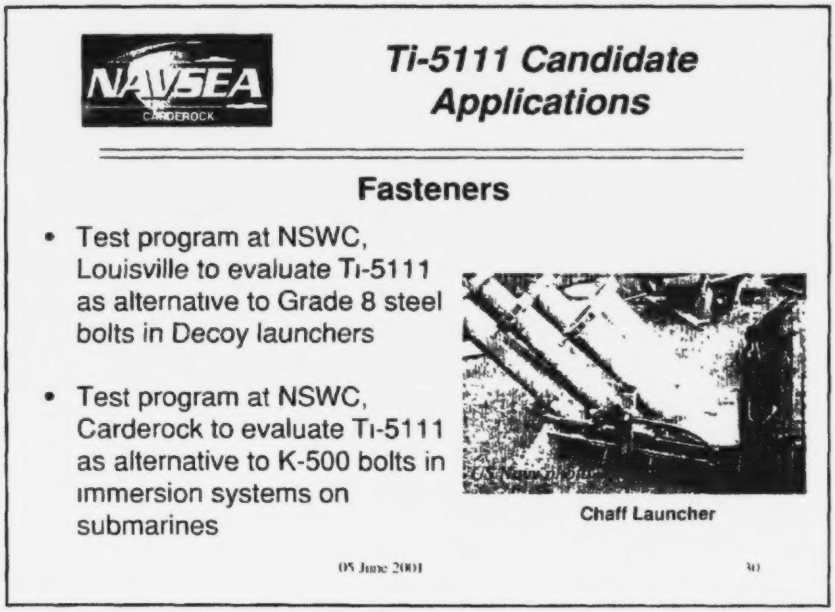

Ti-5111 Candidate Applications

Fasteners

- Test program at NSWC, Louisville to evaluate Ti-5111 as alternative to Grade 8 steel bolts in Decoy launchers
- Test program at NSWC, Carderock to evaluate Ti-5111 as alternative to K-500 bolts in immersion systems on submarines

Chaff Launcher

H516419 ⑦

Experiences with T.I.M.E. Welding: Ontario Research, Techno Scientific, Hyundai, European Investigation, Central Institute of Welding, Aichi Sangyo, and subsequent experiences in DND: 1980s to present

by

J.G. Church, P. Eng.
Weld-Process International Ltd.

and

J.R. Matthews, PhD, P.Eng.
DREA Canada

Abstract

This paper deals on a historic level with the T.I.M.E. Welding Process, a process characterized by a unique control of plasma formed from the ionized gases used in the welding gas mixture.

The experiences of John Church, with T.I.M.E. Welding are described. His work with Ontario Research, Techno Scientific, Hyundai, a European Investigation, the Central Institute of Welding, the Aichi Sangyo Co, and his patent experiences in Japan are presented with data and historical perspectives.

Subsequent experiences in DND from the 1980s to the present are also presented along with Dynamic Tear impact test data to frame the process against other welding methods.

Introduction

John Church and Weld Process International have spent the last 20 years introducing the T.I.M.E. process around the world and subjecting the process to a variety of evaluations from every corner of the globe. The process has endured evaluations at the Welding Institute, Ontario Research, Techno Scientific, in Europe, at the Central Institute of Welding, Hyundai, the Aichi Sangyo Co, Japanese patent bureaucracy, General Dynamics and others. In each instance the process endured the scrutiny and survived with a comment typified by the following… "the process is technically superior to all others evaluated, but…"

The "but" was the story of this Canadian process. In Canada the "but" was the collective thinking that there must be something wrong with someone patenting a gas mixture. In other countries the "but" was the cost analysis and traditional gas metal arc welding lack of fusion (GMAW LOF) concerns.

The process produced exceptional toughness at all times despite the fact that the owners were marketing it for its productivity. Wire feed rates of 15 to 35 m/min were introduced world wide. The weldments were superior in all positions even with standard GMAW equipment. Its acceptance in central Europe and the far east was strong but the British, North American and Canadian acceptance was very slow coming.

DREA was introduced to the process by Mirek Macecek around 1980 to 1982. Mirek had been using the process on robots that he was supplying to the automotive industry and couldn't say enough positive about the process. He showed us a six inch thick narrow gap weldment that was completely free of LOF encouraging us to believe that maybe this process was different.

The more we tested it the more we were convinced that the process was extremely special. In comparative test after comparative test for 20 years the T.I.M.E. process always outperformed the competition. In the past 12 years DREA also set out to resolve the LOF issue and has published our findings in Materials Evaluation April 2001 [1]. Our study shows that when you intentionally introduce 50 mm and 100 mm lack of fusion discontinuities in T.I.M.E. welds of HY100 that the weldments still pass explosion bulge tests because of the superb low temperature transition performance. We are convinced that toughness requirements in submarine weldments can be met without sacrificing weldmetal strength. In other words overmatched weldments and high toughness are both possible and LOF is not a problem. John Church would add that the process reduces the incidence of LOF over normal GMAW as well, even in all position with standard welding machines.

In this paper we present test results that were attained during the early years when the T.I.M.E. process was evaluated around the world. We then present test results at DREA and conclude with some recent results from National Steel Car in Hamilton where it endured its most recent evaluation, and at FMF Cape Scott, where it is involved in a comparison of SMAW and FCAW welding recommended for the Victoria Class Submarines.

Background

The T.I.M.E. Process [2-4] was developed in 1980 by John Church after many years of research and development of gas mixtures for shielding and metal transfer. (John Church started his career in welding in the 1940's. He was responsible for some of Canada's original work in pipeline welding in the late forties. He worked for 18 years in the early part of his career for Lincoln Electric and in more recent years has become a lifetime member of the American Welding Society.) The process is a gas metal arc welding process that employs a special gas and a specially designed nozzle. The process produces welds that are very clean [5] with enhanced weldment toughness. The gas in combination with the nozzle has a surprising influence on the arc. This influence is the subject of a number of patents and continuations (Patent Nos. 4,463,243; 4,572,942; 4,464,560; and 4,524,863; Docket Nos. 1909,015 and 1909,016) describing the precision four-part gas mixture of helium, argon, carbon dioxide and oxygen used for shielding and metal transfer control. The gas mixture flow is controlled directionally through the gas diffuser to interact at the arc. High speed cine photography, demonstrated at the Welding Institute, has shown that a unique stable plasma is produced at the end of the electrode to transfer the droplets from the electrode in an axial spray transfer (linear concentric) pattern into the weld [2]. The ionized plasma suppresses the rotation of the electrode and prevents lateral wire movement during metal transfer. With standard gases, metal transfer from the electrode is not concentric with the electrode and at critical wire feed speeds, the metal transfer creates an unbalanced effect on the electrode, which causes a motion to take place near the end of the electrode. On the other hand the T.I.M.E. process suppresses this motion since the T.I.M.E. gases produce a plasma that reacts concentrically with the electrode, and the resultant of gravity forces, pinch forces, plasma stream forces, surface tension forces and arc forces, remain unidirectional [2]. The droplet transfer from the electrode is stable. The energy from the transferred metal droplets combines with the arc energy in a concentric pattern contributing to the fusion-penetration profile of the deposit [3]. The unique control of the metal transfer allows welding in all positions.

T.I.M.E. Gas

When molten metal is deposited into the weld pool, it must be shielded in order to prevent contamination. An envelope of gases surrounds the molten metal as the electrode transfers into the pool. The envelope of gas prevents the oxygen, the nitrogen and hydrogen from the atmosphere contaminating the weld metal and producing porosity.

When the G.M.A. process was first developed, the metallurgist and manufacturer reached backwards in time to the analysis of transferring metal from the stick electrode – the S.M.A.W. Process. In transferring metal from a cellulose electrode, the glob of molten metal in transfer is surrounded by a gas shield which is mainly carbon dioxide. The carbon dioxide comes from the flux in the electrode in a chemical reduction process at the arc.

The first MIG welding was shielded with carbon dioxide directed around the wire. The atmosphere was excluded by means of this CO_2 shielding.

The CO_2 process was somewhat satisfactory and it was used for several years. However, metallurgists found there was sufficient carbon pick up in the weld deposit to produce an unsatisfactory quality deposit. Today, CO_2 is not used where quality control, appearance and physical properties of the weld metal are significant.

Investigation of the literature related to the evolution of the GMA Process revealed that improving physical properties of the weld has been foremost in the design of gases. Patent data confirms conclusively the developments in the process were directed to improve the quality of the weld deposit.

Shielding gases were changed from CO_2 to Argon and Argon based mixtures. They now consist of Argon, Argon/ CO_2, Argon/ O_2 and Argon/ CO_2/ O_2 in combinations of percentages and each gas mixture produces a difference in the quality of the material deposit and in the characteristics of the arc.

In an arc, the voltage pulls the electron (which is part of the atom structure of the gas), out of its orbit. The ion or positive charge remaining seeks to reform the atomic structure.

The ionized gas in motion produces a plasma energy. When plasma is at the arc, it does not stay constant in one location but it moves around the electrode and from one side to the other. Plasma conducts the energy from the power source called the power energy across the arc.

The power energy of welding energy is amperage multiplied by voltage. The secondary energy is produced by the plasma.

There are two energy levels at the arc: the energy level produced by the amperage and voltage of the power source plus the energy level produced by the plasma determined by the gas mixtures used for shielding.

As plasma moves, its energy under the electrode moves. Its moving effect is to cause the electrode to melt momentarily in the location of its presence.

This change in direction of the droplet transfer causes some of the problems that were associated in the past with the GMAW welding.

Incomplete penetration and/or lack of fusion or cold lap as it is commonly called in the GMA welding process has been caused by inconsistent energy at metal transfer. It has been for this reason that many industries have not allowed the use of the GMA welding process.

The plasma energy moves on one side or the other of the electrode and it melts a droplet from that side of the electrode. If the plasma moves to another side of the electrode, it melts that side of the electrode and causes the droplet of metal to fall from that side of the electrode.

This plasma movement causes a flip-flop of the metal droplets transferring from the end of the electrode into the pool. This causes the inconsistency with respect to the energy level, the penetration variation and the irregular fusion characteristic at the end of that electrode.

Now the T.I.M.E. gas as described in its patent overcomes the plasma motion and stabilizes it. The plasma energy aligns with the power energy and the total energy direction is in line with the electrode causing the axial droplet transfer and consistent penetration and fusion.

The flip-flop plasma energy producing droplets of metal flip flopping from one side of the electrode or the other is replaced by in line energy and axial droplet transfer. This is the remarkable difference of the T.I.M.E. Gas compared to other shielding products and is responsible for its ease of welding and out of position welding even with standard welding machines.

Materials

The HY 80 steel plates used in this study were supplied to MIL 16216 specifications. All other steels were supplied to ASTM specifications. The 16 mm dynamic tear toughness of the HY steel plate at –29C was approximately 2000 joules with the notch oriented in the transverse direction, and was approximately 1200 joules with the notch oriented in the longitudinal direction. While normal quality weldments of HY 80 steel have 16 mm dynamic tear toughness at –29C in the range of 600 to 900 joule range, values equivalent to the longitudinal toughness for the base plate (1200 joules) would be preferred and are the target for weldment improvement for this steel. Lincoln LA100 wires and the TIME process often meet this target.

Early test evaluations

In Tables 1a to 1j data are presented for the early evaluations of the T.I.M.E. Process.

Ontario Research was the first organization to be involved in extended testing of the process. Welding was conducted on an A.S.T.M. A 36 steel, Table 1a, an HY100 Q.T. Steel, Tables 1b and 1d, and a Cr Mo 387 Grade 22 Q. & T. steel, Tables 1c and 1e. These results demonstrated excellent low temperature notch toughness and significant improvements over other gas mixtures.

Techno Scientific was the next company to evaluate and use the T.I.M.E. process, Table 1f. Mirek Macecek was combining the T.I.M.E. process with American robots and selling them to the automotive industry. The results were completely successful. It was Mirek who would later introduce the process to DREA.

The next organization to evaluate the process was Hyundai Ship Research Center, Table 1g. These people were impressed with the high productivity, high wire feed speeds, and quality of results at these speeds. Despite the productivity the impact results continued to impress.

John Churches next experiences were in Europe. The process was subjected to a number of evaluations. It was the subject of a European Investigation, Table 1h. ER 70 S-6 wires, Table 1h, and ER 80 S-N12 wires, Table 1i, were evaluated. A report, I.I.W.-Doc XXI-1238-91, T.I.M.E. Process 1991 ASME 11/C SFA S.18 showed that the low temperature impact properties were retained with the process under high productivity procedures.

Over the years many more companies evaluated the process and many are using it routinely. Companies that switch to the process do not go back. General Dynamics included the T.I.M.E. process in an eighteen process comparison and told us that the T.I.M.E. process had clearly outperformed the other processes. Bombardier uses the process in its car business and has experienced trouble free usage for 17 years.

One of the most significant test results came when the process was subjected to a Japanese Patent Application. Twelve gas mixtures were evaluated as part of the overall assessment of the patent by the patent authority, Table 1j (Overall assessment of varied constituents percentages combinations of the Ar, He, CO_2, O_2 quad gas mixture.) The optimized T.I.M.E. gas composition produced the best results. (composition 9 in Table 1j). The excellent results are even more impressive when one notes the wire feed rates of 15 and 35 m/min. Figure 1 shows the impact results for these 12 compositions.

Figure 2 shows the combined results for the impact tests of weldments detailed in Tables 1a to 1j. These results are exceptional when it is realized that productivity was the primary focus in these evaluations (not toughness).

There are many more industries around the world who have evaluated and used this process. In each case it has out-performed all other processes in the past 20 years of evaluations.

DREA evaluations and experiences

Techno Scientific was the company that introduced the process to DREA. Mirek Macecek was combining the T.I.M.E. process with American robots and selling them to the automotive industry. The results were completely successful. He showed DREA a section from a 6 inch thick narrow gap butt joint which was particularly clear of defects and had very uniform heat markings. DREA then paid Techno Scientific to produce all position weldments of HY80 steel for explosion bulge and notch impact tests. The results were sensational.

Figure 3 presents results of Dynamic Tear testing of T.I.M.E. Weldments in the early 1980s at DREA and comparison to other testing activities. These are lower bound results with questionable crack path results thrown out. This was our first complete comparison of the process. Clearly the process had caught our eye.

In the next few years we set up a comparison trial for HY80 and HY100 with the T.I.M.E. process and another promising Canadian process FM pulse welding. The trial was controlled with third party supervision and WIC, Weld Process and Fleet, welding in controlled situations. Once again the T.I.M.E. placed first.

The five million dollar Canadian Steel and Welding Development project at MIL Davie was the next project to highlight the value of T.I.ME. The project manager intentionally left T.I.M.E. out of the evaluations. His test results were predictable. There were considerable failures of explosion and DT impact tests for the various weld processes evaluated. As expected the higher strength SMAW were prone to failure and incidences of failure were noted throughout the test matrix with one exception. The welds produced with the Mil Davie robot were not failing. At the end of the day it was learned the the robot was fitted with T.I.M.E. welding. The process exceeded the others despite the attemps to bar it from the program.

In the following years T.I.M.E. welding of HY steel was overshadowed by evolution of welding machines. First were the analog pulsed, then digital pulsed. DREA bought and evaluated analog machines from around the world but eventually isolated Fronius pulsed analog machines as the best. It is these machines and standard gases that gave T.I.M.E. the best run for its money. However the T.I.M.E. process still prevailed.

In recent years digital pulsed machines have arrived and DREA evaluated them with the help of Fleet. The Powerwave and the Miller machines were the best overall but digital machines have more uniformity than the earlier analog machines and so many machines are acceptable. FMF Cape Scott has recently acquired Miller Phoenix machines and has been evaluating them throughout the winter of 2000.

In the past winter DREA has assisted FMF in evaluating two UK recommended weld processes for use on our new Victoria class submarines and has sponsored Fleet to do a heat input controlled study of 100s1 wire and the T.I.M.E. process [6]. John Church has completed a full spectrum series of welds with NSC this past winter including 90 and 100s1 strength level HY 80 weldments. Figure 4 presents these results in a generalized form. Once again after 21 years the T.I.M.E. process excels. In a subsequent paper the added advantage of T.I.M.E. welds over these other processes will be highlighted [7].

Summary

The T.I.M.E. Process has been evaluated around the world for 20 years and has out-performed the competition in productivity and flexibility while maintaining the highest reported impact toughness.

References

[1] J.R. Matthews, C.V. Hyatt, and J.F. Porter, "Future Treatment of Weld Acceptance: The Significance of Incomplete Fusion Discontinuities in Low Structural Transition Temperature GMAW Weldments, Materials Evaluation, April, 2001.

[2] M.H. Rodwell, "Evaluation of the TIME MIG Welding System", Project Report LD22983/1/83, Welding Institute, Cambridge, U.K., 1983

[3] Aichi Sangyo, "Welding Characteristics of a New Welding Process, T.I.M.E. Process", Prepared by the Aichi Sangyo Co. Ltd., Japan, July 1989

[4] M.Macecek, "All Position Welding of HY80 Plate with T.I.M.E. Process", DREA Contractor Report 88/419, 1988

[5] J.R. Matthews, J.F. Porter, J. Church, M. Macecek, "An Evaluation of T.I.M.E. Welding of HY 80 Plate," The Welding Journal,70, February 1991.

[6] D.S. Begg and J.R. Matthews, "Toughness Envelope Definition of Pulsed Gas Metal Arc Welds in HY80 Steel", 9th CF/DRDC Meeting on Naval Applications Of Materials Technology, June 2001

[7] J. R. Matthews and John Porter, "Essential testing in Submarine Pressure Hull Weld Acceptance: Victoria Class Subs", 9th CF/DRDC Meeting on Naval Applications Of Materials Technology, June 2001

Table 1a. Physical Properties of T.I.M.E. Weld (Ontario Research Foundation): A.S.T.M. A 36

Date	AWS (.045)	Shield	Y.P. psi	Tensile psi	Elongation %	Impact
July 81 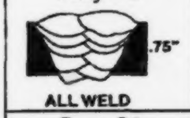	S6	CO_2 75Ar 25 CO_2 T.I.M.E.	65600 67700 65100	82600 83100 77900	29 28.5 33.0	31.5 ftlb @-20 °F 30 ftlb @-20 °F 88 ftlb @-20 °F
Sept 81 	SG SG SG	T.I.M.E. T.I.M.E. T.I.M.E.	78500 61500 61500	94000 75500 75500	26.5 29.0 29.0	71.6 ftlb @ 0 °F 50.8 ftlb @-20 °F 67.3 ftlb @-20 °F
Nov 81 	SG	T.I.M.E.	69400	80000	26.5	56.1 ftlb @-20 °F
Dec 81 	SG	T.I.M.E.	73500	85600	27	89 ftlb @-20 °F 51 ftlb @-40 °F 57 ftlb @-60 °F

Table 1b. Physical Properties of T.I.M.E. Weld (Ontario Research Foundation): Development HY100 Q.T. Steel

Date	AWS (.045)	Shield	Y.P. psi	Tensile psi	Elongation %	Impact
May 82 	S6	T.I.M.E. T.I.M.E. T.I.M.E.	122800 19600	131500 130400	17 17.5	40.8 ftlb @-60 °F 43.6 ftlb @-60 °F 60.4 ftlb @-60 °F
June 82 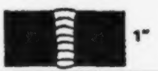	S6 (.035) S6 (.045)	T.I.M.E. T.I.M.E.				63.3 ftlb @-20 °F 70 ftlb @ -20 °F
Apr 82 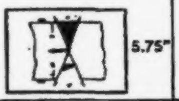	S110 (.045) Airco Ax110	T.I.M.E.	103600 106200 113200	123200 118900 127100	Side bends OK	92 ftlb @-60 °F 87.3 ftlb @-60 °F 63.5 ftlb @-60 °F
July 82 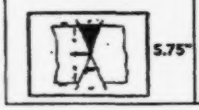	S110 (.045)	T.I.M.E.	142900 152400	85600	14 21	

Table 1c. Physical Properties of T.I.M.E. Weld (Ontario Research Foundation): Cr Mo Development 387 Grade 22

Date	AWS (.045)	Shield	Y.P. psi	Tensile psi	Elongati on %	Impact
Aug 82 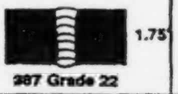 1.75" 387 Grade 22	S6 (.045)	T.I.M.E.				61 ftlb @-20 °F
Aug 82 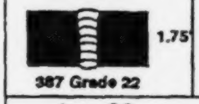 1.75" 387 Grade 22	S6 (.045)	T.I.M.E.				68.5 ftlb @-60 °F 85.5 ftlb @-60 °F 79 ftlb @-60 °F 103 ftlb @-60 °F
Aug 82 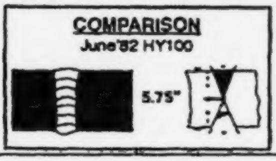 COMPARISON June'82 HY100 5.75"	S6 (.045)	T.I.M.E.		72600 83820 85380 81790 131000	Bends OK 16	95 ftlb @-60 °F 79 ftlb @-60 °F

Table 1d. Physical Properties of T.I.M.E. Weld (Ontario Research Foundation): A36

Date	AWS (.045)	Shield	Y.P. psi	Tensile psi	Elongati on %	Impact
Nov 82 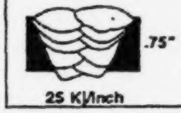 .75" 25 KJ/inch	E70S2	T.I.M.E.	78400	88400	27	92.5 ftlb @-0 °F 85.5 ftlb @-20 °F 79 ftlb @-40 °F 103 ftlb @-60 °F

Table 1e. Physical Properties of T.I.M.E. Weld (Ontario Research Foundation): Cr Mo 387 Grade 22 Q. & T.

Date	AWS (.045)	Shield	Y.P. psi	Tensile psi	Elongation %	Impact
Nov 82 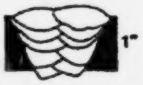	70S2(.035)	T.I.M.E. 2	106600	115700	19.5	22 ftlb @-40 °F
	70S2(.035)	T.I.M.E. 1	82400	106000	23.0	24.5 ftlb @-40 °F
	70S2(.035)	T.I.M.E. 1	97500	110700	17.5	37.5 ftlb @-40 °F
	70S2(.035)		99000	108500	19.5	37.3 ftlb @-40 °F
Nov 82 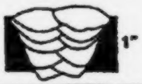	S110	T.I.M.E.	72700	85900	26.5	54.8 ftlb @-40 °F
Jan 83 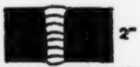	S110(.045)	T.I.M.E.	154000	85400		73 ftlb @-40 °F
		T.I.M.E.	85400	83600		75 ftlb @-40 °F
				85700		

Table 1f. T.I.M.E. Narrow Gap Process Oct 83

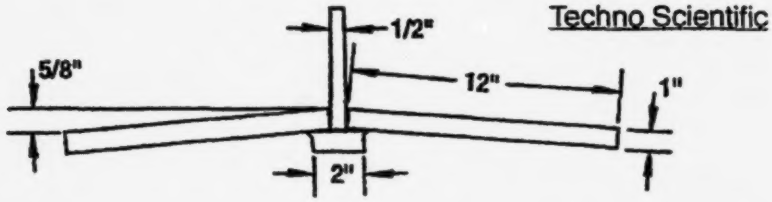

Date	AWS (.045)	Shield	T.I.M.E.	Impact
Oct 83	70S6	P1 #2	T.I.M.E. 1	23 ftlb @-65 °F
		P1 #3		31 ftlb @-65 °F
		P1 #4		21.5 ftlb @-65 °F
Oct 83	100	P2 #2	T.I.M.E. 1	48 ftlb @-65 °F
	S110	P2 #3		76.5 ftlb @-65 °F
		P2 #4		53 ftlb @-65 °F
Oct 83	100	P3 #2	T.I.M.E. 2	50 ftlb @-65 °F
	S110	P3 #3		53 ftlb @-65 °F
		P3 #4		45 ftlb @-65 °F

Table 1g. T.I.M.E. Narrow Gap Process S-6 Electrode Sept. 84 Hyundai Ship Research Center

Date	Welding Conditions			Sequence	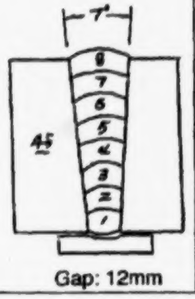	Impact
	Current (A)	Voltage (V)	WFS (m/min)			
Sept 84	360	35	16	Narrow Gap maximization		Face
Sept 84	400	36	21			92 joules@-20°C
Sept 84	400	36	21			44 joules@-40°C
Sept 84	400	36	21			Root
Sept 84	400	36	21			125 joules@-20°C
Sept 84	400	36	21			113 joules@-40°C

Recommended current is 400 amps
Slag removal is required after 2-3 passes
Spatter is no problem
Straight wire feeding is required for arc stability
Maximum welding distance at one time is 7 m

Table 1h. European Investigation I.I.W.-Doc XXI-1238-91, T.I.M.E. Process 1991 ASME 11/C SFA S.18 Mechanical Properties ER 70 S-6 1.2 mm wire

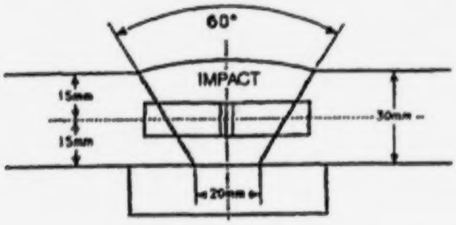

Date	Wire feed speed m/min	Current/ voltage	Travel mm/ min	Heat Input kJ/mm	Yield Elongation	Impact @-30 °C
1991 18% CO2 12 passes	11.4	300 amps/ 30.5 volts	330	1.66	476MPa 30 %	90 joules
1991 T.I.M.E. 12 passes	11.4	300 amps/ 30.5 volts	330	1.66	484MPa 30.4 %	77 joules
1991 T.I.M.E. 12 passes	15	360 amps/ 33.5 volts	440	1.644	492MPa 30.2 %	114 joules
1991 T.I.M.E. 10 passes	20	385 amps/ 36 volts	500	1.66	492MPa 27.6 %	85 joules
1991 T.I.M.E. 10 passes	25	460 amps/ 39 volts	650	1.65	496MPa 31.8 %	115 joules
1991 T.I.M.E. 9 passes	35	495 amps/ 48 volts	350	4.07	408MPa 30.8 %	107 joules

Table 1i. European Investigation I.I.W.-Doc XXI-1238-91, T.I.M.E. Process 1991 ASME 11/C SFA S.18 Mechanical Properties Low Temperature Steels ER 80 S-N12

Date	Wire feed speed m/min	Yield MPa	Tensile MPa	%	Impact Temp	Impact joules
1991 2.5% Ni	25	539	642	24.4	RT -40 -60	173 106 57
1991 NiCrMo	20	830	895	20.2	RT -20 -40	132 84 52

Table 1j. Japanese Patent Application: T.I.M.E. Gas Standards: Overall assessment of varied constituents percentages combinations of the Ar, He, CO2, O2 quad gas mixture

	Constituent Gas Percentages Combination (%)				Weld condition			Contents in Weld Metal (%)			Impact
	Ar	He	CO2	O2	Wire feed speed m/min	Weld Current (A)	Weld voltage (V)	Mn	Si	O2	Ft lbs @-60 °F
1	30	60	10	0	15	350	39	1.20	.6	.036	14.5
					35	560	52	1.10	.5	.040	21.7
2	50	40	10	0	15	360	38	1.15	.6	.037	14.5
					35	570	51	1.10	.6	.040	21.7
3	62	30	8	0	15	380	35	1.10	.7	.035	14.5
					35	590	48	1.10	.6	.040	14.5
4	60	30	8	1.2	15	360	35	1.15	.7	.050	28.9
					35	580	48	1.18	.6	.050	21.7
5	70	20	8.5	1.5	15	380	37	1.20	.7	.035	36.2
					35	590	46	1.25	.7	.040	28.9
6	60	31	8.2	0.8	15	360	35	1.25	.75	.030	39.8
					35	480	47	1.28	.7	.030	34.7
7	62	30	6	2	15	360	36	1.15	.6	.050	28.9
					35	580	48	1.10	.6	.050	14.5
8	60	33.5	6	0.5	15	340	36	1.30	.8	.025	43.4
					35	460	48	1.31	.8	.025	34.7
9	65	26.5	8	0.5	15	330	35	1.33	.8	.023	47.0
					35	450	47	1.32	.8	.024	36
10	65	26	8.8	0.2	15	340	34	1.32	.8	.020	49
					35	480	47	1.33	.8	.020	28.9
11	51.5	40	8	0.5	15	320	37	1.30	.8	.025	39.8
					35	440	49	1.30	.8	.025	28.9
12	61	35	3	1	15	320	39	1.28	.7	.030	28.9
					35	440	50	1.25	.75	.035	27.5

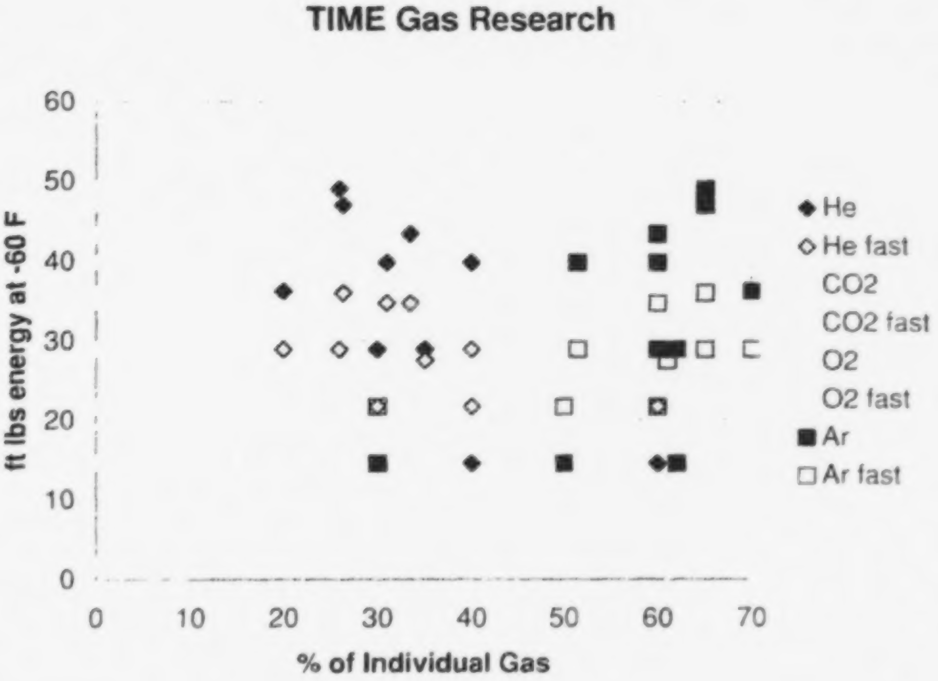

Figure 1: Results of Japanese Patent Application Testing. The highest impact energy results came from the T.I.M.E. gas composition at both 15 and 35 m/min wire feed.

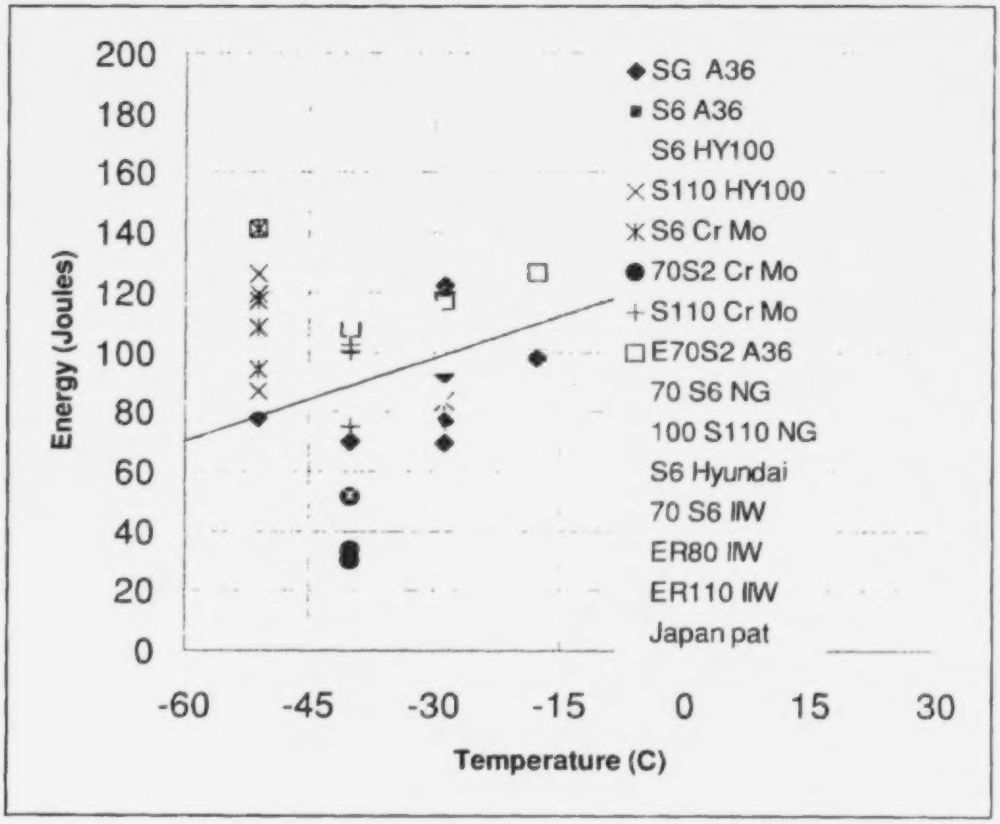

Figure 2: Results of Charpy Testing of T.I.M.E. Weldment combined from all test activity mentioned in this report. These results are exceptional when it is realized that productivity was the primary focus in these evaluations (not toughness).

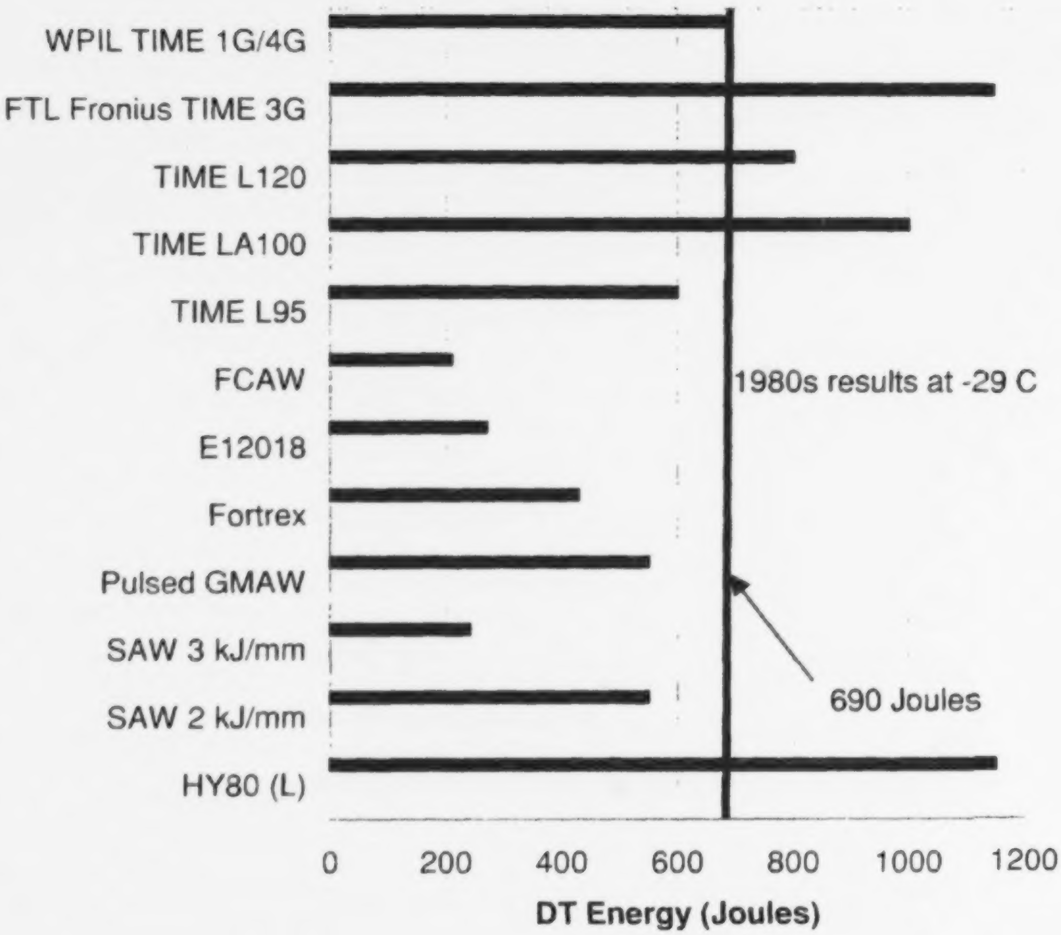

Figure 3: Results of Dynamic Tear Testing of T.I.M.E. Weldments in the early 1980s at DREA and comparison to other testing activities. These are lower bound results with questionable crack path results thrown out.

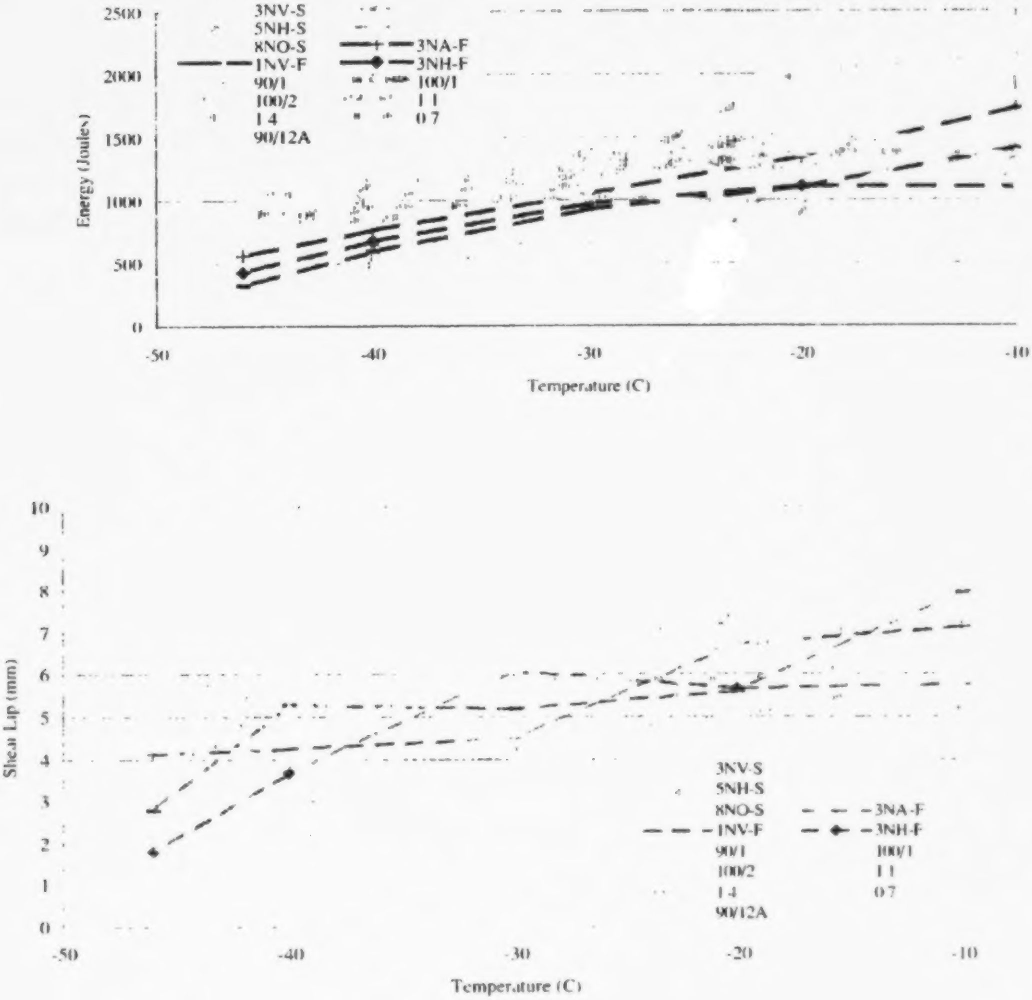

Figure 4: Comparison of T.I.M.E. (solid), SMAW (short dash) and FCAW (long dash) welds. The T.I.M.E. welds are 100 (thick line) and 90 level. The SMAW and FCAW are 90 level.

MISSING LINKS

1950 - Inter Provincial Pipeline

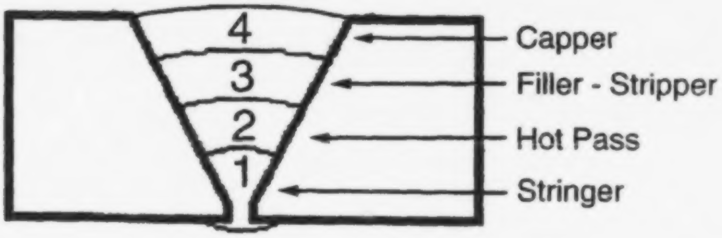

4
3
2
1
Capper
Filler - Stripper
Hot Pass
Stringer

Sparling Davis - 26" Diameter Pipe
Saskatchewan River Crossing

Trans Canada Section

MISSING LINKS #2

Storage Tank Fabrication

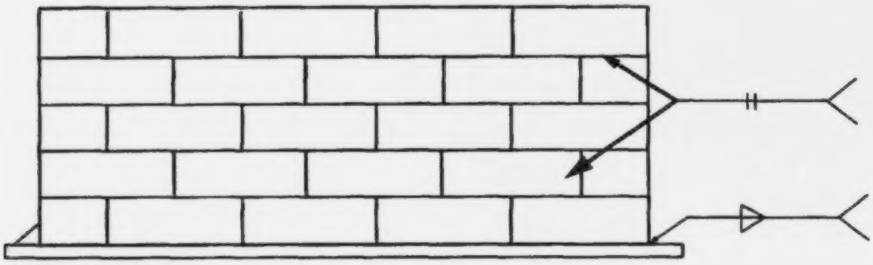

Manitoba Bridge

Spray Transfer For Verticals D.C. + V.E.
Selection For Bottoms And Floors D.C. - V.E.

	A	B	C
Fillet Welds 90%	6012	6011	6015
	6020	6013	7018
	6030	6014	7024

Manufacture's Differences

Size - Electrode - Fillet Size
Fillet Shape

UNDESIRABLE FILLET WELD PROFILES:

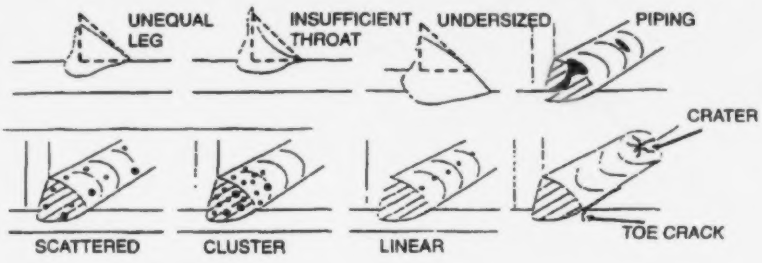
UNEQUAL LEG
INSUFFICIENT THROAT
UNDERSIZED
PIPING
CRATER
SCATTERED
CLUSTER
LINEAR
TOE CRACK

Rules For Productivity
- Largest size elecrode possible
- Highest current possible
- Direct electrode into weld bead

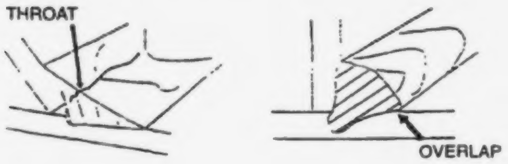
THROAT
OVERLAP

Missing Link
- Bead shape determined the weld quality
- Current density responsible for bead shape and quality
- Smaller electrodes, more productive (7/32, 1/4, 5/16)

Melt Off Rate
Arc speed
Quality
Heat input

LINCOLN ELECTRIC COMPANY

John Lincoln
James F. Lincoln
M.N. Vuchnich
R. Alison

World's Largest Supplier Of Arc Welding

G.E.
Westinghouse
Linde
Airco
Hobart
Miller

T.I.G. - M.I.G. - 1950 Alexander Lesnewich - T.I.G. & M.I.G. Argon

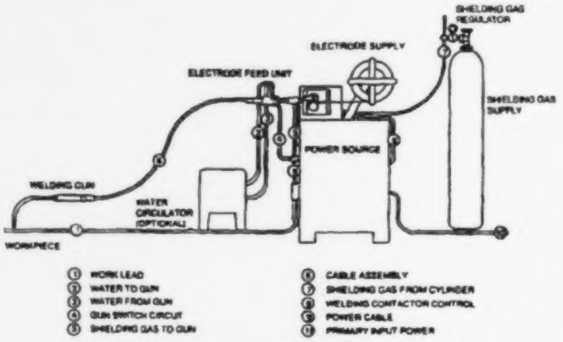
SHIELDING GAS REGULATOR
ELECTRODE SUPPLY
ELECTRODE FEED UNIT
SHIELDING GAS SUPPLY
POWER SOURCE
WELDING GUN
WATER CIRCULATOR (OPTIONAL)
WORKPIECE
① WORK LEAD
② WATER TO GUN
③ WATER FROM GUN
④ GUN SWITCH CIRCUIT
⑤ SHIELDING GAS TO GUN
⑥ CABLE ASSEMBLY
⑦ SHIELDING GAS FROM CYLINDER
⑧ WELDING CONTACTOR CONTROL
⑨ POWER CABLE
⑩ PRIMARY INPUT POWER

Diagram of Gas Metal Arc Welding Equipment

Yenni
Bemier - He / Argon

Craig - GMAW
Gas & Fluxstream

Kaesmacher - Triple Deoxidized Solid Wire

Wolfe
Lesnewich
Tuthill - Transfer Time *
Alloy Electrode ArCo2
Chemistry
C .5
Mn 1.4 - 2.26
Si .29 - .49
Ni 1.56 - 3
Cr .12 -.16
Mo .38 -.6
Impact 55ft.#@-60°F

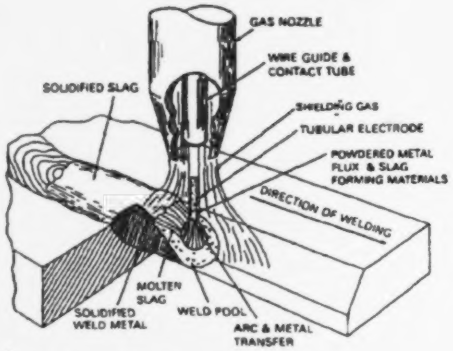
GAS NOZZLE
WIRE GUIDE & CONTACT TUBE
SOLIDIFIED SLAG
SHIELDING GAS
TUBULAR ELECTRODE
POWDERED METAL FLUX & SLAG FORMING MATERIALS
DIRECTION OF WELDING
MOLTEN SLAG
SOLIDIFIED WELD METAL
WELD POOL
ARC & METAL TRANSFER

Gas Shielding Flux Cored Arc Welding

Linde vs Lincoln

↓

Praxair

Inner Shield

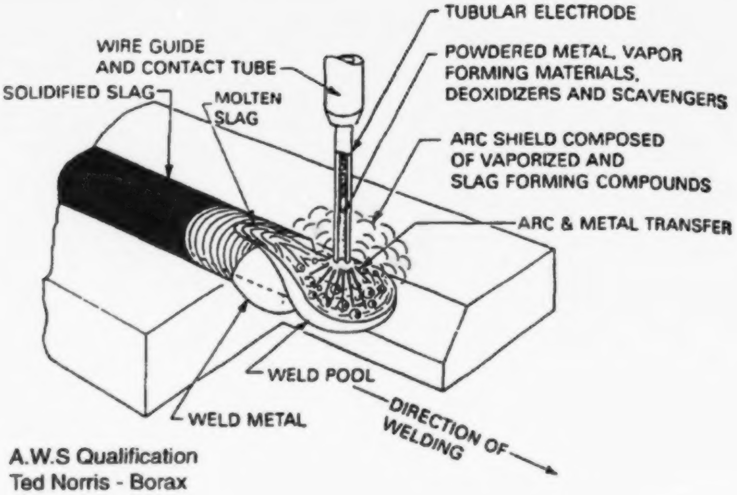
TUBULAR ELECTRODE
WIRE GUIDE AND CONTACT TUBE
POWDERED METAL, VAPOR FORMING MATERIALS, DEOXIDIZERS AND SCAVENGERS
SOLIDIFIED SLAG
MOLTEN SLAG
ARC SHIELD COMPOSED OF VAPORIZED AND SLAG FORMING COMPOUNDS
ARC & METAL TRANSFER
WELD POOL
WELD METAL
DIRECTION OF WELDING

A.W.S Qualification
Ted Norris - Borax

Patent Data

Smoke
Metal Transfer

Globs
Batch Control

Mirrors
Force Selling - Force Feeding

Windsor: Patric

- M.O.R. Weld standards - Howard Almost, E. E. Hart, C. Black, J. Chretien
Massey - John Deere - International Harvester, D.Bridge
National Steel Car
Conversion - Program 3

Departure Time
- Fan Club
- Company Man
- Hands On Vision

Philosophy Mix
- Enlightened Conscience - Bacon, Spinoza, Voltare, Spencer, Berkeley, Hegel, etc.
Religion is supposed to be a friend of man yet it is still in comflict as it has been throughout history
17 Years - Pension $200/month
Destiny

Company
- Seek First Food & Clothing & Kingdon
Still waiting

Flux Cored Wire
- Hobart - Auto TIG
- Solid Wire Dangerous

1973 - Plasmig
- 3 part gas
Copied from Linde A.G. Germany - Format
First N.A. 3 part gas
Stargon - Linde

1975 - Arbed
- .045 Flux Cored - Current Density
Solid Wire - M. Ferguson

LINK OBJECTIVES

Join Up The Missing Links
Metal Transfer
Bead Shape
Melt Off Rate Control
Productivity
Solid Wire

} *Quality*

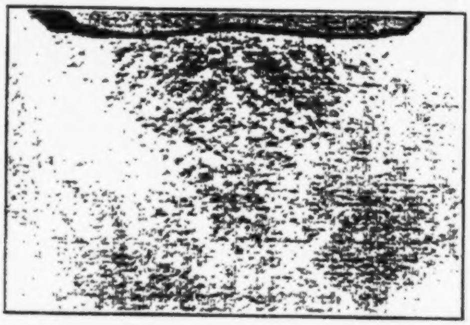

Gas Mixes

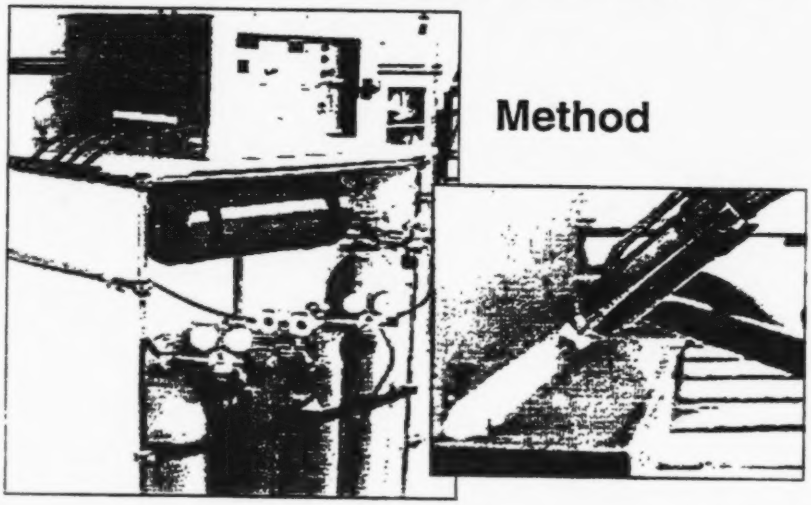

Method

Simet Mixer - No record - Pressure readings
Fillet Welds

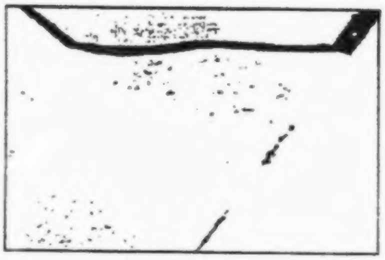

2 Gas - 3 Gas - 4 Gas

Mixing Program

After AWS Tests & Impacts
Marketing (One man show)
Lazard Freres - Welding Institute

INDUSTRY CONVERSION - WELDING ENGINEERS - BORN AGAIN

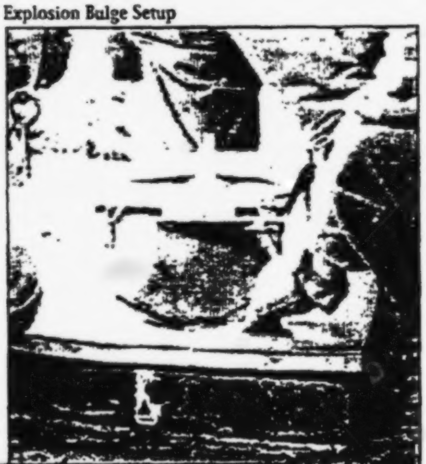

Explosion Bulge Setup

Typical Explosion Bulge Response

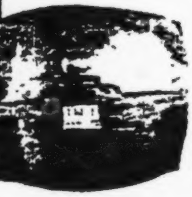

Lack Of Fusion In The Bulge Test

Bombardier
Massey Ferguson (53 page report)
General Dynamics etc.
Japan
Korea
Europe

Marketed through gas - Liquid Carbonic

Revolution - Linde
Praxair
BOC
Liquid Air

Out Welding - Research in gas distribution technology

Dr. Matthews - Research since 1982

- Extend A.W.S Tests
- Dynamic Tear Tests
- Transition Temperatures
- Flaw Inclusions
- L of F Effects
- Explosion Bulge Test

"WELD TOUGHNESS"

MISSING LINK!!

Publication - Future Treatment Of Weld Acceptance:

- Review of Bombardier World Countries
  - Canada
  - Japan
  - Europe
  - Korea
- Historic Review - No Failures - Coincidence or Science
- National Steel Car - Guaranteed Weld
  - Full Support - Dr. Matthews
    - Glen McMillan
    - Austrian Society

NATIONAL STEEL CAR

Guaranteed TIME™ Welding Process Development

Standards

Base Metal	CSA G 40.21.92.60WT - CAT 3 - See test certificate
Base Metal Thickness	One inch
Filler Metal	AWS ER 480S6 Onorm en 440.92 .045 inches
Gas Flow Rate	40-45 Cu.ft/hour
Welding EQT	a) Constant Voltage 450 Ampere 100% duty cycle power b) Wire Feeder range 250 inches/minute to 1,000 inches/minute (Read out control of wire feed speed)
Gun Cable	Bernard 600 ampere special design (Patented Diffuser) - see print
Primer	See specification

Process Development Joint Design

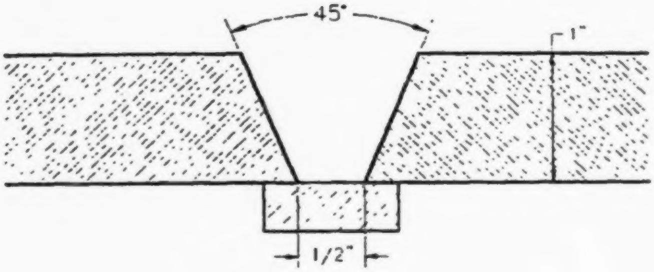

Test for TIME™ Quality Analysis

Test 1 Reduced gas flow rate to develop excess porosity in the weld metal
Test 2 Primer coated plate (See certificate)
Test 3 No preheat (low wire feed speed) (360"/min)
Test 4 No preheat (high wire feed speed) (600"min)
Test 5 Electrode selection - See electrode data
Test 6 Rust coated plate

Scope of Testing

- 6 All Weld Metal Tests to National Steel Car's admissible range and conforming to ASME Boiler and pressure Vessel Code. Section II Part C S.F.A. 5 - 18 1998 Edition 1999 ADDENDA identical to AWS A5.18 in accordance with ANSI/AWS D15-1-93 European Onorm En 288-7.
- 6 Radiograph tests to ASME ANSI/AWS D15-1-98
- 3 Sets Charpy V Notch Impact Tests to ASME Boiler and Pressure Vessel Code Section II. Part C Sta. 18 1998 Edition 1999 ADDENDA identical to AWS A5.18 European Onorm En 288-7.
- 4 Sets Hardness Traverse Tests.

Date of Welding: December 1999 and January 2000

Qualification of National Steel Car's Guaranteed Weld Process

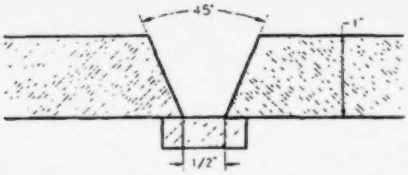

	Induced Porosity	Pnmer	No Preheat	No Preheat	Electrode Selection	Rust
Wire Feed Speed (inch/min)	607	380	330	607	600	380
Current (Amps)	375-430	290-300	290-300	380-420	330-360	280-300
Voltage (volts)	34.9	29.4	29 4	34.9	34.0	29.4
Welding speed (inch/min)	33-50	12-38	12-18	20-26	17-27	15-34
Energy input (KJ/inch)	16-24	13-36	33-49	31-46	27-40	15-40
Stick out	1/4"	1 1/4"	1 1/4"	1 1/4"	1 1/4"	1 1/2"
Flow rate (cu"/hr)	20-30	40-45	40-45	40-45	40-45	40-45
Direction of welding	Neutral	Neutral	Neutral	Neutral	Neutral	Neutral
Operator (S.J. Khamvong)	SJK	SJK	SJK	SJK	SJK	SJK
NSC Permissible range						
Elongation in 2"	26	29	26	26	26	28
Yield strength	77500	71000	77000	78500	76000	71500
Ultimate tensile strength	90000	85000	89500	90000	89500	86000
Parent metal tensile	85000-90000					
Parent metal yield	60000					
Hardness base	87 88 86	88 89 88	83 81 83	82 86 83	79 80 82	71 78 80
Hardness HAZ	96 95 93	96 97 96	94 94 86	95 97 93	98 96 93	92 97 95
Weld Metal	92 95 92	93 90 93	93 96 92	95 97 94	86 90 95	87 86 89
NSC Permissible range						
Charpy V notch impact (20 degree)			74, 86, 62	89, 107 106	82, 90, 94	104, 130, 109
Charpy V notch impact (40 degree)			80, 44	62,50	71, 67	79, 96
					-	-
Chemistry analysis	Carbon				0 78	0 73
	Manganese				1.26	1.24
	Silicon				0.69	0.72
	Phosphorus				0.01	0.01
	Sulphur				0.011	0.01
Wire speed	380-600 inches/min					
Strength	85000-90000 PSI					
Toughness	74-114ft @ 20°F 61-82ft @ 40° F					
Hardness	82-93 Rockwell					
Weld matrix behaviour	Meets National Steel Car's guaranteed quality					

	Porosity	Primer	No Preheat	No Preheat	Ideal Wire	Rust
	Test 1	**Test 2**	**Test 3**	**Test 4**	**Test 5**	**Test 6**
Base	87 88 86	88 89 96	83 81 83	82 86 83	79 80 82	71 78 80
HAZ	96 95 93	96 97 96	94 94 86	95 97 93	98 96 93	92 97 95
Weld	92 95 92	93 90 93	93 96 92	95 97 94	86 90 95	87 86 89

Allowable 35 HRC European HV 10 345

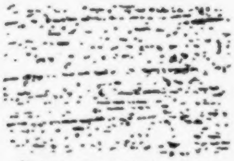
[illegible] x100

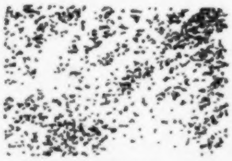
[illegible] x100

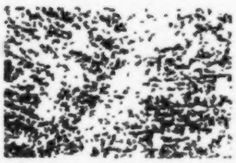
[illegible] Base Metal [illegible] x100

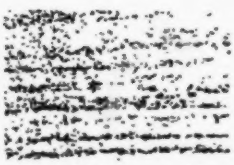
[illegible]

Process Procedure Qualification

Radiograph Test

Discontinuity search for porosity, slag inclusion, lack of fusion, lack of penetration and cracks to acceptable levels or non acceptable levels.

Porosity	Position		Evaluation
7	Horizontal	Acceptable	Fulfilled
8	Overhead	Acceptable	Fulfilled
9	Vertical	Acceptable	Fulfilled
10	Gravity	Acceptable	Fulfilled
11	20º Bevel incomplete gouge	Non Acceptable (Lack of Fusion)	Fulfilled
15	20º Bevel complete gouge	Acceptable	Fulfilled
16	Fillet Weld	Acceptable	Fulfilled

Qualification of Procedures

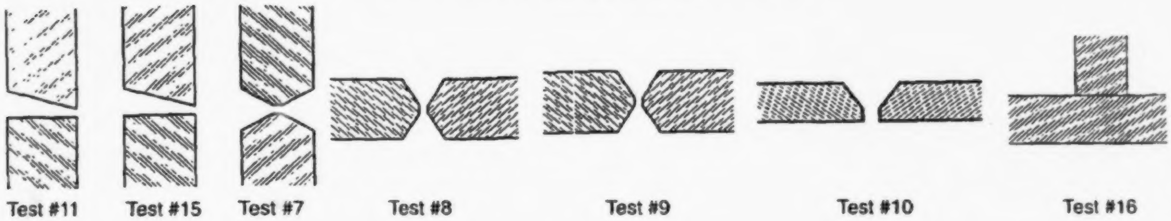

	Test #11	Test #15	Test #7	Test #8	Test #9	Test #10	Test #16
Wire Feed Speed (inch/min)	380	380	330	200-360	280-440	213-365	400-780
Current (Amps)	260-330	290-330	290-315	125-260	115-300	175-260	300-420
Voltage (volts)	29.3	29.3	29.3	17.5-27.5	17.5-30	21.1-29	30-34
Welding speed (inch/min)	8.25	7-22	13-22	14-40	24-33	8-20	10-46
Energy input (KJ/inch)	26-58	24-56	29-40	12-14	13-23	21-28	14-54
Stick out	1 1/4"	1 1/4"	3/4"	3/4"	3/4"	1/2"	1"
Direction of welding	Neutral	Neutral	Neutral	35 degree leading	Neutral	5 degree leading	30 degree leading
Flow rate (cu"/hr)	20-30	40-48	40-45	40-45	40-45	40-45	40-45
Operator (S.J. Khamvong)	SJK	SJK	SJK	SJK	SJK	SJK	SJK
X-ray	L.O.F	V	V	V	V	V	V
Tranverse weld tensile							
Yield strength	62540	65988	66991	50195	48930	72592	
Ultimate tensile	85809	84739	85799	77967	78669	101266	
Yield strength	62459	67159	65634	47124	48454	72866	
Ultimate tensile	85707	85239	85493	76831	77754	101935	
Yield strength	60773	66914	67376				
Ultimate tensile	85329	85495	85882				
Yield strength	62684		67287				
Ultimate tensile	85011		85364				
Side Bends							

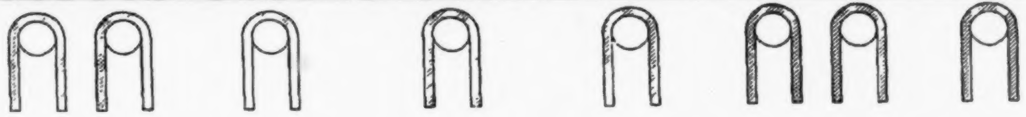

Note: According to ANSI/AWS D15-1-93 the bend tests requires a pin diameter of 2" for this material. The 1 1/2" diameter pin used in the test produces a more severe bend condition and the specimens pass both requirements

National Steel Car

Guaranteed™ Welding Process

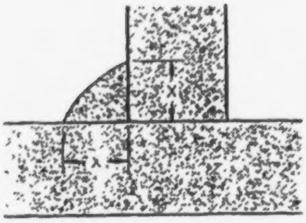

Fillet Weld

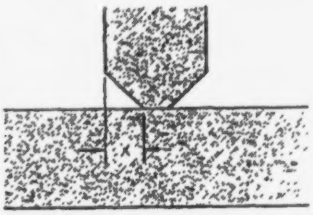

Partial Penetration Weld

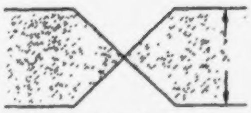

Full Penetration Weld

- Joint Geometry Definition
- Electrode Type (AWS ER 480 S6) Praxair
- Weld Position - Flat, Horizontal, Vertical Overhead - Fillet or Bevel
- Pass Number - all
- Electrode Diameter - .045 inches
- Current (Amps) 115-450
- Arc Voltage (Volts) 17.5-34
- Wire Feed Speed (i.p.m.) 200-600
- Weld size X inches mimimum/maximum 3/16"- 2.3/8" is the maximum size for any single pass fillet
- Pass Type - Stringer beads
- Shielding Gas Time - Argon, Oxygen, Helium, Carbon Dioxide
- Cup Size 3/4" 40-45 cu"/hour flow
- Power source constant voltage - rectifier

Travel Angle - Use a push technique

Push Technique

The torch travel angle of 5 degrees to 35 degrees (push angle) "leading" and an electrode stick out of 7/8" to 1 1/8" shall be used.

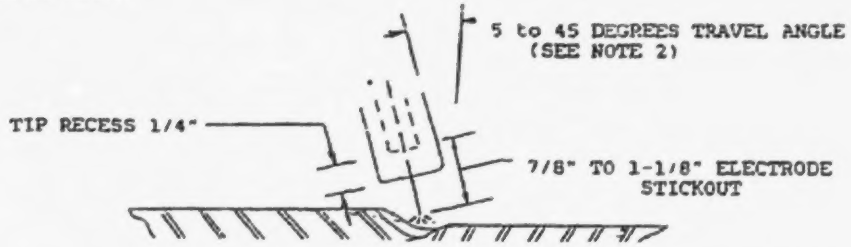

Note: Tip recess can be changed from 1/8" to 1/4" to provide proper stick out dimensions for welding root passes in deep groove joints.

Note: Use a travel angle of 5 degrees - 20 degrees for all flat position welds.
For welds in the horizontal position the travel angle can be increased to 35 degrees.

Note: A TIME™ Gas Diffuser with correct port holes must be used.

GUARANTEED PROCESS COMPARISON

Tools:

Plate – Electrodes – Weld Operators

Welding wire supplied by National Steel Car (Peter Szilak) from current stock for Dynamic Tear Tests.

1 carton FABCOR 80XLS 1/16 inch diameter
1 carton FABCOR RXR XLS 1/16 inch diameter
1 carton FABCOR XL71 1/16 inch diameter

Welding wire supplied by Praxair NS115CF 0.045 inch diameter

Shielding gas - 82%Ar 18% CO_2 for RXR XLS supplied by Praxair
Shielding - CO_2 for 80XLS & XL71 supplied by Praxair
Shielding gas TIME - 26.5% He 8% CO_2 0.5% O2 65.5%Ar by Praxair.

Plate CSA G40.21 92-40WT CAT3 supplied by National Steel Car
Plate CSA G40.21 92-40WT CAT3 beveled and prepared by National Steel Car

Welding operators

Welding of 80XLS – RXR XLS – XL71 – NS115 CF with CO_2 82-18- TIME by John Khamvong of National Steel Car

Welding of NS115 & TIME by Dennis Derry (Weld Process) and Dave Rogalsky (Skill Weld)

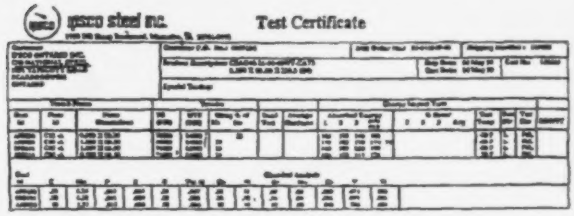

ipsco steel inc.

Test Certificate

Weld Procedure:

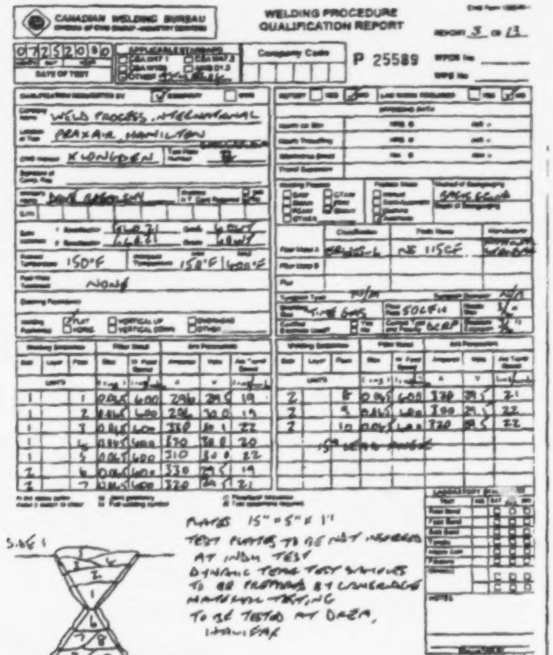

CANADIAN WELDING BUREAU

WELDING PROCEDURE QUALIFICATION REPORT

REPORT 3 OF 13

0 7 2 5 2 0 0 0

DATE OF TEST

Company Code

P 25589

Company Name WELD PROCESS, INTERNATIONAL
Location of Test PRAXAIR, HAMILTON
KLONGDEN
DAVE RAGALSKY
150°F
158°F | 400°F
NONE
NS 115CF
TIME GAS
50 CFH
DCRP

1		1	0.045	600	296	29.5	19
1		2	0.045	600	296	30.0	19
1		3	0.045	600	330	30.1	22
1		4	0.045	600	370	30.0	20
1		5	0.045	600	310	30.0	22
2		6	0.045	600	330	29.5	19
2		7	0.045	600	320	29.5	21

2		8	0.045	600	330	29.5	21
2		9	0.045	600	300	29.5	22
2		10	0.045	600	320	29.5	22

PLATES 15" × 5" × 1"
TEST PLATES TO BE NDT INSPECTED AT INDU TEST
DYNAMIC TEAR TEST SAMPLES TO BE PREPARED BY CAMBRIDGE MATERIAL TESTING
TO BE TESTED AT DREA, HALIFAX

SIDE 1
SIDE 2
ROOT OPENING 3/32"

Witness A.W.S.:

CANADIAN WELDING BUREAU
A Division of the CWB Group
7250 West Credit Avenue, Mississauga, Ontario L5N 5N1
(905) 542-1312, Fax: (905) 542-1318; WEB: www.cwbgroup.com

December 4, 2000

Mr. John Church
Weld Process International Ltd.
1206-2261 Lake Shore Blvd. W.
Etobicoke, Ontario
Canada M8V 3X1

Dear Mr. Church;

Re: Witnessing Welding of Plates for Dynamic Tear Testing

This is to confirm with you that we have witnessed welding of plates on July 25, 2000 and November 30, 2000.

Please find enclosed a copy of the witnessed records (13 pages) for your file.

Thank you for your cooperation.

Yours truly,
CANADIAN WELDING BUREAU

Alice Y. Lau, P.Eng.
Manager, Product Certification

N.D.T. Inspection:

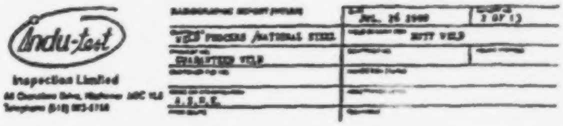

Indu-test
Inspection Limited

JUL. 26 2000
3 OF 13
WELD PROCESS / NATIONAL STEEL
BUTT WELD
GUARANTEED WELD
A.S.M.E.

Dynamic Tear

Designation: E 604 – 83 (Reapproved 1994)

AMERICAN SOCIETY FOR TESTING AND MATERIALS

Standard Test Method for Dynamic Tear Testing of Metallic Materials[1]

This standard is issued under the fixed designation E 604; the number immediately following the designation indicates the year of original adoption or, in the case of revision, the year of last revision. A number in parentheses indicates the year of last reapproval. A superscript epsilon (ε) indicates an editorial change since the last revision or reapproval.

This standard has been approved for use by agencies of the Department of Defense.

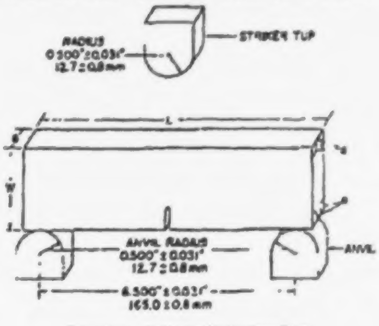

Dimensions and Tolerance for Specimen Blank

Dynamic Tear Test Results (Joules)

Plant Approved Procedures 400"-600"/W.F.S. 400"-780" Advertised

Temp. °C	Base Metal G.40.21-60WT	National Steel Car			T.I.M.E.			T.I.M.E. With Defects			Best M. Core	T.I.M.E. With Chemistry		
		80 x L A	R x R A	XL 71 A	420 A	400 A	600 A	400 NA	400 NA	780 NA	400 A	400 A	400 A	400 A
0° C	1000	M C 400	M C 480	F.C. 1000	1300	1600	1250	1160	800	650	950		1600	
-20° C	250	110	310	400	800	570	550	300	680	700	650	1650	1500	1400
-30° C	235	150	200	325	400	370	600	230	400	290	450	1200	1300	1300
-50° C				Not tested with defects				Defective welds Ductile plastic			Not tested with defects	1000	1300	1100
												New spectrum of fracture resistance		

Acceptable Radiography A
Not Acceptable (NA) - Porosity visible on surface
- 3/16 lack of fusion
- Lack of fusion & porosity (no heat control)

Note: No weld was treated for defect removal

#516420 ⑧

Molecular Magnets – Addressing Defence Signature Needs in 2010

by

Sandra M. Nevill and Carmen Lucas
Defence Research Establishment Atlantic

Abstract

Canadian ships must be protected from weapons that can damage or destroy the vessel. Ships are identified and targeted according to their signatures. One of these signatures, the radar cross section, may be reduced through the use of radar absorbing materials.

Ideal radar absorbing materials have equal permittivity and permeability. Unfortunately, although there are materials available having permittivity few materials having permeability are available. But two novel material types could be investigated for EM signature control. The first type, molecular magnets, is polymer-like materials being developed currently for their data storage capabilities. The second type is materials having negative permeability and/or negative permittivity. These materials are left-handed and have unique properties. An investigation of these materials will be undertaken in the search for EM signature control materials. Of further consideration are the potential advantages these novel radar absorbing materials might have over current technology.

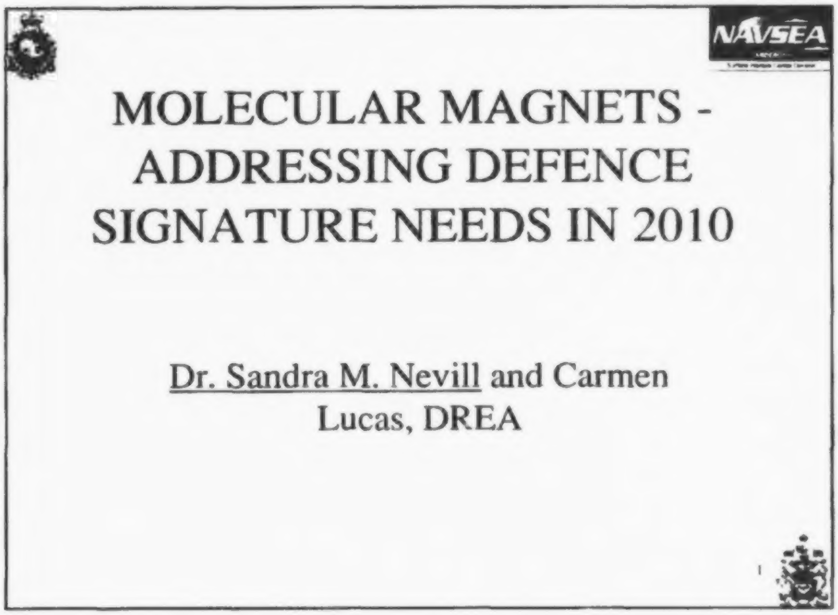

MOLECULAR MAGNETS - ADDRESSING DEFENCE SIGNATURE NEEDS IN 2010

Dr. Sandra M. Nevill and Carmen Lucas, DREA

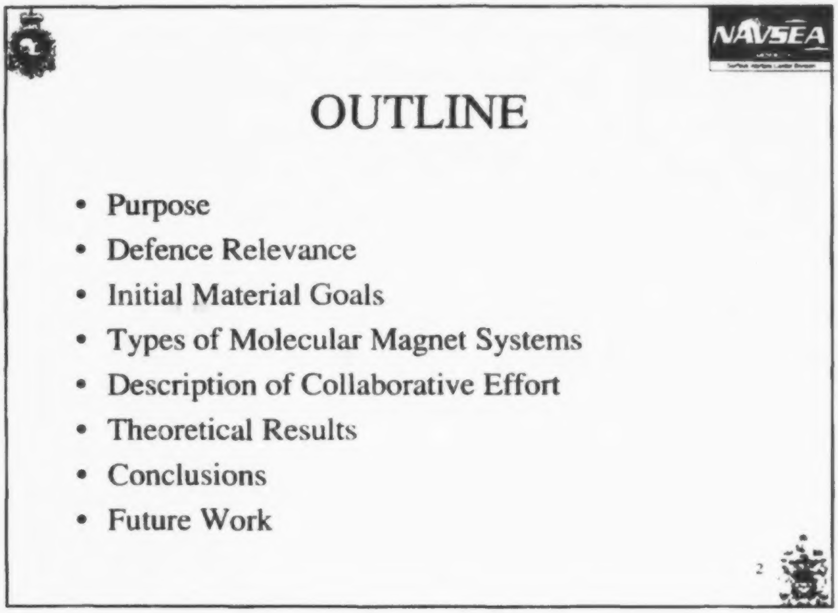

OUTLINE

- Purpose
- Defence Relevance
- Initial Material Goals
- Types of Molecular Magnet Systems
- Description of Collaborative Effort
- Theoretical Results
- Conclusions
- Future Work

PURPOSE

- To fabricate a stable polymer-like organic magnet with a T_c higher than room temperature.
- Direct research and development toward energy absorption (imaginary μ) in the gigahertz region.

DEFENCE RELEVANCE

- Useful radar absorbing materials would have adjustable permittivity and adjustable permeability.
- Current materials having significant permeability tend to have high permittivity as well.
- Need improved performance in terms of frequency range and attenuation.

LONG-TERM DEFENCE GOALS

- To develop an environmentally stable magnetic material with high permeability but low permittivity for EM signature control
- Will be developed through a collaboration amongst molecular magnetism experts for defence purposes

DESCRIPTION OF COLLABORATIVE EFFORT

- We are requesting funding from the Office of Naval Research (ONR) for this collaborative effort.
- This funding would be in addition to a currently funded TIF – a more generalized effort to develop materials for EM signature control through DL(P).
- Approximately 25 molecular magnetism experts will work together to develop a room temperature stable molecular magnet to be used for EM signature control.
- This effort is a unique concept of academics collaborating because they will be sharing ideas before they are published.

NAVSEA

BENEFITS TO GROUP ARRANGEMENT

- Molecular magnets for signature control should be developed by the experts in molecular magnetism in conjunction with the experts in signature control.
- Research into molecular magnetism is not a technology that needs to be developed in-house.
- Able to use current research (used for mass storage) as a stepping stone for defence purposes.

NAVSEA

INITIAL MATERIAL GOALS

- Magnetic moments equal to or greater than that of iron oxide (Fe_3O_4 6000 gauss).
- Permittivity less than that of current magnetic materials (5 + 0j).
- Tc greater than room temperature, preferably above 340K.
- Coercivity at that temperature.
- Air stability.

TYPES OF MOLECULAR MAGNET SYSTEMS

- Organic, organometallic, inorganic, liquid crystals and Langmuir-Blodgett films.
- Tc for purely organic systems less than 50K.
- Very few systems have Tc's greater than 150K.
- Few systems are available that are air stable at room temperature.

PERMITTIVITY AND PERMEABILITY GOALS

- Would expect complex permeabilities of 3 and loss tangents of 1-3
- Permittivities would not be expected to have any imaginary parts but to have real values of approximately 5

CAPABILITIES

- Hypothetically, what types of materials is it possible to develop? Can materials be fabricated that will reduce reflections by 50-60 dB?
- Are there other considerations for these materials, such as thickness, weight, and frequency range coverage?

REFLECTIVITY VERSUS PERMEABILITY

$D/\lambda = 0.1$
F=10 GHz
$\varepsilon = 5 - j0$

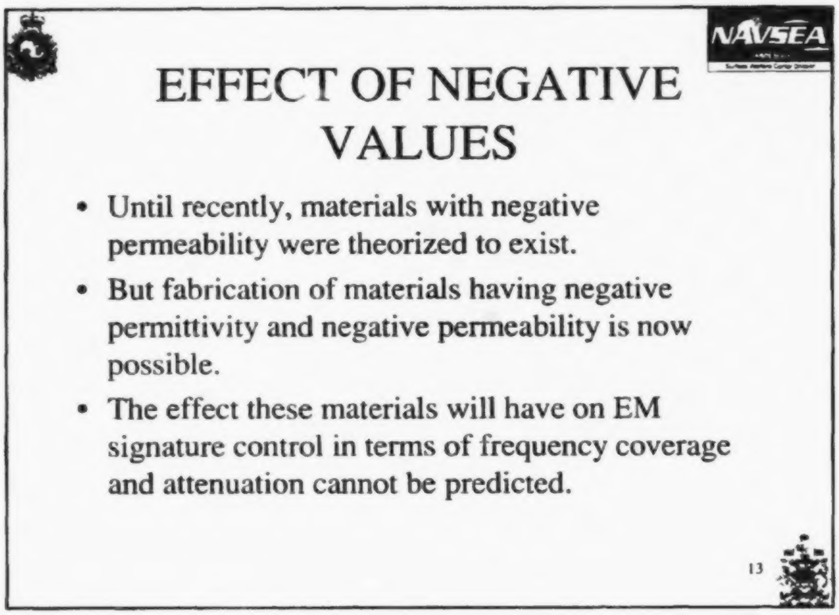

EFFECT OF NEGATIVE VALUES

- Until recently, materials with negative permeability were theorized to exist.
- But fabrication of materials having negative permittivity and negative permeability is now possible.
- The effect these materials will have on EM signature control in terms of frequency coverage and attenuation cannot be predicted.

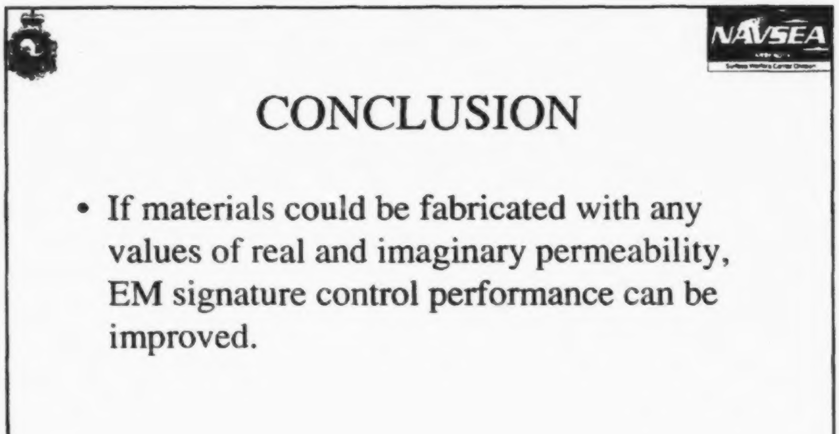

CONCLUSION

- If materials could be fabricated with any values of real and imaginary permeability, EM signature control performance can be improved.

FUTURE WORK

- Continue theoretical calculations but develop permittivity and permeability equations that are frequency dependent allowing a more realistic view.
- As a consequence, be able to follow values of permittivity and permeability over 1-20 GHz.

ACKNOWLEDGEMENTS

- Thank you to Carmen Lucas for starting to make these calculations and being forced to continue!
- Thank you to Canada, particularly Dr. Harold Merklinger and Dr. Warren Nethercote for giving me this opportunity to work with the US experts.
- Thank you to Dr. Vincent Castelli and the US DOD for allowing an international collaboration.
- Thank you to Professor Robin Hicks for introducing me to molecular magnets.

516421 (9)

Essential testing in Submarine Pressure Hull Weld Acceptance: Victoria Class Subs

by
J.R. Matthews and John F. Porter
DREA Canada

Abstract

There is a growing interest in welding and weld approval issues for the Victoria Class submarines. It was accordingly requested by NDHQ DGMEPM that we provide a presentation at this conference on this subject.

There are two main issues. The first is testing for weld approval. DREA recommends that Dynamic Tear transition testing and Explosion bulge testing be the primary special tests for approvals. The first addresses all impact issues and the latter addresses all explosive strain issues. The Australians and the Americans use these two tests but the British rely more on CTOD and crack starter bulge tests.

The second issue is choice of weld process. For 18 years DREA has been able to meet the strength, impact and explosive strain requirements for submarine welds [1]; first with conventional T.I.M.E. welding (1982), then with analog pulsed GMAW using TIME gas or C5 or C10 gas (1988) and more recently pulsed digital T.I.M.E. GMAW (1998) as well. [2]

The underlying technical issue is strength. The Australians, the British and the Americans lowered the strength of the weld to improve the impact performance. The Australians went to E10018 and managed to find consumables that passed the tests (DT and explosion bulge). The British as it turned out lowered their strength from E11018 which they used on the first two Upholders to E9016 for the last two. That's a 20,000 psi strength reduction to promote improved toughness and to pass the impact tests. The Americans have dropped to E10018 more recently. There are two concerns; first, will the reduced strength result in undermatching and strain concentration in the welds and failed tensile and failed explosion bulge, and second, is it really necessary to drop the strength to find a weldment with acceptable toughness.

The test that shows if dropping the strength is OK is the explosion bulge. But the British stopped using the test. In Canada, John Porter has efficiently conceived an underwater test and carried out this test for 15 years. TIME welding is a real alternative to dropping the strength of the weld.

FMF Cape Scott has been conducting a test program this past winter to evaluate these issues and to compare the performance of the UK recommended E9016 and FCAW consumables to the TIME process.

[1] J.R. Matthews, C.V. Hyatt, and J.F. Porter, "Future Treatment of Weld Acceptance: The Significance of Incomplete Fusion Discontinuities in Low Structural Transition Temperature GMAW Weldments, Materials Evaluation, April 2001

[2] D.S. Begg and J.R. Matthews, "Toughness Envelope Definition of Pulsed Gas Metal Arc Welds in HY80 Steel", 9th CF/DRDC Meeting on Naval Applications Of Materials Technology, June 2001

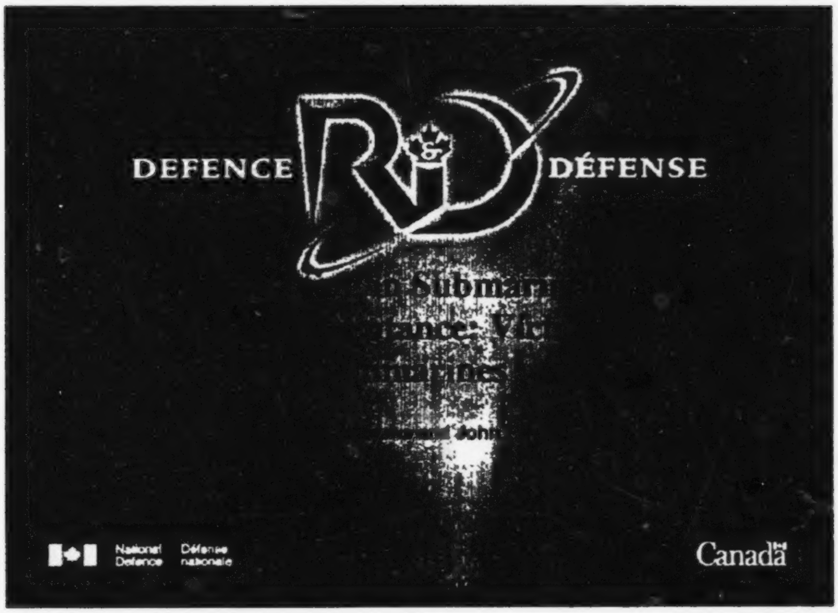

DEFENCE R&D DÉFENSE

n Submari
rance: Vic
marines

John

National Defence Défense nationale

Canada

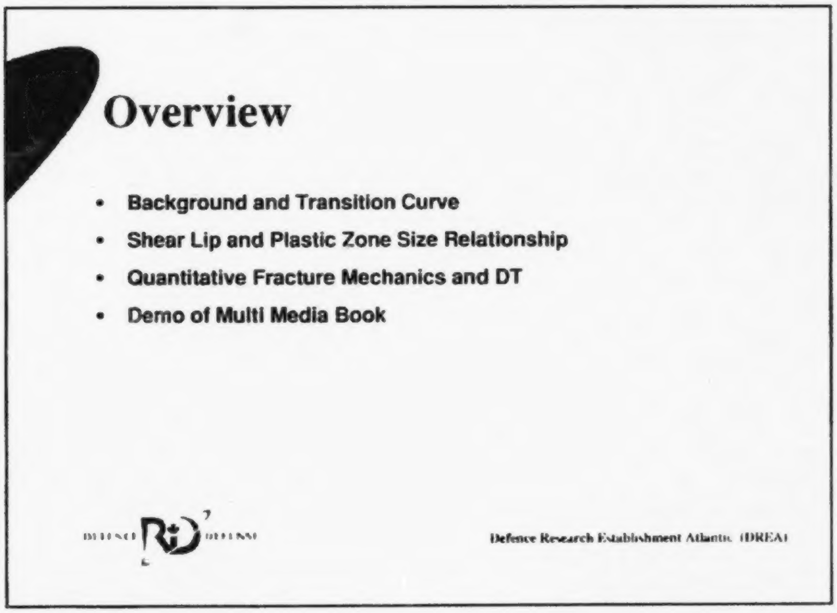

Overview

- Background and Transition Curve
- Shear Lip and Plastic Zone Size Relationship
- Quantitative Fracture Mechanics and DT
- Demo of Multi Media Book

DEFENCE R&D DÉFENSE

Defence Research Establishment Atlantic (DREA)

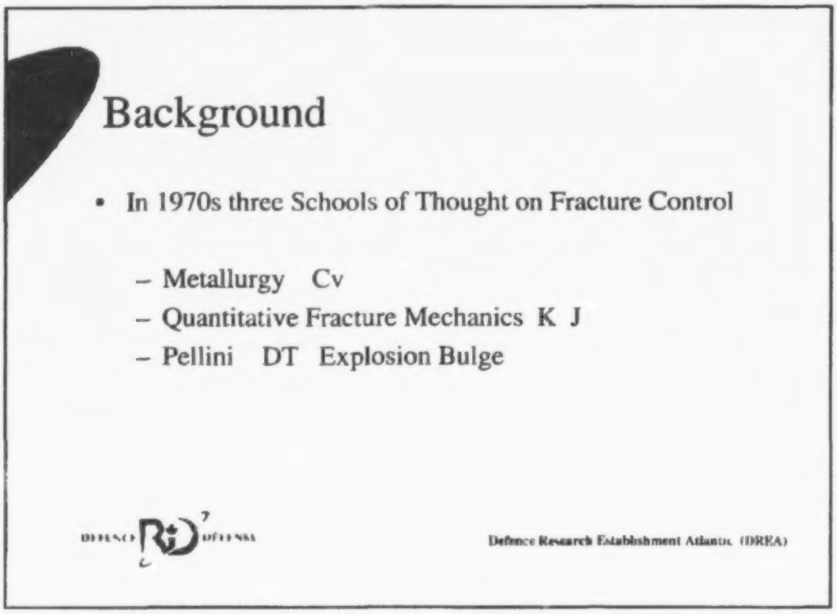

Background

- In 1970s three Schools of Thought on Fracture Control
  - Metallurgy Cv
  - Quantitative Fracture Mechanics K J
  - Pellini DT Explosion Bulge

Defence Research Establishment Atlantic (DREA)

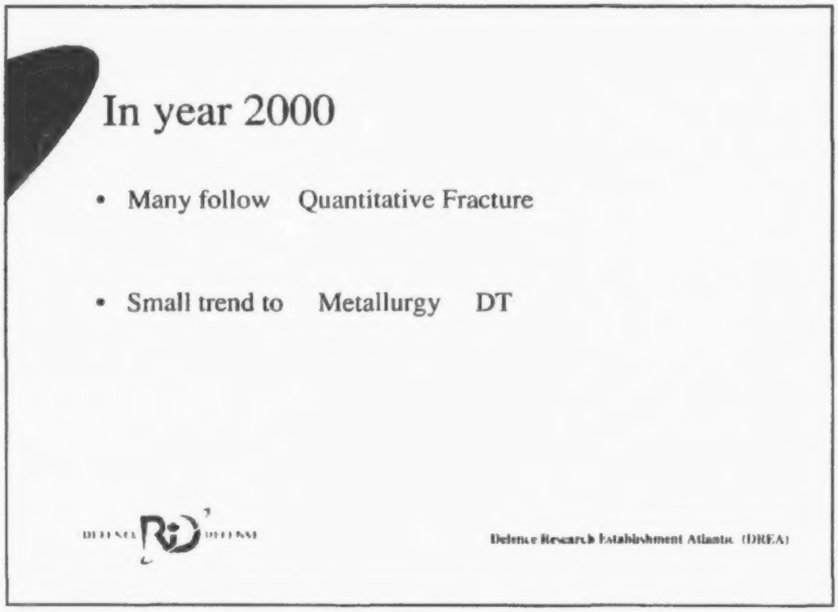

In year 2000

- Many follow Quantitative Fracture
- Small trend to Metallurgy DT

Defence Research Establishment Atlantic (DREA)

Universal Fracture Property

- Plastic Zone Size ryc
- Energy itself DTE
- Stretch zone width SZW
- Shear Lip s

Defence Research Establishment Atlantic (DREA)

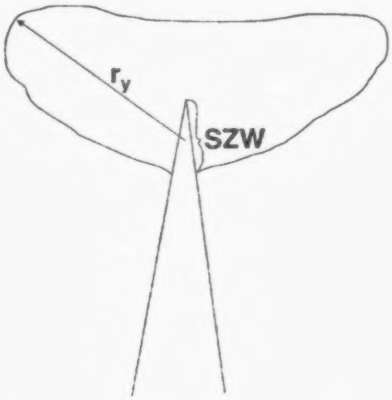

Defence Research Establishment Atlantic (DREA)

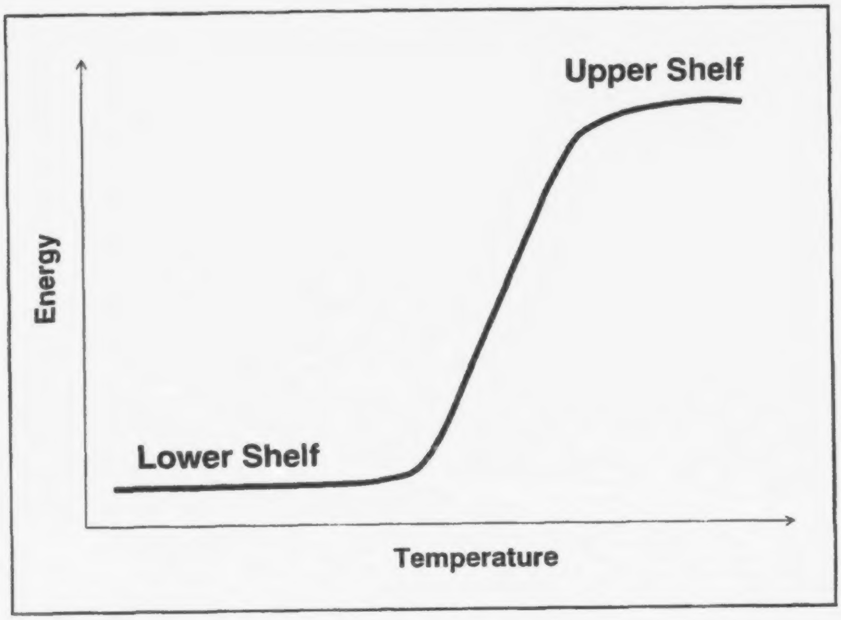
Upper Shelf
Energy
Lower Shelf
Temperature

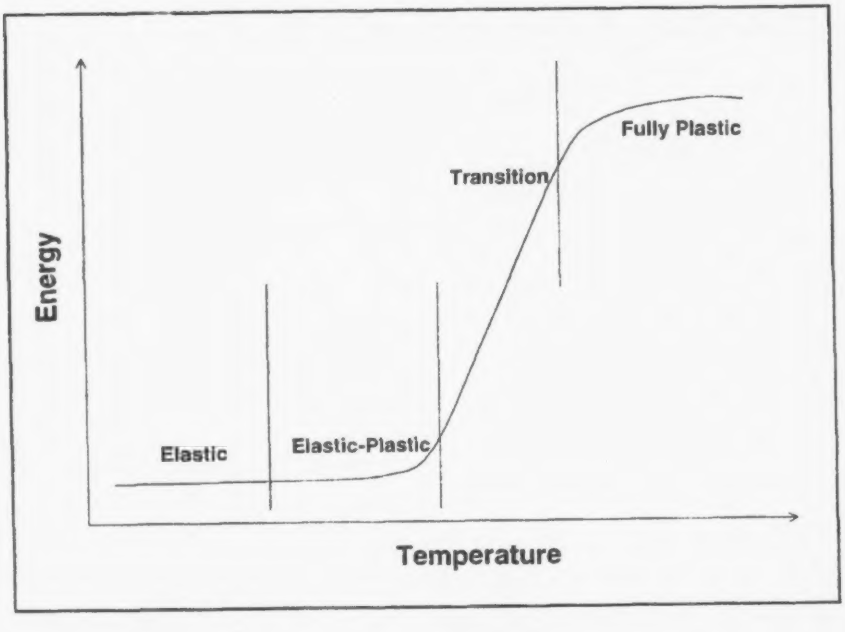
Fully Plastic
Transition
Energy
Elastic
Elastic-Plastic
Temperature

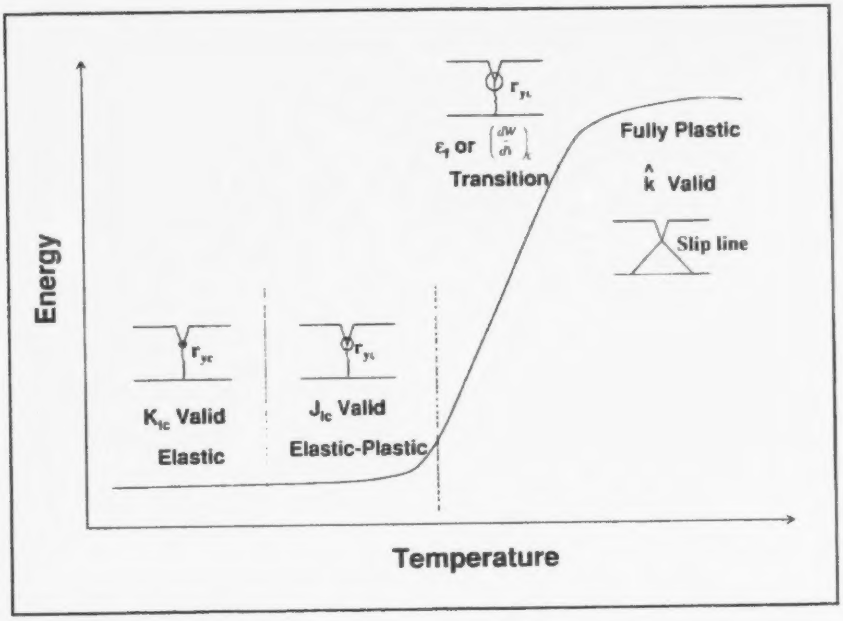
r_{yc}
ε_f or $\left(\frac{dW}{dA}\right)_c$
Transition
Fully Plastic
$\hat{k}$ Valid
Slip line
Energy
r_{yc}
r_{yc}
K_{Ic} Valid
Elastic
J_{Ic} Valid
Elastic-Plastic
Temperature

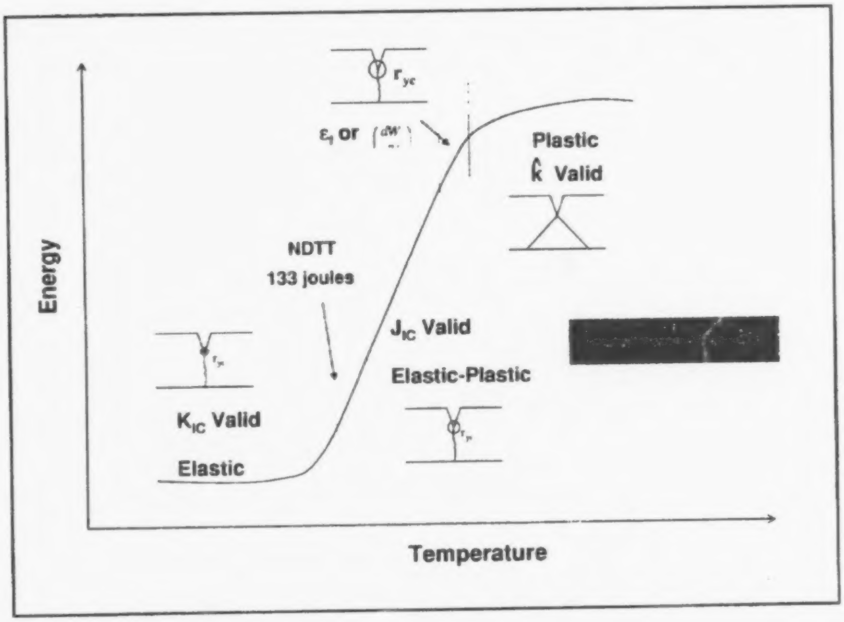
r_{yc}
ε_f or $\left(\frac{dW}{dA}\right)$
Plastic
$\hat{k}$ Valid
Energy
NDTT
133 joules
J_{IC} Valid
Elastic-Plastic
r_{yc}
K_{IC} Valid
Elastic
r_{yc}
Temperature

[redacted]

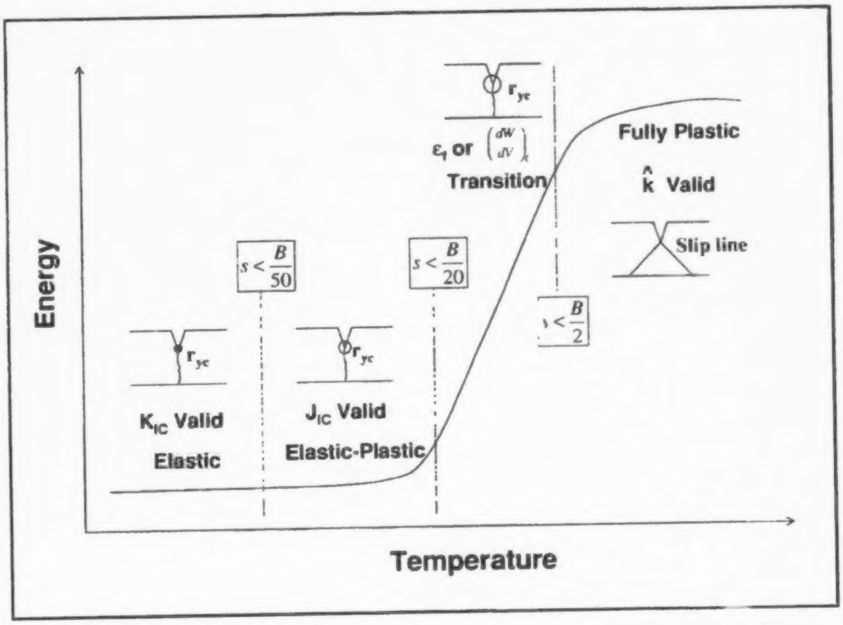

Shear Lip Size

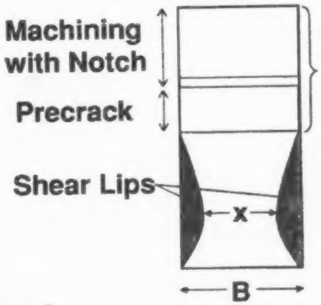
Machining with Notch
Precrack
Shear Lips
x
B

0.45 < a/W < 0.55

$$s = \frac{B - x}{2}$$

Defence Research Establishment Atlantic (DREA)

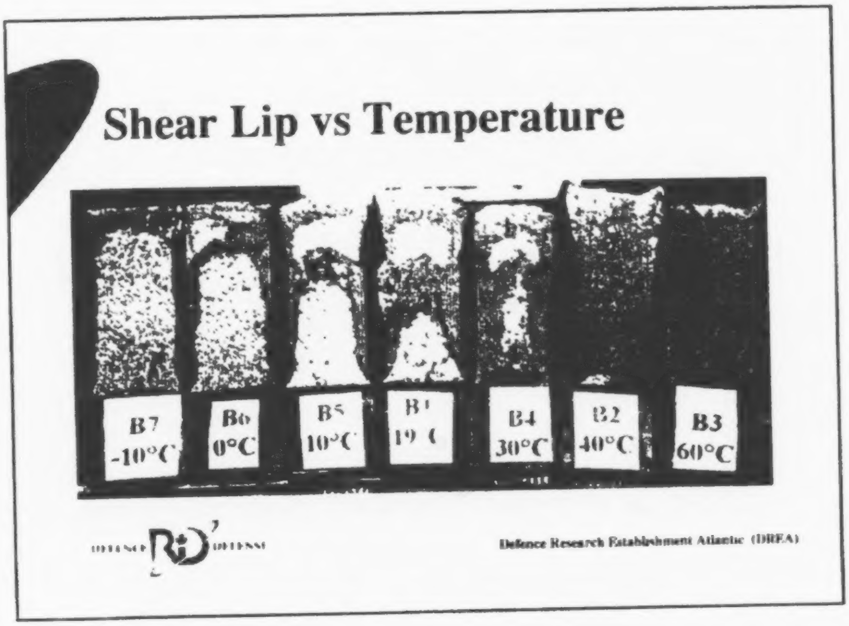

Shear Lip vs Temperature

B7
-10°C
B6
0°C
B5
10°C
B1
19°C
B4
30°C
B2
40°C
B3
60°C

Defence Research Establishment Atlantic (DREA)

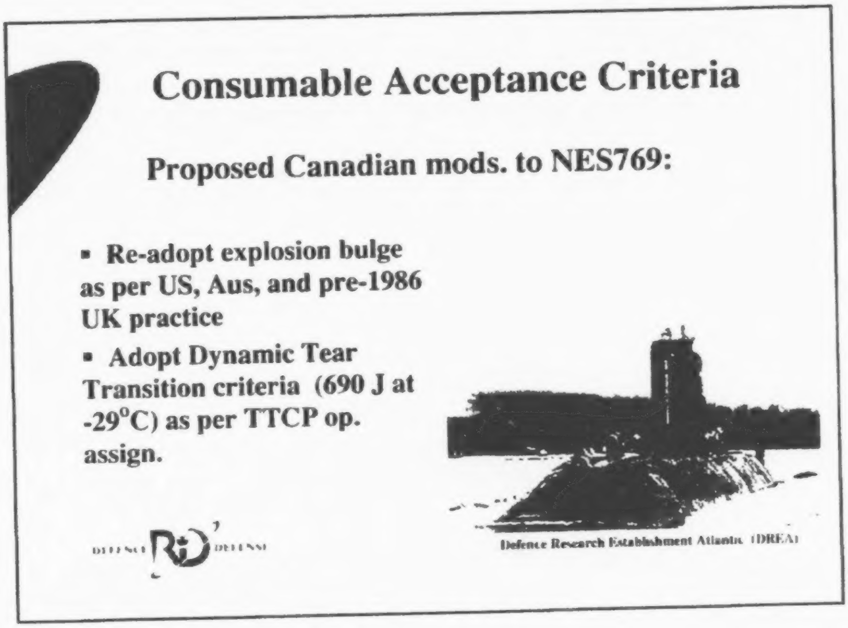

Consumable Acceptance Criteria

Proposed Canadian mods. to NES769:

- **Re-adopt explosion bulge as per US, Aus, and pre-1986 UK practice**
- **Adopt Dynamic Tear Transition criteria (690 J at -29°C) as per TTCP op. assign.**

Defence Research Establishment Atlantic (DREA)

Why Conduct Explosion Bulge Trials ?

Only trial that adequately evaluates the full weldment system's ability to withstand high deformation plasticity without failure.

Explosion Bulge - Features

Full Weldment System:

- Full scale samples,
- Indiscriminately loads all elements of weldment equally,
- Interaction of weldment elements in a manner consistent with platform behaviour (weld metal mismatch effects)

High deformation plasticity:

- As per grounding, collision, explosive attack
- Up to 16% thinning required

Failure:

- Very non-ambiguous

Defence Research Establishment Atlantic (DREA)

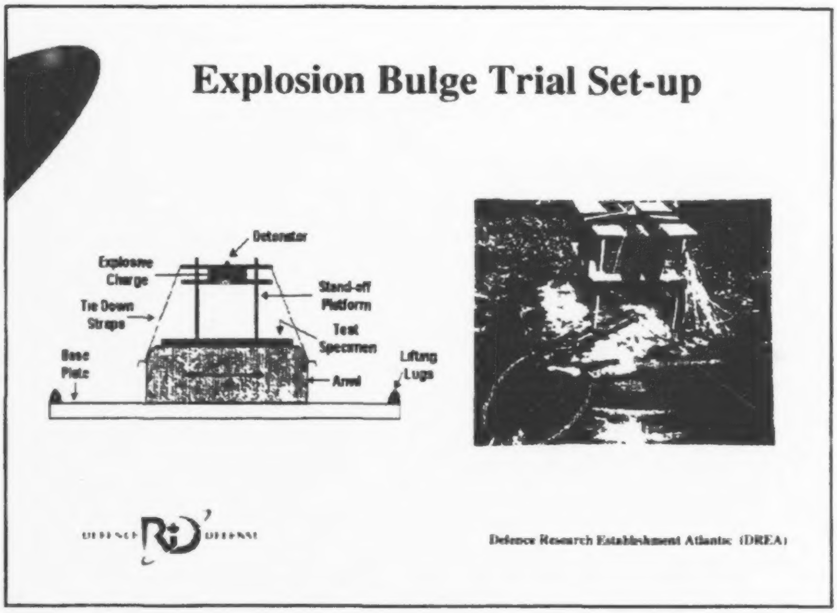

Explosion Bulge Trial Set-up

Detonator
Explosive Charge
Tie Down Straps
Stand-off Platform
Test Specimen
Base Plate
Anvil
Lifting Lugs

Defence Research Establishment Atlantic (DREA)

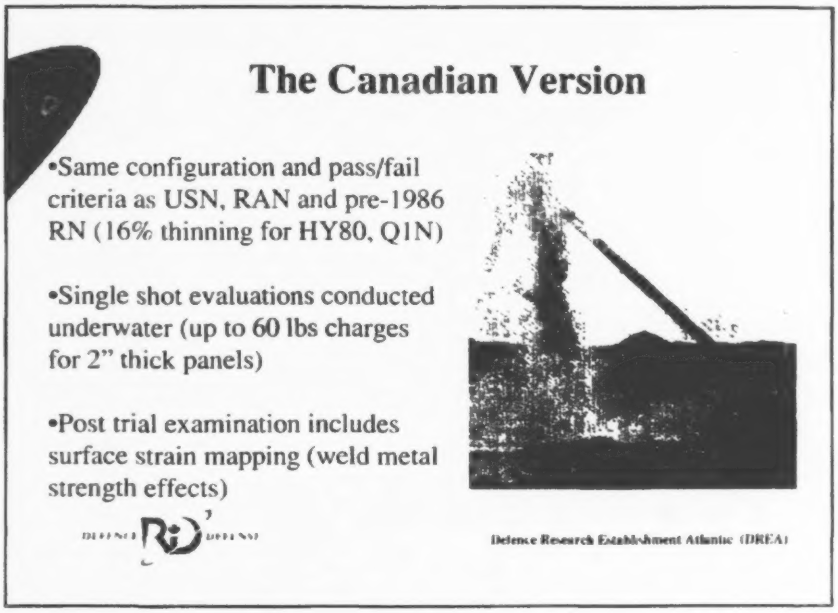

The Canadian Version

- •Same configuration and pass/fail criteria as USN, RAN and pre-1986 RN (16% thinning for HY80, Q1N)
- •Single shot evaluations conducted underwater (up to 60 lbs charges for 2" thick panels)
- •Post trial examination includes surface strain mapping (weld metal strength effects)

Defence Research Establishment Atlantic (DREA)

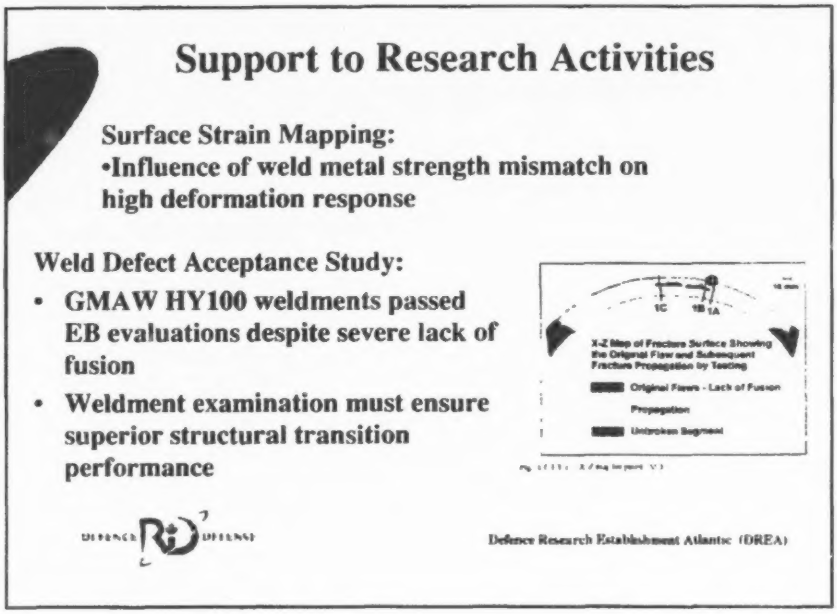

1C
1B
1A
10 mm
X-Z Map of Fracture Surface Showing the Original Flaw and Subsequent Fracture Propagation by Testing
Original Flaws - Lack of Fusion
Propagation
Unbroken Segment

Support to Research Activities

Surface Strain Mapping:

•Influence of weld metal strength mismatch on high deformation response

Weld Defect Acceptance Study:

- **GMAW HY100 weldments passed EB evaluations despite severe lack of fusion**
- **Weldment examination must ensure superior structural transition performance**

Defence Research Establishment Atlantic (DREA)

Conclusion

> **“At the head of this family of tests stands the explosion bulge test which has a high degree of realism in the submarine context” – J.C. Ritter**

#516422 (10)

Advanced Materials Solutions to the Aging Aircraft Problem

by

K.I. McRae

Air Vehicles Research Section
Defence and Civil Institute of Environmental Medicine
Ottawa, Ontario, Canada

Abstract

The Air Vehicles Research Section of DCIEM is responsible for the delivery of all R&D that directly concerns the CF aircraft in the areas of aircraft structures and materials, aeropropulsion, aerodynamics and flight mechanics. The requirement to retain and maintain CF fleets for extended periods of time beyond their normal lives has put most of these aircraft in the "aging" category. This has required the development of novel approaches and concepts in order to reduce the costs involved in this long-term maintenance effort. This paper will describe several of these recent approaches that are currently under development from the advanced materials perspective. These will include:

- a methodology for the in-situ application of a novel heat treatment for 7075-T6 aluminum alloys and the application of a thermal spray coating in order to reduce the incidence of stress corrosion cracking of major aircraft structural components;
- the development of advanced coatings for the replacement of current coatings that involve toxic application processes, such as chromium and cadmium;
- the development of novel techniques for nondestructive evaluation, particularly for the detection of hidden corrosion;
- the application of "smart structures" technology for the development of an instrumented composite patch for metallic aircraft structure; and
- development of new metrics for the quantification of corrosion as well as methods for assessing the interaction of corrosion and fatigue damage.

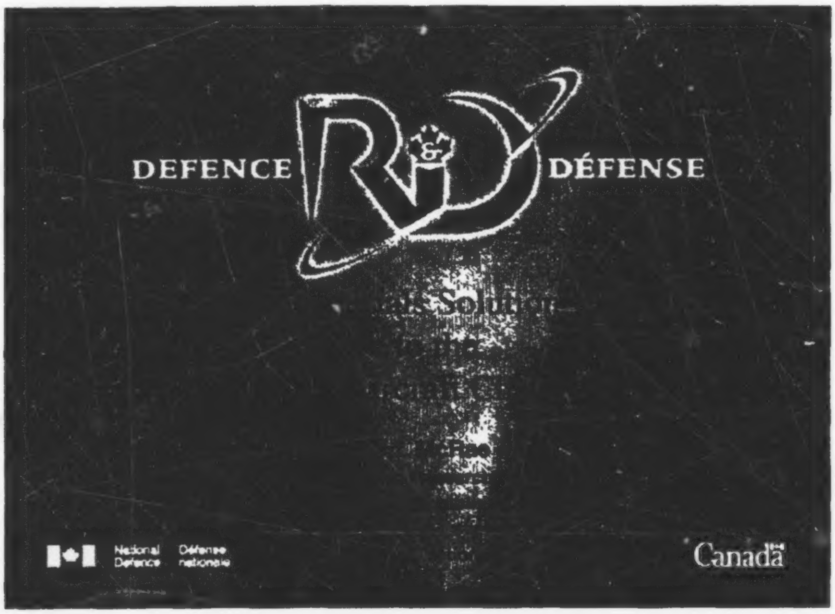

DEFENCE R&D DÉFENSE

[illegible]

National Defence Défense nationale

Canada

Presentation Outline

- The Aging Aircraft Challenge
- R&D Program Delivery
- Airframe structural repair technologies
- Engine life assessment and life extension
- Advanced materials research
- Novel NDT techniques
- Advanced structural integrity concepts
- Conclusion

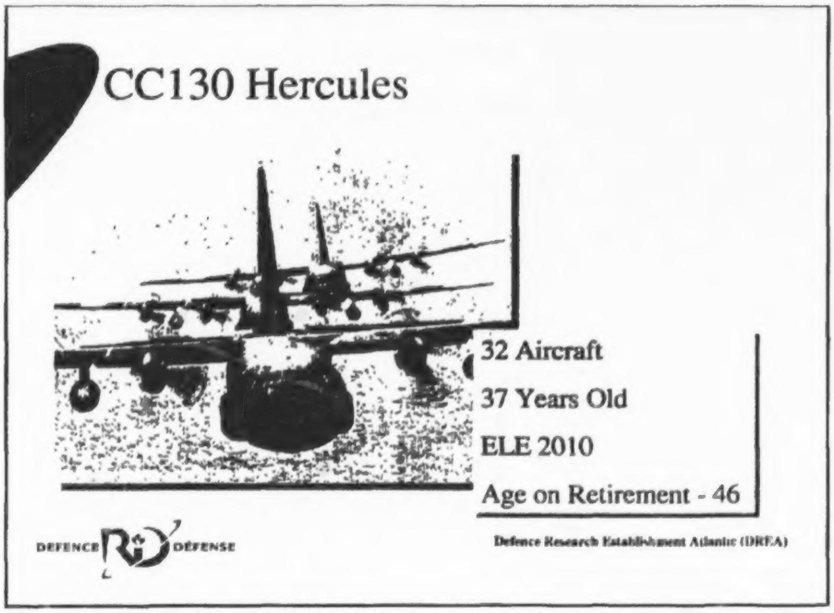

CC130 Hercules

32 Aircraft

37 Years Old

ELE 2010

Age on Retirement - 46

Defence Research Establishment Atlantic (DREA)

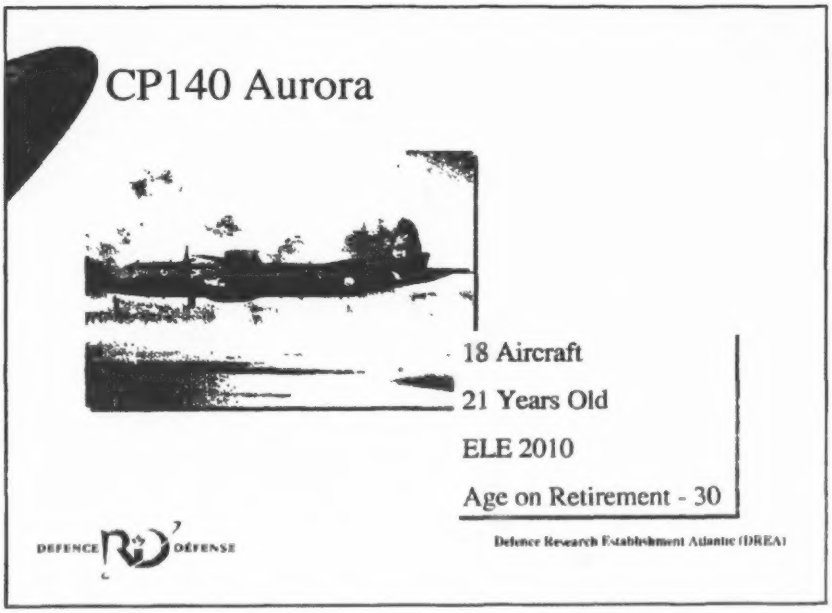

CP140 Aurora

18 Aircraft

21 Years Old

ELE 2010

Age on Retirement - 30

Defence Research Establishment Atlantic (DREA)

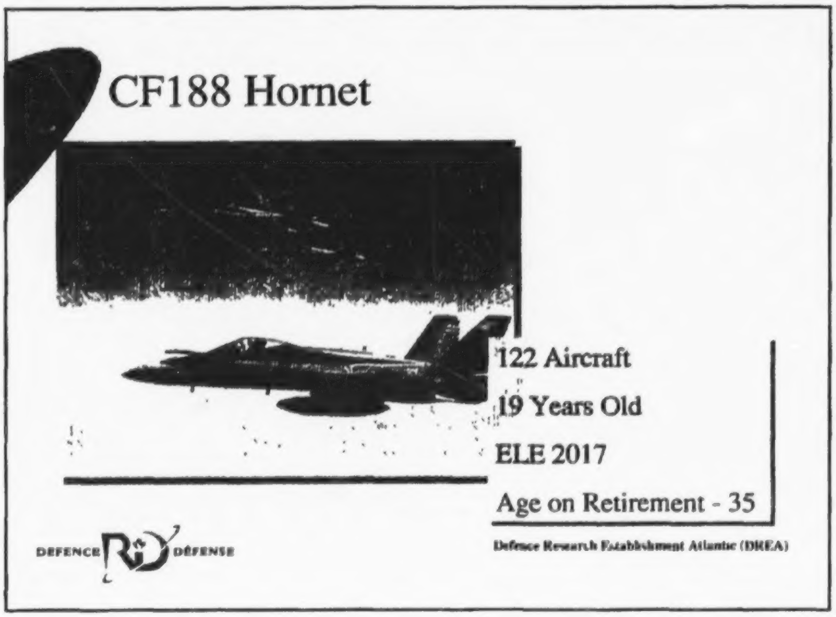

CF188 Hornet

- 122 Aircraft
- 19 Years Old
- ELE 2017
- Age on Retirement - 35

DEFENCE R&D DÉFENSE

Defence Research Establishment Atlantic (DREA)

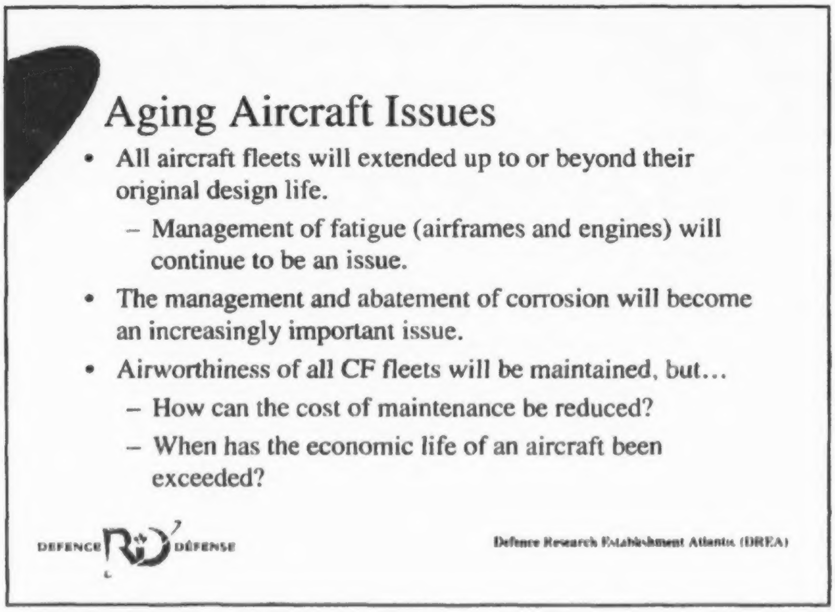

Aging Aircraft Issues

- All aircraft fleets will extended up to or beyond their original design life.
  - Management of fatigue (airframes and engines) will continue to be an issue.
- The management and abatement of corrosion will become an increasingly important issue.
- Airworthiness of all CF fleets will be maintained, but…
  - How can the cost of maintenance be reduced?
  - When has the economic life of an aircraft been exceeded?

DEFENCE R&D DÉFENSE

Defence Research Establishment Atlantic (DREA)

Program Delivery

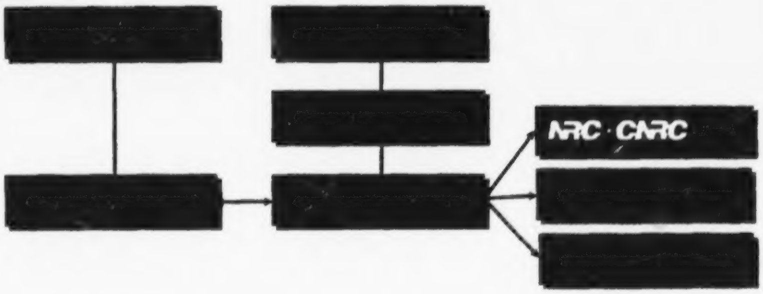

Air Vehicles Technologies

DRDC has structured four projects within the Air Vehicles Technologies Thrust to address these problems:

- Aeropropulsion/Gas Turbine Technologies
- Aircraft Structures and Materials
- Aerodynamics and Flight Mechanics
- D6214 Gas Turbine Repairs/reworks (complete)

Airframe Structural Repair

- Robotic control of shot peening to increase fatigue life
    - improved process control and decreased variability
- Composite patch for fatigue life enhancement
    - CF188 Bulkhead (Y470 Location X-19)
    - Improved patch adhesion and durability
        - sensing of load bearing capacity
- Novel heat treatments
    - in-situ RRA for CC130 sloping longeron

Defence Research Establishment Atlantic (DREA)

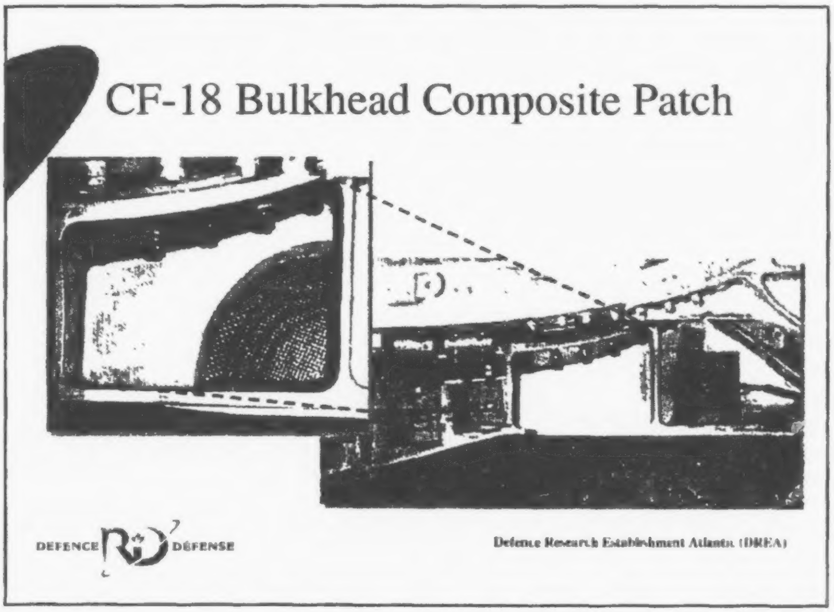

CF-18 Bulkhead Composite Patch

Defence Research Establishment Atlantic (DREA)

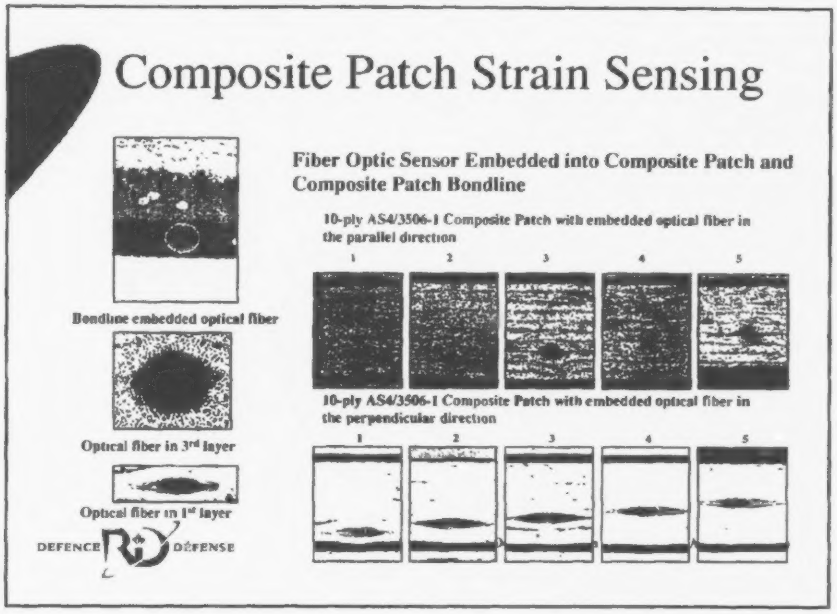

Composite Patch Strain Sensing

Fiber Optic Sensor Embedded into Composite Patch and Composite Patch Bondline

10-ply AS4/3506-1 Composite Patch with embedded optical fiber in the parallel direction

1
2
3
4
5

10-ply AS4/3506-1 Composite Patch with embedded optical fiber in the perpendicular direction

1
2
3
4
5

Bondline embedded optical fiber

Optical fiber in 3rd layer

Optical fiber in 1st layer

DEFENCE DÉFENSE

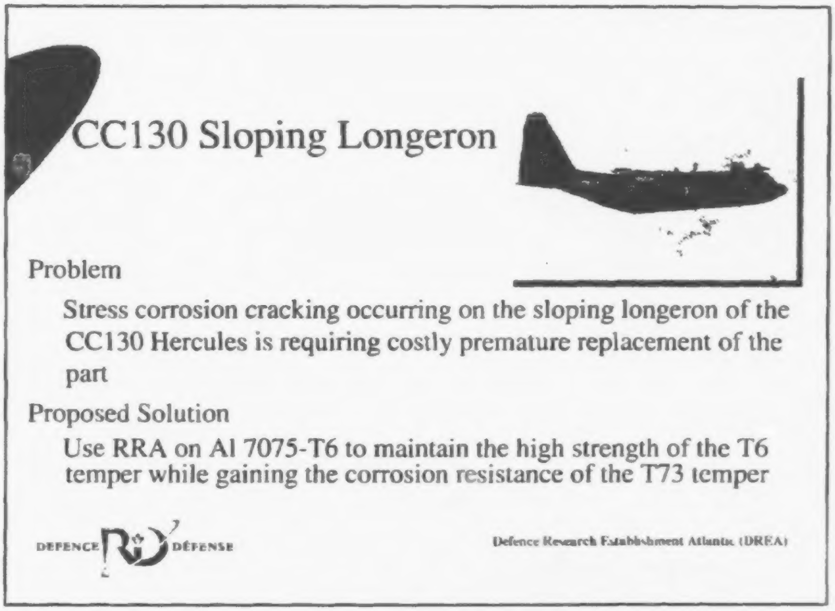

CC130 Sloping Longeron

Problem

Stress corrosion cracking occurring on the sloping longeron of the CC130 Hercules is requiring costly premature replacement of the part

Proposed Solution

Use RRA on Al 7075-T6 to maintain the high strength of the T6 temper while gaining the corrosion resistance of the T73 temper

DEFENCE DÉFENSE

Defence Research Establishment Atlantic (DREA)

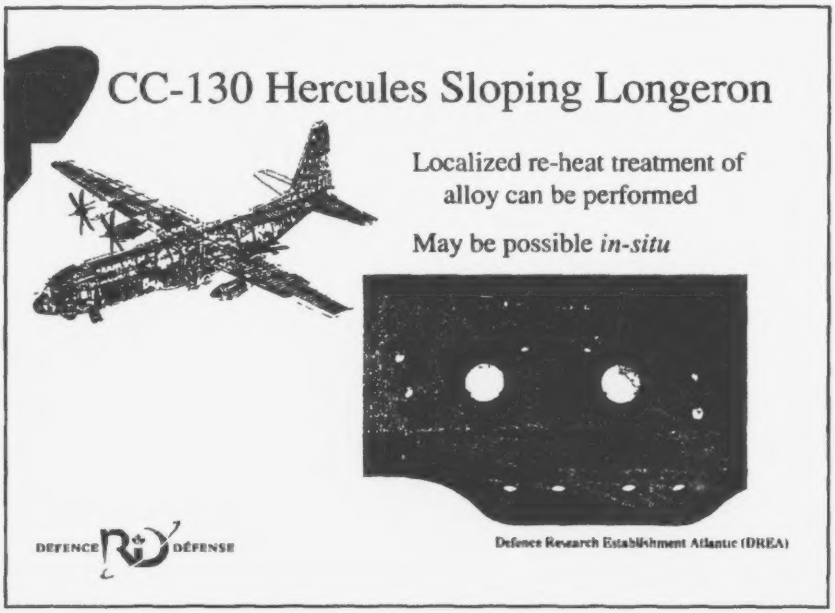

CC-130 Hercules Sloping Longeron

Localized re-heat treatment of alloy can be performed

May be possible *in-situ*

DEFENCE DÉFENSE

Defence Research Establishment Atlantic (DREA)

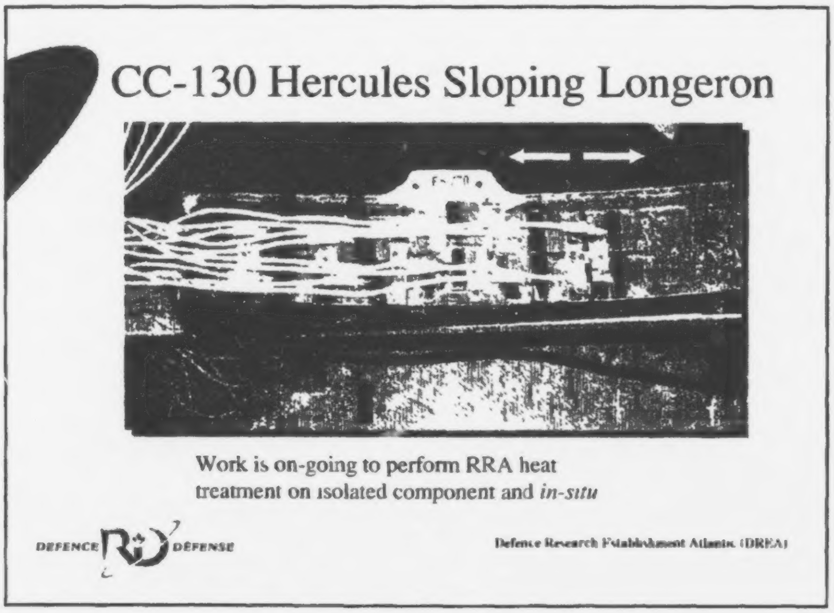

CC-130 Hercules Sloping Longeron

Work is on-going to perform RRA heat treatment on isolated component and *in-situ*

DEFENCE DÉFENSE

Defence Research Establishment Atlantic (DREA)

Engine Life Extension

- Completion of D6214 Major Project
  - Repair, Re-works and Certification Methodologies for F404 (CF-18)
- Damage tolerance and life extension methodologies for:
  - T56 (CC-130 and CP-140)
  - J-85 CAN 40 (Tutor)
  - NENE X (T-33)

D6214 Project Objectives

- Develop a qualification methodology for new repairs. (YN01)
- Implement this method by qualifying a number of advanced repair techniques on the F404 engine. (YN02)
- Contracted to Orenda Aerospace Corporation and NRC/IAR

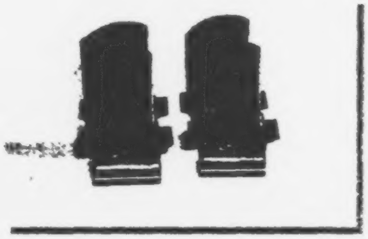

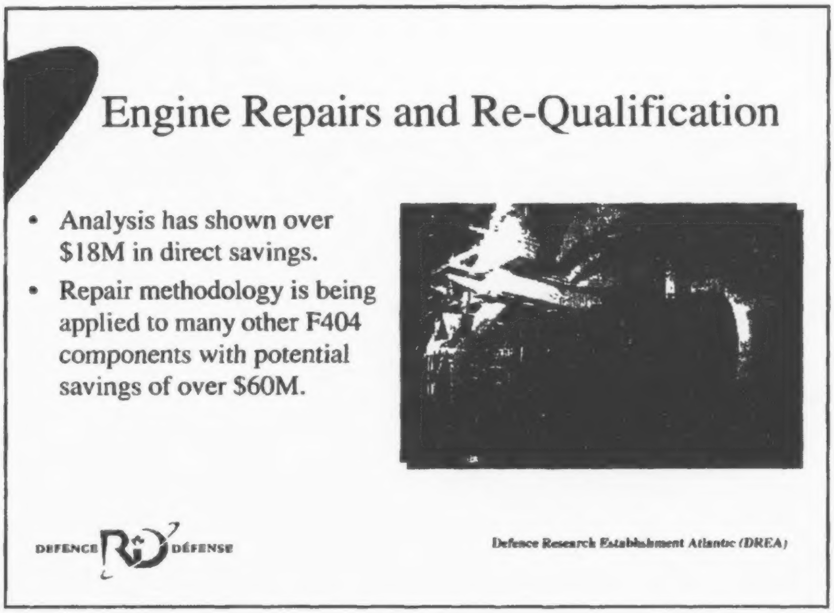

Engine Repairs and Re-Qualification

- Analysis has shown over $18M in direct savings.
- Repair methodology is being applied to many other F404 components with potential savings of over $60M.

DEFENCE R&D DÉFENSE

Defence Research Establishment Atlantic (DREA)

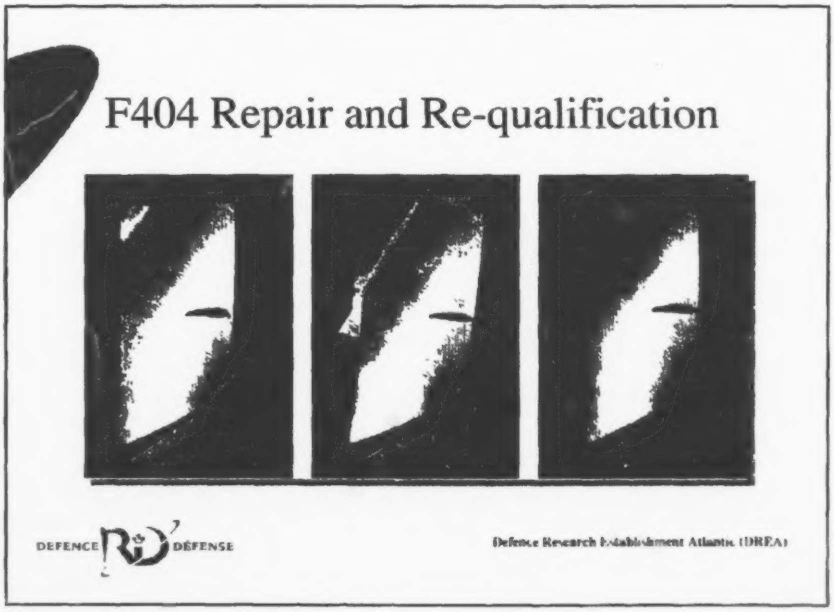

F404 Repair and Re-qualification

DEFENCE R&D DÉFENSE

Defence Research Establishment Atlantic (DREA)

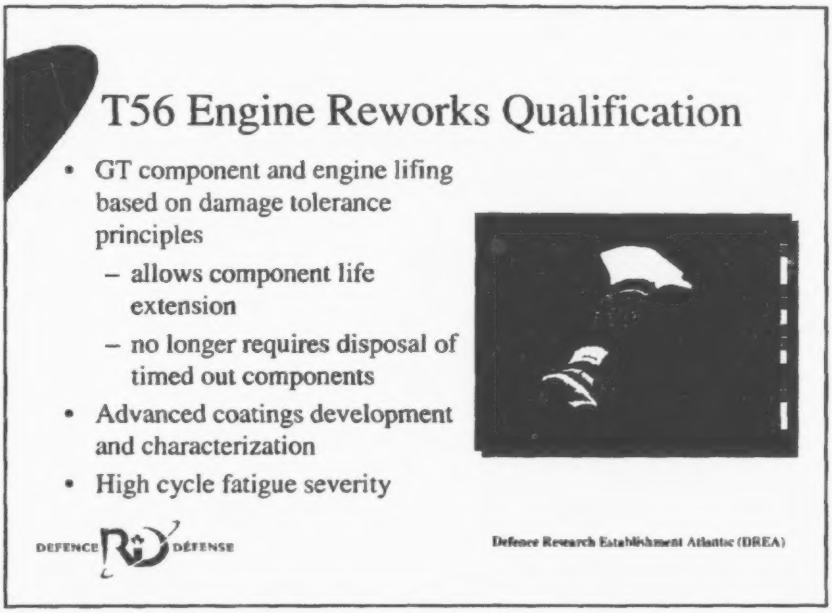

T56 Engine Reworks Qualification

- GT component and engine lifing based on damage tolerance principles
  - allows component life extension
  - no longer requires disposal of timed out components
- Advanced coatings development and characterization
- High cycle fatigue severity

DEFENCE DÉFENSE

Defence Research Establishment Atlantic (DREA)

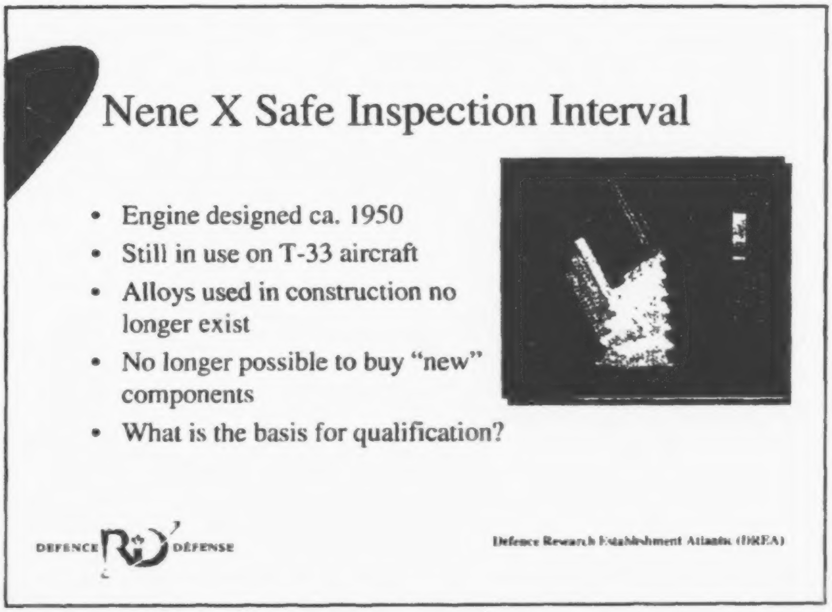

Nene X Safe Inspection Interval

- Engine designed ca. 1950
- Still in use on T-33 aircraft
- Alloys used in construction no longer exist
- No longer possible to buy "new" components
- What is the basis for qualification?

DEFENCE DÉFENSE

Defence Research Establishment Atlantic (DREA)

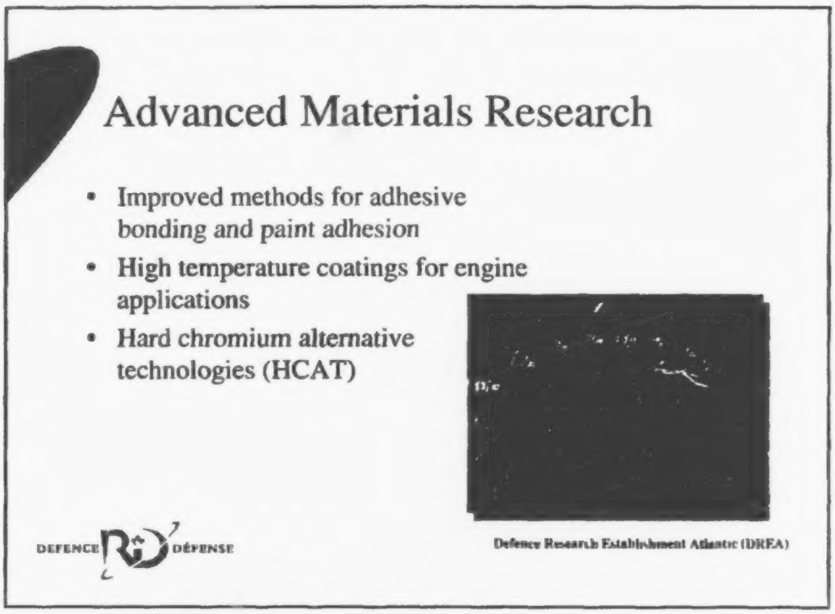

Advanced Materials Research

- Improved methods for adhesive bonding and paint adhesion
- High temperature coatings for engine applications
- Hard chromium alternative technologies (HCAT)

DEFENCE R&D DÉFENSE

Defence Research Establishment Atlantic (DREA)

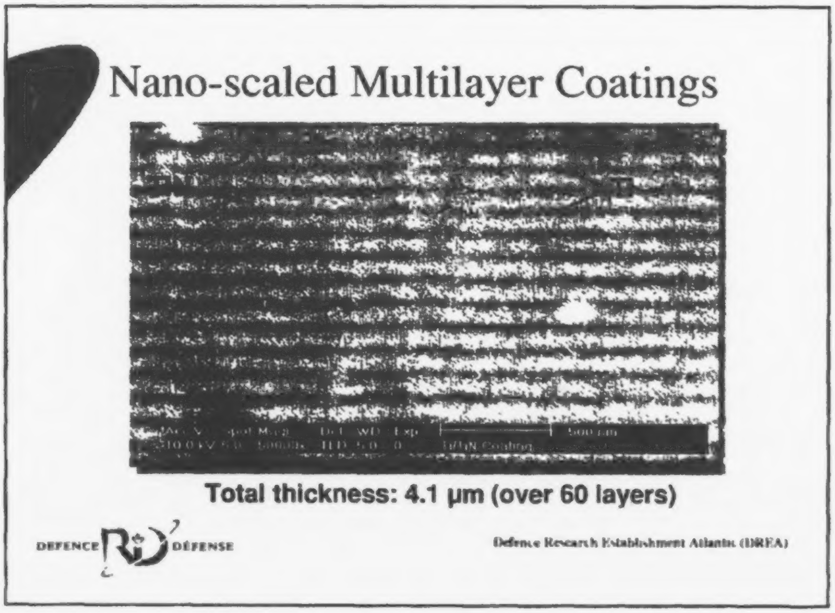

Nano-scaled Multilayer Coatings

Total thickness: 4.1 μm (over 60 layers)

DEFENCE R&D DÉFENSE

Defence Research Establishment Atlantic (DREA)

Hard Chromium Alternatives

- US DoD and DND joint program to replace hard chrome on landing gears
- Elimination of Cr^{6+} from the environment
- WC-Co and WC-CoCr coatings applied by HVOF spraying

DEFENCE DÉFENSE

Defence Research Establishment Atlantic (DREA)

C-HCAT

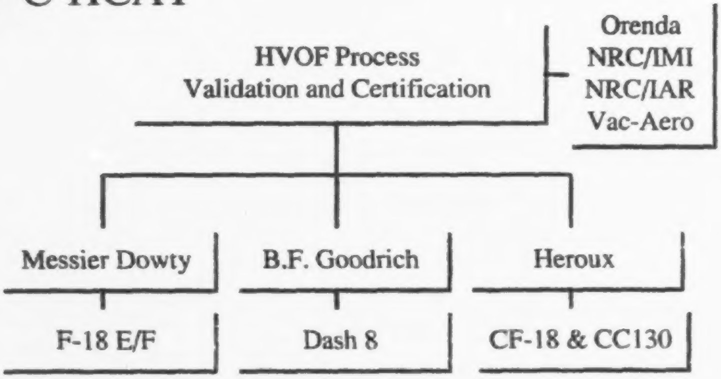

HVOF Process
Validation and Certification

Orenda
NRC/IMI
NRC/IAR
Vac-Aero

Messier Dowty
F-18 E/F

B.F. Goodrich
Dash 8

Heroux
CF-18 & CC130

DEFENCE DÉFENSE

Defence Research Establishment Atlantic (DREA)

Novel NDT Techniques

- Edge-of-light (NRC/IAR)
- Dual frequency eddy current
- Pulsed eddy current
- Laser ultrasonics
- CF-18 Rudder water ingress
- Cracks under fasteners

DEFENCE R&D DÉFENSE

Defence Research Establishment Atlantic (DREA)

Multi-layer Structure

Many difficulties are encountered by scanning an eddy current probe

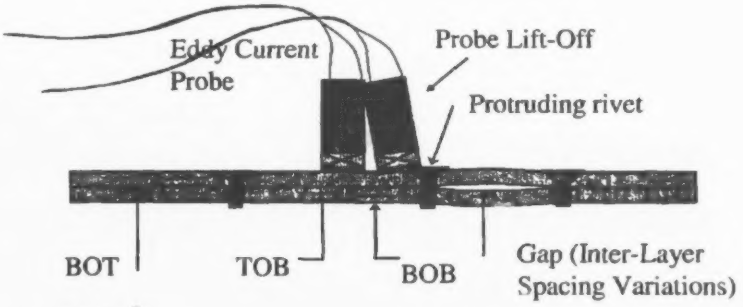

Eddy Current Probe

Probe Lift-Off

Protruding rivet

BOT

TOB

BOB

Gap (Inter-Layer Spacing Variations)

DEFENCE R&D DÉFENSE

Defence Research Establishment Atlantic (DREA)

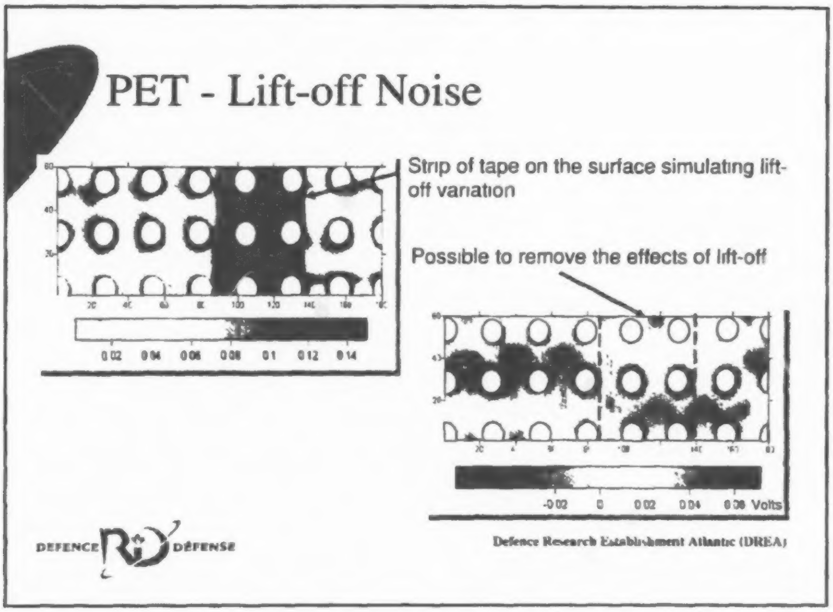

PET - Lift-off Noise

Strip of tape on the surface simulating lift-off variation

Possible to remove the effects of lift-off

DEFENCE DÉFENSE

Defence Research Establishment Atlantic (DREA)

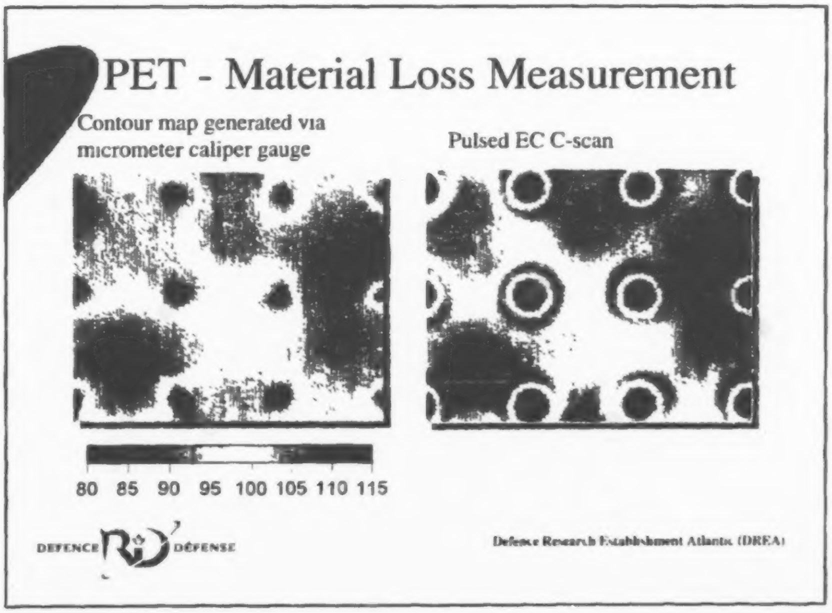

PET - Material Loss Measurement

Contour map generated via micrometer caliper gauge

Pulsed EC C-scan

DEFENCE DÉFENSE

Defence Research Establishment Atlantic (DREA)

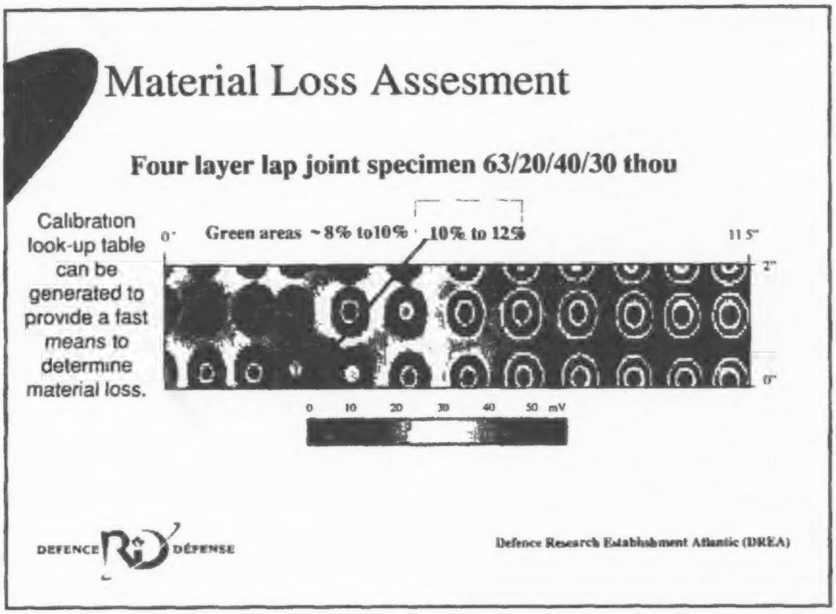

Material Loss Assesment

Four layer lap joint specimen 63/20/40/30 thou

Calibration look-up table can be generated to provide a fast means to determine material loss.

Green areas ~8% to10%

10% to 12%

0"
11.5"
2"
0"
0
10
20
30
40
50 mV

DEFENCE DÉFENSE

Defence Research Establishment Atlantic (DREA)

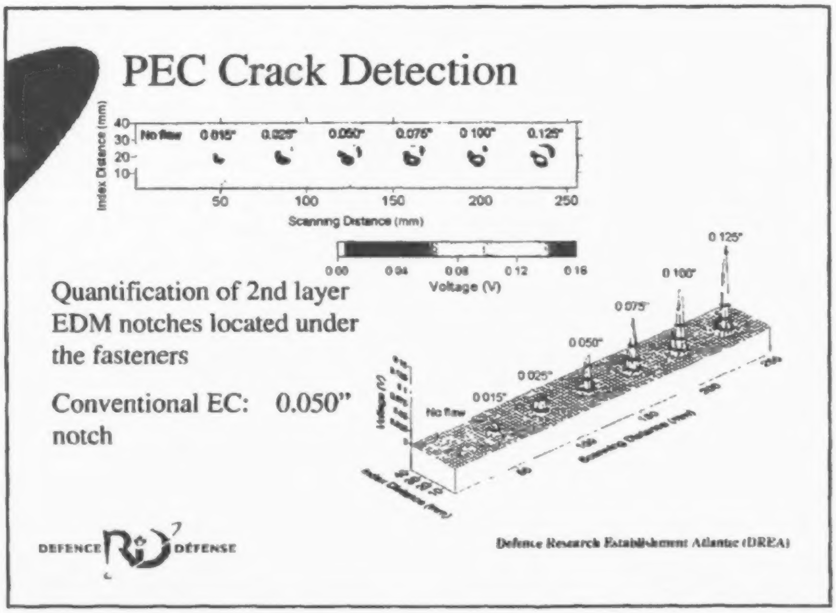

PEC Crack Detection

Quantification of 2nd layer EDM notches located under the fasteners

Conventional EC: 0.050" notch

Index Distance (mm)
40
30
20
10
No flaw
0.015"
0.025"
0.050"
0.075"
0.100"
0.125"
50
100
150
200
250
Scanning Distance (mm)
0.00
0.04
0.08
0.12
0.16
Voltage (V)
No flaw
0.015"
0.025"
0.050"
0.075"
0.100"
0.125"
Voltage (V)
Scanning Distance (mm)
Index Distance (mm)

DEFENCE DÉFENSE

Defence Research Establishment Atlantic (DREA)

Life Cycle Management Issues

- Effect of corrosion pillowing
- Probabilistic reliability assessment
  - fly to a known level of reliability
  - integration with corrosion effects
  - probability of detection (POD) from in-service data

Defence Research Establishment Atlantic (DREA)

Pillowing Cracks

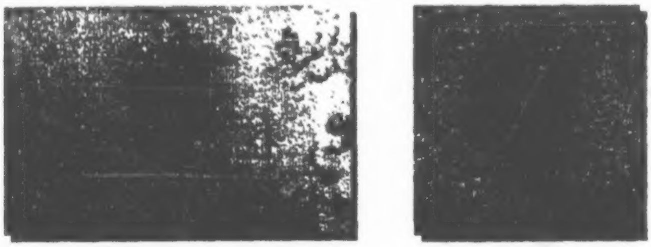

- Cracks found in first layer. Panel was only subjected to the sustained stress caused by the corrosion pillowing.
- These types of cracks have never been found in lap joints that have been disassembled immediately after being subject to accelerated corrosion protocol.

Defence Research Establishment Atlantic (DREA)

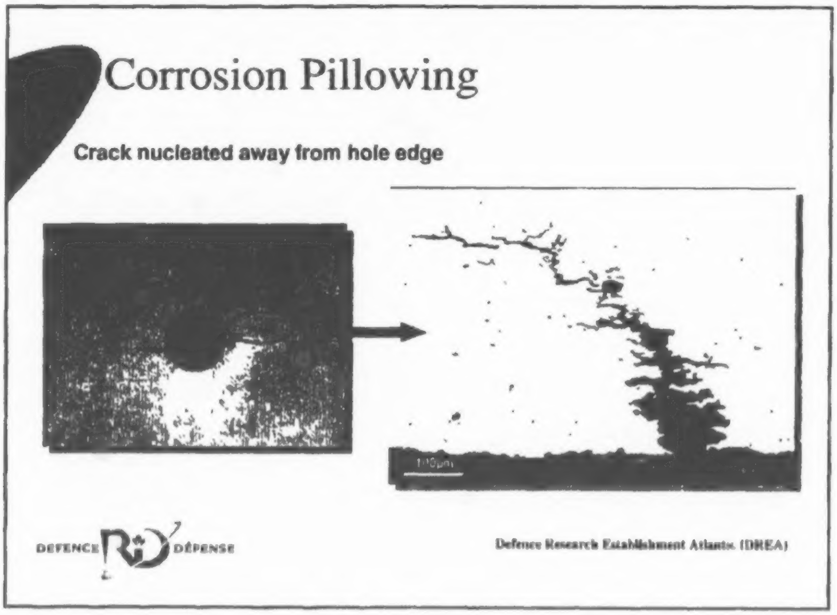

Corrosion Pillowing

Crack nucleated away from hole edge

100μm

DEFENCE DÉFENSE

Defence Research Establishment Atlantic (DREA)

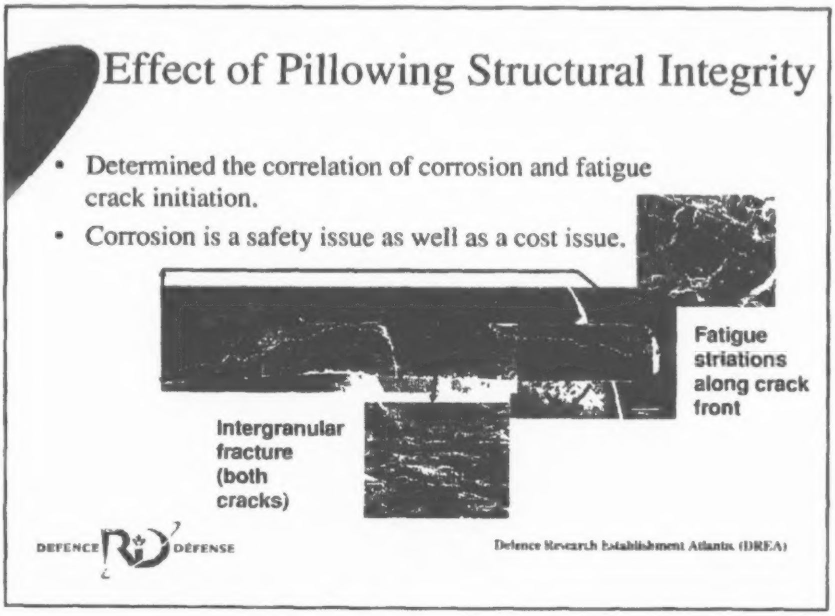

Effect of Pillowing Structural Integrity

- Determined the correlation of corrosion and fatigue crack initiation.
- Corrosion is a safety issue as well as a cost issue.

Fatigue striations along crack front

Intergranular fracture (both cracks)

DEFENCE DÉFENSE

Defence Research Establishment Atlantic (DREA)

#516423 (11)

Transmission Electron Microscopy of Martensitic Phases in Laser-Welded Nickel Aluminum Bronze Alloys

by

J.C. Bennett[1] and C.V. Hyatt[2]

[1]Department of Physics, Acadia University, Wolfville, Nova Scotia, B0P 1X0
[2]Defence Research Establishment Atlantic, Dockyard Laboratory, FMO Halifax,
Halifax, Nova Scotia B3K 2X0

Abstract

Laser cladding of nickel aluminum bronze alloy components offers the potential to improve performance such as corrosion and wear resistance. The attendant rapid cooling results in the formation of non-equilibrium microstructures, including martensitic phases. The development of these microstructures is investigated using transmission electron microscopy for a range of conventional and non-conventional nickel aluminum bronze alloys. The TEM observations indicate that only the disordered β' or 9R martensitic phase is formed under these conditions, with considerable morphological variation related to nominal composition and thermal history.

Transmission Electron Microscopy of Martensitic Phases in Laser Welded [illegible] Alloys

[illegible] MA

[illegible]

[illegible]alvin Hyatt
D.R.E.A.

ACADIA

Outline

- Materials Investigated
- Objectives
- Phase Diagram
- Microstuctures
  - ➢ *Varying Al concentration*
  - ➢ *Effects of small alloying additions*
- Conclusions

ACADIA

Nickel Aluminum Bronze Alloys

- **NAB alloys are widely used for marine components**
- **Suffer damage in service from corrosion and cavitation**
- **D.R.E.A. (C.V. Hyatt et al.) has developed laser cladding techniques to apply a NAB overlayer to worn components**
  - **reclamation not replacement**
  - **improved corrosion and wear resistance, etc.**

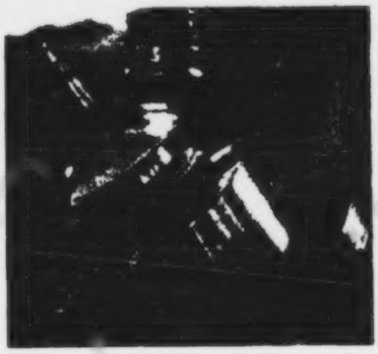

Goal to develop optimum consumable alloy

High cooling rates and novel compositions

↓

little relevant data available

Objective

Use TEM to characterize microstructure developed in terms of phase distributions, precipitates, structural defects, etc. for varying:
- Al concentration
- alloying additions; major (Ni, Fe) and minor (Ti, Zr, Cr)
- heat inputs

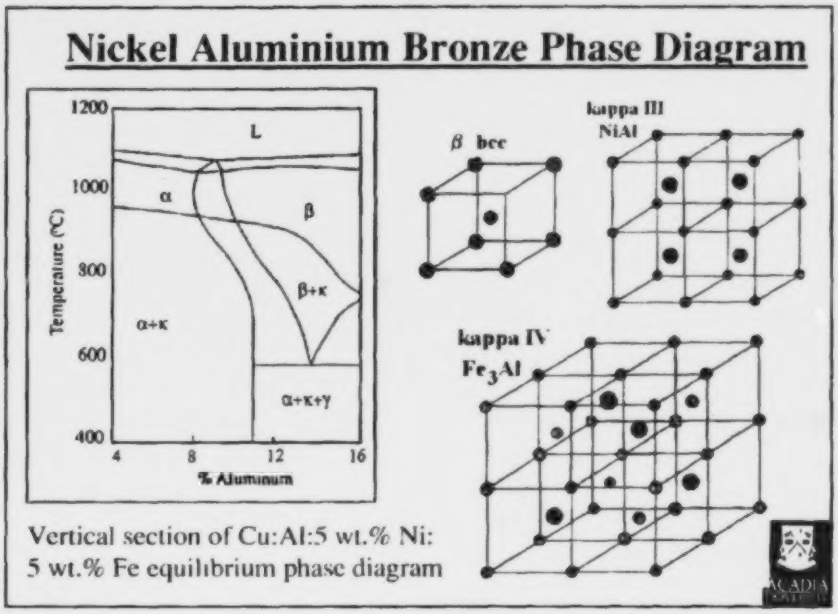

Nickel Aluminium Bronze Phase Diagram

1200
1000
800
600
400
Temperature (°C)
L
α
β
β+κ
α+κ
α+κ+γ
4
8
12
16
% Aluminum
β bcc
kappa III
NiAl
kappa IV
Fe_3Al
ACADIA

Vertical section of Cu:Al:5 wt.% Ni: 5 wt.% Fe equilibrium phase diagram

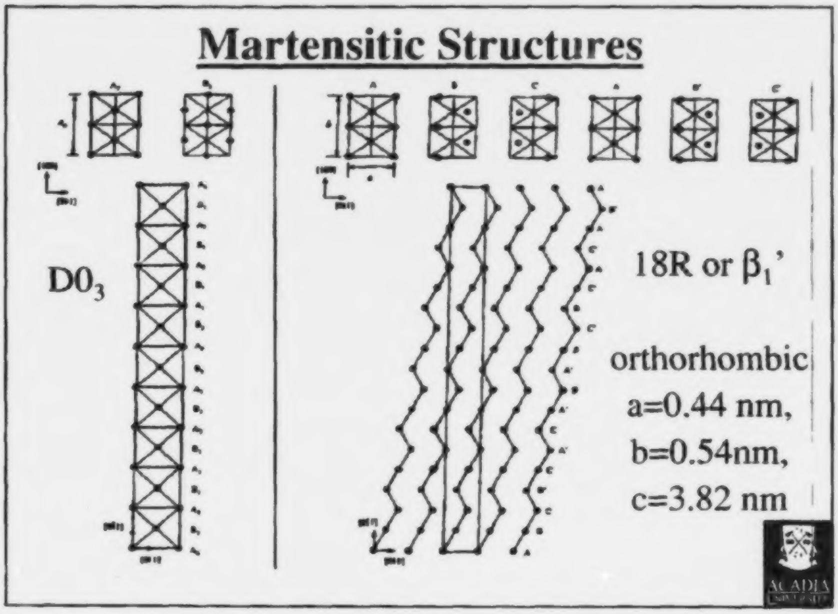

Martensitic Structures

$D0_3$

18R or β_1'

orthorhombic
a=0.44 nm,
b=0.54nm,
c=3.82 nm

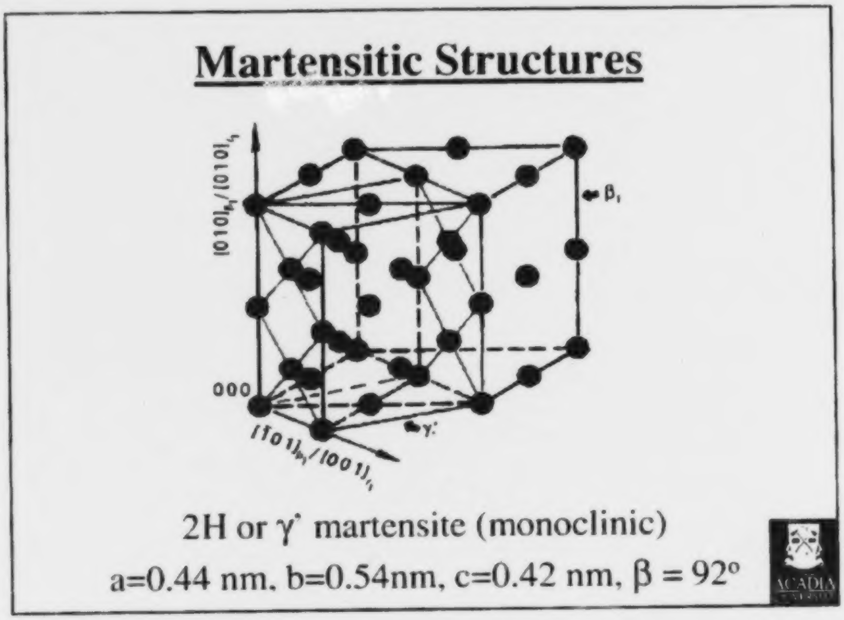
$[010]_{\gamma_1'}/[010]_{\beta_1}$
β_1
000
γ_1'
$[\bar{1}01]_{\gamma_1'}/[001]_{\beta_1}$

Martensitic Structures

2H or γ' martensite (monoclinic)

a=0.44 nm, b=0.54nm, c=0.42 nm, β = 92°

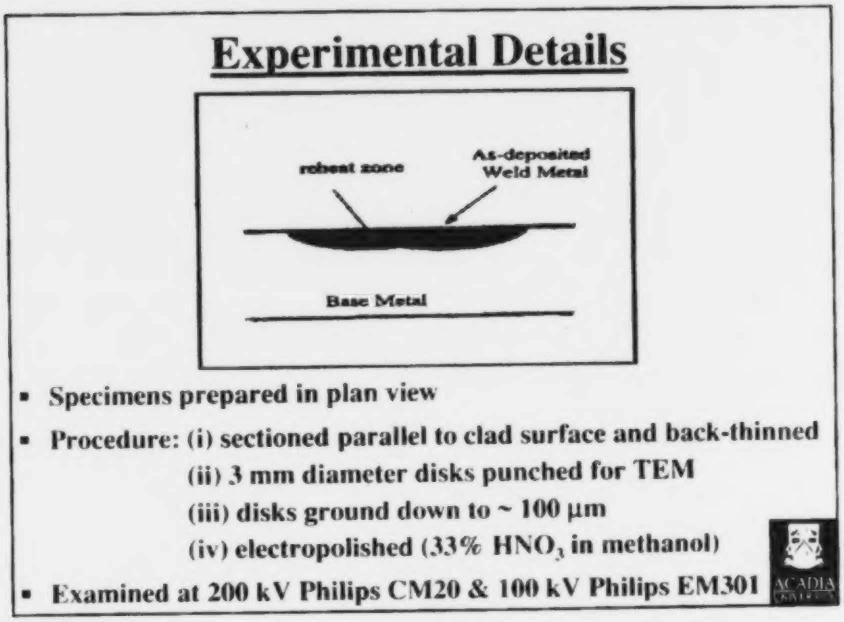
reheat zone
As-deposited Weld Metal
Base Metal

Experimental Details

- Specimens prepared in plan view
- Procedure: (i) sectioned parallel to clad surface and back-thinned
  (ii) 3 mm diameter disks punched for TEM
  (iii) disks ground down to ~ 100 μm
  (iv) electropolished (33% HNO_3 in methanol)
- Examined at 200 kV Philips CM20 & 100 kV Philips EM301

Effect of varying Al
Cu:x wt% Al (Ni/Fe =0.69-0.75)

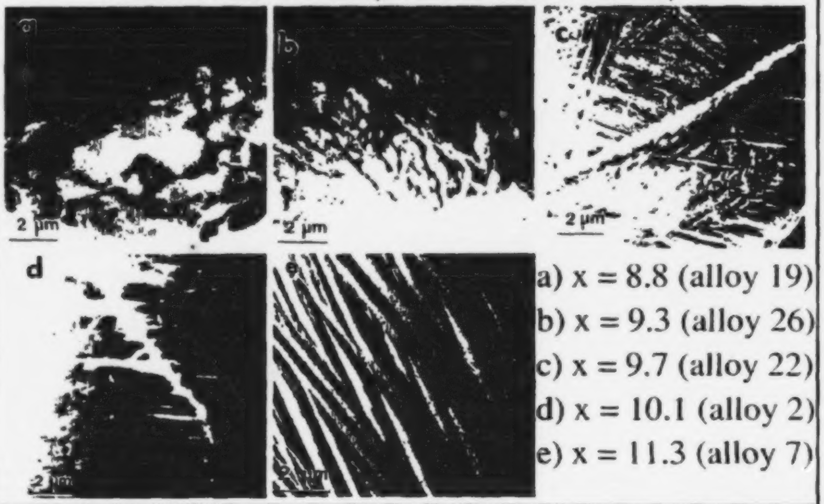

a) x = 8.8 (alloy 19)
b) x = 9.3 (alloy 26)
c) x = 9.7 (alloy 22)
d) x = 10.1 (alloy 2)
e) x = 11.3 (alloy 7)

Alloy 19
Cu:8.8 wt%Al:4.6 wt%Ni:6.2 wt%Fe:1.1 wt%Mn

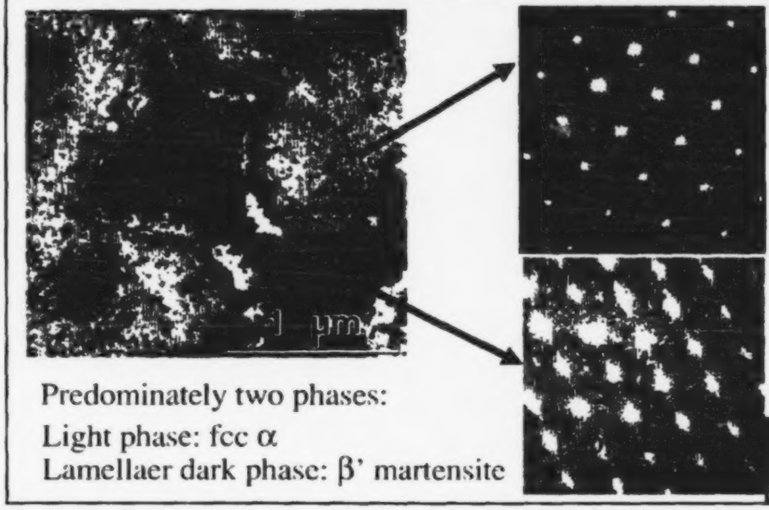

Predominately two phases:
Light phase: fcc α
Lamellaer dark phase: β' martensite

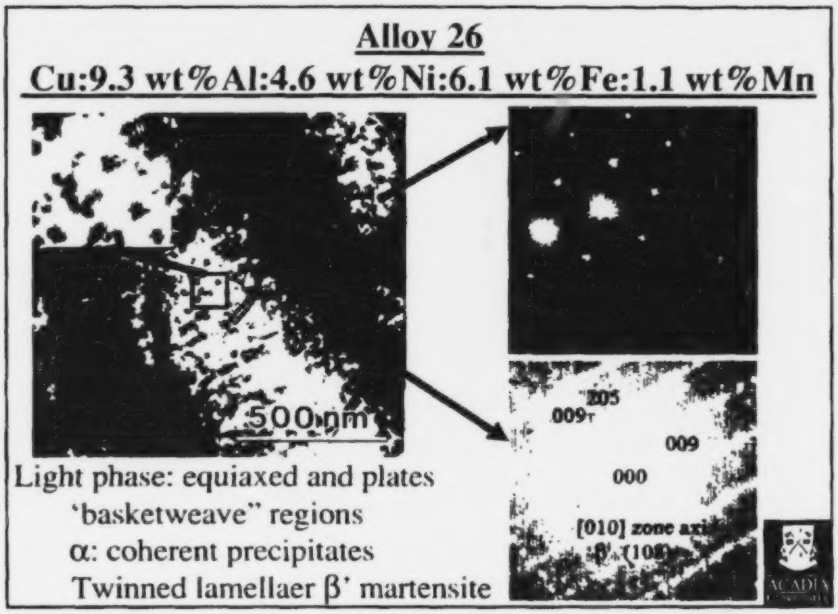

Alloy 26

Cu:9.3 wt%Al:4.6 wt%Ni:6.1 wt%Fe:1.1 wt%Mn

500 nm
205
009T
009
000
[010] zone axi
β' (10

Light phase: equiaxed and plates
'basketweave" regions
α: coherent precipitates
Twinned lamellaer β' martensite

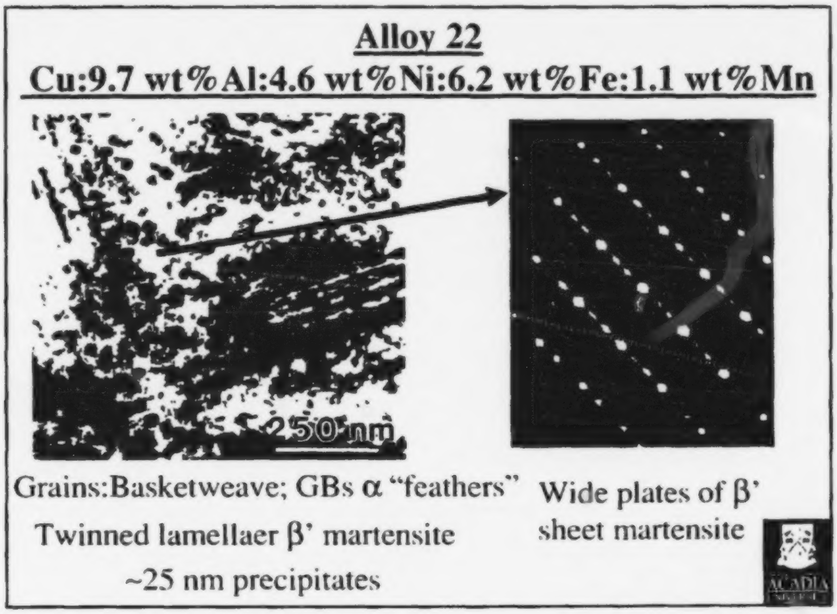

Alloy 22

Cu:9.7 wt%Al:4.6 wt%Ni:6.2 wt%Fe:1.1 wt%Mn

Grains:Basketweave; GBs α "feathers"
Twinned lamellaer β' martensite
~25 nm precipitates

Wide plates of β'
sheet martensite

Alloy 7

Cu:11.3 wt%Al:4 wt%Ni:5.8 wt%Fe:0.95 wt%Mn

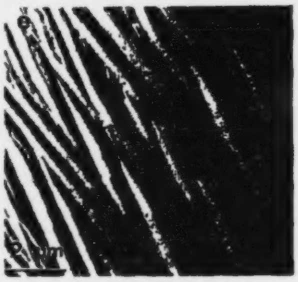

- Parallel sided plates
- Essentially no α phase
- sheet and lamellaer β'
- similar twinning
- differ only in domain size

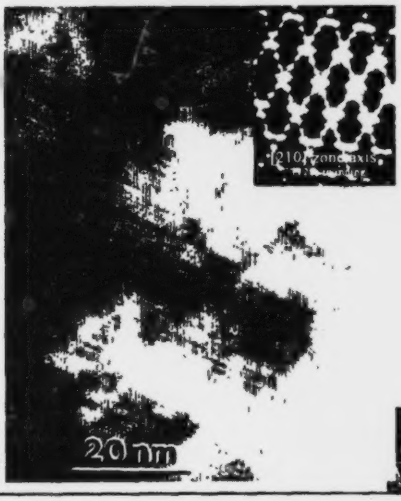
[210] zone axis
20 nm

Effect of varying Al

Cu:x wt% Al (Ni/Fe =0.94-1.06)

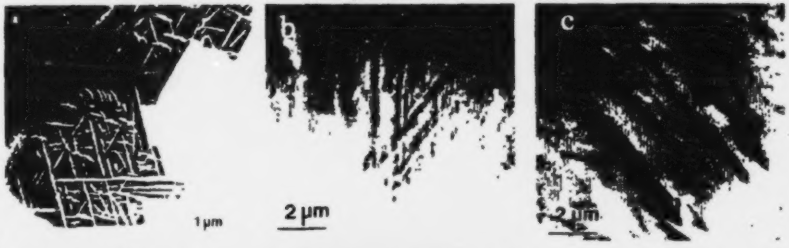
b
c
1 μm
2 μm
2 μm

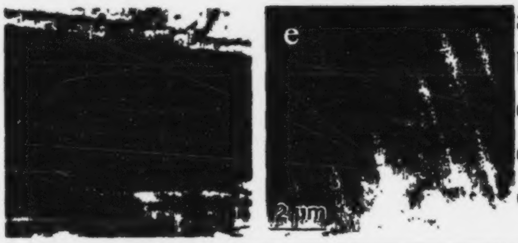

a) x = 9.1 (alloy 3)
b) x = 10.1 (alloy 4)
c) x = 10.7 (alloy 11)
d) x = 11.3 (alloy 12)
e) x = 12.2 (alloy 15)

Alloy 3

Cu:9.3 wt%Al:5 wt%Ni:4.7 wt%Fe:1.1 wt%Mn

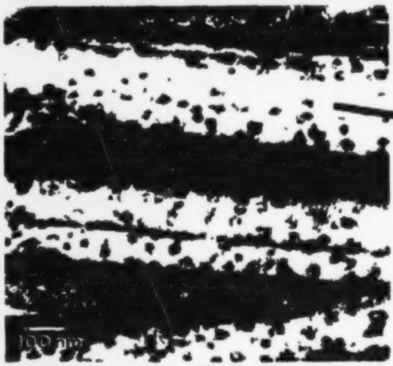

"Basketweave" regions

Sheet martensite and twinned lamellaer martensite

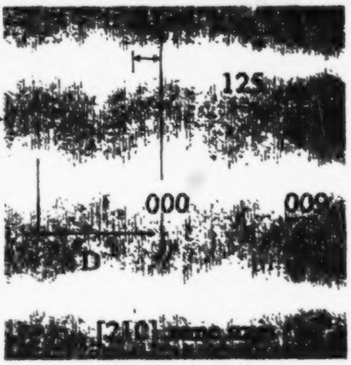

9R martensite

Streaking indicates random faulting

Alloy 4

Cu:10.1 wt%Al:3.8 wt%Ni:3.9 wt%Fe:1wt%Mn

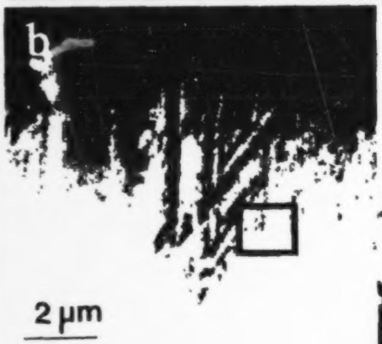

Parallel sided plates

Sheet and twinned lamellaer martensite (9R)

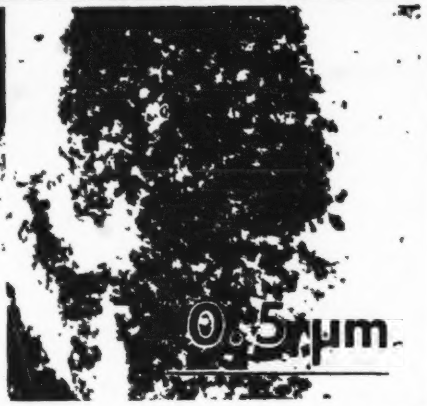

High density of ~50 nm precipitates

Alloy 12
Cu:10.7 wt%Al:4.7 wt%Ni:4.7wt%Fe:1.1 wt%Mn

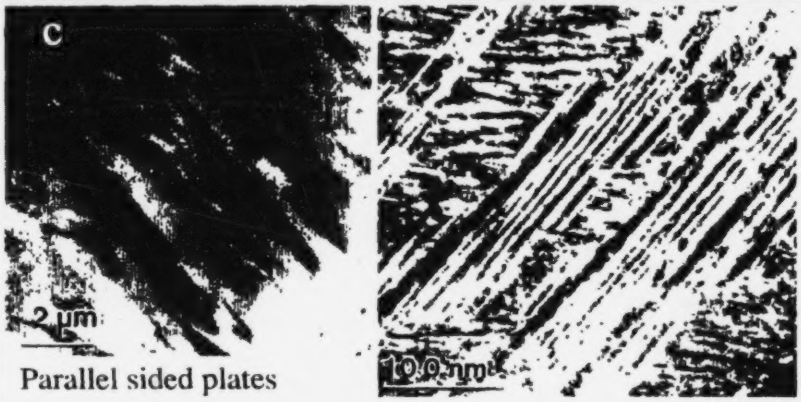

Parallel sided plates

Sheet and twinned
lamellaer martensite (9R)

Very fine twin domains
(< 20 nm width)

Alloy 12
Cu:11.3 wt%Al:4.1 wt%Ni:4.3wt% Fe:1 wt%Mn

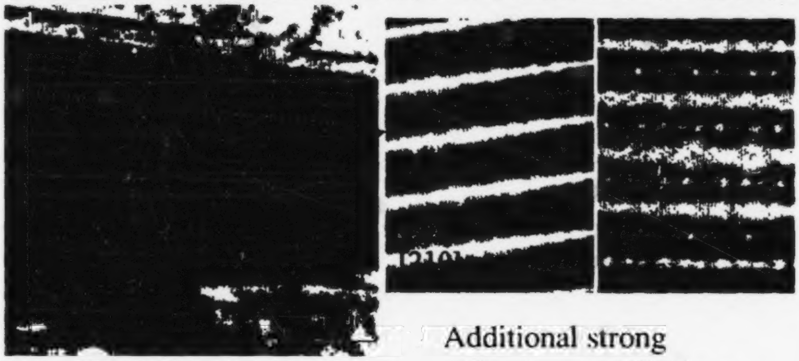

Parallel sided plates

Sheet and twinned
lamellaer martensite (9R)

Additional strong
reflections in [010] z.a.

Alloy 15
Cu:12.2 wt%Al:4.1 wt%Ni:4.3wt% Fe:1 wt%Mn

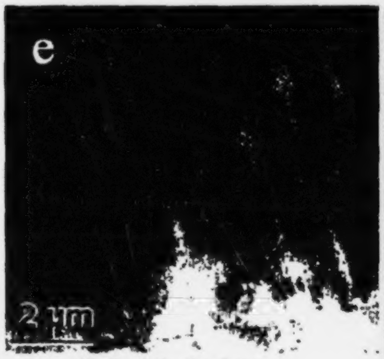

Parallel sided plates

Sheet and twinned
lamellaer martensite (9R)

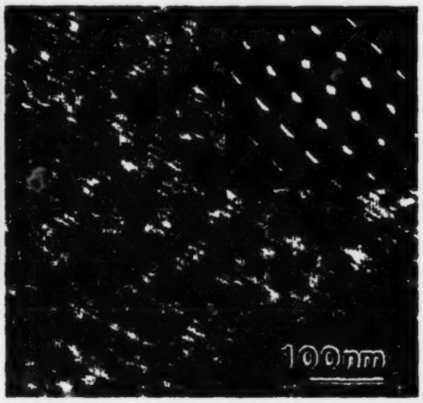

Very fine twin domains
(< 10 nm width)

Effect of varying Al
Cu:x wt% Al (Ni/Fe =1.4)

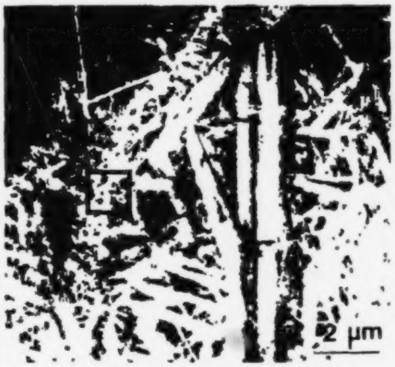

x = 9.2 (alloy 5)

Basketweave texture
Sheet and lamellaer β'

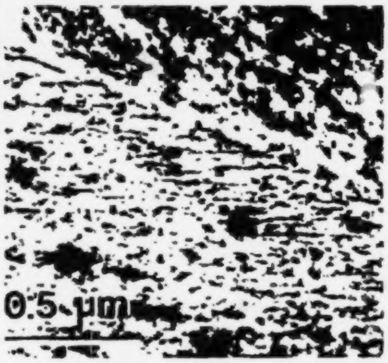

α phase on GBs

Colonies of elongated
Ni rich κ_{III} precipitates

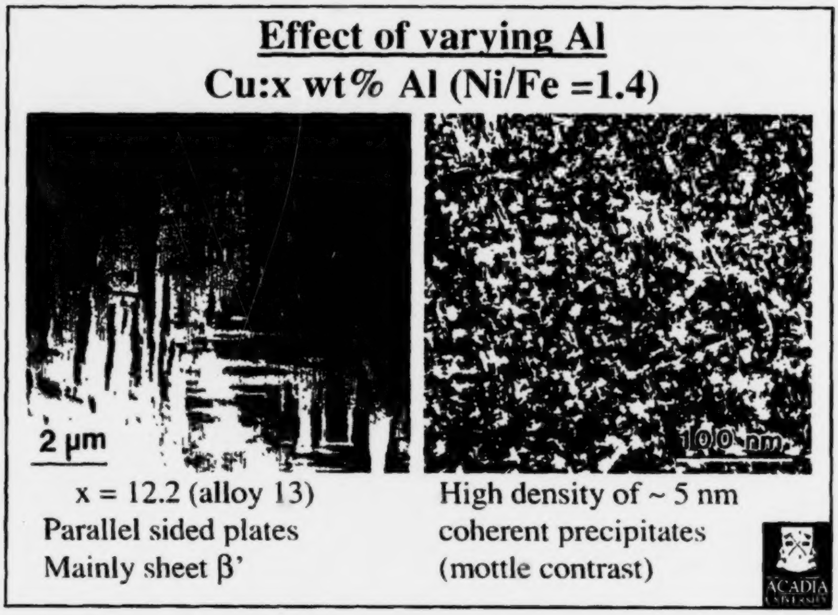

Effect of varying Al
Cu:x wt% Al (Ni/Fe =1.4)

x = 12.2 (alloy 13)
Parallel sided plates
Mainly sheet β'

High density of ~ 5 nm
coherent precipitates
(mottle contrast)

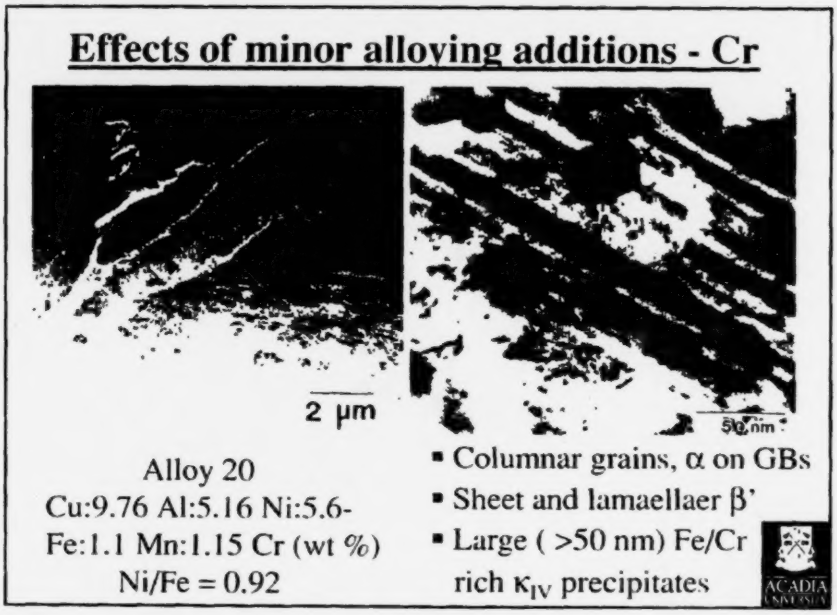

Effects of minor alloying additions - Cr

Alloy 20
Cu:9.76 Al:5.16 Ni:5.6-
Fe:1.1 Mn:1.15 Cr (wt %)
Ni/Fe = 0.92

- Columnar grains, α on GBs
- Sheet and lamaellaer β'
- Large (>50 nm) Fe/Cr rich κ_{IV} precipitates

Effects of minor alloying additions - Cr

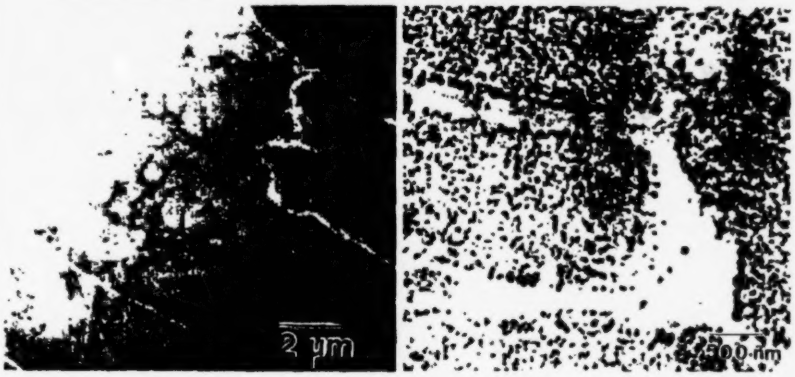

Alloy 25
Cu:9.64 Al:5.1 Ni:6.3 Fe:
1.1 Mn:1.72 Cr (wt %)
Ni/Fe = 0.81

- Cellular solidification structure
- Precipitate free zones

Effects of minor alloying additions - Cr

Alloy 25

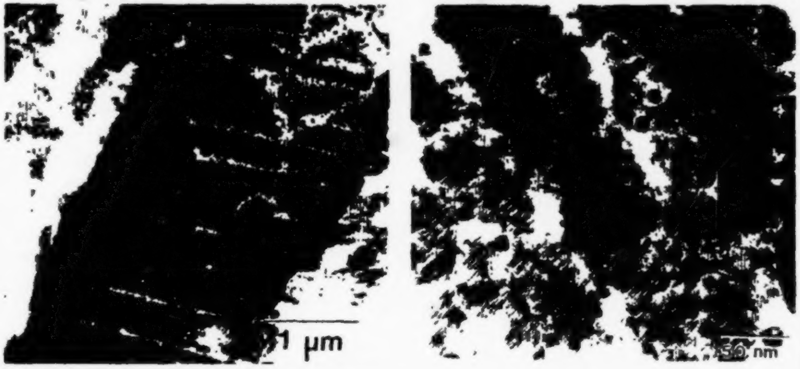

- Grain interiors are β' (9R)
- Martensite plates are continuous through the precipitate free zones

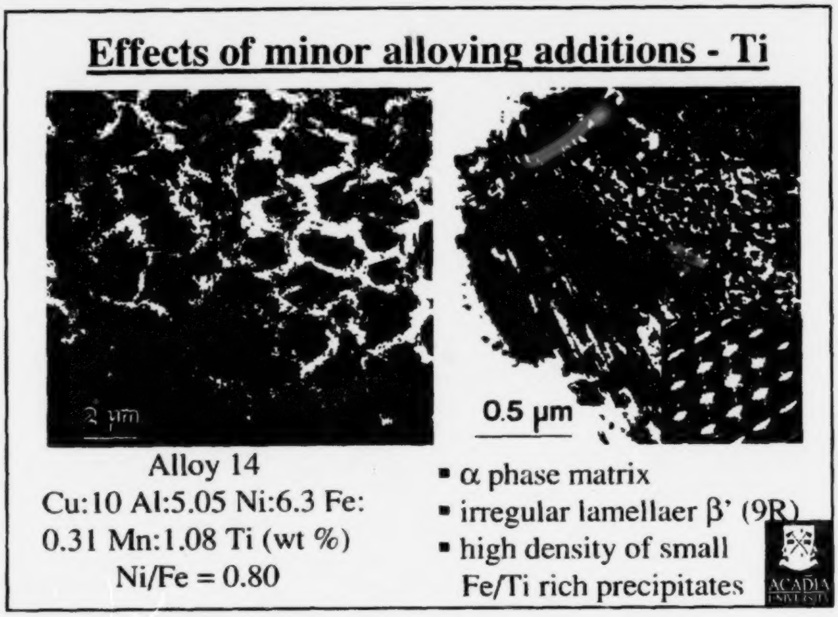

Effects of minor alloying additions - Ti

Alloy 14
Cu:10 Al:5.05 Ni:6.3 Fe:
0.31 Mn:1.08 Ti (wt %)
Ni/Fe = 0.80

- α phase matrix
- irregular lamellaer β' (9R)
- high density of small Fe/Ti rich precipitates

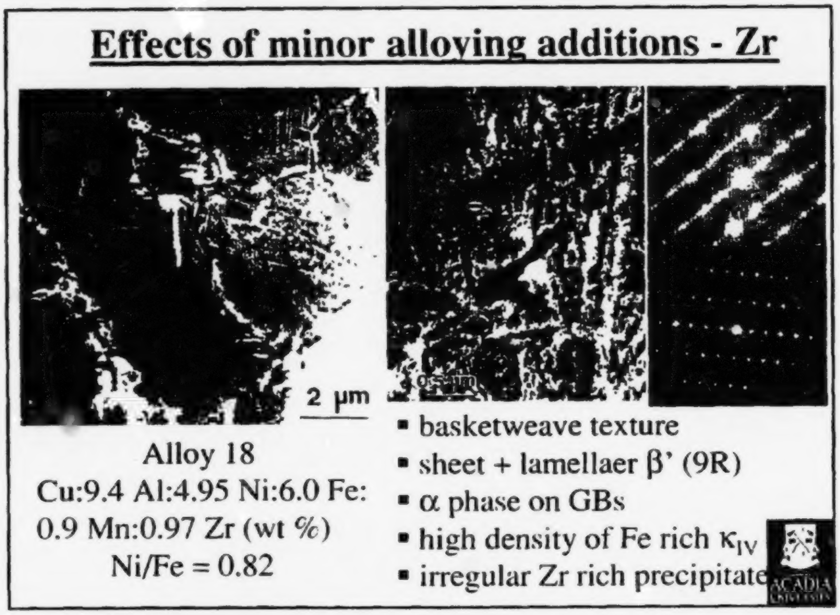

Effects of minor alloying additions - Zr

Alloy 18
Cu:9.4 Al:4.95 Ni:6.0 Fe:
0.9 Mn:0.97 Zr (wt %)
Ni/Fe = 0.82

- basketweave texture
- sheet + lamellaer β' (9R)
- α phase on GBs
- high density of Fe rich κ_{IV}
- irregular Zr rich precipitate

Effects of minor alloying additions - Cr, Ti, Zr

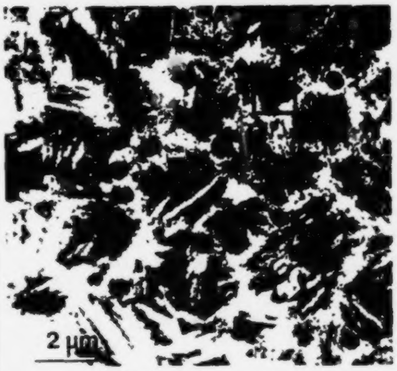

- no visible GBs
- two main phases: i) α matrix
  ii) irregular β' particles (9R lamellaer martensite)

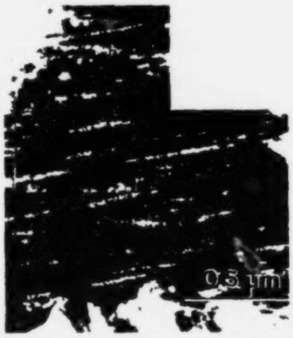

Alloy 27
Cu:9.3 Al:4.9 Ni:5.3 Fe: 1.1 Mn: 0.31 Cr: 0.23 Ti: 0.23 Zr (wt %)
Ni/Fe = 0.92

Effects of minor alloying additions - Cr, Ti, Zr

Alloy 27

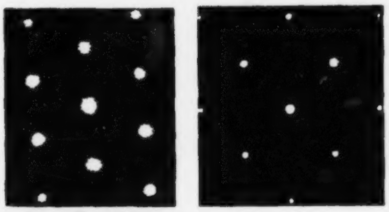

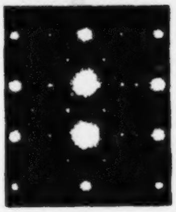

A: BF image
B: [111], C: [100], D: [110] zone axis SAED from large Fe rich κ_{IV} precipitates

Precipitates: (i) small (<50 nm) and (ii) large (>100 nm) κ_{IV} type; (iii) irregular Zr rich

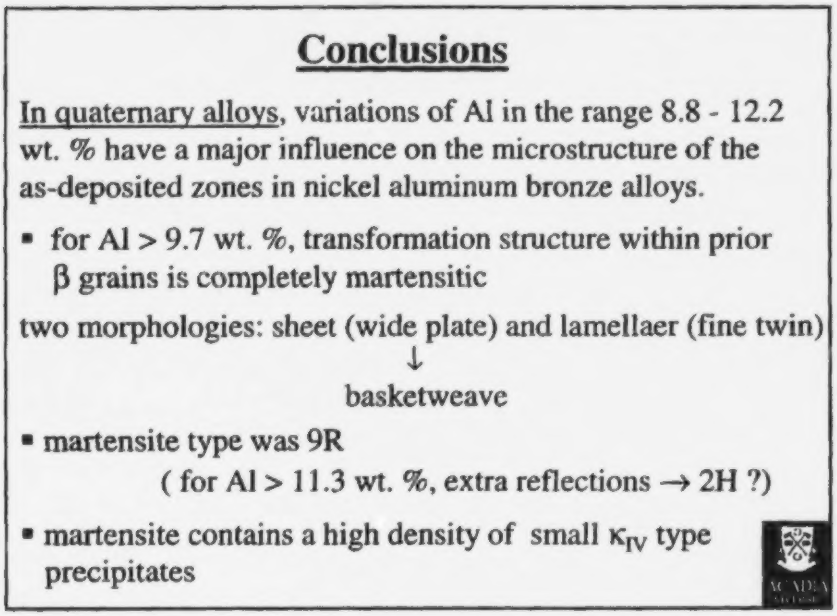

Conclusions

In quaternary alloys, variations of Al in the range 8.8 - 12.2 wt. % have a major influence on the microstructure of the as-deposited zones in nickel aluminum bronze alloys.

- for Al > 9.7 wt. %, transformation structure within prior β grains is completely martensitic

two morphologies: sheet (wide plate) and lamellaer (fine twin)
↓
basketweave

- martensite type was 9R
  (for Al > 11.3 wt. %, extra reflections → 2H ?)
- martensite contains a high density of small κ_{IV} type precipitates

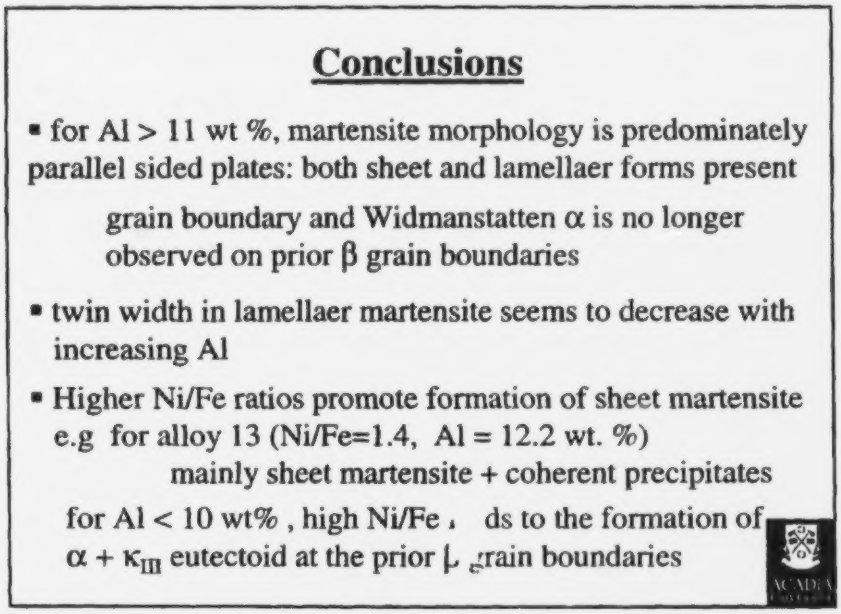

Conclusions

- for Al > 11 wt %, martensite morphology is predominately parallel sided plates: both sheet and lamellaer forms present

  grain boundary and Widmanstatten α is no longer observed on prior β grain boundaries

- twin width in lamellaer martensite seems to decrease with increasing Al
- Higher Ni/Fe ratios promote formation of sheet martensite e.g for alloy 13 (Ni/Fe=1.4, Al = 12.2 wt. %)
  mainly sheet martensite + coherent precipitates

  for Al < 10 wt% , high Ni/Fe leads to the formation of α + κ_{III} eutectoid at the prior β grain boundaries

Conclusions

- Additions of Cr, Ti and Zr result in changes in:
  - i) major phases present
  - ii) precipitate type, number, coherency
- Cr: - cellular solidification structure and columnar grains
  - entirely martensitic (both sheet and lamellaer; 9R)
  - Fe/Cr rich κ_{IV} type precipitates
  - precipitate free zones
- Ti: - no obvious grain structure
  - irregular, lamellaer β' martensite plates in α matrix
  - Fe/Ti rich κ_{IV} type precipitates
- Zr: - probably little influence on majority phases
  - forms complex intermetallic precipitates; undetectable in majority phases

#516424 (12)

A New Fracture Criterion For Piezoelectric Solids

by

S. Xu
University of Manitoba
(joined Martec May 30th 2001)

Abstract

(abstract not available at time of printing)

A New Fracture Criterion for Piezoelectric Solids*

Steven Xu

University of Manitoba

** This work was supported by the Natural Sciences and Engineering Research Council of Canada (NSERC)*

Outline

- Motivation
- Literature review
- Proposed new fracture criterion
- Conclusion

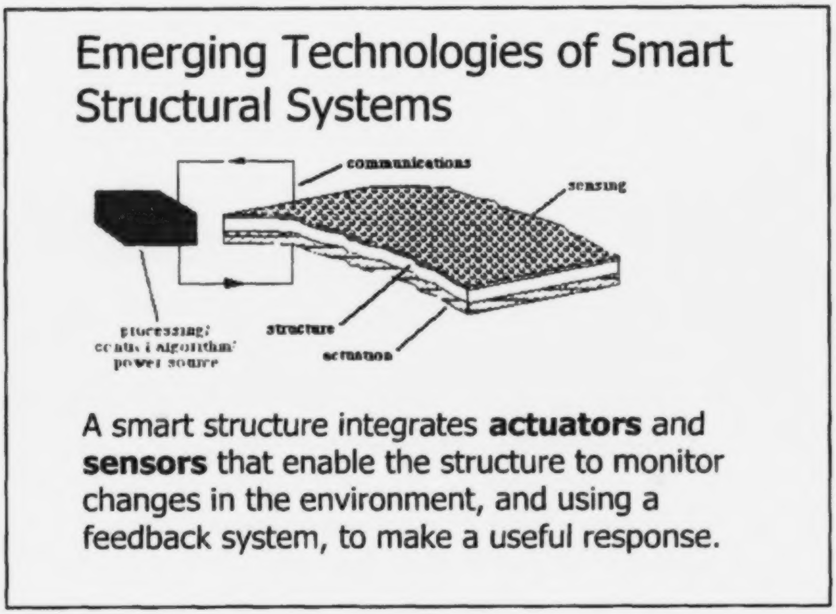

Emerging Technologies of Smart Structural Systems

communications
sensing
processing/
control algorithm/
power source
structure
actuation

A smart structure integrates **actuators** and **sensors** that enable the structure to monitor changes in the environment, and using a feedback system, to make a useful response.

Sensor/Actuator Materials

- Optical fibers
- Magnetostrictive materials
- Shape memory alloys
- Electrorheological fluids
- Piezoelectric materials

Sensor/Actuator Materials

- Optical fibers
- Magnetostrictive materials
- Shape memory alloys
- Electrorheological fluids
- Piezoelectric materials ⟶ most widely used
  - ✓ Fast electromechanical response
  - ✓ Low power requirements

composite shell
distributed piezoelements

Applying piezoactuators to damp vibrations of composite beams (Kawiecki, 1998)

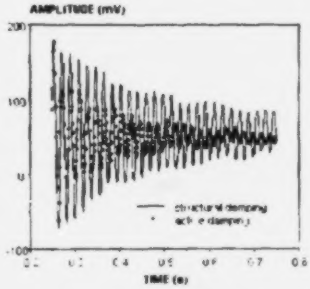

damping coefficient of vibrations was increased from 0.012 to 0.1.

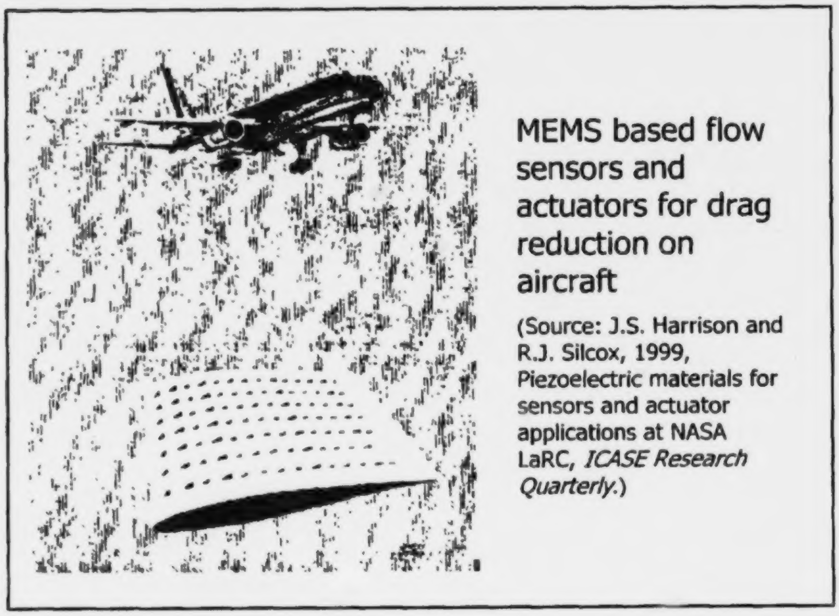

MEMS based flow sensors and actuators for drag reduction on aircraft

(Source: J.S. Harrison and R.J. Silcox, 1999, Piezoelectric materials for sensors and actuator applications at NASA LaRC, *ICASE Research Quarterly*.)

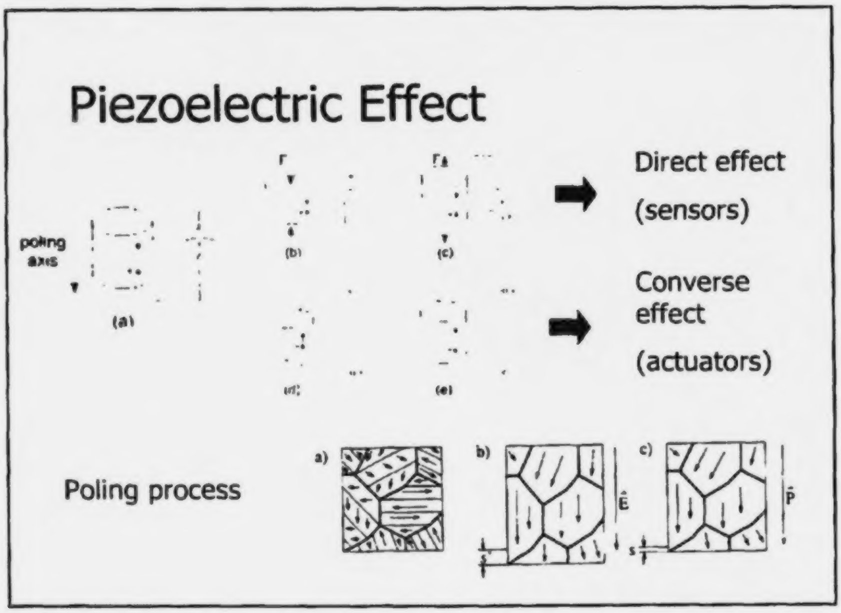

Piezoelectric Effect

➡ Direct effect

(sensors)

➡ Converse effect

(actuators)

Poling process

Equations Governing Piezoelectric Effects

$$\{\sigma\}=[c]\ \{s\}-[e]^T\ \{E\}$$

$$\{D\}=[e]\ \{s\}+[\varepsilon]\ \{E\}$$

For PZT-4:

$$[e]=\begin{bmatrix} 0 & 0 & 0 & 0 & 13.44 & 0 \\ 0 & 0 & 0 & 13.44 & 0 & 0 \\ -6.98 & -6.98 & 13.88 & 0 & 0 & 0 \end{bmatrix}\ (C/m^2)$$

⟶ Unimorph patch PZT actuator

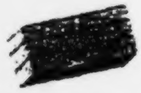

⟶ Multilayer plate-like PZT actuator

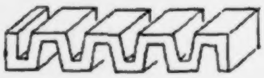

⟶ Multilayer spring-like PZT actuator

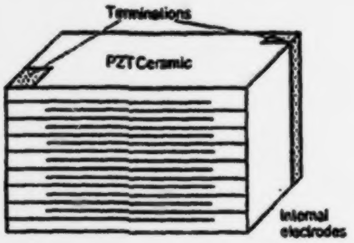
Terminations
PZT Ceramic
Internal electrodes

⟶ Multilayer PZT actuator stack

Concerns about Using Piezoelectric Materials

- Brittle in nature and susceptible to fracture
- Unavoidable presence of defects during manufacturing process
- Fatigue degradation and service performance are related to internal voids and cracks (Park and Carman*, 1997;* Barsoum, 1997; *etc*)

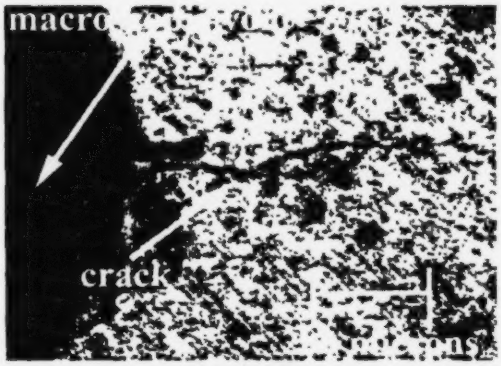

Photograph of a Piezoelectric

Specimen Containing Defects

(Park and Carman, 1997)

Optical micrograph of an impermeable crack

(Lynch, *et al*, 1995)

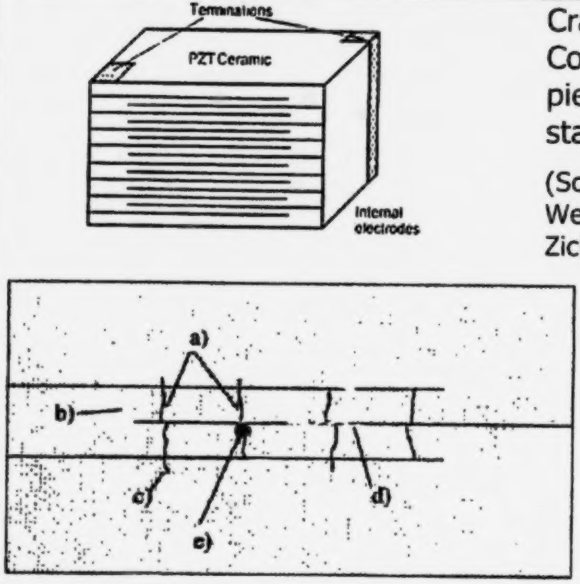
Terminations
PZT Ceramic
Internal electrodes
a)
b)
c)
d)
e)

Crack Configurations in piezoactuator stack

(Schneider G.A., Weitzing, H. and Zickgraf, 1996)

Literature Review of Fracture Criteria

- Previous work
  - Pak, 1992
  - Park and Sun, 1995
  - Kumar and Singh, 1996
- Restrictions
  - Special crack orientation
  - Isotropic fracture toughness
  - Self-similar crack extension

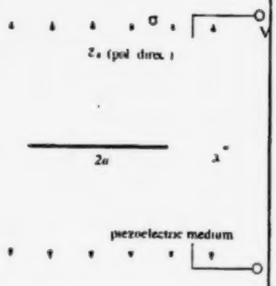
σ
V
z₃ (pol direc.)
2a
x
piezoelectric medium

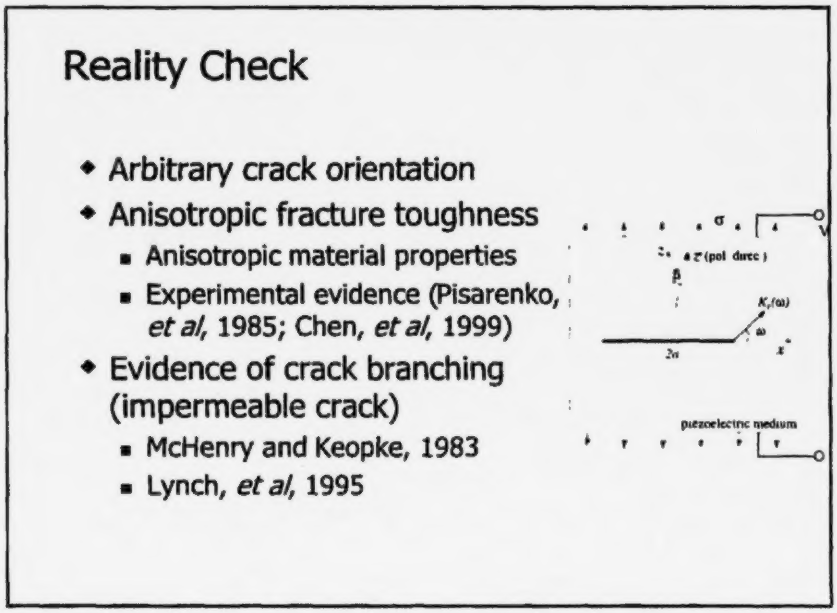

Reality Check

- Arbitrary crack orientation
- Anisotropic fracture toughness
  - Anisotropic material properties
  - Experimental evidence (Pisarenko, *et al*, 1985; Chen, *et al*, 1999)
- Evidence of crack branching (impermeable crack)
  - McHenry and Keopke, 1983
  - Lynch, *et al*, 1995

σ
V
z (pol direc)
β
$K_I(\omega)$
ω
2a
x^*
piezoelectric medium

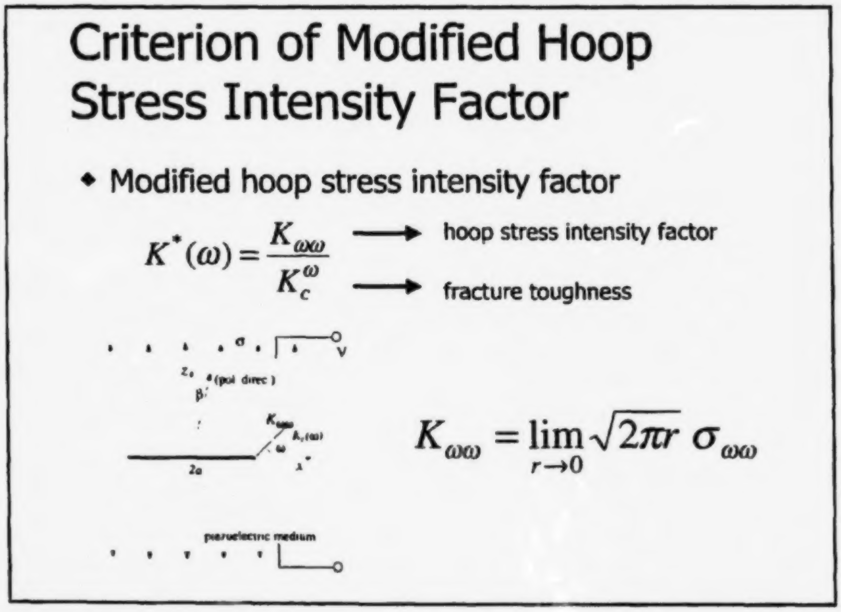

Criterion of Modified Hoop Stress Intensity Factor

- Modified hoop stress intensity factor

$$K^*(\omega) = \frac{K_{\omega\omega}}{K_c^{\omega}}$$

$K_{\omega\omega}$ ⟶ hoop stress intensity factor

K_c^{ω} ⟶ fracture toughness

$$K_{\omega\omega} = \lim_{r\to 0}\sqrt{2\pi r}\,\sigma_{\omega\omega}$$

σ
V
z (pol direc)
β
$K_{\omega\omega}$
$k_I(\omega)$
ω
2a
x^*
piezoelectric medium

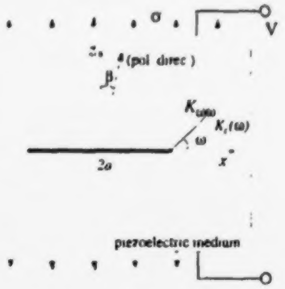
σ
V
(pol direc)
β
$K_{\omega\omega}$
$K_{r}(\omega)$
ω
2a
x^*
piezoelectric medium

- Crack propagation direction α

$$K^*(\alpha) = Max \quad K^*(\omega)$$

- Crack propagation initiates when

$$K_{\alpha\alpha} \geq K_c^\alpha$$

Anisotropy of Fracture Toughness

- Experimental data are available for K_0 and K_{90} (*e.g.* Pisarenko, *et al*, 1985)

Piezoelectric ceramics	**K_0** (MPa.m$^{1/2}$)	**K_{90}** (MPa.m$^{1/2}$)	**K_0/K_{90}**
I	1.50	0.70	2.14
II	1.82	0.77	2.36
III	1.52	1.38	1.10

- A simple model of fracture toughness

$$K_c^\omega = K_0 \sin^2(\omega + \beta) + K_{90} \cos^2(\omega + \beta)$$

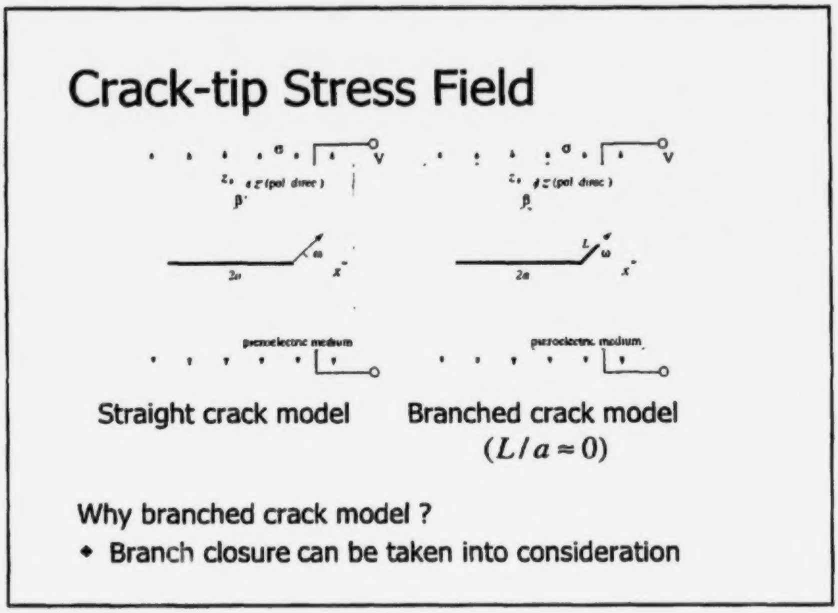

Crack-tip Stress Field

σ
V
z (pol. direc.)
β
2a
ω
L
x
piezoelectric medium

Straight crack model

Branched crack model

$(L/a \approx 0)$

Why branched crack model ?

- Branch closure can be taken into consideration

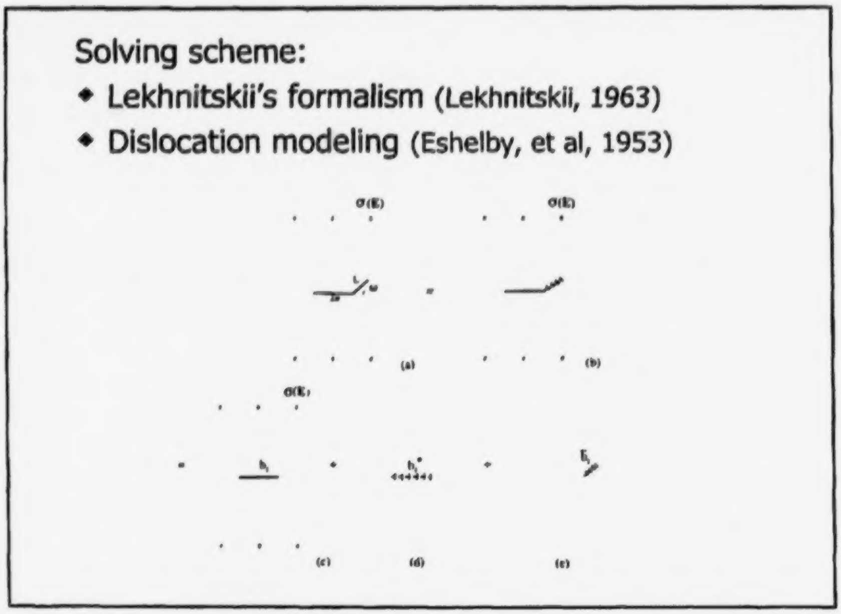

Solving scheme:

- Lekhnitskii's formalism (Lekhnitskii, 1963)
- Dislocation modeling (Eshelby, et al, 1953)

σ(E)
L
ω
2a
=
(a)
(b)
σ(E)
=
b_i
+
b_i^*
+
$\bar{b}_j$
(c)
(d)
(e)

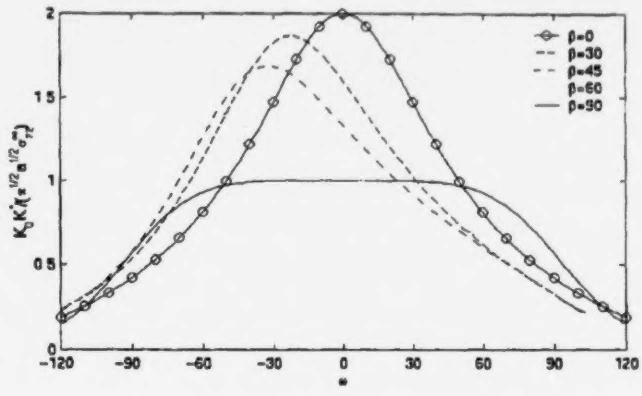

Variation of modified hoop stress intensity factor under remote tension loading in PZT-4 (impermeable crack, $K_0/K_{90}=2$)

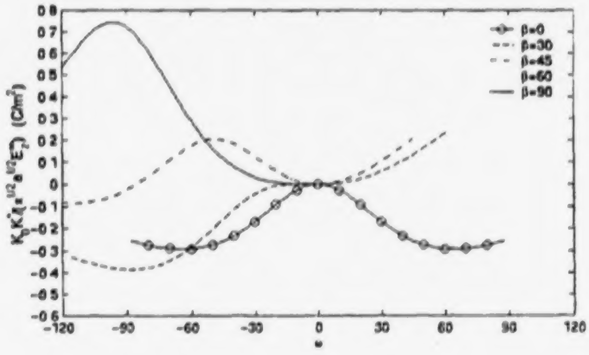

Variation of modified hoop stress intensity factor under positive electric field loading in PZT-4 (impermeable crack, $K_0/K_{90}=2$)

- Even in a symmetric case, a crack may deviate from the straight extension path, which qualitatively agrees with experimental finding (McHenry and Keopke, 1983)
- Currently, a quantitative verification of proposed fracture criterion is not possible due to lack of experimental data

Straight Crack Model VS Branched Crack Model

- Two models have similar trends
- Requirement of an open branch can only be considered by the branched crack model

e.g. Prediction for electric loading, crack orientation β=45 (*deg*)

Straight crack model	106 *(deg)*
Branched crack model	45 *(deg)*

Reason: Branch closure happens when branch angle is larger than 45 (deg)

Isotropic fracture toughness VS anisotropic fracture toughness

- Quite different branching angles are predicted

e.g. Prediction for tensile loading, crack orientation β=30 (*deg*)

Isotropic fracture toughness	0 *(deg)*
Anisotropic fracture toughness	-22 *(deg)*

Future Work

- Domain switching at the crack tip

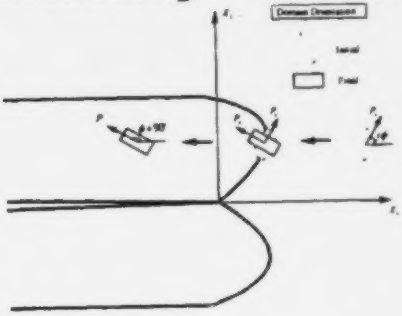

$$K_c = K_c(\theta,\ \sigma^{\infty},\ E^{\infty})$$

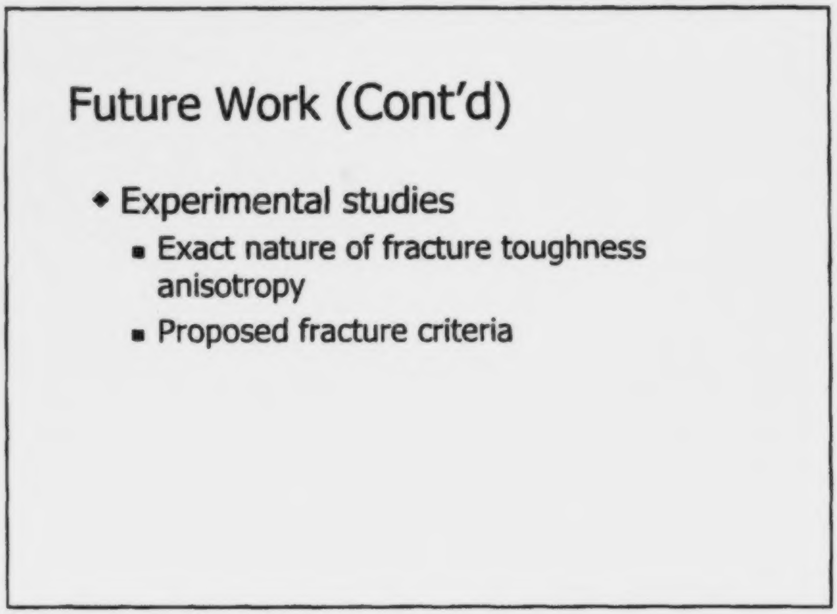

Future Work (Cont'd)

- Experimental studies
  - Exact nature of fracture toughness anisotropy
  - Proposed fracture criteria

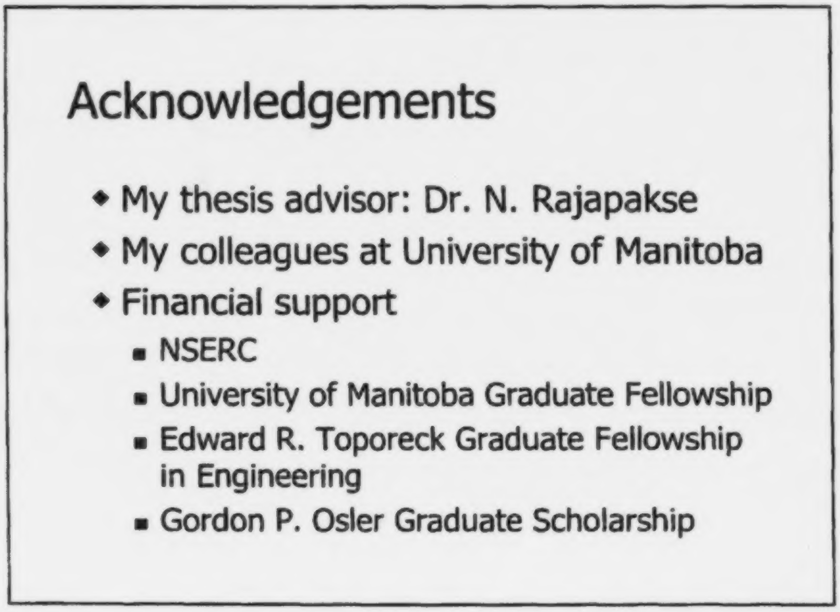

Acknowledgements

- My thesis advisor: Dr. N. Rajapakse
- My colleagues at University of Manitoba
- Financial support
  - NSERC
  - University of Manitoba Graduate Fellowship
  - Edward R. Toporeck Graduate Fellowship in Engineering
  - Gordon P. Osler Graduate Scholarship

#516425 (15)

Advances in Hydrogen Management for High Strength Steel

Yeong-Do Park[1], Chad Lensing[1], Iman Maroef[1], David L. Olson[1], and Zamir Gavra[2]

[1] Center for Welding, Joining, and Coatings Research
Colorado School of Mines, Golden, CO, USA
[2] Nuclear Research Center, Beer-Sheva, ISRAEL

ABSTRACT

Recent advances in hydrogen management for high strength steel welds are reviewed and show promise for higher performance low hydrogen welding consumables.

INTRODUCTION

High strength low alloy (HSLA) steels are known to be susceptible to hydrogen cracking. Also, the hydrogen assisted cracking in HSLA steel welds is considered to take place when all the necessary conditions for cracking are satisfied simultaneously. These conditions include the combination of unacceptable diffusible hydrogen content, high tensile stress, high hardness or a susceptible microstructure, and a temperature ranging between –50 and 100 °C [1, 2, 3, 4, 5]. One of the main practices to make a HAC resisting high strength steel weldment is to reduce the amount of diffusible hydrogen. Another common practice is the pre- or post- weld heat treatment. However, heat treatments are cost intensive and, in some critical cases, not effective. Alternative methods based on metallurgical principles have been studied and offer both for technological and economic merits.

This paper focuses on the recent advances in hydrogen management in high strength steel, particularly on three strategies. First of all, proper selection of weld metal martensite (ferrite) start temperature is introduced. Second, Irreversible weld metal hydrogen traps, such as yttrium addition, have been demonstrated to be effective in managing diffusible hydrogen content, and thus the susceptibility for hydrogen assisted cracking. The influence of the welding parameters on yttrium transferability across the welding arc and on hydrogen trapping behavior in the weld deposition is presented to assist in transferring this advancement to welding practice. Finally, the use of fluoride additions to the welding consumables also has been shown to effectively reduce the weld metal hydrogen content. This paper also discussed about the role of retained austenite in the higher strength steel weld metal in storing and supplying diffusible hydrogen in the weld deposit and its behavior during changes in service temperature is reported.

I. PROPER SELECTION OF WELD METAL MARTENSITE START TEMPERATURE.

The steel weld hydrogen content is dependent on both the hydrogen source and the ability of the weldment to transport hydrogen from the weld metal to the heat affected zone. The transport aspect becomes important because hydrogen atoms have to migrate across two different phases during cooling, mainly austenite and ferrite (martensite). Austenite (FCC) has high hydrogen solubility but low diffusion rate of hydrogen, which in contrast to ferrite and martensite that have orders of magnitude higher hydrogen diffusion coefficients than austenite [6]. As a result of the different hydrogen diffusivities between the two phases, a non-uniform distribution of hydrogen can result across the weldment depending on austenite decomposition behavior of the alloys [7,8]. Evidence of this resulting localized hydrogen distribution can be seen in the laser induced breakdown spectroscopy data for hydrogen spectral emission scans across a weldment as shown in Figure 1 [9]. The apparent localization of hydrogen in this figure may due to the effect of residual stress associated with the weld fusion line, which is known to promote attraction for hydrogen [1]. The effect of hydrogen damage is magnified when the location of the susceptible microstructures (martensite) overlaps the local high hydrogen content.

Proper alloying elements and their contents in the consumable are to be used to insure maximum hydrogen transport away from the weldment (weld metal and HAZ) during the welding thermal cycle. As an alloying dependent parameter, the martensite start temperature (M_s) can be used as an indicator for effective transport of hydrogen. A large difference between the M_s (weld metal) and M_s (base metal) will indicate difficulties in hydrogen transport in the weldment and the tendency for high localization in hydrogen contents. Thus the M_s is a measure of both the microstructure evolution and the ability to have a combination of microstructures suitable for rapid hydrogen transport [7, 8, 10, 11].

Granjon [7] introduced a conceptual model that describes how the austenite-ferrite (or austenite-martensite) phase transformation in steel weldment affects the resulting hydrogen distribution. Two cases are illustrated in Figure 2. When the austenite-martensite transformation in the fusion zone (weld metal) occurs at a higher temperature than the heat affected zone diffusible hydrogen will segregate in the heat affected zone just under the fusion line. This HAZ region is often the location of underbead cracking in high strength steel weldments. On the other hand, when the martensite transformation in the heat affected zone occurs at a higher temperature than in the fusion zone, it is possible that excess hydrogen may accumulate in the weld metal. This situation could promote weld metal hydrogen cracking or micro-fissuring.

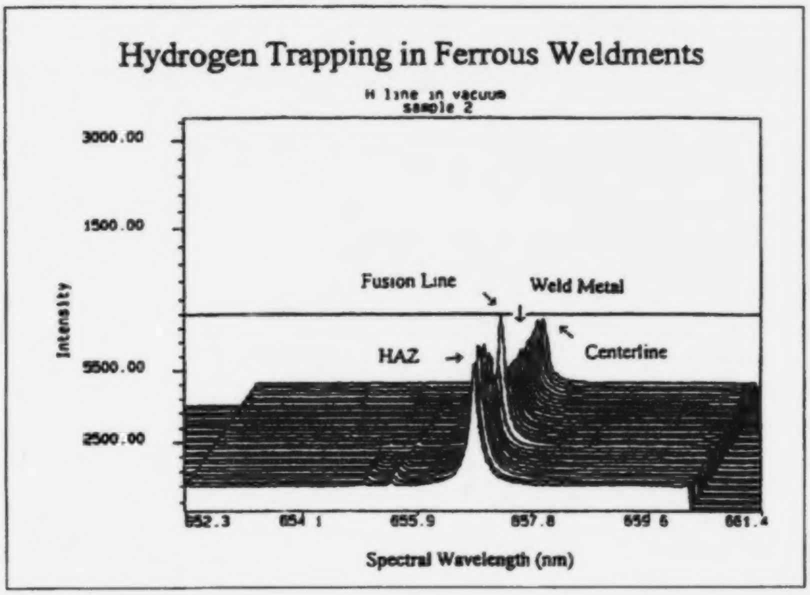

Figure 1. Non-uniform distribution of hydrogen across the center line of a weldment. Intensities of the hydrogen spectral emission are proportional to the hydrogen concentration [9].

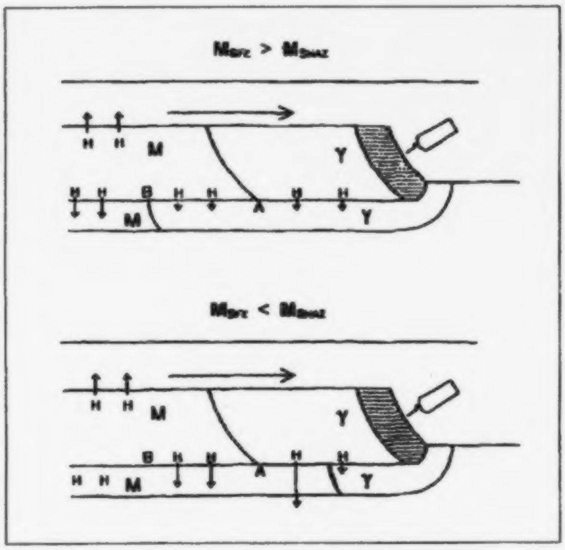
$M_{SFZ} > M_{SHAZ}$
H
H
M
Y
H
H
B
H
H
A
H
H
M
Y
$M_{SFZ} < M_{SHAZ}$
H
H
M
Y
B
H
H
H
H
A
H
H
M
Y

Figure 2. Illustration of hydrogen diffusion at different martensite start temperature for weldment and base metal [7].

CASE 1: WELD METAL WITH LOWER M_s TEMPERATURE THAN THE HAZ.

This case can be described as a situation where the weld metal is overmatched with respect to the base metal. The weld metal with higher alloying content exhibits a higher strength than the base metal, hence its martensite start temperature is depressed to below that of the base metal. While the austenite in the HAZ has begun transforming, the austenite in the weld metal remains unchanged. At this point, the HAZ immediately adjacent to the fusion zone will transport hydrogen at a higher rate than that in the weld metal. If the HAZ martensite start temperature (M_s) is sufficiently high, hydrogen will be able to migrate a significant distance into the parent metal. Especially if the transformation occurs at a moderately elevated temperature, the situation described can potentially reduce the localized hydrogen content in the hard microstructure adjacent to the fusion line, thus reducing the hydrogen cracking susceptibility. However, the hydrogen transport cannot proceed extensively until the weld metal transforms because austenite has the ability of storing high hydrogen contents but can not transport it fast enough to the fusion line. If the weld metal M_s temperature is too low, then the hydrogen transport from the weld metal is limited. Very little hydrogen can reach the heat affected zone adjacent to the fusion line that may eventually lead to weld metal cracking.

CASE 2: HAZ WITH LOWER M_s TEMPERATURE THAN THE WELD METAL.

This case can be described as a situation where the weld metal is undermatched with respect to the base metal. Since the heat affected zone transforms from austenite to ferrite/martensite at lower temperatures and at a later time than the weld metal, the HAZ becomes an austenite diffusion barrier for hydrogen transport. A high hydrogen accumulation in the heat affected zone adjacent to the fusion line results. This situation promotes underbead hydrogen cracking.

To evaluate the ability of using the martensite start temperature as a hydrogen cracking index, the diffusible hydrogen content was plotted as a function of the calculated weld metal martensite start temperature for welds made on the same high strength low alloy steel (Figure 3) [12]. Figure 3 illustrates a demarcation line between the cracked and the uncracked weldments.

From the application of the M_s temperature, it is possible to obtain a ΔM_s expression, and the sign and magnitude of this ΔM_s expression will better describe the hydrogen diffusion behavior:

$$\Delta M_s = M_{s(WM)} - M_{s(BM)}$$

If $\Delta M_s < 0$, hydrogen accumulation will be in the weld metal. If $\Delta M_s > 0$, hydrogen accumulation in the HAZ is possible and underbead cracking may occur. Selection of the alloy additions has to be determined to achieve only a slightly higher martensite start temperature of the weld metal than that of the HAZ, for maximum hydrogen transport to the base metal. In addition, the absolute martensite start temperatures of the weld metal and the HAZ should be high enough to facilitate rapid hydrogen transport in the martensite phase.
Since hydrogen is also known to migrate to regions of high residual tensile strength which

most often in the heat affective zone adjacent to the fusion line, the use irreversible traps may sufficiently immobilize the hydrogen to prevent delayed underbead cracking.

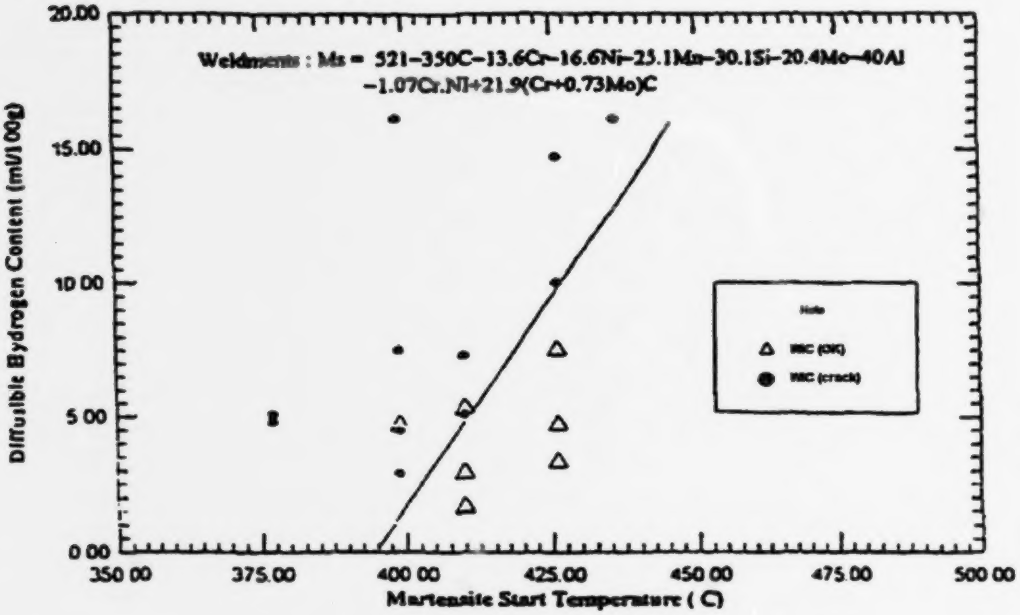

Figure 3. Conceptual illustration of cracking prediction [11].

II. DIFFUSIBLE HYDROGEN CONTROL BY IRREVERSIBLE HYDROGEN TRAPS

II-1 Rare Earth Metal Additions to the Weld Metal

It is known that inclusions in steel which contain elements on the left side of the transition metal series or rare earth elements have interfaces at which hydrogen is allowed to spend long resident times. Elemental additions, which allow for extremely long interfacial resident times, are classified as irreversible hydrogen traps. These weld metal irreversible hydrogen traps binds up the hydrogen at high temperatures and potentially reduces the diffusible hydrogen content [13, 14, 15].

The role of hydrogen trapping, especially strong traps, in high strength steel welding was investigated by adding selected rare earth metals to the weld metal. These additions were made during gas metal arc (GMA) welding using metal cored wires. The selected rare earth metals were neodymium and yttrium, which were inserted into the metal cored GMA-wire consumables in powder form as iron-neodymium or iron-yttrium intermetallic compounds. The powder size selected for the wire manufacturing was between -35 to -70 mesh.

Diffusible hydrogen measurements using ferro-yttrium additions to the metal cored wire are shown for two levels (1000 and 2000 ppm) of addition in Figure 4 [13]. This set of measurements also utilizes welding parameters which yields 1.5 kJ/mm and an argon-0.1 pct hydrogen shielding gas. Figure 4 clearly shows the direct proportionality of diffusible hydrogen reduction with higher amounts of yttrium. Almost 90 pct. diffusible hydrogen reduction can be achieved when welding with the wires that yield 2000 ppm weld metal yttrium. These results implies that addition of yttrium can be tailored to achieve a specific target value of reduction of the diffusible hydrogen content, as long as the other aspects of mechanical integrity of the weld joint are not severely affected.

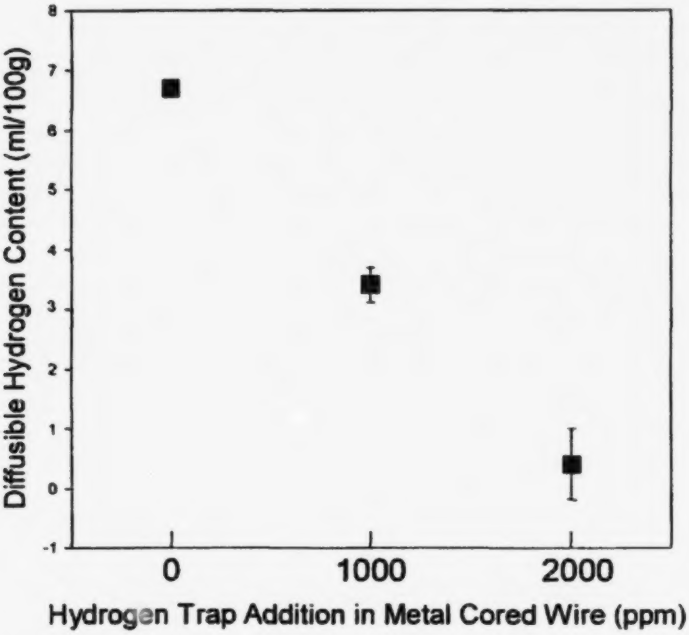

Fig. 4. Diffusible hydrogen content of HSLA steel weld sample GMA welded with mild steel formulated metal cored wires containing ferro-yttrium additions and with 0.1 pct H_2 in argon shielding gas [13].

Diffusible hydrogen measurements have effectively demonstrated the potential use of a hydrogen trapping concept in the hydrogen management of high strength steel welding. However, this measurement can not distinguish the performance of a strong trap site from a weak trap. The ice water quenching procedure stipulated by the AWS specification does not enable one to evaluate the hydrogen trapping performance of individual trap sites in the weld sample, especially above the critical hydrogen cracking temperature (100 °C). Any kind of trap will perform well in such a condition. The accelerated reduction of diffusible hydrogen that is expected from the use of a strong trap can be evaluated by the hydrogen thermal desorption analysis. This measurement technique analyzes the release of hydrogen from various trap sites at characteristic temperatures during a constant heating rate of the weld samples. The methodology applied in this analysis provides an easy way to evaluate a specific trap without excessive interference from other traps coexisting in the weld samples. Hydrogen thermal desorption analysis was used to show that the reduction is directly associated with the hydrogen trapping of the rare earth metal additions in the weld metal. It also served the purpose of showing the strength (binding energy) of the trap sites of interest, as a direct indication of its capacity to provide accelerated reduction of the diffusible hydrogen.

The hydrogen thermal desorption of yttrium containing high purity iron weld metal is shown in Figure 5.a., while that for HSLA 100 steel weld metal is in Figure 5.b [13]. Table 1 reports the chemical composition of HSLA steel and Iron used in this investigation. Also shown in these figures are hydrogen desorption of reference samples, which did not contain yttrium. Both hydrogen thermal desorptions were obtained after the measurement of diffusible hydrogen. They show the presence of hydrogen desorption with peaks at 600 °C and at 800 °C at 4°C/min (550 and 750 °C at 3°C/min). These desorption peaks indicate the presence of two kinds of strong trap sites in the weld metal. These desorption peaks also show that the reduction of diffusible hydrogen occurs because part of the total hydrogen was partitioned to the trap sites. The data suggests that on cooling, the yttrium containing weld deposits traps significant amount of the hydrogen at high temperature leaving the remaining hydrogen for the reversible traps and lattice sites. Identification of the trap sites present in the weld samples with electron microscopy and X-ray diffraction analysis indicates that the 600 °C desorption peak originated from Y_2O_3 inclusions and the 800 °C peak from Fe_2Y second phase.

Table I- Chemical Composition of HSLA Steel and Armco Iron Base Metal the Each Sample (wt-%)

	C	Mn	P	Si	Cr	Ni	Mo	Cu	Al	V	N	Ti
Armco Iron	0.004	1.19	0.009	0.06	0.03	0.007	0.003	0.014	0.006	<0.002	0.004	<0.002
HSLA Steel	0.06	0.83	0.01	0.35	0.57	3.42	0.62	1.64	–	-	–	-

The hydrogen thermal desorption analysis has shown the high binding energy of the rare earth metal associated trap sites, as indicated by high desorption peak temperature. It also shows the potential use of the rare earth metal additions to provide accelerated reduction of diffusible hydrogen during welding cooling cycle. However, evaluation of these trap sites needs to be further pursued to assess the kinetics aspects of hydrogen release and trapping of these trap sites. The binding energy only relates to the driving force of the hydrogen capturing, but not the rate.

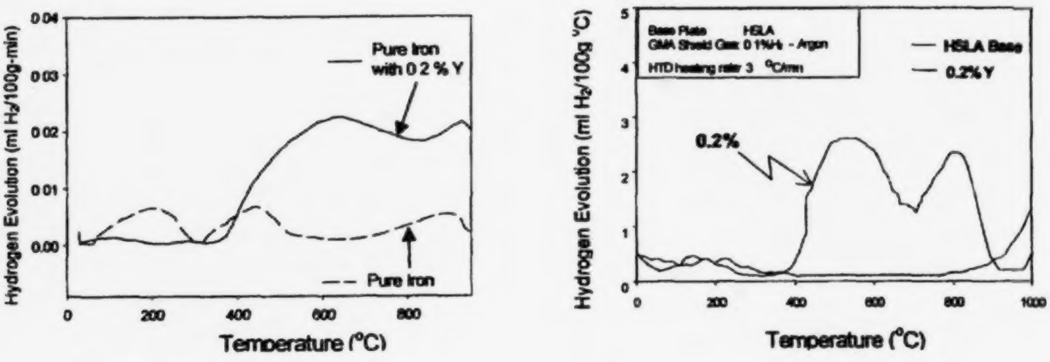

(a) (b)

Fig. 5. Hydrogen thermal desorption of weld metal GMA welded with 0.5 pct. H_2 in argon shielding gas and 600 ppm addition in the weld metal. (a). High purity iron base metal (4 °C/min) (b). HSLA steel base metal (3 °C/min) [13].

II-2. Influence of Welding Process Parameters on the Hydrogen Trapping Effectiveness of Yttrium Addition

Yttrium ferro-additions have demonstrated the significant reduction in diffusible hydrogen content. Experiments were performed on pure iron and high strength low alloy steel weld metal and the proper yttrium content for its effective use has been determined. Also, the recovery of yttrium from the welding consumable to the weld pool has been measured for these experimental wires. The optimum set of welding process parameters for the effective use of the yttrium additions has been determined and demonstrated [16].

The addition of yttrium in the welding arc allows lower voltages and currents for the welding arc due to the lower ionization potential of yttrium than that of argon. These welds were made with 0.1 percent hydrogen in argon shield gas and the welding voltage at 30 volts. The effect on yttrium additions to the amount of heat, i.e. heat input, can be seen in figure 6. The heat inputs ranged from 1.3 to 2.7 kJ per millimeter. The heat input is an indication of the cooling rate that the weld pool will experience. At slower cooling rates, or larger heat inputs, more time is available for diffusion of hydrogen to be trapped by yttrium type traps and the effusion of hydrogen from the weld pool.

The effect of adding 650 ppm of yttrium was to increase the diffusible hydrogen content, as shown in Figure 6. This increase suggests that yttrium reacted with all of the available oxygen and the law of mass action for the oxygen-hydrogen reaction results in higher diffusible hydrogen content. With 3000 or 6000 ppm yttrium additions in the metal cored wired, there was sufficient yttrium to overcome the oxygen-hydrogen inverse relationship for the water reaction. The formation of the yttrium oxide inclusion is readily available for hydrogen trapping thus reducing the diffusible hydrogen content to low levels.

A metal transfer mode plot (Figure 7) was made for gas metal arc (GMA) welding process with a corresponding mapping of diffusible hydrogen contents. The ANSI/AWS A4.3-93 standard was used with gas chromatography to measure diffusible hydrogen contents of HSLA 100 steel welds. Metal cored steel wires with yttrium as a weld metal hydrogen trap were used. Depending on yttrium and sulfur contents yttrium oxide and/or yttrium oxy-sulfide inclusions form in the weld metal. The metal transfer modes were observed and recorded during welding and mapped accordingly with the welding voltage and current. Heat input ranged from 1.4 to 3 kJ/mm and shows a range less than one up to 4 ml of hydrogen per 100 g weld deposit. The effects of voltage, current, travel speed, polarity, and oxygen levels have also been examined. An optimum operating window is shown for welds made resulting in less than one ml of hydrogen (per 100 g deposit) content as shown in Figure 7. In the spray mode, yttrium is effectively transferred across the arc and has the necessary time during transfer across this arc for this size of droplet to produce sufficient yttrium compounds to serve as hydrogen trapping site.

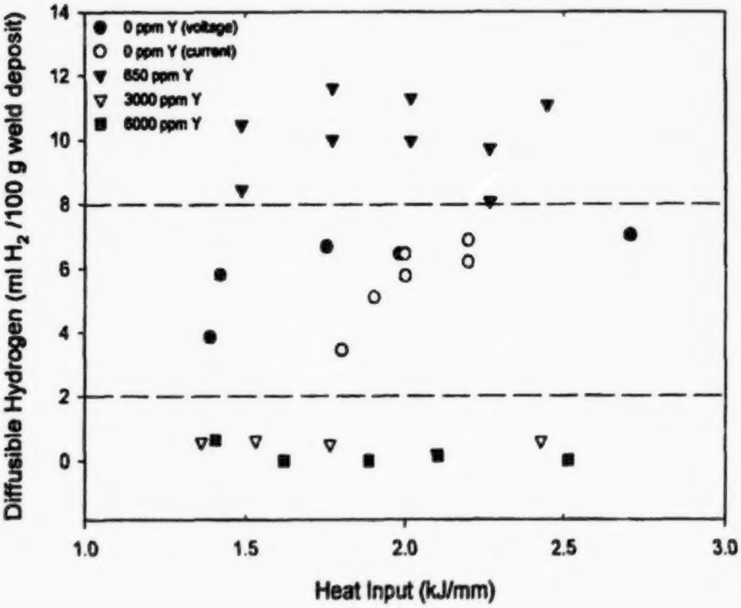

Figure. 6 The effect of heat input on the diffusible hydrogen content with yttrium hydrogen trap additions to metal cored steel wire. Welds made with 0.1 percent hydrogen in argon shield gas on high strength low alloy steel baseplate [16].

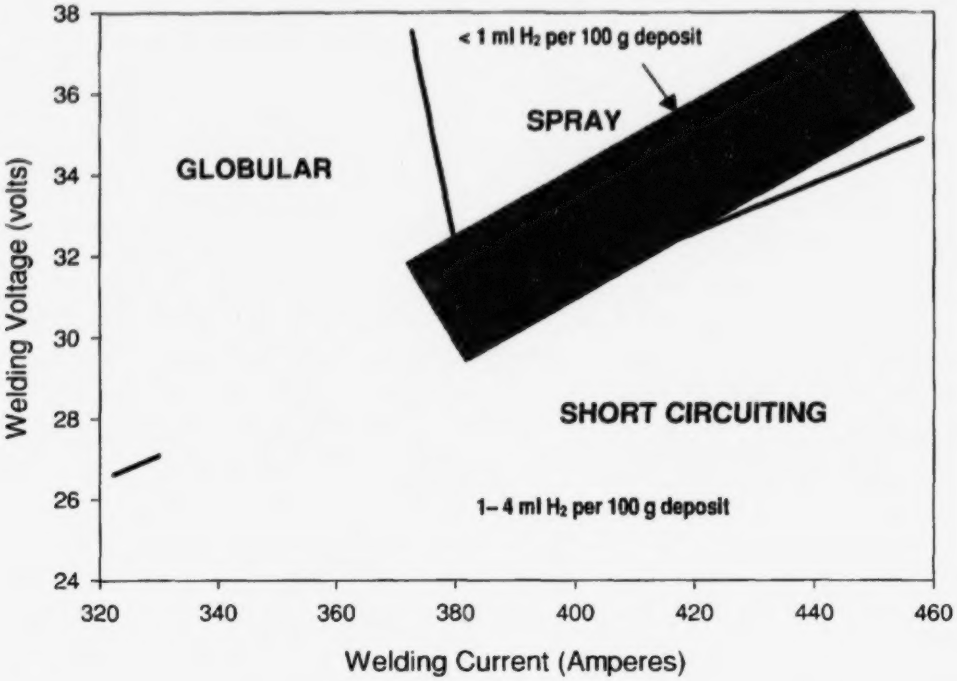

Figure 7. Metal transfer mode – weld metal diffusible hydrogen content plot on a GMA welded HSLA steel with HSLA metal cored steel wire containing 1600 ppm yttrium [16]

Thermal desorption curve for HSLA 100 steel welds made with yttrium additions to a HSLA steel metal cored wire with zero and four percent oxygen in a shielding gas of argon-0.1% hydrogen shows less trapped hydrogen for the four percent oxygen addition. The welds made with no oxygen additions have three peaks. Peak 1 is for a typical of microvoids (a reversible trap), Peak 2 is for a yttrium oxide trap (an irreversible trap), and Peak 3 is for yttrium-oxy-sulfide trap (an irreversible type trap). HSLA steel welds were made at 25 volts and with a wire feed speed of 240 ipm. High oxygen content shows a higher trapped (residual) hydrogen content in the weld metal and also the formation of primarily yttrium oxide inclusions. An increase in the hydrogen content suggests that increasing the shielding gas oxygen content significantly alters the size and distribution of weld metal inclusions and thus the available interfacial trap sites.

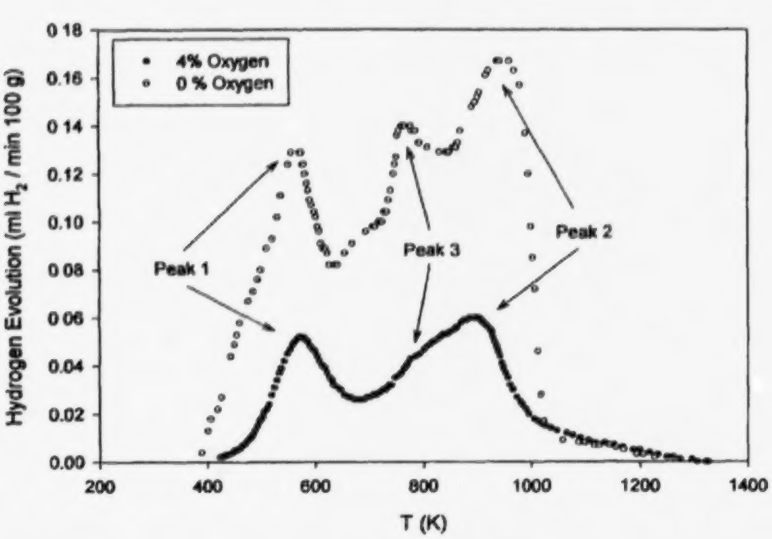

Figure 8. Thermal desorption curve for spray and globular transfer mode. Peak 1 is associated with microvoids; Peak 2 is yttrium oxy-sulfide, and Peak 3 as yttrium oxide [16].

III. HYDROGEN REDUCTION WITH FLUORIDE ADDITIONS

Hydrogen absorption can be minimized through the formation of water vapor or hydrogen fluoride in a thermo-chemical reaction with oxygen or fluorine, respectively, in the welding plasma. Increasing fluorine gas will decrease the amount of hydrogen available to enter the weld deposit as shown in Fig 9. These gases will be generated from selected fluxes that easily decompose during arc heating.

Fluorspar (CaF_2) is believed to dissociate at high temperatures to produce fluorine, and consequently shifts the reaction in Equation 1 to the right, resulting in reduced hydrogen in the arc.

$$F_2 + H_2 \leftrightarrows 2HF \qquad \text{(Eq. 1)}$$

However, it is also recognized that the decomposition of CaF_2 is not particularly active so that most of CaF_2 remains in the slag. Therefore, researchers have been searching for other fluorides more efficient in weld metal hydrogen reduction [17, 18].

Tsuboi et al. [19] observed a reduction of diffusible hydrogen with the addition of Na_3AlF_6 to the welding flux. At eight percent fluoride additions, the diffusible hydrogen level was 4 ml/100g of the deposited metal, which was thirty percent lower than that obtained using CaF_2. Pokhodnya et al. [18] also reported the effectiveness of complex fluorides such as Na_2SiF_6, Na_2TiF_6, K_2SiF_6, and K_2TiF_6 by using Flux Cored Arc Welding (FCAW). Similarly, Matsushita and Liu investigated diffusible hydrogen control in steel weld metal with fluoride additions in welding flux. Figure 10 illustrates the results of diffusible hydrogen content in the steel weld metal deposited with experimental wires that contained 5% K_3AlF_6, 7.5% K_3AlF_6, and 10% K_3AlF_6 additions. The addition of K_3AlF_6 was found to be more effective than that of CaF_2 for hydrogen reduction [21]. Johnson and Liu [20] reported that MnF_3 was able to reduce diffusible hydrogen in welds performed on primer-coated steel plates.

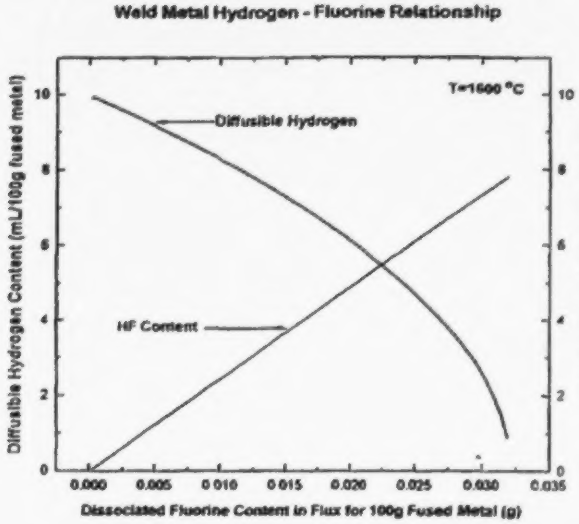

Weld Metal Hydrogen - Fluorine Relationship

Figure 9. Thermo-chemical reaction between fluorine and hydrogen in the welding plasma [2].

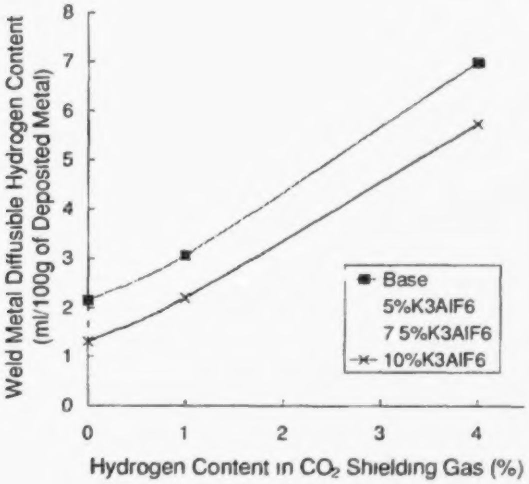

Figure 10. Steel weld metal diffusible hydrogen content given by Base 5% K_3AlF_6, 7.5 K_3AlF_6, and 10% K_3AlF_6 wires [21].

IV. ROLE OF RETAINED AUSTENITE IN HYDROGEN MANAGEMENT

Retained austenite was found to be an intraphase hydrogen trapping site which has relatively high binding energy. To identify retained austenite as an intraphase hydrogen trapping site, four samples with different austenite volume fraction were prepared: AISI type 304 stainless steel, super duplex stainless steel, dual phase steel (12 vol. pct. retained austenite), high strength low alloy (HSLA) steel weld deposit (4 vol. pct. and 0 vol. pct. retained austenite). Each of the samples was charged with 99.9 purity of hydrogen by using gaseous charging. The thermal desorption analysis was employed to observe the hydrogen trapping and detrapping behavior [22, 23, 24].

The hydrogen desorption of the four samples are shown in Figure 11. As clearly shown in this figure, all of the hydrogen desorption has a peak approximately at 600 °C. The corresponding amount of desorbed hydrogen decreased as the volume fraction of austenite decreased. The relationship between the amount of the desorbed hydrogen and the volume fraction of austenite is linear, as shown in Figure 12. These results led to a conclusion that retained austenite behaves as a strong hydrogen trap whose trapping capacity is directly proportional to its volume. Retained austenite is considered as a bulk hydrogen trap which may also contain more than one kind of hydrogen trap sites besides its lattice sites [22].

The exact nature of the interaction between hydrogen and retained austenite, which is manifested by such a high thermal desorption, is not clearly understood. It is worth noticing that there is a different situation of hydrogen desorption between the AISI 304 stainless steel sample and the HSLA steel weld sample. In the former sample, austenite remained stable during the course of thermal heating. Hydrogen seemed to be released from some type of trap sites, most likely dislocations and grain boundaries. Also, hydrogen degassed out of the sample by diffusing sluggishly through the stable austenite phase. In the HSLA steel sample, hydrogen may be released simply due to the progression of retained austenite dissolution during the course of thermal heating. Also in the HSLA steel sample, hydrogen transports more easily though the ferrite matrix. However its desorption was very similar to the AISI 304 stainless steel as seen by its similar peak temperature. An ongoing study is still being carried out to clarify the hydrogen-trapping characteristic of retained austenite [22].

Retained austenite is not only a diffusion-controlled trap but also a meta-stable phase. The dual phase steel (12 vol. pct. retained austenite) was investigated to observe the effects of reduced temperature by using thermal desorption analysis. When the reduced temperature were applied on hydrogen charged specimens, the thermal desorption analysis exhibited a shifting of hydrogen peak to lower temperature as shown in Figure 13(a). The measured retained austenite content as function of quenching temperature is shown Figure 13(b). This result suggests that microstructural transformation associated with changes in service conditions can result in a high diffusible hydrogen content in the resulting martensite phase, which is known as the most susceptible microstructure to hydrogen assisted cracking (HAC). Demonstration of the hydrogen trapping capacity and the metastability of retained austenite suggests that the amount of allowable retained austenite needs to be related to the amount of hydrogen pick up and the expected service condition [23].

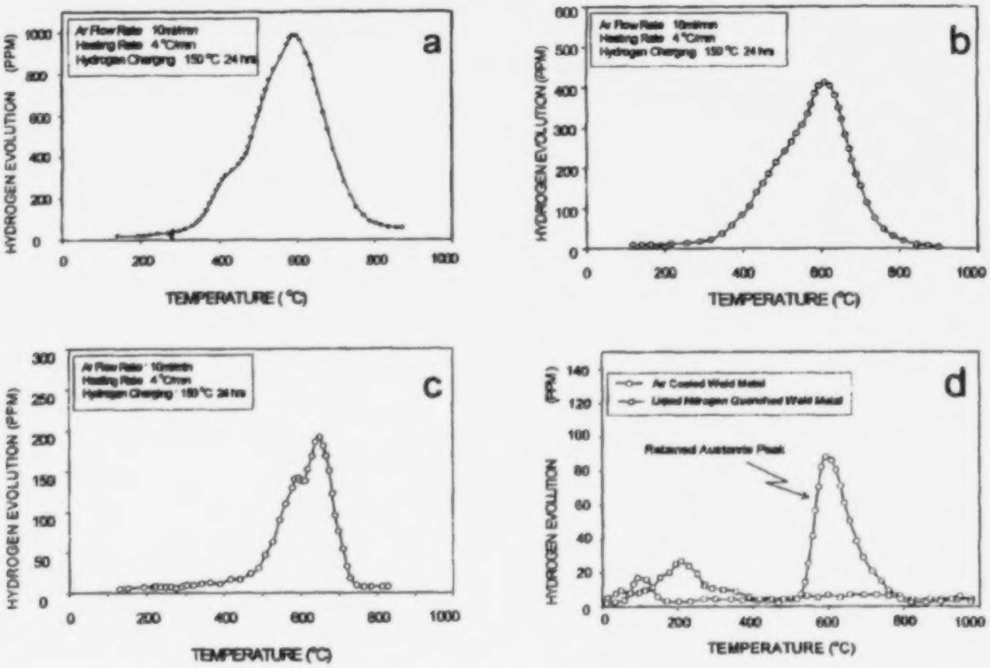

Fig. 11. Thermal desorption analysis for dual phase steel which is quenched in liquid nitrogen after charging; a-type 304 stainless steel b. superduplex stainless steel c. dual phase steel d. HSLA weld metal [22].

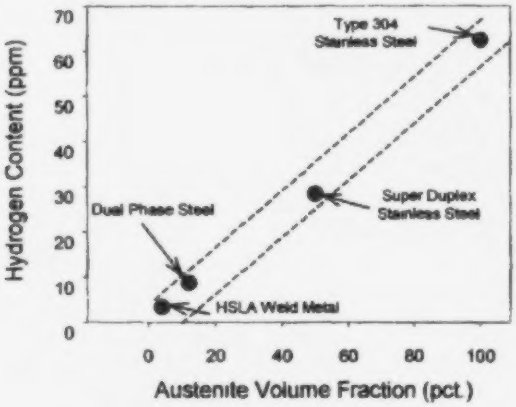

Fig. 12. The relationship between the amount of hydrogen release by desorption with the volume fraction of austenite (22).

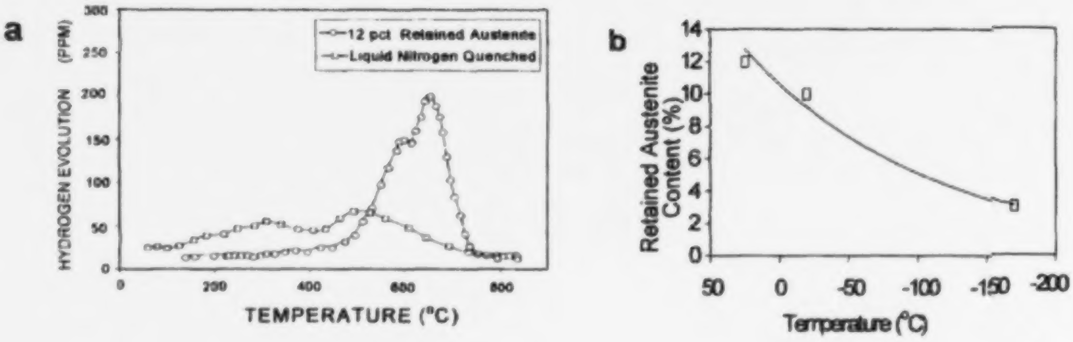

Figure 13. a-Thermal desorption analysis for dual phase steel which is quenched in liquid nitrogen after charging. b-The measured retained austenite content as function of quenching temperature [23].

SUMMARY

Diffusible hydrogen content in high strength low alloy steels welding can be better managed with modifications to the low hydrogen welding consumables. The welding consumable alloy content needs to allow the weld metal to transform from austenite to ferrite/martensite at slightly higher temperature than the base metal does. This practice will allow for the best dispersal of hydrogen from the weld deposit and minimizing the tendency of localizing the hydrogen in the heat affected zone at the fusion line. The use of weld metal hydrogen traps will both reduce the total diffusible hydrogen content and also minimize the hydrogen distribution near the fusion line. The use of complex metal fluorides in the welding consumable to achieve small but sufficient amounts of fluorine to the welding plasma can produce hydrogen fluoride, thus reducing the amount of hydrogen source available for the weld pool or the resulting the weld deposit. Also, the presence of retained austenite was found to influence the ability to control weld metal hydrogen in high strength low alloy steels.

CONCLUSIONS

1. Three modifications to low hydrogen welding consumables have been suggested to be use separately or all together to assist in achieving very low diffusible hydrogen contents in high strength low alloy steel welds.

2. Retained austenite in weld metal is a unpredictable hydrogen source, which upon austenite decomposition, due to thermal experiences may deliver unacceptable local amounts of hydrogen to hard phase transformation products and may resulting in increase of hydrogen cracking susceptibility.

Acknowledgements : The authors acknowledge and appreciate the support of the U.S. Army Research Office.

REFERENCES

1. N. Yurioka, and H. Suzuki, "Hydrogen Assisted Cracking in C-Mn and Low Alloy Steel Weldments", International Materials Review, 35 (4): 217 – 249, (1990).
2. D.L Olson, I. Maroef, C. Lensing, R.D. Smith, W.W. Wang, S. Liu, T. Wildeman, and M, Eberhart, "Hydrogen Management in High Strength Steel Weldments" Proc. the Joint Seminar, Hydrogen Management in Steel Weldments. eds. J.L. Davidson, and D.L. Olson, pp. 1-20. WTIA., (1996).
3. I. Maroef, D.L. Olson, M. Eberhart, G.R. Edwards, " Weld Metal Hydrogen Trapping", Review paper Submitted to International Materials Review, ASM Intrl. Materials Park, OH, (2001).
4. M.D. Clark and D.L. Olson, "The Role of Welding Parameters in Hydrogen Management", Proc. Of Hydrogen Management of High Strength Steel Welds, pp. 215-228, CANMET, Ottawa, Ontario, Canada, (1999).
5. W.J. Engelhard, D.L. Olson, and B. Mishra, "Dissolution of Gaseous Hydrogen in High Strength Steels at Elevated Temperature", Conf. Proc. of Advanced and Specialty Materials, pp. 133-140, ASM, Materials Park, OH (1998).
6. T.H. Bollinghaus, H. Hoffmeister, and C. Middel, "Scatterbands for Hydrogen Diffusion Coefficients in Steels Having a Ferritic or Martensitic Microstructure and Steels Having an Austenitic Microstructure at Room Temperature", Welding in the World (UK), vol. 37, no. 1, pp. 16-23, (1996).
7. H. Granjon, "Cold Cracking in Welding of Steels", Intl. Symposium on Cracking and Fracture in Welds, Conf. Proc. Japan Welding Society, IB, 1.1., (1971).
8. B.A. Graville, "Hydrogen Cracking Sensitivity of HSLA Steels", The Metallurgy, Welding and Qualification of Microalloyed (HSLA) Steel Weldments, 127, (1990).
9. R.D. Smith II, D.L. Olson, T.R. Wildeman, and D.K. Benson, "Fiber Optic Sensor for Diffusible Hydrogen Determination in High Strength Steel," Proceedings from Photonics West 2000, SPIE, San Jose, California, pp. 174-184, (2000).
10. W.W. Wang, S. Liu, and D.L. Olson, "Consequences of Weld Undermatched and Overmatching: Non-Uniform Hydrogen Distribution", Proceedings of OMAE, vol. III-Materials Engineering, pp. 403-409, Florence, Italy, (1996).
11. W.W. Wang. R. Wong, S. Liu, and D.L. Olson, "The Use of Martensite Start Temperatures for Hydrogen Control", Proc. of Shipbuilding Welding Conf., TMS, Cleveland, OH, October, pp. 17-31, Weld Automation in Shipbuiling, TMS, Warrendale, PA, (1996).
12. D.L. Olson, S. Liu, W. Wang, R. Pieters, and S. Ibarra, "Martensite Start Temperature as a Weldability Index", in Conf. Proc. On "Research Trends in Welding Science and Technology", pp. 615-620, Gatlinburg, Tennessee, ASM Intl., Materials Park, OH, (1996).
13. I.S. Maroef, Y.D. Park, C. Lensing, A. Landau, and D.L. Olson, "Hydrogen Trapping of High Strength Steel Weld Metal", ASM International, Materials Park, OH, Joining of Advanced and Specialty Materials II (USA), pp. 284-291, Apr. (2000).

14. I.S. Maroef and D.L. Olson, "Fundamental Aspects of Hydrogen Trapping in Steel Weld Metal", in Joining of Advanced and Specialty Materials II, ASM International, Materials Park, OH, Joining of Advanced and Specialty Materials II (USA), pp. 227-235, Apr. (2000).
15. I.S. Maroef and D.L. Olson, "The Effect of Composition, Hydrogen Traps and Thermal on Hydrogen and Distribution in Steel", ASM International, Materials Park, OH, Joining of Advanced and Specialty Materials II (USA), pp. 543-551, Apr. (2000).
16. C. Lensing, "Utilization of Yttrium Hydrogen Trap and Welding Parameters in Managing Hydrogen Content in Welding High Strength Low Alloy Steel", Ph. D. Thesis, Colorado School of Mines, (2001).
17. S. Liu, D.L. Olson, and S. Ibara, "Electrode Formulation to Reduce Weld Metal Hydrogen and Porosity", Intl. Conf. On Offshore Mechanics and Arctic Engineering, ASME-OMAE, pp. 291-298, (1994).
18. I.K. Pokhodnya, "Hydrogen behavior in welded joints. E.O. Paton Electric Welding Institute, National Academy of Sciences of Ukraine, Ukraine, Kiev, (1996).
19. J. Tsuboi, S. Nakano, and K. Sato, "The Behavior of Hydrogen in Arc Welding." The Welding Journal of Japan, 42-3, pp. 189-201, (1973).
20. K.S. Johnson, S. Liu, and D.L. Olson, "Hydrogen Control and Microstructural Refinement of Structural Steel Welds Using Fluoride-Containing FCAW Electrodes", Proc. 17the Intern. Conf. On Offshore Mechanics and Arctic Engineering, ASME/OMAE, Paper OMAE-98-2801, Lisbon, Portugal, July 6-10, (1998).
21. M. Matsushita and S. Liu, "Hydrogen Control in Steel Weld Metal by Means of Fluoride Additions in Welding Flux", Welding Journal, 79(10), pp. 295s-303-s, (2000).
22. Y.D. Park, I. Maroef, A. Landau, and D.L. Olson, "Hydrogen Trapping and Cracking Susceptibility with Different Restraint Stress Severity in Retained Austenite of High Strength Steel Welds", 20th ASM Heat Treating Society Conference 9-12 October, St. Louis, Missouri, USA, (2000).
23. Y.D. Park, I. Maroef, A. Landau, and D.L. Olson, "Retained Austenite as a Hydrogen Trap in Steel Welds", Manuscripts Accepted to Welding Journal, (2001).
24. Y.D. Park, A. Landau, I.S. Maroef, G.R. Edward, D.L. Olson, "The Role of Retained Austenite in the Hydrogen Management of High Strength Steel Welds", ASM International, Trends in Welding Research (USA), pp. 31-36, June (1998).

#516426 ⑰

Failure Analysis of Nickel Aluminium Bronze Hydraulic Couplings

by

D.P. Edwards, S.P. Lynch, J.L. Davidson and R.B Nethercott,
Aeronautical and Maritime Research Laboratory, Australia.

Abstract

A significant proportion of nickel aluminium bronze couplings (Cu-5Ni-5Fe-10Al) used in a Cu-Ni hydraulic piping system, manufactured from extruded barstock and of several designs suffered cracking after 1-4 years of service. Cracks first appeared in a design that incorporated a crimped lock nut. Couplings were subjected to hydraulic pressure and pressure fluctuations. The internal surfaces of couplings were exposed to hydraulic fluid and the external surfaces were exposed to either seawater or air. Cracks initiated from a variety of sites within the coupling body including threads and sharp radii and occurred from both external and internal surfaces, and propagated in longitudinal and circumferential directions.

Microstructures ranged from a fine grained α-matrix with a dispersion of κ-phases to larger grain sizes with lamellar κ_{III} at grain boundaries and dispersed κ_{II} and κ_{IV} within the α-matrix. Cracking failures were observed across the full range of microstructures examined. Fracture surface observations revealed (due to changes in the degree of corrosion) clear evidence of progression markings on couplings exposed to seawater, whereas for couplings cracked in air, progression markings were less distinct.

SEM examination of fractures showed that intergranular cracking occurred for all coupling designs and crack initiation sites, regardless of whether cracking occurred in air or seawater. Observations of couplings cracked in air showed regions of faint progression markings and fatigue striations on the intergranular facets together with colonies of κ-phase precipitates and depressions from precipitate sites. Analysis of fractures using surface-analytical techniques (e.g. XPS) failed to detect any contaminants that might have promoted intergranular cracking.

Laboratory fatigue tests using compact-tension specimens have in air reproduced the observed fracture surface in limited regions, but fracture was predominantly transgranular. Exposure of specimens to ammonia environments, known to sometimes promote intergranular cracking in copper-based alloys, produced a tarnished transgranular fracture surface in contrast to the contamination-free intergranular fracture surfaces produced in service.

The evidence overall indicates that failure occurs by fatigue. In the case of crimped couplings, high residual tensile stresses are believed to develop within the lock nut and be responsible for the reduction in the effective fatigue life. However, a source of cyclic stress within the piping system responsible for the fatigue cracks within couplings has not been found. Strain gauging of couplings and Cu-Ni pipe has failed to measure any significant cyclic strains in service. Under consideration is the possibility that the pumps and motors within the hydraulic system are the source of low-amplitude, ultra-high frequency loading or resonances that are transmitted by the hydraulic fluid.

To reduce the likelihood of further coupling failures a new wire-lock nut system has since replaced all crimped couplings. Recommendations have been made that NAB couplings could be replaced with stainless steel on the basis that it may have improved fatigue strength in the very high cycle regime and a higher damping capacity.

Failure Analysis of Nickel Aluminium Bronze Hydraulic Couplings.

D.P Edwards, S.P. Lynch, J.L Davidson, R.B. Nethercott

Aeronautical and Maritime Research Laboratory

Maritime Platforms Division

Australia

DEPARTMENT OF DEFENCE
DEFENCE SCIENCE & TECHNOLOGY ORGANISATION DSTO

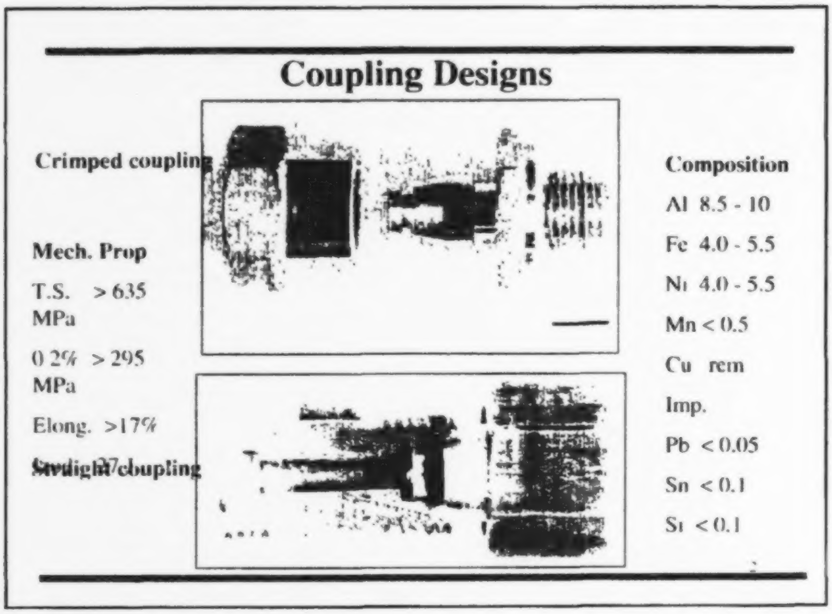

Coupling Designs

Crimped coupling

Mech. Prop

T.S. > 635 MPa

0.2% > 295 MPa

Elong. >17%

[illegible]

Straight coupling

Composition

Al 8.5 - 10

Fe 4.0 - 5.5

Ni 4.0 - 5.5

Mn < 0.5

Cu rem

Imp.

Pb < 0.05

Sn < 0.1

Si < 0.1

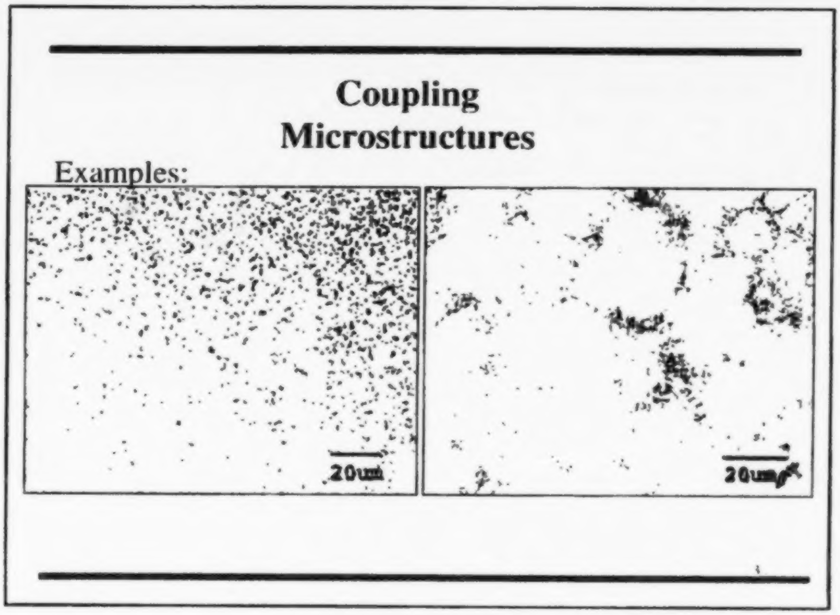

Coupling Microstructures

Examples:

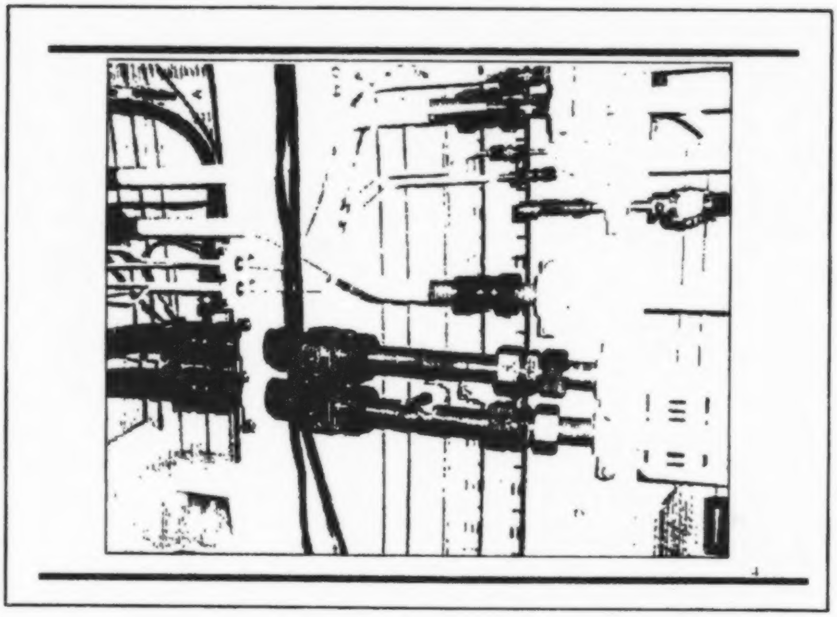

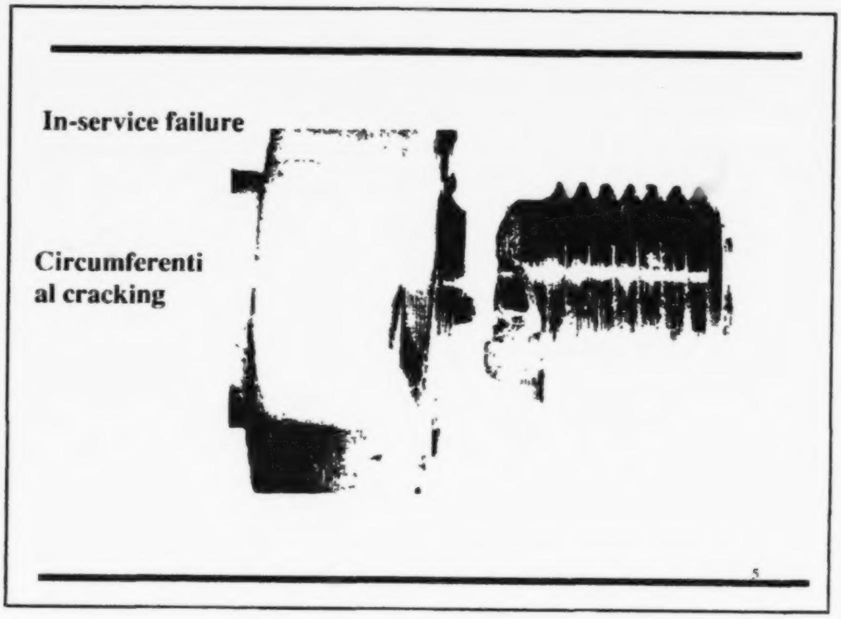

In-service failure

Circumferential cracking

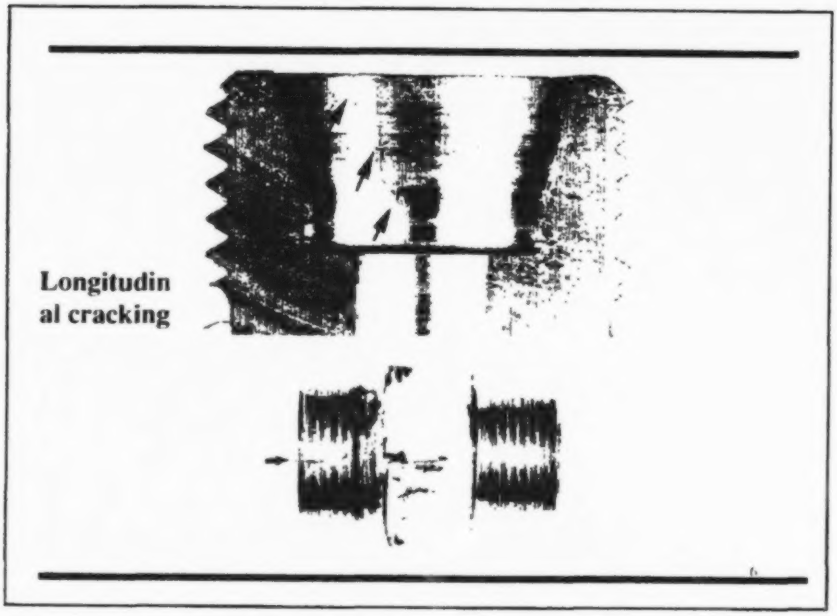

Longitudinal cracking

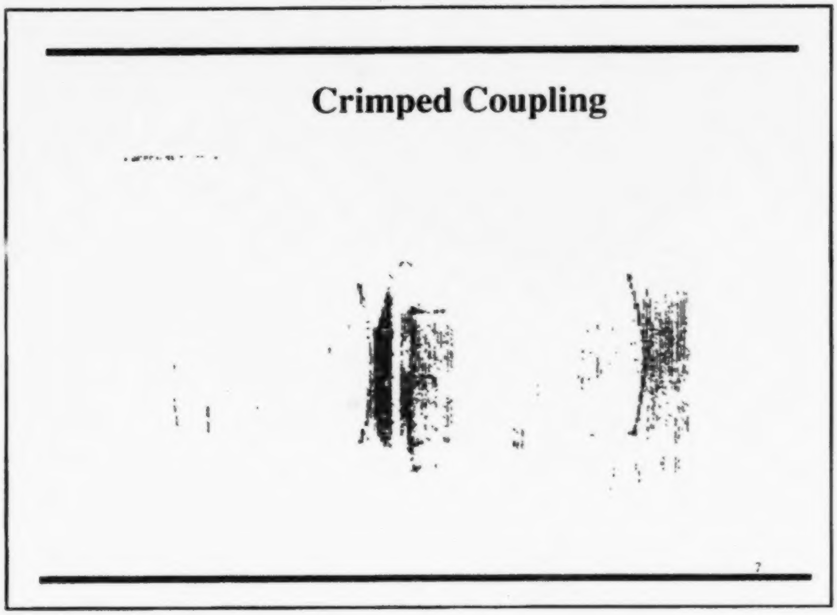

Crimped Coupling

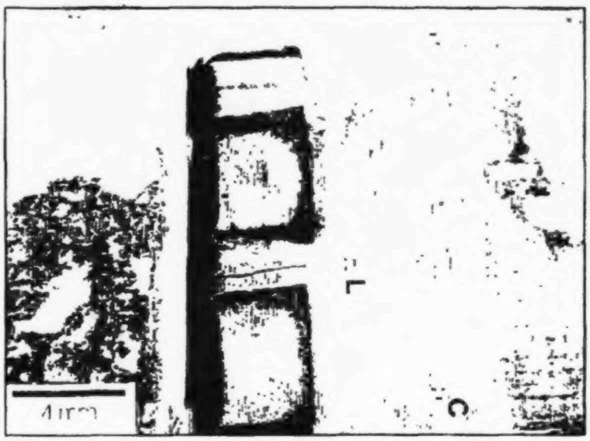

Crack Initiation Sites

Straight and Male-stud coupling

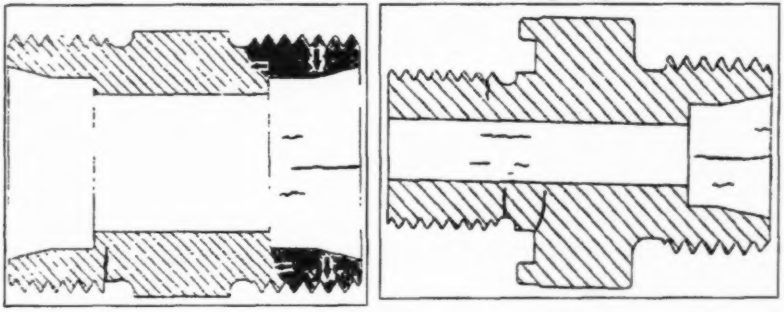

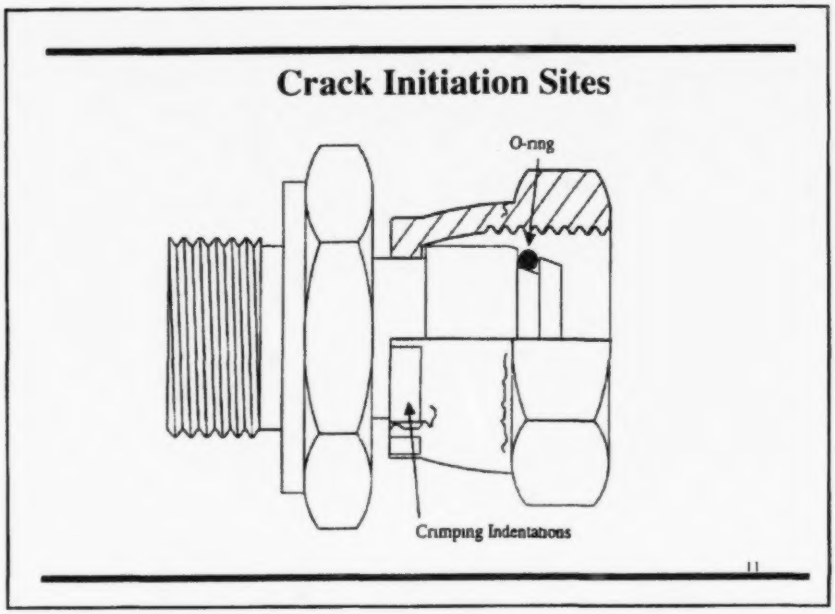

Crack Initiation Sites

O-ring
Crimping Indentations

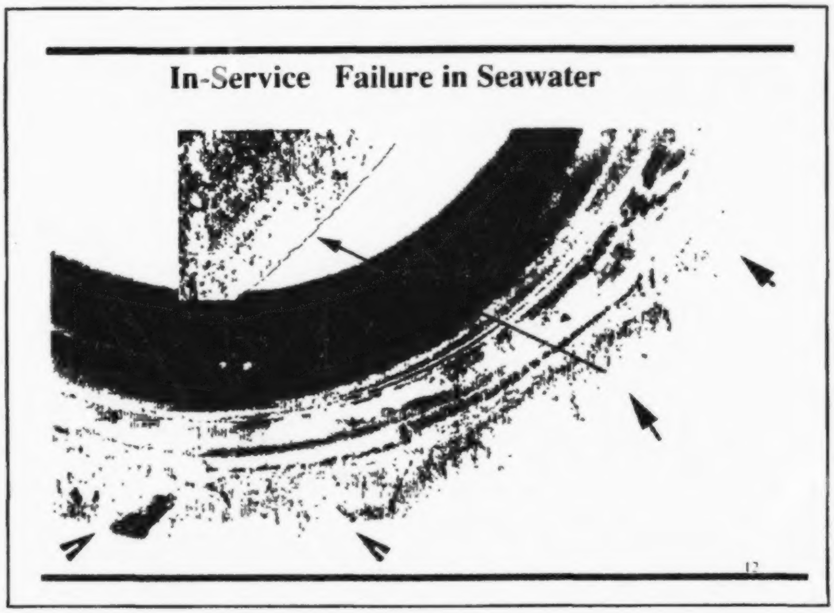

In-Service Failure in Seawater

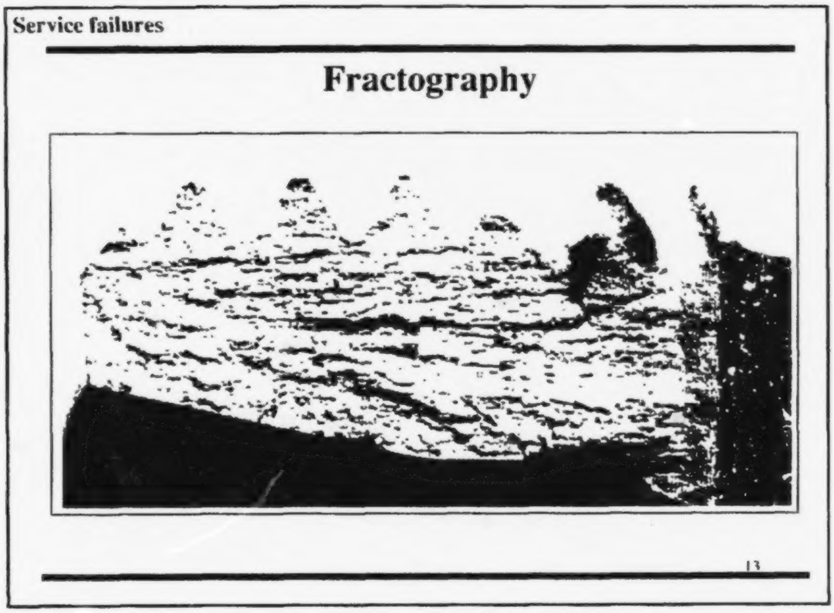

Service failures

Fractography

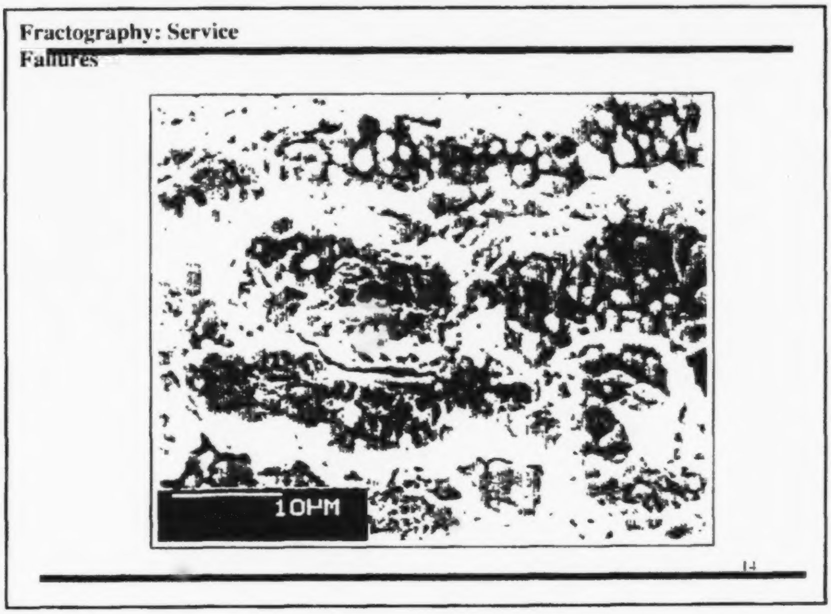

Fractography: Service Failures

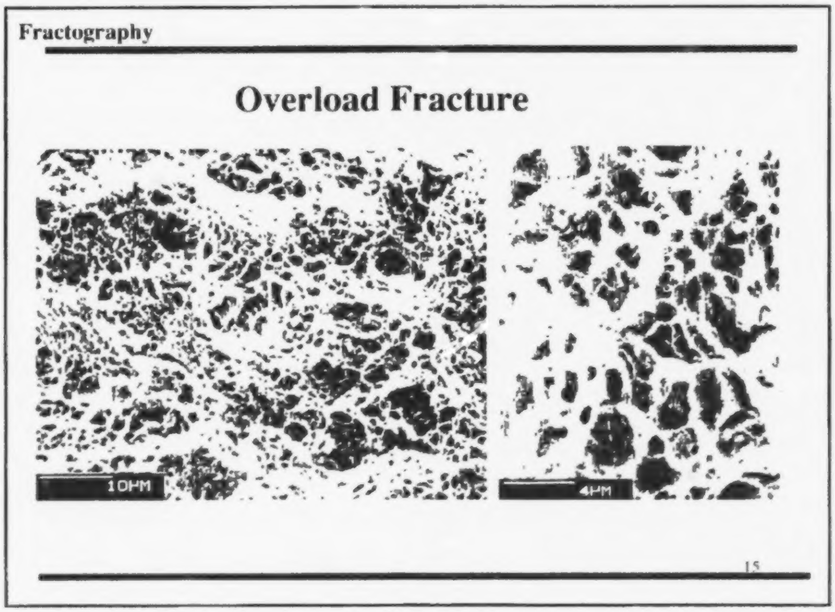

Fractography

Overload Fracture

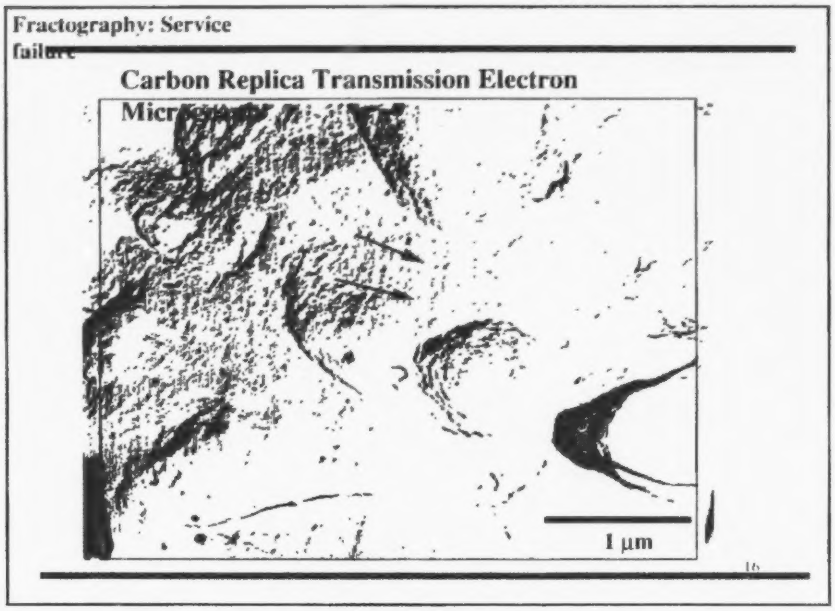

Fractography: Service failure

Carbon Replica Transmission Electron Micr

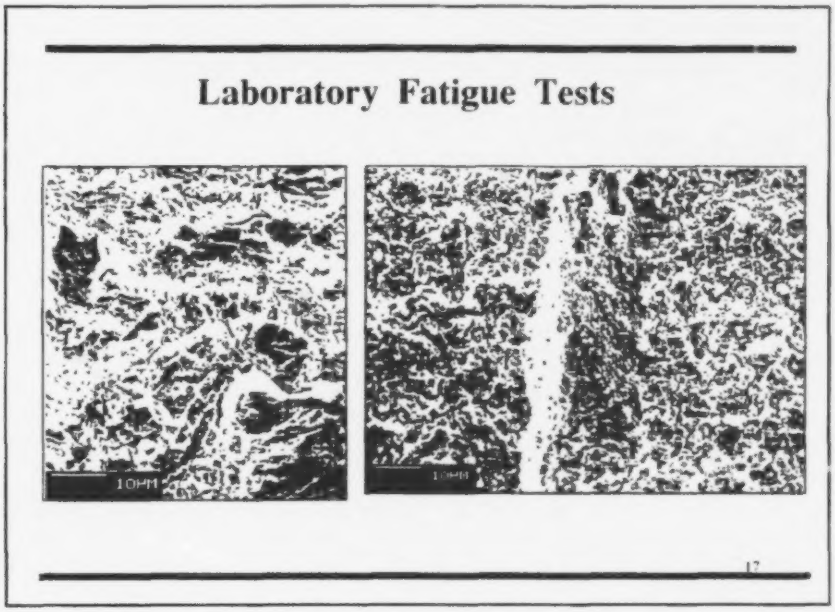

Laboratory Fatigue Tests

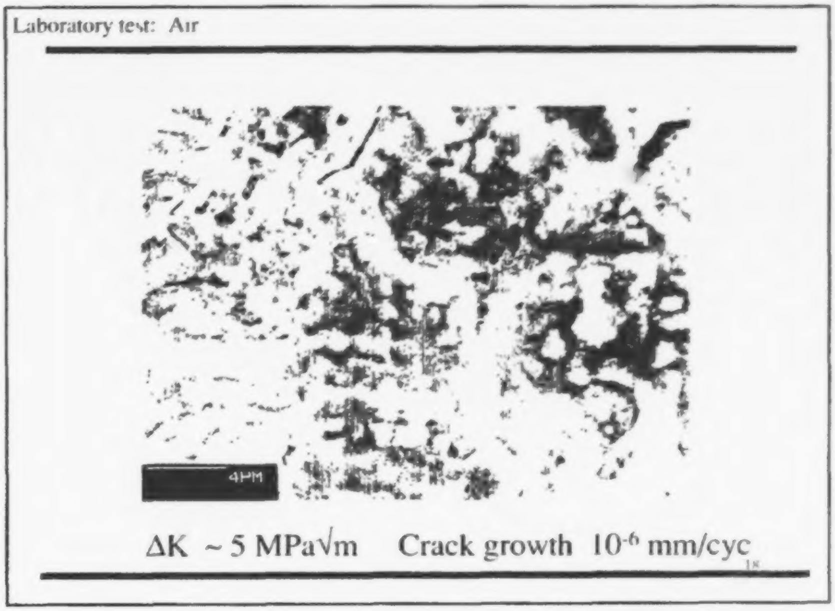

Laboratory test: Air

$\Delta K \sim 5$ MPa$\sqrt{m}$ Crack growth 10^{-6} mm/cyc

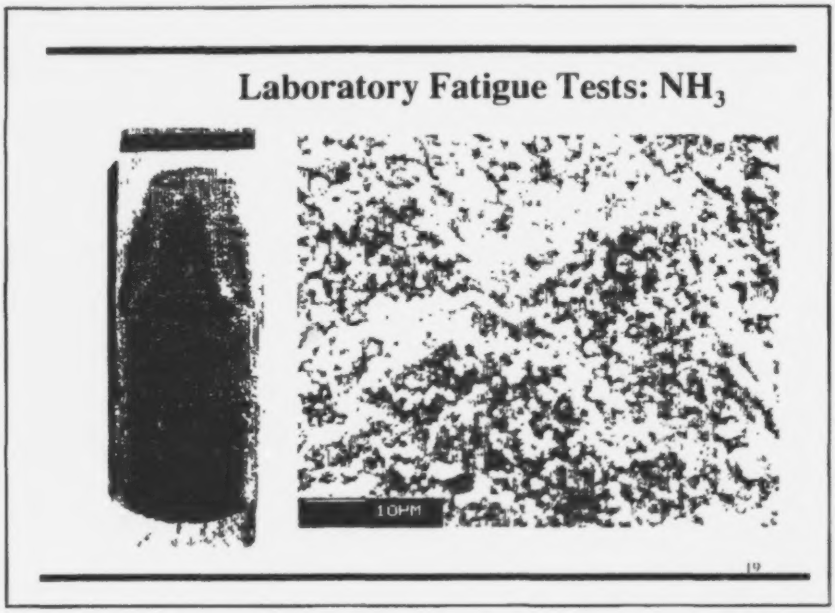

Laboratory Fatigue Tests: NH_3

Summary : Mode and Cause

Failure Mode: Fatigue (intergranular)
- progression markings
- striations

Cause:

Crimped design: residual stress
Male-stud, straight coupling: ??

Loading: low amplitude stress, high freq.

Source of cyclic stress: ???????

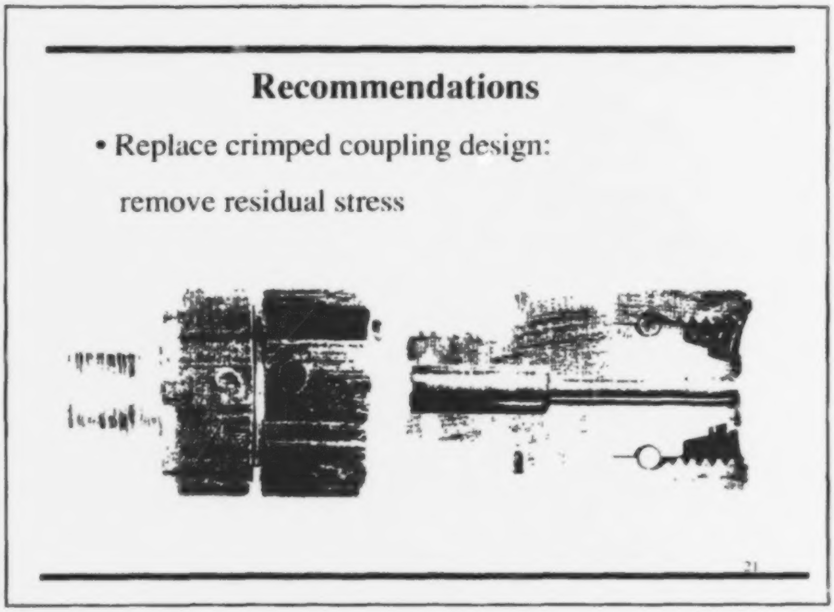

Recommendations

- Replace crimped coupling design:
  remove residual stress

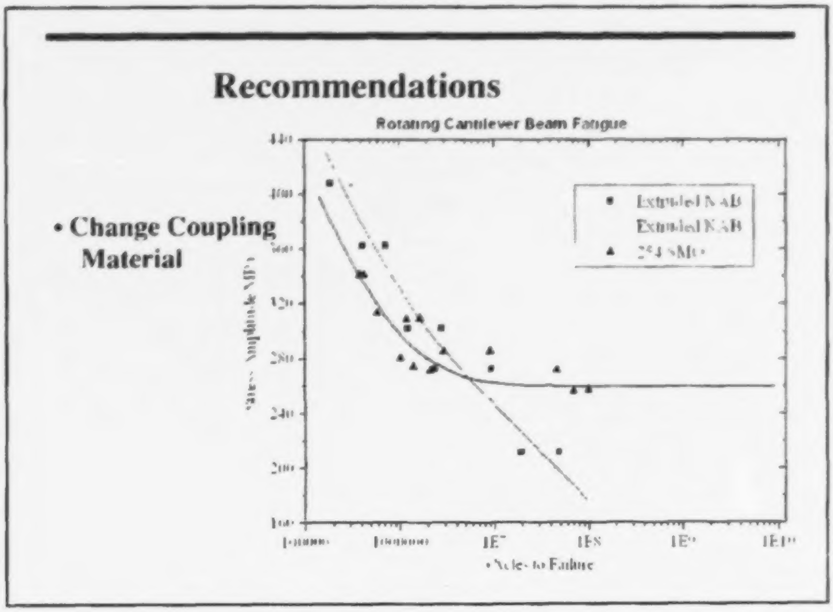

Recommendations

- **Change Coupling Material**

Recommendations

Ensure compliance with installation procedure:
use specified torque ratings

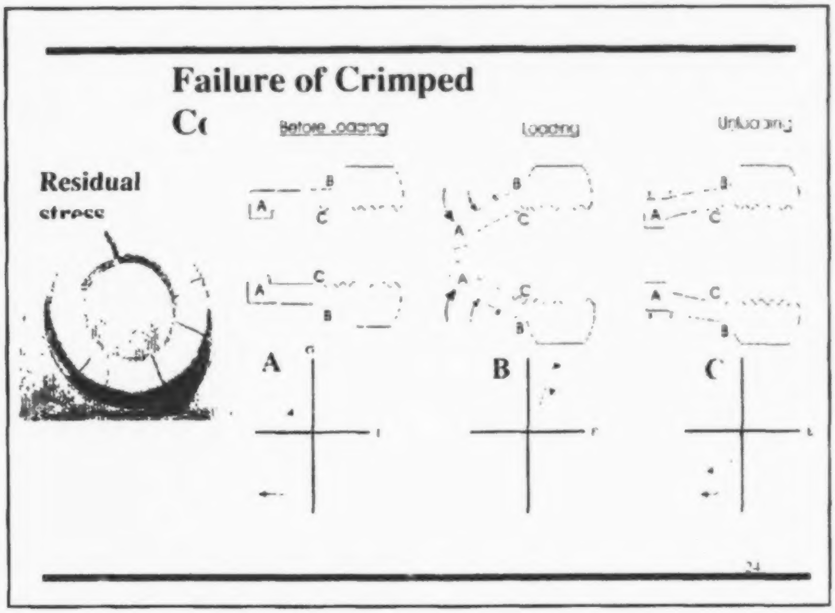

Failure of Crimped C

Residual
stress
Before Loading
Loading
Unloading
A
B
C
A
B
C

#516427 (15)

Review of R and D on Cupronickels and Ni-Al Bronzes at the Materials Technology Laboratory, Canmet

by

Mahi Sahoo

Program Manager, Sustainable Casting
Materials Technology Laboratory (MTL)
Canmet
Ottawa, Ontario

Abstract

A significant amount of research and development work was performed at MTL/Canmet in the late nineteen seventies and early eighties on high strength copper-base alloys such as cupronickels and Ni-Al bronzes for shipboard systems. The need for these studies arose from the nonweldability and poor mechanical properties of the long freezing range tin bronze valves and fillings used at that time as well as the need for improved impingement corrosion resistance associated with the use of high pressure, compact piping system. This work was then extended to propeller castings involving Mn-Ni-Al bronzes, Ni-Al bronzes and high damping Sonoston (Cu-Mn) Alloys. The significant achievements on these alloys will be described together with the efforts distributed towards technology transfer to Canadian foundries.

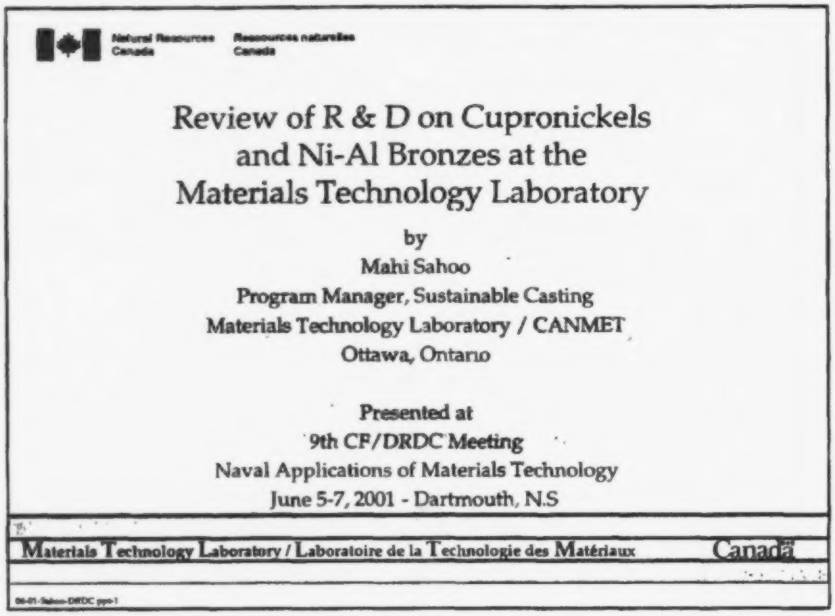

Natural Resources Canada   Ressources naturelles Canada

Review of R & D on Cupronickels and Ni-Al Bronzes at the Materials Technology Laboratory

by
Mahi Sahoo
Program Manager, Sustainable Casting
Materials Technology Laboratory / CANMET
Ottawa, Ontario

Presented at
9th CF/DRDC Meeting
Naval Applications of Materials Technology
June 5-7, 2001 - Dartmouth, N.S

Materials Technology Laboratory / Laboratoire de la Technologie des Matériaux   Canadä

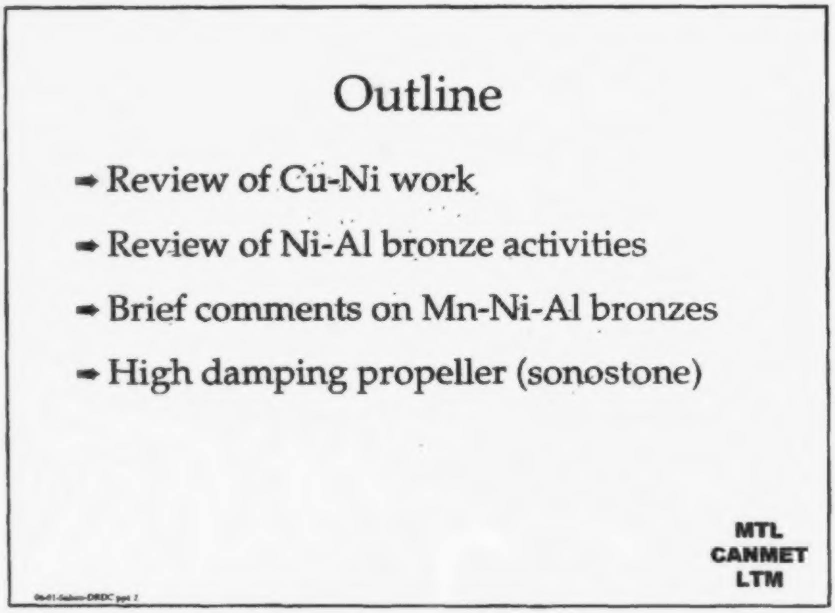

Outline

- Review of Cu-Ni work
- Review of Ni-Al bronze activities
- Brief comments on Mn-Ni-Al bronzes
- High damping propeller (sonostone)

MTL
CANMET
LTM

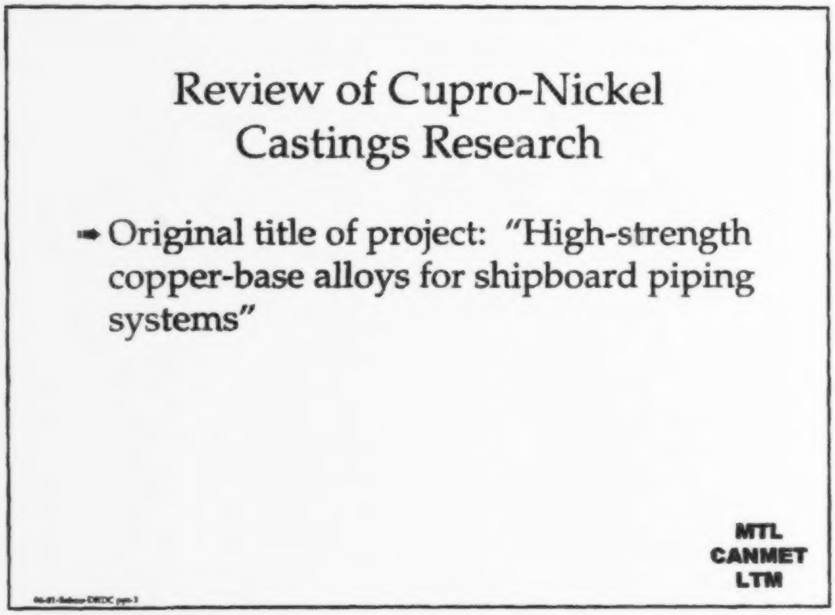

Review of Cupro-Nickel Castings Research

- Original title of project: "High-strength copper-base alloys for shipboard piping systems"

MTL
CANMET
LTM

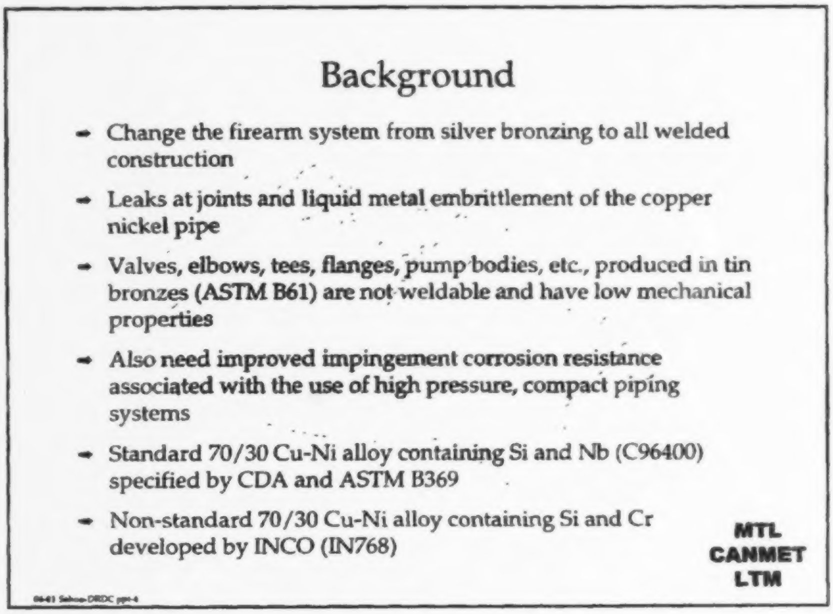

Background

- Change the firearm system from silver bronzing to all welded construction
- Leaks at joints and liquid metal embrittlement of the copper nickel pipe
- Valves, elbows, tees, flanges, pump bodies, etc., produced in tin bronzes (ASTM B61) are not weldable and have low mechanical properties
- Also need improved impingement corrosion resistance associated with the use of high pressure, compact piping systems
- Standard 70/30 Cu-Ni alloy containing Si and Nb (C96400) specified by CDA and ASTM B369
- Non-standard 70/30 Cu-Ni alloy containing Si and Cr developed by INCO (IN768)

MTL
CANMET
LTM

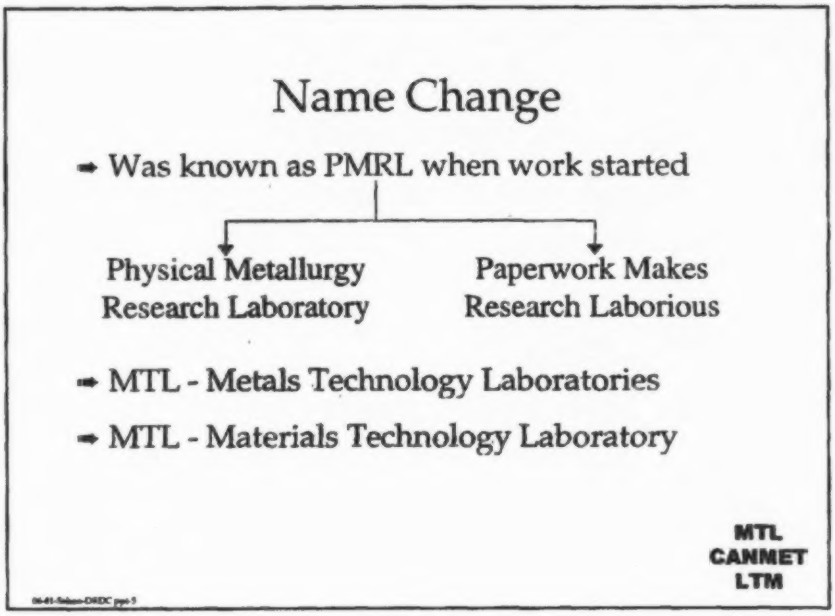

Name Change

- Was known as PMRL when work started

Physical Metallurgy Research Laboratory

Paperwork Makes Research Laborious

- MTL - Metals Technology Laboratories
- MTL - Materials Technology Laboratory

MTL
CANMET
LTM

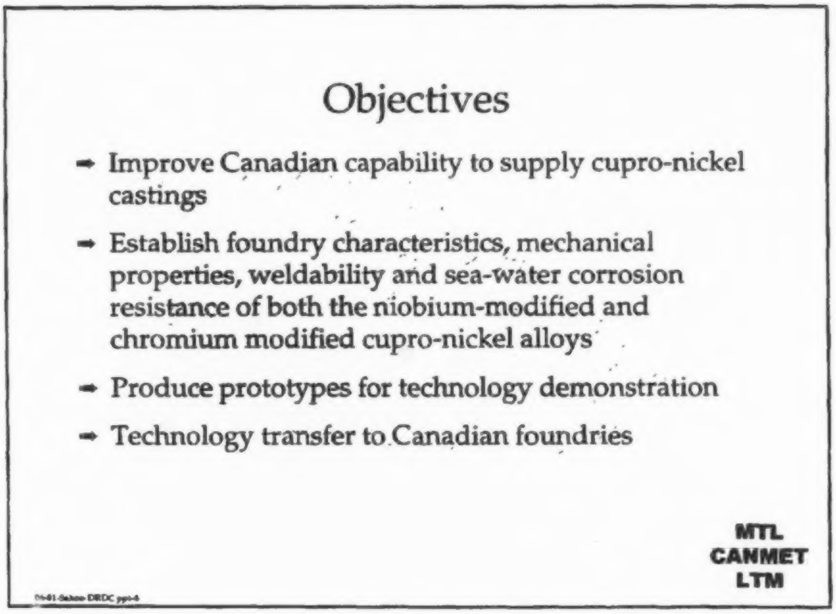

Objectives

- Improve Canadian capability to supply cupro-nickel castings
- Establish foundry characteristics, mechanical properties, weldability and sea-water corrosion resistance of both the niobium-modified and chromium modified cupro-nickel alloys
- Produce prototypes for technology demonstration
- Technology transfer to Canadian foundries

MTL
CANMET
LTM

- Project duration: 1977-1982

MTL
CANMET
LTM

Composition Ranges

	Ni	Si	Nb	Fe	Mn	Pb
C96400†	28-32	0.7 max	1.5 max	0.3-1.5	1.5 max	0.01 max
IN768‡	28-33	0.3-0.5	--	1.0 max	0.4-1.0	0.01 max

† MTL work: 0.2-0.5% Si and 0.6-1.0% Nb for C96400

‡ 1.4-2.0% Cr; 0.05-0.15% Zr; 0.10% max Ti; 0.07% max C and 0.02% max S

MTL
CANMET
LTM

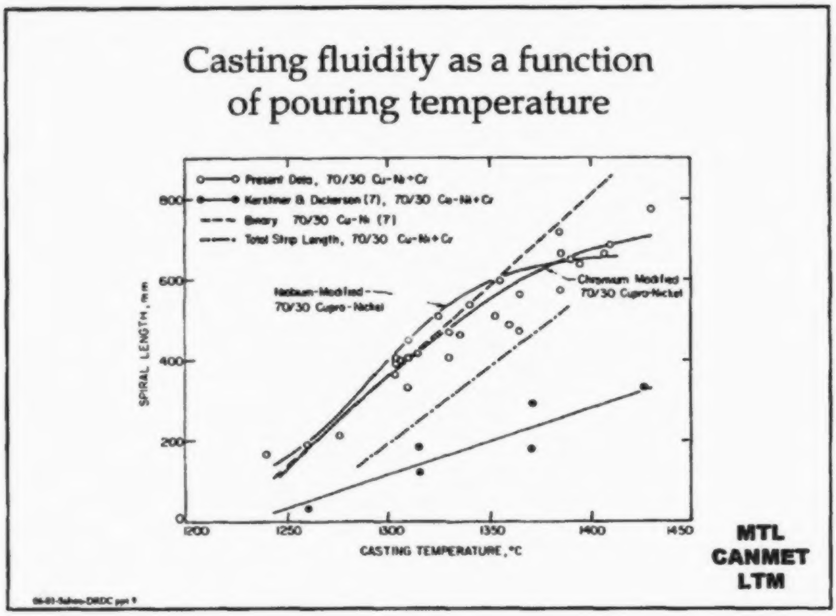

Casting fluidity as a function of pouring temperature

MTL
CANMET
LTM

06-01-Sahoo-DRDC ppt 9

Weldability

- Automatic gas-metal-arc welding (GMAW)
- Hot cracking sensitivity of IN768 using Varestraint listing
- Welded samples supplied to DREA for erosion-corrosion tests

MTL
CANMET
LTM

06-01-Sahoo-DRDC ppt 10

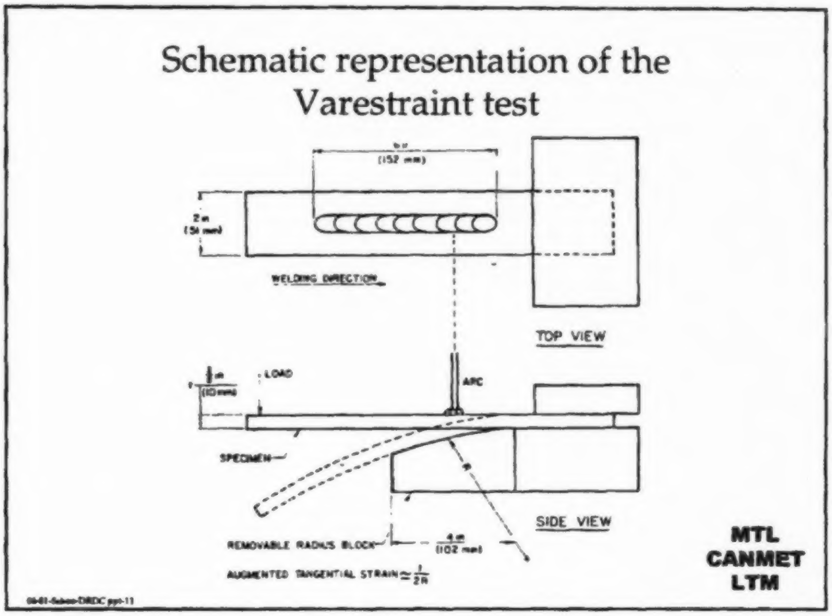

Schematic representation of the Varestraint test

6 in
(152 mm)
2 in
(51 mm)
WELDING DIRECTION
TOP VIEW
3/8 in
(10 mm)
LOAD
ARC
SPECIMEN
R
SIDE VIEW
REMOVABLE RADIUS BLOCK
4 in
(102 mm)
AUGMENTED TANGENTIAL STRAIN ≃ t/2R

**MTL
CANMET
LTM**

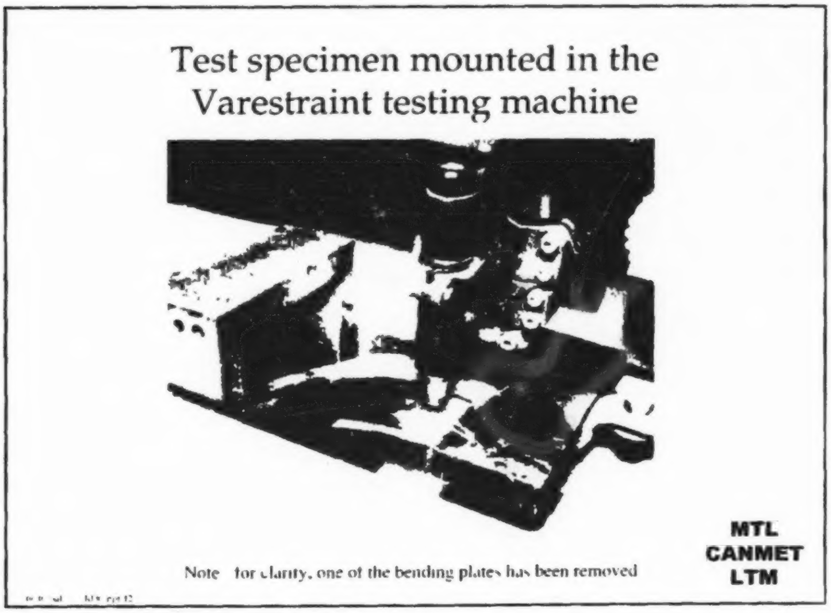

Test specimen mounted in the Varestraint testing machine

Note   for clarity, one of the bending plates has been removed

**MTL
CANMET
LTM**

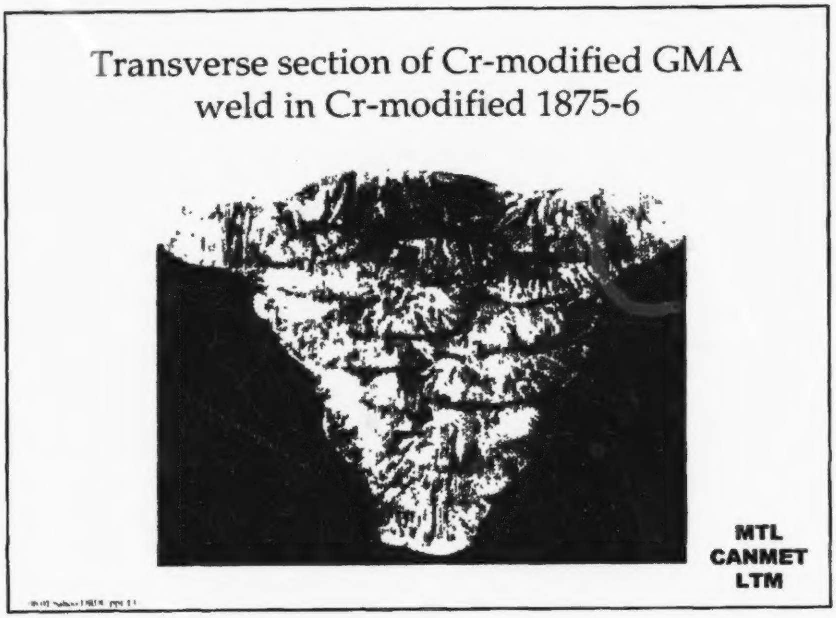

Transverse section of Cr-modified GMA weld in Cr-modified 1875-6

MTL
CANMET
LTM

[illegible]

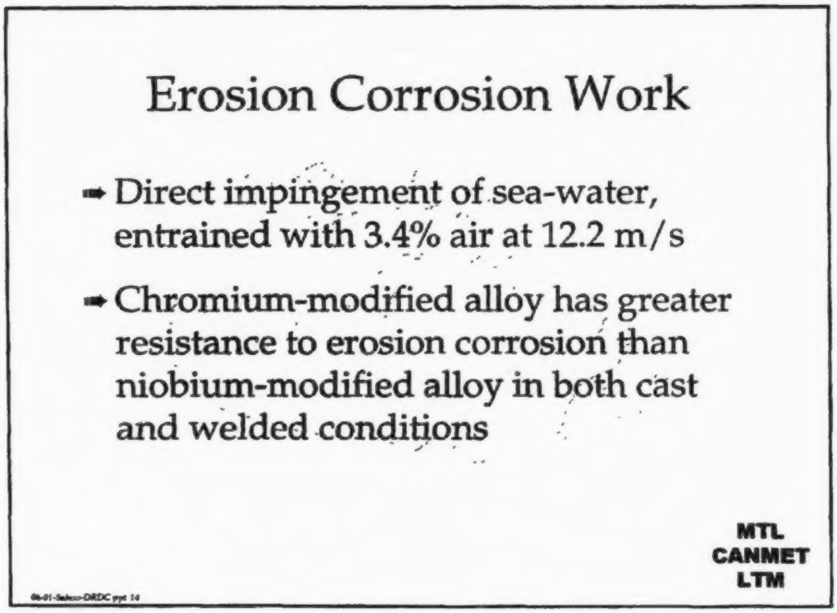

Erosion Corrosion Work

- Direct impingement of sea-water, entrained with 3.4% air at 12.2 m/s
- Chromium-modified alloy has greater resistance to erosion corrosion than niobium-modified alloy in both cast and welded conditions

MTL
CANMET
LTM

06-01-Sahoo-DRDC.ppt 14

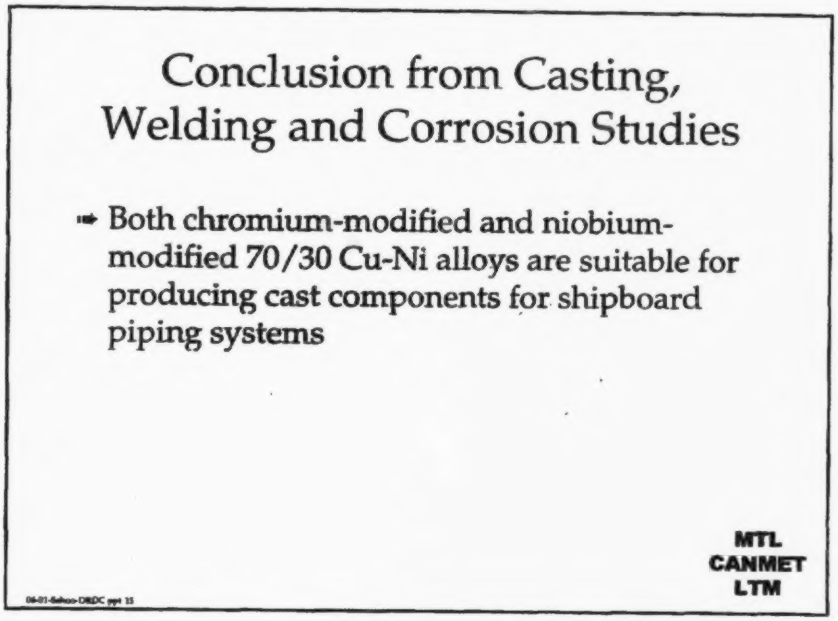

Conclusion from Casting, Welding and Corrosion Studies

- Both chromium-modified and niobium-modified 70/30 Cu-Ni alloys are suitable for producing cast components for shipboard piping systems

MTL
CANMET
LTM

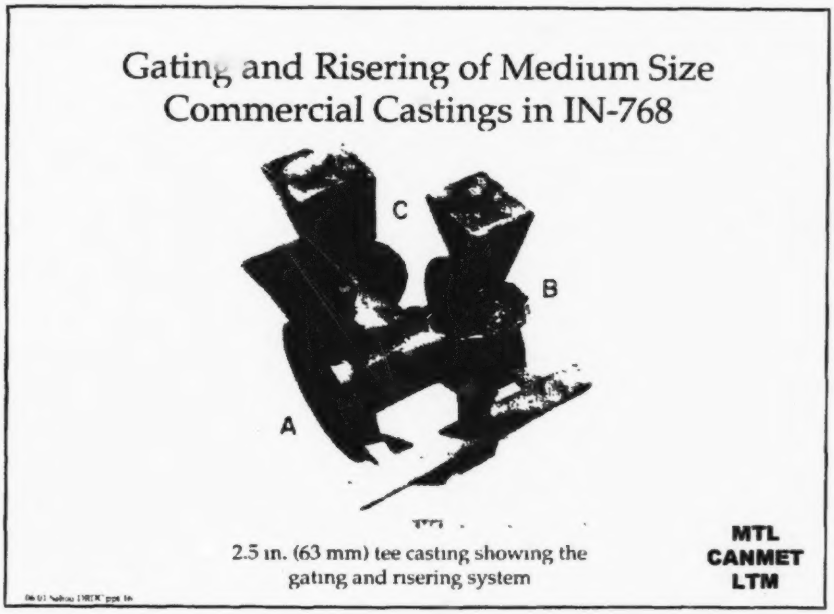

Gating and Risering of Medium Size Commercial Castings in IN-768

2.5 in. (63 mm) tee casting showing the gating and risering system

MTL
CANMET
LTM

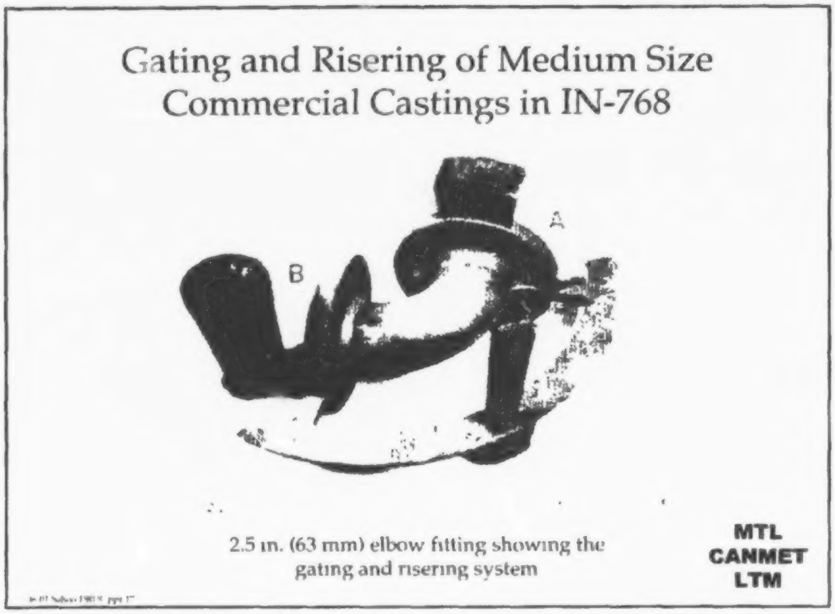

Gating and Risering of Medium Size Commercial Castings in IN-768

2.5 in. (63 mm) elbow fitting showing the gating and risering system

MTL
CANMET
LTM

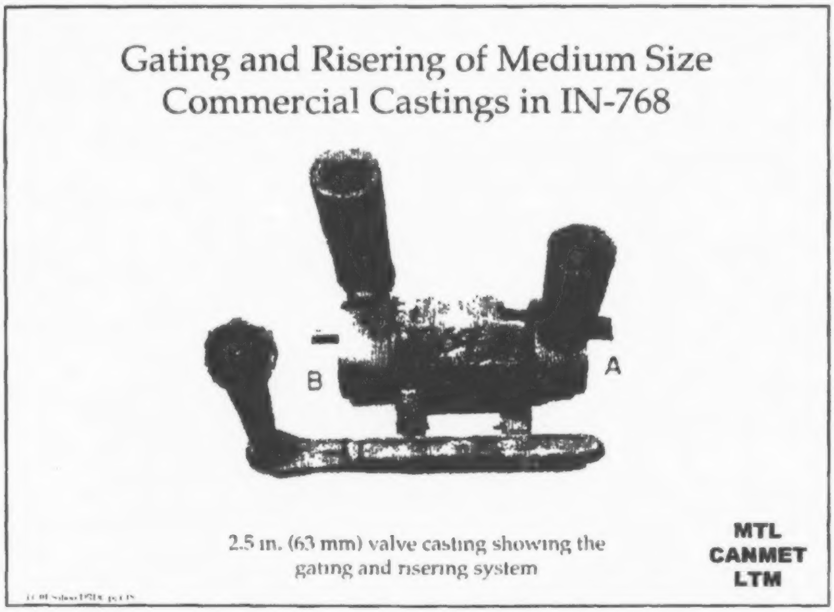

Gating and Risering of Medium Size Commercial Castings in IN-768

2.5 in. (63 mm) valve casting showing the gating and risering system

MTL
CANMET
LTM

Technology Demonstration

- Workshop on cast copper alloy at Ottawa, 1979, 45 attendees from all across Canada
- As a practical sequel to the earlier studies and workshop, Chief of Engineering and Maintenance at DND (DND-CEM) requested MTL to provide technical support to obtain from Canadian sources two ship's sets each of 8 large cast manifolds, in niobium-modified 90/10 (C96200) and 70/30 (C96400) cupro-nickel
- Contract signed with a southern Ontario foundry

MTL
CANMET
LTM

Casting Requirements

- The specifications for the castings were:
  - air-pressure test at 50 psi (345 kPa) before machining,
  - radiographic inspection to level 2 of ASTM E272,
  - proof (water) pressure test to 400 psi (2760 kPa) after machining, and
  - composition limits and mechanical properties of separately-cast test bars conforming to ASTM B369-78 for alloys C6200 (90/10 Cu-Ni) and C96400 (70/30 Cu-Ni)
- Established gating and risering system
- MTL established melting practice was employed

MTL
CANMET
LTM

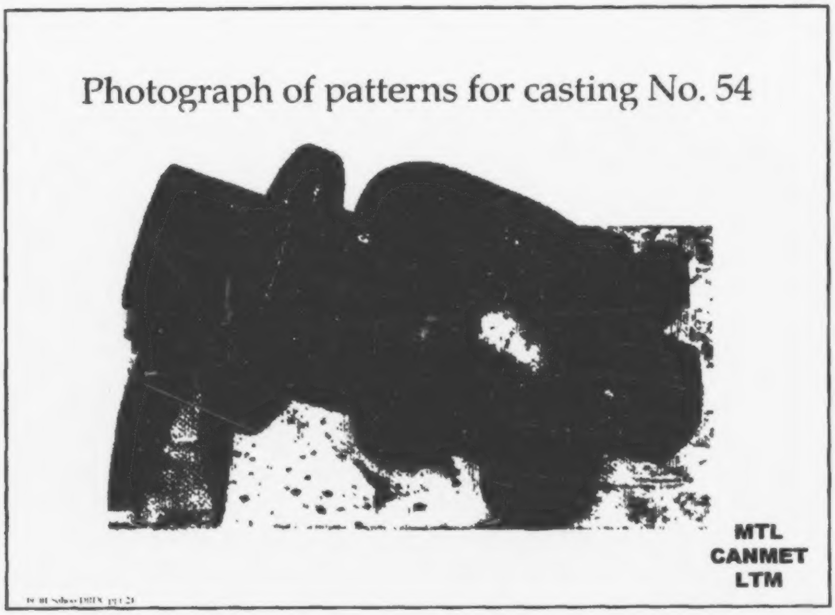

Photograph of patterns for casting No. 54

MTL
CANMET
LTM

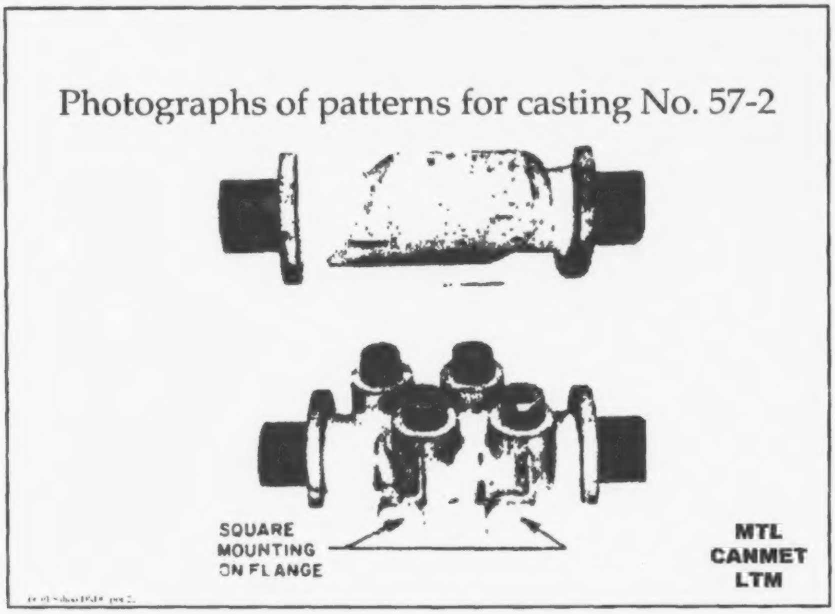

Photographs of patterns for casting No. 57-2

SQUARE
MOUNTING
ON FLANGE

MTL
CANMET
LTM

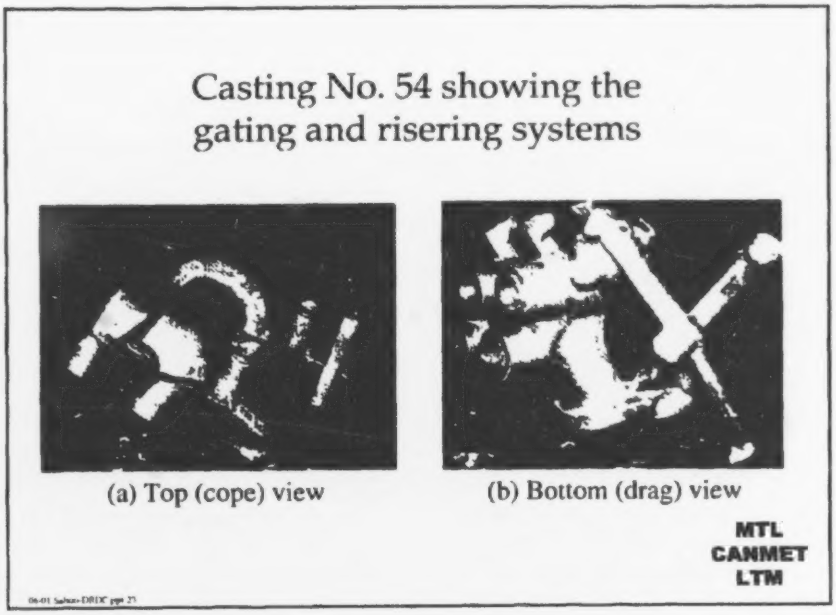

Casting No. 54 showing the gating and risering systems

(a) Top (cope) view

(b) Bottom (drag) view

MTL
CANMET
LTM

06-01 Sahoo-DRDC ppt 23

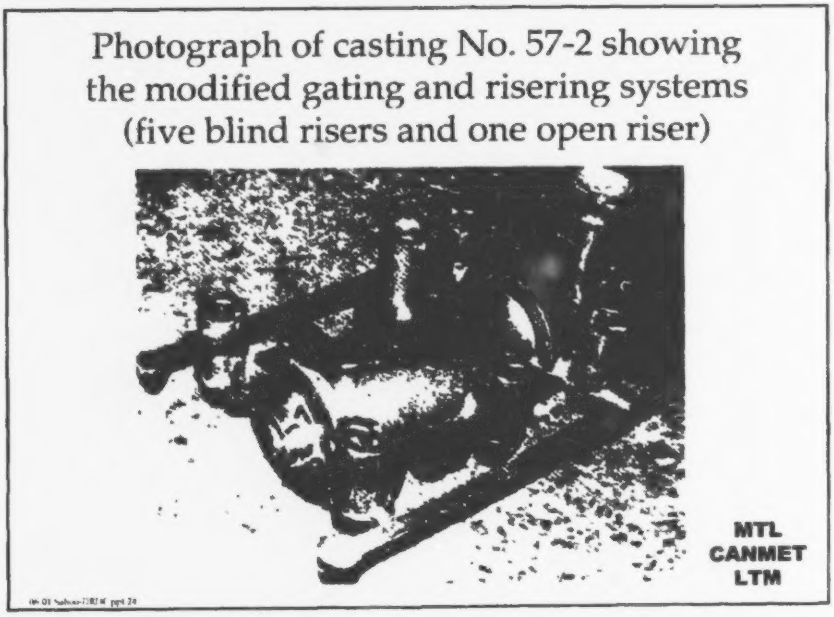

Photograph of casting No. 57-2 showing the modified gating and risering systems (five blind risers and one open riser)

MTL
CANMET
LTM

06-01 Sahoo-DRDC ppt 24

Technology Demonstration

- Production of a six-valve chest casting in C96400 (Nb-modified 70/30 Cu-Ni)
- Requirements same as before
- Shock tested at Montreal

MTL
CANMET
LTM

Photos of the used six-valve chest casting

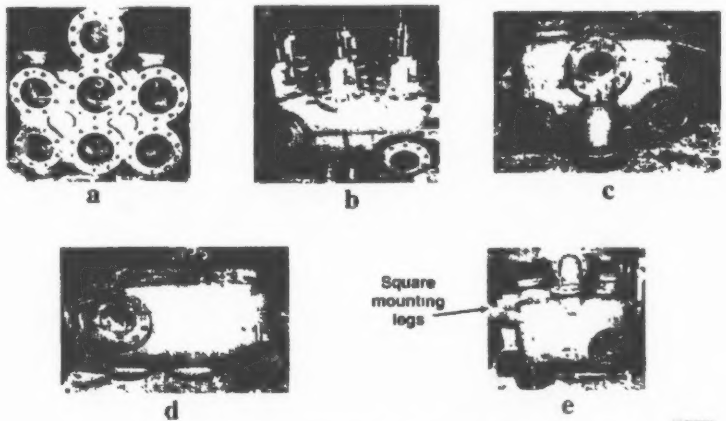

A, b, c, d, view 180° from C, Ie, view of "top", 90° from d Photos a-c are taken successively as the casting is turned through 180° Other views as indicated

MTL
CANMET
LTM

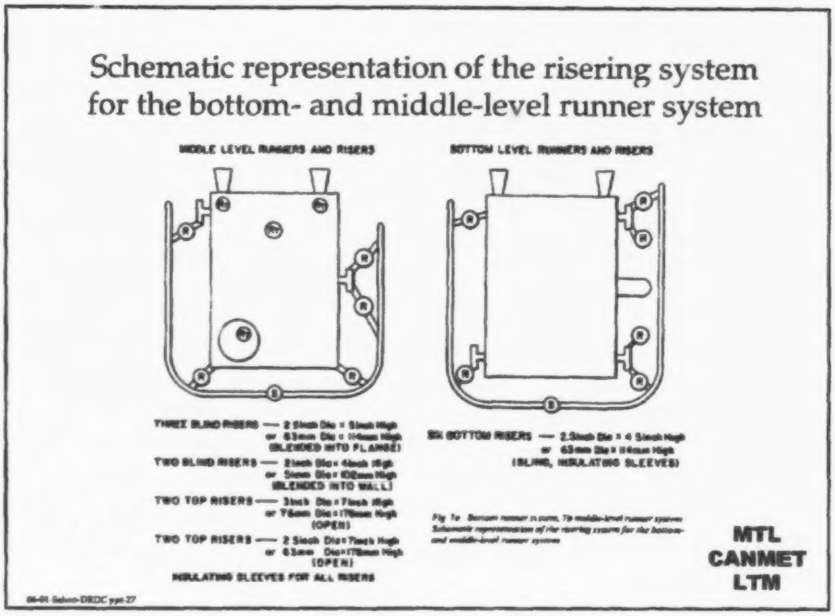

Schematic representation of the risering system for the bottom- and middle-level runner system

MIDDLE LEVEL RUNNERS AND RISERS
BOTTOM LEVEL RUNNERS AND RISERS
R
S
THREE BLIND RISERS — 2.5inch Dia × 5inch High or 63mm Dia × 114mm High (BLENDED INTO FLANGE)
TWO BLIND RISERS — 2inch Dia × 4inch High or 51mm Dia × 102mm High (BLENDED INTO WALL)
TWO TOP RISERS — 3inch Dia × 7inch High or 76mm Dia × 178mm High (OPEN)
TWO TOP RISERS — 2.5inch Dia × 7inch High or 63mm Dia × 178mm High (OPEN)
INSULATING SLEEVES FOR ALL RISERS
SIX BOTTOM RISERS — 2.5inch Dia × 4.5inch High or 63mm Dia × 114mm High (BLIND, INSULATING SLEEVES)

MTL
CANMET
LTM

Nickel-Aluminum Bronzes

- Approached by DREA to focus attention on Ni-Al bronzes (alloy C95800)
- Perform weldability evaluation
- Supply welded samples to DREA for erosion corrosion work

MTL
CANMET
LTM

- ➡ Project duration: 1979-1984

MTL
CANMET
LTM

Composition Ranges for C95800

- ➡ 8.5 to 9.5% Al
- ➡ 4 to 5% Ni
- ➡ 3.5 to 4.5% Fe*
- ➡ 0.8 to 1.5% Mn
- ➡ 79.0% min Cu

*Fe content shall not exceed Ni content

- ➡ Mechanical properties:
  - 85 ksi (585 MPa) UTS
  - 35 ksi (240 MPa) YS
  - 15% Elong

MTL
CANMET
LTM

Workplan Proposed to DREA

- Systematic study of the effects of composition and corrosion-inhibiting heat treatment on the mechanical properties, especially at the low Al (~8.5% Al) end of the composition range.
- Produce concast rods (22 mm diam)
- Simulate the sand-cast microstructure by homogenizing at 1000°C for 2 h followed by furnace cooling at 4°C/min to 555°C and then air cooling

MTL
CANMET
LTM

Composition Matrix

Ni-Al bronze alloying levels in
continuously cast bar stock

	Target wt %	Actual wt %
Nickel – fixed	4.5	4.01-4 6
Iron – 3 levels at each of 2 Mn levels	3.5 4.5 5.0	2.96-5.13
Manganese – 2 levels	0.8 1.3	0.65-1.26
Aluminum – 3 levels for each Fe level	8.25 8.75 9.25	8.09-9.9

MTL
CANMET
LTM

Vertical section of the Cu-Al-Ni-Fe system at 5% Ni, 5% Fe

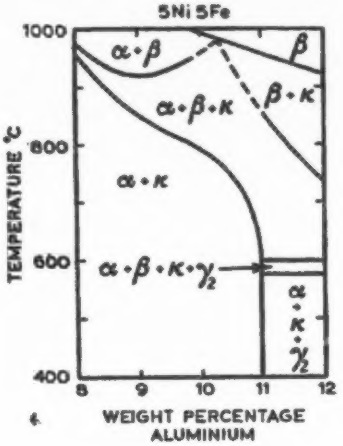

MTL
CANMET
LTM

Microstructure for Ni-Al Bronzes

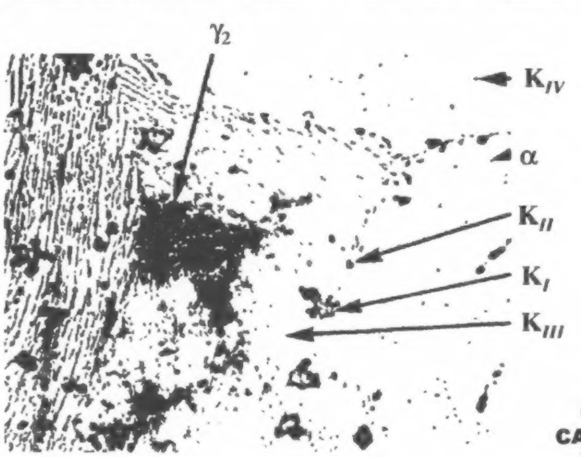
γ₂
K_IV
α
K_II
K_I
K_III

MTL
CANMET
LTM

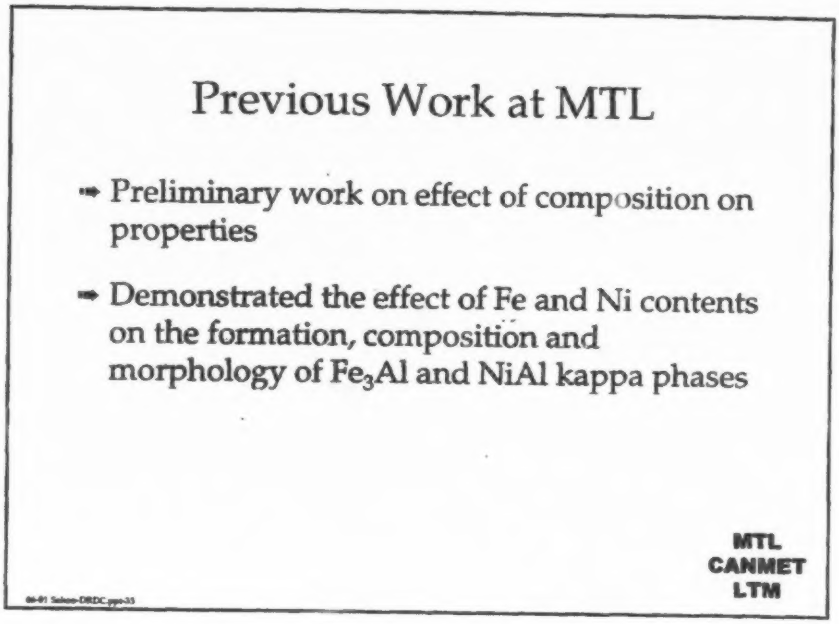

Previous Work at MTL

- Preliminary work on effect of composition on properties
- Demonstrated the effect of Fe and Ni contents on the formation, composition and morphology of Fe_3Al and NiAl kappa phases

MTL
CANMET
LTM

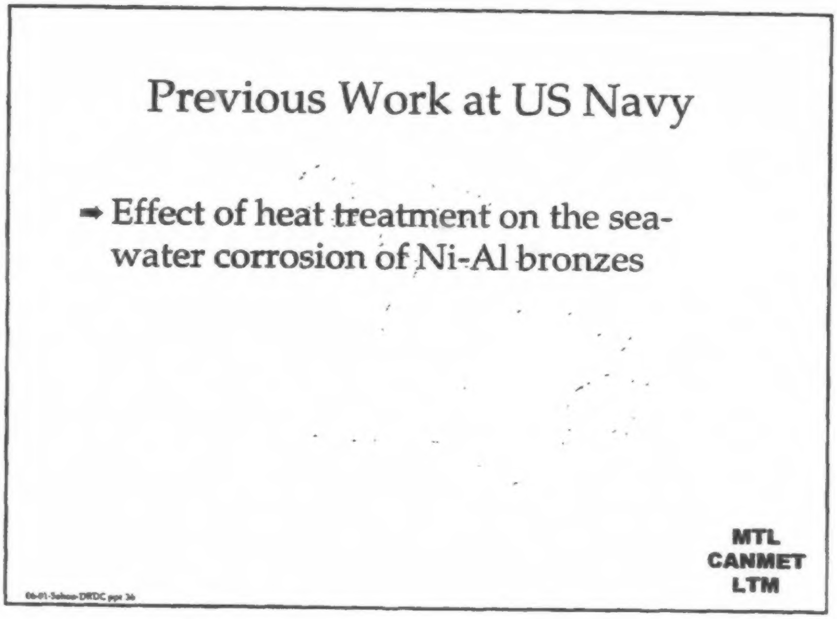

Previous Work at US Navy

- Effect of heat treatment on the sea-water corrosion of Ni-Al bronzes

MTL
CANMET
LTM

Heat Treatments

- 700°C, 6 h air cool
- Also at 600 and 650°C
- Time: 6 to 8 h

MTL
CANMET
LTM

Optical micrographs of sand-cast and
700°C heat treated NAB alloy

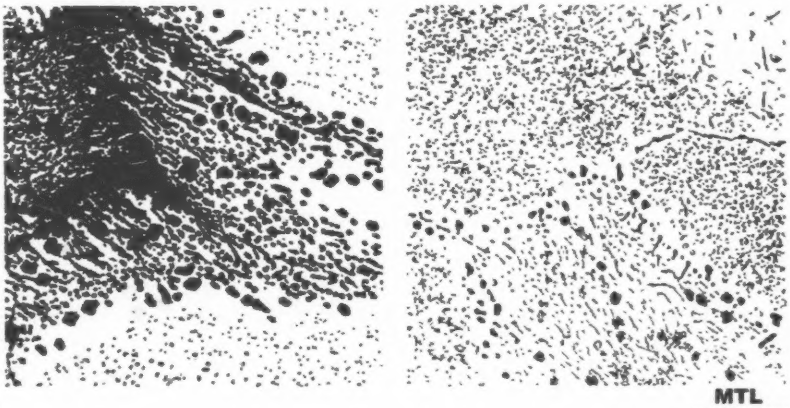

MTL
CANMET
LTM

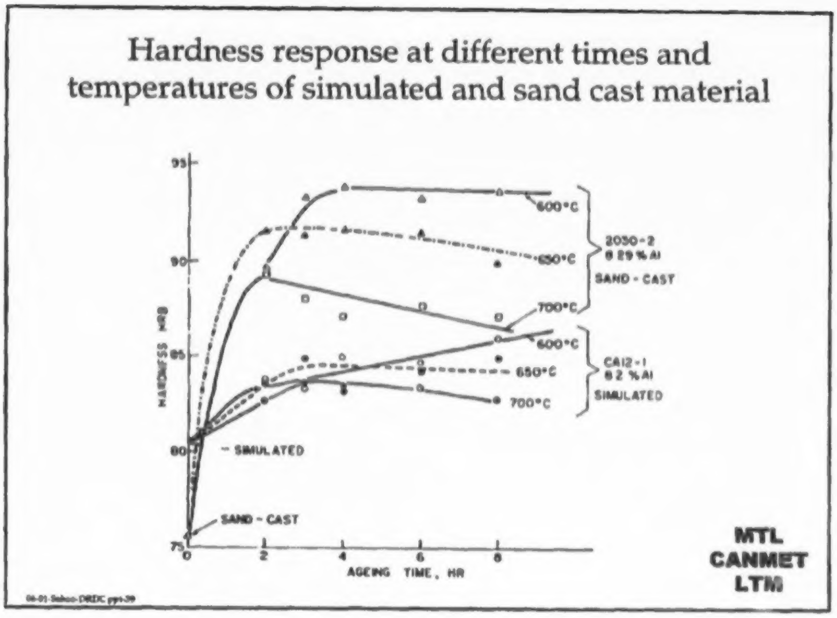

Hardness response at different times and temperatures of simulated and sand cast material

MTL
CANMET
LTM

Presence of the Dark Etching Phase (γ_2) in Simulated and Sand Cast Alloys

As-cast condition	Cast + 700°C, 6 h
Present at >8.8% Al even with as little as 0.7% Mn	(i) At >9.25% Al, γ_2 cannot be removed with as little as 0.8% Mn (ii) At 9.0-9.25% Al, γ_2 cannot be removed at >1.0% Mn (iii) At <9.0% Al, γ_2 can be removed provided <1.2% Mn

MTL
CANMET
LTM

Effect of Corrosion Inhibiting Heat Treatment

- Complete or partial removal of γ_2 depending on Al and Mn contents
- γ_2 becomes discontinuous at high end of Al
- Precipitation strengthening
- Better response to precipitation at the low end of Al and greater increases in strength
- Easy to meet ASTM specified mechanical properties

MTL
CANMET
LTM

Recommendations

- Produce castings at low Al levels (range 8.5%) which contain little or no γ_2 phase; hence inherently good corrosion resistance
- Heat treat at 700°C to improve the mechanical properties

MTL
CANMET
LTM

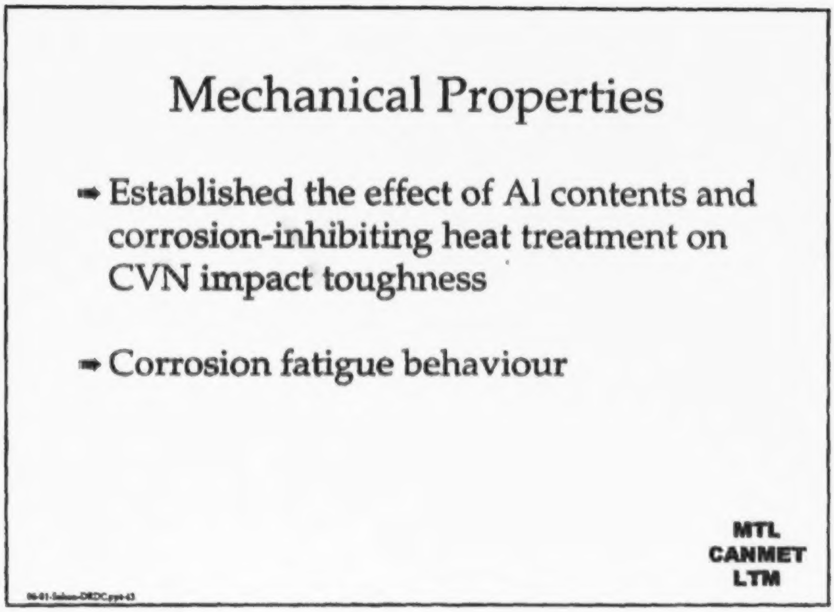

Mechanical Properties

- Established the effect of Al contents and corrosion-inhibiting heat treatment on CVN impact toughness
- Corrosion fatigue behaviour

MTL
CANMET
LTM

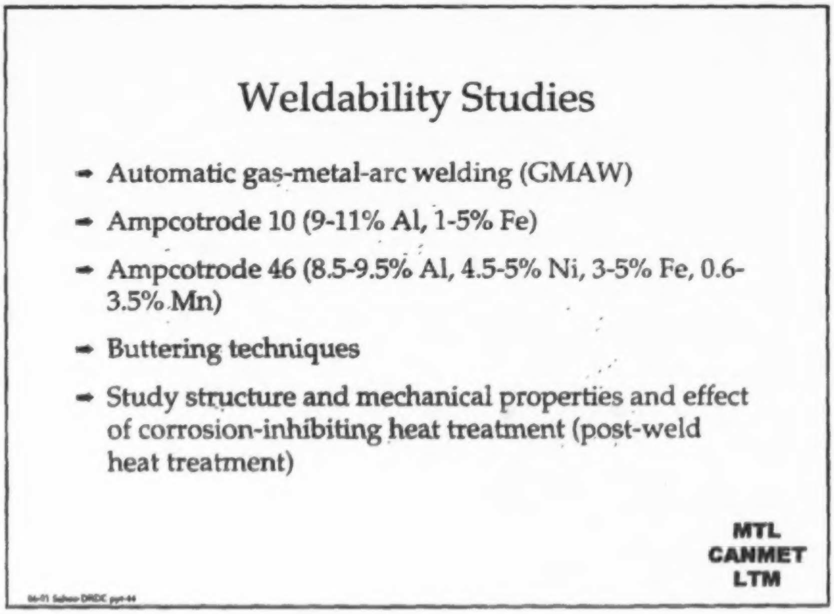

Weldability Studies

- Automatic gas-metal-arc welding (GMAW)
- Ampcotrode 10 (9-11% Al, 1-5% Fe)
- Ampcotrode 46 (8.5-9.5% Al, 4.5-5% Ni, 3-5% Fe, 0.6-3.5% Mn)
- Buttering techniques
- Study structure and mechanical properties and effect of corrosion-inhibiting heat treatment (post-weld heat treatment)

MTL
CANMET
LTM

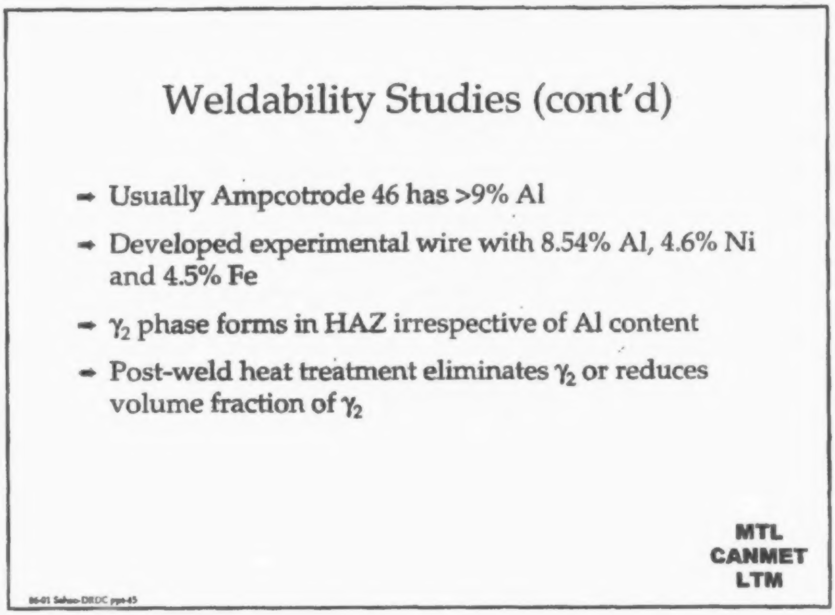

Weldability Studies (cont'd)

- Usually Ampcotrode 46 has >9% Al
- Developed experimental wire with 8.54% Al, 4.6% Ni and 4.5% Fe
- γ_2 phase forms in HAZ irrespective of Al content
- Post-weld heat treatment eliminates γ_2 or reduces volume fraction of γ_2

MTL
CANMET
LTM

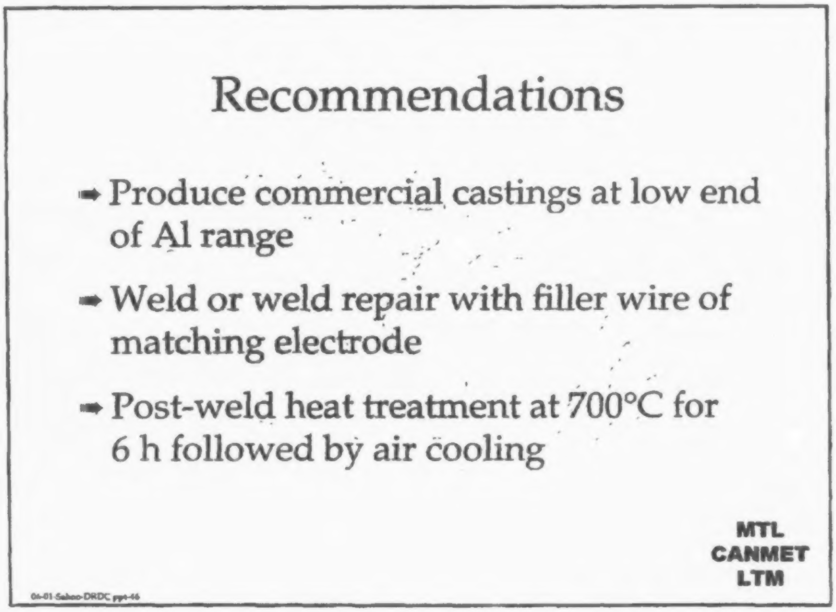

Recommendations

- Produce commercial castings at low end of Al range
- Weld or weld repair with filler wire of matching electrode
- Post-weld heat treatment at 700°C for 6 h followed by air cooling

MTL
CANMET
LTM

Effect of Slow Cooling

- Concast rods, >100°C/min
- Keel block, 7°C/min
- Simulation of concast after heating to 1000°C, 5°C/min
- Large propeller (8000 kg), 0.1-0.2°C/min
- UTS, YS and % Elong in thicker sections are about 75% of those for separately cast keel block test bars
- Effect of 700°C, 6 h heat treatment on structure and mechanical properties

MTL
CANMET
LTM

06-01-Sahoo-DRDC.ppt-47

Schematic representation of the single-blade controllable-pitch propeller showing the location from which a piece weighing about 200 lb (90 kg) was removed

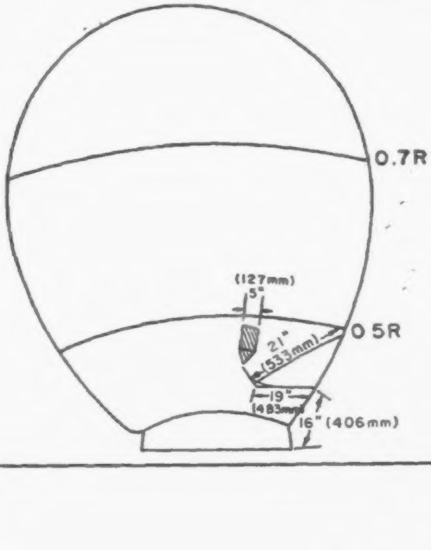

MTL
CANMET
LTM

06-01 Sahoo-DRDC ppt-48

Influence of cooling rate on the mechanical properties of Ni-Al bronze alloy No. 20-1 and sand-cast No. 2104-5

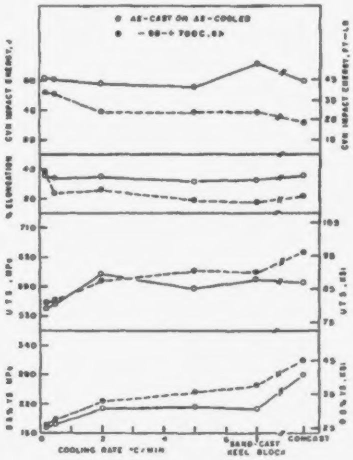

MTL
CANMET
LTM

Fracture Toughness

- Sand-cast plates (7°C/min)
- Slowly cooled at 0.2°C/min
- Propeller blade (0.1°C/min)
- J_{IC} testing technique (ASTM E-813)
- Effect of 700°C, 6 h heat treatment on J_{IC}

MTL
CANMET
LTM

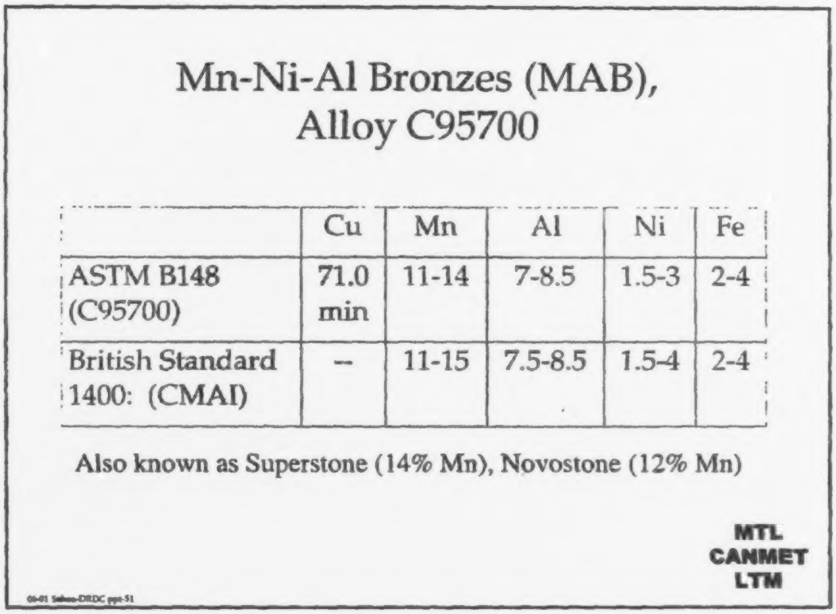

Mn-Ni-Al Bronzes (MAB), Alloy C95700

	Cu	Mn	Al	Ni	Fe
ASTM B148 (C95700)	71.0 min	11-14	7-8.5	1.5-3	2-4
British Standard 1400: (CMAI)	--	11-15	7.5-8.5	1.5-4	2-4

Also known as Superstone (14% Mn), Novostone (12% Mn)

MTL CANMET LTM

06-01 Sahoo-DRDC ppt-51

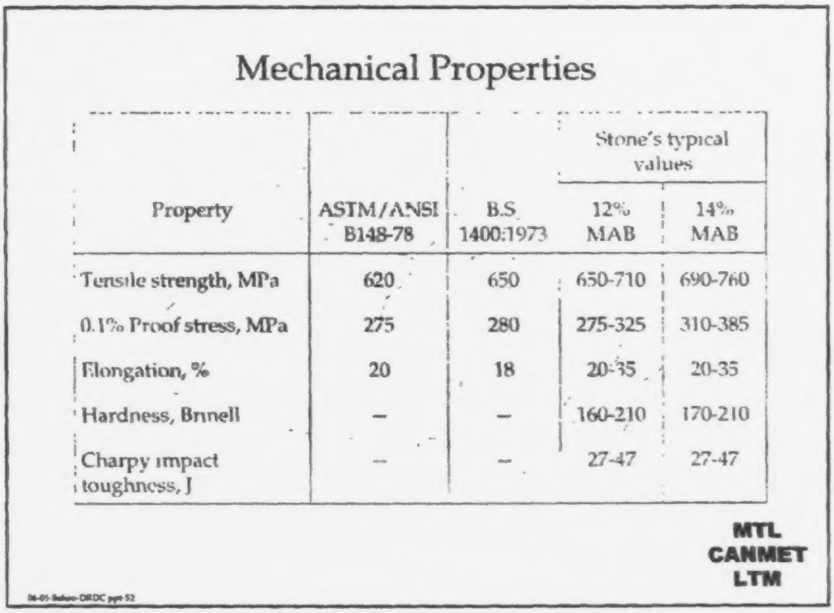

Mechanical Properties

Property	ASTM/ANSI B148-78	B.S. 1400:1973	Stone's typical values	
			12% MAB	14% MAB
Tensile strength, MPa	620	650	650-710	690-760
0.1% Proof stress, MPa	275	280	275-325	310-385
Elongation, %	20	18	20-35	20-35
Hardness, Brinell	–	–	160-210	170-210
Charpy impact toughness, J	–	–	27-47	27-47

MTL CANMET LTM

06-01-Sahoo-DRDC ppt-52

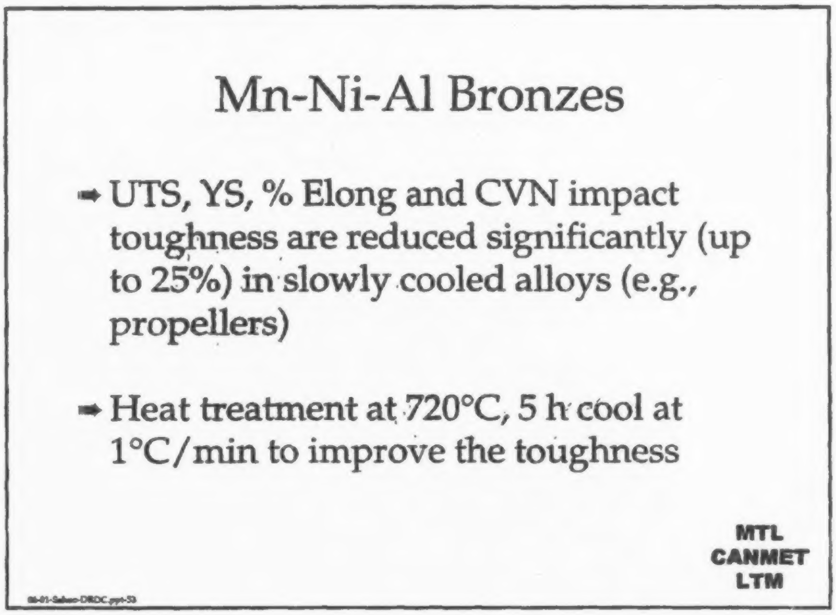

Mn-Ni-Al Bronzes

- UTS, YS, % Elong and CVN impact toughness are reduced significantly (up to 25%) in slowly cooled alloys (e.g., propellers)
- Heat treatment at 720°C, 5 h cool at 1°C/min to improve the toughness

MTL
CANMET
LTM

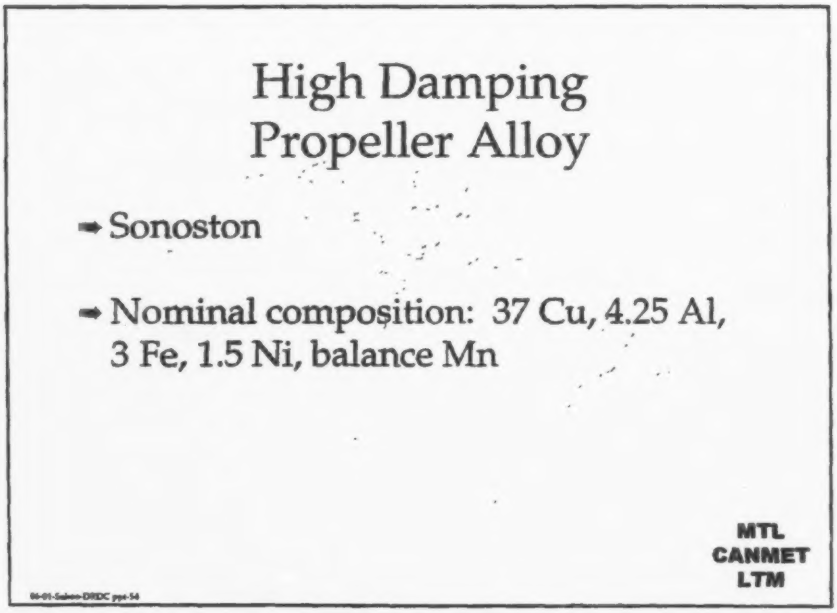

High Damping Propeller Alloy

- Sonoston
- Nominal composition: 37 Cu, 4.25 Al, 3 Fe, 1.5 Ni, balance Mn

MTL
CANMET
LTM

#516428 (16)

Copper based alloy fastener materials - stress corrosion studies

by

J C Galsworthy, DERA, MoD, UK
K J A Mawella, STGMT, DPA, MoD, UK

Abstract

There is the potential for cost effective use of high strength copper nickel alloys for fasteners in submerged naval applications. Now that alloys with strengths equivalent to the previously used steel fasteners are available with the potential of good corrosion performance their wider use is sought.

However, one initial specific application of Marinel has resulted in a small incidence of stress corrosion failures which on further examination instigated laboratory stress corrosion studies to understand the problem.

It was concluded that the deformation and thermal cycle associated with the hot heading manufacturing process developed a microstructure susceptible to unexpected chemical species. This was compounded by an assemble cleaning procedure which used an ammonia based cleaning solution.

The use of machined fasteners and the removal of the cleaning solution has reduced the incidence of stress corrosion failures in this application. Additional tests have shown that Marinel and Nibron Special have similar stress corrosion response in the environments selected. Both materials have potential for platform cost reduction through wider use in submerged naval structures.

Introduction

There is a recognised requirement for corrosion resistant fasteners for marine and naval use. Many applications call for a combination of strength and corrosion resistance, together with electrochemical compatibility. Resistance to other failure mechanisms is also paramount, such as stress corrosion cracking and hydrogen embrittlement.

There can be upwards of 30,000 fasteners in a submarine or minesweeper requiring regular inspection and renewal. A majority being made of a copper alloy for corrosion resistance and compatibility. The constant attempts to reduced life cycle costs for naval vessels has begun to address these fastener issues. Life cycle costs being potentially reduced by the use of alternative copper based alloys.

The introduction of some alloys have seen subsequent service problems. This paper presents some of the investigations and the background stress corrosion studies conducted by the UK MoD into alternative copper based alloy fasteners for these challenging naval applications.

Background

Many naval applications have relied on Nickel Aluminium Bronze (NAB) fasteners, or when magnetic properties dictate, Aluminium Silicon Bronze (ASB) is used. The service performance of these materials have been generally good but the NAB fasteners suffer from selective phase corrosion so require regular inspection and renewal, and ASB fasteners have had a checkered history with periodically intergranular failures of small batches due to stress corrosion cracking as a result of overstressing. The strength of both these materials is low, much lower than steel, necessitating the continued use of low alloy steel fasteners in some applications which corrode when exposed to seawater, especially in conjunction with copper based alloy components.

High strength copper-nickel alloys as corrosion resistant fasteners with strength levels equivalent to typical steel fasteners have the potential to enhance naval structures and reap cost benefits.

The early development of high strength copper nickel alloys stem from observations made on the age-hardening effect of aluminium on the basic copper-nickel composition. Initial alloys had poor grain size control and inconsistent properties but through the addition of grain refining elements and better process control viable alloys were marketed. This led to the DGS357 and NES835 specification material based on Hiduron 191. Increases in strength were continually sought and further developments within the copper alloy industry resulted in other alloys, such as Marinel and Nibron Special.

The use of Marinel in one specific application resulted in a small number of unexpected failures attributed to stress corrosion cracking. The attempts to understand the reasons for and the prevention of these failures lead to laboratory stress corrosion tests to simulate the perceived service environment on this alloy and subsequently on a potential alternative, Nibron Special.

Marinel

Marinel was a proprietary alloy developed and originally produced by Langley Alloys Ltd, part of Langley Group PLC. It is a copper based alloy with 18% Ni which, controlled additions of aluminium, manganese and iron, together with additions of chromium and niobium, develops a good combination of strength and ductility following controlled working and ageing treatment. The principal strengthening agent is Ni_3Al precipitates, supplemented by further strengthening from Ni_3Nb, NiNbSi and $Ni_{16}Nb_6Si_7$ precipitates. The increased strength of Marinel over the previous NES835 alloy enabled some specific naval design applications to utilise this high strength alloy.

One application of this alloy has been for the securing bolts for the external submerged fixing of a glass reinforced plastic structure. However a number of instances of fastener failures were encountered which on examination exhibited an intergranular morphology and were attributed to stress corrosion cracking, despite the absence of the environments normally expected to give rise to this mode of failure in this and similar copper based alloys. It was considered that sensitisation of the material by the heat cycle employed during the hot heading process could have rendered the material susceptible to stress corrosion. This sensitisation being to a wider range of environments, and possibly less aggressive environments than those typically considered detrimental to this material, such as mercury, amines and hydrogen sulphide.

The immediate recommendation was for the replacement of hot headed fasteners by fasteners machined from bar stock, but work was also put in hand to attempt the identification of the environmental component causing the stress corrosion cracking observed. The following chemical species were identified as being present in or associated with the bolted assembly:

1. Seawater – ever present in submerged joints.
2. Araldite – used to secure the bolt bushes, can generate amines on curing.
3. Loctite – used to lock the bolts, considered chemically inert.
4. Termalene grease – reportedly used in some assemblies.
5. Micro – a propriety cleaner/detergent containing a small percentage of ammonia – used in pre-cleaning the bolts.

A series of uniaxial, constant load, laboratory stress corrosion tests were undertaken. The environments being selected as:

1. Aerated natural seawater.
2. Araldite AV100 epoxy resin plus 2.5% Araldite hardener HV100.
3. Loctite 242.
4. Termalene grease (molybdenum disulphide type).
5. 10:1 solution of seawater and Micro.

These tests were carried out on as supplied material and material heat treated to simulate the hot headed microstructure. Test loads being 91 to 99% of the 0.2% proof stress of the material in the tested condition. Test durations were up to over 8000 hours if failure hadn't occurred, after which time surface examination and longitudinal sections of the specimens were examined for cracking.

Of the specimen/environment combinations evaluated only one suffered complete failure, this being the heat treated sample exposed to 10:1 seawater/Micro solution at 91% PS after 6300 hours. Surface cracking was observed in a heat treated sample in aerated seawater after over 8000 hours. No other samples exhibited observable surface cracking, and sections showed no cracking and only minor corrosion on the seawater/Micro exposed samples.

Although not an exhaustive series of tests, the conclusions of this study were that cracking only occurred in the simulated hot headed material either in the seawater/Micro solution when failure occurred or in aerated seawater when surface cracking was observed. The other environments did not induce cracking. The seawater/Micro solution also caused surface corrosion on the samples.

An instruction to the fleet to prohibit the use of this ammonia containing cleaning solution was issued. This, together with the earlier recommendation to replace hot headed fasteners, has resulted in the elimination of failures in machined Marinel fasteners attributed to stress corrosion, except for one specific incidence involving bar stock with very coarse niobium rich precipitates.

Marinel is now manufactured and marketed by Langley Alloys Division of Meighs Ltd. As a consequence of the problems experienced in the Marinel alloy and with the aim of obtaining a more consistent product the current supplier has introduced Marinel+. It is understood that Marinel+ contains reduced levels of iron and niobium, and is subject to tighter controls in respect of both composition and heat treatment than had been previously applied to Marinel. The effectiveness of these changes have yet to be fully assessed by UK MoD.

Nibron Special

Nibron Special is a proprietary copper alloy containing 14.5% nickel with controlled additions of aluminium, iron and manganese. The strengthening is from Ni_3Al precipitation through controlled rolling and heat treatment. This alloy has been marketed as having equivalent strength and applications to Marinel.

To provide a potential second material source for designs requiring high strength copper alloy a study of the properties and performance of Nibron Special has been conducted. Whilst this contained comparison of a wide range of material properties, including mechanical and corrosion performance, one area of particular concern was its potential behaviour in the equivalent environment under which Marinel was found susceptible to stress corrosion cracking.

An identical procedure of uniaxial, constant load, laboratory stress corrosion test was conducted on as supplied and simulated hot headed Nibron Special material. The environments in this investigation were however restricted to aerated natural seawater and seawater/Micro solution, as these had shown cracking in Marinel. As a control and check against the Marinel previously evaluated in this way, two heat treated Marinel specimens from the original batch were tested simultaneously with these Nibron Special specimens.

None of the Nibron Special or Marinel control specimens failed during the testing. After 8760 hours tests were removed, examined and sectioned. The Marinel control specimens showed extensive intergranular cracking to a depth of 30μm in seawater and 75μm in seawater/Micro solution on the section examined. This being consistent with the earlier observations but without repeat of the earlier failure.

The as supplied Nibron Special specimens exhibited negligible attack in seawater with minor cracking to 25μm in seawater/Micro. The simulated hot headed Nibron Special specimens showed very small cracks of less than 20μm in seawater but evidence of extensive intergranular cracking extending to depths of up to 90μm in the seawater/Micro solution.

It was concluded that the simulated hot headed microstructure in Nibron Special had increased susceptibility to stress corrosion cracking in the environments evaluated. The seawater/Micro solution was the more aggressive environment. The Nibron Special results were comparable with the Marinel results in the control tests and earlier studies.

Discussion

The initial introduction of high strength copper nickel alloys in submerged naval applications has encountered a minor incidence of service failures. In the specific application examined the failure rate attributed to stress corrosion was less than 5% and then restricted to specific batches of fasteners.

The microstructure of these high strength materials is engineered by additions of alloying elements combined with controlled working and specific heat treatments. This leads to the optimum microstructure and properties as promoted by the suppliers. Hot heading is a standard bolt forming process for conventional materials due the reduced bar stock diameter requirements and the cost effective use of material. The alternative machining process does have cost penalties and material wastage. However with these advanced copper based materials it is not surprising that subsequent thermal and deformation cycles introduced to produce the hot head are likely to alter the optimum microstructure. In this case it has been clearly illustrated that this altered microstructure directly lead to an unanticipated susceptibility to stress corrosion cracking.

Certain chemical species are known to initiate stress corrosion cracking in copper nickel alloys. These have been documented elsewhere and include mercury, amines and hydrogen sulphide. Assessment of the specific assembly procedure did not identify the presence of any of these specific known species, however as shown in the studies, the presence of the ammonia based cleaning solution used in the joint assemble showed a detrimental effect.

The reported studies have clearly shown that the simulated hot headed microstructure is susceptible to stress corrosion cracking in the identified seawater/Micro solution and this is considered the most likely cause of the premature failure of the service fasteners.

The relatively low incidence of failure may be explained by the batch to batch variations in microstructure produced, the change in microstructure along the fastener length and the likelihood of the presence of the residual cleaner species at a specific susceptible region.

Despite only the single incidence of failure in the laboratory tests, the Marinel test results from both studies are mutually supporting and comparable with the Nibron Special results.

The remedial actions to move to machined bolts with the optimum microstructure recommended by the supplier and the removal of the ammonia based cleaning solution are the immediate outcome of this work.

Conclusions

Despite the development of high strength copper nickel alloys with significantly higher strength levels than previously available, their introduction to wider naval use has been restrained due to unexpected service failures in one specific submerged application. An understanding of this specific problem was essential to suggest remedial action and to re-establish confidence in these generic materials to promote their wider use.

Assessment of the original failures and the supporting laboratory studies have concluded that the specification of hot headed Marinel bolts which changed the optimum material microstructure into one susceptible to stress corrosion in an unexpected environment and a cleaning procedure which introduced this specific environment were the most probable causes of the problems encountered. This supplemented by improved material process control introduced by the suppliers of these high strength materials now offers the potential of their wider use, provided this is cost effective and carefully considered to avoid similar problems to those encountered above.

Comparisons on Marinel and Nibron Special show the two alloys to be broadly comparable in their mechanical and corrosion performance, especially in their stress corrosion behaviour determined in the reported studies. Both alloys are potential candidates for these high strength naval applications.

Acknowledgements

This work was conducted by DERA under funded from STGMT, DPA, MoD UK. The assistance of colleagues at DERA is acknowledged in conducting the work reported, especially C Roberts, T Shucksmith and C Caldwell.

Hiduron 191, Marinel and Marinel+ are tradenames of Langley Alloys Division of Meighs Ltd. Nibron Special is a tradename of Columbia Metals Ltd.

© British Crown Copyright 2001/DERA

Published with the permission of the Defence Evaluation and Research Agency on behalf of Controller of Her Majesty's Stationery Office.

Table 1
Nominal Compositions

Wt%	Cu	Ni	Al	Fe	Mn	Cr	Nb
Marinel	balance	18	2	1	5	0.5	0.6
Nibron Special	balance	14.5	3	1.5	0.3		

Table 2
Mechanical Properties

Material	Condition	0.2% PS (MPa)	UTS (MPa)	Elongation (%)
Marinel	Spec. Min	700	870	15
	As supplied	791	1002	16
	Simulated Hot Headed	660	956	22
Nibron Special	Spec. Min	630	850	12
	As supplied	767	916	
	Simulated Hot Headed	592	794	

#516429 (17)

Canadian Navy Pollution Abatement Overview

by

LCdr Peter Hartley, NDHQ, DMSS 4-8

Abstract

Concern for the environment is a key issue on the Canadian National Agenda and a major concern for the Department of National Defence. This presentation will review the environmental regulations the Canadian Navy strives to meet and the departmental policy statement on pollution prevention. It will also list the methods and pollution abatement equipment the navy is using to implement the policy onboard navy ships. The brief will also introduce the Canadian navy involvement with the NATO community.

Maritime Environmental Protection in the Canadian Navy

by: LCdr Peter Hartley

Introduction

- **Concern for the Environment - key issue on the Canadian National Agenda commenced late '80s**
- **Green Plan / Code of Environmental Stewardship - Gov't Leadership Role**
- **Federal Departments would set the example**
- **Nav Ops affected by Environmental Regs**

Applicable Regulations

- **International Waters: International Convention for the Prevention of Pollution from Ships - MARPOL 73/78**
- **Territorial Waters: Canada Shipping Act**
- **Canadian Fisheries Act**
- **Great Lakes & Western Segment of St Lawrence Seaway: Great Lakes Sewage Pollution Prevention Regulations**

Regulations (Continued)

- **MARPOL 73/78: Warships are exempt**
- **Canada Shipping Act: Warships are exempt**
- **Great Lakes Sewage Pollution Prevention Act: Warships are exempt**

However

- 'it is CF and DND policy that the letter and spirit of all applicable federal environmental laws shall be met or exceeded and, whenever possible, compatibility with provincial and international standards shall be ensured'

Solid & Liquid Waste Streams

- **Solid Waste**
    - **Plastics - anything that has plastic in it**
    - **Garbage - Metal, glass, paper, cardboard, non-oily rags, floating dunnage**
    - **Food Waste**
- **Liquid Waste**
    - **Black Water - drains from toilets & urinals**
    - **Grey Water - galley, laundry, sink & shower drains**
    - **Oily Water/ Bilge Water**

Amount of Solid Waste Produced

- estimated that a frigate generates about 2.7 cu-m/day/man of waste products. This can be broken down as follows:
  - Food: 7.0%
  - Paper/Cardboard: 44.2%
  - Metal & Glass: 11.5%
  - Plastics: 37.3%

Solid Waste Discharge Regulations iaw MARPOL 73/78

- **Plastics - Discharge is prohibited**
- **Non-Pulped Garbage - Shall not be disposed of at sea within 25 nm from any coastlines or anywhere in MARPOL Special Areas**
- **Pulped Garbage shall not be disposed of within 3 nm from coastlines or within 12 nm when in MARPOL Special Areas**

Solid Waste Discharge Regulations (Cont'd)

- **Pulped Food Waste - Shall not be disposed of within 3 nm from coastlines, or within 12 nm when in MARPOL Special Areas, unless operational requirements dictate otherwise**
- **Non-Pulped Food Waste - Shall not be disposed of within 12 nm from coastlines including MARPOL Special Areas**

Solid Waste Handling Equipment

- **Plastic Waste Processor consisting of:**
    - **Compress/melt units**
    - **Storage racks**
- **Shredder & Shredder/Compactor**
- **Pulper**
- **Bag Sealing System**
- **Galley Garbage Grinder (garberator)**

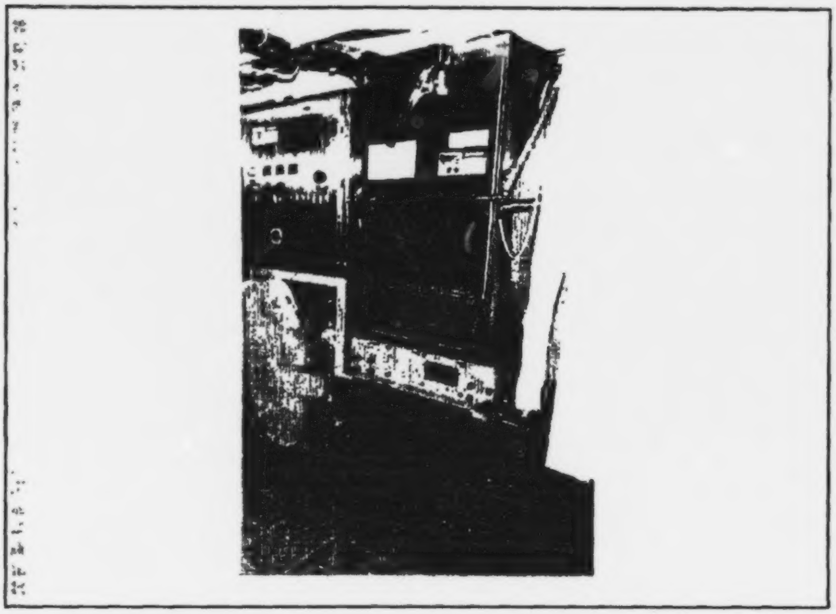

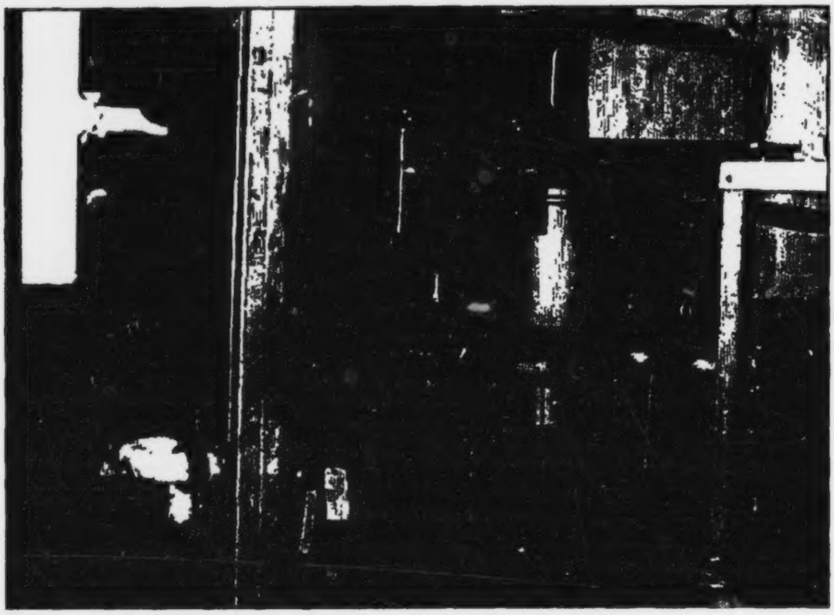

Black Water Discharge Regulations

- Discharge prohibited in inland waters
- In Harbour - Ships must comply with local regulations
- At Sea:
    - 0 - 12 nm - Effluent must be treated using a certified system & ship underway at speed greater than 4 knots
    - Beyond 12 nm of any coast - Untreated discharge permitted, at moderate rate, if ship underway at speed greater than 4 knots

National & International Effluent Standards for Type II MSDs

Authority					Sample Size	Statistic Type
	CFU (/100 ml)	TSS (mg/l)	BOD (mg/l)	Chlorine (mg/l)		
CSA	200	50	50	(.5-1.0)	40	Absolute
MARPOL	250	100	50		40	Geometric Mean
USCG	200	150	N/A	N/A	40	Arithmetic @95%
		CFU = Colony forming units (fecal coliform) TSS = Total Suspended Solids BOD = Biochemical Oxygen Demand				

Grey Water Discharge Regs

- **Grey Water discharge is not presently regulated by either the CSA or MARPOL 73/78 providing that no hazardous waste or chemicals are mixed with laundry or washplace drains.**
- **Nevertheless, many port authorities and coastal states do regulate the discharge of grey water**

Black & Grey Water Systems

- **All ships are fitted with Vacuum Collection Holding & Transfer Systems**
- **Omnipure sewage treatment plants being procured for IROQUOIS and PROTECTEUR Class ships**
- **The Omnipure sewage treatment plant on HFX Class ships has being upgraded**

Oily Waste Water Discharge

- **Oily waste water shall only be discharged overboard after treatment with oil separating or oil filtering equipment, and only if:**
  - **less than 5 ppm in inland waters**
  - **less than 15 ppm outside of inland waters**
  - **system has an Oil Content Monitor**
- **Discharge is prohibited in Arctic waters**

Oily Waste Water Equipment

- **Only those oily water separators fitted with an oil content monitor (and recirculation line) that prevent the discharge of effluent which exceeds the limits are acceptable**
- **Ships not fitted with OCMs must post a sentry at the discharge point to ensure the effluent shows no visible oil sheen**

Oily-Water Separator & Oil-Content Monitor

- **The Hydromem Oil-Water Separator & Oil-Content Monitor was procured and delivered**
- **The OWS & OCM were certified Sep 98**
- **Installations are in progress**

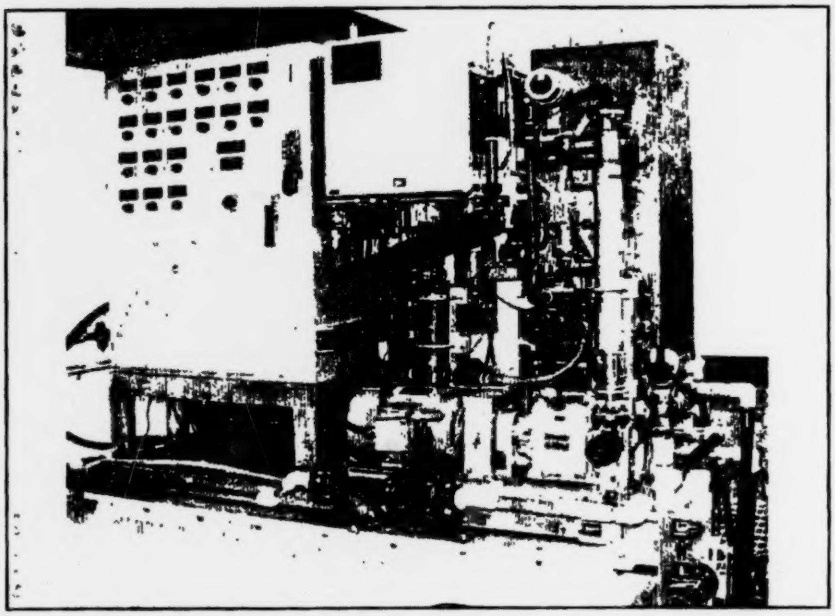

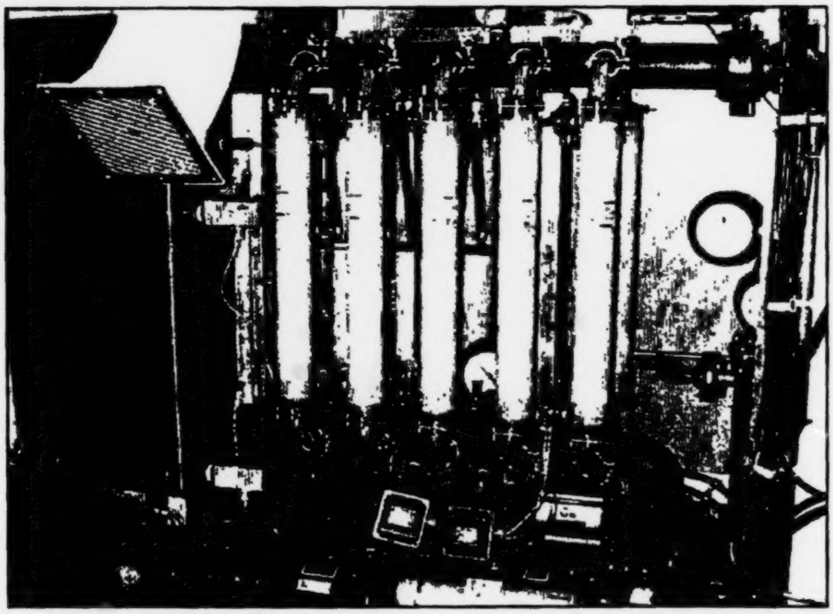

NATO - Special Working Group 12

- Formed to bring NATO experts together to discuss and share information concerning Maritime Environmental Protection
- Work together to save time and money
- Exchange Test & Evaluation information
- Identify opportunities for co-operation
- Oil Spill Expert Team
- Expert Workshops

Environmentally Sound Ships

- The long term goal for NATO navies is to develop environmentally sound ships; not just compliant ships.
- Unrestricted world-wide ops, including ports, littoral areas and restricted seas, free from the constraints of national or international legislation
- Where possible, systems will be designed for zero discharge

E.S.S - Cont'd

- Where zero discharge is not feasible or appropriate, discharges will be environmentally benign
- All waste held onboard will be acceptable for disposal ashore

What's Coming Next

- Ban on the use of TBT anti-fouling paints by 2008
- Ballast water management
- Air Emission controls
- Solid and Liquid Waste management. Green Ship Index in Europe. Ships will be ranked and monitored. The higher the ranking, the lower the port service costs

#516430 (18)

IMPACT OF OPERATIONAL PARAMETERS ON A MEMBRANE BASED BILGE WATER TREATMENT SYSTEM

By Marco Nottegar
Naval Engineering Test Establishment
LaSalle, Quebec, Canada H8R 1Z2

INTRODUCTION

In an effort to balance environmental discharge requirements with acceptable bilge water treatment rates the Canadian Navy has investigated the appropriateness of a membrane based shipboard bilge water treatment system. Initial results have revealed that the effluent (membrane permeate) has achieved the 15 mg/L (beyond 12 nautical miles) and 5 mg/L (within inland waters) requirements but difficulty has been experienced in sustaining adequate discharge rates.

In order to optimize membrane permeation rates (flux) two important aspects of a membrane based system need to be addressed: pre-treatment and membrane operational parameters. This paper addresses the impact of membrane operational parameters on membrane flux. Specifically, the impact of cross-flow conditions and pressure will be examined.

THEORY

Many theoretical models exist to describe membrane flux behaviour. One model is the "resistive model" which expresses membrane flux as (1):

$$J = \frac{\Delta P}{\mu R_{total}} \qquad (1)$$

where: J = membrane flux;
ΔP = trans-membrane pressure;
μ = viscosity; and
R_{total} = total system resistance.

The total system resistance is the sum of various resistive components, which include the intrinsic resistance of the membrane, the resistance associated with the boundary layer and the resistance associated with membrane fouling. The overall system resistance can be expressed as:

$$R_{total} = R_{mem} + R_{bl} + R_{foul} \qquad (2)$$

where: R_{mem} = intrinsic membrane resistance;
R_{bl} = boundary layer resistance; and
R_{foul} = fouling resistance;

The benefit of using the resistive model is that it allows for an easy means of quantifying the various resistive components.

The intrinsic membrane resistance is dependent on the membrane's characteristics and independent of feed concentration and operating conditions. Specifically, a membrane's resistance is determined by its overall pore area and structure plus its interaction with the liquid it is treating (in the case of bilge water treatment the hydrophilic/hydrophobic nature of the membrane).

The boundary layer resistance is the result of concentration polarization of the solute at the membrane surface, resulting in an additional resistance to flux. The impact of flow conditions on the boundary layer resistance is identified through an examination of the phenomena of concentration polarization, whereby membrane flux is expressed as (2):

$$J = k \ln\left(\frac{C_{bl}}{C_{bulk}}\right) \qquad (3)$$

where: k = mass transfer coefficient;
C_{bl} = concentration at the boundary layer resistance; and
C_{bulk} = bulk concentration.

The mass transfer coefficient is dependent on hydraulic conditions, that is laminar or turbulent flow, and therefore it can be affected the membrane hollow fibre diameter and the bilge water velocity. The mass transfer coefficient, and therefore flux, is related to Reynolds Number as follows (1):

$$k \alpha \mathrm{Re}^{0.33} \quad \text{for laminar flow conditions} \qquad (4)$$

$$k \alpha \mathrm{Re}^{0.85} \quad \text{for turbulent flow conditions} \qquad (5)$$

$$\mathrm{Re} = \frac{V d_h \rho}{\mu} \qquad (6)$$

where: V = membrane cross-flow velocity;
d_h = hydraulic diameter, which is the hollow fibre diameter in this case; and
ρ = liquid density.

While we cannot control the density or viscosity of the bilge water it is possible to alter the membrane cross-flow velocity (through pump size) and the diameter of the hollow fibre (during the design/selection of the membrane) and therefore control the mass transfer coefficient. Additionally, equations (4) and (5) reveal that increasing the Reynolds number increases the mass transfer coefficient and therefore membrane flux, but the significant increase in membrane flux occurs when flow conditions change from laminar to turbulent flow.

The fouling resistance is caused by the interaction of the boundary layer with the membrane. Accordingly, membrane fouling is also affected by the flow conditions and trans-membrane pressure.

Figure 1 provides a graphical representation of the impact that hydraulic conditions and trans-membrane pressure have upon membrane flux. In Figure 1 it can be seen that for a membrane processing pure water flux is directly proportional to the trans-membrane pressure. However, for a membrane processing contaminated water the flux reaches a point where it becomes pressure independent. This is due to the boundary layer formation being proportional to the applied trans-membrane pressure. Therefore when the boundary layer dominates any increases in trans-membrane pressure are offset by a subsequent increase in boundary layer resistance. While Figure 1 does not incorporate membrane fouling it still provides important information as to the onset and impact of fouling because it is known that the fouling becomes greater when the boundary layer is thicker/denser(5). Therefore fouling is greatest when flux is pressure independent.

Figure 1: Membrane Flux vs. Trans-Membrane Pressure Relationship

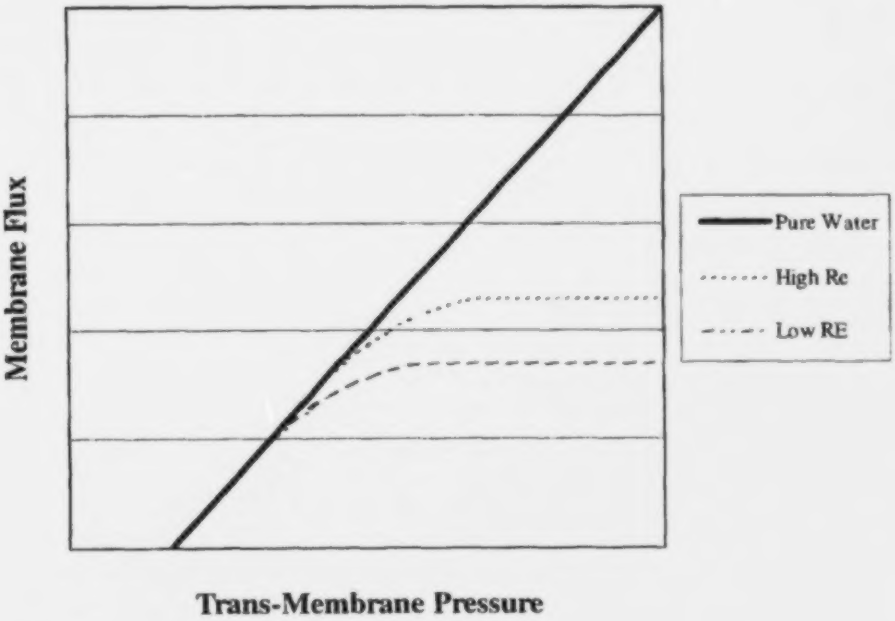

Figure 1 also shows the impact that flow conditions have upon flux. That is, more turbulent flow, as identified by the Reynolds number, allows for increased flux. Reviewing equations (3), (4) and (5) it can be seen that this is the result of membrane flux being directly proportional to the mass transfer coefficient, which is directly proportional to the Reynolds number.

METHODOLOGY

The test runs were conducted using the test rig shown in Figure 2. This test rig employed a single pass membrane configuration. Adjustments to the By-Pass Valve allowed for the control of the membrane cross-flow velocity, and the membrane inlet pressure. Adjustments to the Permeate Valve allowed for the control of the permeate pressure.

Figure 2: Experimental Test Rig

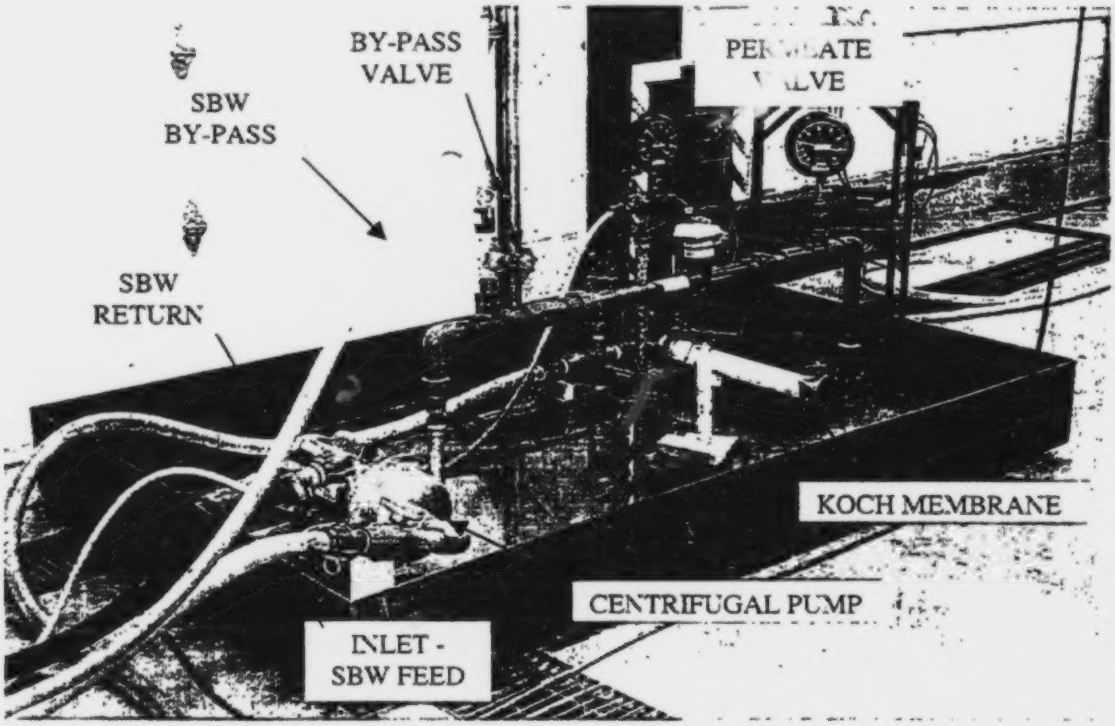
BY-PASS VALVE
PERMEATE VALVE
SBW BY-PASS
SBW RETURN
KOCH MEMBRANE
CENTRIFUGAL PUMP
INLET - SBW FEED

Unless otherwise noted each test run was comprised of the following three runs:

a. Pure Water Permeate (PWP) Run. To determine the intrinsic resistance of the membrane prior to a Synthetic Bilge Water (SBW) Run;
b. Synthetic Bilge Water (SBW) Run; and
c. Post-SBW PWP Run. This PWP run was conducted after flushing the test rig with approximately 50L of water. The purpose of this water flush is to remove the boundary layer from the membrane and the contaminants present in the test rig. The purpose of this run was to determine the degree of fouling experienced by the membrane, by determining the membrane plus the fouling resistance.

Two hollow fibre membranes were tested, these being the KOCH HF15-45-XM50 and WIMCO S-32516 membrane. Table 1 identifies the major characteristics of these two membranes.

Table 1: Membrane Characteristics

Membrane	**Membrane Material**	**Hollow Fibre Internal Diameter (m)**	**Number of Hollow Fibres**	**Membrane Area (m^2)**	**MWCO (Daltons)**
KOCH	PAN	$1.14*10^{-3}$	650	1.39	50,000
WIMCO	Modified PAN	$1.60*10^{-3}$	230	0.675	50,000

Notes: PAN = polyacrylonitrile
MWCO = Molecular Weight Cut-Off

A Synthetic Bilge Water mixture containing approximately 2000 mg/L of oils was used for the SBW runs. This SBW mixture was prepared with the following constituents:

a. 2000 mg/L of Oils. These oils were comprised of:
    i. 50% new naval distillate,
    ii. 20% new diesel engine lubricating oil,
    iii. 20% used diesel engine lubricating oil,
    iv. 10% new hydraulic oil;
b. 500 mg/L of Surfactants. These surfactants were comprised of:
    i. 80% high emulsifying surfactant (i.e. ALCONOX),
    ii. 10% Corrosion Removal Compound,
    iii. 10% Aqueous Film Forming Foam (AFFF);
c. 250 mg/L of solids. These solids were comprised of:
    i. 80% course grade AC test dust,
    ii. 10% ferric oxide,
    iii. 10% carbon black; and
d. The remaining 99.725% of the SBW was water, with a 50/50 mix of fresh and seawater. Accordingly, the salt content of this 50/50 mixture is approximately 18,000 mg/L.

All of the above components were added and the SBW was mixed for approximately 15 minutes prior to conducting the SBW Run.

NOTE

> Oil-in-water analysis was conducted in accordance with EPA method 1664. However, the results proved to be suspect and therefore are not addressed in this paper. In accordance with EPA method 1664 the extractant used is n-hexane. It is suspected that the reason for the problematic oil-in-water results is due to n-hexane not having the ability to sufficiently to adequately break down the emulsions caused by the surfactant used in the preparation of the SBW.

TEST RESULTS AND DISCUSSION

The goal of the testing was to examine the impact of hydraulic flow conditions and trans-membrane pressure on membrane flux.

Hydraulic Flow Conditions

To examine the impact of a membrane's hydraulic flow conditions on its flux two variables were examined:

a. cross-flow velocity of the SBW through the membrane; and
b. hollow fibre diameter.

In essence the purpose of the both of these tests was to determine the impact of hydraulic flow conditions, as defined by the Reynolds Number, on flux capacity. While Reynolds numbers do not exactly predict hydraulic flow conditions they do provide a good guide of the type of hydraulic flow conditions present. The general rule is that:

a. laminar flow is present with a Reynolds number no greater than 2300;
b. turbulent flow is present with a Reynolds number greater than 4000; and
c. a transition from laminar to turbulent flow occurs when the Reynolds number is between 2300 to 4000.

The examination of the cross-flow velocity was conducted exclusively with the KOCH membrane. The examination of the impact of the hollow fibre diameter was conducted by comparing the performance of the KOCH and WIMCO membranes.

With the exception of the SBW Run conducted with a membrane cross-flow velocity of 87L/min (23.0 US gpm) all of the SBW Runs were conducted for a duration of 240-minutes. However, in order to properly compare fouling resistance all of the results will be presented based upon a 180 minute run duration.

Cross-Flow Velocity

Figure 3 displays the results of the test runs, conducted with varying cross-flow velocities through the KOCH membrane. This graph shows a marginal increase in flux with an increase in cross-flow velocity. However, examining these results may be somewhat misleading as the membrane resistance varies from run to run as a result of "irreversible membrane fouling" (i.e. the limitations of the cleaning procedure employed). To remove this variable the resistances attributed to the SBW boundary layer and fouling have been determined through PWP runs, conducted before and after the SBW run. Table 2 identifies these resistive components and allows for a cross-referencing of these resistive components against the hydraulic flow conditions present during each SBW Runs. Figure 4 graphically represents these resistive components versus the cross-flow velocity.

Figure 3: SBW Runs – Varying Membrane Cross-Flow Velocity

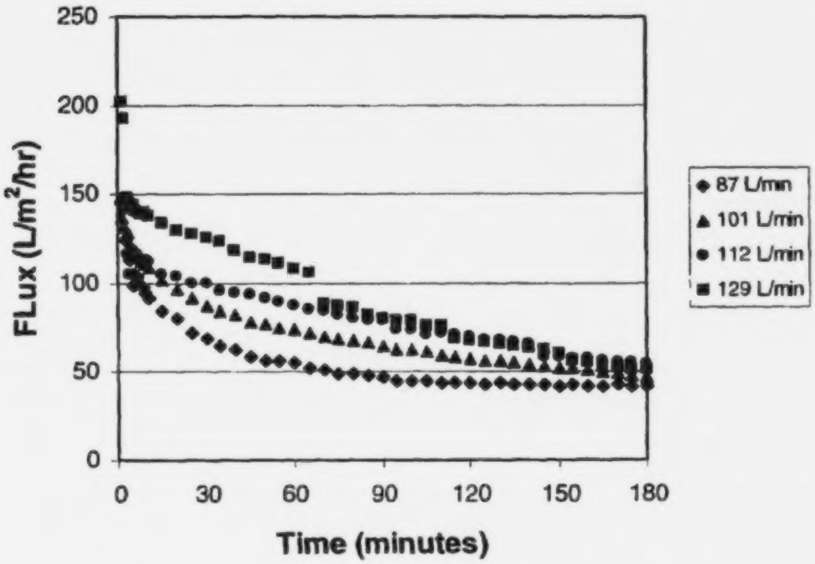

Examining Table 2 and Figure 4 it can be seen that the boundary layer and fouling resistance appear to decrease as the cross-flow velocity is increased. The boundary layer resistance has a slight spike upwards for the test run conducted at 112 L/min and the fouling resistance increased rather substantially for the 129 L/min run. However, these inconsistencies could be attributed to one of two factors:

a. difficulty in preparing identical batches of SBW; and
b. limited variance in hydraulic flow conditions (i.e. Reynolds number).

Table 2: SBW Runs – Varying Membrane Cross-Flow Velocity

Cross-Flow Velocity		Reynolds Number	Trans-Membrane Pressure	Resistive Components (10^{15} m^{-1})			
(L/min)	(m/s)	(-)	(psi)	R_{total}	R_{mem}	R_{bl}	R_{foul}
87	2.18	2772	9.50	6.39	1.55	2.18	2.66
101	2.52	3206	8.88	5.21	1.44	1.59	2.19
112	2.79	3555	9.00	4.64	1.60	1.83	1.20
129	3.22	4098	9.25	5.00	1.34	1.37	2.29

Generally, it appears that the flux increases with increasing in cross-flow velocity. However, the ability to alter the hydraulic flow conditions with the same membrane is limited to the operating range of the membrane. Specifically, for the KOCH membrane the maximum membrane inlet pressure is 30 psi and these test runs were conducted with the membrane inlet pressure ranging from 19 to 24 psi. Therefore any further increases in membrane cross-flow velocity are limited, especially considering that pressure is proportional to the square of velocity.

NOTE

> It should also be noted that testing conducted by the Carderock Division, Naval Surface Warfare Center used a cross-flow velocity of 4 m/s (5). This cross-flow velocity is higher than that which can be obtained with the KOCH membrane, given its maximum inlet pressure rating of 30psi.

Figure 4: Boundary Layer and Fouling Resistances for Varying Membrane Cross-Flow Velocity

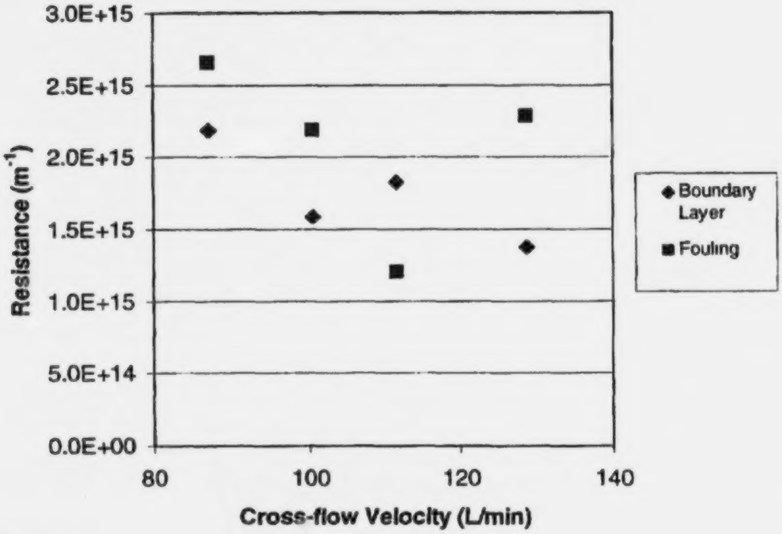

Hollow Fibre Diameter

As identified above the ability to vary the cross-flow velocity with the KOCH membranes is limited. Therefore in order to further examine the impact of varying hydraulic flow conditions has on membrane performance two different membranes were compared. These two membranes were the KOCH and WIMCO membranes. These two membranes had a number of differences, with the two primary differences being different hollow fibre diameters and membrane material. Therefore some but not all of the different flux capacities can be attributed solely to the different fibre diameter.

The test runs for both membranes were conducted with a trans-membrane pressure of approximately 11 psi. The test runs were conducted such that the KOCH and WIMCO membranes had Reynolds numbers of approximately 3500 and 6600 respectively. With a Reynolds number of approximately 3500 it is most likely that the KOCH membrane is operating with a flow in the transition stage between laminar and turbulent flow. However, the WIMCO membrane does appear to be operating with turbulent flow.

As seen from Figure 5 the WIMCO membrane had a much greater flux than the KOCH membrane. Part of the reason that the WIMCO membrane demonstrated a greater flux can be attributed to its material of construction. This is demonstrated by its greater PWP flux; i.e. its lower membrane resistance. The membrane resistance of the KOCH and WIMCO membranes are approximately $1.27*10^{15}$ m^{-1} and $0.52*10^{15}$ m^{-1}, respectively.

Figure 5: SBW Runs – Varying Membranes

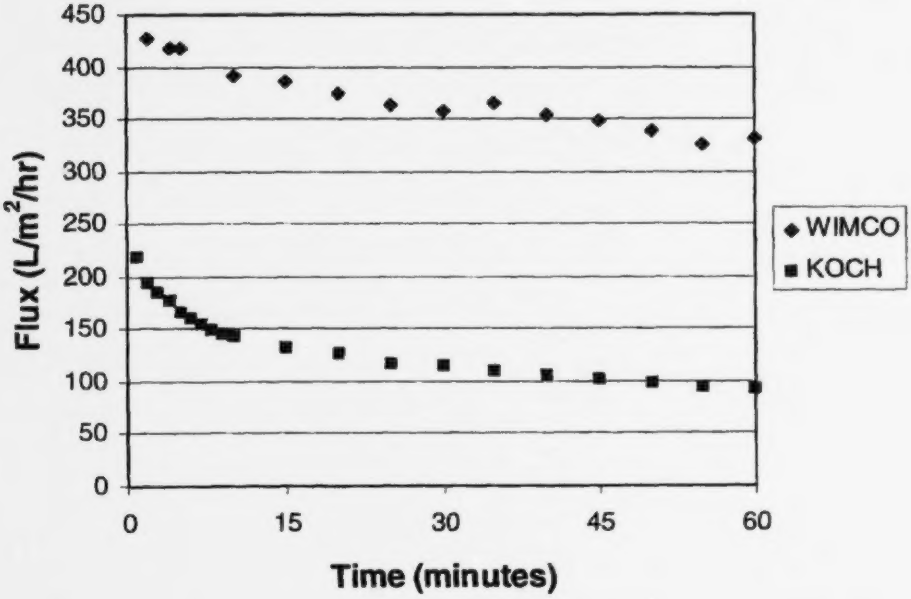

However, examination of the boundary layer and fouling resistances provides an insight into the hydraulic flow conditions. Figure 6 plots the combination of the boundary layer and fouling resistances over the duration of the run. (Unfortunately, when these two membranes were tested a post-SBW PWP run was not conducted and therefore the boundary layer and fouling resistance could not be separated.) It can be noted from Figure 6 that:

a. the WIMCO membrane very quickly (within approximately 15 minutes) achieves a lower cumulative resistance than the KOCH membrane; and

b. the WIMCO membrane cumulative resistance stabilized much more quickly (within approximately 5 minutes) than the KOCH membrane.

Figure 6: Boundary Layer and Fouling Resistances for Varying Membranes

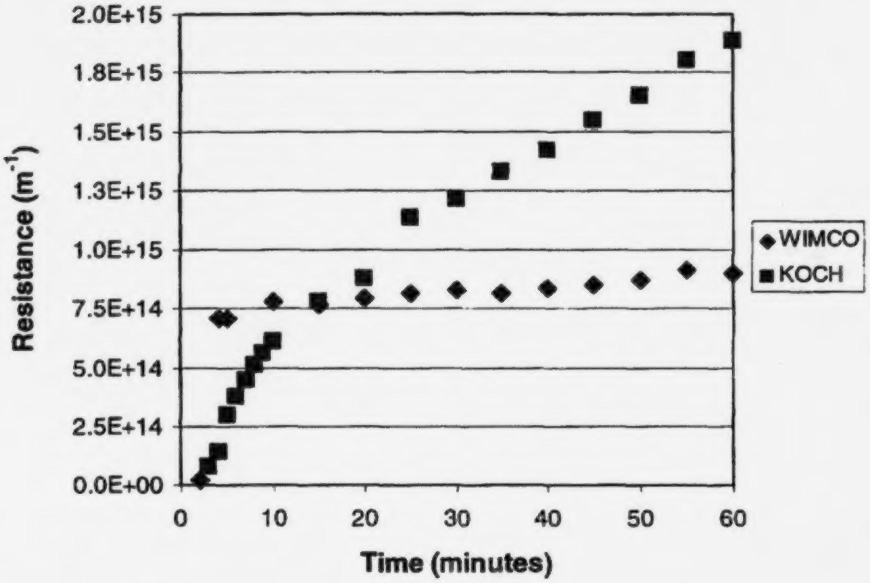

These trends highlight some important points regarding the operation of these two membranes. First, the WIMCO membrane likely experiences much less fouling than the KOCH membrane. This is revealed because the resistance associated with WIMCO membrane increases at a much lower rate than that of the KOCH membrane. Secondly, a steadily increasing non-membrane resistance is indicative of non-turbulent flow and conversely relatively consistent non-membrane resistance is indicative of turbulent flow (3). Accordingly, the KOCH resistance appears to demonstrate non-turbulent flow conditions. While the WIMCO membrane appears to demonstrate turbulent flow conditions.

Trans-Membrane Pressure

The effect of trans-membrane pressure on flux was examined by conducting 4 test runs, with the KOCH membrane, at trans-membrane pressure varying from 7.5 to 12.375 psi. For all these test runs the cross-flow velocity was maintained at approximately 129L/minute (34 USgpm), equating to a Reynolds number of approximately 4100.

As discussed above, in the examination of the hydraulic flow conditions, it was noted that the boundary layer and fouling resistances were greater than the membrane resistance. Therefore membrane theory predicts that it is these resistive factors, and not the membrane resistance, that will determine membrane flux. Therefore reducing trans-membrane pressure should result in an increased flux, due to decreased fouling. However, a quick review of Figure 7 does not substantiate this hypothesis as the test runs conducted at the higher trans-membrane pressures (9.25 and 12.375 psi) have significantly higher flux than the test runs conducted at the lower trans-membrane pressures.

Figure 7: SBW Runs – Varying Trans-Membrane Pressure

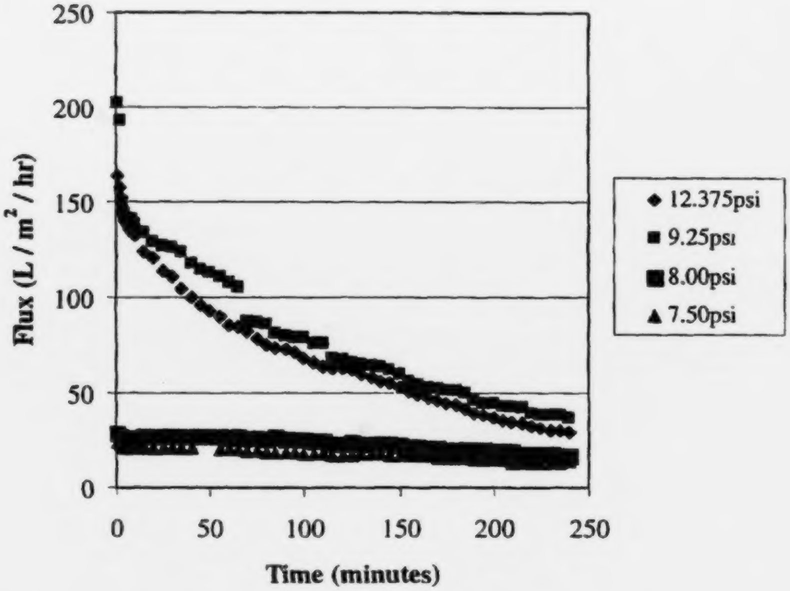

Parting out the membrane resistance and examining the boundary layer and fouling resistances is done in Figure 8. Here we see that the fouling resistance does decrease with decreasing trans-membrane pressure, as predicted by membrane theory. However, the boundary layer resistance is somewhat puzzling. Rather than continually decreasing with a decreasing trans-membrane pressure, as predicted by membrane theory, it is greatest at the lowest trans-membrane pressure.

The easy answer to explain this unexpected behaviour would be to assign this anomaly to the difficulty with creating similar batches of SBW and/or a lack of reproducible values from only four test runs. Therefore the test runs may not be providing accurate/reproducible results. However, it is my opinion that these results do represent actual conditions as other results have generally supporting membrane theory and were subject to the same conditions.

Figure 8: Boundary Layer and Fouling Resistances for Varying Trans-Membrane Pressures

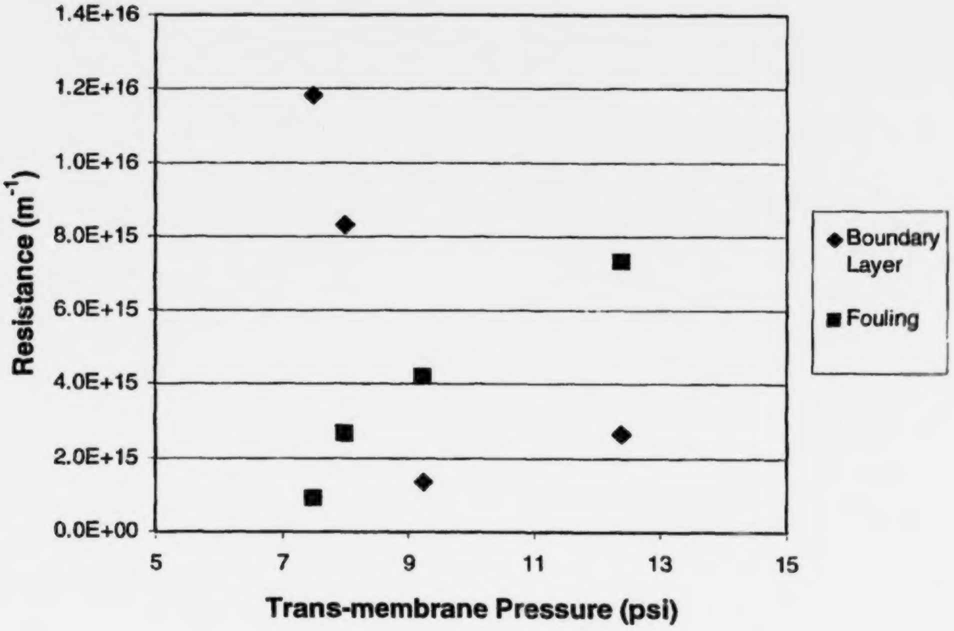

A closer examination of the operation, and the manner in which these trans-membrane pressures were achieved may provide a clue to this unexpected behaviour. To conduct these trans-membrane pressures test runs, at approximately the same cross-flow velocities, the required permeate pressure was created by adjusting the permeate valve. For the runs with trans-membrane pressures of less than 9 psi the membrane outlet pressure was less than the permeate pressure. Although for the 9 psi run the membrane outlet pressure was almost equal the permeate pressure. This is shown in Figure 9. When the permeate pressure is greater than the membrane outlet pressure the flux is reversed for a portion of the length of the membrane. That is, fluid is flowing from the permeate side to the inside of the fibre as to the normal flow pattern. Figure 9 shows that the boundary layer resistance rapidly increases when the permeate pressure exceeds the membrane outlet pressure. However, when the permeate pressure does not exceed the membrane fibre outlet pressure –"normal operation" - the boundary layer resistance reacts as expected.

Figure 9: Membrane and Permeate Pressures for Varying Trans-Membrane Pressures Runs

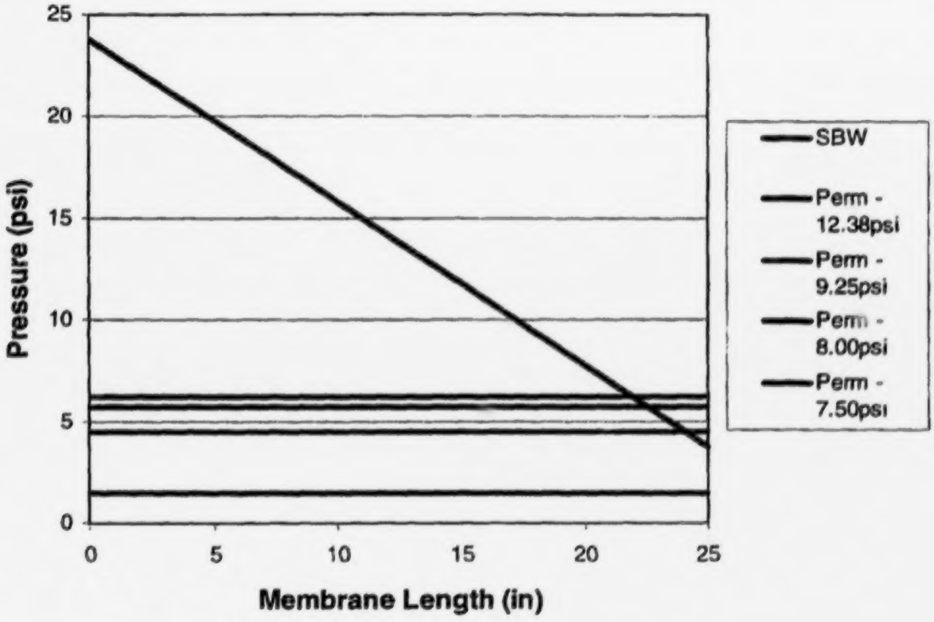

While the boundary layer resistance has this unique characteristic when the permeate pressure exceeds the membrane outlet pressure it is important to note, from Figure 8, that the fouling resistance continually and substantially decreases with a lower trans-membrane pressure. This characteristic is corroborated by testing conducted by the Carderock Division, Naval Surface Warfare Center which found that a "high fouling rate is a result of overfluxing the membranes" (5).

Accordingly, it would appear that the optimal operating conditions would be derived by running at the lowest possible trans-membrane pressure, without having the permeate pressure exceed the membrane outlet pressure.

Additionally, membrane design can have a substantial impact on ensuring the lowest possible trans-membrane pressure. Two possible means of designing a membrane to operate with a low trans-membrane pressure include:

a. increasing the membrane's cross-sectional area. This requires a balancing of trans-membrane pressure and hydraulic flow conditions; and/or
b. decreasing membrane length.

CONCLUSION

The membrane testing conducted revealed that it is the boundary layer and fouling resistances, not the membrane resistance, that are the limiting factors in determining membrane flux.

Accordingly, the importance of operating in turbulent flow conditions and minimizing trans-membrane pressure were proven to be critical in maximizing membrane flux.

With respect to trans-membrane pressure it was also revealed that increasing the permeate pressure beyond the membrane outlet pressure was counter productive, at least with respect to boundary layer conditions. Therefore permeate pressure should not exceed the membrane outlet pressure.

Varying operating conditions (such as cross-flow velocity and the membrane inlet, outlet and permeate pressures) allows for one to operate within a trans-membrane pressure range. However, it is during the membrane design that this trans-membrane pressure range is determined. A membrane's cross-sectional area (affected by the hollow fibre diameter in the case presented) and membrane length are some of the design factors which can influence the trans-membrane pressure range.

REFERENCES

1. Eykamp, W., "Mircofiltration and Ultrafiltration" in "Membrane Separation Technology. Principles and Applications", R.D. Noble and S.A. Stern, Eds., Elsevier Science B.V. (1995), pp. 1-43.
2. Mulder, M., "Polarization Phenomena and Membrane Fouling" in "Membrane Separation Technology. Principles and Applications", R.D. Noble and S.A. Stern, Eds., Elsevier Science B.V. (1995), pp. 45-83.
3. Porter, M., "Handbook of Industrial Membrane Applications", Noyes Publications, Park Ridge, New Jersey, U.S.A. (1990), pp. 136-229.
4. Technical Literature from Osmonics, Inc., "Select Engineering Principles of Crossflow Membrane Technology", 01 March 1990.
5. Tompkins, K.T., et al, "Ultrafiltration Membrane Polishing System for Shipboard Treatment of Oily Wastewater", Carderock Division, Naval Surface Warfare Center, not dated.

516431 ⑲

Studies on Micro and Ultrafiltration in Oily Wastewater Purification

A.Y. Tremblay and T.H. Li
University of Ottawa, Dept. of Chemical Engineering
Ottawa, ON.

D. E. Veinot
Defence Research Establishment Atlantic
Dockyard Laboratory(A), Halifax, NS.

ABSTRACT

A series of ultrafiltration (UF) and microfiltration (MF) tests were performed on an oily wastewater mixture whose composition closely resembled that of wastewaters accumulating in a ship's bilge. The wastewater was found to contain a substantial amount of dissolved solids, defined as particles measuring less than 0.45 micron, which cannot be accounted for as dissolved salts alone. These oily wastewaters are by nature difficult to treat with membrane processes. The presence of used lubricating oils in a ship's bilges implies that particles of soot will be present in this wastewater. In order to offer a better representation of actual bilge water, synthetic wastewater mixtures were prepared using used lubricating oils.

Experimental results indicate that free oil is present in this type of wastewater. The wastewater was found to contain mechanical emulsions, chemical emulsions and particles of soot that can act as nucleating sites for oil. The size of the particles causing the flux decline was determined from cake filtration theory. Excessive pump shear was found to reduce the size of these particles by half causing a reduction in membrane performance. Once dispersed, the particles causing this further reduction in flux decline did not readily aggregate over a 24 hour period.

Tests were performed to verify that free oil was not irreversibly coating the surface of the membrane leading to this flux decline. A UF membrane was placed in a stir cell and free oil was poured directly onto its surface. The results indicate that new oil does not readily remain on the surface of the membrane. To determine the affinity of used oil for the membrane, the test described above was repeated with used oil. After a period of 24 hours in the stir cell, 90 % of the membrane surface was free of oil and just as clean as at the beginning of the test. These tests indicate that the membrane can recover from the de-phasing of free oil at its surface.

The oil content of the permeate was determined for a series of UF membranes placed in cross-flow test cells. The quality of the permeate was relatively independent of the molecular weight cut-off of the membrane. Contrary to expectations, membranes having the smallest pore size had the lowest oil retention. The UF membrane having the lowest pore radius of 2 nm should have retained oil emulsions expected to be two to three orders of magnitude greater. This suggests that some free oil is dispersed in the wastewater at a molecular level. In the presence of a cake, free oil is scrubbed clean from

solution as it passes through the cake. The results further support cake dominated filtration where the presence of a hydrophobic cake at the surface of the membrane enhances the separation of free oil by capturing it in its structure.

Objectives

- Determine factors that affect the UF and MF of oily wastewaters.
- Focus on wastewaters containing:
- – mixture of 50/50, fresh water:seawater
- – presence of new vs. used oils.
- New vs. Used Oil
  - Microscopic examination of bilge water
  - Particle measurements using light scattering
  - Solids content in used oil
- Study oil de-phasing at the surface of the membrane.
- Determine oil removal as a function of membrane pore size (MWCO).

Oily Wastewater used in the permeation experiments – Synthetic Bilge Water

- oils – 2000 ppm;
- – 50% naval distillate (diesel fuel),
- – 40% naval diesel engine lubricating oil and,
- – 10% hydraulic oil.
- detergents and surfactants - 500 ppm.
- – 90% Canadian Navy standard oil and grease detergent (CLEANBREAK),
- – 10% Canadian Navy standard corrosion removal compound (OSTREM Rust Stain Remover).
- water - Composed of a 50/50 mixture of fresh and sea water.

New oil vs. Used oil

- New oil
- – oils are mainly aliphatic hydrocarbons (hydrophobic)
- Used oil
- – many oxidized chains (more hydrophylic)
- – contains soot
- – other particulates

Synthetic Bilge Water

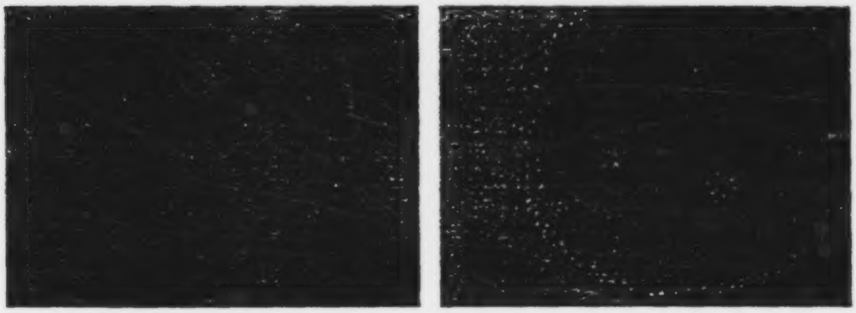

New Oil

Used Oil

50 µm

Microscopic examination of synthetic bilge water

- New oil - simple oil in water emulsion.
- Used oil - more complex water in oil in water emulsion.
- Used oil - possibility of forming reverse miscelles at the surface of the membrane

Determining the solids content in Used Oil

- Dissolve oil in hexane
- Filter using 0.45 micron PVDF filters.
- Particle content >0.45 µm = 4.9 % by wt. used oil.
- Particle content 0.02 to 0.45 µm = 0.72 % by wt.
- Total = 5.62 % by wt. used oil.

Bilge water can contain a large amount of dissolved solids in a range that is difficult to treat by membrane technologies.

- In a 6 % oil in water solution given very good dispersion,
- there is a potential to have (6 *0.72 % = 0.04 % dissolved solids in solution)
- assuming s.g. =1, gives 400 mg/L of dissolved particles in the 0.02 to 0.45 µm range.

Study effects of shear and aging on bilge water

Study the effect of shearing - aging
Shear => circulating wastewater in a centrifugal pump for 1/2 hour
Shear wastewater - rest 1/2 hour - test
Take same wastewater 24 hours later - shear – test

GN (10.0 kD) membrane
aging for
1/2 hour 24 hours

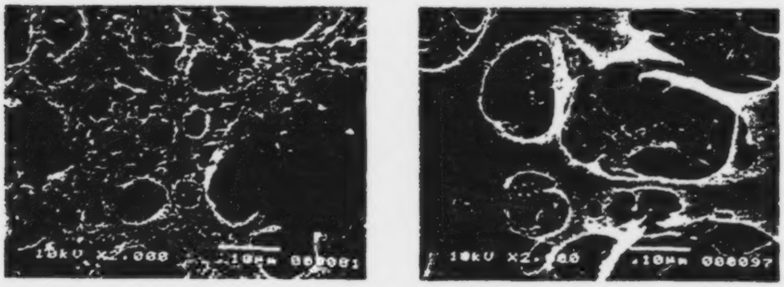
10kV X2,000 10µm 000081
10kV X2,000 10µm 000097

GN (10.0 kD) membrane
aging for
1/2 hour 24 hours

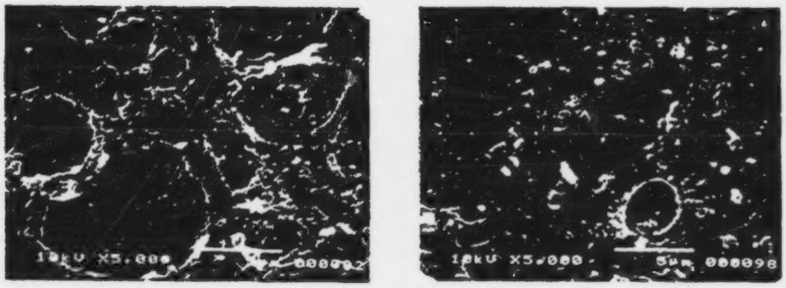
10kV X5,000
10kV X5,000 5µm 000098

The size of the particles causing the flux decline was determined from cake filtration theory.

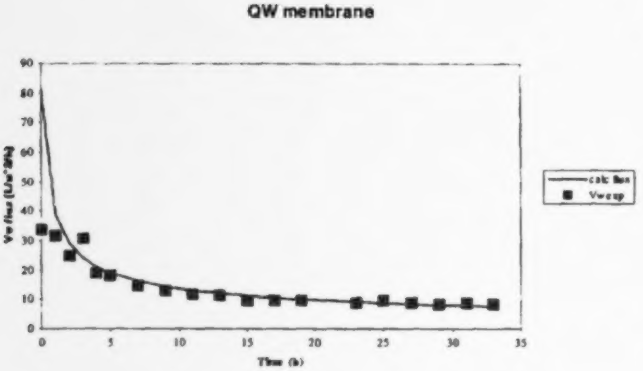

30,000 Daltons, MWCO, Radius = 6.4 nm

Shear effects on the radius of particles forming the filter cake at the surface of the membrane.

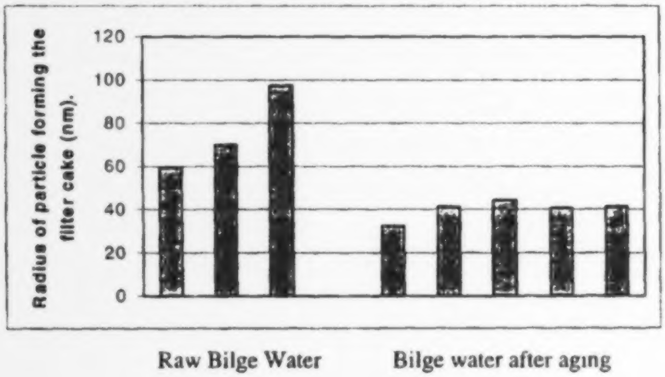

Conclusions from shearing and aging

- Shearing and aging reduced size of the particles found in synthetic bilge water.
- Once the bilge water was sheared, settling was not found to be a significant factor affecting the size of particles in bilge water.
- Excessive pump shear was found to reduce the size of these particles by half causing a reduction in membrane performance.

Tests to determine the influence of oil-membrane surface interactions

Objectives

- verify that free oil was not irreversibly coating the surface of the membrane
- perform experiments where free oil was poured directly onto the surface of the membrane prior to the permeation run.

Method

- Experiment conducted in a 7.0 cm diameter stir cell, QW (30 kD) membrane selected.
- The membrane was initially wet with water.
- Water droplets were completely removed from its surface.
- The membrane was placed in the stir cell and oil was poured directly onto the membrane until it was coated by a 1/8" thick layer.
- The oil covered membrane was then allowed to sit for 5 minutes.
- The stir cell was filled with synthetic bilge water and a standard permeation experiments carried out at 50 psig.

Plot of bilge water permeate flux vs. time for a membrane flooded with oil.

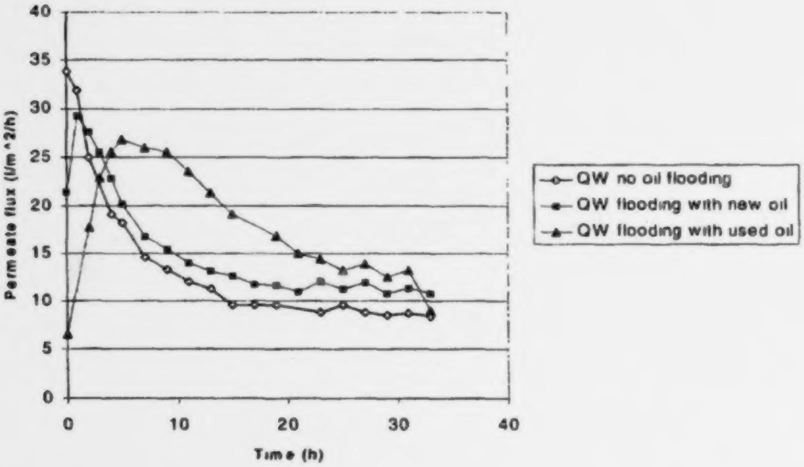

Plot of bilge water permeate flux vs. time for a membrane flooded with oil.

Conclusion- oil-membrane surface interactions

- The membrane can recover from a sudden exposure to oil.
- Hydrophilic membrane materials do exist, (QW membrane), that reduce or eliminate free oil as a cause of irreversible membrane fouling.
- These tests also indicate that the membrane can recover from the de-phasing of free oil at its surface.

The ability of membranes to separate oil and grease (O&G)

Analyze permeate from cross-flow tests

- operate test cells at a cross-flow velocity of from 1 to 1.8 m/s.
- Membranes were tested at 50 psig.
- Bilge water concentration of hexane extractable Oil and Grease EPA 1664 = 73 mg/L

Results from oil removal tests

- All membranes produce a permeate that meets and greatly exceeds the discharge regulation of 15 mg/L oil and grease for a feed concentration of 73 mg/L oil and grease.
- The quality of the permeate was relatively independent of the molecular weight cut-off of the membrane.

Plot of O&G Concentration in the permeate vs. MWCO of the membrane

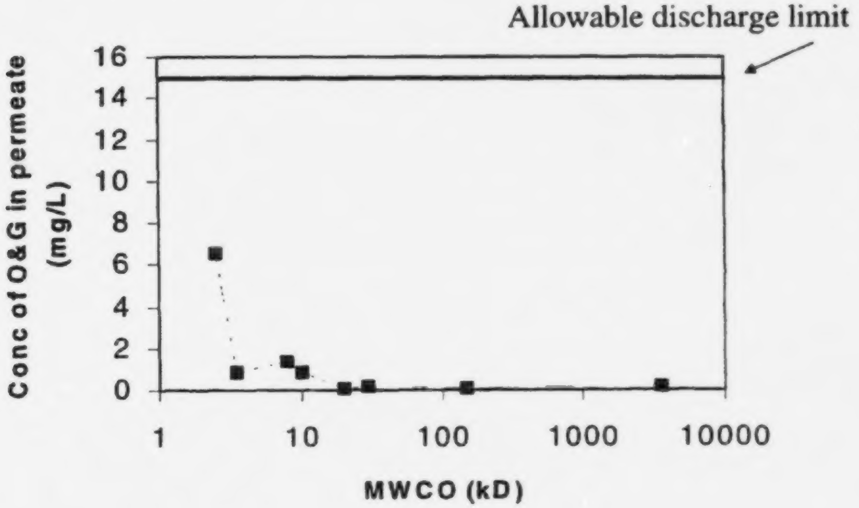

- The pore radius of the GH membrane is 2.0 nm which should have separated 4.0 nm particles.
- The cake enhances the separation of free oil by capturing it in its structure.
- Suggests oil is dispersed at the molecular level or is destabilized on contact with the membrane but is scrubbed clean from solution as the feed passes through the cake.
- The state of the emulsified oil be it chemical or mechanical forming the cake will affect the separation process.

The cake layer acted as a dynamic membrane.

- This type of membrane can be formed dynamically and regenerated.
- Given proper conditioning of the bilge water, membranes having a large pore size can be used to treat this wastewater.

Conclusions Summary

- New oil - simple oil in water emulsion.
- Used oil - more complex water in oil in water emulsion.Used oil - possibility of forming reverse miscelles at the surface of the membrane
- Excessive pump shear was found to reduce the size of problematic particles by half causing a reduction in membrane performance.
- The membrane can recover from a sudden exposure to oil.
- These tests also indicate that the membrane can recover from the de-phasing of free oil at its surface.
- The wastewater was found to contain a substantial amount of dissolved solids, defined as particles measuring less than 0.45 micron, which cannot be accounted for as dissolved salts alone.
- The presence of used lubricating oils in a ship's bilges implies that particles of soot will be present in this wastewater.
- The results further support cake dominated filtration where the presence of a hydrophobic cake at the surface of the membrane enhances the separation of free oil by capturing it in its structure.

Acknowledgements

- Defence Research Establishment Atlantic (DREA/CRDA) - DND.

#516.434 (20)

The Influence of Colloids and Fine Particles on Membrane Performance

A.Y. Tremblay, M. Nottegar, and H. Peng
University of Ottawa, Dept. of Chemical Engineering
Ottawa, ON.
(tremblay@uottawa.ca)

D. E. Veinot
Defence Research Establishment Atlantic
Dockyard Laboratory(A), Halifax, NS.
(veinot@drea.dnd.ca)

ABSTRACT

The influence of colloids and fine particles on the performance of ultrafiltration (UF) and microfiltration (MF) membranes in treating an oily wastewater mixture containing used oil was studied. The composition of this wastewater closely resembled that of wastewaters accumulating in a ship's bilge. Several membranes having molecular weight cut-offs (MWCO) spanning the full range of commercially available UF pore sizes were tested in thin channel cross-flow test cells.

The size and distribution of particles present in this wastewater was determined from dynamic light scattering (DLS) measurements, direct observations of the cake layer at the surface of the membrane and the modeling of experimentally obtained flux decline curves. The DLS measurements indicate that the synthetic bilge water prepared from used oil contains a bimodal distribution with mean radii at 89 nm and 1,340 nm. Particles in the lower distribution had radii ranging from 70 to 100 nm while those in the larger distribution ranged from 900 to 2,200 nm. The results obtained from all three techniques were in excellent agreement. Permeate flux was found to be severely affected by the presence of the smaller particles as their dimension is precisely in the range that is the most difficult to treat by cross-flow membrane filtration.

The results of the UF cross-flow tests show a substantial drop in flux for the largest pore radius tested (70 nm pore radius) versus that of a membrane having a smaller 14 nm pore radius. This suggests the entrapment of the 70-100 nm radius particles within the membrane having a 70 nm radius causing pore blockage and the serious flux decline observed for this membrane. Under these circumstances, the membrane to be used in this application should have a pore radius that is below the smaller particle distribution of 70-100 nm radius or well above a 100 nm particle radius. The microfiltration tests support these findings as pore blockage was found to be prevalent for MF membranes having a pore radius of 100 nm. MF membranes with pore radii just below this threshold performed extremely well. The results indicate that the accumulation of the sub-micron particles present in bilge water at the surface of the membrane and within membrane pores dominates membrane performance. The selection of the proper membrane pore size, particularly in MF, is critical to the success of membrane technology in this application.

Look at Concentration polarization

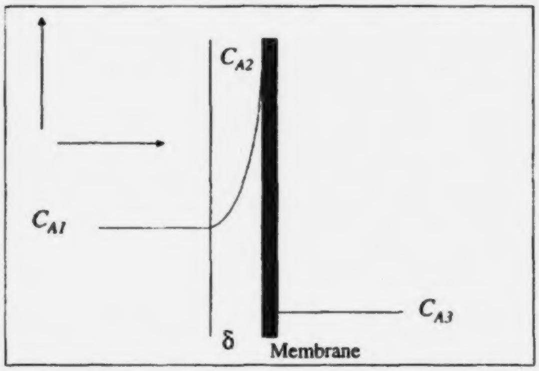

$$J = \frac{N_B}{c_1} = k \ln\left[\frac{C_{A2} - C_{A3}}{C_{A1} - C_{A3}}\right]$$

In the case where $C_{A3} << C_{AI}$. and $C_{A3} << C_{A2}$ (high separation)

then,

$$J = k \ln\left[\frac{C_{A2}}{C_{A1}}\right]$$

Gives rise to the gel model;

$$J = k \ln\left(\frac{C_g}{Cb}\right)$$

Where.

C_b is the bulk or feed concentration and
C_g is the concentration of a gel at the surface of the membrane

$C_g =$ 22 wt % for gelatin at 70°C,
28 wt % for human albumin,
60 wt % electrodeposition primer,
60 wt % styrene butadiene latex

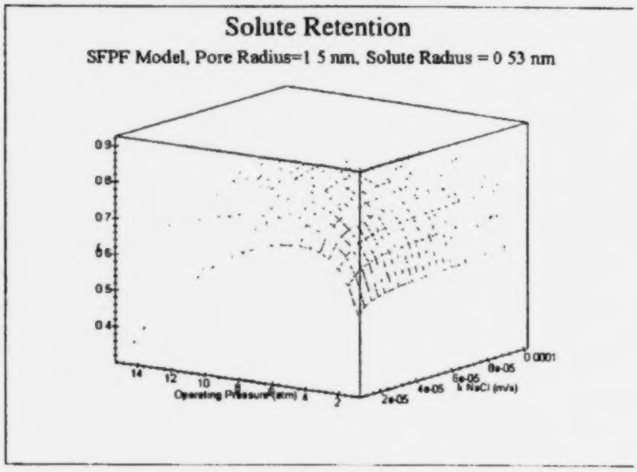
Solute Retention
SFPF Model, Pore Radius=1 5 nm, Solute Radius = 0 53 nm
0 9
0 8
0 7
0 6
0 5
0 4
14
12
10
8
6
4
2
Operating Pressure (atm)
2e-05
4e-05
6e-05
8e-05
0 0001
k NaCl (m/s)

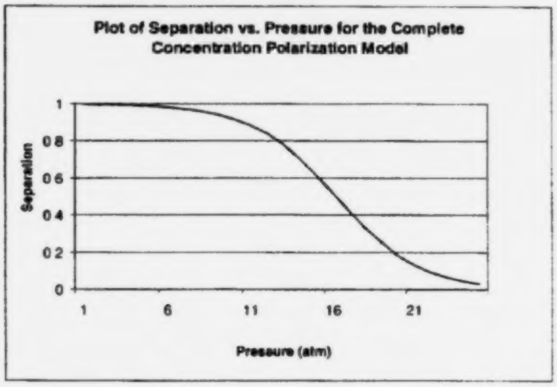
Plot of Separation vs. Pressure for the Complete Concentration Polarization Model
Separation
1
0 8
0 6
0 4
0 2
0
1
6
11
16
21
Pressure (atm)

Influence of Colloidal Particulate Size on Membrane Performance and Cost

Film theory models based on Brownian back-transport from the membrane under predict permeate flux by as much as two orders of magnitude for colloidal suspensions.

Transport mechanisms for colloids and particles must be used in addition to Brownian diffusion to predict permeate flux in ultrafiltration and microfiltration.

Additional transport mechanisms are:
- shear-induced diffusion
- convective transport tangential to the membrane surface
- inertial lift

Brownian diffusivity

$$D_{brn} = \frac{kT}{6\pi\mu a_p}$$

Where k is Boltzmann's constant, a_p = particle radius, ϕ = particle volume fraction, T is temperature and γ is the local shear rate

Shear diffusivity

$$D_{shear} = \dot{\gamma}\ a_p^2\ (0.33\phi^2(1 + 0.5e^{8.8\phi}))$$

Where: a_p = particle radius,
ϕ = particle volume fraction,
T = temperature and
$\dot{\gamma}$ = local shear rate.

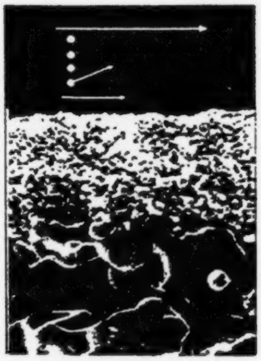

Lower Shear

Highest Shear at the surface of the membrane

Particles move from a region of higher shear to one of lower shear

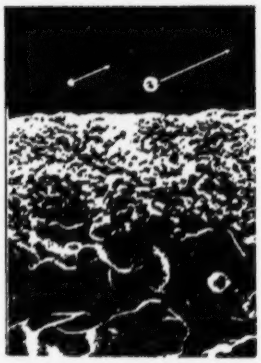

Diffusion away from the membrane is proportional to the square of the particle size.

$$D_{shear}\ \alpha\ a_p^2$$

The Diffusivity of a particle in solution is given by the sum of its Brownian and shear diffusivities.

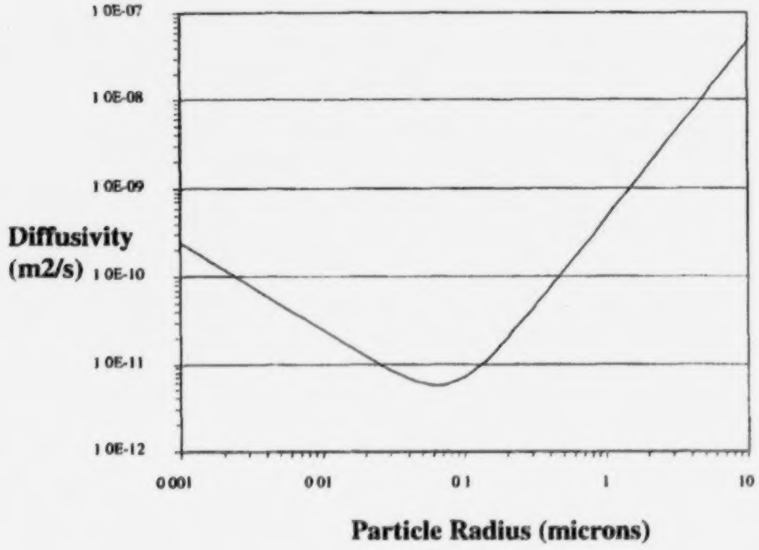

Effect of Particle Size on Permeate Flux

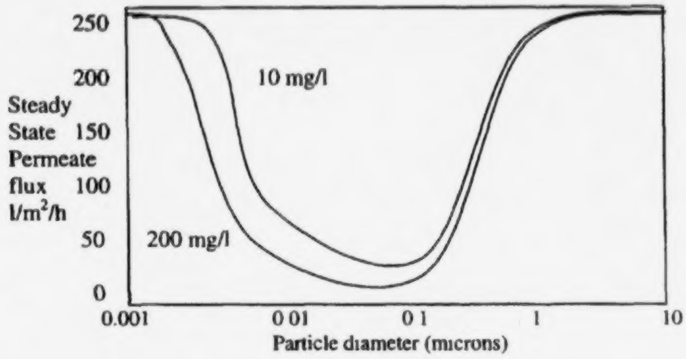

MWCO of membrane is 100,000 Daltons
Feed pressure = 100 kPa

Particle size distribution in synthetic bilge water

- Perform DLS (dynamic light scattering) measurements to determine the particle size distribution in synthetic bilge water.
- Compare bilge water prepared using new oil vs. used oil.

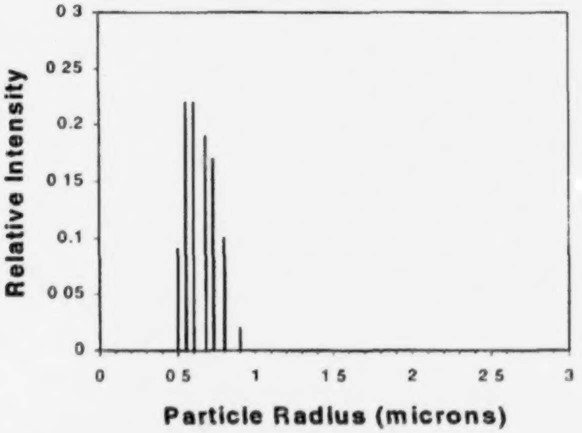

Particle size distribution for synthetic bilge water produced from new oil. Mean = 0.646 µm

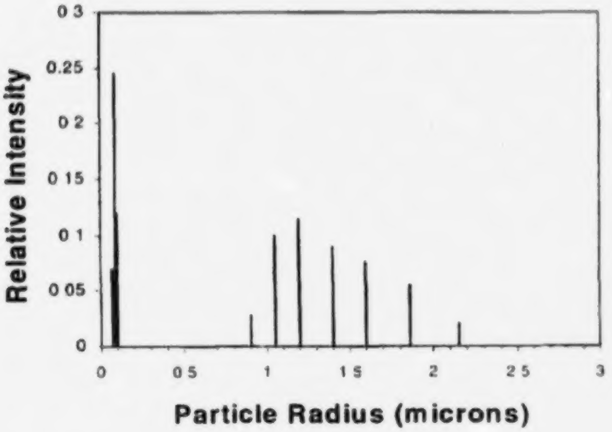

Particle size distribution for bilge water produced from used oil.

New Oil

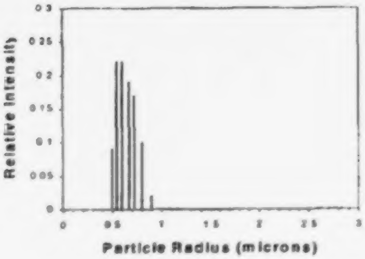

Used Oil

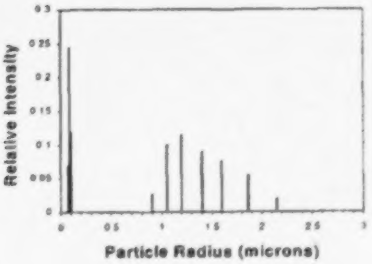

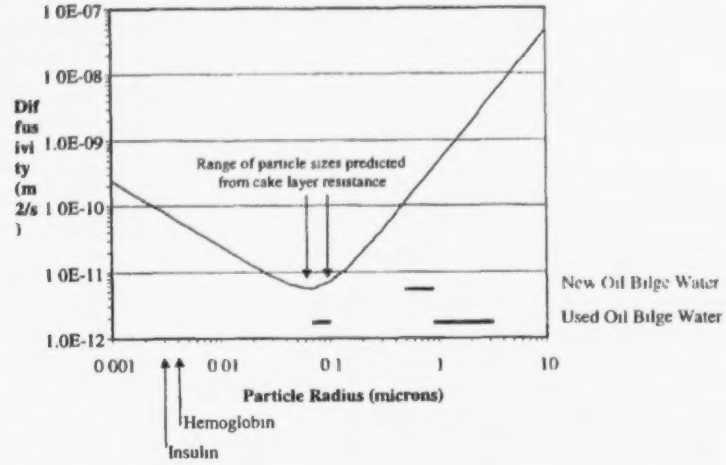

Look at the surface of Ultrafiltration membranes fouled with synthetic bilge water prepared from used oil.

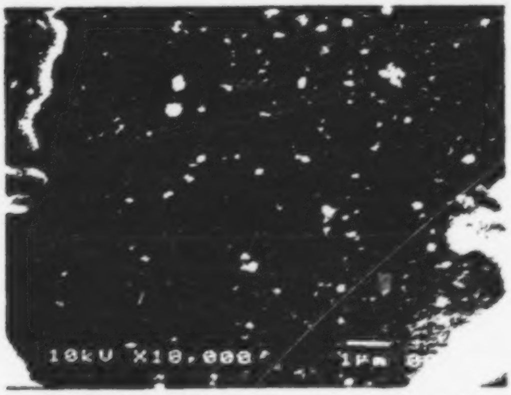
10kV X10,000
1µm

Surface of a 3.5kD MWCO membrane, pore radius 0.0022 µm.

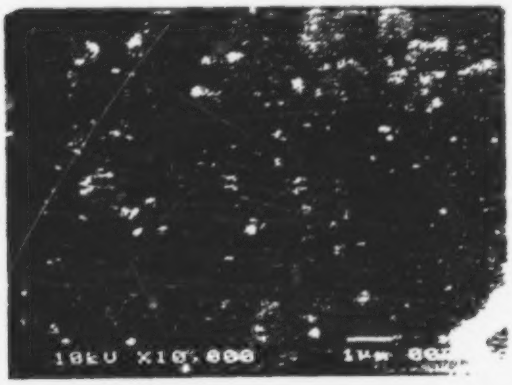
10kV X10,000
1µm

Surface of a 8kD MWCO membrane, pore radius 0.0033 µm.

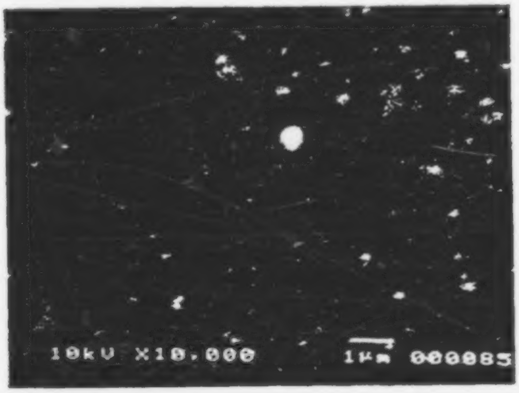
10kV X10,000
1µm 000085

SEM of the surface of a 10kD MWCO, pore radius 0.0037 µm

Soot vs. Carbon Black

Look at size and specific gravity carbon black

- commercially available, average particle sizes ranging from 8 to 100 nm
- specific gravity of 1.7 to 1.9 (Columbian Chem. Co., 1997).
- the carbon black particles can aggregate into larger units measuring several microns.

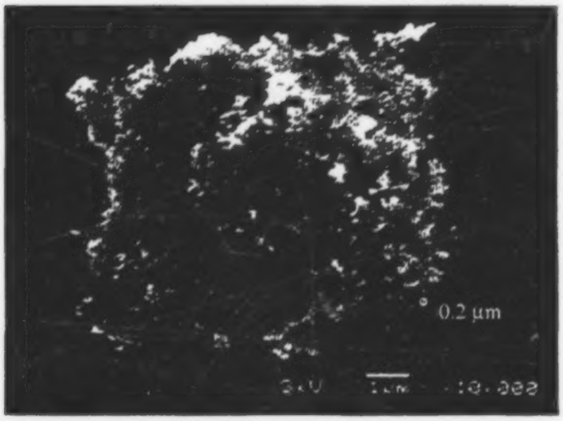

Carbon black aggregated particle (International Steering Committee for Black Carbon Reference Materials)

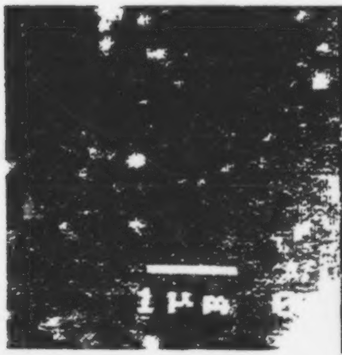

Membrane filter cake

Aggregated soot.

Can we define an optimum pore size for this application ?

Flat sheet membranes in a thin channel x-flow module

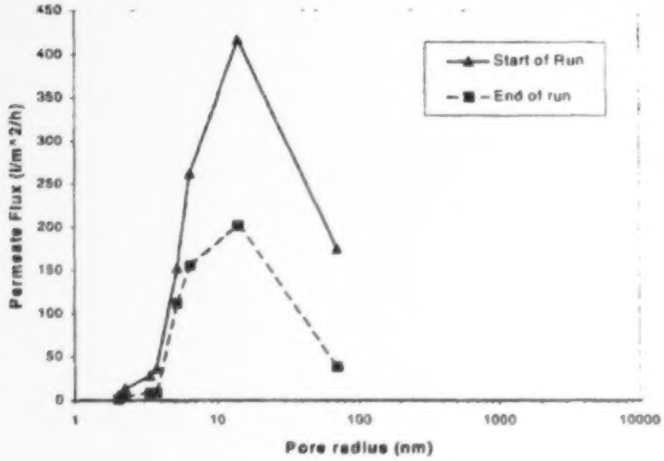

Flat sheet membranes in a thin channel x-flow module and DLS measurements for used oil

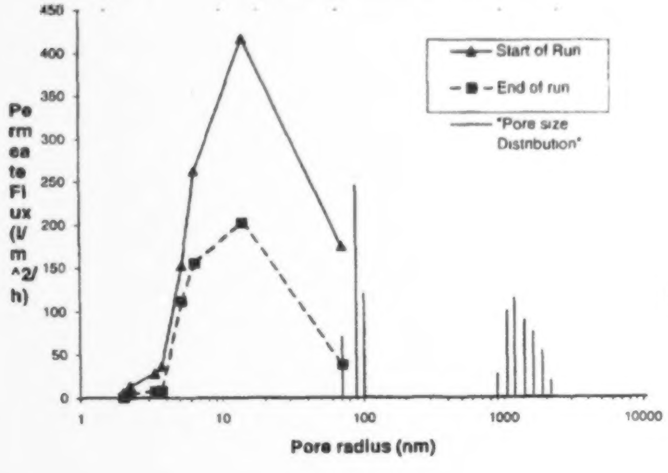

Used oil

Conclusions (defining an optimal pore size).

- Pore blinding was observed when a 3,600 kDalton membrane was used.
- Membranes having pore sizes above 0.1 microns could be used to allow for the passage of the 0.1 micron soot.
- Upper limit would be that observed for the passage of oil through the membrane.

Module Testing

- Comparison of polymeric & ceramic membrane modules
- Pre-treatment – coalescence

Membrane Modules

- Polymeric:
  - KOCH CM:
    - 50K MWCO, polyacrylonitrile
  - CERAMEM:
    - 0.005micron, silica selective layer with an alumina porous substructure\\

Initial Flux Rates

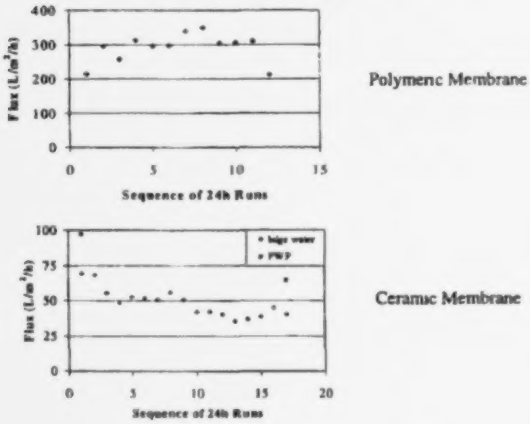

Pretreatment by Coalescence
Polymeric Membrane - Used Bilge Water

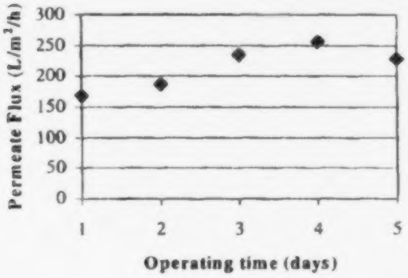

Conclusions (module testing)

- The polymeric membrane (Koch CM) appears to be more resistant to pore plugging than the ceramic membrane
- Flux Enhancement:
  - Backflushing - offers marginal improvement, for these UF membranes, but not as much as anticipated due to nature of cake layer.
  - Coalesence pre-treatment is effective in enhancing permeate flux.

Testing of new small tube membranes Carbo-cor (Koch membranes) tubular modules.

Flat sheet and tubular membranes (solid circles) with
DLS measurements for used oil

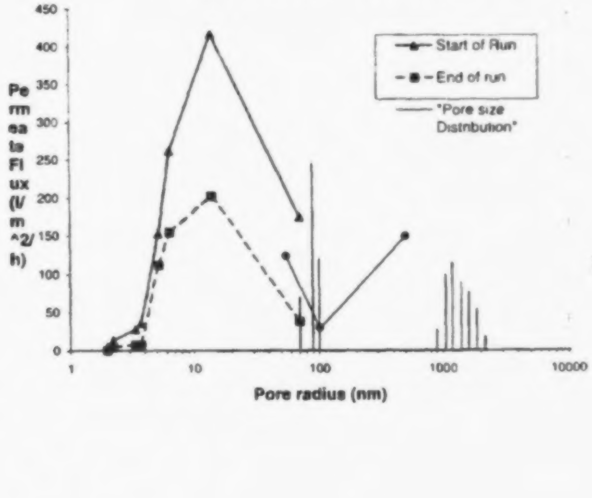

Used oil

Precipitation of sparingly soluble salts.

```
                 ----------- EQUILIBRATED MASS DISTRIBUTION -----------

  Name              DISSOLVED              SORBED               PRECIPITATED
                  mol/L      percent      mol/L      percent      mol/L      percent

F-1            3.753E-05    100.0    0.000E+00       0.0    0.000E+00       0.0
Cl-1           2.849E-01    100.0    0.000E+00       0.0    0.000E+00       0.0
Na+1           2.445E-01    100.0    0.000E+00       0.0    0.000E+00       0.0
SO4-2          1.590E-02    100.0    0.000E+00       0.0    0.000E+00       0.0
Mg+2           2.715E-02     97.5    0.000E+00       0.0    6.889E-04       2.5
Ca+2           4.628E-03     87.0    0.000E+00       0.0    6.889E-04      13.0
K+1            5.171E-03    100.0    0.000E+00       0.0    0.000E+00       0.0
Br-1           4.308E-04    100.0    0.000E+00       0.0    0.000E+00       0.0
Sr+2           8.021E-05    100.0    0.000E+00       0.0    0.000E+00       0.0
H2O            4.642E-06    100.0    0.000E+00       0.0    0.000E+00       0.0
H+1            2.160E-04    100.0    0.000E+00       0.0    0.000E+00       0.0
CO3-2          2.346E-04     14.6    0.000E+00       0.0    1.378E-03      85.4
```

Evidence of Magnesium and Calcium carbonate precipitates in used modules from HMC ships.

The following slides are the Scanning Electron Micrographs of clean and used membrane along with the Electron Diffractive X-ray (EDX) scans of the new and used membranes.

These results indicate that in addition to soot, sparingly soluble precipitates are present in the cake and within the membrane as evidenced by the Ca and Mg present in the EDX of the used membranes.

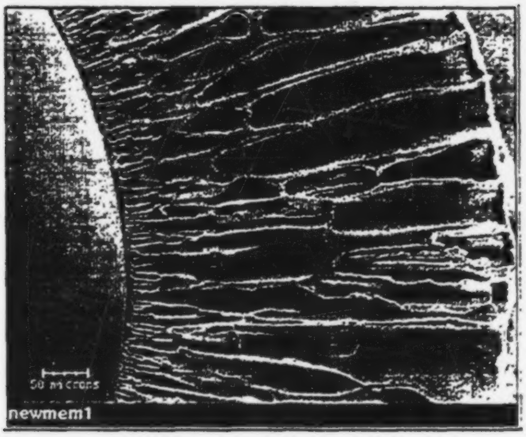
50 microns
newmem1

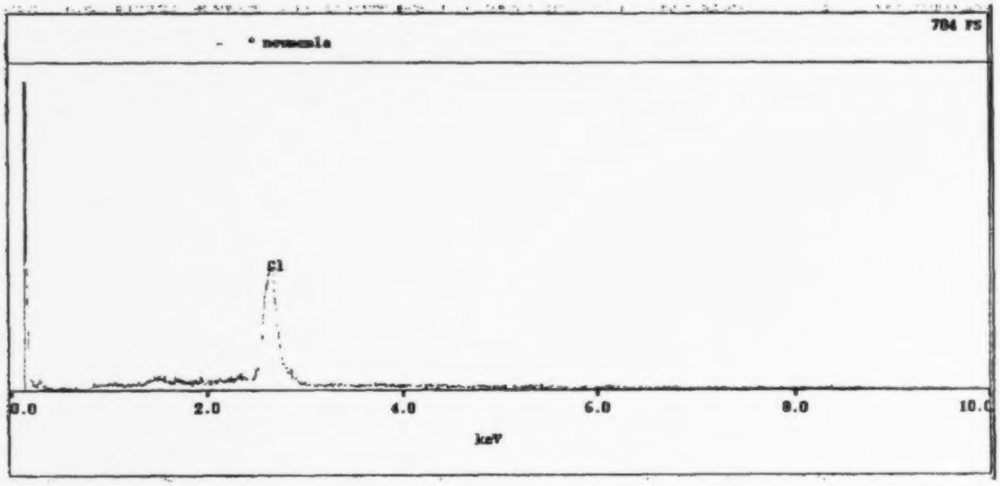
* newmem1a
784 FS
Cl
0.0
2.0
4.0
6.0
8.0
10.0
keV

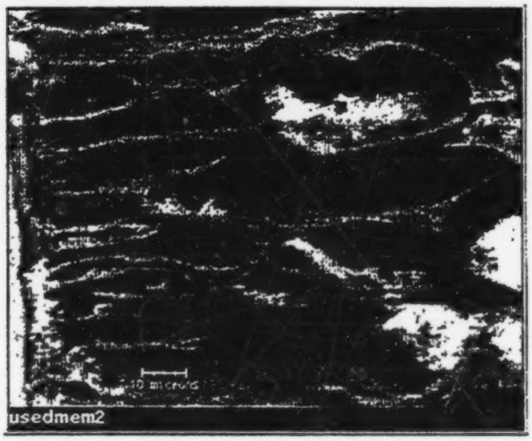
10 microns
usedmem2

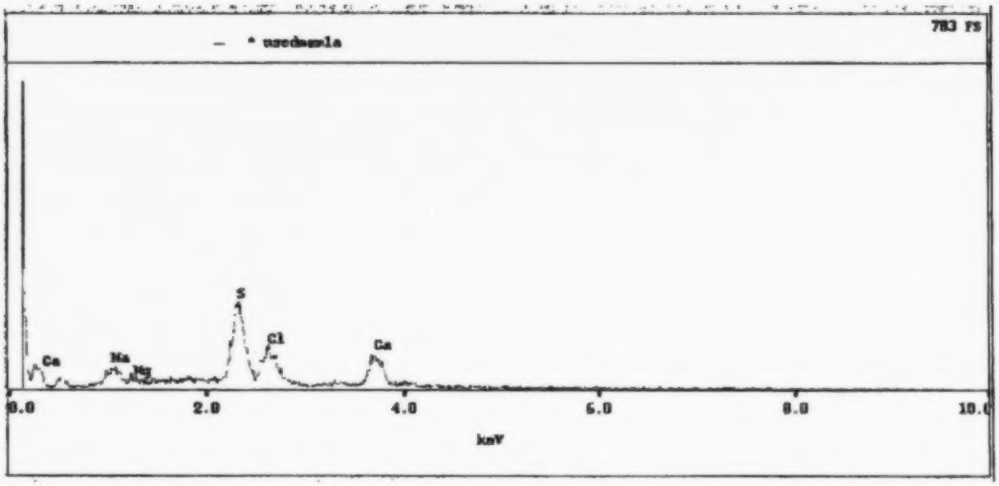

ACKNOWLEGMENTS

- Defence Research Establishment Atlantic (DREA/CRDA) - DND.

#516436 (21)

CPF Biofouling Investigations

B.M. Zwicker[1], G.R. Pelletier[2], J.F. Porter[2]

(1) Department of Fisheries & Oceans, Bedford Institute of Oceanography
(2) Defence Research Establishment Atlantic, Dockyard Lab

Abstract

The seawater cooling systems on the Canadian Patrol Frigates (CPF) have been experiencing serious problems with marine fouling, primarily due to the ingestion of blue mussel (*Mytilus edulis*) larvae. Defence Research Establishment Atlantic Dockyard Laboratory (DREA/DL) has undertaken a development project to investigate the factors that govern the degree of the marine fouling problem and to devise solutions and systems to reduce or eliminate their occurrence.

To control biofouling, many different techniques have been employed over the years with varying results. Some successful methods are under scrutiny due to their environmental effects. Any proposed solution must take into consideration the safety of the CPF crew, while being environmentally conscience and having minimal negative effects on non-target organisms. Research now focuses on finding methods that discourage or repel the settlement of biofouling organisms, rather than extermination.

DREA/DL have constructed a seawater system that mimics some characteristics of the CPF auxiliary seawater circulating system (ASWC), used to supply a source of cooling water to various onboard equipment. Studies using the DREA/DL seawater system have been conducted on three different biofouling chemical treatments; hypochlorite, copper ion, and iodine.

Static seawater studies investigating the physical response of juvenile and adult mussels to chemical treatment determined that hypochlorite and copper ion had a lower effective concentration than iodine in discouraging mussel settlement.

Follow-up studies on hypochlorite and copper treatment utilizing the DREA/DL seawater system examined the effect of concentration with respect to electrical current and seawater flow rate. Hypochlorite treatment results indicate that current and flow rate have a similar effect on seawater concentration. However, results for the copper treatment were quite different due to the effect of the Cu/Ni piping on the seawater copper concentrations.

1.0 Introduction

The accumulation of organisms on surfaces immersed in water, referred to as biofouling, is a natural process in both freshwater and marine environments. The study of marine biofouling dates back centuries and is still being investigated presently. Much of the work has been undertaken by the shipping industry, which still incurs large financial losses due to biofouling every year. Most of these losses are due to the biofouling found on the hull of ships which cause (1) additional drag on the ship, (2) increased concern regarding structural damage and repair, and (3) expense of removing biofouling.

Although seawater provides a medium for the transport of ships, it also provides a source of cooling water for the equipment onboard these ships. The internal walls of the piping in these cooling water systems are another site for biofouling accumulation. This accumulation causes decreased flow rates affecting the system efficiency. If the biofouling is allowed to accumulate indefinitely, it will lead to the eventual failure of the cooling water system.

The Canadian Patrol Frigate (CPF), like many ships, uses seawater for cooling a variety of equipment throughout the ship. This requires an extensive cooling water system, which was designed to respond to the varying cooling needs onboard the CPF. Unfortunately, this also provides a wide array of seawater flow rate conditions for biofouling accumulation to occur. Settlement sites will be based chiefly on the requirements of the biofouling organism, leading to the accumulation of different organisms in different locations in the cooling water system.

The problem of biofouling accumulation in the cooling water system of the CPF's is predominantly due to blue mussel (*Mytilus edulis*) infestation. The problem became serious enough on several occasions that the cooling water system had to be shutdown, dismantled and manually cleaned. Obviously, this was not a practical long-term solution to this mussel infestation problem. Another solution was vital for both financial and operational reasons.

This solution had to meet a number of criteria and limitations related to the existing cooling water system on the CPF's along with other considerations such as:

(1) the health and safety of the crew;
(2) the space and storage restrictions (onboard a CPF);
(3) the costs must be practical;
(4) the negative effect on the cooling water system had to be minimal; and
(5) the potential negative affects on non-target organisms and the environment.

With all these concerns, finding an effective solution that meets all the requirements would be a very difficult task.

With the problem organism and the requirements of an adequate solution identified. The next step was to become familiar with the problem organism and any existing methods for preventing infestation. This lead to an extensive literature search providing information on the blue mussel and methods of controlling infestation (Chou et.al., 1999). To determine which of these potential methods or treatments was most likely to fulfill all the necessary requirements would involve testing. Several of the most promising chemical treatments for discouraging mussel settlement were selected for laboratory testing (Part 1).

While these studies were being completed, the design and construction of a seawater system was underway at the Defence Research Establishment Atlantic (DREA) Dockyard Lab. This seawater system was designed and constructed for the purpose of investigating the CPF biofouling problem, consequently, its design was similar to a CPF cooling water system. The material used in the construction of the CPF cooling water system was copper/nickel (90% Cu/10% Ni) piping in an attempt to minimize problems related to biofouling. The DREA/DL seawater system was constructed primarily of the same material (90/10 Cu, Ni); however, due to accessibility and adaptability requirements, some PVC valves and piping were included. Time and supply constraints resulted in the use of copper T-joints and elbows during construction of the seawater system.

Once construction was complete and the system was operational, preliminary mussel exposure tests using chemically treated seawater derived from the seawater system were undertaken. The three chemical treatments initially tested were chlorine (electrochemically generated hypochlorous acid/hypochlorite and related compounds from seawater), copper (electrochemically generated from sacrificial anodes) and an iodine solution (injected into seawater system).

The results were incomplete since seawater chemical concentration could not be determined during testing. Chemical concentration could not be determined since on-site analysis equipment (for hypochlorite) was not available and the system lacked two properly functioning flow meters. During the time required to address the problems preventing the determination of chemical concentration, the assessment of the iodine treatment was sacrificed in favour of a control line.

The two remaining chemical treatments (hypochlorite and copper) being evaluated are generated electrochemically (from the seawater), which means that chemical production is electrically based. Knowledge of electrical current and seawater flow rate are the two primary factors required (in this case) for studying chemical concentration, since electrical current determines the rate of chemical production and seawater flow rate dictates the dilution factor.

The concentration study investigated the possibility of estimating chemical concentration based on the knowledge of seawater flow rate and electrical current. Concentration was monitored while either seawater flow rate or electrical current is varied. The resulting data was plotted and examined in an attempt to provide a simple method (relationship) for predicting concentration.

2.0 Background

Mussels are bivalve molluscs belonging to the family Mytilidae. The common or blue mussel (*Mytilus edulis*) is among the most abundant and widely distributed invertebrate species inhabiting intertidal and shallow subtidal waters in the North Atlantic. Range limitations seem to be governed mainly by temperature; elevated water temperature limits their southern distribution.

The mussel life cycle (see Figure 1) includes a free-swimming larval stage, which through metamorphosis will develop into an immature adult and becomes sessile. This process involves the search for an adequate settlement site, followed by initial and then permanent attachment. Attachment is accomplished through a series of secreted byssal threads, providing resilient, long-term anchorage.

The cooling water system provides many suitable areas for mussel settlement and growth, leading to the blockage problems experienced by the CPF's. Once mussel colonies are established, removal is difficult, while mussel extermination is only a partial solution. Chemical treatment is capable (over extended periods) of killing the established mussels, but after death, the shells and byssal threads remain. Manual cleaning is the only effective method of shell removal in a CPF cooling water system. The other problem with exterminating established mussel colonies is their high resistance to chemical treatment compared with the majority of other marine organisms. Adult mussels have the ability to completely isolate themselves from their environment through shell closure. Respiration and nutritional needs will eventually force the mussel to re-open its shell. However, this isolation period allows the mussel to survive conditions, which would be detrimental to most other marine organisms.

Since eliminating adult mussel infestation is difficult and impacts the local environment, an alternate method was essential. Rather than deal with an established colony, prevention of mussel settlement would be a logical approach, eliminating the need for shell removal. Chemical treatment can be used to discourage mussel settlement rather than exterminating a live colony.

2.1 Part 1: Laboratory Mussel Study

Once the mussel has selected a site for settlement, the mussel foot is crucial for attachment. The foot (Figure 2) provides the initial attachment until a byssal thread can be excreted for a more secure, permanent attachment. The production and attachment of a series of byssal threads then follows. Without the aid of the foot, mussel attachment would not be possible.

To observe the effectiveness of chemical treatment in preventing mussel settlement, a simple experiment was designed to monitor the physical response of the mussel to chemical exposure. The two physical responses noted were whether the exposed mussel remained in a relaxed state (mussel valve open enough for respiration and feeding) and whether the foot was active or remained withdrawn inside the mussel shells (valve). Based on these two parameters the effectiveness of a chemical treatment against mussel settlement can be evaluated.

The laboratory tests were conducted at various chemical concentrations, providing an approximate effective concentration against mussel settlement. However, laboratory results do not necessarily apply in actual field trials, but do provide a good basis for field applications.

2.2 Part 2: Seawater System Mussel Study

The laboratory mussel study was followed by similar experiments where the chemically treated seawater was derived from the DREA/DL seawater system, rather than being manually prepared. The seawater system mussel studies also involved monitoring the physical response (valve and foot activity) of the mussel to chemical exposure. Assessment was identical to the method used in Part 1.

The study concerned the evaluation of three chemical treatment (copper, hypochlorite and iodine) systems associated with the DREA/DL seawater system. The tests conducted were only preliminary in nature, since chemical concentration could not be determined in the treated seawater removed from the seawater system.

2.3 Part 3: Seawater System Concentration Study

The preliminary results from the seawater system mussel study looked at mussel response, but lacked any information regarding chemical concentration. Following some modifications to the seawater system and the acquisition of some additional analysis equipment, chemical concentration in the treated seawater could be properly monitored. Previous laboratory work (Part 1) supplied effective concentrations (for hypochlorite and copper) for preventing mussel settlement. Now could these concentrations be attained in the DREA/DL seawater system with the associated treatment equipment?

The determination of concentration of an element or compound in seawater is often a very difficult process. The two chemicals in question, hypochlorite and copper, although generated through a similar method, differ in many ways. Since copper is an element, the concentration can be fairly easily monitored by analyzing for total copper in the seawater sample. Chlorine as hypochlorite presents a much different problem. Hypochlorite will react (normally through oxidation) with a variety of chemicals present in seawater, resulting in less reactive or non-reactive forms of chlorine. Once the chlorine is in a non-reactive form it no longer offers any protection against biofouling. This is further complicated by the fact that seawater naturally contains chlorine (primarily in the ionic chloride form). These facts indicate a need for a rapid yet selective analysis, for the more reactive forms of chlorine. The practical solution was a portable chlorine analyzer, which chiefly detects the chemical compounds of chlorine, which offer some degree of biofouling protection (hypochlorite and some less reactive chlorine compounds).

There are many variables (i.e. electrical current, seawater flow rate, pH, temperature, salinity, other chemicals present, etc.) which play a role in determining the hypochlorite and copper concentration in the treated seawater. Some variables play a larger role than others do in determining concentration; however many of them are not easy to alter in a cooling water system. The two (controllable) variables playing the greatest role in determining concentration for the two treatment systems under consideration are: applied electrical current and seawater flow rate. Altering either variable will effect the chemical concentration in the treated seawater.

To study the effects of electrical current and seawater flow rate on chemical concentration, only one variable can be altered during an experiment. The results should provide the individual relationship between the altered variable and the chemical concentration in the treated seawater. Examination of the two relationships separately will provide some insight into predicting the chemical concentration present in the treated seawater. However, since other variables (i.e. temperature, pH, salinity, mixing, etc.) have not been considered, the prediction of concentration in this manner, can only be considered a good estimate.

3.0 Materials

All experiments were conducted at the Bedford Institute of Oceanography (BIO) or at the Defence Research Establishment Atlantic Dockyard Laboratory (DREA/DL). In either case, ambient Halifax harbour seawater was used for all experiments and mussel storage. The seawater contained adequate oxygen and nutrients for long-term mussel growth and survival. The juvenile (adult) blue mussels (8-17 mm) used in all chemical exposure experiments were collected from the shoreline (intertidal zone) of Halifax harbour (in close proximity of BIO).

3.1 Part 1: Laboratory Mussel Study

These chemical exposure (of mussels) experiments were performed at BIO, in 250-ml polypropylene beakers (Canadawide Scientific) using 200-ml of seawater. The beakers were fitted with plastic meshing (inside) to prevent the test mussel from sinking to the bottom of the beaker. This was necessary to facilitate stirring, which was accomplished through the use of a Nalgene Star Head™ magnetic stir bar (Fisher Scientific) and a magnetic stirrer (Barnstead/Thermolyne). Temperature was monitored using a thermometer (Fisher Scientific) in a separate beaker. Mussel shell length was determined with a steel ruler (Westcott) prior to experimentation.

All chemical solutions were prepared by dissolving solids (except for sodium hypochlorite and hydrogen peroxide) in distilled water using 100-ml volumetric flasks (Pyrex, Kimax). The chemicals used were: (1) benzalkonium chloride (Aldrich Chemical Co.), (2) cupric (copper) sulfate (Fisher Scientific), (3) didecyldimethylammonium bromide (Aldrich Chemical Co.), (4) dodecyltrimethylammonium bromide (Aldrich Chemical Co.), (5) ferrous (iron) sulfate (Baker & Adamson), (6) hydrogen peroxide (Fisher Scientific), (7) iodine (Fisher Scientific, foil-wrapped, parafimed, glass-stopper bottle kept refrigerated to prevent degassing), (8) nickel sulfate (Fisher Scientific), (9) potassium permanganate (BDH Chemicals), (10) sodium hypochlorite (Aldrich Chemical Co.), and (11) zinc sulfate (Fisher Scientific). Chemical solutions were added to the test seawater (in one or two aliquots) using an Eppendorf™ tip ejector pipette (Brinkmann Instruments, Model 4700).

The timing of experimental duration and observations was accomplished using a digital timer (Fisher Scientific).

3.2 Part 2: Seawater System Mussel Study

The chemical exposure tests performed and materials used were identical to those in "3.1 Laboratory Mussel Study", except all work was performed at DREA/DL using chemically treated seawater from the seawater system. The DREA/DL seawater system consists of three independent lines that are connected to a common seawater intake and drainpipe. As shown in Figures 3a & b, each line runs approximately 13 feet and is made up of 4", 2", and 1.5" diameter piping. The 4" piping is PVC, while the other two diameters are 90/10 Cu/Ni piping. Due to accessibility and adaptability requirements, PVC valves and piping was necessary. Also, because of time and supply constraints, copper T-joints and elbows had to be used. This setup permits the evaluation of three different antifouling treatment systems simultaneously.

The material used in the construction of the CPF cooling water system is primarily copper/nickel (90% Cu/10% Ni) piping. The antifouling properties of Cu/Ni piping have been investigated and well documented. Present theory attributes the antifouling properties of Cu/Ni piping to an oxidation layer that forms on the surface of the pipe, upon immersion in seawater. For this reason, the DREA/DL seawater system was constructed primarily of 90/10 Cu/Ni piping.

Three different commercially supplied chemical treatments were evaluated. They were copper [Andover Management Inc. (Cathelco)], electrochemically generated from sacrificial anodes], hypochlorite [Royal Military College (RMC)/Huron Technologies, electrochemically generated from seawater], and iodine [IO Gold (injection of premixed solution)].

3.3 Part 3: Seawater System Concentration Study

The two remaining treatment systems installed on the seawater system offer protection against biofouling by producing either hypochlorite or copper. The system producing the hypochlorite was provided jointly by the Royal Military College (RMC) and Huron Technologies, while Andover Management Inc. (Cathelco) provided the copper producing system.

The equipment provided by RMC/Huron Tech. (Line C) comprised of an in-line hypochlorite package designed for swimming pool use, which had been adapted for this particular application. It consisted of an in-line electrolytic cell (2" diameter) constructed with electrodes that are thin sheets protected by a grating at either end of the cell. By reversing polarity of the electrodes periodically, calcareous deposits should be prevented from accumulating on the electrodes. The electrical current was provided for the cell by a regulated DC power supply (Sterling Instruments L3210).

The Cathelco anti-fouling system installed on the DREA/DL seawater system (Line A) consisted of the following equipment: one EB/NS/2W control panel; one electrode tank, made of heavy duty PVC to suit the existing piping; two type 2525/100 combination anode/cathodes; and one "Techcessories" 13.5 DC 6.5A power supply. Additional combination anode/cathodes were purchased at the time of installation. The electrode tank was fitted with a metal screen, in July/2000.

The hypochlorite concentration was monitored using a HI 93701 Free Chlorine ISM analyzer (Hanna Instruments) based on a recommendation from RMC/Huron Tech. The determination of copper in the treated seawater samples was accomplished using an inductively coupled plasma atomic emission spectrophotometer (ICP-AES) manufactured by Varian (Liberty Series II).

4.0 Methods

4.1 Part 1: Laboratory Mussel Study

The chemical exposure experiments performed, used 200-ml of stirred, seawater that varied from 8° to 20.5°C, over the experimental period. Temperature was recorded at the start and completion of the experimental period, and the mussel shell length was recorded before placement of the mussel in the test beaker.

Prior to the addition of the chemical solution to the test seawater (dosing), the test mussel was required to be in 'an active state'. The mussel valve had to be open with the mussel foot extended outside the valve. Once the mussel was in the 'active state', the chemical solution was added and the timer initiated. Mussels were individually tested and response was noted after the initial 15-sec. (to allowing for mixing), for a period of

10 or 15-min. After which they were removed from the treated seawater and placed in untreated seawater for long-term (14 days) mortality observations.

Estimates of effective concentrations are based on the mussel response data, which was calculated as follows:

(1) % time foot retracted = (time foot retracted / exp. time) x (100)
(2) % time valve shut = (time valve shut / exp. time) x (100)

In addition, the presence of initial byssal attachment was noted for all test mussels.

4.2 Part 2: Seawater System Mussel Study

This study utilized the same experimental procedure as the (4.1 Part 1) Laboratory Mussel Study, with one significant difference. The chemically treated seawater used in the mussel exposure tests was derived from the DREA/DL seawater system. A 200-ml aliquot of chemically treated seawater was removed from one of the three seawater lines. All three lines (A, B, and C) are equipped with a different chemical treatment (copper, iodine, and hypochlorite) and two different sampling locations (taps). Treated seawater samples were removed and tested from both tap locations: identically located on each line at the midway (mid tap) and end (end tap) points. Seawater used for testing the control mussels was removed from the holding tanks, which were supplied with untreated seawater.

The test mussel was placed in the beaker containing the 200-ml aliquot of treated seawater with the simultaneous initiation of the timer. Mussel responses were noted for a 15-minute period, followed by inspection for initial byssal attachment. Then the test mussels were placed in untreated seawater and returned to BIO (within 1-3 days) for a post-treatment observation period of 14-days.

The comparison of the effectiveness of each chemical treatment in preventing mussel settlement was based on the existing system parameters. The electrical current for the copper (6 mamps) and hypochlorite (2 amps) generating equipment and the injection rate for the iodine equipment remained constant throughout the experimental period. The determination of chemical concentration was not possible for several reasons.

There was a lack of a quick, on-site chlorine (hypochlorite) analysis and two of the treatment lines [copper (Line A) and iodine (Line B)] were not equipped with accurate flow meters. Hypochlorite is rather unstable (requiring immediate analysis) and chemical concentration is dependent on seawater flow rate (dilution factor).

4.3 Part 3: Seawater System Concentration Study

The effect on the chemical concentration in treated seawater by electrical current and seawater flow rate was investigated. The concentration study involved altering two variables (electrical current and seawater flow rate) individually, while recording the affect on chemical concentration in the treated seawater. For each experiment, ten treated seawater samples (~175-ml) were collected in 250-ml polypropylene beakers (Canadawide Scientific), discarding the first aliquot (~175-ml) of seawater to clear the tap of any stagnant seawater. Since sample collection taps are located on top of the copper piping, occasionally sample collection required (depending on seawater flow rate) partial closure of a drain valve on the line being tested. The seawater sample was then either rapidly (1-2 minutes) analyzed in the case of hypochlorite, or acidified ($pH \leq 2$)

using nitric acid (HNO_3, Fisher Scientific, trace metal grade) and stored at 4°C until analyzed, in the case of copper.

The hypochlorite analysis required a 10-ml aliquot of the treated seawater and the remainder of the treated seawater sample was used for temperature determination (digital thermometer, BCR Industries, model ET-10). Ten concentration determinations were obtained for each experiment performed. At high enough concentrations (> 2.5 ppm free chlorine) the treated seawater sample required dilution (1:1) with distilled water using a pipette (Oxford). Prior to dilution the distilled water was insured to be void of free chlorine by testing. One set of experiments required monitoring concentration at different seawater flow rates (~ 4, 6, 7, 10, 15, and 20 USGPM) while the electrical current of the treatment equipment remained constant (0.9 amps). The other set of experiments altered electrical current (0.5, 1.0, 1.5, 2.0, and 2.5 amps) while maintaining a steady seawater flow rate (10 USGPM). The data from each experiment was averaged and used to generate a scatter plot, illustrating the relationship between the individual variables and the hypochlorite concentration in the treated seawater.

Prior to sample copper analysis the equipment (ICP-AES) was allowed to properly warm-up and stabilize (~ 30 minutes) and then was calibrated. Following the preparation of the equipment, samples were removed from storage (4°C) and shaken prior to analysis. Due to a printer-related problem, results were recorded manually in a lab book. The 125-ml polyethylene bottles (Nalgene HDPE) used for sample storage were cleaned before sample collection by soaking (≥ 24 hours) in a dilute nitric acid (~10% v/v Fisher reagent grade) solution. The copper treatment system (Cathelco) had an additional sampling site located at the top of the anode tank, allowing for sample collection at either the copper line tap located just downstream from the anode tank, or the top of the anode tank (see Figures 3a & b). These sampling sites will be referred to as "tap" (copper line tap) or "pot" (top of anode tank). The sacrificial combination anode/cathodes were occasionally removed (i.e. during maintenance) and weighed using an analytical balance (Denver Instruments, TR-6101) to verify proper weight loss.

All related experimental readings (electrical current, seawater flow rate, time, and temperature) were recorded just preceding treated seawater collection for chemical analysis. Flow rate readings are approximate since small fluctuations in meter readings were common during the experimental collection period. Temperature data was obtained immediately after the 10-ml test aliquot of treated seawater was removed.

The equipment provided by both companies was designed to be very low maintenance over an extended period of time. Unfortunately, since the in-line electrolytic cell (hypochlorite) was intended for swimming pool use, it's design caused some blockage problems due to mussel shells. Closing off that seawater line (C) and disconnecting the cell and removing the shells before reconnection and reopening the line rectified this problem. This problem was easy to detect by monitoring seawater flow rate, when blockage occurred, the flow rate was reduced significantly. The screen located in the electrode tank of the Cathelco system also required periodic cleaning, however, when it was in need of cleaning, it had little affect on the seawater flow rate. This was the only routine maintenance performed on either of the two treatment systems.

5.0 Results

5.1 Part 1(A): Laboratory Mussel Study

The initial evaluation of the eleven chemicals (tested singularly or in combination) for discouraging mussel settlement was completed at a concentration of 50 ppm (μg/g). The results of these experiments are ranked and summarized in Table 1. None of the treatments proved to be effective in preventing mussel settlement when compared to the control.

To determine the concentration range at which the chemical treatments became effective in preventing mussel settlement, individual mussels were tested at increasing concentrations. The results of these tests are presented in Table 2. Results indicate an effective concentration (bold), based on a comparison with control mussel responses.

5.1a.1 Sodium Hypochlorite

The sodium hypochlorite treatment was evaluated at the following concentrations: 0.1, 0.15, 0.2, 0.4, 0.5, 1.0, and 5.0 ppm, with the results summarized in Table 2. The mussel response at 0.1 and 0.15 ppm was not significantly different from the control group. At the 0.2 ppm level, the % time foot retracted and valve shut, noticeably increased then decreased at the 0.4 and 0.5 ppm level. The response substantially increased at the 1.0 ppm level (98 % for time foot retracted and 50 % for time valve shut), then at 5.0 ppm, the ideal results (100 % for time foot retracted and 99 % for time valve shut) were obtained. Initial byssal attachment occurred only in the 0.15 ppm sodium hypochlorite treatment. All 7 of the mussels exposed to sodium hypochlorite survived the long-term (14-day post-treatment) mortality test period.

5.1a.2 Iodine

Results for iodine treatment tested at concentrations of 0.1, 0.15, 0.2, 0.3, 0.6, 0.9, and 1.2 ppm, are summarized in Table 2. The mussel response at all concentrations tested did not vary significantly. The time the foot was retracted ranged from 22 % (0.6 ppm) to 61 % (0.1 ppm) and the time the valve was shut ranged from 0 % (0.1, 0.15, 0.3, 0.6, 0.9, and 1.2 ppm) to 6 % (0.2 ppm). Initial byssal attachment occurred only at the 0.15 ppm iodine concentration. The survival rate for the iodine treated mussels was very good: no fatalities during the 14-day post-treatment period. Since mussel responses at the tested iodine concentrations did not differ significantly from the control group, an effective concentration was not attained.

5.1a.3 Potassium Permanganate

Mussel responses for potassium permanganate concentrations of 0.2, 0.6 and 0.8 ppm are found in Table 2. Mussel response at 0.2 ppm potassium permanganate did not differ significantly from the control group. Response at the 0.6 ppm (85 % for time foot retracted, 38 % for time valve shut) level was considerably better than the control mussels, however, the 0.8 ppm treatment was even better (100 % for time foot retracted and time valve shut), suggesting further testing at higher (>0.8 ppm) concentrations was unnecessary. Initial byssal attachment did not occur at any of the concentrations tested. One of the mussels exposed to potassium permanganate died during the 14-day post-treatment period.

5.1a.4 Benzalkonium Chloride

Benzalkonium chloride was tested at 0.2, 0.4, 0.6, 1.0, 2.5, and 5.0 ppm to determine mussel response (Table 2). At the 0.2, 0.4, 0.6 and 1.0 ppm levels, responses were similar to the control mussels. Only at the 2.5 ppm (55 % for time foot retracted, 39 % for time valve shut) and 5.0 ppm (74 % for time foot retracted, 20 % for time valve shut) were the results noticeably better than the control group, however, improvement was still not sufficient enough to be considered effective. Initial mussel byssal attachment occurred at 0.2, 0.4 and 2.5 ppm benzalkonium chloride with all exposed mussels surviving the 14-day post-treatment period.

5.1a.5 Dodecyltrimethylammonium Bromide

Four different concentrations of dodecyltrimethylammonium bromide (0.5, 1.0, 2.5 and 5.0) were tested to investigate mussel response. Results at the 0.5, 1.0 and 2.5 ppm levels, were similar to the control group responses. Only at the 5.0 ppm level did results (63 % for time foot retracted, 14 % for time valve shut) improve in comparison to the control group, however, no concentration tested could be considered effective. No mussels exposed to dodecyltrimethylammonium bromide initiated byssal attachment, and all mussels exposed survived the 14-day post-treatment period.

5.1a.6 Didecyldimethylammonium Bromide

Mussel responses at concentrations of 0.5, 1.0, 1.5, 2.5 and 5.0 ppm didecyldimethylammonium bromide were investigated and the results are in Table 2. At 0.5 ppm, mussel response resembled control group results, however, better results were obtained at 1.0 ppm (87 % for time foot retracted and 0 % for time valve shut), 1.5 ppm (72 % for time foot retracted and 1 % for time valve shut), and 2.5 ppm (96 % for time foot retracted and 2 % for time valve shut). Near ideal results were obtained from the 5.0 ppm treatment, where mussel responses were: 96 % for time foot retracted and 72 % for time valve shut. None of the mussels exposed to didecyldimethylammonium bromide initiated byssal attachment and no fatalities occurred during the 14-day post-treatment period.

5.1a.7 Cupric Sulfate

Mussel responses at the first three concentrations (0.1, 0.2 and 0.3 ppm) of cupric sulfate (Table 2) tested, were not significantly different from the control mussel group. However, response improved at the 0.4 ppm level (63 % for time foot retracted, 26 % for time valve shut), while ideal results were obtained at the 0.6 ppm level (100 % for time foot retracted and time valve shut). Initial mussel byssal attachment was found in three (0.1, 0.3 and 0.4 ppm) of the cupric sulfate solutions tested, while all mussels exposed to cupric sulfate survived the 14-day post-treatment period.

5.1a.8 Sodium Hypochlorite + Zinc Sulfate

Mussel response for the combination of sodium hypochlorite (NaOCl) and zinc sulfate (as Zn) was determined at the following concentrations: 0.2 ppm NaOCl / 0.2 ppm Zn, 0.5 ppm NaOCl / 0.2 ppm Zn, 0.5 ppm NaOCl / 0.4 ppm Zn, 1.0 ppm NaOCl / 0.4 ppm Zn, and 1.0 ppm NaOCl / 0.8 ppm Zn. Mussel response at all (except 0.2 ppm

NaOCl/0.2 ppm Zn) of the combined concentrations evaluated, showed improvement over the control group (Table 2). However, mussel response did not correlate to an increasing (combined) chemical concentration, since the 1.0 ppm NaOCl / 0.4 ppm Zn combination gave better results than the 1.0 ppm NaOCl / 0.8 ppm Zn combination. Initial byssal attachment was established by 3 of the test mussels, at the following concentrations: 0.2 ppm NaOCl / 0.2 ppm Zn, 0.5 ppm NaOCl / 0.4 ppm Zn, and 1.0 ppm NaOCl / 0.4 ppm Zn. There were no fatalities in the mussels exposed to the sodium hypochlorite/zinc sulfate solutions over the 14-day post-treatment period.

5.1a.9 Sodium Hypochlorite + Nickel Sulfate

Mussel response for the combination of sodium hypochlorite (NaOCl) and nickel sulfate (as Ni) was assessed at the following concentrations: 0.2 ppm NaOCl / 0.2 ppm Ni, 0.5 ppm NaOCl / 0.2 ppm Ni, 0.5 ppm NaOCl / 0.4 ppm Ni, 1.0 ppm NaOCl / 0.4 ppm Ni, and 1.0 ppm NaOCl / 0.8 ppm Ni (Table 2). Mussel response results for sodium hypochlorite/nickel sulfate was similar to the sodium hypochlorite/zinc sulfate results. There was no correlation between mussel responses and increasing (combined) chemical concentrations. For example, the results of mussel response were better for 1.0 ppm NaOCl / 0.4 ppm Ni, than for 1.0 ppm NaOCl / 0.8 ppm Ni. Mussel byssal attachment was initiated in the 0.5 ppm NaOCl / 0.4 ppm Ni treatment only, with all exposed mussels surviving the 14-day post-treatment period.

5.1a.10 Sodium Hypochlorite + Cupric Sulfate

The combination of sodium hypochlorite (NaOCl) and cupric sulfate (Cu) was tested at the following concentrations: 0.2 ppm NaOCl / 0.2 ppm Cu, 0.5 ppm NaOCl / 0.2 ppm Cu, 0.5 ppm NaOCl / 0.4 ppm Cu, 0.75 ppm NaOCl / 0.4 ppm Cu, and 1.0 ppm NaOCl / 0.4 ppm Cu. Results for mussel responses (Table 2) were very good (in comparison to the control), displaying a relationship between mussel response and increasing chemical concentration. The % time foot retracted was essentially the same (96, 94, 100) for the three most concentrated solutions (0.5 ppm NaOCl / 0.4 ppm Cu, 0.75 ppm NaOCl / 0.4 ppm Cu, 1.0 ppm NaOCl / 0.4 ppm Cu), however, the % time valve shut showed a gradual increase (63, 74, 100) as the concentration of the test solution increased. Mussel byssal attachment was initiated only in the 0.2 ppm NaOCl / 0.2 ppm Cu test solution. All the mussels exposed to sodium hypochlorite/cupric sulfate test solutions, survived the 14-day post-treatment period.

5.1a.11 Sodium Hypochlorite + Cupric Sulfate + Zinc Sulfate

Exposure experiments were carried out at the following (Table 2) levels: 0.2 ppm NaOCl / 0.1 ppm Cu, Zn (each); 0.5 ppm NaOCl / 0.1 ppm Cu, Zn; 0.5 ppm NaOCl / 0.2 ppm Cu, Zn; 1.0 ppm NaOCl / 0.2 ppm Cu, Zn; and 1.0 ppm NaOCl / 0.4 ppm Cu, Zn. Mussel responses were similar to the control group, up to a concentration of 0.5 ppm NaOCl / 0.2 ppm Cu, Zn, at which point, the results improved significantly. Conversely, mussel responses did not significantly improve at the two higher (combined) concentrations. 0.5 ppm NaOCl / 0.2 ppm Cu, Zn produced the following mussel responses: 100 % for time foot retracted and 32 % for time valve shut. While, 1.0 ppm NaOCl / 0.4 ppm Cu, Zn produced marginally better overall mussel responses of: 95 % for time foot retracted and 64 % for time valve shut. Three of the mussels tested (0.2

ppm NaOCl / 0.1 ppm Cu, Zn; 0.5 ppm NaOCl / 0.1 ppm Cu, Zn; 1.0 ppm NaOCl / 0.4 ppm Cu, Zn) established initial byssal attachment. Mussel mortality was zero, for mussels exposed to sodium hypochlorite/cupric sulfate/zinc sulfate test solutions, over the 14-day post-treatment period.

5.1a.12 Hydrogen Peroxide + Iron Sulfate

Exposure experiments were completed for this chemical combination at the following concentrations: 0.125 ppm H_2O_2 / 0.05 ppm Fe, 0.25 ppm H_2O_2 / 0.1 ppm Fe, 1.25 ppm H_2O_2 / 1.25 ppm Fe, 2.5 ppm H_2O_2 / 1.25 ppm Fe, 3.75 ppm H_2O_2 / 1.25 ppm Fe, and 5.0 ppm H_2O_2 / 1.25 ppm Fe (Table 2). Mussel responses were comparable to the control until the concentration reached 2.5 ppm H_2O_2 / 1.25 ppm Fe, where response results were: 92 % for time foot retracted and 35 % for time valve shut. Less favourable responses were observed for the 3.75 ppm H_2O_2 / 1.25 ppm Fe test solution, before obtaining near perfect results for the 5.0 ppm H_2O_2 / 1.25 ppm Fe solution (100 % for time foot retracted and 93 % for time valve shut). None of the test mussels initiated byssal attachment during chemical exposure, or perished during the 14-day post-treatment period.

5.1 Part 1(B): Laboratory Mussel Study

Based on the results found in Table 2 and some of the other important factors (i.e. health risks, cost, ease of handling, availability, etc.), seven treatments were selected for further assessment. A range of four different concentrations, for each treatment were chosen and ten (10) mussels were tested at each concentration along with a control set. The results of these experiments can be found in Tables 3 – 31 and all results are summarized in Table 32.

5.1b.1 Control

The average response for the 10 control mussels (Table 3) over the 10-min. observation time was: 31 ± 15 % for time foot retracted, and 0 ± 0 % for time valve shut. Three of the test mussels (nos. 3, 9, and 10) initiated byssal attachment. The variability of individual mussel response can be demonstrated by examining the minimum and maximum response times. The minimum was 5 % (mussel no.3), while the maximum was 53 % (mussel no.5) for time foot retracted. For % time valve shut, all mussels had an identical result of 0 %. There was no mussel mortality during the 14-day period following testing.

5.1b.2 Sodium Hypochlorite (0.5 - 1.5 ppm)

Average mussel responses for the 0.5 ppm sodium hypochlorite treatment (Table 4) were: 75 ± 28 % for time foot retracted, and 32 ± 23 % for time valve shut, with one mussel (no.3) initiating byssal attachment. Individual mussel responses in this group ranged from 13 % (mussel no.4) to 100 % (mussel nos.2 and 6) for time foot retracted, and 0 % (mussel nos.2 and 4) to 70 % (mussel no.1) for time valve shut. The 14-day post-treatment mortality test produced no mussel fatalities.

Average mussel responses for the 0.75 ppm sodium hypochlorite treatment (Table 5) were: 79 ± 27 % for time foot retracted, 39 ± 26 % for time valve shut, with one mussel (no.6) initiating byssal attachment. Individual mussel responses ranged from

16 % (mussel no.6) to 100 % (mussel no.8) for time foot retracted, and 3 % (mussel no.6) to 80 % (mussel no.4) for time valve shut. All mussels survived the 14-day post-treatment mortality test.

Sodium hypochlorite treatment at the 1.0 ppm level (Table 6) produced average mussel responses of: 81 ± 32 % for time foot retracted, 57 ± 33 % for time valve shut, with two mussels (nos.5 and 8) initiating byssal attachment. Individual mussel responses ranged from 21 % (mussel no.5) to 100 % (mussel nos.2, 3, 6, 7 and 9) for time foot retracted, and 12 % (mussel no.5) to 100 % (mussel no.6) for time valve shut. No mussel mortality occurred over the 14-day post-treatment period.

Sodium hypochlorite treatment at the 1.5 ppm level (Table 7) produced average mussel responses of: 100 ± 0 % for time foot retracted, 92 ± 17 % for time valve shut, with no mussel initiating byssal attachment. Individual mussel responses were identical (100 %, for all mussels) for time foot retracted, and ranged from 47 % (mussel no.9) to 100 % (mussel nos.1, 3, 5, 6, 7 and 8) for time valve shut. No mussel fatalities were observed over the 14-day post-treatment period.

5.1b.3 Cupric Sulfate (0.5 - 1.5 ppm)

Average mussel responses for the 0.5 ppm cupric sulfate treatment (Table 8) were: 74 ± 23 % for time foot retracted, 52 ± 28 % for time valve shut, with two mussels (nos.7 and 10) initiating byssal attachment. Individual mussel responses ranged from 37 % (mussel no.10) to 100 % (mussel nos.2, 3 and 8) for time foot retracted, and 18 % (mussel no.9) to 96 % (mussel no.3) for time valve shut. No mussel mortality occurred over the 14-day post-treatment period.

Cupric sulfate treatment, at the 0.75 ppm level (Table 9), produced average mussel responses of: 78 ± 22 % for time foot retracted, 61 ± 23 % for time valve shut, with one mussel (no.9) initiating byssal attachment. Individual mussel responses ranged from 35 % (mussel no.5) to 100 % (mussel nos.2, 4 and 10) for time foot retracted, and 32 % (mussel no.5) to 100 % (mussel nos.2 and 10) for time valve shut. No mussel mortality was observed over the 14-day post-treatment period.

Average mussel responses for the 1.0 ppm cupric sulfate treatment (Table 10) were: 90 ± 13 % for time foot retracted, 76 ± 23 % for time valve shut, with no mussels initiating byssal attachment. Individual mussel responses ranged from 66 % (mussel no.5) to 100 % (mussel nos.1,4,6 and 9) for time foot retracted, and 35 % (mussel no.10) to 100 % (mussel nos.1,6 and 9) for time valve shut. The 14-day post-treatment period yielded no mussel mortality.

Average mussel responses for the 1.5 ppm cupric sulfate treatment (Table 11) were: 92 ± 16 % for time foot retracted, 87 ± 21 % for time valve shut, with no mussels initiating byssal attachment. Individual mussel responses ranged from 57 % (mussel no.9) to 100 % (mussel nos.1, 2, 3, 4, 6, 7, and 8) for time foot retracted, and 39 % (mussel no.9) to 100 % (mussel nos.1, 2, 6, 7 and 8) for time valve shut. No mussel fatalities were observed over the 14-day post-treatment period.

5.1b.4 Potassium Permanganate (0.5 - 1.5 ppm)

Potassium permanganate treatment, at the 0.5 ppm level (Table 12), produced average mussel responses of: 82 ± 17 % for time foot retracted, 35 ± 20 % for time valve shut, with no mussels initiating byssal attachment. Individual mussel responses ranged from 51 % (mussel no.5) to 100 % (mussel nos.7 and 9) for time foot retracted, and 0 % (mussel no.1) to 56 % (mussel no.7) for time valve shut. No mussel mortality was observed over the 14-day post-treatment period.

Average mussel responses for the 0.75 ppm potassium permanganate treatment (Table 13) were: 72 ± 28 % for time foot retracted, 44 ± 26 % for time valve shut, with no mussels initiating byssal attachment. Individual mussel responses ranged from 3 % (mussel no.10) to 97 % (mussel no.8) for time foot retracted, and 0 % (mussel no.10) to 82 % (mussel no.9) for time valve shut. The 14-day post-treatment period yielded no mussel mortality.

Average mussel responses for the 1.0 ppm potassium permanganate treatment (Table 14) were: 92 ± 6 % for time foot retracted, 68 ± 18 % for time valve shut, with no mussels initiating byssal attachment. Individual mussel responses ranged from 79 % (mussel no.9) to 100 % (mussel no.1) for time foot retracted, and 48 % (mussel no.10) to 100 % (mussel no.1) for time valve shut. No mussel fatalities were observed over the 14-day post-treatment period.

Average mussel responses for the 1.5 ppm potassium permanganate treatment (Table 15) were: 95 ± 5 % for time foot retracted, 69 ± 18 % for time valve shut, with no mussels initiating byssal attachment. Individual mussel responses ranged from 84 % (mussel no.3) to 100 % (mussel nos.1,5 and 10) for time foot retracted, and 30 % (mussel no.3) to 97 % (mussel no.5) for time valve shut. No mussel mortality occurred over the 14-day post-treatment period.

5.1b.5 Didecyldimethylammonium Bromide (2.5 - 10 ppm)

Average mussel responses for the 2.5 ppm didecyldimethylammonium bromide treatment (Table 16) were: 65 ± 22 % for time foot retracted, 11 ± 12 % for time valve shut, with two mussels (nos.6 and 9) initiating byssal attachment. Individual mussel responses ranged from 15 % (mussel no.6) to 92 % (mussel no.2) for time foot retracted, and 0 % (mussel nos.1, 6 and 8) to 37 % (mussel no.2) for time valve shut. The 14-day post-treatment period yielded no mussel mortality.

Average mussel responses for the 5.0 ppm didecyldimethylammonium bromide treatment (Table 17) were: 77 ± 23 % for time foot retracted, 27 ± 19 % for time valve shut, with no mussel initiating byssal attachment. Individual mussel responses ranged from 30 % (mussel no.6) to 100 % (mussel no.10) for time foot retracted, and 0 % (mussel no.6) to 73 % (mussel no.1) for time valve shut. No mussel fatalities were observed over the 14-day post-treatment period.

Average mussel responses for the 7.5 ppm didecyldimethylammonium bromide treatment (Table 18) were: 84 ± 14 % for time foot retracted, 49 ± 20 % for time valve shut, with one mussel (no.1) initiating byssal attachment. Individual mussel responses ranged from 55 % (mussel no.1) to 100 % (mussel no.10) for time foot retracted, and 19 % (mussel no.1) to 85 % (mussel no.9) for time valve shut. No mussel mortality occurred over the 14-day post-treatment period.

Didecyldimethylammonium bromide treatment, at the 10 ppm level (Table 19), produced average mussel responses of: 95 ± 5 % for time foot retracted, 73 ± 17 % for time valve shut, with no mussels initiating byssal attachment. Individual mussel responses ranged from 87 % (mussel nos.6 and 8) to 100 % (mussel nos.3, 5 and 7) for time foot retracted, and 47 % (mussel no.1) to 100 % (mussel no.7) for time valve shut. No mussel mortality was observed over the 14-day post-treatment period.

5.1b.6 Hydrogen Peroxide (5.0 - 15 ppm)

Average mussel responses for the 5.0 ppm hydrogen peroxide treatment (Table 20) were: 86 ± 10 % for time foot retracted, 60 ± 23 % for time valve shut, with one mussel (no.5) initiating byssal attachment. Individual mussel responses ranged from 64 % (mussel no.5) to 97 % (mussel no.3) for time foot retracted, and 0 % (mussel no.3) to 75 % (mussel nos.9 and 10) for time valve shut. No mussel mortality occurred over the 14-day post-treatment period.

Hydrogen peroxide treatment, at the 7.5 ppm level (Table 21), produced average mussel responses of: 88 ± 16 % for time foot retracted, 76 ± 16 % for time valve shut, with two mussels (nos.6 and 9) initiating byssal attachment. Individual mussel responses ranged from 53 % (mussel no.9) to 100 % (mussel no.3) for time foot retracted, and 41 % (mussel no.9) to 91 % (mussel no.7) for time valve shut. No mussel mortality was observed over the 14-day post-treatment period.

Average mussel responses for the 10 ppm hydrogen peroxide treatment (Table 22) were: 88 ± 15 % for time foot retracted, 73 ± 15 % for time valve shut, with one mussel (no.6) initiating byssal attachment. Individual mussel responses ranged from 58 % (mussel no.3) to 100 % (mussel no.7) for time foot retracted, and 52 % (mussel no.3) to 95 % (mussel no.4) for time valve shut. No mussel fatalities were observed over the 14-day post-treatment period.

Average mussel responses for the 15 ppm hydrogen peroxide treatment (Table 23) were: 90 ± 11 % for time foot retracted, 81 ± 12 % for time valve shut, with no mussel initiating byssal attachment. Individual mussel responses ranged from 60 % (mussel no.6) to 99 % (mussel no.7) for time foot retracted, and 53 % (mussel no.6) to 93 % (mussel no.1) for time valve shut. No mussel mortality occurred over the 14-day post-treatment period.

5.1b.7 Sodium Hypochlorite + Cupric Sulfate (0.25 - 0.75 ppm each)

Average mussel responses for the 0.25 ppm (each) sodium hypochlorite + cupric sulfate combination treatment (Table 24) were: 86 ± 24 % for time foot retracted, 73 ± 33 % for time valve shut, with one mussel (no.5) initiating byssal attachment. Individual mussel responses ranged from 40 % (mussel no.5) to 100 % (mussel nos.2, 3, 4, 6, 7 and 10) for time foot retracted, and 10 % (mussel no.1) to 100 % (mussel nos.6 and 7) for time valve shut. No mussel fatalities were observed over the 14-day post-treatment period.

Average mussel responses for the combination of 0.50 ppm sodium hypochlorite + 0.25 ppm cupric sulfate (Table 25) were: 95 ± 6 % for time foot retracted, 62 ± 31 % for time valve shut, with no mussel initiating byssal attachment. Individual mussel responses ranged from 84 % (mussel no.5) to 100 % (mussel nos.1, 2, 7 and 9) for time foot retracted, and 18 % (mussel no.1) to 100 % (mussel nos.2 and 9) for time valve shut. No mussel mortality was observed during the 14-day post-treatment period.

Average mussel responses for the 0.50 ppm (each) sodium hypochlorite + cupric sulfate combination treatment (Table 26) were: 85 ± 24 % for time foot retracted, 74 ± 35 % for time valve shut, with no mussel initiating byssal attachment. Individual mussel responses ranged from 47 % (mussel no.9) to 100 % (mussel nos.1, 5, 6, 7, 8 and 10) for time foot retracted, and 16 % (mussel no.9) to 100 % (mussel nos.1, 5, 6, 7 and 10) for time valve shut. No mussel mortalities were observed over the 14-day post-treatment period.

Average mussel responses for the 0.75 ppm (each) sodium hypochlorite + cupric sulfate combination treatment (Table 27) were: 100 ± 1 % for time foot retracted, 91 ± 7 % for time valve shut, with no mussel initiating byssal attachment. Individual mussel responses were all 100 % (except for mussel no.7) for time foot retracted, and ranged from 83 % (mussel nos.9 and 10) to 100 % (mussel nos.1, 2 and 3) for time valve shut. All ten mussels survived the 14-day post-treatment period.

5.1b.8 Iodine (1.5 - 6.0 ppm)

Iodine treatment, at the 1.5 ppm level (Table 28), produced average mussel responses of: 77 ± 18 % for time foot retracted, 20 ± 17 % for time valve shut, with no mussel initiating byssal attachment. Individual mussel responses ranged from 44 % (mussel no.1) to 100 % (mussel no.3) for time foot retracted, and 0 % (mussel nos.3 and 6) to 44 % (mussel nos.4 and 9) for time valve shut. Mussel survival rate was 100 % over the 14-day post-treatment period.

Average mussel responses for the 3.0 ppm iodine treatment (Table 29) were: 80 ± 23 % for time foot retracted, 39 ± 35 % for time valve shut, with one mussel (no.9) initiating byssal attachment. Individual mussel responses ranged from 44 % (mussel no.5) to 100 % (mussel nos.1, 3, 6, 7 and 8) for time foot retracted, and 0 % (mussel no.9) to 87 % (mussel no.3) for time valve shut. The 14-day post-treatment period yielded no mussel mortality.

Average mussel responses for the 4.5 ppm iodine treatment (Table 30) were: 94 ± 10 % for time foot retracted, 66 ± 21 % for time valve shut, with no mussel initiating byssal attachment. Individual mussel responses ranged from 68 % (mussel no.8) to 100 % (mussel nos.2, 4, 5 and 10) for time foot retracted, and 33 % (mussel no.8) to 91 % (mussel nos.2, 5 and 10) for time valve shut. No mussel mortality occurred over the 14-day post-treatment period.

Average mussel responses for the 6.0 ppm iodine treatment (Table 31) were: 94 ± 13 % for time foot retracted, 72 ± 26 % for time valve shut, with no mussel initiating byssal attachment. Individual mussel responses ranged from 60 % (mussel no.2) to 100 % (mussel nos.1, 4, 5, 7, 8, 9 and 10) for time foot retracted, and 26 % (mussel no.2) to 100 % (mussel no.5) for time valve shut. No mussel fatalities were observed over the 14-day post-treatment period.

5.2 Part 2: Seawater System Mussel Study

The experimental method used in Part 1 (Laboratory Mussel Study) was used to assess the three chemical treatment systems associated with the DREA/DL seawater system. Tests were completed for the two different tap locations (mid and end) affiliated with each treatment system along with a control set. The results can be found in Tables 33 – 39, and summarized in Table 40. There were no mussel mortalities during the 14-day post-treatment period.

5.2.1 Control

The mussels from the control group (Table 33) were tested using seawater derived from the holding tank (untreated). The average responses of 10 control mussels over the 15-min. observation time were 47 ± 23 % (time foot retracted) and 5 ± 6 % (time valve shut). Three of the mussels (mussel nos. 3, 9, and 10) initiated byssal attachment during the test period. Individual mussel response was variable as evident in the minimum and maximum % of time of physical responses: results ranged from a low of 17 % (mussel no.5) to a high of 100 % (mussel no.2) for % time foot retracted, and 1 % (mussel nos.4 and 7) to 20 % (mussel no.1) for % time valve shut.

5.2.2 Hypochlorite (End Tap)

Average mussel responses for the hypochlorite (end tap) treatment (Table 34) were 100 ± 0 % for time foot retracted and 99 ± 1 % for time valve shut. No mussel initiated byssal attachment. Individual mussel responses were 100 % (for all 10 mussels) for time foot retracted, and ranged from 97 % (mussel nos.1 and 10) to 100 % (mussel nos.3, 4, 5, 6, 7 and 8) for time valve shut.

5.2.3 Iodine (End Tap)

Average mussel responses for the iodine (end tap) treatment (Table 35) were 70 ± 23 % for time foot retracted, 33 ± 34 % for time valve shut, with two mussels (nos.5 and 7) initiating byssal attachment. Individual mussel responses ranged from 30 % (mussel no.5) to 100 % (mussel nos.1 and 3) for time foot retracted, and 2 % (mussel no.6) to 93 % (mussel no.3) for time valve shut.

.2.4 Copper (End Tap)

The copper (end tap) treatment (Table 36), produced average mussel responses of: 66 ± 23 % for time foot retracted, 23 ± 16 % for time valve shut, with two mussels (nos.5 and 8) initiating byssal attachment. Individual mussel responses ranged from 24 % (mussel no.5) to 93 % (mussel no.9) for time foot retracted, and 2 % (mussel no.1) to 51 % (mussel no.9) for time valve shut.

5.2.5 Hypochlorite (Mid Tap)

Average mussel responses for the hypochlorite (mid tap) treatment (Table 37) were (almost identical for all mussels): 100 ± 0 % for time foot retracted, 100 ± 1 % for time valve shut, with no mussel initiating byssal attachment.

5.2.6 Iodine (Mid Tap)

Iodine (mid tap) treatment (Table 38), produced average mussel responses of: 67 ± 30 % for time foot retracted, 38 ± 27 % for time valve shut, with two mussels (nos.4 and 5) initiating byssal attachment. Individual mussel responses ranged from 27 % (mussel no.5) to 100 % (mussel no.1) for time foot retracted, and 6 % (mussel no.5) to 89 % (mussel no.6) for time valve shut.

5.2.7 Copper (Mid Tap)

Average mussel responses for the copper (mid tap) treatment (Table 39) were: 64 ± 28 % for time foot retracted, 20 ± 14 % for time valve shut, with two mussels (nos.2

and 4) initiating byssal attachment. Individual mussel responses ranged from 15 % (mussel no.2) to 100 % (mussel no.5) for time foot retracted, and 1 % (mussel no.2) to 35 % (mussel no.3) for time valve shut.

5.3 Part 3: Seawater System Concentration Study

The results of the hypochlorite concentration experiments conducted to investigate the effect on seawater concentration with respect to (1) flow rate and (2) electrical current can be found in Tables 41-51, with the results summarized in Tables 52 and 53. The data from the summary tables has been plotted (Conc. vs. Flow Rate and Conc. vs. Electrical Current) in Figures 4 and 5.

The original experimental plan for investigating treated seawater copper concentration was identical to the hypochlorite concentration study. However, initial and follow-up results, found in Table 54, indicated that there was another variable playing an important role in seawater copper concentrations. For this reason, the original experimental plan was replaced with work that focused on the identification of this unknown variable. The weight loss of the sacrificial copper anodes was monitored throughout the experimental period to ensure the equipment was functioning properly. Shown in Figure 6a & b are photographs of the anodes. The anode weight loss measurements are found in Table 55, while Figure 7 outlines this data graphically.

6.0 Discussion

6.1 Part 1: Laboratory Mussel Study

Prior to discussing the experimental results a number of key issues should be considered. These issues pertain to the interpretation of the results, which must be done cautiously, for the following reasons:

(1) the great variation in response, between individual mussels, to chemical exposure (as illustrated by the experimental results);
(2) the enormous difference that temperature can play in mussel response and chemical reactivity;
(3) the unknown difference in response, between mussels of differing levels of development (i.e. larval vs. juvenile adult);
(4) the inability to determine mussel health prior to chemical exposure;
(5) the vast difference between laboratory and field conditions;
(6) variability of water conditions can dramatically influence chemical effectiveness (i.e. pH, salinity, organic carbon and naturally occurring chemical concentrations); and
(7) number of test mussels was inadequate for proper statistical assessment.

None of the individual or combination chemical treatments proved to be effective at the ~ 50 ppb level (Table 1), and the elevated treatments (Table 2) involved only one mussel at each concentration, therefore, the discussion will be limited to the seven chemical treatments at effective concentrations (Tables 4 - 31).

A comparison of responses between the chemically exposed and control mussel results (Table 32) verify that all the chemicals tested, displayed some degree of success in discouraging mussel settlement, however, effective concentrations vary significantly between chemical treatments. Most displayed a relationship between concentration and effectiveness, i.e. effectiveness increased with increasing chemical concentration.

Sodium hypochlorite exhibited some degree of settlement discouragement at the 0.5 ppm level, with effectiveness increasing with elevated concentration. This culminated with almost ideal mussel responses (100 ± 0 % for time foot retracted and 92 ± 17 % for time valve shut) at the 1.5 ppm sodium hypochlorite concentration. Results indicate that the effective concentration is between 0.5 - 1.5 ppm NaOCl for controlling mussel settlement.

Sodium hypochlorite is an oxidant, and like most oxidants, is not selective. Meaning that, sodium hypochlorite will react with any oxidizeable substance it comes in contact with, thereby, affecting more than just the target organism. This environmental concern is compounded by the chemical reaction with naturally-occurring organic matter in seawater, producing some biologically harmful compounds (i.e. trichloromethanes). Most oxidants are also temperature-dependent, being more effective at increased temperatures, and sodium hypochlorite is rather pH-dependent. Sodium hypochlorite is commonly available as a liquid, providing a product that is easy and relatively safe to handle. In comparison to other chemical treatments, sodium hypochlorite is inexpensive, with virtually no known detrimental affects on equipment.

Published literature concerning the effects on mussels from exposure to sodium hypochlorite, concentrated on mortality results. Rajagopal et al (1995) studied the effects of chlorine on the green mussel, *Perna viridis*, and found that smaller mussels were less tolerant than larger mussels, and filtration rate, foot activity and byssal thread production decreased with increasing chlorine concentration.

Cupric sulfate behaved similarly to sodium hypochlorite, providing some level of settlement discouragement at the 0.5 ppm level. Increasing cupric sulfate concentration produced improved levels of settlement discouragement. The results for cupric sulfate treatment at the 1.0 ppm level (90 ± 13 % for time foot retracted, 76 ± 23 % for time valve shut) were similar to the 1.5 ppm level (92 ± 16 % for time foot retracted, 87 ± 21 % for time valve shut), indicating that ~1.0 ppm Cu should be adequate for discouraging settlement.

Cupric sulfate (or copper) is not an oxidant, but like most oxidants is not selective, thereby, negatively affecting more than just the target organism. This is compounded by the concern linked to copper accumulation in the marine environment. Copper toxicity appears to be temperature-dependent and to a lesser extent, pH-dependent. Aqueous copper is relatively safe, easy to handle, with essentially no known equipment concerns, however, treatment would be costly in comparison to sodium hypochlorite.

The literature contains many studies on the effects of copper exposure to mussels, with several examining the sublethal effects. Davenport & Manley (1978) used a flow-through seawater system, at 15°C, to expose adult (30-60mm) mussels to various concentrations of copper. They determined that complete mussel valve closure occurs around 0.2 ppm Cu. Conversely, Stromgren (1982) used a flow-through seawater system (8-15°C) to expose adult (19-29mm) mussels to various copper concentrations, reporting permanent valve closure at 0.005 ppm Cu. Manley (1983) reported a negative effect on mussel respiration, filtration and ventilation in response to copper exposure using a flow-through seawater (14°C) system. Beaumont et al. (1987) reported that a copper concentration of 0.4 ppm produced a 50 % mortality rate in mussel larvae (veligers), over a 15-day period, using static, seawater (15°C) tests.

Results for potassium permanganate experiments were less predictable. Mussel responses were quite good at the 0.5 ppm level (82 ± 17 % for time foot retracted, 35 ± 20 % for time valve shut), however, response dropped at the 0.75 ppm level (72 ± 28 % for time foot retracted, 44 ± 26 % for time valve shut). Followed by improved, but almost identical responses at the 1.0 ppm (92 ± 6 % for time foot retracted, 68 ± 18 % for time valve shut) and 1.5 ppm (95 ± 5 % for time foot retracted, 69 ± 18 % for time valve shut) levels. This suggests the effective concentration (to discourage mussel settlement) is ~1.0 ppm $KMnO_4$.

Potassium permanganate is a solid oxidant, which generates a dark purple colour in solution, and suffers the same problem as other oxidants: a lack of selectivity. Aqueous solutions are easy and relatively safe to handle, although use would be more costly than sodium hypochlorite. No information regarding equipment and environmental effects could be found.

The literature contained only freshwater mortality studies of zebra mussel (*Dreissena polymorpha*) exposure to potassium permanganate. Klerks & Fraleigh (1991) used zebra mussels (14-16mm) in a flow-through system to determine exposure at 1.0 ppm and 2.5 ppm $KMnO_4$, produced a 50 % mortality rate in 49.8 and 10.7 days respectively. Matisoff et al. (1991) concluded that >2 ppm potassium permanganate was required in a flow-through system to cause zebra mussel mortality.

Mussel responses to didecyldimethylammonium bromide exposure reflected treatment concentration. Settlement discouragement increased and was most effective at 10 ppm level (95 ± 5 % for time foot retracted and 73 ± 17 % for time valve shut), the highest concentration tested.

Didecyldimethylammonium bromide is a surfactant categorized as a quaternary ammonium salt. Surfactants do not disperse evenly throughout the bulk of a solution, rather they tend to congregate at the liquid/solid interfaces. For this reason, field tests would be more appropriate than static, laboratory experiments to assess the effectiveness against mussel settlement. Didecyldimethylammonium bromide is a solid that suffers somewhat from solubility problems, but once in solution, it is easy and relatively safe to handle. The mode of chemical reaction responsible for discouraging mussel settlement is not well understood, although it is believed to be related to charge (anion/cation). Unlike most other chemicals tested, didecyldimethylammonium bromide does not appear to be pH-dependent, although it is somewhat temperature-dependent. There is concern over toxicity to non-target organisms, and the long-term effects on equipment and the environment have not been studied. Presently, cost is the largest drawback to treatment with didecyldimethylammonium bromide.

The literature lacked any studies pertaining to the chemical exposure of mussels to didecyldimethylammonium bromide, however, several other quaternary ammonium salts have been examined. These freshwater studies assessed the effectiveness in controlling zebra mussel infestation. Most reports (Martin et al., 1993; McMahon et al., 1993; Khalanski, 1993) agree that a concentration of 1-8 ppm, of the particular quaternary ammonium salt studied, is required to cause mussel mortality.

The results for treatment with hydrogen peroxide were rather puzzling. Mussel responses at 5.0 ppm (86 ± 10 % for time foot retracted, 60 ± 23 % for time valve shut) were not significantly different from 15 ppm (90 ± 11 for time foot retracted, 81 ± 12 % for time valve shut), with 7.5 and 10 ppm giving similar results. Implying that the control of mussel settlement may be possible with $\leq$ 5.0 ppm hydrogen peroxide.

Hydrogen peroxide is another oxidant suffering from a selectivity and temperature-dependence problem. It is available as a liquid, therefore handling and use is relatively safe and simple. Questions remain regarding storage and affects of long-term use on equipment and the environment, however, presently, the major drawback of hydrogen peroxide treatment is cost.

The literature contained two reports that studied the effectiveness of hydrogen peroxide against mussel infestation. One study (Nishimura et al., 1988) investigated the inhibition of mussel settlement using a laboratory flow-through, seawater system, while the other (Ikuta et al., 1988) examined the prevention of mussel fouling in the field. Authors from both studies concluded that 1.0 - 4.0 ppm hydrogen peroxide was necessary to prevent mussel settlement.

The 0.25 ppm (each) sodium hypochlorite + cupric sulfate combination treatment produced very good mussel responses (86 ± 24 % for time foot retracted, 73 ± 33 % for time valve shut), but responses were practically ideal (100 ± 1 % for time foot retracted, 91 ± 7 % for time valve shut) at the 0.75 ppm (each) concentration. Indicating that adequate control of mussel settlement may be achieved at 0.25 ppm (each), however, 0.75 ppm (each) would provide an even better probability of settlement control.

Refer to previous discussion regarding the chemical characteristics of these two individual compounds. Keeping in mind, that most drawbacks (i.e. environmental concerns, cost, etc.) would be reduced due to the use of lower concentrations of each chemical.

Two different studies were found in the literature regarding biofouling control using this combination. Knox-Holmes (1993) determined that the copper/chlorine treatment was more effective than equivalent treatments with chlorine, copper or chlorine/aluminum for controlling both micro and macrofouling in a continuously, flowing seawater system. Strauss (1989) used a similar procedure to determine that the copper/chlorine combination was significantly more effective than chlorine alone for inhibiting micro and macrofouling. There was no published literature pertaining solely to the discouragement of mussel settlement using the copper/chlorine combination.

The last chemical assessed using this technique was iodine. Mussel responses were directly related to concentration with gradual improvement up to the 4.5 ppm level. Results were very good, but did not differ significantly between the 4.5 ppm (94 ± 10 % for time foot retracted, 66 ± 21 % for time valve shut) and 6.0 ppm (94 ± 13 % for time foot retracted, 72 ± 26 % for time valve shut) iodine treatments. Implying that 4.5 ppm iodine may be adequate to discourage mussel settlement.

Iodine, another solid oxidant (non-selective) suffers from solubility problems and behaves similar to chlorine in solution. One advantage of iodine over chlorine; iodine does not react with seawater to form harmful compounds (i.e. trichloromethanes) that are produced by chlorine. Aqueous iodine is relatively safe and easy to handle, however, due to degassing (I_2) iodine solutions must be kept in a closed environment to minimize losses. There is no information regarding the long-term effects on equipment and the environment from iodine use. The major drawback with iodine treatment is cost, being much more expensive than chlorine at effective concentrations.

There was no information in the published literature pertaining to the use of iodine in controlling mussel settlement or biofouling.

6.2 Part 2: Seawater System Mussel Study

Since experimental seawater chemical concentrations were not determined, results will only be discussed in a comparative manner between the three treatments.

Initial tests were completed on the end tap location on each system. Mussel response results were excellent for the hypochlorite treatment (100 ± 0 % for time foot retracted, 99 ± 1 % for time valve shut). Results were inferior (lower) from the iodine (70 ± 23 % for time foot retracted, 33 ± 34 % for time valve shut) and copper (66 ± 23 % for time foot retracted, 23 ± 16 % for time valve shut) treatments.

Mid tap sites provided similar mussel response results to the end tap tests. The hypochlorite (100 ± 0 % for time foot retracted, 100 ± 1 % for time valve shut) results were superior to the iodine (67 ± 30 % for time foot retracted, 38 ± 27 % for time valve shut) and copper (64 ± 28 % for time foot retracted, 20 ± 14 % for time valve shut) results.

Without knowledge of the chemical concentration (copper, hypochlorite and iodine) in the test seawater, the hypochlorite treatment produced the most desirable mussel responses. Unfortunately, the validity of these results depends primarily on the chemical concentration. For example, the hypochlorite concentration could have been significantly higher than either the iodine or copper concentration, explaining the superior results.

6.3 Part 3: Seawater System Concentration Study

Since seawater is such a complex solution, determining the concentration of many chemicals (or elements) can be difficult, involving the effects of numerous variables (i.e. pH, temperature, reactivity, salinity, solubility, etc.). However, in the case of chemical treatment (dosing), many of these variables have a minimal effect, since seawater chemical concentration is artificially elevated. For dosing, the primary variables governing seawater concentration (usually) are the amount of chemical added and the volume of seawater. For this study, the two primary variables were applied electrical current (amount of chemical) and the seawater flow rate (volume).

The primary variables were examined individually, where the first set of hypochlorite experiments involved altering seawater flow rate (volume), while maintaining a constant electrical current (amount of chemical). The results (Table 52) were plotted (Figure 4), illustrating the gradual drop in hypochlorite concentration as the flow rate of seawater increases. The results for the experiments where electrical current was changed while maintaining a constant seawater flow rate (Table 53) was also plotted (Figure 5), with a similar effect on hypochlorite concentration. As electrical current decreases, so does the seawater concentration of hypochlorite. Although the results for both experiments were anticipated, neither provided a simple (i.e. linear) relationship for estimating seawater hypochlorite concentration.

If experimental data was generated over a wide range of values for both seawater flow rate (with constant current) and electrical current (with constant flow rate), then the plotted data could be used to predict approximate hypochlorite seawater concentrations. For safe, economical chemical treatment to prevent mussel settlement, seawater chemical concentration is a vital piece of information. Otherwise, treatment might be inadequate, failing to prevent settlement; or over-treatment, which will result in wasted revenue and an increased risk of harm to the environment, equipment and non-target organisms.

The intention of these experiments was to investigate the potential of predicting seawater chemical concentration based on current and flow rate, not to calibrate the test equipment, since it was a prototype intended for experimental purposes only. The in-line design of the hypochlorite generator (cell) would not be appropriate for CPF installation. The generator has grating located at either end (to protect electrodes) which repeatedly caused restricted seawater flow rate problems. The accumulation of a small number of mussel shells (~ 6) on the inlet grating could cause a 75% decrease in seawater flow through the cell. Closing the line (Line C), disconnecting the cell and manual removal of the shells was the only remedy to this problem, which would be impractical for CPF use. A screen or strainer located upstream from the generator would help; however the screen/strainer would need periodic removal for cleaning (also not practical). For this reason, an alternative to an in-line generator, such as an injection system, would be recommended for CPF use.

Another important fact deserving consideration is reactivity. Since hypochlorite is a fairly strong oxidant, it will react with a variety of naturally occurring compounds found in seawater. This in turn will decrease the hypochlorite concentration, perhaps below effective concentrations. The products of some of these reactions are ineffective in preventing mussel settlement. Therefore monitoring hypochlorite concentration only at the source of (hypochlorite) generation will not be adequate for an extensive seawater system.

The same two variables (electrical current, flow rate) were to be investigated for their effect on concentration in the copper treatment experiments. The initial plan was to duplicate the experiments performed for the hypochlorite study; however, this was not completed. Since initial copper concentration measurements caused some concern, a more thorough preliminary study was justified. This study was designed to confirm that the seawater copper concentration was altered by varying the electrical current. The first step was to determine the natural (or background) concentration of copper in seawater, which lead to the unexpected discovery. Some seawater samples were collected from the control (B) line as part of this study and compared with samples taken from the copper treatment (A) line. The results (Table 54) for these samples were unexpected, indicating a need for an explanation. The concentration of copper in seawater taken from the treatment (A) line was higher than what the manufacturer's literature suggested for that applied current; although, even more surprising was the copper concentration in the seawater removed from the control line. It had a higher copper concentration than the two treated seawater samples. The copper had to be coming from somewhere in the seawater system since the copper concentration in Halifax harbour water was comparable to naturally occurring levels in industrialized harbours.

Further tests lead to an explanation of these unexpected results. The elevated copper levels were a result of the Cu/Ni piping and the copper joints that were used in the seawater system. The seawater passing through these pipes and joints was picking up copper from their internal walls. The oxidation layer that forms on copper when it is immersed in seawater, is not tightly bound and will slough off, exposing fresh, unoxidized metal. The elevated copper must be due to one or both of the sources: (1)

oxidation layer or (2) freshly exposed metal. The majority of data found in Table 54, where elevated copper concentrations seem to be related to seawater flow rate, supports this theory. Except for the odd result, copper concentrations are higher in the samples collected during elevated flow rates.

The results also indicate that the amount of copper produced by the treatment equipment is insignificant (at lower settings) compared to the copper concentration provided by the oxidation of the Cu/Ni pipes. The literature supplied by the manufacturer of the copper treatment equipment, states that the effective copper concentration for combating biofouling is only slightly higher than natural levels. If this information is accurate, then the pipes are providing more than sufficient levels of copper for adequate protection against biofouling. The only areas of concern would be areas of reduced flow or stagnant seawater.

These results were obtained using the DREA/DL seawater system, which was constructed of the same Cu/Ni piping used in the CPF cooling water system. However, the DREA/DL seawater system also includes some copper joints not present on CPF cooling water systems. If the contribution from these copper joints is minimal, then similar seawater copper levels can be expected in CPF cooling water piping. This should be confirmed by obtaining seawater samples from several CPF cooling water systems. Ideally, samples would be obtained from two ships under similar service conditions; one equipped with copper treatment (Cathelco), the other without. This would verify elevated seawater copper concentrations and the contribution (if any) from the treatment equipment.

7.0 Conclusions/Recommendations

7.1 Part 1: Laboratory Mussel Study

All the chemicals tested for discouragement of mussel settlement were effective; however, some were only effective at relatively high concentrations. The choice of biofouling chemical treatment must take the following criteria into consideration: high effectiveness at low concentration; relative safeness and ease of handling, storage and maintenance; cost-effectiveness; and equipment and environment-friendliness. The top three treatments (in no particular order), based on the above criteria and the experimental results are:

(1) sodium hypochlorite + cupric (copper) sulfate,
(2) sodium hypochlorite, and
(3) cupric (copper) sulfate.

7.2 Part 2: Seawater System Mussel Study

It is clearly apparent from the results that the hypochlorite treatment is substantially more effective than either the iodine or copper treatments. However, this does not account for chemical concentration, which could vary significantly between the individual treatments. Without the concentration information these results are essentially inconclusive. This should be rectified prior to any further assessment of the chemical treatment equipment associated with the DREA/DL seawater system.

Once seawater chemical concentration (for hypochlorite, copper and iodine) can be monitored, the next step would be individual treatment optimization by altering (decreasing/increasing) chemical addition and/or system flow rate.

7.3 Part 3a: Seawater System Concentration Study

The hypochlorite concentration study results indicate that chemical concentration can be reasonably estimated (for the equipment and seawater system tested), with knowledge of applied electrical current and seawater flow rate. Any installation of a hypochlorite treatment system will require calibration of the equipment to insure adequate chemical concentration for preventing mussel settlement and infestation. It is recommended that redesigned hypochlorite treatment system be installed on a CPF, followed by appropriate studies. Such as, the rate of degradation should be monitored throughout the cooling water system and prior to discharge. If chemical reactions (with naturally occurring seawater compounds) cause a decrease in the hypochlorite concentration, adequate protection against mussel settlement could be compromised.

The concentration study results for the copper treatment (Cathelco) system and the hypochlorite system differed significantly. The copper concentration results indicate that the primary source of copper was not the Cathelco system, but rather the Cu/Ni piping itself. Further copper ion concentration measurements should be performed. Seawater samples should be taken from two different CPF's (a CPF with Cathelco and one without Cathelco) under similar service conditions. Adequate copper levels in DREA/DL cooling seawater appear to be achieved by controlling the flow rate; however, with regards to a CPF, areas of stagnant or minimal flow may require additional biofouling protection.

Since the results of the concentration study of copper indicate the piping is the main source of copper, then there must be elevated copper in all Cu/Ni piping. This means that the hypochlorite treatment would also include elevated copper in the seawater. Both chemicals possess antifouling properties, so in combination they may have a significantly lower effective concentration against mussel settlement. This possible synergistic effect of the (copper/hypochlorite) combination should be studied using the DREA/DL seawater system, or after hypochlorite treatment installation on a CPF.

The final recommendation would be to continue to investigate alternate methods of discouraging mussel settlement. Since both copper and hypochlorite are regulated compounds, stricter regulations could lead to concentrations too low to effectively discourage mussel settlement.

8.0 Acknowledgements

The authors would like to thank the following individuals and agencies: Dr. Bob Klassen and Dr. Pierre Roberge (RMC) for supplying the hypochlorite equipment installed on the DREA seawater system and their useful input on a number of technical issues. Martin Yeatman (Andover Mgmt. Inc.) who provided the copper treatment equipment (Cathelco) and also provided some technical assistance. Gary Fisher (DREA) for his guidance and technical support on sample preparation and analysis. Chester Mappin and his crew (pipe-fitters) from FMF Cape Scott for continuous technical and mechanical support throughout this investigation.

9.0 References

Beaumont, A.R., G. Tserpes and M.D. Budd. 1987. Some effects of copper on the veliger larvae of the mussel *Mytilus edulis* and the scallop *Pecten maximus* (Mollusca, Bivalvia). Mar. Environ. Res., 21: 299-309.

Chou, C.L., B. Zwicker, J.F. Porter, and G.R. Pelletier. 1999. Potential biofouling strategies against blue mussel (*Mytilus edulis*) infestation in a cooling water system. Can. Tech. Rep. Fish. Aquat. Sci. 2283: vi + 89 p.

Davenport, J. and A. Manley. 1978. The detection of heightened sea-water copper concentrations by the mussel *Mytilus edulis*. J. Mar. Biol. Ass. U.K., 58: 843-850.

Ikuta, S., K. Nishimura, T. Yasunaga, S. Ichikawa and Y. Wakao. 1988. Biofouling control a using synergistic hydrogen peroxide and ferrous ion technique. Off. Proc. Intern. Water Conf., 49th Ann. Meeting, Pittsburgh, PA, p449-458.

Khalanski, M. 1993. Testing of five methods for the control of zebra mussels in cooling circuits of power plants located on the Moselle river. EDF (Electricite de France), p22.

Klerks, P.L. and P.C. Fraleigh. 1991. Controlling adult zebra mussels with oxidants. J. Am. Water Works Assn., Vol. 83, 12: 92-100.

Knox-Holmes, B. 1993. Biofouling control with low levels of copper and chlorine. Biofouling, 7: 157-166.

Manley, A.R. 1983. The effects of copper on the behavior, respiration, filtration and ventilation of *Mytilus edulis*. J. Mar. Biol. Ass. U.K., 63: 205-222.

Martin, I.D., G.L. Mackie and M.A. Baker. 1993. Control of the biofouling mollusc, *Dreissena polymorpha* (Bivalvia: Dreissenidae), with sodium hypochlorite and with polyquaternary ammonia and benzothiazole compounds. Arch. Environ. Contam. Toxicol., 24: 381-388.

Matisoff, G., A. Greenberg, G. Gubanich and J. Ciaccia. 1991. Effects of potassium, chloramine, and chlorine dioxide on control of adult zebra mussels. J. Shellfish Res., Vol. 11, 1:232.

McMahon, R.F., B.N. Shipman and D.P. Long. 1993. Laboratory efficacies of nonoxidizing molluscicides on the zebra mussel (*Dreissena polymorpha*) and the Asian clam (*Corbicula fluminea*). In: Zebra Mussels: Biology, Impacts, and Control, edited by T.F. Nalepa and D.W. Schloesser, CRC Press, Inc., Boca Raton, Florida, pp.575-598.

Nishimura, K., T. Yasunaga, S. Ichikawa and Y. Wakao. 1988. Development of a new antifouling method for a marine cooling water system. Mar. Biol., 99: 145-150.

Rajagopal, S., V.P. Venugopalan, K.V.K. Nair and J. Azariah. 1995. Response of green mussel, *Perna viridis* (L.) to chlorine in the context of power plant biofouling control. Mar. Fresh. Behav. Physiol., 25: 261-274.

Stewart, P.L. 1994. Environmental requirements of the blue mussel (*Mytilus edulis*) in eastern Canada and its response to human impacts. Can. Tech. Rep. Fish. Aquat. Sci. 2004: x + 41p.

Strauss, S.D. 1989. New methods, chemicals improve control of biological fouling. Power, 1: 51-52.

Stromgren, T. 1982. Effect of heavy metals (Zn,Hg,Cu,Cd,Pb,Ni) on the length growth of *Mytilus edulis*. Mar. Biol., 72: 69-72.

TABLE 1: Summary of Treatments at ~ 50 ppb

Chemical Treatment	Av Mussel Size(mm)	Av. Temp (°C) Start	End	Av. Time Foot Retracted (sec)	Av. Time Valve Shut (sec)	Av. % Time Foot Retracted	Av % Time Valve Shut
Cupric Sulfate	13	14.4	18.0	377	43	42 ± 18	5 ± 8
Sodium Hypochlorite + Cu	14	13.5	17.7	340	0	38 ± 15	0 ± 0
Benzalkonium Chloride	14	13.7	16.9	337	28	37 ± 16	3 ± 9
Iodine	14	12.7	16.7	308	1	34 ± 19	0 ± 1
Potassium Permanganate	13	13.6	16.9	308	17	34 ± 17	2 ± 4
Dodecyltrimethylammonium Bromide	13	14.1	17.5	297	7	33 ± 25	1 ± 3
Didecyldimethylammonium Bromide	14	14.6	18.3	273	5	31 ± 28	1 ± 2
Control	13	13.3	17.2	271	1	30 ± 17	0 ± 0
Sodium Hypochlorite + Zn	14	13.4	17.0	256	0	29 ± 15	0 ± 0
Sodium Hypochlorite + Ni	13	13.6	17.6	264	0	29 ± 19	0 ± 0
Sodium Hypochlorite + Zn + Cu	14	13.3	17.1	202	0	23 ± 10	0 ± 0
Sodium Hypochlorite	14	9.5	15.1	188	15	21 ± 12	2 ± 3
Hydrogen Peroxide + Fe	14	11.6	16.2	191	0	21 ± 10	0 ± 0
Hydrogen Peroxide	14	9.6	14.9	176	0	20 ± 10	0 ± 0

TABLE 2 Determination of Effective Concentration for Chemical Treatment (> 50 ppb)

Chemical Treatment	Conc (ppb/ppm)	Mussel Size (mm)	Temp. (°C) Start	End	Time Foot Retracted (s)	Time Valve Shut (s)	% Time Foot Retracted	% Time Valve Shut	Initial Byssal Attachment
Sodium Hypochlorite	~ 100 ppb	12	14.0	18.0	425	0	47	0	no
	~ 150 ppb	16	12.0	16.0	382	0	42	0	yes
	~ 200 ppb	13	13.0	17.0	782	317	87	35	no
	~ 400 ppb	16	13.0	17.0	531	263	59	29	no
	~ 500 ppb	15	13.0	17.0	379	0	42	0	no
	~ 1.0 ppm	16	12.0	16.5	885	454	98	50	no
	~ 5.0 ppm	13	13.0	17.5	900	892	100	99	no
Iodine	~ 100 ppb	14	13.0	17.5	549	0	61	0	no
	~ 150 ppb	14	12.0	17.0	291	0	32	0	yes
	~ 200 ppb	13	14.0	18.0	366	52	41	6	no
	~ 300 ppb	13	12.5	17.5	373	0	41	0	no
	~ 600 ppb	15	13.0	17.5	195	0	22	0	no
	~ 900 ppb	14	14.0	19.0	356	0	40	0	no
	~ 1.2 ppm	16	15.0	20.0	334	0	37	0	no
Potassium Permanganate	~ 200 ppb	15	12.0	18.0	413	0	46	0	no
	~ 600 ppb	15	12.0	16.5	767	342	85	38	no
	~ 800 ppb	15	14.0	18.5	900	900	100	100	no
Benzalkonium Chloride	~ 200 ppb	12	14.0	18.0	717	0	80	0	yes
	~ 400 ppb	15	13.0	17.0	210	0	23	0	yes
	~ 600 ppb	13	13.0	17.0	197	0	22	0	no
	~ 1.0 ppm	16	12.0	16.5	310	79	34	9	no
	~ 2.5 ppm	13	13.0	16.5	494	352	55	39	yes
	~ 5.0 ppm	12	11.0	15.5	669	177	74	20	no
Dodecyltrimethylammonium Bromide	~ 500 ppb	12	13.0	17.0	332	0	37	0	no
	~ 1.0 ppm	13	12.0	16.0	154	0	17	0	no
	~ 2.5 ppm	12	13.0	17.5	215	0	24	0	no
	~ 5.0 ppm	13	12.5	17.0	563	125	63	14	no
Didecyldimethylammonium Bromide	~ 500 ppb	13	12.0	16.0	338	0	38	0	no
	~ 1.0 ppm	16	11.0	15.0	781	0	87	0	no
	~ 1.5 ppm	12	11.0	15.0	648	10	72	1	no
	~ 2.5 ppm	13	12.0	17.0	864	21	96	2	no
	~ 5.0 ppm	14	13.0	17.0	862	646	96	72	no
Cupric Sulfate	~ 100 ppb	13	11.0	16.5	366	68	41	8	yes
	~ 200 ppb	16	14.0	18.5	491	339	55	38	no
	~ 300 ppb	14	13.0	17.5	229	62	25	7	yes
	~ 400 ppb	16	12.0	17.0	567	236	63	26	yes
	~ 600 ppb	14	13.0	17.0	900	897	100	100	no

Table 3: Control

Mussel No.	Mussel Size(mm)	Temperature (°C) Start	End	Time Foot Retracted (sec)	Time Valve Shut (sec)	% Time Foot Retracted	% Time Valve Shut	Initial Byssal Attachment
1	13	10 0	12 0	224	0	37	0	no
2	16	10 0	12 0	194	0	32	0	no
3	15	10 0	12 0	28	0	5	0	yes
4	15	10 0	12 0	296	0	49	0	no
5	16	11 0	13 5	320	0	53	0	no
6	13	9 5	11 5	170	0	28	0	no
7	13	10 5	12 5	148	0	25	0	no
8	17	9 5	11 0	128	0	21	0	no
9	12	9 5	11 0	99	0	17	0	yes
10	13	10 0	12 0	267	0	45	0	yes
Average	14	10 0	12 0	187	0	31 ± 15	0	

Table 4: Sodium Hypochlorite (~ 0.50 ppm)

Mussel No.	Mussel Size(mm)	Temperature (°C) Start	End	Time Foot Retracted (sec)	Time Valve Shut (sec)	% Time Foot Retracted	% Time Valve Shut	Initial Byssal Attachment
1	14	12 0	13 5	567	418	95	70	no
2	16	12 0	14.0	600	0	100	0	no
3	13	12 0	14 0	295	31	49	5	yes
4	17	12 0	14.0	75	0	13	0	no
5	15	12 0	14 0	392	284	65	47	no
6	13	12 0	14 5	600	200	100	33	no
7	16	12 0	13 5	350	255	58	43	no
8	14	11 5	13 0	548	243	91	41	no
9	15	12 0	14 0	546	253	91	42	no
10	14	12 0	13 5	525	238	88	40	no
Average	15	12 0	13 8	450	192	75 ± 28	32 ± 23	

Table 5: Sodium Hypochlorite (~ 0.75 ppm)

Mussel No.	Mussel Size(mm)	Temperature (°C) Start	End	Time Foot Retracted (sec)	Time Valve Shut (sec)	% Time Foot Retracted	% Time Valve Shut	Initial Byssal Attachment
1	16	12 0	13 5	587	332	98	55	no
2	15	10 5	12 5	564	92	94	15	no
3	16	12 5	14 0	520	200	87	33	no
4	15	12 5	14 0	521	480	87	80	no
5	16	12 0	14 0	435	225	73	38	no
6	15	12 0	14 0	96	18	16	3	yes
7	16	10 5	12 5	586	362	98	60	no
8	15	10 0	13.0	600	389	100	65	no
9	13	12 0	14 0	560	209	93	35	no
10	14	12 0	13 5	288	55	48	9	no
Average	15	11 6	13 5	476	236	79 ± 27	39 ± 26	

Table 6: Sodium Hypochlorite (~ 1.0 ppm)

Mussel No.	Mussel Size(mm)	Temperature (°C) Start	End	Time Foot Retracted (sec)	Time Valve Shut (sec)	% Time Foot Retracted	% Time Valve Shut	Initial Byssal Attachment
1	14	12 5	14 0	551	356	92	59	no
2	13	12 0	14 0	600	525	100	88	no
3	12	13 0	15 0	600	368	100	61	no
4	14	12 5	14 0	553	126	92	21	no
5	13	11 0	12 5	126	71	21	12	yes
6	13	11 0	13 0	600	600	100	100	no
7	15	12 0	13 5	600	539	100	90	no
8	12	11 5	13 0	145	74	24	12	yes
9	12	13 0	14 5	600	436	100	73	no
10	14	12 5	14 0	468	325	78	54	no
Average	13	12 1	13 8	484	342	81 ± 32	57 ± 33	

Table 7: Sodium Hypochlorite (~ 1.5 ppm)

Mussel No.	Mussel Size(mm)	Temperature (° C)		Time Foot Retracted (sec)	Time Valve Shut (sec)	% Time Foot Retracted	% Time Valve Shut	Initial Byssal Attachment
		Start	End					
1	17	12.0	14.0	600	600	100	100	no
2	15	12.0	14.0	600	505	100	84	no
3	13	12.0	14.0	600	600	100	100	no
4	16	12.0	14.0	600	519	100	87	no
5	13	12.0	14.0	600	600	100	100	no
6	16	11.0	13.0	600	600	100	100	no
7	15	11.0	13.0	600	600	100	100	no
8	15	12.5	15.0	600	600	100	100	no
9	14	12.0	14.0	600	284	100	47	no
10	12	13.0	14.5	600	586	100	98	no
Average	15	12.0	14.0	600	549	100 ± 0	92 ± 17	

Table 8: Cupric Sulfate (~ 0.50 ppm)

Mussel No.	Mussel Size(mm)	Temperature (° C)		Time Foot Retracted (sec)	Time Valve Shut (sec)	% Time Foot Retracted	% Time Valve Shut	Initial Byssal Attachment
		Start	End					
1	15	11.0	13.5	410	316	68	53	no
2	14	11.5	13.5	600	567	100	95	no
3	14	11.0	13.0	600	577	100	96	no
4	15	12.5	14.0	371	220	62	37	no
5	13	12.0	13.5	360	218	60	36	no
6	15	12.0	14.0	552	327	92	55	no
7	15	10.5	13.0	273	162	46	27	yes
8	15	10.5	12.5	600	417	100	70	no
9	17	10.5	13.0	427	107	71	18	no
10	16	12.5	14.0	221	181	37	30	yes
Average	15	11.4	13.4	441	309	74 ± 23	52 ± 28	

Table 9: Cupric Sulfate (~ 0.75 ppm)

Mussel No.	Mussel Size(mm)	Temperature (° C)		Time Foot Retracted (sec)	Time Valve Shut (sec)	% Time Foot Retracted	% Time Valve Shut	Initial Byssal Attachment
		Start	End					
1	17	11.5	13.5	420	294	70	49	no
2	14	11.0	12.5	600	600	100	100	no
3	14	12.5	14.0	578	316	96	53	no
4	15	12.0	14.0	600	249	100	42	no
5	17	12.0	13.5	210	190	35	32	no
6	16	12.0	13.5	385	325	64	54	no
7	15	12.0	13.5	394	309	66	52	no
8	12	12.0	14.0	510	368	85	61	no
9	15	13.0	14.5	410	370	68	62	yes
10	14	12.0	14.0	600	600	100	100	no
Average	15	12.0	13.7	471	362	78 ± 22	61 ± 23	

Table 10: Cupric Sulfate (~ 1.0 ppm)

Mussel No.	Mussel Size(mm)	Temperature (° C)		Time Foot Retracted (sec)	Time Valve Shut (sec)	% Time Foot Retracted	% Time Valve Shut	Initial Byssal Attachment
		Start	End					
1	16	12.0	13.5	600	600	100	100	no
2	13	12.0	14.0	573	540	96	90	no
3	16	12.0	14.0	519	432	87	72	no
4	15	12.0	13.5	600	481	100	80	no
5	12	10.5	12.0	394	291	66	49	no
6	17	11.0	12.5	600	600	100	100	no
7	15	11.5	13.0	574	463	96	77	no
8	14	12.0	13.5	518	350	86	58	no
9	17	12.0	14.0	600	600	100	100	no
10	15	12.0	14.0	412	210	69	35	no
Average	15	11.7	13.4	539	457	90 ± 13	76 ± 23	

Table 11: Cupric Sulfate (~ 1.5 ppm)

Mussel No.	Mussel Size(mm)	Temperature (°C) Start	End	Time Foot Retracted (sec)	Time Valve Shut (sec)	% Time Foot Retracted	% Time Valve Shut	Initial Byssal Attachment
1	13	12.5	14.5	600	600	100	100	no
2	16	11.0	13.0	600	600	100	100	no
3	15	10.5	13.0	600	577	100	96	no
4	15	11.5	13.5	600	510	100	85	no
5	16	11.5	13.0	571	499	95	83	no
6	17	11.0	13.5	600	600	100	100	no
7	16	11.5	13.5	600	600	100	100	no
8	14	10.5	13.0	600	600	100	100	no
9	15	11.0	13.0	339	234	57	39	no
10	16	11.0	13.5	402	383	67	64	no
Average	15	11.2	13.4	551	520	92 ± 16	87 ± 21	

Table 12: Potassium Permanganate (~ 0.50 ppm)

Mussel No.	Mussel Size(mm)	Temperature (°C) Start	End	Time Foot Retracted (sec)	Time Valve Shut (sec)	% Time Foot Retracted	% Time Valve Shut	Initial Byssal Attachment
1	16	11.0	13.0	476	0	79	0	no
2	15	11.5	13.5	505	310	84	52	no
3	15	11.5	13.0	565	228	94	38	no
4	16	11.0	13.0	517	231	86	39	no
5	12	11.5	13.5	307	120	51	20	no
6	15	10.0	12.0	487	284	81	47	no
7	17	10.0	12.0	600	336	100	56	no
8	13	11.5	13.0	537	231	90	39	no
9	15	11.0	13.0	600	305	100	51	no
10	13	11.0	12.5	340	37	57	6	no
Average	15	11.0	12.9	493	208	82 ± 17	35 ± 20	

Table 13: Potassium Permanganate (~ 0.75 ppm)

Mussel No.	Mussel Size(mm)	Temperature (°C) Start	End	Time Foot Retracted (sec)	Time Valve Shut (sec)	% Time Foot Retracted	% Time Valve Shut	Initial Byssal Attachment
1	16	10.5	12.0	452	370	75	62	no
2	15	10.0	12.0	286	40	48	7	no
3	15	10.0	12.0	478	267	80	45	no
4	15	11.0	12.5	452	147	75	25	no
5	17	10.5	12.0	524	384	87	64	no
6	16	11.0	13.0	522	310	87	52	no
7	17	10.5	12.5	487	249	81	42	no
8	16	10.5	12.5	580	370	97	62	no
9	13	11.0	12.5	540	493	90	82	no
10	17	11.0	12.5	15	0	3	0	no
Average	16	10.6	12.4	434	263	72 ± 28	44 ± 26	

Table 14: Potassium Permanganate (~ 1.0 ppm)

Mussel No.	Mussel Size(mm)	Temperature (°C) Start	End	Time Foot Retracted (sec)	Time Valve Shut (sec)	% Time Foot Retracted	% Time Valve Shut	Initial Byssal Attachment
1	15	10.5	12.5	600	597	100	100	no
2	15	11.0	13.0	577	521	96	87	no
3	17	11.0	13.0	564	475	94	79	no
4	14	10.0	12.5	565	395	94	66	no
5	14	10.0	12.0	552	474	92	79	no
6	13	10.5	12.5	521	305	87	51	no
7	15	10.5	12.5	589	330	98	55	no
8	17	11.0	13.0	512	340	85	57	no
9	13	12.0	13.5	473	317	79	53	no
10	14	10.5	13.0	556	285	93	48	no
Average	15	10.7	12.8	551	404	92 ± 6	68 ± 18	

Table 15: Potassium Permanganate (~ 1.5 ppm)

Mussel No.	Mussel Size(mm)	Temperature (° C)		Time Foot Retracted (sec)	Time Valve Shut (sec)	% Time Foot Retracted	% Time Valve Shut	Initial Byssal Attachment
		Start	End					
1	17	10.5	12.5	600	487	100	81	no
2	14	11.0	13.0	581	491	97	82	no
3	13	10.5	12.5	501	181	84	30	no
4	18	10.0	12.5	558	402	93	67	no
5	13	10.0	12.0	600	579	100	97	no
6	14	10.0	12.0	574	451	96	76	no
7	15	10.0	12.0	529	420	88	70	no
8	12	10.0	12.0	565	328	94	55	no
9	17	10.0	12.0	556	344	93	57	no
10	14	10.0	12.0	600	442	100	74	no
Average	15	10.2	12.3	566	413	95 ± 5	69 ± 18	

Table 16: Didecyldimethylammonium Bromide (~ 2.5 ppm)

Mussel No.	Mussel Size(mm)	Temperature (° C)		Time Foot Retracted (sec)	Time Valve Shut (sec)	% Time Foot Retracted	% Time Valve Shut	Initial Byssal Attachment
		Start	End					
1	17	10.0	11.5	392	0	65	0	no
2	13	10.0	12.0	554	219	92	37	no
3	12	10.0	12.0	297	47	50	8	no
4	15	9.5	11.5	342	12	57	2	no
5	17	11.0	13.0	502	95	84	16	no
6	11	10.0	12.0	87	0	15	0	yes
7	12	9.5	12.0	464	93	77	16	no
8	14	10.0	12.0	472	0	79	0	no
9	14	10.0	11.5	392	88	65	15	yes
10	13	9.5	11.0	381	78	64	13	no
Average	14	10.0	11.9	388	63	65 ± 22	11 ± 12	

Table 17: Didecyldimethylammonium Bromide (~ 5.0 ppm)

Mussel No.	Mussel Size(mm)	Temperature (° C)		Time Foot Retracted (sec)	Time Valve Shut (sec)	% Time Foot Retracted	% Time Valve Shut	Initial Byssal Attachment
		Start	End					
1	14	10.0	12.0	579	436	97	73	no
2	13	9.5	11.5	561	133	94	22	no
3	13	9.5	11.5	522	248	87	41	no
4	12	10.0	12.0	263	103	44	17	no
5	13	9.5	11.5	447	199	75	33	no
6	14	10.0	12.0	181	0	30	0	no
7	12	10.0	12.0	496	146	83	24	no
8	13	10.0	12.0	459	124	77	21	no
9	12	10.0	11.5	498	177	83	17	no
10	13	11.0	13.0	600	136	100	23	no
Average	13	10.0	11.9	461	170	77 ± 23	27 ± 19	

Table 18: Didecyldimethylammonium Bromide (~ 7.5 ppm)

Mussel No.	Mussel Size(mm)	Temperature (° C)		Time Foot Retracted (sec)	Time Valve Shut (sec)	% Time Foot Retracted	% Time Valve Shut	Initial Byssal Attachment
		Start	End					
1	14	10.0	12.0	331	115	55	19	yes
2	14	9.5	11.0	495	273	83	46	no
3	15	10.0	12.0	520	439	87	73	no
4	15	9.0	11.0	566	256	94	43	no
5	14	9.0	11.0	435	310	73	28	no
6	11	9.5	11.5	410	266	68	44	no
7	13	10.0	12.0	553	283	92	47	no
8	17	10.0	12.0	538	259	90	43	no
9	13	10.0	12.5	571	510	95	85	no
10	15	10.5	13.0	600	393	100	66	no
Average	14	9.8	11.8	502	310	84 ± 14	49 ± 20	

Table 19: Didecyldimethylammonium Bromide (~ 10 ppm)

Mussel No.	Mussel Size(mm)	Temperature (°C)		Time Foot Retracted (sec)	Time Valve Shut (sec)	% Time Foot Retracted	% Time Valve Shut	Initial Byssal Attachment
		Start	End					
1	15	10.0	12.0	571	280	95	47	no
2	12	10.5	12.0	558	472	93	79	no
3	14	9.0	11.0	600	425	100	71	no
4	12	10.5	12.5	572	361	95	60	no
5	16	10.0	12.0	600	534	100	89	no
6	13	10.0	12.0	519	495	87	83	no
7	14	9.5	12.0	600	600	100	100	no
8	18	9.5	11.0	519	294	87	49	no
9	13	10.0	11.5	596	452	99	75	no
10	16	10.0	12.0	588	456	98	76	no
Average	14	9.9	11.8	572	437	95 ± 5	73 ± 17	

Table 20: Hydrogen Peroxide (~ 5.0 ppm)

Mussel No.	Mussel Size(mm)	Temperature (°C)		Time Foot Retracted (sec)	Time Valve Shut (sec)	% Time Foot Retracted	% Time Valve Shut	Initial Byssal Attachment
		Start	End					
1	14	9.5	11.5	522	426	87	71	no
2	13	9.5	11.0	538	391	90	65	no
3	16	10.0	12.0	579	0	97	0	no
4	16	10.0	12.0	462	405	77	68	no
5	15	9.0	11.0	383	263	64	44	yes
6	16	9.0	11.0	507	382	85	64	no
7	14	9.0	11.0	561	422	94	70	no
8	13	10.0	12.0	472	429	79	72	no
9	15	9.5	11.5	543	452	91	75	no
10	16	9.5	11.5	559	450	93	75	no
Average	15	9.5	11.5	513	362	86 ± 10	60 ± 23	

Table 21: Hydrogen Peroxide (~ 7.5 ppm)

Mussel No.	Mussel Size(mm)	Temperature (°C)		Time Foot Retracted (sec)	Time Valve Shut (sec)	% Time Foot Retracted	% Time Valve Shut	Initial Byssal Attachment
		Start	End					
1	14	10.0	12.0	571	515	95	86	no
2	13	9.0	11.0	567	542	95	90	no
3	14	10.0	12.5	600	450	100	75	no
4	14	10.0	12.0	557	488	93	81	no
5	15	9.5	11.5	567	498	95	83	no
6	15	9.0	11.0	365	330	61	55	yes
7	12	10.0	12.5	574	544	96	91	no
8	15	10.0	12.0	563	487	94	81	no
9	13	9.0	11.5	316	246	53	41	yes
10	15	9.0	11.5	559	483	93	81	no
Average	14	9.6	11.8	524	458	88 ± 16	76 ± 16	

Table 22: Hydrogen Peroxide (~ 10 ppm)

Mussel No.	Mussel Size(mm)	Temperature (°C)		Time Foot Retracted (sec)	Time Valve Shut (sec)	% Time Foot Retracted	% Time Valve Shut	Initial Byssal Attachment
		Start	End					
1	18	10.0	12.0	457	337	76	56	no
2	15	10.0	12.0	585	417	98	70	no
3	16	10.0	12.0	350	312	58	52	no
4	14	10.0	12.0	595	567	99	95	no
5	16	9.5	12.0	544	425	91	71	no
6	14	10.0	12.0	420	371	70	62	yes
7	16	11.0	13.0	599	407	100	68	no
8	14	11.0	13.0	574	558	96	93	no
9	16	11.0	13.0	588	524	98	87	no
10	12	10.0	12.0	569	472	95	79	no
Average	15	10.3	12.3	528	439	88 ± 15	73 ± 15	

Table 23: Hydrogen Peroxide (~ 15 ppm)

Mussel No.	Mussel Size(mm)	Temperature (° C)		Time Foot Retracted (sec)	Time Valve Shut (sec)	% Time Foot Retracted	% Time Valve Shut	Initial Byssal Attachment
		Start	End					
1	17	10.0	12.0	584	560	97	93	no
2	16	10.0	12.0	538	490	90	82	no
3	16	10.0	12.0	545	467	91	78	no
4	13	9.5	12.0	529	501	88	84	no
5	17	10.0	12.5	570	438	95	73	no
6	16	10.0	12.5	362	320	60	53	no
7	13	11.0	13.0	594	551	99	92	no
8	14	10.0	12.0	538	488	90	81	no
9	14	11.5	13.5	582	519	97	87	no
10	17	11.0	13.0	571	513	95	86	no
Average	15	10.3	12.5	541	485	90 ± 11	81 ± 12	

Table 24: Sodium Hypochlorite + Cupric Sulfate (~ 0.25 ppm each)

Mussel No.	Mussel Size(mm)	Temperature (° C)		Time Foot Retracted (sec)	Time Valve Shut (sec)	% Time Foot Retracted	% Time Valve Shut	Initial Byssal Attachment
		Start	End					
1	17	10.0	12.0	246	61	41	10	no
2	13	9.5	11.5	600	571	100	95	no
3	13	10.0	12.5	600	490	100	82	no
4	16	11.0	13.5	600	579	100	97	no
5	16	10.0	12.0	241	169	40	28	yes
6	14	10.0	12.0	600	600	100	100	no
7	15	10.5	12.5	600	600	100	100	no
8	13	11.0	13.5	528	357	88	60	no
9	17	10.0	12.0	556	349	93	58	no
10	18	10.0	11.5	600	575	100	96	no
Average	15	10.2	12.3	517	435	86 ± 24	73 ± 33	

Table 25: Sodium Hypochlorite (~ 0.50 ppm) + Cupric Sulfate (~ 0.25 ppm)

Mussel No.	Mussel Size(mm)	Temperature (° C)		Time Foot Retracted (sec)	Time Valve Shut (sec)	% Time Foot Retracted	% Time Valve Shut	Initial Byssal Attachment
		Start	End					
1	15	9.0	11.5	600	107	100	18	no
2	17	9.5	11.5	600	599	100	100	no
3	15	11.0	13.0	520	262	87	44	no
4	16	11.0	13.0	538	226	90	38	no
5	17	10.0	12.0	502	131	84	22	no
6	12	10.0	12.0	588	521	98	87	no
7	14	11.0	13.5	600	331	100	55	no
8	14	10.5	13.0	571	378	95	63	no
9	15	11.0	13.0	600	600	100	100	no
10	14	10.0	12.0	591	544	99	91	no
Average	15	10.3	12.5	571	370	95 ± 6	62 ± 31	

Table 26: Sodium Hypochlorite + Cupric Sulfate (~ 0.50 ppm each)

Mussel No.	Mussel Size(mm)	Temperature (° C)		Time Foot Retracted (sec)	Time Valve Shut (sec)	% Time Foot Retracted	% Time Valve Shut	Initial Byssal Attachment
		Start	End					
1	13	10.0	12.5	600	598	100	100	no
2	17	10.0	12.0	340	218	57	36	no
3	15	10.5	13.0	580	362	97	60	no
4	17	11.0	13.0	287	177	48	30	no
5	15	10.0	12.5	600	600	100	100	no
6	16	9.5	11.5	600	600	100	100	no
7	13	10.0	12.0	600	600	100	100	no
8	15	11.0	13.0	600	565	100	94	no
9	15	10.0	12.0	284	94	47	16	no
10	16	9.5	11.5	600	600	100	100	no
Average	15	10.2	12.3	509	441	85 ± 24	74 ± 35	

Table 27: Sodium Hypochlorite + Cupric Sulfate (~ 0.75 ppm each)

Mussel No.	Mussel Size(mm)	Temperature (° C) Start	End	Time Foot Retracted (sec)	Time Valve Shut (sec)	% Time Foot Retracted	% Time Valve Shut	Initial Byssal Attachment
1	13	11.0	13.0	600	600	100	100	no
2	16	10.5	13.0	600	600	100	100	no
3	15	10.0	12.0	600	600	100	100	no
4	16	10.0	11.5	600	505	100	84	no
5	14	10.0	12.0	600	547	100	91	no
6	14	9.5	12.0	600	533	100	89	no
7	17	10.0	12.0	587	546	98	91	no
8	14	9.5	11.5	600	550	100	92	no
9	13	10.0	11.5	600	497	100	83	no
10	16	9.5	11.5	600	499	100	83	no
Average	15	10.0	12.0	599	548	100 ± 1	91 ± 7	

Table 28: Iodine (~ 1.5 ppm)

Mussel No.	Mussel Size(mm)	Temperature (° C) Start	End	Time Foot Retracted (sec)	Time Valve Shut (sec)	% Time Foot Retracted	% Time Valve Shut	Initial Byssal Attachment
1	16	10.0	11.5	266	87	44	15	no
2	13	10.0	11.5	488	60	81	10	no
3	13	10.0	12.0	600	0	100	0	no
4	15	10.0	12.0	518	262	86	44	no
5	15	10.0	12.0	363	108	61	18	no
6	13	10.0	12.0	586	0	98	0	no
7	15	10.0	12.0	553	73	92	12	no
8	13	11.0	13.0	442	234	74	39	no
9	14	10.0	12.0	384	266	64	44	no
10	14	10.0	11.5	441	81	74	14	no
Average	14	10.1	12.0	464	117	77 ± 18	20 ± 17	

Table 29: Iodine (~ 3.0 ppm)

Mussel No.	Mussel Size(mm)	Temperature (° C) Start	End	Time Foot Retracted (sec)	Time Valve Shut (sec)	% Time Foot Retracted	% Time Valve Shut	Initial Byssal Attachment
1	13	10.5	13.0	600	430	100	72	no
2	16	10.0	12.0	367	134	61	22	no
3	14	10.5	12.5	598	532	100	87	no
4	16	11.0	13.5	326	67	54	11	no
5	16	10.5	12.0	266	96	44	16	no
6	15	10.0	12.0	600	485	100	81	no
7	14	10.5	12.5	600	78	100	13	no
8	16	11.5	13.5	600	77	100	13	no
9	15	9.0	11.0	353	0	59	0	yes
10	17	10.0	12.0	511	448	85	75	no
Average	15	10.4	12.4	482	235	80 ± 23	39 ± 35	

Table 30: Iodine (~ 4.5 ppm)

Mussel No.	Mussel Size(mm)	Temperature (° C) Start	End	Time Foot Retracted (sec)	Time Valve Shut (sec)	% Time Foot Retracted	% Time Valve Shut	Initial Byssal Attachment
1	12	10.0	11.5	594	288	99	48	no
2	17	11.0	12.5	600	544	100	91	no
3	14	10.0	12.0	587	464	98	77	no
4	13	9.5	11.0	600	291	100	49	no
5	16	10.0	11.5	600	543	100	91	no
6	12	10.0	11.5	560	320	93	53	no
7	13	10.5	12.0	583	397	97	66	no
8	15	10.0	12.0	407	199	68	33	no
9	15	11.0	13.0	536	360	89	60	no
10	12	10.0	12.0	598	546	100	91	no
Average	14	10.2	11.9	567	395	94 ± 10	66 ± 21	

Table 31: Iodine (~ 6.0 ppm)

Mussel No.	Mussel Size(mm)	Temperature (°C) Start	End	Time Foot Retracted (sec)	Time Valve Shut (sec)	% Time Foot Retracted	% Time Valve Shut	Initial Byssal Attachment
1	17	10 0	12 0	600	373	100	62	no
2	14	9 5	11 5	361	156	60	26	no
3	12	10 0	12 0	558	321	93	54	no
4	14	11 0	13 0	600	517	100	86	no
5	12	10 5	12 0	600	597	100	100	no
6	16	9 5	11 0	509	241	85	40	no
7	13	9 5	11 0	600	494	100	82	no
8	14	11 0	13 5	600	593	100	99	no
9	15	10 0	12 0	600	587	100	98	no
10	13	9 5	11 5	600	459	100	77	no
Average	14	10 1	12 0	563	434	94 ± 13	72 ± 26	

Table 32: Summary of Chemical Treatments at Effective Concentrations

Chemical Treatment & (Table Nos)	Conc (ppm)	Av. Mussel Size(mm)	Av Temp (°C) Start	End	Av. Time Foot Retracted (sec)	Av. Time Valve Shut (sec)	Av. % Time Foot Retracted	Av. % Time Valve Shut
Control (3)		14	10 0	12 0	187	0	31 ± 15	0
Sodium Hypochlorite (4 - 7)	~ 0 50	15	12 0	13 8	450	192	75 ± 28	32 ± 23
	~ 0 75	15	11 6	13 5	476	236	79 ± 27	39 ± 26
	~ 1 0	13	12 1	13 8	484	342	81 ± 32	57 ± 33
	~ 1 5	15	12	14	600	549	100 ± 0	92 ± 17
Cupric Sulfate (8 - 11)	~ 0 50	15	11 4	13 4	441	309	74 ± 23	52 ± 28
	~ 0 75	15	12 0	13 7	471	362	78 ± 22	61 ± 23
	~ 1 0	15	11 7	13 4	539	457	90 ± 13	76 ± 23
	~ 1 5	15	11 2	13 4	551	520	92 ± 16	87 ± 21
Potassium Permanganate (12 - 15)	~ 0 50	15	11 0	12 9	493	208	82 ± 17	35 ± 20
	~ 0 75	16	10 6	12 4	434	263	72 ± 28	44 ± 26
	~ 1 0	15	10 7	12 8	551	404	92 ± 6	68 ± 18
	~ 1 5	15	10 2	12 3	566	413	95 ± 5	69 ± 18
Didecyldimethylammonium Bromide (16 - 19)	~ 2 5	14	10 0	11 9	388	63	65 ± 22	11 ± 12
	~ 5 0	13	10 0	11 9	461	170	77 ± 23	27 ± 19
	~ 7 5	14	9 8	11 8	502	310	84 ± 14	49 ± 20
	~ 10	14	9 9	11 8	572	437	95 ± 5	73 ± 17
Hydrogen Peroxide (20 - 23)	~ 5 0	15	9 5	11 5	513	362	86 ± 10	60 ± 23
	~ 7 5	14	9 6	11 8	524	458	88 ± 16	76 ± 16
	~ 10	15	10 3	12 3	528	439	88 ± 15	73 ± 15
	~ 15	15	10 3	12 5	541	485	90 ± 11	81 ± 12
Sodium Hypochlorite + Cupric Sulfate (24 - 27)	~ 0 25 each	15	10 2	12 3	517	435	86 ± 24	73 ±33
	~ 0 50 + ~ 0 25	15	10 3	12 5	571	370	95 ± 6	62 ± 31
	~ 0 50 each	15	10 2	12 3	509	441	85 ± 24	74 ± 35
	~ 0 75 each	15	10 0	12 0	599	548	100 ± 1	91 ± 7
Iodine (28 - 31)	~ 1 5	14	10 1	12 0	464	117	77 ± 18	20 ± 17
	~ 3 0	15	10 4	12 4	482	235	80 ± 23	39 ± 35
	~ 4 5	14	10 2	11 9	567	395	94 ± 10	66 ± 21
	~ 6 0	14	10 1	12 0	563	434	94 ± 13	72 ± 26

Table 33: Control

Mussel No.	Mussel Size(mm)	Temperature (° C) Start	End	Time Foot Retracted (sec)	Time Valve Shut (sec)	% Time Foot Retracted	% Time Valve Shut	Initial Byssal Attachment
1	15	9.0	10.5	471	176	52	20	no
2	14	9.5	10.5	900	41	100	5	no
3	16	9.5	10.5	467	26	52	3	yes
4	12	9.0	10.0	506	9	56	1	no
5	13	9.0	10.5	151	41	17	5	no
6	15	9.5	10.5	467	25	52	3	no
7	15	9.5	10.0	206	10	23	1	no
8	12	9.5	10.5	311	26	35	3	no
9	16	9.0	10.0	358	37	40	4	yes
10	13	9.0	10.0	421	69	47	8	yes
Average	14	9.3	10.3	426	46	47 ± 23	5 ± 6	

Table 34: Hypochlorite Treatment (End Tap)

Mussel No.	Mussel Size(mm)	Temperature (° C) Start	End	Time Foot Retracted (sec)	Time Valve Shut (sec)	% Time Foot Retracted	% Time Valve Shut	Initial Byssal Attachment
1	14	15.5	16.0	900	874	100	97	no
2	16	15.5	16.0	900	881	100	98	no
3	15	15.0	15.5	900	900	100	100	no
4	17	16.5	17.0	900	900	100	100	no
5	14	16.5	17.0	900	896	100	100	no
6	15	16.5	17.0	900	900	100	100	no
7	16	17.0	17.5	900	900	100	100	no
8	14	16.5	17.5	900	900	100	100	no
9	15	17.0	17.5	900	889	100	99	no
10	13	16.5	17.0	900	870	100	97	no
Average	15	16.3	16.8	900	891	100 ± 0	99 ± 1	

Table 35: Iodine Treatment (End Tap)

Mussel No.	Mussel Size(mm)	Temperature (° C) Start	End	Time Foot Retracted (sec)	Time Valve Shut (sec)	% Time Foot Retracted	% Time Valve Shut	Initial Byssal Attachment
1	15	16.5	17.5	900	741	100	82	no
2	14	12.0	13.0	691	66	77	7	no
3	15	12.0	13.0	900	840	100	93	no
4	14	12.5	14.0	398	54	44	6	no
5	14	12.0	13.5	272	62	30	7	yes
6	17	12.0	13.0	592	17	66	2	no
7	13	14.5	15.0	477	265	53	29	yes
8	13	14.5	15.0	662	63	74	7	no
9	15	14.5	15.0	661	520	73	58	no
10	13	14.0	15.0	732	330	81	37	no
Average	14	13.5	14.4	629	296	70 ± 23	33 ± 34	

Table 36: Copper Treatment (End Tap)

Mussel No.	Mussel Size(mm)	Temperature (° C) Start	End	Time Foot Retracted (sec)	Time Valve Shut (sec)	% Time Foot Retracted	% Time Valve Shut	Initial Byssal Attachment
1	14	15.5	16.5	778	17	86	2	no
2	13	15.0	15.5	537	153	60	17	no
3	16	11.5	13.0	708	328	79	36	no
4	15	11.5	12.5	806	348	90	39	no
5	13	12.5	13.5	213	103	24	11	yes
6	14	12.0	13.0	395	58	44	6	no
7	12	12.0	13.0	613	260	68	29	no
8	14	11.0	12.5	358	64	40	7	yes
9	15	11.0	13.0	838	459	93	51	no
10	15	13.0	14.0	651	247	72	27	no
Average	14	12.5	13.7	590	204	66 ± 23	23 ± 16	

Table 37: Hypochlorite Treatment (Mid Tap)

Mussel No	Mussel Size(mm)	Temperature (°C) Start	End	Time Foot Retracted (sec)	Time Valve Shut (sec)	% Time Foot Retracted	% Time Valve Shut	Initial Byssal Attachment
1	14	10.0	11.0	900	900	100	100	no
2	15	10.0	11.0	900	900	100	100	no
3	11	10.0	11.0	900	900	100	100	no
4	13	10.0	10.5	900	900	100	100	no
5	12	9.5	10.5	900	900	100	100	no
6	13	9.5	10.5	900	900	100	100	no
7	11	9.5	10.5	900	900	100	100	no
8	16	9.5	11.0	900	883	100	98	no
9	12	10.0	11.0	900	900	100	100	no
10	14	10.0	11.0	900	900	100	100	no
Average	13	9.8	10.8	900	898	100 ± 0	100 ± 1	

Table 38: Iodine Treatment (Mid Tap)

Mussel No.	Mussel Size(mm)	Temperature (°C) Start	End	Time Foot Retracted (sec)	Time Valve Shut (sec)	% Time Foot Retracted	% Time Valve Shut	Initial Byssal Attachment
1	13	9.5	10.5	900	606	100	67	no
2	13	9.5	10.5	878	491	98	55	no
3	12	9.5	10.5	750	321	83	36	no
4	12	9.5	10.5	303	138	34	15	yes
5	11	9.0	10.5	239	58	27	6	yes
6	16	9.5	10.0	858	797	95	89	no
7	13	9.0	9.5	578	149	64	17	no
8	17	9.0	10.0	266	140	30	16	no
9	13	9.0	10.0	847	495	94	55	no
10	16	9.0	10.0	425	247	47	27	no
Average	14	9.3	10.2	604	344	67 ± 30	38 ± 27	

Table 39: Copper Treatment (Mid Tap)

Mussel No	Mussel Size(mm)	Temperature (°C) Start	End	Time Foot Retracted (sec)	Time Valve Shut (sec)	% Time Foot Retracted	% Time Valve Shut	Initial Byssal Attachment
1	15	9.5	10.5	525	285	58	32	no
2	15	9.5	10.5	131	11	15	1	yes
3	12	9.5	10.5	868	315	96	35	no
4	16	9.0	10.5	256	23	28	3	yes
5	15	9.5	10.5	900	103	100	11	no
6	15	9.5	10.5	667	271	74	30	no
7	13	9.0	10.0	547	288	61	32	no
8	17	9.0	10.0	451	24	50	3	no
9	15	9.5	10.5	758	285	84	32	no
10	13	9.5	10.5	683	207	76	23	no
Average	15	9.4	10.4	579	181	64 ± 28	20 ± 14	

Table 40: Summary of Seawater System Treatments

Chemical Treatment & (Table Nos)	Tap Position	Av. Mussel Size(mm)	Av. Temp (°C) Start	End	Av. Time Foot Retracted (sec)	Av. Time Valve Shut (sec)	Av % Time Foot Retracted	Av % Time Valve Shut
Control (33)		14	9.3	10.3	426	46	47 ± 23	5 ± 6
Hypochlorous Acid (34)	End	15	16.3	16.8	900	891	100 ± 0	99 ± 1
Iodine (35)	End	14	13.5	14.4	629	296	70 ± 23	33 ± 34
Copper (36)	End	14	12.5	13.7	590	204	66 ± 23	23 ± 16
Hypochlorous Acid (37)	Mid	13	9.8	10.8	900	898	100 ± 0	100 ± 1
Iodine (38)	Mid	14	9.3	10.2	604	344	67 ± 30	38 ± 27
Copper (39)	Mid	15	9.4	10.4	579	181	64 ± 28	20 ± 14

Table 41. Concentration of Free Chlorine at
Seawater Flow Rate of ~ 4 USGPM

Sample No.	Flow Rate (USGPM)	Equip. Settings		Temp. (°C)	Free Cl (mg/L)*
		(volts)	(amps)		
1	4.2	12.4	0.9	18.5	0.86
2	4.3	12.4	0.9	18.4	0.74
3	4.3	12.4	0.9	18.4	0.88
4	4.2	12.4	0.9	18.4	0.72
5	4.2	12.4	0.9	18.4	0.73
6	4.0	12.4	0.9	18.4	0.77
7	4.0	12.4	0.9	18.5	0.90
8	4.0	12.4	0.9	18.4	0.97
9	4.1	12.4	0.9	18.6	0.84
10	4.1	12.4	0.9	18.5	0.84
avg	4.1	12.4	0.9	18.5	0.83
std dev	0.12	0.00	0	0.07	0.083

* mg/L = ppm

Table 42. Concentration of Free Chlorine at
Seawater Flow Rate of ~ 6 USGPM

Sample No.	Flow Rate (USGPM)	Equip. Settings		Temp. (°C)	Free Cl (mg/L)*
		(volts)	(amps)		
1	6.1	12.3	0.9	17.9	0.95
2	6.1	12.4	0.9	17.6	0.80
3	6.4	12.4	0.9	17.6	0.78
4	6.1	12.4	0.9	17.4	0.63
5	6.2	12.4	0.9	18.0	0.89
6	6.2	12.3	0.9	18.3	0.67
7	6.2	12.3	0.9	18.4	0.59
8	6.2	12.3	0.9	18.5	0.61
9	6.2	12.3	0.9	18.5	0.57
10	6.1	12.3	0.9	18.4	0.62
avg	6.2	12.3	0.9	18.1	0.71
std dev	0.09	0.05	0	0.42	0.136

mg/L = ppm

Table 43. Concentration of Free Chlorine at
Seawater Flow Rate of ~ 7 USGPM

Sample No.	Flow Rate (USGPM)	Equip. Settings		Temp. (°C)	Free Cl (mg/L)*
		(volts)	(amps)		
1	7.0	12.0	0.9	18.4	0.81
2	7.0	11.9	0.9	18.4	0.59
3	7.0	11.9	0.9	18.5	0.77
4	7.1	11.9	0.9	18.4	0.65
5	7.1	11.9	0.9	18.6	0.56
6	7.1	11.9	0.9	18.6	1.02
7	7.0	11.7	0.9	18.6	0.37
8	7.0	11.8	0.9	18.6	0.48
9	7.1	11.9	0.9	18.5	0.4
10	7.1	12.0	0.9	18.7	0.67
avg	7.1	11.9	0.9	18.5	0.63
std dev	0.05	0.09	0	0.11	0.199

mg/L = ppm

Table 44. Concentration of Free Chlorine at
Seawater Flow Rate of ~ 10 USGPM

Sample No.	Flow Rate (USGPM)	Equip. Settings		Temp. (°C)	Free Cl (mg/L)*
		(volts)	(amps)		
1	10.1	11.9	0.9	17.2	0.69
2	10.0	12.1	0.9	17.0	0.75
3	9.9	12.1	0.9	17.0	0.84
4	9.9	12.3	0.9	17.0	0.88
5	10.0	12.2	0.9	17.2	0.97
6	10.1	12.3	0.9	17.1	0.91
7	10.4	12.1	0.9	17.1	0.70
8	9.7	12.2	0.9	17.3	0.86
9	10.0	12.3	0.9	17.3	0.69
10	10.3	12.4	0.9	17.4	0.60
avg	10.0	12.2	0.9	17.2	0.79
std dev	0.20	0.14	0	0.14	0.119

mg/L = ppm

Table 45. Concentration of Free Chlorine at
Seawater Flow Rate of ~ 15 USGPM

Sample No.	Flow Rate (USGPM)	Equip. Settings		Temp. (°C)	Free Cl (mg/L)*
		(volts)	(amps)		
1	15.0	12.1	0.9	17.0	0.62
2	15.0	12.1	0.9	16.9	0.43
3	15.1	12.1	0.9	16.8	0.47
4	14.8	12.1	0.9	16.8	0.46
5	15.1	12.1	0.9	16.8	0.70
6	15.0	12.1	0.9	16.7	0.61
7	15.0	12.1	0.9	16.7	0.62
8	14.9	12.1	0.9	16.8	0.54
9	14.9	12.1	0.9	16.7	0.65
10	15.2	12.1	0.9	16.8	0.46
avg	15.0	12.1	0.9	16.8	0.56
std dev	0.12	0.00	0	0.09	0.096

mg/L = ppm

Table 46. Concentration of Free Chlorine at
Seawater Flow Rate of ~ 20 USGPM

Sample No.	Flow Rate (USGPM)	Equip. Settings		Temp. (°C)	Free Cl (mg/L)*
		(volts)	(amps)		
1	20.0	12.1	0.9	17.0	0.52
2	20.4	12.0	0.9	16.9	0.45
3	19.9	12.0	0.9	16.9	0.32
4	20.1	12.0	0.9	16.9	0.48
5	20.2	11.4	0.9	16.8	0.53
6	20.3	11.7	0.9	16.9	0.49
7	20.1	11.8	0.9	16.9	0.61
8	20.0	11.9	0.9	16.9	0.62
9	19.8	12.0	0.9	16.6	0.47
10	19.7	12.0	0.9	16.8	0.53
avg	20.1	11.9	0.9	16.9	0.50
std dev	0.22	0.21	0	0.11	0.085

mg/L = ppm

Table 47. Concentration of Free Chlorine at Electric Current of 0.5 amps

Sample No	Flow Rate (USGPM)	Equip. Settings		Temp (° C)	Free Cl (mg/L)*
		(volts)	(amps)		
1	10.1	8.7	0.5	17.5	0.73
2	9.8	8.9	0.5	17.4	0.43
3	10.0	9.0	0.5	17.4	0.46
4	10.2	9.0	0.5	17.4	0.55
5	10.0	9.0	0.5	17.4	0.42
6	10.0	8.9	0.5	17.3	0.46
7	10.2	9.0	0.5	17.2	0.51
8	9.9	9.0	0.5	17.4	0.44
9	9.8	9.0	0.5	17.6	0.60
10	9.9	9.0	0.5	17.5	0.47
avg	10.0	9.0	0.5	17.4	0.51
std dev	0.14	0.10	0	0.11	0.097

mg/L = ppm

Table 48. Concentration of Free Chlorine at Electric Current of 1.0 amps

Sample No.	Flow Rate (USGPM)	Equip Settings		Temp. (° C)	Free Cl (mg/L)*
		(volts)	(amps)		
1	9.8	12.8	1.0	17.5	0.77
2	10.2	12.8	1.0	17.3	0.82
3	10.1	12.8	1.0	17.3	0.80
4	10.1	12.8	1.0	17.5	0.59
5	10.3	12.8	1.0	17.4	0.77
6	10.5	12.8	1.0	17.6	0.78
7	9.7	12.8	1.0	17.7	0.78
8	10.1	12.8	1.0	17.7	0.64
9	10.0	12.8	1.0	17.6	0.79
10	9.9	12.8	1.0	17.6	0.79
avg	10.1	12.8	1.0	17.5	0.75
std dev	0.24	0.00	0	0.15	0.075

* mg/L = ppm

Table 49. Concentration of Free Chlorine at Electric Current of 1.5 amps

Sample No	Flow Rate (USGPM)	Equip Settings		Temp (° C)	Free Cl (mg/L)*
		(volts)	(amps)		
1	9.8	14.9	1.5	17.7	0.78
2	10.3	14.9	1.5	17.5	0.79
3	10.5	14.9	1.5	17.4	0.66
4	9.9	14.9	1.5	17.3	1.01
5	10.1	14.9	1.5	17.4	1.15
6	9.8	14.9	1.5	17.3	1.19
7	9.9	14.9	1.5	17.3	0.93
8	10.3	14.9	1.5	17.4	0.94
9	9.9	14.9	1.5	17.5	1.04
10	10.2	14.9	1.5	17.4	1.01
avg	10.1	14.9	1.5	17.4	0.95
std dev	0.25	0.00	0	0.12	0.167

mg/L = ppm

Table 50. Concentration of Free Chlorine at Electric Current of 2.0 amps

Sample No	Flow Rate (USGPM)	Equip. Settings		Temp (° C)	Free Cl (mg/L)*
		(volts)	(amps)		
1	10.2	15.6	2.0	17.4	2.02
2	9.8	15.6	2.0	17.5	1.90
3	10.3	15.6	2.0	17.6	2.03
4	9.7	15.6	2.0	17.5	1.96
5	10.1	15.6	2.0	17.6	2.21
6	9.7	15.6	2.0	17.6	2.13
7	10.2	15.6	2.0	17.4	1.88
8	10.1	15.6	2.0	17.5	2.19
9	10.3	15.6	2.0	17.5	2.38
10	9.6	15.5	2.0	17.6	2.29
avg	10.0	15.6	2.0	17.5	2.10
std dev	0.27	0.03	0	0.08	0.168

mg/L = ppm

Table 51. Concentration of Free Chlorine at Electric Current of 2.5 amps

Sample No	Flow Rate (USGPM)	Equip. Settings		Temp. (° C)	Free Cl (mg/L)*
		(volts)	(amps)		
1	9.7	16.1	2.5	17.8	3.02
2	10.3	16.0	2.5	17.8	2.66
3	10.2	16.0	2.5	17.7	2.94
4	9.6	16.0	2.5	17.7	3.28
5	10.1	16.0	2.5	17.6	3.30
6	9.7	16.0	2.5	17.8	3.22
7	9.8	16.0	2.5	17.7	3.52
8	10.0	16.0	2.5	17.7	2.92
9	10.1	16.0	2.5	17.6	3.36
10	9.7	15.6	2.5	17.7	3.12
avg	9.9	16.0	2.5	17.7	3.13
std dev	0.25	0.13	0	0.07	0.253

mg/L = ppm

Table 52. Summary of Conc. of Free Chlorine for Flow Rate Tests

Table No.	Flow Rate (USGPM)	Equip. Settings		Temp. (o C)	Free Cl (mg/L)*
		(volts)	(amps)		
1	4.1	12.4	0.9	18.5	0.83
2	6.2	12.3	0.9	18.1	0.71
3	7.1	11.9	0.9	18.5	0.63
4	10.0	12.2	0.9	17.2	0.79
5	15.0	12.1	0.9	16.8	0.56
6	20.1	11.9	0.9	16.9	0.50

Table 53. Summary of Conc. of Free Chlorine for Electric Current Tests

Table No.	Flow Rate (USGPM)	Equip. Settings		Temp (o C)	Free Cl (mg/L)*
		(volts)	(amps)		
7	10.0	9.0	0.5	17.4	0.51
8	10.1	12.8	1.0	17.5	0.75
9	10.1	14.9	1.5	17.4	0.95
10	10.0	15.6	2.0	17.5	2.10
11	9.9	16.0	2.5	17.7	3.13

Table 54: Seawater Copper Concentrations for Concentration Study

Sample	Flow Rate (USGPM)	Seawater Copper Concentrations (ppm)				
		Experimental Values				Theoretical Values
		Aug. 21	Aug. 24	Aug. 29	Aug. 30	
Harbour Water			0.007			
Strainer Blank			0.005		0.008	
Pump Blank				0.004	0.001	
Control Blank (mid tap)	~ 7				0.012	
Control Blank (mid tap)	~ 15			0.21		
Control Blank (end tap)	~ 7				0.021	
Control Blank (end tap)	~ 12		0.15			
Control Blank (end tap)	~ 20	0.48				
0.12 (tap)	~ 5			0.14		0.13
0.12 A (tap)	~ 15		0.18			0.042
0.12 B (tap)	~ 15		0.092			0.042
0.12 (tap)	~ 17				0.033	0.037
0.12 (tap)	~ 20	0.57				0.032
0.12 (tap)	~ 25			0.093		0.025
0.12 (pot)	~ 5			0.13		0.13
0.12 (pot)	~ 17				0.012	0.037
0.12 (pot)	~ 25			0.042		0.025
0.48 A (tap)	~ 15		0.21			0.17
0.48 B (tap)	~ 15		0.22			0.17
0.48 (tap)	~ 20	0.23				0.13

Table 55: Cathelco Anode Weight Measurements.

	Date	Anode 1 (gram)	Anode 2 (gram)	Difference			Wastage/day	
				Anode 1	Anode 2	days	Anode 1	Anode 2
Test 1 new anode	Oct 99	1031	1031					
	6/16/00	990.4	972.8	40.6	58.2	175	0.232	0.333
Test 2 new anode	6/16/00	1031.4	1031					
	11/8/00	999.9	998.8	31.1	32.2	56	0.555	0.575
	8/23/00	974.2	986.3	25.7	12.5	12	2.142	1.042
	5/9/00	926.1	952.7	48.1	33.6	13	3.7	2.585
	9/14/00	894.8	923.3	31.3	29.4	9	3.478	3.267
	9/26/00	837.4	898.4	57.4	24.9	12	4.783	2.075
	3/10/00	797.2	865.7	40.2	32.7	7	5.743	4.671

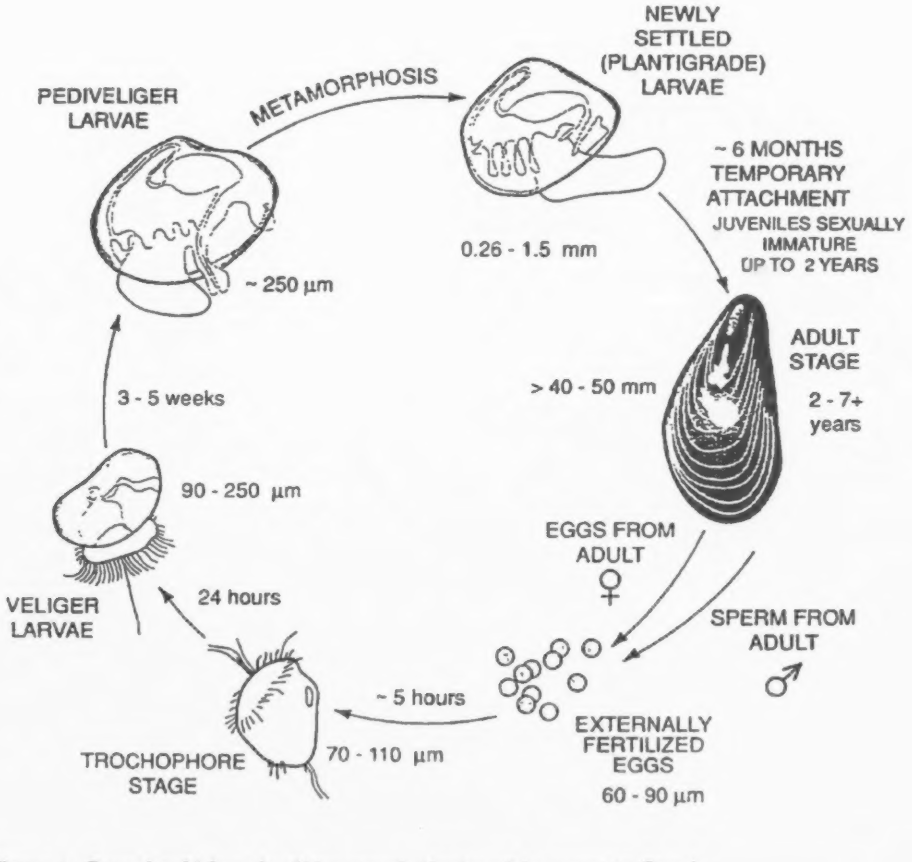
NEWLY SETTLED (PLANTIGRADE) LARVAE
PEDIVELIGER LARVAE
METAMORPHOSIS
~ 6 MONTHS TEMPORARY ATTACHMENT
JUVENILES SEXUALLY IMMATURE UP TO 2 YEARS
0.26 - 1.5 mm
~ 250 µm
ADULT STAGE
> 40 - 50 mm
2 - 7+ years
3 - 5 weeks
90 - 250 µm
EGGS FROM ADULT ♀
SPERM FROM ADULT ♂
VELIGER LARVAE
24 hours
~ 5 hours
EXTERNALLY FERTILIZED EGGS
60 - 90 µm
TROCHOPHORE STAGE
70 - 110 µm

Figure 1. Generalized life cycle of blue mussel, *Mytilus edulis*, in eastern Canada (Adapted from Stewart 1994)

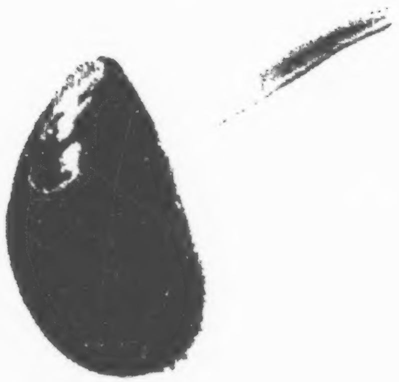

Figure 2. Blue mussel in 'active state', with foot fully extended.

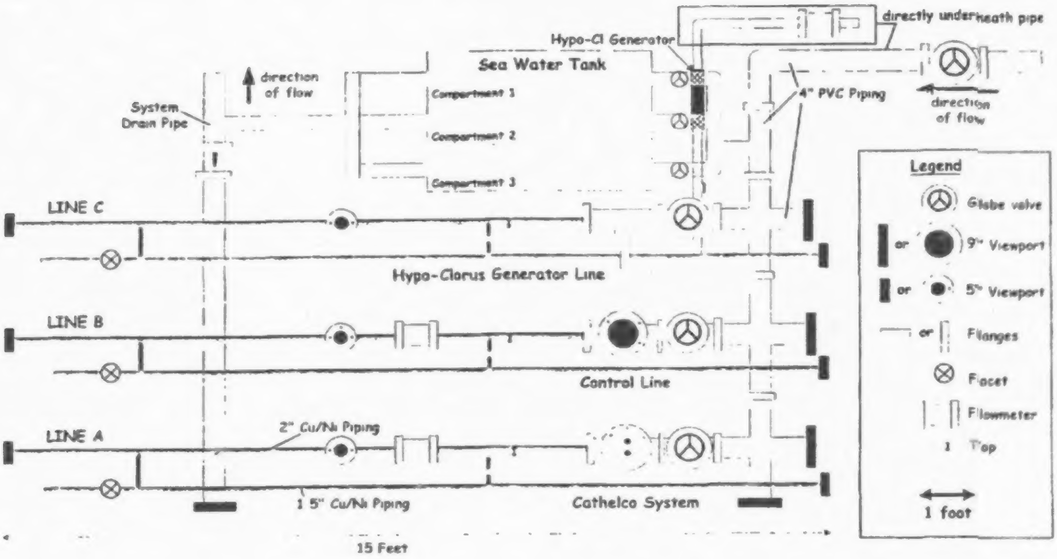
directly underneath pipe
Hypo-Cl Generator
Sea Water Tank
direction of flow
System Drain Pipe
Compartment 1
Compartment 2
Compartment 3
4" PVC Piping
direction of flow
LINE C
Hypo-Clorus Generator Line
LINE B
Control Line
LINE A
2" Cu/Ni Piping
1.5" Cu/Ni Piping
Cathelco System
15 Feet
Legend
Globe valve
or 9" Viewport
or 5" Viewport
or Flanges
Facet
Flowmeter
1 Tap
1 foot

Figure 3a. Top view DREA/DL Seawater System

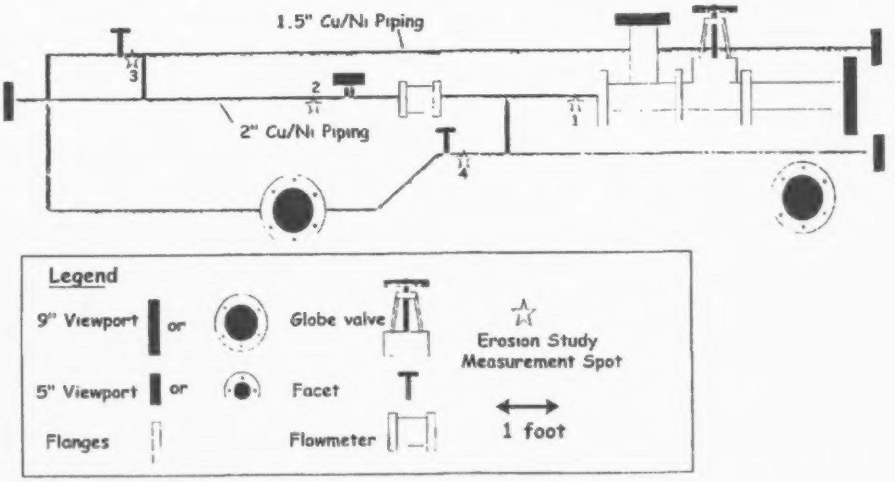
1.5" Cu/Ni Piping
3
2
1
2" Cu/Ni Piping
4
Legend
9" Viewport or
5" Viewport or
Flanges
Globe valve
Facet
Flowmeter
Erosion Study Measurement Spot
1 foot

Figure 3b Side view DREA/DL Seawater System

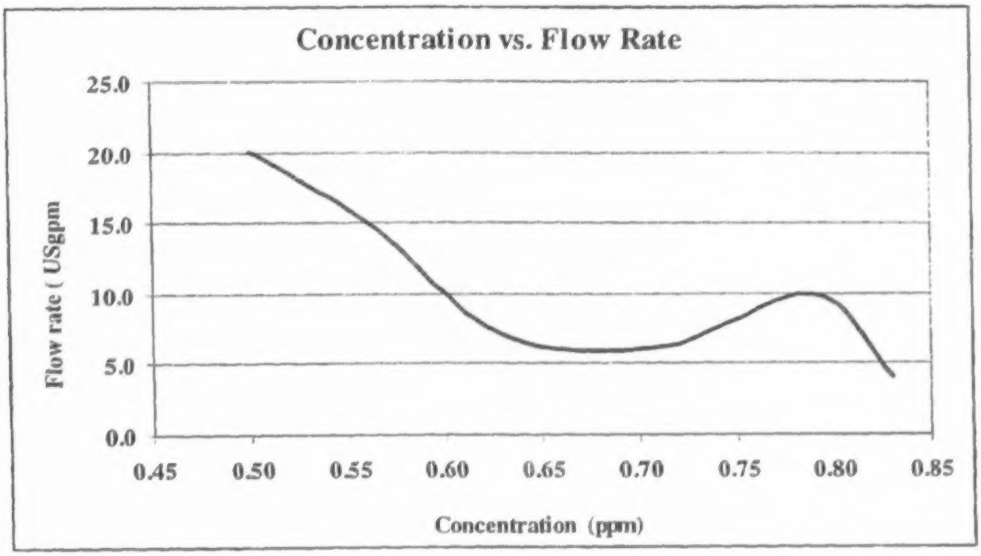

Figure 4. Concentration versus Flow Rate for the Hypochlorite Treatment.

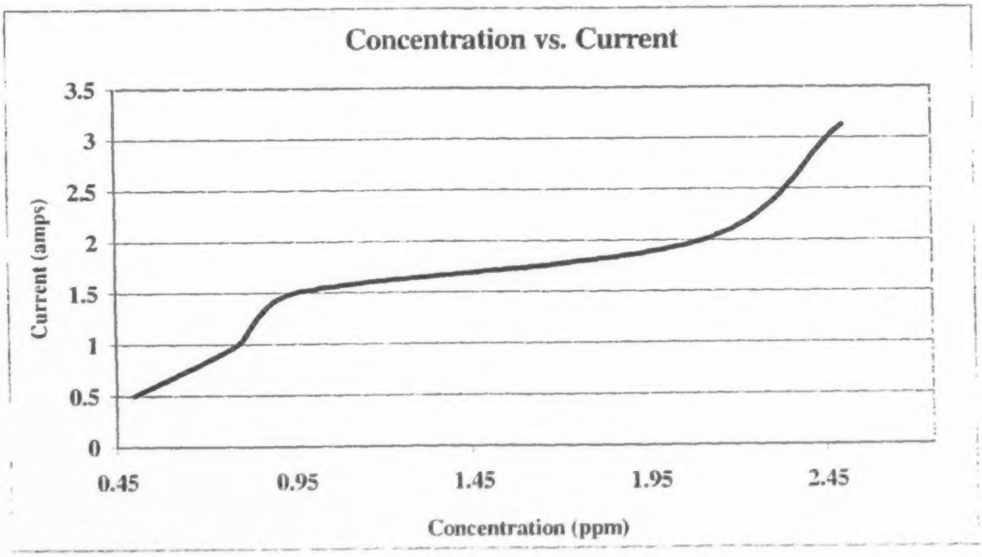

Figure 5. Concentration versus Electric Current for the Hypochlorite Treatment.

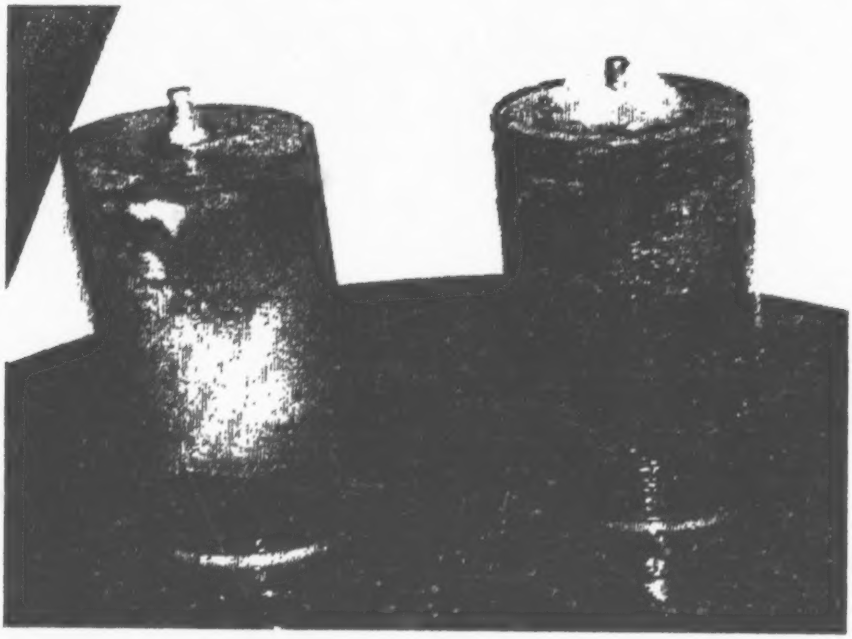

Figure 6a. Cathelco Anodes attached to assembly cover (June 26/00).

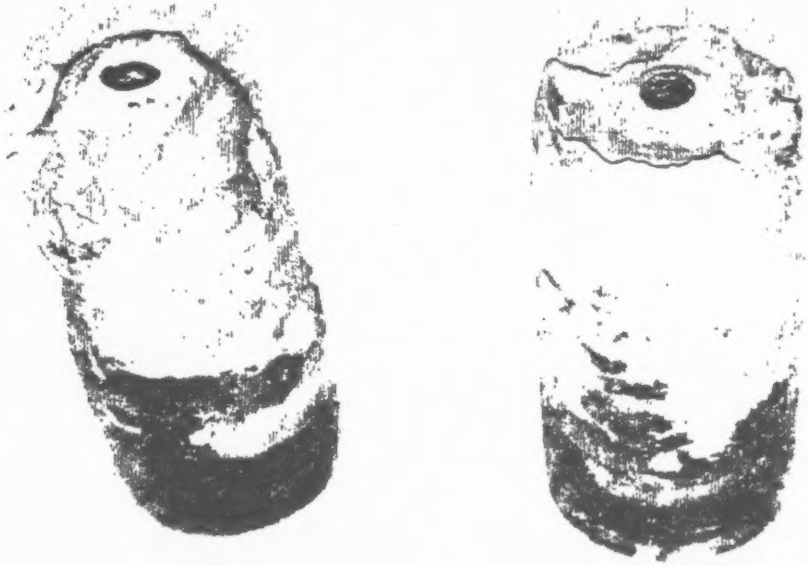

Figure 6b. Cathelco Anodes 1 and 2 (Oct. 3/00).

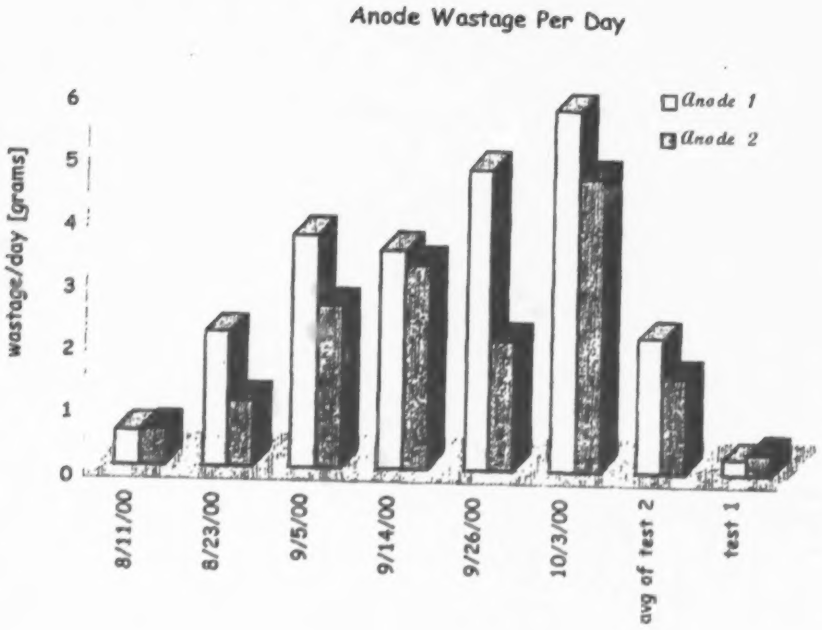

Figure 7. Cathelco Anode weight loss measurements.

#516437 (22)

The Manufacture of Submarine Valves from Wrought Steel using the Electron Beam Welding Process

Alan Aitchison, Principal Welding Engineer, BAE SYSTEMS Marine, United Kingdom and
Chris Punshon, Electron Beam Applications Section Manager, TWI, United Kingdom.

Abstract

MOD and BAE have been concerned for many years about the integrity and mechanical properties achievable in high strength steel castings used for submarine construction. This has resulted in extended delivery times due to the necessity to repair components prior to installation and less stringent fracture toughness requirements being specified for castings than for the wrought components of the submarine hull. Considerable development work has been carried out over a period spanning many years to assess the feasibility of using electron beam welding for the fabrication of high quality hull valves from wrought Q1N steel. The toughness properties of EB welds in this material have been examined using a range of test methods ranging from standard charpy V-notch and CTOD tests to bulge explosion test. Behaviour of welds in the as welded, stress relieved and fully heat treated conditions has been assessed and will be discussed briefly.

The main body of the paper will describe the production route for two sets of typical components that will be used in the current MOD submarine build programme. Topics covered will include the weld procedure approval work, EB welding of the components, machining, NDE and post weld heat treatment of the completed valves. On completion of the fabricated valve body, the internal sections are clad with Monel by the Hot Wire TIG process prior to fitting of the internal mechanical gear. Details of this operation will be also discussed.

INTRODUCTION

BAE SYSTEMS has been assessing the use of electron beam welding for the fabrication of marine valves for many years in conjunction with MOD (UK) and TWI. [1,2,3,4]. The latter are a company that specialises in contract R&D in welding and joining technology and also offers a unique sub contract EB welding capability in the UK to its Industrial member companies. The facility offers a range of both high vacuum and reduced pressure, large capacity EB welding chambers that use the TWI designed high power 100kW-RF electron beam gun.

Traditionally, the manufacturing method for steel valves and hull penetrations has been sand castings and experience has shown repeatedly that it is difficult to meet the exacting Naval requirements using this method. Most of the valves are of Category 1 status which, by definition, means that malfunction may lead to loss of life or the submarine. Historically some of the cast valves produced have extensive weld repairs and on account of the large wall thickness of the castings it is probable that large defects may still be present despite having been subject to X-Ray inspection. In consequence, considerable delays have been experienced between ordering and receiving a fully fitted out valve ready for installation into the submarine. Furthermore it has been found to be difficult to attain similar reliable mechanical property values, especially with respect to charpy impact values at -84°C as required in plate and forgings . Notably, after checking that both static and dynamic CTOD values were acceptable in castings at the -5°C test temperature MOD decided to reduce the impact property specification requirements to 100 Joules at -20°C. **Table 1** compares the Naval Specification (NES 736) requirements for chemical compositions and mechanical properties for Wrought Plates, Forgings and Castings.[5].

Extensive work has been carried out on Q1N steel, the principal hull plating and cast material for both nuclear and diesel electric submarines built to British Naval Specification requirements. These trials have determined that, at present, EB welds need to be fully quench and tempered after welding to achieve consistent charpy impact toughness values equivalent to the parent plate.[6,7,8,9] In addition, work at DERA has shown that satisfactory corrosion fatigue properties have been attained. [10,11] **Figure 1** shows a very large EB welded component that simulated a hull valve for a nuclear submarine that was checked by NDE and Time of Flight UT and was considered acceptable to the existing MOD requirements for nuclear submarine components.

In conjunction with this work all the relevant parties were actioned to produce a Specification to support the electron beam welding of Q1N steel production components to be used on the Astute submarine build. (Basic details of Astute Submarine in **Table 2**) This resulted in BAE Systems Specification 855 [12] that has been approved by the Design Authority and was intended to be used as the basic document for EB welding components for use on the Astute class submarine.)

BAE Technical Department redesigned a limited number of marine valves to be made from wrought plate based on original Castings drawings with active participation by TWI to ensure there would be minimal problems in producing the components. This paper discusses the extensive testing carried out before the official weld procedures were produced together with the product route to fabricate the said valves.

Electron Beam Welding Chambers and Guns

Throughout the programme the majority of the welding work was carried out using TWI's large chamber ($150m^3$) EB welding facility. This machine, shown in Fig. 2 was, at that time fitted with TWI's 100 kW RF excited diode type electron gun which has been designed

specifically for long duration, high power welding operations on high value components where consistency and reliability of performance are essential.
The working volume of the chamber measures ~8metres in length x 3.6metres x 3.6metres and the NC controlled work-piece manipulator has a static capacity of 20 tonnes, thus large components can be accommodated.

The pumping time for this large chamber, however, is of the order of 1 hour and therefore to explore methods for improving productivity, the possibility of using the latest Reduced Pressure EB welding technology was tested. With this method the work chamber is pumped to a coarse vacuum pressure of ~1mbar in contrast to 0.001mbar in the high vacuum equipment and significant time- savings are possible. In addition, for particularly large components, local sealing can be used. TWI's latest 100kW Reduced Pressure EB welding facility is shown in Fig. 3.This equipment can also be operated at high vacuum.

Electron Beam Welding – Welding position

There are several preferred welding positions for EB welding that can be briefly described as:-

Circular welds in a planetary configuration in which the incident electron beam is parallel to the axis of rotation. **Figure 4 a**
Circular welds in a circumferential butt configuration in which the incident electron beam is perpendicular to the axis of rotation. **Figure 4 b**
Linear welds. **Figure 4 c**
Partially penetrating welds in which the joint face is fully fused but the electron beam does not penetrate the entire material thickness. **Figure 4d**

The preferred position for welding Q1N steel valve type components has been where the beam is always perpendicular to the axis of the component since this allows control over the molten weld metal. The fusion zone width of the actual weld has been selected to ensure that the risk of missed joint defects is reduced especially since Q1N steel is prone to magnetic beam deflection problems if degaussing precautions are not undertaken prior to welding.

Assessment of Mechanical Properties in EB welds made in QIN Steel

Whilst considerable amount of technical data has been amassed there are several high points that are worth underling to underline the potential of the process.
The basic principle of approving electron beam welded NQ1 steel panels has been agreed in the early 1990's but several events caused further work that assessed the welds to BSEN standards and also new bulge explosion test types at DERA Scotland.

Effects of PWHT on Mechanical Properties of EB Q1N Steel Weldments

This particular aspect of development work concerned the repair of a thick section of Q1N steel forging on the Vanguard Class submarine. A series of test welds were made in 130mm thick Q1N steel to produce sufficient material to examine the effects of as welded and post weld heat treated weldments. [13]

The results in effect summed up the whole spectrum of EB welds in Q1N steel with respect to weld conditions –AW; SR and Q&T.

Values from the as welded EB welds produced high hardnesses in the FL and WM, around 420 –450HV, whilst acceptable cross tensiles of 720 –725 N/mm^2 were achieved. The charpy specimens were tested at -50°C and lay between 51 –76 Joules, above the minimum required by NES 770 –Weld Acceptance Criteria [14] Successful side bend tests were obtained over a 4T diameter former and 180° angle.

A further section of the 150mm EB weld was stress relieved at 610°C for six hours and water quenched and this affected the tensile strength by reducing the values to 700N/mm2 but the side bend tests were similar to the as welded test results. The charpy values were considerably reduced to between 27 and 62 Joules, evidence of the temper embrittlement effect that can occur with this material when using single run welds in thick plate.

However the excellent results from the Q&T post weld heat treatment tests were as expected with as parent plate hardness values through the fusion line (FL) and weld metal (WM) being around 227 HV. No defects were found in the 4 side bend tests and the through thickness charpy tests at -50°C realised values between 202 to 261 Joules. These values were typical of as received parent plate properties. A synopsis of the test results achieved for the Vanguard repair work has been detailed in **Table 3**

The production welds were carried out successfully with some minor SMAW repairs to the root areas where some deflections from the weld joint had occurred due to magnetic effects.

The components welded have been in service now for several years with no problems recorded for any reason.

Cosmetic TIG Weld Repairs of EB Welds in Q1N Steel

One common problem with EB autogenous welds in thick material has been the occurrence of under flush welds that required possible dressing and welding by a standard arc welding process. A small programme of work using the TIG process with Argon shielding gas was devised to assess the fracture toughness properties of the cosmetic repair welds on the surface of the original EB welds. The American Linde 95 solid bare wire was selected and two areas along the EB weld were ground down to 3 and 7 mm depth respectively and repaired using the aforementioned wire as a filler material.

Tests were then made with the welds in the as welded and fully heat treated conditions comprising of hardness surveys and charpy tests at -50°C test temperature for the latter condition only.

Table 4 lists the properties obtained and shows weld and fusion line to have hardnesses up to 425VPD in the as welded condition and down to 240 –250HV in the fully heat treated condition. The charpy values at the weld centre line were around 230 –250 Joules at -50°C for both depths of repair welds. Agreement with MOD was reached to use this cosmetic repair technique on production EB welded components should the occasion arise. **Figure 5** is a photo-macrograph of a section through a cosmetic TIG weld repair on the cap of an EB weld in Q1N steel

Effects on Weld Performance of Slope Down Flaws

Concern had been raised about the slope down-slope up flaws found in circular EB welded components over 50 mm thick and MOD requested that a HTE (Hull Toughness Element) test be carried out. This test was a variant of the flawed bulge explosion test (FBE) that had a uni-axial as opposed to a bi-axial bulge that occurred after the explosive charge had been detonated. This very deep searching defect assessment test had a definite pass –no pass criteria in that any defect must not exceed 50mm from the original fatigue crack length after receiving the explosive charge.

Accordingly BAE contracted TWI [15] to produce a 90mm thick Q1N steel panel with deliberately introduced slope flaws that were considerably more severe than those anticipated to occur in production components. These flaws of spiking phenomena occur more so in Q1N steel than other low alloy steels since it is more susceptible to solidification cracking when welding autogenously. Every attempt should be made to minimise the occurrence of these flaws by increasing the radius of the weld penetration cavity tip by determining the rate of beam power current decay coupled to beam focus and oscillation parameters.

The 90mm thick panel was machined either side down to 50mm thickness, to confirm to the standard HTE test plate thickness, and fully heat treated by quench and tempering before checking the weld flaws position by NDE (RT). This enabled DERA to position the machined notch and fatigue crack right in the centre of the flaws strung in a sloping fashion through the centre of the weld length. The test made with a 190-gramme charge under sea water at a test temperature of -5°C was successful.[16]. The initial surface crack did extend by 40 mm from the flaw indications area. Details of the test are listed in **Table 5**. On opening up the panel the extent of the pre-existing defects can be seen together with the machined notch and fatigue crack, **Figure 6.** MOD agreed to allow flaws in production components welded by EBW as long as they did not exceed those exhibited in the HTE panel and this information was added to the requirements of Specification 855.

The Use of Reduced Pressure Electron beam Welding For QIN Steel Components

All of the previous R&D and production work with EBW had been conducted using the high vacuum EB process. However the recent development of Reduced Pressure EB welding (RPEBW) has opened up several advantages that centre around the rapid pump down associated with this variant. The reduced pump down times of 10 minutes in place of 50 –60 minutes normally required considerably reduced the waiting times and associated costs that arose from the use of high vacuum EB chambers. BAE commissioned TWI [17] to examine the feasibility of using RPEBW as an alternative route for welding Q1N steel components. Several QIN steel panels were welded using the low vacuum EB process in plates from 55 to 90mm thickness, in both linear and circumferential butt welds. Both weld types achieved sound welds with no flaws in the 55mm thick welds but there were some slope down flaws in the other thicker weldments.

The bend specimens from as welded and Q&T condition weldments were satisfactory over 180° around a 4T diameter former. Charpy values were above 200Joules from the fully heat treated EB welded panel and the crystallinity values on tests carried out at -50°C were all deemed acceptable to the requirements of BAE Specification 855. **Table 6** lists the side bend and charpy tests carried out in the as welded and fully quench and tempered conditions.

Further to this work it was decided to contract DERA to perform an HTE Test on a 50 mm thick Q1N steel fully heat treated weldment with slope down flaws in the middle of the weld length. The ensuing machined notch and fatigue crack ensured that the effect of the flaws in the weld would be severely tested and the result after testing the panel in the standard underwater explosion test was considered satisfactory and well above minimum values set by DERA. A series of trials involving the SIFT test [18] gave excellent values down to -80°C. The test combines a drop weight and CTOD type specimen together with a temperature transition that fully evaluates a reliable measurement of fracture toughness. Professor Sumpter, DERA has summarised the basic facts of both the HTE and SIFT tests in Appendix 1 of this paper.

Weld Procedure Suite of Electron Beam Welds in Q1N Steel Ranging From 30mm to 150mm Thickness

TWI were given a contract to approve a set of Welding Procedures based on Specification 855 and BSEN 288 Part Three weld procedure requirements prior to the placing of a contract to project manage sets of valves for use in the construction of the Astute Class Submarine Build Programme. The procedures were also based on the explosive bulge panels tested by DERA on contract work from MOD.

A complete set of procedures was eventually approved using 38 mm; 70 mm; 100mm and 130mm Q1N steel plates with the basic EB welding parameters listed in **Table 7** for the entire thickness range. After full Q&T heat treatment the panels were sectioned with respect to cross tensiles, side bends and charpy tests at +20°C and -50°C.

The charpy tests at the lower test temperature consistently achieved values between 230 and 270 Joules in the weld metal and over 200J in the fade out area. The side bends were tested satisfactory over a 4 T diameter former to a 180° angle. Cross tensiles produced values between 726 and 757 N/mm². The complete set of test results have been summarised in **Table 8**. **Table 9** lists the individual plate range approved for each weld procedure plate thickness.

TWI also produced a set of shielded metal arc welding procedures for repairs to EB welds in QIN steel prior to PWHT. The test repair weld depths were 10 and 40mm depth in 53mm thick EB welds in Q1N steel. The welding parameters and mechanical test results have been listed in **Table 10** and cover the repair range of 10mm to 80mm deep weld repairs prior to PWHT.

This set of EB welds and SMAW repair weld procedures formed the basis for any production work on Q1N steel that was associated with the Astute build or any new components required for refit work on British nuclear submarines.

Production Aspects

Once BAE had decided to place a contract on TWI for the production of several electron beam welded marine valves for the Astute class submarine the amount of paperwork and specifications increased dramatically.

A complete set of drawings for the valves was sent with the order that detailed blank sizes, component dimensions and the finished machined surface dimensions in the areas clad by Monel. Copies of Specification 855 (Electron Beam Welding of Q1N Steel Components) and Specification 706 Section 22 (Cladding of Hull Valves with Monel) [19]. were also sent to TWI. **Figure 7** shows a basic drawing configuration as supplied to TWI for EB welding the blanks together.

The prime form for the Institute to adhere to was called a QASOR (Quality Assurance Statement of Requirements) that detailed the relevant Naval/BAE Specifications to be consulted and the types of tests/instructions that needed to be adhered to and signed against as being completed. **Table 11** for example of a QASOR form.

BAE employed a computer driven Compass contract system that needed to detail a unique number for every part and complete component for a particular item on the submarine.

This enabled MOD to have full traceability of all material and components during the complete service life of the submarine that in the case of the valves involved identifying them back to the original steel cast number. The actual Blank Identification list for one component has been listed in **Table 12** where the varying unique numbers ensured all parts were traceable from cast number, plate number, blank number and raw material number.

The blanks for the fabricated valves were cut from the relevant Q1N steel plates as shewn in **Figure 8** in the Main Steel Production Shop on a Messer Greisheim oxy acetylene profile cutting machine. Extreme care was made to ensure a good, smooth finish to the cut sidewalls of the blanks. Before removing the blanks from the network plate they were soft nosed stamped with a Compass Contract number and a unique blank number for this particular work package as indicated in the Blank Identification form discussed previously. **Figure 9**.

On shipping the blanks to Granta Park the Institute were obliged to produce a Quality Plan Traveller that detailed the operation, type of examination, department involved, Control Document titles up to signing of the traveller by TWI and BAE to accept that the work had been carried out to the relevant specifications and work requirements. **Table 13.**

All of this work was based on the approved Welding Procedures for the EB welding of Q1N steel plate from 30mm to 143mm thickness and the SMAW repair procedures of EB welded joints prior to PWHT.

TWI decided to use the larger of the main EB welding chambers available, the EB2 Facility with the 100kW RF Gun. Each blank was cleaned free of oil and grime as well as being passed through a degaussing ring to reduce possible magnetic effects deflecting the electron beam. A sacrificial bar or 'beam stopper' made from carbon manganese bar stock was positioned to run through the centre of the weld to 'soak up' any excess beam power that inevitably occurs when welding thick section steels. The effects of this excess power on the bar are clearly illustrated in **Figure 10**. **Figure 11** shows a collection of machined parts awaiting to be EB welded. The next view, **Figure 12** shows the machined sections set up ready for welding and illustrating the close fit-up between the sections. After the first pair of blanks had been welded together and checked by UT through the top surface rather than directly at the weld as per normal practice, the next blank was positioned and EB tack welded prior to completing the main weld run. (Prior to testing there was considerable checking of the parameters and **Figure 13** shows the various linear and round rings used). **Figure 14** shows a component part EB welded in the EB2 chamber. This system was used until the complete component had been welded together. **Figure 15** shows a completed valve after EB welding with a section cut from an experimental test showing the EB welds. Once a component had been completely welded the individual welds were closely assessed on the outer and inner surfaces and where necessary dressed by grinding to ensure good surfaces for RT inspection at Hi Tec Ltd of Sheffield

TWI had been contracted to organise the post weld machining operations to remove excess plate material to the drawing requirements and prior to being fully heat treated to the requirements of NES 736 Part 3 by Hi-Tec Ltd of Sheffield. In essence, this is a Naval Material specification for Q1N steel castings but used on the advise of MOD to perform the required quench and temper PWHT on the EB welded wrought steel valves. This also involved placing sections of the actual plate sections in with the furnace load to enable tensile and charpy tests to be made to ensure the material had been restored to its original mechanical properties. The sections were forwarded to BAE and the tests showed that the heat treatment had been successful with respect to 0.2% Proof Stress values of for the 130mm and 80mm plate thicknesses. The charpy tests were actually tested at –84°C instead of the –20°C requirement for casting, but still achieved values between 246 – 257 Joules. **Table 14** for full details of the mechanical tests.

The RT inspection of the welds was undertaken using an 8 MeV linear accelerator or'Linac' unit that was capable of detecting any defects as per the requirements of Specification 855.

Once the NDE had been completed and all paperwork signed off that the work had been carried out to the QA Traveller Plan the machined and test components were sent to Forth Tool and Valve Ltd in Glenrothes, Scotland, a company specialising in world class cladding of offshore components. Their expertise was centred upon an in-house designed Hot wire TIG facility that utilised 2 x 1.2mm diameter TIG wires being fed into the weld pool aided by a small super imposed current. This creates a very controlled, smooth layer of Monel cladding that enabled values of iron to be below the statutory 3% limit at the finished-machined surface. **Table 15** lists the basic weld history data used to clad the valves. **Figure 16** is a general view of the cladding made on Q1N steel rings and illustrates the small rippled interface so typical of this type of precision cladding techniques.

References

1. Electron beam welding of cast and wrought Q1N steel, ARE TM 88202: 1988. John Bird and John Galsworthy.

2. A limited investigation into the effect of Electron Beam Welding on Q1N/HY80 Steel. Alan Aitchison. WDLR No 135

3. An Alternative Production Route for Steel Submarine Pressure Hull Components J C Galsworthy and A. Aitchison . DRA(MAR) TM (MTMS) 91406: 1991

4. Development of Methods for Improved Submarine Component Quality Using the Electron Beam Welding Process. C Punshon and T Szluha. TWI Report 3893/1/88

5. NES 736 Naval Engineering Standard. Requirements for Q1 Navy Quality Steel
   Part 1 –Plates Part 2 – Forgings Part 3 - Castings

6. Toughness Tests on EB welded Joints in Q1N and Q2N Materials. C Punshon, TWI Report 3401/2/90

7. The properties of Electron Beam Weldments in Cast and Wrought Q1N steel. J Bird and J Galsworthy. Paper 15 in the Proceeding of the 2nd International Conference on Power Beam Technology, Stratford on Avon, UK. September 1990. TWI 1991

8. An Alternative Fabrication Method for Thick Walled Marine Components Using The EB Welding Process. C Punshon and A Aitchison. Paper 12. As per ref 9 Conference.

9. Electron Beam Welding High Strength Marine Valves from Wrought Steel A Aitchison, C Punshon and J Bird. JOM Seminar, Helsingor, June 1995

10. Low Frequency Corrosion Fatigue of EB Weldments in Q1N Steel Plate. J Galsworthy. ARE TM(UMM) 86417:1986

11. Stress Corrosion Evaluation of EB Weldments in Q1N Steel. ARE TM (UMM) 89418:1990

12. BAE Specification 855 –Electron Beam Welding Of Marine Components Cosmetic TIG. A Aitchison.

13. Repair to Vanguard Forging. WDLR Report No 211. A. Aitchison BAE

14. NES 770 Welding And Fabrication of Q1N, HY80 and QT35 Steels

15. An Investigation into the Effects of Slope Down Indications on Weld Quality when EB Welding Q1N Steel. WDLR 326 A Aitchison.

16. Procedure for Underwater Bulge Explosion Tests MTL MO9- DERA

17. Reduced Pressure Electron Beam Welding on NQ1 Steel –Initial Tests For BAE Systems, Report Number 12319/1/00, June 2000. C SPunshon

18. Simplified Fracture Toughness Measurements by Drop Weight Loading. JDG Sumpter -ECF 12 –Fracture from Defects Seminar

19. BAE Specification 706 Section 22 –Monel Cladding of Marine Valve Components

Appendix One

Summary of Test Results for a Q1N steel Reduced Pressure Electron Beam Weld

By Professor J D G Sumpter, DERA, Rosyth

Two types of tests were undertaken to determine the defect tolerance effect of the slope down weld run of a reduced pressure electron beam weld

An HTE (Hull Toughness Element) tested at -5°C.
SIFT (Simplified Fracture Toughness) tests at a range of temperatures down to -80°C.

The objective of the HTE is to demonstrate that hull integrity under explosive loading, at the minimum conceivable operating depth, in the presence of a realistic weld defect. A 50 mm long by 4 mm deep machine notch is inserted at the surface centreline of the weld. This is then extended in depth by cyclic loading until the total crack depth is 7.5 mm. A weld would not be allowed to enter service with a surface-breaking defect un-repaired, but it is also conceivable that an undetected sub-surface defect might break surface after fatigue cycling. Knowledge that the submarine welds can tolerate defects of this size is also useful for setting NDE standards. The HTE test has replaced the traditional Pellini bulge test for submarine approval in the UK.

The ideal result from the HTE test is that there should be no crack extension from the fatigue crack under explosive loading. This is seldom achieved in arc welds, and a 'pass' in the HTE test is awarded as long as the surface crack extension at the end of the test does not exceed 50 mm. However in the case of the EB weld, the ideal result was achieved, and there was no evidence of any crack extension from the fatigue crack, even at its deepest point (inspected by breaking open the panel at low HTE approval test margin.

This high tolerance defect was also reflected in the SIFT tests. This test is a non-standard test developed at DERA Rosyth. The specimen has a standard fatigue cracked, fracture mechanics, three point loading geometry, but is loaded to a set deflection under drop weight loading without instrumentation. The idea of the test is to provide a simple laboratory alternative to the HTE test, but one that requires less specialist equipment than a dynamics fracture mechanics test. No load or displacement measurements are taken on the specimen during the test, it is simply loaded to a set deflection and the crack extension noted. In this way it is analogous to the HTE test. An advantage over the HTE test is that it can be carried out over a range of low temperatures to determine the safety margin on the brittle to ductile transition for operations at -5°C.

In the case of the RPEB weld, the SIFT tests were approximately 45mm square with a crack depth of about 18 mm. The cracks were located at the weld centreline. The set deflection was chosen to give a J value of 1MN/n at the stop distance. This represents a very high value of defect tolerance. SIFT tests were started at –5°C., but when no crack extension was observed, the temperature was lowered progressively to –40°C., -60°C. and finally –80°C. Even at –80°C. there was no significant crack extension from the fatigue crack. This demonstrates the very high toughness performance of the RPEB welds, which is essentially the same as that of the QIN steel parent plate.

The following sketch shows the basic set-up of the SIFT test.

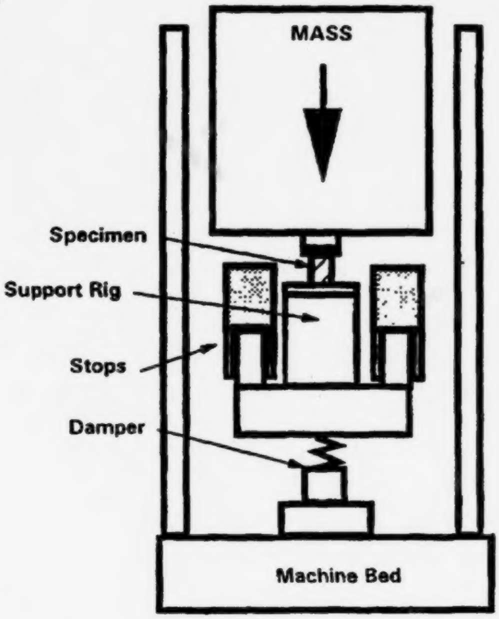
MASS
Specimen
Support Rig
Stops
Damper
Machine Bed

Figure 1 Schematic of test rig

Q1N Steel Plates NES 736 Part 1	Q1N Steel Castings NES 736 Part 3	Q1N Steel Forgings NES 736 Part 2
<0 18	<0 20	<0 18
0 10 - 0 40	0 55 - 0 75	0 10 - 0 40
<0 015*	<0 010*	<0 015*
<0 015*	<0 010*	<0 015*
0 15 - 0 35	> 0 50	0 15 - 0 35
2 25 - 3 25	2 50 - 3 25	2 25 - 3 25
1 00 - 1 80	1 35 - 1 65	1 00 - 1 80
0 20 – 0 60	< 0 60	0 20 – 0 60
>0 015	0 01 – 0 03	>0 015
<0 020	<0 020	0 02
<0 020	<0 030	<0 020
<0 20	<0 20	<0 20
<0 03	<0 03	<0 03
<0 01	<0 01	<0 01
<0 005	<0 005	<0 005
<0 010	<0 010	<0 015
<0 02	<0 02	<0 02
<0 025	<0 018	<0 025
~16 mm 550- 690 -16 mm 550 -655	550 minimum	547- 655
20 minimum	16 minimum	20 minimum - L 18 minimum - T
55 minimum - L 50 minimum - T	35 minimum	55 minimum L 50 minimum - T
90J 60mm plate 70J 60mm plate	100J	68J 150mm forging >150mm forging by agreement

Q1N STEEL WROUGHT PLATE, FORGINGS AND CASTINGS SPECIFICATION PROPERTIES

TABLE 2 SSN ASTUTE CLASS SPECIFICATIO

(Obtained from Internet site
– //naval-technology com/projects/astute/specs htm)

Crew	110 (including 12 officers)
Displacement	6,600 tons (surfaced)
Dimensions	
Length	91 7m
Beam	10 4m
Draught	10m
Speed	29 knots (dived)
Missiles	
Submarine Launched Cruise Missile	Tomahawk Block III
Surface- o – Surface Missile	Sub Harpoon
Torpedoes	6 x 21 inch torpedo tubes for missiles and Spearfish torpedo – total of 36 carried
Combat Data System	BAE Sema SMCS
Countermeasures	ESM, Decoys
Radar	I-band navigation radar
Sonar	Thompson Sintra Type 2076
Propulsion	
1 Rolls Royce PWR 2Nuclear	
2 GEC Turbines	
2 Diesel Alternators	
1 Emergency Drive Motor	

TABLE 3 TEST RESULTS FROM 150mm THICK Q1N STEEL WELDED BY THE ELECTRON BEAM WELDING PROCESS FOR THE VANGUARD CLASS SUBMARINE BUILD PROGRAMME

Electron Beam Welding Parameters used in Weld Procedure Trials	
Accelerating Voltage	140 kV
Beam Current	320 mA
Travel Speed	100 mm/min
Stand off Distance	250 mm

	As Welded Condition	Stress Relieved Condition 610°C for 6 Hours, WQ	Quench and Tempered Condition 920°C FOR 6 HOURS,WQ 640°C for 5 Hours, WQ
Cross Tensiles, N/mm²	725 722 721	699 698 707	742 733 734
Side Bend, 4T Dia Over 180° Angle	3 with no defects 1 with 1mm slit after full bend	3 with no defects 1 with 3mm split after full bend	4 with no defects
Hardness, VPD	243 PM 450 FL 410 Weld	216 PM, 276 FL, 283 Weld	228 PM, 227 FL, 227 Weld
Charpy, Joules -50°C	51 76 68	41 27 62	Cap 226 216 202 22mm below surface 224 220 230 42mm below surface 244 261 249
CTOD Tests -5°C mm	0 97 1 04 0 98 1 22 1 21 1 07	2 12 2 07 2 07 1 66 1 89 1 50	1 42 1 76 1 73 1 20 1 20 1 32

[illegible] FOR REPAIR WELDS OF
RON BEAM WELDED QIN STEEL PANELS

RON BEAM WELDING PARAMETERS	
ATE THICKNESS	80mm**
NE TYPE	EB 11
R VACUUM	5 X 10-3 BAR
I TYPE	RF 100kW
POSITION	HV
ING VOLTAGE	150kV
CURRENT	160Ma
) SPEED	125MM/mm
IL CURRENT	Top off Bottom 1-60 – 1 45
CILLATION	PATTERN –CIRCULAR 70Hz 30 POINTS

chined down to 50MM thickness for HTE test

PARAMETERS USED FOR TIG REPAIRS	
SOURCE	MG 450 AC/DC RECTIFIER
PE AND SIZE	LINDE 95, 1 6mm DIAMETER
GAS	ARGON
EMPERATURE	70°C
G CURRENT	120A AND DC-ve
VIDTH OF TEST 1	3mm DEEP, 7mm WIDE
VIDTH OF TEST 2	6mm DEEP, 11mm WIDE
UNS TEST 1	7
UNS TEST 2	11

RDNESS SURVEYS ACROSS REPAIR WELD AREAS		
	AS WELDED Vn)	AFTER Q & T*** Vn)
	212- 237	242 - 258
E	311 – 425	240 - 256
L	360 - 373	233 - 245

FOR 2 HOURS, WQ AND 640°C FOR 2 HOURS, WQ

-50°C TEST TEMPERATURE FROM Q&T TIG REPAIRS OF EB WELDS		
E	3mm DEEP TIG REPAIR	6 MM DEEP TIG REPAIR
	244 249 250 249 249 245	228 242 248 252 253 245

TABLE 5 DATA ON THE HTE QIN STEEL ELECTRON BEAM WELDED PANEL

(PART OF THE ASSESSMENT OF SLOPE DOWN/UP FLAWS IN EB WELDS)

DETAILS FROM THE DERA HTE TEST ON EB WELDED QIN STEEL PANEL	
MATERIAL	ELECTRON BEAM WELD
SIDE NOTCHED	ROOT
NOMINAL TEST TEMPERATURE	-5°C
CHARGE WEIGHT	190 gm
NO OF SHOTS	1
WATER DEPTH	2.1 m
DEPTH OF BULGE	13 46 mm
INCREASE IN NOTCH WIDTH	1 92 mm
INITIAL SURFACE CRACK LENGTH	56 12 mm
FINAL SURFACE CRACK LENGTH	96 85 mm
PASS/FAIL	PASS
PHOTOGRAPH OF FLAW AREA	FIGURE XX

CHARPY VALUES OBTAINED FROM HTE EB WELDED QIN STEEL PANEL	
TEST TEMPERATURE °C	JOULES
-20°C	196 195 204
-50°C	184 191 191 185199 195 197 194 202
-75°C	163 172 165 175 190 168
-84°C	146 138 154 181 180 172
-100°C	163 168 145 155 131 150

TABLE 6 REDUCED PRESSURE ELECTRON BEAM WELDING TEST RESULTS

RPEBW WELDING PARAMETERS	
Panel Number	W26
Panel Thickness	90mm
Accelerating Voltage	175kV
Beam Current	180mA
Travel Speed	150 mm/min
Focus	Top 1 67 Bottom 0 6
Work Distance	230 mm
Beam Deflection	8 points at 72 Hz O Pattern

Charpy Test Results from RPEBW QIN Steel 90mm Weld				
Test Temperature/ Charpy Position	As Welded Condition Joules	Crystallinity %	Quenched and Tempered Condition Joules	Crystallinity %
-50°C				
Outer	64 41 58	79	202,204 222	0
Middle	56, 26, 36 53, 68 42	86	233, 235 229 242, 236 236	0
Inner	34 48 61	84	228, 241 236	0
-84°C				
Outer			239 230 150	
Middle			195, 219 211 222, 218 224	
Inner			215 270 236	
-100°C				
Outer			216 208 195	
Middle			216 72, 186 203 220 96	
Inner			178 128 177	

TABLE 7 WELDING PARAMETERS USED IN THE ELECTRON BEAM WELDING PROCEDURE TESTS FOR QIN STEEL 30 -143mm THICK.

ALL WELDS WERE MADE WITH THE JOINTS IN THE HORIZONTAL WELDING POSITION

TWI REF NUMBER & MATERIAL THICKNESS mm	ACCEL VOLTAGE V	BEAM CURRENT mA	TRAVEL SPEED mm/min	FOCUS COIL CURRENTS		WORK DIST mm	BEAM DEFLECTIONS Ampl Freq.
				F1A	F2A		
W31 38mm	150	120	150	0 5	1 504	300	5 POINTS AT 2mm DIAMETER AT 70hZ
W38 53mm	150	150	150	0 5	1 504	300	5 POINTS AT 2mm DIAMETER AT 70hZ
W40 70mm	150	200	125	0 5	1 504	300	5 POINTS AT 2mm DIAMETER AT 70hZ
W43 100mm	150	250	100	0 5	1 504	300	5 POINTS AT 2mm DIAMETER AT 70hZ
W44 136mm	150	250	125	0 5	1 504	300	5 POINTS AT 2mm DIAMETER AT 70hZ

THE SLOPE UP DOWN DEGREES FOR ALL WELDS WERE 30° UP 5° OVERLAP AND 30° DOWN

MECHANICAL PROPERTY TEST RESULTS FROM ELECTRON ELDED OIN STEEL PLATE WELD PROCEDURE TRIALS

TEST TYPE	TEST RESULTS
OSS TENSILE DE BEND ARPY +20°C ARPY -50°C	726 730, 724 726 N/mm² 4 x SB. 120° over 4T Diameter Former 260 WM, 260 FL, 229 Fade In/Out, 272 Fade In/Out FL. 234 253 247 WM, 262, 273 282 FL. 192,130 133 Fade In/Out, 258, 260, 304 Fade In/Out FL.
OSS TENSILE DE BEND ARPY J +20°C ARPY J -50°C	696, 690, 664 665 N/mm² 4 off, 120° over 4T Diameter Former 264 WM 278 FL, 260 Fade in / out, 297 Fade in / out FL. 267 246 248 WM, 278, 272, 248 FL.
OSS TENSILE DE BEND ARPY +20°C ARPY -50°C	744 743, 733, 734, 735, 735 N/mm² 8 x SB over 120° over 4T Diameter Former 234 WM 238 FL, 303 Fade In/Out, 270 Fade In/ Out FL. 246 238, 241 WM, 282, 230, 316 FL.
OSS TENSILE DE BEND HARPY +20°C HARPY -50°C	740 743 746, 737, 737, 741, 730, 749 N/ mm² 12 x SB from Top, Middle & Bottom, 120° over 4T Diameter Former 273 WM, 226 FL, 289 Fade In/ Out, 220 Fade In/ Out FL. 312 316, 304 WM, 334 319, 319 FL.
OSS TENSILE DE BEND HARPY +20°C HARPY -50°C	

PLATE THICKNESS RANGES AS DERIVED FROM ELECTRON BEAM WELDING PROCEDURE

WEL PLATE THICKNESS mm	EB WELD PLATE RANGE* mm
38	30 - 42
53	42 - 58
70	56 - 77
100	80 - 110
136	109 - 150
MAW WELD REPAIR 10mm DEEP AIR IN 53mm EB WELD)	SMAW WELD REPAIR OF EB WELD 5mm TO 20mm DEEP
MAW WELD REPAIR 40mm DEEP AIR IN 53mm EB WELD	SMAW WELD REPAIR OF EB WELD 20mm TO 40mm DEEP

LE 11 TYPICAL OASOR FORM

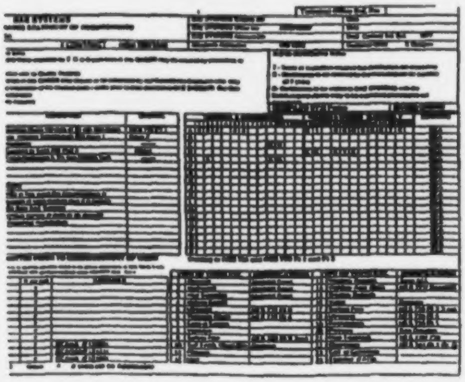

TABLE 10 SHIELDED METAL ARC WELDING PARAMETERS AND MECHANCIAL PROPERTIES OBTAINED IN THE REPAIR OF ELECTRON BEAM WELD PROCEDURES FOR OIN STEEL

REPAIR DETAILS

ORIGINAL PLATE THICKNESS -MM	DEPTH OF SMAW WELD REPAIR OF EB WELD -MM
53 mm	10 mm
53 mm	40 mm

WELDING PARAMETERS

WELDING PARAMETER	ACTUAL VALUES
ELECTRODE TYPE	TUFMET [illegible] - E 12018-G
ELECTRODE SIZE, mm	4mm
POWER TYPE	DC+
WELDING CURRENT, A	170-180A
ARC VOLTAGE, V	23 - 25V
TRAVEL SPEED mm/min RUN OUT LENGTH mm	
HEAT INPUT, kJ/mm	1.09 - 2.47

POST WELD HEAT TREATMENT

HEAT TREATMENT
920°C FOR 4 HOURS, WQ 640°C FOR 4 HOURS, WQ

MECHANICAL PROPERTIES

TEST TYPE	EB53 [illegible] - 10mm REPAIR	EB53 [illegible] - 40mm REPAIR
CROSS TENSILE	749 733 N/mm²	
SIDE BEND 4T DIA FORMER A120°	4 OFF - SATISFACTORY	4 OFF SATISFACTORY
CHARPY J +20°C	[illegible]	[illegible]
CHARPY J -50°C	[illegible]	[illegible]
HARDNESS HV10	[illegible]	[illegible]

TABLE 12 LIST OF BLANKS FOR EB WELDING OF VALVES CONTRACT WITH TWI

ITEM & BLANK NO	CAST HEAT NO	QN PLATE & NO	RAW MATL NO	THICKNESS MM	SIZE O/DIA ID MM	RAW MATL PIECE PART NO	DESCRIPTION	AFFIRMATION OF IDENTITY	
								BAE	TWI
A10	H0758	10127	14200272	130	360/56	30027406	FLANGE	✓	
A11	H0758	10127	14200272	130	360/56	30027406	FLANGE	✓	
A12	H0758	10127	14200272	130	360/56	30027406	FLANGE	✓	
A13	H0758	10127	14200272	130	360/56	30027406	FLANGE	✓	
B14	H2907	10033	14240499	80	280/56	30027407	RING	✓	
B15	H2907	10033	14240499	80	280/56	30027407	RING	✓	
B16	H2907	10033	14240499	80	280/56	30027407	RING	✓	
B17	H2907	10033	14240499	80	280/56	30027407	RING	✓	
D18	H2907	10033	14240499	80	370/150	30027408	RING	✓	
D19	H2907	10033	14240499	80	370/150	30027408	RING	✓	
D20	H2907	10033	14240499	80	370/150	30027408	RING	✓	
D21	H2907	10033	14240499	80	370/150	30027408	RING	✓	
E22	H0758	10126	14200272	130	370/150	30027409	RING	✓	
E23	H0758	10126	14200272	130	370/150	30027409	RING	✓	
E24	H0758	10126	14200272	130	370/150	30027409	RING	✓	
E25	H0758	10126	14200272	130	370/150	30027409	RING	✓	
C26	H0758	10069	14200272	[illegible]	[illegible]	30027410	FLANGE	✓	
C27	H0758	10069	14200272	[illegible]	[illegible]	30027410	FLANGE	✓	
C28	H0758	10069	14200272	[illegible]	[illegible]	30027410	FLANGE	✓	
C29	H0758	10069	14200272	[illegible]	[illegible]	30027410	FLANGE	✓	
							SIGNATURE AND DATE	21/11/12	

WELDING ENGINEERS
BAE SYSTEMS
BARROW-IN-FURNESS
21/11/12

TABLE 13 QUALITY PLAN / TRAVELLER FORM

Op No	Rev No	Component/Operation	Examination Description	Dept/Individual Responsible	Control Doct	Approval Required	Verifying Document	Reqd for LTR	Inspection/Approval		
									TWI	BAE SYS	Subcon't
21		Heat Treatment		Manuf Dept	Proc No HT122	yes	This QP				
22		Inspect	Rad and check heat treat charts	NDE Dept	RAD Proc No XR/120 Acc Std NS855	yes	This QP NDE HT Record HT Chart	yes			H
23		Assemble LTR Doc Pack (doc pack retained by TWI)		QA Dept/TWI		yes	This QP		H	H	H
24		Prepare Valve body for despatch		Stores Dept							
25		Despatch Valve Body this QP and matl certs to FT+V		Stores Dept and QA			This QP				
26	Cladding and machining to be performed by Forth Tool and Valve Ltd in accordance with their QP SFE(0)										
27		Assemble LTR doc pack	Review for accuracy and completeness	Subcon't/TWI/ BAESYS	QASOR	yes			H	H	H
28		Prepare valve body for despatch		Despatch Dept							
29		Release valve and LTR		TWI/ BAESYS	F12111	yes	This QP F12111	yes	H	H	
30		Despatch Valve Body and Doc Pack to CTIW BAES		Stores Dept and QA	F12111						

TABLE 14 COMPARISON OF MECHANICAL PROPERTIES OF AS RECEIVED QIN STEEL PLATES FROM THE MILL & TEST COUPONS AFTER PWHT OF THE PRODUCTION VALVES

PLATE NUMBER	HEAT TREATMENT	PROOF STRESS N/mm^2	TENSILE STRENGTH N/mm^2	ELONGN %	R of A %	CHARPY JOULES @-84°C
AS RECEIVED N10033 80mm CPN20027411	QUENCH °C TEMPER °C	624 598 596 590	737 719 716 712	23 23 24 24	79 79 78 79	224 206 210 228 256 272 248 260 216 216 218 272
AS RECEIVED N10169 130mm N10169		628 621 611 614	738 746 724 726	23 23 23 23	23 23 23 23	254 256 214 264 256 266 254 270 246 198 246 238 244 216 260 200 256 242
PWHT TEST COUPON 80mm N10033		602	714	24	81	257 253 257
PWHT TEST COUPON 130mm N10169		594	711	23	81	246 251 246

TABLE 15 BASIC DETAILS OF MONEL OVERLAYING PROCEDURE ONTO ELECTRON BEAM WELDING QIN STEEL COMPONENTS

	WELDING PARAMETRS
PROCESS	PULSE SUPERIMPOSED GTAW TWIN HOT WIRES
WIRE TYPE	MONEL 67
AWS CLASSIFICATION	ER NiCu-7
SIZE	1 2mm
NO OF WIRES	2
GAS TYPE	HIGH PURITY ARGON
FLOW RATE	12-14l/min
WIRE POLARITIES	DC-ve
WELDING MACHINE	FTV COMPUTERISED HOT WIRE TIG SYSTEM
BASIC CHARACTERISTICS	PEAK 235A BASE 150 SIC 35A FOR 50mS
WIRE FEED SPEED	1350mm/min 1st PASS 1650 mm/min 2nd PASS
TRAVEL SPEED	1st &2nd LAYERS 380mm/min +/-50
BEAD TYPE	STRINGER BEAD
OSCILLATION	N/A
PASS TYPE	MULTIPLE

SIC = SUPER IMPOSED CURRENT

TEST TYPE	NO	RESULTS
SIDE BEND	4	4T DIA, 180° ANGLE PASS
HARDNESS	L	174 WM 300 FL 227 PM
MACRO	T	190 WM 294 FL 220 PM
FE CONTENT@ 3mm FROM FB		2 62%
WELD CHEMISTRY		C 0 07, Si 0 97, P 0 01, S 0 004, Ni 63, Al 0 51, Cu 26 6, Ti 2 28

L = LONGITUDINAL
WM = WELD METAL
PM = PARENT PLATE

T = TRANSVERSE
FL = FUSION LINE
FB = FUSION BOUNDARY

Fig 1

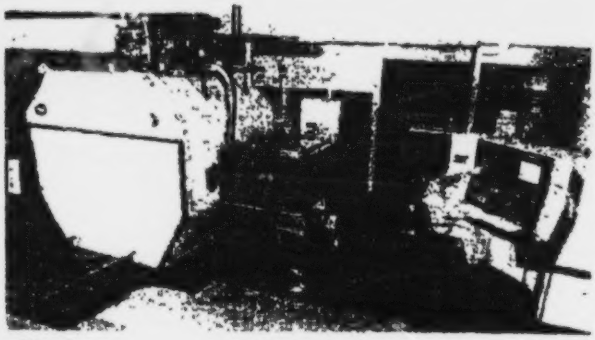

Fig 2

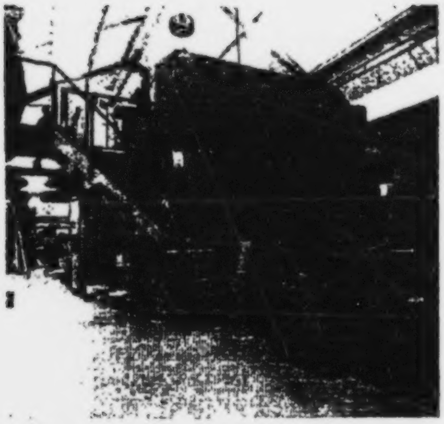

Fig 3

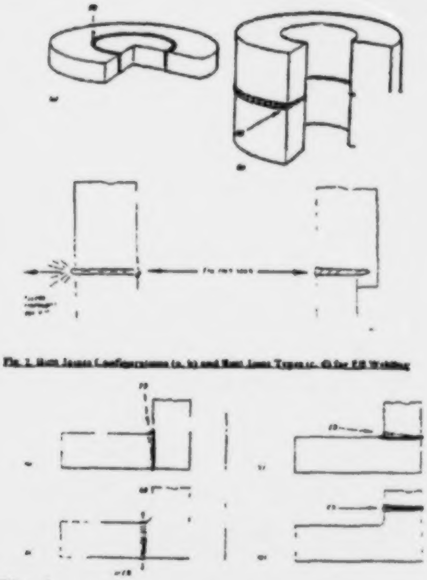
Fig. 2. Butt Joint Configurations (a, b) and Butt Joint Types (c, d) for FS Welding

Fig 4

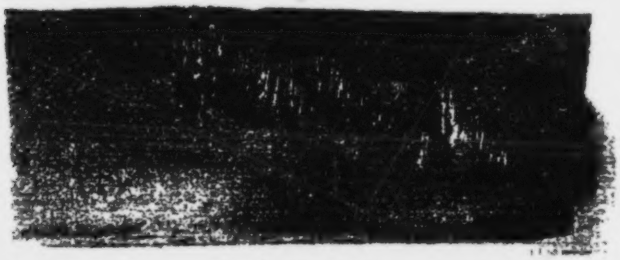

Fig 5

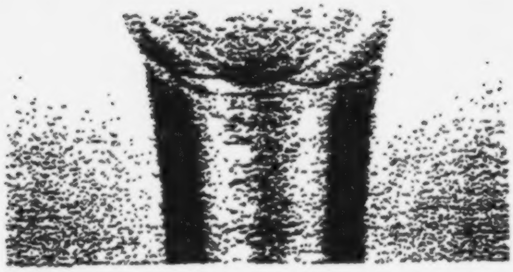
Fig 6

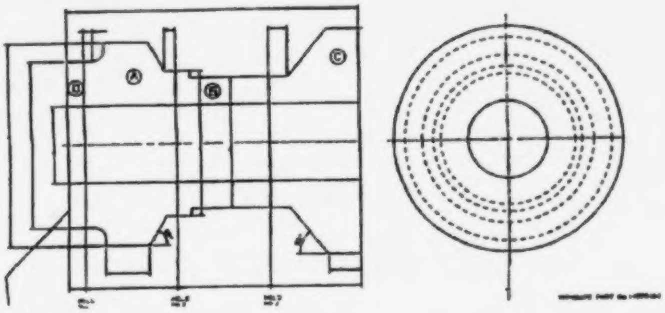

Fig 7

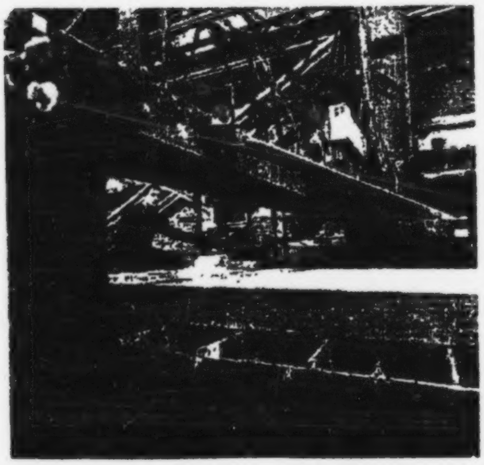
Fig 8

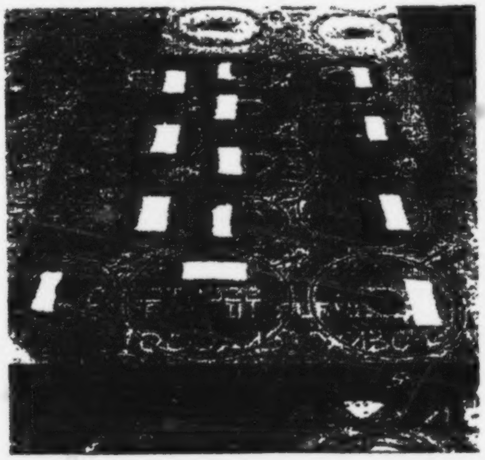
Fig 9

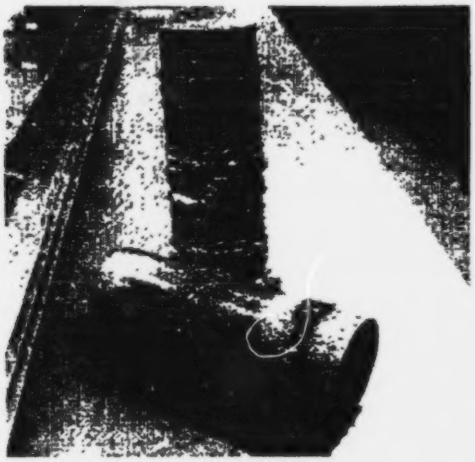

Fig 10

Fig 11

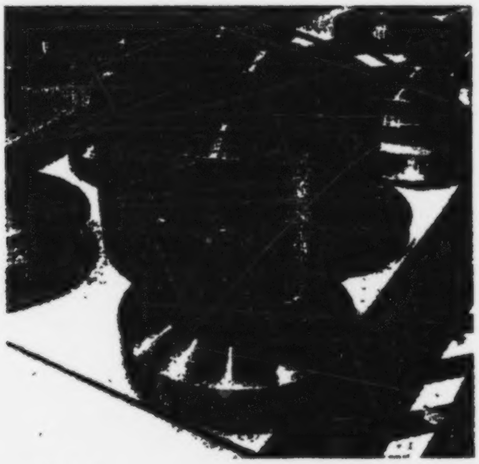

Fig 12

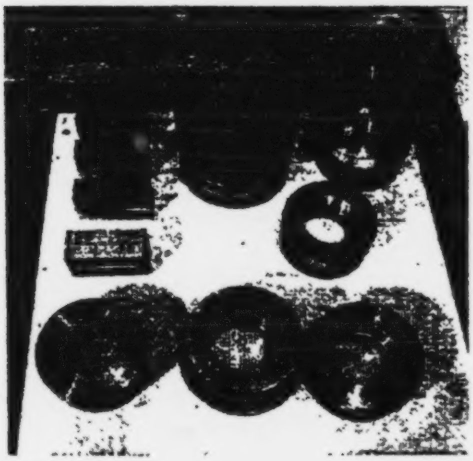

Fig 13

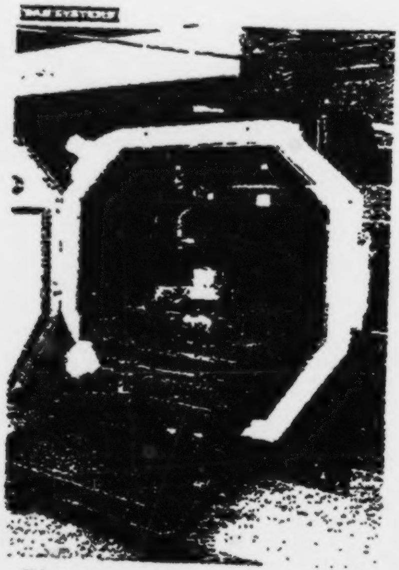
BAE SYSTEMS

Fig 14

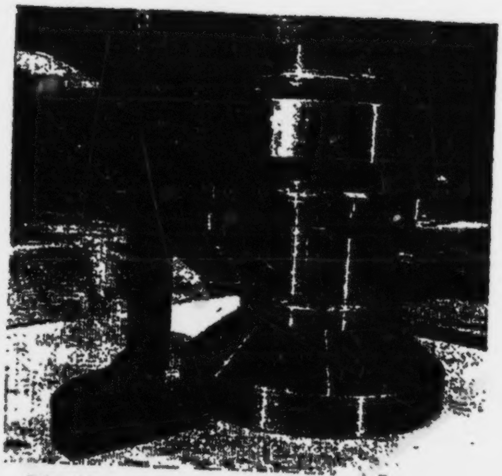

Fig 15a

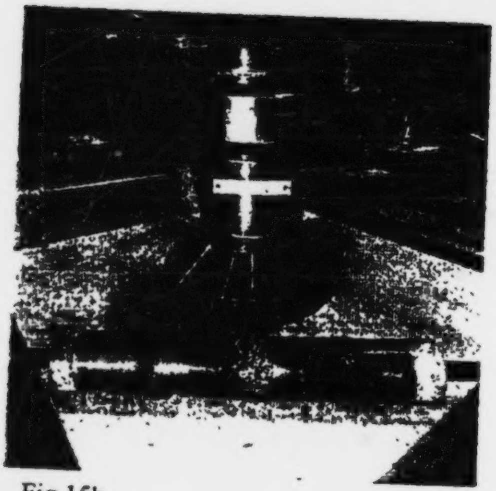

Fig 15b

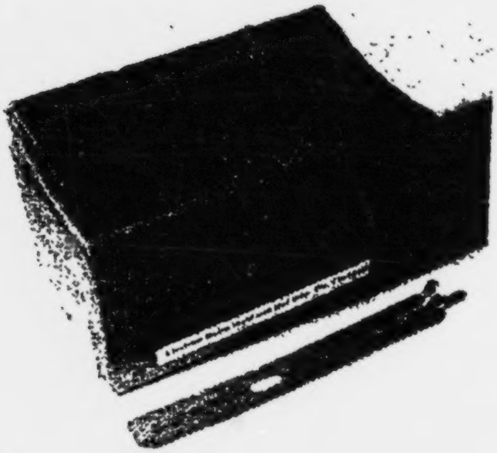

Fig 16

#516438 (23)

Studies on the effect of impurity elements on the mechanical properties and weldability of alloy C95800

M. Sadayappan, M Letts, R. Zavadil and M Sahoo
568 Booth Street, Ottawa, Ontario K1A 0G1

Abstract

At present, there is no consensus on the maximum allowable limits for impurity elements in aluminum bronze castings which could adversely affect the ductility and promote cracking during welding and heat treatment. This work was carried out to evaluate the effect of some impurity elements on the mechanical properties and heat treatment of two most popular aluminum bronze alloys namely, C95800 and C95400. In addition the cracking in the heat affected zone (HAZ) during welding of alloy C95800 was investigated.

Selected impurity elements (Pb, Zn, Sn, Bi, Se, Cr, Si and Be) were added as one, two or three element combinations in alloy C95800. The mechanical properties were evaluated under as-cast and heat treated conditions. The as-cast strengths (UTS and YS) were always above the ASTM specified limits. However, the ductility (% elongation) was reduced to just above and in some cases below the minimum specified value. The heat treatment, which is recommended for improving the sea water corrosion resistance, marginally increases strength but reduces the ductility. Only Pb, Sn and Bi appear to be the impurity elements to have any major impact on the %elongation. The maximum combined content of lead and bismuth should be less than 0.06% to achieve good ductility. Tin content should be controlled below 0.1% when present together with lead and bismuth.

The weldability of alloy C95800 was assessed by conducting full bend test. However, it was found out that this test could not be used to predict the cracking in heat affected zone (HAZ). The simulation of the HAZ, using a Gleeble 2000 weld simulator, was found to be more representative than the bend test. Of all the impurity elements tested only lead and bismuth were found to promote cracking in the HAZ. The other impurity elements (Zn, Sn, Se, Cr, Si and Be) did not have any significant effect on HAZ cracking. Based on the results for various combinations of the impurity elements and microstructural observations the limits to prevent HAZ cracking in C95800 can be specified as follows: Lead - 0.05%, Zinc - 1.2%, Tin - 0.3%, Bismuth - 0.03%, Selenium - 0.035%, Silicon - 0.25%, Chromium - 0.1% and Beryllium - 0.1%

Combining the results from the mechanical properties and weldability the new limits for the impurity elements in alloy C95800 are as follows:

Lead	0.01%	Zinc	1.2%
Tin	0.1%	Bismuth	0.03%
Selenium	0.035%	Silicon	0.1%
Chromium	0.1%	Beryllium	0.1%

Natural Resources Canada Ressources naturelles Canada Canada

Impurity Elements in Aluminum Bronze Alloy C95800

M. Sadayappan and M. Sahoo
Materials Technology Laboratory
Natural Resources Canada

Supported by US DOE/NRCan

Natural Resources Canada Ressources naturelles Canada Canada

Introduction

- Three year project (Dec. 1996 - Dec.1999)
- Sponsored by U S Department of Energy and Natural Resources Canada
- The limits on impurity elements in Ni-Al bronze C95800 to be determined

Natural Resources Canada Ressources naturelles Canada Canada

Introduction

- Impurity elements
  - Affect mechanical properties of C95800
  - Promote weld cracking in HAZ
- ASTM specification B 148-95
  - Range for major alloying additions - Al, Fe, Ni, Mn
  - Two impurity elements Si, Pb
- Anticipated impurity elements
  - Pb, Zn, Sn, Cr, Be, Si, Bi, Se

Natural Resources Canada Ressources naturelles Canada Canada

Composition

CDA C95800 and ASTM B148-95

Element	Al	Fe	Ni	Mn
Range	8.5 - 9.5	3.5 - 4.5	4.0 - 5.0	0.8 - 1.5

Impurity	Pb	Si
Limit	0.03	0.1

Natural Resources Canada　Ressources naturelles Canada　Canada

Literature

- Review done by AFS in 1993
- Si, Pb, Sn, Mg, Bi, Sb and Cd reduce ductility
- Only Si and Sn increase strength
- Zn has no significant effect on mechanical properties
- No agreement on safe limits
- Susceptible for cracking in heat affected zone of weld or during heat treatment

---

Natural Resources Canada　Ressources naturelles Canada　Canada

Objective

- To evaluate effect of impurity elements on
  - Mechanical properties
  - Heat treatment
  - HAZ cracking during welding

of Aluminum Bronze C95800

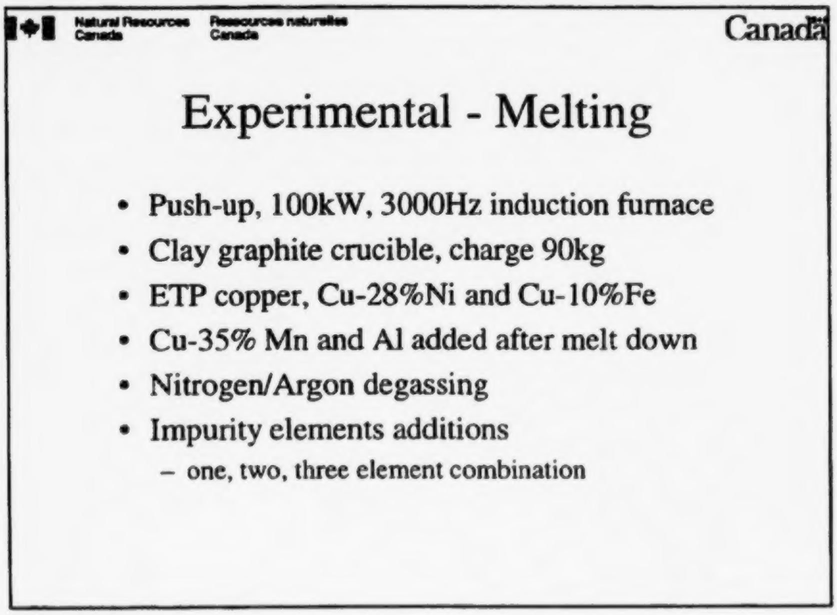

Natural Resources Canada Ressources naturelles Canada

Canada

Experimental - Melting

- Push-up, 100kW, 3000Hz induction furnace
- Clay graphite crucible, charge 90kg
- ETP copper, Cu-28%Ni and Cu-10%Fe
- Cu-35% Mn and Al added after melt down
- Nitrogen/Argon degassing
- Impurity elements additions
  - one, two, three element combination

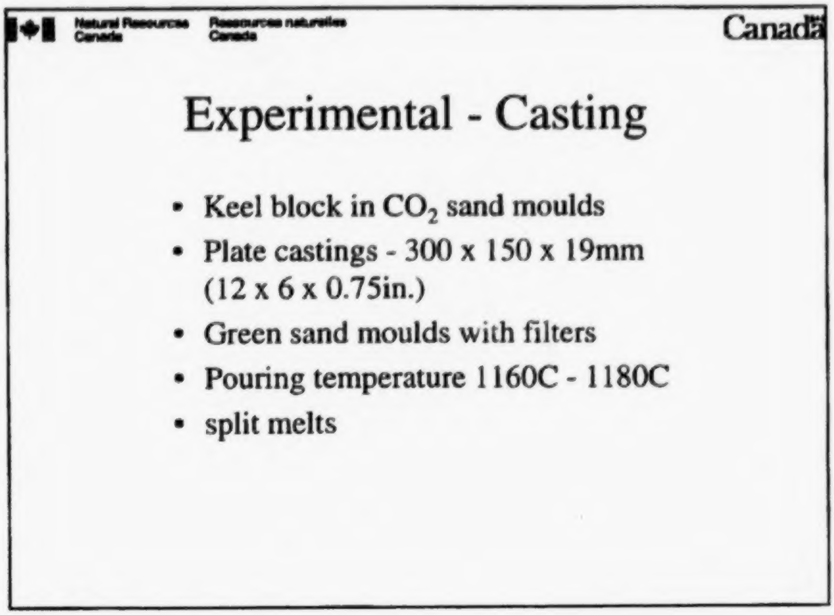

Natural Resources Canada Ressources naturelles Canada

Canada

Experimental - Casting

- Keel block in CO_2 sand moulds
- Plate castings - 300 x 150 x 19mm (12 x 6 x 0.75in.)
- Green sand moulds with filters
- Pouring temperature 1160C - 1180C
- split melts

Natural Resources Canada Ressources naturelles Canada Canada

Composition

Alloy	Range	Composition, %			
		Al	Fe	Ni	Mn
C95800	ASTM	8.5 - 9.5	3.5 - 4.5	4.0 - 5.0	0.8 - 1.5
	Experimental	9.0	4.0 - 4.5	4.0 - 4.7	1.0

Natural Resources Canada Ressources naturelles Canada Canada

Impurity elements

Single Element	Two Elements	Three Elements
Lead	Lead + Zinc	Lead + Tin + Bismuth
Zinc	Lead + Tin	
Tin	Lead + Bismuth	
Bismuth	Lead + Silicon	
Selenium	Bismuth + Selenium	
Silicon	Bismuth + Silicon	
Chromium		
Berylium		

Based on AFS monitoring committee recommendations

Natural Resources Canada Ressources naturelles Canada Canada

Property Evaluation

- Microstructure
- Heat Treatment - 700C for 6hrs, air cool
- Properties
  - Tensile strength
  - Yield strength
  - % Elongation
- Weldability
  - Bend test
  - Gleeble analysis

Natural Resources Canada Ressources naturelles Canada Canada

Summary

Mechanical properties

As-Cast alloys

- The UTS was above ASTM minimum - 585 MPa
- YS was above ASTM minimum - 215 MPa
- Ductility was reduced by impurity elements but remained above the 15% minimum in most cases.
- Silicon reduced ductility
- Combination of Pb-Sn and Pb-Bi-Sn reduced strength and ductility

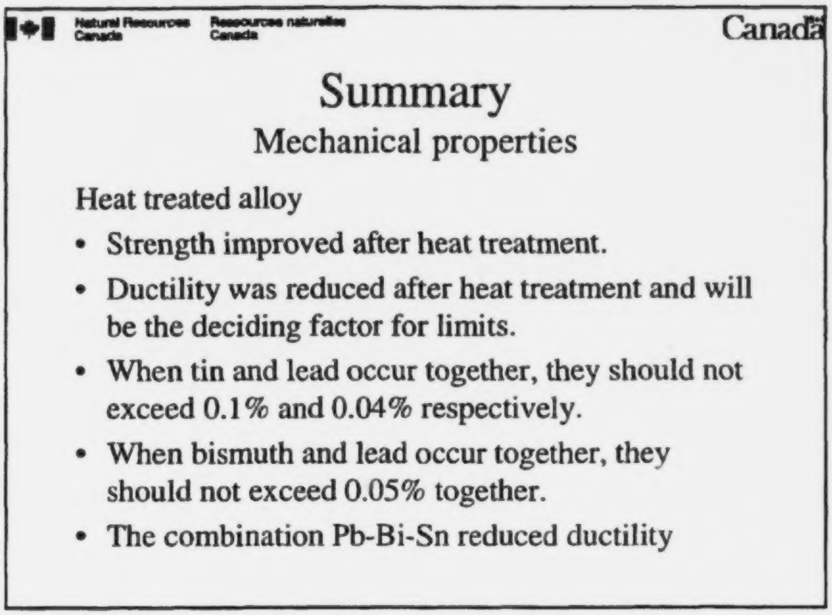

Natural Resources Canada Ressources naturelles Canada

Canada

Summary

Mechanical properties

Heat treated alloy

- Strength improved after heat treatment.
- Ductility was reduced after heat treatment and will be the deciding factor for limits.
- When tin and lead occur together, they should not exceed 0.1% and 0.04% respectively.
- When bismuth and lead occur together, they should not exceed 0.05% together.
- The combination Pb-Bi-Sn reduced ductility

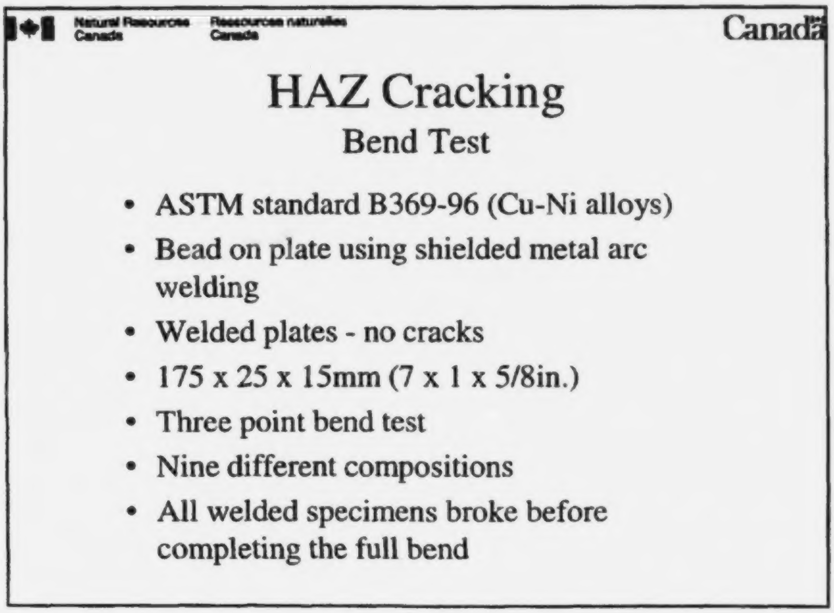

Natural Resources Canada Ressources naturelles Canada

Canada

HAZ Cracking

Bend Test

- ASTM standard B369-96 (Cu-Ni alloys)
- Bead on plate using shielded metal arc welding
- Welded plates - no cracks
- 175 x 25 x 15mm (7 x 1 x 5/8in.)
- Three point bend test
- Nine different compositions
- All welded specimens broke before completing the full bend

Natural Resources Canada Ressources naturelles Canada Canada

HAZ Cracking

Gleeble Simulation

Temperature, C		Cooling	Observation	
Preheat	Soak		Macrostructure	Microstructure
-	1000	Water	Cracks, Porosity	
	992		No cracks	Allotriomorphic α
	950		No cracks	Allotriomorphic α
-	1005	Air	Cracking	
135	984	Water	No cracks	Allotriomorphic α
140	1017	Air	No cracks	Allotriomorphic α
145	990	Slow	No cracks	HAZ
140	948	Slow	No cracks	HAZ

Natural Resources Canada Ressources naturelles Canada Canada

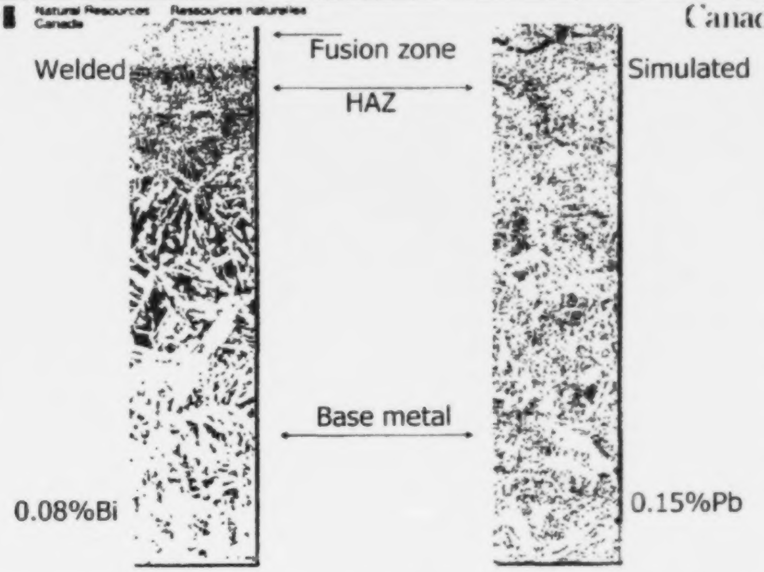

Natural Resources Canada Ressources naturelles Canada Canada

HAZ Cracking

Effect of Pb and Bi

Alloy	Temp. C	Observation
0.1% Pb	963 984 1014	No cracks
0.15% Pb	875	Lost control cracks
	-	Lost control cracks
0.03%Bi	958 994 1005	No cracks
0.08% Bi	980	Sample cracked
	980	Sample broke

Natural Resources Canada Ressources naturelles Canada Canada

Pb distribution

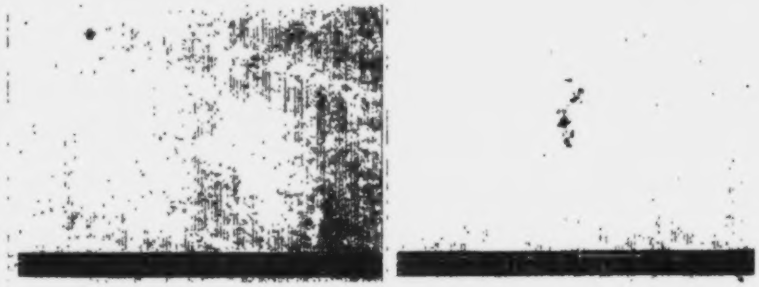

As-cast

HAZ

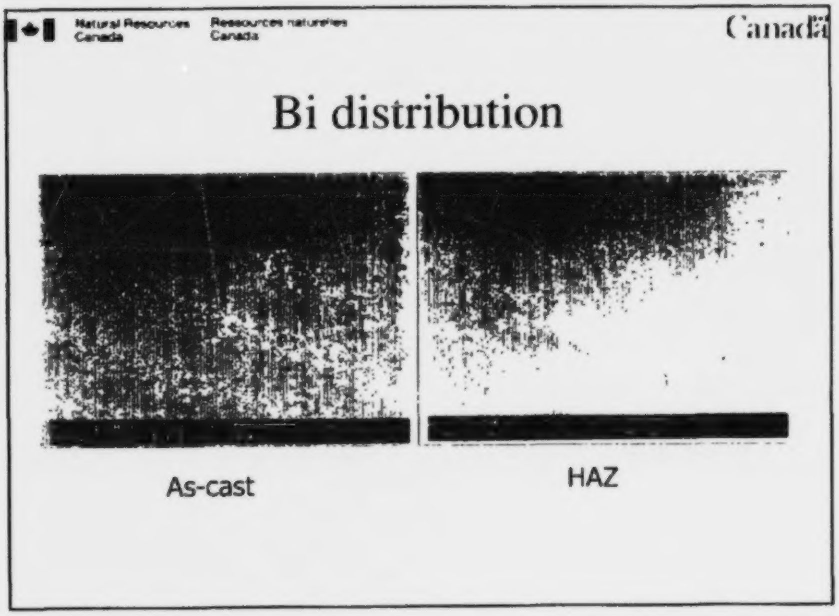

Natural Resources Canada Ressources naturelles Canada Canada

Bi distribution

As-cast

HAZ

Natural Resources Canada Ressources naturelles Canada Canada

Other elements

- Other impurity elements, namely Zn, Sn, Si, Cr, Be, and Se did not have any effect on HAZ
- In multiple impurity elements
  - Pb and Bi promoted cracking in low levels

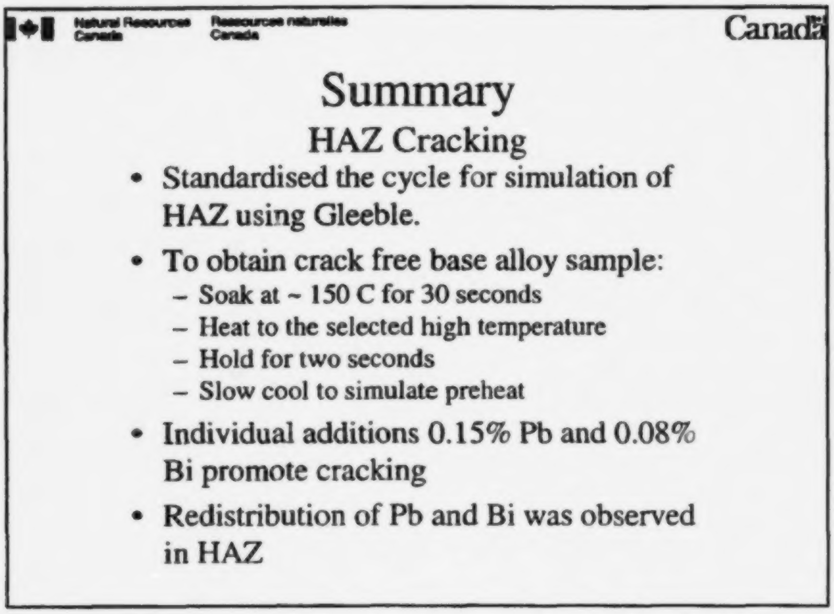

Natural Resources Canada Ressources naturelles Canada Canada

Summary

HAZ Cracking

- Standardised the cycle for simulation of HAZ using Gleeble.
- To obtain crack free base alloy sample:
  - Soak at ~ 150 C for 30 seconds
  - Heat to the selected high temperature
  - Hold for two seconds
  - Slow cool to simulate preheat
- Individual additions 0.15% Pb and 0.08% Bi promote cracking
- Redistribution of Pb and Bi was observed in HAZ

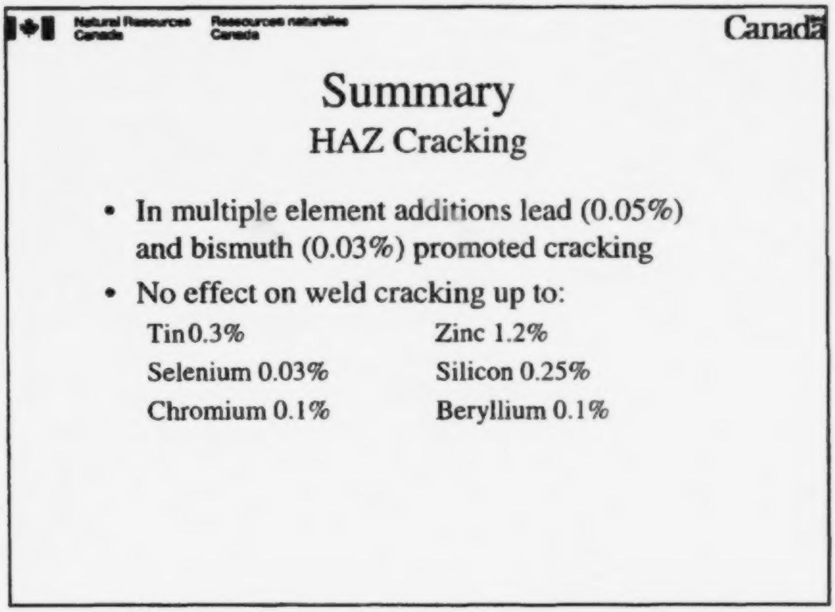

Natural Resources Canada Ressources naturelles Canada Canada

Summary

HAZ Cracking

- In multiple element additions lead (0.05%) and bismuth (0.03%) promoted cracking
- No effect on weld cracking up to:

Tin 0.3% Zinc 1.2%
Selenium 0.03% Silicon 0.25%
Chromium 0.1% Beryllium 0.1%

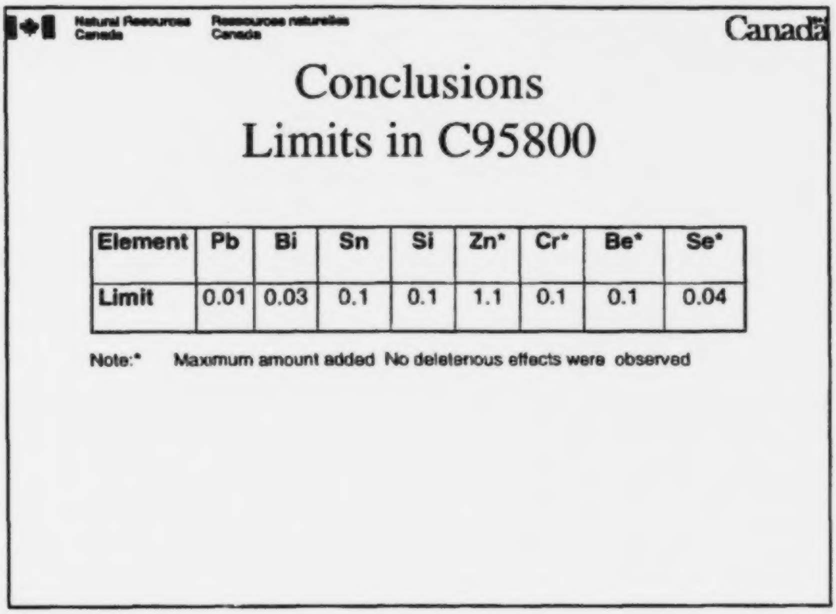

Natural Resources Canada
Ressources naturelles Canada

Canada

Conclusions
Limits in C95800

Element	Pb	Bi	Sn	Si	Zn*	Cr*	Be*	Se*
Limit	0.01	0.03	0.1	0.1	1.1	0.1	0.1	0.04

Note:* Maximum amount added No deleterious effects were observed

#516439 (24)

Low Heat Input Welding and Cladding of Nickel Aluminum Bronze and Related Alloys

by

Calvin Hyatt

Defence Research Establishment Atlantic
Defence Research and Development Canada
P.O. Box 1012, Dartmouth, Nova Scotia, Canada, B2Y 3Z7

Abstract

Low heat input welding and cladding of the nickel aluminum bronze and related alloys, which find wide use in naval applications, offers advantages of a low distortion, a potential for improved properties and a minimum impact on nearby heat sensitive materials. In this presentation, the Defence Research Establishment Atlantic's research on laser, arc and electron beam welding and cladding of nickel aluminum bronze and related alloys will be summarized, with emphasis on the laser cladding studies. Details of the microstructures will be given in the presentation, including how they are influenced by composition and welding procedural variables. Properties important for these materials—corrosion, crevice, cavitation-erosion, erosion-corrosion, stress corrosion, corrosion fatigue, wear, hardness and ductility—will also be discussed, with mention of how these properties are related to microstructure. Results of simulated and actual submarine service will be presented. In summary, the presentation will show that with proper procedural control and consumable selection, the most complex of parts can be clad and that the clad properties meet or exceed those of the base material.

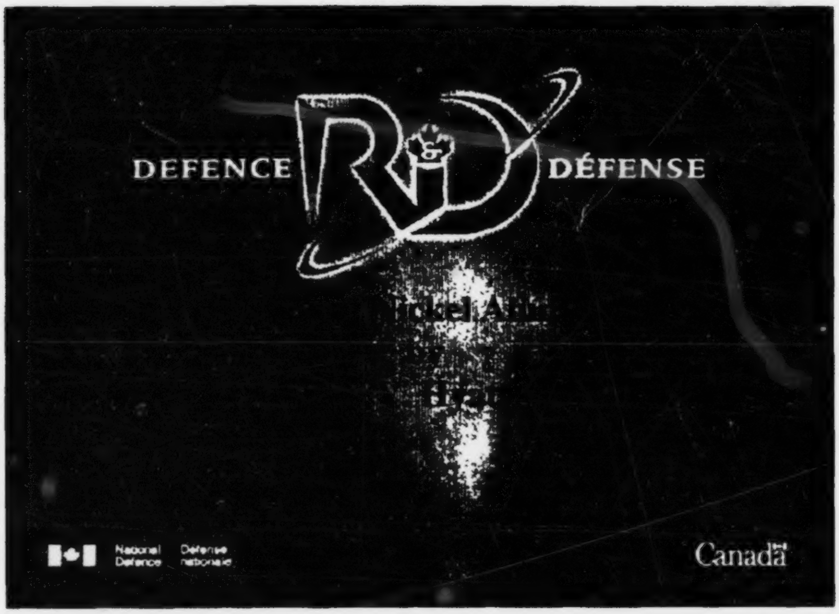

DEFENCE R&D DÉFENSE

[illegible]ickel Al[illegible]

[illegible]

National Defence Défense nationale

Canada

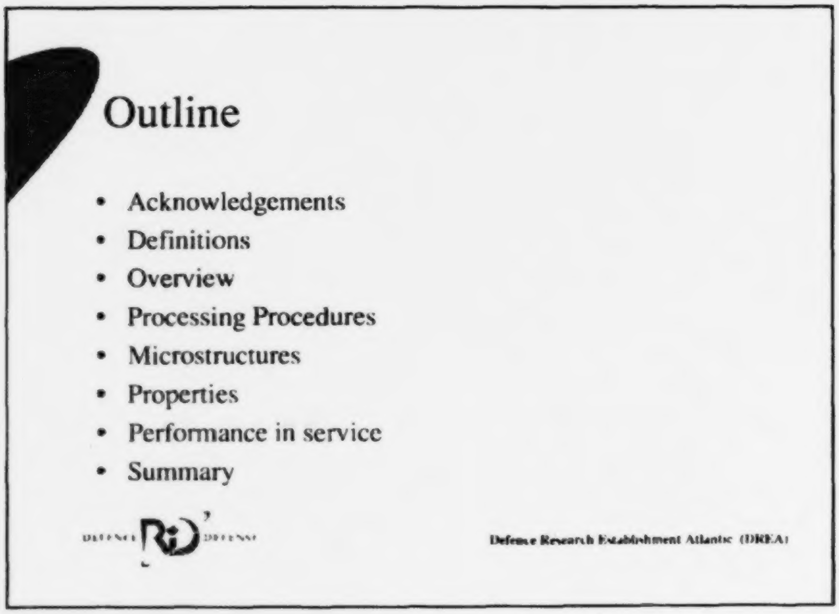

Outline

- Acknowledgements
- Definitions
- Overview
- Processing Procedures
- Microstructures
- Properties
- Performance in service
- Summary

DEFENCE R&D DÉFENSE

Defence Research Establishment Atlantic (DREA)

Collaborators

- J. Gianetto, Dr. M. Sahoo, Dr. G. Botton, Materials Technology Laboratory, NRCAN-Casting,forming, Special techniques
- Prof. P. Roberge and Dr. B. Klassen, Royal Military College, Corrosion
- Dr. Xue, NRC, Advanced Manufacturing Institute, Laser welding)
- Ken Magee, Alberta Laser Institute, Laser Welding
- Dr. C Bennett, Acadia University, Transmission Electron Microscopy
- Dr. A. Majumdar, DSTO, Australia

Overview

- Purpose of the work was answer the question: Can laser cladding be used to surface engineer (improve) and/or repair components of ships and submarines
- Reason: Such components a major cost driver,security of (quick) supply a concern.
- In this talk: show laser cladding does work for nickel aluminum bronze

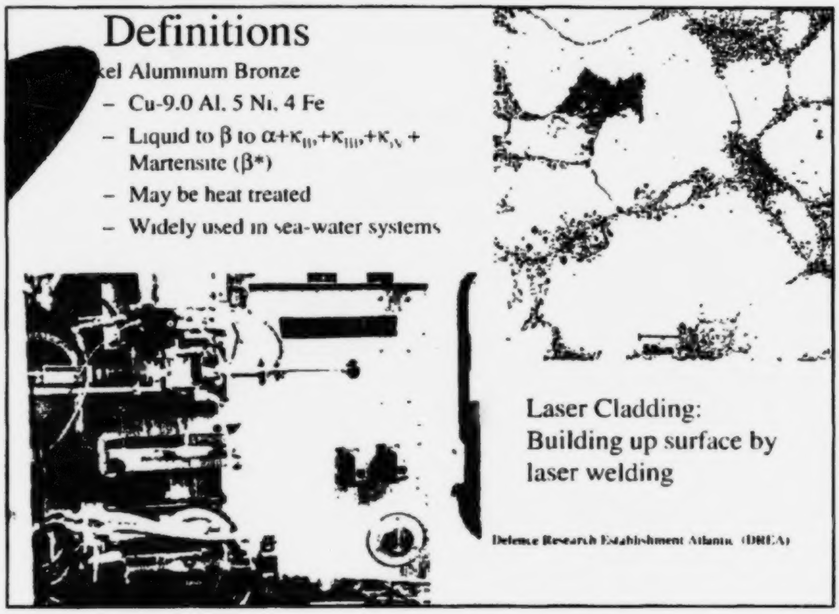

Definitions

- kel Aluminum Bronze
  - Cu-9.0 Al, 5 Ni, 4 Fe
  - Liquid to β to $\alpha+\kappa_{II}+\kappa_{III}+\kappa_{IV}$ + Martensite (β*)
  - May be heat treated
  - Widely used in sea-water systems

Laser Cladding:
Building up surface by laser welding

Defence Research Establishment Atlantic (DREA)

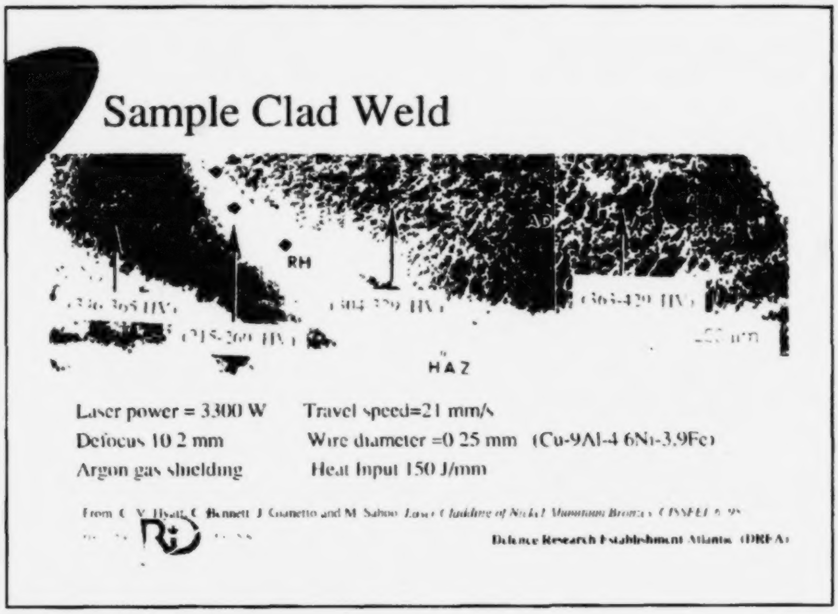

Sample Clad Weld

AD
RH
(336-365 HV)
(304-329 HV)
(365-420 HV)
(215-260 HV)
HAZ

Laser power = 3300 W Travel speed=21 mm/s
Defocus 10 2 mm Wire diameter =0 25 mm (Cu-9Al-4 6Ni-3.9Fe)
Argon gas shielding Heat Input 150 J/mm

From C. V. Hyatt, C. Bennett, J. Gianetto and M. Sahoo *Laser Cladding of Nickel Aluminum Bronzes* [illegible]

Defence Research Establishment Atlantic (DREA)

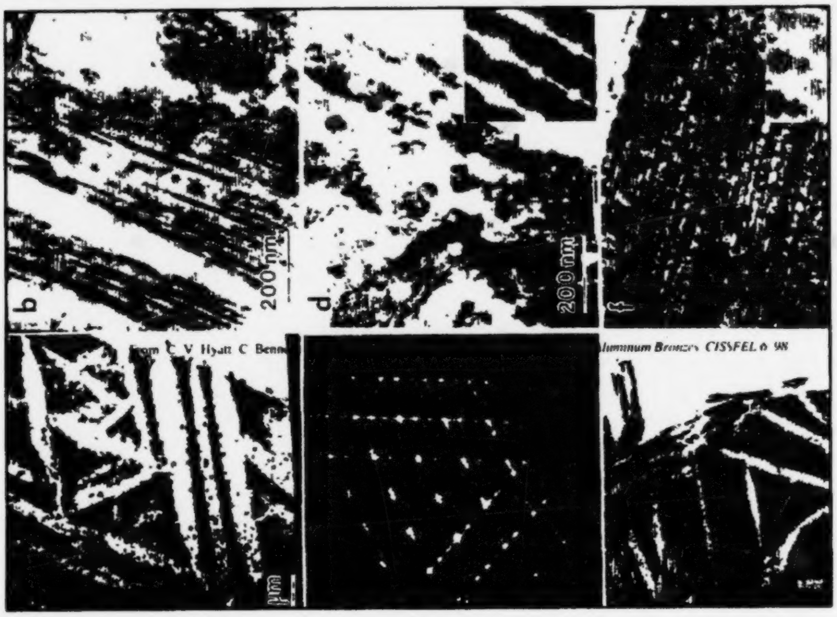

From C V Hyatt C Benn … luminum Bronzes CISSFEL 6 98

Processing

- Arc weld cladding
  - Micro-TIG, Micro-Plasma (thick section fusion problem)
  - Pulsed GMAW (quite good if you want a thick deposit)
- Arc-Spark (will it match laser welding?)
- Laser cladding (wire and powder, helium and Argon shielding)
  - alloying
  - processing conditions
  - component geometry

Arc weld details L. Malik, *Low Heat Input Arc Welding of Nickel Aluminum Bronze*. DREA CR/96/411

DEFENCE R&D DEFENSE

Defence Research Establishment Atlantic (DREA)

Processing

Alloying effects

7 conduction mode welding conditions 20 to 300 J/mm

1 keyhole mode weld

Various valve and impeller castings

Cladding from 42.5 to 600 J/mm

Nickel Aluminum Bronze Alloy Compositions

Series	Melt #	Sample	Cu	Ni	Fe	Mn	Al	Cr	Ti	Zr	Ni/Fe
C	100 95-2	1	76.45	5.06	6.20	0.35	8.70		2.24		0.82
B	125 95-3	2	79.60	3.80	5.50	1.00	10.10				0.69
B	128 95-1	3	80.10	5.00	4.70	1.10	8.10				1.06
B	125 95-1	4	81.20	3.80	3.90	1.00	10.15				0.97
B	128 95-2	5	78.60	6.50	4.60	1.10	9.20				1.41
B	133 95-1	6	78.00	4.70	3.80	1.30	12.20				1.24
B	132 95-3	7	77.95	4.00	5.80	0.95	11.30				0.69
A	124 95-1	8	80.20	4.60	4.80	1.10	8.30				0.96
A	124 95-3	9	77.30	4.60	4.60	1.00	12.80				1.00
C	103 95-3	10	75.44	4.95	6.10	0.36	8.60		3.55		0.81
A	124 95-2	11	78.60	4.70	4.70	1.10	10.70				1.00
B	132 95-1	12	79.30	4.10	4.30	1.00	11.30				0.95
B	133 95-2	13	76.40	5.80	4.20	1.30	12.20				1.40
C	103 95-1	14	77.20	5.05	6.30	0.31	10.00		1.08		0.80
B	133 95-3	15	74.00	6.10	6.50	1.20	12.20				0.94
B	132 95-2	16	78.60	4.10	5.00	1.00	11.30				0.82
B	128 95-3	17	77.60	6.50	5.70	1.00	9.20				1.14
C	114 95-1	18	77.83	4.95	6.02	0.83	9.40			0.97	0.82
A	136 95-1	19	79.30	4.60	6.20	1.10	8.80				0.74
C	137 95-2	20 [illegible]	77.23	5.16	5.60	1.10	9.76	1.15			0.92
C	137 95-1	21	78.71	5.19	4.78	1.10	9.61	0.61			1.09
A	136 95-3	22	78.40	4.60	6.20	1.10	8.70				0.74
D	140 95-2	23	78.95	4.70	5.00	1.00	8.30	0.60	0.44	0.41	0.94
	140 95-3	24 [illegible]					7.80				
C	137 95-3	25 [illegible]	76.14	5.10	6.30	1.10	9.64	1.72			0.81
A	136 95-2	26	78.80	4.60	6.10	1.10	9.30				0.75
D	140 95-1	27	78.63	4.90	5.30	1.10	9.38	0.31	0.23	0.23	0.92

Characterization of base castings described in G McMahon, J A Gianetto and M Sahoo, *Microstructural Characterization of Sand Cast Ni-Al Bronzes* C V Hyatt, E Robichaud, J R Matthews, *Mechanical Properties of Experimental Ni-Al Bronzes*

Defence Research Establishment Atlantic (DREA)

etry:

ery complex parts can be clad normal and non-normal incidence, low dilution.

Dissimilar materials

Thin sections cause difficulties

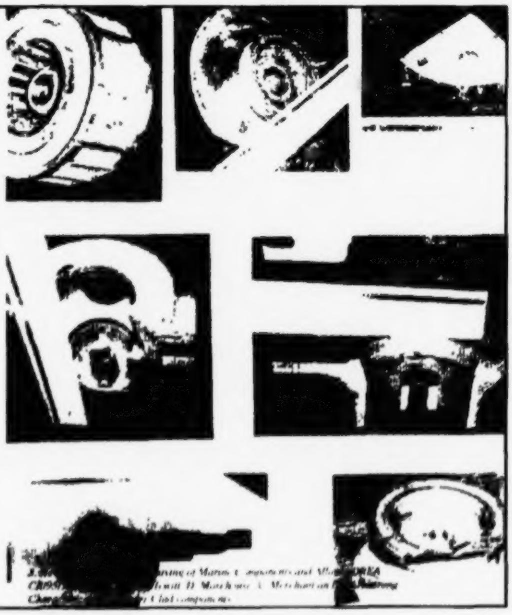

[illegible]

Outline

- Acknowledgements
- Definitions
- Overview
- Processing Procedures
- Microstructures
  - Transformation data
  - Heat Input
  - Composition
  - Heterogeneity
- Properties
- Performance in service

Defence Research Establishment Atlantic (DREA)

Transformation data

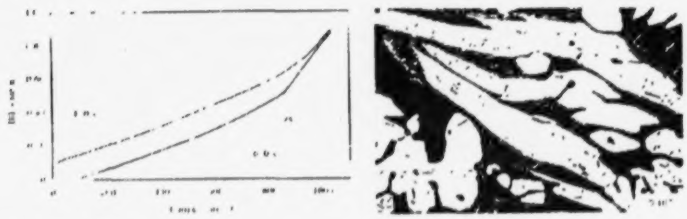

- (Ms 170 °C.
- 400 °C precipitation
- Widmanstatten α

Defence Research Establishment Atlantic (DREA)

From C. V. Hyatt, C. Bennett, J. Gianetto and M. Sahoo *Laser Cladding of Nickel Aluminum Bronzes* CISSLLE 6/98

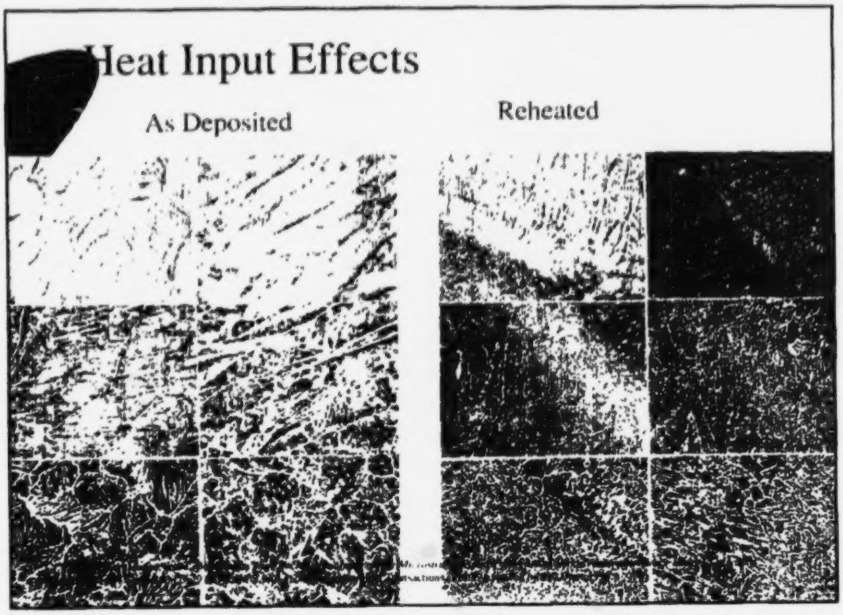

Heat Input Effects

As Deposited

Reheated

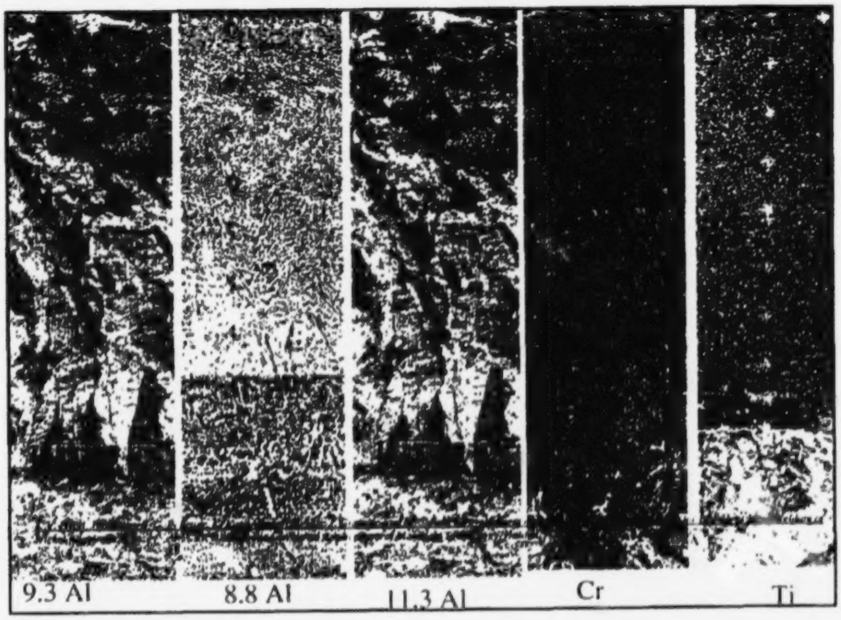
9.3 Al
8.8 Al
11.3 Al
Cr
Ti

Composition Variation

- An advantage of the laser method is homogenization of the surface but, are there micro-scale changes in composition? YES:
  - -flares from intermetallics (makes autogenous surfacing at low heat input less effective)
  - -interpass fusion line
  - -underlying cellular structure

Papers in progress
Gianetto, Packwood et al , Bennett and Hyatt

Defence Research Establishment Atlantic (DREA)

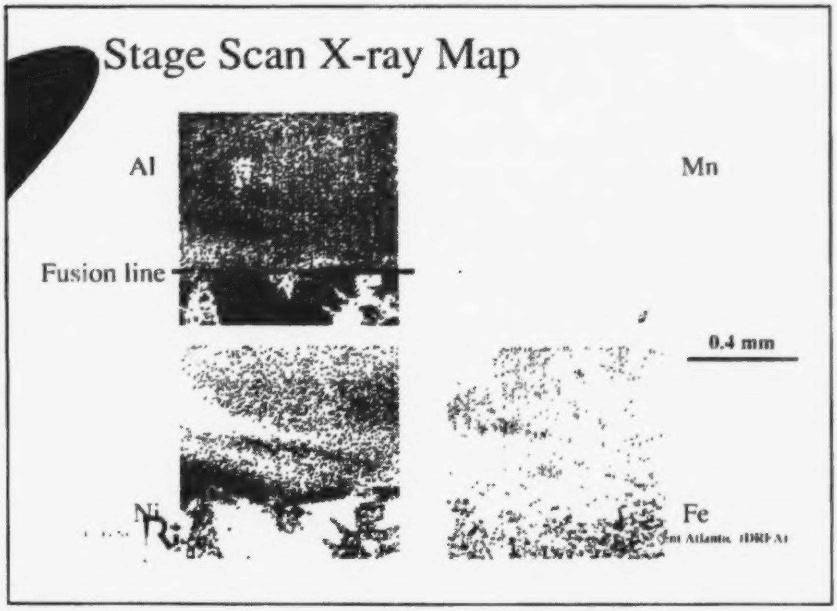

Stage Scan X-ray Map

...nt Atlantic (DREA)

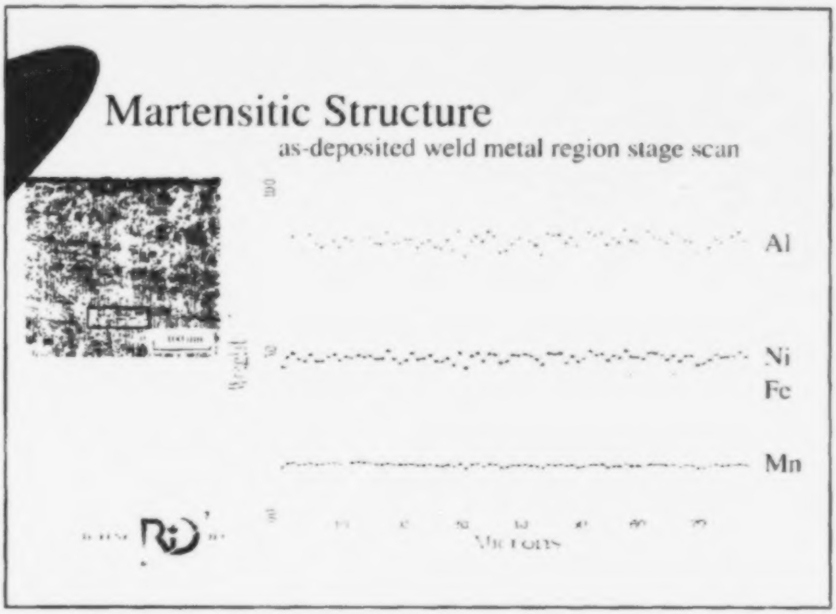

Martensitic Structure

as-deposited weld metal region stage scan

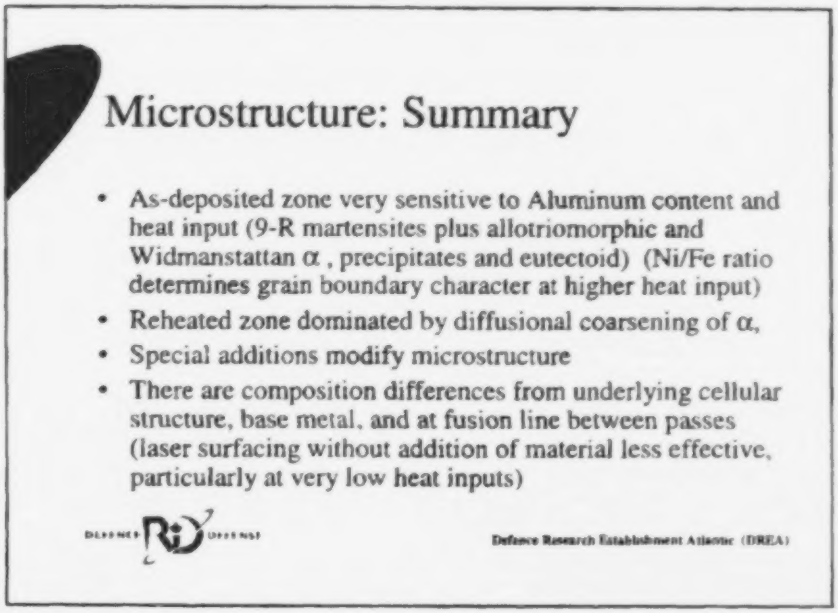

Microstructure: Summary

- As-deposited zone very sensitive to Aluminum content and heat input (9-R martensites plus allotriomorphic and Widmanstattan α , precipitates and eutectoid) (Ni/Fe ratio determines grain boundary character at higher heat input)
- Reheated zone dominated by diffusional coarsening of α,
- Special additions modify microstructure
- There are composition differences from underlying cellular structure, base metal, and at fusion line between passes (laser surfacing without addition of material less effective, particularly at very low heat inputs)

Defence Research Establishment Atlantic (DREA)

Outline

- Acknowledgements
- Definitions
- Overview
- Processing Procedures
- Structures
- Properties
  - Hardness (Varies with position in weld, thermal history,composition)
  - Weldability (does it crack on welding?, high Al, high Ni-change in martensite)
  - Ductility
  - Corrosion (Laboratory, long term, stress corrosion)
  - Erosion-Corrosion
  - Wear
  - Cavitation-Erosion
  - Corrosion Fatigue
- Performance in service

DEFENCE R&D DEFENSE

Defence Research Establishment Atlantic (DREA)

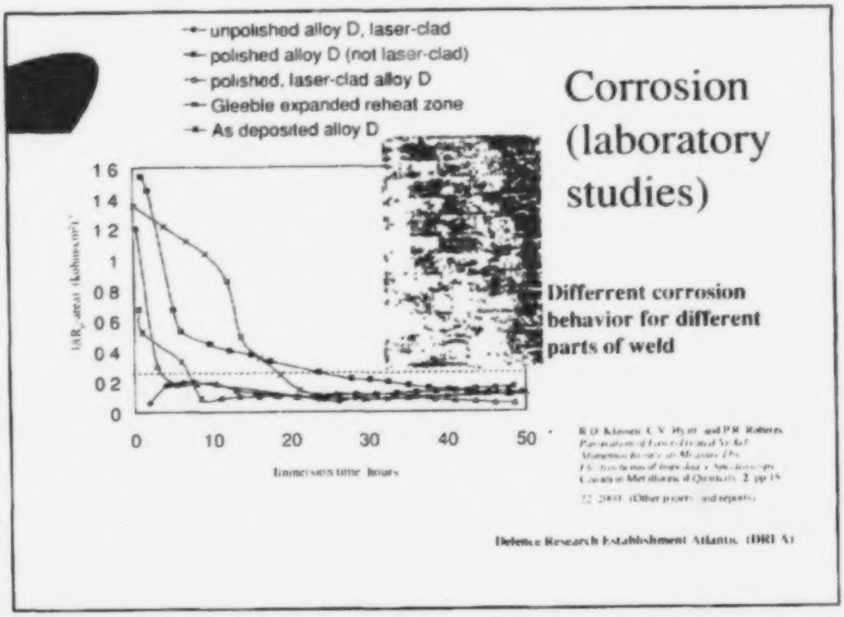

Corrosion (laboratory studies)

Different corrosion behavior for different parts of weld

- R D Klassen, C V Hyatt and P R Roberts, [illegible] Canadian Metallurgical Quarterly, 2, pp 15-22, 2003 (Other papers and reports)

Defence Research Establishment Atlantic (DREA)

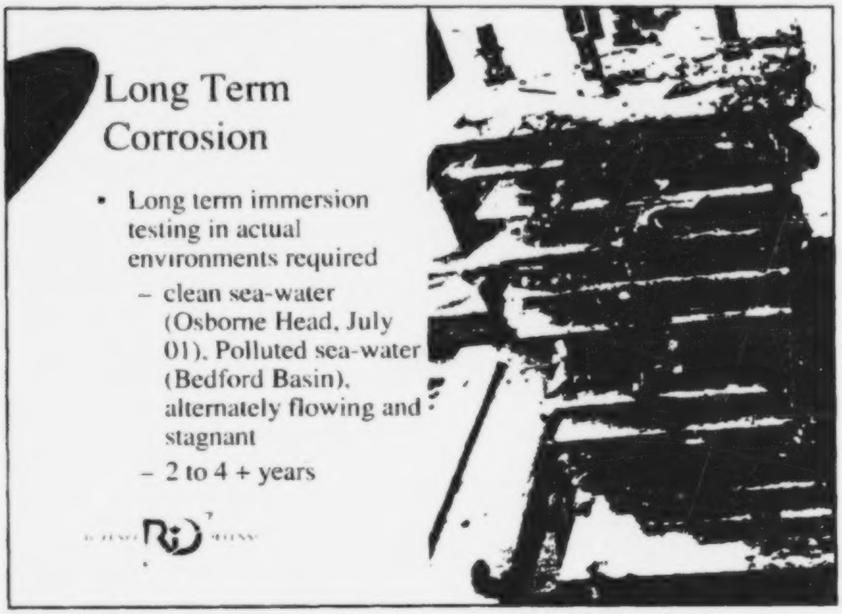

Long Term Corrosion

- Long term immersion testing in actual environments required
  - clean sea-water (Osborne Head, July 01). Polluted sea-water (Bedford Basin), alternately flowing and stagnant
  - 2 to 4 + years

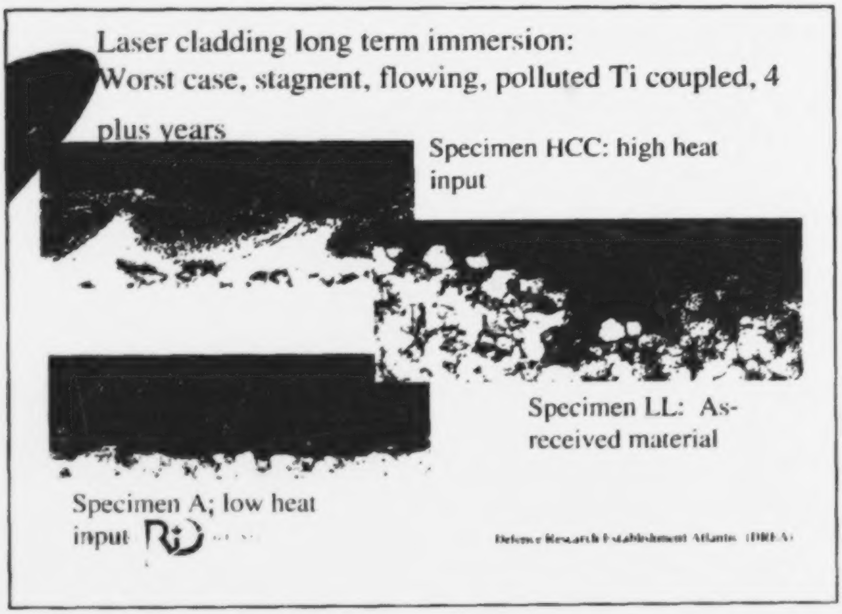

Laser cladding long term immersion: Worst case, stagnent, flowing, polluted Ti coupled, 4 plus years

Specimen HCC: high heat input

Specimen LL: As-received material

Specimen A; low heat input

Defence Research Establishment Atlantic (DREA)

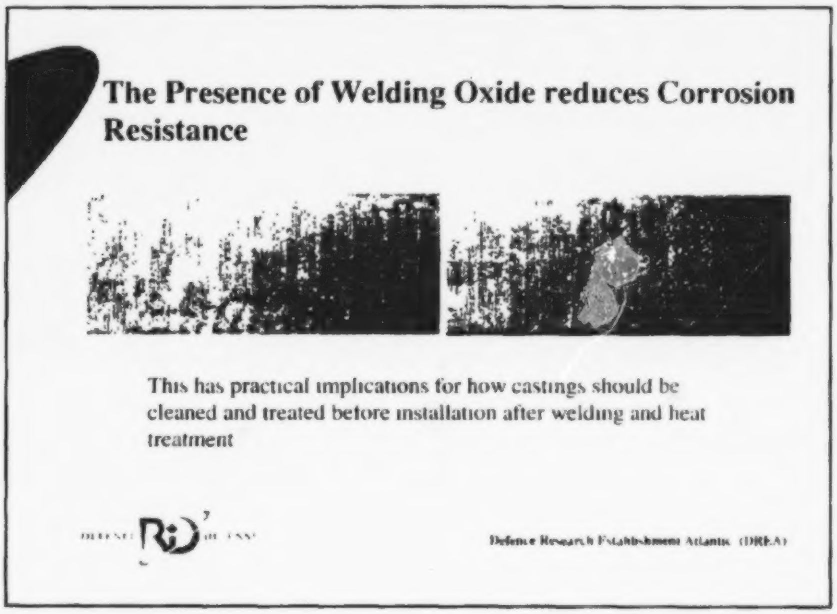

The Presence of Welding Oxide reduces Corrosion Resistance

This has practical implications for how castings should be cleaned and treated before installation after welding and heat treatment

Defence Research Establishment Atlantic (DREA)

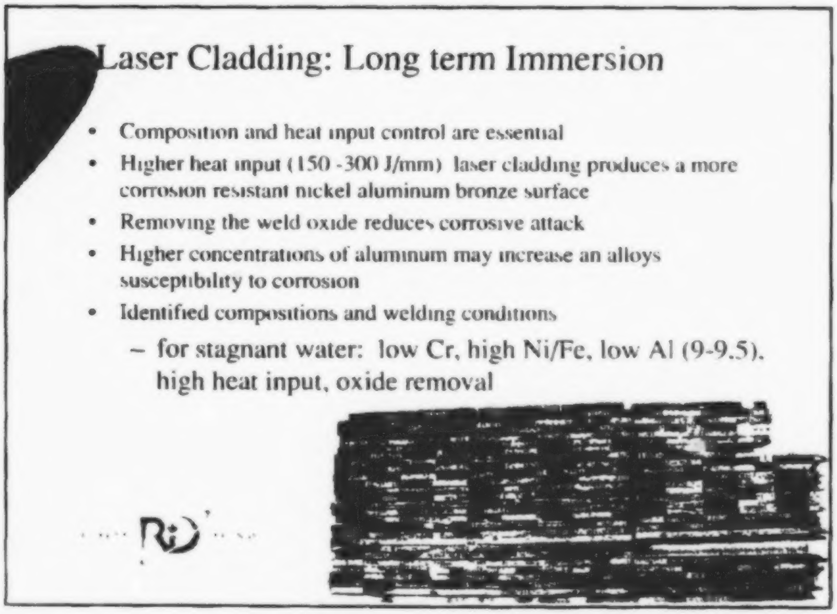

Laser Cladding: Long term Immersion

- Composition and heat input control are essential
- Higher heat input (150 -300 J/mm) laser cladding produces a more corrosion resistant nickel aluminum bronze surface
- Removing the weld oxide reduces corrosive attack
- Higher concentrations of aluminum may increase an alloys susceptibility to corrosion
- Identified compositions and welding conditions
  - for stagnant water: low Cr, high Ni/Fe, low Al (9-9.5), high heat input, oxide removal

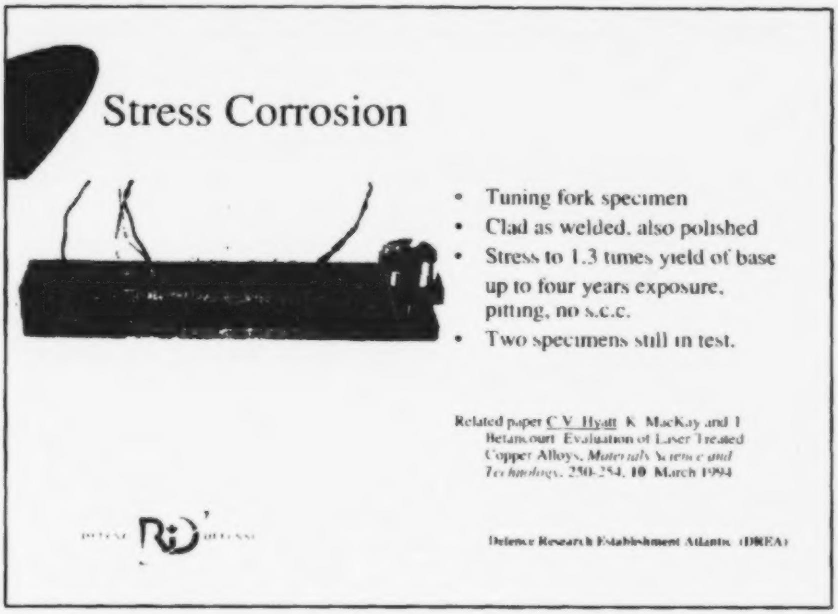

Stress Corrosion

- Tuning fork specimen
- Clad as welded, also polished
- Stress to 1.3 times yield of base up to four years exposure, pitting, no s.c.c.
- Two specimens still in test.

Related paper C.V. Hyatt, K. MacKay and I. Betancourt, Evaluation of Laser Treated Copper Alloys, *Materials Science and Technology*, 250-254, 10 March 1994

Defence Research Establishment Atlantic (DREA)

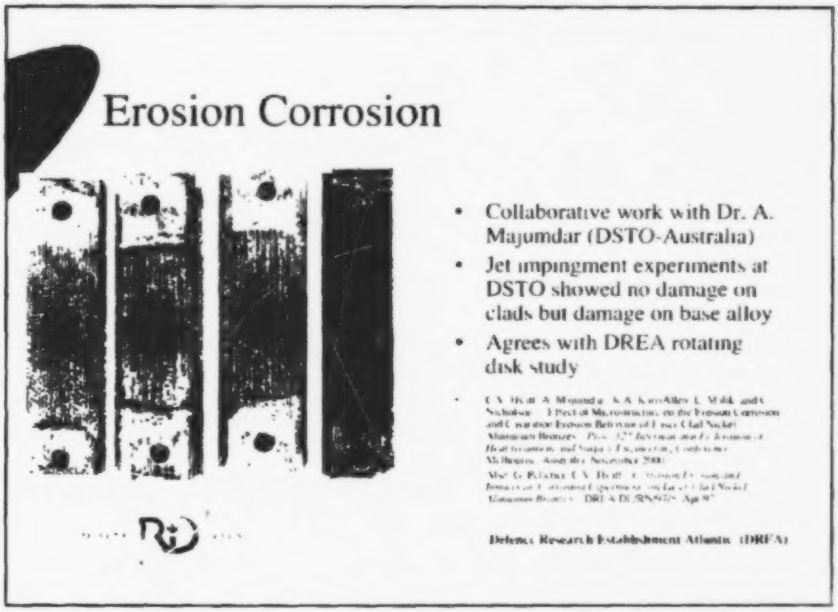

Erosion Corrosion

- Collaborative work with Dr. A. Majumdar (DSTO-Australia)
- Jet impingment experiments at DSTO showed no damage on clads but damage on base alloy
- Agrees with DREA rotating disk study
- [illegible]

Defence Research Establishment Atlantic (DREA)

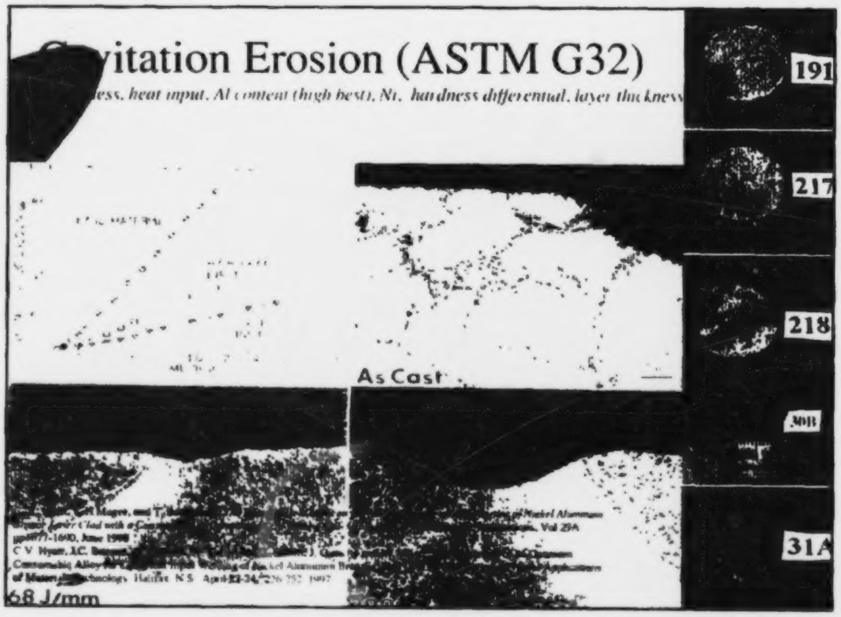

...vitation Erosion (ASTM G32)

...ess, heat input, Al content (high best), Ni, hardness differential, layer thicknes

As Cast

68 J/mm

191
217
218
30B
31A

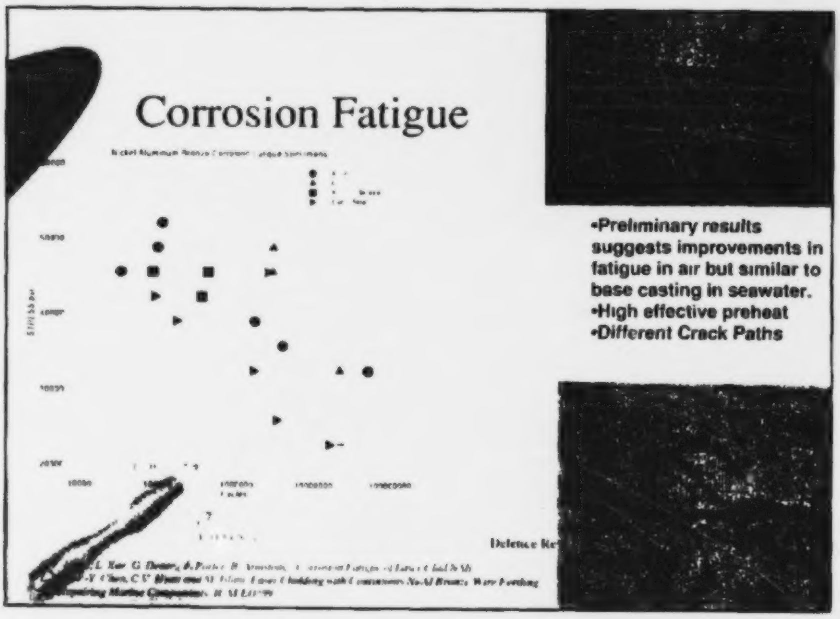

Corrosion Fatigue

- Preliminary results suggests improvements in fatigue in air but similar to base casting in seawater.
- High effective preheat
- Different Crack Paths

Defence Re

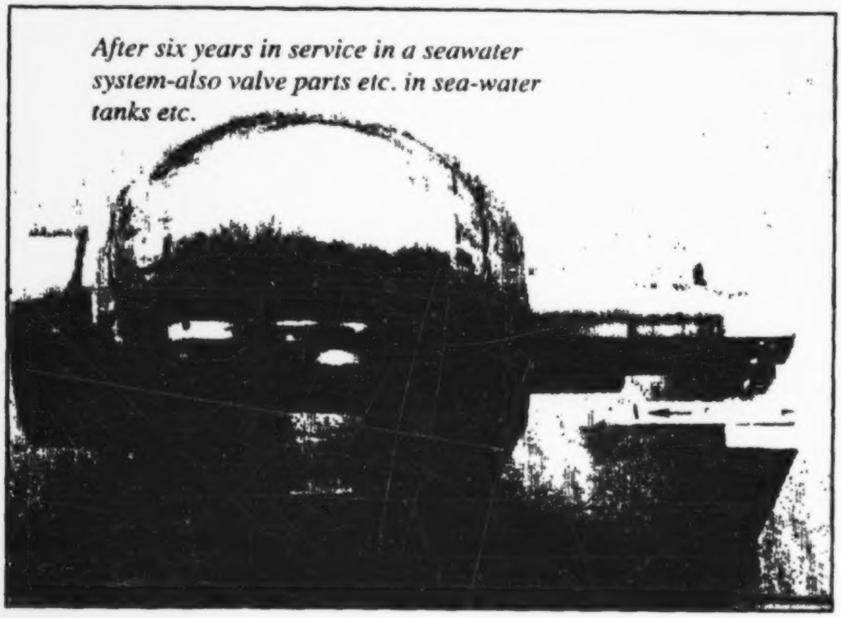

After six years in service in a seawater system-also valve parts etc. in sea-water tanks etc.

Summary: It works

- Most complex of parts can be clad
  - good weldability except for high Al/high Ni (cracking)
- Microstructure a mix of martensites, α, and precipitates
  - reheated zone is dominated by diffusional coarsening of α, heat affected zone by base structure.
  - Composition variations at fusion line, from underlying cell structure, and from base metal intermetallics affect corrosion behaviour.
  - Surface melting less appropriate
- Properties at least match base casting…(corrosion, corrosion fatigue)
  - In some cases much better (eg. Cavitation).
  - No problems with stress corrosion cracking (only one alloy considered)
  - Ductility matching base requires low enough Al/high enough heat to give α

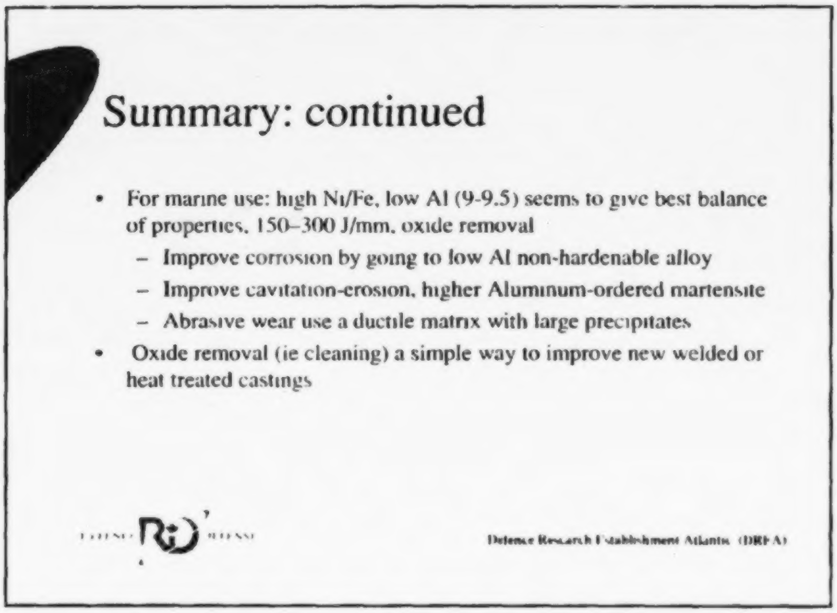

Summary: continued

- For marine use: high Ni/Fe, low Al (9-9.5) seems to give best balance of properties, 150–300 J/mm, oxide removal
  - Improve corrosion by going to low Al non-hardenable alloy
  - Improve cavitation-erosion, higher Aluminum-ordered martensite
  - Abrasive wear use a ductile matrix with large precipitates
- Oxide removal (ie cleaning) a simple way to improve new welded or heat treated castings

Defence Research Establishment Atlantic (DREA)

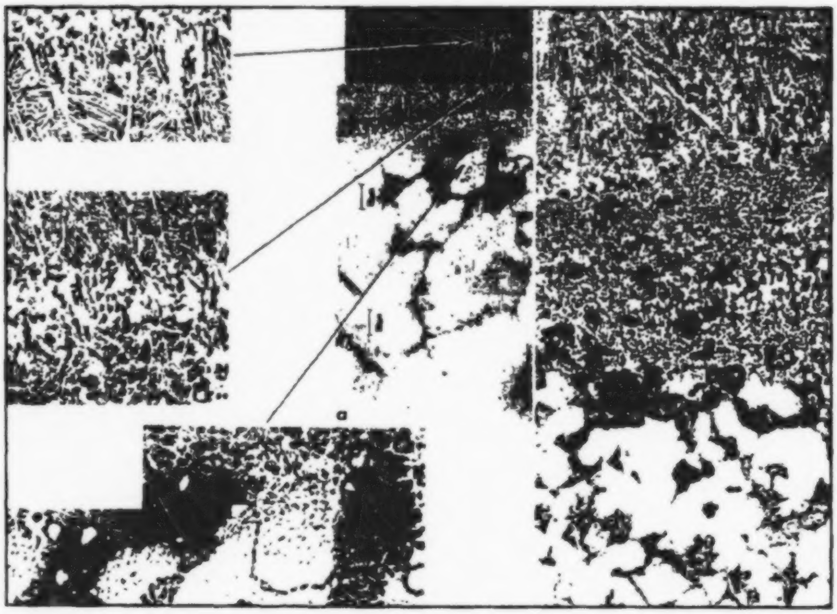

#516 440 (25)

Synthesis and Characterization of Magnetic Shape Memory Materials

by

M.A. Gharghouri† and C. Hyatt††

† Dept. of Mining and Metallurgical Engineering, Dalhousie University, P.O. Box 1000,
Halifax, N.S., Canada B3J 2X4
†† Defense Research Establishment Atlantic, P.O. Box 1012,
Dartmouth, N.S., Canada B2Y 3Z7

Abstract

Magnetic shape memory alloys give significant recoverable strain due to the reorientation of martensite plates by the motion of twin boundaries as a result of an applied magnetic field. The presence or extent of the effect is a function of such variables as the martensite morphology, the mobility of twin boundaries, the volume magnetostriction, and the magnetic susceptibility. The effect can occur at high frequencies and at easily achievable temperatures. These materials thus show great promise for use in actuators and sensors for a variety of applications. An introduction to this class of materials is provided, and preliminary work to synthesize and characterize nickel-based magnetic shape memory materials is described.

Synthesis and Characterization of Magnetic Shape Memory Materials

Michael Gharghouri
Mining & Metallurgical Engineering, Dalhousie University

Calvin Hyatt
Defence Research Establishment Atlantic

Outline

- Introduction
  - Active materials and their applications
- Magnetic properties of matter
  - Background
  - Paramagnetism and ferromagnetism
- Magnetostriction
  - Mechanism of magnetostriction
  - Limitations
- Magnetic shape memory materials
  - Background - martensite formation and morphology
  - Mechanism of MSM effect (Ni_2MnGa, FeNiCoTi)
- Preliminary work

Introduction - active materials

- Active materials are used to:
  - activate switches (close circuits)
  - effect changes in a structure
    - helicopter rotors
    - biomimetic active hydrofoils
- Requirements of active materials:
  - sensible operating temperatures
  - large strains
  - high frequencies
  - strength and toughness
- Classes of active materials:
  - electrostrictives
  - magnetostrictives
  - magnetic shape memory

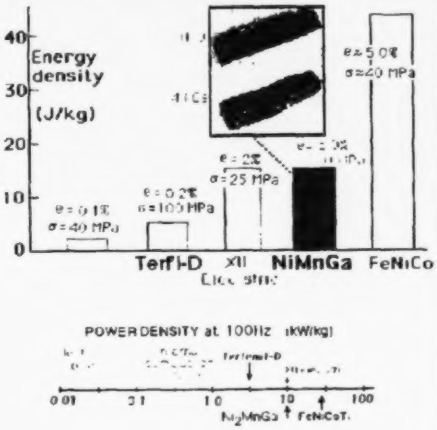

Magnetic properties of matter

- Simplest magnetic structure = magnetic dipole
  - *Examples.* current loop, bar magnet, solenoid, elementary particles
  - electron ⇒ "spin" magnetic moment + "orbital" magnetic moment
- Magnetic dipole moment (μ)
  - N & S poles which are inseparable and are not sharply defined
  - Dipole experiences a torque when exposed to an applied **B** ($\tau = \mu \times \mathbf{B}$)

Paramagnetism and ferromagnetism

- PARAMAGNETISM
  - In most atoms and ions, $\Sigma\mu_{electron} = 0 \Rightarrow$ non-magnetic
  - In some cases, the magnetic moments do not cancel completely so the atom / ion has an overall magnetic moment.
    - Elementary dipoles tend to align in an applied field **BUT** thermal agitation interferes
      - $\mu_{max} = N\mu$ (N = # of atoms, μ = atomic magnetic moment)
      - In practice, $\mu_{actual} << \mu_{max}$
    - Magnetization M = magnetic dipole moment per unit volume ($M = \mu / V$)

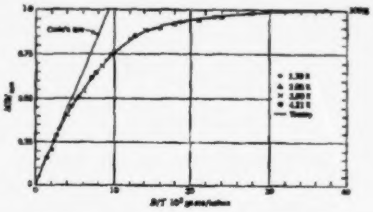

Paramagnetism and ferromagnetism

- FERROMAGNETISM
  - Fe, Co, Ni can achieve a high degree of magnetic dipole alignment even at elevated temperatures.
  - This effect is due to "exchange coupling" between adjacent atoms, which causes the magnetic alignment to be "locked-in"
  - Exchange coupling disappears above the Curie Temperature (1043 K for Fe)

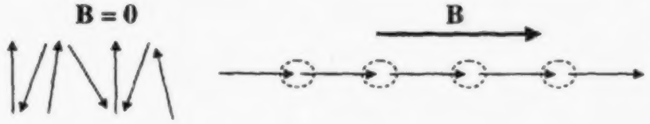

Magnetization of ferromagnetic materials

- Saturation magnetization is generally achieved at very high applied field B_0.
  - Magnetic domains - regions in which magnetic dipoles are aligned
- When a magnetic field is applied:
  - Favorably oriented domains grow at the expense of unfavorably oriented domains.
  - Orientation direction of dipoles in a domain can become closer to the field direction.

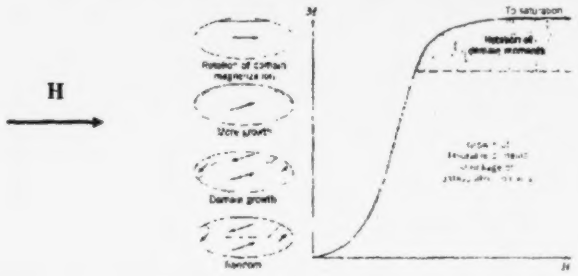

Ferromagnetism

- Magnetization curves are anisotropic
  - There is an easy direction of magnetization

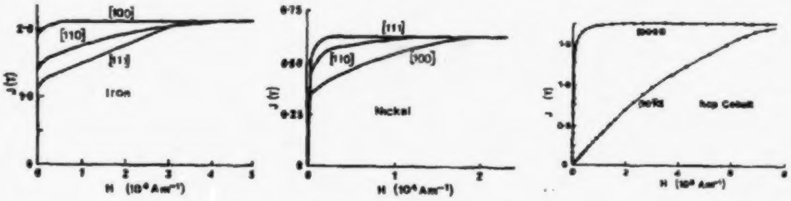

Magnetostriction

- When the magnetic electron spin dipole moments of the atoms in a solid are aligned, the length of the bonds between the atoms changes.
  - Shape and volume of a ferromagnetic solid change as it is magnetized.
- Magnetostriction = reversible strain along the axis of magnetization.
  - Usually saturates at the same time as magnetization
  - Anisotropic because:
    1) The magnetization curve is anisotropic
    2) Elastic properties are anisotropic.
  - Appears to provide the clearest magnetic indication of the stress state of a sample.

Magnetostriction - limitations

- Saturation magnetostriction is relatively low (max < 1%).
- Large fields are needed to induce appreciable strains (2 kOe)
- Useful frequency range is limited by development of eddy currents
- Materials are very brittle in tension.
- Terfenol-D - must be mechanically biased in compression.

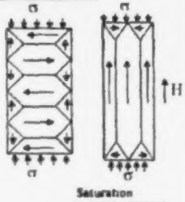

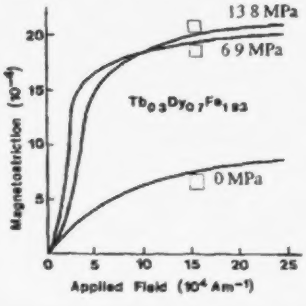

Material	Saturation magnetostriction λ_s (10^{-6})
Iron	−7
Fe−3 2% Si	+9
Nickel	−33
45 Permalloy, 45% Ni−55% Fe	+27
82% Ni−18% Fe Permalloy	0
Permendur, 49% Co−49% Fe−2% V	+70
87% Fe−13% Al Alfer	+30
Magnetite, Fe_3O_4	+40
Cobalt ferrite, $CoFe_2O_4$	−110
Cobalt ferrite, $Co_{1.1}Fe_{1.9}O_4$	−250
$SmFe_2$	−1560
$TbFe_2$	+1753
$Tb_{0.3}Dy_{0.7}Fe_{1.93}$ (Terfenol D)	+2000
$Fe_{66}Co_{18}B_{15}Si_1$ (amorphous)	+35
$Co_{72}Fe_3B_6Al_3$ (amorphous)	0

Magnetic Shape Memory Effect (MSME)

- **Magnetostriction** - expansion or contraction of interatomic bonds (elastic,0.2%)
- **MSME** - movement of twin boundaries in twinned martensite (plastic, 6%)
- Martensite:
  - Forms by a diffusionless transformation (no change in composition)
    - steels, nickel aluminum bronzes, NiMnGa, FeNiCoTi
  - Transformation from cubic to tetragonal structure
  - Transformed region appears coherent with the surrounding parent phase.
    - The habit planes are macroscopically undistorted, and are often irrational

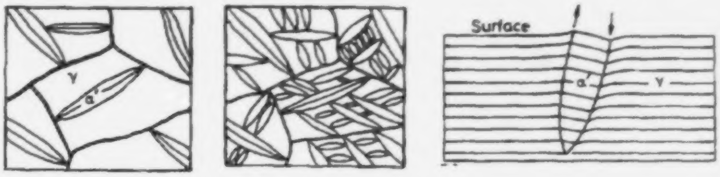

Martensite crystallography

- How do the invariant planes arise ???
- The strain on nucleation of a martensite region within the parent phase is accommodated (elastic energy is minimized) by a shear deformation:
  - slip
  - formation of an ensemble of twin variants
    - internally twinned martensite
    - more likely in a lath-type martensite morphology

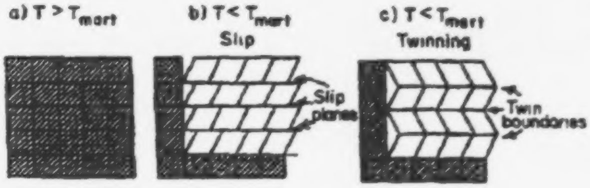

The magnetic shape memory effect

- If one twin type is favored over the other, the habit plane and the shape of the martensite plate must change.
- In MSM materials, there is a field-induced redistribution of the twin variants in the martensite.

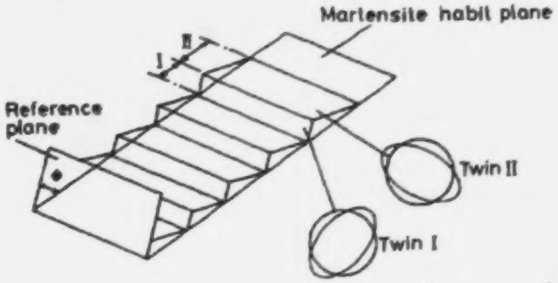
Martensite habit plane
II
I
Reference plane
Twin II
Twin I

The magnetic shape memory effect

- The MSM effect is only appreciable if the magnetic anisotropy is sufficiently high
  - It is easier to re-orient the crystal than to rotate the magnetization away from the easy axis
  - More likely to move twin boundaries than to rotate the magnetization within the unfavorably oriented internal twins

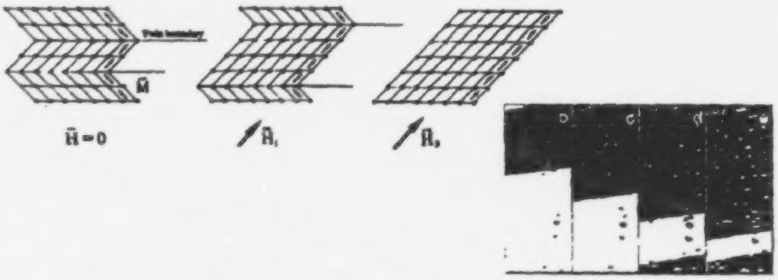
$\vec{M}$
$\vec{H} = 0$
$\vec{H}_1$
$\vec{H}_2$

Factors affecting the MSM effect

- Alloying elements
  - hinder twin boundary motion
  - stabilize martensite phase
  - favor lath or plate martensite morphology
  - affect T_C and M_S temperatures

Work output $\propto \frac{M_S^2 H^2}{4Ce_0^2}\left(1-\frac{M_S H}{4K_u}\right)$

- Plastic deformation prior to martensite formation
  - affect martensite morphology (heterogeneous nucleation)

Stress is limited by $M_S H$

- Prior austenite grain size
  - limit size of martensite laths
- Crystallographic texture
  - max strain for highly textured material (single crystal)
- Mechanical bias
  - max strain if starting structure consists only of unfavorable twin variant

---

Preliminary work

- Goal: to produce and test magnetostrictive and MSM materials
  - Polycrystals
  - Directionally solidified samples
- Made polycrystalline NiMnGa, FeAlGa
- Setup for directional solidification
- First lattice images of Terfenol-D

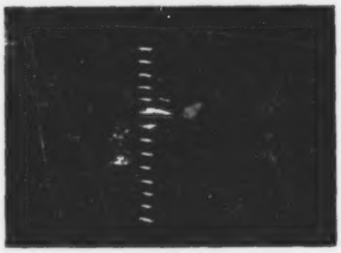

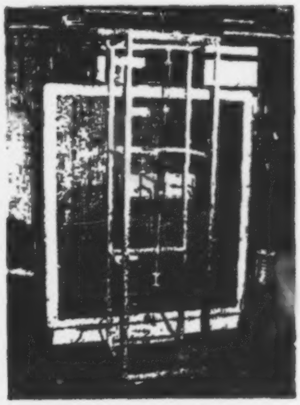

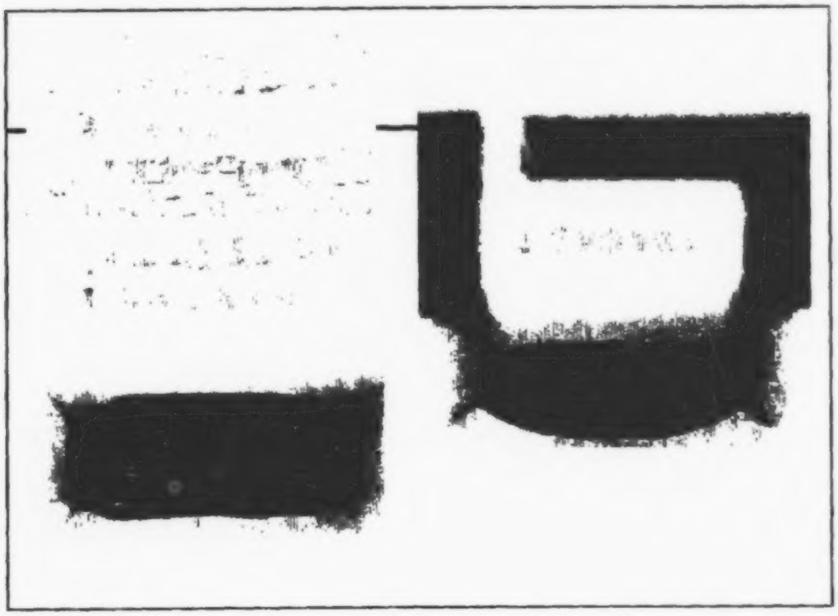

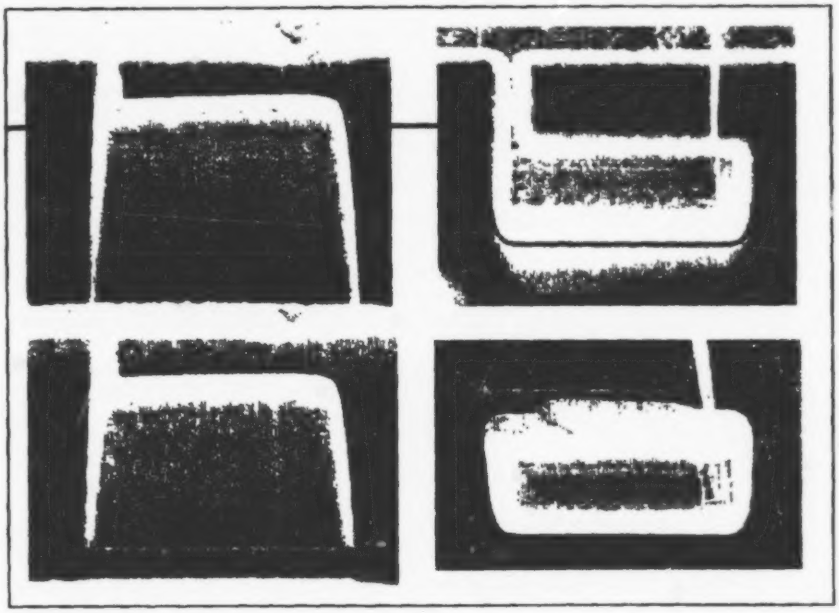

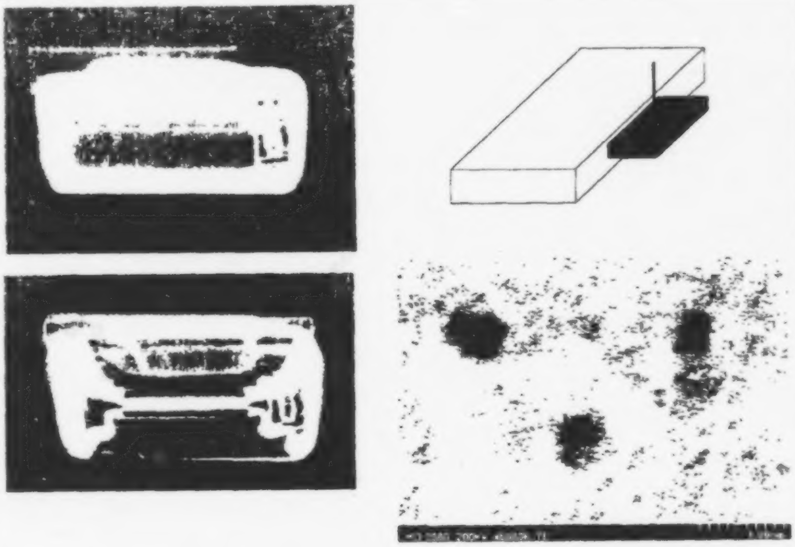

Summary - magnetostriction vs. MSM effect

- Field-induced strain is due to different processes.
  - MSM - twin boundary motion
    - Strain is tied to the crystallography
  - Magnetostrictives
    - Strain is tied to M (magnetization rotates relative to crystallography)
- Effects of magnetocrystalline anisotropy
  - MSM materials - field-induced strains increase with increasing magnetocrystalline anisotropy
  - Magnetostrictives - field-induced strains decrease with increasing magnetocrystalline anisotropy
- Saturation magnetization
  - Critical to both mechanisms
- Potential strains and energy density
  - MSM materials - up to ≈6% predicted, ≈715 kJ m^{-3}
  - Magnetostrictives - up to ≈0.2% achieved, ≈120 kJ m^{-3}

#516441 (26)

Application of Advanced Laser Consolidation Process for the Manufacturing of Complex FSP Shells

L. Xue, A. Theriault, M.U. Islam, C.J. Purcell*

Integrated Manufacturing Technologies Institute
National Research Council Canada
800 Collip Circle, London, Ontario N6G 4X8

*Defence Research Establishment Atlantic
9 Grove Street, P.O.Box 1012, Dartmouth, Nova Scotia B2Y 3Z7

Abstract

The Integrated Manufacturing Technologies Institute (IMTI) of NRC has developed a novel process called "Free-Form Laser Consolidation" that produces functional net-shape components layer by layer directly from CAD models by using a laser beam to melt and re-solidify the injected powder (or wire). As opposed to conventional machining processes, this computer-aided manufacturing (CAM) technology can build complete parts or features on an existing component by adding instead of removing material. IMTI has investigated laser consolidation of Fe-, Ni- and Co-base alloys, and the work is underway on Ti-alloys. Laser consolidated (LC) IN-625 is metallurgically sound, free of cracks or porosity. The "as-consolidated" IN-625 samples has surface finishes of the order of 1~2 •m (Ra) and dimensional accuracy of around 0.05 mm. The tensile properties of the laser-consolidated IN-625 alloy are comparable to the respective wrought materials. The microstructure of the laser-consolidated samples is similar to the rapidly solidified materials. Laser consolidation is a promising process for manufacturing functional net-shape components.

The folded shell projector (FSP) is a compact flextensional sound source being developed at DREA for low frequency sonar applications including active towed arrays and sonobuoys. The design radiates from a thin walled cylindrical shell with superimposed corrugations. The prototype was built by electroforming, followed by NC machining. This process was expensive and time-consuming, and offered limited choices for the shell material.

An investigation of the laser consolidation process for manufacturing the FSP shell was completed in FY 99/00. Advances in laser consolidation achieved by IMTI permit the free-form production of the FSP shell directly from a CAD file delivered over the Internet. Four shells have been built of IN-625 alloy to validate the process, and assembled into FSPs. The calibration results reveal that the laser consolidated FSPs show substantial improvements over the electroformed prototype. The investigation included changing the design of the shell during the program, proving that rapid design evolutions are readily accommodated since no hard tooling is required. The LC IN-625 shells have wall thickness typically 0.8 mm. The process parameters have been optimized for high accuracy and surface finish, with wall thickness tolerances in most sections of less than 0 02 mm.

Laser consolidation offers designers the possibility that soon they will be able to "print" functional prototypes directly from their computers. Being able to form complex components whose composition is changed as the part is being built up, represents a significant future opportunity for transducer designers. A key implication for defence manufacturing is that small production runs of thin wall superalloy parts will no longer have tooling as the main cost driver.

NRC · CNRC

Advanced Laser Consolidation Process for Manufacturing Complex FSP Shells

L. Xue, A. Theriault and M.U. Islam (NRC/IMTI)
C. Purcell (DRDC/DREA)

9th CF/DRDC Meeting on Naval
Applications of Materials Technology
June 5-7, 2001, Dartmouth, N.S.

NRC · CNRC

Outline:

- Introduction
  - process description, advantages, current state of the technology
- Functional Properties of LC Materials
  - accuracy, finish, strength, microstructure, etc.
- Manufacturing of FSP shells by Laser Consolidation
  - shell designs, data transfer, dimensional inspection, sensor assembling & testing
- Other Potential Applications of the Technology
- Implications for Defence
- Conclusions

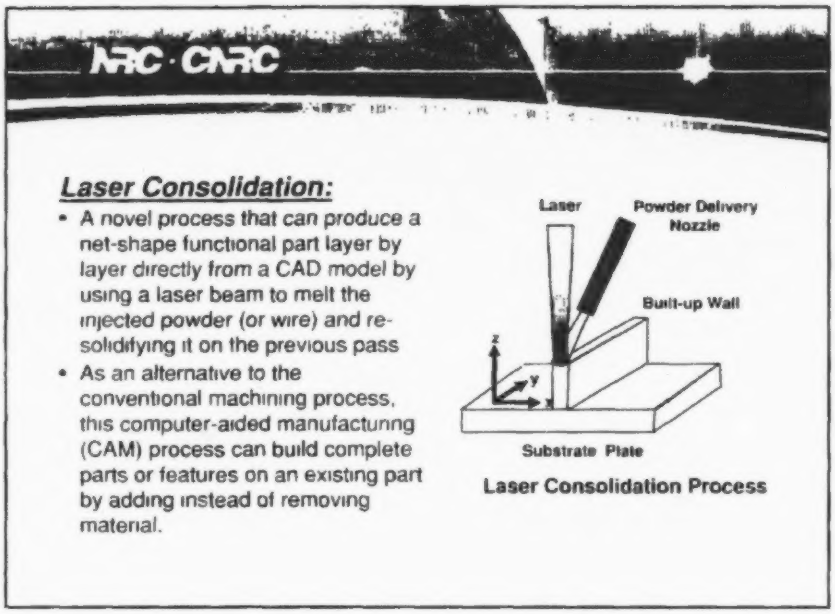

Laser Consolidation:

- A novel process that can produce a net-shape functional part layer by layer directly from a CAD model by using a laser beam to melt the injected powder (or wire) and re-solidifying it on the previous pass
- As an alternative to the conventional machining process, this computer-aided manufacturing (CAM) process can build complete parts or features on an existing part by adding instead of removing material.

Laser Consolidation Process

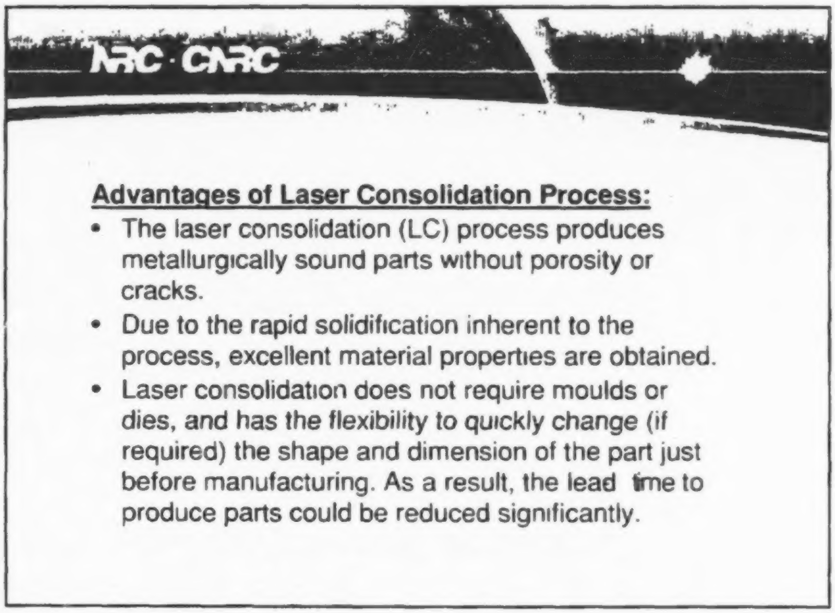

Advantages of Laser Consolidation Process:

- The laser consolidation (LC) process produces metallurgically sound parts without porosity or cracks.
- Due to the rapid solidification inherent to the process, excellent material properties are obtained.
- Laser consolidation does not require moulds or dies, and has the flexibility to quickly change (if required) the shape and dimension of the part just before manufacturing. As a result, the lead time to produce parts could be reduced significantly.

NRC · CNRC

IMTI's Laser Consolidation - Dimensional Accuracy

Hollow Square Tube:

Wall Thickness - 0 775 ± 0 025 mm
Wall Height - 20 785 ± 0 38 mm
Parallelness - 0 048 mm (opposite walls)
Squareness - 90 00° ± 0 02°
Perpendicularity - 89 92° ± 0 15°

Cylinder:

Cylinder ID - 37.041 ± 0.048 mm
Cylinder OD - 38 631 ± 0 033 mm
Height - 20 790 ± 0 069 mm
Circularity - ± 0 043 mm (ID & OD)

Conical Sample with 10° angle:

Angle - 9 93° ± 0 07°
Circularity - ± 0 043 mm (ID & OD)

Note: Samples were made from IN-625 alloy powder All values are averages of at least 6 measurements.

- **LC IN-625 samples showed excellent dimensional accuracy and surface finish.**

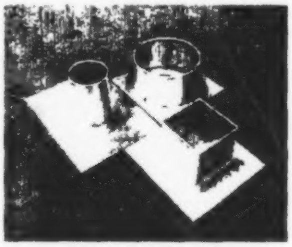

Surface Finish - 1-2 μm Ra

NRC · CNRC

Laser Consolidation - Mechanical Properties

- **The LC IN-625 material is stronger than the respective cast materials and comparable to wrought materials.**

Materials		$\sigma_{0.2}$ (MPa)	σ_{UTS} (MPa)	δ (%)
LC IN-625	Horizontal	518±9	797±8	31±2
	Vertical	477±10	744±20	48±1
Cast IN-625		350	710	48
Wrought IN-625		490	855	50

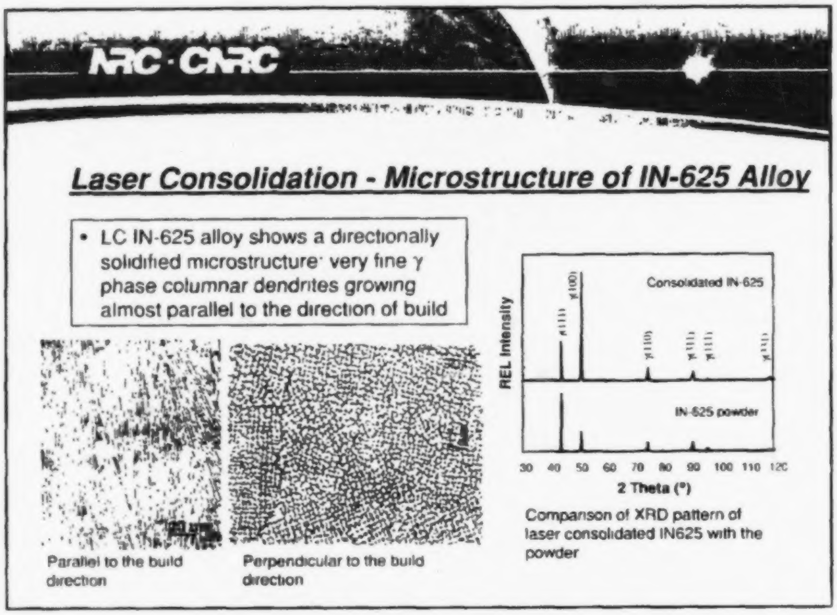
NRC · CNRC
REL Intensity
γ(111)
γ(100)
Consolidated IN-625
IN-625 powder
30 40 50 60 70 80 90 100 110 120
2 Theta (°)
20 μm

Laser Consolidation - Microstructure of IN-625 Alloy

- LC IN-625 alloy shows a directionally solidified microstructure: very fine γ phase columnar dendrites growing almost parallel to the direction of build

Parallel to the build direction

Perpendicular to the build direction

Comparison of XRD pattern of laser consolidated IN625 with the powder

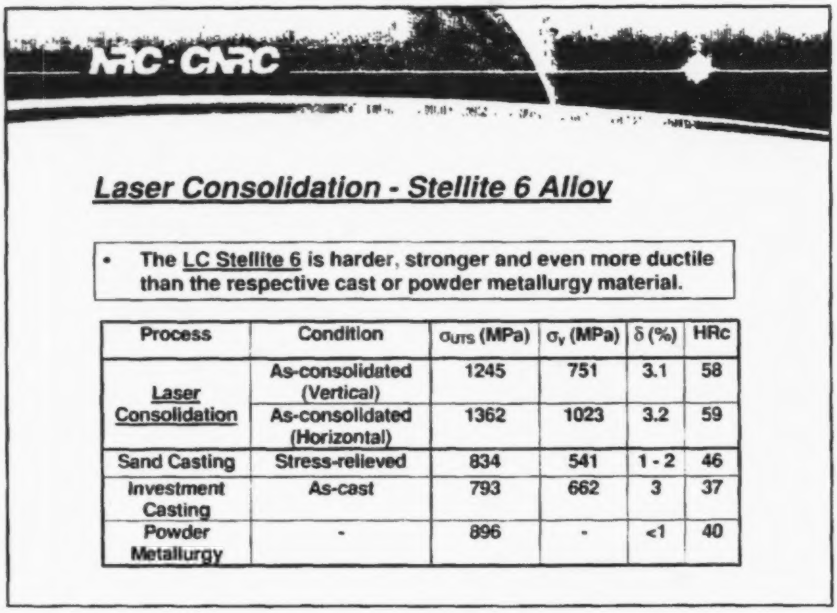

Laser Consolidation - Stellite 6 Alloy

- **The LC Stellite 6 is harder, stronger and even more ductile than the respective cast or powder metallurgy material.**

Process	Condition	σ_{UTS} (MPa)	σ_y (MPa)	δ (%)	HRc
Laser Consolidation	As-consolidated (Vertical)	1245	751	3.1	58
	As-consolidated (Horizontal)	1362	1023	3.2	59
Sand Casting	Stress-relieved	834	541	1 - 2	46
Investment Casting	As-cast	793	662	3	37
Powder Metallurgy	-	896	-	<1	40

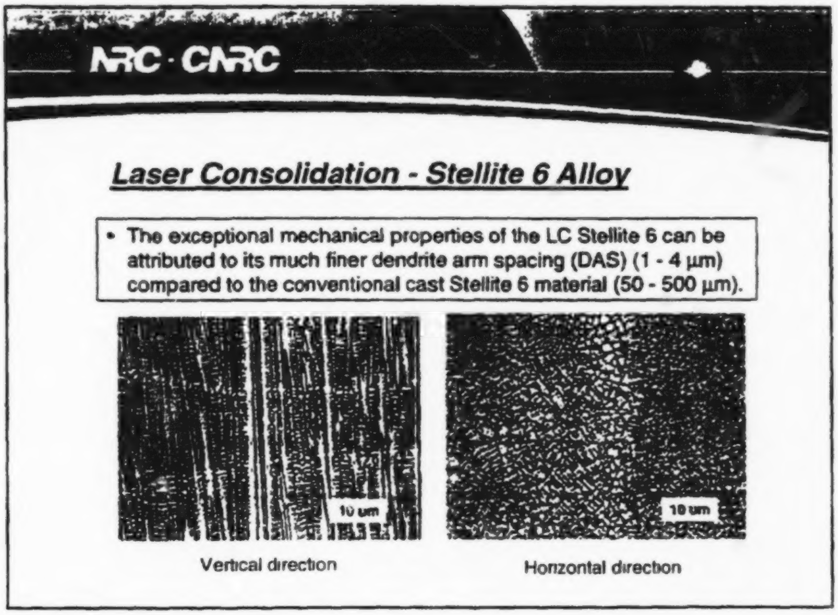

NRC · CNRC

Laser Consolidation - Stellite 6 Alloy

- The exceptional mechanical properties of the LC Stellite 6 can be attributed to its much finer dendrite arm spacing (DAS) (1 - 4 μm) compared to the conventional cast Stellite 6 material (50 - 500 μm).

Vertical direction

Horizontal direction

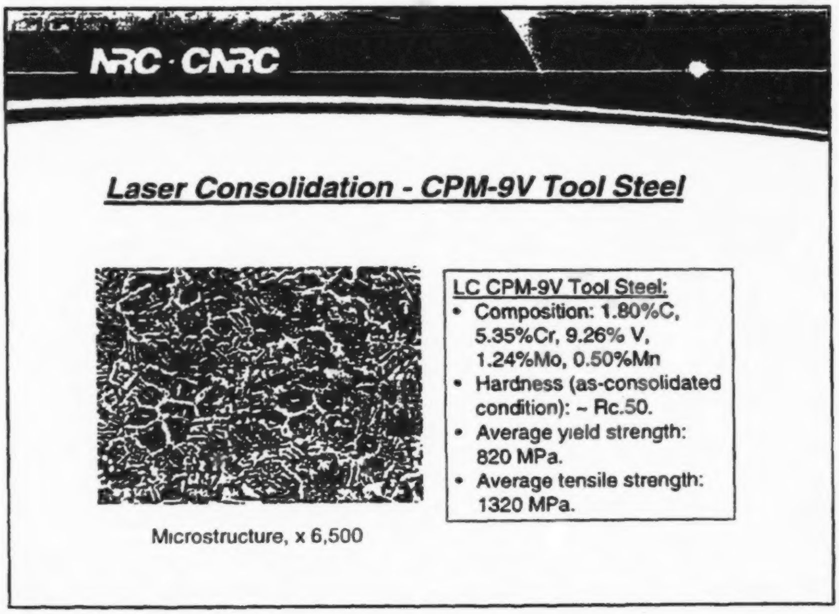

NRC · CNRC

Laser Consolidation - CPM-9V Tool Steel

Microstructure, x 6,500

LC CPM-9V Tool Steel:

- Composition: 1.80%C, 5.35%Cr, 9.26% V, 1.24%Mo, 0.50%Mn
- Hardness (as-consolidated condition): ~ Rc.50.
- Average yield strength: 820 MPa.
- Average tensile strength: 1320 MPa.

NRC · CNRC

Laser Consolidation - CPM-9V Tool Steel

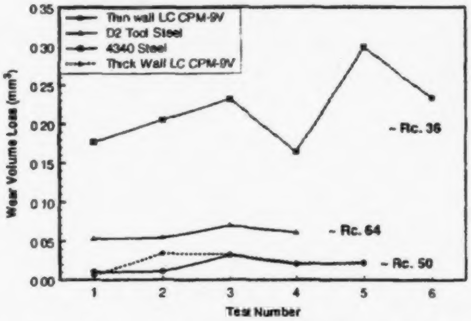

- **Under test conditions, the wear resistance of LC CPM-9V is almost triple compared to heat treated D2 and almost one order of magnitude better compared to 4340 steel.**

Pin-on-disk wear test against 1/4" WC ball under 500g load at 0.28m/s for 8000m.

NRC · CNRC

Laser Consolidation - Residual Stresses

- The LC IN-625 material exhibits significant magnitude of residual compressive stresses along the horizontal direction, while the residual compressive stresses along the vertical direction is relatively low.

Method	Residual Stress (MPa)	
	Horizontal Direction	Vertical Direction
X-Ray Diffraction	-412	-147
Hole-Drilling	-349	-42

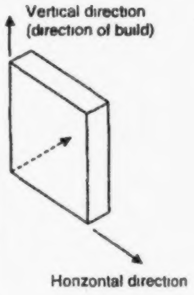

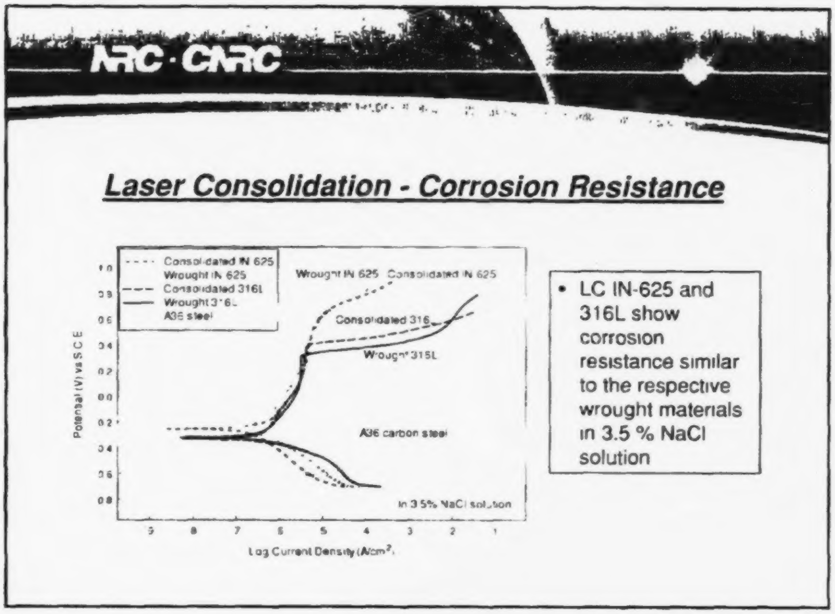

Laser Consolidation - Corrosion Resistance

- LC IN-625 and 316L show corrosion resistance similar to the respective wrought materials in 3.5 % NaCl solution

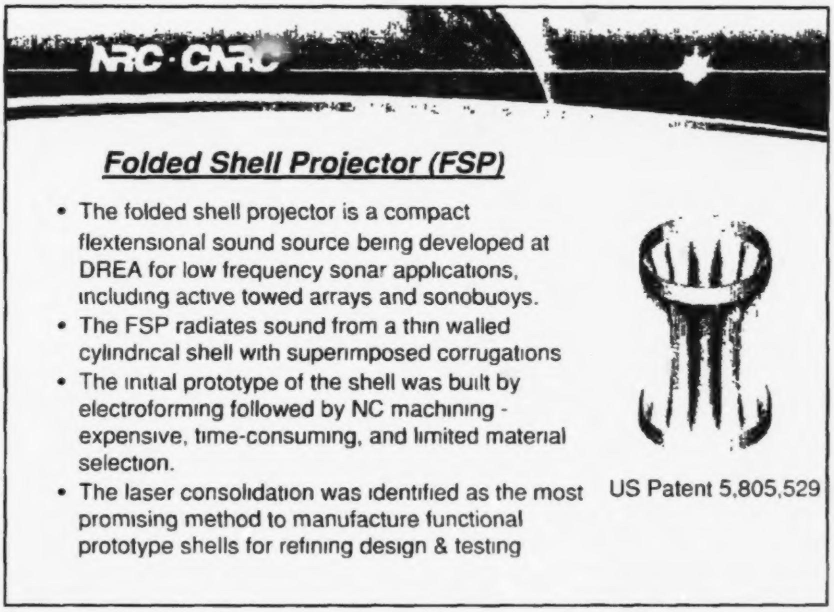

Folded Shell Projector (FSP)

- The folded shell projector is a compact flextensional sound source being developed at DREA for low frequency sonar applications, including active towed arrays and sonobuoys.
- The FSP radiates sound from a thin walled cylindrical shell with superimposed corrugations
- The initial prototype of the shell was built by electroforming followed by NC machining - expensive, time-consuming, and limited material selection.
- The laser consolidation was identified as the most promising method to manufacture functional prototype shells for refining design & testing

US Patent 5,805,529

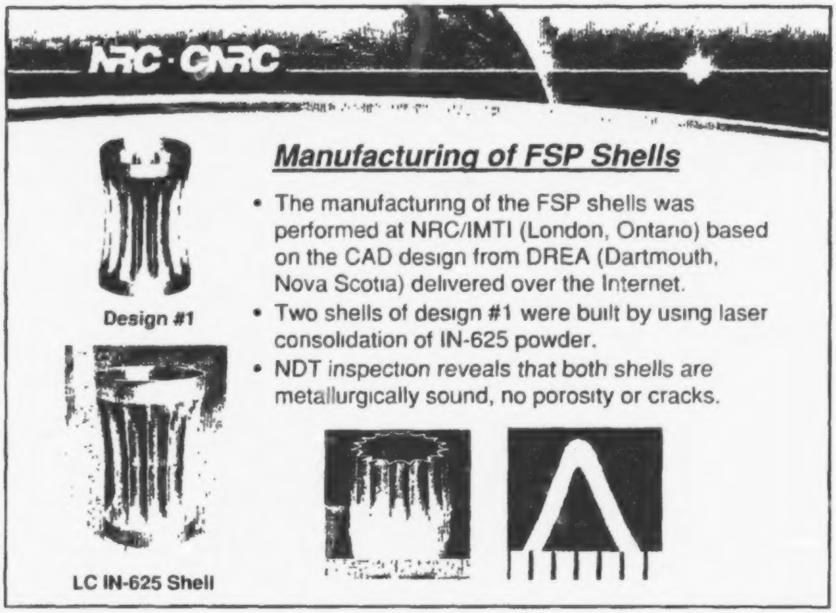

NRC · CNRC

Manufacturing of FSP Shells

- The manufacturing of the FSP shells was performed at NRC/IMTI (London, Ontario) based on the CAD design from DREA (Dartmouth, Nova Scotia) delivered over the Internet.
- Two shells of design #1 were built by using laser consolidation of IN-625 powder.
- NDT inspection reveals that both shells are metallurgically sound, no porosity or cracks.

Design #1

LC IN-625 Shell

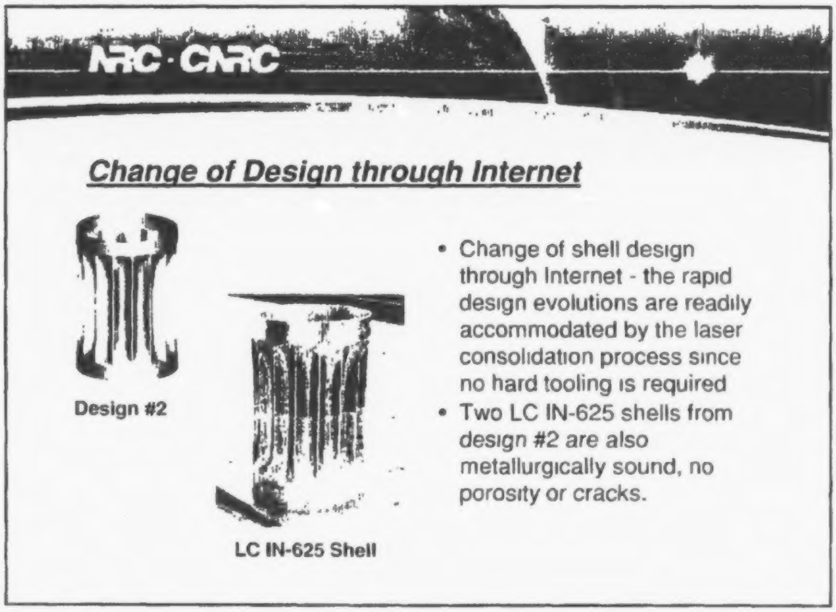

NRC · CNRC

Change of Design through Internet

- Change of shell design through Internet - the rapid design evolutions are readily accommodated by the laser consolidation process since no hard tooling is required
- Two LC IN-625 shells from design #2 are also metallurgically sound, no porosity or cracks.

Design #2

LC IN-625 Shell

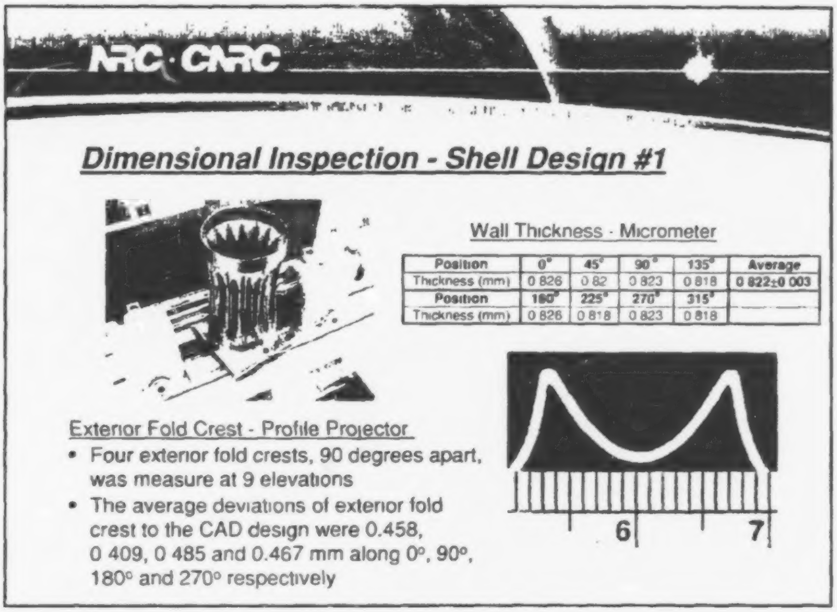

NRC·CNRC

Dimensional Inspection - Shell Design #1

Wall Thickness - Micrometer

Position	0°	45°	90°	135°	Average
Thickness (mm)	0 826	0 82	0 823	0 818	0 822±0 003
Position	180°	225°	270°	315°	
Thickness (mm)	0 826	0 818	0 823	0 818	

Exterior Fold Crest - Profile Projector

- Four exterior fold crests, 90 degrees apart, was measure at 9 elevations
- The average deviations of exterior fold crest to the CAD design were 0.458, 0 409, 0 485 and 0.467 mm along 0°, 90°, 180° and 270° respectively

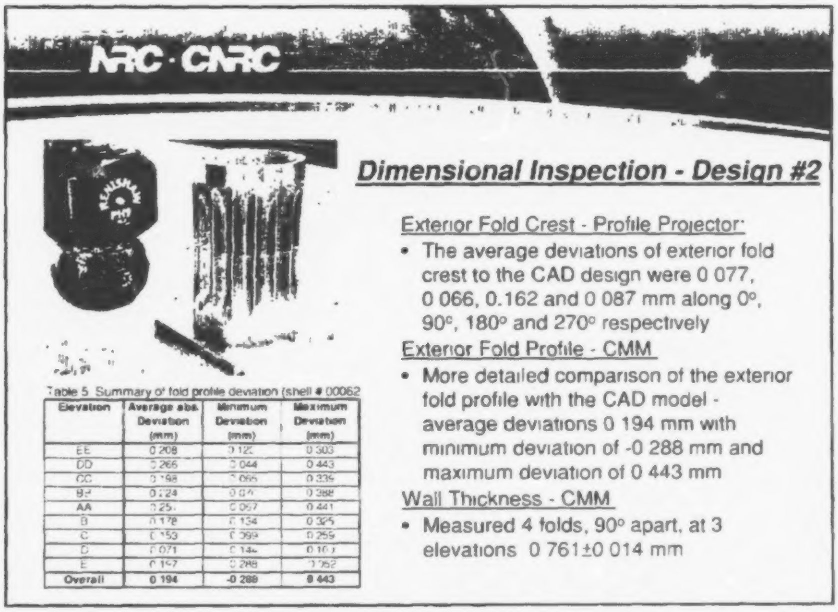

NRC·CNRC

Dimensional Inspection - Design #2

Table 5 Summary of fold profile deviation (shell # 00062

Elevation	Average abs. Deviation (mm)	Minimum Deviation (mm)	Maximum Deviation (mm)
EE	0 208	[illegible]	0 303
DD	0 266	0 044	0 443
CC	0 198	0 066	0 339
BB	0 224	[illegible]	0 388
AA	0 251	0 057	0 441
B	0 178	0 134	0 325
C	0 153	0 099	0 259
D	0 071	0 144	[illegible]
E	0 157	0 288	[illegible]
Overall	0 194	-0 288	0 443

Exterior Fold Crest - Profile Projector:

- The average deviations of exterior fold crest to the CAD design were 0 077, 0 066, 0.162 and 0 087 mm along 0°, 90°, 180° and 270° respectively

Exterior Fold Profile - CMM

- More detailed comparison of the exterior fold profile with the CAD model - average deviations 0 194 mm with minimum deviation of -0 288 mm and maximum deviation of 0 443 mm

Wall Thickness - CMM

- Measured 4 folds, 90° apart, at 3 elevations 0 761±0 014 mm

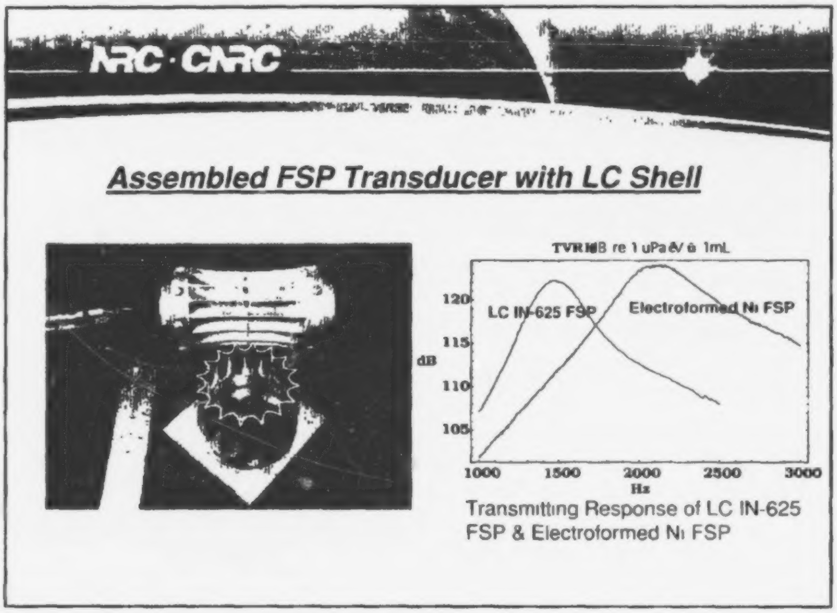

NRC · CNRC

Assembled FSP Transducer with LC Shell

TVR dB re 1 uPa/V @ 1m
120
115
110
105
dB
LC IN-625 FSP
Electroformed Ni FSP
1000
1500
2000
2500
3000
Hz

Transmitting Response of LC IN-625 FSP & Electroformed Ni FSP

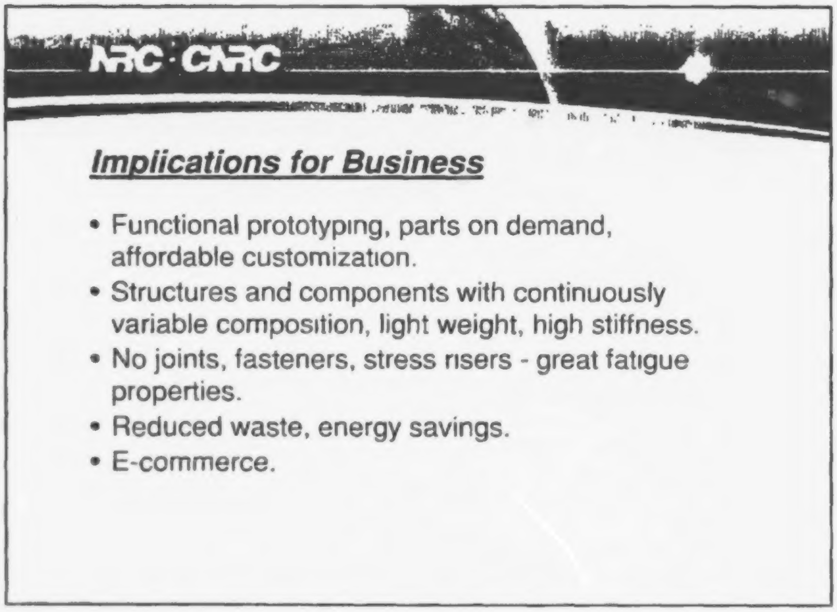

NRC · CNRC

Implications for Business

- Functional prototyping, parts on demand, affordable customization.
- Structures and components with continuously variable composition, light weight, high stiffness.
- No joints, fasteners, stress risers - great fatigue properties.
- Reduced waste, energy savings.
- E-commerce.

NRC · CNRC

Potential Applications in Defence Area

Laser consolidation/cladding and other laser based technologies may have many potential applications in the defence areas to improve equipment performance, shorten prototyping cycle, and reduce maintenance cost and time:

- Navy - functional prototyping, build spare parts and repair expensive parts
- Air force - repair turbine blades, build parts, etc.
- Army - functional prototyping, build spare parts and repair expensive parts

---

NRC · CNRC

Summary:

- NRC/IMTI has developed a unique laser consolidation process and is currently leading the technology development for producing high quality net shape components (2 patents obtained and 1 pending).
- By using laser consolidation process, fully functional complex FSP shells were produced and design changes were incorporated quickly – this proves that laser consolidation can have many potential applications in the defence areas .
- NRC/IMTI will like to work collaboratively with DND/DRDC to further explore its applications in defence related areas and to transfer this exciting new manufacturing technology to Canadian industry suppliers for DND.

#516442 (27)

The Effects Of Decaying Marine Organisms On The Corrosion Of Copper-Nickel Alloys In Sea Water

by

D. R. Lenard and R. R. Welland

Defence Research Establishment Atlantic Dockyard Laboratory (Pacific)
CFB Esquimalt
PO BOX 17000 STN FORCES VICTORIA BC V9A 7N2

Abstract

Recent changes in construction techniques and operational practice have resulted in a number of failures of copper-nickel components in sea water systems, including perforation of 70/30 heat exchanger tubes that was attributed to exposure to sulfide-polluted, stagnant sea water during shutdowns. In an effort to understand the mechanism of these failures, 70/30 copper-nickel specimens were exposed to flowing sea water until protective films were developed. Some of the specimens were then buried in organic debris that had been allowed to accumulate at the bottom of the tank. These specimens were then re-exposed to flowing sea water after two weeks. Corrosion rates were monitored throughout the experiment using linear polarization resistance. The corrosion rate increased by an order of magnitude when the specimens were re-exposed to flowing sea water. The results also suggest that repair of damaged protective films may take longer than initial film formation.

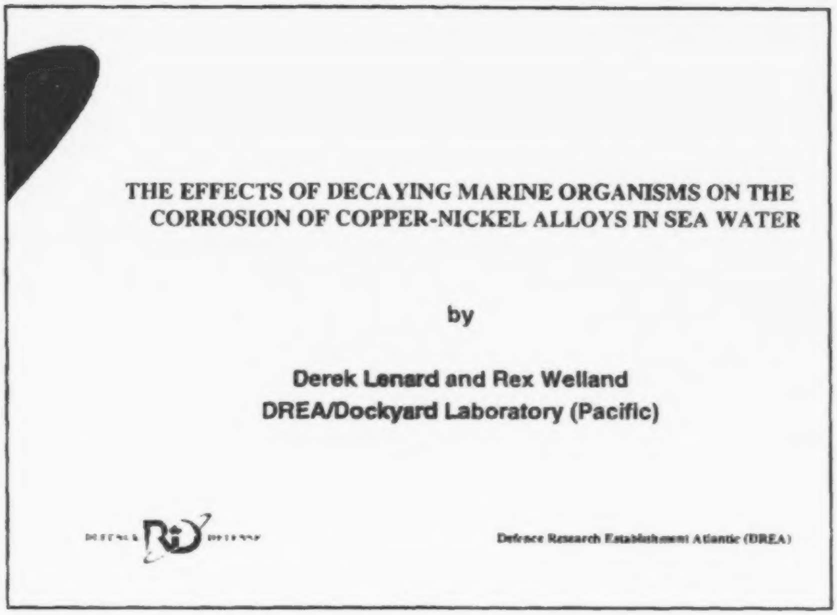

THE EFFECTS OF DECAYING MARINE ORGANISMS ON THE CORROSION OF COPPER-NICKEL ALLOYS IN SEA WATER

by

Derek Lenard and Rex Welland
DREA/Dockyard Laboratory (Pacific)

Defence Research Establishment Atlantic (DREA)

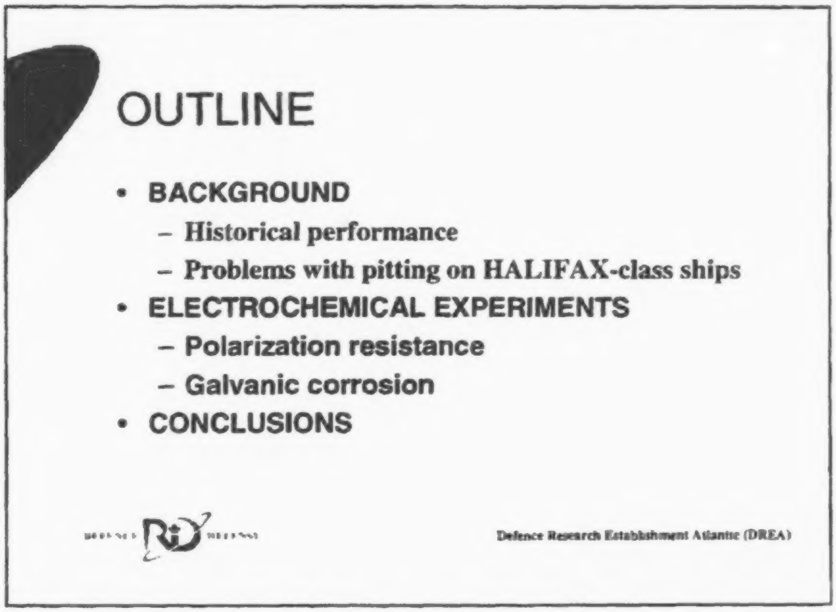

OUTLINE

- **BACKGROUND**
  - **Historical performance**
  - **Problems with pitting on HALIFAX-class ships**
- **ELECTROCHEMICAL EXPERIMENTS**
  - **Polarization resistance**
  - **Galvanic corrosion**
- **CONCLUSIONS**

Defence Research Establishment Atlantic (DREA)

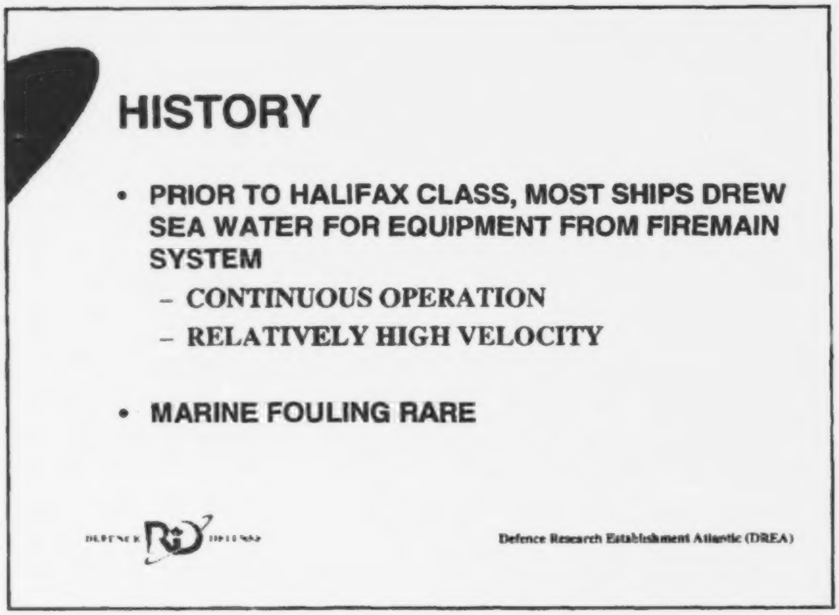

HISTORY

- PRIOR TO HALIFAX CLASS, MOST SHIPS DREW SEA WATER FOR EQUIPMENT FROM FIREMAIN SYSTEM
  - CONTINUOUS OPERATION
  - RELATIVELY HIGH VELOCITY
- MARINE FOULING RARE

Defence Research Establishment Atlantic (DREA)

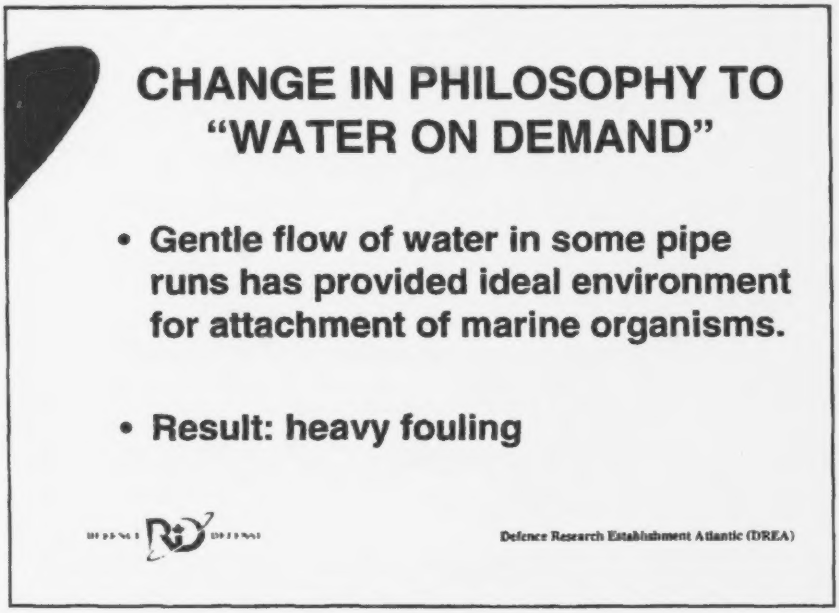

CHANGE IN PHILOSOPHY TO "WATER ON DEMAND"

- Gentle flow of water in some pipe runs has provided ideal environment for attachment of marine organisms.
- Result: heavy fouling

Defence Research Establishment Atlantic (DREA)

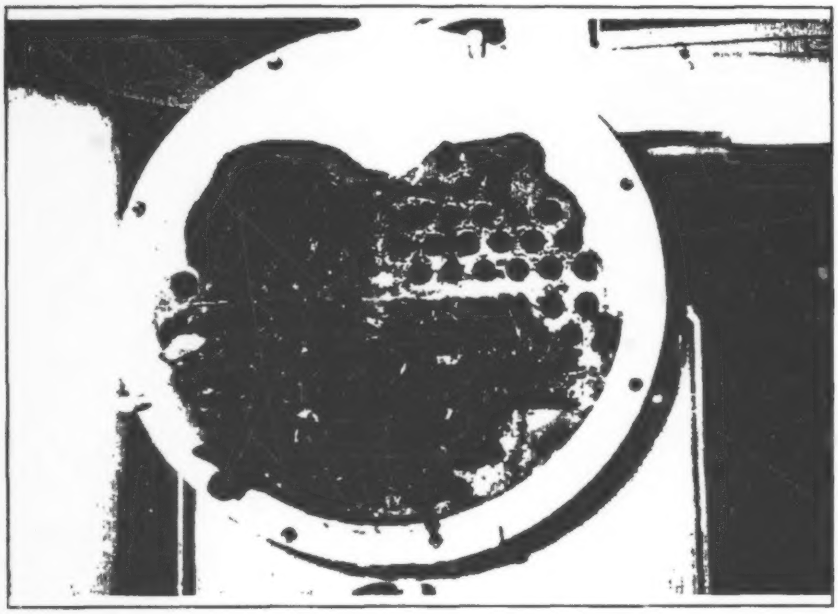

- Blockage on the supply side of a chiller 3 months after a previous cleaning. Most of the material consisted of the remnants of mussels and hydroids that were killed by exposure to fresh water during a visit to Portland, OR. The dead shells broke away from other parts of the system and were trapped at the tube plate. However, this material formed a base for new growth and live four-day old mussels were found in the debris in mid-December, well outside their normal attachment season.

CHANGE IN PHILOSOPHY TO "WATER ON DEMAND"

- Sea water flow shut off when equipment not in use. Fouling organisms die from lack of oxygen.
- Sulfides released from decaying organisms interfere with protective films on Cu-Ni alloys.

Defence Research Establishment Atlantic (DREA)

PITTING OF 70-30 COPPER-NICKEL

- IN ADDITION TO CAUSING OTHER PROBLEMS, HAS FOULING CONTRIBUTED TO PITTING OF 70-30 COPPER-NICKEL ALLOYS?
- PITTING FAILURES HAVE OCCURRED IN DIESEL LUBE OIL COOLERS, AIR EMISSION COOLERS AND HYDRAULIC OIL COOLERS.
- WHAT IS THE MECHANISM?

Defence Research Establishment Atlantic (DREA)

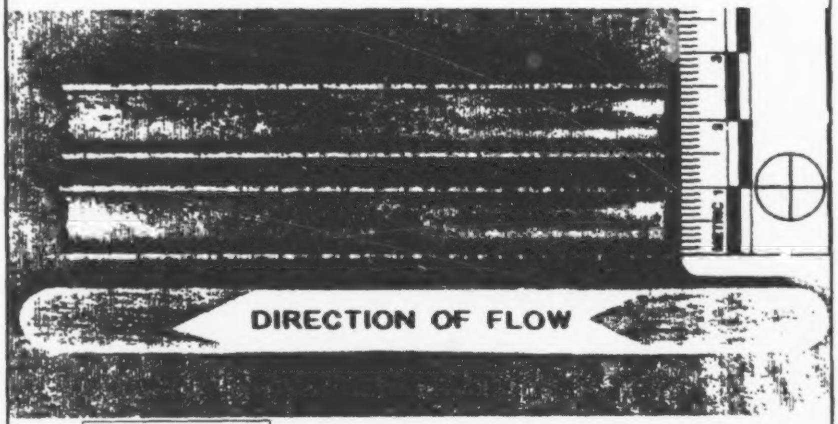

PITTING IN A HYDRAULIC OIL COOLER

- Leak developed after 15 months
- Constant flow of sea water through cooler at sea.
- Flow shut off in port, leaving cooler full of stagnant sea water.
- Temperature of oil entering cooler normally 30 - 40 Celsius
- If temperature reaches 65 C, alarm activated: never happened.

Defence Research Establishment Atlantic (DREA)

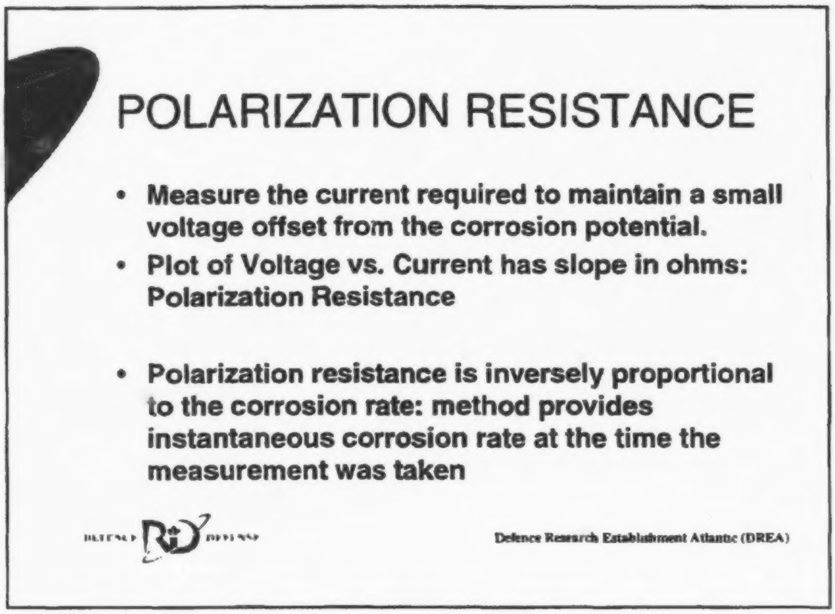

POLARIZATION RESISTANCE

- **Measure the current required to maintain a small voltage offset from the corrosion potential.**
- **Plot of Voltage vs. Current has slope in ohms: Polarization Resistance**
- **Polarization resistance is inversely proportional to the corrosion rate: method provides instantaneous corrosion rate at the time the measurement was taken**

Defence Research Establishment Atlantic (DREA)

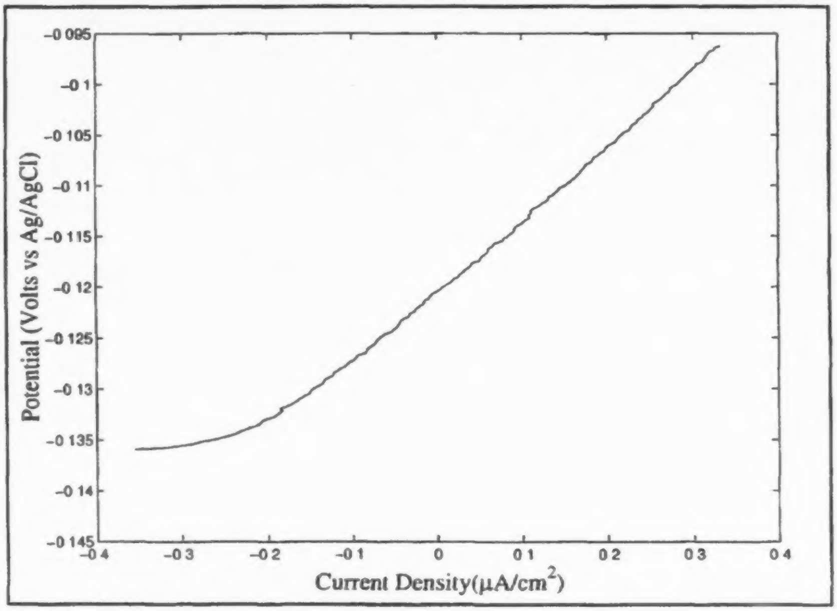

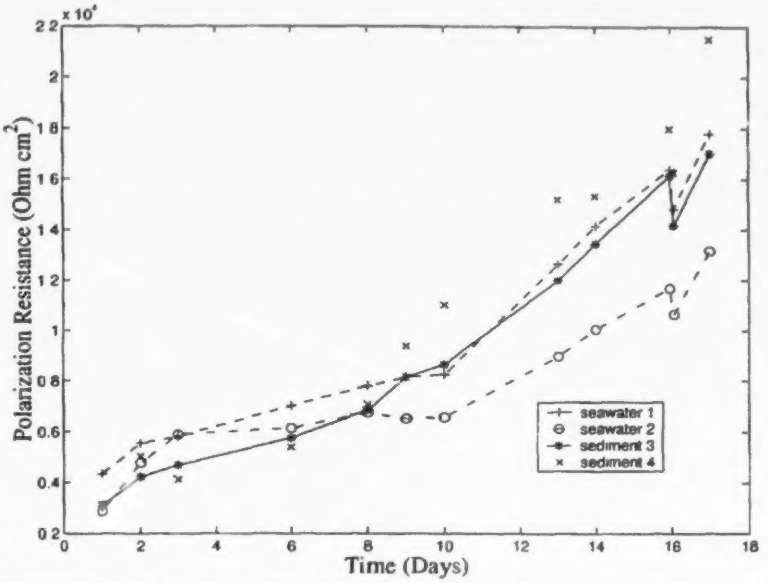

- Polarization resistance measurements for 4 specimens of 70-30 Cu-Ni that, at this point, had been continuously exposed to flowing sea water. Observe the decrease in polarization resistance (increase in corrosion rate) that occurred on Day 16, one hour after the sea water delivery pumps were changed. The switchover introduced a small amount of sulfide (from marine organisms that have died in the stagnant line) into the water in the tank for a few minutes. Note that, in this case, the interruption in the development of the protective film is temporary and any damage is repaired by continuing exposure to clean sea water.

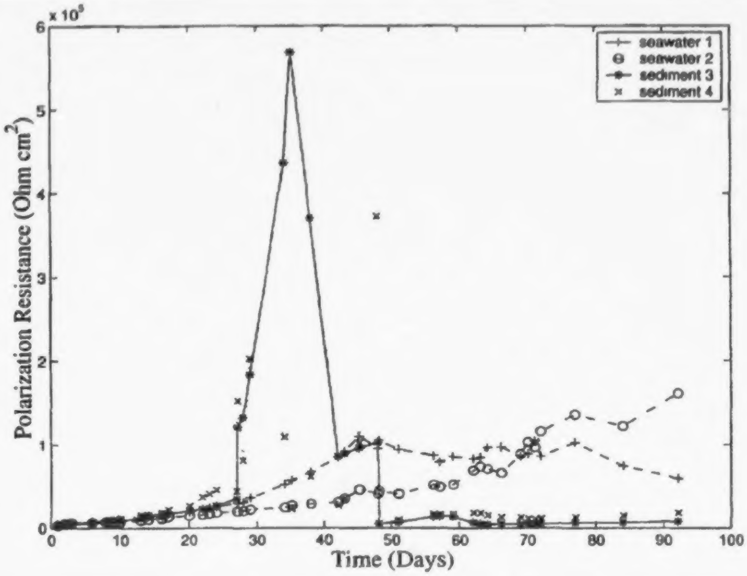

- Polarization resistance measurements for 4 specimens of 70-30 Cu-Ni. Until Day 27, all specimens were exposed to clean, flowing sea water, with the brief exception of the introduction of a small amount of sulfide on Day 16, as described in a previous slide. On Day 27, specimens 3 and 4 were lowered into organic debris that had been allowed to accumulate at the bottom of the exposure tank. The immediate increase in polarization resistance (decrease in corrosion rate) is associated with the lack of oxygen in the sediment. The sediment was loosely packed and had little effect on the solution resistance (iR drop). On Day 48, specimens 3 and 4 were lifted back into the flowing sea water.

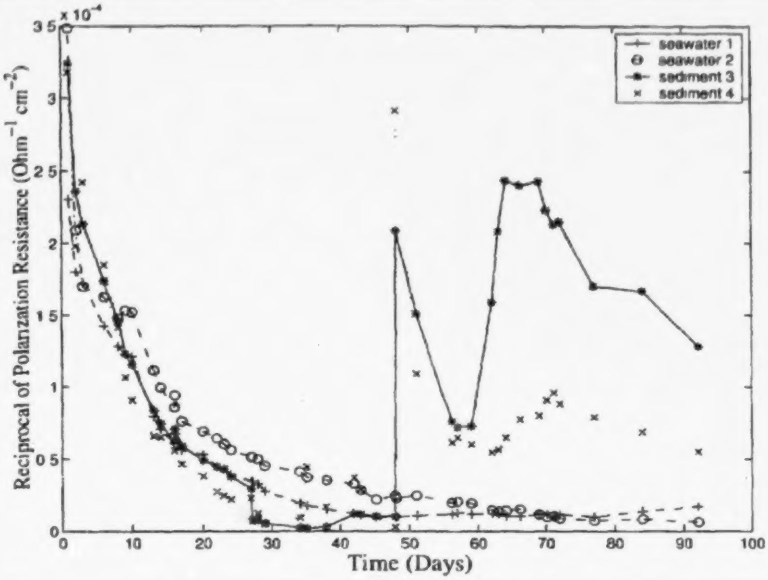

- Same data as previous graph, but y-axis converted to reciprocal of polarization resistance, which is directly proportional to corrosion rate. Note the sharp increase in corrosion rate when specimens 3 and 4 are re-exposed to flowing sea water. They show at least an order of magnitude higher corrosion rates than the control specimens that were continuously exposed to flowing sea water. Furthermore, these specimens do not develop protective films as quickly as they did when first exposed to sea water at the start of the experiment. Fully protective films did not develop even after another 45 days of exposure to flowing sea water.

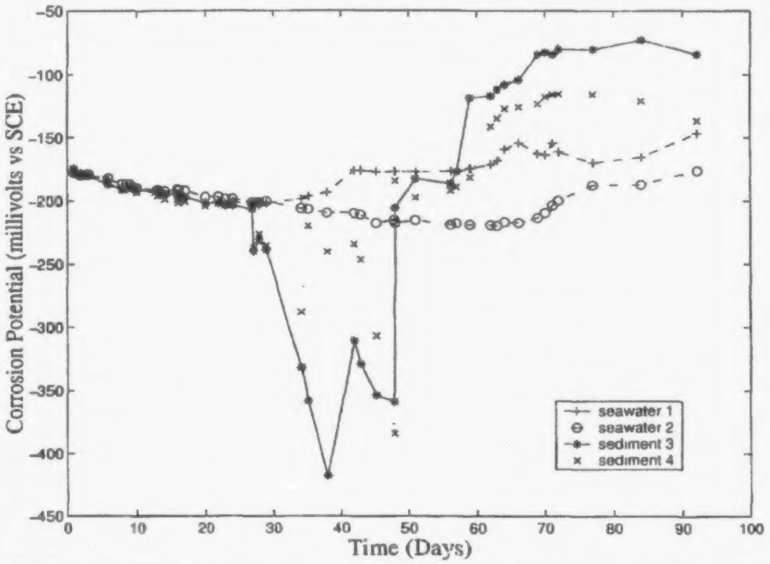

- Plot of corrosion potential for the specimens described on the previous two pages. The shift in corrosion potential for specimens 3 and 4 between Day 27 and Day 48 results from the anaerobic conditions in the sediment. The fluctuations in corrosion potential during this time period suggest the possibility of biological activity within the sediment.

GALVANIC CORROSION

- **USE "ZERO-RESISTANCE AMMETER" TO MEASURE CURRENT FLOW BETWEEN INDIVIDUAL SPECIMENS IN A PAIR AS A RESULT OF DIFFERENT EXPOSURE CONDITIONS.**
- **ATTEMPT TO DETERMINE CONDITIONS UNDER WHICH GALVANIC CORROSION WILL OCCUR**

- Specimens of 70-30 Cu-Ni that were 1 cm wide by 18 cm long were coated with two coats of an underwater epoxy paint so that 1 cm^2 of Cu-Ni was exposed on one side. Pairs of specimens were placed in the sea water tank so that the exposed faces were 2 cm apart as shown in the next photograph. All specimens exposed to flowing sea water for 21 days. Of the six pairs, on Day 21, two sets of pairs were lowered into the organic debris and for three pairs, only one specimen in each pair was lowered into the debris. The sixth pair served as a control and remained exposed to flowing sea water. After another 21 days, one specimen from each pair was lifted back into the flowing sea water. A silver-silver chloride reference electrode was placed between each specimen pair.

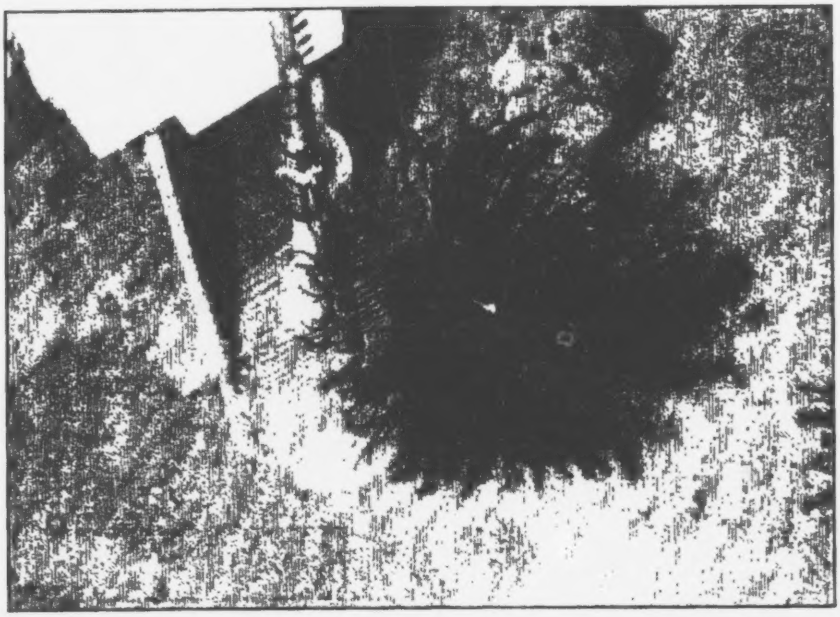

- General arrangement for measuring galvanic corrosion. In the above photograph, fecal matter from a sabellid worm (Eudistylia vancouveri) can be seen to be contributing to the organic debris on the bottom of the tank.

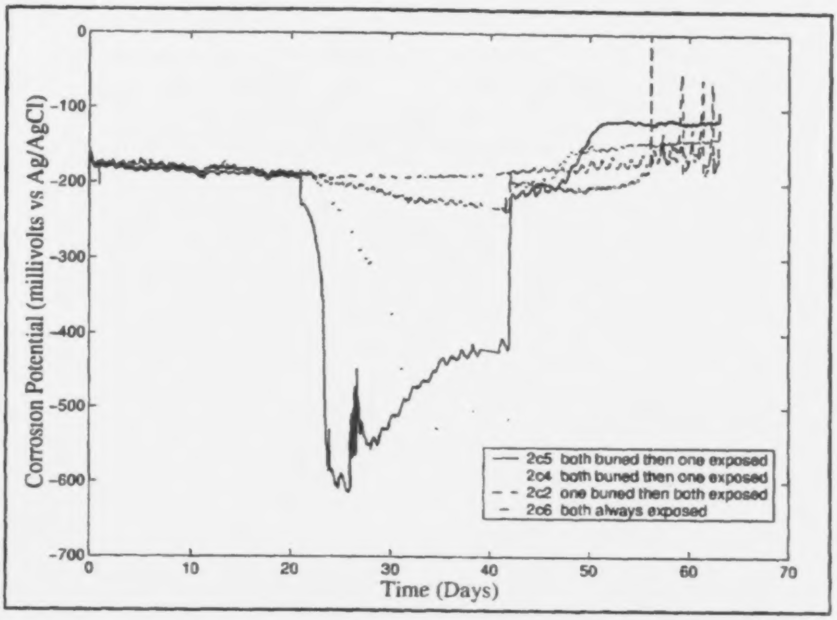

- As observed during the polarization resistance measurements, there was a marked shift in the corrosion potential for the two pairs of specimens for which both members of the pair had been lowered into the debris between Day 21 and Day 42. No such dramatic shift was observed for any of the three pairs in which only one specimen was lowered into the debris or for the control. The sharp spikes in the potential for specimen 2c2 (dotted line) after Day 56 were caused by a sea cucumber (Eupentacta quinquesemita) crawling up and down the reference electrode.

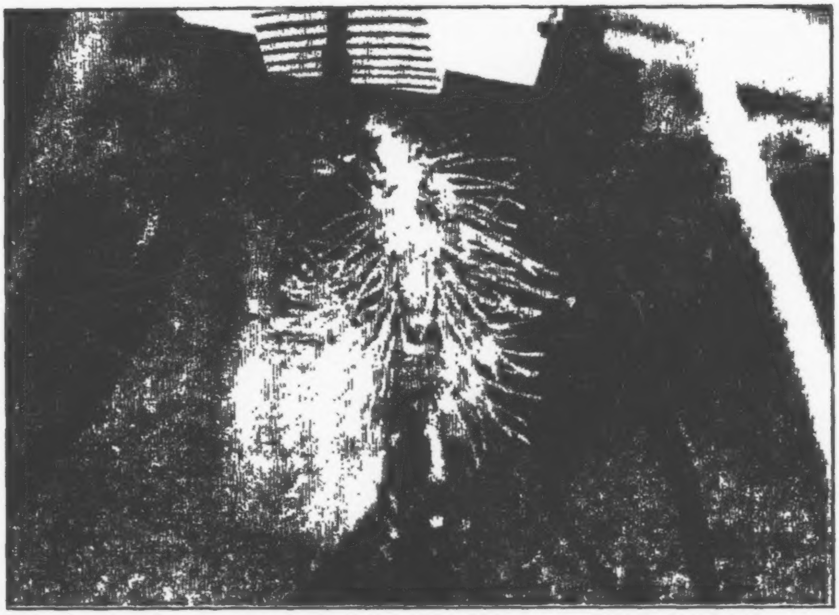

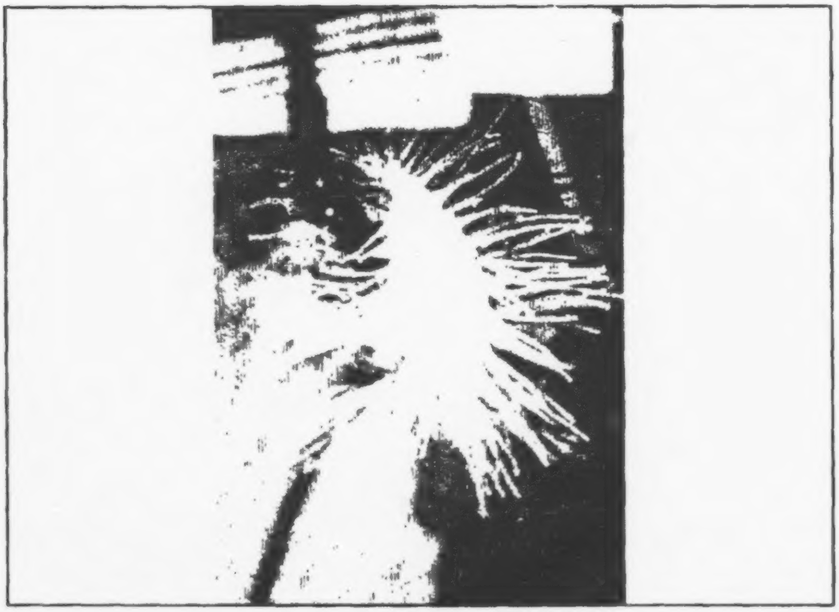

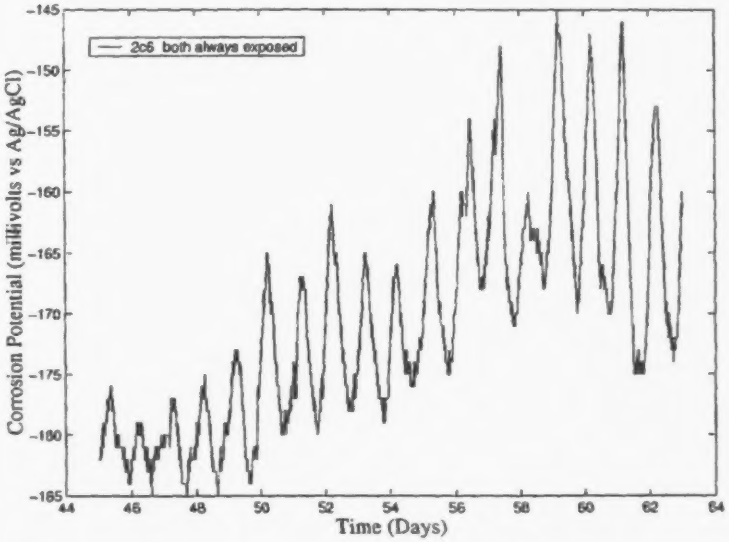

- Blow up of the region of the previous graph between Day 45 and Day 63 for the control cell (2c6). The daily variation is presumed to be caused by variations in the oxygen concentration as a function of biological activity.

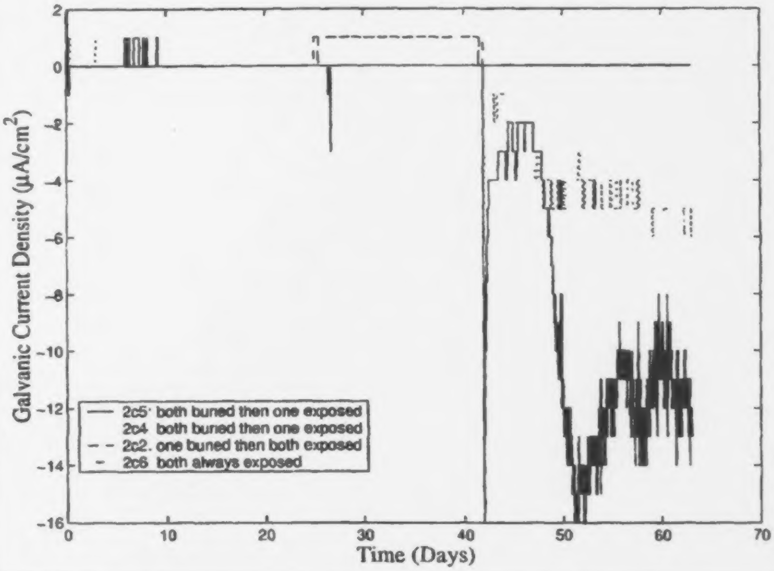

- Substantial galvanic current was observed for the two pairs of specimens in which both members of the pair had been buried in the organic debris (2c4 and 2c5). This current was observed as soon as one member of each pair was lifted back into the flowing sea water and persisted throughout the remainder of the experiment. The direction of current was determined to be such that the specimen that remained buried in the sediment suffered accelerated corrosion. This conclusion was supported by the fact that the specimens in these pairs that were lifted back into the sea water were rapidly fouled, indicating that the cathodic protection resulting from the galvanic current prevented the release of copper ions, which have biocidal properties, from these specimens

Defence Research Establishment Atlantic (DREA)

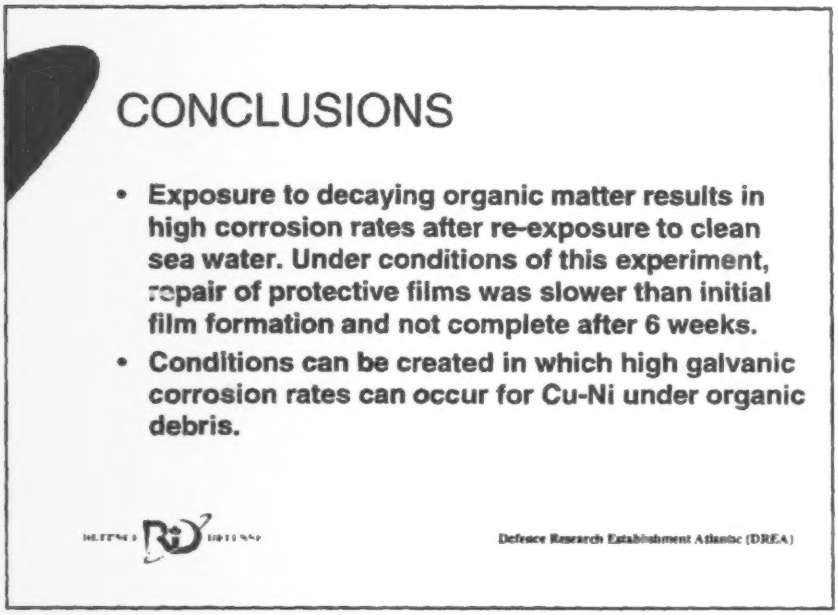

CONCLUSIONS

- **Exposure to decaying organic matter results in high corrosion rates after re-exposure to clean sea water. Under conditions of this experiment, repair of protective films was slower than initial film formation and not complete after 6 weeks.**
- **Conditions can be created in which high galvanic corrosion rates can occur for Cu-Ni under organic debris.**

Defence Research Establishment Atlantic (DREA)

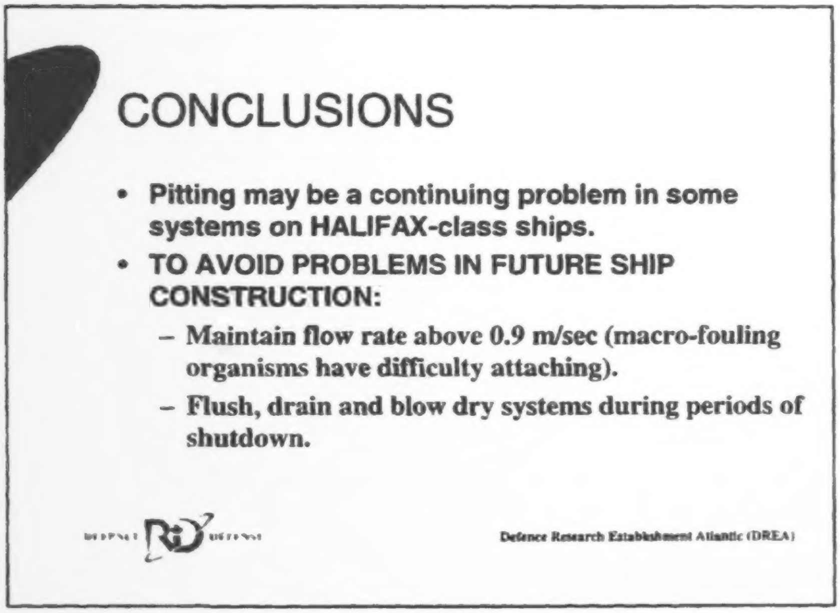

CONCLUSIONS

- **Pitting may be a continuing problem in some systems on HALIFAX-class ships.**
- **TO AVOID PROBLEMS IN FUTURE SHIP CONSTRUCTION:**
  - **Maintain flow rate above 0.9 m/sec (macro-fouling organisms have difficulty attaching).**
  - **Flush, drain and blow dry systems during periods of shutdown.**

Defence Research Establishment Atlantic (DREA)

#516443 (38)

An Overview of the DREA Program for Modelling Impressed Current Cathodic Protection Systems

KarisAllen, K.J.[1], Brennan, D.[2], MacKay, K.D.[2] and Porter, J.F.[3]

ABSTRACT: A comprehensive program was conducted to develop two independent methodologies for generating hull potential profiles for impressed current cathodic protection systems (ICCP). The two methodologies developed were physical scale modelling (PSM) and computer simulations using CPBEM and BEASY boundary element software suites. A 1/100 scale model of the Canadian Patrol Frigate (CPF) was fabricated and instrumented for comparison with the computer simulations. The results indicate that both CPBEM and BEASY computer simulations were in good agreement with the potentials generated by the PSM/ICCP model. For the quiescent tests conducted, the potentials predicted by CPBEM and BEASY were generally within 15 millivolts and 35 milivolts of the PSM potentials, respectively. For the dynamic tests conducted, both CPBEM and BEASY produced potentials within 35 millivolts of the PSM potentials.

1. INTRODUCTION

1.1 General

Paint and preservation combined with cathodic protection is the mainstay of preventative measures employed by marine engineers for the interior and exterior corrosion protection of marine hull forms. The Canadian Navy has historically been a world leader in the development of innovative hardware for marine based cathodic protection (CP) systems. However, the design of these cathodic protection systems is still based on past experience, empirical relationships and engineering judgement. Owing to this inexact method of designing CP systems, a majority of the systems designed for marine hull forms have required modifications to correct various deficiencies. These deficiencies lead to increased current requirements in order to adequately protect the hull. Also, empirical design often results in areas of over protection and under protection which leads to increases in long term maintenance costs.

A typical impressed current cathodic protection system (ICCP) consists of three parts; the structure to be protected (cathode), the anode which provides the protection, and the electrolyte (i.e. seawater). For mobile marine based platforms, the anode is normally fixed to the hull of the structure. A reference electrode is also fixed to the hull in a position remote to the anode. The potential at the reference electrode is maintained at a predetermined level by adjusting the potential at the anode via a suitable feedback control system. The focus of this study is to develop two independent methodologies for the generation of ICCP hull potential profiles.

[1] Research Engineer, FACTS Engineering, PO Box 20039 Halifax, NS, Canada, B3R 2K9
[2] Research Engineer, Martec Ltd., 1888 Brunswick St. Halifax, NS, Canada, B3J 3J8
[3] Defence Scientist, DREA, PO Box 1012, Dartmouth, NS, Canada, B2Y 3Z7

1.2 Physical Scale Modelling

Physical scale modelling of cathodically protected marine structures provides acceptable approximations of global hull potential profiles. It has been shown that large structures subjected to cathodic polarization can be physically modelled by maintaining a linear relationship between the model size (ie 1/100 scale) and electrolytic medium conductivity. As a first approximation, the hull form is modelled as a perfectly coated system (ie electrically insulating). This is usually accomplished by fabricating the hull of the model from insulating materials such as FRP or PVC. In this configuration, polarization of the uncoated propeller surface area accounts for a majority of the current demand from the ICCP system. The anode current required to protect the hull increases as hull velocity increases. Under normal service conditions, this is the result of the increased rate of oxygen transfer to the cathodic surfaces. Incorporating hull velocity effects into physical scale modelling is usually accomplished by dimensionally modelling fluid velocity.

The Canadian Patrol Frigate (CPF), the structure of interest for this study, is cathodically protected using a two zone impressed current system. The forward zone consists of two impressed current anodes with a controlling reference electrode located forward with respect to the anodes. The stern zone is again comprised of two anodes located in front of the propellers with the reference electrode controlling the anodes located aft of the propellers (designated as aft-aft). Optionally, the aft anodes can be controlled using a reference electrode (designated as mid-aft) located between the forward and aft anodes. While both zones are controlled independently from each other, potential fields interact throughout the center portion of the ship. For this study, replication of the CPF control system was adopted. The system was configured with two independently controlled zones with PID logic controlling anode currents based on predetermined reference electrode potentials. Also, several non-controlling reference electrodes were located along the longitudinal axis of the model to provide a more detailed map of the global hull potential profile.

The production of the physical scale model is a multi-step procedure. First, a 1/100 scale male PSM plug was manufactured using a CAD/CAM facility and the line offsets for the structure. The male plug was constructed from high density styrofoam. Once completed, the exterior surface of the plug was coated with a layer of fibreglass mesh adhered to the plug using an epoxy resin to increase the damage tolerance of the plug. In the second step, a female mould was fabricated by suspending the male mould (plug) in a prefabricated casting box using a commercially available casting mortar. In the final step, the physical scale model was fabricated using the female mould. To provide the through hull penetrations required to instrument the model with reference electrodes and anodes, a lattice structure, which was laid on top of the mould and referenced to the bow of the model, was constructed. Polished steel rods were inserted through holes machined into this lattice where a hull penetration was required (see Figure 1). Once the model was fully cast using a cold cure epoxy, it was allowed to fully cure prior to removal from the mould. The through hull penetrations were subsequently machined to remove any spurs formed during the casting process. Imperfections observed on the hull surface were filled with an epoxy based filler.

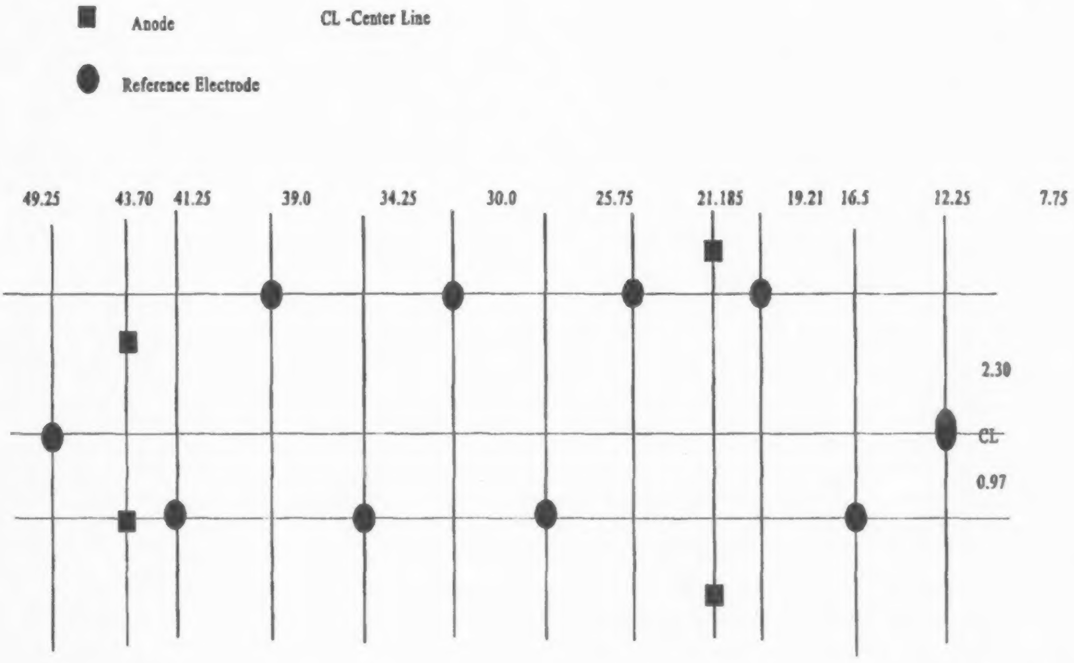

Note: All Dimensions Shown are in Inches

Figure 1 - Anode and reference electrode sensor positions for the PSM model constructed

Two nickel aluminium disks 44 mm in diameter and 3 mm in thickness were machined to simulate the propeller area. The disks were attached to a constant speed AC motor via an epoxy coated steel shaft and ratio pulleys to provide the desired rotational velocity to the disks. Controlling the rotational velocity of the disks was achieved by varying the ratio of the drive pulleys. The disk shafts penetrated the rear wall of the PSM/ICCP flow tank (as opposed to penetrating the model) owing to the constructional simplicity afforded by this approach.

1.3 Computer Modelling

A number of investigators have been applying various computational methods to the design of cathodic protection systems. The basic mathematical problem is defined by the Laplace equation and is straightforward to solve. A detailed discussion of the Laplace equation and the boundary conditions as applied to cathodic protection and galvanic corrosion analysis can be found in publications by Zamani et al. [1,2] and Brebbia and Dominquez [3]. An excellent state-of-the-art survey article outlining the development of finite difference, finite element and boundary element methods for galvanic analysis has been prepared by Munn [4]. The advantage of the finite difference method is its reduced storage requirements, but its disadvantage is that curved or oblique boundaries cannot be readily accommodated. Because of the flexibility of its element shapes and orientations, the finite element method is more suitable for problems with complex geometries or with inhomogeneous material (electrolyte) properties. The main disadvantage is its inability to represent infinite domains. The boundary element method provides direct solutions for boundary points only (solutions at other points are obtained as a post-processing step) and for that reason is more suitable for modelling infinite domains. Its advantage over finite element methods reduces as domain boundary complexity increases. BEASY-CP, a software program developed and marketed by Computational Mechanics Inc. of Billerica, Maine and the CPBEM program developed by Defence Research Establishment Atlantic are two typical boundary element software packages that can be used by the designer to predict the potential levels both on a structure and in the electrolyte, and to determine the current levels on the structure and anodes.

The analysis problem under consideration will be the prediction of the electric potential distribution in an electrolyte medium due to the presence of submerged dissimilar metals or externally applied impressed currents. The conservation of charge within an electrolyte is the basis of the mathematical formulation used in cathodic protection analysis. The governing equilibrium equation reduces to the Laplace equation expressed in terms of the electrical potential for certain idealized conditions. The Laplace equation is valid for steady state conditions, a uniform homogenous electrolyte, and no charge sources or sinks in the electrolyte.

Several improvements have recently been incorporated into the CPBEM code to achieve an increasingly precise modelling of the propeller that serves as a cathode. Originally, the propeller was approximated by an arbitrary strip of boundary element panels at the aft end of the ship hull. Collectively, these panels had approximately the same area as the surface area of the propeller blades. The strip form of the cathode provided a reasonable approximation of the potential current densities everywhere except in aft portions of the ship near the cathode strip. Unfortunately, in practice some severe corrosion problems developed in that area of the ship hull. Consequently, the propeller strip was replaced by an approximation of an actual propeller in order to improve the resulting potentials on the portion of the hull near the propeller. Two forms of propeller approximation were considered. The simpler of the two was a disk that was approximately equivalent to the actual propeller. This type of propeller model was used by De Giorgi et al. [5]. The second propeller approximation was a detailed propeller model with five distinct blades. Both approximations showed conditioning problems as blade thickness was decreased which necessitated the implementation of a hypersingular boundary element formulation within CPBEM. In the second propeller approximation, some simplification in the shape of the propeller blades was also required in order to achieve convergence.

2.0 EXPERIMENTAL PROGRAM

2.1 Procedure for Generating Potentiodynamic Polarization Resistance Data

Analytical modelling requires electrochemical data for the relevant materials systems as part of the input data. The information required is generated by conducting polarization resistance measurements for the structural material systems under service conditions. In the case of CPF, the hull form is coated 350 WT and the propellers are manufactured from nickel aluminium bronze (NAB). The propellers are left uncoated and thus generate the majority of the current requirements for the aft zone of the system. Hull velocities can range from static conditions to approximately 30 knots. The kinetics of the reactions governing the polarization resistance of these materials are dependent on velocity of the seawater passing along the hull and over the propellers. It, therefore, becomes necessary not only to produce static flow polarization curves, but also dynamic flow polarization resistance curves for these materials

Initial PSM trials used an epoxy hull form combined with NAB propellers. Thus, for these comparison trails, only NAB polarization resistance data was required as input data to the computational model. NAB specimens were machined with a diameter of 9.50 mm and a height of 12.70 mm. Dielectric epoxy was applied to the bottom surface of specimens tested at velocity to maintain constant velocity conditions over the exposed surface area for the rotating tests. Prior to conducting a test sequence, the exposed specimen surface area was polished to a 600 grit finish. The polarization resistance instrumentation was verified using 430 stainless steel calibration specimens tested in accordance with the procedure detailed in ASTM G-5.

Prepared NAB specimens were immersed in an electroylte of naturally occurring seawater for testing. Once immersed, the specimens were preexposed under open circuit potential conditions for 55 minutes, at which time the open circuit potential was recorded. Subsequent to preexposure, an impressed current potential sweep of -0.6 V/hr was impressed at the reference electrode to generate the polarization resistance relationship for the material. Tests were conducted for specimen rotational velocities tested ranging from quiescent flow conditions to approximately 2.33 m/s. Specimen current requirements and saturated calomel reference electrode potentials were digitized with 16 bits of resolution and bussed to a microprocessor for subsequent post processing.

2.2 Physical Scale Modelling (PSM) Procedure

The following section details the experimental procedure conducted prior to and during the PSM trials. Prior to inserting the ten Ag/AgCl reference electrodes into the model, the accuracy of each reference electrode was verified by checking the open circuit potential against a precision grade saturated calomel electrode. Once calibration of each electrode was verified, it was inserted into the appropriate hull penetration in the epoxy model so that the sensor tip was flush with the outer surface of the model. Four high density graphite impressed current anodes (two aft and two forward) were inserted in the remaining hull penetrations. Once inserted and positioned, the electrodes/anodes were sealed into the model using a silicone based sealant to minimize the egress of seawater from any incomplete fit between the model and the electrode/anodes. Prior to sealing the top of the model tank, the NAB propeller disk surfaces were polished using 600 grit emery paper. The top of the PSM tank with the model attached was then sealed and the reference electrodes and the anodes were connected to the close coupled hardware using shielded coax wire with BNC connections. To provide a check on the aft and forward currents being recorded by the microprocessor based data acquisition system, an analog current meter was placed in series between the anode and the close coupled hardware.

Prior to initiating the testing sequence, The PSM inner tank was filled with 1/100 (approx 400 μmho/cm) scale electrolyte with naturally occurring seawater as the base. The inner tank water circulation and the aeration pumps were activated for 24 hours prior to testing to ensure oxygen saturation of the electrolyte.

Four ICCP test configurations were evaluated using the PSM facility. Table 1 contains the details of the reference electrode combinations used during the trials. The four combinations chosen were selected to approximate the current configurations available to CPF ICCP operators. For each configuration, three applied potentials (at the appropriate controlling reference electrode) were evaluated, namely -0.6V, -0.8V and -1.0V with respect to a Ag/AgCl reference. At each applied potential, the ten reference electrode voltages and two anode currents were recorded for subsequent analysis.

Table 1 - Experimental test matrix for ICCP/PSM model configurations.

Configuration No.	Reference Electrode Controlling Forward Anodes	Reference Electrode Controlling Aft Anodes	Propeller Velocity (RPM)
1	Ref 2	Ref 10 (aft-aft)	0
2	Ref 2	Ref 8 (mid-aft)	0
3	Ref 2	Ref 10 (aft-aft)	3450
4	Ref 2	Ref 8 (mid-aft)	3450

3.0 RESULTS AND DISCUSSION

3.1 Polarization Resistance Results

The graphs in Figures 2 and 3 show the combined (triplicate trial) potentiodynamic polarization resistance data collected for the nickel aluminum bronze specimen tests with naturally occurring seawater as the electrolytic medium for the quiescent and 2.33 m/s flow conditions, respectively. For the quiescent cathodic polarization resistance tests conducted, the current density increased from approximately 2 μA/cm^2 to 100 μA/cm^2 as the applied potential was increased from -300 mV to -600 mV verses a saturated calomel reference electrode (SCE). From -600 mV to 1100 mV only a minimal increase was observed in the current density. As the applied potential was increased above 100 mV the current density again resumed an increasing relationship. As the seawater velocity was increased to 2.33 m/s the magnitude of the current density at the -600 mV knee showed an increasing trend from 100 μA/cm^2 for quiescent flow to 1500 μA/cm^2 at 2.33 m/s.

In general, from the tests conducted, the ASTM G-5 potentiodynamic test procedure showed excellent reproducibility. The triplicate tests conducted at each combination of test variables showed only minimal variation between tests.

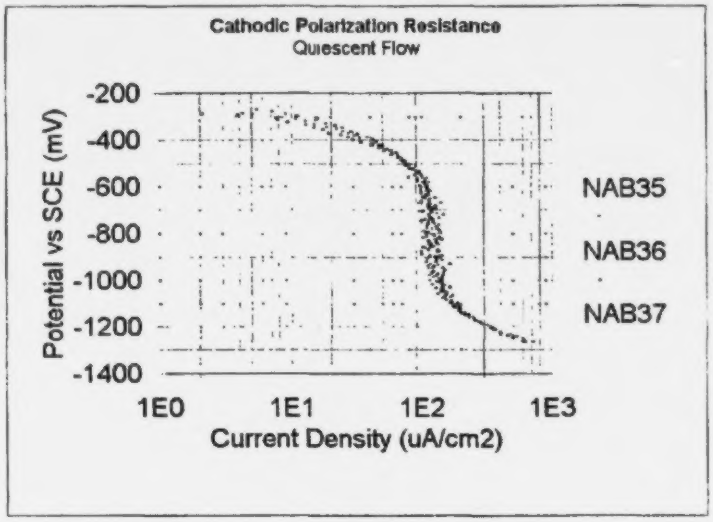

Figure 2 - Cathodic Polarization resistance relationship obtained for NAB for quiescent electrolyte flow conditions.

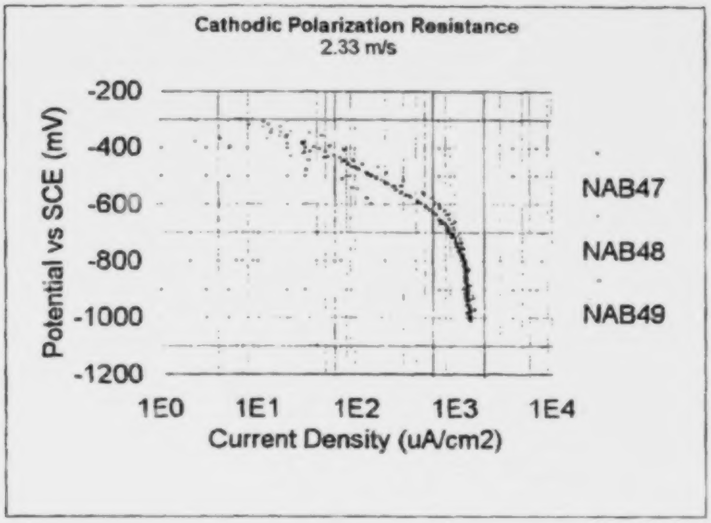

Figure 3 - Cathodic Polarization resistance relationship obtained for NAB for 2.33 m/s electrolyte flow

3.2 Physical Scale Modelling Results

Tables 2 through 5 contain the longitudinal reference electrode potentials and aft anode current demand for the two differing ICCP model anode/references electrode configurations under static and dynamic conditions. Tables 5.1 and 5.2 contain the results for trials where reference electrode 10 was used as the feedback signal (aft-aft configuration for CPF) for 0 and 3450 RPM propeller velocities, respectively. Tables 5.3 and 5.4 contain the results for the configurations where reference electrode 8 was used as the feedback signal (mid-aft configuration for CPF) for 0 RPM and 3450 RPM propeller velocities, respectively. For each configuration and velocity combination, the results for three differing tests at potentials bracketing the operational range of acceptable protection were recorded. For all configurations and velocities tested, the data indicates that as the applied potential increases, the current demand increases. Since the NAB propellers are the only exposed metallic structure during these trails, this observation is consistent with the cathodic NAB polarization resistance data generated and presented in the previous section.

For the two static trials (0 RPM propeller velocities), the developed feedback control circuitry provided stable control of the model currents. However, for the dynamic test conducted at 3450 RPM a minor oscillation was observed in the command/feedback relationship. The likely source of this oscillation is intermittent shaft grounding at higher rotational velocities.

Table 2 - 0 RPM Velocity, Reference Ag/AgCl, Conductivity 415-420 µmho/cm, Feedback Ref 10

Cmd (V)	Cur (A)	Ref 1 (mV)	Ref 2 (mV)	Ref 3 (mV)	Ref 4 (mV)	Ref 5 (mV)	Ref 6 (mV)	Ref 7 (mV)	Ref 8 (mV)	Ref 9 (mV)	Ref 10 (mV)
-0.60	1.185	638	646	638	648	639	646	641	657	664	606
-0.80	2.29	845	848	845	850	845	848	849	858	896	792
-1.00	3.15	1061	1065	1060	1067	1061	1067	1067	1078	1111	980

Table 3 - 3450 RPM Velocity, Reference Ag/AgCl, Conductivity 415-420 µmho/cm, Feedback Ref 10

Cmd (V)	Cur (A)	Ref 1 (mV)	Ref 2 (mV)	Ref 3 (mV)	Ref 4 (mV)	Ref 5 (mV)	Ref 6 (mV)	Ref 7 (mV)	Ref 8 (mV)	Ref 9 (mV)	Ref 10 (mV)
-0.60	1.91	666	667	667	667	667	664	668	680	683	605
-0.80	2.80	854	856	854	856	853	855	853	887	921	787
-1.00	3.70	*1228	1240	1237	1238	1213	1235	1236	1271	1299	1114

* Input data showed significant variation (observation of command/feedback relationship experienced oscillation).

Table 4.- 0 RPM Velocity, Reference Ag/AgCl, Conductivity 415-420 µmho/cm, Feedback Ref 8

Cmd (V)	Cur (A)	Ref 1 (mV)	Ref 2 (mV)	Ref 3 (mV)	Ref 4 (mV)	Ref 5 (mV)	Ref 6 (mV)	Ref 7 (mV)	Ref 8 (mV)	Ref 9 (mV)	Ref 10 (mV)
-0.60	0.93	601	603	603	603	601	603	605	606	614	582
-0.80	1.95	778	783	783	783	782	783	782	791	813	728
-1.00	2.58	946	944	944	943	948	943	941	990	1000	869

Table 5 - 3450 RPM Velocity, Reference Ag/AgCl, Conductivity 415-420 µmho/cm, Feedback Ref 8

Cmd (V)	Cur (A)	Ref 1 (mV)	Ref 2 (mV)	Ref 3 (mV)	Ref 4 (mV)	Ref 5 (mV)	Ref 6 (mV)	Ref 7 (mV)	Ref 8 (mV)	Ref 9 (mV)	Ref 10 (mV)
-0.60	1.28	597	600	600	600	598	600	601	605	615	571
-0.80	1.86	875	887	853	843	876	841	867	*818	890	787
-1.00	2.76	972	949	981	959	948	946	966	*1000	1020	902

* Input data showed significant variation (observation of command/feedback relationship experienced oscillation).

In general, it is observed that potentials remain relatively constant to the fore of reference electrode 7 which is located in front of the aft anodes. This observation is consistent with the position of the propellers which is aft of the aft anodes combined with the high dielectric capacity of the hull form. It is also observed that the current demand required by the propellers produces an area of decreased potential aft of the propellers. For the configurations which used the mid-aft reference electrode as the feedback signal, the level of protection behind the propellers (for a -0.8V command signal) is reduced to marginal levels for the static test conducted. The data indicates that positioning the feedback reference electrode aft of the propellers resolves under protection issues behind the propellers but has the effect of increasing the level of potential fore of the rear anodes. For the -0.8 V static test conducted, these levels did not, however, increase to the level where paint degradation would be expected to be significant.

Increasing the velocity for a given configuration has the effect of increasing the current demand required to protect the propellers which again is consistent with the trends observed in the polarization resistance tests conducted on the NAB propeller material. This increased current demand for the dynamic tests results in an longitudinal potential profile with marginally higher levels of applied potentials to the fore of the aft anodes.

3.3 Computer Modelling Results

Figure 4 represents a typical comparison between the potentials predicted by the computer model and recorded PSM potentials using the ASTM G5 potentiodynamic polarization resistance data as input to the computer model. Using the ASTM G5 data generally did not result in a good correlation between the computer and PSM results. This observation was attributed to the inability of a "short term test" to predict current densities which accurately reflect field observations.

For this study, the NAB propellers were the only galvanically active metal attached to the model, thus polarization resistance data used as input to the computer model was generated directly from the propellers attached to the PSM model. This was achieved by using the computer model to accurately assess the potential difference between the propeller material and an adjacent reference electrode. The polarization curve data used in the analysis is provided below in Table 6. This data was obtained directly from the experimental analysis, and represents the static, or quiescent case (i.e. zero propeller velocity).

For the purposes of this study, numerical simulations were performed in order to predict the effect of varying the anode current. The anode current levels were considered consistent with those generated with the PSM model. Typical contour plots of the surface potentials for selected trials are provided in Figures 5 through 7.

Table 6 - Polarization Curve Data

Potential (mV)	Current Density (micro A / cm2)
547.9	14.79
562.6	18.85
656.9	31.02
708.5	36.43
775	41.04
864.7	50.11

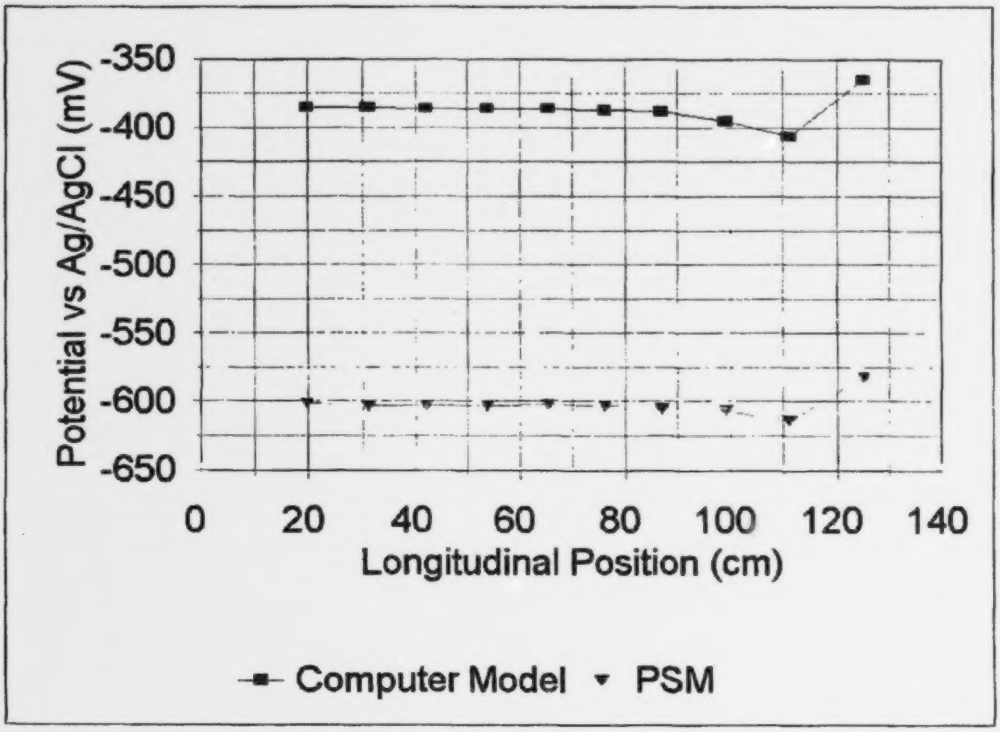

Figure 4 - Hull potentials along the longitudinal axis of the PSM model compared to the computer simulation using potentiodynamic polarization data generated using ASTM G5 (Quiescent flow with reference electrode 8 feedback potential of -0.6V).

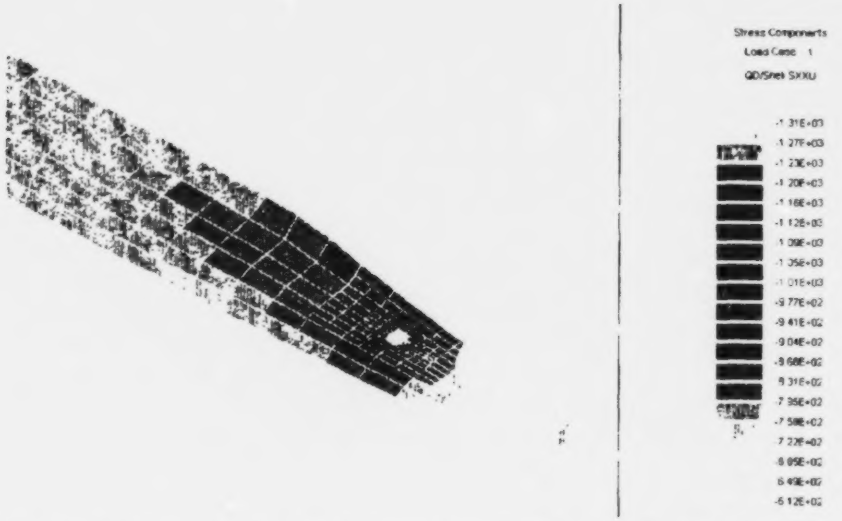
Stress Components
Load Case 1
QD/Shell SXXU
-1 31E+03
-1 27E+03
-1 23E+03
-1 20E+03
-1 16E+03
-1 12E+03
-1 09E+03
-1 05E+03
-1 01E+03
-9 77E+02
-9 41E+02
-9 04E+02
-8 68E+02
-8 31E+02
-7 95E+02
-7 58E+02
-7 22E+02
-6 85E+02
-6 49E+02
-6 12E+02

Figure 5.- Surface potentials computed for anode current of 1.95 mA (quiescent polarization data).

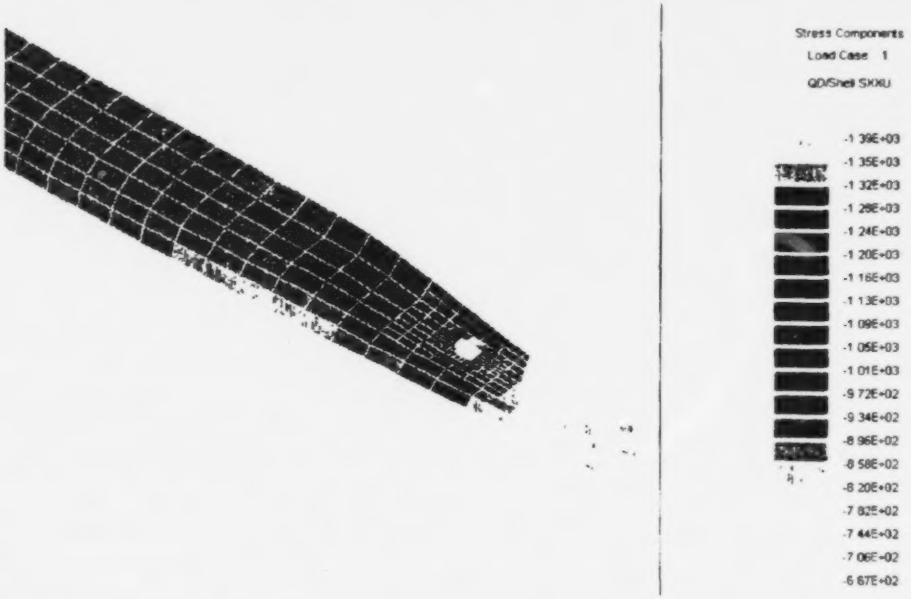
Stress Components
Load Case 1
QD/Shell SXXU
-1 39E+03
-1 35E+03
-1 32E+03
-1 28E+03
-1 24E+03
-1 20E+03
-1 16E+03
-1 13E+03
-1 09E+03
-1 05E+03
-1 01E+03
-9 72E+02
-9 34E+02
-8 96E+02
-8 58E+02
-8 20E+02
-7 82E+02
-7 44E+02
-7 06E+02
-6 67E+02

Figure 6 - Surface potentials computed for anode current of 2.29 mA(quiescent polarization data).

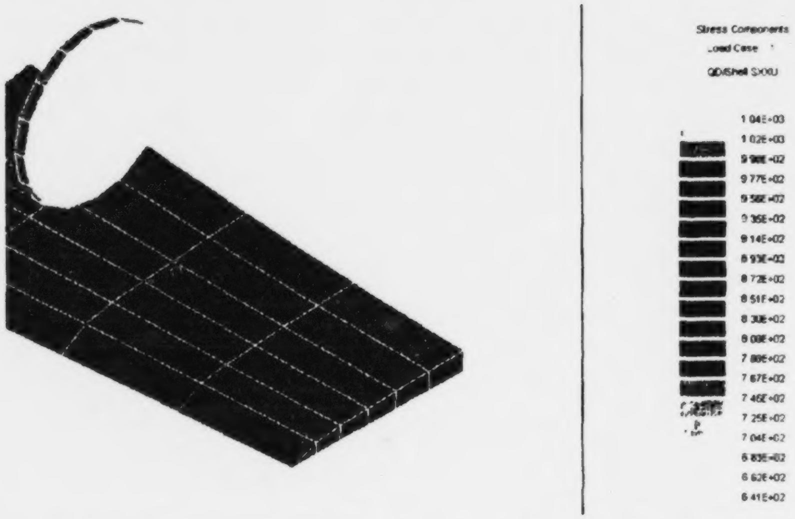
Stress Components
Load Case 1
QD/Shell SXXU
1.04E+03
1.02E+03
9.98E+02
9.77E+02
9.56E+02
9.35E+02
9.14E+02
8.93E+02
8.72E+02
8.51E+02
8.30E+02
8.09E+02
7.88E+02
7.67E+02
7.46E+02
7.25E+02
7.04E+02
6.83E+02
6.62E+02
6.41E+02

Figure 7 - Surface potentials computed for anode current of 2.80 mA(dynamic polarization data).

The primary objective of this study was to develop two independent methodologies for generating hull potential profiles for impressed current cathodic systems (ICCP). In the execution of experimental program, results were generated by both physical scale modelling (PSM) and computer simulations. Codes utilized to generate the computer simulations included both CPBEM (a code developed by DREA/DL) and BEASY (a software code which has been used as a benchmark code by several NATO countries). This section compares PSM and the analytical results generated for the PSM configurations evaluated.

Figures 8 - 13 and 14 - 19 are graphical comparisons of the PSM, CPBEM and BEASY results for the quiescent and dynamic PSM model configurations tested, respectively. For the quiescent tests, both the CPBEM and BEASY results show good agreement with the PSM potentials. In general, potentials generated by CPBEM were within 35 mV of the potentials recorded using the PSM modelling methodology. BEASY generally produced a closer agreement with the PSM results than CPBEM. Potentials generated by BEASY were normally within 15 mV percent of the respective PSM potential. It has been postulated that the non-linearity of the polarization resistance data used as input may account for a portion of the differences observed between the two codes. Incorporating a more sophisticated solver algorithm into the CPBEM code would bring the agreement within the accuracy exhibited by BEASY for these trials.

Similar to the quiescent tests, both CPBEM and BEASY predictions produced excellent agreement with the PSM potentials recorded for the dynamic configurations evaluated. In general, both CPBEM and BEASY were within 35 mV of the potentials recorded using the PSM facility. In the dynamic case, the absence of a difference between the performance of CPBEM and BEASY is attributed to the electrical noise generated by the contact used to ground the propeller shafts to the ICCP hardware.

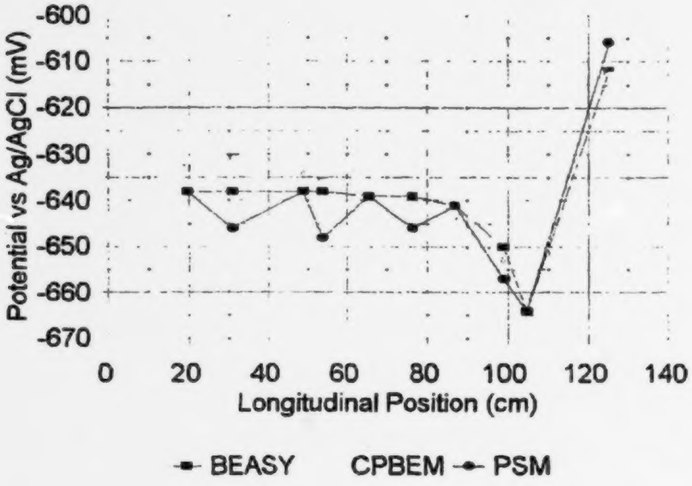

Figure 8 - Hull potentials along the longitudinal axis of the PSM model compared to the CPBEM and BEASY predictions. Model configuration (Quiescent flow with reference electrode 10 feedback potential of 0.6V).

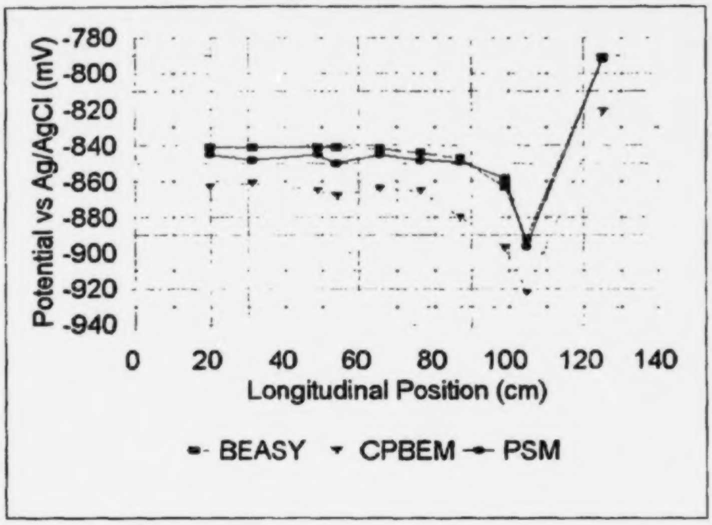

Figure 9 - Hull potentials along the longitudinal axis of the PSM model compared to the CPBEM and BEASY predictions. Model configuration (Quiescent flow with reference electrode 10 feedback potential of 0.8V).

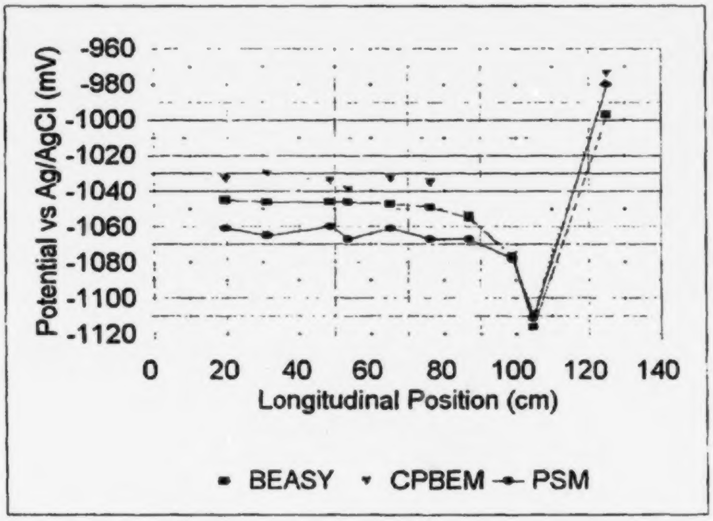

Figure 10 - Hull potentials along the longitudinal axis of the PSM model compared to the CPBEM and BEASY predictions. Model configuration (Quiescent flow with reference electrode 10 feedback potential of 1.0V).

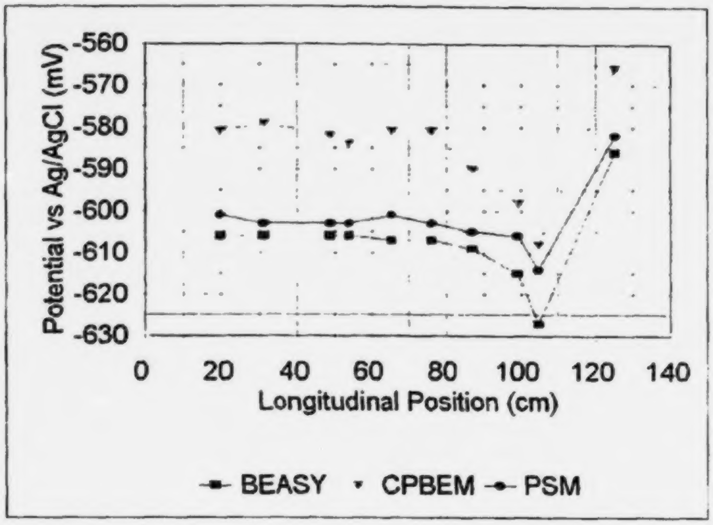

Figure 11 - Hull potentials along the longitudinal axis of the PSM model compared to the CPBEM and BEASY predictions. Model configuration (Quiescent flow with reference electrode 8 feedback potential of 0.6V).

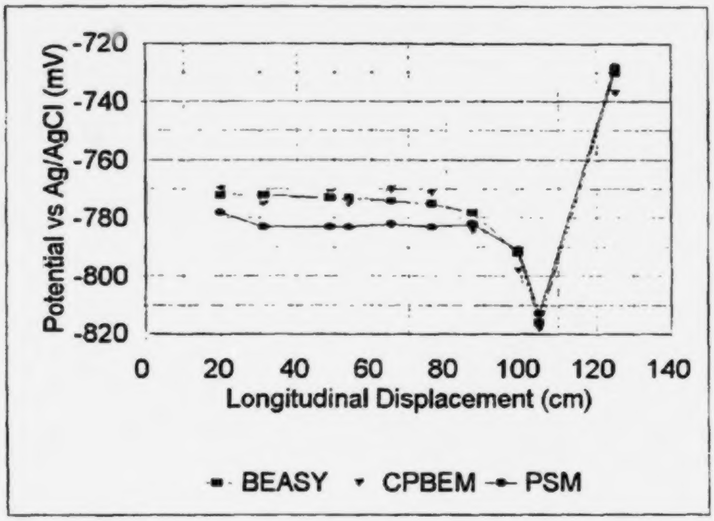

Figure 12 - Hull potentials along the longitudinal axis of the PSM model compared to the CPBEM and BEASY predictions. Model configuration (Quiescent flow with reference electrode 8 feedback potential of 0.8V).

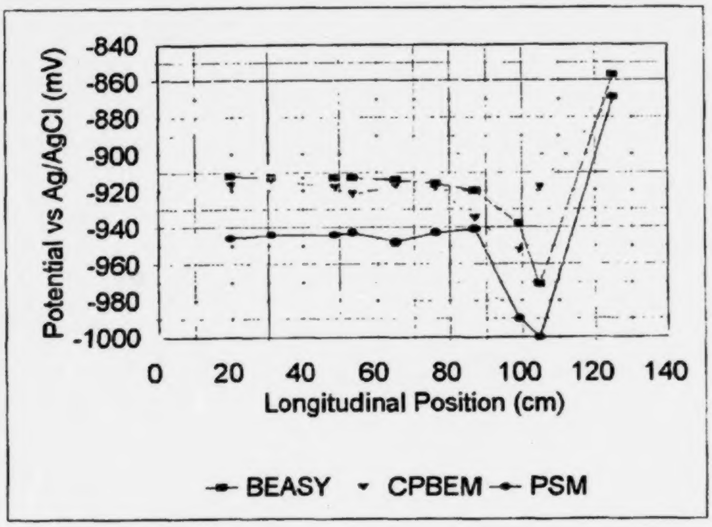

Figure 13 - Hull potentials along the longitudinal axis of the PSM model compared to the CPBEM and BEASY predictions. Model configuration (Quiescent flow with reference electrode 8 feedback potential of 1.0V).

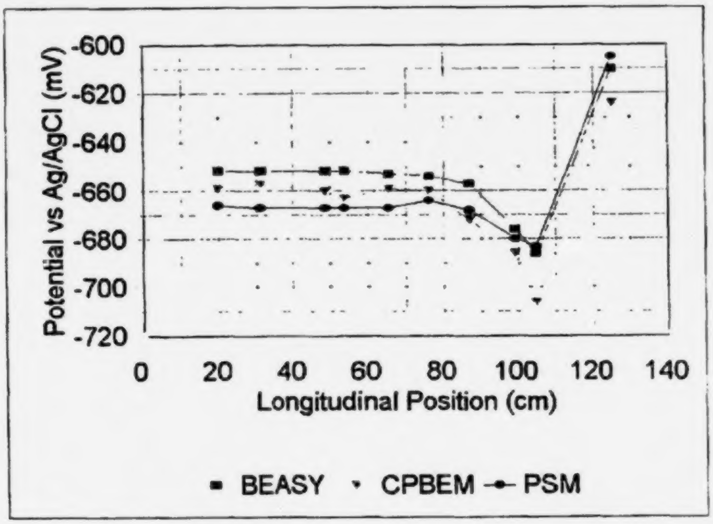

Figure 14 - Hull potentials along the longitudinal axis of the PSM model compared to the CPBEM and BEASY predictions. Model configuration (Dynamic flow with reference electrode 10 feedback potential of 0.6V).

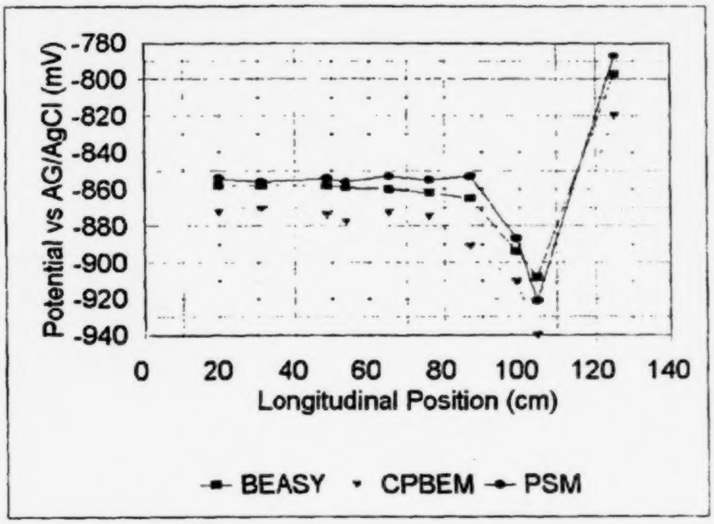

Figure 15 - Hull potentials along the longitudinal axis of the PSM model compared to the CPBEM and BEASY predictions. Model configuration (Dynamic flow with reference electrode 10 feedback potential of 0.8V).

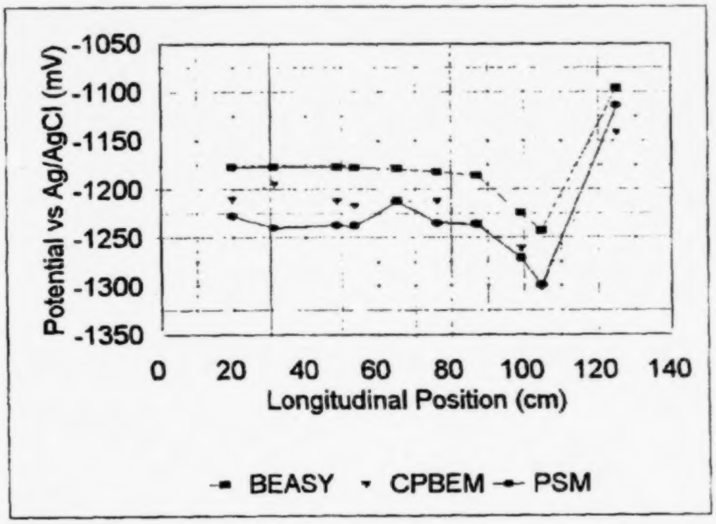

Figure 16 - Hull potentials along the longitudinal axis of the PSM model compared to the CPBEM and BEASY predictions. Model configuration (Dynamic flow with reference electrode 10 feedback potential of 1.0V).

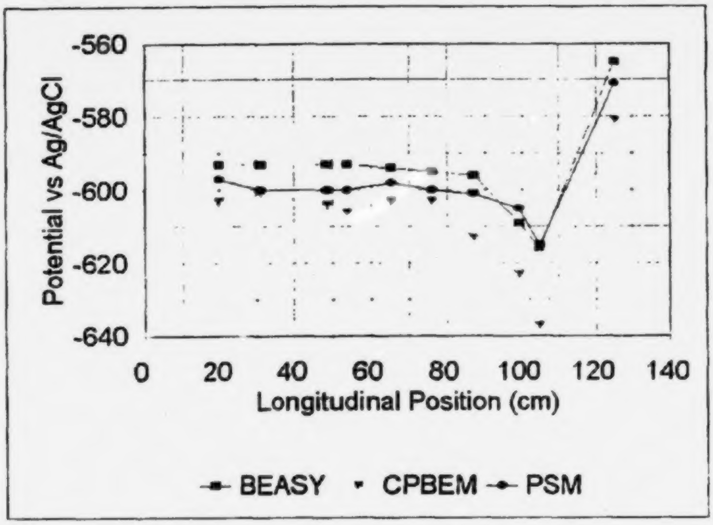

Figure 17 - Hull potentials along the longitudinal axis of the PSM model compared to the CPBEM and BEASY predictions. Model configuration (Dynamic flow with reference electrode 8 feedback potential of 0.6V).

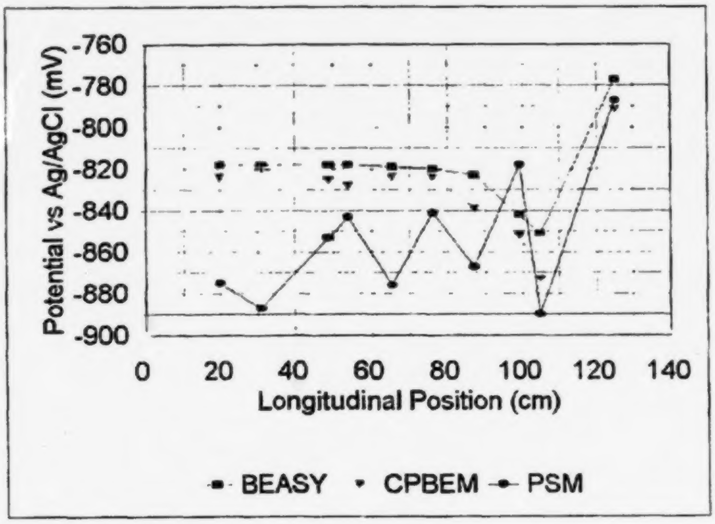

Figure 18 - Hull potentials along the longitudinal axis of the PSM model compared to the CPBEM and BEASY predictions. Model configuration (Dynamic flow with reference electrode 8 feedback potential of 0.8V).

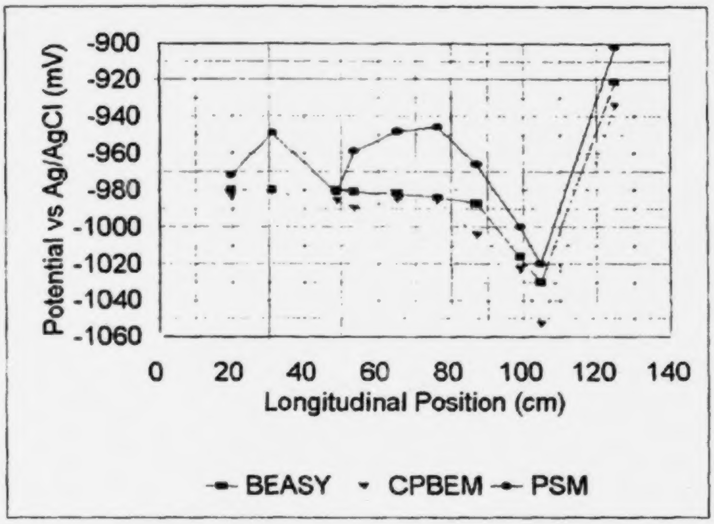

Figure 19 - Hull potentials along the longitudinal axis of the PSM model compared to the CPBEM and BEASY predictions. Model configuration (Dynamic flow with reference electrode 8 feedback potential of 1.0V).

4.0 CONCLUSIONS

A comprehensive program was conducted to develop two independent methodologies for generating hull potential profiles for impressed current cathodic protection systems. The two methodologies developed were physical scale modelling and computer simulations using CPBEM and BEASY software suites. A 1/100 scale model of CPF was fabricated and instrumented for comparison with the computer simulations. Several inferences can be drawn from the results generated from this study. These inferences include:

Both CPBEM and BEASY computer simulations were in good agreement with the potentials generated by the PSM/ICCP model. For the quiescent tests conducted, the potentials predicted by CPBEM and BEASY were generally within 35 mV and 15 mV of the PSM potentials, respectively. For the dynamic tests conducted, both CPBEM and BEASY produced potentials within 35 mV of the PSM potentials.

Both the PSM and computer simulation test results indicate that an area of marginal protection occurs behind the propellers if the mid-aft reference electrode is used to control the aft anode current output. By positioning the feedback reference electrode aft of the propellers this area of marginal cathodic protection is significantly reduced without increasing the potential over the rest of the structure to levels which would result in paint degradation.

5.0 REFERENCES

[1] N.G. Zamani, J.F. Porter and A.A. Mufti. A Survey of Computational Efforts in the Field of Corrosion Engineering. Int. J. Numer. Methods in Engng., Vol 23, pp. 1295-1311 (1986).

[2] N.G. Zamani. Boundary Element Simulation of the Cathodic Protection System in a Prototype Ship. Applied Math. and Comp., Vol 26, pp. 119-134 (1988).

[3] C.A. Brebbia and J. Dominquez. Boundary Elements - An Introductory Course. McGraw-Hill, New York (1989).

[4] R.S. Munn. A Review of the Development of Computational Corrosion Analysis for Spatial Corrosion Modelling Through its Maturity in the Mid-1980's. pp. 215-228, Computer Modelling in Corrosion, ASTM STP 1154, Ed. by R.S. Munn. ASTM (1992).

[5] V.G. De Giorgi, E.D. Thomas, A.I Kaznoff, "Numerical Simulation of Impressed Current Cathodic Protection (ICPP) Systems Using Boundary Element Methods," in R.S. Munn ed., pp. 265-276, "Computer Modelling in Corrosion," ASTM Special Technical Publication 1154, Philadelphia, USA, 1992.

#516444 (29)

Fatigue Crack Growth in 350WT Steel Subjected to Intermittent Tensile Overloads & Compressive Underloads

by
P.A.Rushton[1], F. Taheri[2], and D.C. Stredulinsky[3]

[1]Advanced Research & Emerging Technologies Division, Martec Limited, Halifax, NS, Canada
[2]Civil Engineering Department, Dalhousie University, Halifax, NS, Canada
[3]Structural Acoustics & Strength Group, Defense Research Establishment Atlantic, Dartmouth, NS, Canada

Abstract

Previous investigations have shown that significant crack growth retardation in 350WT steel may be realized through the application of tensile overloads. However, the application of compressive underloads may appreciably reduce the retardation produced by previous tensile overloads. Unfortunately, compressive underloads are commonly neglected in practice, or, at best, dealt with via an empirically adjusted stress ratio (R). Therefore, a combined experimental and analytical/numerical fatigue testing program was undertaken with the objective of investigating the effects of intermittently applied tensile overloads (OL) and compressive underloads (UL) on fatigue crack growth in center-cracked 350WT steel specimens. A significant amount of knowledge has been gained regarding this overload/underload interaction, the subsequent fatigue crack growth behavior, and the analytical and numerical characterization of such behavior.

Experimental fatigue testing was performed on a total of 16 specimens, in which the stress ratio (R), the overload ratio (OLR), and the overload-to-underload ratio (OL/UL) were systematically varied. Modifications to the commonly used Wheeler model were proposed, allowing consideration of compressive underloading effects. The results of the proposed modifications will be included in a future publication.

A previously proposed exponential delay model was revised to include the effects of not only overload ratio, but also stress ratio and overload/underload ratio. Although seemingly complex, the resulting delay model may be easily incorporated into any existing crack growth model for constant amplitude loading, and has been shown to yield fatigue life predictions which are generally in good agreement with the experimental data. Details of the revised delay model are to be included in a future publication.

In addition to a discussion of the experimental program, the current briefing will focus on a nonlinear FE analysis (using the NISA FE package) which was also performed, subjecting a typical specimen to a simple OL/UL sequence. The results of this FE investigation validated the proposed existence of a crack tip 'compressive plastic zone' under compressive loading, the size of which is typically smaller than that produced by an equivalent tensile overload. The analysis also predicted a zone of tensile yielding at the crack tip upon removal of this compressive underload, further substantiating the experimentally observed phenomena of crack growth acceleration and reduction in retardation. The size of these compression-induced 'yield zones' were found to depend not only on the relative magnitude of the compressive underload and preceding tensile overload, but also on the assumed crack face separation (δ_0).

Fatigue Crack Growth in 350WT Steel Subjected to Intermittent Tensile Overloads & Compressive Underloads

by

Philip Rushton, Martec Limited
Farid Taheri, Daltech University
David Stredulinsky, DREA

Outline

- Introduction
- Brief Review of Fracture Mechanics
- Motivation for Research
- Approach
  - Experimental
  - Analytical/Numerical
- Discussion of Results
  - Experimental
  - Analytical/Numerical
- Conclusions
- Acknowledgements

Introduction: Why Consider Research on Fracture?

- Cost of Fracture is Enormous ($$$)
- Consequences of Fracture Worse Today
- Knowledge of Crack Growth Behavior Essential
  - Safer, More Cost-Effective Design Practices
  - Improve Fabrication & Quality Control Measures
  - Assess Inspection, Maintenance & Repair
- Interaction of Tensile & Compressive Loading
  - Compressive Loading Data is Scarce
  - Effects of Compressive Loading Often Neglected
  - May Yield Unconservative Life Predictions

Theories of Fracture Mechanics

- Two Main Branches of Fracture Mechanics
  - Linear Elastic Fracture Mechanics (LEFM)
  - Elastic Plastic Fracture Mechanics (EPFM)
- LEFM w/Linear Elastic Materials (Minimal Yielding)
  - Stress Intensity Factor (K):

$$K = \sigma Y \sqrt{\pi a} \ (\mathrm{MPa}\sqrt{m})$$

- EPFM Used w/Large-Scale Plastic Deformation
  - J-Integral (Rice): Accounts for N/Linear Material Behavior

$$J = \frac{K_{EQ}^2}{E}$$

Fatigue Crack Propagation

- Small Cracks & Flaws Inevitable
- Some Type of Crack Growth Analysis Required
  - Establish Intervals for Inspection, Maintenance/Repairs, etc.
  - Project/Forecast Remaining Useful Life of Components
  - Ultimately, Maintain Structural Integrity

Fatigue Crack Propagation

- FCP Models Describe Growth Rate, **da/dN = *f* (ΔK, R)**
  - Most Describe Stable Region II Growth
  - Model Disadvantages: Number & Nature of Curve Fitting Parameters Used to Describe *f* (ΔK, R)
  - Most Parameters Lack Physical Significance
- **Paris' Law** (Early 1960's): $\frac{da}{dN} = C_P(\Delta K)^{m_P}$
  - Simple ⇒ Only 2 Parameters (m_P= Slope, C_P= Intercept)
  - Does Not Account for Near-Threshold$^{(I)}$ Growth, Rapid/Unstable Growth$^{(III)}$, or Stress Ratio ($R=\sigma_{min}/\sigma_{max}$)
  - Additional Capabilities ⇒ More Parameters (Forman, Walker)

Fatigue Crack Propagation

- **Zheng & Hirt Model** (1983):
  - Δa_i = Distance Over Which Max. Normal Stress Exceeds Material Fracture Stress
  - No Empirical Parameters ⇒ Simple Tensile Testing Req'd

$$\frac{da}{dN} = \frac{(\Delta K - \Delta K_{th})^2}{2\pi E \sigma_{ult} (1 + RA)[-\ln(1 - RA)]}$$

- **Effects of Load Interaction** is an Important Aspect to Consider:
  - Tensile Overloads (OL) ⇒ Crack Growth Retardation
  - Compressive Underloads (UL) ⇒ Crack Acceleration
  - OL + UL ⇒ Combination of Retardation & Acceleration

Fatigue Crack Propagation

- **Wheeler Model** (1972):
  - Quantifies Crack Growth Retardation Using Factor ϕ_R
  - Retardation IF Current PZ Lies w/in Boundary of a Previous PZ
  - Applied to ANY FCP Model ⇒ $\mathbf{(da/dN)_R = \phi_R \cdot} f\,\mathbf{(\Delta K, R)}$
  - **Empirical** Shaping Exponent 'm': Value That "Best Fits" Data

$$\phi_R = \begin{cases} \left[\dfrac{r_{pi}}{a_{OL} + r_{pOL} - a_i}\right]^m & , a_i + r_{pi} \le a_{OL} + r_{pOL} \\ 1 & , a_i + r_{pi} \ge a_{OL} + r_{pOL} \end{cases}$$

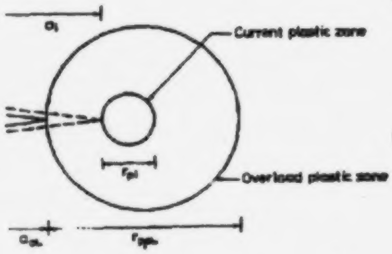

Fatigue Life Assessment Techniques

- Closed Form Integration of $da/dN = f(\Delta K, R)$
- Numerical Integration:
  - 1% Rule, Midpoint Rule, etc.
  - Cycle-by-Cycle Integration
  - Piecewise-Linear Integration

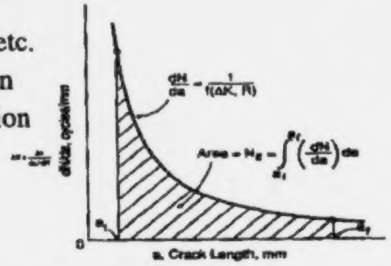

$$\Delta N \cong \frac{\Delta a}{da/dN}$$

- Cumulative Damage Theories
  - Failure Based On Progressive Damage Accumulation (D_1)

Motivation for Research

- DREA: Fatigue Problems w/350WT, No da/dN-ΔK Data
- Phase I: Obtain Baseline CAL Data for 350WT
  - Zheng & Hirt Shown Promising But Highly Dependent on K_{th}
  - Intermittent Tensile Overloads ($OLR = \sigma_{max,OL}/\sigma_{max,CAL}$)
  - Delay Model Proposed to Quantify Retardation (N_D)
- Phase II: Semi-Random Loading
  - Investigate Tensile & Compressive Loading
    - Effects of Compressive Loading on Retardation
    - Insight Into Load Interaction Effects in 350WT
    - Improve Fatigue Life Predictions
  - Evaluate K_{th} (Zheng & Hirt)

Experimental Approach

- Specimens: 300mmx100mmx5mm Plates w/EDM Starter Notch of 2a = 20mm
- Category 5 Steel Common in Bridges, Offshore Structures, and Hulls of Halifax Class Frigates
- All Testing Performed iaw ASTM E647
  - Threshold Testing to Evaluate K_{th}
  - Tensile & Compressive Overloading: Variations in R, OLR and OL/UL Ratio
- Instron UTM (±100kN Dynamic Capacity)
- Mitutoyo Travelling Microscope (10X Magnification)

Experimental Approach: Loading Sequence & Test Setup

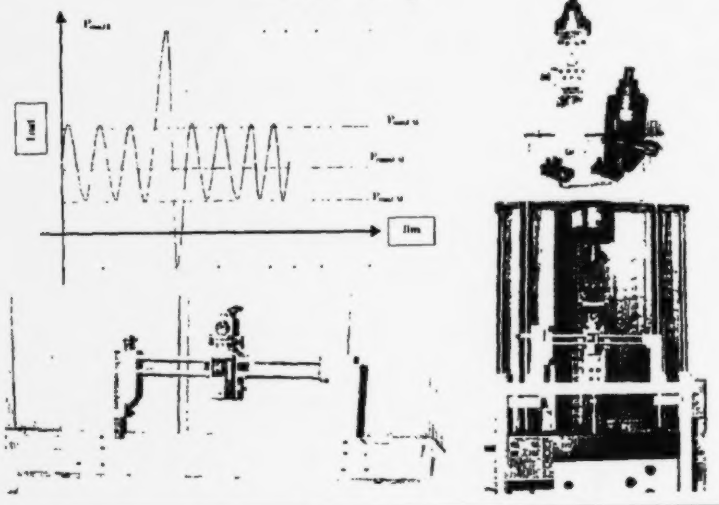

Numerical Approach

- Quantify Effects of Load Interaction
  - Correlate Experimental Results w/Predictions Using Existing Models
- Propose Modifications to Better Account for Compressive Loading Effects
- FE Analysis: Investigate Crack Tip Plasticity Under Typical Overload - Underload Sequence
- Revise Previous Delay Model Incl. OLR, R, & OL/UL

Experimental Results: Threshold Testing

- Average K_{th} = 5.6 MPa√m (vs 6.00 MPa√m Suggested)
- Growth Rates Over-predicted by Zheng & Hirt Model
- Fatigue Life Under-predicted w/Experimental K_{th}

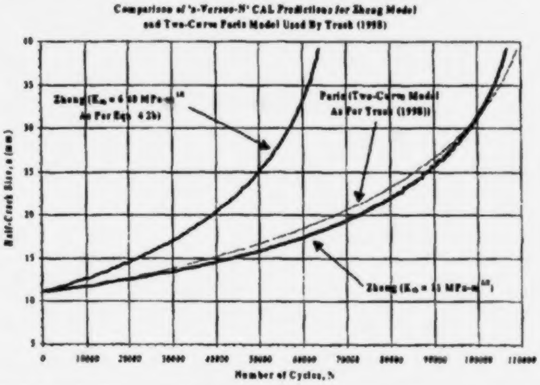
Comparison of 'a-Versus-N' CAL Predictions for Zheng Model and Two-Curve Paris Model Used By Trask (1998)

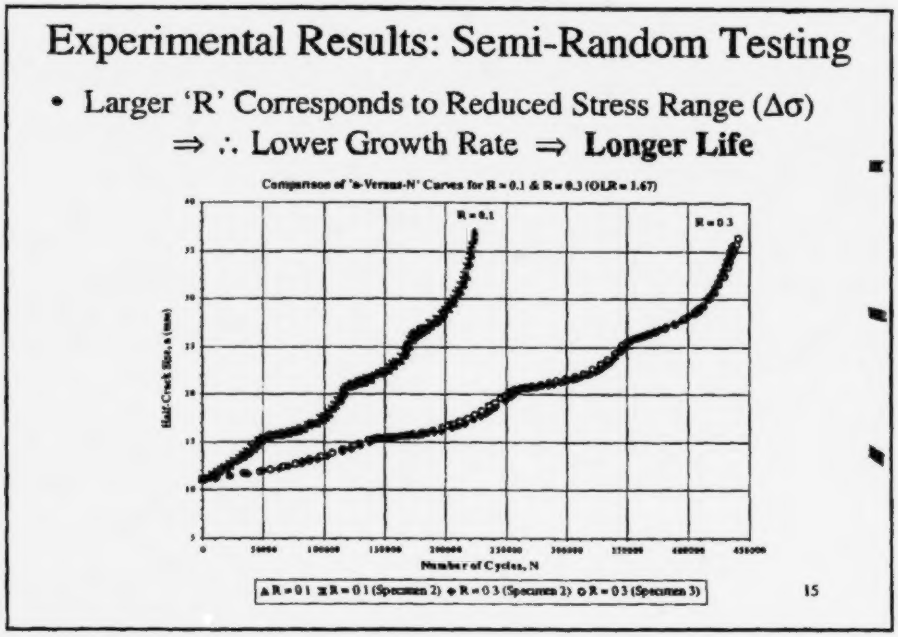

Experimental Results: Semi-Random Testing

- Larger 'R' Corresponds to Reduced Stress Range (Δσ) ⇒ ∴ Lower Growth Rate ⇒ **Longer Life**

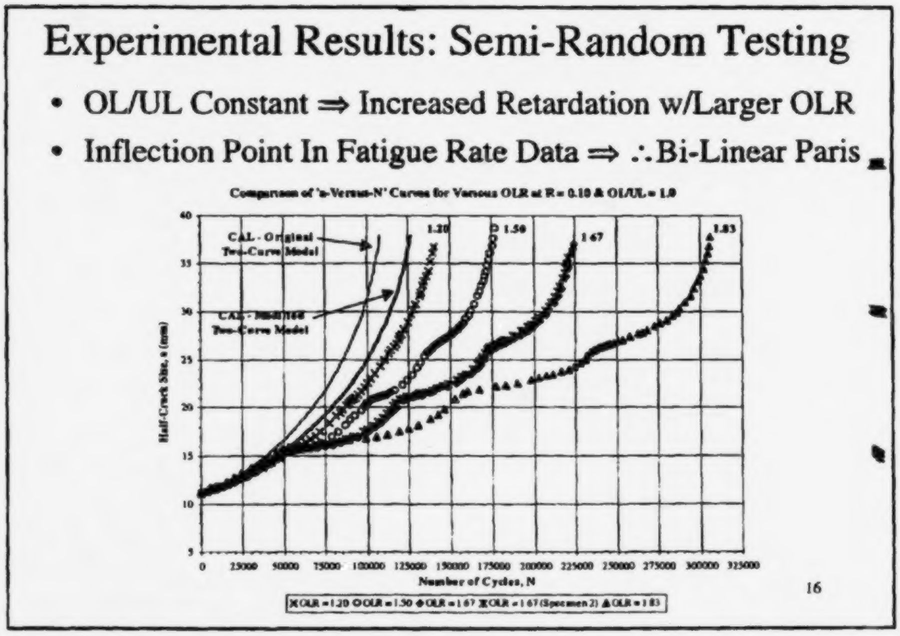

Experimental Results: Semi-Random Testing

- OL/UL Constant ⇒ Increased Retardation w/Larger OLR
- Inflection Point In Fatigue Rate Data ⇒ ∴Bi-Linear Paris

Experimental Results: Semi-Random Testing

- Maintained Constant OLR & Varied OL/UL Ratio
  - Post-Overload Retardation Was Greatly Affected
  - Suggests a **Compressive Plastic Zone** @ Crack Tip

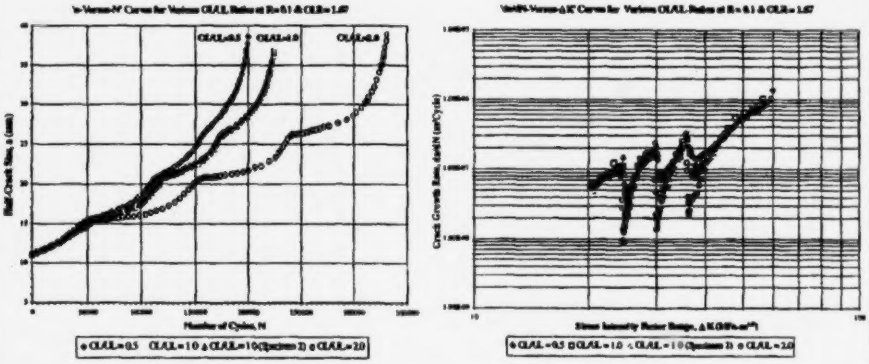

Numerical Results: Semi-Random Testing

- Larger UL's (ie., Smaller OL/UL) ⇒ Less Retardation
  - Min. Post-OL Growth Rate is Higher % of Equiv't. CAL Rate

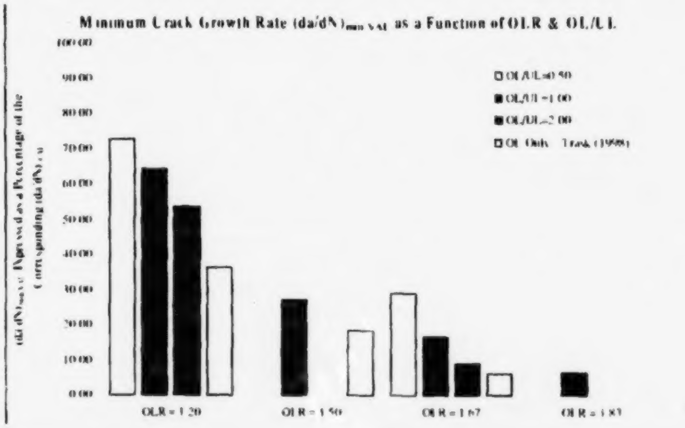

Numerical Results: Wheeler Predictions

- Excellent Fatigue Life Predictions Obtained w/Wheeler Model & Bi-Linear Paris Approximation
  - <1% Error in 11 of 16 Specimens, >5% Error for 2 Specimens

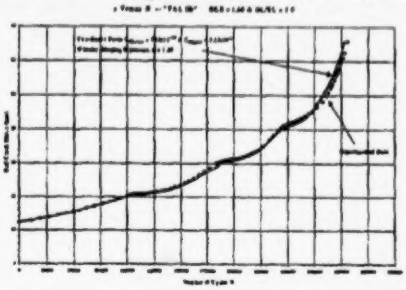

- Shaping Exponent 'm' **Empirical** in Nature
  - Trial & Error to Determine 'Best Fit' to Data
  - Potential Shown in Polynomial Regression of m=*f*(OLR)[19]

Numerical Results: Modified Wheeler Model

- Crack Growth Acceleration Typically Neglected in Practice
- Modifications: Account for Reduction in Retardation
  - Incorporate an 'Effective' Plastic Zone, $r_{\mathrm{eff}} = r_p - r_{cp}$
  - Result: Smaller Overall PZ ⇒ Less Growth Retardation Predicted

$$\phi_R^{T-C} = \begin{cases} \left[\dfrac{r_{\mathrm{eff}i}}{(a_{OL}+r_{\mathrm{eff}OL}-a_i)}\right]^m, & a_i+(r_{pi}-r_{cpi})<a_{OL}+(r_{pOL}-r_{cpUL}) \\ 1, & a_i+(r_{pi}-r_{cpi})\ge a_{OL}+(r_{pOL}-r_{cpUL}) \end{cases}$$

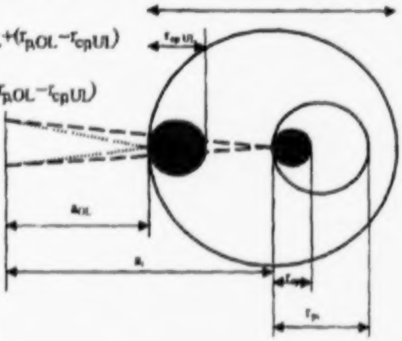

- Proposed Compressive PZ:

$$r_{cp} = \frac{1}{\alpha\ \pi}\left(\frac{\Delta K_{UL}}{2\cdot\sigma_{yld}}\right)^2$$

  - $\Delta K_{UL} = K_{\min,CAL} - K_{UL}$
- <2% Error in Life Predictions

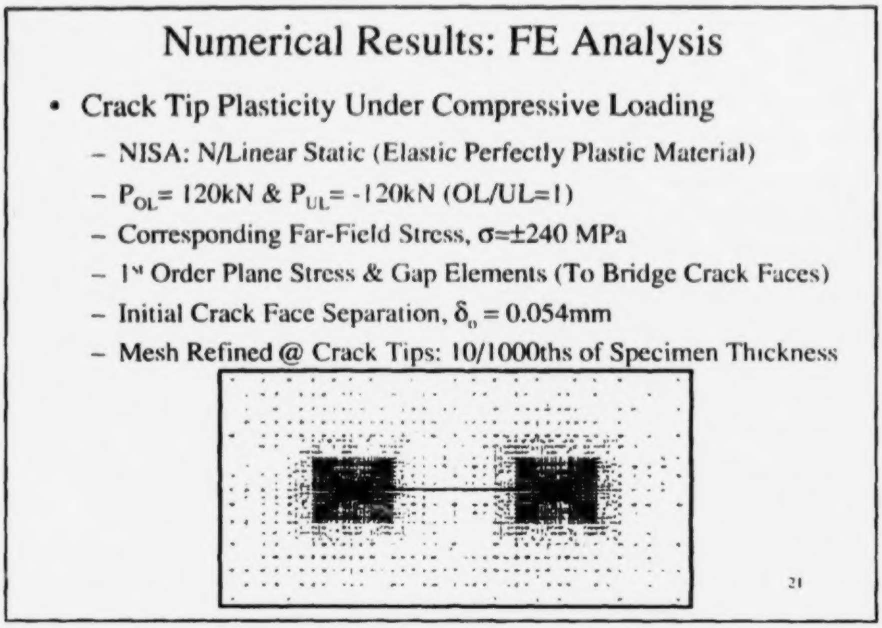

Numerical Results: FE Analysis

- Crack Tip Plasticity Under Compressive Loading
  - NISA: N/Linear Static (Elastic Perfectly Plastic Material)
  - P_{OL}= 120kN & P_{UL}= -120kN (OL/UL=1)
  - Corresponding Far-Field Stress, $\sigma=\pm240$ MPa
  - 1^{st} Order Plane Stress & Gap Elements (To Bridge Crack Faces)
  - Initial Crack Face Separation, $\delta_0 = 0.054$mm
  - Mesh Refined @ Crack Tips: 10/1000ths of Specimen Thickness

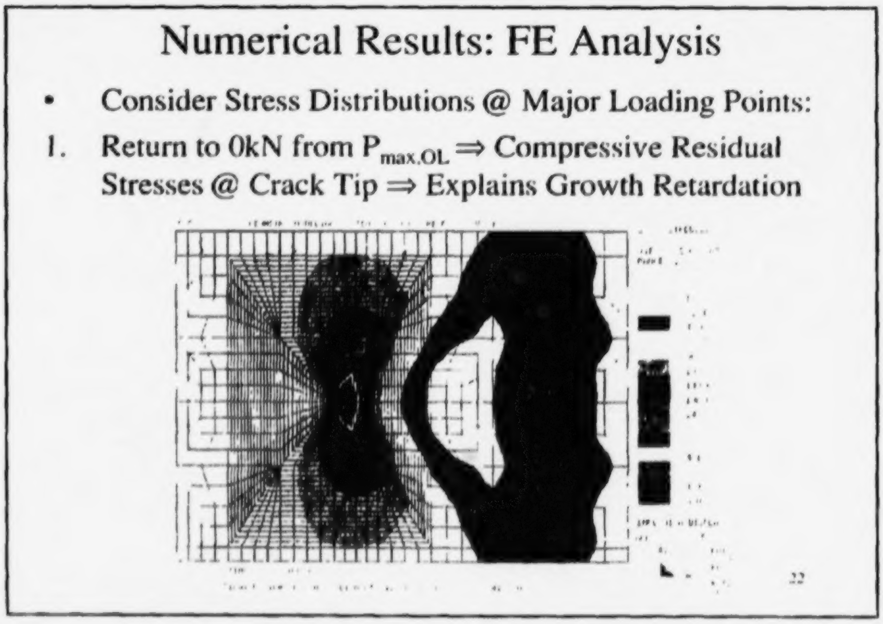

Numerical Results: FE Analysis

- Consider Stress Distributions @ Major Loading Points:

1. Return to 0kN from $P_{max.OL} \Rightarrow$ Compressive Residual Stresses @ Crack Tip $\Rightarrow$ Explains Growth Retardation

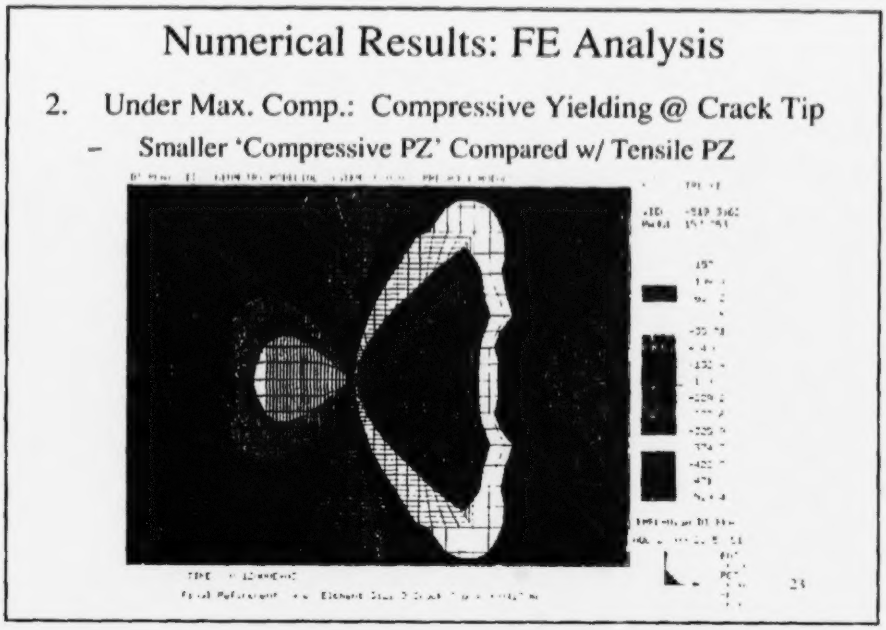

Numerical Results: FE Analysis

2. Under Max. Comp.: Compressive Yielding @ Crack Tip
   - Smaller 'Compressive PZ' Compared w/ Tensile PZ

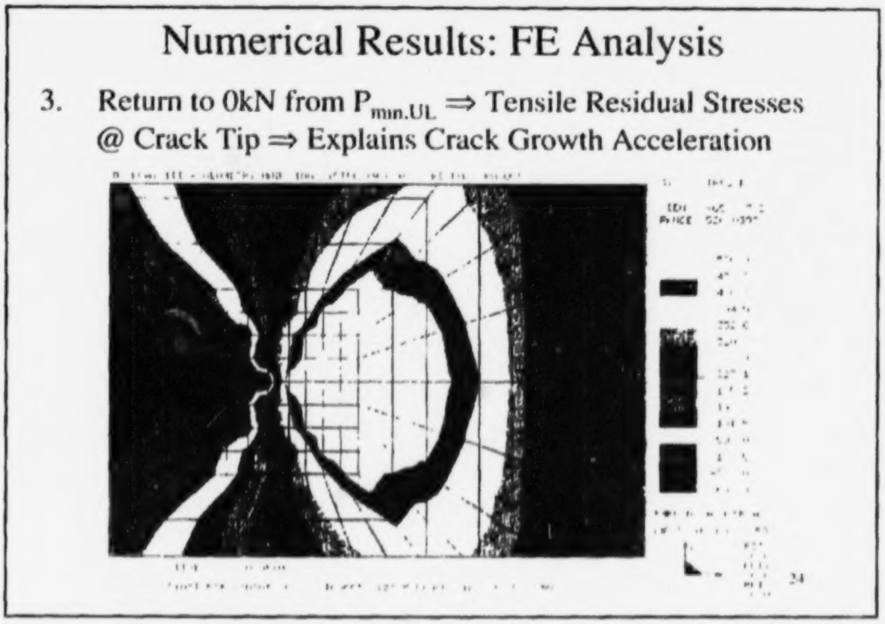

Numerical Results: FE Analysis

3. Return to 0kN from $P_{min,UL}$ ⇒ Tensile Residual Stresses @ Crack Tip ⇒ Explains Crack Growth Acceleration

Numerical Results: FE Analysis

- Results Based on Crack Face Separation, $\delta_o = 0.054$mm
- $\therefore$Reduced Separation to $\delta = 0.0054$mm (i.e., 1/10 δ_o)
  - Identical Trends Under Tensile Loading, As Expected
  - Smaller Plastic Zones Predicted Under Compression
- $\therefore$ Size of Compressive Yield Zones Depends on:
  - Magnitude of Both Compressive Underload (UL) & Preceding Tensile Overload (OL)
  - Assumption of Average Crack Face Separation, δ
    - ($\delta \approx 200\mu$m May Be a More Realistic Assumption)

Numerical Results: Exponential Delay Model

- Trask (1998): Proposed an Exponential Delay Model To Predict Retardation (N_D) as f(OLR)
- In Conjunction w/Paris' Law, This Delay Model Yields a Life Prediction of:

$$N_{if} = \int_{a_i}^{a_f} \frac{da}{C_P \Delta K^{m_P}} + N_{OL} \cdot N_D$$

Where: $N_D = f(\text{OLR})$

- Objective: Revise This Delay Model Such That

$$N_D = f(\text{OLR, R, OL/UL})$$

Numerical Results: Exponential Delay Model

- First Plotted $\mathrm{Log}_{10}[N_D]$ as a Function of OLR
  - Found Similar Slopes @ All Stress Ratios (R) & OL/UL Ratios

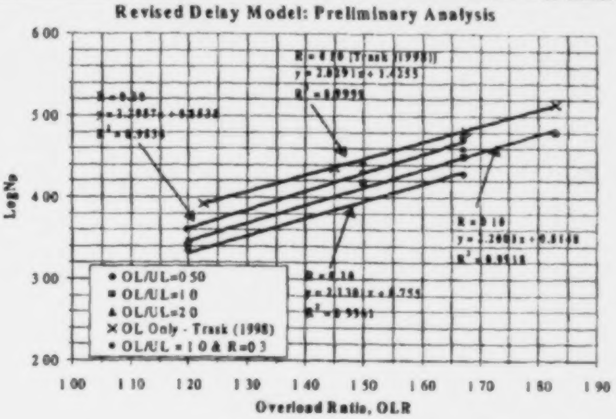

Numerical Results: Exponential Delay Model

- Suggested @ Constant OL/UL, Data for Different Stress Ratios (R) May Be Consolidated Onto a Single Curve:
  - $\mathrm{Log}_{10}[N_D(1\text{-}R)^2]$ vs OLR ⇒ Consolidation Achieved (Red)

$$\mathrm{Log}_{10}[N_D(1\text{-}R)^2] = \mu(\mathrm{OLR}) + \beta$$

  - Resulting Curve w/Slope Similar to Unconsolidated Curves

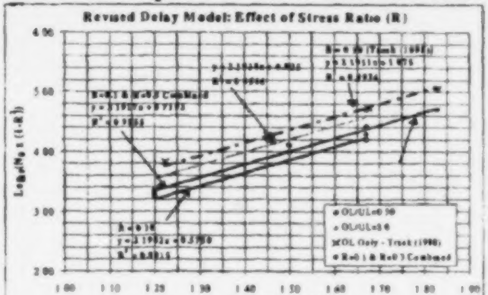

Numerical Results: Exponential Delay Model

- Suggests That Each OL/UL May Have Unique Intercept
  - Express Intercept 'β' as f(OL/UL)
  - Least Squares Regression of β-vs-OL/UL
- Finally, $N_D = f$(OLR, R, OL/UL) Expressed As

$$N_D = \frac{10^{m \cdot OLR + \left[a\left(\frac{OL}{UL}\right)^2 + b\left(\frac{OL}{UL}\right) + c\right]}}{(1-R)^2}$$

- Recall Paris' Life Prediction: $N_{if} = \int_{a_i}^{a_f} \frac{da}{C_P \Delta K^{m_P}} + N_{OL} \cdot N_D$
- Average of 3.25% Error in Fatigue Life Predictions

Conclusions

- Threshold Testing: Average $K_{th} = 5.6$ MPa√m
- Valuable Insight Into Load Interaction in 350WT
- Excellent Life Predictions w/Wheeler & Paris
  - Potential in Expressing Wheeler 'm' as f(OLR)
- Variation in UL Greatly Affects Growth Retardation
  - @ Constant OLR, Larger UL Yields Less Retardation
    - Suggesting Crack Tip Plasticity Under Compressive Load
    - FE Analysis Confirmed Crack Tip 'Compressive Plastic Zone'
- Revisions to Trask's Exponential Delay Model
  - Multi-Parameter Model Includes OLR, R, and OL/UL
  - Life Predictions Agreed Well w/Experimental Data

Acknowledgements

- Research Funded Through Financial Support From Defense Research Establishment Atlantic (DREA) and National Science & Engineering Research Council of Canada (NSERC)
- Sincere Thanks & Appreciation to Dr. Farid Taheri (Daltech)
- Appreciation Extended to Dr. David Stredulinsky (DREA), Mr. John Porter (Halifax Dockyard), and Dr. Graeme Lee (Daltech)
- Special Thanks to David Trask, and Civil Dept. Technicians Mark MacDonald and Blair Nickerson

#516445 (30)

Minor Corrosion - Major Mechanical Failures

by J.C. Thornley

RPC
Fredericton, New Brunswick, Canada

ABSTRACT

Fatigue cracking is recognized as a major cause of component breakage in service. However, there is frequently a failure to differentiate between failures resulting from fatigue in air and failures resulting from corrosion fatigue. Not differentiating between them often leads to the mechanical aspects of the failure being addressed but with the corrosion aspects being neglected.

The consequences of failing to provide adequate corrosion protection to several components from various commercial vessels will be illustrated with some case histories. The case histories cited are concerned with the cracking or the complete breakage of tail shafts, rudder stocks and shell plating from such vessels as tugs, fishing boats and ferries. In all cases, if adequate corrosion protection had been provided to prevent the minor amount of corrosion that did take place it is strongly believed that the resulting mechanical failures would have been averted.

Other case histories will be used to illustrate those situations where corrosion protection by cathodic protection, might not be effective in reducing the probability of cracking.

1.0 INTRODUCTION

Each individual component failure, with few exceptions, is unique in some respect or other. Despite the uniqueness of individual component failures, patterns of shared characteristics emerge from groups of failure investigations. These shared characteristics might, for example, link individual failures from pulp mills, thermal generating stations and from ships of various kinds. In this article the single shared characteristic that has been taken from several apparently diverse mechanical failures is that of the "corrosion fatigue" cracking mechanism. Case histories illustrating the points covered will be drawn wholly from the marine industry but similar sets of case histories, illustrating the same points, could be taken from other industries.

Corrosion fatigue cracking is cracking in a component as a result of that component being subjected to oscillating or fluctuating loading while in a corrosive environment. In contrast "ordinary" fatigue cracking would be the cracking of that same material tested in air.[1]

In this article the materials that will be considered are steels. The oscillating stresses needed to cause steels to fail by corrosion fatigue cracking are lower, and often drastically lower, than those stresses which will cause failure by in-air fatigue cracking (ref. 1, 2). It seems that this was first recognized in the 1920's. The reduction in fatigue strength caused by replacing air by a corrosive environment can be dramatic. Some results showing the sort of reduction in fatigue strength that can come from simultaneous fatigue loading and corrosion are shown in Figure 1. There it can be seen that a 0.5% carbon steel has a fatigue strength of about 380 MPA at 10^8 cycles, when loaded in air. If those one hundred million load cycles are applied while the steel corrodes freely in a salt spray the fatigue strength falls to about 35 MPA. The simultaneous corrosion lowers the long term fatigue strength of the steel to about 10% of its in-air fatigue strength. More corrosion resistant materials are affected to a lesser degree but there is often still a fatigue strength reduction. For example, a steel similar to type 304 stainless steel might lose about 35% of its fatigue strength at 10^8 cycles when tested in salt spray rather than in air (Figure 2, Ref. 1).

---

[1] Even in air, changes in relative humidity can have effects on the fatigue properties of some materials but that will not be discussed here.

For certain materials and structures the damaging effects of the corrosive environment can be alleviated by applying a suitable form of corrosion protection (Refs. 3, 4). One form of protection that has been found to be generally effective has been cathodic protection, and an example of the effectiveness of the classical cathodic coating, hot-dip galvanizing, is illustrated in Figure 3. The right sort of corrosion protection can return the fatigue strength of a steel from desperately low levels back up to its fatigue strength in air, or close to that value.

However, although all of this has been known for more than sixty years (refs. 1, 2, 3), corrosion fatigue failures still continue to occur in situations where they could have been prevented. The following case histories illustrate this point.

2.0 CASE HISTORIES: MARINE FAILURES BY CORROSION FATIGUE

2.1 Carbon Steel Tail Shaft Failures

A fracture face resulting from the breakage of the shaft of a controllable pitch propeller is shown in Figure 4 (case history #1). In the photograph in Figure 4 both the hollow tail shaft and the pitch control rod, set in the centre of the shaft, are seen to be broken. Our concern is with the failure of the tail shaft.

The fracture face of the tail shaft can visibly be divided into two separate areas. One, the upper area of Figure 4, is relatively flat and smooth. The other area, the lower area of Figure 4 is rougher and is dull rather than shiny. The flat area takes up about 70% of the whole fracture face and has a series of gently curved, approximately parallel lines on it. These markings are typical of the markings known as "beach marks" and which appear on fatigue crack fracture faces. They can be used to locate the area where cracking started. Doing that on this fracture face we see that there is substantial corrosion in the area where cracking started. If we take longitudinal sections through the shaft surface in this corroded area where cracking started, features such as those shown in Figure 5 can be seen. Here we have corrosion pits with associated cracks. These cracks become increasingly narrow with increasing distance below the shaft's outer surface until they become sharp cracks (Figure 6). This observation is typical of corrosion fatigue cracking, particularly with materials that are relatively low in corrosion resistance, such as plain carbon steels.

Corrosion fatigue cracking does not appear to be the same problem with carbon steel shafts driving fixed propellers. The difference appears to be that carbon steel shafts driving fixed propellers are equipped with corrosion resistant liners, such as bronze, from forward of the packing box, through the stern tube, completely to the forward face of the propeller hub. That is, the carbon steel on a fixed propeller is designed to not come into contact with seawater. In the case of a CP propeller's tail shaft, a liner is also used but the liner often stops a few inches forward of the flange to which the CP propeller is fitted. These few inches of exposed carbon steel are in contact with seawater and may not receive cathodic protection. These few inches of steel are, therefore, often subjected to corrosion fatigue conditions and, periodically, there are tail shaft failures as a consequence of the absence of corrosion protection. In the case here the vessel was in the Atlantic off Cape Breton. Others have been operating elsewhere in the western North Atlantic or off the west coast of Newfoundland at the time of the failure. Each of the incidents known to us, where corrosion fatigue has been involved, have been single screwed vessels and all have been towed to safety.

2.2 Stainless Steel Tail Shaft Failures

Stainless steel tailshafts also do not always receive cathodic protection. Sometimes it is not recognized that the application of cathodic protection to stainless steel tailshafts is important. In fact, the importance of using cathodic protection probably depends, amongst other things, on the proportion of time that a vessel is in service. Stainless steels, in general, have good resistance to fast flowing seawater but many of them have relatively poor resistance to stagnant seawater. Therefore, stainless steel tail shafts on vessels which are in service almost continuously will be expected to corrode relatively little in comparison with otherwise identical tailshafts on vessels which are idle for substantial periods.

This was demonstrated several years ago by the failures of several tailshafts made from the stainless steel often known as 17-4 PH (UNS S17400). These stainless steel tailshafts had been fitted to fishing boats equipped with fixed pitch propellers and which operated in the Gulf of St. Lawrence. They tended to be idle during the winter and some of them sat in the ice. In this idle period corrosion pitting developed. This pitting can continue once the vessel had returned to service. Therefore, when the vessel is operating we have the conditions for corrosion fatigue cracking. Even though stainless steels are more resistant to corrosion fatigue cracking than carbon steels, the tailshafts of two vessels failed (Figure 7, case history #2), and cracking was discovered in at least one other (Figure 8, case history #3). We have seen similar cases of tailshaft failures from vessels fitted with unprotected type 316 stainless steel tailshafts. The failure to apply cathodic protection to these tailshafts puts them at risk from corrosion fatigue cracking and, although they don't all fail as a consequence of not utilizing suitable corrosion protection, some of them do fail.

2.3 Rudder Stock Failures

These failures were on a ferry and there had been two rudder stock failures before the third one was investigated metallurgically. A sketch of the rudder stock is shown in Figure 9. The fracture face on the recovered part of the rudder stock is shown in Figure 10 (case history #4). There were three areas on the fracture face that could clearly be distinguished one from the other. Two of these areas were smooth and the other, the central part of the fracture face, was quite rough. It appeared that two corrosion fatigue cracks had grown across the shaft from approximately opposite sides until the cross section was reduced to about 50% of its original area. The remaining cross section then failed by brittle fracture, in a single overload. (The failures of the first two rudder stocks were not examined. It is understood that they were both blamed on striking an underwater object. It is quite probable, however, that those two earlier failures were also a consequence of corrosion fatigue cracking.)

Longitudinal sections were taken through what appeared to be the cracking origins. Corrosion pits, some of them associated with shallow cracks, were seen in the resulting sections. These were the same as those shown earlier in Figure 4 and are typical of corrosion fatigue cracking in carbon steels. Again, all of the features indicate that the failure is by corrosion fatigue cracking and not by simple in-air fatigue cracking. Allowing the steel to corrode freely has reduced its fatigue strength by as much as 90%. As in the other cases cited, the metal loss due to corrosion has been minor. However, the corrosion has had the effect of allowing cracks to form when they would otherwise have been absent.

2.4 Shell Plating

It is mechanical components such as shafts that fail most frequently from fatigue cracking and corrosion fatigue cracking. However, any component that is subjected to an oscillating or fluctuating load is at risk from fatigue cracking and any component which also sees corrosion simultaneously is at risk from corrosion fatigue cracking. The photograph in Figure 11 shows cracking in some shell plating.

Below the water line, shell plating is normally protected from corrosion by a combination of coating and cathodic protection. The cathodic protection prevents corrosion at those sites where the coating is damaged. If the cathodic protection fails for some reason, corrosion can take place at those sites where the coating is damaged. It is believed that this was the cause of the cracking seen in Figure 11 (case history #5). For various reasons, the cathodic protection had failed on at least some parts of this vessel. This allowed us to enter the realm of corrosion fatigue cracking. One thing that should be noted is that there are groups of cracks. It is quite common for corrosion fatigue cracking to result in groups of cracks rather than single individual cracks.

2.5 Other Vessel Components and Inspection Procedures

RPC have also been involved with corrosion fatigue failures in rudders, boilers and other vessel components. Corrosion fatigue cracking on rudders should also be preventable by suitable corrosion protection but is complicated by rudders being welded structures. Preventing corrosion fatigue cracking inside boilers is a different matter. It depends on operation and on boiler water chemistry control and the cracking may not be readily detectable. In one case that we were involved with a boiler explosion resulted from corrosion fatigue cracking, with crew fatalities. The boiler had been inspected a short time previously, without the cracking being discovered. In some of the other cases cited it is also quite possible that existing cracks had escaped detection during surveys prior to failure.

One major reason for corrosion fatigue cracks escaping detection is that layers of corrosion product and other sorts of corrosion damage often hide the cracking. It is not immediately recognized that corrosion makes cracking more likely and the layers of corrosion product are not always removed prior to an inspection. This means that cracks can remain hidden. Therefore, when critical components, such as tailshafts and boiler drums, are being inspected it is important to remove corrosion products. In some cases it might also be necessary to grind to smooth metal or to abrasive blast to white metal in order to perform a decent inspection. The cracking seen in the tail shaft in Figure 7 (Case History #3) was only visible after much of the corrosion pitting on the shaft surface had been removed. Dye penetrant inspection was used for crack detection on that shaft. On the original pitted surface only pitting was revealed by dye penetrant examination, no cracks were seen. The surface being inspected was a mass of corrosion pits and these pits very effectively obscured the cracks. When most of the pitting had been removed the crack indications became plainly visible.

3.0 EXCEPTIONS TO THE BENEFICIAL EFFECTS OF CATHODIC PROTECTION

In each of the case histories presented it is strongly believed that, if the components involved had been cathodically protected they would probably not have cracked or failed as they did. This is not always the case. Applying cathodic protection to a component that operates under oscillating loads in a corrosive environment will not always prevent it from cracking. One thing should be said immediately: The case histories presented were concerned with the smooth surfaces of steels that were relatively soft. Here "relatively soft" means that their ultimate tensile strengths were less than about 1000 MPA (150 ksi). We will now look at the implications for a component which is either not smooth or which is hard.

3.1 Welded or Cracked Components

When we have components without smooth surfaces, the benefit of corrosion protection in preventing corrosion fatigue cracking can be much less than is the case when smooth, or relatively smooth, surfaces are involved. There has been considerable disagreement in the past about the benefits of cathodic protection in delaying corrosion fatigue cracking. An international conference was convened in Halifax in 1986 (ref. 5) just to consider whether cathodic protection was a benefit or a detriment with regard to corrosion fatigue cracking. This conference was almost exclusively directed towards fatigue at welded joints. On a more practical level, welded structures, particularly those involving load carrying fillet welds, quite regularly fail by fatigue cracking even when those structures have been well protected by hot-dip galvanizing. An example is shown in Figures 12 and 13 (case history #6). Here we have two weld locations on a marine structure. At each spot there are two fatigue cracks that have started at weld toes and have grown into the steel. The steel is not corroded at all because it has been effectively hot dip galvanized. The galvanizing has effectively prevented corrosion but it has not prevented cracking.

Welds reduce the fatigue resistance of steel to the same degree (numerically) that operating in a corrosive environment reduces fatigue cracking resistance. In this case of cracking at these welds the zinc may have kept the structure at its in-air fatigue strength but that fatigue strength, at welds, has been too low for the actual service and we have had cracking.

Structures which already contain cracks may also fail to benefit by the application of cathodic protection. The effects of cathodic protection on crack growth rates have been determined by several investigators. Some investigators have found little effect of cathodic protection on crack growth rates while others have found that the application of cathodic protection to samples with growing cracks in them has accelerated crack growth. The voltage to which the protected structure is polarized and the strength of the steel may determine whether that protection is beneficial or detrimental in its affects on crack growth rate (refs. 6, 7). Therefore, corrosion protection should be applied when a part is new, or early in its life. If the component has already started to crack there may be no benefit to its application, or it may be positively detrimental.

3.2 Components made from High Strength Steels

Here, high strength steels are those which have strengths greater than about 160 to 170 ksi (1100-1200 MPA). For these steels, corrosion protection by cathodic protection is generally positively detrimental, with or without oscillating loading. Cathodic protection normally results in the liberation of some hydrogen, some of which migrates into the steel. With relatively soft steels this hydrogen generally causes no damage. High strength steels, however, can suffer from hydrogen induced cracking. This cracking is usually intergranular rather than transgranular. These very high strength seels can crack by this mechanism even without cathodic protection. The application of cathodic protection to high strength steels simply exacerbates an already possible cracking mechanism. A high density of manganese sulphide inclusions, as in certain free cutting steels, may make this cracking even more likely and may allow it to occur at lower strength levels than in a steel with a low level of those manganese sulphide inclusions (8).

4.0 CONCLUSIONS

1. Simultaneous corrosion and oscillating loading can cause smooth steel components to fail at as little as 10% of the oscillating stress necessary to cause failure in dry air.

2. The need for applying corrosion protection to prevent mechanical failures is not always recognized. A consequence of this is that some components fail quite unnecessarily by corrosion fatigue cracking.

3. The most effective corrosion protection for preserving in-air fatigue properties is cathodic protection via anodes, impressed current, galvanizing or by metal spraying with a metal anodic to the substrate. (The substrate will normally be steel so that metal spraying with zinc and/or aluminum will normally be applicable.)

4. Certain welded components may still fail by fatigue cracking even though they are adequately protected against corrosion. The greatest benefit is obtained when smooth new components of suitable design receive cathodic protection.

5. Components that already have cracks in them are unlikely to benefit by the application of cathodic protection if the objective of that cathodic protection is to arrest cracking.

6. Steels with ultimate tensile strengths exceeding about 160 to 170 ksi (1100 to 1200 MPA) may crack by hydrogen cracking if they receive cathodic protection when placed in a corrosive environment.

REFERENCES

1. H.J. Gough and D.G. Sopwith, Engineering, vol 136, pp 75 to 78, July 1933.

2. D.J. McAdam, Trans. Am. Soc. for Steel Treating, vol 11, pp 355 to 390, 1927.

3. D.G. Sopwith and H.J. Gough, J. Iron and Steel Inst., vol 135, pp 315 to 339, 1937.

4. A. Royez and J. Pomey, Revue de Metallurgie, vol 56, pp 122 to 128, 1959.

5. Ed. O. Vosikovsky and K. Leewis, "Cathodic Protection" a + or - in corrosion fatigue", pub. Canmet (M39-19/1896E) Sept. 1986.

6. C.E. Jaske, D. Bruek, J.E. Slater and W.E. Anderson, "Corrosion Fatigue of Structural Steels in Seawater for Offshore Applications", ASTM STP 642: Symposium on Corrosion Fatigue, Denver, Colorado, Nov. 1976.

7. A. Stacey, "Research on High Strength Structural Steels", http://www.orf.co.uk/ORF-articles/issue119/119research.htm (01 02 23)

8. J.C. Thornley, Prak. Metall. 34 pp 472 to 477 (1997).

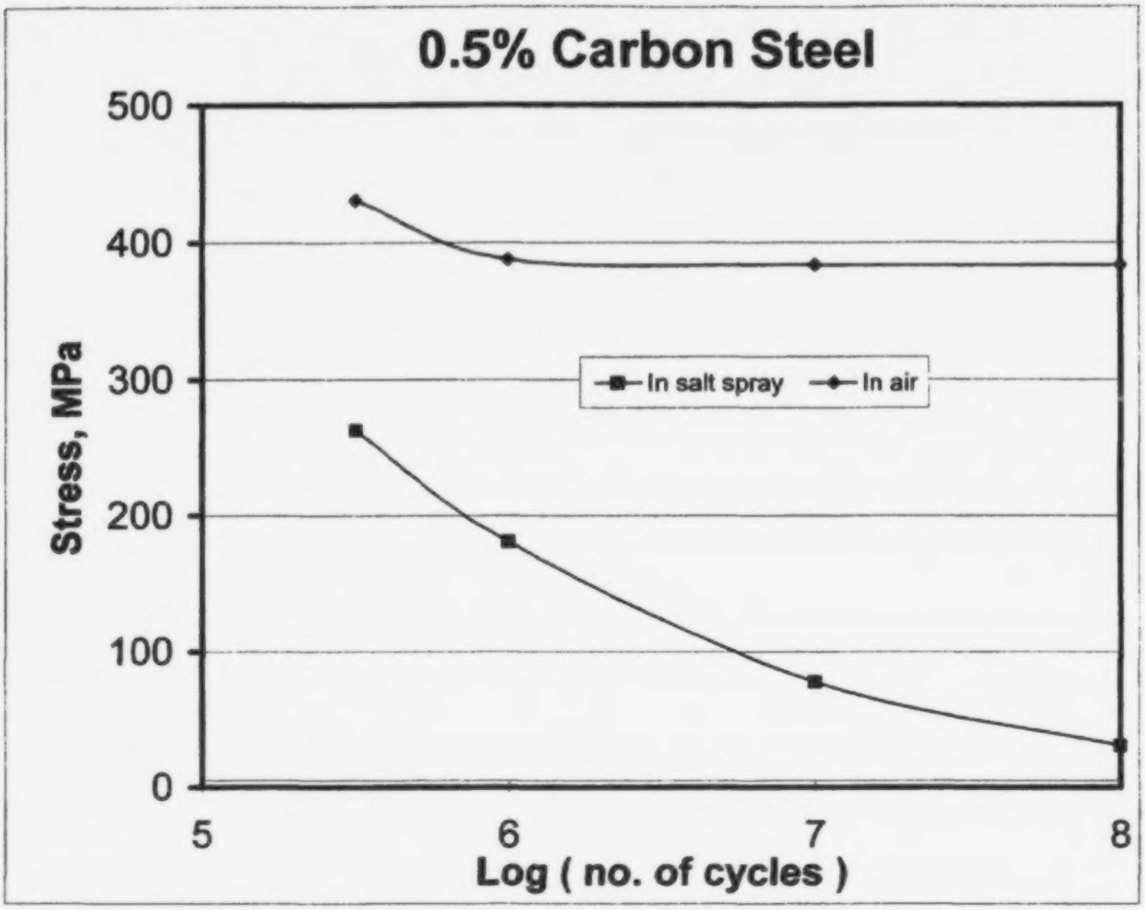

Figure 1.
The rotating bending fatigue strength of this 0.5% carbon steel falls drastically if the test environment is changed from air to salt spray. At 10^7 cycles the fatigue strength of the steel falls to 20% of its in-air value as a consequence of carrying out the testing in salt spray.
(From: H.J. Gough and D.G. Sopwith, Engineering, vol 136, pp 75 to 78, July 1933.)

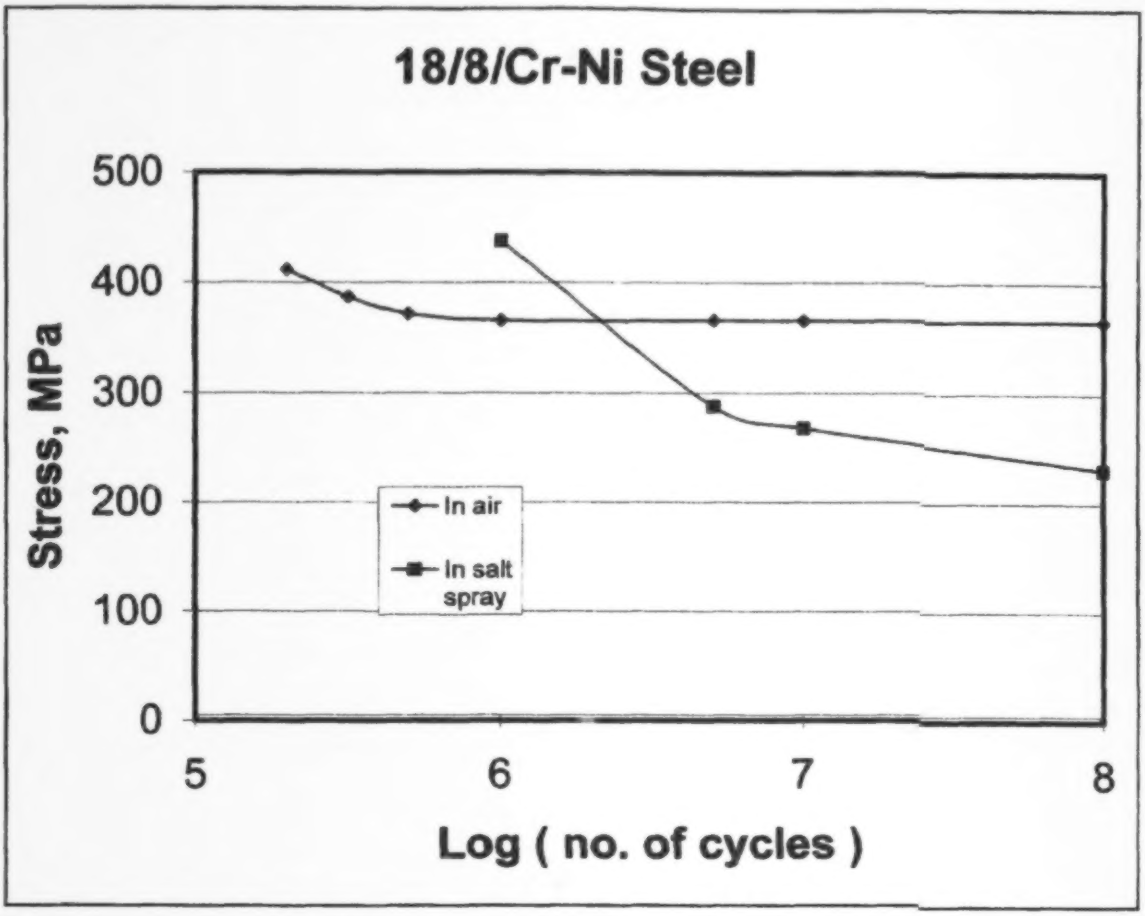

Figure 2.
When a steel similar to type 304 stainless steel is fatigue tested in a salt spray environment rather than in air, its drop in fatigue resistance (about 35%) is less than that of a plain carbon steel but it is still detrimentally affected to a significant degree.
(From: H.J. Gough and D.G Sopwith, Engineering, vol 136, pp 75 to 78, July 1933.)

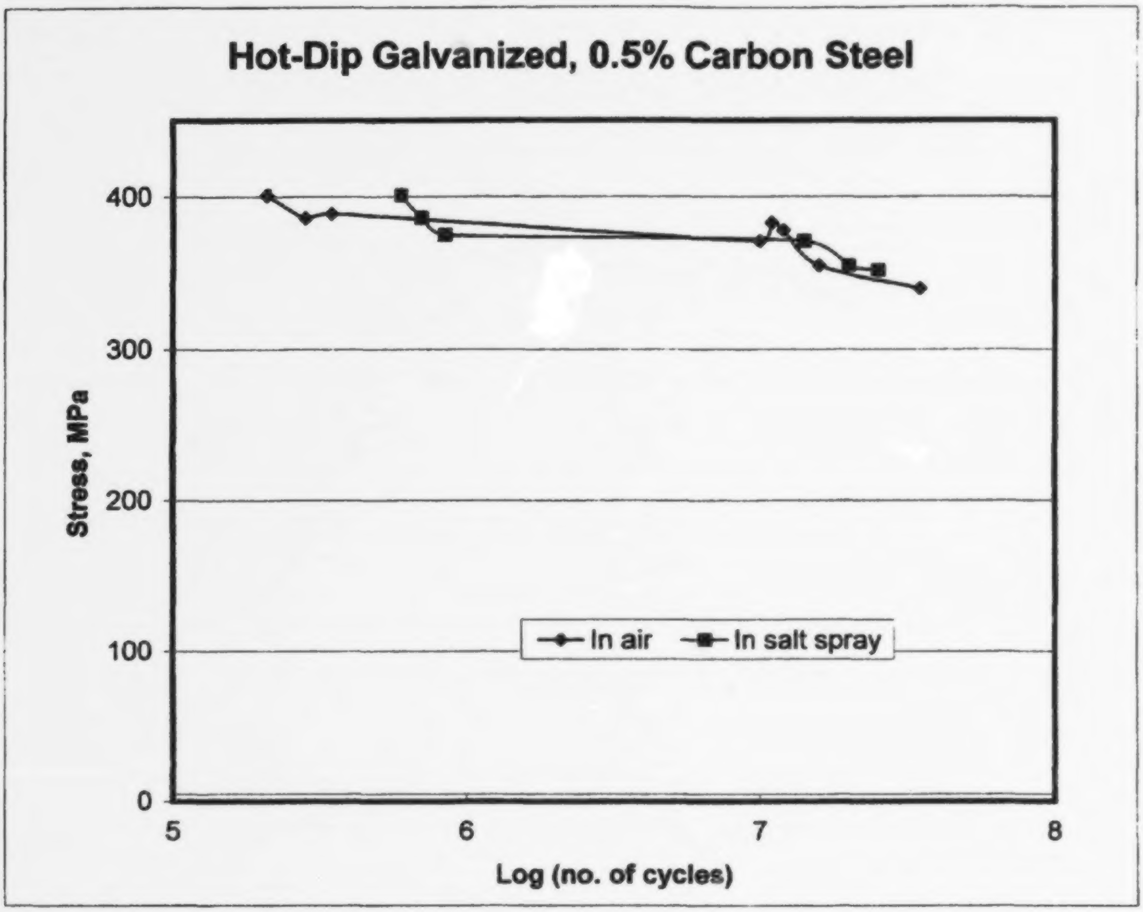

Figure 3.
Hot dip galvanizing, and some other methods of corrosion protection, can prevent the fatigue strength of carbon steels from deteriorating when they are exposed to salt water.
(Taken from D.G. Sopwith and H.J. Gough, J. Iron and Steel Inst., vol 135, pp 315 to 339, 1937.)

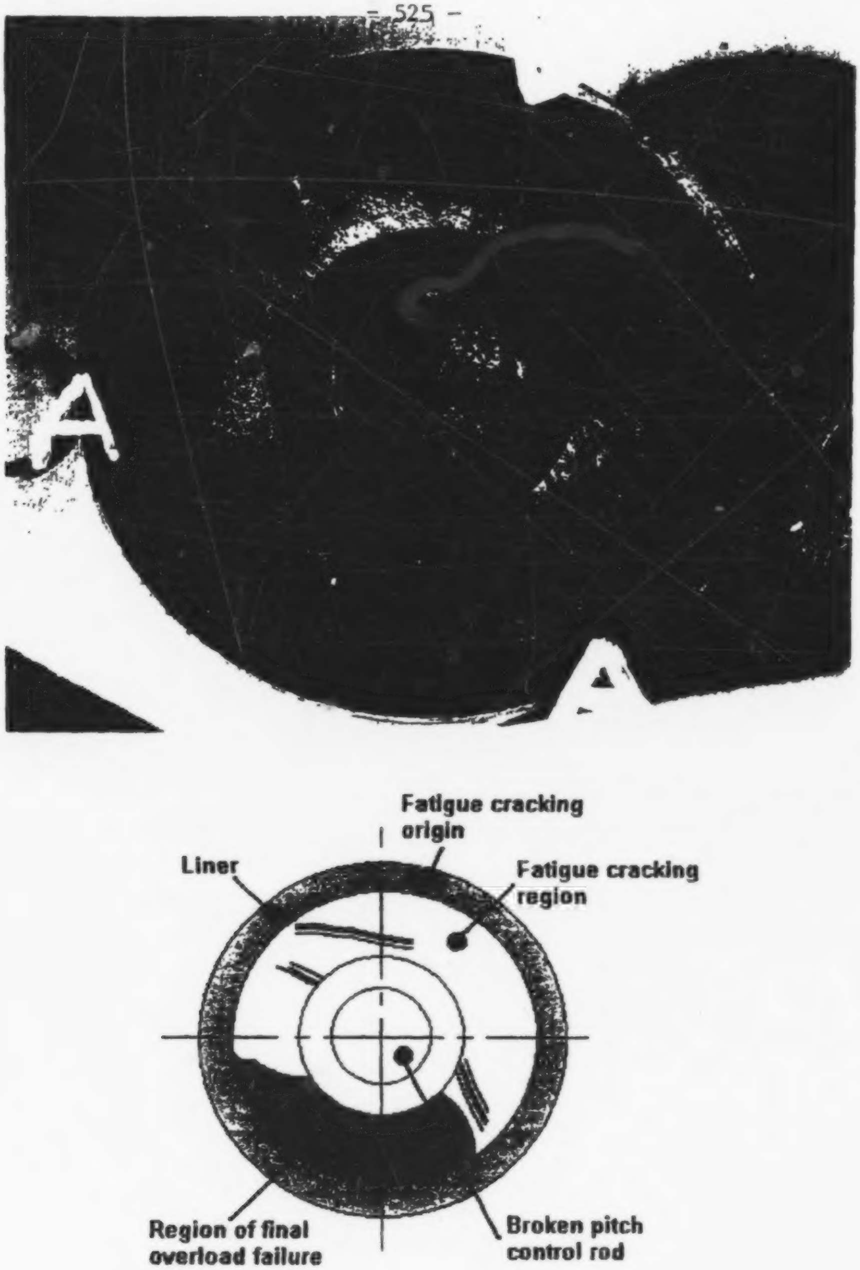
A
A
Fatigue cracking origin
Liner
Fatigue cracking region
Region of final overload failure
Broken pitch control rod

Figure 4. The photograph shows one fracture face of a broken tail shaft driving a controllable pitch propeller. The sketch below indicates the various areas of this fracture face. About 70% of the tail shaft had cracked through, by fatigue cracking, prior to final failure. (Case History #1)

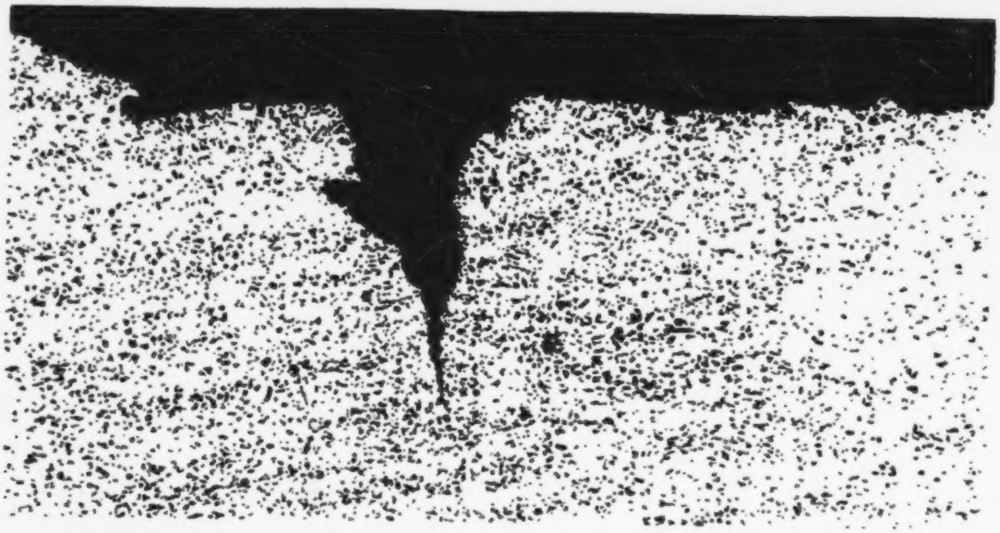

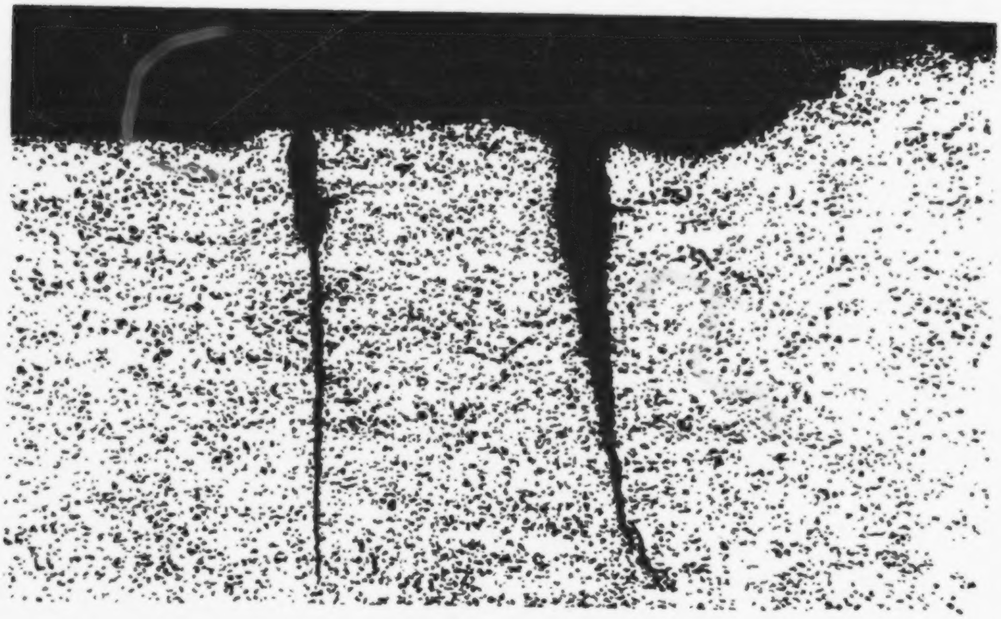

Figure 5.
Magnifications: 20x
Each of these photomicrographs shows cracking extending into the shaft from the surface. The cracks originate in corrosion pits and as they become deeper and longer, they become progressively sharper. (See Figure 6). (Case History #1)

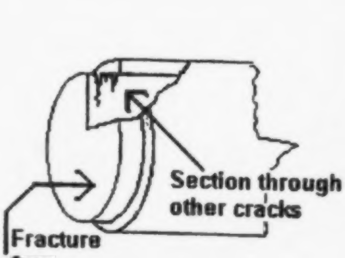
Section through other cracks
Fracture face

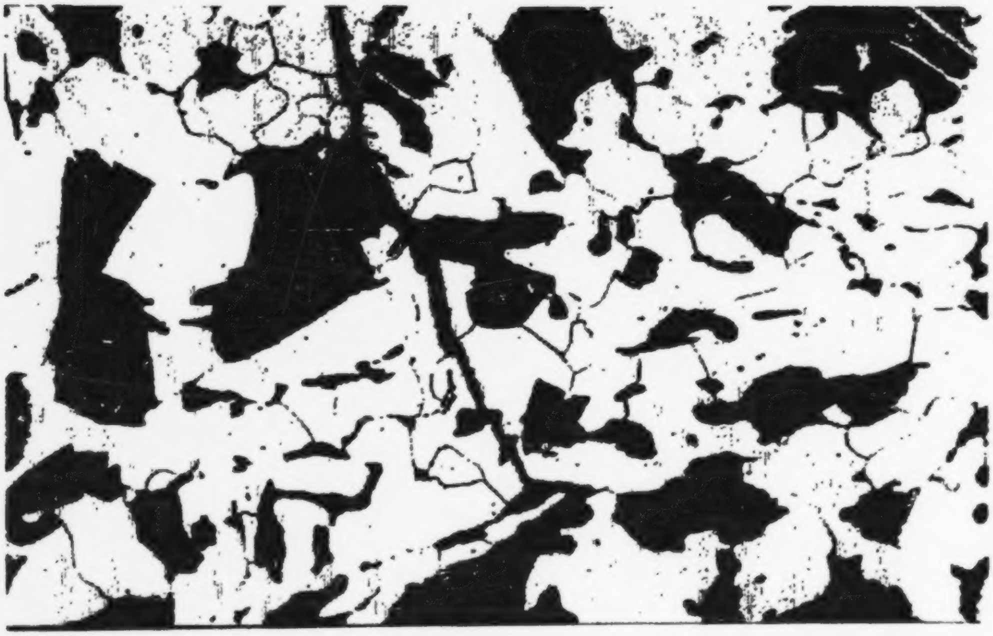

Figure 6.
Magnification 500x.
This photomicrograph shows the tip of one of the cracks in Figure 5. The crack tip is narrow and the cracking is transgranular. That is, the cracking progresses across grains rather than around them. (Case History #1)

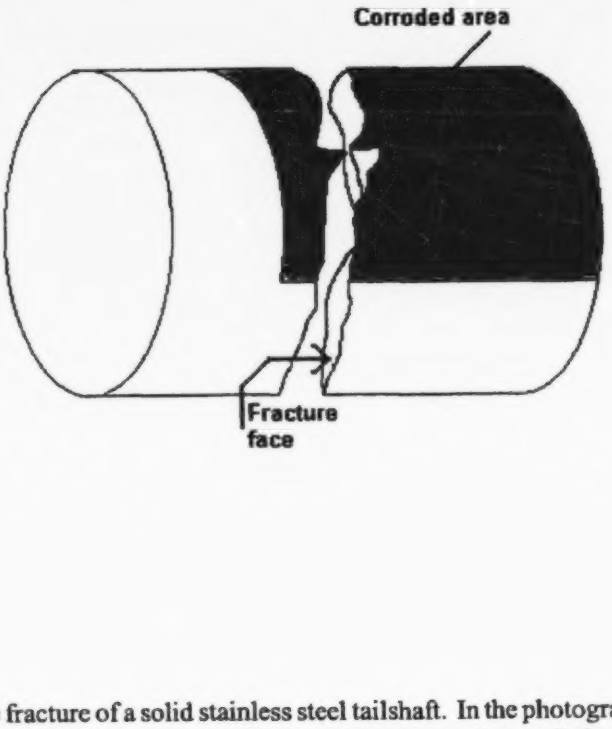

Figure 7.
Here we have the fracture of a solid stainless steel tailshaft. In the photograph note that the corroded area lies within rectangular boundaries. This would correspond to a tail shaft bearing position, within the stern tube, while the vessel was lying idle in the water. This is crevice corrosion. The corrosion fatigue cracking originated in this area of crevice corrosion cracking. (Case History #2)

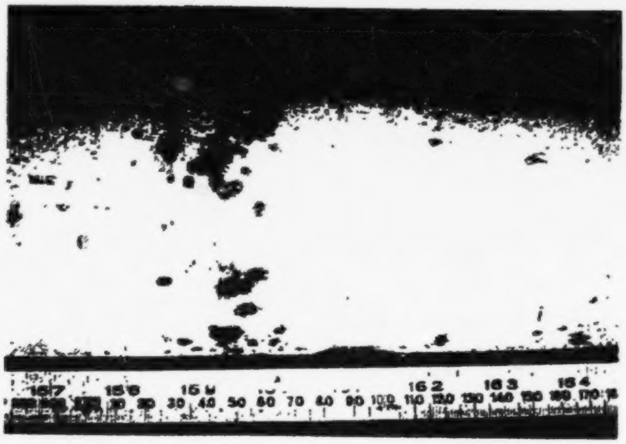

When the shaft was first examined all that was seen were many indications from corrosion pits.

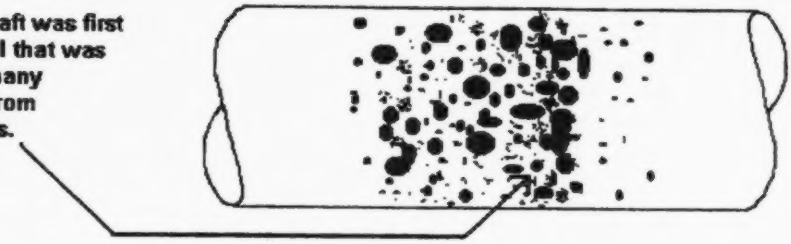

When 1 or 2 mm had been ground from the shaft, locally, linear indications were seen clearly. It is believed that these dye indications were being produced by cracks.

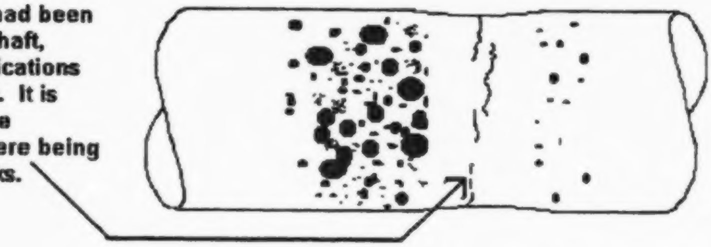

Figure 8.
On two vessels the tail shaft had failed as is shown in Figure 7. At this time two other vessels fitted with the same tailshafts were hauled out of the water. The tailshafts on these were damaged by pitting corrosion. Dye penetrant examination on the shafts at this time showed this pitting but did not reveal any cracking. When some of the pitting was removed, by grinding away 1 or 2 mm from the shaft surface, cracking was seen. (Case History #3)

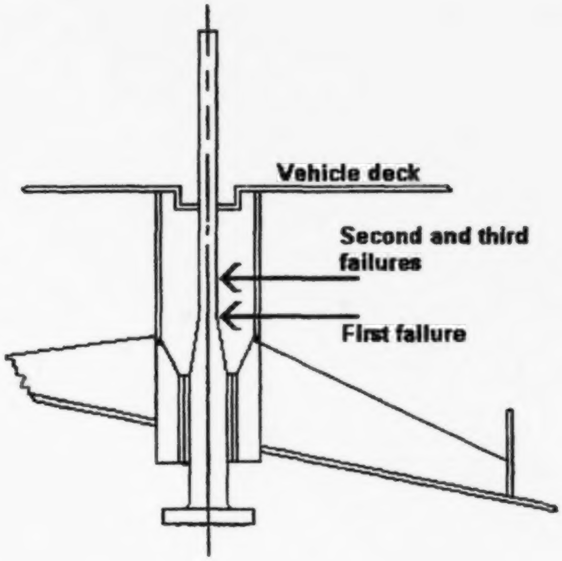
Vehicle deck
Second and third failures
First failure

Figure 9.
This sketch shows a rudder post that failed on three separate occasions over a five year period. The first two failures were blamed on striking submerged objects. The third was investigated metallurgically and proved to have resulted from corrosion fatigue cracking. (Case History #4)

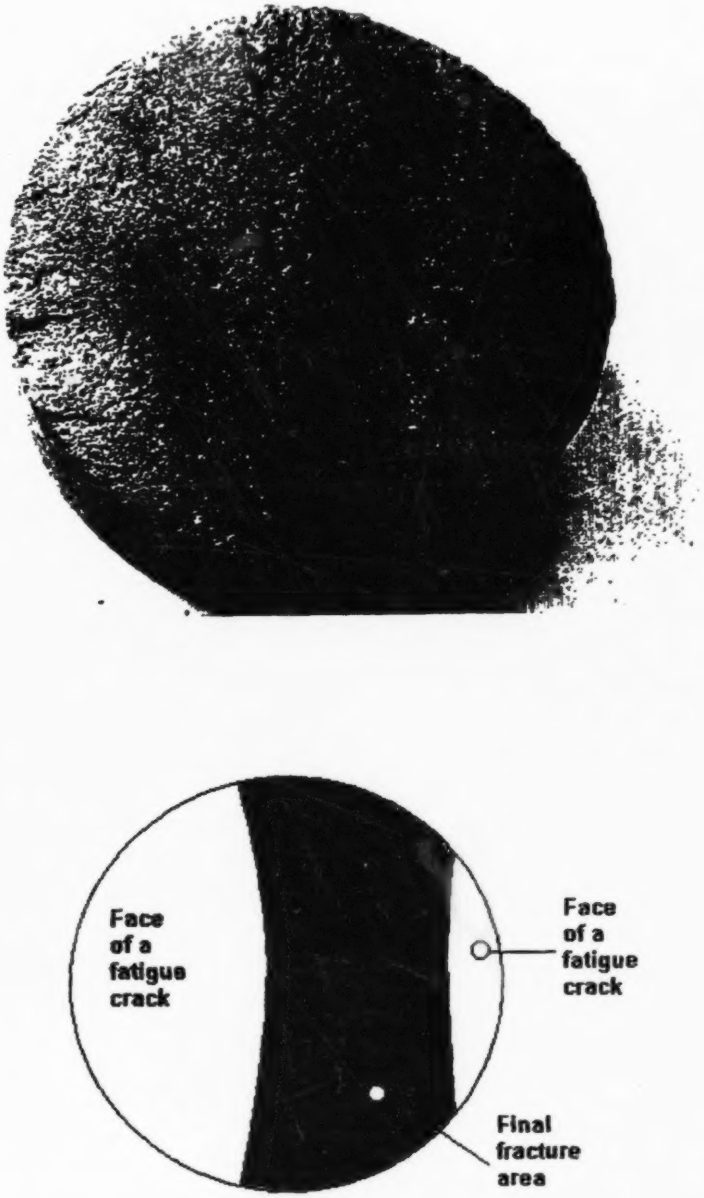
Face of a fatigue crack
Face of a fatigue crack
Final fracture area

Figure 10.
Fracture face of the rudder post after cleaning it in inhibited acid.. (Case History #4)

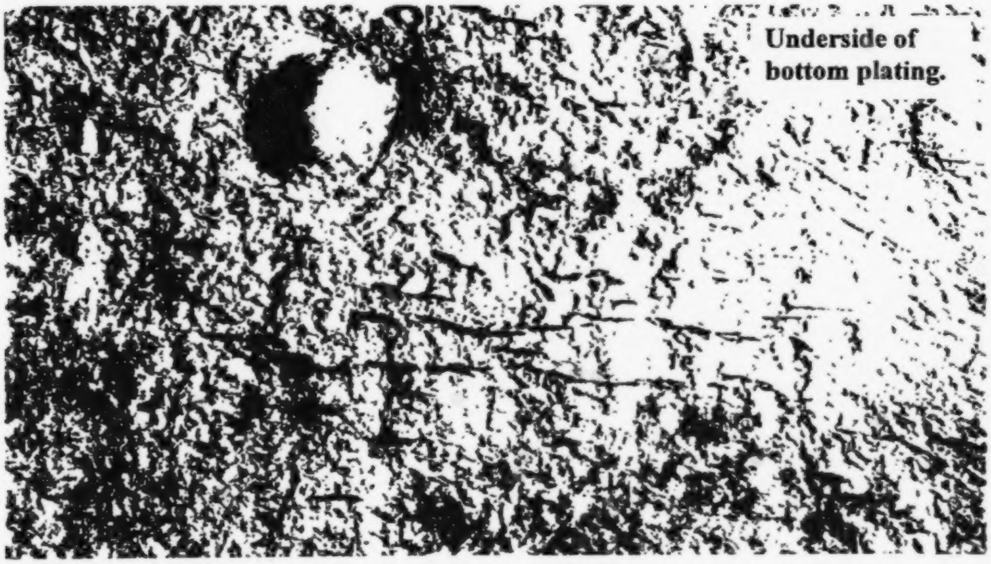

Figure 11.
10x Magnification. This photograph shows cracking in the bottom plating of a vessel. In the laboratory the cracks could only be seen after the rust adhering to the surface had been removed using a suitable acid solution. (In the field the adherent rust could have been removed in some other way to make these cracks visible.) (Case History #5)

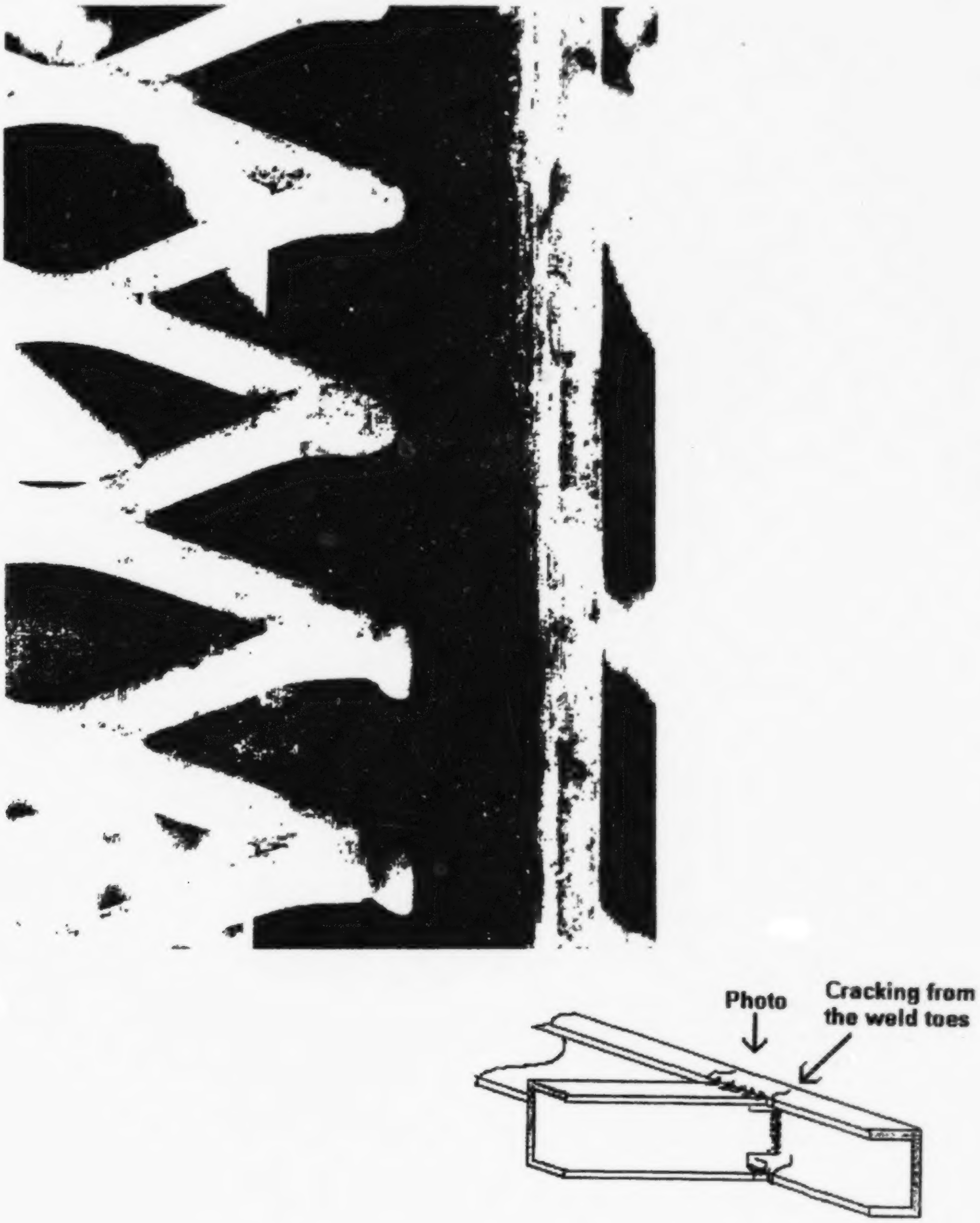
Photo
Cracking from the weld toes

Figure 12.
This welded marine structure cracked badly by fatigue cracking despite being galvanized and despite being almost completely free from corrosion. (Case History #6)

#516446

(31)

Diesel Dilemmas

by

Danny O. Morehouse, John F. Porter and John A. Hiltz

Defence Research Establishment Atlantic, Dockyard Laboratory, Halifax, N.S

Abstract

The application of diesel engines for propulsion and electrical generation on naval platforms is not new in concept and application but is becoming the general rule. This has led to design changes that have transformed the diesel into a high revving more output per pound prime mover. Maintaining robustness while delivering the required output, in as light and as small a package as possible, is a challenging task. When one factors in the problems associated with the integration with other manufacturer's systems, variations of lubricants and fuels utilized, as well as, design oversights and varied maintenance/operational environments, the odds of providing a trouble-free power plant with longevity diminishes. This presentation will cover a few of the more interesting failure investigations seen in the last five to ten years involving naval platform prime movers. Similarities will become apparent and ways of preventing future problems addressed.

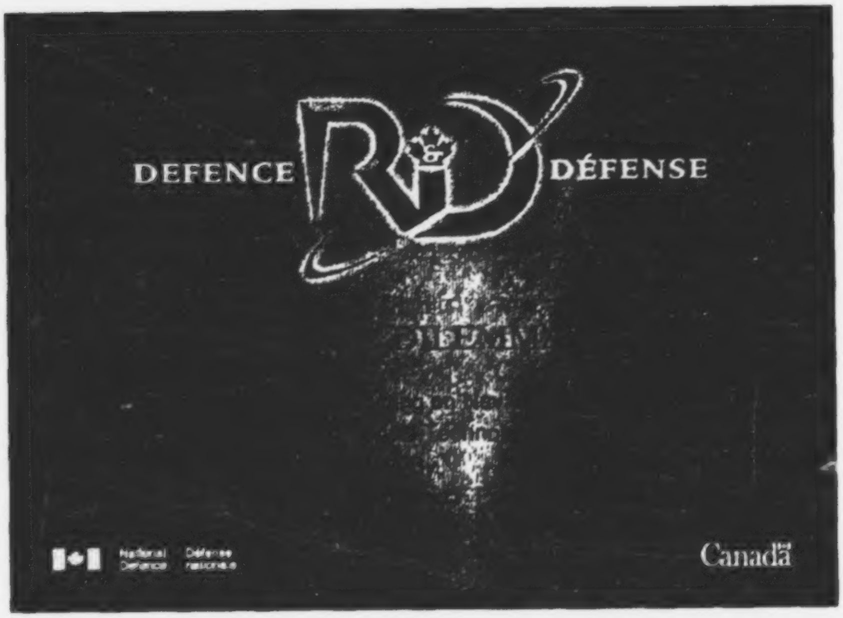

DEFENCE R&D DÉFENSE

National Defence Défense nationale

Canada

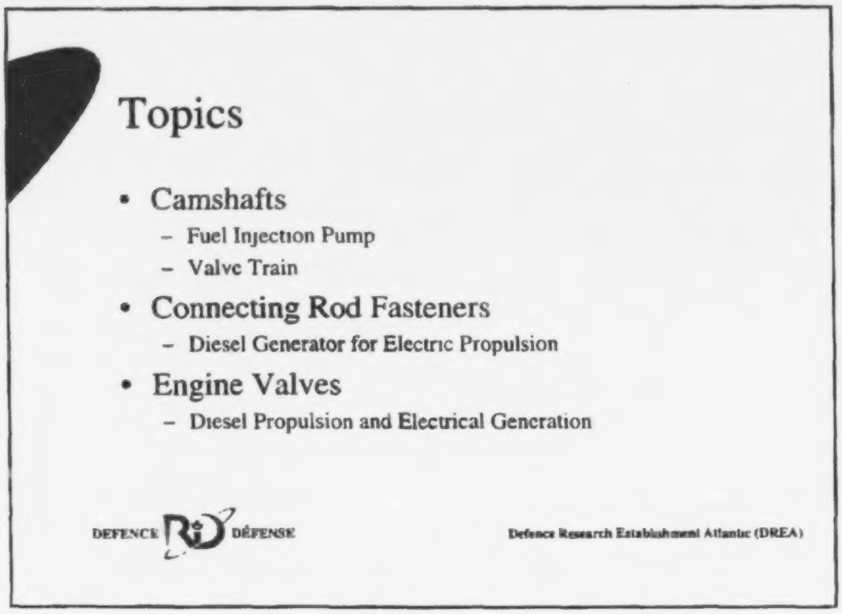

Topics

- Camshafts
  - Fuel Injection Pump
  - Valve Train
- Connecting Rod Fasteners
  - Diesel Generator for Electric Propulsion
- Engine Valves
  - Diesel Propulsion and Electrical Generation

DEFENCE R&D DÉFENSE

Defence Research Establishment Atlantic (DREA)

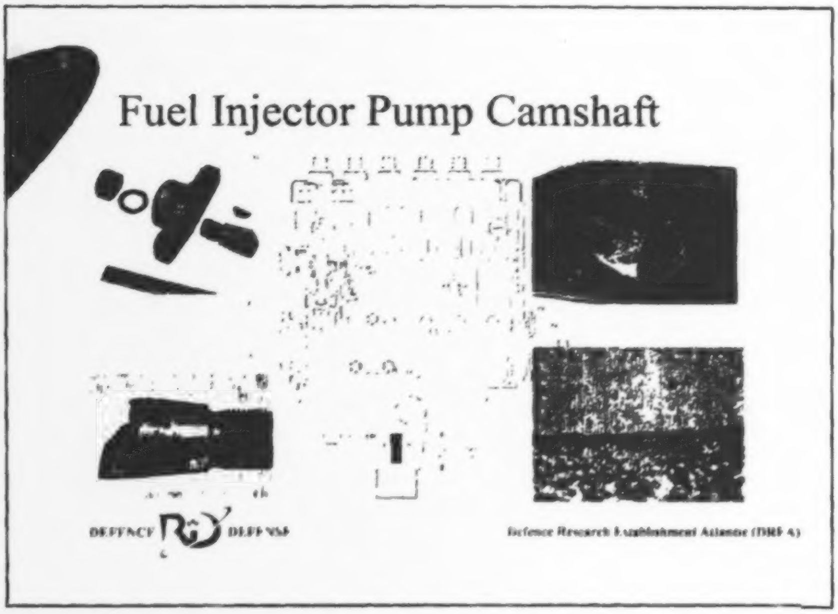

Fuel Injector Pump Camshaft

DEFENCE DEFENSE

Defence Research Establishment Atlantic (DREA)

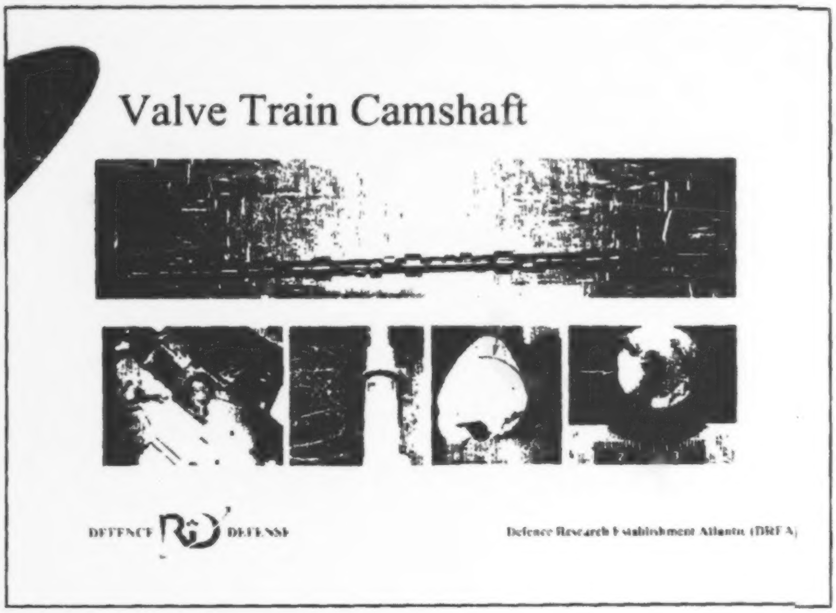

Valve Train Camshaft

DEFENCE DEFENSE

Defence Research Establishment Atlantic (DREA)

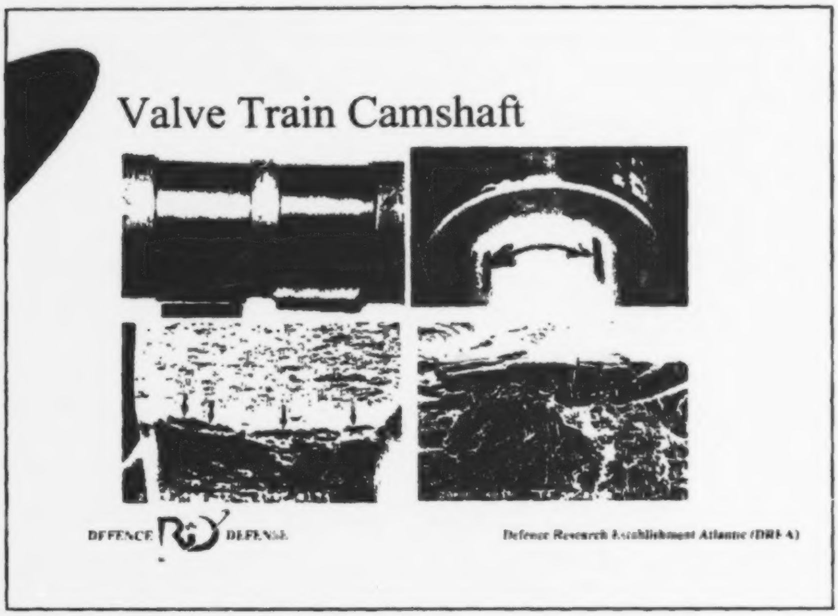

Valve Train Camshaft

DEFENCE DEFENSE

Defence Research Establishment Atlantic (DREA)

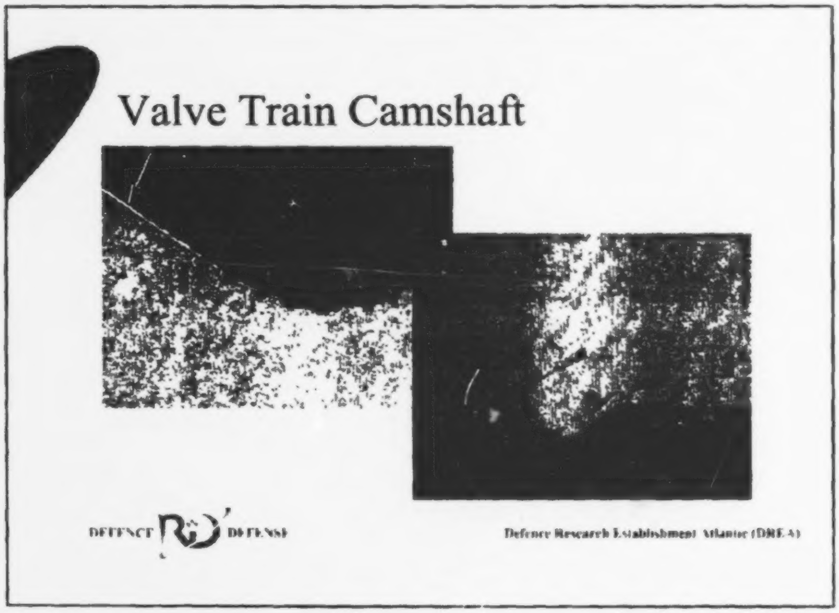

Valve Train Camshaft

DEFENCE DEFENSE

Defence Research Establishment Atlantic (DREA)

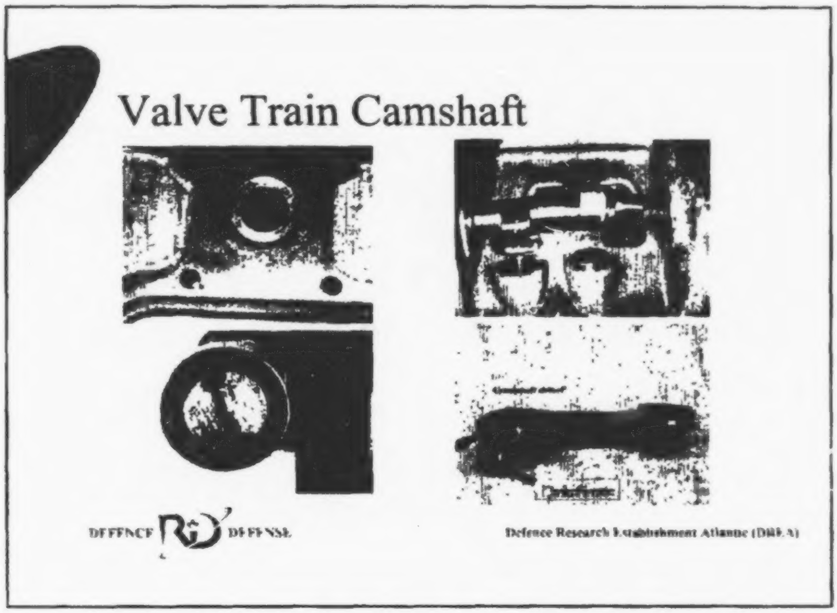

Valve Train Camshaft

DEFENCE DEFENSE

Defence Research Establishment Atlantic (DREA)

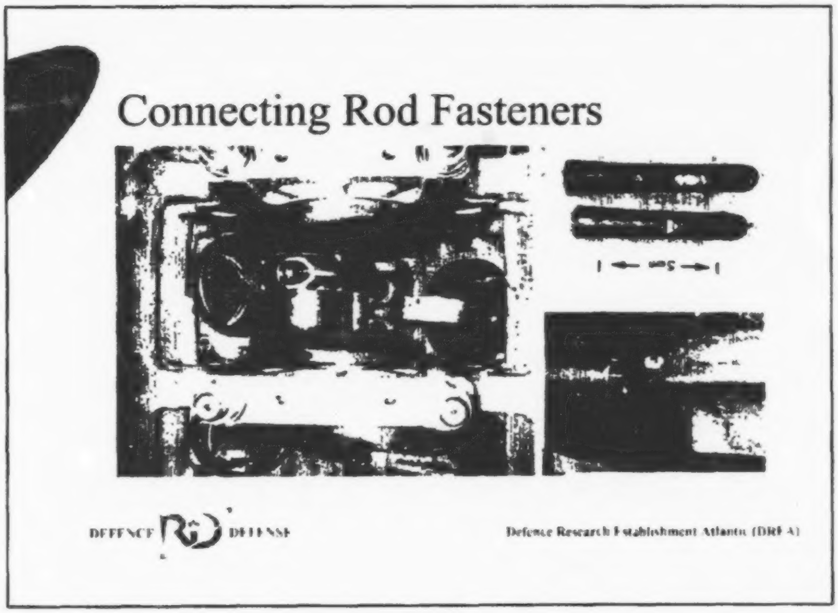

Connecting Rod Fasteners

DEFENCE DEFENSE

Defence Research Establishment Atlantic (DREA)

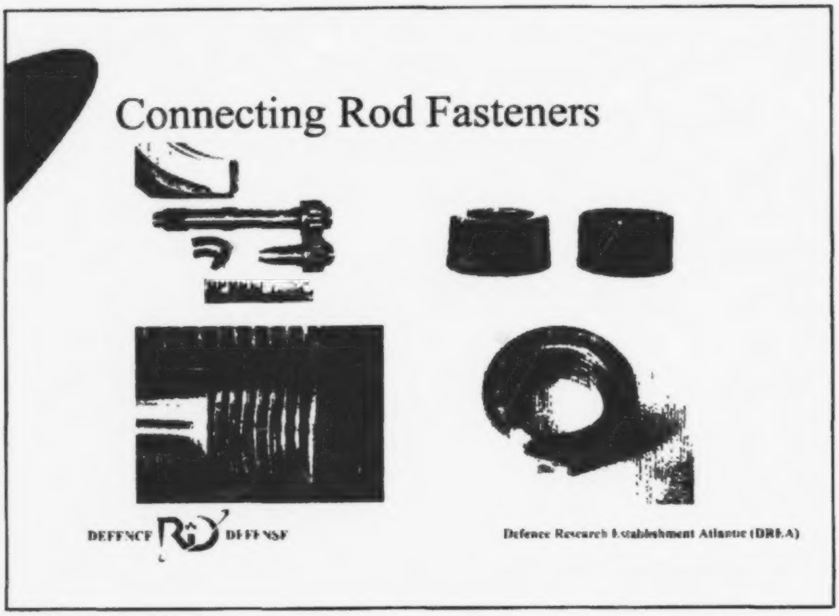

Connecting Rod Fasteners

DEFENCE DEFENSE

Defence Research Establishment Atlantic (DREA)

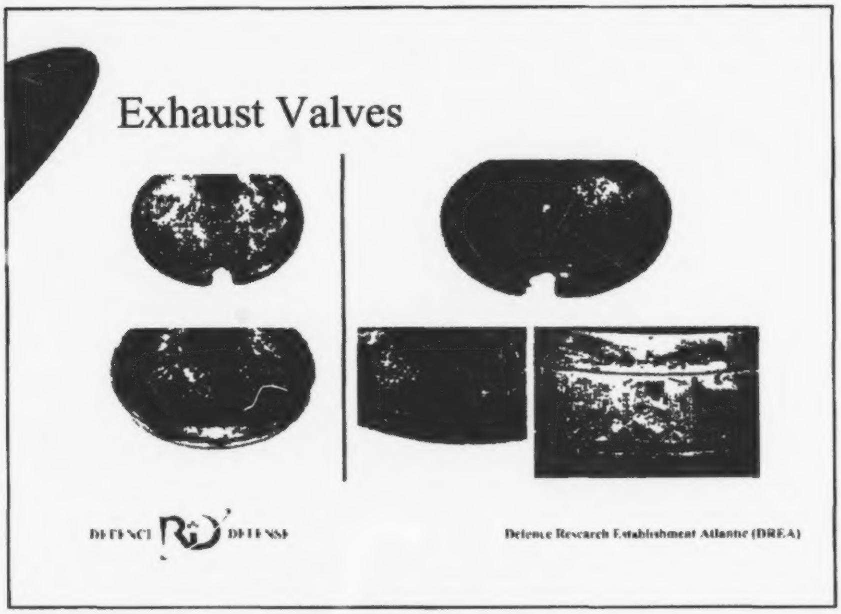

Exhaust Valves

DEFENCE DEFENSE

Defence Research Establishment Atlantic (DREA)

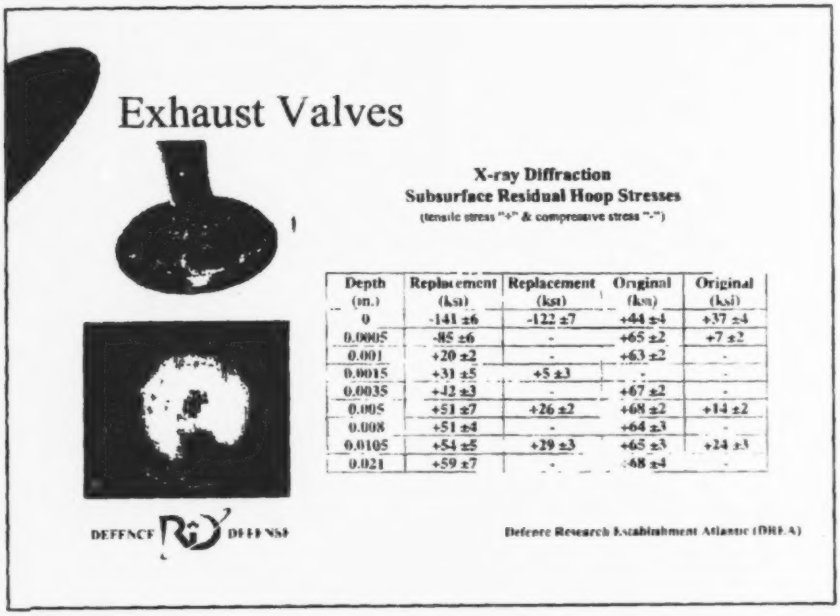

Exhaust Valves

X-ray Diffraction
Subsurface Residual Hoop Stresses
(tensile stress "+" & compressive stress "-")

Depth (in.)	Replacement (ksi)	Replacement (ksi)	Original (ksi)	Original (ksi)
0	-141 ±6	-122 ±7	+44 ±4	+37 ±4
0.0005	-85 ±6	-	+65 ±2	+7 ±2
0.001	+20 ±2	-	+63 ±2	-
0.0015	+31 ±5	+5 ±3	-	-
0.0035	+42 ±3	-	+67 ±2	-
0.005	+51 ±7	+26 ±2	+68 ±2	+14 ±2
0.008	+51 ±4	-	+64 ±3	-
0.0105	+54 ±5	+29 ±3	+65 ±3	+24 ±3
0.021	+59 ±7	-	+68 ±4	-

DEFENCE DEFENSE

Defence Research Establishment Atlantic (DREA)

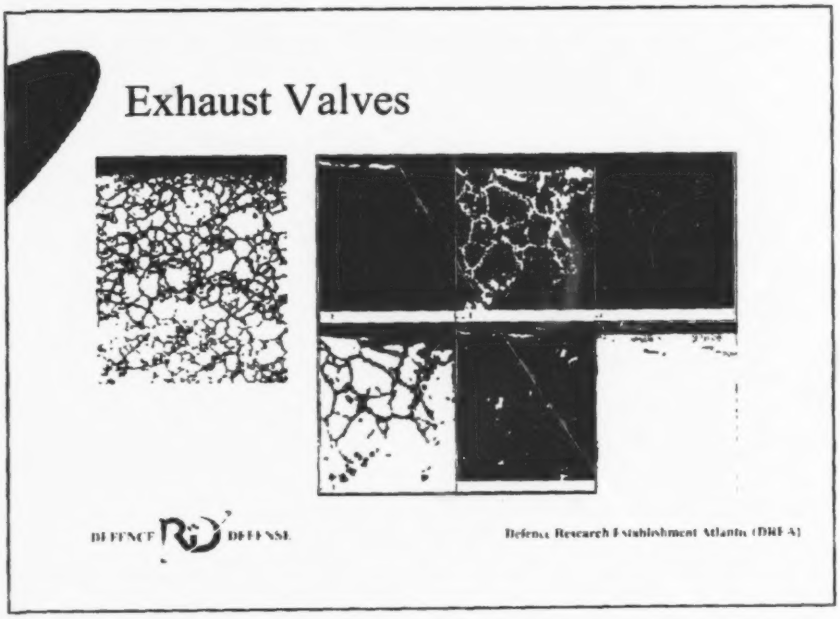

Exhaust Valves

DEFENCE DEFENSE

Defence Research Establishment Atlantic (DREA)

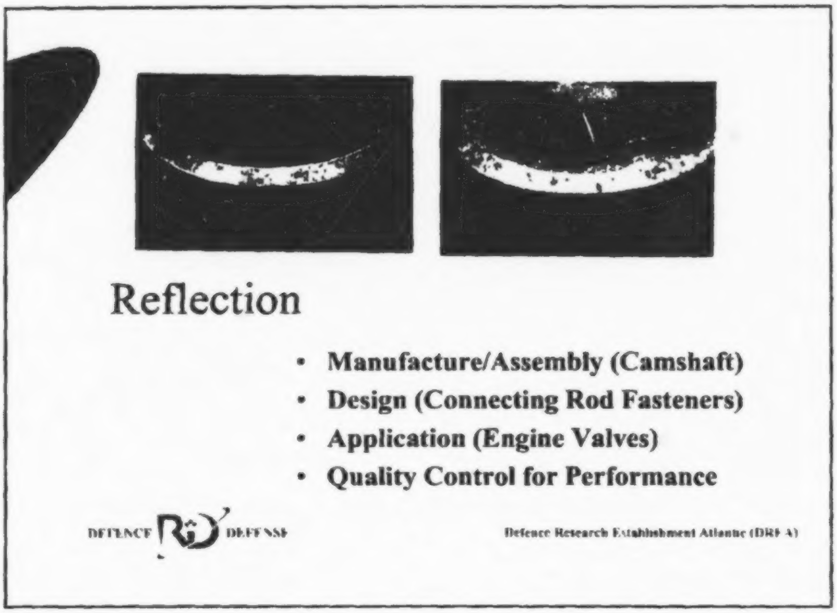

Reflection

- Manufacture/Assembly (Camshaft)
- Design (Connecting Rod Fasteners)
- Application (Engine Valves)
- Quality Control for Performance

DEFENCE DEFENSE

Defence Research Establishment Atlantic (DREA)

ULTRASONIC WELD TESTING AND IMAGING USING PORTABLE AUTOMATED ARM

A. CHAHBAZ, A. CYR, R. SICARD
A. PELLETIER AND M. BRASSARD

TEKTREND INTL , NDT TECHNOLOGY AND DEVELOPMENT
2001 ST REGIS BLVD , MONTREAL, QUE , H9B 2M9
research@tektrend com

DR. J. R. MATTHEWS

DOCKYARD LABORATORY ATLANTIC
DREA, HALIFAX, N S B3K 5X5
jim.matthews@drea dnd ca

ABSTRACT

Automated and manual ultrasonic techniques are rapidly becoming as popular as conventional radiographic techniques for weld testing applications, However, for automated ultrasonic techniques, inspection cycle time and defect/data interpretation represent important factors.

In this work, we describe the use of portable automated PC-based ultrasonic scanner to inspect simulated and real naval construction welds. The system is a self-contained single unit in which all electronic boards are mounted in the system server workstation. The system offers advanced analysis and interpretation capabilities, and can display the raw and interpreted inspection results in a realistic 3D representation.

We also examine the resulting scan images from two inspection setups used to improve inspection reliability and defect interpretation in terms of detectability of weld defects. We then averaged and reconstructed the images using a Syntactic Aperture Focusing Technique SAFT technique with an attenuation correction factor introduced to improve resolution for long propagation paths.

The Syntactic Aperture Focusing Technique (SAFT) makes it possible to increase the signal-to-noise ratio by averaging several shifted reflections from the same defect point. Lateral resolution is therefore improved, especially for long probe-to-defect distances. Moreover, the resolution remains constant along the beam axis, avoiding beam width perturbations and providing the user with a reconstructed image that makes defect interpretation easier.

INTRODUCTION

The three most popular methods for weld inspection are Radiography, Ultrasonic Angle Beam Pulse-Echo and Time-of-Flight Diffraction. The last two methods have their own advantages and drawbacks, and do not provide full characterization of weld defects. Advanced processing techniques such as SAFT, are required to assist in characterization and precise flaw imaging.

In this work, we investigate multi-path SAFT algorithm using Ultrasonic Angle Beam Pulse-Echo to detect common pipeline weld defects (lack of fusion, lack of penetration and slag inclusion) and compare it to TOFD and time-of-flight results. Using beam width limitation with the implemented SAFT algorithm, we achieved reasonable computation time for SAFT imaging. And to improve the ultrasonic beam resolution, an attenuation correction factor was introduced.

NDI TECHNIQUES FOR WELD EVALUATION

Manual and automated ultrasonic techniques are rapidly becoming as popular as conventional radiographic techniques. They offer great potential for weld inspection since they can be employed on in service complex welded components. The most commonly used techniques are Ultrasonic Angle Beam Pulse-Echo and Time-of-Flight Diffraction. The advantages and drawbacks of these techniques are described in Table 1:

Table 1. *Advantages and drawbacks of ultrasonic PE and TOFD*

Pulse-Echo
Advantages
▪ Good sizing accuracy in the weld axis. ▪ Excellent POD for various well oriented defects.
Drawbacks
▪ Very sensitive to defect orientation. ▪ Weak response with off-angle planar and volumetric flaws. ▪ Need to have "echo dynamics" information (need to use several angles simultaneously to insure defect coverage). ▪ In some cases, poor defect-sizing information is obtained because it is based on reflected signal amplitude.

TOFD
Advantages
▪ Once a defect is identified, vertical sizing is very accurate. ▪ Often used as a safety net for some critical defects. ▪ Improve assessment of mismatch (high-low).
Drawbacks
▪ Very weak response (low SNR) from defect tips diffraction. ▪ Classical TOFD use the assumption that the flaw is positioned symmetrically between the probes, which is rarely true. ▪ Bad spatial resolution because of wide beam spread ▪ Dead zone effect near the entry surface.

TOFD
▪ Diffraction is more complex than reflection. Unlike PE method, it becomes difficult to analyze results for complex situations (due to mode conversions etc...).
▪ Requires a second axis of motion (D-Scan) to define the side of weld on which the defects occurs.
▪ Optimum probe center spacing can result in probe interference with weld cap.
▪ Mismatch conditions can mask defects in back wall signal.
▪ TOFD data are relatively big as multi-channel PE data.

SAFT DATA ACQUISITION, PRINCIPLES AND ADVANTAGES

For automated ultrasonic techniques, inspection cycle time and defect/data interpretation represent important factors. The system used in our experimentation is an automated self-contained ultrasonic unit[1]. It features a data acquisition module, advanced analysis and interpretation capabilities, and can display the raw and interpreted inspection results in a realistic representation.

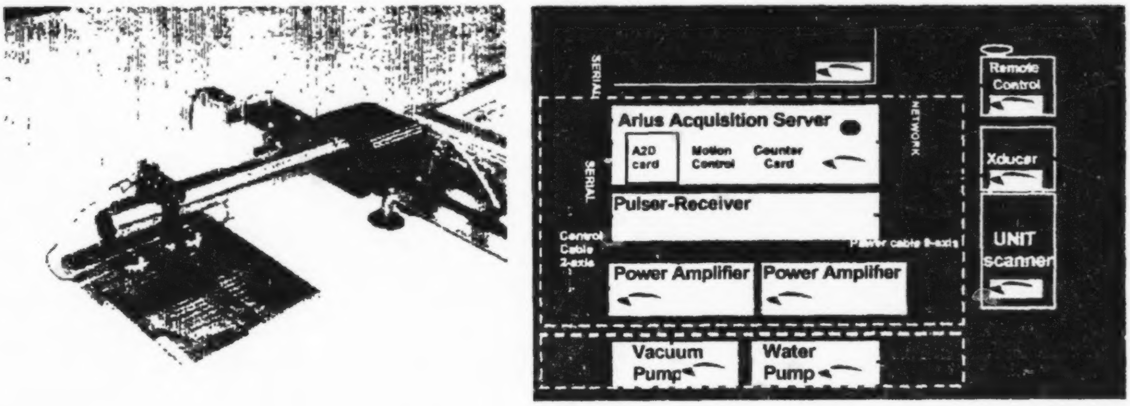
SERIAL
Remote Control
Arius Acquisition Server
A2D card
Motion Control
Counter Card
NETWORK
Xducer
SERIAL
Pulser-Receiver
Control Cable 2-axis
Power cable 8-axis
UNIT scanner
Power Amplifier
Power Amplifier
Vacuum Pump
Water Pump

Figure 1. System configuration and setup for weld testing

The complete system comprises the hardware and software modules with

The software also includes simple and multi-SAFT imaging modules. The principle of conventional SAFT is to extrapolate for each transducer position and provide the sum of energy reflected and transmitted at all transducer positions (Figure 2). The extrapolation process, called back-propagation, sums up in phase signals received due to scattering on defects and signals received due stochastic noise are averaged. The great advantage of SAFT is the increase of lateral resolution, which becomes theoretically constant along the material depth. Resolution evaluation is usually provided by the estimation of the PSF (Point Spread Function) width and height resulting from SAFT processing on a point-like defect response[2].

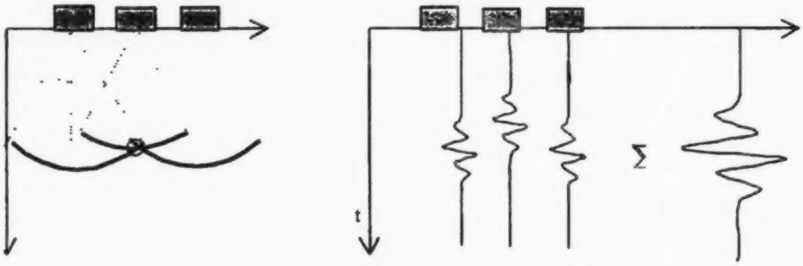

Figure 2. *SAFT extrapolation principle*

With SAFT imaging, resolution and signal-to-noise enhancement depend strictly on the acquisition aperture size. Therefore, *increasing the effective aperture* is the key to benefiting from SAFT's advantages. There are several practical ways to do this, including wide beam transducers, multiple wave paths including boundary reflections, pitch-catch configuration and fusion of reconstructed images acquired through different apertures. In this experimental work and since welded structures are inspected, multi-path SAFT algorithm was implemented and tested[3]. With this technique, multiple wave paths with boundary reflections are used to improve resolution of classical SAFT by increasing the effective aperture and information focusing. The same formulation as conventional SAFT :s used for multi-path process but summated on several paths (Figure 3).

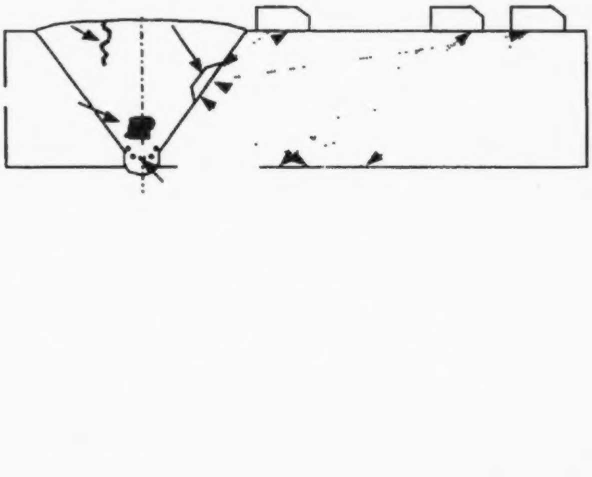

Using boundary reflections with multi-paths SAFT, long aperture paths are involved. Hence, an attenuation correction factor composed of the incident and scattering coefficients was introduced to the formulated mult-path SAFT algorithm to compensate for attenuation caused by spreading and absorption losses. Moreover, a beam width limitation was also implemented to reduce calculation time.

INSPECTION RESULTS AND WELD EVALUATION

In the scope of this work, experiments were conducted on simulated carbon steel construction weld containing four common pipeline weld flaws (Figure 4). Tests were first performed with TOFD technique and then conventional pulse-echo method to apply the multi-path SAFT. Figure 5 shows the TOFD results presented in B-scan, using color scale level. Inspection was performed on the specimen along the Y-direction using single pass in pitch-catch at 5 MHz with 0.25" angle beam transducer to generate 65° shear waves.

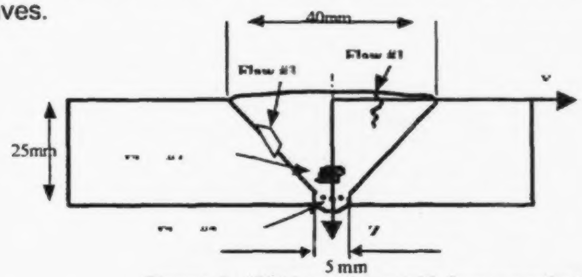

Figure 4. Weld specimen with four manufactured flaws

Table 2. Flaws dimension and location

Flaw #	Description	Distance from reference to indication		Flaw depth	Flaw height	Flaw length
		"X"	"Y"	"Z"		
1	Longitudinal crack	-0.2"	2.0"	Surface breaking	0.4"	0.5"
2	Lack of penetration	0.0"	4.75"	0.9"	0.1"	0.4"
3	Lack of fusion	0.35"	6.75"	0.3"	0.2"	0.5"
4	Slag inclusion	0.0"	9.5"	0.75"	0.1"	0.5"
Note: Flaw no. 2 is surface breaking on backwall						

Results in figure 5 show the TOFD indications from the detected defects. The relatively high amplitude of the diffracted and reflected mode represents indication of flaws. Table 3 compares the measured and the real dimension of the detected flaws. Size and depth of the detected flaws with TOFD was calculated with simple Pythagorean principles[4].

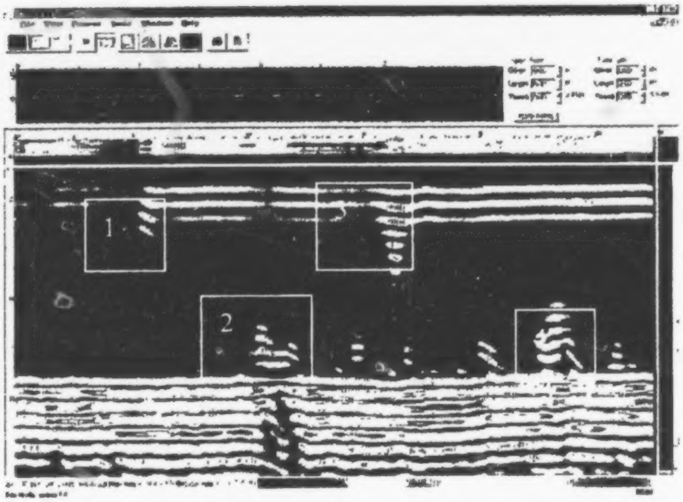

Figure 5. TOFD B-scan with color scale levels

Table 3. Flaw characterization with TOFD

Flaw	T_1	T_2	Depth			Heigth		
			Measured	Real	Error	Measured	Real	Error
1	N/a	17.14 μs	N/a	N/a	N/a	0.41"	0.4"	+0.01"
2	18.06 μs	18.48 μs	0.77"	0.9"	-0.13"	0.13"	0.1"	+0.03"
3	16.86 μs	17.54 μs	0.17"	0.3"	-0.13"	0.42"	0.2"	+0.22"
4	17.86 μs	18.48 μs	0.71"	0.75"	-0.04"	0.19"	0.1"	+0.09"

A second set of tests was performed in pulse-echo at 5 MHz with 0.25" angle beam transducer at 60°. Several lines of scans were performed and recorded. Figure 6 shows the C-scan results of the inspection displayed as conventional 0° pulse-echo scan. Each point on the C-scan originates from a different transducer position.

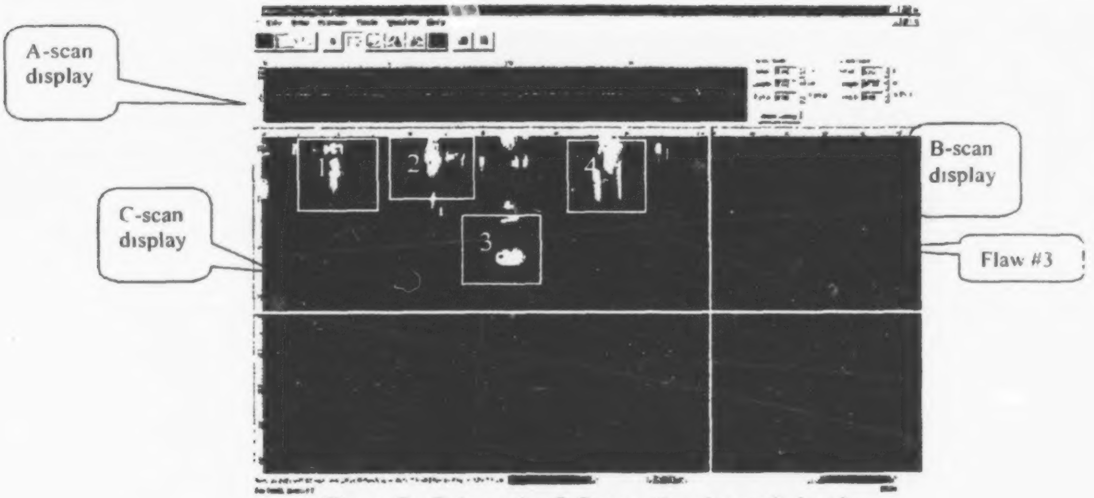

Figure 7. Pulse-echo C-Scan with color scale levels

Table 4. Flaw characterization with PE

Flaw	Depth			Heigth		
	Measured	Real	Error	Measured	Real	Error
1	N/a	N/a	N/a	0.35"	0.4"	0.05"
2	0.80"	0.9"	0.1"	0.11"	0.1"	0.01"
3	0.10"	0.3"	0.20"	0.13"	0.2"	0.07"
4	0.74"	0.75"	0.01"	0.26"	0.1"	0.16"

For each detected flaw with the pulse-echo setup, the time-of-flight was taken to calculate the distance and depth by simple trigonometric approach. Next, the welded construction was scanned using a 2.25 MHz 0.25" diameter probe at 45^0 for the Multi-path SAFT evaluation. Only flaws number 2, 3 and 4 were inspected for the multi-path SAFT. Flaw 1 is not deep enough; thus, with the SAFT we could obtain any increase in the lateral resolution.

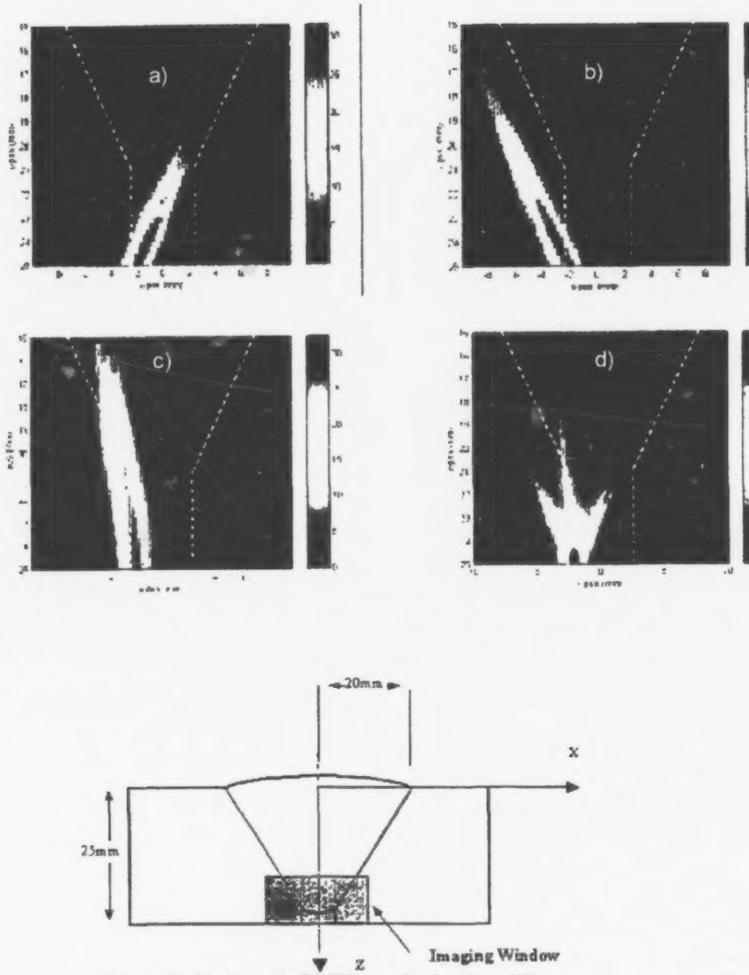

Figure 8. Multi-path SAFT results for flaw #2

Lack of penetration results were computed with paths (0,0), (1,1), (0,1) (1,0). Focusing effect of the multi-path image reconstruction is shown in Figure 8d where all paths were considered. Accuracy in the flaw sizing was highly improved when using all wave paths to reconstruct the flaw at a threshold of –6dB. Setting the threshold was arbitrary, however, an important parameter to accurately calculate the size of the flaw.

Figure 9 shows images of lack of fusion weld flaws computed with single and multi-paths at 10° beam spread angle. In Figure 8a, wave path (0,0) was employed for the image reconstruction. However, paths (0,0), (0,1) and (1,1) were considered for the computation of Figure 8b. It was clearly noted that, the contributions of all paths were week compared to path (1,1). This was caused by the highly oriented nature of the lack of fusion flaw.

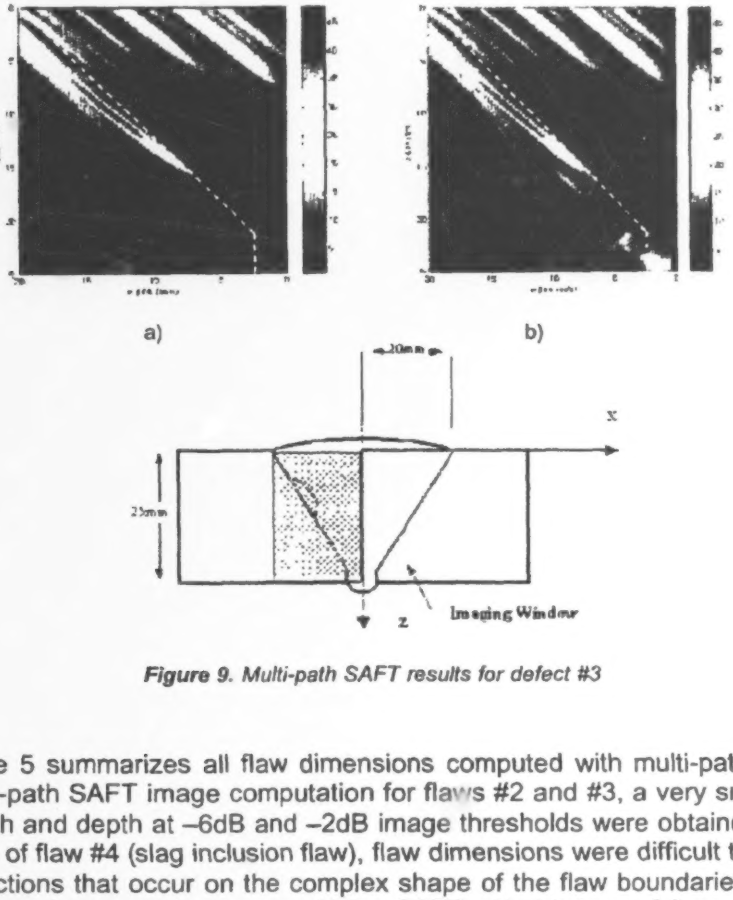

a)

b)

Figure 9. Multi-path SAFT results for defect #3

Table 5 summarizes all flaw dimensions computed with multi-path SAFT. From the multi-path SAFT image computation for flaws #2 and #3, a very small error in the flaw length and depth at –6dB and –2dB image thresholds were obtained. However, in the case of flaw #4 (slag inclusion flaw), flaw dimensions were difficult to obtain. The multi-reflections that occur on the complex shape of the flaw boundaries make it difficult to interpret the computed image. Using SAFT with this type of flaws requires careful and more appropriate signal acquisition.

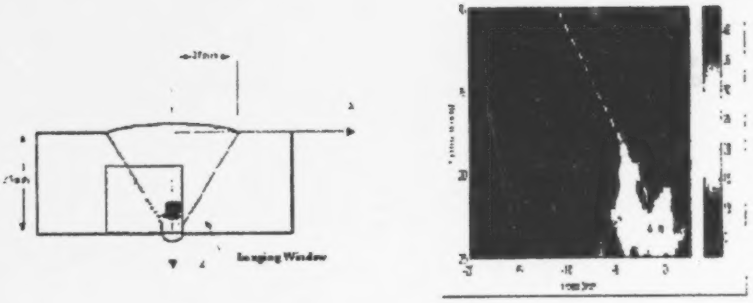

Figure 10. Multi-path SAFT results for defect #4

Table 5. Flaw characterization with SAFT using PE setup

Flaw	Depth			Height		
	Measured	Real	Error	Measured	Real	Error
1	N/a	Surface	N/a	N/a	0.4"	N/a
2	0.903"	0.935"	0 03"	0.09"	0.1"	0.01"
3	0 29"	0.3"	0.005"	0.19"	0.2"	0.004"
4	N/a	0.75"	N/a	N/a	0.1"	N/a

CONCLUSIONS

The principle of multi-path SAFT was investigated using pulse-echo setup to detect common pipeline weld defects. SAFT results were compared to TOFD and time-of-flight tests.

Compared to the TOFD and PE results, the multi-path SAFT algorithm presented good accuracy for two flaws. The use of the reconstruction helped to increase focusing and the effective testing aperture. In the case of highly oriented or complex surface flaw, the SAFT theoretical accuracy could not be reached, since, only some few scattered rays are received. Improvement of the inspection mode while using SAFT should help to improve the accuracy. Currently, a split angle pitch-catch version of the algorithm is being tested.

Critical algorithm parameters have also been identified (reconstructed image threshold, beam width limitation, wave velocity and wedge delay). Our experimental results showed that, a practical use of the multi-path SAFT requires a specific and careful testing procedure to calibrate these critical parameters.

REFERENCES

---

[1] PANDA system see http://www.tektrend.com/products/products/panda.html

[2] R.N Thomson, Transverse and longitudinal resolution of the synthetic aperture focusing technique, ULTRASONICS, Jan. 1984

[3] F. Ganansia, A.Chahbaz and K. Mborokih, "Experimental Evaluation of Weld Defects Using Multi-Path SAFT," QNDE, Montreal. 25 July 1999

[4] J.P. Charlesworth, J.A.G. Temple," Engineering Application of Ultrasonic TOFD" RSP, Johon Wiley

#516448 (3.3)

Reference Temperatures for 350WT and A517 Plate and Welds

by

J. Morrison[1], X. Wu[2], and D.A. Hull[3]

[1] Dockyard Laboratory (Pacific), Victoria, BC
[2] Bombardier Aerospace, Montreal, PQ
[3] Engineering Material Research, Downsview, ON

Abstract

An experimental program at the Dockyard Laboratory (Pacific) and Engineering Material Research is assessing whether master curve technology can provide an effective way of quantifying hull toughness for warship cleavage fracture control.

Reference temperature and master curve determinations have been made for CSA350WT and ASTM A517 steel plates and welds using the ASTM test method E1921. This procedure generates K_{Jc} toughness transition curves statistically from the analysis of toughness data populations. The effect of orientation and loading rate on cleavage crack initiation toughness has been studied using both servo-hydraulic and drop tower instrumentation.

In almost all cases the toughness data generated met the validity requirements of the standard. Comparisons have been made with notched bar impact test energies and nil ductility transition temperatures. The results have also been evaluated in terms of the expected toughness requirement for a ship structural detail.

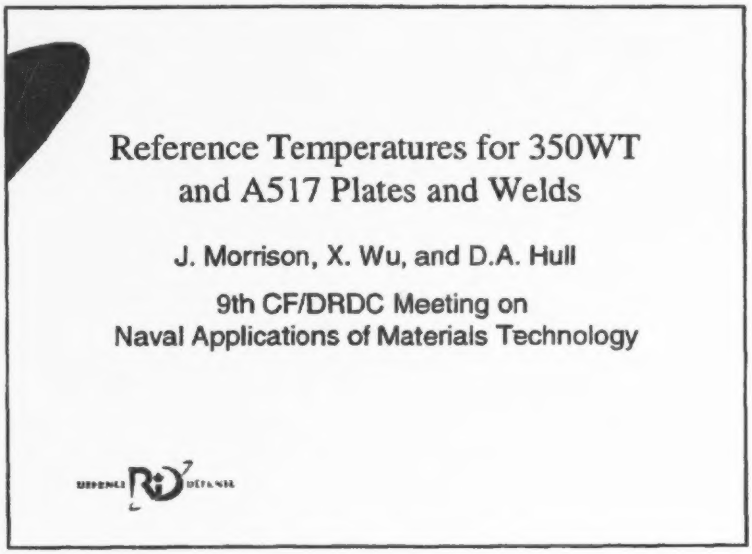

Reference Temperatures for 350WT and A517 Plates and Welds

J. Morrison, X. Wu, and D.A. Hull

9th CF/DRDC Meeting on
Naval Applications of Materials Technology

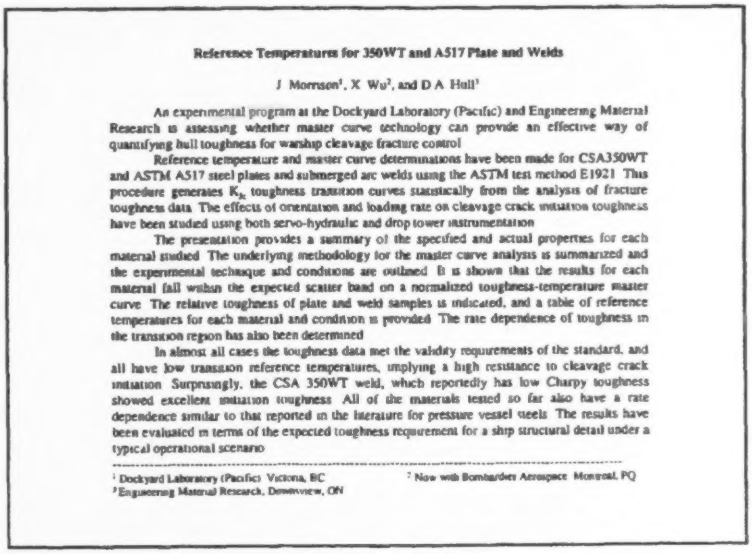

Reference Temperatures for 350WT and A517 Plate and Welds

J Morrison[1], X Wu[2], and D A Hull[3]

An experimental program at the Dockyard Laboratory (Pacific) and Engineering Material Research is assessing whether master curve technology can provide an effective way of quantifying hull toughness for warship cleavage fracture control

Reference temperature and master curve determinations have been made for CSA350WT and ASTM A517 steel plates and submerged arc welds using the ASTM test method E1921 This procedure generates K_{Jc} toughness transition curves statistically from the analysis of fracture toughness data The effects of orientation and loading rate on cleavage crack initiation toughness have been studied using both servo-hydraulic and drop tower instrumentation

The presentation provides a summary of the specified and actual properties for each material studied The underlying methodology for the master curve analysis is summarized and the experimental technique and conditions are outlined It is shown that the results for each material fall within the expected scatter band on a normalized toughness-temperature master curve The relative toughness of plate and weld samples is indicated, and a table of reference temperatures for each material and condition is provided The rate dependence of toughness in the transition region has also been determined

In almost all cases the toughness data met the validity requirements of the standard, and all have low transition reference temperatures, implying a high resistance to cleavage crack initiation Surprisingly, the CSA 350WT weld, which reportedly has low Charpy toughness showed excellent initiation toughness All of the materials tested so far also have a rate dependence similar to that reported in the literature for pressure vessel steels The results have been evaluated in terms of the expected toughness requirement for a ship structural detail under a typical operational scenario

---

[1] Dockyard Laboratory (Pacific) Victoria, BC

[2] Now with Bombardier Aerospace Montreal, PQ

[3] Engineering Material Research, Downsview, ON

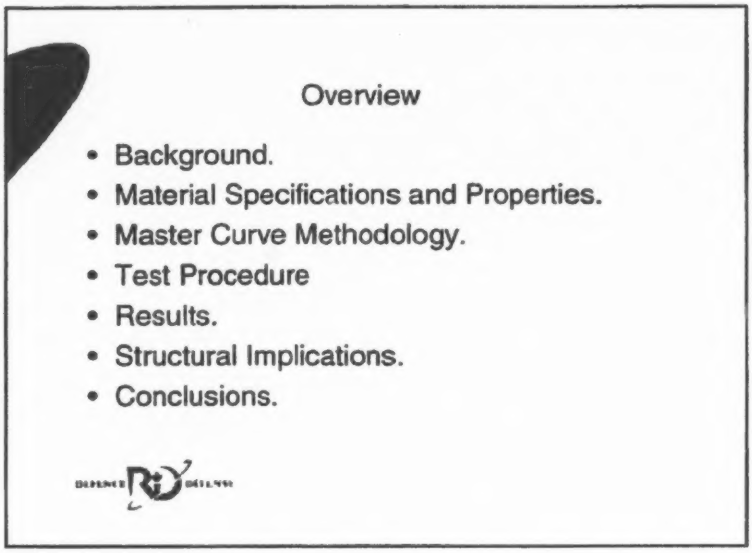

Overview

- Background.
- Material Specifications and Properties.
- Master Curve Methodology.
- Test Procedure
- Results.
- Structural Implications.
- Conclusions.

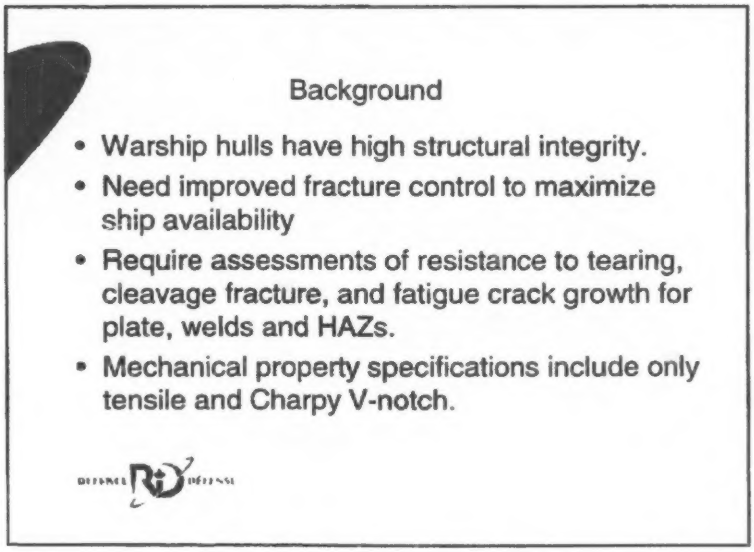

Background

- Warship hulls have high structural integrity.
- Need improved fracture control to maximize ship availability
- Require assessments of resistance to tearing, cleavage fracture, and fatigue crack growth for plate, welds and HAZs.
- Mechanical property specifications include only tensile and Charpy V-notch.

- Limited thickness invalidates K_{Ic} tests.
- Can master curve methods quantify brittle fracture resistance of ship steels?
- Would the results be useful for material selection/qualification and structural integrity assessment?
- What criteria or correlations would be appropriate for naval applications?

Specification -CSA 350WT

- CSA G40.21 Grade 350WT Cat 5 plate. (6mm-30mm)
- Chemical composition (wt %):

C	P	S	Nb+V	Mn	Si
0.22max	0.03max	0.04max	0.1max	0.8-1.5	0.15-0.4

- Mechanical properties

Yield stress (MPa)	350 min.
UTS (MPa)	480-650
elongation (%)	22 min.
Charpy V @ -40°C (J)	40 min.

(additional Charpy requirements 65 J @ +20°C & 20J @ -60°C)

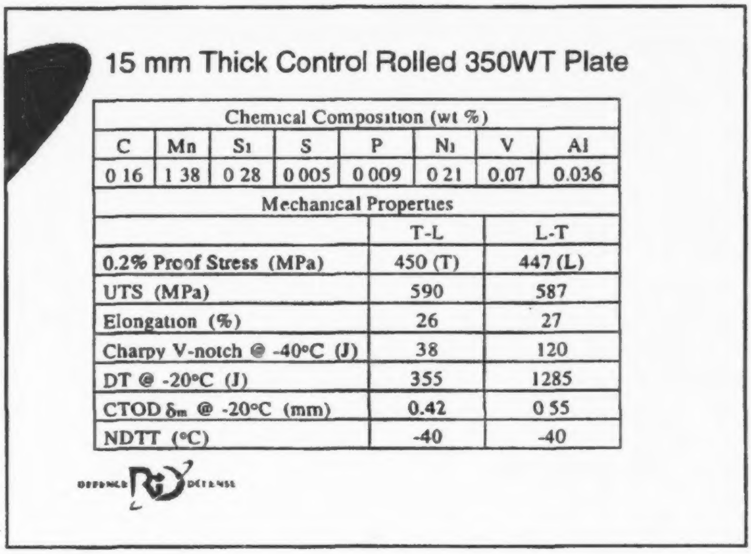

15 mm Thick Control Rolled 350WT Plate

Chemical Composition (wt %)							
C	Mn	Si	S	P	Ni	V	Al
0.16	1.38	0.28	0.005	0.009	0.21	0.07	0.036

Mechanical Properties		
	T-L	L-T
0.2% Proof Stress (MPa)	450 (T)	447 (L)
UTS (MPa)	590	587
Elongation (%)	26	27
Charpy V-notch @ -40°C (J)	38	120
DT @ -20°C (J)	355	1285
CTOD δ_m @ -20°C (mm)	0.42	0.55
NDTT (°C)	-40	-40

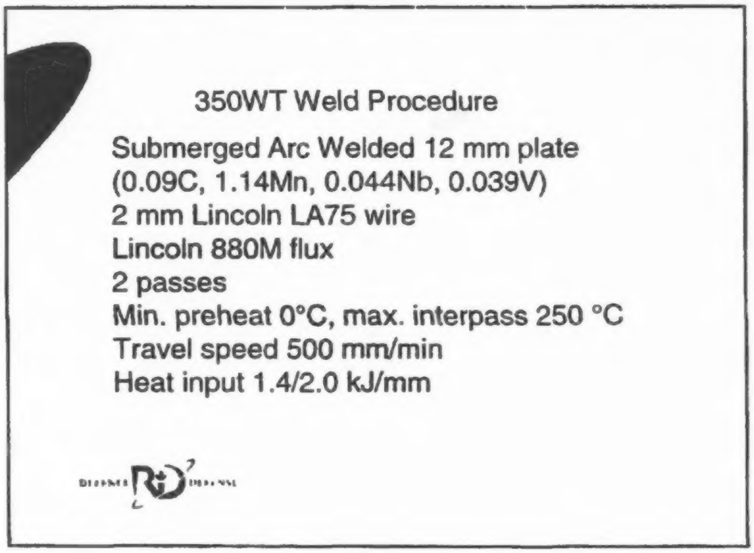

350WT Weld Procedure

Submerged Arc Welded 12 mm plate
(0.09C, 1.14Mn, 0.044Nb, 0.039V)
2 mm Lincoln LA75 wire
Lincoln 880M flux
2 passes
Min. preheat 0°C, max. interpass 250 °C
Travel speed 500 mm/min
Heat input 1.4/2.0 kJ/mm

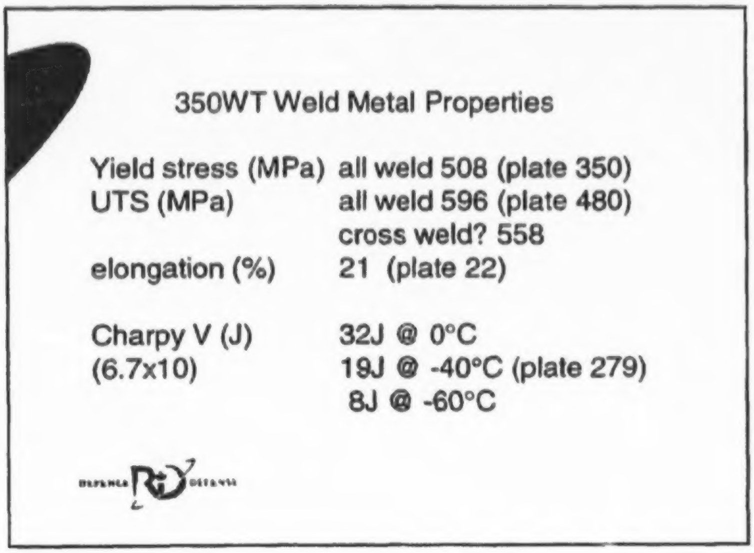

350WT Weld Metal Properties

Yield stress (MPa)	all weld 508 (plate 350)
UTS (MPa)	all weld 596 (plate 480) cross weld? 558
elongation (%)	21 (plate 22)
Charpy V (J) (6.7x10)	32J @ 0°C 19J @ -40°C (plate 279) 8J @ -60°C

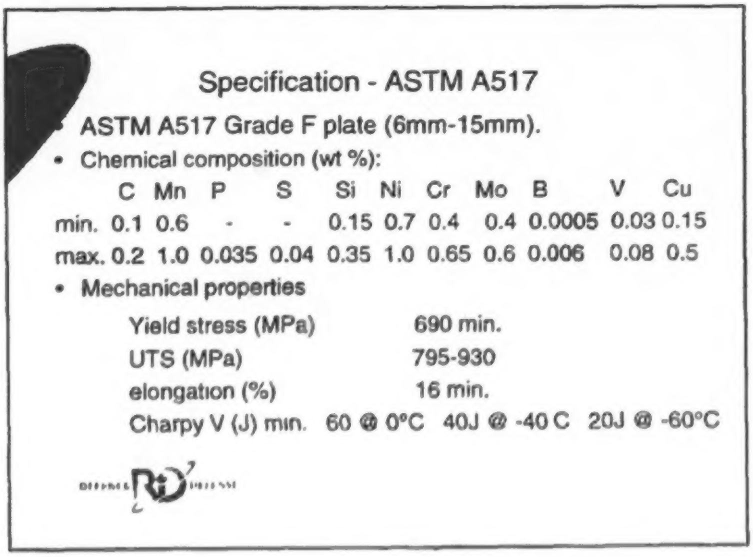

Specification - ASTM A517

- ASTM A517 Grade F plate (6mm-15mm).
- Chemical composition (wt %):

	C	Mn	P	S	Si	Ni	Cr	Mo	B	V	Cu
min.	0.1	0.6	-	-	0.15	0.7	0.4	0.4	0.0005	0.03	0.15
max.	0.2	1.0	0.035	0.04	0.35	1.0	0.65	0.6	0.006	0.08	0.5

- Mechanical properties

Yield stress (MPa)	690 min.		
UTS (MPa)	795-930		
elongation (%)	16 min.		
Charpy V (J) min.	60 @ 0°C	40J @ -40 C	20J @ -60°C

10 mm ASTM A517 Plate

Chemical Composition (wt %)

C	Mn	Si	S	P	Cr	Ni	Mo	Al	Cu
0.13	0.76	0.31	0.001	0.017	0.46	0.86	0.43	0.04	0.40

Mechanical Properties

0.2% Proof Stress (MPa)	769
UTS (MPa)	816
Elongation (%)	22
Charpy V-notch @ -40°C (J)	159

ASTM A517 Weld Procedure

Submerged Arc Welded 10 mm plate
3.2 mm L-Tec 120 wire
Oerlikon OP121TT flux
2 passes
Min. preheat 0°C, max. interpass 150 °C
Travel speed 500 mm/min
Heat inputs 1.7/2.2 kJ/mm

A517 Weld Metal Properties

Yield stress (MPa)	all weld 613
UTS (MPa)	all weld 781 cross weld? 815
elongation (%)	21
Charpy V (J) min. (7.5x10)	101J @ 0°C 71J @ -40°C 45J @ -60°C

Master Curve Methodology

- Cleavage fracture toughness is characterized by a weakest link model and a three parameter Weibull description of the distribution and size of initiation sites. Cleavage failure probability is given by:

$$P_f = 1 - \exp\left(- \left(\frac{K_I - K_{min}}{K_0 - K_{min}} \right)^4 \right)$$

- The shift parameter (K_{min}) provides a lower bound toughness. An empirical estimate for ferritic steels is 20 MPa√m.

- K_0 is the data fitting parameter, and can be used to calculate the population median

$$K_0 = \left[\sum_{j=1}^{N} (K_{Jc(i)} - K_{min})^4 / (N - 0.3068)^{1/4} \right] + K_{min}$$

$$K_{Jc(med)} = (K_0 - K_{min})[\ln 2]^{1/4} + K_{min}$$

- The weakest link model also quantifies the size effect on fracture toughness.

The "Master Curve" assumes that the temperature dependence of cleavage toughness is the same for all ferritic steels.

$$K_{Jc(med)} = 30 + 70\exp[0.019(T - T_0)]$$

The "Reference Temperature" T_0 provides an index at which the median toughness for a 25 mm thick specimen is 100 MPa√m.

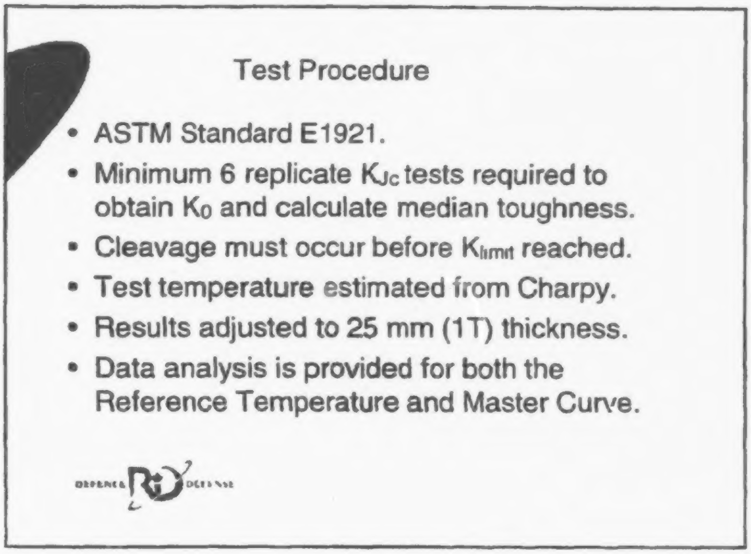

Test Procedure

- ASTM Standard E1921.
- Minimum 6 replicate K_{Jc} tests required to obtain K_0 and calculate median toughness.
- Cleavage must occur before K_{limit} reached.
- Test temperature estimated from Charpy.
- Results adjusted to 25 mm (1T) thickness.
- Data analysis is provided for both the Reference Temperature and Master Curve.

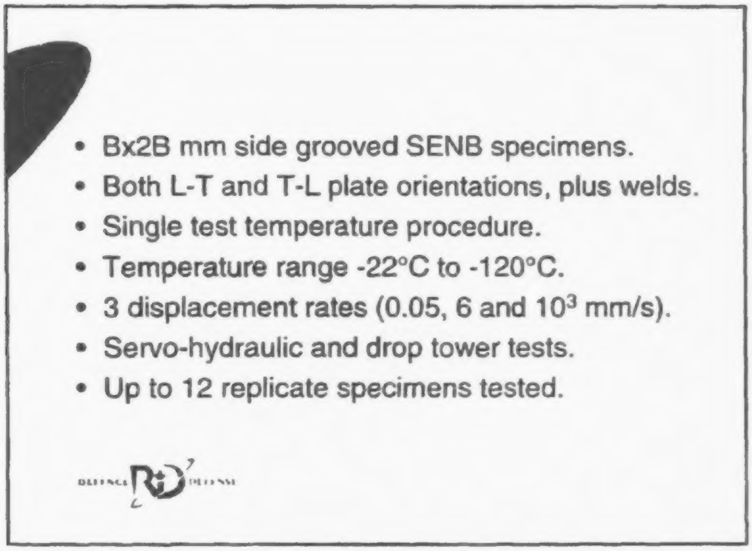

- Bx2B mm side grooved SENB specimens.
- Both L-T and T-L plate orientations, plus welds.
- Single test temperature procedure.
- Temperature range -22°C to -120°C.
- 3 displacement rates (0.05, 6 and 10^3 mm/s).
- Servo-hydraulic and drop tower tests.
- Up to 12 replicate specimens tested.

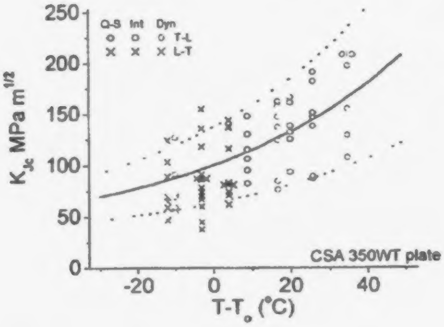
Q-S
Int
Dyn
T-L
L-T
250
200
150
100
50
0
K_{Jc} MPa $m^{1/2}$
-20
0
20
40
T-T_o (°C)
CSA 350WT plate

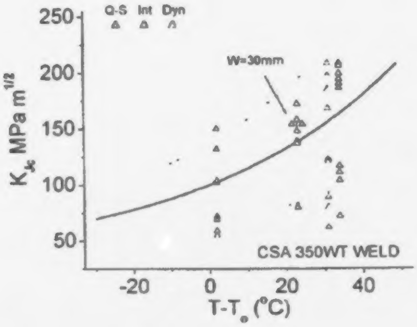
Q-S
Int
Dyn
250
200
150
100
50
K_{Jc} MPa $m^{1/2}$
W=30mm
-20
0
20
40
T-T_o (°C)
CSA 350WT WELD

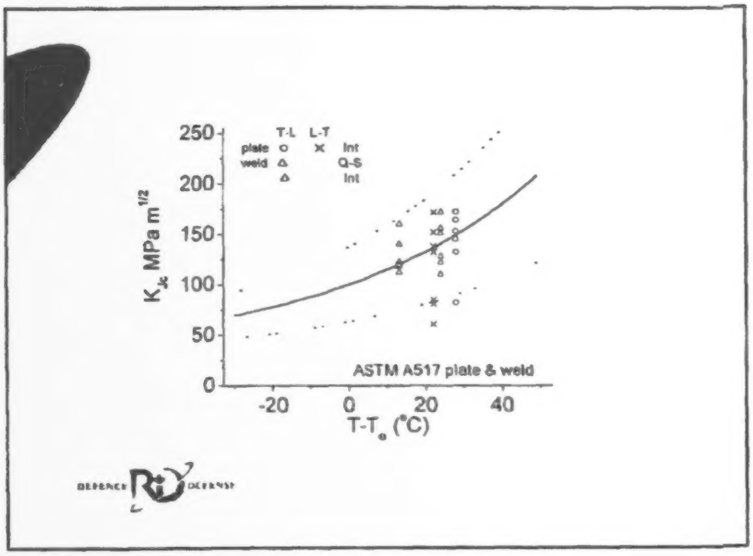
250
200
150
100
50
0
K_Jc MPa m^1/2
T-L
L-T
plate ○ × Int
weld △ Q-S
△ Int
ASTM A517 plate & weld
-20
0
20
40
T-T_o (°C)

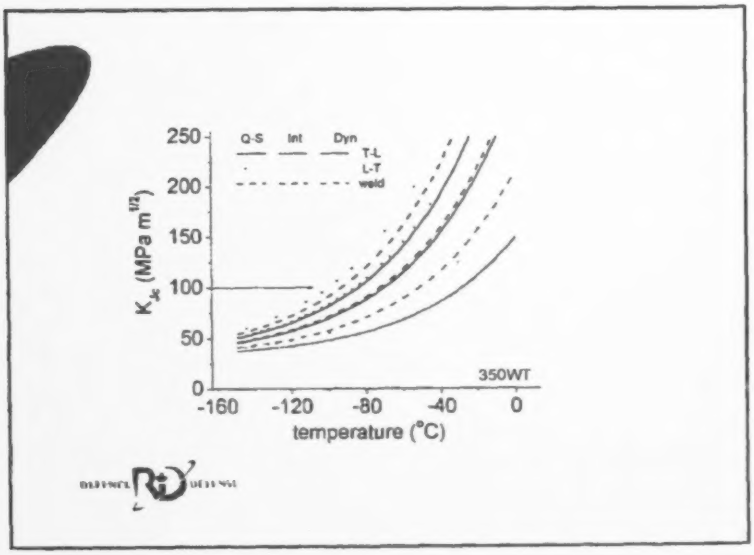
250
200
150
100
50
0
K_Jc (MPa m^1/2)
Q-S
Int
Dyn
T-L
L-T
weld
350WT
-160
-120
-80
-40
0
temperature (°C)

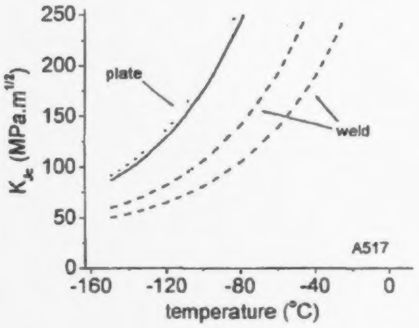

Reference Temperature Summary

material	testing speed		
	quasi-static	intermediate	dynamic
	reference temperature °C		
350WT plate T-L	-76	-70	-39
T-L	-84	-73	-28
350WT plate L-T	-100	-86	-46
350WT SAW weld 20x10	-93	-72	-51
30x10	-94	-	-
ASTM A517 plate T-L	-	-138	TBD
ASTM A517 plate L-T	-	-142	TBD
ASTM A517 SAW weld	-104	-83	TBD

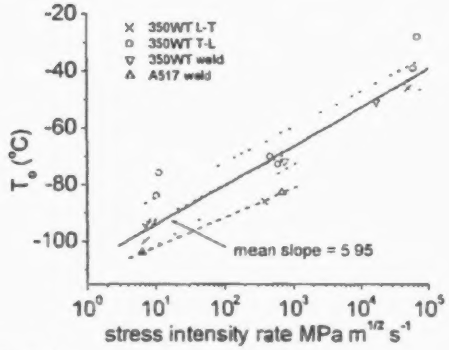

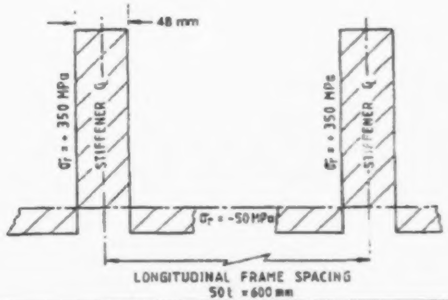
48 mm
σr = + 350 MPa
STIFFENER ℄
σr = + 350 MPa
STIFFENER ℄
σr = -50 MPa
LONGITUDINAL FRAME SPACING
50 t = 600 mm

Longitudinal stiffener detail (Sumpter (1991))

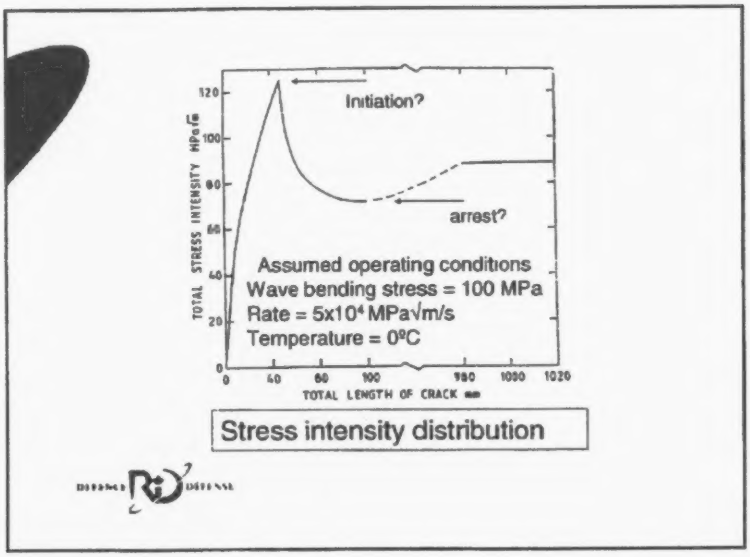

Assumed operating conditions
Wave bending stress = 100 MPa
Rate = 5x10⁴ MPa√m/s
Temperature = 0ºC

Stress intensity distribution

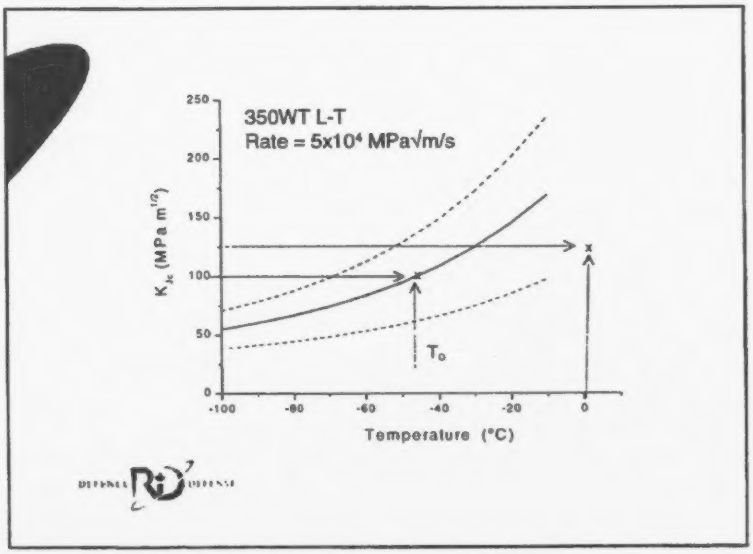

350WT L-T
Rate = 5x10⁴ MPa√m/s

Use of Master Curves in Fracture Control

- T_0 can provide a better reference temperature baseline than that from from Charpy (e.g. minimum energy or fibrosity), or drop weight tests (RT_{NDT}).
- Successful predictions of structural element performance have been made using the master curve (US Navy).
- Determination of safety margins for upper shelf behaviour at lowest service temperatures
- Comparison of constraint effects for flaw tolerance assessment.

Conclusions

The reference temperature procedure has been used to quantify the brittle fracture resistance of ship plate and welds.

- The master curve provided a reasonable description of the various sets of K_{Jc} data.
- The rate dependence of K_{Jc} is similar to that reported elsewhere.
- These plates and welds should have a high resistance to brittle fracture initiation under ship operating conditions.

#516449 ③④

Master Curve Description of the Crack Arrest Toughness of 350WT Steel

by

J. Morrison[1], L. N. Pussegoda[2], R. B. Nethercott[3], and J.D. Sumpter[4]

[1]DREA Dockyard Laboratory (Pacific), Victoria, BC, Canada.
[2]Fleet Technology Ltd, Kanata, ON, Canada
[3]Aeronautical and Maritime Research Laboratory, Melbourne, Australia
[4]DERA, Rosyth, United Kingdom

Abstract

The measurement of crack arrest fracture toughness is difficult and expensive, particularly if a representative structural element is to be tested, and the underlying theory is controversial. Small specimen test methods have been developed, but applying these to ship plate presents special challenges, primarily because the limited thickness precludes plane strain conditions in the specimen. A collaborative Operating Assignment under TTCP MAT Group Panel 1 (Metallic Materials and Processes) has recently assessed a small specimen crack arrest test method for ship plate.

As part of this assignment the crack arrest toughness of 15 mm thick CSA 350WT plate has been determined using a full thickness compact specimen test procedure. A crack arrest master curve has been calculated from this data, and provided a good description of the data scatter. Comparisons were made between the crack arrest reference temperature T_{Ka}, and the crack arrest temperature estimated from NDTT. The data have also been analyzed using expected service loading for a simple structural detail.

The results suggest that the proposed procedures can be used to generate useful data from ship plate for structural integrity assessment, although the technique will always require careful optimization of specimen design and testing conditions.

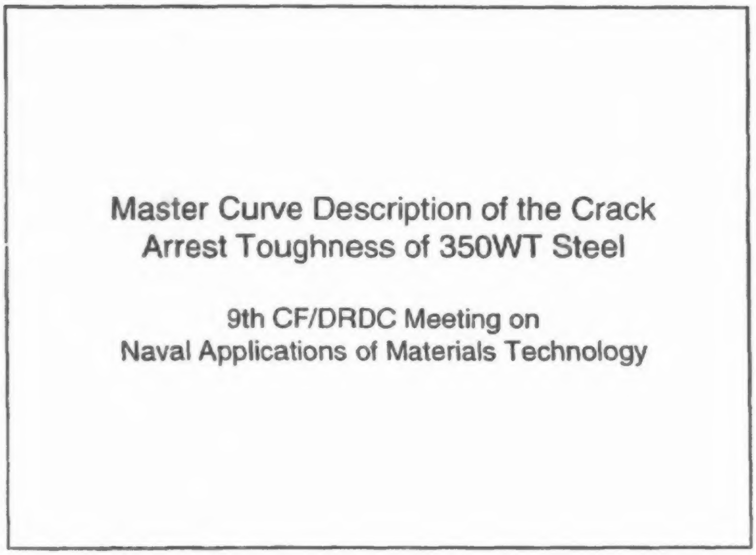

Master Curve Description of the Crack Arrest Toughness of 350WT Steel

9th CF/DRDC Meeting on
Naval Applications of Materials Technology

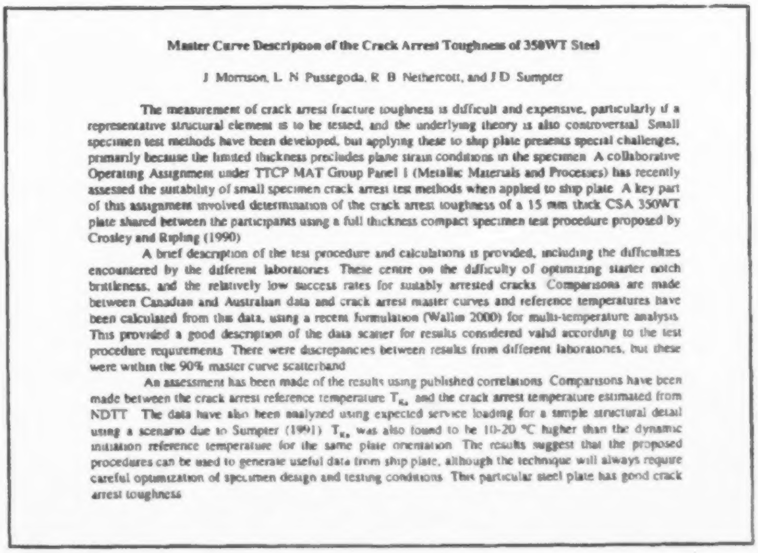

Master Curve Description of the Crack Arrest Toughness of 350WT Steel

J Morrison, L N Pussegoda, R B Nethercott, and J D Sumpter

The measurement of crack arrest fracture toughness is difficult and expensive, particularly if a representative structural element is to be tested, and the underlying theory is also controversial Small specimen test methods have been developed, but applying these to ship plate presents special challenges, primarily because the limited thickness precludes plane strain conditions in the specimen A collaborative Operating Assignment under TTCP MAT Group Panel I (Metallic Materials and Processes) has recently assessed the suitability of small specimen crack arrest test methods when applied to ship plate A key part of this assignment involved determination of the crack arrest toughness of a 15 mm thick CSA 350WT plate shared between the participants using a full thickness compact specimen test procedure proposed by Crosley and Ripling (1990)

A brief description of the test procedure and calculations is provided, including the difficulties encountered by the different laboratories These centre on the difficulty of optimizing starter notch brittleness, and the relatively low success rates for suitably arrested cracks Comparisons are made between Canadian and Australian data and crack arrest master curves and reference temperatures have been calculated from this data, using a recent formulation (Wallin 2000) for multi-temperature analysis This provided a good description of the data scatter for results considered valid according to the test procedure requirements There were discrepancies between results from different laboratories, but these were within the 90% master curve scatterband

An assessment has been made of the results using published correlations Comparisons have been made between the crack arrest reference temperature T_{Ka} and the crack arrest temperature estimated from NDTT The data have also been analyzed using expected service loading for a simple structural detail using a scenario due to Sumpter (1991) T_{Ka} was also found to be 10-20 °C higher than the dynamic initiation reference temperature for the same plate orientation The results suggest that the proposed procedures can be used to generate useful data from ship plate, although the technique will always require careful optimization of specimen design and testing conditions This particular steel plate has good crack arrest toughness

TTCP Operating Assignment on Crack Arrest Toughness of Ship Plate

Contributors

J. Morrison (Focus Officer)
DREA/DL(P)
Victoria, BC, Canada

J.D. Sumpter
DERA
Rosyth, Scotland

R. Nethercott
AMRL
Melbourne, Australia

N Pussegoda
Fleet Technology Ltd
Kanata, ON, Canada

Overview

- Background/program.
- Material properties.
- Crack arrest test procedure/problems.
- K_a^* master curve.
- Crack Arrest Master Curve/Correlations.
- Structural Implications.
- Conclusions.

Background

- Limited thickness invalidates K_{Ia} tests.
- Is it possible to measure a useful crack arrest toughness under non plane strain conditions?
- How well would the master curve describe the crack arrest data?
- Would the results be useful for material selection and structural integrity assessment?

Program

Australia.
  - Compact crack arrest (CCA) specimen testing (plate).
  - Low temperature tensile properties.
  - Efffect of prestrain on crack initiation.

Canada
  - Characterization of steel plate.
  - CCA specimen testing (plate plus HAZ).
  - Evaluation of different brittle weld crack starters.

United Kingdom
  - Review of crack arrest theory and application.
  - Dynamic crack initiation tests.
  - Crack arrest trials using both wedge and pin loaded specimens.

15 mm 350WT plate

Chemical Composition (wt %)

C	Mn	Si	S	P	Ni	V	Al
0.16	1.38	0.28	0.005	0.009	0.21	0.07	0.036

Mechanical Properties

	T-L	L-T
0.2% Proof Stress (MPa)	450 (T)	447 (L)
UTS (MPa)	590	587
Elongation (%)	26	27
Charpy V-notch @ -40°C (J)	38	120
DT @ -20°C (J)	355	1285
CTOD δ_m @ -20°C (mm)	0.42	0.55
NDTT (°C)	-40	-40

350WT Weld

Submerged Arc Welded 15 mm plate
Orientation: transverse.
Butt weld with one straight edge.
Lincoln LA75 wire Lincoln 880M flux
6 passes, Travel speed 435 mm/min
Min. preheat 20°C, max. interpass 200°C
Heat input 3.4 kJ/mm
VHN Hardness: Plate-198,
CGHAZ-221
Weld-209

Heat Affected Zone Properties

Charpy V (J)	140J @ -25°C	
	138J @ -35°C	
	95J @ -40°C	
	50J @ -45°C	
CTOD mm	0.55 @ -5°C	SD = 0.40
	0.79 @ -15°C	SD = 0.47

Crack arrest test procedure

- Tests carried out by FTL and AMRL.
- ASTM E1221 requires plane strain.
- Followed Crosley and Ripling (1990) procedure for specimens with full product thickness.

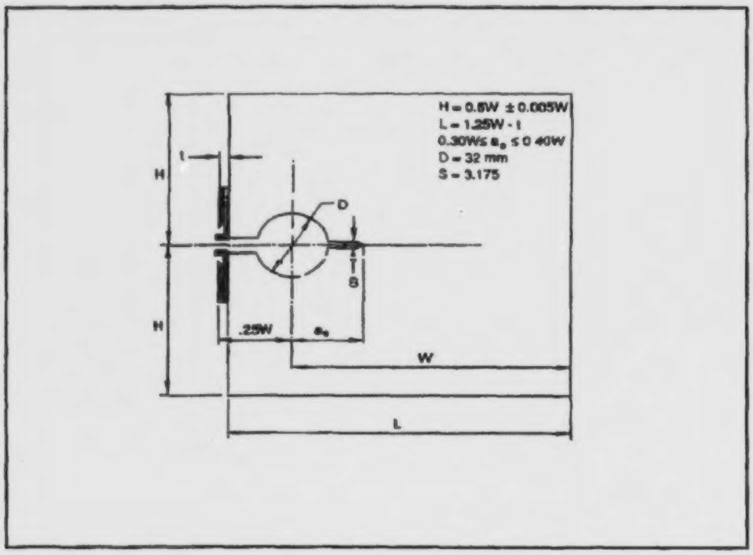
$H = 0.6W \pm 0.005W$
$L = 1.25W - t$
$0.30W \leq a_o \leq 0.40W$
$D = 32$ mm
$S = 3.175$
t
H
D
S
H
.25W
a_o
W
L

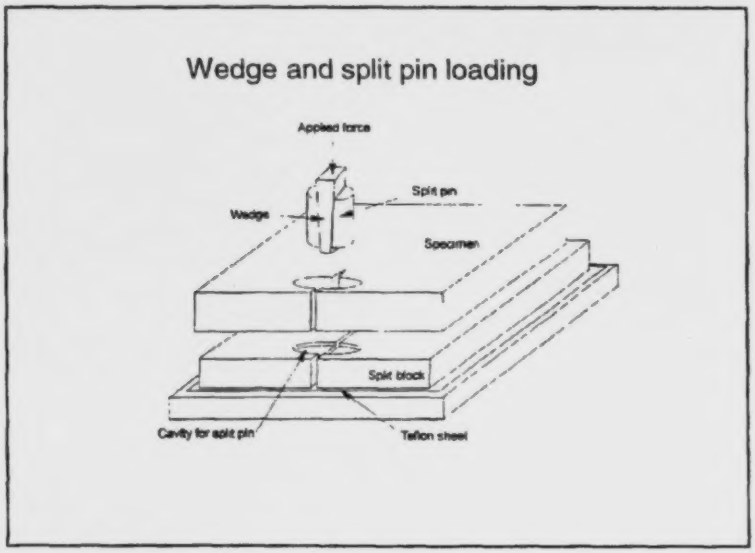

Wedge and split pin loading

Applied force
Split pin
Wedge
Specimen
Split block
Cavity for split pin
Teflon sheet

Crack arrest test parameters

- Modified compact specimen W=150 to 300mm.
- Brittle crack starter.
  Brittle weld deposit or strain aged embrittled.
- Test temperature range -10°C to -30°C.
- K_a^* considered "valid" if crack runs and arrests within defined CMOD and a/W limits.

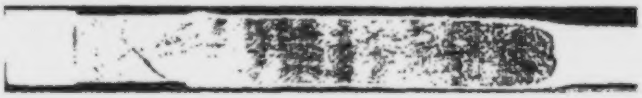

Crack arrest expressions

- Specimens dimensions:

$$W \geq 2.83(K_v/\sigma_{ys})^2$$

where K_v is a starting estimate of toughness

- CMOD limits:

$$\delta = K_v\sqrt{W}/E\ f(a/W)$$

for $a/W = 0.525$ (min.) and 0.8 (max.)

$f(a/W)$ is same as in ASTM 1221

- Preliminary toughness:

$$K_a = \delta\ E\ f(a/W)/\sqrt{W}$$

- Plasticity correction:

$$K_a^* = K_a[1 - 0.105\phi^2(1 - (a/W)^{0.5})]$$

where $\phi = E\delta/1.5\sigma_{ys}W$

Problems in crack arrest testing

- Requires large specimens.
- Low to moderate success rates. Method originally conceived for quality assurance.
- Difficult to optimize brittle starter for specimen toughness and test temperature.
- Monotonic vs. repeated loading?
- Plasticity corrections.

FTL results

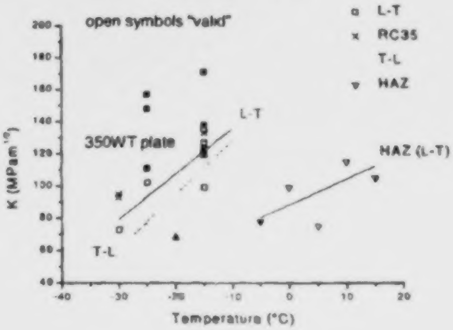

Combined AMRL and FTL K_a* results

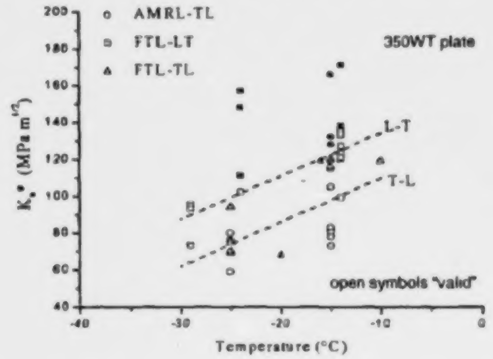

Reference temperature fit for T_{Ka} (Wallin 2000)

- K_a does not follow the Weibull distribution used for K_{Jc} (slope=4, K_{min}= 20 MPa√m). Need alternative algorithm (Wallin 2000).
- If K_a distribution is log normal, the multi-temperature fit for plane strain K_{Ia} is given by:

$$\sum_{i=1}^{n} \frac{\ln K_{Ia_i} \cdot \exp\{0.019 \cdot [T_i - TK_{Ia}]\}}{30+70 \cdot \exp\{0.019\,[T_i - TK_{Ia}]\}} -$$

$$\sum_{i=1}^{n} \frac{\ln(30+70 \cdot \exp\{0.019 \cdot [T_i - TK_{Ia}]\}) \cdot \exp\{0.019\,[T_i - TK_{Ia}]\}}{30+70\,\exp\{0.019 \cdot [T_i - TK_{Ia}]\}} = 0$$

K_a^* master curve

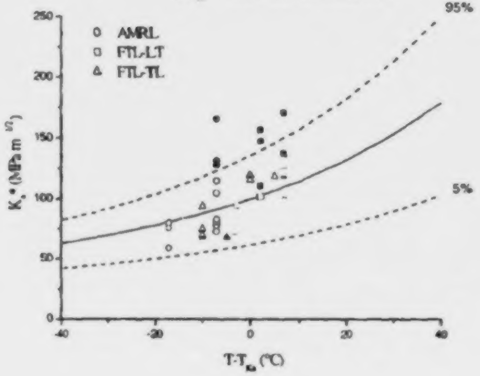

Crack arrest reference temperatures

Orientation	Source	T_{Ka} (°C)
L-T	FTL	-27
T-L	AMRL	4
	FTL	-15
	Combined	-3

(multi-temperature analysis)

Are these K_a^* values sensible?

1. T_{ka} and Crack Arrest Temperature (CAT).

CAT estimation e.g. Wiesner & Hayes (1996)

$$CAT = [NDTT+10] + [\ln\sigma/0.046-105] + [1.53(B-5)^{1/13}-190]$$

applied stress correction thickness correction

at 450 MPa yield stress & B = 15 mm

$$CAT \sim NDTT + 30°C \sim -10°C$$

taking an average T_{ka} of -15°C for T-L and L-T
median $K_a^* \sim 107$ MPa$\sqrt{m}$ at CAT

2. Normalization to dynamic yield stress.
e.g. Sumpter (1986)

At NDTT:

$$0.075 \leq K_{Ia}/\sigma_{yd} \leq 0.118 \sqrt{m}$$

for $K_a^* = 74$ MPa$\sqrt{m}$ and $\sigma_{yd} = 630$ MPa

$$K_a^*/\sigma_{yd} = 0.117 \sqrt{m}$$

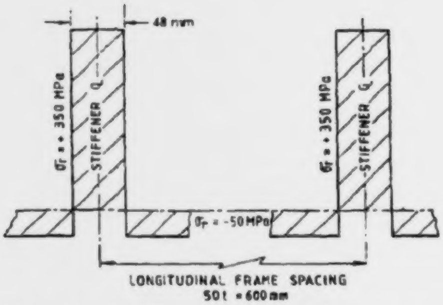
48 mm
σr = + 350 MPa
STIFFENER ℄
σr = + 350 MPa
STIFFENER ℄
σr = -50 MPa
LONGITUDINAL FRAME SPACING
50t = 600 mm

Longitudinal stiffener detail (Sumpter (1991))

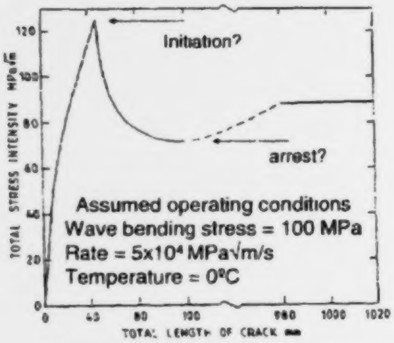

Stress intensity distribution

- For $T_{ka} = -15°C$ (average of T-L and L-T),
  $K_a^* = 70$ MPa√m at -44°C.
- NDTT is -40°C.
- At 0°C 70 MPa√m is on 4% tolerance bound.

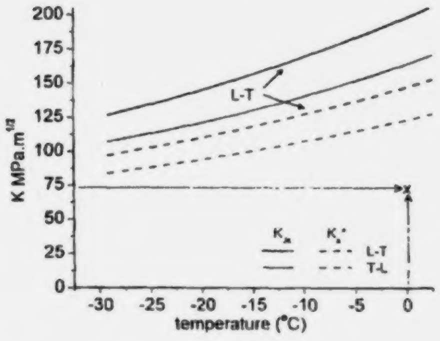

Conclusions

- A full thickness specimen procedure was used to characterize the crack arrest toughness of a ship plate.
- The master curve provided a reasonable description of K_a^* data.
- T_{ka}^* was 10-20°C higher than a dynamic T_o, and is roughly equal to a CAT predicted from NDTT.
- 350WT steel should have a high resistance to cleavage crack propagation under ship operating conditions.

#516450 35

Assessment of Meta-Lax on ASTM A517 and HY80 Weldments

by

G.R. Pelletier *, J.F. Porter +, G.M.C. Lee *

* Department of Metallurgical Engineering, Dalhousie University
+ Defence Research Establishment Atlantic Dockyard Laboratory

Abstract

Defence Research Establishment Atlantic Dockyard Laboratory (DREA/DL) purchased for assessment purposes, Meta-Lax stress-relieving equipment from Bonal Technologies Inc. Claims are that Meta-Lax will relieve thermal stresses within metal components by using non-destructive sub-harmonic vibration, thus improving the mechanical properties of weldments when applied during welding.

This technology was assessed by comparing the shielded metal arc welding (SMAW) weldments of ASTM A517 and HY80 steels. Five ASTM A517 steel plates and two HY80 steel plates were welded. Charpy V-Notch and Dynamic Tear impact tests specimens were removed from each welded plate and tested at temperatures ranging from 25°C to -40°C. The fractured Charpy V-Notch specimen surfaces were further examined with a scanning electron microscope (SEM). Metallography specimens were mounted, polished and etched. Rockwell Macro-Hardness tests were performed on specimens from each plate.

The Charpy V-Notch and Dynamic Tear impact tests did not provide conclusive results with regards to the Meta-Lax process. However, the specimens that had the benefit of the Metalax process had consistently lower hardnesses.

1.0 Introduction

Prior to the construction or repair of any ship or submarine serious consideration must be given to the welding of any metal. When metals are welded together several problems can result due to the mechanics of welding. One such problem, and perhaps one of the most significant is that of stress. Several different techniques, such as pre-heat and post-heat treatments have been employed for many decades to relieve stresses incurred during welding. Many different apparatus have been designed as replacements to high-cost heat treatment processes. One such apparatus is Meta-Lax.

Meta-Lax is stress-relieving equipment manufactured by Bonal Technologies Inc. of Southfield, Michigan, USA. Bonal Technologies claims that Meta-Lax will relieve thermal stresses within metal components by using non-destructive sub-harmonic vibration. These thermal stresses, which create problems of distortion and pre-mature cracking are said to be reduced by the Meta-Lax "stress-relieving" process. It has also been alleged that this technology will significantly improve the mechanical properties of weldments when applied during welding. Vibrating metals immediately before they undergo solidification will produce smaller grains. Mechanical vibrators attached to a welding table construes a simple application of this principle.

Several promotional reports have concluded that savings could be achieved with Meta-Lax, and that such savings justified investment. It has been suggested that naval shipyards that encounter excessive welding rework, poor weld quality, or labor intensive pre/post-weld heat treatments would benefit from this technology [1]. The equipment is portable and shipboard application is feasible. The equipment may be used on small to very large components.

Defence Research Establishment Atlantic Dockyard Laboratory (DREA/DL) has purchased this equipment for the purpose of assessment. This technology was assessed by comparing the shielded metal arc welding (SMAW) weldments of ASTM A517 and HY80 steels. Five ASTM A517 steel plates were welded (three plates were welded with the Meta-Lax equipment, two without), and two HY80 steel plates were welded (one plate was welded with the Meta-Lax equipment and one without).

Metallography, hardness, dynamic tear and Charpy V-Notch impact test specimens were removed from each welded plate. The dynamic tear and Charpy V-Notch specimens were tested at temperatures ranging from 25°C to -40°C.

The fractured Charpy V-Notch specimen surfaces were also examined with a scanning electron microscope (SEM). The recorded fractographs were examined with respect to testing temperature and whether they were welded with or without the Meta-Lax process.

Primary testing revealed minor differences between the specimens that received the Metalax treatment and those that did not.

2.0 Background

2.1 Meta-Lax

Meta-Lax is a process developed by Bonal Technologies, which claims to relieve thermal stress within metal components by using nondestructive sub-harmonic vibrations. The name is a combination of **metal** and **relax**ation. The Meta-Lax process induces mechanical energy in a work piece by means of vibration. Different levels of induced energy will have different effects on metal. Bonal states that with vibration, as with heat, there exists an optimum energy level that will result in stress relief [2].

When the Meta-Lax process is used during welding, the process is referred to as "weld conditioning". Meta-Lax weld conditioning supposedly relieves thermal stresses as they are introduced during weld solidification. This procedure apparently produces several desirable benefits for the weld metal and the heat affected zone (HAZ).

According to Bonal Technologies, the following are results that can be expected when their equipment is used during welding [3].

1. Reduce Weld Distortion (up to 95%)
2. Reduce Weld Cracking (up to 95%)
3. Reduce Porosity
4. Increase Ductility (up to 400%)
5. Reduce Preheat Temperature
6. Deeper Weld Penetration
7. Faster Welding
8. Easier to Weld Vertical & Overhead
9. Reduce Spatter
10. Increase in Impact Energies

Pictured in Figure 1 is the Meta-Lax equipment. Figure 1a is the control console, it is used to set the frequency of vibration and monitors the vibrational energy. The "foot" of the harmonic peak is the target zone; it is supposedly the optimal level for vibrational stress relief. This 'foot' is located approximately 1/3 up the base of the harmonic curve. This target zone is easily located with the use of a graphical chart display (Figure 1b). The force inducer that creates the sub-harmonic vibrations is pictured in Figure 1c. The force inducer is clamped to a worktable or directly to a work piece. A transducer picks up the vibrational energy and directs it to the control console.

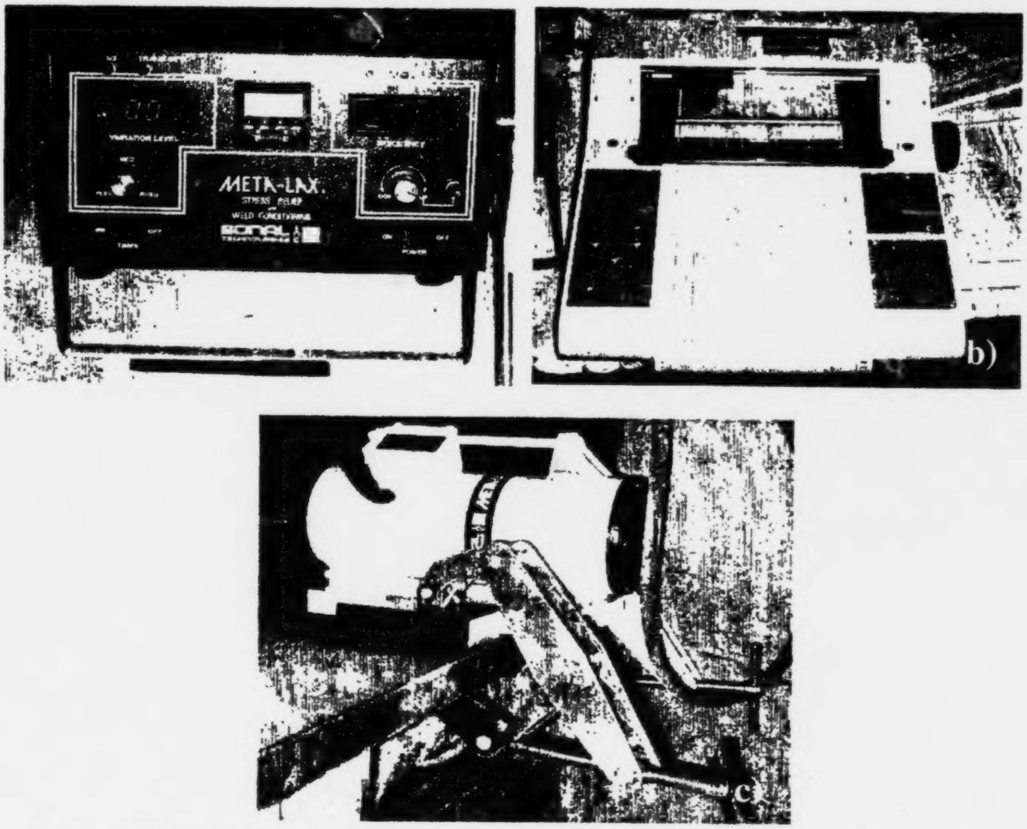

Figure 1. Meta-Lax equipment, a) control console; b) graphical display: c) force inducer.

2.2 Testing

The examination of the weldment microstructures, combined with various mechanical test data, provides much information about materials and their weldments. To properly assess any material, standard procedures and tests are common practice.

2.2.1 Charpy V-Notch Impact Test

Notch toughness is measured by impact tests, which involves a weight striking a specially prepared sample. The minimum force or absorbed energy required to fracture or break the specimen is recorded. The Charpy V-Notch impact test (ASTM Standard E23) is the easiest, fastest and most economical means of recording impact energy.

In the Charpy V-Notch impact test a pendulum is raised to a standard height and is released to strike the specimen. The energy absorbed during fracture is measured by the loss of energy of the pendulum. The tests are performed at different temperatures so that a transition curve of energy absorbed versus temperature can be plotted.

2.4.2 Dynamic Tear

Dynamic tear specimens are tested in a vertical drop-tower loading frame from a height of 1.52 m. The total energy a specimen absorbs during separation is recorded with the use of an instrumented tup (calibrated load cell). The tup is connected to a signal conditioner and from there to a computer, where the data is converted from load-time to load-displacement, using conservation of energy principles. The dynamic tear test (ASTM E604) is the most effective way of predicting structural performance of a given material.

Figure 2 is a representation of a typical transition curve [4]. These curves can be constructed from impact energy data obtained from either Charpy V-Notch or a dynamic tear tests. As can be seen the curve is divided into 4 sections: fully plastic fractures; transition fractures; elastic-plastic fractures; and fully elastic fractures. Fractures in the upper regions of the curve are ductile, while fractures in the lower regions of the curve are brittle.

In designing against brittle fractures it is of extreme importance that the minimum service temperature of the structure's steel coincide with the upper shelf of the structural transition curve [5]. It is therefore necessary to determine the structural transition of a steel and to design within the minimum service temperature of the surroundings and selected materials.

Transition curves can also be constructed from the shear lip width measurements obtained from the tested impact specimens. The shear lip information is equivalent to the energy information for characterizing the toughness of carbon and low alloy steels and their weldments [6]. Because the shear lip data is always available for re-examination and inexpensive to obtain, it is the preferred method for evaluating the transition behaviour of steels and their weldments.

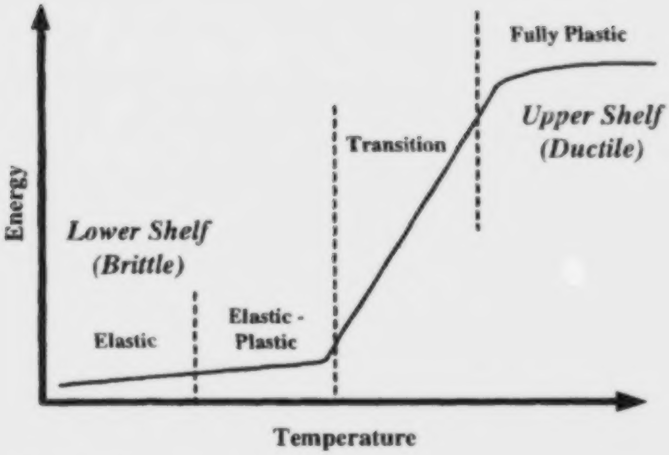

Figure 2. Transition Curve.

2.2.3 Hardness Test

Hardness is a measure of a material's ability to resist localized plastic deformation as a result of indentation. There are several different types of hardness test. Even so, they all push an indenter into the surface of a specimen, under controlled loads and rate of application. The hardness number is determined by the amount of indentation or penetration in the material [7].

Rockwell tests are the most popular hardness test performed because of its simplicity. Depending on the type of indenter and its respective applied load, several different Rockwell scales are possible. The different scales allow for a wide range of metals and alloys to be tested (from very soft to very hard metals).

3.0 Material

Two steels were used in this study: ASTM A517 Grade F steel and HY80 steel. Both steels were purchased from the Metal Stores at Fleet Maintenance Facility Cape Scott (FMFCS). Table 1a lists the composition of both steels. The ASTM A517 steel was 12 mm thick, while the HY80 steel was 25mm thick.

The ASTM A517 Grade F steel is a mill-heat-treated, high yield strength, quenched, and tempered alloy steel. It is primarily used for welded structures that require weight reduction and good toughness properties.

The HY80 is also mill-heat-treated steel, which is used for very high strength, high-toughness structural fabrications such as submarine, pressure vessels and nuclear reactors. The 80 correspond to the minimum yield strength (ksi). As with the ASTM A 517, HY80 steel carbon content is kept low to achieve weldability.

Lincoln welding electrodes (E11018M) were used to weld both the ASTM A517 and HY80 steels (diameters of 1/8" and 5/32"). Table 1b lists the composition of the electrodes.

Table 1a. Steel Compositions.

	C	Mn	P	S	Si	Ni	Cr	Mo	Cu	Fe
ASTM A517 (F)	0.1-0.2	0.6-1.0	0.035 max	0.04 max	0.15-0.35	0.7-1.0	0.40-0.65	0.4-0.6	0.15-0.50	bal.
HY 80	0.16	0.33				2.27	1.51	0.48		bal.

Table 1b. Welding Electrode Composition.

	C	Mn	P	S	Si	Ni	Cr	V
E11018M	0.1	1.3-1.8	0.03 max	0.03 max	0.6	1.25 - 2.5	0.4	0.05

4.0 Method

Prior to the commencement of experimental work a training session was held. The 12 hours training session was given by Tom Hebel, President of Bonal Technology. Basic Meta-Lax stress relieving principles, as well as equipment set-up and operation were covered. FMFCS machinists and welders, DREA/DL personnel, and professors from the Department of Metallurgical Engineering at Dalhousie University attended the session.

Upon completion of the classroom training hands-on training took place at FMFCS Welding Shop. Experience was gained with equipment set-up, pre-stress relieving, and weld conditioning.

4.1 Plate Preparation

The 10 X 4 feet ASTM A517 and 7 X 2 feet HY80 steel sheets were sent to the Welding Shop at FMFCS to be flamed cut. The ASTM A517 plates were cut into welding coupons of 1 X 5 feet, while the HY80 plates were cut into welding coupons of 1 X 3.5 feet. The proper edge preparations were machined on all welding coupons. Two different edge preparations were used: bevel (single V) and square and bevel (also known as the 1/2 K).

4.2 Welding

The welding process used for this study was shielded metal arc welding (SMAW), sometimes called stick welding. SMAW is a highly versatile manual method used for welding complex shapes in difficult positions. It is possible to rely upon SMAW for large structures, and particularly for smaller, more complex structures. However, SMAW is most frequently used in combination with more cost efficient welding methods for larger structures (i.e. flux core arc welding [FCAW] and submerged arc welding [SAW]).

All plates were pre-heated prior to welding, with the exception of Plate 5. The plates were welded in the 1G position (flat position), with a root opening of 5 mm. It was necessary to place strong backs onto the HY80 steel. During welding the interpass temperature, current, voltage, weld length, and weld time was recorded, and the heat input calculated.

The Meta-Lax process was applied to some of the plates as they were welded. A sub-harmonic frequency of 34-35 Hz was used. Plate 7 was pre-stress relieved prior to welding at a frequency of 35 Hz for 15 minutes. Shown in Table 2 are the different parameters that were used for each plate.

Table 2. Steel Plates Parameters.

	ASTM A517 Steel					HY 80	
Plate	**Plate 3**	**Plate 4**	**Plate 5**	**Plate 6**	**Plate 7**	**Plate A**	**Plate B**
Edge Preparation	Bevel	Bevel	Bevel	Square & Bevel	Square & Bevel	Square & Bevel	Square & Bevel
Preheat (C)	Torch	52	No Preheat	50	52	121	121
Avg. Heat Input (KJ/mm)	1.622	1.763	1.589	1.532	1.541	1.680	1.615
Metalax	No	34-35 Hz	34-35 Hz	No	Pre-Stress Relief (35 Hz for 15 min), 33 Hz	No	34-35 Hz

Once welding was completed, the plates were sent to the DREA/DL Radiography Shop for inspection of the weld metals. No defects were found. The welded plates were then sent to the Machine Shop at FMFCS so that specimens could be machined from all plates. Outlined in Figure 3 are the type and location of specimens removed.

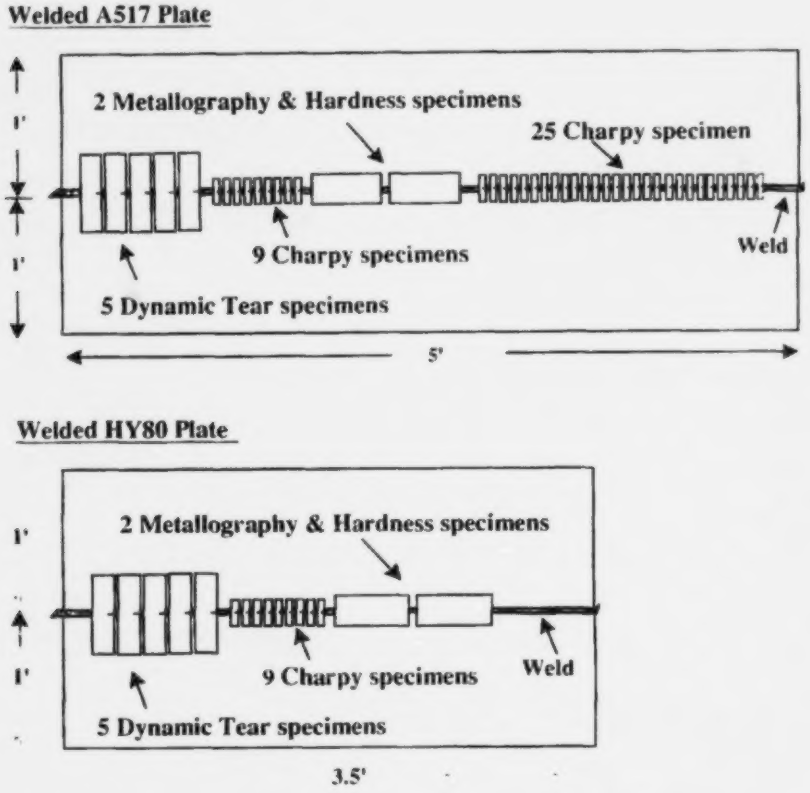
Welded A517 Plate
1'
1'
2 Metallography & Hardness specimens
25 Charpy specimen
9 Charpy specimens
Weld
5 Dynamic Tear specimens
5'
Welded HY80 Plate
1'
1'
2 Metallography & Hardness specimens
9 Charpy specimens
Weld
5 Dynamic Tear specimens
3.5'

Figure 3. Machining Outline of Testing Specimens (a) A517 steel, (b) HY80 steel.

4.3 Charpy V-Notch Specimens

The Charpy V-Notch specimens were machined and notched by FMFCS Machine Shop. To ensure that the weldment of each specimen was located in the center, the specimens were first machined longer than necessary (≈3"). The weldment of each specimen was then etched with a 4% nital solution. The specimens were finally machined to their correct length, guaranteeing that the weldment was located in the center of each specimen. Shown in Figure 4 are the dimensions of the Charpy V-Notch impact specimens. Plates 3, 4 and 5 and Plates A and B were notched in the weld metal as outlined in the ASTM Standard E23, while Plates 6 and 7 were notched in the heat-affected zone (HAZ) as outlined in the Canadian Standards (Supplement No. 1-M1989).

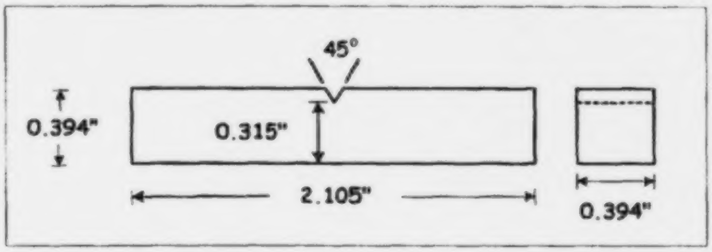

Figure 4. Charpy V-Notch Impact Specimen dimensions.

Prior to testing the specimens were held in a cooled methanol bath for approximately 20 minutes at each testing temperature. Testing temperatures ranged from 25°C to -40°C.

4.4 Dynamic Tear Specimens

The dynamic tear specimens were machined by the FMFCS Machine Shop and notched by the FMFCS Tool and Die Shop. To ensure that the weldment of each specimen was located in the center, the specimens were first machined longer than necessary (≈8.5"). The weldment of each specimen was then etched with a 4% nital solution. The specimens were finally machined to their correct length, guaranteeing that the weldment was located in the center of each specimen. All specimens were notched in the center of the weldment using an EDM, the notch was then pressed with an knife-edge using an Instron. Shown in Figure 5 are the dimensions of the dynamic tear impact specimens.

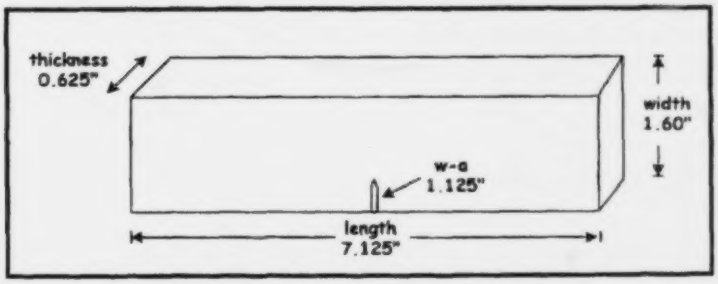

Figure 5. Dynamic Tear Impact Specimen dimensions.

The dynamic tear impact specimens were tested in accordance with ASTM Standard E604. Prior to testing the specimens were held in a cooled methanol bath for approximately 20 minutes at each testing temperature. Testing temperatures ranged from 0°C to -40°C.

The shear lip data was obtained by measuring, with the use of digital calipers, the distance between the two shear lips on the fractured dynamic tear specimens. This value was subtracted from the original specimen width, and divided by two to obtain the average shear lip width.

4.5 Metallography Specimens

The metallography specimens were machined by the FMFCS Machine Shop. Two specimens (3" X 6") were removed from each plate. A metallography specimen from each plate was cut as shown in Figure 6.

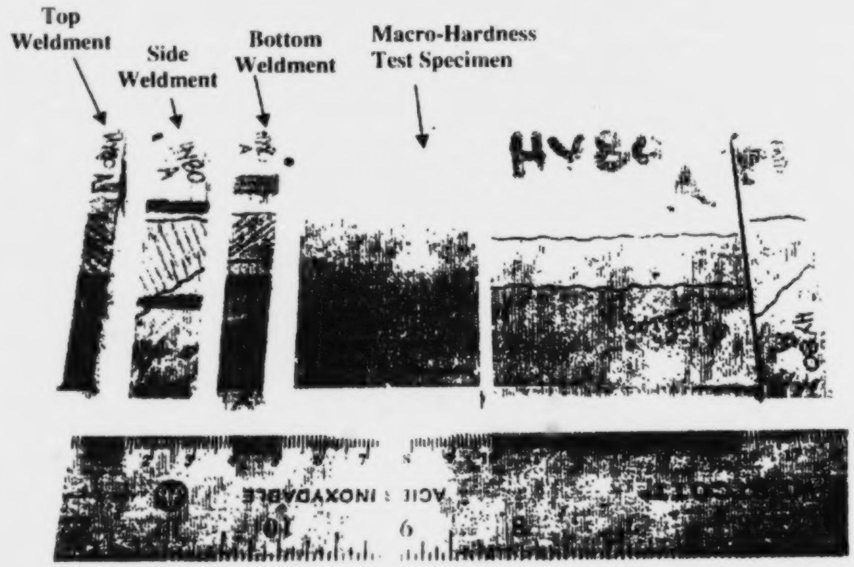

Figure 6. Sectioning of Metallography Specimen.

Three weldment specimens were removed from each metallography specimen. These weldment specimens represent a top, bottom, and side view of the weldment. The specimens were mounted in an automated Buehler™ Mounter with Epomet™ molding compound. Once the mounted specimens were cool, identification was etched onto the backside of the mounts. Groups of six specimens were polished simultaneously on the Buehler automated polisher.

The specimens were then etched using a 5% nital solution (HNO_3 and methanol). The specimens were then examined under an optical microscope and micrographs were obtained for each specimen.

4.5 Hardness Specimens

Transverse weld macro-hardness tests were preformed on a section of the metallography specimens (Figure 6). The Rockwell C scale was used (conical diamond indenter and 150 Kg applied load). Starting 10 mm from the edge parallel to the weldment, thirteen reading were taken at 5 mm intervals across the top weldment of each specimen, as shown in Figure 7. An extra reading was taken at each HAZ, for a total of 15 indentations per specimen.

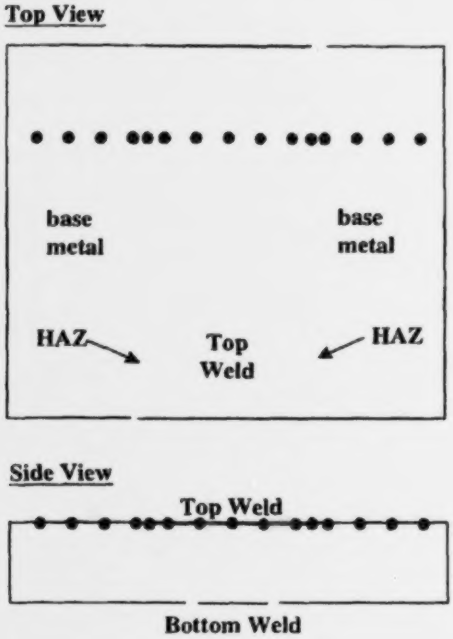

Figure 7. Rockwell Macro-Hardness Test Specimens (Top Weldment).

4.7 Fractography Examination

Once the Charpy V-Notch specimens were tested, one half of the tested specimen was cut to remove the fracture surface. The smaller fracture surface specimens were washed using warm soapy water, rinsed with methanol and then acetone, and blown dried with hot air.

Specimens were mounted onto SEM stubs using conductive carbon glue. The fracture surface of the ASTM A517 specimens tested at 25°C and -30°C, and the fracture surface of the HY80 specimens tested at 0°C and -30°C were observed with the SEM at several magnifications.

5.0 Results

5.1 Charpy V-Notch Impact Test Results

Listed in Tables 3a and 3b are the recorded impact energies for the tested Charpy V-Notch impact specimens. A specimen from Plate 6 (ASTM A517) will have to be re-tested at -20°C, as the tested specimen result is inconsistent (expected human error). Figures 8a to 8c graphically represent the results from Tables 3a and 3b.

Table 3a. ASTM A517 Charpy V-Notch Impact Test Results.

Temp °C	A517 Bevel Preheat Testing Weld No Metalax **Plate 3**	A517 Bevel Preheat Testing Weld Metalax **Plate 4-M**	A517 Bevel No Preheat Testing Weld Metalax **Plate 5-M**	A517 Square & Bevel Preheat Testing HAZ No Metalax **Plate 6**	A517 Square & Bevel Preheat & Pre-Stress Relief Testing HAZ Metalax **Plate 7-M**
25	95	107	96	166	150
10	99	94	84	157	172
0	75	90	73	168	168
-10	83	84	58	140	163
-20	62	73	73	**73 ***	178
-30	66	61	44	145	159
-40	60	62	41	129	104

* to be re-tested

Table 3b. HY80 Charpy V-Notch Impact Test Results.

Temp °C	HY 80 Square & Bevel Preheat No Metalax **Plate A**	HY 80 Square & Bevel Preheat Metalax **Plate B**
10	98	97
0	107	107
-10	91	94
-20	85	92
-30	72	81
-40	70	64

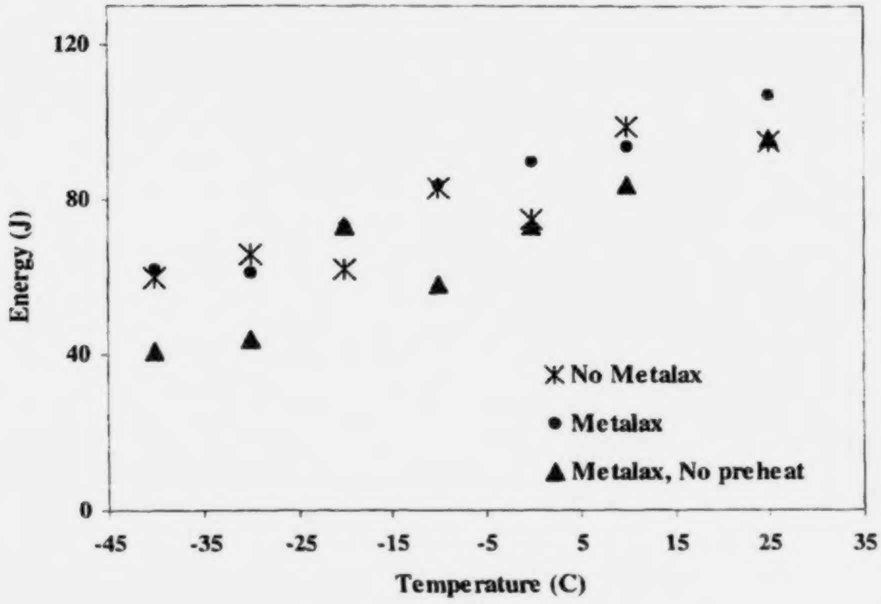

Figure 8a. ASTM A517 Charpy V-Notch Impact Test Results (weld metal).

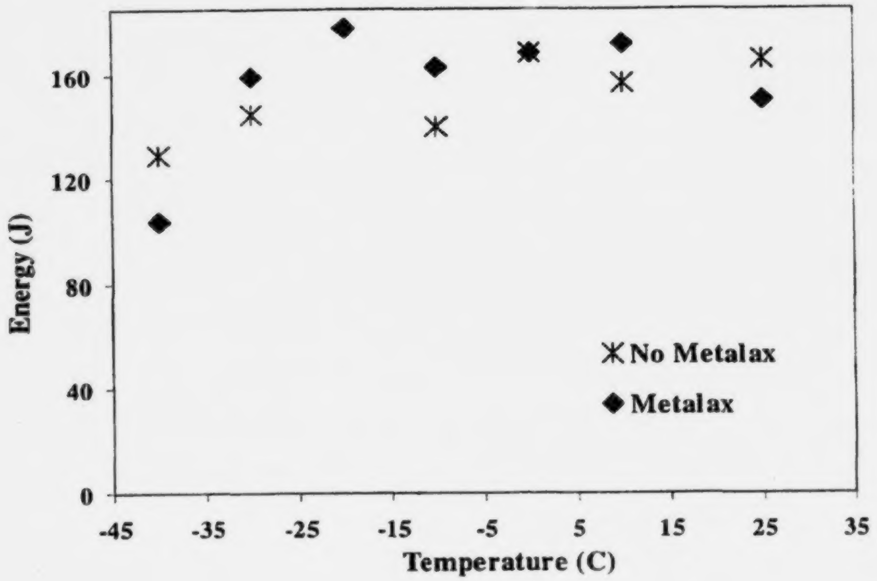

Figure 8b. ASTM A517 Charpy V-Notch Impact Test Results (HAZ).

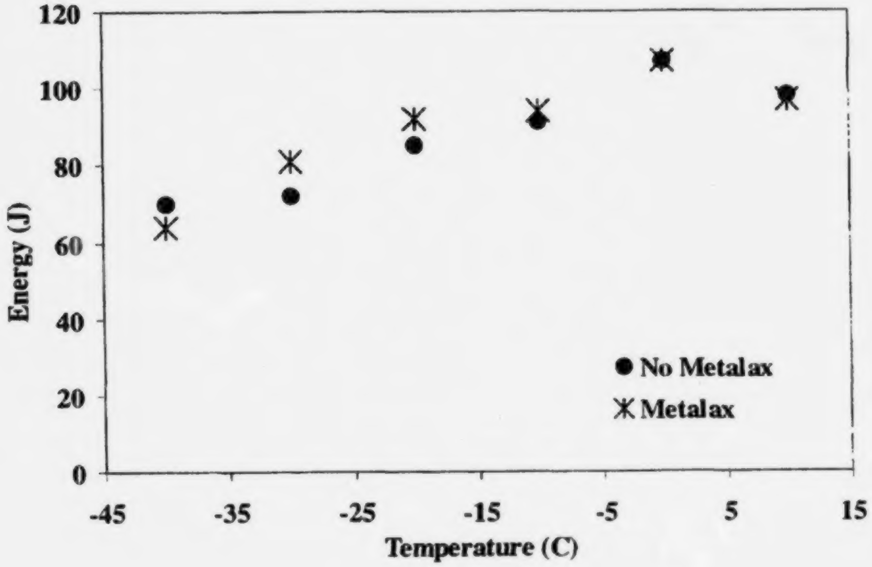

Figure 8c. HY80 Charpy V-Notch Impact Test Results (weld metal).

5.2 Dynamic Tear Test Results

Listed in Table 4 are the recorded impact energies and the shear lip measurements for the tested ASTM A517 dynamic tear specimens. Figures 9a and 9b graphically represent the energy values, while Figure 10a and 10b graphically represents the shear lip measurements.

Table 4. ASTM A517 Steel Dynamic Tear Test Results

	Thickness (mm)	Temp. (C)	Energy (J)	Shear Lip	
				X (mm)	s (mm)
Plate 3					
1	11.82	0	**810**	0.73	**5.55**
2	11.92	-10	**887**	0	**5.96**
3	11.88	-20	**844.6**	0.43	**5.73**
4	11.91	-30	**547.1**	3.67	**4.12**
5	11.93	-40	**571.4**	2.61	**4.66**
Plate 4M					
1	11.73	0	**901**	0	**5.87**
2	11.73	-10	**950**	0.62	**5.56**
3	11.72	-20	**449.5**	4.25	**3.74**
4	11.73	-30	**547.3**	2.45	**4.64**
5	11.74	-40	**593.5**	2.75	**4.50**
Plate 5M					
1	9.46	0	**739**	1.02	**4.22**
2	9.45	-10	**751**	0	**4.73**
3	9.46	-20	**577.1**	1.62	**3.92**
4	9.46	-30	**338.6**	2.69	**3.39**
5	9.46	-40	**142.1**	5.62	**1.92**
Plate 6					
1	7.92	0	**591**	0	**3.96**
2	7.91	-10	**495**	0	**3.96**
3	7.93	-20	**497.5**	0	**3.97**
4	7.92	-30	**565.6**	1.08	**3.42**
5	7.93	-40	**419.6**	1.15	**3.39**
Plate 7M					
1	7.42	0	**510**	0	**3.71**
2	7.41	-10	**500**	0	**3.71**
3	7.42	-20	**n/a**	0.74	**3.34**
4	7.39	-30	**478.8**	0	**3.70**
5	7.4	-40	**465.6**	1.03	**3.19**

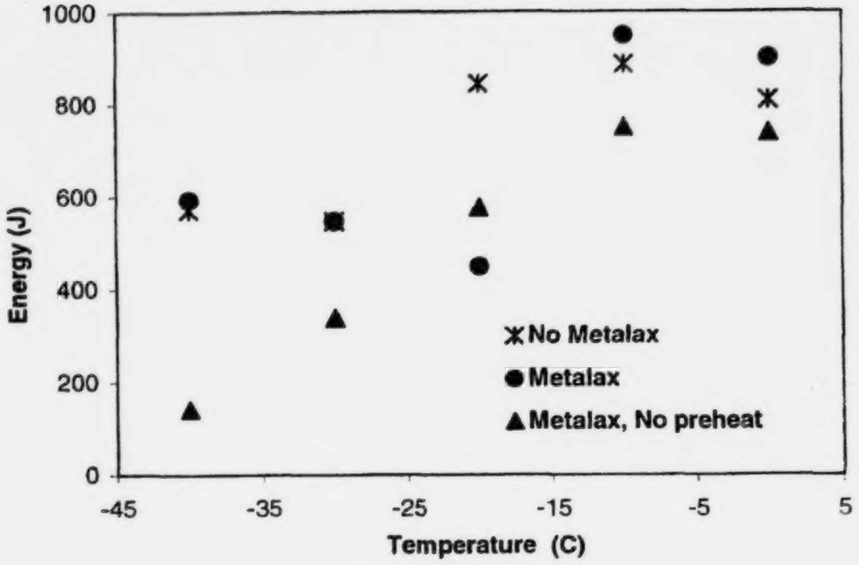

Figure 9a. ASTM A517 Dynamic Tear Test Energy Results (bevel edge).

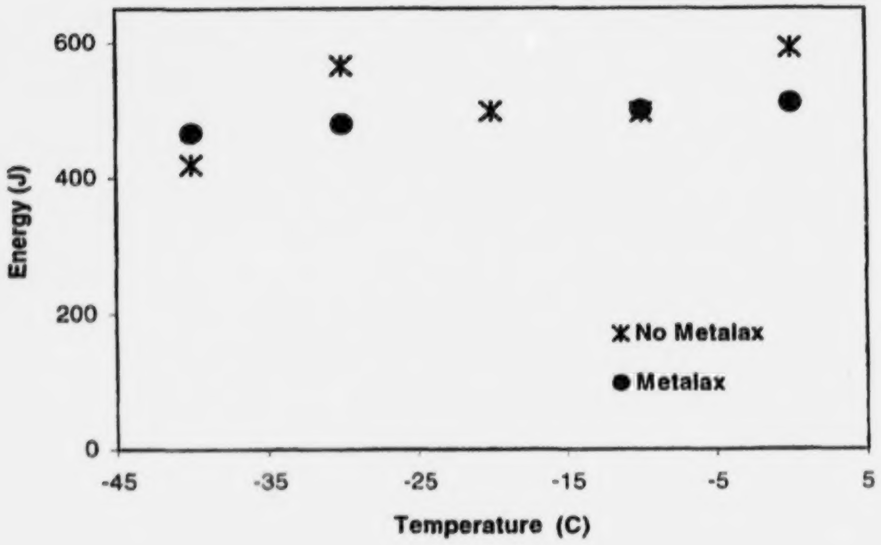

Figure 9b. ASTM A517 Dynamic Tear Test Energy Results (square & bevel edge).

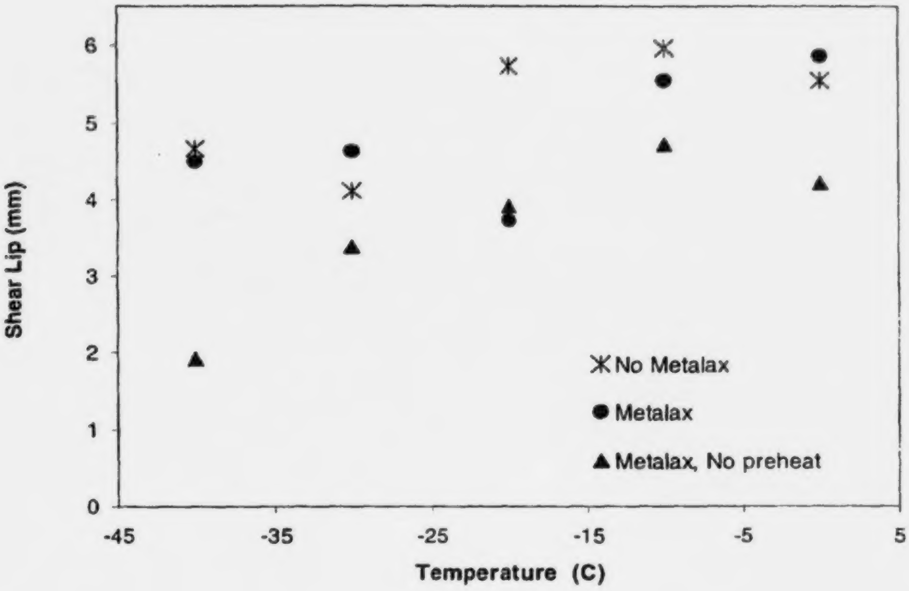

Figure 10a. ASTM A517 Dynamic Tear Test Shear Lip Results (bevel edge).

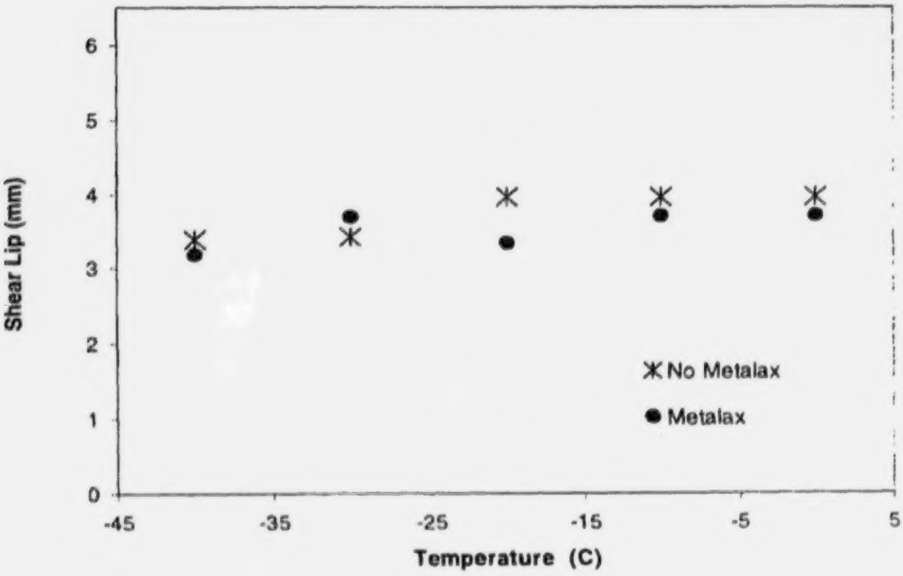

Figure 10b. ASTM A517 Dynamic Tear Test Shear Lip Results (square & bevel edge).

5.3 Hardness Tests

Listed in Tables 5a and 5b are the Rockwell macro-hardness test results for the ASTM A517 and the HY80 steels. The readings with (*) represent the base metal, the readings with (+) represent the HAZ and the readings with (-) represent the weld metal. Figures 11a to 11c graphically represent this data.

Table 5a. ASTM A517 Rockwell Macro-Hardness Test Results.

not cut as others

	A517 Bevel Preheat **No Metalax** **Plate 3**		A517 Bevel Preheat **Metalax** **Plate 4**		A517 Bevel **No Preheat** **Metalax** **Plate 5**		A517 Square & Bevel Preheat **No Metalax** **Plate 6**		A517 Square & Bevel Preheat & Pre-Stress Relief **Metalax** **Plate 7**
1*	25	**1***	24	**1***	23	**1***	23.5	**1***	25
2*	25.5	**2***	24.5	**2***	25.5	**2***	25.5	**2***	26
3*	25	**3***	24.5	**3***	26	**3***	25.5	**3***	26.5
4*	22.5	**4**	25	**4**	25.5	**4***	25	**4***	25
4.5+	32.5	**4.5+**	25.5	**4.5+**	24.5	**4.5+**	30.5	**4.5+**	35
5-	20.5	**5-**	21	**5-**	24.5	**5-**	30.5	**5-**	27.5
6-	26	**6-**	20	**6-**	23	**6-**	23.5	**6-**	24
7-	25	**7-**	20	**7-**	23	**7-**	22.5	**7-**	24.5
8-	24.5	**8-**	19	**8-**	21.5	**8-**	21.5	**8-**	25
9-	24.5	**9-**	18	**9-**	22.5	**9-**	24	**9-**	24.5
9.50+	31	**10+**	23	**10**	24	**10-**	24	**9.5-**	23
10*	23.5	**10.5+**	26	**10.5+**	33.5	**10.5+**	35	**10+**	28
11*	25.5	**11***	26	**11***	25	**11***	24	**11***	25
12*	25	**12***	26	**12***	26	**12***	26	**12***	26
13*	25	**13***	26	**13***	26.5	**13***	25.5	**13***	25

Table 5b. HY80 Rockwell Macro-Hardness Test Results.

	HY 80 Square & Bevel Preheat **No Metalax** **Plate A**		HY 80 Square & Bevel Preheat **Metalax** **Plate B**
1*	27	**1***	27
2*	28	**2***	26
3*	28	**3***	27
4+	44.5	**4+**	35
4.5+	29.5	**4.5+**	19
5-	27.5	**5-**	19
6-	24.5	**6-**	19.5
7-	25	**7-**	23
8-	23	**8-**	19
9-	23	**9-**	23
10+	36	**9.5+**	36
10.5+	32	**10+**	42.5
11*	34	**11***	26.5
12*	28	**12***	27
13*	28	**13***	27

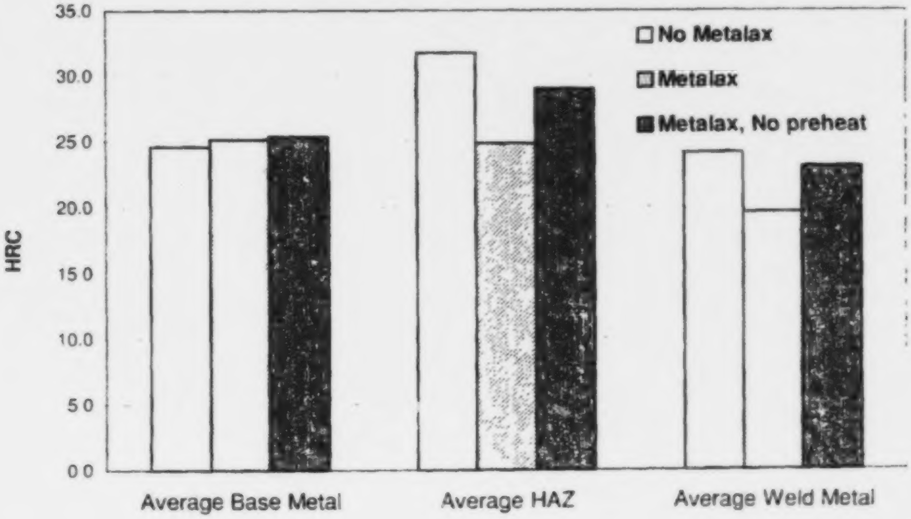

Figure 11a. ASTM A517 Rockwell Macro-Hardness Results (Plates 3, 4 and 5).

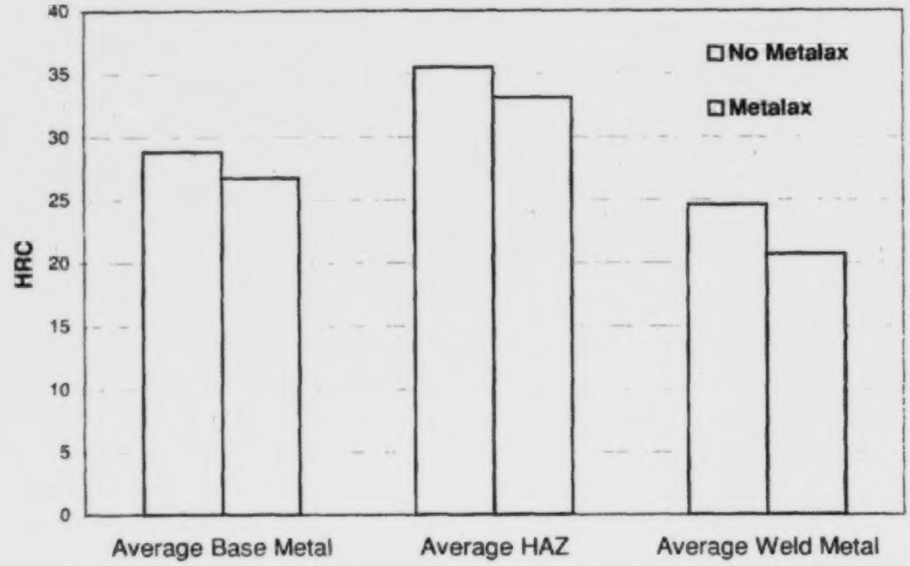

Figure 11b. ASTM A517 Rockwell Macro-Hardness Results (Plates 6 and 7).

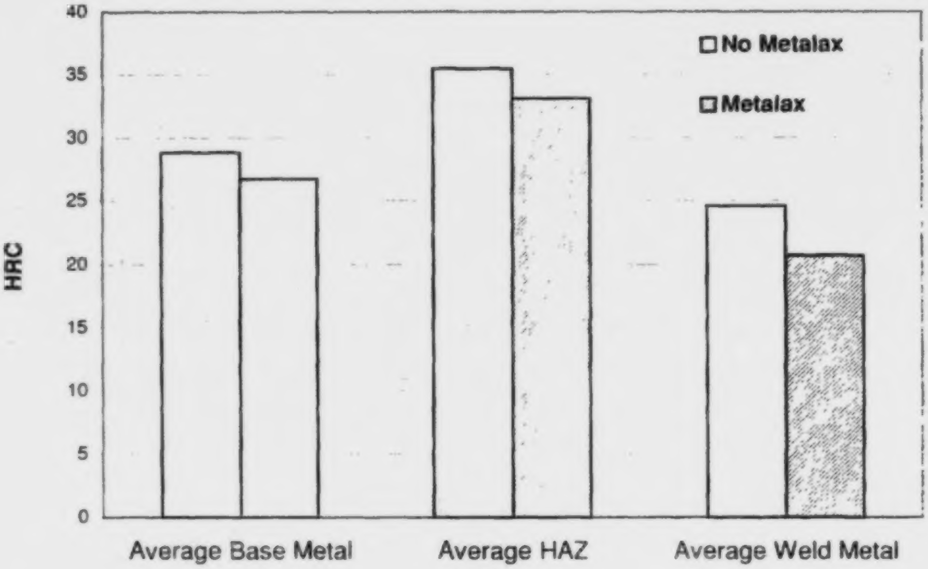

Figure 11c. HY80 Rockwell Macro-Hardness Results (Plates A and B).

5.5 Fractography

All SEM fractographs (Figures 12 to 18), were recorded with an accelerating voltage of 25 kV, a working distance of 15mm, a condenser lens setting of 4, a gun bias of 2, and an aperture setting of 2. All specimens were photographed in the same orientation.

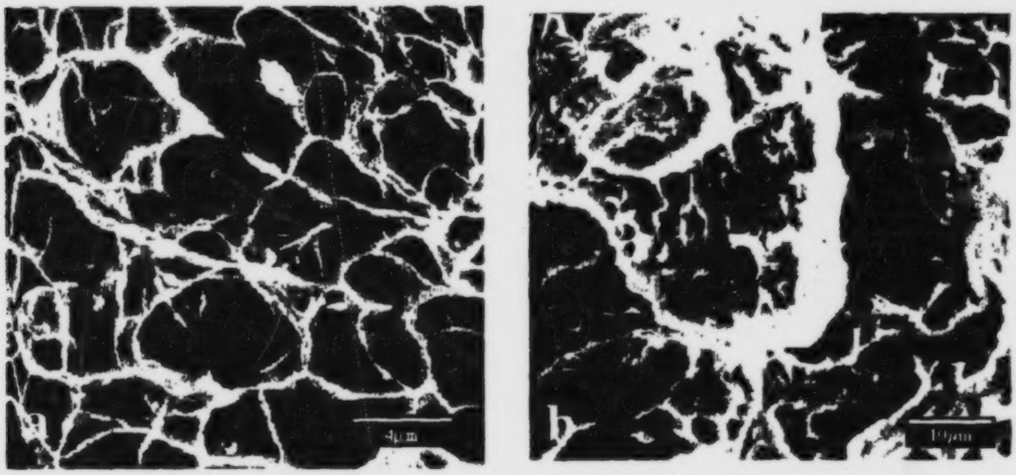

Figure 12. ASTM A517, No Meta-lax, weld metal (Plate 3) Fractographs of tested Charpy V-Notch specimens; a) tested at 25°C, b) tested at -30°C.

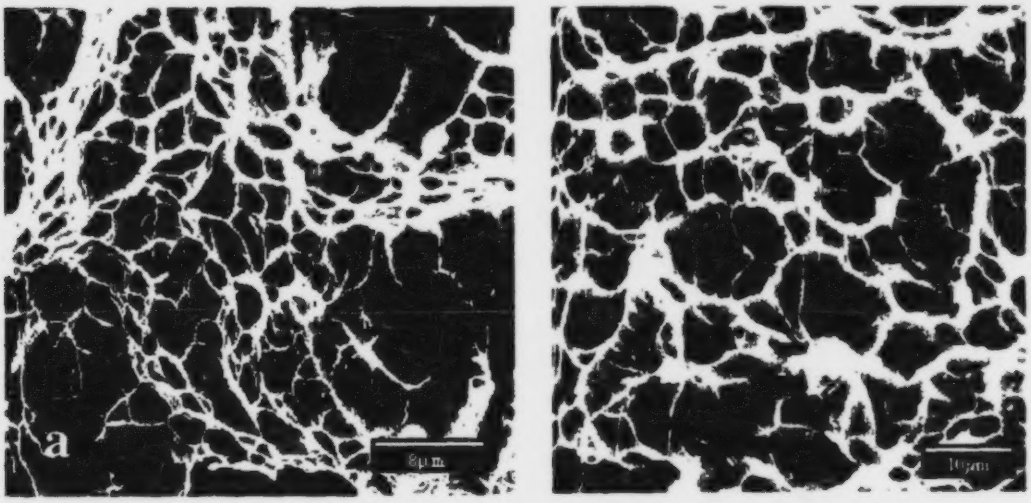

Figure 13. ASTM A517, Meta-Lax, weld metal (Plate 4) Fractographs of tested Charpy V-Notch specimens; a) tested at 25°C, b) tested at -30°C.

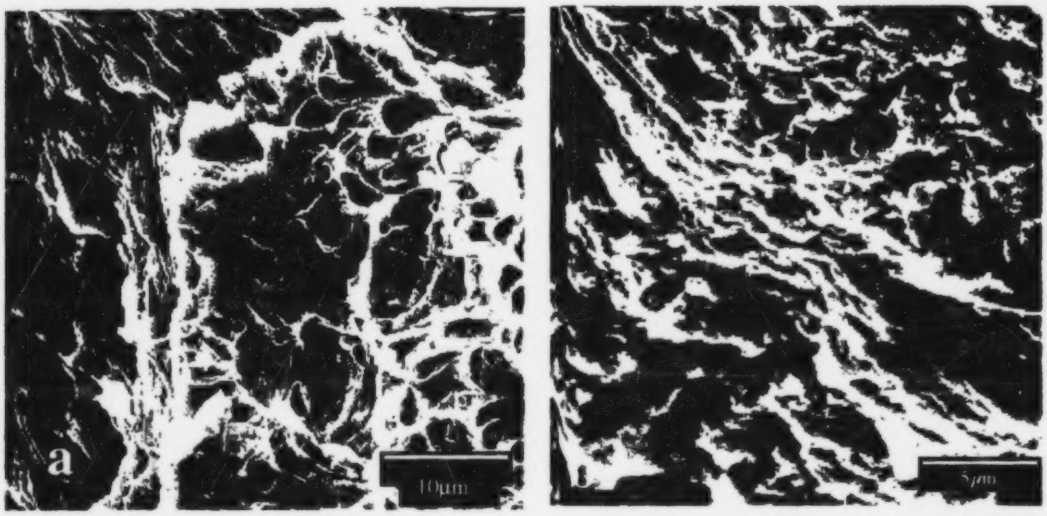

Figure 14. ASTM A517, Meta-Lax, No Preheat, weld metal (Plate 5) Fractographs of tested Charpy V-Notch specimens; a) tested at 25°C, b) tested at -30°C.

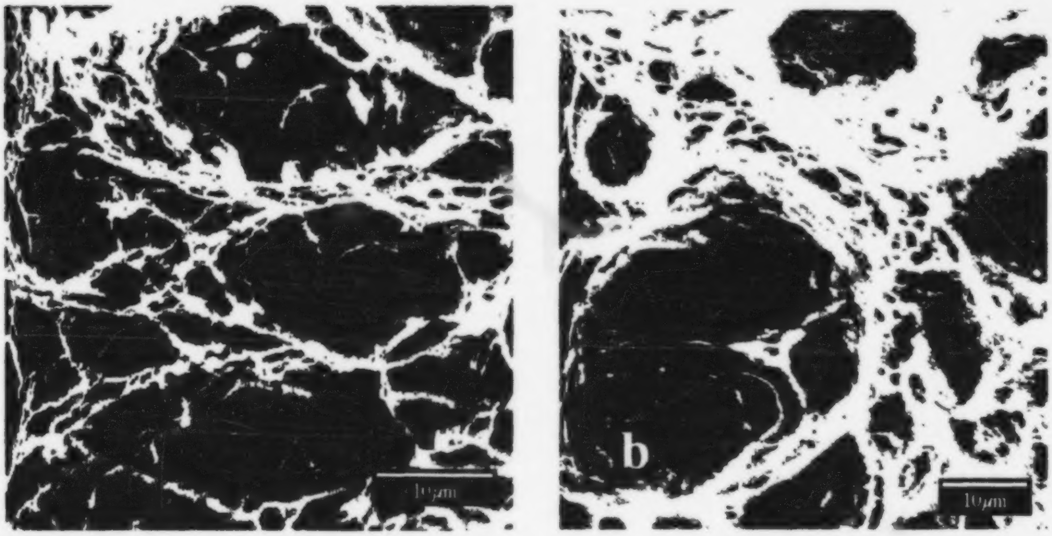

Figure 15. ASTM A517, No Meta-Lax . HAZ (Plate 6) Fractographs of tested Charpy V-Notch Specimens, a) tested at 25°C, b) tested at -30°C.

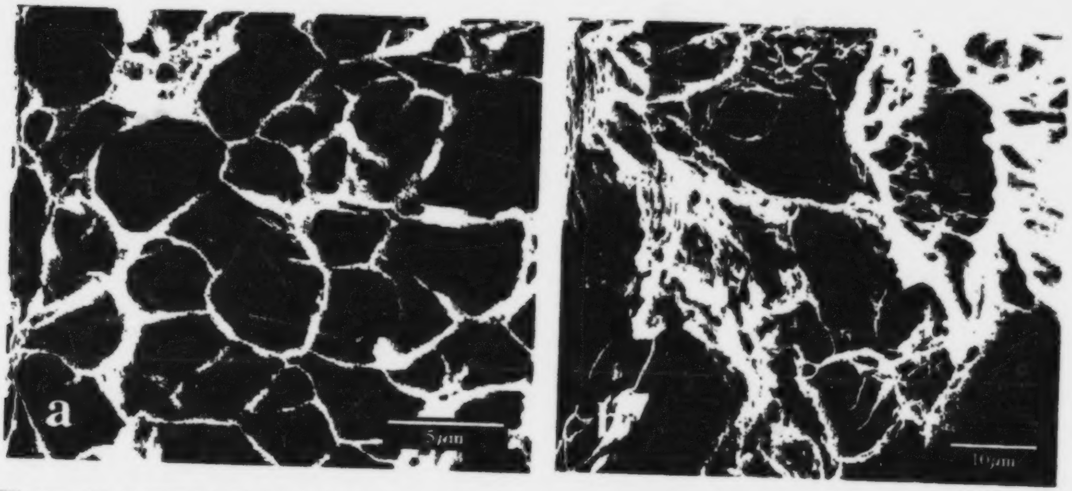

Figure 16. ASTM A517, Meta-Lax, HAZ (Plate 7) Fractographs of tested Charpy V-Notch specimens; a) tested at 25°C, b) tested at -30°C.

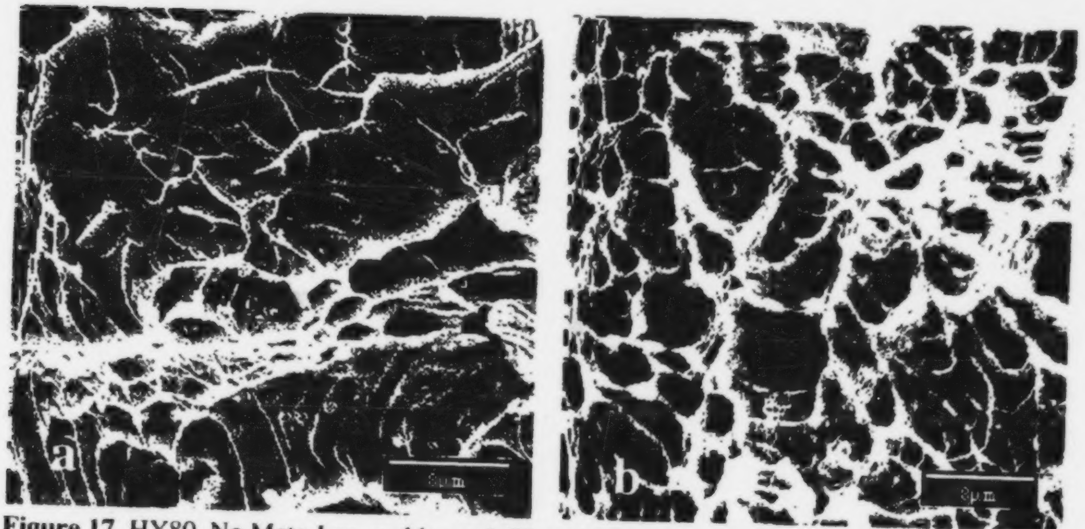

Figure 17. HY80, No Meta-Lax, weld metal (Plate A) Fractographs of tested Charpy V-Notch specimens; a) tested at 0°C, b) tested at -30°C.

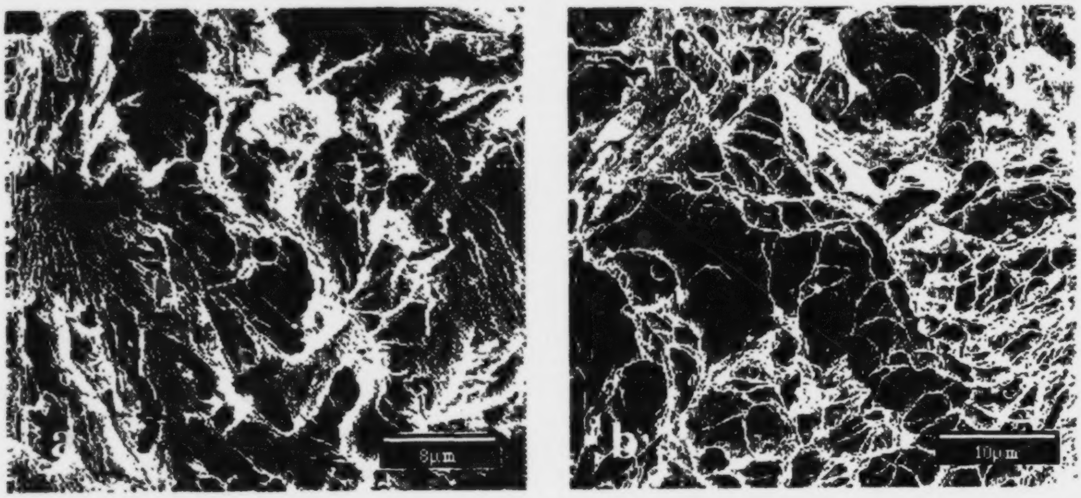

Figure 18. HY80, Meta-Lax, weld metal (Plate B) Fractographs of tested Charpy V-Notch specimens; tested at 0°C, b) tested at -30°C.

6.0 Discussions

Some observations were recorded during the machining of specimens from the welded plates. The machinist responsible for removing the backing bars off the welded steel had several comments with regards to working with the welded plates. Without knowledge of which plate had been welded with the Meta-Lax process, he was able to correctly identify which plate had received the Meta-Lax process. According to the machinist, during machining, there were marked decreases in noise, work piece vibration and distortion with the plate that received the Meta-Lax welding conditioning process. The plate that received no welding conditioning was much more difficult to work with, the backing bar was not as easily removed.

Fleet Technologies are also assessing the Meta-Lax process in an independent investigation into the effects of fatigue crack initiation and growth in butt-welded specimens. They were the recipient of test Plates 1 and 2 (ASTM A517 Grade F steel, exact size and welding procedure as Plate 3 and 4). Plate 2 was welded using the Meta-lax process in order to assess the Meta-Lax equipment while investigating the effect of residual stress and weld toe geometry on variable amplitude loading. Fleet Technology has reported that x-ray diffraction measurements indicated no difference in residual stress reading between plates. However, they did remark that the plate that was welded with the Meta-Lax process was less distorted.

It was anticipated that further comments would forthcoming during the machining of the test specimens, however, several machinists were employed, and no comparison could be made.

6.1 Charpy V-Notch Impact Test

As anticipated, as the testing temperature decreased, the impact energy also decreased (Figure 8). Not anticipated were the impact energies for the HAZ (Plate 6 & 7). The HAZ had better impact energies than the weld metal (Figure 8b). Further work must be done to understand these results.

Plate 5, which was not preheated, but welded with the Meta-Lax process, had the poorest results when compared with Plate 3 (no Meta-Lax) and Plate 4 (Meta-Lax).

The impact test results for the HY80 steel are very similar to those obtained for the ASTM A517 steel. The same welding electrode was used for both steels. Since the notch was placed in the weld metal, similar result should be expected.

In general, the Charpy V-Notch impact test results are not very conclusive with regards to the Meta-Lax process having any effect on the weld metal, the results are so close that they could be thought as being similar. Nonetheless, the Meta-Lax processed specimens recorded slightly better impact results.

6.2 Dynamic Tear Test

Similar to the Charpy V-Notch results, Plate 5, which was not preheated but welded with the Meta-Lax process, had the poorest results when compared with Plate 3 (no Meta-Lax) and Plate 4 (Meta-Lax).

The HY80 steel dynamic tear specimens from Plate B could not be tested due to improper machining. These specimens were not machined with the weldment in the center of the specimen. A safe test could not be guaranteed (specimen could not be mounted properly in test apparatus). Therefore none of the HY80 dynamic tear specimens were tested.

Unlike the Charpy V-Notch impact test results, the specimens welded without the Meta-Lax process recorded slightly better impact results (Figures 9a and 9b). The plates with the bevel edge preparation (Plates 3 and 4) had better dynamic tear results than the plates with the square and bevel edge preparation (Plates 6 and 7).

6.3 Hardness Test

Both the HAZ and the weld metal of the ASTM A517 and HY80 steels had lower hardnesses when they were welded with the Meta-lax process. The Meta-Lax plate that was not pre-heated prior to welding had lower hardnesses than the control plate which was pre-heated prior to welding.

6.4 Fractography

Both transgranular and microvoid coalescence are visible in Figure 12. Shown in Figure 12a is the ASTM A517 specimen tested at 25°C. As expected, the result indicates upper shelf behaviour (Figure 4), hence the dimple microstructure. The dimples appear slightly elongated in the direction of crack propagation. At a testing temperature of -30°C the dimples are no longer present (Figure 12b).

Both images in Figure 13 appear to be ductile fractures evident by the microvoid coalescence. There are differences in the microstructures found in Figures 12b and 13b. Both are ASTM A517 steels, both are tested at -30°C, however Figure 13b was welded with the benefit of the Meta-Lax process.

The specimens in Figure 14 were welded with the Meta-Lax process, however prior to welding, no preheat was employed to the plate. Neither fracture surface appears to be 100% ductile, even at 25°C (Figure 14a). Figure 14a appears to be a combination of both transgranular fracture and microvoid coalescence. Both cleavage facets and elongated dimples are present. As for Figure 14b, no conclusion could be drawn. This fracture surface could not be referenced with any in the literature at hand, nor were there any recognizable distinctive features.

The dimples in Figures 15a and 15b are the largest and the deepest recorded. These Charpy specimens were notched in the HAZ and did not have the benefit of the Meta-Lax process. The observed fracture surface corresponds to the impact energy results from the Charpy tests, which were also the highest obtained. The specimens tested at 25°C and -30°C have similar microstructures, the impact energy readings from the Charpy test were also similar (difference of 37J between 25°C and -30°C).

The micrographs in Figure 16 represent the fracture surfaces of the specimens which were notched in the HAZ and had the benefit of the Meta-Lax process. Figure 16a represents a ductile fracture by microvoid coalescence. Figure 16b appears to be a combination of dimples and cleavage facets. It is difficult to make a clear comparison between Figures 15 and 16, however the specimens from Plate 6 (Figure 15) which were welded without the Meta-lax process, had the larger dimples. Further investigation of these HAZ specimens is necessary. The HAZ impact results were also suspicious, as they were the highest overall.

The fractographs of the HY80 specimens had some similarities. Curiously, the specimens tested at -30°C (Figures 17b and 18b) appear more ductile than those tested at 0° (Figures 17a and 18a). Dimples and cleavage facets are visible in both specimens tested at 0°C . However, the dimples in Figure 18b (Meta-Lax process) appear deeper than those in Figure 17b.

7.0 Conclusions

- The Charpy V-Notch and Dynamic Tear impact tests did not provide conclusive results with regards to the Meta-Lax process.
- Lower impact energies were obtained when pre-heat was neglected prior to welding.
- HAZ & weld metal hardnesses were lowest with plates welded with the Meta-lax process.
- More work is necessary to provide conclusive results with regards to the Meta-Lax process.

8.0 Recommendations

Several Charpy specimens should be tested at the same temperature. The variance between results is too large for relying on solely one test result per temperature. At least 3 specimens should be tested at each temperature. Twenty-five additional Charpy V-Notch Impact specimens have been machined from each welded plate so that further testing can occur.

The weldments of the test plates have very complex microstructures, a result of the micro-alloying and multi-pass welding. It is necessary to re-analyses the weldment microstructure with a metallurgically less complicated steel. Seven low-carbon steel coupons have been machined with a groove so that a one pass SMAW can be deposited. It is expect that these microstructures will set a base for the more complex microstructures of the thicker plates.

9.0 Acknowledgement

Without DREA/DL's support, resources and encouragement this work would not have been possible. I would especially like to thank John Porter, not only for his time and patience as a member of my Master's Committee, but also for his guidance throughout this work. I am grateful to James Matthews for teaching me everything I know about transition curves as well as for the use of his equipment and Vincent Roy for his assistance with the dynamic tear testing.

I would also like to acknowledge the advice and guidance I received from the technicians at the Dockyard Laboratory. Their wealth of knowledge and expertise made this work so much more enjoyable. I am grateful to Dan Morehouse for providing his expertise towards the mechanical tests, Bob Armstrong for teaching me the art of preparing specimens, and Etienne Robichaud and Steve Kavanaugh for keeping me sane. I would like to thank everyone else at the Dockyard Laboratory not involved with this work, your encouragement, comments, and questions have all had a positive effect.

I would like to thank Drs. G.M.C. Lee, M. Gharghouri and M. Laufer from the Department of Metallurgical Engineering, Dalhousie University. Their time and patience as members of my Master's Committee is appreciated.

I would also like to thank Jack Hobbs of Hobbs Engineering for his expertise and advice with regards to welding.

Finally I would like to thank Fleet Maintenance Facility Cape Scott. Especially, Raymond Beazley of the Welding Shop and Paul Swantee of the Tool & Die Shop, their co-operation with this project was invaluable.

10.0 References

1. Bonal Technologies, Technical Support Summary Regarding "Meta-Lax" Stress Relief and Weld Conditioning, Southfield, November 1999.

2. Bonal Technologies.

3. Bonal Technologies.

4. J.R. Matthews, "Ship Fracture", Paper Presented at the 3rd CF/CRAD Meeting on Naval Applications of Material Technology, Halifax, NS. April 22-24, 1997, pp. 409-29.

5. J.R. Matthews, J.F. Porter & G.R. Pelletier, "Recommended Standard For Weld Consumable Approval System For Ships and Submarines", DL(A), August 1998.

6. J. R. Matthews, "Prediction of Ductile Behaviour in Welded Structures (Transition Behaviour, Shear Lip, Notch Acuity and Specimen Size)", The Minerals, Metals & Material Society, 1997.

7. W.D. Callister, "Material Science and Engineering, An Introduction", John Wiley, New York, 1994.

#516451 (36)

Toughness Envelope Definition of Pulsed Gas Metal Arc Welds in HY80 Steel

by

D.S. Begg and J.R. Matthews

Fleet Technology Limited, Kanata, Ontario, Canada
Defence Research Establishment Atlantic, Halifax, Nova Scotia, Canada

Abstract

Over the past decade, Defence Research Establishment Atlantic, has sponsored several projects related to "All Position Gas Metal Arc Welding" as part of their mandate to develop expertise in submarine materials and maintenance technology. These efforts have led to the identification of pulsed GMAW with C5, C10, or T.I.M.E gas combinations as the preferred ones from the perspective of superior weld zone mechanical properties in HY steels.

Previous work was successful in ranking new digital pulsed gas metal arc welding systems for optimal introduction in submarine refit followed by the development of a low heat input benchmark welding procedure for welding HY80 steel in the vertical-up position, using Lincoln's LA100 (ER100S-1) solid wire with T.I.M.E gas (26.5%He, 8%CO_2, 0.5%O_2, Ar Bal).

Although the benchmark is considered a practical procedure for the purposes of submarine repair and modification, it would be advantageous from the point of view of productivity to increase the heat input while maintaining the toughness requirements.

Five welded panels were produced with ER100S-1 solid wire and T.I.M.E gas, and radiographed +/- 20° to normal to verify weld soundness. The heat input used to produce each welded panel spanned the practical range for all position welding with the objective of identifying a level at which the weld metal toughness drops off below the required value. Dynamic tear samples were extracted and tested to develop notch toughness transition curves for each weld heat input.

Toughness Envelope Definition of Pulsed Gas Metal Arc (P-GMA) Welds in HY-80 Steel

by

- D. S. Begg (Fleet Technology Limited)
- Dr. J. R. Matthews (DREA)

presented at

9th CF/CRAD Meeting on Naval Applications of Materials Technology
Dartmouth, N.S., June 5 - 7, 2001

FTL FLEET TECHNOLOGY LTD

Oberon to Upholder

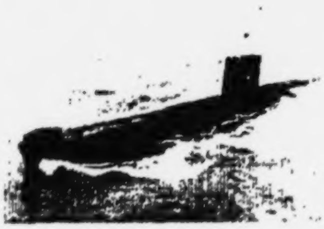

Oberon - QT-28

Upholder - Q1N (HY-80)

FTL FLEET TECHNOLOGY LTD

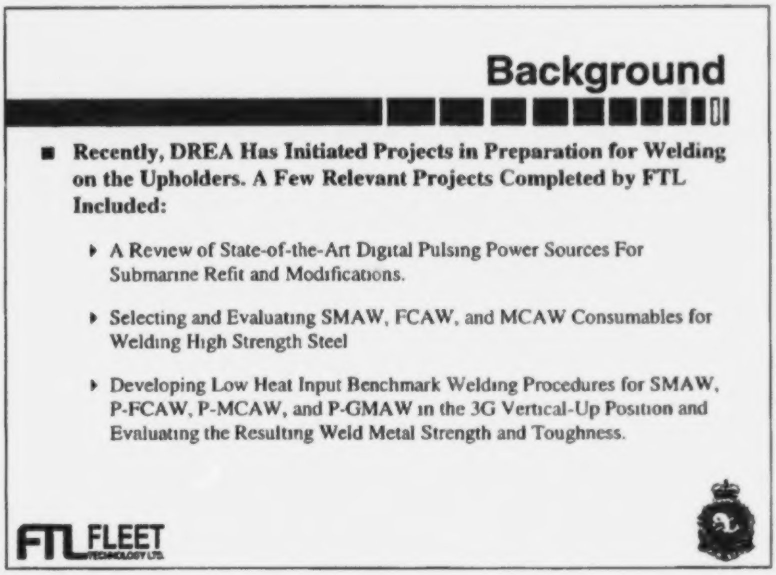

Background

- **Recently, DREA Has Initiated Projects in Preparation for Welding on the Upholders. A Few Relevant Projects Completed by FTL Included:**
  - A Review of State-of-the-Art Digital Pulsing Power Sources For Submarine Refit and Modifications.
  - Selecting and Evaluating SMAW, FCAW, and MCAW Consumables for Welding High Strength Steel
  - Developing Low Heat Input Benchmark Welding Procedures for SMAW, P-FCAW, P-MCAW, and P-GMAW in the 3G Vertical-Up Position and Evaluating the Resulting Weld Metal Strength and Toughness.

FTL FLEET TECHNOLOGY LTD.

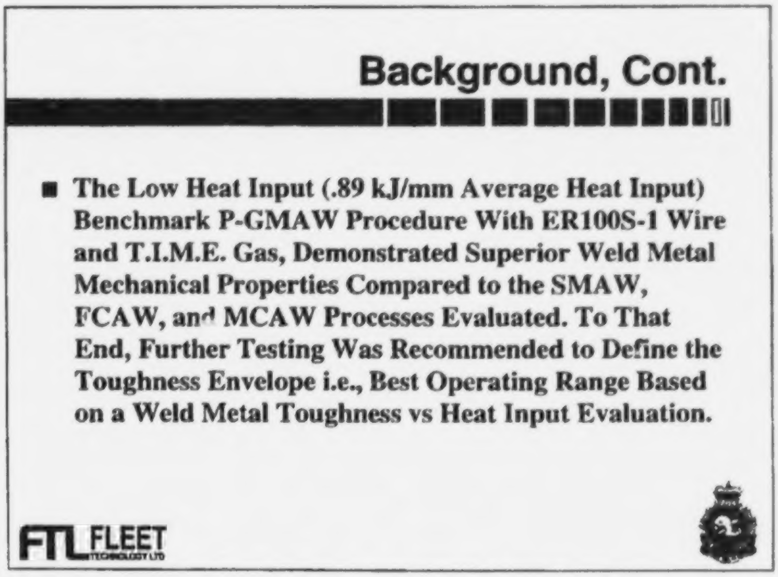

Background, Cont.

- **The Low Heat Input (.89 kJ/mm Average Heat Input) Benchmark P-GMAW Procedure With ER100S-1 Wire and T.I.M.E. Gas, Demonstrated Superior Weld Metal Mechanical Properties Compared to the SMAW, FCAW, and MCAW Processes Evaluated. To That End, Further Testing Was Recommended to Define the Toughness Envelope i.e., Best Operating Range Based on a Weld Metal Toughness vs Heat Input Evaluation.**

FTL FLEET TECHNOLOGY LTD

Objectives

- **Define the Toughness Envelope for Weld Metal in HY-80 Steel As a Function of Heat Input, Using the P-GMAW Process and T.I.M.E. Gas in the 3G Vertical-Up Position.**
- **Secondly, Define the Operating Range Suitable for Producing Sound Welds Using P-GMAW and T.I.M.E. Gas in the 3G Vertical-Up Position.**

FTL FLEET TECHNOLOGY LTD.

Approach

- **Weld Five 1000 mm Long 25 mm Thick HY-80 Test Panels in the 3G Vertical-Up Position and Incrementally Increase Heat Input With Each Subsequent Panel Welded.**
- **Extract and Test Dynamic Tear Specimens From Each Panel to Characterize Weld Metal Toughness at Each of the Five Heat Inputs.**
- **Extract Cross Section from Each Weld to Characterize Hardness as a Function of Heat Input.**

FTL FLEET TECHNOLOGY LTD.

Approach, Cont.

- **Despite Being Rated 2nd in the Power Source Review Project, the Miller Phoenix Power Source With 60M Digital Feeder Was Used to Perform All Welding to Ensure That the Results Are Repeatable With the Miller Phoenix Power Sources at the FMF Cape Scott.**

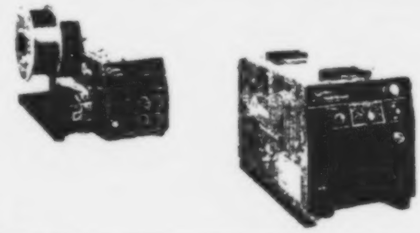

FTL FLEET TECHNOLOGY LTD

Consumable Selection - GMAW

- **1.2 mm Diameter ER100S-1 (Lincoln LA-100) Solid Wire With T.I.M.E. Gas Shielding Was Used Based on Good Performance in Past Test Programs, And, Was the Combination Used in the Benchmark Project.**

FTL FLEET TECHNOLOGY LTD

Procedure Development

- **The Goal Was to Fill up an Entire Panel Joint With Multiple Weld Passes, Each at the Selected Heat Input Level. Each Subsequent Panel Was Then Welded at a Higher Heat Input.**
- **Through Earlier Laboratory Trials Five Heat Inputs Were Selected For 3G Vertical-Up Welding Based on Best Performance in Terms of "Wetting Ability" and Weld Control. The Heat Inputs Selected Were 0.5, 0.7, 0.9, 1.1, and 1.4 kJ/mm.**

FTL FLEET TECHNOLOGY LTD

P-GMAW Procedure Details

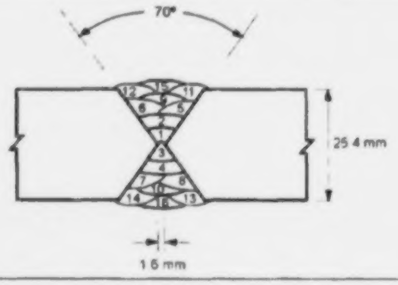

FTL FLEET TECHNOLOGY LTD

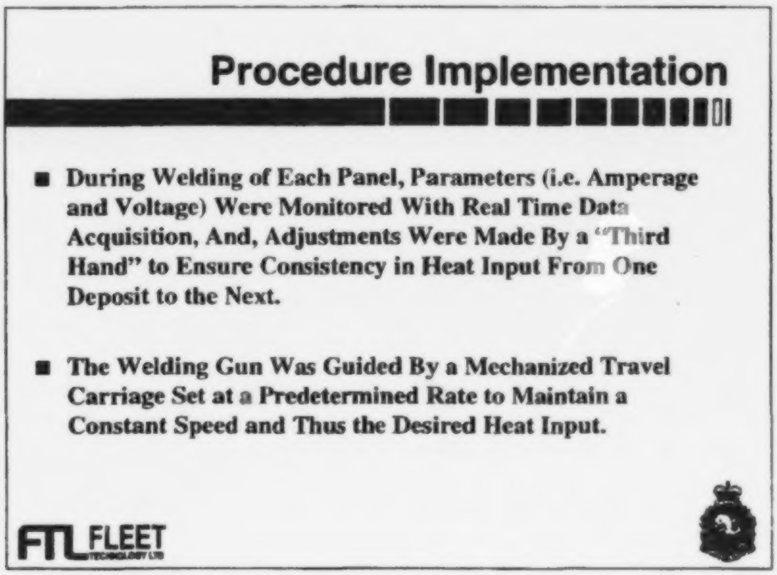

Procedure Implementation

- During Welding of Each Panel, Parameters (i.e. Amperage and Voltage) Were Monitored With Real Time Data Acquisition, And, Adjustments Were Made By a "Third Hand" to Ensure Consistency in Heat Input From One Deposit to the Next.
- The Welding Gun Was Guided By a Mechanized Travel Carriage Set at a Predetermined Rate to Maintain a Constant Speed and Thus the Desired Heat Input.

FTL FLEET TECHNOLOGY LTD

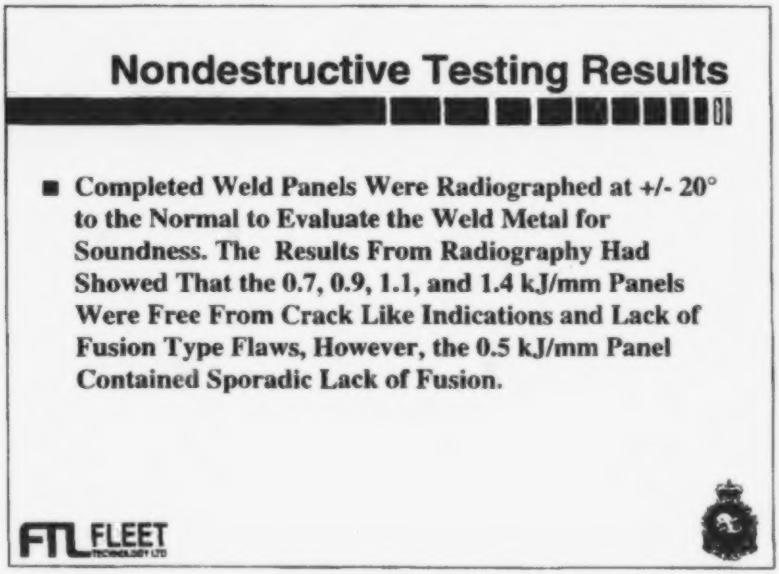

Nondestructive Testing Results

- Completed Weld Panels Were Radiographed at +/- 20° to the Normal to Evaluate the Weld Metal for Soundness. The Results From Radiography Had Showed That the 0.7, 0.9, 1.1, and 1.4 kJ/mm Panels Were Free From Crack Like Indications and Lack of Fusion Type Flaws, However, the 0.5 kJ/mm Panel Contained Sporadic Lack of Fusion.

FTL FLEET TECHNOLOGY LTD

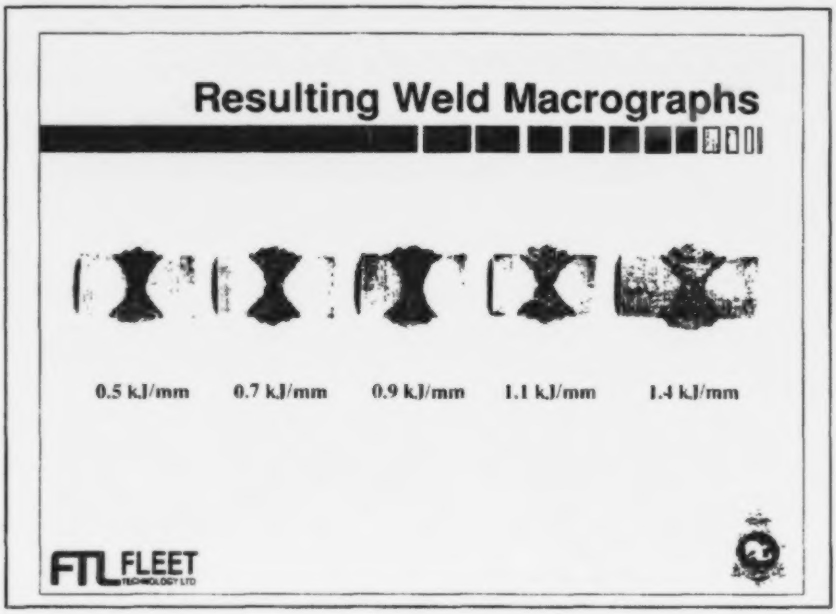

Resulting Weld Macrographs

0.5 kJ/mm

0.7 kJ/mm

0.9 kJ/mm

1.1 kJ/mm

1.4 kJ/mm

FTL FLEET TECHNOLOGY LTD

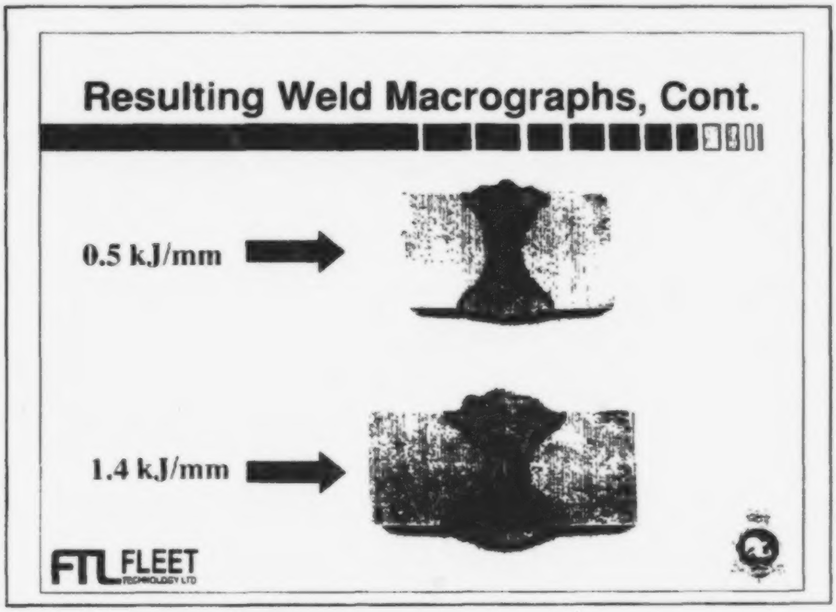

Resulting Weld Macrographs, Cont.

0.5 kJ/mm

1.4 kJ/mm

FTL FLEET TECHNOLOGY LTD

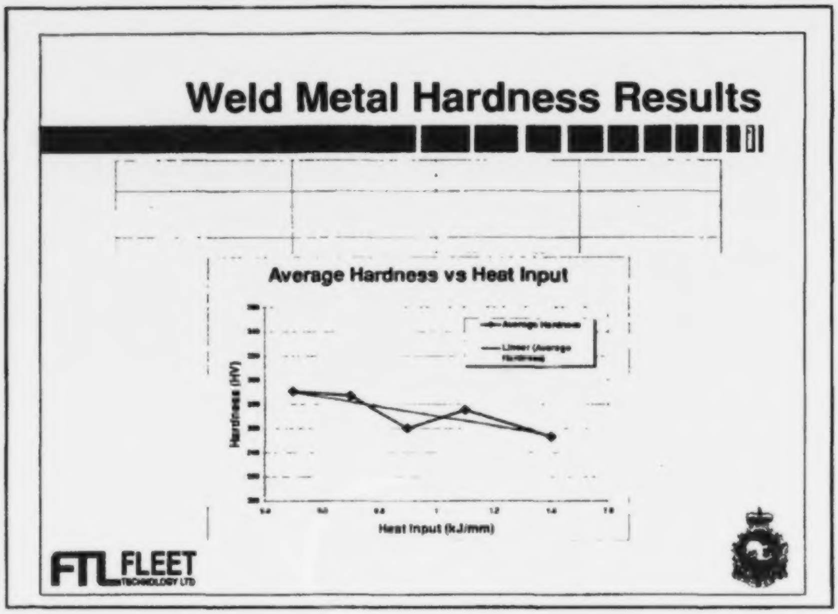

Weld Metal Hardness Results

FTL FLEET TECHNOLOGY LTD

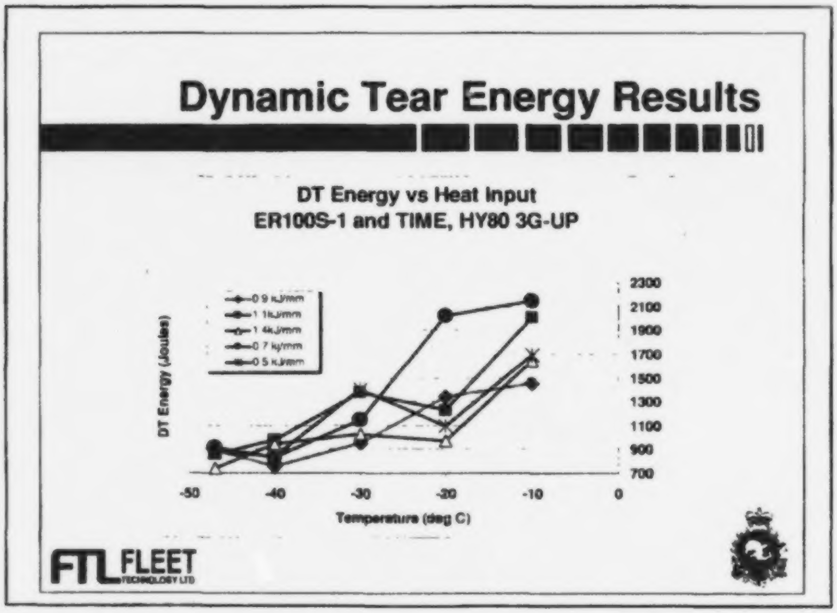

Dynamic Tear Energy Results

DT Energy vs Heat Input
ER100S-1 and TIME, HY80 3G-UP

FTL FLEET TECHNOLOGY LTD

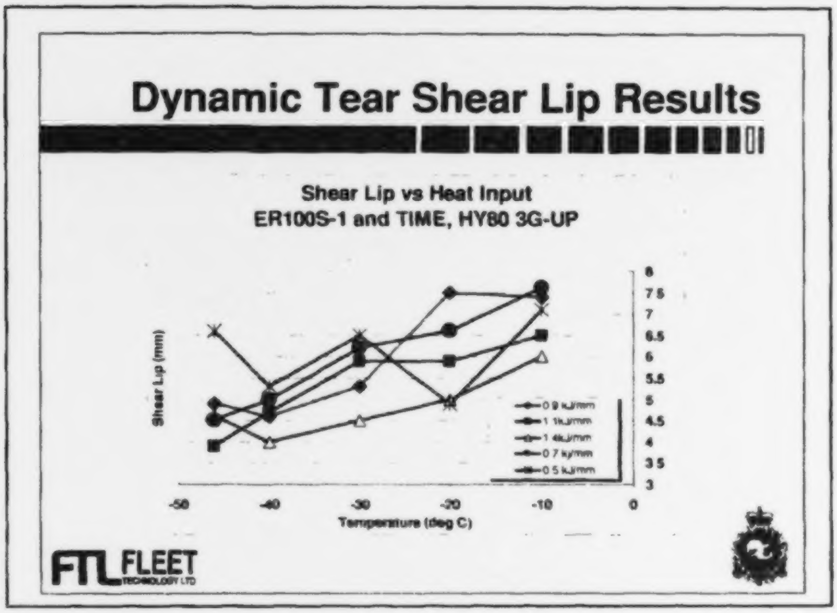

Dynamic Tear Shear Lip Results

Shear Lip vs Heat Input
ER100S-1 and TIME, HY80 3G-UP

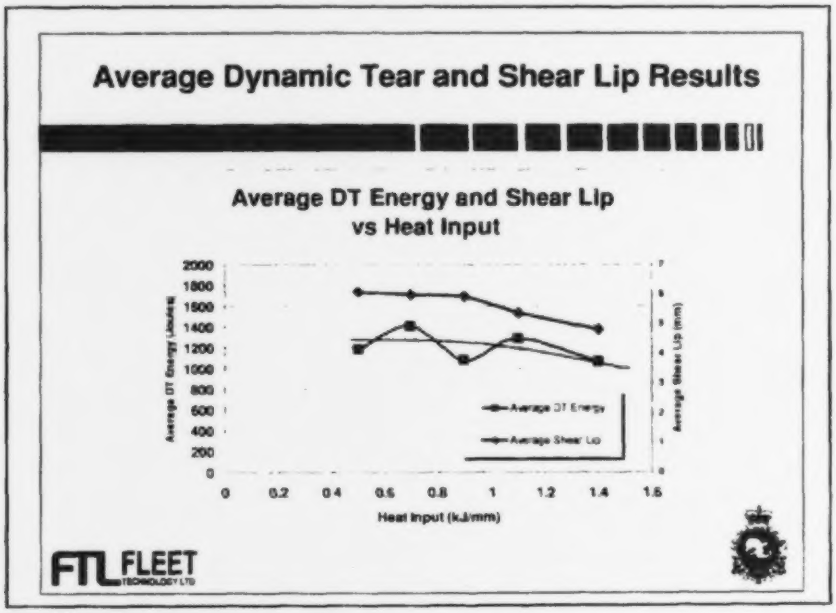

Average Dynamic Tear and Shear Lip Results

Average DT Energy and Shear Lip
vs Heat Input

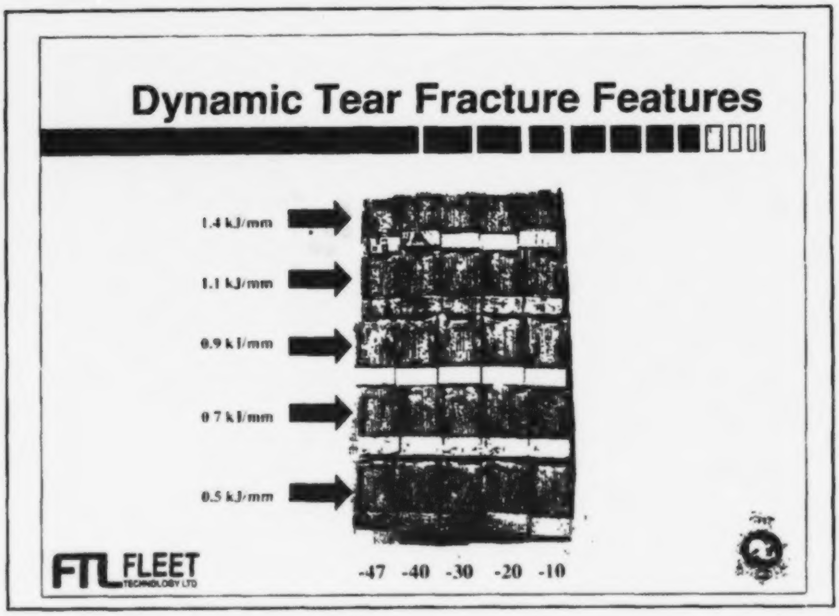

Dynamic Tear Fracture Features

1.4 kJ/mm
1.1 kJ/mm
0.9 kJ/mm
0.7 kJ/mm
0.5 kJ/mm
-47 -40 -30 -20 -10

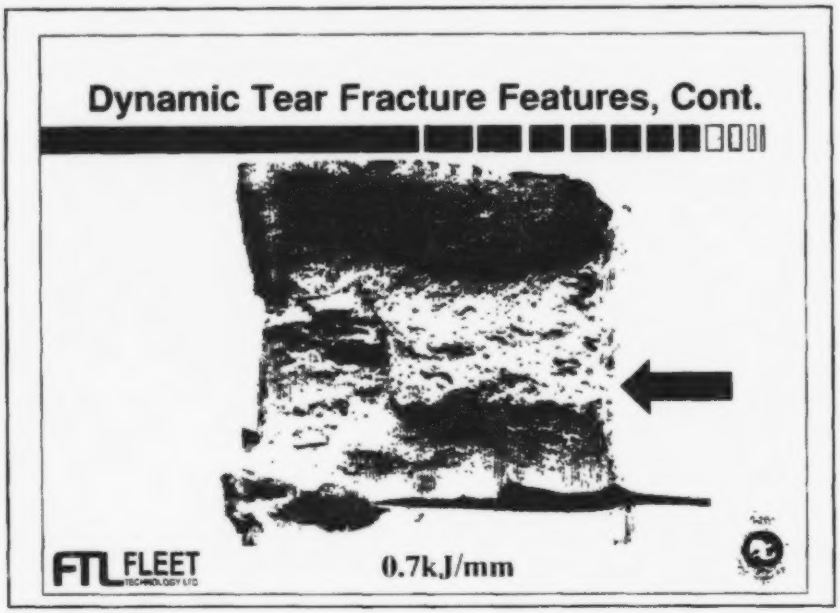

Dynamic Tear Fracture Features, Cont.

0.7kJ/mm

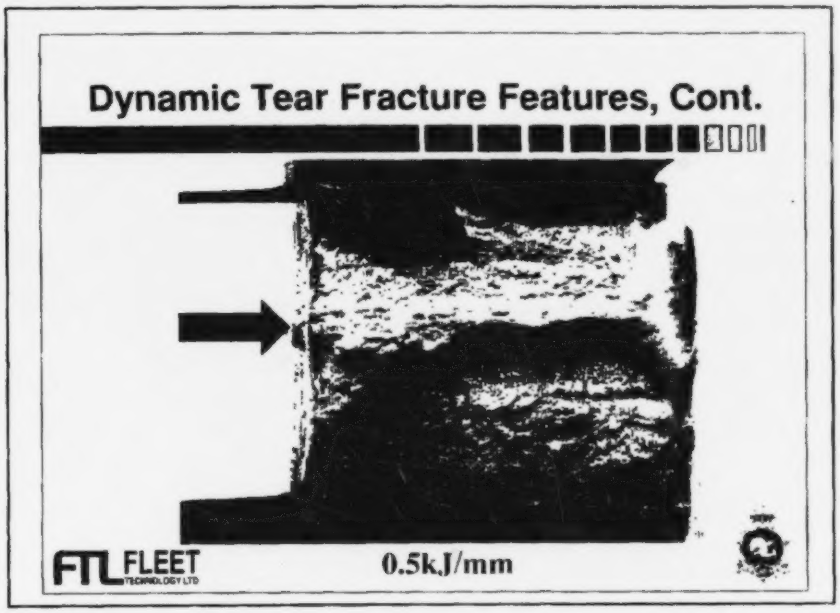

Dynamic Tear Fracture Features, Cont.

0.5kJ/mm

FTL FLEET TECHNOLOGY LTD

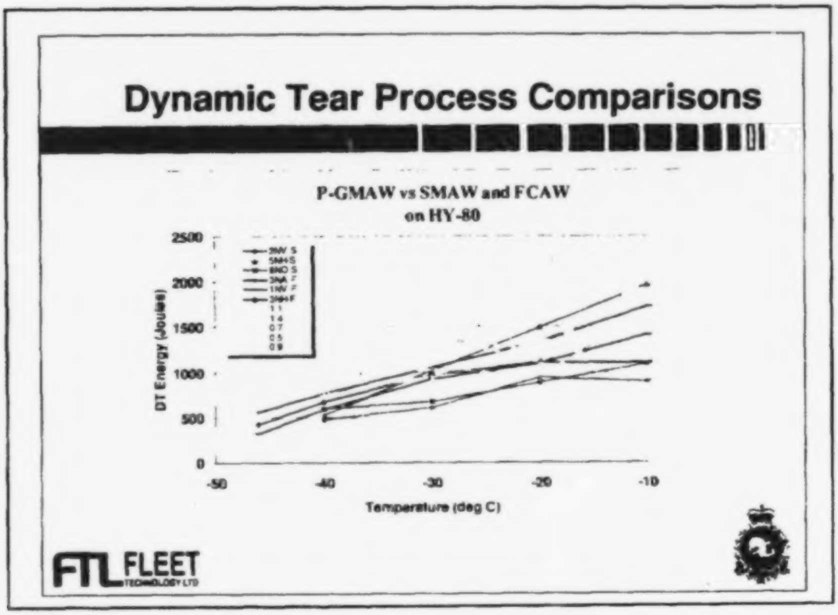

Dynamic Tear Process Comparisons

P-GMAW vs SMAW and FCAW
on HY-80

FTL FLEET TECHNOLOGY LTD

Conclusions

- Based on the Hardness Results, There is a Downward Trend in Hardness With Increasing Heat Input.
- Based on the Shear Lip Results, the Downward Trend in Toughness Begins Around 1 kJ/mm.
- Based on Visual Appearance, the 0.5 and 0.7 kJ/mm Welds Are Tougher Than at Other Heat Inputs, the 0.5 kJ/mm Being the Toughest.
- All of the P-GMAW Welds Produced Meet the 690J at -30°C Toughness Requirement for Dynamic Tear Energy.

Conclusions, Cont.

- Although 0.5 to 1.0 kJ/mm Heat Input Range Provides the Best Toughness Over the Range of Heat Inputs Tested, a Heat Input Range of 0.7 to 1.1 kJ/mm Provides the Best *Operating* Characteristics for 3G Vertical-Up Welding With the Miller Power Source.
- The Dynamic Tear Results From the FTL P-GMAW / T.I.M.E. Welds Exceed the Results for the Recommended E9016 SMAW and the FCAW Tests Recently Conducted at FMF Cape Scott. In Addition the Latter Were at a 100 MPa Lower Strength Level to Optimize Their Toughness.

Recommendations for Future Work

- Analyze Microstructure of Completed Welds to Determine If There Are Any Significant Differences in Weld Metal Microstructure with Increasing Heat Input

- Position of Welding May Influence the Effectiveness of Shielding Gas Coverage, Thus Influencing the Percentage of Nitrogen Entrapped in the Weld Metal and Resulting Toughness. It Is Recommended That the Toughness Be Evaluated in Other Positions As Well (Flat, Horizontal, and Overhead) to Further Define the Toughness Envelope.

- The Lincoln Powerwave, Rated #1 in the Power Source Review Contract, Is Still Recommended for P-GMA Welding Over the Miller Power Source Based on the Lincolns Superior Arc Characteristics and Dynamic Response, and, a More Friendly User Interface.

FTL FLEET TECHNOLOGY LTD.

#516452 (37)

Composite Material Durability for Naval Structures

by

F. Dubois-Artiga*, J. Dalzel-Job**, K J.A. Mawella*** and F. Decobert****

*DCN Indret, France
**DERA Rosyth, Dunfermline, United Kingdom
***DPA, Bristol, United Kingdom
****DGTA, Paris, France

Background

It is well known that composite materials progressively deteriorate with environmental conditions. A marine environment with combined exposure to moisture, salt water and temperature variations seems to be particularly aggressive for polyester matrix/fiberglass reinforced composites used for the manufacturing of ships, especially hulls and superstructures. The ageing effects on composite structures are commonly studied by accelerated ageing tests at elevated temperature, performed on laboratory specimens. However, so far a lack of long term data for natural ageing has prevented a comparison with accelerated ageing to be made so that the consequences for ship durability cannot be assessed.

This paper describes the results of a programme on accelerated ageing of composites, carried out under a British-French collaboration Agreement. Accelerated ageing tests with a temperature of 40°C or 60°C have been carried out by both parties over a period of up to 8000 hours, and will continue up to 24000 hours. Samples are withdrawn from artificial seawater at regular periods and residual characteristics determined by physico-chemical and mechanical tests. In a parallel study, samples located above and below the water-line were drawn from a French minehunter after 17 years of service and tested with the same procedure. A previous programme of residual mechanical tests on material from British minehunters is also referred to in this paper.

The eventual aim of the programme is to achieve a correlation between real time ageing as experienced in service and laboratory accelerated ageing, in order to analyse the real effect of temperature on laminate degradation mechanisms and also to distinguish their acceleration from other modifications to the material The possibility of extrapolating material behaviour over thirty years in order to increase the life duration of ships will be studied.

Introduction

It is well documented in the literature that the mechanical and physical properties of fibre reinforced polymer (FRP) composites degrade after prolonged exposure in aggressive environments such as seawater. Water molecules are able to diffuse into the polymer matrix where the result can be reversible damage, such as matrix plasticisation and swelling or irreversible damage, such as hydrolysis and microcracking. Water may also affect the matrix/fibre interfacial bond and in some instances attack the fibre reinforcement itself. A typical curve of water uptake against time for a polyester resin is given in Figure 1.

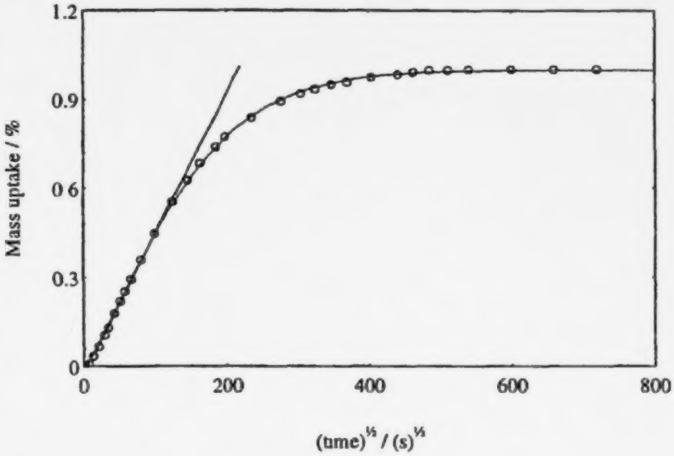

Figure 1. Moisture Diffusion: Crystic 489 resin, 93% RH at 293°C, 0.37mm thick sheet (~ 1 week) (DERA)

The study of long term durability of composites is complex and although accelerated ageing techniques can be used, the accuracy of this approach for predicting marine FRP composite durability has not been assessed. Furthermore, since composite materials for ships are relatively new (HMS WILTON was launched in 1972) very little real-time data for ageing marine FRP is available with which to compare results from accelerated ageing model predictions.

Part 1: Accelerated Ageing Programme

The scope of this programme is to:

- observe mechanical, physical and chemical changes in GRP laminate caused by accelerated ageing in seawater,
- monitor these changes over a time period of 24,000 hours (2yrs 9m)
- achieve a correlation between the real-time ageing of in-service vessels and laboratory accelerated ageing,
- study the possibility of extrapolating material behaviour to thirty years and beyond.

Experimental

Test materials used in this work were laminates typical of minehunter construction used by the French and British Navy. Panels were laid up by hand and the edges sealed with silicon. They did not receive any post cure. The two materials studied were :

- Crystic 489 Polyester resin reinforced with Fothergill YO530 glass woven roving ('DERA laminates')
- Norsodyne 7031T Polyester resin reinforced with Vetrotex S830 glass woven roving ('CESMAN laminates')

Conditioning: The conditioning procedure for accelerated ageing of the laminates was full immersion in artificial seawater maintained at 40°C (DERA procedure) and 60°C (CESMAN procedure). The results are presented on materials aged for up to 4000 hours under DERA procedure and 8000 hours under CESMAN procedure.

Testing : Samples were withdrawn periodically from the conditioning tanks and tested to assess their mechanical properties such as tensile, flexural, compressive and interlaminar shear strength. In addition gravimetric (water uptake) measurements, dynamic mechanical thermal analysis (DMTA) and chemical analysis (Infrared spectrometry) were carried out.

Results

The results of the mechanical tests carried out on both UK and French laminates pre-exposed at 40°C and 60°C are shown in Figures 2 – 16 below. The laboratory carrying out the tests is identified in each case.

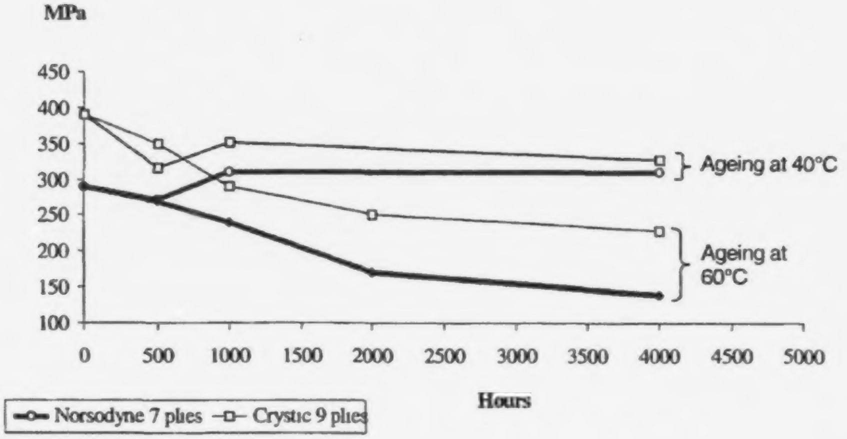

Figure 2. Effect of pre-exposure time at 40°C and 60°C on the tensile strength of French (Norsodyne) and UK (Crystic 489) laminates (DCN)

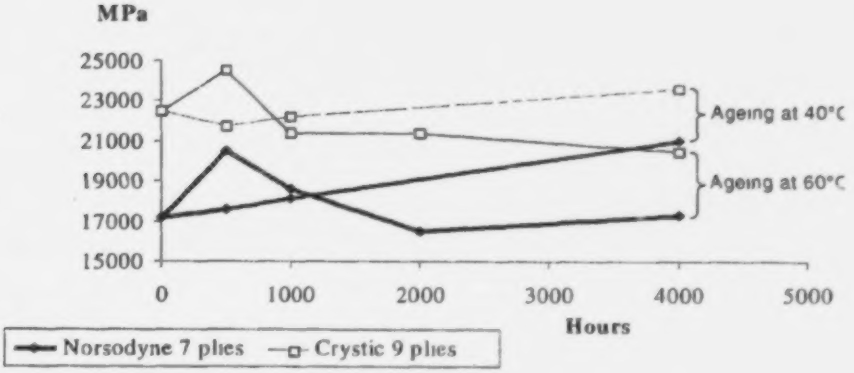

Figure 3. Effect of pre-exposure time at 40°C and 60°C on the tensile modulus of French (Norsodyne) and UK (Crystic 486) laminates (DCN)

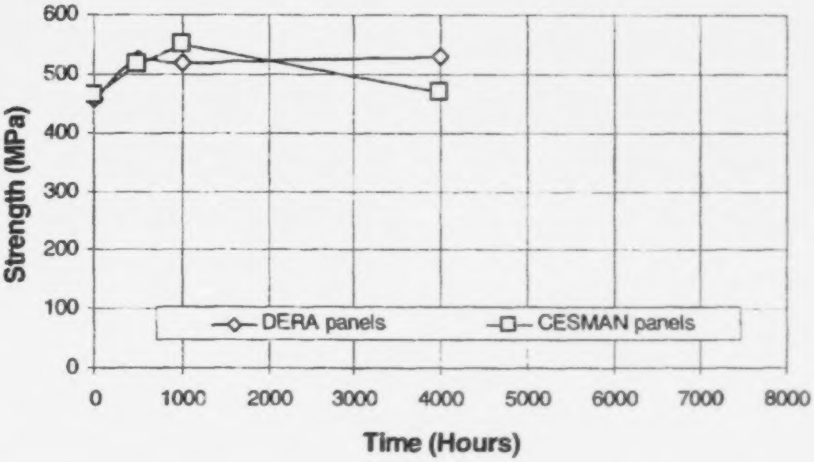

Figure 4. Effect of pre-exposure time on flexural strength of French and UK laminates pre-exposed at 40°C (DERA)

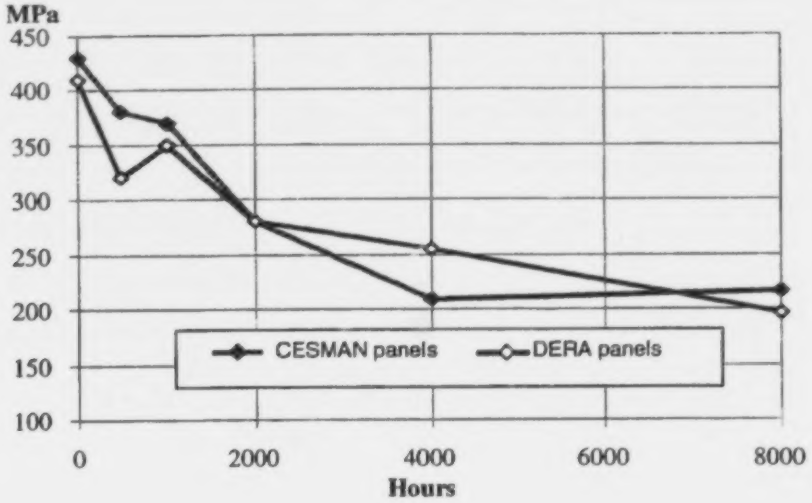

Figure 5. Effect of pre-exposure time on flexural strength of French and UK laminates pre-exposed at 60°C (DCN)

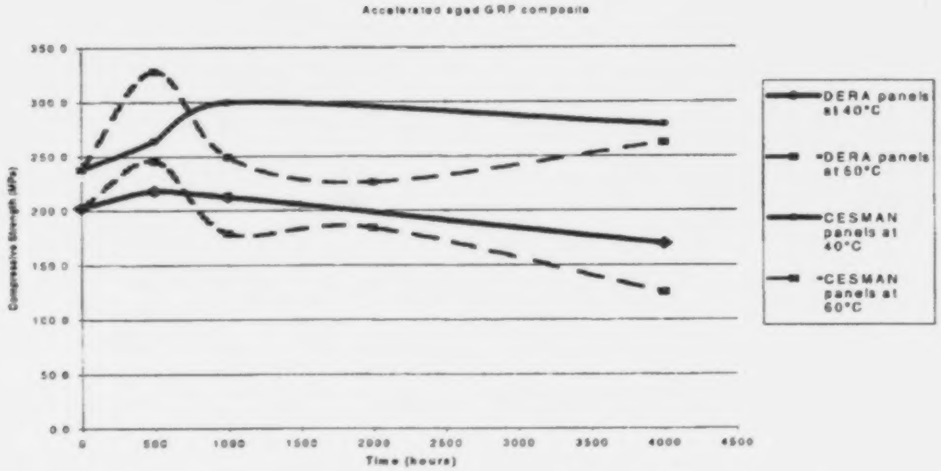

Figure 6 Effect of pre-exposure time on the compressive strength of French and UK laminates pre-exposed at 40°C and 60°C (DERA)

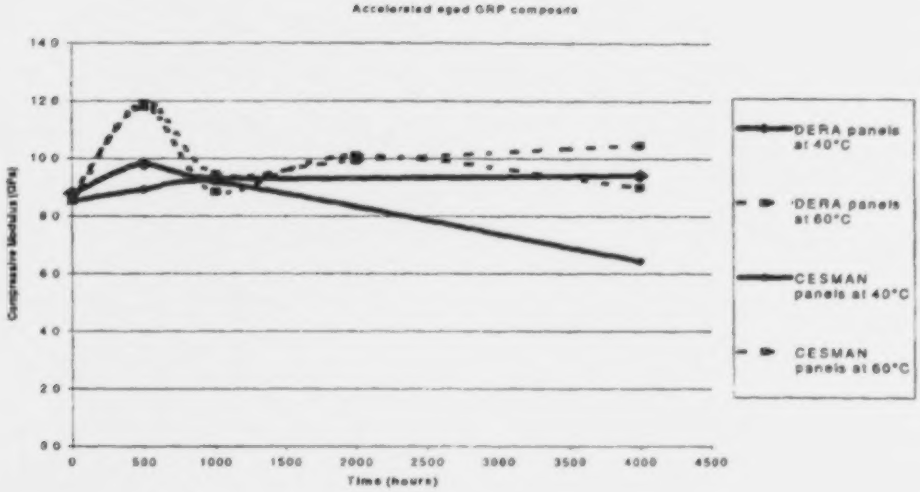

Figure 7 Effect of pre-exposure time on the compressive modulus of French and UK laminates pre-exposed at 40°C and 60°C (DERA)

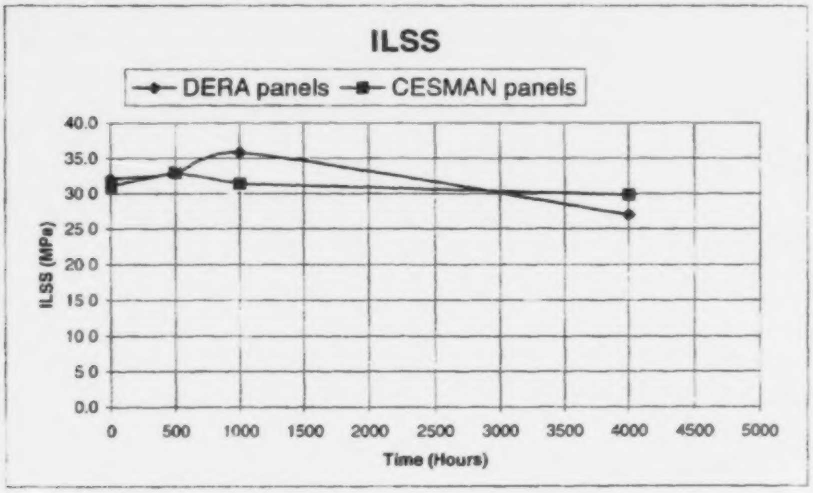

Figure 8 Effect of pre-exposure time on interlaminar shear strength of French and UK laminates pre-exposed at 40°C (DERA)

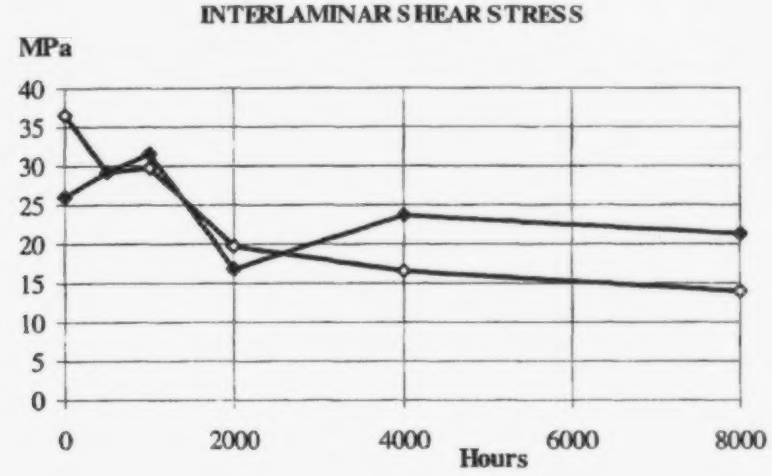

Figure 9 Effect of pre-exposure time on interlaminar shear strength of French and UK laminates pre-exposed at 60°C (DCN)

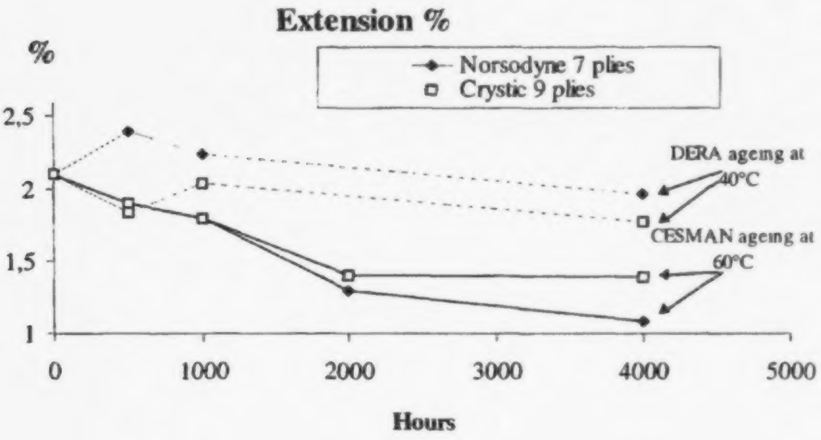

Figure 10 Effect of pre-exposure time on elongation at break of French and UK laminates pre-exposed at 40°C and 60°C (DCN)

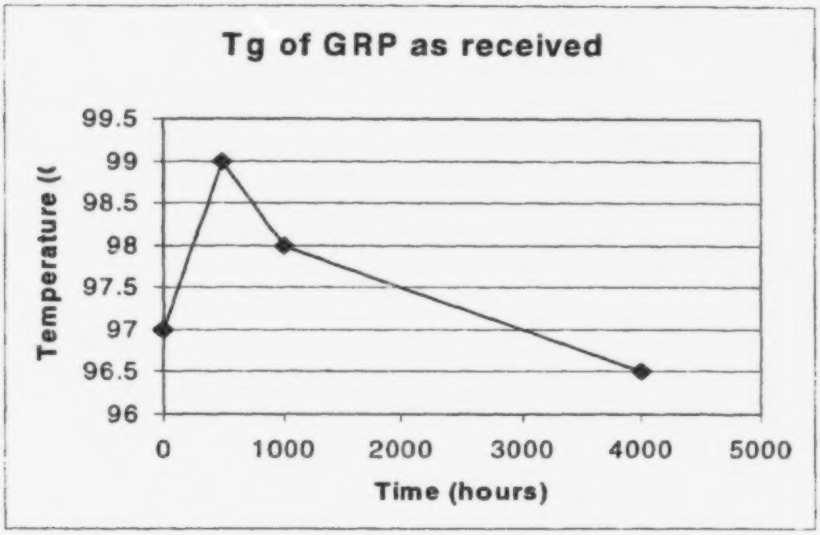

Figure 11 Tg of Crystic 489 resin pre-conditioned at 40°C as a function of pre-exposure time (DERA)

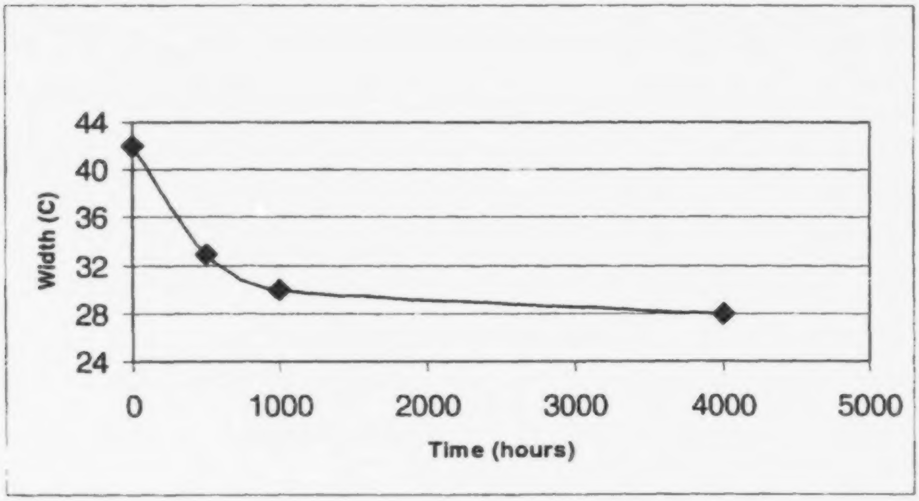

Figure 12. Width of *tan(δ)* of Crystic 489 resin conditioned at 40°C as a function of conditioning time (DERA)

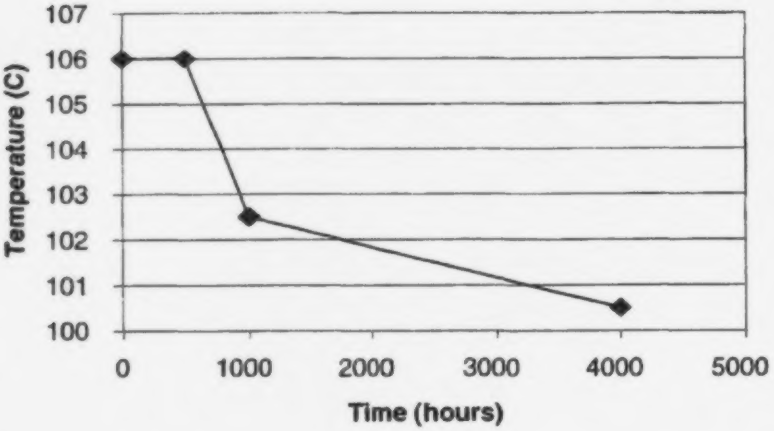

Figure 13 Tg of second DMTA run as a function of conditioning time for Crystic specimens conditioned at 40°C (DERA)

	DSC	(Tg°C)	Fiber	Rate (%)
Ageing (hours)	Norsodyne	Crystic	Norsodyne	Crystic
T0	**112**	**84**	51,1	**60,7**
T500	101	**89**	57,7	62
T1000	98	80	55,3	59
T2000	**105**	82	51,3	59,8
T4000	103	81	52,6	59,6
T8000	103	79	54,9	58,6

Table 1 Tg of Norsodyne and Crystic conditioned at 60°C with a record of fibre rate (%wt) (DCN)

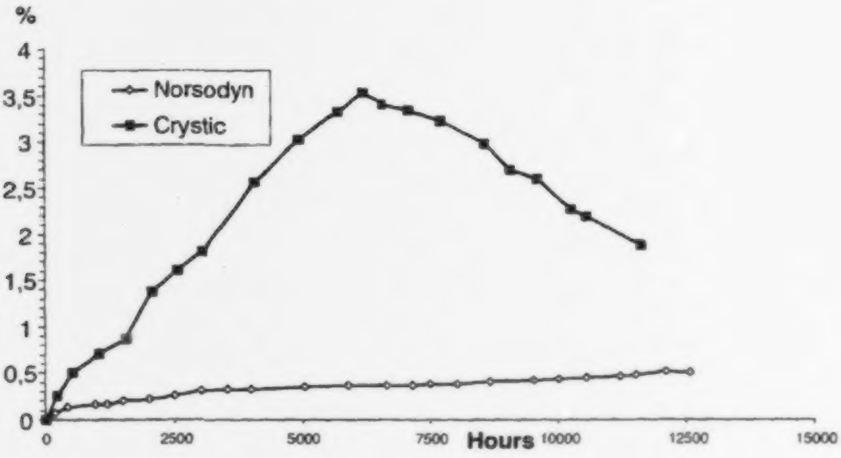

Figure 14 Water sorption (% wt) for Norsodyne and Crystic laminat conditioned at 60°C (DCN)

Discussion of Results

Specimens have been conditioned for up to 8000 hours, and whilst this represents only one-third of the total conditioning time for the programme, certain effects can be clearly seen from the data. In some instances however, the overall trend beyond the initial stages is unclear. Figures 2 to 9 show changes in strength and stiffness of the French and UK materials which have been conditioned at 40°C or 60 °C for either 4000 or 8000 hours. Compression and interlaminar shear (ILS) are both properties that are significantly affected by changes in resin state, whereas tension, and to a lesser extent, flexure are properties dominated by the fibres. For compression and ILS there is an increase in property during the first 500 hours; this is then followed by a decrease. Pre-conditioning at 60 °C has a greater effect on the resin than exposure at 40°C, which is expected.

Degradation of the mechanical properties of the composite can be related to changes in the resin chemical structure as shown by changes in Glass Transition Temperature (Tg) in Figures 11, 12 and 13 and Table 1. Two factors are important here - the density of the cross links between the polymer chains and the degree of plasticisation of the resin.

- Conditioning at 40°C increases the number of cross links, giving a higher Tg as measured by the peak of the tan delta curve (Fig 11). A higher Tg indicates a stronger, more brittle polymer. The Tg appears to rise initially and then fall off with time

- The width of the tan delta peak measured by DMTA measures plasticisation of the resin and Fig 12 shows that ageing appears to remove plasticisation over time.

- Fig 13 shows the Tg measured for samples after a second DMTA analysis. Tg gives an indication of the degree of cross-linking and shows if degradation to the polymer network is taking place. The results show that the Tg starts to drop after about 500 hours.

Changes in mechanical properties can be related to changes recorded in the DMTA analysis as follows:

- Where mechanical properties have increased with exposure time, this is linked to the increase in Tg caused by the post-cure effect from the elevated temperature immersion, which increases the resin cross-linking.

- Over extended time periods (beyond 500 or 1000 hours) the effect of this post cure is lost due to the competing degradation reactions that break the chemical bonds and cross-links

- Resin toughness is reduced over time as low molecular weight material that imparts plasticisation is removed (through post-curing and leaching). Although absorbed water acts as a plasticiser, there is a net reduction in toughness.

Part 2: Mechanical properties of GRP ship hulls

UK/DERA:

In 1994/95 a mid-life update programme was conducted on the Hunt Class Mine Countermeasures Vessels (MCMV). Panels were cut from the superstructure and hull (above and below the water line) of vessels aged 14½, 21,22 and 23 years. Figure 15 shows Tensile strength in the warp direction of the woven fibres. Because of the lack of data between vessel build (year 0) and 14½ years, a linear regression was made on a logarithmic scale for extrapolation to the 40 years of proposed design life. Other properties measured were tensile modulus, compressive and flexural strength and modulus and interlaminar strength. This data, together with the results of the French studies on an eighteen-year old minehunter described below, will be used for the 'real-time' ageing part of the programme.

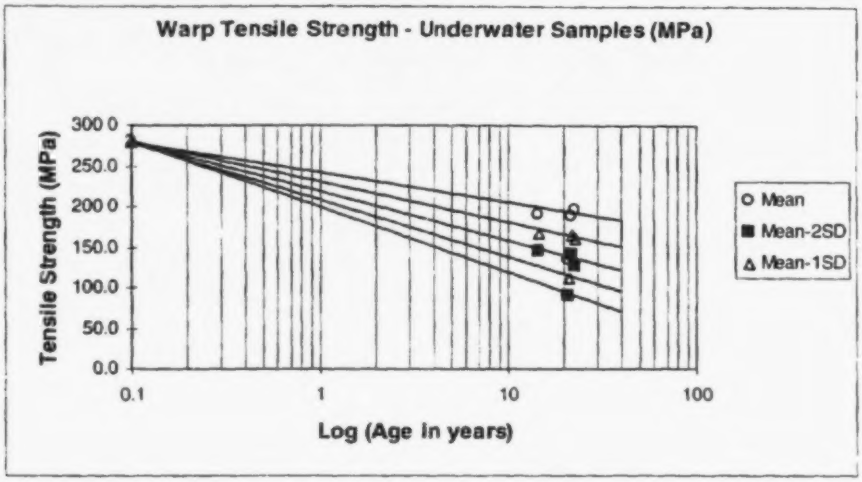

Figure 15 Tensile strength of GRP ship hull laminate extrapolated to 40 years (from the Hunt Class Mid-life Update 1995) (DERA)

France/DCN:

Plates were cut from the French minehunter ANDROMEDE. This ship has a single skin hull which was manufactured 1982/1983 from hand lay-up Tetrahydrophthalic polyester resin NF 294T with a 830 g/m² woven roving glass reinforcement. The outer layers of the hull (grey in colour) were made from 150 g/m² glass mat and 2 woven roving 580 g/m² glass plies with isophthalic polyester resin and gel-coat.

2 plates, each measuring 700 x 300 mm were cut: the first, 18 mm thick, was taken from above the water line and the second, 27 mm thick, taken from below the water line. These are shown schematically in Figure 16.

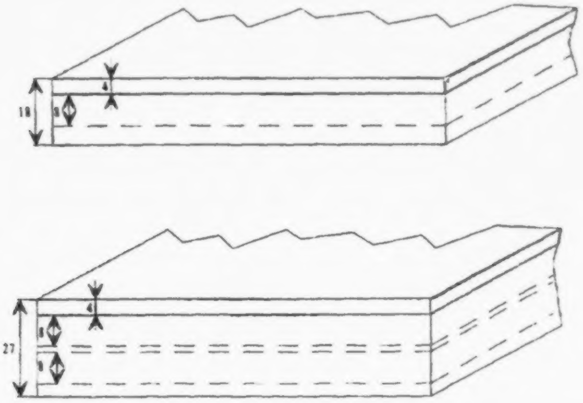

Figure 16 Above- and below- water plates cut from ANDROMEDE.

Characteristics		Air	Water-skin	Water-heart
DSC	Enthalpy J/g	-1	-8	-8
	Tg °C	90	92	89
Fiber rate %		50	47	51
3 Pts Bending	Stress Mpa	250	190	220
	Modulus Mpa	15000	12200	14500
	Deflection mm	6,7	5,9	5,6
Interlaminar shear stress Mpa		22,9	22,6	20,7
Tensile	Stress Mpa	170	125	127
	Modulus Mpa	21900	14600	17900
	Elongation %	0,96	1	1,06
Visco-elastic analysis	Modulus E' Mpa	14000	11200	14300
	Tg °C	111	110	107

Table 2 Mechanical and physical properties of above and below water laminate taken from ANDROMEDE

Environment	Modulus E_t (GPa)	Modulus E_v (GPa)	Validity of tests	σt_r (MPa)	σv_r (MPa)	εt_r (%)	εv_r (%)	Validity of tests
air	**16.4** *(1,1)*	**16,4** *(1,3)*	5/6	**244,6** *(21.6)*	**241,6** *(27,0)*	**1,39** *(0,22)*	**1,29** *(0,20)*	4/6
water (gel-coat side)	**14,2** *(1.5)*	**13,5** (*)	2/4	**219.2** *(11.1)*	(**)	**1,40** *(0.32)*	(**)	1/4
Water (internal side)	**15,3** *(0.7)*	**15,0** *(0.7)*	4/6	**218,7** *(17,0)*	(**)	**1,42** *(0 17)*	(**)	1/6

(*) no significant standard deviation (only 2 values)

(**) : one result

Table 3 Compression properties of above and below water laminate taken from ANDROMEDE

Discussion of results

Compared to the laboratory-manufactured samples described in Part 1 there was a greater degree of scatter in the test results, which would be expected in laminate manufactured industrially.

It is interesting to compare results of air and water-skin samples because they have the same location under the gel-coat. Results from air samples are generally higher than the others with however more significant standard deviations, especially for bending. Water-skin samples show lower values but also have a lower fibre rate (3 to 4 %). Variations of temperature and hygrometry accelerate the ageing of composite materials that induces a plasticisation of the resin and then an increase of the modulus and failure stress with a small strain.

The visco-elastic analysis shows that the Tg of material from water-heart samples is 3°C lower than 2 other withdrawals (this is the same for DSC) and that the modulus for water-heart samples and air samples is higher; the modulus of samples close to the water seems to be affected by this environment.

Correct results were obtained with compression tests for samples from above the waterline but samples from under the water line had only 1 out of 2 correct failures. Lower compression characteristics were found for plates under the waterline compared to those with air exposure. The influence on thickness location is difficult to assess because of the variations of fibre rate.

Conclusions

Glass/polyester composites have been aged in saltwater for up to 8000 hours. Physical and mechanical tests have shown that elevated temperature conditioning has a beneficial post-cure effect, but over time the benefits of this post-cure are overtaken by the degradation effects of moisture uptake and chemical reactions within the resin resulting in overall reductions in strength, stiffness and toughness.

The UK laminate, made from Crystic 489 resin, had a higher fiber content (~60%wt) than the French material (~54%wt). Also, the UK material, had a higher water sorption rate and final total mass than the French Norsodyne laminate. This accounted for the faster decrease in Tg of the UK material during pre-exposure.

The UK material had 2 additional lies of reinforcement compared to French laminates and greater initial mechanical properties. However, despite these differences, the overall trends were similar for both the Norsodyne and Crystic 489 materials between for the test duration of 8000 hours.

To summarise, there was a general decrease of tensile and bending strength, but an increase of tensile and bending modulus at 500h followed by a decrease (post cure effect with increase of resin cross-linking then breaking of chemical bonds with toughness reduction)

When the data for 24,000 hours of conditioning has been obtained, a correlation between accelerated and real time ageing will be carried out and there may be an opportunity in the future to extend this work to include an investigation of the effect of paint coatings on water uptake and consequent property changes.

#516453 (38)

Effect of Time in Service on the Oxidative Induction Time of Shell Rimula X Diesel Lubricating Oil

John A. Hiltz, Irvin A. Keough, and Randall D. Haggett, Defence Research Establishment Atlantic, Dockyard Laboratory, Building D-17, PO Box 99000, Station Forces, Halifax, Nova Scotia, B3K 5X5.

Abstract

Problems with the auxiliary diesel engines on CF Ships, specifically carbon build-up on piston heads, resulted in a systematic study of the engines in an attempt to determine the cause. Analysis indicated that the lubricating oil was suffering from a severe fuel dilution problem. Low load engine operation was thought responsible for these problems and a number of fixes were made. These included the introduction of low load injector nozzles, increasing the engine cooling temperature, raising the charge air temperature and increasing the turbo speed. However, the carbon build-up problem persisted.

The lubricating oil used in these engines, MIL-L-9000H [1], was identified as a potential contributor to the carbon build-up. In particular, the oxidation stability of the oil was questioned. A study of the oxidative stability of the oil [2] indicated that MIL-L-9000H, the oil specified for the propulsion and auxiliary diesel engines on CF Ships, exhibited less oxidation resistance than several commercially available SAE 40 diesel lubricating oils.

In this paper the results of a study of the oxidative stability of Shell Rimula X diesel lubricating oil following service in four diesel generators on HMCS Vancouver are reported.

Introduction

Diesel lubricating oils are composed of base oils, additives and viscosity modifiers. All of these components are susceptible to oxidative degradation. The oxidative degradation process involves the formation of peroxy and alkyl radicals (see Figure 1) and will lead to the complete breakdown of the oil and subsequent equipment failure [3]. To improve stability, oxidation inhibitors, or antioxidants, are added to lubricating oils. Antioxidants work by eliminating the initiation and propagation reactions shown in Figure 1; some decompose hydroperoxides, some scavenge radicals while others deactivate the metal ions that promote hydroperoxide formation [4]. For instance, compounds such as zinc dialkyl dithiophosphates, alkylsulfides, polyalkylsulfides and metal dithiocarbamates act as hydroperoxide decomposers while arylamines and alkylphenols act as radical scavengers.

1. $RH \xrightarrow{O_2/M^{n+}} R^* + HOO^*$

2. (a) $R^* + O_2 \rightarrow ROO^*$

(b) $ROO^* + RH \rightarrow ROOH + R^*$

3. (a) $ROO^* + HOO^* \rightarrow ROOH + O_2$

(b) $ROO^* + R^* \rightarrow ROOR$

(c) $R^* + R^* \rightarrow RR$

1. Initiation – formation of hydroperoxide and alkyl radicals in presence of oxygen and metal ion
2. Propagation – formation of a)alkylperoxide radical and b) regeneration of alkyl radical
3. Termination

Figure 1. Reactions involved in the oxidative degradation of hydrocarbons molecules in lubricating oils.

The operating conditions in a diesel engine, that is, the presence of oxygen and high temperatures, accelerate the oxidative degradation process. The resistance of lubricating oil to oxidative degradation is the most significant property of the oil as it defines the ability of the oil to continue to perform in-service. Two ASTM tests, ASTM D 943 Oxidation Characteristics of Inhibited Mineral Oils (TOST) [5] and ASTM D 2272 Rotating Bomb Oxidation Test (RBOT) [6], have traditionally been used to assess the oxidative stability of lubricating oils. These tests are time consuming. TOST often takes greater than 1500 hours and RBOT between 1 and 45 hours. In addition these tests require 300 mL and 30 grams of sample respectively.

Differential scanning calorimetry has been used to study the oxidative stability of oils [7-13]. An ASTM standard method, ASTM E 1858-97 Determining Oxidation Induction Time (OIT) of Hydrocarbons by Differential Scanning Calorimetry, has recently been published [14]. The advantages of this method are its precision, short analysis time (less than 2 hours) and small sample size (less than a millilitre of oil). The results of OIT testing of oils are used to rank the resistance of oils to oxidative degradation in service. That is, oils with longer OITs will have a greater resistance to oxidative degradation.

In 1999, a study of the oxidative stability of the diesel lubricating oil used in the auxiliary and propulsion diesel engines on CF Ships, MIL-L-9000H, was initiated to determine if the oxidative stability of the oil might be a contributor to carbon build-up in these engines. The results of the study [2] indicated that a number of commercially available marine diesel lubricating oils had OITs greater than MIL-L-9000H. As the engine manufacturer had suggested that the poor oxidative stability of MIL-L-9000H oil might be contributing to carbon build-up in the engines, an Operational Evaluation of Shell Rimula X, a commercial SAE 40 marine diesel lubricating oil recommended by the engine manufacturer was initiated on HMCS Vancouver.

In this paper the affect of time in service of Rimula X on OIT are reported and compared to the results for MIL-L-9000H diesel lubricating oil.

Experimental

Differential Scanning Calorimetry

All differential scanning calorimetry (DSC) was carried out on a TA Instruments Model 2910 modulated differential scanning calorimeter. A pressure cell (TA Instruments) was used for all experiments. Data acquisition and analysis was carried out using Thermal Analysis and Thermal Solutions software (TA Instruments).

The DSC was run under a dynamic atmosphere of oxygen regulated by a flow meter (Tube Cube, Matheson). The pressure cell was charged with 500 psi oxygen and the flow from the cell set at 25 mL/min. Oil samples (~3.0 mg) were analysed in aluminum pans (TA Instruments kit number T80518). The pans were cleaned according to Annex A1 in reference 14.

The temperature programs for the DSC baseline calibration, indium and tin standards and OIT runs are listed in Table 1. The DSC baseline was run without pans. The indium and tin standards were run in closed pans. The indium standard (14.75 mg) had a melt temperature of 156.60°C and a heat of fusion of 28.71 J/g. The tin standard (11.78 mg) had a melt temperature of 231.23 °C and a heat of fusion of 61.24 J/g.

The DSC cell was cleaned after every oxidation induction time run. The cleaning consisted of heating the unsealed cell to 500°C for 20 minutes. OITs were measured as described in reference 14.

Oil Samples

New and used samples of Rimula X SAE 40 (Shell Canada) were received from HMCS Vancouver. The used samples were from diesel generators #1, #2, #3, and #4.

The MIL-L-9000H marine diesel lubricating oils were supplied by PetroCanada.

Rotella T SAE 40 (Shell Canada), IDO Universal #40 (Irving Oil), and Duron SAE 40 (PetroCanada) were received from the Stores System, Base Halifax.

Table 1. DSC temperature programs for instrument calibration, oxidation induction time of oils, and cleaning methods.

Indium Standard: equilibrate at 120, ramp at 1°C/min to 175°C

Tin Standard: equilibrate at 200°C, ramp at 1°C/min to 250°C

DSC Baseline Calibration: Ramp at 40°C/min to 175°C, equilibrate at 175°C, isothermal for 100 minutes

Oxidation Induction Time: same as DSC Baseline but isothermal at 185°C

Clean Method: Ramp at 40°C/min to 500°C, isothermal for 20 minutes

Sample Preparation

Samples were shaken for 1-2 minutes prior to sampling. The sample (3±0.3mg) was transferred from the sample container to the DSC pan using a micropipette (50μL).

Gas Chromatography/Mass Spectrometry (GC/MS) Analysis

GC/MS analysis was carried out on a Hewlett Packard Model 6890 gas chromatograph with a Hewlett Packard Model 5973 mass selective detector (Agilent Technologies). A 30m long x 0.25 mm inside diameter DB5 (5% phenyl-95%methylsilicone stationary phase) capillary column was used for all separations. Helium at a flow rate of 1.0 mL/min was used as the carrier gas.

The GC oven was programmed to hold at 40°C for five minutes, ramp to 150°C at a rate of 8°C/min, then ramp to 300°C at a rate of 10°C/min, and finally to hold at 300°C for 15 minutes.

New and used Rimula X lubricating oil samples were diluted 1 in 250 in hexane and 1μL of the resulting solution analyzed. N-phenylnaphthalene amine was used as an internal standard for antioxidant depletion studies.

Viscosity

Kinematic viscosities of new and used Rimula X diesel lubricating oil sample were measured at 100°C.

Results and Discussion

OITs of MIL-L-9000H and Commercial Diesel Lubricating Oils

The OITs of new samples of three batches of MIL-L-9000H lubricating oils are shown in Table 2. Statistical analysis (analysis of variance [12]) indicated that differences between the OITs for samples from a particular batch of oil and the OITs for the three batches of oil were not significant.

Table 2. Oxidative Induction Times (OITs) of three batches of MIL-L-9000H diesel lubricating oils.

BATCH #/ OIT RUN	#1	#2	#3	#4	Average
Batch 981781	56.24 min	59.03	59.51		58.29
Batch 983486	57.20	57.49			57.34
Batch 991751	59.00	57.33	54.62	57.15	57.05

Analysis of variance indicated that the differences between samples from a batch and between batches were not significant.

The thermograms, that is, plots of heat flow versus time at 185 °C, for the three batches of MIL-L-9000H oils are shown in Figure 2. The thermograms of new and used MIL-L-9000H oils samples (HMCS Toronto) are shown in Figure 3. It can be seen that the OIT of the samples decreases with the number of hours in service, from 57.1 minutes for the new oil to 20.7 minutes for the oil after 377 hours.

A suggestion by the engine manufacturer that the 'poor' oxidative stability of MIL-L-9000H diesel lubricating oils could be contributing to the carbon build up problem led to an analysis of several commercial marine diesel lubricating oils. The results of the analysis of three commercial oils are shown in Figure 4. OIT testing indicated that the oxidative stability of the MIL-L-9000H was inferior to the commercial oils. The engine manufacturer was asked to recommend oils for an operational evaluation in the engine. One of the recommended oils was Shell Rimula X. The results of the operational evaluation of Shell Rimula X in the four diesel generators on HMCS Vancouver are reported in the next section.

Oxidative Induction Time of New and Used Shell Rimula X SAE 40 Marine Diesel Lubricating Oil Samples

The results of the OIT study of Shell Rimula X samples from diesel generators #1, #2, #3 and #4 HMCS Vancouver are shown in Table 3. Plots of the results for the four diesel generators are shown in Figures 5 through 8 respectively.

In general the OITs of the oil samples decreased with time in service. The results for the 546 hour sample from DG #2 and the 139 hour sample from #3 DG do not follow this pattern. That is the OIT for these samples is greater than for the preceding sample. Oil change logs obtained from HMCS Vancouver indicate that there was a complete oil change after 468 operating hours on DG #2. Therefore the sample marked 546 hours was only in service for 78 hours (546 – 468 hours). The oil logs do not indicate an oil change in DG #3 between 50 and 139 hours of operation. However, the OIT and other experimental data (antioxidant concentrations and viscosity) suggest that new oil had been added to this engine.

The short OITs for the 191 and 758 hour samples from DG #1, 463 hour sample for DG #2, 490 and 568 hour samples for DG #3, and the 789 hour sample for DG #4 are indicative of severe loss of oxidative stability. Although OIT has not been correlated with remaining useful life of the oil under 'normal' operating conditions, the results suggest the time that the oil will continue to perform is limited.

Figures 9 and 10 show the OIT results for 2 hour and 50 hour samples from the diesel generators. There was no 2 hour sample from DG #1. Comparison of the OITs indicates that the reduction in oxidative stability of the oil is dependent on the diesel from which it was taken. That is, the reduction in OIT depends on more than operating hours in the engine.

As noted in the Introduction, antioxidants are added to oils to enhance the oxidative stability of lubricating oils. To determine if the reduction in OIT was related to depletion of antioxidants, gas chromatography/mass spectrometry analysis of the oils was carried out.

Antioxidant Depletion

Chromatograms, that is,GC/MS traces, of new and used oil samples from DG #1 and DG #2 HMCS Vancouver are shown in Figures 11 and 12. Analysis of the chromatograms indicated that presence of two hindered phenol-based antioxidants; 2,6-di-tert-butylphenol with a retention time of 4.3 minutes and 4,4'-methylenebis(2,6-di-tert-butylphenol) with a retention time of 20.1 minutes. The peak with a retention time of 14.7 minutes is due to n-phenylnaphthalene amine, which was added as an internal standard to each of the samples.

Table 3. OITs, antioxidant concentrations, and viscosities of Rimula X samples from #1, #2, #3, and #4 diesel generators HMCS Vancouver.

Sample	Time in use hours	OIT minutes	Antioxidant mg/L***	Viscosity cSt
New	0.0	77.3	20.2/2.1	14.9
#1 DG	0.09	71.8	20.2/2.6	14.8
#1 DG	50.0	51.3	3.8/2.3	14.8
#1 DG	121.0	42.8	2 2/1 7	14 6
#1 DG	191.0	11.4	0.2/0.0	17.6
#1 DG	758 0	8.2	0.2/0.0	18.3
New (#2 DG)	0 0	76.6	24 2/2.4	14 8
#2 DG	2.0	73.3	18.8/2.5	14.9
#2 DG	50.0	55.5	3.3/2.4	14.6
#2 DG	463.0	14.6	0.0/0.0	15.3
#2 DG	546.0	45.4*	4.6/2.2	14 5
#2 DG	583.0	30.8	0.2/1.2	14.8
#3 DG	2.0	49.5	20.1/3 1	14.7
#3 DG	50 0	41.6	4.5/2.8	14.9
#3 DG	139 0	72 1**	17.8/3.0	14 8
#3 DG	490.0	8.8	0.7/0 0	17.1
#3 DG	568.0	8.5	0.4/0 0	17 3
#4 DG	2 0	57.8	11.6/2.5	14.8
#4 DG	50.0	49.8	4.8/2.7	14.8
#4 DG	789.0	7.9	0 3/0 0	18 9

*Oil change at 468 hours

**Results suggest oil change prior to sampling

***First number refers to concentration of 2,6-di-tert-butyl phenol and the second number the concentration of 4,4'-methylenebis(2,6-di-tert-butyl phenol).

The depletion of these two antioxidants was followed by comparing the area under their peaks to the area under the internal standard peak. The results of the antioxidant depletion study for DGs #1, #2, #3, and #4 are shown in Table 3.

In general, the area under the antioxidant peaks decreased with the time the oil was in service. However, for the 546 hour sample in DG #2 the concentration of the antioxidants increased relative to the 463 hour sample (see Figure 10). This anomalous behavior was also observed in the OIT analysis. As was noted in the OIT discussion, the oil log for the engine indicated that there had been a complete oil change after 468 hours. Therefore the 546 hour sample had only been in service for approximately 78 hours. The results for the 139 hour sample from DG #3 are also anomalous. However, the result is consistent with the OIT results. That is, an increase in antioxidant concentration should correspond to an increase in OIT.

Viscosity

Several factors can affect the viscosity of lubricating oils including oxidative degradation, fuel dilution, and carbon build-up. The OIT results indicate that oxidative stability of the oil is decreasing with time in service. As oxidative degradation increases, reactions, such as the R* + R* termination reaction shown in Figure 1, can produce higher molecular weight hydrocarbons and a concomitant increase in the viscosity of the fluid. Suspended solids, such as carbon, also increase the viscosity of lubricating oils. In contrast to this, fuel dilution reduces the viscosity of SAE 40 lubricating oils.

The kinematic viscosities of the new and used Rimula X samples are shown in Table 3. The viscosity of the used oils remains constant or decreases slightly and then increases with time in service. For instance, the viscosity of the oil in DG #1 decreased from 14.9 cSt (new) to 14.6 cSt (121 hours) and then increased to 17.6 cSt (191 hours) and 18.3 cSt (758 hours). The decrease is due to fuel dilution of the oil. The increase in fuel dilution of the oil can be seen in Figure 9. The fuel peaks are located between 6 minutes and 16 minutes. As the time in service increases the viscosity increase related to carbon build up or oxidative degradation over rides the decrease due to fuel dilution.

As was observed for the OIT and antioxidant depletion results, viscosity measurement also reflected the change in oil in DG #2 at 468 hours. That is, the viscosity of the 546 hour sample was less than the 463 hour sample.

Conclusions

The OIT of Shell Rimula X diesel lubricating oil is greater than MIL-L-9000 H diesel lubricating. This suggests that under a given set of operating conditions that Rimula X will have superior oxidation resistance compared to MIL-L-9000H oils.

The OIT of Rimula X decreases with the time in service. This reduction has been related to the depletion of antioxidants in the oil.

Fuel dilution and carbon build-up have significant affects on the viscosity of the oil. Fuel dilution leads to a decrease in the viscosity for shorter in service times while carbon build-up leads to an increase in the viscosity of the oil at longer in service times.

The presence of fuel and carbon in the used Rimula X oil suggest that the source of the carbon in the oil is the incomplete combustion of fuel in the engine.

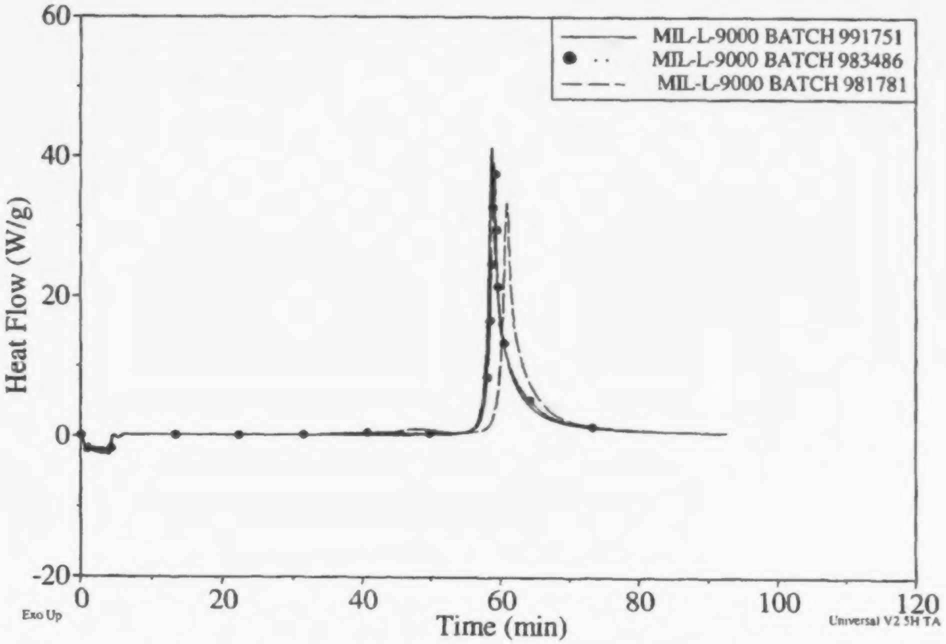

Figure 2. Thermograms of three batches of MIL-L-9000H diesel lubricating oil.

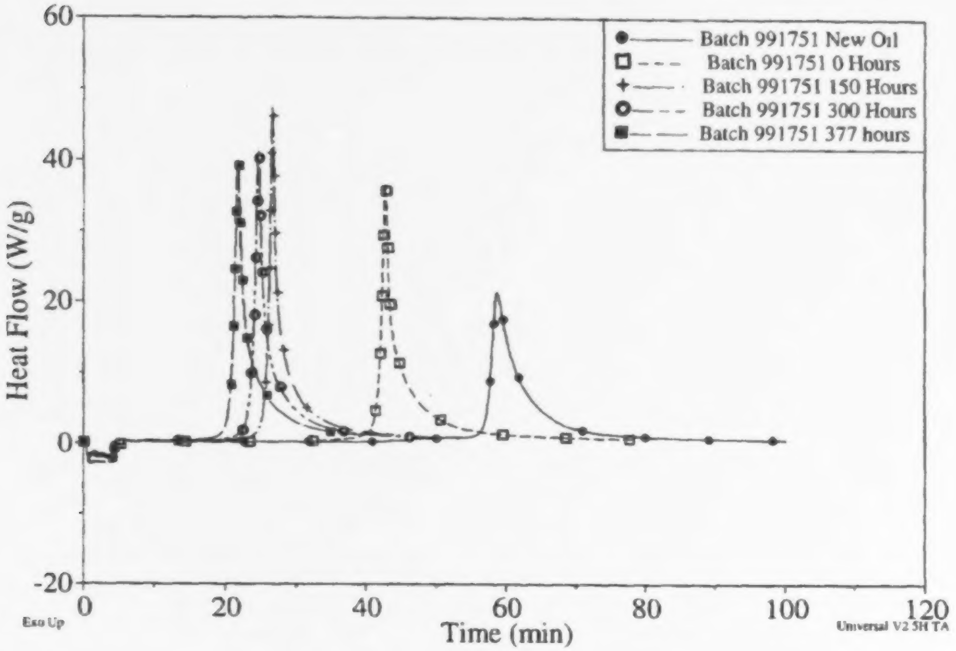

Figure 3. Thermograms of new MIL-L-9000H and MIL-L-9000H after 0, 150, 300, and 3777 hours in #4 DG HMCS Toronto.

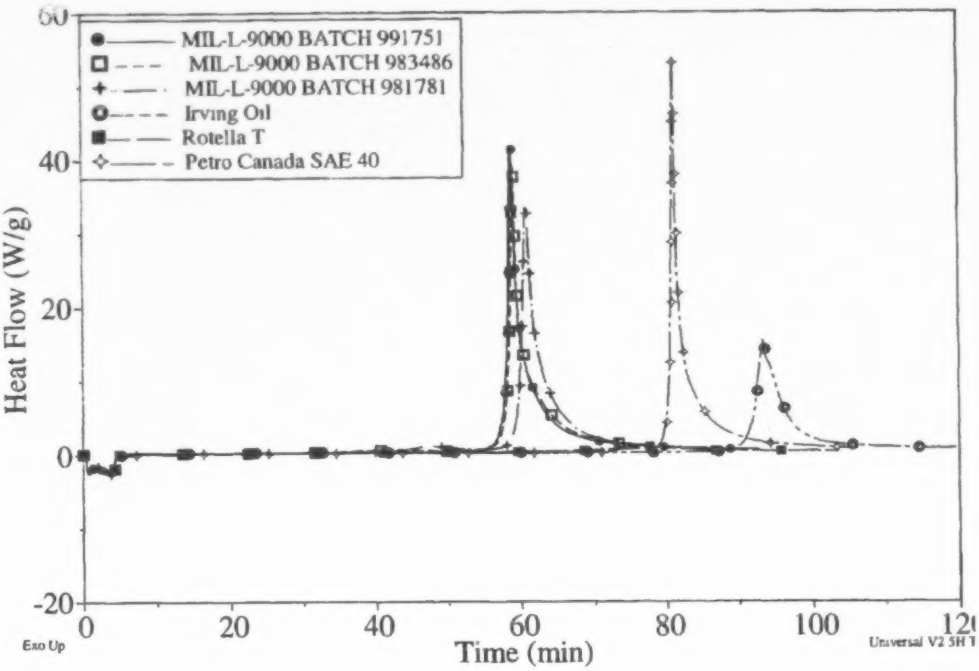

Figure 4. Thermograms of three batches of MIL-L-9000H, Irving Oil IDO Universal #40, Shell Rotella T, and PetroCanada Duron SAE 40 diesel lubricating oils.
]

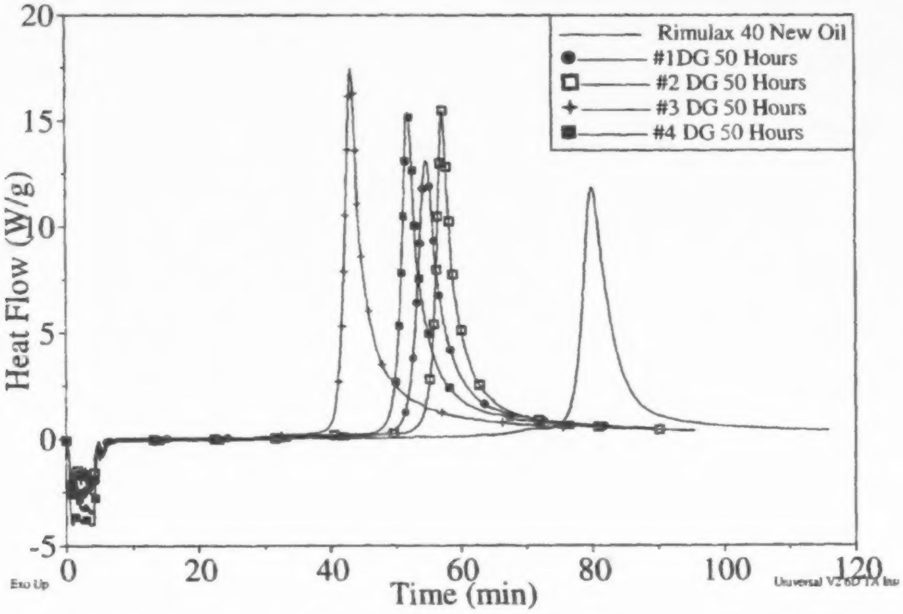

Figure 5. Thermograms of new and used Rimula X diesel lubricating oil samples from DG #1 HMCS Vancouver.

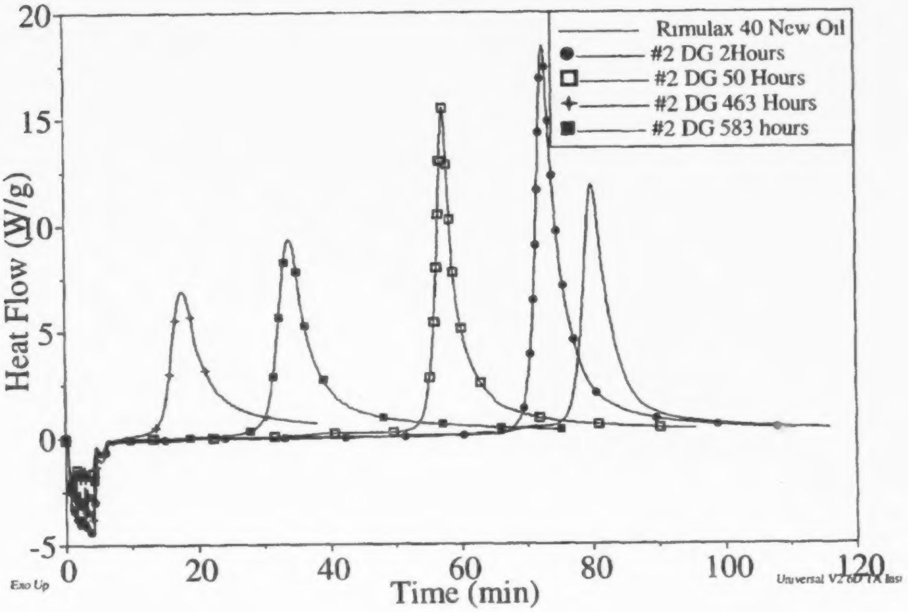

Figure 6. Thermograms of new and used Rimula X diesel lubricating oil samples from DG #2 HMCS Vancouver.

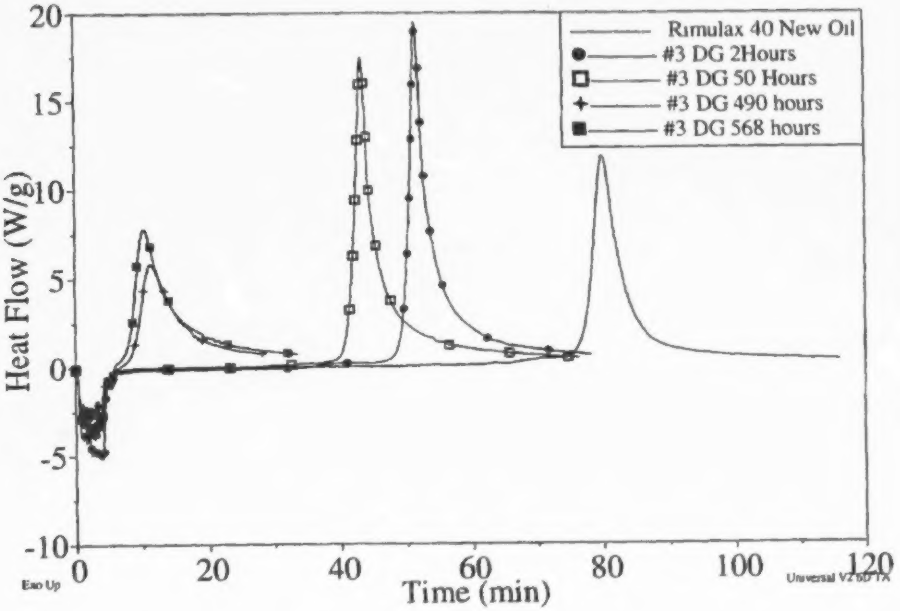

Figure 7. Thermograms of new and used Rimula X diesel lubricating oil samples from DG #3 HMCS Vancouver.

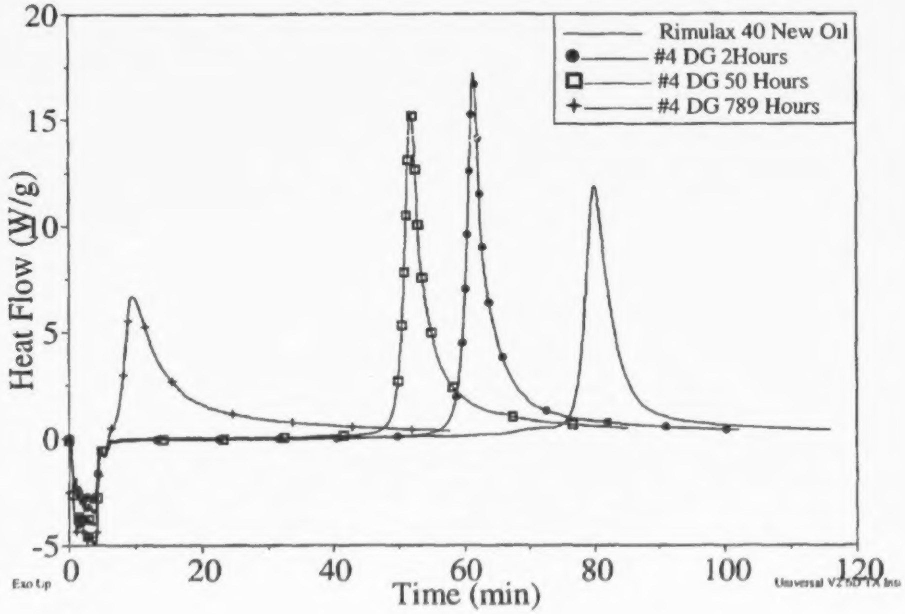

Figure 8. Thermograms of new and used Rimula X diesel lubricating oil samples from DG #4 HMCS Vancouver.

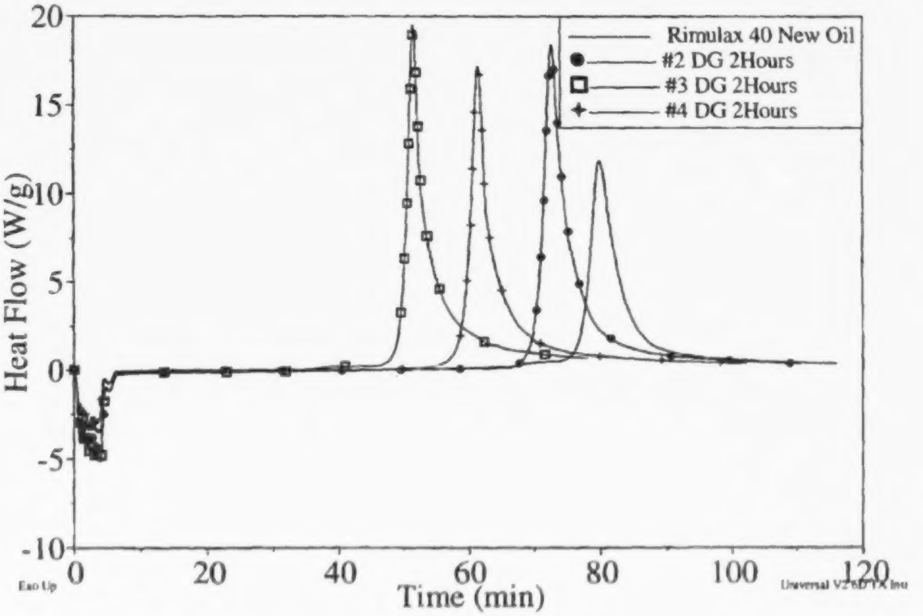

Figure 9. Thermograms of new and 2 h Rimula X diesel lubricating oil samples from DG #2, DG #3, and DG #4 HMCS Vancouver.

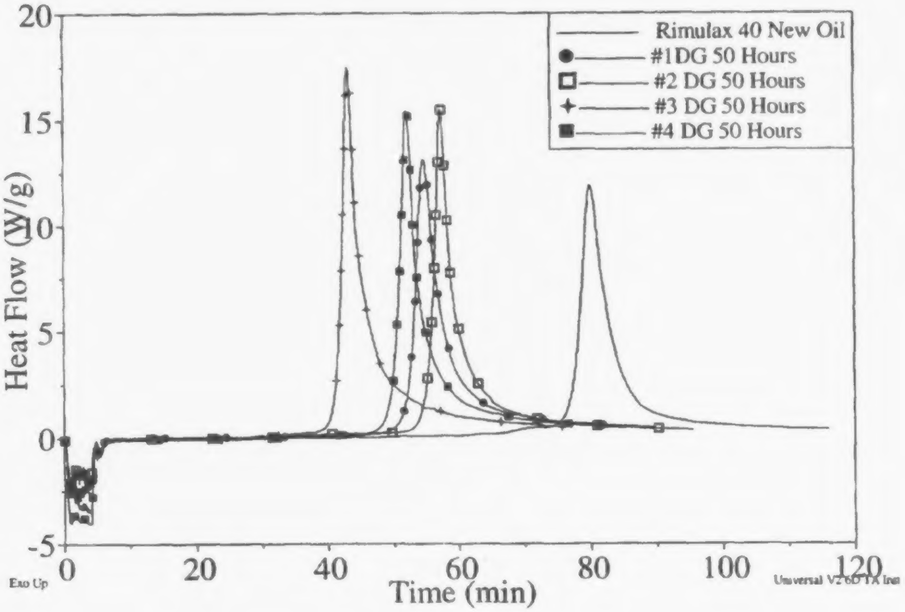

Figure10. Thermograms of new and 50 h Rimula X diesel lubricating oil samples from DG #1, DG #2, DG #3, and DG #4 HMCS Vancouver.

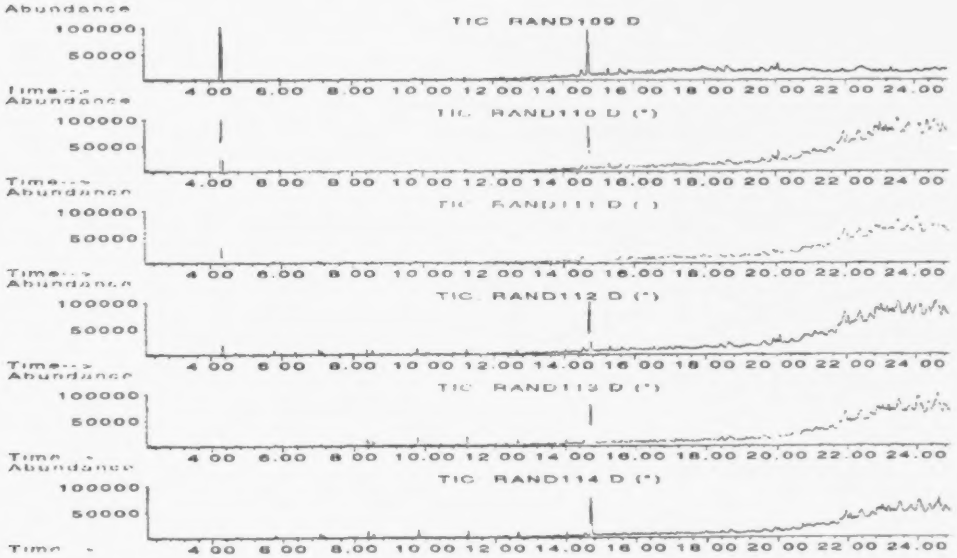

Figure 11. Chromatograms of new and used Rimula X oils samples from DG #1 HMCS Vancouver. From top; new oil, and used oil samples after 0.09 , 50 h, 121 h, 191h, and 758 h in the engine.

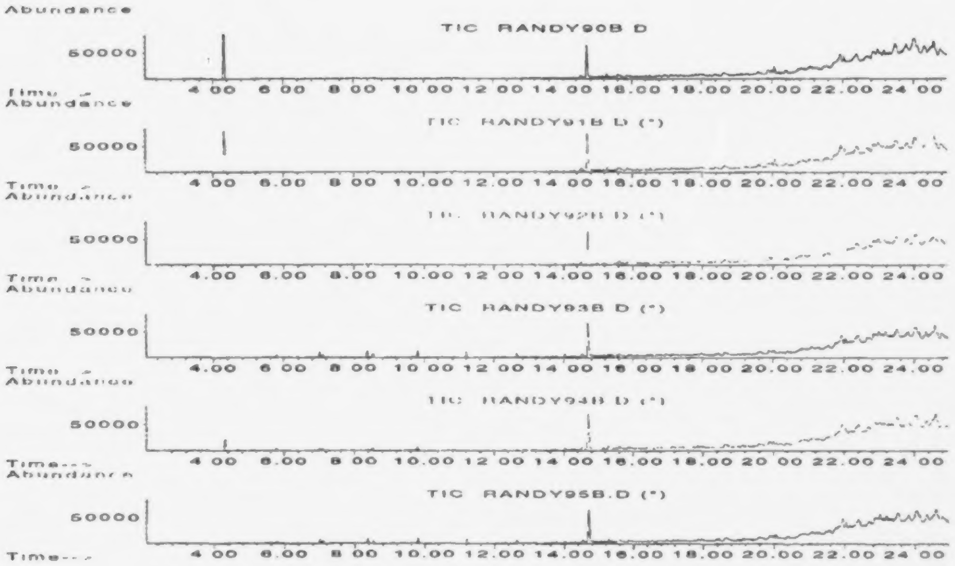

Figure12. Chromatograms of new and used Rimula X oils samples from DG #2 HMCS Vancouver. From top; new oil, and used oil samples after 2 h, 50 h, 463 h, 546 h, 583 h in the engine.

References

1. US Military Specification, MIL-L-9000H, Lubricating Oil, Shipboard Internal Combustion Engine, High Output Diesel, September 1987.
2. John A. Hiltz and Irvin A. Keough, "High Pressure Differential Scanning Calorimetry Study of the Oxidative Stability of Diesel Lubricating Oils", Proceedings of Canadian Thermal Analysis Society 10th Annual Technical Meeting, pages 69-77, Mississauga, Ontario, 23-24 May, 2000.
3. J. C. Cowan, **Applied Polymer Science**, edited by J. K. Craver and R. W. Tess, American Chemical Society, Washington, D.. C. page 517, Chapter 26 (1975).
4. S. Q. A. Rizvi, "Additives for Automotive Fuels and Lubricants:, Journal of the Society of Tribologists and Lubrication Engineers, 33, **55**, No. 4, April 1999.
5. ASTM D 943, Standard Test Method for Oxidation Characteristics of Inhibited Mineral Oils, American Society for Testing and Materials, 100 Bar Harbor Drive, West Conshohocken, PA, USA.
6. ASTM D 2272, Standard Test Method for Rotating Bomb Oxidation Test, American Society for Testing and Materials, 100 Bar Harbor Drive, West Conshohocken, PA, USA.
7. Paul F. Levy, G. Nieuweboer, and L. Semanski, "Pressure Differential Scanning Calorimetry", Thermochimica Acta, **1**, 429-439 (1970).
8. F. Noel, Journal of the Institute of Petroleum, **57**, 354 (1971).
9. R. L. Blaine, "Thermal Characterization of Lube Oils and Greases", Presented at the NLGI 43rd Annual meeting, St. Louis, Missouri, October 1975.
10. J. A. Walker and W Tsang, "Characterization of Lubricating Oils by Differential Scanning Calorimetry", SAE Technical Paper Series 801383, presented at Baltimore, Maryland, October 1980, Society of Automotive Engineers, Inc., Warrendale Pennsylvania.
11. R. E. Kauffman and W. E. Rhine, "Development of a Remaining Useful Life of a Lubricant Evaluation Technique. Part 1: Differential Scanning Calorimetry Techniques", Lubrication Engineering, February, 1988, pages 154-161.
12. E. Gimzewski, "The relationship between oxidation induction temperatures and times for petroleum products", Thermochimica Acta, **198**, 133-140 (1992).
13. W. F. Bowman and G. W. Stachowiak, Application of Sealed Capsule Differential Scanning Calorimetry-Part II Assessing the Performance of Antioxidants and Base Oils", Lubrication Engineering, May 1999, pages 22-29.
14. ASTM E 1858-97, Standard Test Method for Determining Oxidation Induction Time of Hydrocarbons by Differential Scanning Calorimetry, American Society for Testing and Materials, 100 Bar Harbor Drive, West Conshohocken, PA, USA (1997).
15. ASTM D482-91 , "Standard Test Method for Ash from Petroleum Products", American Society for Testing and Materials, 100 Bar Harbor Drive, West Conshohocken, PA, USA (1992).
16. Erwin Kreyszig, **Introductory Mathematical Statistics – Principles and Methods**, Chapter 16, John Wiley and Sons, Toronto, Canada (1970).

#516.454 (39)

Synthesis and Characterization of a Series of Thermoplastic Polyurethanes

by

J.P. Szabo*, D. Cook†, J. Hackett*, and I.A. Keough*

*Defence Research Establishment Atlantic, P.O. Box 1012, Dartmouth, N.S. B2Y 3Z7
†Bodycote Ortech, 2395 Speakman Drive, Mississauga, Ontario L5K 1B3

Abstract

The use of Group Contribution Analysis (GCA) and Group Interaction Modelling (GIM) to model the dynamic mechanical properties of polymers is the subject of an ongoing TTCP (The Technical Cooperation Panel) study. This paper describes the synthesis of 20 phase mixed thermoplastic polyurethanes for the TTCP modelling study, and the characterization of these polymers by dynamic mechanical thermal analysis (DMTA). The polyurethane formulations were synthesized from 4,4'-methylenebis(phenyl isocyanate) or 1,6-diisocyanatohexane, and glycol, polgylcol, or glycol/polyglycol mixtures. The standard "one-shot" batch reaction method was initially tried for several of the formulations, but a number of problems were identified. These included bubble formation in the samples, high exotherms, and fast reaction times. As a result, a solution polymerization/ solution casting method was developed, using N,N-dimethylformamide as a solvent. This approach has several advantages including control of the reaction temperature and rate and the absence of bubble formation in the samples. All 20 of the formulations were successfully prepared in solution, and 15 of the formulations were successfully solvent cast into 1 mm thick film samples for DMTA testing. The dynamic mechanical properties of the solvent cast samples were determined over a range of temperatures and frequencies, and time-temperature superposition was used to produce DMTA master curves. The dependence of the dynamic mechanical properties of on chemical structure is discussed in terms of qualitative factors, such as soft segment molecular weight, and quantitative group contributions.

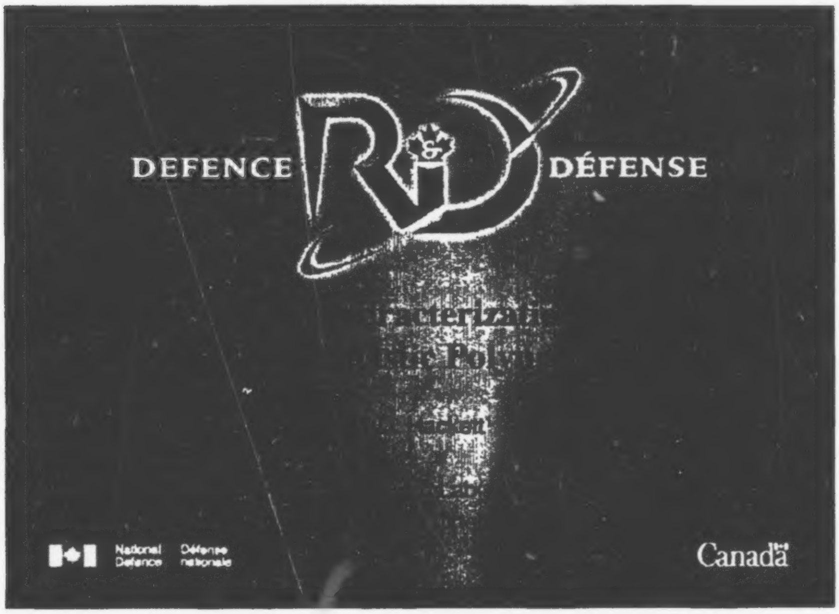

DEFENCE R&D DÉFENSE

racterizati

tic Poly

[illegible]

National Defence Défense nationale

Canada

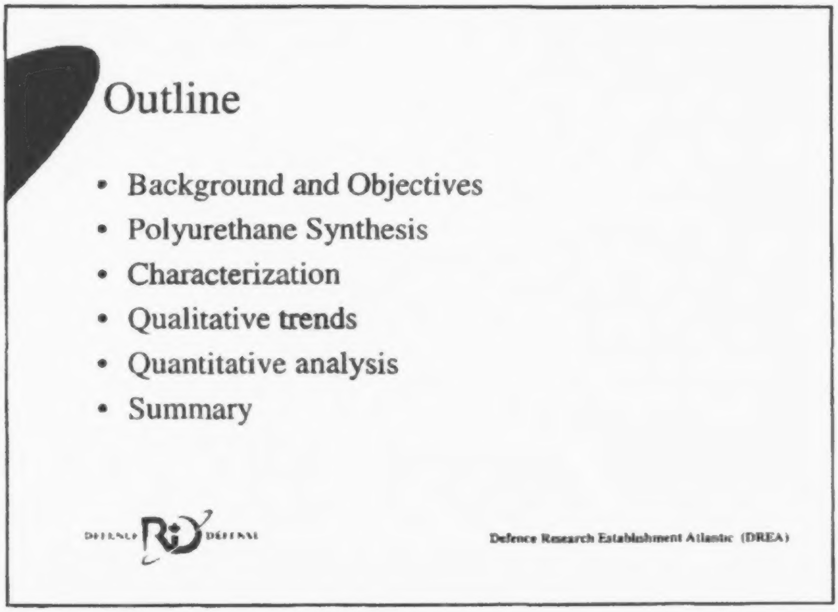

Outline

- Background and Objectives
- Polyurethane Synthesis
- Characterization
- Qualitative trends
- Quantitative analysis
- Summary

DEFENCE R&D DÉFENSE

Defence Research Establishment Atlantic (DREA)

Polymer Modelling

Several semi-empirical methods have been developed:

- **Group Contribution Analysis** (van Krevelen).. Physical properties of polymer determined by sum of contributions from structural groups.
- **Connectivity Index Method** (Jozef Bicerano). Each polymer has a set of 4 indices related to its topology that may be used to derive a wide variety of physical properties.
- **Group Interaction Modelling** (David Porter). Mean field method uses 6 input parameters for each structural sub-unit: ($L, N, M, \theta_1, V_w, E_{coh}$). Relies on above two methods for calculation of V_w and E_{coh}.

Damping Properties

- The damping properties of polymers are a critical aspect of acoustic signature control on naval ships and submarines.
- TTCP Assignment: Objective is to study methods (GIM, GCA) for predicting the dynamic mechanical properties of polymers from their chemical structures.
- Can we predict the height, width, shape, and position of damping peak from structural considerations only?
- As part of this project, a series of thermoplastic polyurethanes have been synthesized and characterized. Limited number of structural sub-groups (5).

Polyurethane Synthesis: One Shot Reaction

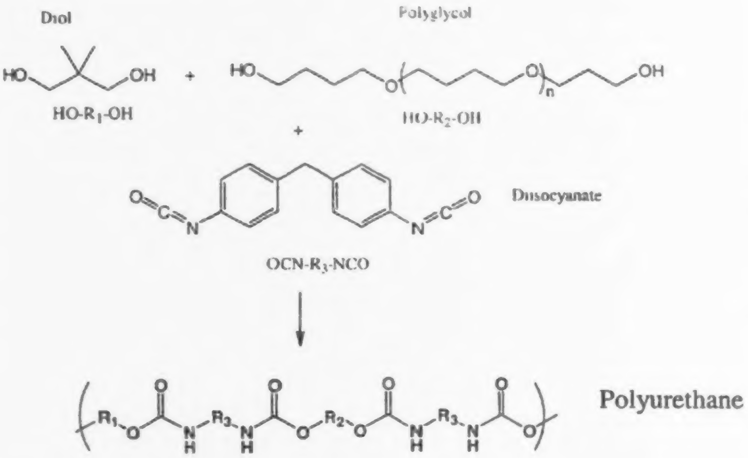
Diol
Polyglycol
HO
OH
+
HO
O
O
n
OH
HO-R$_1$-OH
HO-R$_2$-OH
+
O=C=N
N=C=O
Diisocyanate
OCN-R$_3$-NCO
R$_1$
O
N
H
R$_3$
R$_2$
Polyurethane

Abbreviations

BDO = 1,4'-butanediol

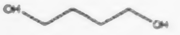

DEG = di(ethylene glycol)

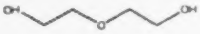

DMPD = 2,2-dimethyl-1,3-propanediol

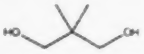

T650, T1000 and T1400
poly(tetramethylene ether glycol) MW 650, 1000 and 1400

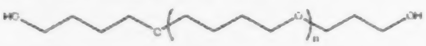

P600 and P1000 = poly(ethylene glycol) MW 600 and 1000

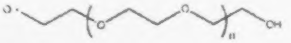

HDI = 1,6-diisocyanatohexane

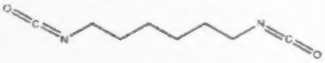

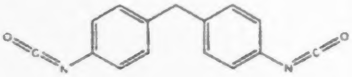

MDI = 4,4' methylenebis(phenyl isocyanate)

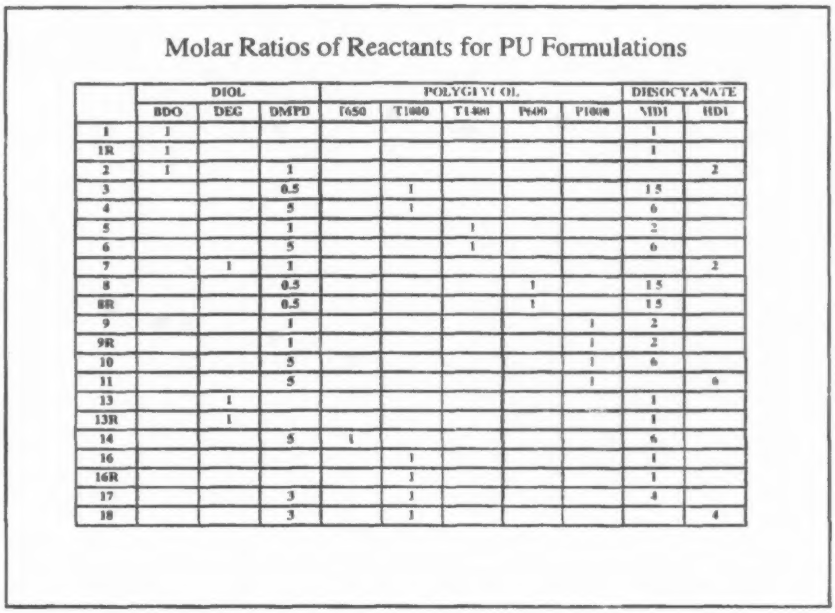

Molar Ratios of Reactants for PU Formulations

	DIOL			POLYGLYCOL					DIISOCYANATE	
	BDO	DEG	DMPD	T650	T1000	T1400	P600	P1000	MDI	HDI
1	1								1	
1R	1								1	
2	1		1							2
3			0.5		1				1.5	
4			5		1				6	
5			1			1			2	
6			5			1			6	
7		1	1							2
8			0.5				1		1.5	
8R			0.5				1		1.5	
9			1					1	2	
9R			1					1	2	
10			5					1	6	
11			5					1		6
13		1							1	
13R		1							1	
14			5	1					6	
16					1				1	
16R					1				1	
17			3		1				4	
18			3		1					4

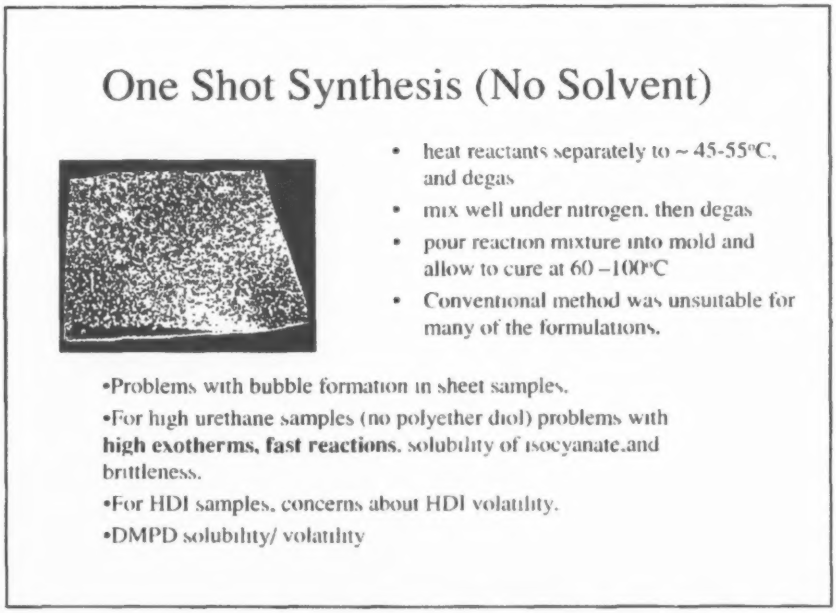

One Shot Synthesis (No Solvent)

- heat reactants separately to ~ 45-55°C, and degas
- mix well under nitrogen, then degas
- pour reaction mixture into mold and allow to cure at 60 – 100°C
- Conventional method was unsuitable for many of the formulations.

•Problems with bubble formation in sheet samples.

•For high urethane samples (no polyether diol) problems with **high exotherms, fast reactions**, solubility of isocyanate.and brittleness.

•For HDI samples, concerns about HDI volatility.

•DMPD solubility/ volatility

Solution Polymerization/ Casting

•A solution polymerization/ casting method was developed using dimethylformamide (DMF) as solvent.
•Problems with high exotherms, rapid reaction times, and bubbles were avoided
•16 out of 21 formulations were successfully cast into 1-2 mm thick films.
•5 formulations did not form satisfactory samples for dynamic mechanical characterization (cracked during film formation).

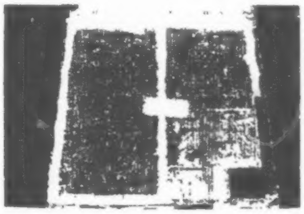

Characterization

- Specimens were characterized by
  - gel permeation chromatography
  - elemental analysis
  - infrared spectroscopy
  - differential scanning calorimetry
  - **dynamic mechanical analysis:**

$$E^{*} = E' + i E''$$

$$\tan\delta = \frac{E''}{E'}$$

E*	complex modulus
E'	storage modulus
E''	loss modulus
tan δ	loss factor

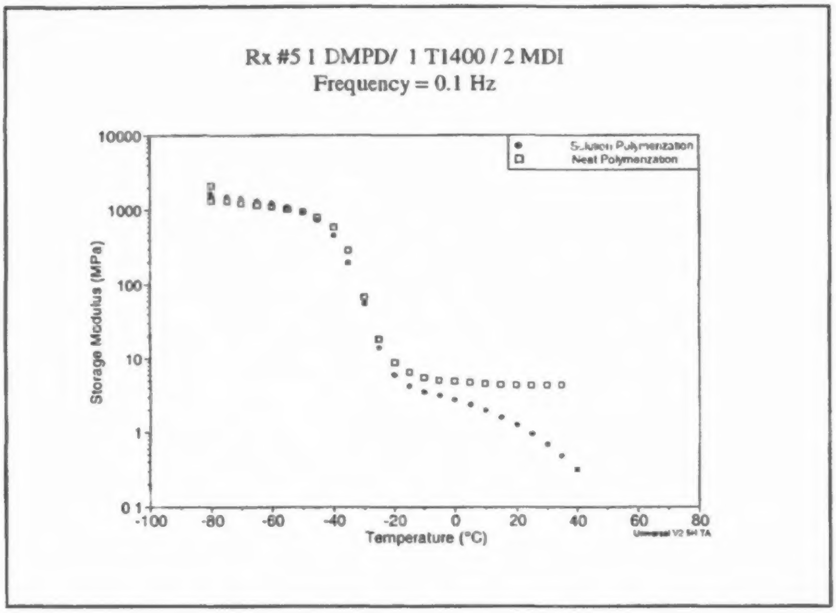

Rx #5 1 DMPD/ 1 T1400 / 2 MDI
Frequency = 0.1 Hz

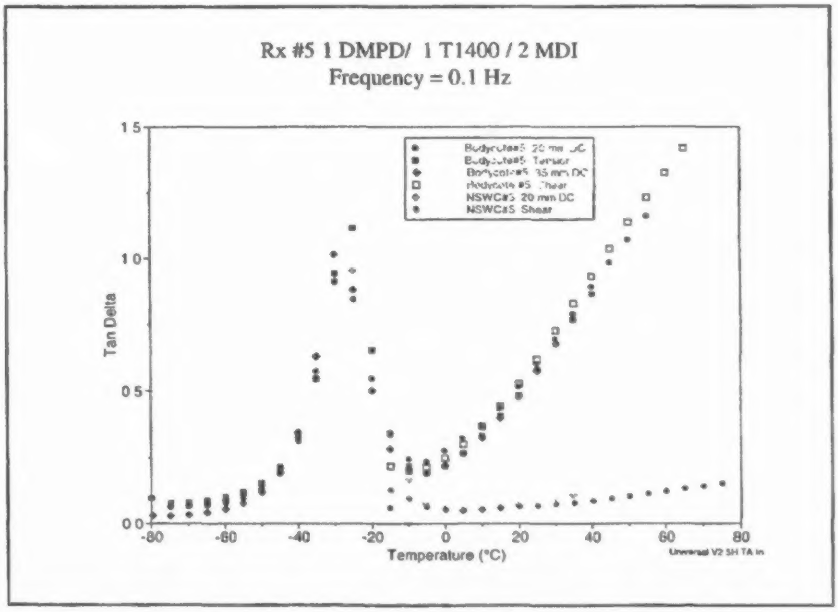

Rx #5 1 DMPD/ 1 T1400 / 2 MDI
Frequency = 0.1 Hz

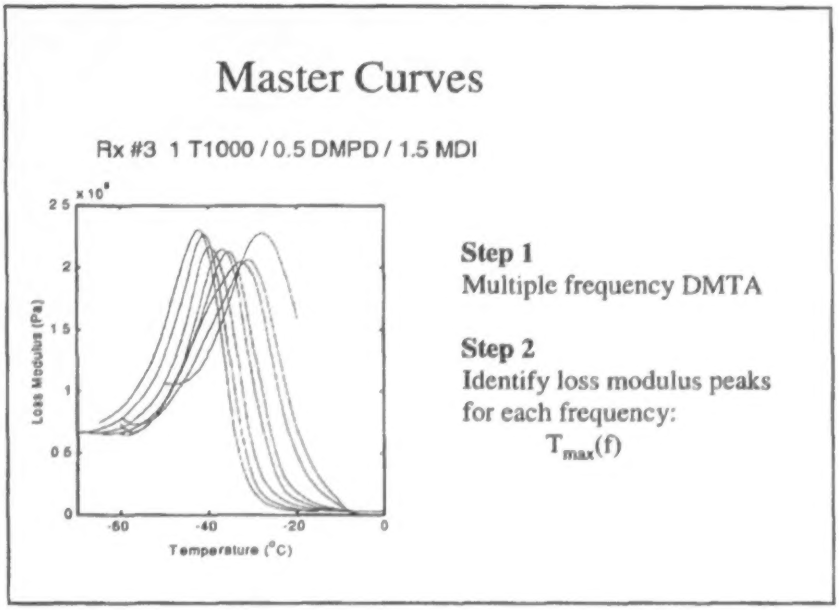

Master Curves

Rx #3 1 T1000 / 0.5 DMPD / 1.5 MDI

Step 1
Multiple frequency DMTA

Step 2
Identify loss modulus peaks for each frequency:
$T_{max}(f)$

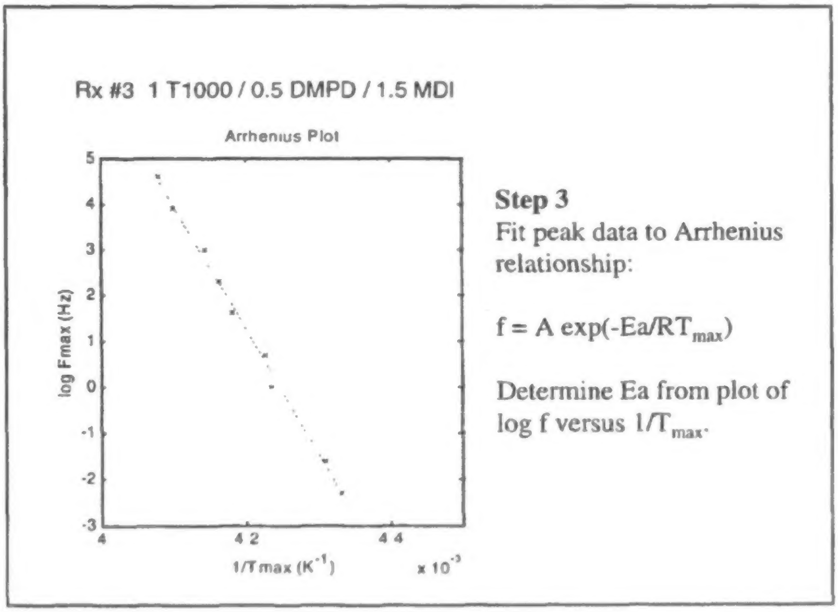

Rx #3 1 T1000 / 0.5 DMPD / 1.5 MDI

Step 3
Fit peak data to Arrhenius relationship:

$f = A \exp(-Ea/RT_{max})$

Determine Ea from plot of log f versus $1/T_{max}$.

Step 4 Calculate shift factors using $\log a_T = -\frac{Ea}{R}\left[\frac{1}{T_r} - \frac{1}{T}\right]$

Step 5 Fit master curves to Havriliak-Negami model

Rx #3 1 T1000 / 0.5 DMPD / 1.5 MDI $T_r = 298$ K

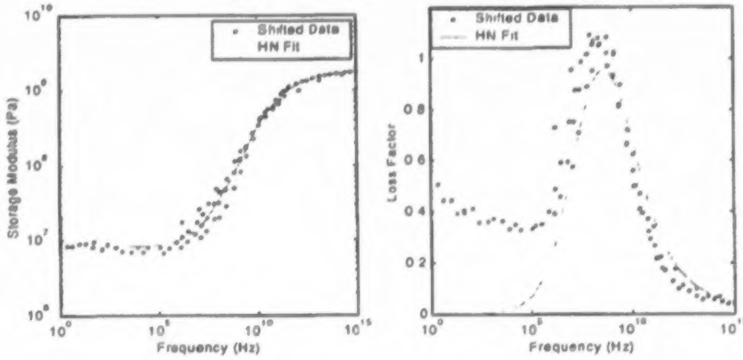

Properties Determined

$$\boxed{E^* = \frac{E_o - E_\infty}{\left[1 + (i\omega\tau)^\alpha\right]^\beta} + E_\infty}$$

Havriliak - Negami Eqn

For 16 formulations studied by DMTA, determined:

- Arrhenius activation energy Ea
- 5 HN parameters at reference temperature T = 298 K
- Height, width, and position of loss factor peak in temperature and frequency domains

No data for 5 of the formulations: 1, 1R, 2, 13, 13R

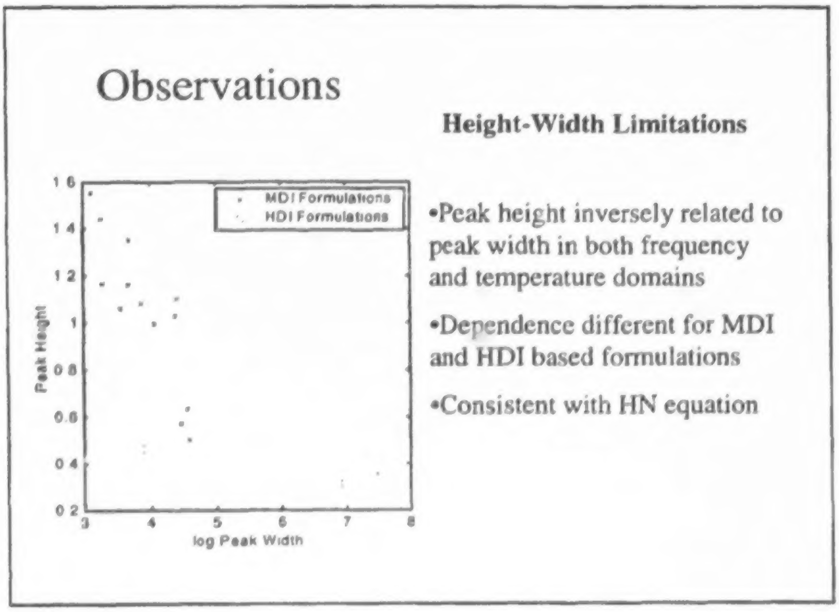

Observations

Height-Width Limitations

- Peak height inversely related to peak width in both frequency and temperature domains
- Dependence different for MDI and HDI based formulations
- Consistent with HN equation

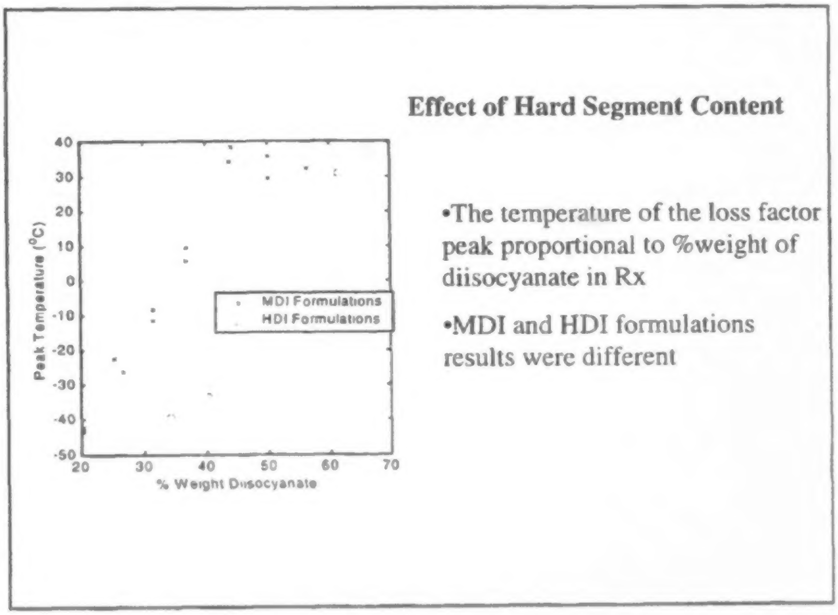

Effect of Hard Segment Content

- The temperature of the loss factor peak proportional to %weight of diisocyanate in Rx
- MDI and HDI formulations results were different

Modelling Damping Properties

- Group Interaction Modelling (GIM)
  - Approach looks promising for dynamic mechanical property prediction.
  - Results published in internal DERA report.
- Group Contribution Analysis (GCA)
  - van Krevelen method used
  - Results of this study with data for 16 polyurethanes are inconclusive
  - May not be large enough set of polymers

Defence Research Establishment Atlantic (DREA)

GCA: Small Groups

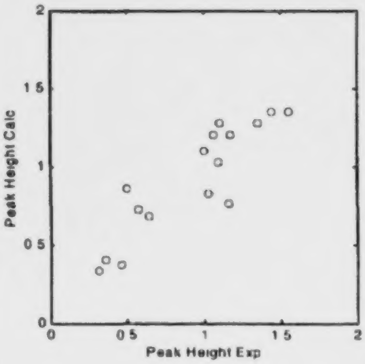

- •Used least squares approach to find group coefficients for 5 small groups in table.
- •Derived coefficients were able to explain experimental data reasonably well, BUT
- •Negative value for dimethyl propane height coefficient does not make physical sense
- •Analysis done with larger groups gave slightly better results

	Group Contributions		
	Height	Width	log(fmax)
Methylene	0.379	5.389	13.533
Ether Oxygen	3.413	-2.446	40.662
Dimethyl Propane	-9.298	9.142	75.982
Phenyl	1.976	0.586	-23.349
Urethane	1.806	8.737	-31.635

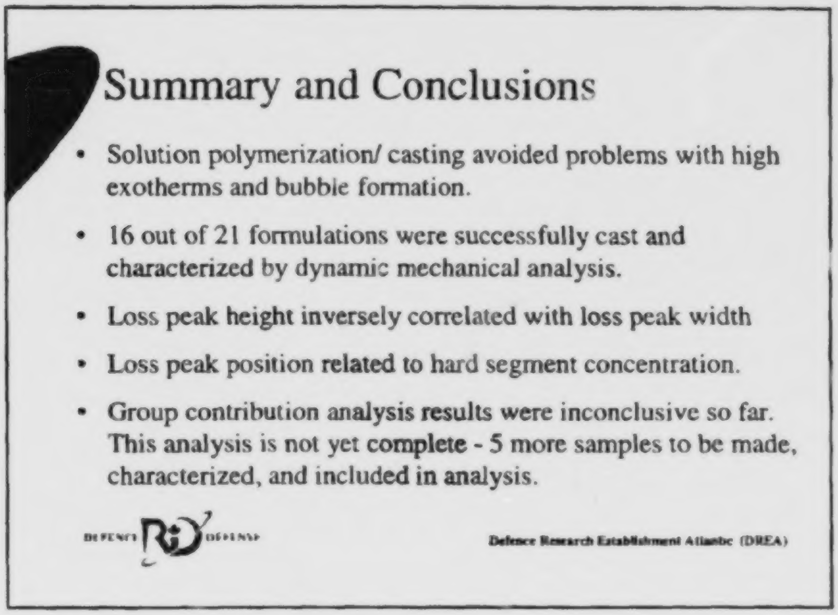

Summary and Conclusions

- Solution polymerization/ casting avoided problems with high exotherms and bubble formation.
- 16 out of 21 formulations were successfully cast and characterized by dynamic mechanical analysis.
- Loss peak height inversely correlated with loss peak width
- Loss peak position related to hard segment concentration.
- Group contribution analysis results were inconclusive so far. This analysis is not yet complete - 5 more samples to be made, characterized, and included in analysis.

Defence Research Establishment Atlantic (DREA)

#516455 (40)

Polymer Actuators Based on Maxwell Forces

by

J.P. Szabo*, B. White†, and J. Leidner†

*Defence Research Establishment Atlantic, P.O. Box 1012, Dartmouth, N.S. B2Y 3Z7
†Bodycote Ortech, 2395 Speakman Drive, Mississauga, Ontario L5K 1B3

Abstract

There are currently two main classes of actuating materials - piezoelectric materials, characterized by high frequency response but very small movements, and shape memory alloys, characterized by very slow response but relatively large movements. Polymeric actuators are an emerging class of materials, which offer the potential to fill the performance gap between piezoelectric materials and shape memory alloys. There are four main classes of polymeric actuators: (i) piezoelectric, (ii) hydrated membranes and hydrogels, (iii) electrostrictive, and (iv) dielectric. In this presentation, the possible applications of dielectric polymers to active noise and vibration control will be presented, along with results of preliminary work to fabricate and characterize these materials. Dielectric actuators based on cast thermoplastic polyurethane films were prepared with brushed-on graphite powder as electrodes. Strains of up to around two percent were measured. This strain corresponds to a stress of approximately 150 kPa. The voltage/strain relationship followed a parabolic relationship as predicted by theoretical considerations. Actuators with similar strain values were prepared by forming longer films and rolling them into tubes.

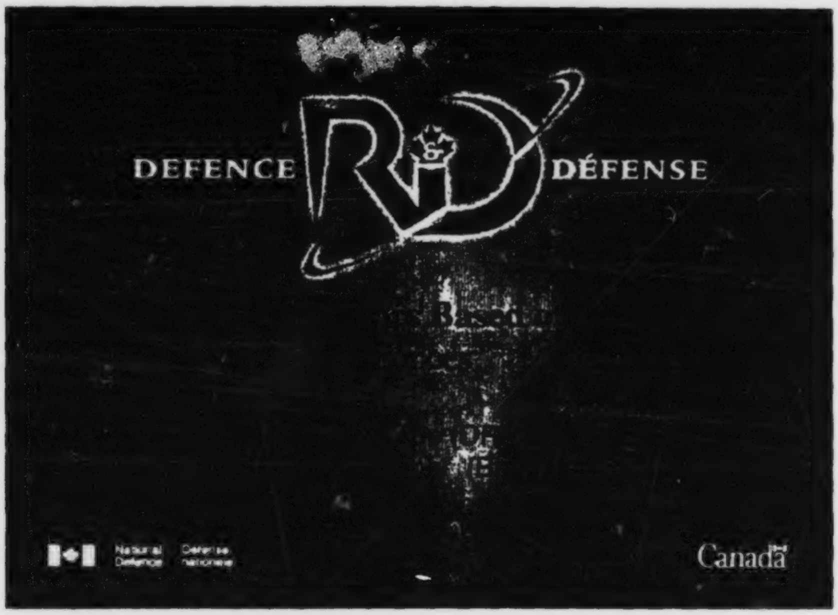

DEFENCE R&D DÉFENSE

National Defence Défense nationale

Canada

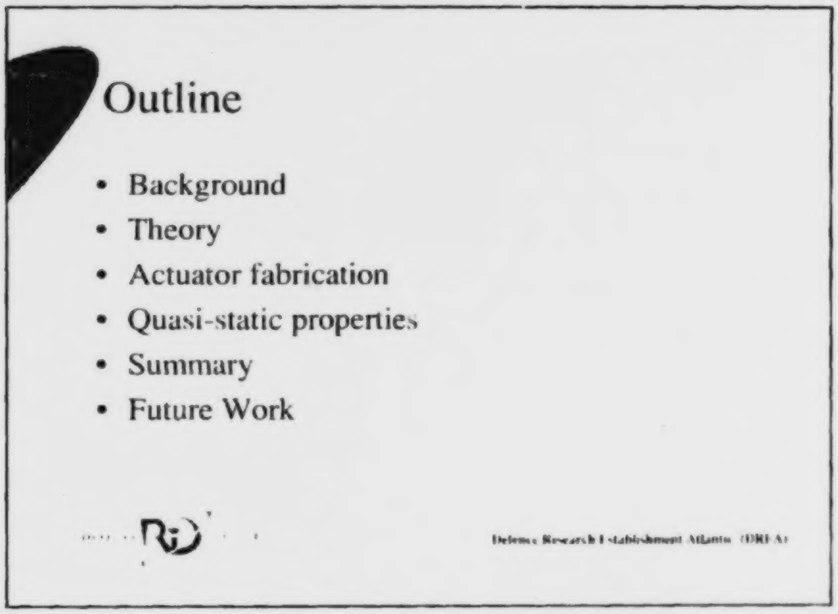

Outline

- Background
- Theory
- Actuator fabrication
- Quasi-static properties
- Summary
- Future Work

Defence Research Establishment Atlantic (DREA)

Types of Actuator Materials

Fast response, low strain
  - Piezoelectric
  - Electrostrictive
  - Magnetostrictive

Slow response, high strain
  - Shape memory alloys

Fast response, high strain
  - Dielectric actuators

Defence Research Establishment Atlantic (DREA)

Background

- Dielectric actuator technology is at a point where the basic phenomenon has been observed and demonstrated.
- Most of the research in the field has been published since 1998, and the bulk of the work has been carried out at SRI, and more recently in Denmark
- Strains of > 100% have been observed in stretched acrylic and silicone films. Frequency response for silicone flat up to 400 Hz.
- Much of the work is directed at "artificial muscles" for robotics.

Defence Research Establishment Atlantic (DREA)

Dielectric Actuators

Maxwell Stress Effect

A voltage potential applied across a thin, non-conducting, elastomeric membrane results in the attraction of two charged surfaces, compression of the elastomer, and a resulting increase in its length.

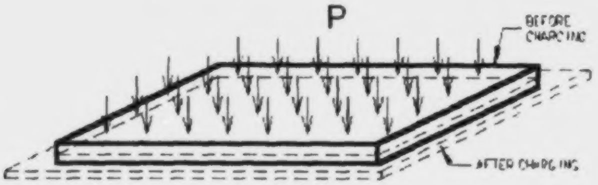

- If a thin film actuator is rolled into a rod then actuation force is along the cylinder axis.
- Elastomeric actuator would be ideal for active vibration isolation.

"Rolled" actuator

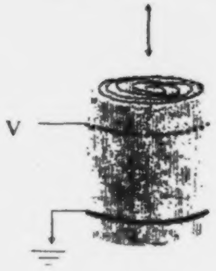

Combined Active/ Passive Vibration Isolation

- Active and passive isolation are complementary
- Works as passive isolator if power fails
- Robust control

Objectives

- Develop simple static models for film actuators
- Select an appropriate dielectric elastomer
- Fabricate a number of film and rod shaped actuators
- Characterize the static strain as a function of applied voltage and film thickness
- This was intended to be preliminary study
- Work was carried out at Bodycote Ortech under contract to DREA

Defence Research Establishment Atlantic (DREA)

Single Layer Model

Strain $\varepsilon_1 = \mu e_0 e V^2/2Yd^2$

Stress $P_1 = \mu e_0 e V^2/2d^2$

Assumptions:
- No constraints on dielectric
- Dielectric is perfectly elastic
- Electrode has no stiffness
- Deformation due only to Maxwell forces

Maximum effects are proportional to
- dielectric permittivity of polymer
- square of the dielectric strength (max voltage per unit thickness)

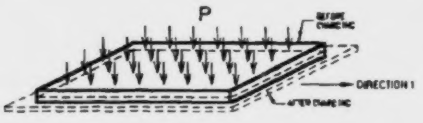

Material Selection

- Graphite electrodes - low stiffness, electrically conductive.
- Elastomer - non-conductive, no pinholes, high dielectric breakdown strength, high dielectric constant, low hardness
- Preliminary film casting experiments were carried out on:

	Manufacturer	Type	Hardness (Shore A)	Dielectric Constant	Dielectric Strength (kV/mm)
FC2123	Dyneon	Fluorinated rubber	71	5.7	40
THV 220	Dyneon	Fluorinated rubber	44	5.7	62
Elastosil RT 601	Wacker	2 component silicone	45	3.1	23
Pellethane 2103-70A	Dow	Thermoplastic polyurethane	[illegible]	[illegible]	25
PLV 6034	Pelseal	2 component fluoroelastomer		3.1	40
SIFEL 5701	Shin Etsu MicroSi	2 component fluorosilicone	71	3.1	23

Film Preparation

- A centrifugal spin caster was designed and built
- Idea was that gas bubbles would be removed under centrifugal force.
- Initial experiments indicated that dimensional accuracy of the drum was inadequate, resulting in non-uniform films.

Decided to use a simple casting procedure, selecting defect free areas:
- Dissolved PU in 8% DMF solution
- Cast films onto glass plates buffed with wax
- Dried films at 60°C for > 8 hours
- Film thicknesses were in the range 25-150 µm

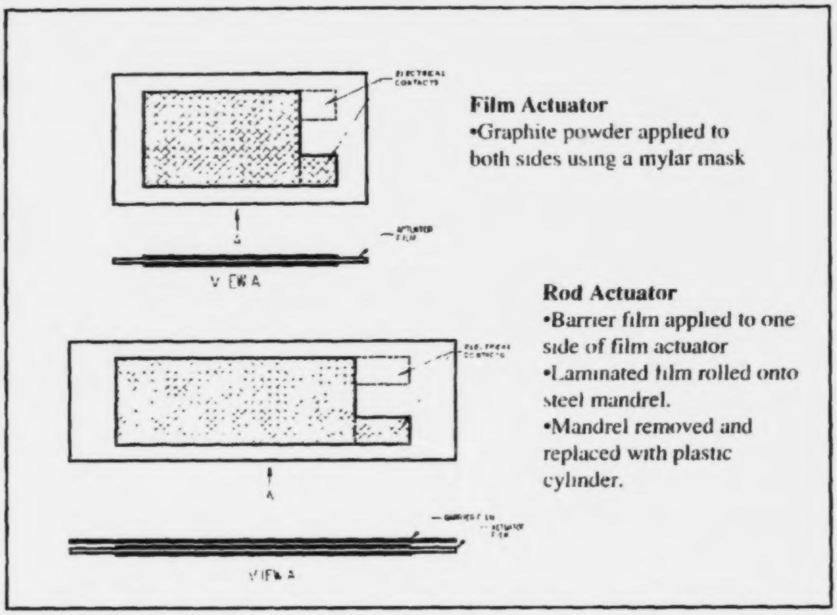
ELECTRICAL CONTACTS
A
ACTUATOR FILM
VIEW A
ELECTRICAL CONTACTS
A
BARRIER FILM
ACTUATOR FILM
VIEW A

Film Actuator

- Graphite powder applied to both sides using a mylar mask

Rod Actuator

- Barrier film applied to one side of film actuator
- Laminated film rolled onto steel mandrel.
- Mandrel removed and replaced with plastic cylinder.

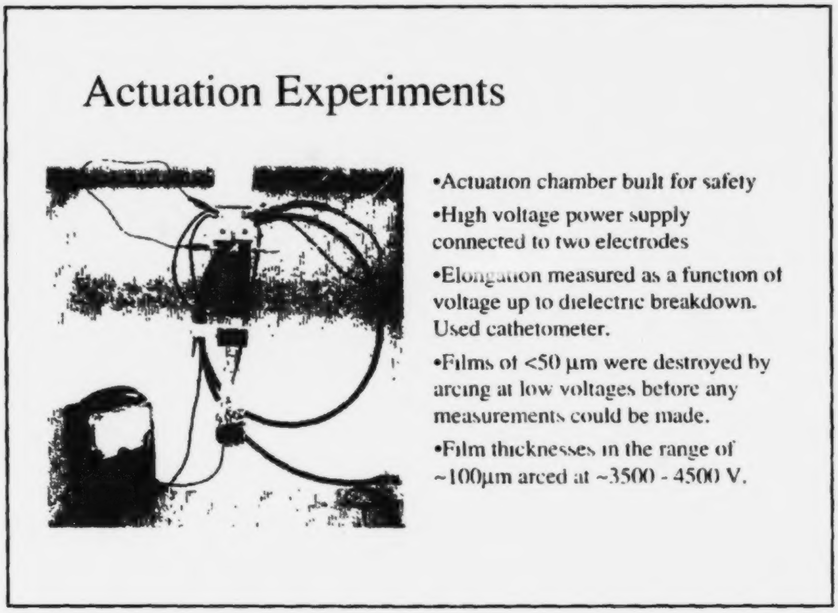

Actuation Experiments

- Actuation chamber built for safety
- High voltage power supply connected to two electrodes
- Elongation measured as a function of voltage up to dielectric breakdown. Used cathetometer.
- Films of <50 µm were destroyed by arcing at low voltages before any measurements could be made.
- Film thicknesses in the range of ~100µm arced at ~3500 - 4500 V.

Film Actuator Data

Note V^2 dependence

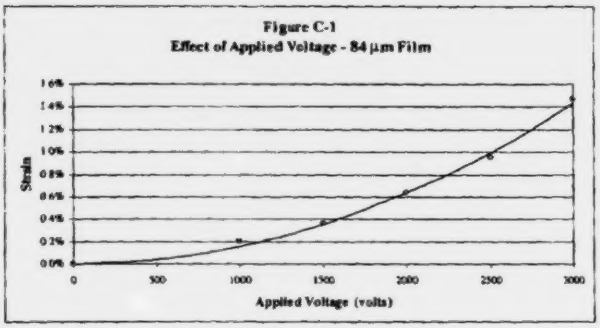

Figure C-1
Effect of Applied Voltage - 84 μm Film

Rod Actuator

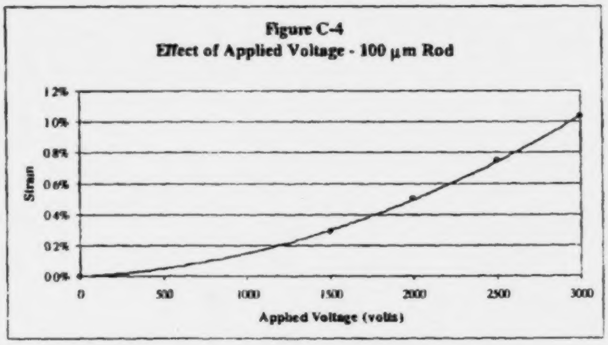

Figure C-4
Effect of Applied Voltage - 100 μm Rod

Instron Stress-Strain Data

ASTM D882-97 Quasi-static Young's modulus = 7.275 MPa

Figure D-1
Stress/Strain Behaviour of Pellethane 2103-70A

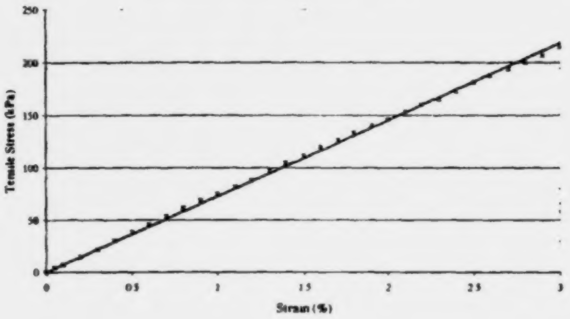

Summary Table

Up to 234 kPa stress observed
Thickness dependence not in accordance with the model
Non-uniformity of film thickness possibly an issue

	Stress (kPa)			
Applied Voltage	84 µm Film 01-05-8518-107	100 µm Film 01-05-8660-7-3	135 µm Film 01-05-8660-9/12	100 µm Rod 01-05-8518-111
0	0	0	0	0
500	3	2	2	
1000	12	8	8	
1500	26	19	19	20
2000	46	33	33	36
2500	72	52	52	56
3000	104	74	75	80
3500	142	101	102	
4000	185	132	133	
4500	234	167	169	

Comparison with Model

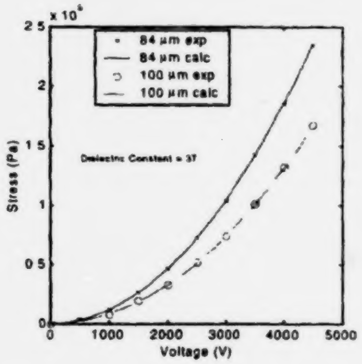

Stress $P_1 = \mu e_0 e V^2/2d^2$

For 84 µm and 100 µm films:

- Model fits data very well using a value of e = 37 for the dielectric constant
- Manufacturer's reported value of e = 7.3
- Difference could be explained by frequency dependence of e.
- Need to measure e(ω)

Summary

- Dielectric actuators based on cast thermoplastic polyurethane films were prepared with brushed-on graphite powder as electrodes.
- Strains of up 2% were measured, which corresponds to a stress of approximately 230 kPa for an 84 µm film.
- The voltage/strain relationship followed a parabolic relationship as predicted by theoretical considerations. Actuators with similar strain values were prepared by forming longer films and rolling them into tubes.
- Experimental data was in accordance with a simple parallel plate capacitor model for two different film thicknesses, using a value of 37 for the dielectric constant of the polyurethane film.

DEFENCE R&D DEFENSE

Defence Research Establishment Atlantic (DREA)

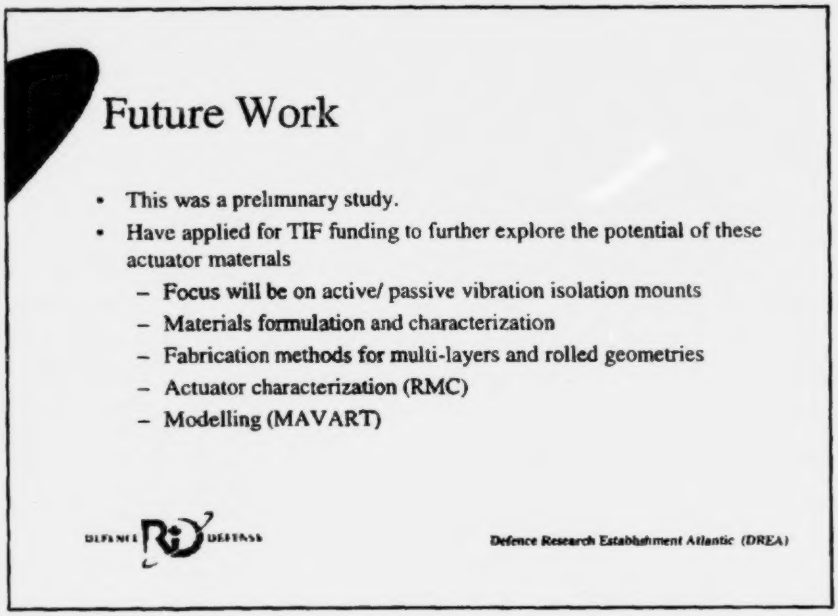

Future Work

- This was a preliminary study.
- Have applied for TIF funding to further explore the potential of these actuator materials
  - Focus will be on active/ passive vibration isolation mounts
  - Materials formulation and characterization
  - Fabrication methods for multi-layers and rolled geometries
  - Actuator characterization (RMC)
  - Modelling (MAVART)

Defence Research Establishment Atlantic (DREA)

#516456 (41)

CPF Heated Window Failures

by

James R Matthews
Vincent Roy
Steve Kavanaugh
Calvin Hyatt
Etienne Robichaud
Dan Morehouse

Dwight Veinot
John Power
Irv Keough
Gary Fisher

Alan Russell
Paul Martin
B.J. Kaye
R.D. Roland

George Watt
Steve Zan
Kevin McTaggart

George Schattschneider

Defence Research Establishment Atlantic
P.O.Box 1012, Dartmouth, Nova Scotia B2Y 3Z7

Abstract

This talk will summarize the findings of the DREA-DL(A) and DREA-DL(P) investigation of the heated window failures on Canadian Patrol Frigates (CPF's). Each CPF has 32 heated windows, distributed throughout the ship as follows: 19 on the bridge, 3 in the flight deck control room, 8 in the landing safety officer shelter (LSO), and 2 on the quarterdeck. This investigation was conducted because of a reported extraordinarily high incidence of failure of these windows on ships throughout the fleet with its associated effects on operational activities and repair costs. The report contains the results of failure investigations on some of these windows together with the findings of laboratory experiments and models that were designed to simulate in-service conditions and gather data in support of the failure investigations. It also contains both short and long term recommendations that, if implemented, will mitigate this failure problem.

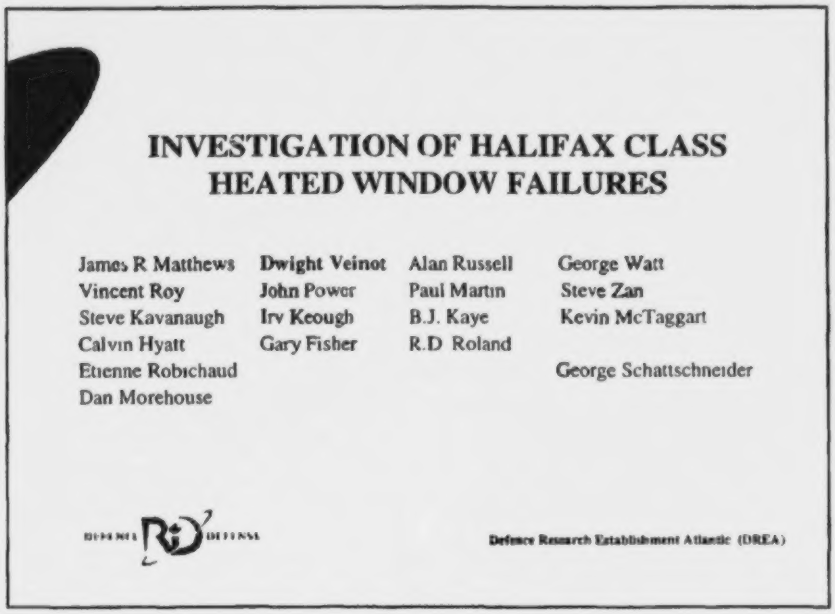

INVESTIGATION OF HALIFAX CLASS HEATED WINDOW FAILURES

James R Matthews
Vincent Roy
Steve Kavanaugh
Calvin Hyatt
Etienne Robichaud
Dan Morehouse

Dwight Veinot
John Power
Irv Keough
Gary Fisher

Alan Russell
Paul Martin
B.J. Kaye
R.D Roland

George Watt
Steve Zan
Kevin McTaggart

George Schattschneider

Defence Research Establishment Atlantic (DREA)

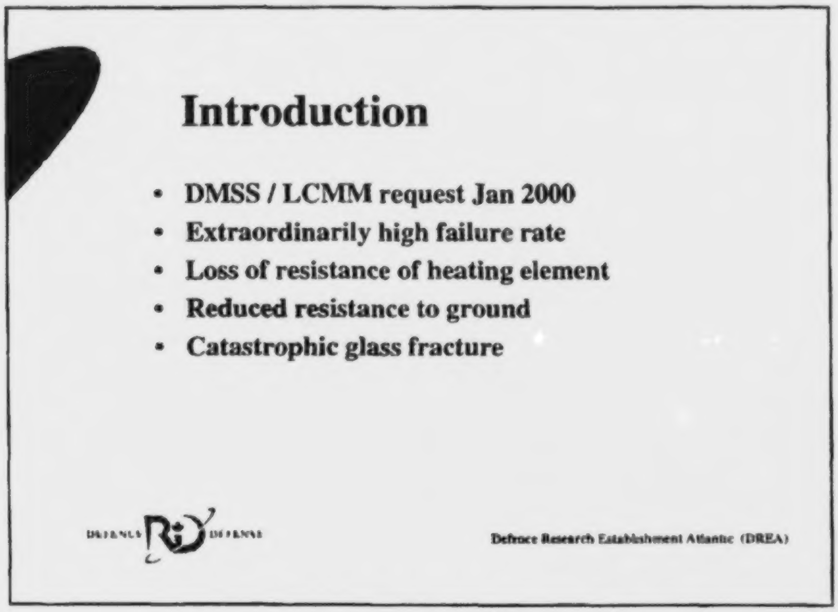

Introduction

- DMSS / LCMM request Jan 2000
- Extraordinarily high failure rate
- Loss of resistance of heating element
- Reduced resistance to ground
- Catastrophic glass fracture

Defence Research Establishment Atlantic (DREA)

Outline

- Heated window construction
- Case failure studies
- Laboratory experiments
- Conclusions
- Recommended remedies

Defence Research Establishment Atlantic (DREA)

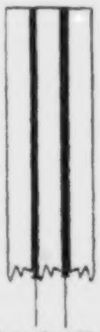
1.5 mm polyvinyl butyral

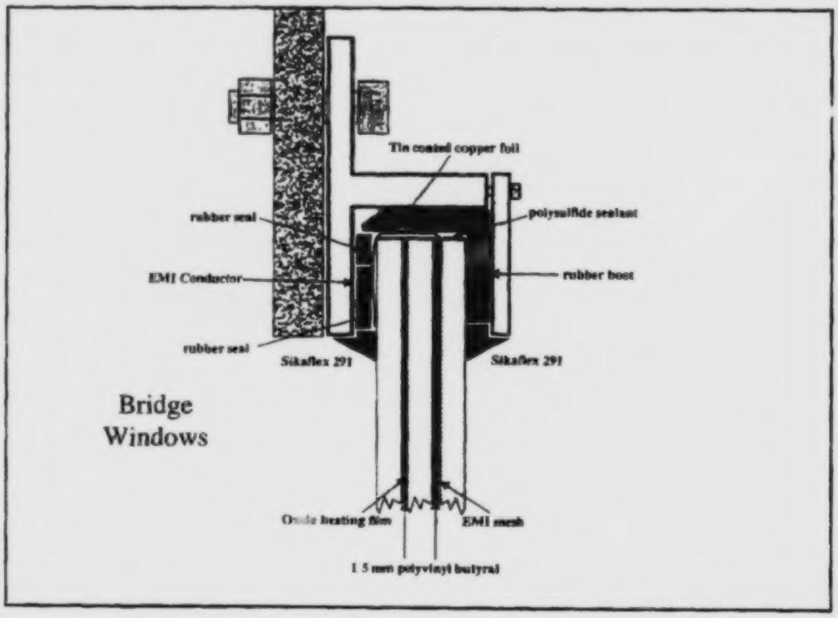
Tin coated copper foil
rubber seal
polysulfide sealant
EMI Conductor
rubber boot
rubber seal
Sikaflex 291
Sikaflex 291
Bridge
Windows
Oxide heating film
EMI mesh
1.5 mm polyvinyl butyral

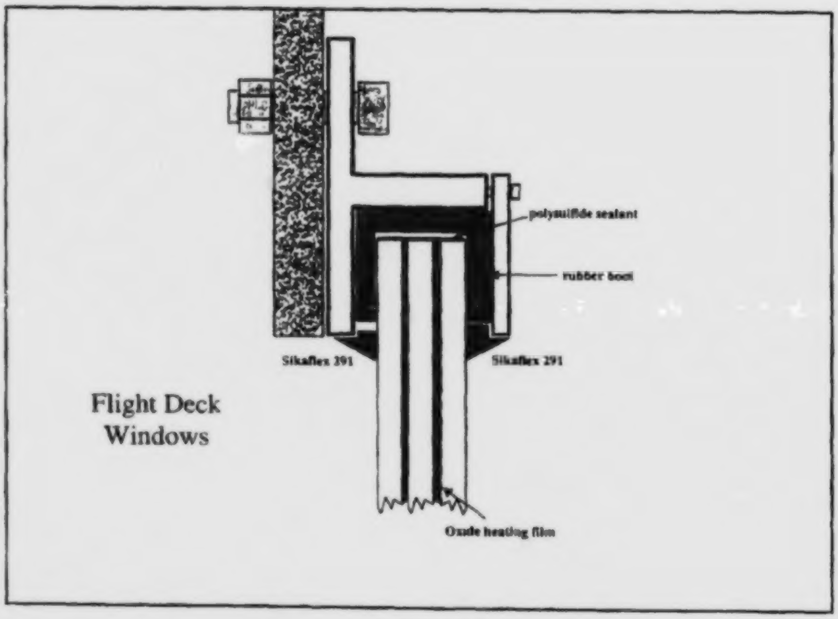
polysulfide sealant
rubber boot
Sikaflex 291
Sikaflex 291
Flight Deck
Windows
Oxide heating film

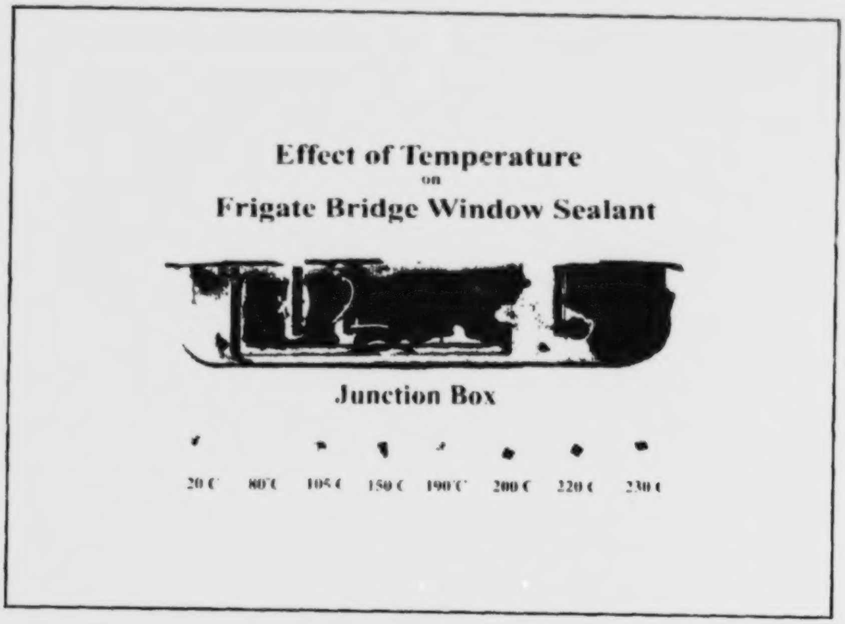

Effect of Temperature
on
Frigate Bridge Window Sealant

Junction Box

20 C
80°C
105 C
150 C
190°C
200 C
220 C
230 C

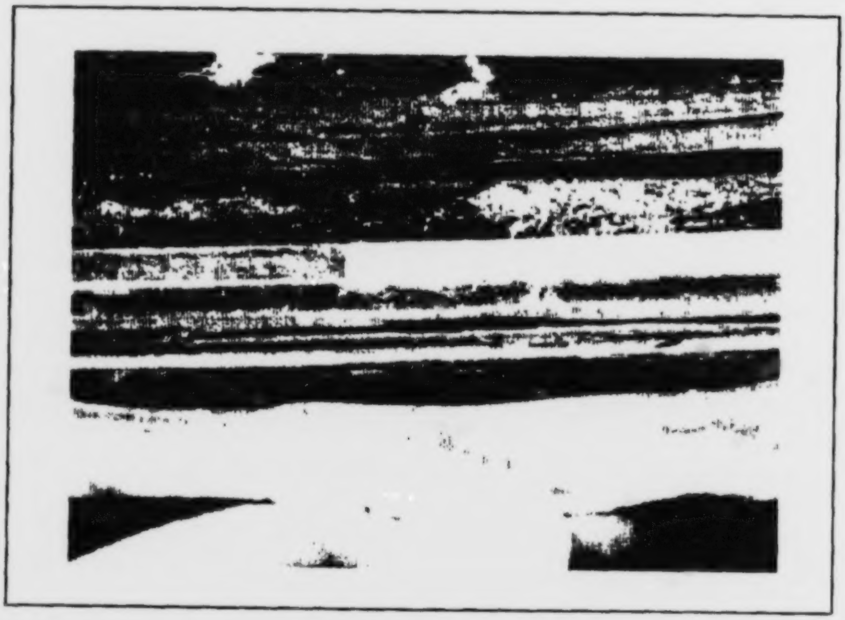

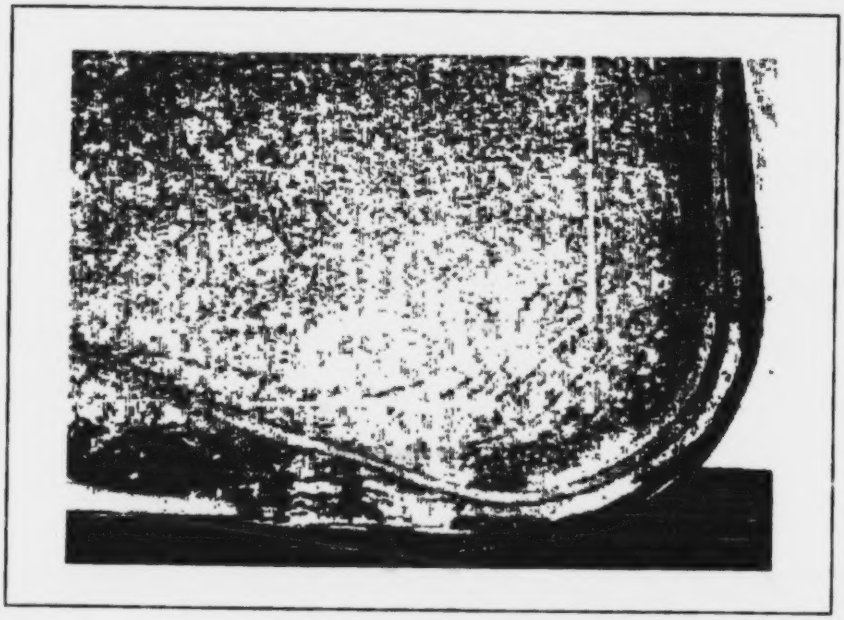

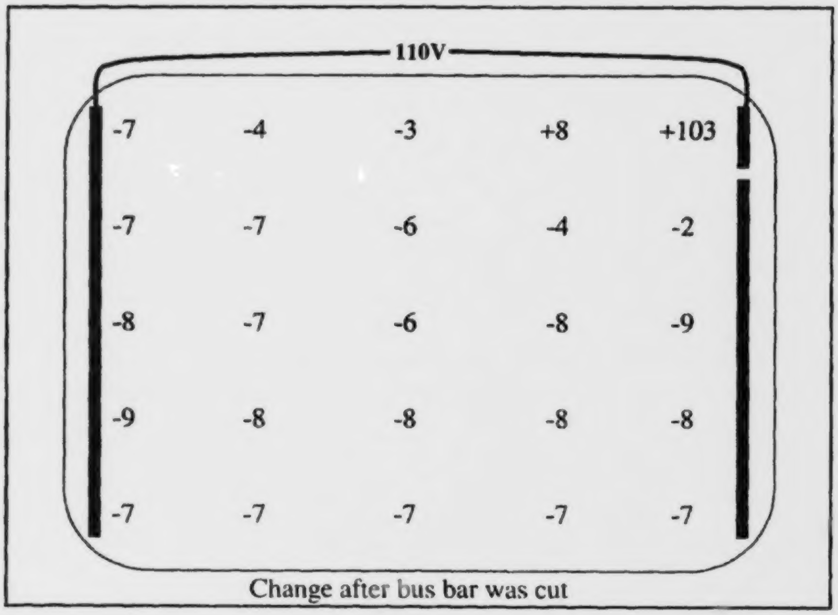
110V
-7 -4 -3 +8 +103
-7 -7 -6 -4 -2
-8 -7 -6 -8 -9
-9 -8 -8 -8 -8
-7 -7 -7 -7 -7

Change after bus bar was cut

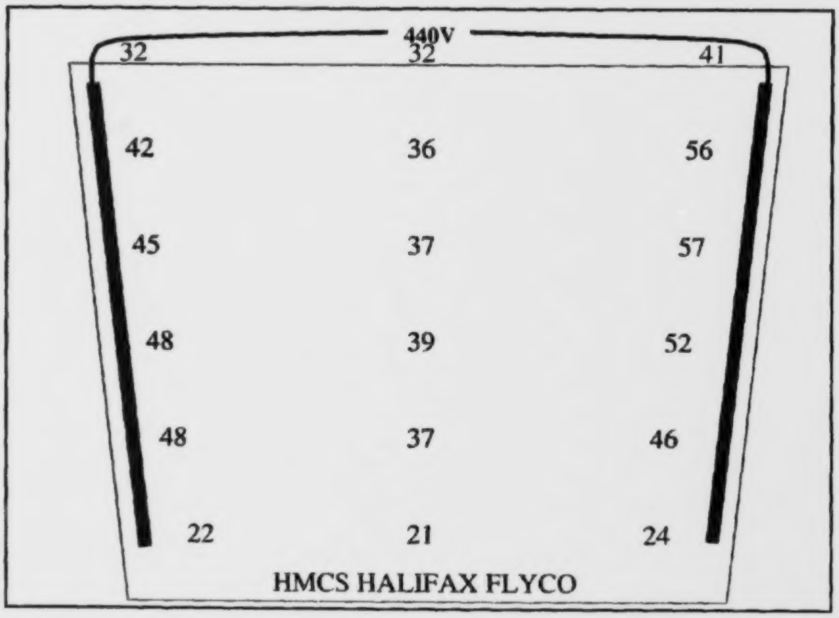
440V
32 32 41
42 36 56
45 37 57
48 39 52
48 37 46
22 21 24

HMCS HALIFAX FLYCO

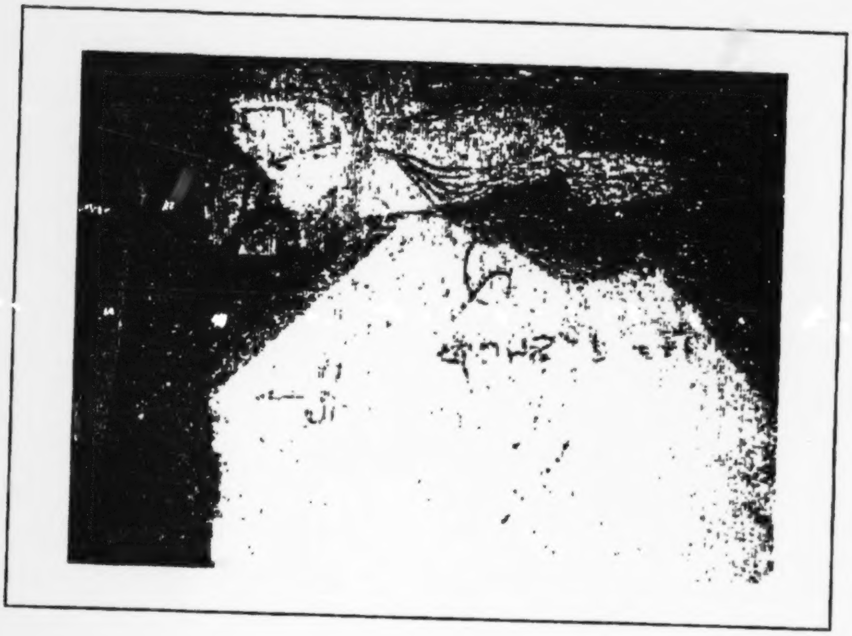

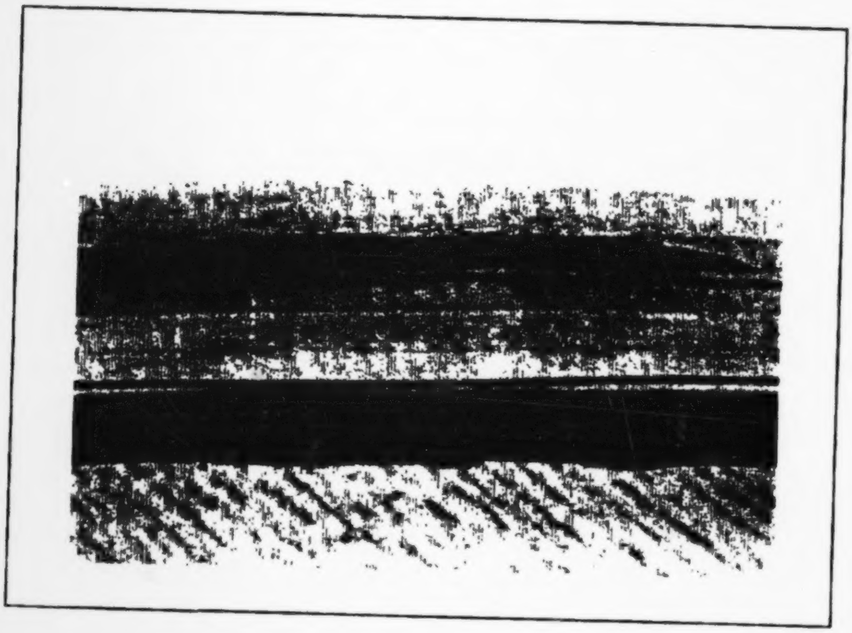

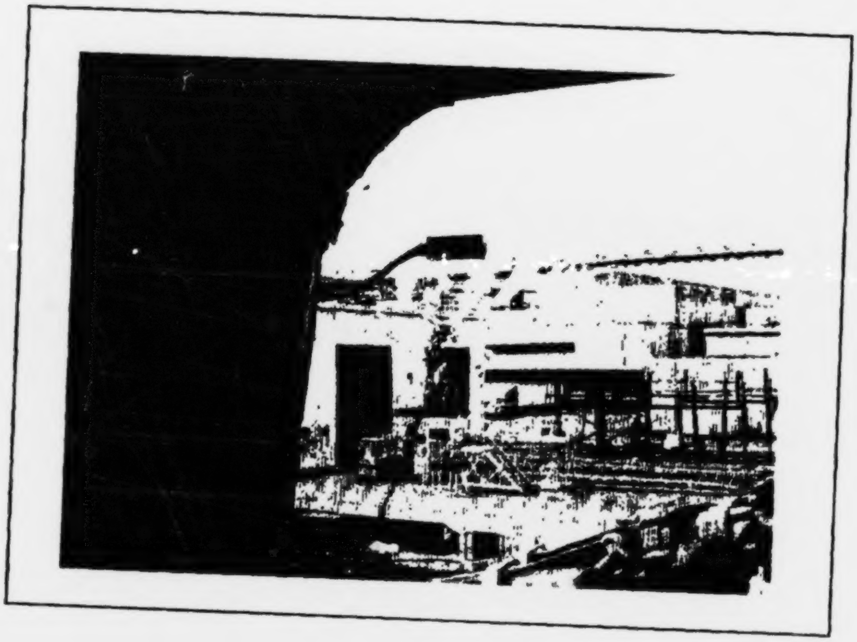

Recommended Remedies

- Bridge windows
  - redesign mechanical seal
  - trim EMI foil
  - don't use glue on rubber seals
  - use UV safe adhesive / sealant (Sikaflex 295UV)
  - eliminate / remove interior insulation
- FLYCO windows
  - locate thermostats on side of windows in regions of greatest heating rate
  - move bus bars in from edge
  - put resistive heater oxide on center pane
  - ensure flatness

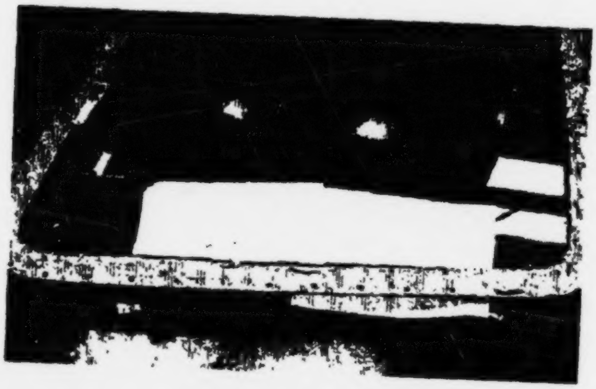

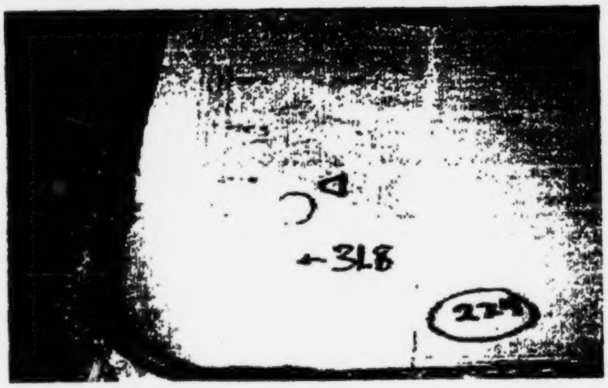

Defence Research Establishment Atlantic (DREA)

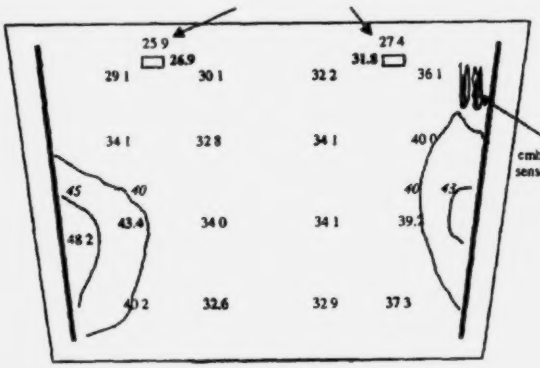
25 9
26.9
27 4
31.8
29 1
30 1
32 2
36 1
34 1
32 8
34 1
40 0
embedded sensors 38 C
45
40
40
43
43.4
48 2
34 0
34 1
39.2
40 2
32.6
32 9
37 3

Defence Research Establishment Atlantic (DREA)

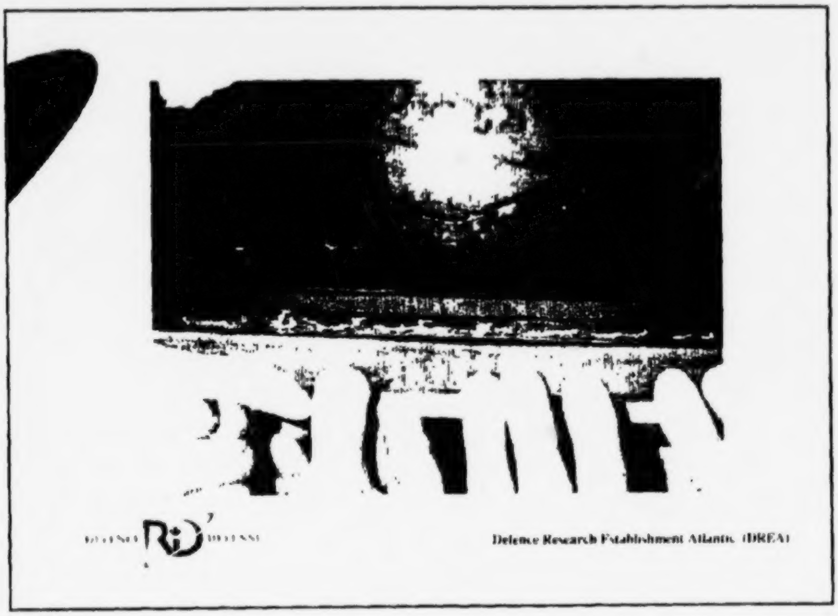

Defence Research Establishment Atlantic (DREA)

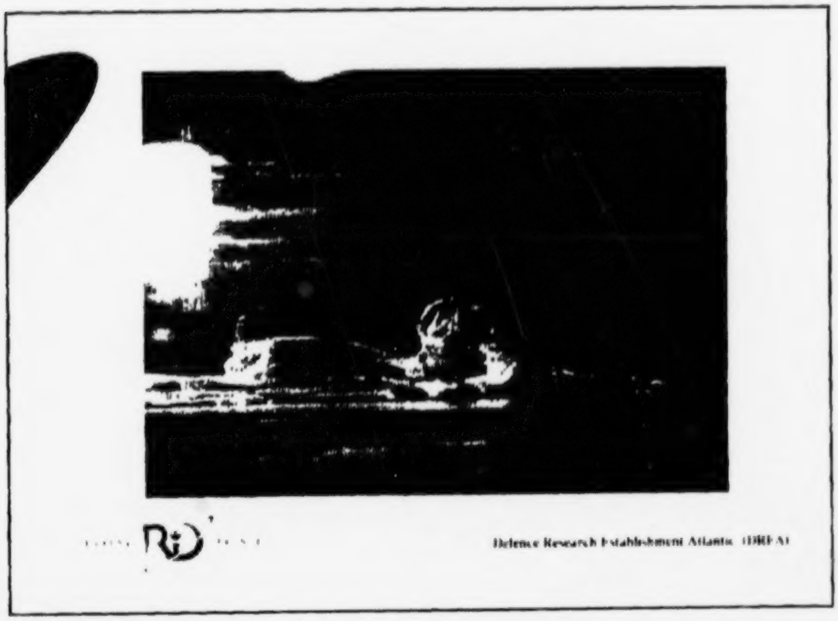

Defence Research Establishment Atlantic (DREA)

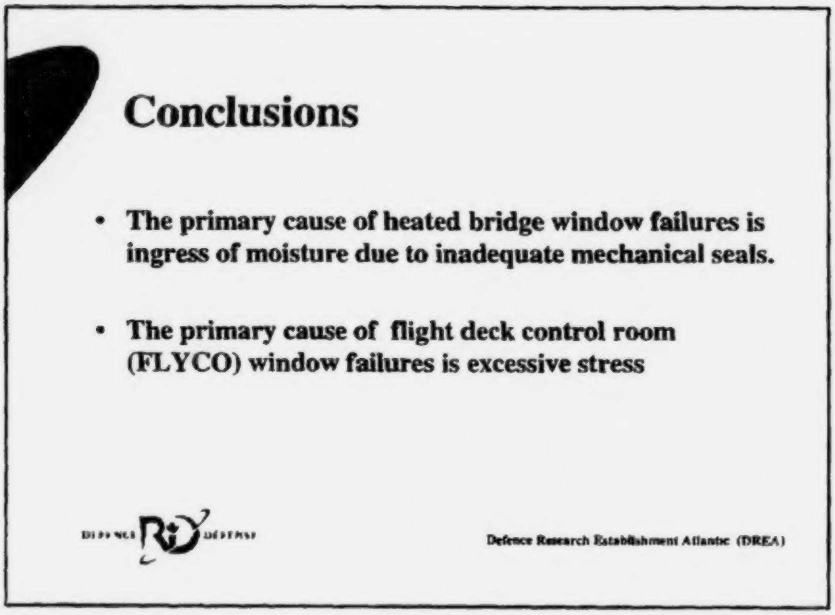

Conclusions

- **The primary cause of heated bridge window failures is ingress of moisture due to inadequate mechanical seals.**
- **The primary cause of flight deck control room (FLYCO) window failures is excessive stress**

Defence Research Establishment Atlantic (DREA)

#516457 (42)

Probabilistic Service Life Assessment of Missile Structures

by

U.O. Akpan[1] and F. Wong[2]

[1]Research and Emerging Technologies Department
Martec Limited, Suite 400, 1888 Brunswick Street, Halifax, N.S., Canada B3J 3J8.

[2] Emergent Energetic Materials
Defence Research Establishment Valcartier

Abstract

Tactical missiles that use solid rocket motors are stored under controlled thermal conditions or deployed at geographical locations under widely varying weather conditions that are best described as random processes. Depending on the storage conditions, a motor may be subjected to changing ambient temperature, solar radiation, wind, rain and snow, resulting in randomly varying induced stresses, strains and cumulative damage which may exceed the strength and strain capacities of the propellant. This could give rise to cracks that could induce failure upon firing. The motivation for service life assessment is the detection of propellant degradation and the prediction of the end life before it actually occurs.

An approach for probabilistic service life assessment of missile systems that incorporates structural degradation due to thermal loading cycles is developed. Probabilistic models for daily thermal load cycles is formulated and incorporated into structural response models for rocket motors. Probabilistic models for a missile structural capacity are proposed and calibrated from measured data. Performance functions for assessing the service life of stored missiles are developed. First Order Reliability Method (SORM) is used to calculate instantaneous reliability of a missile structure. Methodology for computing the time dependent reliability of a degrading missile structure is developed. Sensitivity of the time dependent reliability to system parameters is investigated. Example problems are used for demonstrations.

PROBABILISTIC SERVICE LIFE ASSESSMENT OF MISSILE STRUCTURES

By

U. O. Akpan[1] and F. Wong[2]

[1] Research and Emerging Technologies Department, Martec Limited
1888 Brunswick St. Suite 400, Halifax, NS, Canada

[2] Emergent Energetic Materials
Defence Research Establishment Valcartier, Valcatier, Quebec

The 9th CF/DRDC MEETING on
NAVAL APPLICATIONS OF MATERIAL TECHNOLOGY
5-7 MAY 2001

Defence Research
Establishment Valcartier

Martec Limited
Advanced Engineering and
Research Consultants

PRESENTATION OUTLINE

- MOTIVATIONS/INTRODUCTION
- OBJECTIVE OF STUDY
- PROBABILISTIC MODELS FOR SERVICE LIFE ASSESSMENT
- DEMONSTRATION EXAMPLE
- LIMITATIONS OF APPROACH
- SUMMARY/CONCLUSIONS

Defence Research
Establishment Valcartier

Martec Limited
Advanced Engineering and
Research Consultants

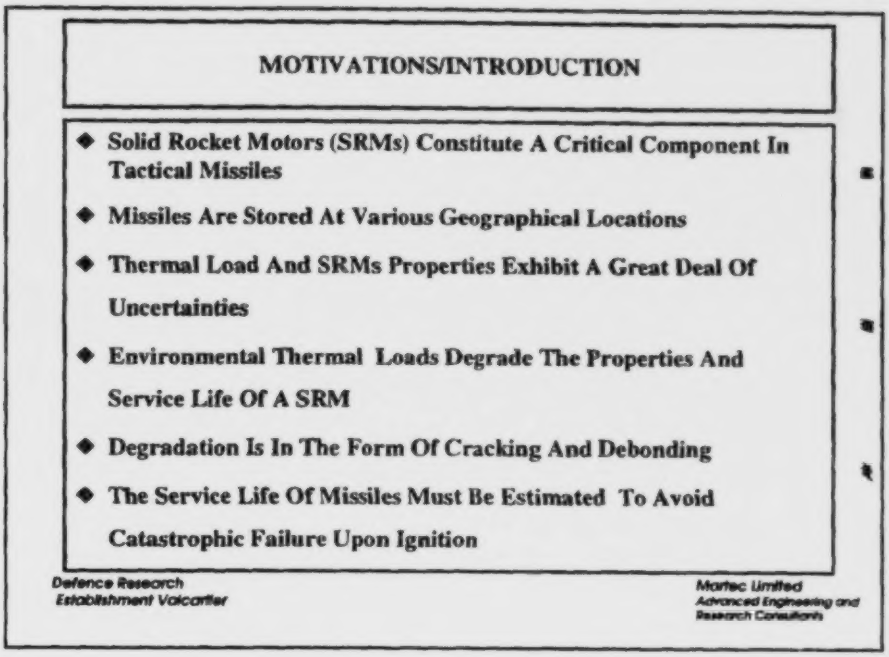

MOTIVATIONS/INTRODUCTION

- Solid Rocket Motors (SRMs) Constitute A Critical Component In Tactical Missiles
- Missiles Are Stored At Various Geographical Locations
- Thermal Load And SRMs Properties Exhibit A Great Deal Of Uncertainties
- Environmental Thermal Loads Degrade The Properties And Service Life Of A SRM
- Degradation Is In The Form Of Cracking And Debonding
- The Service Life Of Missiles Must Be Estimated To Avoid Catastrophic Failure Upon Ignition

Defence Research
Establishment Valcartier

Martec Limited
Advanced Engineering and
Research Consultants

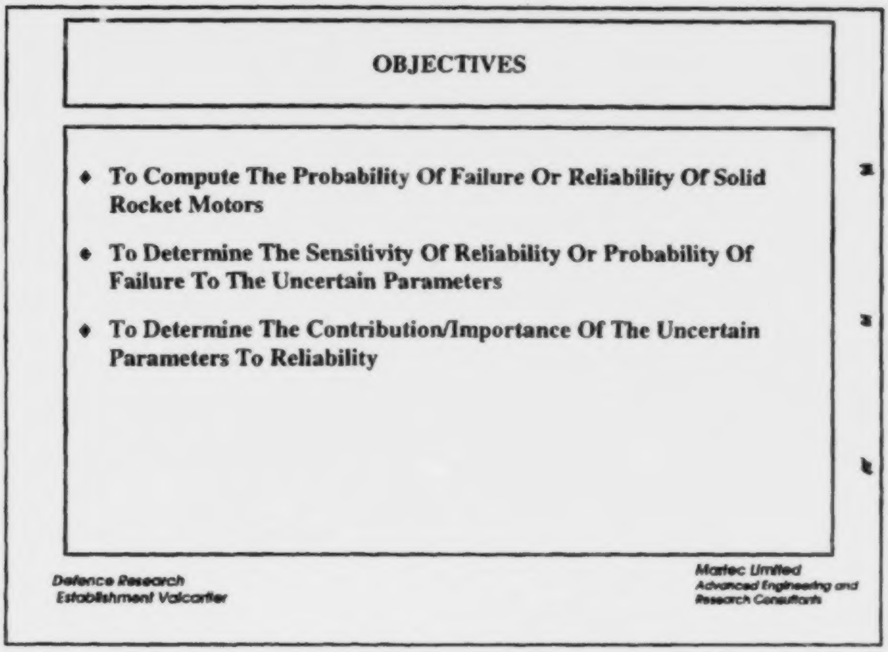

OBJECTIVES

- To Compute The Probability Of Failure Or Reliability Of Solid Rocket Motors
- To Determine The Sensitivity Of Reliability Or Probability Of Failure To The Uncertain Parameters
- To Determine The Contribution/Importance Of The Uncertain Parameters To Reliability

Defence Research
Establishment Valcartier

Martec Limited
Advanced Engineering and
Research Consultants

MERITS OF PROBABILISTIC APPROACH

- Rational, Systematic And Utilizes Available Information On Uncertainties
- Sensitivity To Information
- It Allows For Quantification Of Reliability And Risk, Hence Provides A Framework For Application Of Risk Management Procedures
- Realistic For Decision Making
- Not Overly Conservative/Cost Effective
- Provides A Framework For Systematic Determination Of Overall System Reliability From The Reliability Of Individual Components

RELATIONSHIP BETWEEN PROBABILISTIC AND DETERMINISTIC APPROACH

- Probabilistic And Deterministic Methods Are Not Competing But Complementary Methods Of Engineering Analysis And Decision Making

- Best Probabilistic Methods Are Those That Are Founded On Well-established Deterministic Procedures - Sound Deterministic Before Probabilistic

PROBABILISTIC MODELS FOR SERVICE LIFE ASSESSMENT

- **Models for Thermal Loads**
- **Models for Critical Structural Responses**
- **Models for Structural Capacities**
- **Models for Performance Functions**
- **Algorithms for Computing Instantaneous Reliability**
- **Algorithms for computing Progressive Reliability**

Defence Research
Establishment Valcartier

Martec Limited
Advanced Engineering and
Research Consultants

MODELS FOR THERMAL LOAD

- **Maximum Daily Temperature Modeled by**

$$T(t) = T_m + T_y a(t) + T_d$$

- T_m = Mean Value of Yearly Temperature
- T_y = Yearly Amplitude of Temperature
- T_d = Peak Value of Daily Temperature
- $a(t) = sin(2\pi/\omega(t - t_0))$
- t - Day

Defence Research
Establishment Valcartier

Martec Limited
Advanced Engineering and
Research Consultants

MODELS FOR CRITICAL STRUCTURAL RESPONSE

Schematic Diagram

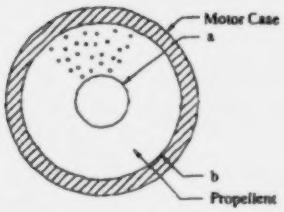

Defence Research
Establishment Valcartier

Martec Limited
Advanced Engineering and
Research Consultants

MODELS FOR CRITICAL STRUCTURAL RESPONSE

- Model can be:
  - Analytical
  - Experimental
  - Numerical

Defence Research
Establishment Valcartier

Martec Limited
Advanced Engineering and
Research Consultants

MODELS FOR CRITICAL STRUCTURAL RESPONSE

- **Critical Structural Responses are:**
    - **Bore Strain / Stress (Bore Cracking)**
    - **Bondline Stress (Debonding)**
- **Analytical Models are Employed in Study**

MODELS FOR CRITICAL STRUCTURAL RESPONSE

- **Bore Strain Formula**

$$\varepsilon_\theta = \log_e\{1+\varepsilon_\theta^1(a)\}$$

- **Bore Stress Formula**

$$\sigma_{rc}(a) = 2E_p\alpha_R\lambda^2\Delta T$$

- **Bondline Stress Formula**

$$\sigma_r(b) = E_p\alpha_R\left(\lambda^2 - 1\right)\Delta T$$

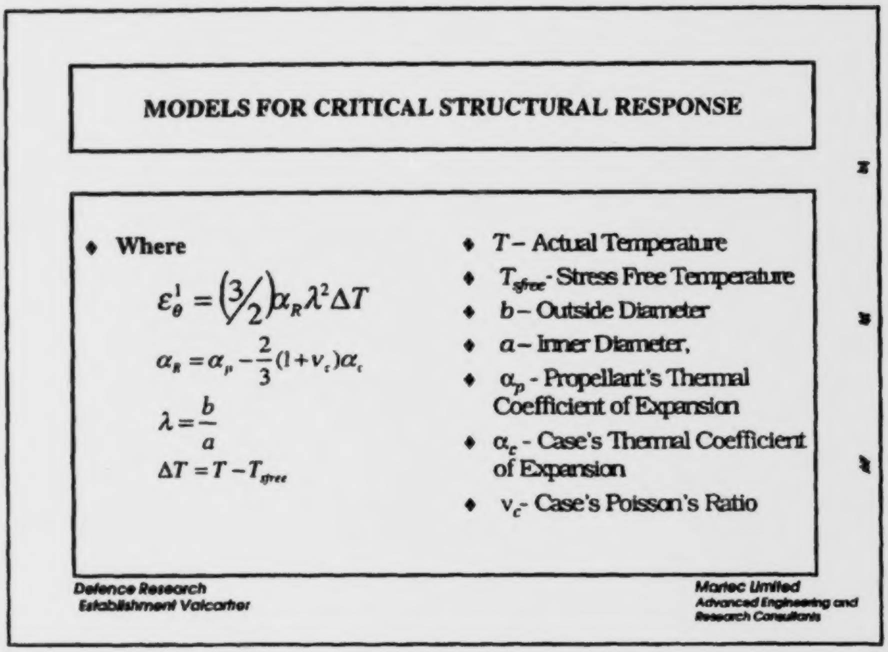

MODELS FOR CRITICAL STRUCTURAL RESPONSE

- **Where**

$$\varepsilon_\theta^1 = \left(\frac{3}{2}\right)\alpha_R \lambda^2 \Delta T$$

$$\alpha_R = \alpha_p - \frac{2}{3}(1+\nu_c)\alpha_c$$

$$\lambda = \frac{b}{a}$$

$$\Delta T = T - T_{sfree}$$

- T – Actual Temperature
- T_{sfree} - Stress Free Temperature
- b – Outside Diameter
- a – Inner Diameter,
- α_p - Propellant's Thermal Coefficient of Expansion
- α_c - Case's Thermal Coefficient of Expansion
- ν_c - Case's Poisson's Ratio

Defence Research
Establishment Valcartier

Martec Limited
Advanced Engineering and
Research Consultants

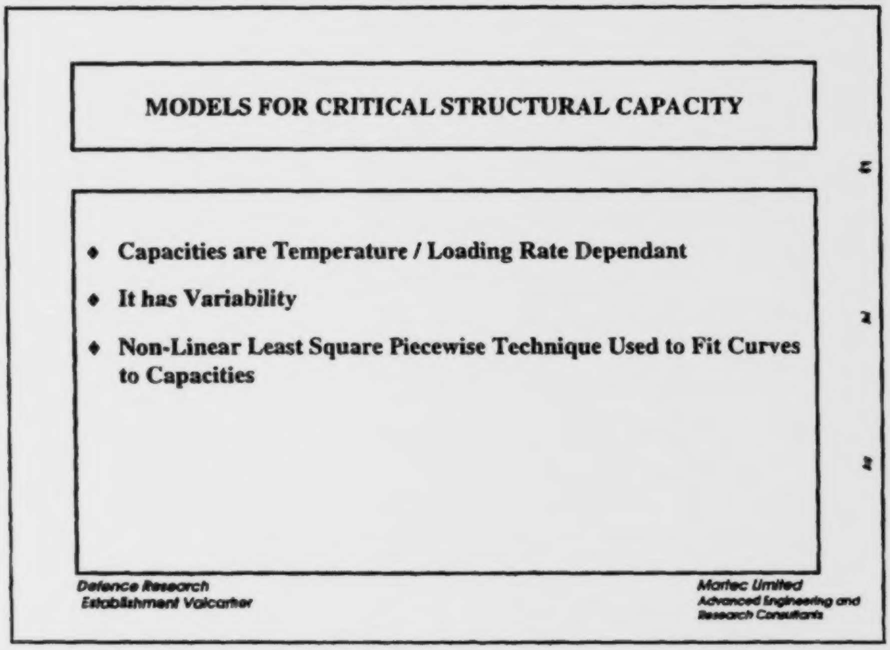

MODELS FOR CRITICAL STRUCTURAL CAPACITY

- **Capacities are Temperature / Loading Rate Dependant**
- **It has Variability**
- **Non-Linear Least Square Piecewise Technique Used to Fit Curves to Capacities**

Defence Research
Establishment Valcartier

Martec Limited
Advanced Engineering and
Research Consultants

MODELS FOR CRITICAL STRUCTURAL CAPACITY

Typical Stress Capacity Plot

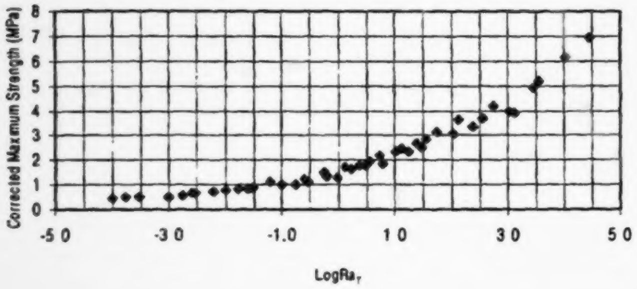

Defence Research Establishment Valcartier

Martec Limited
Advanced Engineering and Research Consultants

MODELS FOR CRITICAL STRUCTURAL CAPACITY

Typical Strain Capacity Plot

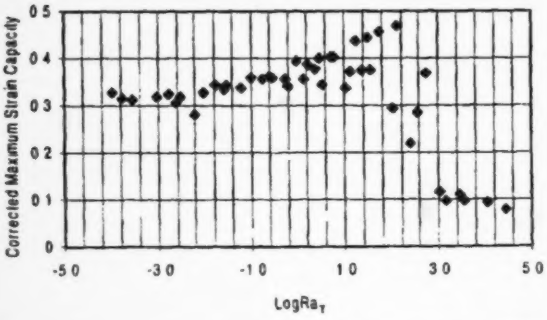

Defence Research Establishment Valcartier

Martec Limited
Advanced Engineering and Research Consultants

MODELS FOR CRITICAL STRUCTURAL CAPACITY

Corrected Maximum Strain Capacities (LogRa$_T$ < −1 61)

Corr Max Strain Cap = 0 328457e$^{0\ 010734 \mathrm{logRa}_T}$

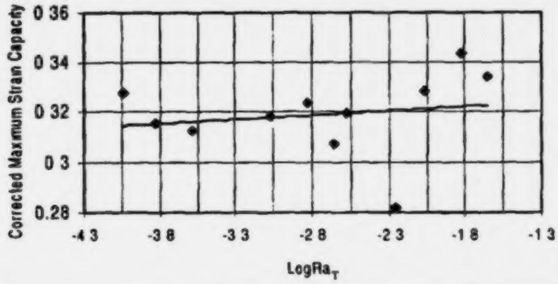

Defence Research Establishment Valcartier

Martec Limited
Advanced Engineering and Research Consultants

MODELS FOR CRITICAL STRUCTURAL CAPACITY

Corrected Maximum Strain Capacities (−1 61 < LogRa$_T$ < 0.24)

Corr Max Stnan Cap = 0 368891e$^{0\ 055073 \mathrm{LogRa}_T}$

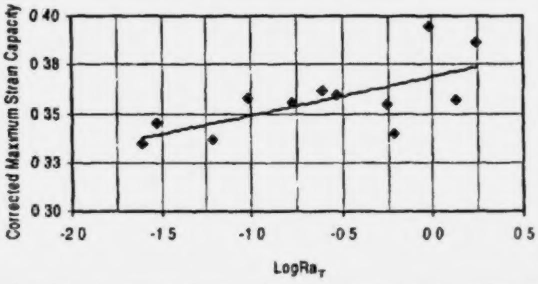

Defence Research Establishment Valcartier

Martec Limited
Advanced Engineering and Research Consultants

MODELS FOR CRITICAL STRUCTURAL CAPACITY

Corrected Maximum Strain Capacities ($0.24 < LogRa_T < 1.74$)

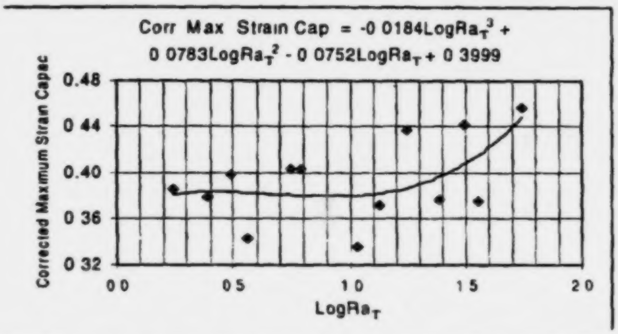

Corr Max Strain Cap = $-0.0184LogRa_T^3 + 0.0783LogRa_T^2 - 0.0752LogRa_T + 0.3999$

Defence Research Establishment Valcartier

Martec Limited
Advanced Engineering and Research Consultants

MODELS FOR CRITICAL STRUCTURAL CAPACITY

Corrected Maximum Strain Capacities ($LogRa_T > 1.74$)

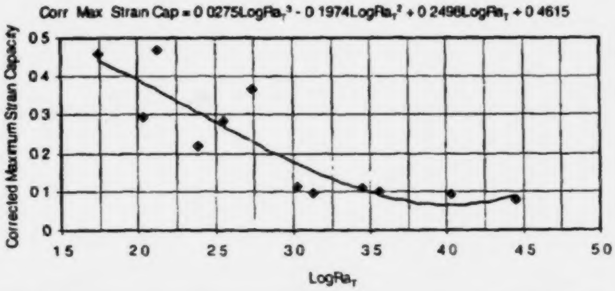

Corr Max Strain Cap = $0.0275LogRa_T^3 - 0.1974LogRa_T^2 + 0.2498LogRa_T + 0.4615$

Defence Research Establishment Valcartier

Martec Limited
Advanced Engineering and Research Consultants

MODELS FOR CRITICAL STRUCTURAL CAPACITY

Corrected Maximum Strength ($LogRa_T < -0.02$)

Corr Max Strength = 1394330 816261e$^{[illegible] LogRa_T}$

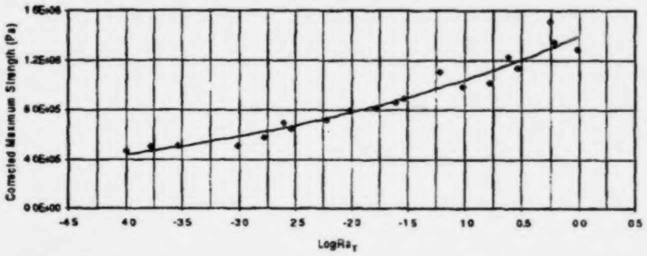

Defence Research Establishment Valcartier

Martec Limited Advanced Engineering and Research Consultants

MODELS FOR CRITICAL STRUCTURAL CAPACITY

Corrected Maximum Strength ($LogRa_T > -0.02$)

Corr Max Strength = 1569233 857262e$^{0\ 336267 LogRaT}$

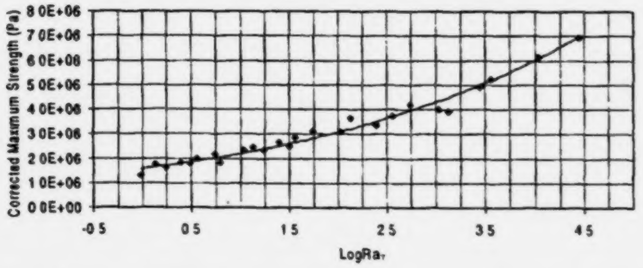

Defence Research Establishment Valcartier

Martec Limited Advanced Engineering and Research Consultants

MODELS FOR PERFORMANCE FUNCTION

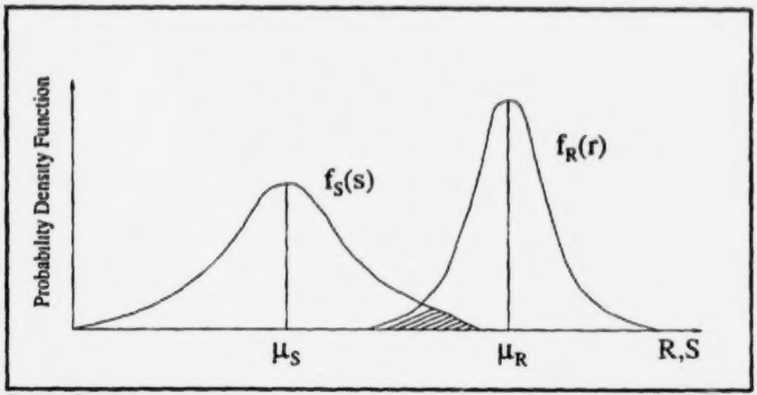

Defence Research
Establishment Valcartier

Martec Limited
Advanced Engineering and
Research Consultants

MODELS FOR PERFORMANCE FUNCTION

- General Performance Functions Can Be Developed

$$g(X(T)) = R(X(t)) - L(X(t))$$

- Instantanious and Time Dependant Reliability Have to be Computed

Defence Research
Establishment Valcartier

Martec Limited
Advanced Engineering and
Research Consultants

ALGORITHM FOR INSTANTENOUS RELIABILITY

$$P_f = \int_{\Omega} f(X(t))dX = \int_{\Omega} f(X_1, X_2....X_n)dX$$

Defence Research
Establishment Valcartier

Martec Limited
Advanced Engineering and
Research Consultants

ALGORITHM FOR PROGRESSIVE / TIME DEPENENT RELIABILITY

- Interested in the Structural Reliabiltiy with Time, $\gamma(t)$

$$\gamma(t) = \exp[-\int_0^t \lambda(\tau)d\tau]$$

- $\lambda(t)$ = Conditions Probability Function

$\lambda(t)\,dt$ = *Prob*[failure between *t* and *t+dt*|no failure up to *t*]

Defence Research
Establishment Valcartier

Martec Limited
Advanced Engineering and
Research Consultants

EXAMPLE: ESTIMATION OF SERVICE MISSILE STORED AT TWO SITES

Values of Material and Geometric Parameters

PARAMETER	TYPICAL VALUE
b	3 21
a	1
α_e	85x10^{-6}/°C
ν_c	0 33
α_c	23.6x10^{-6}/°C
T_{stm}	60°C

Defence Research
Establishment Valcartier

Martec Limited
Advanced Engineering and
Research Consultants

EXAMPLE: ESTIMATION OF SERVICE MISSILE STORED AT TWO SITES

Values of Material and Geometric Parameters

PARAMETERS	SEASONAL VARIATION		DIURNAL CYCLE	
	T_y(C)	T_m(C)	T_d(C)	$\sigma_{Td}(C)$
Alert	20 8	-12 88	-0 35	5 46
Valcartier	17 8	5 8	2 41	4 92

Defence Research
Establishment Valcartier

Martec Limited
Advanced Engineering and
Research Consultants

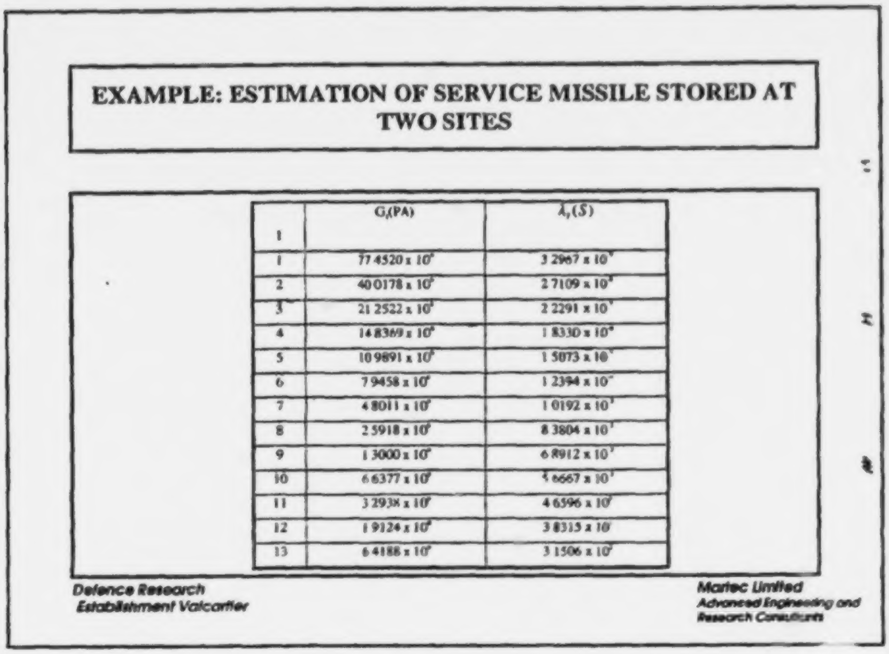

EXAMPLE: ESTIMATION OF SERVICE MISSILE STORED AT TWO SITES

I	G_i(PA)	$\lambda_i(S)$
1	77 4520 x 10[illegible]	3 2967 x 10[illegible]
2	40 0178 x 10[illegible]	2 7109 x 10[illegible]
3	21 2522 x 10[illegible]	2 2291 x 10[illegible]
4	14 8369 x 10[illegible]	1 8330 x 10[illegible]
5	10 9891 x 10[illegible]	1 5073 x 10[illegible]
6	7 9458 x 10[illegible]	1 2394 x 10[illegible]
7	4 8011 x 10[illegible]	1 0192 x 10[illegible]
8	2 5918 x 10[illegible]	8 3804 x 10[illegible]
9	1 3000 x 10[illegible]	6 8912 x 10[illegible]
10	6 6377 x 10[illegible]	5 6667 x 10[illegible]
11	3 2938 x 10[illegible]	4 6596 x 10[illegible]
12	1 9124 x 10[illegible]	3 8315 x 10[illegible]
13	6 4188 x 10[illegible]	3 1506 x 10[illegible]

Defence Research
Establishment Valcartier

Martec Limited
Advanced Engineering and
Research Consultants

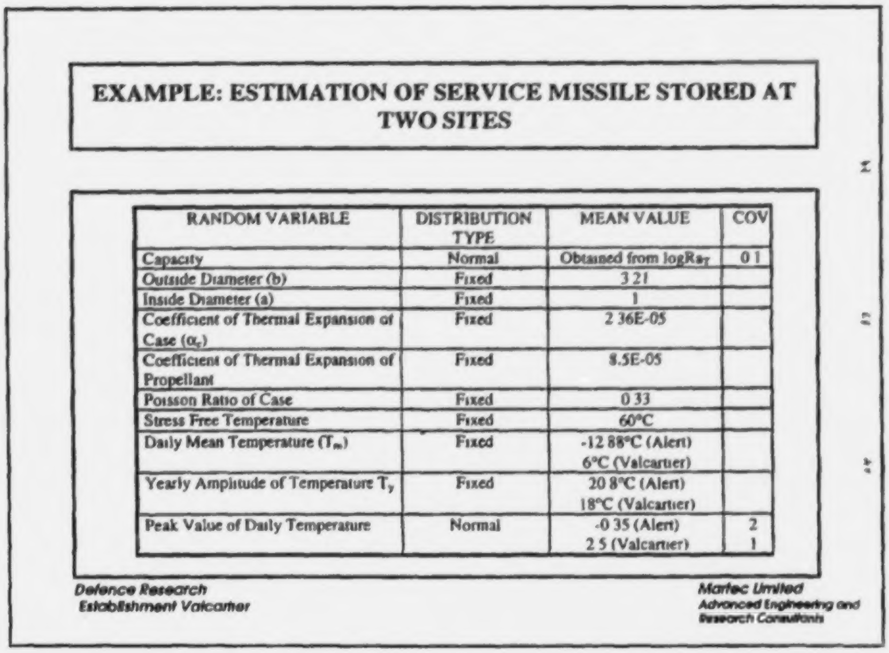

EXAMPLE: ESTIMATION OF SERVICE MISSILE STORED AT TWO SITES

RANDOM VARIABLE	DISTRIBUTION TYPE	MEAN VALUE	COV
Capacity	Normal	Obtained from logR_{aT}	0 1
Outside Diameter (b)	Fixed	3 21	
Inside Diameter (a)	Fixed	1	
Coefficient of Thermal Expansion of Case (α_c)	Fixed	2 36E-05	
Coefficient of Thermal Expansion of Propellant	Fixed	8.5E-05	
Poisson Ratio of Case	Fixed	0 33	
Stress Free Temperature	Fixed	60°C	
Daily Mean Temperature (T_m)	Fixed	-12 88°C (Alert) 6°C (Valcartier)	
Yearly Amplitude of Temperature T_y	Fixed	20 8°C (Alert) 18°C (Valcartier)	
Peak Value of Daily Temperature	Normal	-0 35 (Alert) 2 5 (Valcartier)	2 1

Defence Research
Establishment Valcartier

Martec Limited
Advanced Engineering and
Research Consultants

EXAMPLE: ESTIMATION OF SERVICE MISSILE STORED AT TWO SITES

Summary of Ratio of Daily Critical Response
to Daily Capacity at Alert and Valcartier

	VALCARTIER Range of Values	ALERT Range of Values
$\frac{\sigma_{cr}}{\sigma_r}$	8.89 - 3.72	5.53 - 2.6
$\frac{\sigma_t}{\sigma_t}$	4.0 - 1.68	2.5 - 1.14
$\frac{\varepsilon_f}{\varepsilon_r}$	8.77 - 4.09	5.52 - 2.96

Defence Research
Establishment Valcartier

Martec Limited
Advanced Engineering and
Research Consultants

ESTIMATION OF SERVICE LIFE FOR MISSILES

Probabilistic Results for Valcartier: Instantaneous Probability of Failure
(Based on Strain)

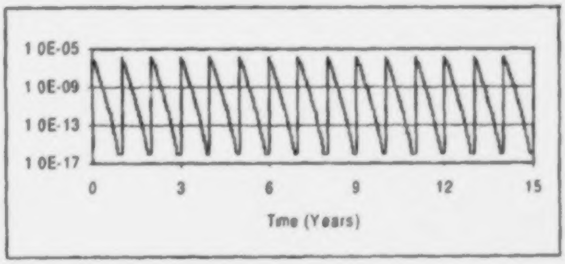

Defence Research
Establishment Valcartier

Martec Limited
Advanced Engineering and
Research Consultants

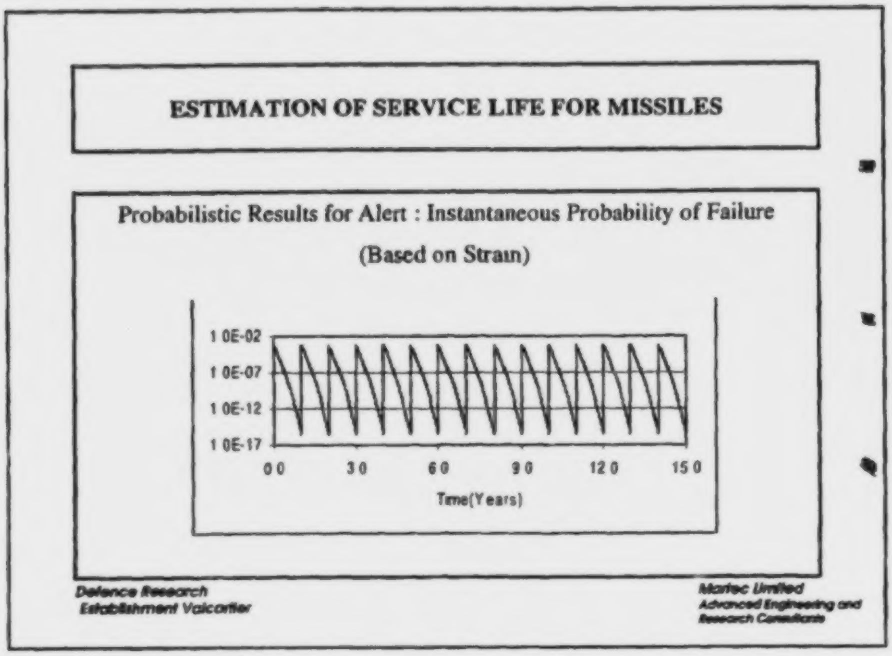

ESTIMATION OF SERVICE LIFE FOR MISSILES

Probabilistic Results for Alert : Instantaneous Probability of Failure

(Based on Strain)

Defence Research
Establishment Valcartier

Martec Limited
Advanced Engineering and
Research Consultants

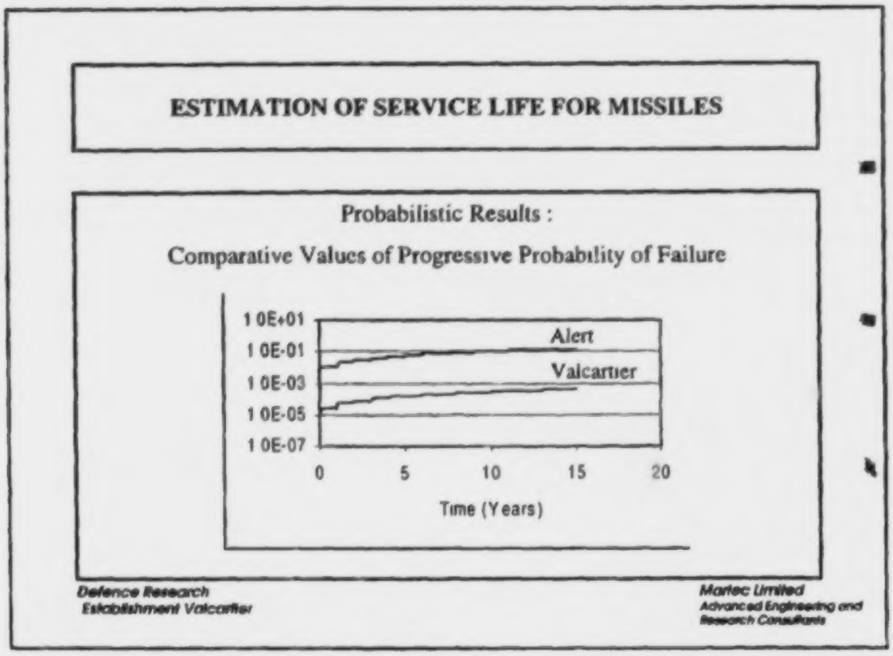

ESTIMATION OF SERVICE LIFE FOR MISSILES

Probabilistic Results :

Comparative Values of Progressive Probability of Failure

Defence Research
Establishment Valcartier

Martec Limited
Advanced Engineering and
Research Consultants

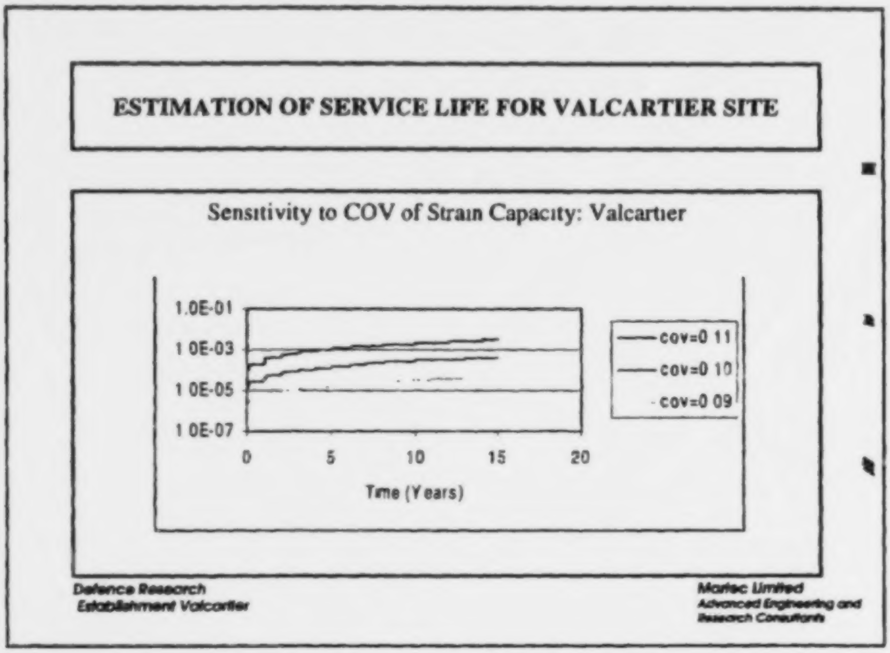

ESTIMATION OF SERVICE LIFE FOR VALCARTIER SITE

Sensitivity to COV of Strain Capacity: Valcartier

Defence Research
Establishment Valcartier

Martec Limited
Advanced Engineering and
Research Consultants

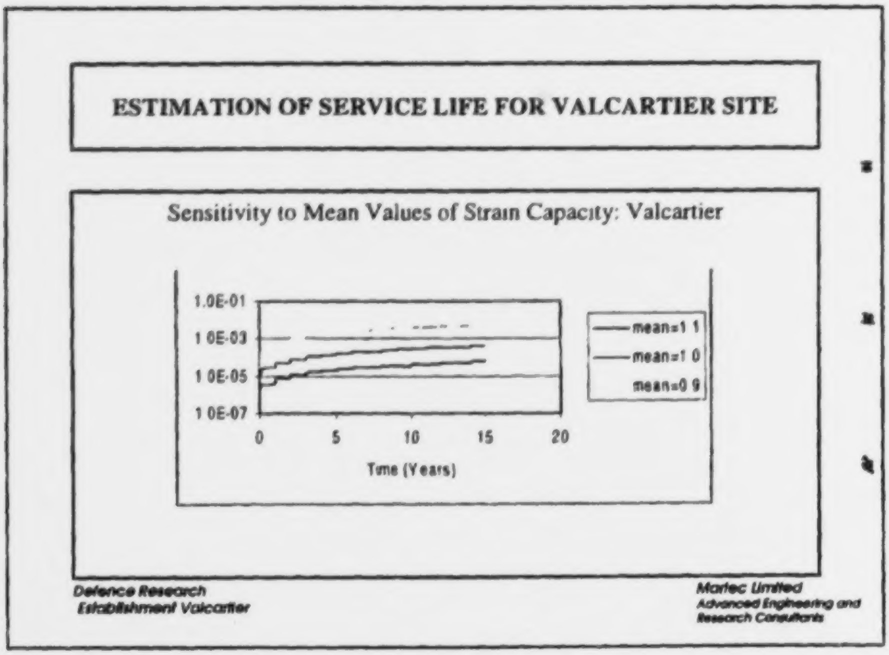

ESTIMATION OF SERVICE LIFE FOR VALCARTIER SITE

Sensitivity to Mean Values of Strain Capacity: Valcartier

Defence Research
Establishment Valcartier

Martec Limited
Advanced Engineering and
Research Consultants

LIMITATION OF RESULTS

- Effect of Cumulative Damage Not Considered
- Probabilistic Distribution for Strain Capacity Assumed and Not Calibrated From Data
- Variables That Affect the Structural Responses Modeled as Fixed Variables

Defence Research
Establishment Valcartier

Martec Limited
Advanced Engineering and
Research Consultants

SUMMARY/CONCLUSIONS

- A Time Dependent Probabilistic Strategy For Assessing the Service Life of Missile Structure Has been Developed
- Example Problems That Demonstrate the Approach Have been Demonstrated
- Limitations of Method Have been Highlighted
- Alternative Probabilistic Service Life Assessment Strategies that Circumvent the Limitations are Being Pursued

Defence Research
Establishment Valcartier

Martec Limited
Advanced Engineering and
Research Consultants

#516.458 (43)

Delayed Cracking in Simulated Submarine Repair Welds

by

N. Pussegoda,(1) A. Dinovitzer(1), Bo Xu(1) and B.A Graville(2)

(1)FTL, Kanata, ON, Canada
(2) Graville Associates, Georgetown, ON, Canada

Abstract

The Graville/FTL hydrogen diffusion and cracking risk models have been used successfully in the past to predict delayed cracking and to demonstrate how changes to the welding procedure can minimise the risk of cracking. The hydrogen diffusion model has been validated from the perspective of predicting the maximum delay time for cracking in a critical location, such as at the root of a notch, in previous work on pipeline welds and HAZ's. The findings reported here in based on Naval steels from the perspective of delayed cracking in welds and HAZ.

Pipeline repair welds carried out using cellulose covered electrodes that give high hydrogen levels, of up to 20 ml/100 gr of deposited weld metal, are susceptible to delayed hydrogen cracking. Higher strength welds, such as shielded metal arc welding of A517 Gr F steel have been found to be susceptible as well under practical welding conditions. The current work has demonstrated that delayed cracking can occur in repair simulations of HY 80 welds made with humidified E11018 electrodes. The maximum times for delayed cracking were reasonably predicted for two repair simulations involving two hydrogen diffusion distances.

FTL FLEET TECHNOLOGY LTD

Delayed Cracking in Simulated Submarine Repair Welds

Fleet Technology Limited, Kanata, Ontario

Presented by N. Pussegoda

Co-authors: A. Dinovitzer, Bo Xu and B.Graville

Funding from DREA

FTL FLEET TECHNOLOGY LTD

Background

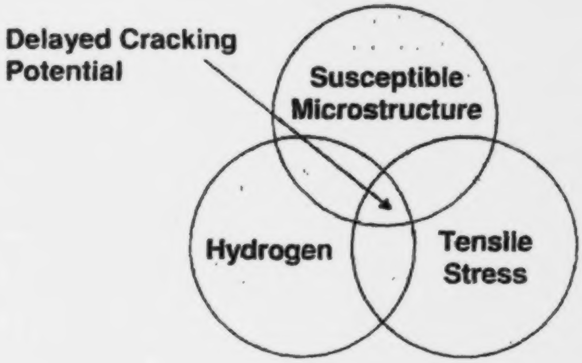

Delayed Cracking Potential

Susceptible Microstructure

Hydrogen

Tensile Stress

FTL FLEET TECHNOLOGY LTD

Background (Cont.)

History

Delayed cracking in welds (cracking tests)

Single pass weld tests - estimate required pre-heat to avoid root pass cracking (WIC)

Moving to higher strength and thicker plate the pre-heat requirement by itself is insufficient to avoid cracking

---

FTL FLEET TECHNOLOGY LTD

Problem and Approach Towards a Solution

Problem

In thicker multi-pass welds distribution of the hydrogen and higher residual (increased yield strength) stresses starts to play a major role

The inter-pass temperature and time (hydrogen distribution) and the welding procedure (residual stresses) play a major role

Problem and Approach Towards a Solution (Cont.)

Approach (FTL/Graville Model)

Use of the local hydrogen concept (finite difference model)

Simulate multi-pass welding procedure
Material and residual stress effect (sensitivity)
Predictive (risk of cracking)

Objective of the Current Work

Validate the model for delayed cracking times using two weld repair simulations (two diffusion distances) in submarine welds

Diffusivity of hydrogen in the material of interest (in weld metal)

Tests (determine delayed cracking times)

FTL FLEET TECHNOLOGY LTD

Diffusivity of Hydrogen

Method

Modified AWS 4.3 procedure.

RT effusion (compared to 45°C)

Hydrogen effusion from sample is monitored over Hg

FTL FLEET TECHNOLOGY LTD

Diffusivity of Hydrogen (Cont.)

Weld

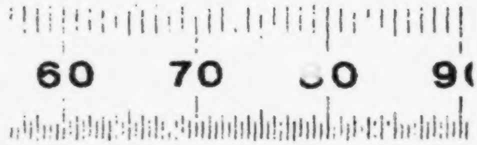

E76018 (E11018) electrode on HY 80 base metal and mild steel (AWS 4.3).

Humidified electrode

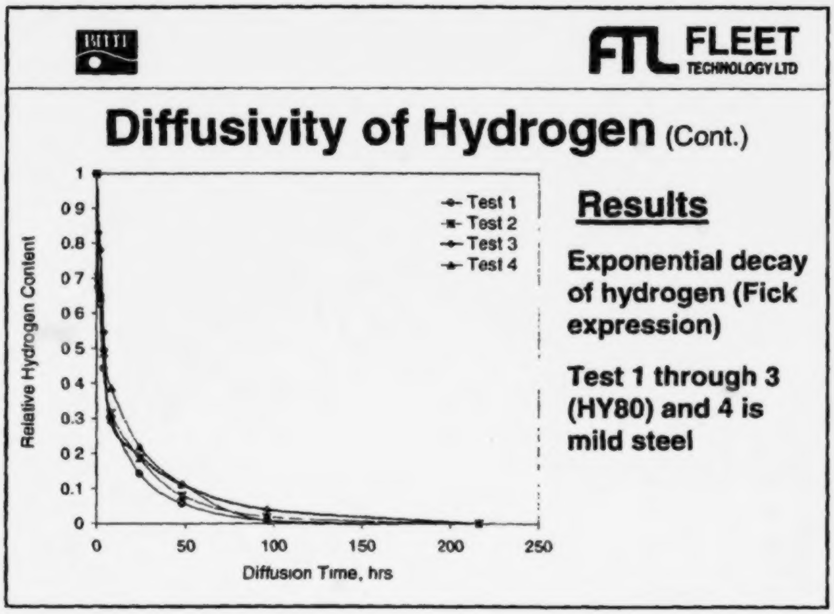

FTL FLEET TECHNOLOGY LTD

Diffusivity of Hydrogen (Cont.)

Results

Exponential decay of hydrogen (Fick expression)

Test 1 through 3 (HY80) and 4 is mild steel

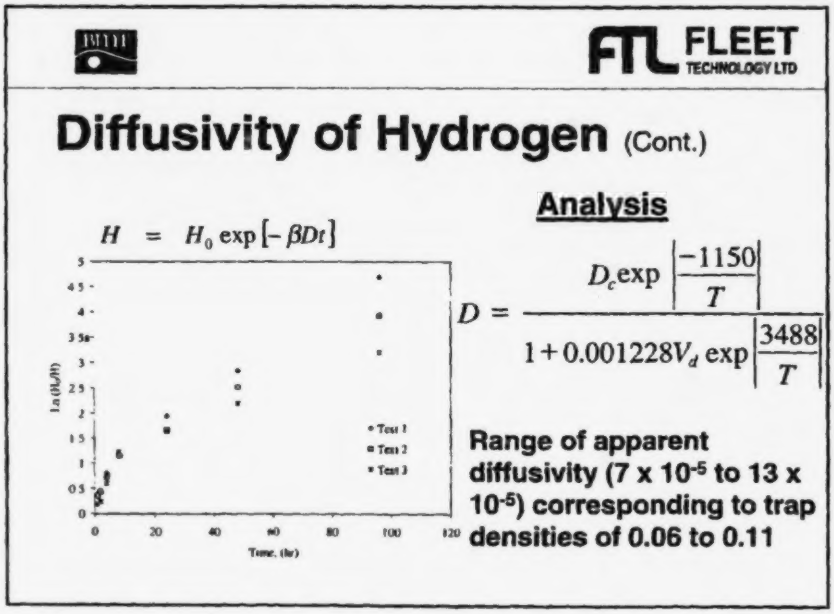

FTL FLEET TECHNOLOGY LTD

Diffusivity of Hydrogen (Cont.)

$$H = H_0 \exp\left[-\beta D t\right]$$

Analysis

$$D = \frac{D_c \exp\left|\frac{-1150}{T}\right|}{1 + 0.001228 V_d \exp\left|\frac{3488}{T}\right|}$$

Range of apparent diffusivity (7 x 10^{-5} to 13 x 10^{-5}) corresponding to trap densities of 0.06 to 0.11

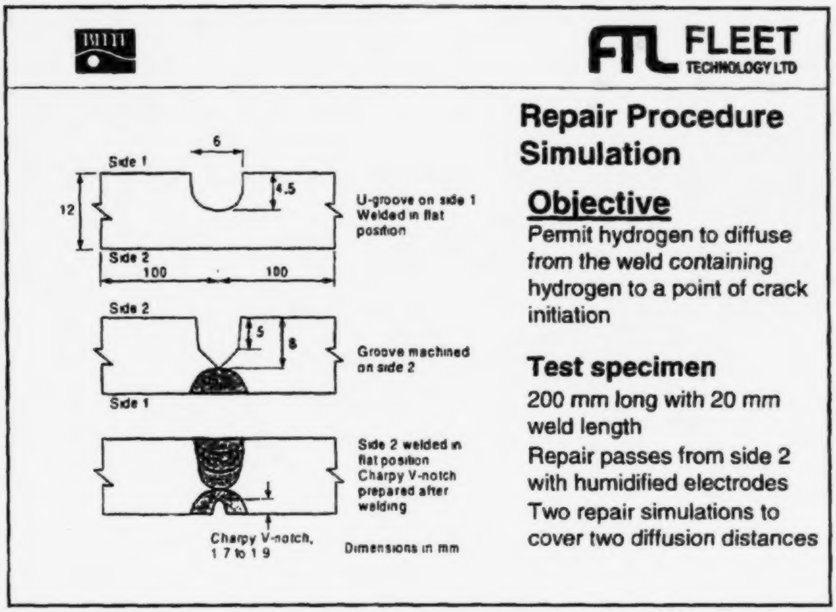
FTL FLEET TECHNOLOGY LTD
6
Side 1
4.5
12
U-groove on side 1 Welded in flat position
Side 2
100
100
Side 2
5
8
Groove machined on side 2
Side 1
Side 2 welded in flat position Charpy V-notch prepared after welding
Charpy V-notch, 1 7 to 1 9
Dimensions in mm

Repair Procedure Simulation

Objective

Permit hydrogen to diffuse from the weld containing hydrogen to a point of crack initiation

Test specimen

200 mm long with 20 mm weld length

Repair passes from side 2 with humidified electrodes

Two repair simulations to cover two diffusion distances

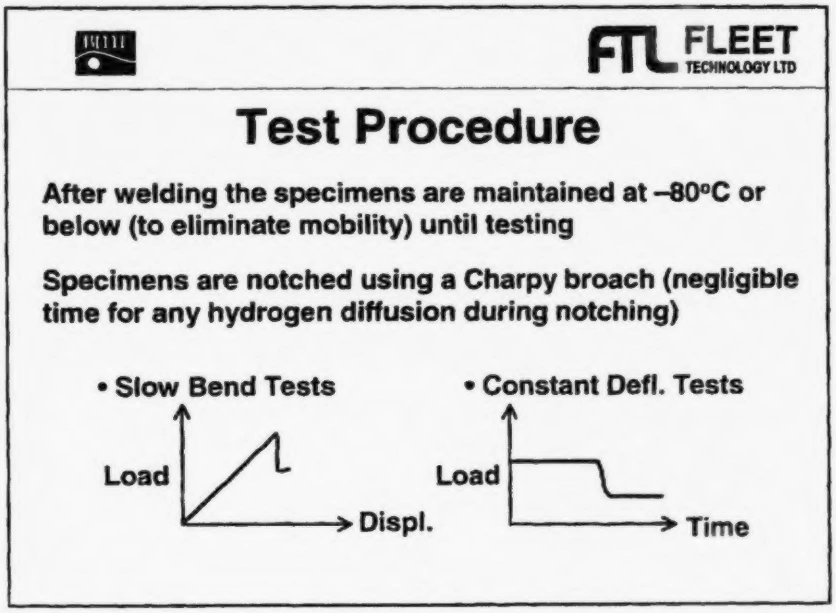
FTL FLEET TECHNOLOGY LTD
Load
Displ.
Load
Time

Test Procedure

After welding the specimens are maintained at –80°C or below (to eliminate mobility) until testing

Specimens are notched using a Charpy broach (negligible time for any hydrogen diffusion during notching)

- **Slow Bend Tests**
- **Constant Defl. Tests**

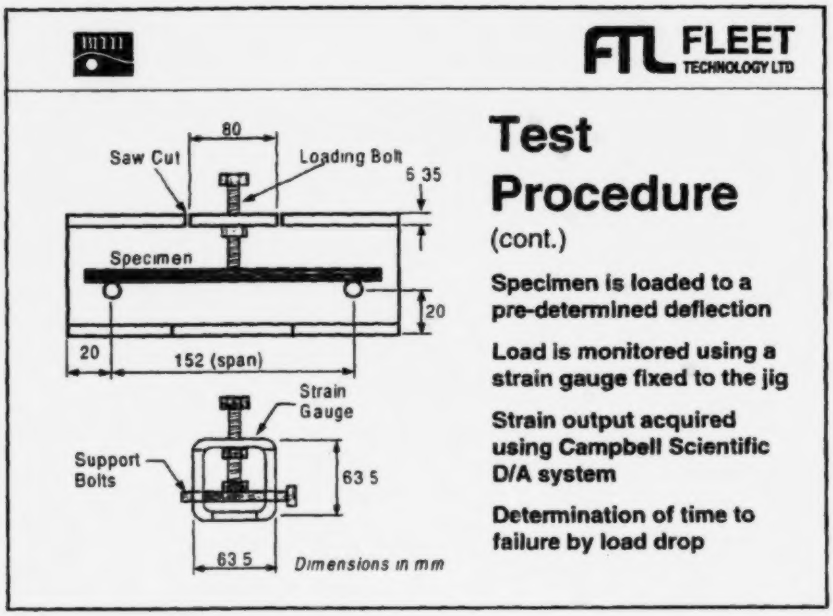
FTL FLEET TECHNOLOGY LTD
80
Saw Cut
Loading Bolt
6 35
Specimen
20
20
152 (span)
Strain Gauge
Support Bolts
63 5
63 5
Dimensions in mm

Test Procedure

(cont.)

Specimen is loaded to a pre-determined deflection

Load is monitored using a strain gauge fixed to the jig

Strain output acquired using Campbell Scientific D/A system

Determination of time to failure by load drop

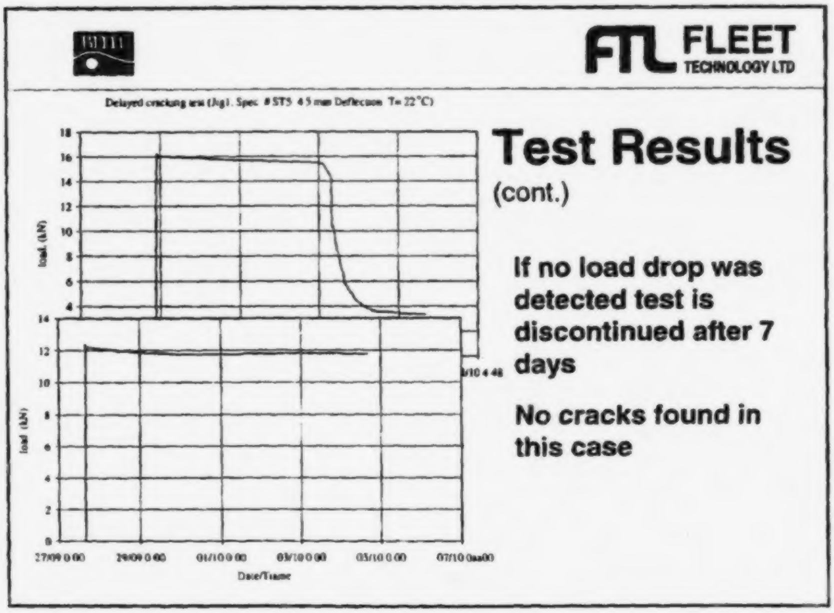

Test Results

(cont.)

If no load drop was detected test is discontinued after 7 days

No cracks found in this case

FLEET TECHNOLOGY LTD

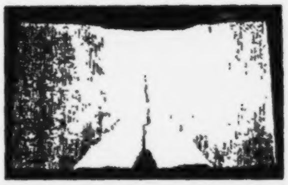

Test Results (cont.)

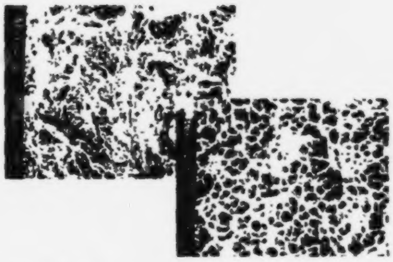

Hydrogen assisted cracking manifests both as quasi-cleavage and/or fine microvoids

FLEET TECHNOLOGY LTD

Concept of Delayed Cracking Time

Cracking occurs when hydrogen from the source diffuses to the site for cracking (below the Charpy notch) and reaches a critical value

At higher values of applied deflection, the critical hydrogen value is lower than at a lower deflection

Therefore for specific hydrogen level there needs to be a threshold deflection below which no cracking will occur.

This concept is used to experimentally determine the maximum delay time for cracking by gradually dropping the applied deflection until no cracking is observed.

FLEET TECHNOLOGY LTD

Prediction of Delayed Cracking

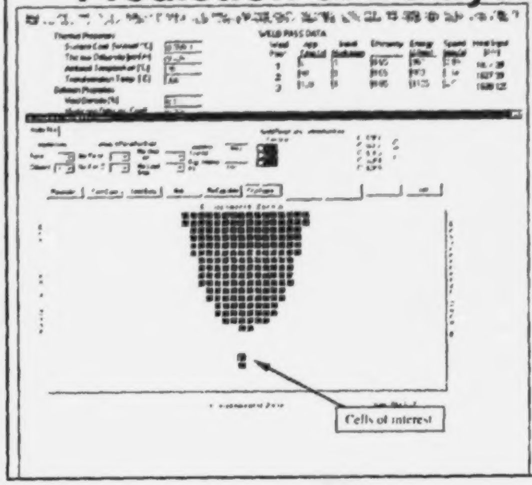

The hydrogen diffusion model

Shows the 3 pass repair simulation

Cell size is 0.5 mm

Relative hydrogen for each pass is unity

Cells where hydrogen level with time is of interest are shown

---

FLEET TECHNOLOGY LTD

Prediction of Delayed Cracking

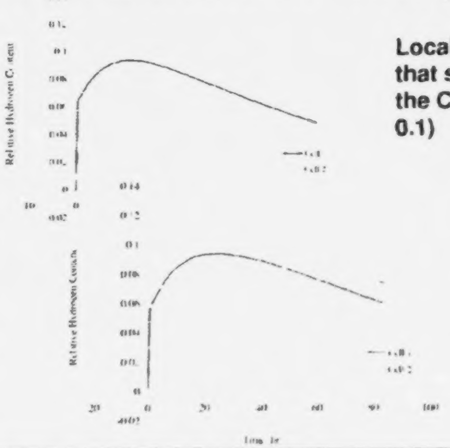

Local hydrogen level at two cells that span the region of the root of the Charpy notch (trap densities 0.1)

Two apparent diffusion rates that represents two trap densities (0.1 and 0.2).

The slower rate resulted in delay times representing the experimentally observed maximum delay for cracking.

FTL FLEET TECHNOLOGY LTD

Critical Hydrogen Curves

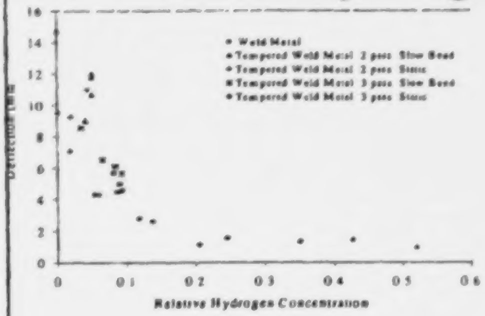

Obtained by combining model predictions and experiments.

Relative hydrogen concentration (abscissa) is from the model.

The deflection is from the experiments.

Displays a high sensitivity to hydrogen in the weld metal

Lower susceptibility due to tempering.

FTL FLEET TECHNOLOGY LTD

Concluding Remarks

Hydrogen effusion experiments performed on standard weld samples were used to determine hydrogen diffusivity.

The model was used to demonstrate the local hydrogen concentration build up and decay at a critical site in a bend specimen for two repair simulations resulting for two diffusion distances

The experimental results were compared with model predictions. The comparison showed that better agreement was obtained with hydrogen diffusivity corresponding to a trap density of 0.2 as in previous work

The relative hydrogen concentration from the model output showed the higher hydrogen susceptibility of the single pass, as-deposited weld metal (from slow bend tests) when compared with the tempered weld (in constant deflection tests)

FLEET TECHNOLOGY LTD

Recommendations

To extend the use of the critical hydrogen curve one has to calibrate the deflection (ordinate) to a stress value as then it would be independent of the specimen geometry.

The critical hydrogen curve is also a function of the material (microstructure). Therefore other susceptible materials associated with high strength submarine welds and HAZ are worthy of evaluation.

Diffusivity from effusion experiments resulted in higher values than those inferred from delayed cracking tests. Alternatives to the bead on plate weld, i.e. one more representative of the weld in the bend specimen is recommended for evaluation.

The above tasks will lead to a database that is necessary to develop more reliable repair procedures with reduced risk of cracking.

#516459 (14)

Crevice Corrosion Susceptibility of Mixtures of Monel and HY-80 Steel

by

Bob Klassen and Pierre Roberge

Dept. of Chem./Chem. Eng.
Royal Military College of Canada
Kingston, Ontario K7K 7B4

Abstract

The crevice corrosion characteristics of mixtures of monel and steel were studied. The technique used for characterizing crevice corrosion was recently developed at RMC. It consists of creating a crevice on the specimen by placing a block with a drilled hole on the surface and then galvanically connecting the specimen to a counter electrode. The current between the specimen and counter electrode is measured as well as the potential between the specimen and a reference electrode.

The main conclusion is that mixing monel with steel up to 5% increases the susceptibility to crevice corrosion and that further additions up to 10% reduces the susceptibility towards the level of virgin monel. There was one important exception to this trend. The sample with 8% steel addition was much higher than its neighbors in this series. One explanation is the passivation scale, that was evident in the scanning electron microscope micrographs for samples with greater than 2% steel, is unstable and subject to removal by processes that are not closely related to the percent iron in the metal. A secondary conclusion is that re-casting monel, without the addition of steel, changed the grain structure from round cells to a dendritic structure but this had no effect on its susceptibility to crevice corrosion.

It appears that a new technique for obtaining the polarization resistance of a sample has been developed. Polarization resistance is a widely accepted index of corrosion rate. The procedure, however, requires further theoretical analysis.

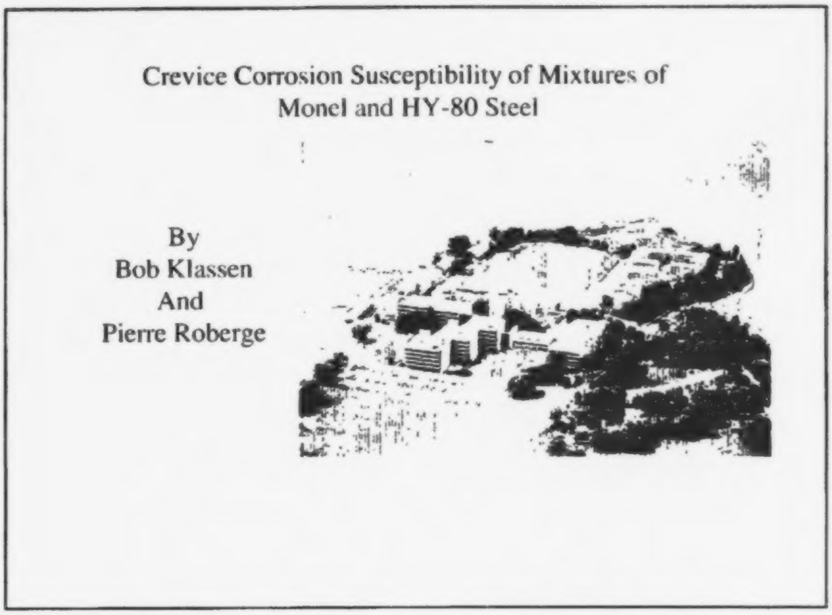

Crevice Corrosion Susceptibility of Mixtures of Monel and HY-80 Steel

By
Bob Klassen
And
Pierre Roberge

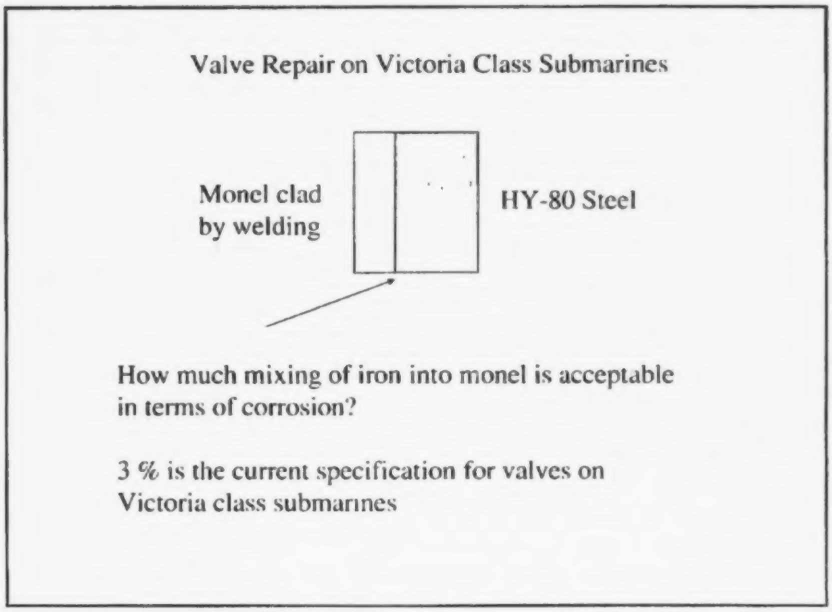

Valve Repair on Victoria Class Submarines

Monel clad
by welding

HY-80 Steel

How much mixing of iron into monel is acceptable in terms of corrosion?

3 % is the current specification for valves on Victoria class submarines

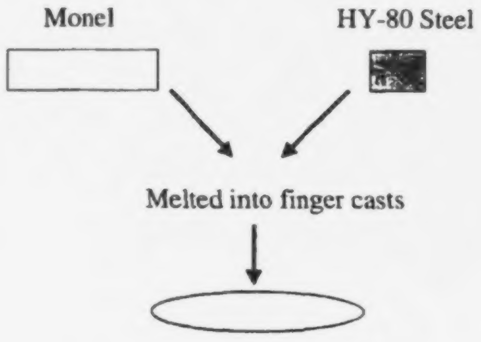

Monel

HY-80 Steel

Melted into finger casts

Series of cast samples, 0 to 10% steel
also virgin (not cast) monel

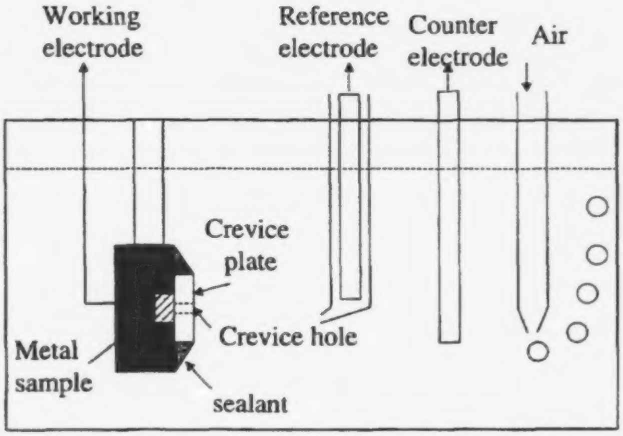
Working electrode
Reference electrode
Counter electrode
Air
Crevice plate
Crevice hole
Metal sample
sealant

Virgin monel, not re-cast

Nickel	65.1%
Copper	31.8%
Iron	1.3%
Silicon	0.5%
Mang.	1.2%

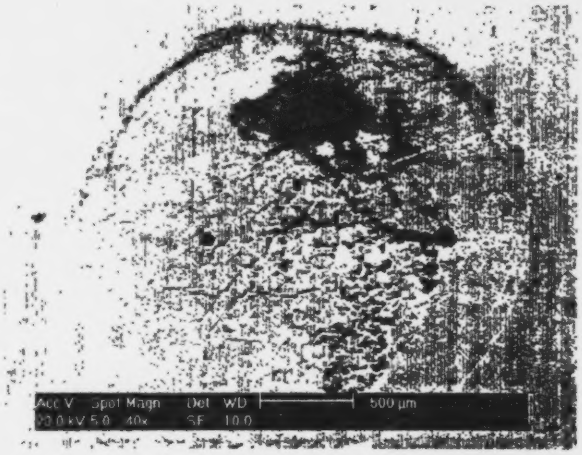
Acc.V Spot Magn Det WD
500 µm
20.0 kV 5.0 40x SE 10.0

Virgin monel, not re-cast

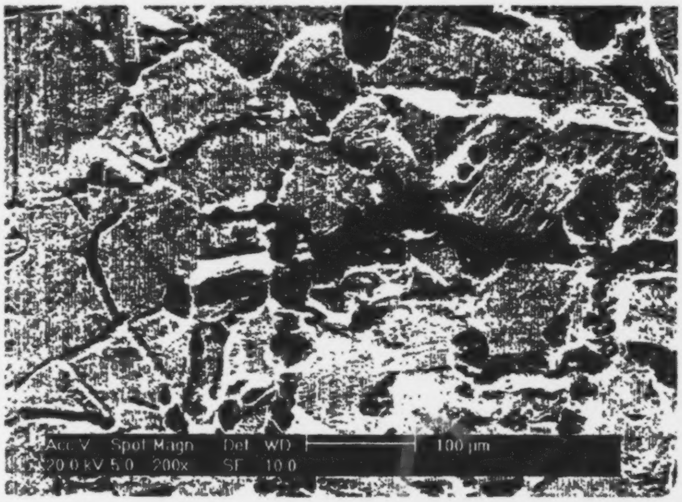
Acc.V Spot Magn Det WD
100 µm
20.0 kV 5.0 200x SE 10.0

Virgin monel, not re-cast

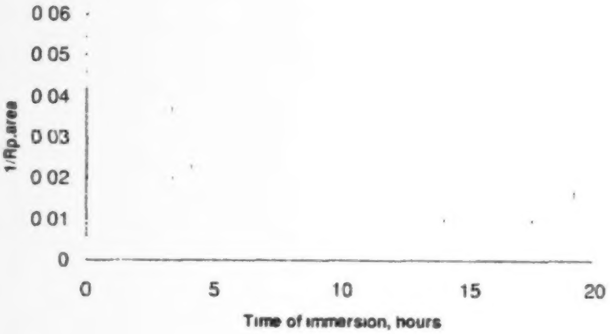

Re-cast monel, no steel added

Nickel	65.3%
Copper	31.6%
Iron	1.4%
Silicon	0.5%
Mang.	1.2%

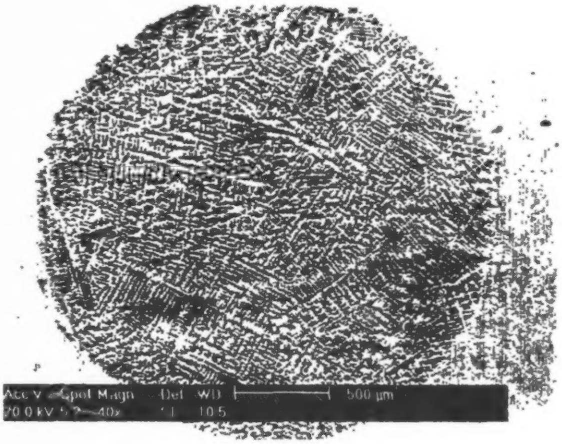
Acc.V Spot Magn Det WD
20.0 kV 40x 10.5
500 µm

Re-cast monel, no steel added

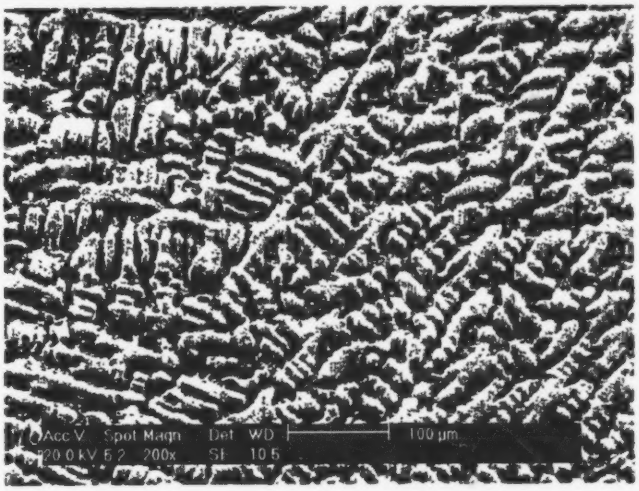
Acc.V Spot Magn Det WD
100 µm
20.0 kV 5.2 200x SE 10.5

Re-cast monel, no steel added

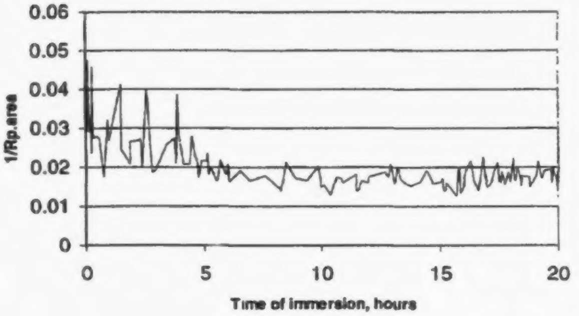

1 % Steel Mixed into Monel

Nickel	64.4%
Copper	30.7%
Iron	2.6%
Silicon	1.0%
Mang.	1.2%

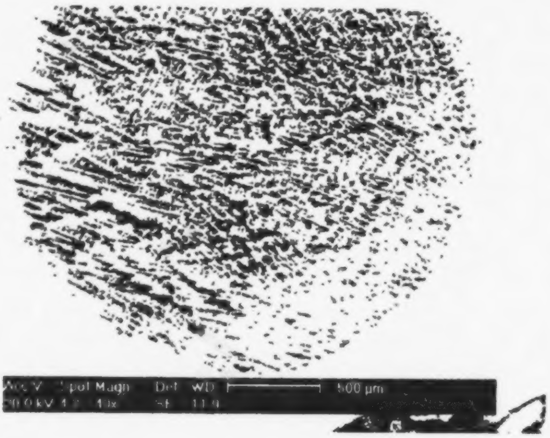
Acc.V Spot Magn Det WD 500 µm
20.0 kV 4.2 10x SE 11.9

1 % Steel Mixed into Monel

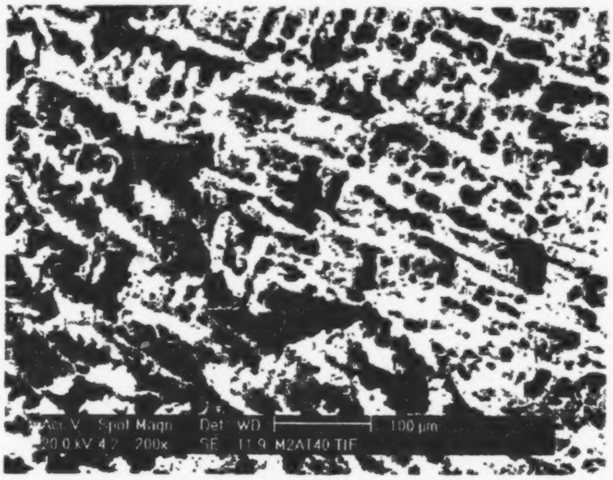
Acc.V Spot Magn Det WD 100 µm
20.0 kV 4.2 200x SE 11.9 M2A140.TIF

1 % Steel Mixed into Monel

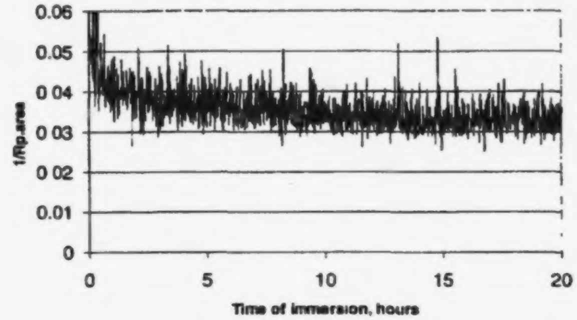

3 % Steel Mixed into Monel

Nickel 62.9%
Copper 30.7%
Iron 4.0%
Silicon 1.2%
Mang. 1.3%

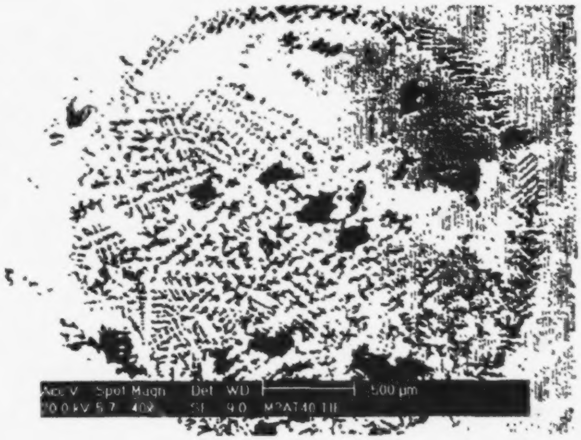
Acc.V Spot Magn Det WD
500 µm
20.0 kV 5.7 40x SE 9.0 M2AT40.TIF

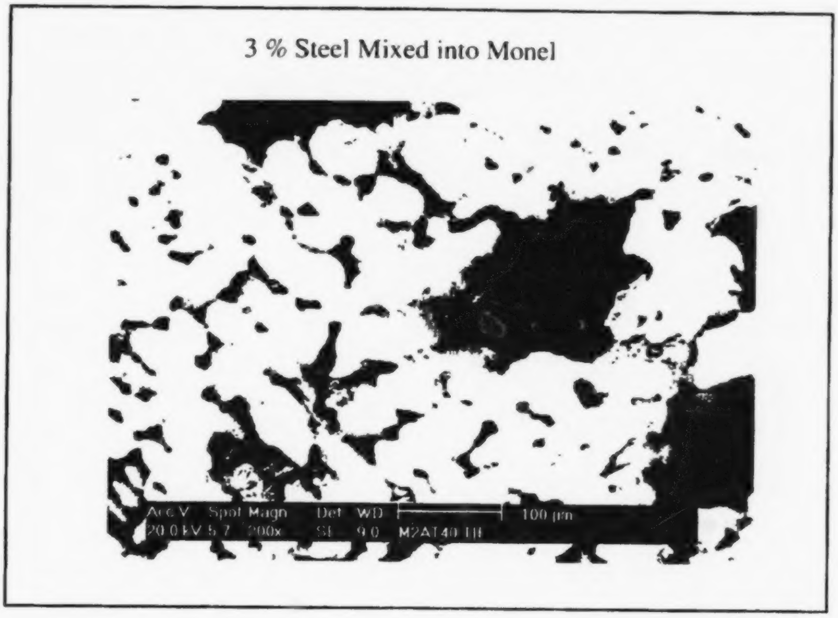
3 % Steel Mixed into Monel

Acc.V Spot Magn Det WD 100 µm
20.0 kV 5.7 200x SE 9.0 M2AT40.TIF

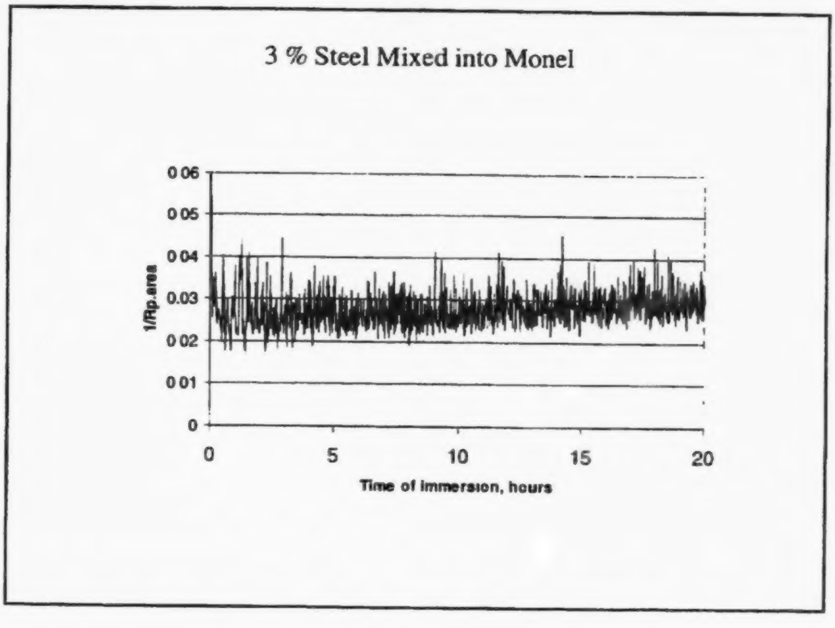
3 % Steel Mixed into Monel

4 % Steel Mixed into Monel

Nickel	61.5%
Copper	30.9%
Iron	5.7%
Silicon	0.8%
Mang.	1.1%

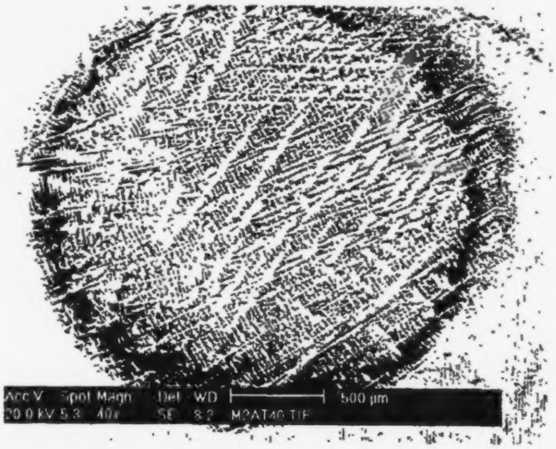
Acc.V Spot Magn Det WD
500 µm
20.0 kV 5.3 40x SE 8.2 M2AT40.TIF

4 % Steel Mixed into Monel

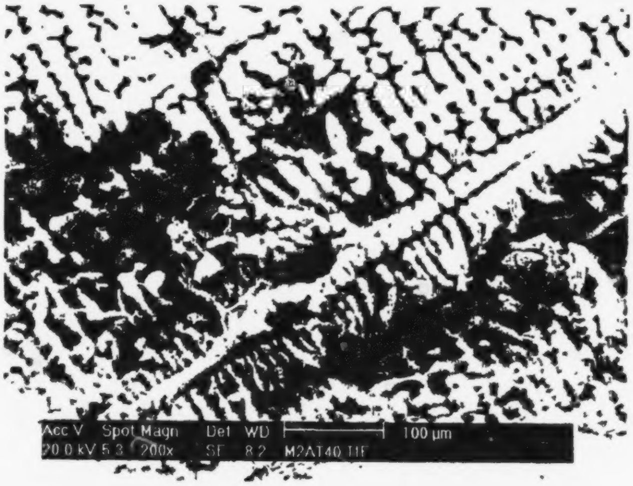
Acc.V Spot Magn Det WD
100 µm
20.0 kV 5.3 200x SE 8.2 M2AT40.TIF

4 % Steel Mixed into Monel

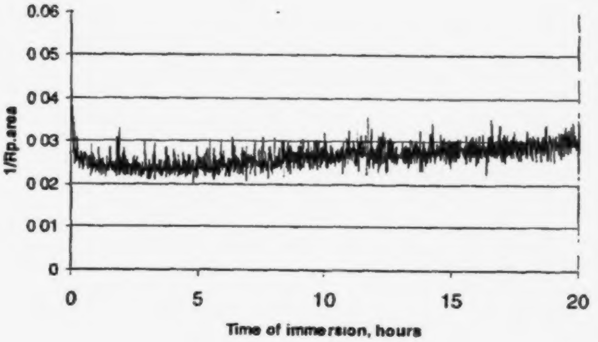

5 % Steel Mixed into Monel

Nickel	61.6%
Copper	29.6%
Iron	6.4%
Silicon	1.2%
Mang.	1.1%

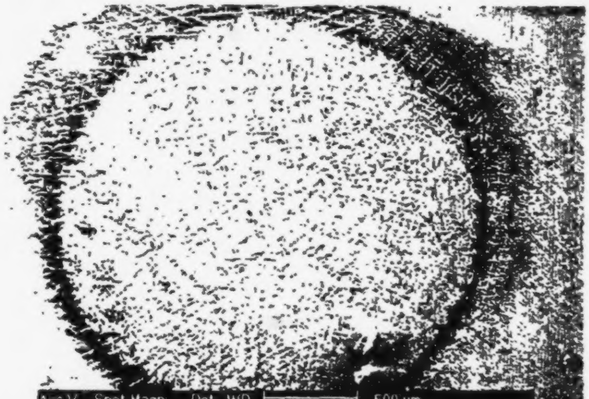
Acc.V Spot Magn Det WD 500 µm
20.0 kV 6.0 40x SE 10.3 M2AT40.TIF

5 % Steel Mixed into Monel

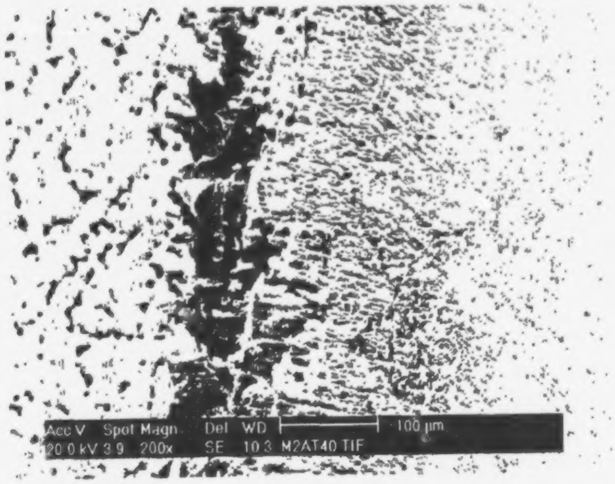
Acc V Spot Magn Det WD 100 µm
20 0 kV 3 9 200x SE 10 3 M2AT40 TIF

5 % Steel Mixed into Monel

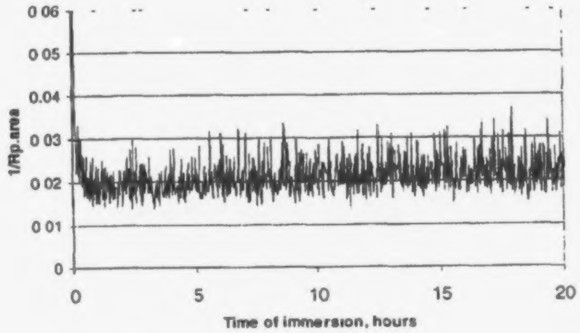

6 % Steel Mixed into Monel

Nickel	61.3%
Copper	29.1%
Iron	7.4%
Silicon	1.0%
Mang.	1.2%

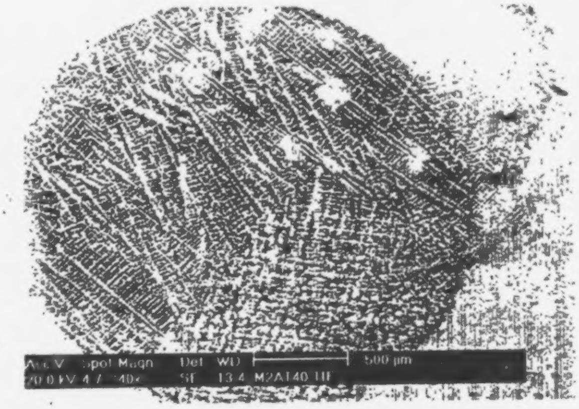
Acc.V Spot Magn Det WD 500 µm
20.0 kV 4.7 40x SE 13.4 M2A140 HF

6 % Steel Mixed into Monel

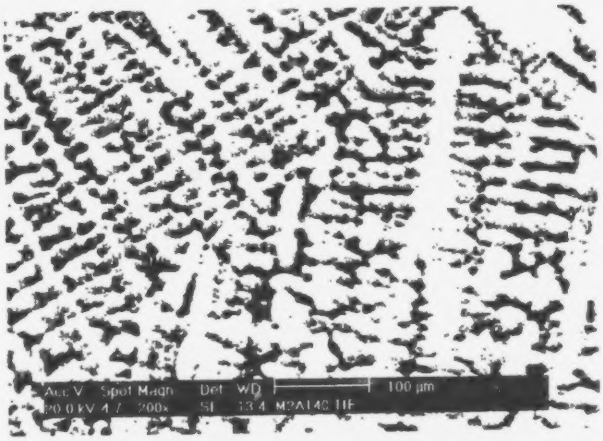
Acc.V Spot Magn Det WD 100 µm
20.0 kV 4.7 200x SE 13.4 M2A140 HF

6 % Steel Mixed into Monel

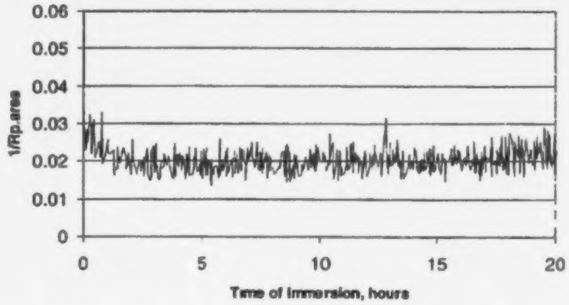

7 % Steel Mixed into Monel

Nickel 60.9%
Copper 29.2%
Iron 8.3%
Silicon 0.8%
Mang. 0.9%

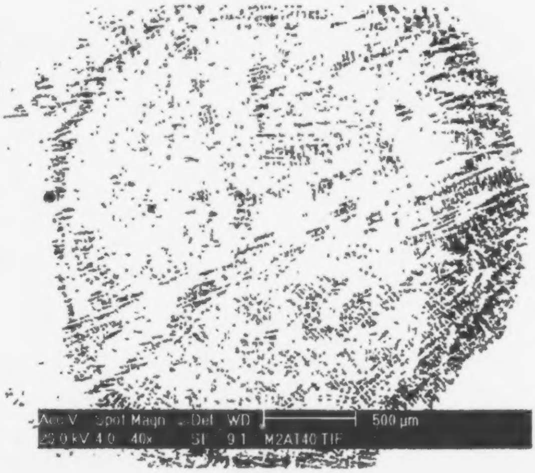
Acc.V Spot Magn Det WD
500 µm
25.0 kV 4.0 40x SE 9.1 M2AT40.TIF

7 % Steel Mixed into Monel

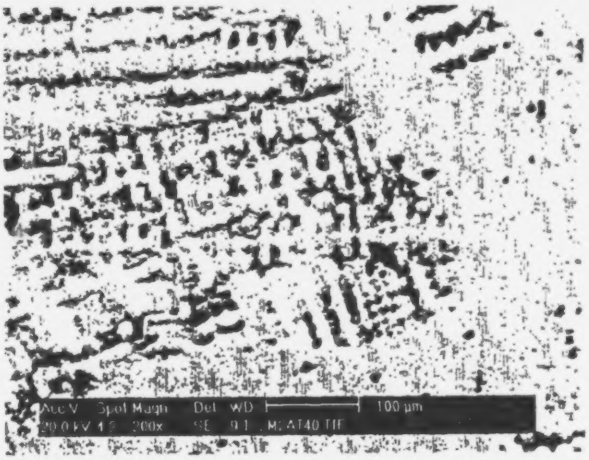
Acc.V Spot Magn Det WD 100 µm
20.0 kV 1.? 200x SE 9.1 M2AT40.TIF

7 % Steel Mixed into Monel

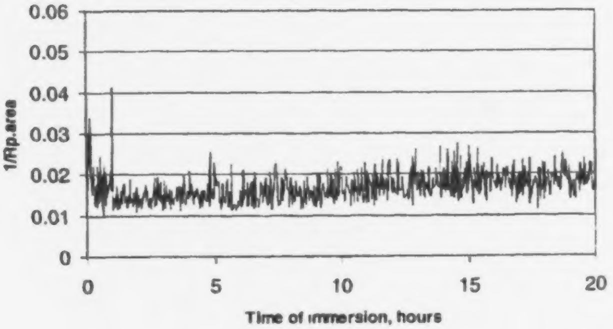

8 % Steel Mixed into Monel

Nickel	59.8%
Copper	29.2%
Iron	9.3%
Silicon	0.4%
Mang.	1.3%

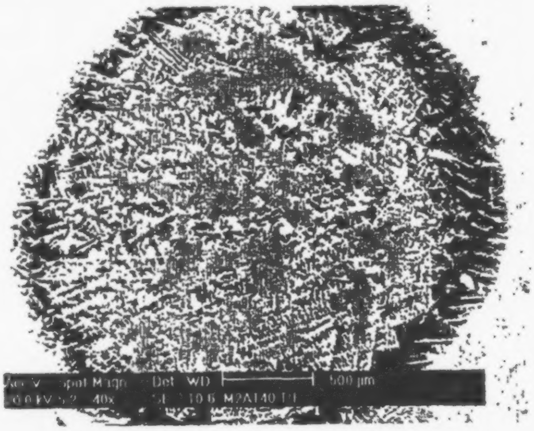
Spot Magn
Det
WD
500 µm
40x
10 6
M2A140

8 % Steel Mixed into Monel

Scale

Nickel	43.4%
Copper	24.4%
Iron	29.6%
Silicon	1.2%
Mang.	1.4%

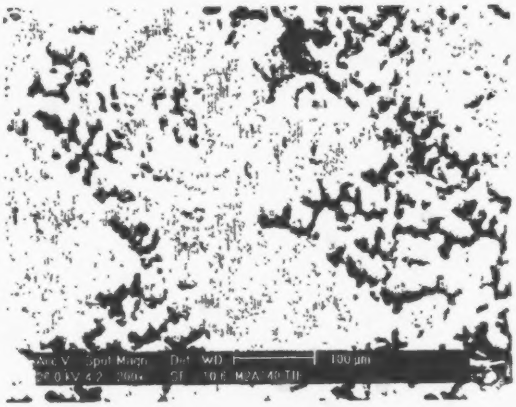
Acc V
Spot Magn
Det
WD
100 µm
4 2
SE
10 6

8 % Steel Mixed into Monel

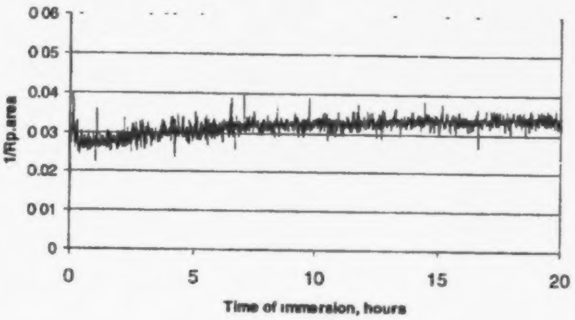

10 % Steel Mixed into Monel

Nickel	59.6%
Copper	28.5%
Iron	10.9%
Silicon	1.0%
Mang.	0.9%

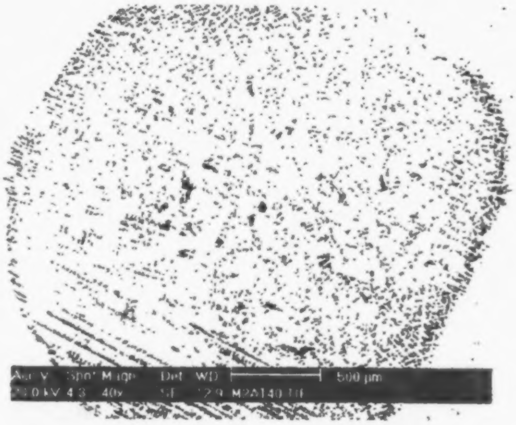
Acc.V Spot Magn Det WD
500 μm
20.0 kV 4.3 40x SE 12.9 M2A140.tif

10 % Steel Mixed into Monel

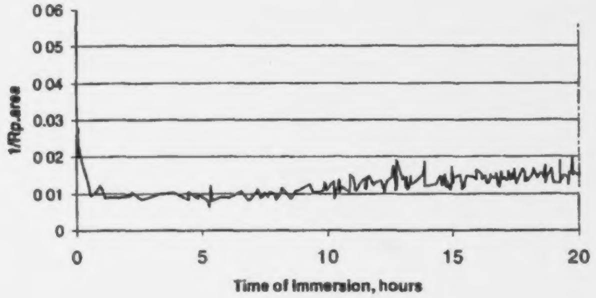

Corrosion Rate vs Iron content

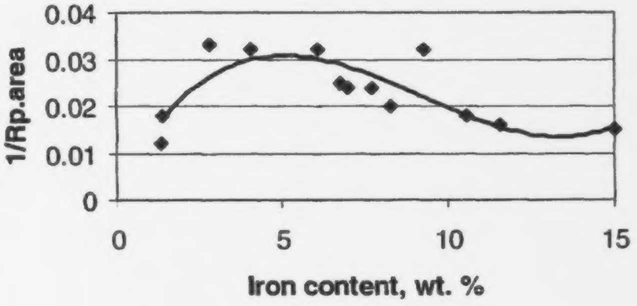

Fraction of area covered by scale and the corrosion rate per unit of unscaled area

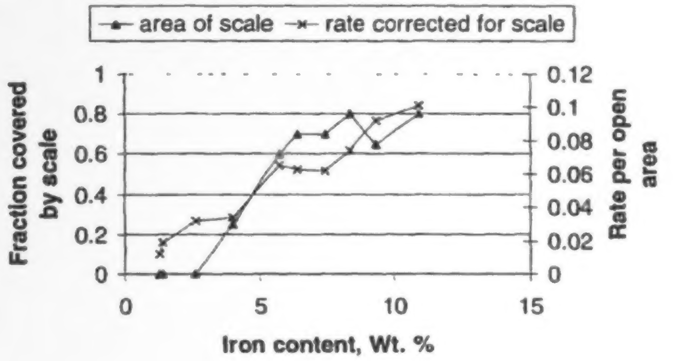

Conclusions

- No advantage to restricting the mixing steel into monel to 3% or less.
- The susceptibility to crevice corrosion peaks at 2-4% steel addition and usually deceases with increasing steel content.
- An unstable, iron-rich scale provides some protection at steel additions greater than 4%.

#516 460 (45)

Crack-tip Blunting and Fracture Resistance of a Ship Plate Steel

by G. Shen*, S. Xu*, J. Morrison and W.R. Tyson***
*** Materials Technology Laboratory (MTL), Natural Resources Canada**
**** Dockyard Laboratory Pacific (DLP), Dept. of National Defence**

Abstract

Fracture resistance curves for a structural steel suitable for ship plate have been measured using single-edge-notch bend (SENB) samples with a/W values of 0.2, 0.5 and 0.7. Supporting calculations using the finite element method (FEM) have been performed, with special attention to the blunting behaviour.

It has been verified, in agreement with other work, that fracture resistance increases with decreasing constraint, i.e. with decreasing a/W over the range of a/W studied in this work. Also, the blunting line slope has been found to depend on constraint, i.e. on yield stress, work hardening coefficient, and a/W. FEM results show that the slope coefficient M varies between the value recommended in ASTM standards (M=2) and that recommended by the European Structural Integrity Society, ESIS (M=4 for the material of this work), but the value is significantly closer to the ESIS figure.

Stretch-zone-width (SZW) measurements have been made on the fracture surfaces. Difficulty was experienced in deriving a reliable value of SZW because of the subjective nature of the determination of the stretch zone in this steel. In particular, if the stretch zone is defined so as to exclude all tearing features such as voids, then a highly conservative result is found for the tearing initiation toughness. This suggests that it may be preferable to define toughness by fitting the resistance curve with a power-law equation and reporting a value of J or CTOD at a chosen value of crack growth, e.g. 0.2 mm, without distinguishing between blunting and tearing contributions to this growth.

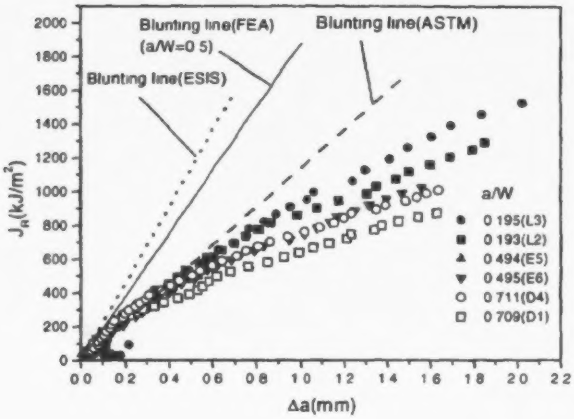

Fig. 1 J-resistance curves for SENB samples

It was found in Fig.1 (the measured J_R curves for SENB sample with different a/W) that the samples with shallow cracks have much higher J resistance than that with deep cracks.

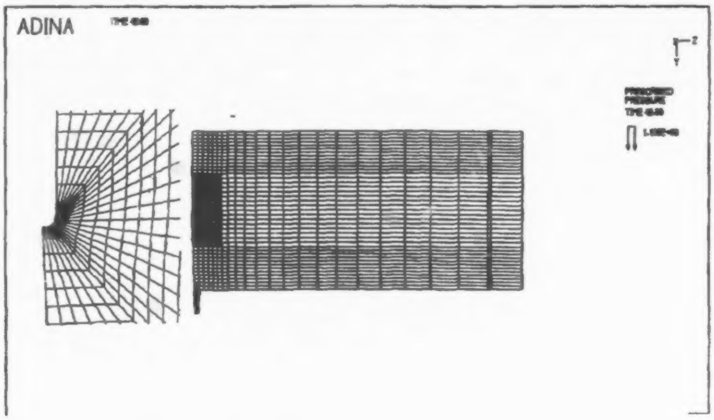

Fig. 2 Finite element mesh used in the calculation and the deformed crack tip mesh

In Fig.2, it is seen the shape of deformed crack tip is closed to a semi-cycle. Therefore, a relevant definition of crack tip opening displacement (δ_t) was used. It is given in Fig.3. This definition was also used to define crack blunting ($\delta_t = 2\Delta a$).

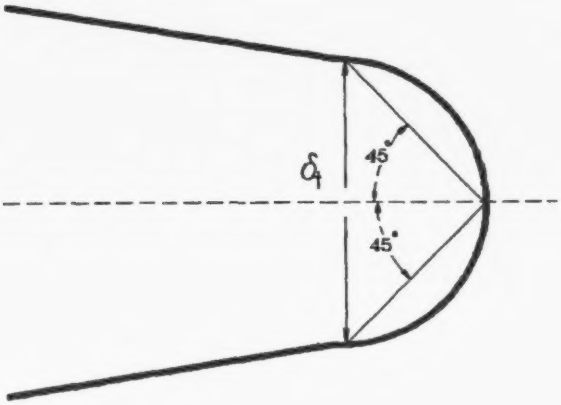

Fig.3 Definition for crack tip opening displacement (δ_t)

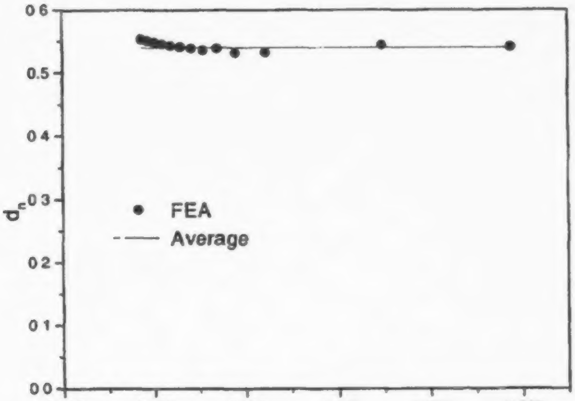

Fig. 4 d_n as a function of normalized J-integral, calculated for actual σ-ε data

In Fig.4, a parameter (d_n) relating the J-integral with CTOD is given. Parameter d_n was calculated by FEA for a SENB sample made of the structural steel CSA G40.21 350WT with a/W=0.5. By using parameter d_n, J-integral and Δa was related and a parameter M(a/W, n) was used to show the slope of a blunting (J-Δa) line.

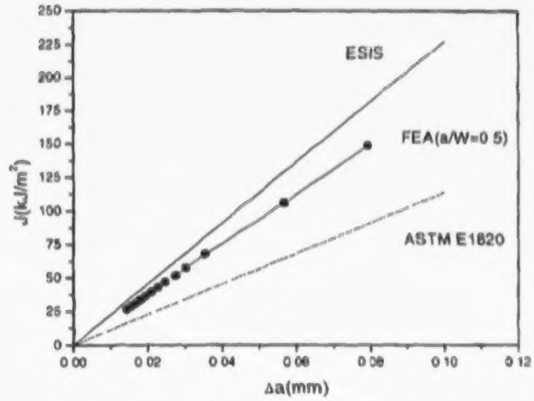

Fig. 5 Blunting line for SENB geometry (a/W=0.5); FEA results calculated using the actual stress-strain data

Fig.5 gives the blunting lines calculated by FEA for a SENB sample with a/W=0.5 and with the material property of the structural steel CSA G40.21 350WT at –30°C (M=3.3) and that given by ASTM 1820(M=2) and by ESIS (M=4). The calculated value is close to that given by ESIS.

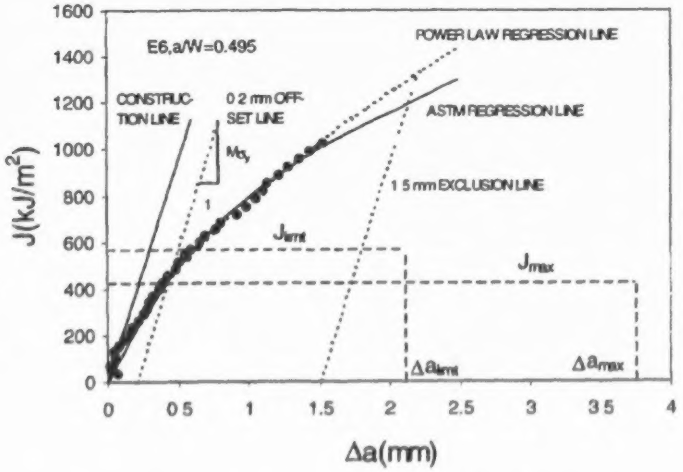

Fig. 6 Resistance curve for sample E6 analysed according to ASTM E 1820

Fig.6 gives resistance curve for sample E6 analysed according to ASTM standard E 1820.

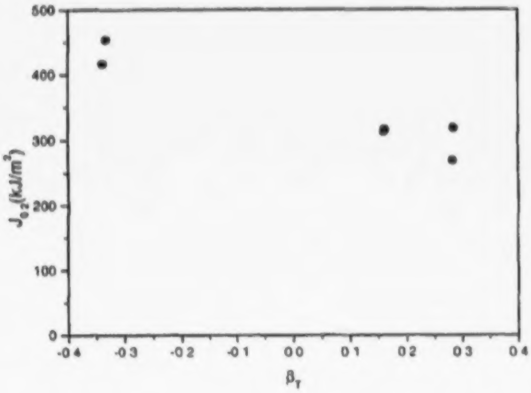

Fig. 7 $J_{0.2}$ vs β_T for SENB samples with different a/W

Fig. 7 shows that the J-resistance (at 0.2 mm crack growth) of samples with different crack depths can be correlated by elastic constraint parameter β_T.

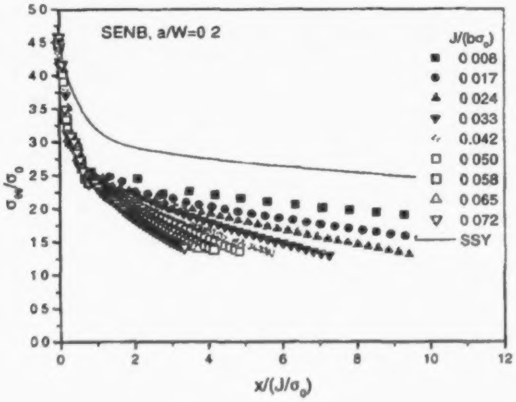

Fig. 8 Normalized crack opening stress as a function of normalized distance from crack tip, a/W=0.2

Fig.8 shows the normalized crack opening stress as a function of normalized distance from crack tip for a SENB sample, a/W=0.2 and the crack tip stress of small scale yielding (SYY) solution. It is seen that the normalized stress at fracture control region ($X/(J/\sigma 0)=2$) of the shallow crack is much lower than that of SYY.

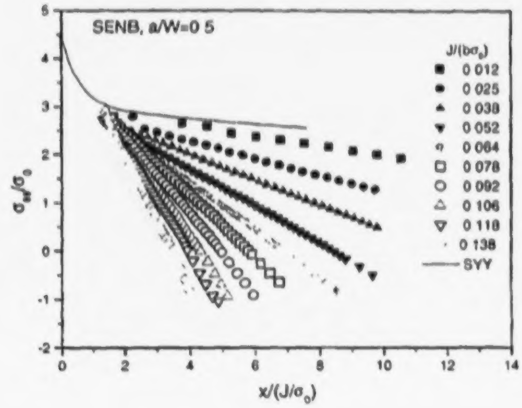

Fig. 9 Normalized crack opening stress as a function of normalized distance from crack tip, a/W=0.5

Fig. 9 is the same figure as Fig. 8, but for a deep crack, a/W=0.5. It is seen that the normalized stress at fracture control region (X/(J/σ0)=2) of the deep crack is close to that of SYY when J-integral is not too high.

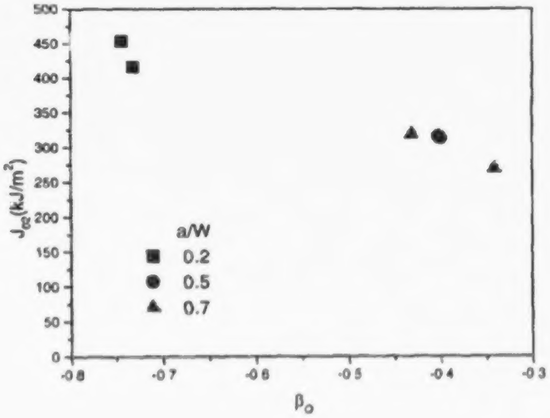

Fig. 10 $J_{0.2}$ as a function of β_Q for SENB samples

Fig. 10 shows that the J-resistance (at 0.2 mm crack growth) of samples with different crack depths can be correlated by plastic constraint parameter β_Q.

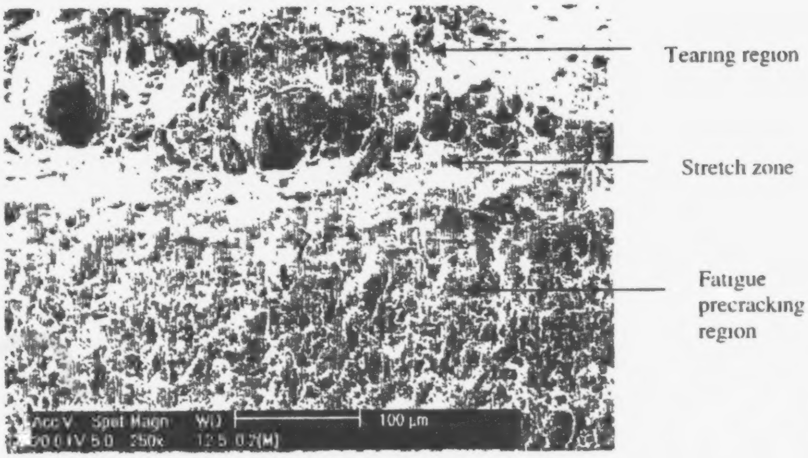
Tearing region
Stretch zone
Fatigue precracking region
Acc.V Spot Magn WD
20.0 kV 5.0 250x 12.5 0.7(M)
100 µm

Fig. 11 SEM fractograph of fatigue precracked region, stretch zone and tearing region near mid-width of sample L2 (a/W=0.2)

Fig. 11 shows SEM fractograph of fatigue precracked region, stretch zone and tearing region near mid-width of sample L2 (a/W=0.2). The SZW was found to be very small – less than 0.1 mm. It was also difficult to define the stretch zone boundaries unambiguously.

Conclusions

The following conclusions can be drawn from the experiments and finite element analyses:

1) Blunting line analysis was conducted by calculating the J-integral and crack tip opening displacement using the finite element method. The results from calculations conducted in the present study agreed with those given by EPRI. The slope of the blunting line for a deep crack ($a/W=0.5$) and a medium-hardening material ($n\approx10$, $\varepsilon_0\approx0.00245$) was found to correspond to $M= J/(\sigma_Y a)\cong3.3$, which lies between values recommended by ASTM E 1820 ($M=2$) and by ESIS ($M=4$ for the present material).
2) The slope of the blunting line $M\sigma_Y$ is a function of material properties (yield stress and strain hardening coefficient) and of constraint. M decreases with increasing strain hardening coefficient n at constant a/W and decreases with decreasing a/W at constant n.
3) The crack tip stress field of a shallow crack is significantly lower than that of small scale yielding under the same applied driving force. The difference increases with increasing applied stress. The crack tip stress field of a deep crack is close to that of small scale yielding under the same applied driving force when the applied crack driving force is small. However, it is lower than that of SSY when the applied load is large.
4) Shallow cracks have significantly higher J-resistance than deep cracks. The J-resistance of SENB samples with different crack depth was well correlated by either β_T, related to the T-stress, or by β_Q , related to the Q parameter.
5) The SZW was found to be very small – less than 0.1 mm – for the present material. However, it was difficult to define the stretch zone boundaries unambiguously. Contrary to expectation, no dependence of SZW on a/W was found; in particular, the SZW was not found to be larger at $a/W=0.2$ than at $a/W=0.5$ or 0.7.

#516461 (46)

Investigation of Plastic Zone Development in Dynamic Tear Test Specimens

by

T.S. Koko[1], B.K. Gallant[1] and J.R. Matthews[2]

[1] Martec Limited, 400-1888 Brunswick Street, Halifax, NS, Canada, B3J 3J8
[2]Dockyard Laboratory Atlantic, Defence Research Establishment Atlantic, P.O. Box 99000, Stn Forces, Bldg D17, Halifax, N.S., B3K 5X5

Abstract

This paper presents on-going investigations on plastic zone development in dynamic tear (DT) type three-point bend specimens used to measure the fracture toughness of marine structural materials. The purpose of the study is to use finite element technology to provide an understanding of the plastic zone development, to determine the upper limit of temperature relative to full size transition curves where elastic plastic fracture becomes invalid. In earlier studies, the authors utilized 2-D finite element models to compute the ratio of crack tip blunting (stretch zone) to plastic zone size (radius) that is used to determine the elastic-plastic fracture toughness. Those studies established the feasibility, as well as limitations, of 2-D finite element modeling for computing the plastic zone development in DT specimens.

In the present study we present efforts geared towards improving the 2-D modeling, as well as investigations into the use of 3-D models to provide estimates of the shear lip size. The ABAQUS finite element software was used to model the elastic-plastic behavior of the specimens. The DT specimen was made of 350WT steel and the crack was induced by pressing the notch, followed by fatigue cracking at a limit load level of 40% of the specimen limit load. The specimen was loaded until fixed amounts of permanent deformation were recorded. Results were obtained in the form of plots, showing the progression of the plastic zone around the crack tip. For each case, the results provide the following: mid point plastic deflection, stretch zone width, plastic zone radius, and shear lip size. The finite element results obtained and how these compare to the experiments in elastic plastic testing are discussed.

ON PLASTIC ZONE DEVELOPMENT IN DYNAMIC TEAR-TYPE TEST SPECIMENS

BY
T.S. KOKO[1], B.K. GALLANT[1] and J.R. MATTHEWS[2]

[1]MARTEC LIMITED, HALIFAX, NS
[2]DREA, DOCKYARD LAB., P O BOX 99000, HALIFAX, NS

PRESENTED AT 9TH CF/CRAD MEETING ON
NAVAL APPLICATIONS OF MATERIALS TECHNOLOGY
HALIFAX, NS, JUNE 7, 2001

Martec Limited
Advanced Engineering and Research Consultants

Outline

- BACKGROUND
- PROBLEM DESCRIPTION
- FINITE ELEMENT MODEL
- RESULTS
- SUMMARY AND CONCLUSIONS

Martec Limited
Advanced Engineering and Research Consultants

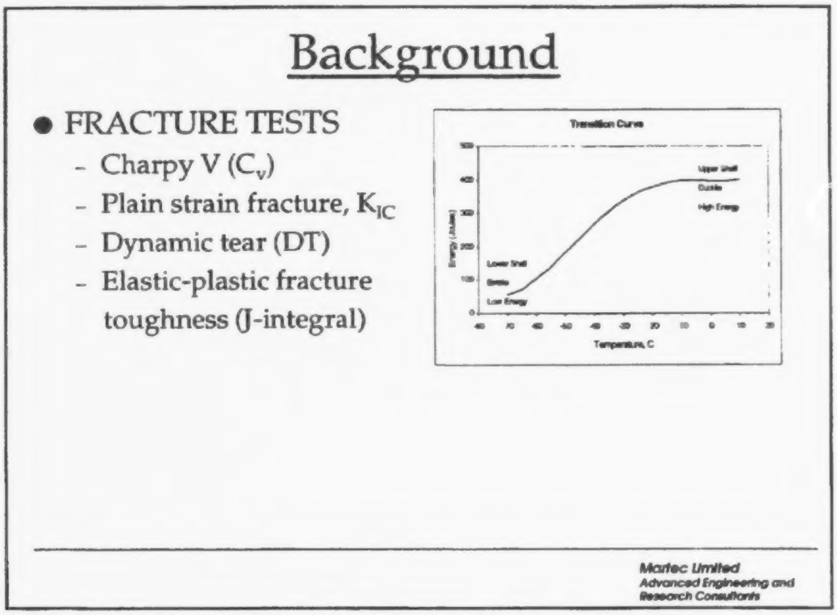
Transition Curve
Energy (Joules)
500
400
300
200
100
0
-80
-70
-60
-50
-40
-30
-20
-10
0
10
20
Temperature, C
Upper Shelf
Ductile
High Energy
Lower Shelf
Brittle
Low Energy

Background

- FRACTURE TESTS
  - Charpy V (C_v)
  - Plain strain fracture, K_{IC}
  - Dynamic tear (DT)
  - Elastic-plastic fracture toughness (J-integral)

Martec Limited
Advanced Engineering and Research Consultants

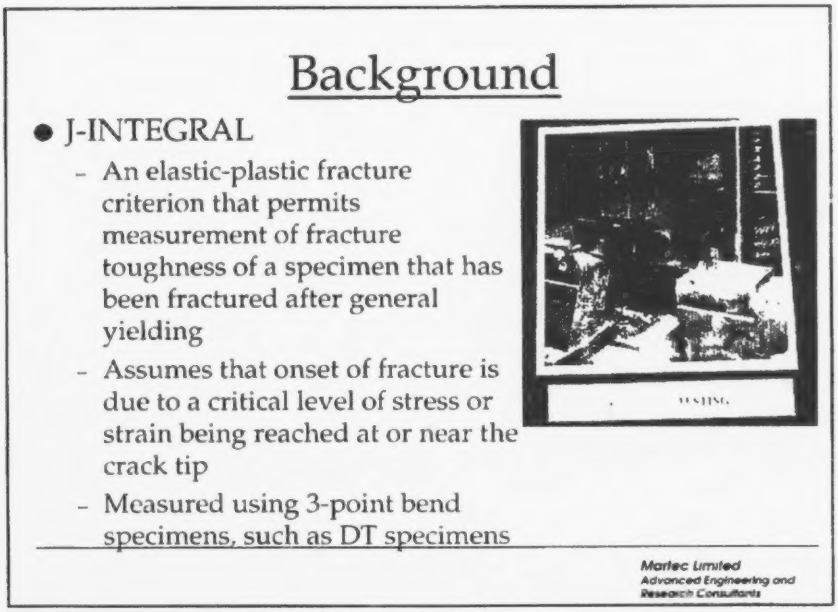

Background

- J-INTEGRAL
  - An elastic-plastic fracture criterion that permits measurement of fracture toughness of a specimen that has been fractured after general yielding
  - Assumes that onset of fracture is due to a critical level of stress or strain being reached at or near the crack tip
  - Measured using 3-point bend specimens, such as DT specimens

Martec Limited
Advanced Engineering and Research Consultants

Background

Definitions:

r_y=Plastic zone radius
Szw = stretch zone width
s = shear lip size

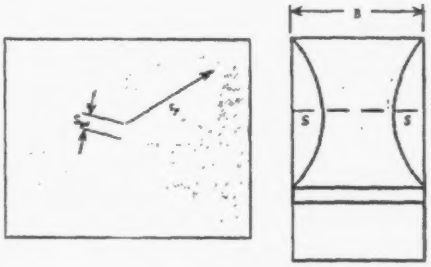

Background

- Definitions:
  - Stretch Zone Width (*SZW*): Distance from crack tip to interface of yield zone with side of crack

$$S_{ZW} = J/(2\sigma_{flow})$$

  - Plastic Zone Radius (*PR*): Maximum extent of plastic zone
  - Ratio: $\beta = r_y / S_{ZW}$
  - Shear-lip size: Distance from the yield surface to original surface on side of specimen (*s*). Assumed to be equal to the critical r_y.

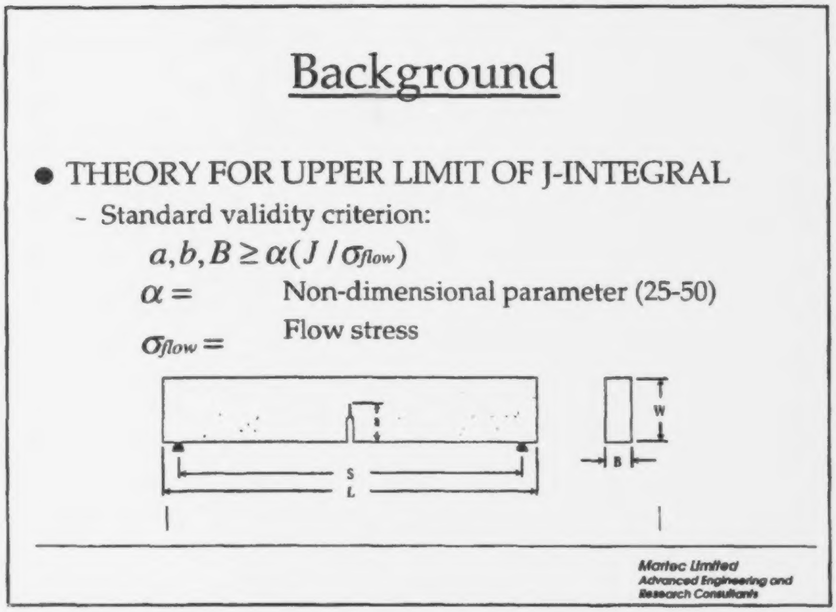

Background

- THEORY FOR UPPER LIMIT OF J-INTEGRAL
  - Standard validity criterion:

$$a,b,B \ge \alpha(J / \sigma_{flow})$$

$\alpha =$ Non-dimensional parameter (25-50)

$\sigma_{flow} =$ Flow stress

Martec Limited
Advanced Engineering and
Research Consultants

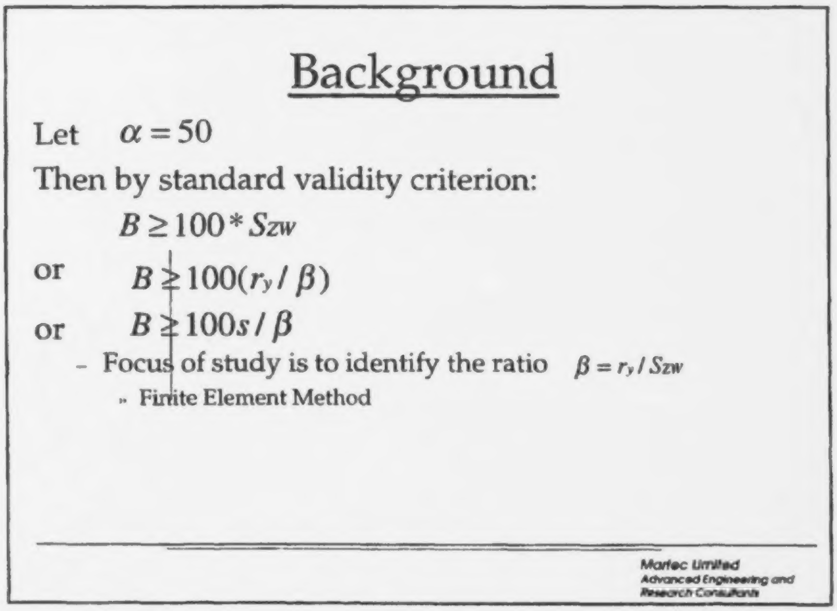

Background

Let $\alpha = 50$

Then by standard validity criterion:

$$B \ge 100 * S_{ZW}$$

or $B \ge 100(r_y / \beta)$

or $B \ge 100s / \beta$

- Focus of study is to identify the ratio $\beta = r_y / S_{ZW}$
  - Finite Element Method

Martec Limited
Advanced Engineering and
Research Consultants

Objectives

- Investigate The Plastic Zone Development in DT Test Specimens
  - To provide an understanding of the ratio of the plastic zone size (radius) to crack tip blunting (stretch zone)
  - To determine the upper limit where elastic plastic fracture becomes invalid

Objectives

- Scope of this presentation
  - Influence of material models
  - Specimen geometry
  - Influence of mesh configuration
  - 3-D modeling

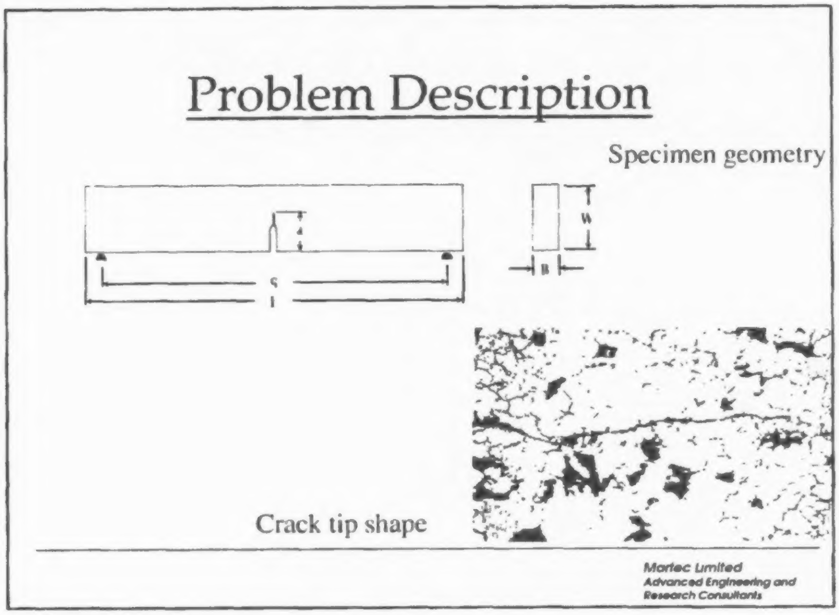

Problem Description

Specimen geometry

Crack tip shape

Problem Description

Dimensions	Specimen		
	Standard DT	Non-Standard	DT with 1" x 2" Bar
Beam Length, L (mm)	181 00	125 00	225 00
Beam Span, S (mm)	164 00	100 00	200 00
Crack Length, a (mm)	14 00*	12 50**	14 00*
Beam Width, W (mm)	41 00	25 00	50 00
Beam Thickness, B (mm)	8 00	12 50	25 00

- Standard DT and non-standard specimens under quasi-static loading
- 350WT and 304 stainless steel materials
- Crack tip shape is that of a fatigue crack, followed by a blunted fatigue crack
- Require plastic zone development using FE analysis

Finite Element Model

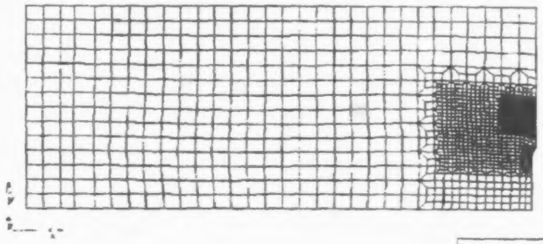

Typical FE Mesh for half of beam

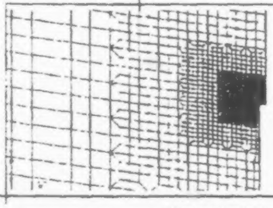

Detailed mesh the around crack tip

Martec Limited
Advanced Engineering and Research Consultants

Finite Element Model

- Highlights of FE Model:
  - Assumes symmetry
  - Geometry of crack carefully modeled
  - Mesh consists of 4000 quad elements (2-D model)
  - Smallest element size approx. 0.1×10^{-3} mm near crack tip
  - ABAQUS FE code utilized
  - Large displacement, large strain, elastic-plastic formulations
  - Load applied as displacement at center of beam
  - Incremental analysis procedure (> 5000 increments typical)

Martec Limited
Advanced Engineering and Research Consultants

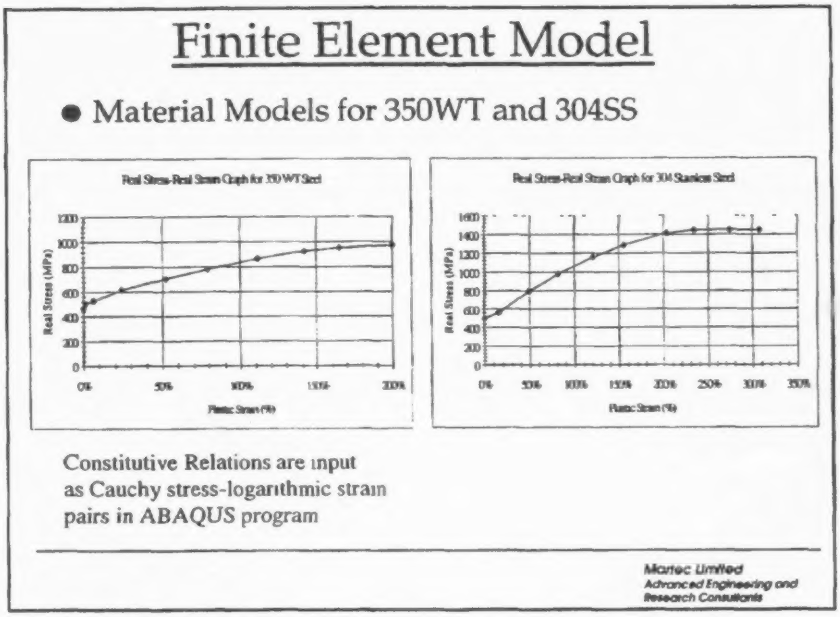

Finite Element Model

- Material Models for 350WT and 304SS

Constitutive Relations are input
as Cauchy stress-logarithmic strain
pairs in ABAQUS program

Martec Limited
Advanced Engineering and
Research Consultants

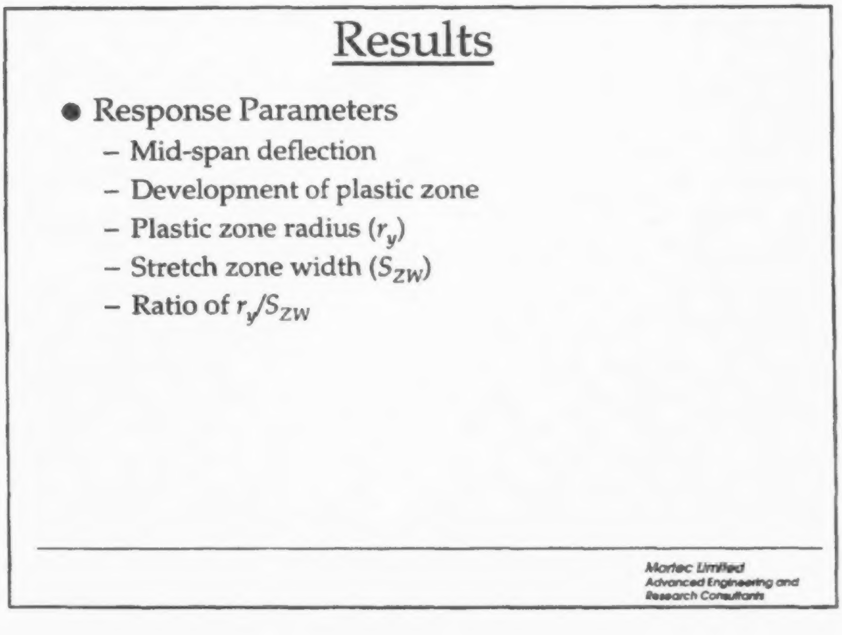

Results

- Response Parameters
  - Mid-span deflection
  - Development of plastic zone
  - Plastic zone radius (r_y)
  - Stretch zone width (S_{ZW})
  - Ratio of r_y/S_{ZW}

Martec Limited
Advanced Engineering and
Research Consultants

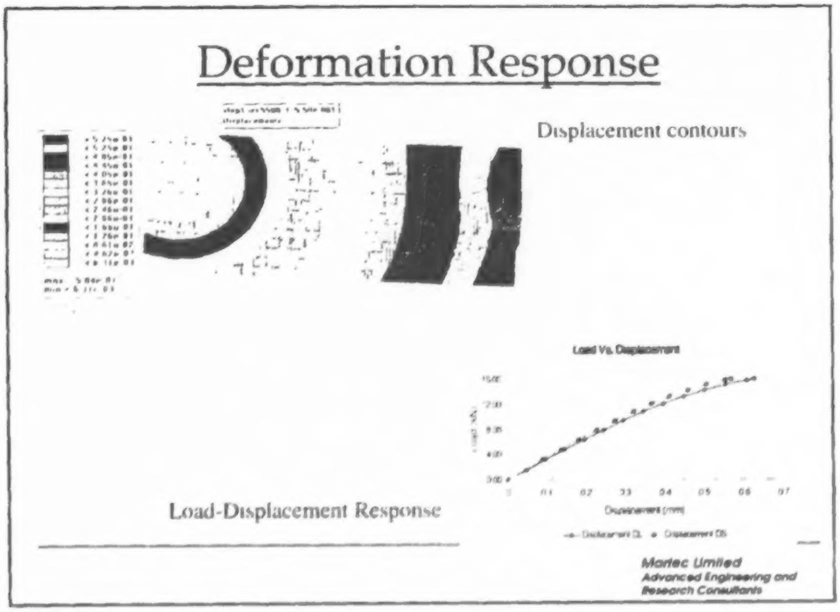

Deformation Response

Displacement contours

Load-Displacement Response

Load Vs. Displacement
0.1
0.2
0.4
0.5
0.6
0.7
Displacement (mm)

Martec Limited
Advanced Engineering and Research Consultants

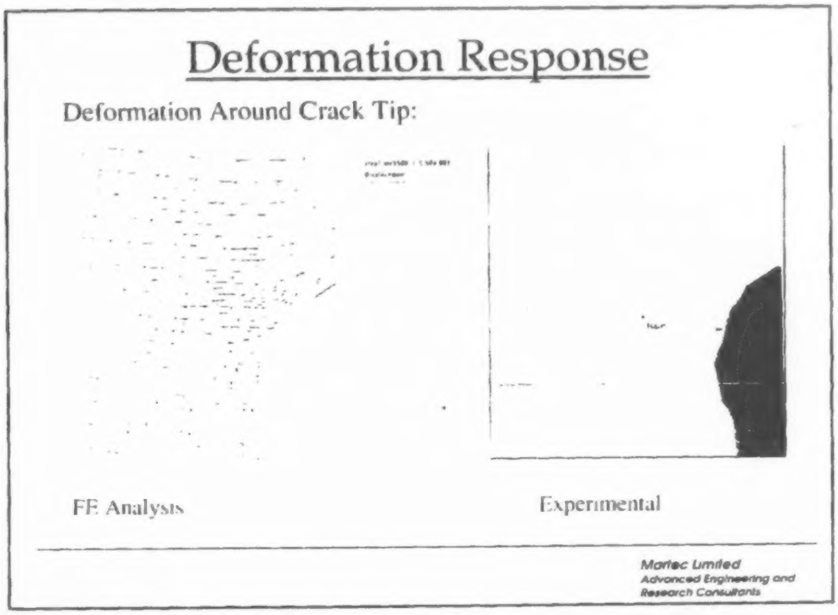

Deformation Response

Deformation Around Crack Tip:

FE Analysis

Experimental

Martec Limited
Advanced Engineering and Research Consultants

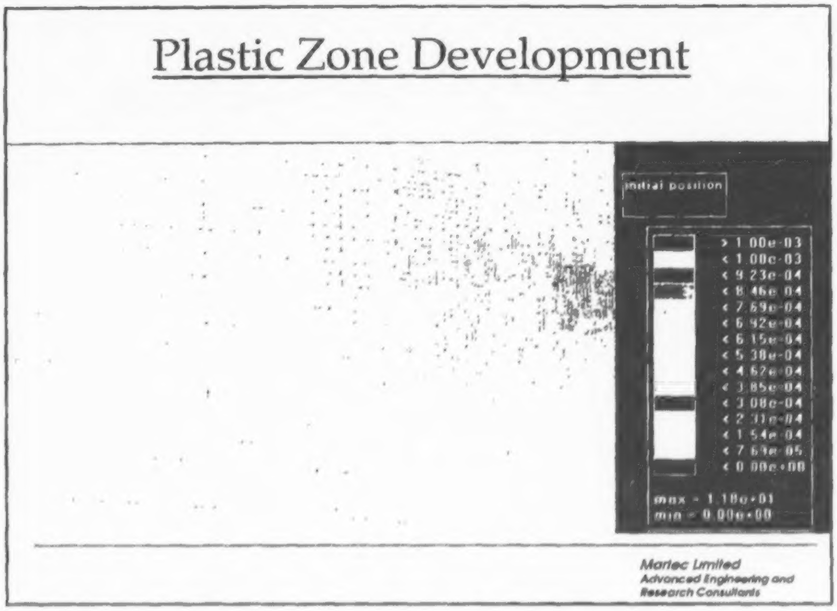

Plastic Zone Development

Martec Limited
Advanced Engineering and Research Consultants

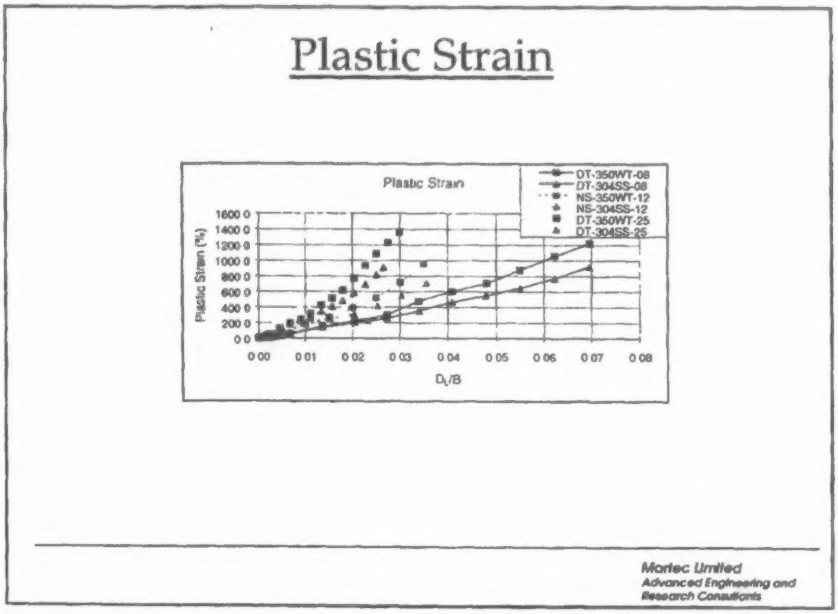

Plastic Strain

Martec Limited
Advanced Engineering and Research Consultants

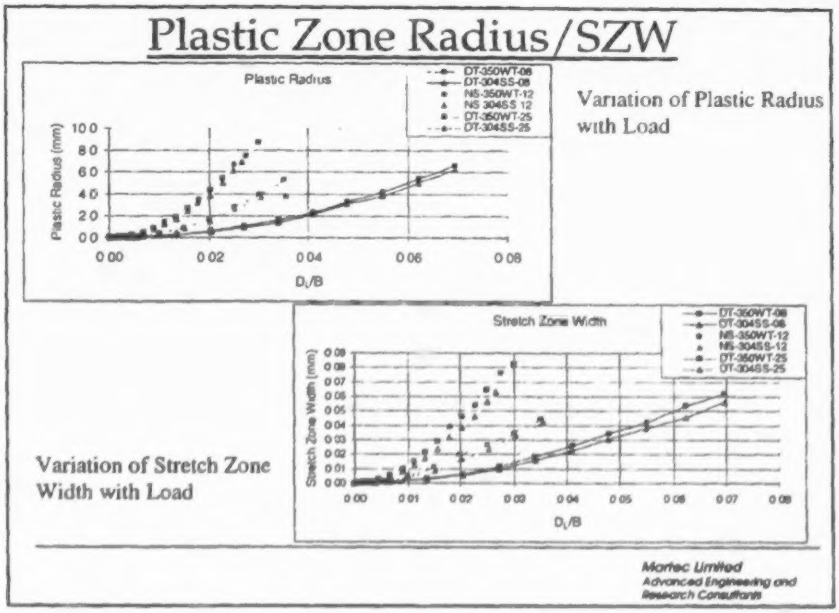

Plastic Zone Radius/SZW

Variation of Plastic Radius with Load

Variation of Stretch Zone Width with Load

Martec Limited
Advanced Engineering and Research Consultants

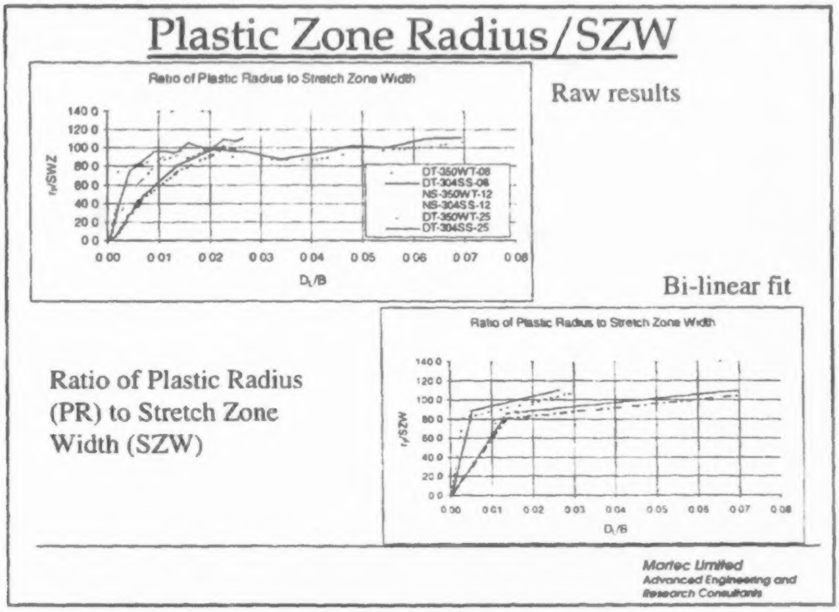

Plastic Zone Radius/SZW

Raw results

Bi-linear fit

Ratio of Plastic Radius (PR) to Stretch Zone Width (SZW)

Martec Limited
Advanced Engineering and Research Consultants

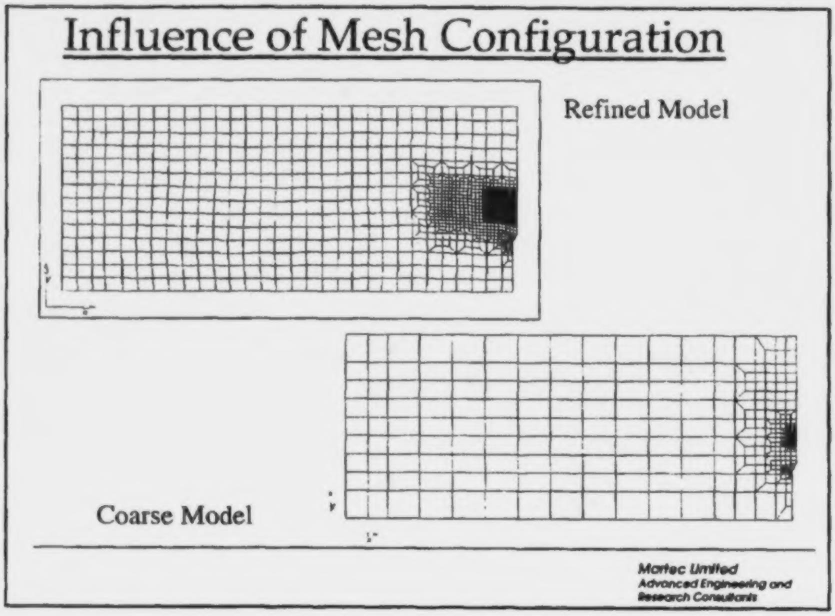

Influence of Mesh Configuration

Refined Model

Coarse Model

Martec Limited
Advanced Engineering and Research Consultants

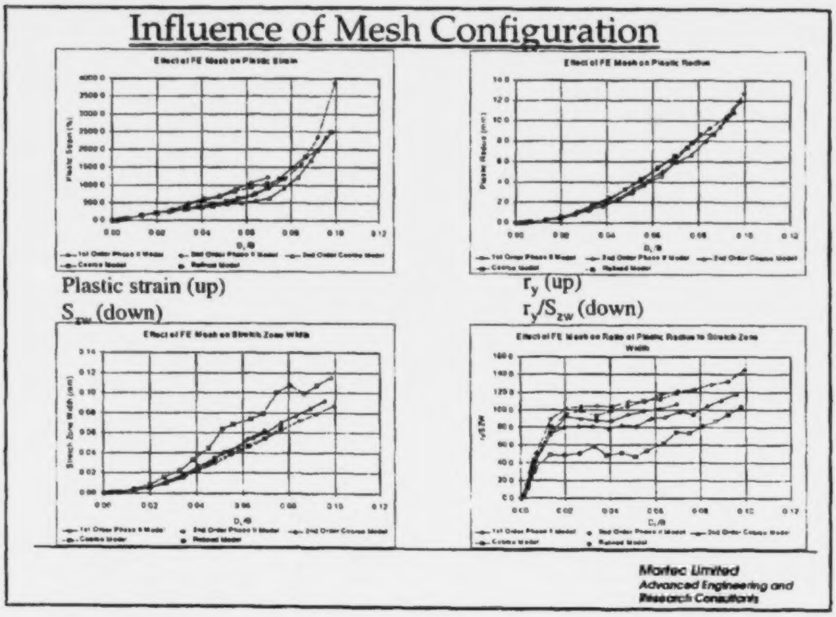

Influence of Mesh Configuration

Plastic strain (up)
S_{zw} (down)

r_y (up)
r_y/S_{zw} (down)

Martec Limited
Advanced Engineering and Research Consultants

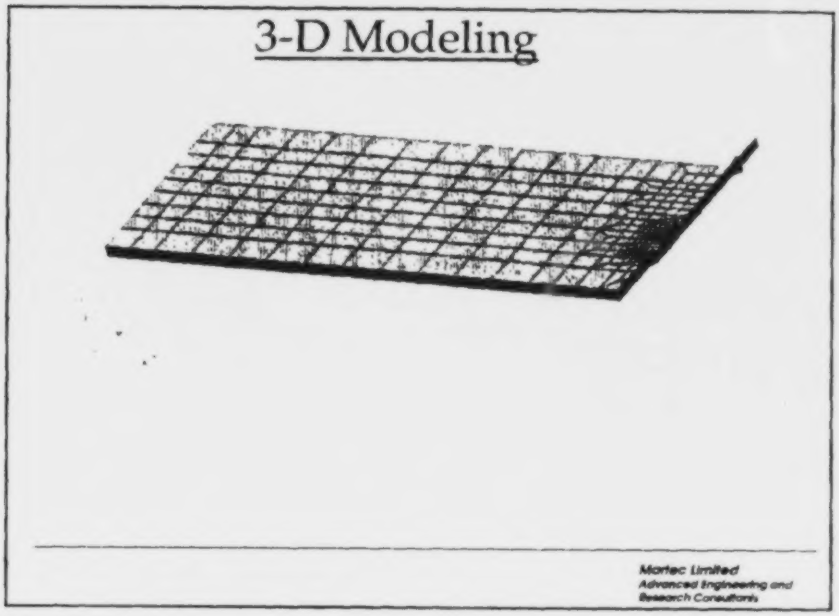

3-D Modeling

Martec Limited
Advanced Engineering and Research Consultants

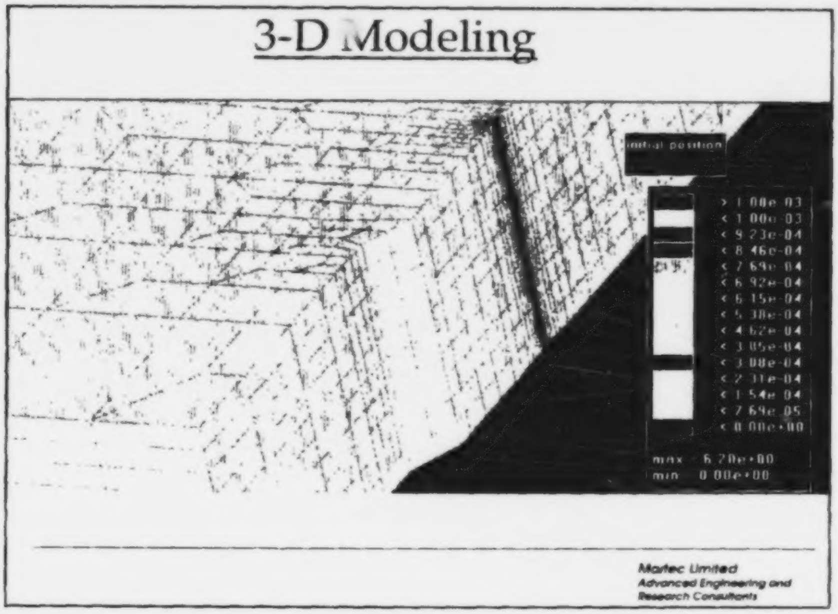

3-D Modeling

initial position
> 1.00e-03
< 1.00e-03
< 9.23e-04
< 8.46e-04
< 7.69e-04
< 6.92e-04
< 6.15e-04
< 5.38e-04
< 4.62e-04
< 3.85e-04
< 3.08e-04
< 2.31e-04
< 1.54e-04
< 7.69e-05
< 0.00e+00
max 6.20e+00
min 0.00e+00

Martec Limited
Advanced Engineering and Research Consultants

Summary & Conclusions

- Presented FE analysis of development of plastic zone in DT test specimens (350WT and 304 SS materials)
- Maximum plastic strain, plastic zone radius (r_y) and S_{ZW} increase parabolically with load
- Maximum plastic strain, r_y and S_{ZW} increase with specimen thickness (for given D_L/B)
- Ratio r_y/SZW increases with plasticity and exhibit bilinear behaviour

Summary & Conclusions

- Ratio r_y/SZW
  - increases with plasticity and exhibit bilinear behaviour
  - is affected by mesh configuration

#516462 (47)

Production and Maintenance of Nickel Aluminium Bronze Submarine Seawater System Castings

By J. Bird

Former Head of Materials Technology
Directorate of Naval Architecture, Procurement Executive,
UK Ministry of Defence

ABSTRACT

With the transfer of the Victoria Class (UK Upholder class) submarines to Canada there will be a requirement to maintain the NAB submarine seawater system castings in a serviceable condition. Consequently it will be necessary to replace some castings due to degradation in service. This paper describes the modern techniques used in the UK to manufacture NAB components, the methods employed to confirm the integrity of the castings and where acceptable the means to reclaim flawed castings. In addition the paper details the methods used to examine castings which show evidence of selective phase corrosion in service, the main cause of the degradation of NAB castings in submarine seawater systems. Also described are the Validation and Revalidation procedures used to ensure new NAB castings are acceptable for service in seawater systems and NAB castings which have seen prolonged service are acceptable for continued service.

INTRODUCTION

The Canadian government is replacing their ageing O & P fleet with the more modern, former UK Upholder class submarines, Upholder, Unseen, Ursula, and Unicorn. The submarines were built between 1986 and 1990, the former at VSEL Barrow in Furness, now BAE Systems, the latter three at Cammell Lairds in Birkenhead. These boats, now the HMCS Victoria class, have been renamed HMCS Chicoutimi, HMCS Victoria, HMCS Cornerbrooke and HMCS Windsor respectively with delivery of the last boat being completed sometime in late 2001 or early 2002.

Before the acquisition of the submarines by Canada, Marconi Marine (VSEL) in Barrow in Furness, were contracted to bring the boats up to an operational condition, the boats having been mothballed for a number of years. At this time an examination of the submarine seawater systems indicated that significant degradation of the NAB castings had occurred whilst the submarines were decommissioned. Consequently it was necessary for extensive refurbishment to be carried out. During upgrading the NAB castings in the seawater systems were revalidated in accordance with a combination of the requirements laid down in DPT 1312 (1) and NES 872 Part 3 (2), the latter being the specification currently used in the production of NAB castings for submarine seawater systems. In particular the identification of selective phase corrosion was carried out using silver nitrate solution, see Section 7 Validation/Revalidation. The method was regarded by BAE Systems as the most effective method of identifying selective phase corrosion.

The identification of selective phase corrosion in NAB components led to the items being either refurbished by effectively removing the areas subject to selective phase corrosion damage or replacing the defective castings as appropriate. On the basis of a number of conversations with company personnel it is the authors' belief that for HMCS Victoria the majority of the NAB components examined were replaced. Further as a consequence of discussions with the casting manufacturer, Meigh's Limited, the author believes that items were manufactured specifically as replacements for scrapped defective NAB castings. The first boat in the class, HMCS Chicoutimi, was originally commissioned in 1989, HMCS Victoria in 1990, HMCS Cornerbrooke in 1991, and HMCS Windsor in 1993. The times between launch and commissioning varied, the maximum was 2½ years for HMCS Chicoutimi. HMCS Victoria was the second of the class to be built, launched and commissioned. Consequently castings in HMCS Chicoutimi and HMCS Victoria would be expected to exhibit similar levels of corrosion but those in HMCS Cornerbrooke and HMCS Windsor should be less severely affected.

During future operations in Canadian waters selective phase corrosion problems in NAB components will undoubtedly arise which will require the establishment of an appropriate upkeep regime. This regime should include the provision of high integrity NAB replacement items, manufactured either in the UK or Canada, as well as the application of established refurbishment procedures in order to maintain existing NAB castings in an acceptable condition for continued service.

This paper details the UK manufacturing route for the production of NAB castings including the procedures used for the identification of casting imperfections, radiographic, ultrasonic and dye penetrant techniques. The means and methods used, when deemed appropriate, to reclaim flawed castings are identified together with examples of the approved weld procedures, equipment and materials.

The paper notes that materials when subjected to long term immersion in seawater show degradation to a greater or lesser extent, including crevice corrosion and dissimilar metal joints. The well-documented (3,4,5,6) mechanism of selective phase corrosion, identified with the degradation of NAB components is noted and the accepted means of remedial action discussed. This includes the latest requirements for the Validation and Revalidation of NAB components, NES 872 (7,8,2,9). It has been stated that forged NAB components may be less susceptible to selective phase corrosion. Work carried out in the 1970's indicated that the structure of heat treated forged material contained a more isolated distribution of the β phase within the α grains and non continuous κ_{III} phase such that no significant selective phase corrosion occurred in extended corrosion testing. This behaviour has been reflected in the service performance of some forged NAB components such as the main ballast tank valves, 'Kingston's'.

MANUFACTURE

Nickel Aluminium Bronze castings are manufactured in accordance with NES 747. This latest specification has been divided into five parts, Part 1, Centrifugally cast NAB (10). Part 2, NAB castings where welding is permitted on the wetted surface (11).

Part 3, for commercial NAB castings (12), Part 4, for NAB castings where welding is not permitted on the wetted surface (13) and Part 5, Design and manufacture of Nickel-Aluminium Bronze Sand Castings (14). NES 747 Part 3, commercial NAB castings, is directed towards the application of NAB castings for surface ship propellers and NAB castings not in contact with seawater etc. This part should not be used for submarine first level castings and NAB castings in contact with seawater.

1. Melting and Casting.

The manufacture of Nickel Aluminium Bronze castings should be carried out in accordance with NES 747, published in five parts (10,11,12,13,14). All castings made to this specification would be made from ingot, the composition of which is laid down in the specification, ultra low impurity virgin material or approved scrap. Approved scrap in these circumstances would mean the foundries own scrap arising from the production of castings to NES 747. It is more clearly defined as scrap that is derived from nickel aluminium bronze, the composition of which has been established with regard to the complete range of both the alloying elements and impurity elements and was segregated and identifiable to the satisfaction of the MoD (PE)/AA. The UK NAB founders have used per-alloyed ingot for many years, in preference to all virgin melts, in order to ease the compositional control problems in their foundries. The founders have relied to a considerable extent on the compositional accuracy of the ingot to guarantee the final casting composition.

The specification, NES 747, does not call for any defined metal melting or foundry practice and melting can be carried out in both oil fired and electric induction furnaces. However the manufacturer of replacement NAB items for the Victoria class, Meigh's Ltd., prefers to melt in electric induction furnaces. The molten metal would be cast into resin bonded sand moulds prepared using wooden patterns to define the casting shape and as necessary pre-formed cores of the correct dimensions. In the majority of cases, Meigh's limited, use bottom pouring, through ceramic foam filters, and occasionally Semi-Durville mould rotation techniques. In order to ensure casting integrity, production verification uses FDA simulation of mould filling and subsequent solidification to confirm the individual production methods employed with each casting.

2. Analysis.

The specified analysis requirements detailed in NES 747 Parts 1,2,3 and 4 for NAB ingot and castings are given in Tables 1 and 2 respectively. There are slight differences between the ingot and casting analyses with respect to aluminium and particularly manganese. The maximum and minimum values for these elements in the ingot analysis are slightly higher than in the specified casting analysis in order to take account of unavoidable losses, the result of oxidation during melting and casting.

A comparison of the casting analyses for the various NAB specifications Table 2 shows there are no differences in the major alloying elements. There are some differences in the allowable impurity elements; zinc, lead and tin and the total allowable impurities but these generally show a tightening of the requirements. These changes in impurity levels have been incorporated in the specification in order to improve weldability. This tightening of the requirements is also reflected in the specified compositions for NAB ingot under the various parts of NES 747.

When replacement NAB castings require to be purchased for the Victoria class, Part 2 of NES 747 would probably be the most applicable part of the specification to use. This part is preferred by the UK ship builder because of the extra cost inherent in the application of NES 747 Part 4. This extra cost is the risk premium demanded by the founder in order to ensure sound casting bores, not requiring upgrading by weld repair. The use of NES 747 Part 4 requires the founder to cast significant numbers of any item in order to ensure castings with acceptable soundness after machining. Both the original NAB castings installed in the seawater systems of the Upholder class and the replacement castings, purchased for the refurbishment, were all purchased to NES 747 Part 2.

3. Mechanical Properties.

The specified mechanical properties for castings manufactured to the various parts of NES 747 are given in Table 3. With respect to NAB castings for seawater systems, the only differences in the mechanical property requirements relate to the 0.2% proof stress and ultimate tensile strength in NES 747 Part 1 compared with Parts 2 and 4. The lower property requirements in NES 747 Part 1 exists because centrifugally cast material, due to the inherent coarseness of the metallurgical structure, grain size, is not capable of developing the higher 0.2% proof stress and UTS requirements.

The 250MPa 0.2% proof stress and 620MPa UTS requirement is a recent inclusion in the latest issue of NES 747 and was incorporated in an attempt to improve NAB casting quality for submarine applications. Of necessity, by increasing the 0.2% proof stress requirement it was believed that the founder would have to improve his foundry practice in order to meet the new requirements. The specified strength requirements are little different to those detailed in NES 747 Part 3 but in the latter case the increases are associated with a decrease in the specified percentage elongation requirement.

NAB castings manufactured in accordance with the NES 747 specification require heat treatment necessitating soaking the castings at 675°C ±15°C for a minimum of 6 hours. All heat treatment furnaces must be qualified to the requirements laid down in NES 746, (15). Originally the qualification procedures were supervised using MoD personnel but latterly this requirement has proved onerous with regard to providing the necessary support to the furnace qualification work. Consequently therefore, the MoD has decided that the manufacturer should be satisfied that the required heat treatment is carried out in a furnace generating the required thermal characteristics. These characteristics necessitate an acceptable uniformity of temperature throughout the furnace and consequently an acceptable uniformity of temperature in the castings and associated test pieces. The latter requirements should be monitored, by attaching the appropriate number of suitably placed thermocouples onto the castings. The current requirements laid down in NES 746, were based on BS 2M54, (16). However, SAE-AMS-H6875, (17), the commercial replacement for the US Mil 6875 specification, for the control of heat treatment furnaces, would also be appropriate. Heat treatment should be carried out in order to reduce the susceptibility of the material to selective phase corrosion whilst in contact with seawater and in particular to reduce the susceptibility of the heat affected zones of weld repairs to this phenomenon.

4. Integrity.

4a. Requirements

All castings manufactured to the NES 747 'Requirements for Nickel Aluminium Bronze Castings and Ingots' should be Class 1, Class 2 or Class 3 as defined in NES 863, including amendment 1, (18). The current descriptions of these classes dependent on the service conditions are:

Class 1.	A casting the failure of which would lead to uncontrollable flooding, the total immobilisation of the ship or submarine or present a serious hazard to personnel. This class of casting has very high standards of inspection and acceptance and is intended for use in critical parts of surface ships and submarines.
Class 2.	A casting the failure of which would lead to severe but controllable flooding, the serious disruption of weapons systems, the main propulsion machinery or its attendant auxiliaries including generators.
Class 3.	All other castings. Class III castings may only be used where their failure would not constitute an immediate significant hazard.

The integrity of the as NAB castings should be determined in accordance with NES 863, 'Requirements for the Classification, Dimensions, Tolerances and General Standards of Acceptance for Copper and Nickel Alloy Castings' (18) and the relevant part of NES 747. The associated non-destructive examination carried out in order to demonstrate the required integrity should be as specified in NES 729 Parts 1-5 (19, 20, 21, 22, 23). The inspection of castings in general involves the use of radiography, Part I, to identify sub surface flaws and dye penetrant examination, Part 4, to locate surface breaking defects such as porosity. Radiography may be carried out using an Iridium or Cobalt source. In most cases shallow surface breaking casting defects, identified using dye penetrant techniques, would be blended out whilst the larger surface breaking flaws would excavated for weld repair.

It is the casting designer's responsibility to indicate on reference diagrams, for Class 1 and Class 2 castings, the regions to be examined by non-destructive testing. These regions are to be identified as Critical Test Regions and Test Regions and are described in accordance with the following principles:

Critical Test Region.

Applies to those regions of a Class 1 casting that may be highly stressed as a result of operating conditions, taking into account whether or not the item is resiliently mounted.

Test Regions.

Applies to those regions of a Class 2 casting not designated as a Critical Test Region and those regions of a Class 2 casting which may be highly stressed as a result of the operating conditions, taking into account whether or not the item is resiliently mounted.

Non-Designated Region

Applies to all regions of a Class 2 casting not designated as a Test Region and to all regions of a Class 3 casting.

In all cases the casting design should aim to minimise the need for machining (NES 863).

4b. Examination/Acceptance

Castings made to the relevant parts of NES 747, parts 1,2 and 4, require to be examined visually, using dye penetrant, radiographic and ultrasonic means. The shipbuilder has a preference to use NES 747 Part 2 for the main proportion of NAB castings rather than Part 4 due to the greater difficulty and cost of complying with Part 4, weld repair not being permitted on the wetted surface. It is the authors' opinion that using NES 747 Part 4 could add considerably to the manufacturing costs.

4b1. Dimensions

Dimensionally all NAB castings should be within the tolerances stated on the casting drawings. Should no tolerance be stated then the following positive and negative deviations with respect to thickness would be acceptable under NES 863:

a. For thickness of <20 mm +3 mm
b. 20 mm to 40 mm +15%
c. >40 mm +6 mm
d. ≤50 mm −10%
e. >50 mm 5 mm

d. & e. would apply, provided the reduced section was free from sub-surface defects in Critical Test and Test regions. In addition the cumulative local reduction in section should not exceed 20 % or the total defective area should not be greater than 20 % of the total area of the casting in non-designated regions. Additionally the blending out of surface defects should not exceed 10% for designated regions and not greater than 20 % of any non-designated region.

4b2. Visual

All castings are to be 100% examined visually and, where necessary, at up to X5 magnification to identify and record all surface imperfections. All surfaces to be clean and free from linear defects. Rounded forms of surface defects should not be accepted in Critical Test and Test regions but maybe acceptable in non-designated regions. Round defects would be deemed to have an aspect ratio of 3:1 or less.

4b3. Liquid Penetrant

It is recommended that 100% liquid penetrant examination to NES 729 Part 4 (22) should carried out before final machining in order to mitigate against the possibility of unnecessary machining of defective Class 1 and Class 2 castings. Where practicable 100% liquid penetrant inspection should be undertaken on all surfaces of Class 1 and Class 2 castings in their final finished condition. Defects identified as cracks, chain-like porosity and oxide inclusions should not be accepted.

Isolated pinhole porosity could be acceptable except on sealing surfaces, against a running shaft. In these cases the more stringent requirement is to be clearly stated on the contract documents which are subject to discussion between purchaser and manufacturer of the castings.

Clustered pinpoint porosity and other defects, identified using Liquid Penetrant examination, could be accepted provided:

a. the maximum size of the bleed out for any indication, in a specified time scale, was ≤ 3 mm in diameter.

b. the sum of all the individual diameters of all indications did not exceed 24 mm in an area of 70 mm x 70 mm for sections up to 50 mm thick.

c. the sum of the diameters of all indications in sections greater than 50 mm thick did not exceed 36 mm in an area of 70 mm x 70 mm.

It should be noted that fine porosity and shrinkage, can affect the susceptibility of the material to selective phase corrosion.

4b4. Radiography/Ultrasonics

The manufacturer should carry out either 100% radiographic or 100% ultrasonic examination of Critical Test regions and Test Regions.

Radiography should be carried out in accordance with NES 729 Part 1, all sub-surface imperfections being identified for further assessment. On a sample basis, in order to establish the satisfactory general quality of castings, Non-Designated regions may be radiographically examined. Examples of this may include:

1. Lowly stressed Class 2 castings.
2. Sample positions on large Class 2 and Class 3 castings.
3. Batch supply of Class 3 castings

Ultrasonic examination should be carried out in compliance with NES 729 Part 5, all subsurface defects being identified for further assessment. If ultrasonic examination were to be used it should be confirmed, in selected areas, by radiography. Confirmation should be achieved with a minimum of 10% radiography of the total area inspected. It should be noted that due to the possibly large grain structure inherent in cast NAB the effectiveness of the ultrasonic examination might be seriously impaired as a consequence of beam attenuation.

Sub-surface defects such as cracks, hot tears, cold shuts and lack of fusion when welded etc. would not be acceptable but filamentary shrinkage, oxides and sponginess could be accepted provided:

a. in Critical Test regions the local reduction in thickness did not exceed 5% of the contract drawing thickness and the defective area did not exceed 10% of the region.

b. in Test regions the local reduction in section thickness did not exceed 10% of the contract drawing thickness and the total defective area did not exceed 20 % of the region.

c. isolated imperfections, shrinkage cavities, gas holes and rounded inclusions would be acceptable provided the total local reduction in thickness together with other sub-surface defects did not exceed 10% of the contract drawing thickness in the Critical Test Regions and 20% in Test regions.

d. When examination is by sample inspection the cumulative local reduction in section thickness, as a result of sub-surface defects in any position, should not exceed 20% of the contract drawing section thickness with the total defective area not exceeding 20% of the total area examined.

4b5. Combined Requirements

Imperfections such as filamentary shrinkage, oxides, sponginess micro-porosity isolated shrinkage cavities, gas holes and rounded inclusions should be separated by 2.25 times the contract drawing thickness in way of the defect or 1.25 times the length of the larger adjacent defect whichever is greater. Defects with a closer approach than stated above should be considered as single defect with an overall length equivalent to the distance between the furthest extremities of the two defects.

4b6. Pressure Testing

When required, castings should be subjected to a specified water pressure test for a minimum of fifteen minutes in which time there should be no evidence of leakage.

5. Repair.

5a. Blending

Unacceptable surface imperfections may be blended out by a suitable process, machining, pneumatic chipping or grinding. The contract drawing section must not be reduced by more than 5 mm for a section thickness >50 mm or by more than 10% for section thickness ≤50 mm. The total blended area including fairing should not exceed

10% of any designated test region or 20 % of a non-designated region. The sides of the depression must be smooth with a minimum radius of three times the maximum depth of the blending, the remaining section under the depression must be free of sub-surface defects as revealed by radiography or ultrasonics, in Critical Test and Test Regions.

5b Welding

5b1 Dimensional Defects

Repair by welding in order to correct casting dimensions and machining errors would be acceptable using an approved procedure within the following limits:

1. Weld deposit thickness restricted to 20% of contract drawing thickness for sections between 12mm and 50mm and to 10mm for sections greater than 50mm in thickness.
2. Total area of deposit in Critical Test Regions and Test Regions restricted to 10% of the inner or outer surface area of the region not including the flange thickness and webs.
3. Weld repair in non-designated areas restricted to 20% of inner and outer surface areas not including flange thickness and webs.

5b2. Surface and Sub-Surface

Rectification of unacceptable surface and sub-surface defects may be achieved by welding using an approved procedure within the following limits:

1. In Critical Test and Test regions the area of repair should be restricted to 10% of the surface area of the region not including flange thickness and webs.
2. For non-designated regions the area of repair should not exceed 20% of the inner or outer surface area of the region not including flange thickness and webs.
3. Any individual repair should not exceed 5% of the test area of the repair in Critical Test Regions.
4. No individual repair should exceed 10% of the test area in Test Regions.

5b3 Combined Defects

For repairs which seek to correct dimensional errors and surface and sub-surface defects the following requirements would be applicable:

1. The total area of weld repair in Class 1 and Class 2 castings should not exceed 10% Of the surface area of the casting excluding the flange thickness and webs.

2. The total area of combined repair should not exceed 20% of the surface area of Class 3 castings excluding the flange thickness and webs.

5b4 NES 747 Part 4 Variations

The requirements for the correction of dimensional errors surface and sub-surface defects by blending and welding are equivalent to those defined in NES 747 Part 2 with the following exceptions:

1. No welding is allowed on any wetted surface.
2. Welding is not allowed on sections less than 12mm thick.
3. When welding from a non-wetted surface the depth of closest approach to the wetted surface should not be less than 10mm.

5c. Impregnation

Recovery by impregnation, in accordance with Def Stan 03-1 (24), is not acceptable for Class 1 castings. However, impregnation could be accepted with written approval for Class 2 castings and is acceptable for Class 3 castings. The foregoing would only be acceptable provided the original area of leakage does not exceed 10% of the test region in Class 2 castings and 10% of the total area pressure tested in Class 3 castings.

5d. Special Repairs

Circumstances may arise where repairs would be required but at the same time the repairs would be more extensive than would be permitted by the specification. In these circumstances if an effective economical repair were possible the contractors repair procedures would need to be submitted to the acceptance authority for approval.

WELDING REQUIREMENTS

The main NAB casting imperfections include cracks, hot tears, cold shuts, porosity, shrinkage, included sand, oxide film, laps and imprecise casting dimensions. Imperfections not meeting the requirements of the NES 747 specification together with other minor defects should be repaired, where appropriate, by welding in accordance with NES 771, 'Requirements, Procedure and Inspection for Weld Repair of Copper Alloy and Nickel Alloy Castings' (25).

Weld repair of NAB castings may only be undertaken after the approval of a written weld procedure, based on welder or procedure qualification, by the Quality Assurance Representative. It is preferable for welding to be carried out in the flat position with where necessary weld run-on and run-off plates, made of the same material as that being welded. The GMA or GTA processes, using 99.95% minimum pure Argon as the shielding gas, have been approved for the welding of NAB. The welding consumables approved for use with these processes are Bostrand AT246 and Stubbs A 3444 wires. The deposits should be laid using a preheat temperature of 50°C-100°C with a maximum interpass temperature of 200°C.

All weld repairs should be post weld heat treated to minimise the susceptibility of the weld HAZ to selective phase corrosion in the sea water environment. The heat treatment used consists of, as with the standard casting heat treatment, holding the component at 615°C for a minimum of 6 hours followed by air cooling in still air. The validation of the heat treatment furnace should be carried out in accordance with DG SHIPS 746 or similar (15, 16, 17).

The NES 771 (25) specification details welder qualification requirements, the development of an approved written weld procedure and the necessary NDT to be carried out. The welding procedures require to be qualified under a number of headings:

a. repairs for dimensional rectification with excavation depths not exceeding 10 mm need to be qualified using a restrained test plate which should not be less than 320 mm x 125 mm x 25 mm in size.

b. repairable defects greater than 10 mm in depth require procedures to be qualified using restrained test plates which measure not less than 320 mm x 250 mm x 40 mm in size.

c. in those circumstances where a. and b. would not adequately simulate the required weld repair the test plate should be designed to embody all the essential features of the repair, regarding access, restraint and heat dissipation.

In addition to the above it is a requirement within the specification for destructive tests to be carried out, including:

a. Transverse tensile tests.
b. All weld metal tensile test.
c. Side bend test.
d. An etched macro section at x10 magnification.

Following the successful completion of the destructive and non-destructive tests, the weld procedure and the test results should be submitted to the inspecting authority for approval. Welder qualification should be carried out using one or all of the weld test assemblies, used as appropriate, for weld procedure approval

VALIDATION/REVALIDATION

NAB castings in contact with seawater, in addition to complying with a particular part of NES 747, are subject to additional requirements. The additional requirements were originally mandated in order to ensure that the effects of selective phase corrosion on the integrity of the NAB submarine seawater systems components could be adequately managed. For critical castings, where failure in service would create an unacceptable hazard, the castings should be validated to determine their suitability for service. The policy of validation has been in operation for a considerable number of years within the British Navy. For all classes of submarine the NAB manufacturing data records are used for validation, as detailed in NES 872, 'Procedures for First Level Nickel Aluminium Bronze Castings'. The data records should include:

Visual Examination record sheet
Weld repair and Defect recording sheet

Radiographic Interpretation Record Sheet
Dye Penetrant Examination Record Sheet
Sketches of weld repair areas
Records of dimensional checks
Validation Certificate

Following validation an items should be identified by H, if it has been heat treated, and or A, if it has been weld repaired, a unique radiographic number, the material specification and VAL followed by the date of validation, e.g. HA34567X/747NA/VAL/14/7/88. The validation data and QA certificate of compliance should accompany the casting and the 'lead' Dockyard should hold these data when the casting has been fitted to the vessel. Additionally an identical pack should be kept by the repair/manufacturing facility as a record as support to future validations.

The specification NES 872, is a Category 1 document and as such should be applied to all NAB castings for submarine construction and refit. The specification is published in four parts, Parts 1 'Policy', Part 2 'Validation', Part 3 'Re- validation' and Part 4 'Inspections Outside of Refit Period'. These requirements should be applied to all replacements for the NAB components in the seawater systems of the Canadian 'Victoria' Class submarines.

The latest versions of the NES Specifications are divided into Categories 1, 2 or 3, in order to define their applicability in construction and refit as compared with possible alternative commercial specifications:

Category 1.	If not applied could have a Critical affect on the vessel with respect to its safety, its compliment or third parties, operational performance of the vessel, its systems or equipment.
Category 2.	If not applied could have significant affect on vessel safety, its compliment or third parties, operational performance of the vessel, its systems or equipment, through life costs and support.
Category 3.	If not applied could have a minor affect on MoD best practice and fleet commonality, corporate experience and knowledge and current support practice.

The following is a short synopsis of Parts 1, 2, 3 and 4 of NES 872 as they would be applied to the supply of replacement NAB castings for Victoria Class submarines:

NES 872 Part 1, "Policy" (7).

This document defines Critical Castings, affecting submarine safety, as all First Level castings in contact with seawater. The castings need to be manufactured as either Class 1 or 2, in accordance with NES 747 Parts 1,2 or 4. Such castings should be categorised in accordance with NES 863 (18), identified and listed in the NAB register.

NAB castings listed in the NAB register should be validated and revalidated in accordance with Parts 2 and 3 of NES 872. The design authority should determine the periodicity of revalidation. As necessary, higher risk castings should be selected for examination during docking periods, inspected and the requisite action taken in accordance with NES 872 Part 4.

During a refit period, all NAB castings listed in the NAB register should be revalidated in accordance with NES 872 part 3, replaced with NAB castings in accordance with NES 872 Part 2, or CNC to NES 824 (26, 27) as required. Welding would not normally be allowed on revalidation.

Non critical castings should only to be replaced when defective. Revalidation would require, with the agreement of the design authority, the replacement of castings where it was physically impossible or not economically viable to revalidate.

The NAB register, in order to monitor, control the inspection and the replacement of First Level Quality Assured NAB castings contains all the concessions, Departures from Design Intent and Certificates of non-conformity. Deviations, which directly affect the structure, geometry or pressure boundary integrity of each casting component, are of particular importance.

During build, the shipbuilder would prepare the NAB register, for a particular boat, of all the appropriate castings and supply a copy of the register to the requisite authorities including the submarine commanding officer. It is the commanding officers responsibility to keep the submarines copy of the NAB register up to date following any work undertaken outside refit. Between refits it is the responsibility of the mechanical engineering officer to maintain the master copy. All changes as a result of necessary work should be noted. During a docking period it would the responsibility of the docking period contractor to update the master copy of the NAB register in accordance with the design authorities requirements.

Whilst in refit, it would be responsibility of the refitting contractor to update the NAB register of the submarine in accordance with the design authority requirements. At the end of the refit period the registers should be audited along with the First Level Quality Assurance documentation. The Master Register should be issued to the submarine and the design authority.

The complete Quality Documentation including a copy of the validation certificate, Weld Repair Recording Sheets, Wall Thickness Recording Sheets, sketches and photographs of the castings listed in the NAB register should be sent to the Through Life Records Contractor. These records must be updated and maintained as castings are replaced.

NES 872 Part 2, "Validation" (8).

The document details the finger print examinations required on new First Level NAB castings prior to installation in the submarine. Drawings with dimensions, including wall thickness and all non-conformance documentation (concessions, departures from design intent etc) affecting casting integrity are required by the validation contractor. Also required are the weld repair recording sheet, a gridded sketch of the casting, a wall thickness recording sheet and a validation certificate by the personnel carrying out the inspection.

Information on the size and location of weld repairs and wall thickness measurements, which must meet the requirements of NES 747 Parts 1, 2 and 4, provide the baseline for the through life monitoring process of NAB castings. Ultrasonic means of thickness checking must be supported by approved written procedures. All areas of weld repair exposed to seawater should be sketched or photographed; sized and cross-referenced via grid based sketches to an identifiable position within the casting.

Quality Assurance Documentation should include results of all tests performed, weld procedure details, records of weld repair, and wall thickness data. Record sheets, which are to be available for audit, should be annotated with the ship fitting number, description and unique radiographic number. Finally the validation certificate should be completed when the NDE is complete to the requirements of NES 747 Parts 1, 2 or 4.

Following validation the individual cast NAB items should identified by stamping using the radiographic number followed by VAL plus date and prefixed with A for weld repaired and H for heat treated, e.g. HA 4567X/747NA/VAL/14/7/88. When a casting has been fitted to a vessel a copy of the validation certificate together with a full set of the accompanying QA records should be held by the Through Life Records Contractor and as such should be available for future revalidation of the component.

NES 872 Part 3, "Revalidation" (2).

The document identifies the actions to be taken when it has been found necessary to revalidate first level NAB castings because of very severe selective phase corrosion problems periodically encountered with the use of NAB in submarine seawater systems. It was to these requirements that all the NAB castings in the seawater systems of the Victoria class submarines were upgraded, before the boats were transferred to the Canadian Navy.

During a refit period all NAB castings listed in the NAB register, should be revalidated in accordance with NES 872 Part 3 (2). Castings not revalidated but rejected, should be replaced with NAB castings which have already been revalidated, new NAB castings that have been validated in accordance with NES 872 Part 2 (8), or replaced with Copper Nickel Chrome Castings to NES 824 (26).

In addition to the examination of NAB castings during refit a number of first level "High Risk" castings should be revalidated at the intermediate docking periods to NES 872 Part 4 "Inspections Outside Refit Periods" (9). On the basis of the findings of the examination a judgement should be made as to the condition of the remaining high-risk castings. The details of the examinations to be undertaken using NES 872 Part 4 directly mirror the requirements in NES 872 Part 3.

Revalidation has been aimed at establishing the suitability of a casting, with regard to freedom from general and selective phase corrosion, the acceptability of any weld repairs and the maintenance of an adequate wall thickness, for continued service, following dressing to remove the corroded regions. Non-critical castings, those not on the NAB register, should only replaced when defective.

When the NAB castings selected for revalidation have been removed from the seawater systems they will be covered, on the seawater-wetted surface, to varying degrees with bio-fouling and calcareous deposits. Before revalidation can take place therefore these extraneous items must be removed by: -

a. Hydro-jetting with or without abrasives.
b. Dry blasting with Alumina grit.

c. Using a chemical dip.

Following the use of these treatments the presence of selective phase corrosion would be indicated on the cleaned surface of the casting by the presence of a difficult to remove layer of re-deposited copper. This layer must and should be effectively removed by abrasion leaving no re-deposited copper on the surface to give false indications of selective phase corrosion.

Subsequent to the abrasive cleaning, the identification of selective phase corrosion should be confirmed by the use of a freshly prepared 10% silver nitrate solution. Application of the solution must be carried within one hour of dry abrasion of the surface, because the surface develops an oxide resistant film, resistant to the silver nitrate etch. Regions of selective phase corrosion are subsequently identified by the presence of a black deposit after treatment with the Silver Nitrate solution. The black deposit is composed of metallic silver formed as a result of silver from the silver nitrate solution, replacing the copper, which was originally deposited during of the selective phase corrosion process.

In order to remove the selective phase corrosion, the areas indicated by the black deposit should be repeatedly ground, using tungsten carbide burrs or grinding wheels, to a maximum 1mm depth at a time. The areas should then be etched until no further black deposits of silver develop on the application of the silver nitrate solution.

An alternative treatment to the above would to first degrease the casting using a detergent containing hot water wash followed by immersing in a brightening agent (Ardrox 160 containing a mixture of 29% Chromic and 4% Sulphuric acids). This procedure, which must be carried out with fresh solution, will etch the surface, delineating the areas of weld repair and selective phase corrosion if present. After etching the various areas can be identified from their appearance: -

a. Parent Metal -- Mid Grey.

b. Weld Metal -- Dark Grey or Black.

c. HAZ selective phase corrosion -- Greyish Green.

d. Plug corrosion -- Copper coloured or Greenish Grey.

As with the first procedure for the identification and removal of selective phase corrosion, repeated grinding and the use of Ardrox 160 etch should ensure the removal of corrosion revealing the underlying sound material. However in the light of experience the technique employing the 10% silver nitrate solution has been preferred by the UK fabricator.

Following the removal of all the selective phase corrosion the ground areas should need to be thickness gauged. Thickness gauging should be carried out using calibrated callipers and the remaining wall thickness should only be accepted provided it was more than 90% of the finished machine drawing thickness.

For some of the larger castings it could be economic to carry out a life assessment on initially rejected castings in order to justify a further commission or to calculate the maximum justifiable life. Life assessment should be carried out using the probabilistic approach with NABWETLIFE; a MoD developed code, or a deterministic approach using finite element analysis and fracture mechanics. The probabilistic approach would be more suitable for thinner castings. The author does not know whether the Victoria class NAB castings are identified in the existing NABWETLIFE submarine specific database together with the inspection time-scales.

Rejected castings should not normally weld repaired, however on occasion, this action could be deemed appropriate, especially when only a single replacement casting were required. Should weld repair be approved this should be carried out in accordance with NES 771 (25) taking due consideration with respect to possible distortions arising from weld repair. After completing the weld repair it would be a requirement of the specification to heat-treat the repaired castings so as to minimise the susceptibility of the weld HAZ to selective phase corrosion. This heat treatment would be waived provided the consequences of so doing, HAZ corrosion in seawater, have been recognised and accepted.

Alternative means of reclamation could be appropriate and these would include the use of sleeves, fillers and coatings but all these options would be subject to design authority approval.

SUMMARY

NAB castings have been manufactured in the UK over the past thirty years. Consequently, a large amount of experience has been generated regarding the manufacture of high integrity NAB castings for submarine seawater systems. Experience in the production of NAB casting is believed to exist in Canada. It is to be expected therefore that the requirements for the production of Victoria Class seawater system castings could be met.

Questions have been raised from time to time regarding the size, shape and complexity of NAB castings for submarine seawater systems. In particular it is believed that the overall weight of such castings could be reduced if the designs were related directly to the properties of NAB and not, as at present a development of original designs based on gunmetal. The final shape of the castings is dependent on the requirement to cast NAB to a shape, which will result in a high integrity casting. Using a combination of FDA techniques, to simulate mould filling, solidification and improving pattern accuracy, with pattern equipment NC milled from CAD data of the casting profile, casting size and shape could be optimised. The process would include data on contraction rates obtained from a prototype. In such circumstances the patterns would be constructed from damage resistant, durable materials and the final castings would be optimised as regards manufacture and fitness for purpose.

The requirement to heat treat NAB castings to reduce the risk of selective phase corrosion in a seawater environment is a necessity where weld repair has been carried out but its effectiveness in other circumstances is debatable.

The integrity of NAB castings in seawater systems is important not only to carry the design loads but in particular the provision of wetted surfaces that are free of unacceptable defects. NAB is susceptible to crevice corrosion, which can eventually lead to extensive selective phase corrosion. The presence of shrinkage porosity in the wetted surface of a NAB casting provides a pre-existing crevice to initiate early selective phase attack. Consequently it is highly desirable to minimise the amount of porosity on machined seawater wetted surfaces.

It is allowable for identified defects to be repaired by blending, welding or impregnation, as appropriate, within clearly defined criteria. However, the necessity to carry out these procedures should be restricted as far as possible by ensuring optimised, high integrity NAB castings, using simulation techniques, are manufactured. Repair by welding must be accompanied by an approved procedure incorporating both welder and procedure approvals.

In order to manage NAB castings in service, as a result of the susceptibility of the material to selective phase corrosion problem, procedures have been put in place that will guarantee the life of any particular NAB casting with respect to the submarine commissions. The procedures cover the means of surveying as manufactured castings in order to identify dimensions, record the position of any repairs and report overall casting integrity. In addition the means of identifying the presence selective phase corrosion is identified, the action to be taken to remove such damage and the revalidation of such castings for continued service. These procedures are now described in NES 872 Parts 1, 2, 3, and 4, (7, 8, 2, 9). The application of these procedures ensures new NAB castings are acceptable for service in seawater systems and NAB castings, which have seen prolonged service, are still acceptable for continued service.

If the corrosion performance of forged NAB, as indicated in the introduction, is significantly superior to cast NAB, then this contention should be tested in extensive trials, so that if substantiated, acceptable forged items could be procured as NAB casting replacements. Clearly many items because of their shape would be difficult to forge. However such items could be redesigned to assist in the forging process as cast items now are designed to some extent with casting in mind. Redesign of components may have an additional benefit in that weight would be reduced compared with the cast product but higher machining costs may result when using forged components, which ultimately may mitigate against the widespread use of forged NAB components.

TABLES

	Main Alloying Elements					Impurities						Total Impurities
	Al	Fe	Ni	Mn	Zn	Zn	Pb	Sn	Si	Mg	Cr	
NES 747 Part 1 min	8.9	4.0	4.5	1.0								
Ingot max	9.6	5.0	5.5	1.4		0.05	0.01	0.05	0.05	0.05	0.01	0.20
NES 747 Part 2 min	8.9	4.0	4.5	1.0								
Ingot max	9.6	5.0	5.5	1.4		0.05	0.01	0.05	0.05	0.05	0.01	0.20
NES 747 Part 3 min	8.8	4.0	4.0									
Ingot max	10.0	5.5	5.5	1.5	0.5		0.01	0.1	0.1	0.05	0.01	0.20
NES 747 Part 4 min	8.9	4.0	4.5	1								
Ingot max	9.6	5.0	5.5	1.4		0.05	0.01	0.05	0.05	0.05	0.01	0.20

Nickel content is to be greater than iron content.

Table 1. Ingot Composition.

Source	Main Alloying Elements					Impurities						Total Impurities
	Al	Fe	Ni	Mn	Zn	Zn	Pb	Sn	Si	Mg	Cr	
NES 747 Part 1 min	8.8	4.0	4.5	0.75								
Casting max	9.5	5.0	5.5	1.3		0.05	0.01	0.05	0.10	0.05	0.01	0.25
NES 747 Part 2 min	8.8	4.0	4.5	0.75								
Casting max	9.5	5.0	5.5	1.3		0.05	0.01	0.05	0.10	0.05		0.25
NES 747 Part 3 min	8.8	4.0	4.0									
Casting max	10	5.5	5.5	1.5	0.5		0.01	0.10	0.10	0.05	0.01	0.30
NES 747 Part 4 min	8.8	4.0	4.5	0.75								
Casting max	9.5	5.0	5.5	1.3		0.05	0.01	0.05	0.10	0.05	0.01	0.25

Nickel content is to be greater than iron content.

Table 2. Casting Composition.

Source	0.2% PS		UTS		Elong.
	tsi	N/mm^2	tsi	N/mm^2	%
NES 747 Part 1 min		230		600	15
NES 747 Part 2 min		250		620	15
NES 747 Part 3 min		250		640	13
NES 747 Part 4 min		250		620	15

Table 3. Mechanical Property Requirements.

REFERENCES

1. DG SHIPS 1312 Revalidation Procedure for Submarine Nickel Aluminium Bronze Castings, which have had previous service involving, contact with seawater.
2. NES 872 Part 3 Procedures for First Level Nickel Aluminium Bronze Castings Part 3 Revalidation
3. Heidersback R. "Clarification of the Mechanism of the Dealloying Phenomena". Corrosion Vol. 24. No 2. February 1968.
4. Rowlands JC, Brown TRHM. "Preferential Phase Corrosion of Cast Al Bronzes with Complex Microstucture in Seawater. Fourth International Congress on Marine Corrosion and Fouling. Centre de Researches d'Etudes Oceanographiques, Juan-Les-Pins, Boulogne, France 1976 p 475-479.
5. Rowlands JC "Studies on the Preferential Phase Corrosion of Cast Nickel Aluminium Bronze in Sea water". 8th International Congress on Metallic Corrosion, 1981. Vol. II. Mainz, West Germany, 6-11 September 1981.
6. Jones RL, Rowlands JC "Recent Research and Development on Copper Alloys at Admiralty Research Establishment, Holton Heath". Copper Alloys in the Marine Environment Conference, Birmingham, 1-2 April 1985.
7. NES 872 Part 1 Procedures for First Level Nickel Aluminium Bronze Castings. Part 1. Policy.
8. NES 872 Part 2 Procedures for First Level Nickel Aluminium Bronze Castings. Part 2. Validation.
9. NES 872 Part 4 Procedures for First Level Nickel Aluminium Bronze Castings. Part 4. Inspections Outside of Refit Period.
10. NES 747 Part 1 Nickel Aluminium Bronze Naval Alloy Centrifugally Cast.
11. NES 747 Part 2 Nickel Aluminium Bronze Naval Alloy Ingots and Sand Castings with Weld Repair Permitted to the Wetted Surface.
12. NES 747 Part 3 Nickel Aluminium Bronze Commercial Alloy Ingots and Sand Castings.
13. NES 747 Part 4 Nickel Aluminium Bronze Naval Alloy Sand Castings with Welding Restricted to the Non-Wetted Surface (Class 1 and Class 2 Castings Only).
14. NES 747 Part 5 Design and Manufacture of Nickel-Aluminium-Bronze Sand Castings
15. NES 746 Approval and Control of Heat Treatment Furnaces
16. BS 2M54 Specification for the Temperature Control in the Heat Treatment of Metals.
17. SAE-AMS-H6875 Heat Treatment of steel Raw Materials
18. NES 863 Requirements for the Classification, Dimensions,

		Tolerances and General Standards of Acceptance for Copper and Nickel Alloy Castings.
19.	NES 729 Part 1	Requirements for Non-Destructive Examination Methods. Radiography.
20.	NES 729 Part 2	Requirements for Non-Destructive Examination Methods. Magnetic Particle.
21.	NES 729 Part 3	Requirements for Non-Destructive Examination Methods. Eddy Current.
22.	NES 729 Part 4	Requirements for Non-Destructive Examination Methods. Liquid Penetrant.
23.	NES 729 Part 5	Requirements for Non-Destructive Examination Methods. Ultrasonics.
24.	Def Stan 03-1	Impregnation of Porous Castings.
25.	NES 771	Requirements, Procedure and Inspection for Weld Repair of Copper Alloy and Nickel Alloy Castings
26.	NES 824 Part 1	Copper Nickel Chrome Sand Castings and Ingots Part 1. Production Requirements
27.	NES 824 Part 2	Copper Nickel Chromium Sand Castings Part 2. Guide to Production Methods

Note! The opinions expressed in the paper are those of the author alone. The paper is an extract from the work carried out by the author for DREA in 2000, originally detailed in the report entitled 'Victoria Class Submarine System Valve Bodies' and presented at DREA on Tuesday 3rd October 2000.

#516463 48

Probabilistic Risk Assessment of Aging Ship Structures

by

U. O. Akpan[1], T. S. Koko[1], B. Ayyub[2] and T.E. Dunbar[1]

[1]Research and Emerging Technologies Department
Martec Limited, Suite 400, 1888 Brunswick Street, Halifax, N.S., Canada B3J 3J8.
[2]Professor of Civil Engineering, University of Maryland, College Park, Maryland

Abstract

Aging ship structures experience several damage modes especially corrosion, which is regarded as one of most important damage modes. Corrosion manifests itself in several forms, including, general corrosion, pitting and grooving. It is a continuous degradation process in uncoated steel and usually resumes after the coating has broken down. It is a major threat to the structural integrity of aging vessels, especially tanker structures and bulk carriers, many of which continue to operate beyond their design service life. The importance of monitoring and mitigating corrosion growth has been recognized by classification societies of ship owners and International Maritime Organizations. Standards for assessing the structural integrity of aging vessels are being developed by the various agencies.

An approach for risk assessment of the ultimate strength of a ship hull structure in the presence of corrosion is developed. Corrosion growth is modeled as a time dependent random function that decreases the thickness of ship hull structural members with time. Second Order Reliability Method (SORM) is used to calculate instantaneous reliability of the primary hull structure. Methodology for computing the time dependent reliability of a corroding ship structure is developed. Sensitivity of the time dependent reliability of the structure to statistical and probabilistic description of the corrosion growth parameters is investigated. An example problem involving a corroding tanker structure is used for demonstration.

PROBABILISTIC RISK ASSESSMENTS OF AGING SHIP STRUCTURES

By

U. O. Akpan[1] , T. S. Koko[1] , B. M. Ayyub[2] and T. Dunbar[1]

[1] Research and Emerging Technologies Department, Martec Limited
1888 Brunswick St. Suite 400, Halifax, NS, Canada

[2] BMA Engineering Inc.
Potomac, Maryland, USA

The 9th CF/DRDC MEETING on
NAVAL APPLICATIONS OF MATERIAL TECHNOLOGY
5-7 MAY 2001

BMA Engineering Inc

Martec Limited
Advanced Engineering and Research Consultants

PRESENTATION OUTLINE

- MOTIVATIONS/INTRODUCTION
- OBJECTIVE OF STUDY
- MODELS FOR PROBABILISTIC RISK ASSESSMENT
- DEMONSTRATION EXAMPLE
- LIMITATIONS OF RESULTS
- CONCLUSIONS

BMA Engineering Inc

Martec Limited
Advanced Engineering and Research Consultants

MOTIVATIONS/INTRODUCTION

- Most Aging Ship Structures Operate Beyond Their Design Life
- Several Damage Modes That Affect Structural Integrity Are Experienced By These Structures
- Prominent Among Them Is Corrosion
- Corrosion Manifest In Several Forms, Including, General Corrosion And Pitting
- The Impact of Corrosion on Structural Integrity Has to be Estimated
- Uncertainty is Associated With Corrosion Modeling

BMA Engineering Inc

Martec Limited
Advanced Engineering and Research Consultants

OBJECTIVES

- To Develop A Time Dependent Probabilistic Risk Methodology For Assessing The Impact Of Corrosion On Ultimate Strength Of Aging Ship Structures
- To Assess The Sensitivity Of Ship Structures To Probabilistic Descriptions Of Corrosion Growth Parameters

BMA Engineering Inc

Martec Limited
Advanced Engineering and Research Consultants

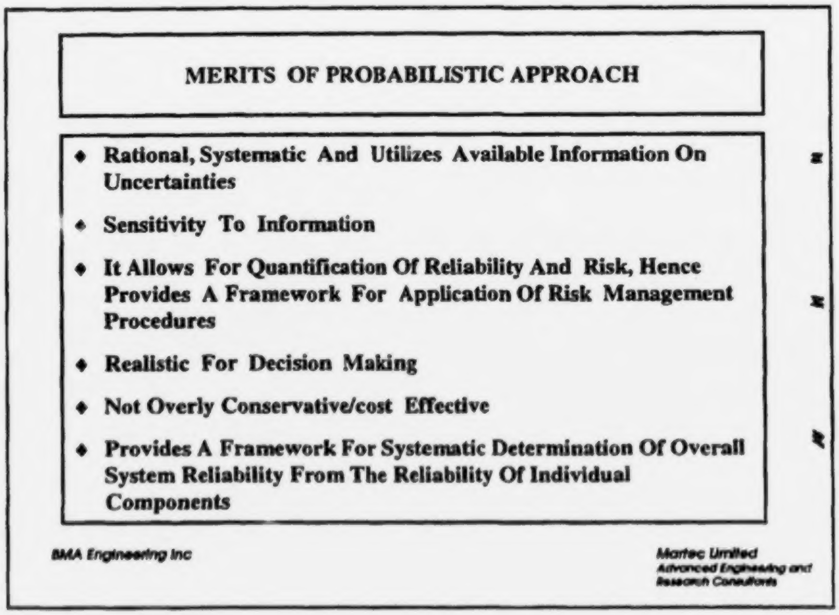

MERITS OF PROBABILISTIC APPROACH

- Rational, Systematic And Utilizes Available Information On Uncertainties
- Sensitivity To Information
- It Allows For Quantification Of Reliability And Risk, Hence Provides A Framework For Application Of Risk Management Procedures
- Realistic For Decision Making
- Not Overly Conservative/cost Effective
- Provides A Framework For Systematic Determination Of Overall System Reliability From The Reliability Of Individual Components

BMA Engineering Inc

Martec Limited
Advanced Engineering and
Research Consultants

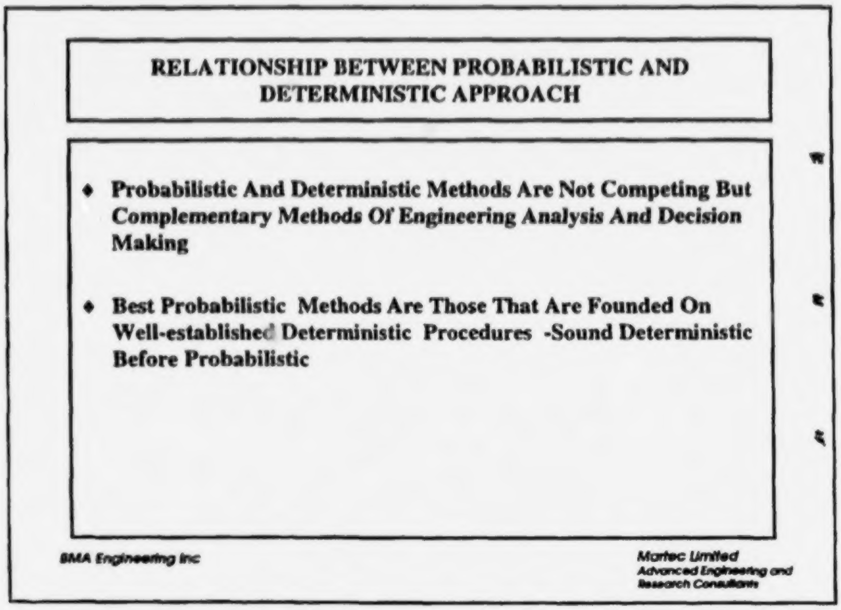

RELATIONSHIP BETWEEN PROBABILISTIC AND DETERMINISTIC APPROACH

- Probabilistic And Deterministic Methods Are Not Competing But Complementary Methods Of Engineering Analysis And Decision Making
- Best Probabilistic Methods Are Those That Are Founded On Well-established Deterministic Procedures -Sound Deterministic Before Probabilistic

BMA Engineering Inc

Martec Limited
Advanced Engineering and
Research Consultants

MODELS FOR PROBABILISTIC RISK ASSESSMENT

Time Dependent Ultimate Strength Limit State

$$g(t) = U(t) - L(t)$$

$$U(t) = M_u(t)$$

$$L(t) = M_{sw}(t) + M_w(t)$$

$M_u(t)$ - **Ultimate Hull Girder Bending Moment Capacity**

$M_{sw}(t)$ - **Still Water Bending Moment**

$M_w(t)$ - **Wave Bending Moment**

MODELS FOR PROBABILISTIC RISK ASSESSMENT

- **Formula For Ultimate Hull Girder Bending Moment Capacity**
  - ⇒ **Analytical**
  - ⇒ **Complicated Numerical Models (FEM)**
- **Review of Formulas Provided in Mansour, 1997**

MODELS FOR PROBABILISTIC RISK ASSESSMENT

- **Mansour and Hoven Model (1994) is used in Current Study**

$$M_u(t) = \phi\sigma_u Z(t)$$

ϕ **- Buckling Knock Down Factor (Non-dimensional)**

σ_u **- Ultimate Strength**

$Z(t)$ **- Midship Hull Elastic Section Modulus**

- **Corrosion Affects The Hull Girder Capacity by Reducing the Section Modulus** $Z(t)$

MODELS FOR PROBABILISTIC RISK ASSESSMENT

- **Modeling the Effect of Corrosion**
- **General Corrosion is Considered**
- **It Reduces the Section Modulus by Thinning the Thickness of the Primary Structural Members**
- **Thickness Reduction r(t) is Modeled as:**

$$r(t) = C_1(t - t_0)^{c_2}$$

- **t_0 - Coating Life (Years); t - Vessel Age (Years); C_1 - Annual Corrosion Rate and C_2 is taken as 1**

MODELS FOR PROBABILISTIC RISK ASSESSMENT

- **Modeling the Effect of Corrosion**

$$M_u(t) = \phi\sigma_u \begin{cases} Z(r(t_0)) & t \le t_0; \quad r(t_0) = 0 \\ Z(r(t)) & t > t_0; \quad r(t) > 0 \end{cases}$$

- **Formulas for Calculating the Section Modulus are Available in Standard Text (Hughes, 1983)**

MODELS FOR PROBABILISTIC RISK ASSESSMENT

- **Load Modeling - Still Water Bending Moment**
- **IACS Design Formula is Used**

$$M_{sw}(t) = \begin{cases} +14.97CL^2B(8.167 - C_b)(lb-in) & hogging \\ -64.88CL^2B(0.7 + C_b)(lb-in) & sagging \end{cases}$$

$$C = \begin{cases} 2.917x10^{7}L & L < 3540\,in \\ 1.559x10^{-1} - \left(\frac{11810-L}{1420375}\right)^{1.5} & 3540 < L < 11810\,in \\ 1.559x10^{-1} & 11810 < L < 13780\,in \\ 1.559x10^{-1} - \left(\frac{L-13780}{2139840}\right)^{1.5} & L > 13780\,in \end{cases}$$

- **L is the Length; B is the Breadth; C_b is the Block Coefficient**

MODELS FOR PROBABILISTIC RISK ASSESSMENT

- **Procedure for Computing Wave Induced Bending Moments**
  - **(1) Identification of Ship Route**
  - **(2) Computation of Ocean Wave Statistics**
  - **(3) Calculation of Bending Moment Using Either Linear or Second Order Strip Theory**
- **A Simplified Direct Method Based on Precalculated Seakeeping Tables is Used (Loukakis and Chryssaatomidis (1985))**
- **Given the Major Dimensions and Operational Profile of the Vessel, The Value of the Wave Induced Bending Moments can be Read from The Sea-Keeping Tables**

BMA Engineering Inc

Martec Limited
Advanced Engineering and Research Consultants

MODELS FOR PROBABILISTIC RISK ASSESSMENT

Limit State Function for Ultimate Strength Capacity

$$g(t) = x_u \phi \sigma_u Z(t) - x_{sw} M_{sw}(t) - x_w x_s M_s(t)$$

x_u - Random Variable Representing Modeling Uncertainty in Ultimate Strength

x_{sw} - Uncertainty in Still Water Bending

x_s - Uncertainty in Wave Bending Moment

x_w - Accounts for Non-linearity in Wave Bending Moment

Typical Values Provided by Mansour & Hoven (1994)

BMA Engineering Inc

Martec Limited
Advanced Engineering and Research Consultants

MODELS FOR PROBABILISTIC RISK ASSESSMENT

Instantaneous Probability of Failure

$$P_f(t)=\int_{\Omega} f(x(t))dx$$

- **FORM, SORM, Monte Carlo Simulation**
- **Available in COMPASS**

MODELS FOR PROBABILISTIC RISK ASSESSMENT

Time Dependent Probability Of Failure

$$\gamma_p(t)=\exp\left(-\int_0^t \lambda(\tau)d\tau\right)$$

$$h(t)=\frac{P_f(t)}{RL(t-1)}$$

$$RL(t)=\exp\left(-\int_0^t \frac{P_f(\tau)}{RL(\tau-1)}d\tau\right)$$

$$P_{ft}(t)=1-RL(t)$$

DEMONSTRATION EXAMPLE

- A Corroding Tanker Structure id Considered
- Hull and Structural Detail of a Corroding Tanker Structure

Principal Dimensions of a Tanker Vessel

Item	Dimension
Length (*L*)	721' 10"
Breadth (*B*)	125'
Depth (*D*)	57'
Draft (*T*)	44' 2"
Block Coefficient	0 75

BMA Engineering Inc

Martec Limited
Advanced Engineering and
Research Consultants

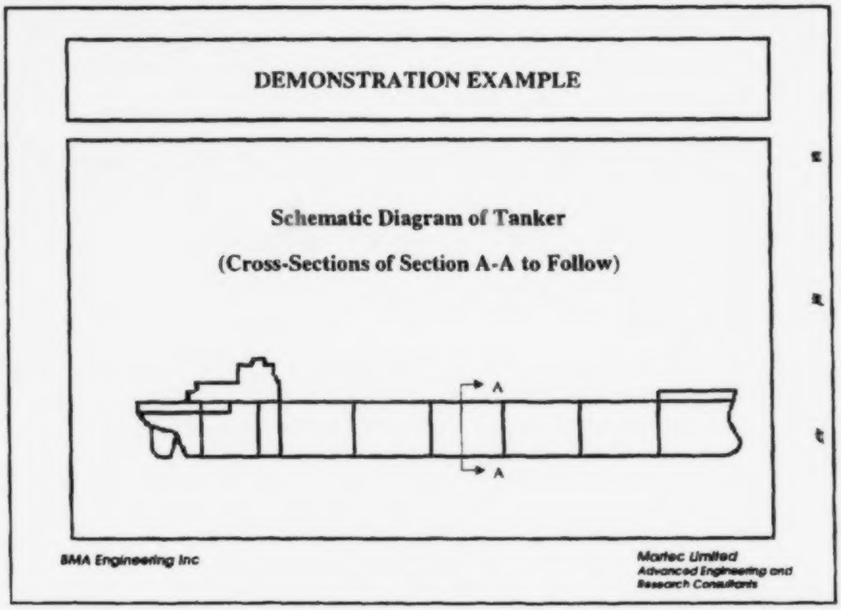

DEMONSTRATION EXAMPLE

Schematic Diagram of Tanker

(Cross-Sections of Section A-A to Follow)

BMA Engineering Inc

Martec Limited
Advanced Engineering and
Research Consultants

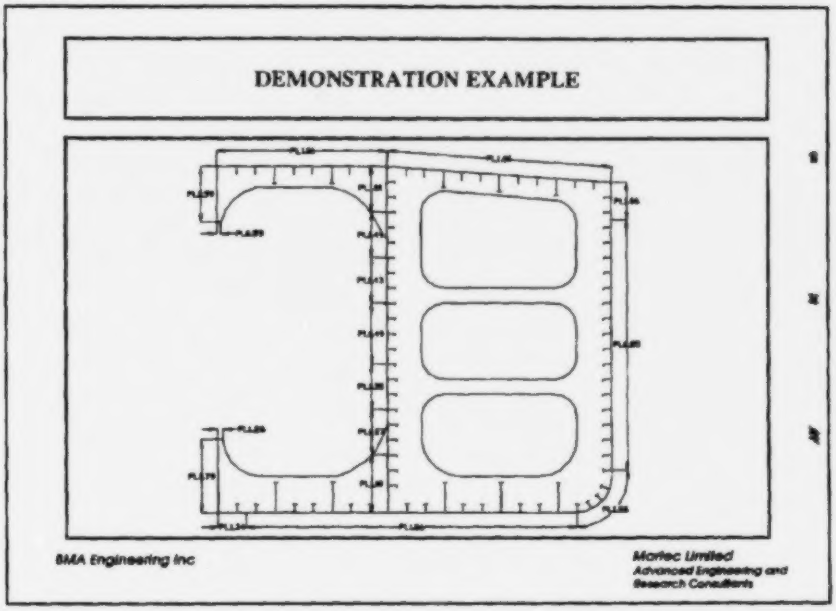

DEMONSTRATION EXAMPLE

BMA Engineering Inc

Martec Limited
Advanced Engineering and
Research Consultants

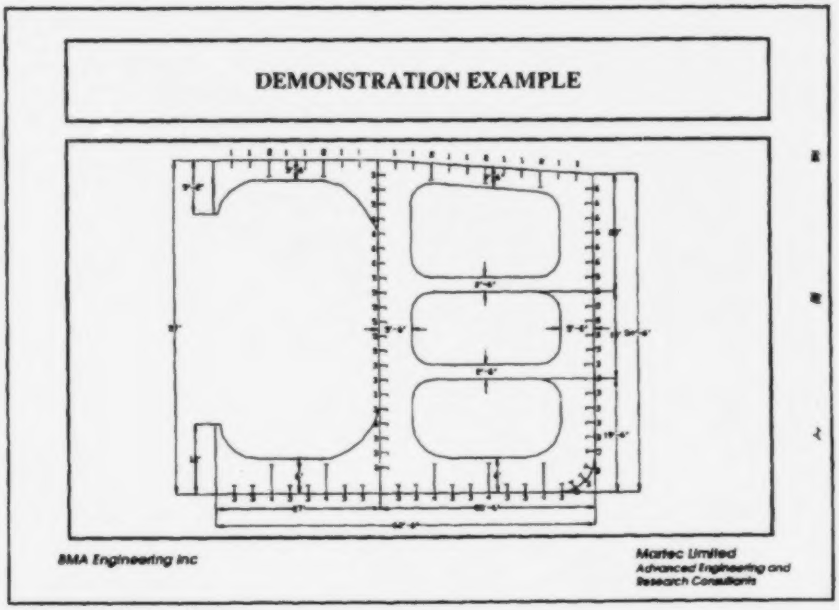

DEMONSTRATION EXAMPLE

BMA Engineering Inc

Martec Limited
Advanced Engineering and
Research Consultants

DEMONSTRATION EXAMPLE

Stiffener Dimensions

Stiffener Dimensions (Inches)		
Stiffener #	Web	Flange
1	17.7x1.40	
2	39.4x0.63	15.75x0.63
3	18.3x0.71	7.50x1.00
4	48.0x0.63	13.8x1.00
5	14.6x0.63	3.94x0.63
6	11.7x0.45	3.94x0.63

DEMONSTRATION EXAMPLE

Typical Corrosion Rates for Tanker Members (TSCF, 1997)

Corrosion Rates						
	Mean		Minimum		Maximum	
Location	mm/yr	in/yr	mm/yr	in/yr	mm/yr	in/yr
Deck Plating	0.065	2.5591E-03	0.03	1.1811E-03	0.10	3.9370E-03
Deck Longitudinals (Web)	0.065	2.5591E-03	0.03	1.1811E-03	0.10	3.9370E-03
Side Shell Plating	0.030	1.1811E-03	0.03	1.1811E-03	0.03	1.1811E-03
Side Shell Plating Longitudinals (Web)	0.030	1.1811E-03	0.03	1.1811E-03	0.03	1.1811E-03
Bottom Shell Plating	0.170	6.6929E-03	0.04	1.5748E-03	0.30	1.1811E-02
Bottom Shell Longitudinals (Web)	0.065	2.5591E-03	0.03	1.1811E-03	0.10	3.9370E-03
Longitudinal Bulkhead Plating	0.065	2.5591E-03	0.03	1.1811E-03	0.10	3.9370E-03
Longitudinal Bulkhead Longs (Web)	0.065	2.5591E-03	0.03	1.1811E-03	0.10	3.9370E-03

DEMONSTRATION EXAMPLE

Probabilistic Characteristics of Random Variables

Random Variable	Mean Value	Coefficient of Variation (COV*)	Distribution Type
Ultimate Stress, σ_u	40.8 ksi	0.1	Lognormal
Knockdown Factor, c	0.95		Fixed
Stillwater Moment, M_{sw}	1.817×10^{10} lb-in	0.4	Normal
Wave Induced Moment, M_w	2.837×10^{10} lb-in	0.1	Extreme

DEMONSTRATION EXAMPLE

Probabilistic Characterization of Random Variables (Mansour & Hoven, 1994)

Random Variable	Distribution Type	Mean	Coefficient of Variation (COV*)
x_u	Normal	1.0	0.15
x_{sw}	Normal	1.0	0.05
x_w	Normal	0.9	0.15
x_s	Normal	1.15	0.03

DEMONSTRATION EXAMPLE

Corrosion Rates			
Location	Mean (in/yr)	Coefficient of Variation	Distribution Type
Deck Plating	2.5591E-03	0.5	Weibull
Deck Longitudinals (Web)	2.5591E-03	0.5	Weibull
Side Shell Plating	1.1811E-03	0.1	Weibull
Side Shell Plating Longitudinals (Web)	1.1811E-03	0.1	Weibull
Bottom Shell Plating	6.6929E-03	0.5	Weibull
Bottom Shell Longitudinals (Web)	2.5591E-03	0.5	Weibull
Longitudinal Bulkhead Plating	2.5591E-03	0.5	Weibull
Longitudinal Bulkhead Longs (Web)	2.5591E-03	0.5	Weibull

BMA Engineering Inc

Martec Limited
Advanced Engineering and Research Consultants

DEMONSTRATION EXAMPLE

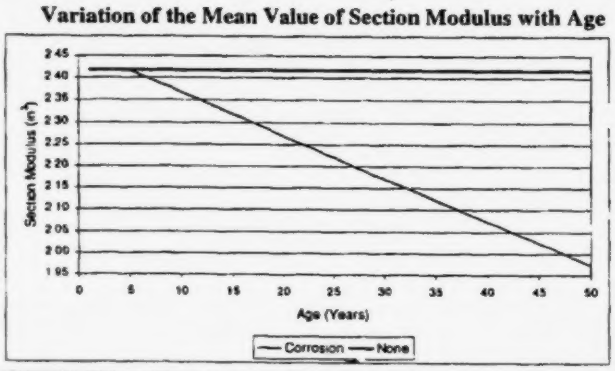
Variation of the Mean Value of Section Modulus with Age

BMA Engineering Inc

Martec Limited
Advanced Engineering and Research Consultants

DEMONSTRATION EXAMPLE

Instantaneous and Time Dependent Probabilities of Failure for a Tanker with Corrosion

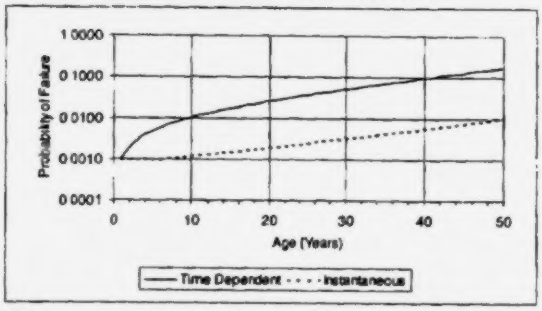

BMA Engineering Inc

Martec Limited
Advanced Engineering and
Research Consultants

DEMONSTRATION EXAMPLE

Effect of Corrosion Growth Rate on a Ship's Section Modulus

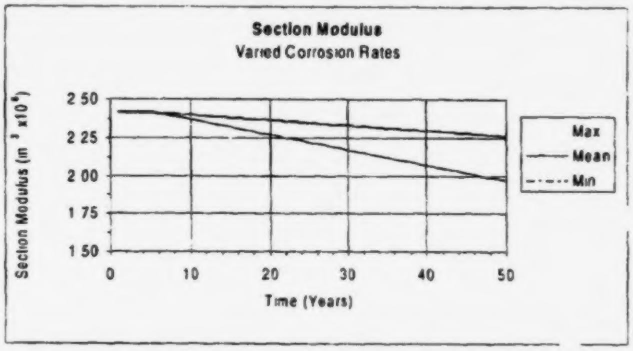

BMA Engineering Inc

Martec Limited
Advanced Engineering and
Research Consultants

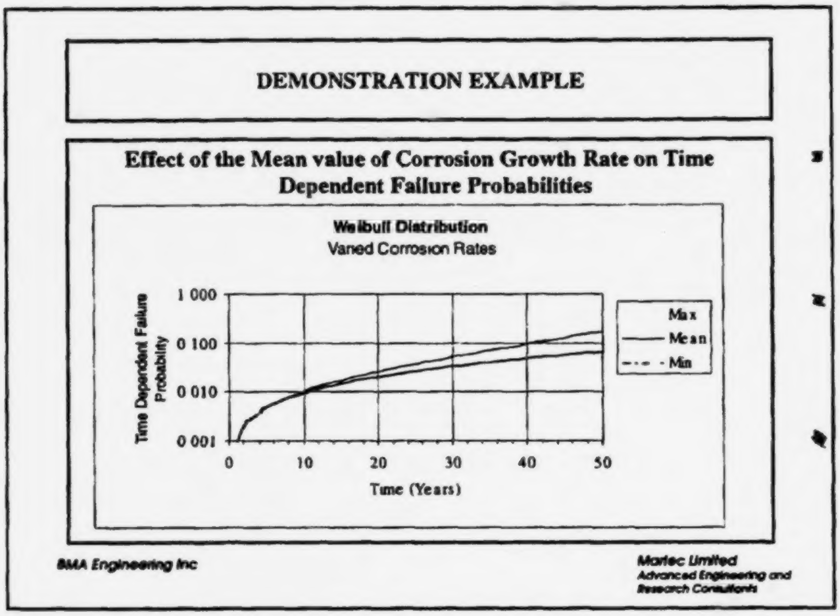

DEMONSTRATION EXAMPLE

Effect of the Mean value of Corrosion Growth Rate on Time Dependent Failure Probabilities

Weibull Distribution

Varied Corrosion Rates

BMA Engineering Inc

Martec Limited
Advanced Engineering and Research Consultants

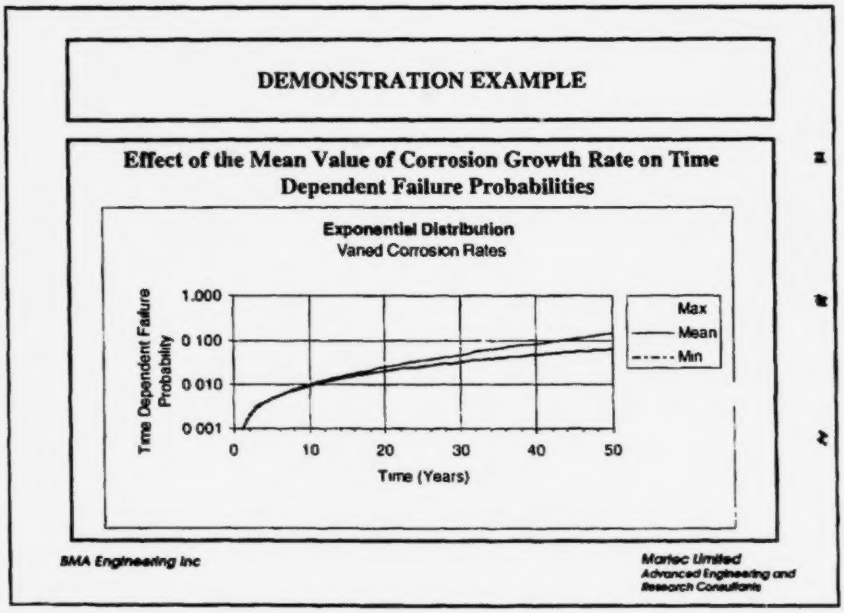

DEMONSTRATION EXAMPLE

Effect of the Mean Value of Corrosion Growth Rate on Time Dependent Failure Probabilities

Exponential Distribution

Varied Corrosion Rates

BMA Engineering Inc

Martec Limited
Advanced Engineering and Research Consultants

DEMONSTRATION EXAMPLE

Effect of Probability Distribution of Corrosion Growth Rates on Time Dependent Failure Probabilities of an Aging Tanker

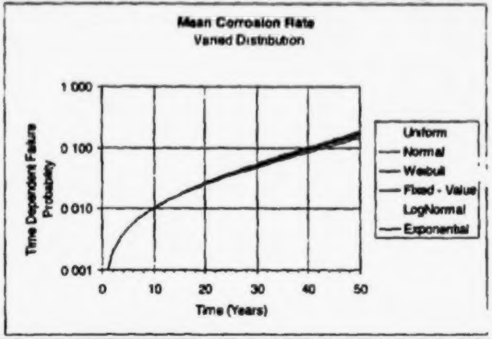

BMA Engineering Inc

Martec Limited
Advanced Engineering and Research Consultants

LIMITATIONS OF RESULTS

- **Renewal of Structural Members Not Included**
- **Pitting / Cracks Not Considered**
- **Rate of Corrosion Growth Assumed to be Time Invariant**

BMA Engineering Inc

Martec Limited
Advanced Engineering and Research Consultants

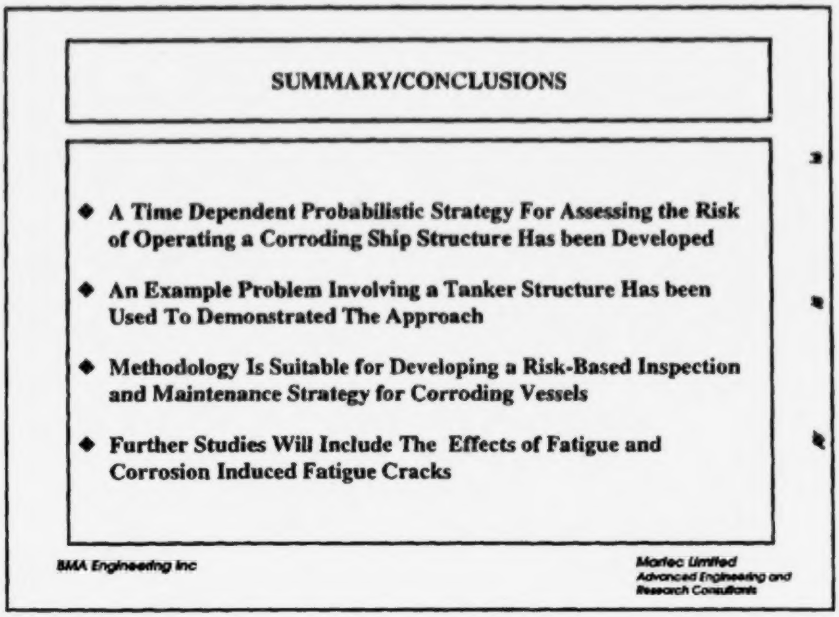

SUMMARY/CONCLUSIONS

- A Time Dependent Probabilistic Strategy For Assessing the Risk of Operating a Corroding Ship Structure Has been Developed
- An Example Problem Involving a Tanker Structure Has been Used To Demonstrated The Approach
- Methodology Is Suitable for Developing a Risk-Based Inspection and Maintenance Strategy for Corroding Vessels
- Further Studies Will Include The Effects of Fatigue and Corrosion Induced Fatigue Cracks

BMA Engineering Inc

Martec Limited
Advanced Engineering and Research Consultants

#516464 (49)

A Neural Network Analysis of HSLA Steels

by

E. A. Metzbower
U. S. Naval Research Laboratory
Code 6320
Washington DC 20375-5320
USA

E. J. Czyryca
Naval Surface Warfare Center
Carderock Division
Code 6140
West Bethesda, MD 20817-5700
USA

and

H.K.D.H. Bhadeshia
University of Cambridge

Abstract

A neural network analysis has been performed on a data set from several programs that the U. S. Navy funded in order to determine the composition and properties of HSLA steels. The input variables were the chemical elements, plate thickness, austenitizing and tempering temperatures, and a parameter which assess the cooling rate from those temperatures. The outputs consisted of the yield and ultimate tensile strength, elongation, and Charpy V-notch values at either –1 or –51 °C. The data was sorted into two sets: one with a yield strength of approximately 550 MPa; and the other with a yield strength of approximately 690 MPa. The neural network technique used a Bayesian framework and allowed the estimation of error bars which warn when the data are sparse or locally noisy. After the neural network was trained, a best model was determined. The single best model sometimes generalizes poorly on unseen data. A committee of best models was then used to make predictions that are more reliable than the single best model. Several compositions were evaluated at different thickness and different yield strengths to assess the effect of changes in composition on the properties of the plate.

A Neural Network Analysis of HSLA Steels

E. A. Metzbower
Naval Research Laboratory
E. J. Czyryca
Naval Surface Weapons Center
Carderock Division
H. K. D. H. Bhadeshia
University of Cambridge

Outline

- Introduction
- Neural Networks
- Results
- Predictions
- Conclusions

Introduction

- HSLA Steels
  - 550-900 MPa (80-130 ksi)
  - Low Carbon < 0.05 wt%
  - Compositional change with thickness
  - Cu dispersion strengthened
  - Ni ensures good fracture toughness
  - Can be welded with low preheat/interpass temperatures

Neural Network Concept

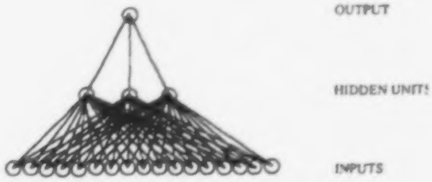

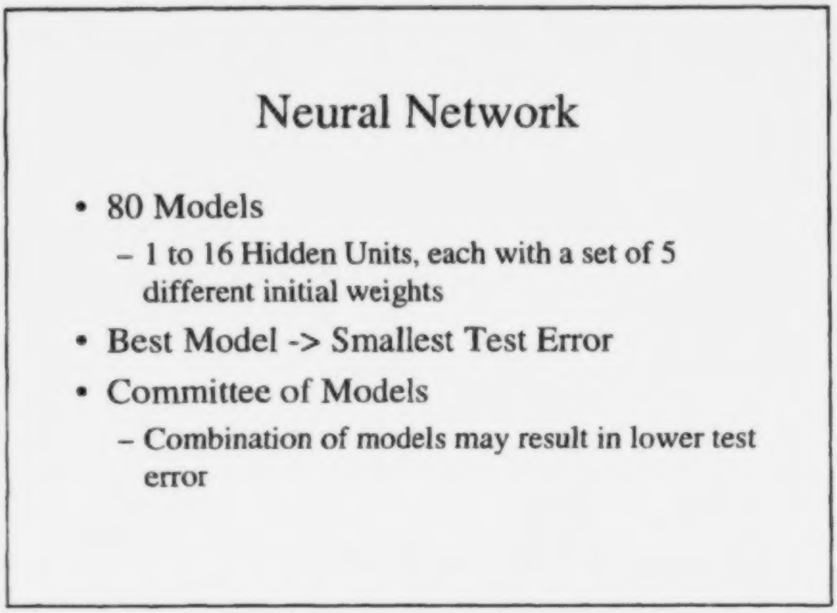

Neural Network

- 80 Models
  - 1 to 16 Hidden Units, each with a set of 5 different initial weights
- Best Model -> Smallest Test Error
- Committee of Models
  - Combination of models may result in lower test error

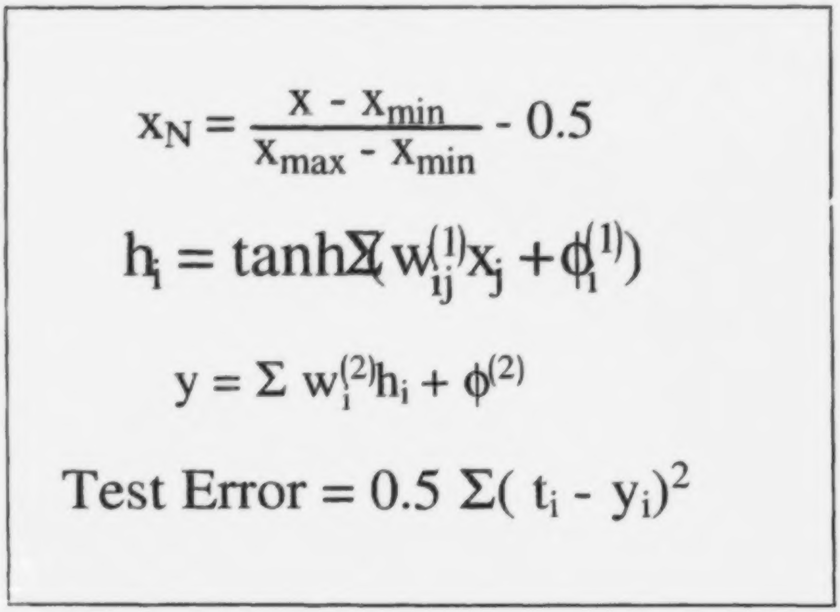

$$x_N = \frac{x - x_{min}}{x_{max} - x_{min}} - 0.5$$

$$h_i = \tanh(\Sigma w_{ij}^{(1)} x_j + \phi_i^{(1)})$$

$$y = \Sigma\, w_i^{(2)} h_i + \phi^{(2)}$$

$$\text{Test Error} = 0.5\, \Sigma(t_i - y_i)^2$$

Input and Output for 550 MPa HSLA Steel

Input	Minimum	Maximum	Mean	Std Dev
C	0 025	0 064	0 0501	0 0097
Mn	0 5	1 4	0 8751	0 3561
Si	0 13	0 36	0 2499	0 0603
Cr	0 22	0 83	0 6133	0 1419
Ni	0 86	2 52	1 6454	0 5542
Mo	0 19	0 66	0 3662	0 1596
Cu	0 74	1 26	1 1027	0 0799
Nb	0 003	0 3	0 0434	0 0599
Al	0 017	0 07	0 0310	0 0105
N	0 0	0 01	0 0033	0 0045
P	0 0	0 013	0 0033	0 0047
S	0 0	0 01	0 0028	0 0043
Thickness	13	51	24 0204	16 8100
Austenite Temp	899	927	901 5714	8 1278
Cooling Rate	4	10	6 8163	3 0098
Temper Temp	538	704	614 5510	39 2613
Cooling Rate	4	10	9 4490	1 7417
YS / MPa	521 3	617	572 1867	28 3776
UTS / MPa	637	792	706 6667	32 4036
Elongation / %	20 3	32	27 1296	1 8681
CVN@-51EC / J	3	286 1	85 1917	48 3516

Neural Network Calculates

- Yield Strength
- ° Ultimate Tensile Strength
- Elongation
- Charpy V-Notch Value
  - @-18°C (0°F)
  - @-51°C (-60°F)

Number of Data Used in Neural Networks

	550 MPa	690 MPa
Yield Strength	98	150
Ultimate Strength	96	150
Elongation	98	150
CVN@-18EC		64
CVN@-51EC	84	88

- Results

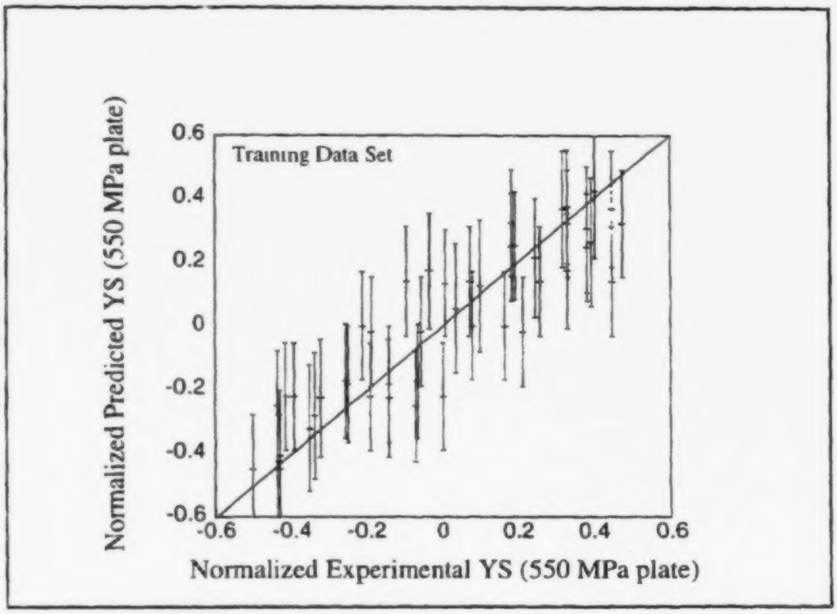
Training Data Set
Normalized Predicted YS (550 MPa plate)
Normalized Experimental YS (550 MPa plate)
0.6
0.4
0.2
0
-0.2
-0.4
-0.6
-0.6
-0.4
-0.2
0
0.2
0.4
0.6

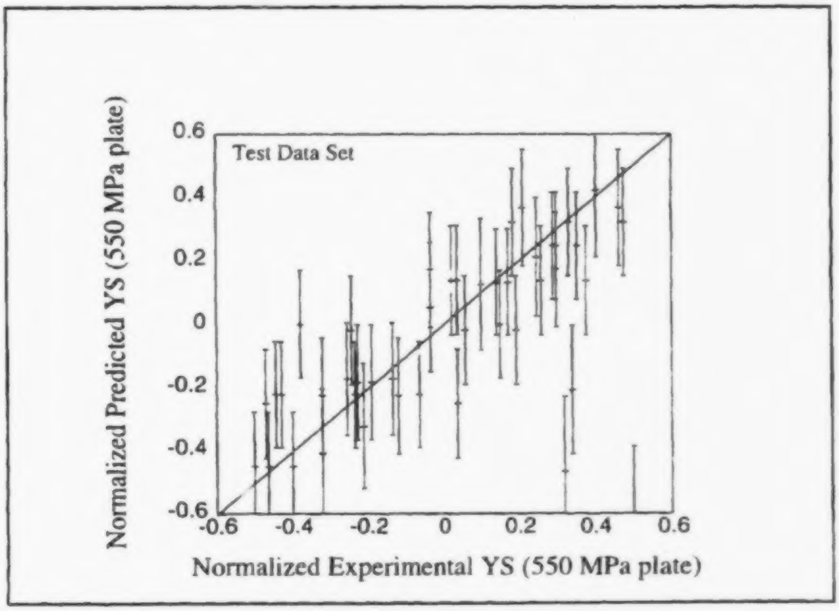
Test Data Set
Normalized Predicted YS (550 MPa plate)
Normalized Experimental YS (550 MPa plate)
0.6
0.4
0.2
0
-0.2
-0.4
-0.6
-0.6
-0.4
-0.2
0
0.2
0.4
0.6

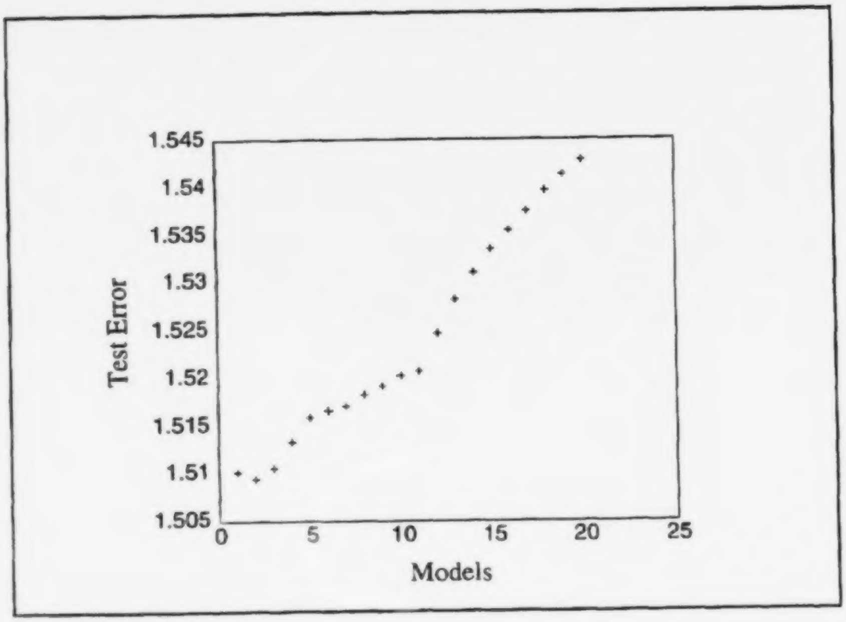
Test Error
1.545
1.54
1.535
1.53
1.525
1.52
1.515
1.51
1.505
0
5
10
15
20
25
Models

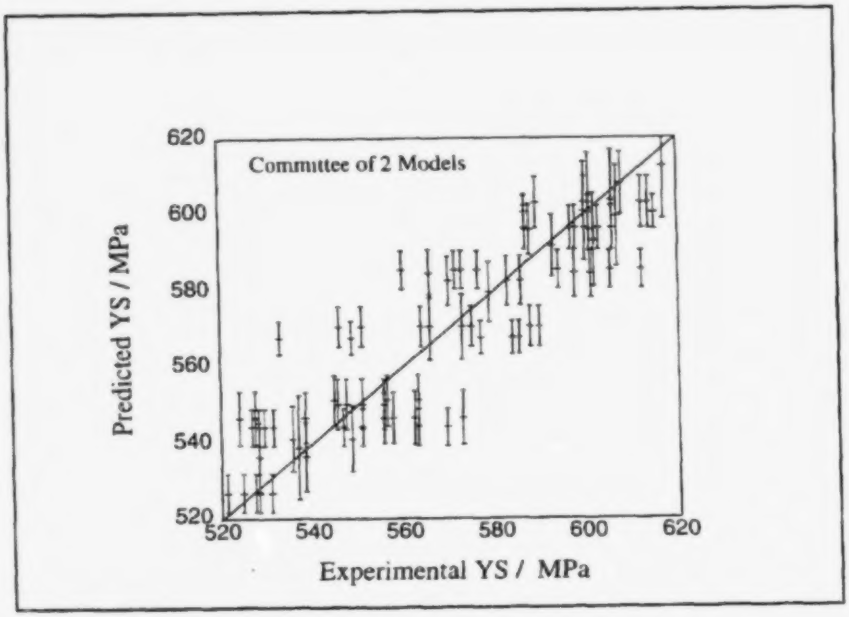
Committee of 2 Models
Predicted YS / MPa
620
600
580
560
540
520
520
540
560
580
600
620
Experimental YS / MPa

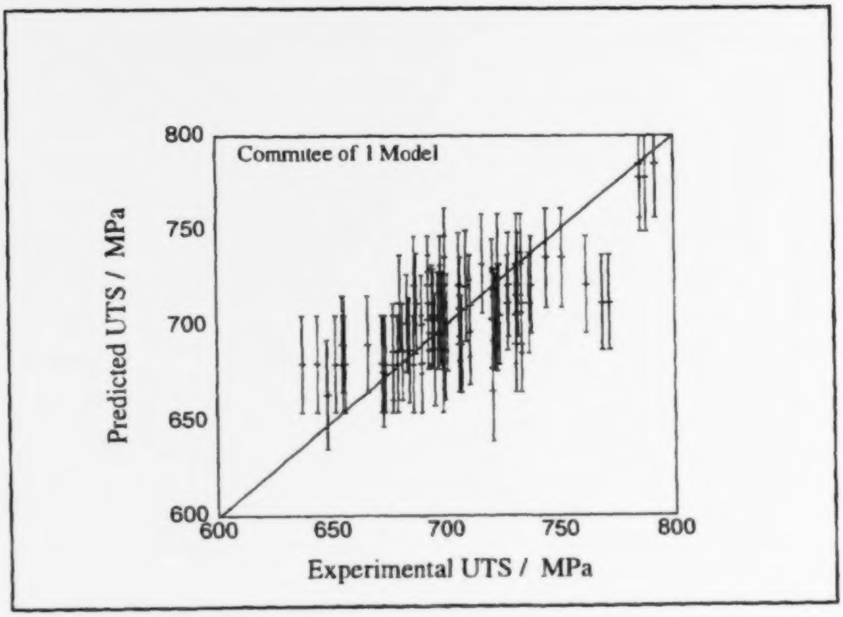
Committee of 1 Model
Predicted UTS / MPa
Experimental UTS / MPa
600
650
700
750
800
600
650
700
750
800

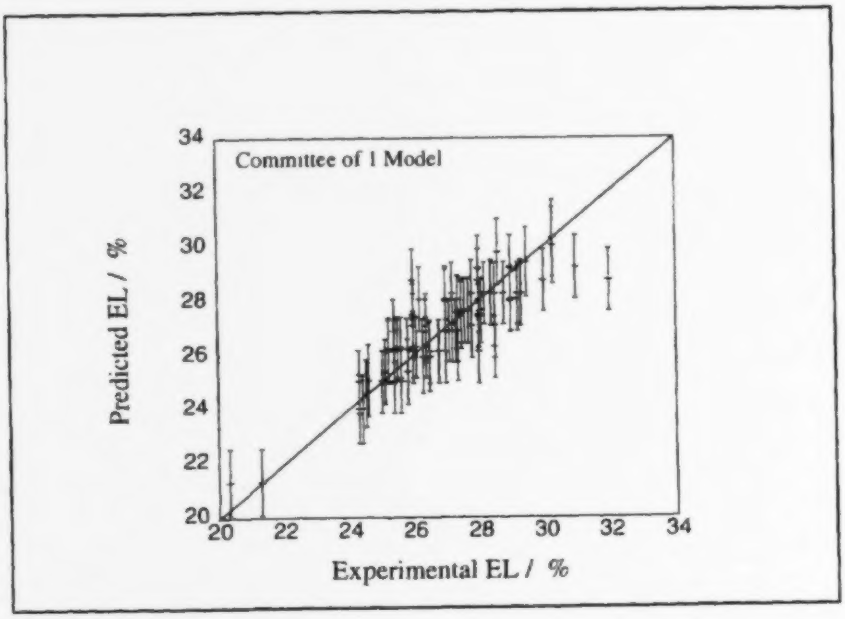
Committee of 1 Model
Predicted EL / %
Experimental EL / %
20
22
24
26
28
30
32
34
20
22
24
26
28
30
32
34

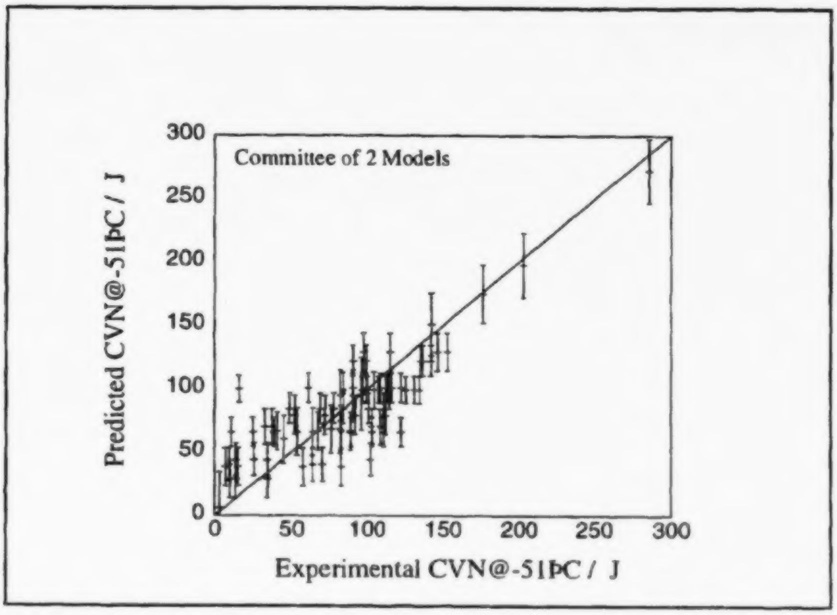

Predictions

Chemistry for 550 MPa Plate

Input	25 mm	50 mm	50 mm / A736
C	0.04	0.04	0.04
Mn	0.60	1.00	1.50
Si	0.30	0.30	0.30
Cr	0.65	0.60	Nil
Ni	0.90	2.00	0.90
Mo	0.20	0.50	0.20
Cu	1.20	1.20	1.20
Nb	0.045	0.030	0.020
Al	0.020	0.020	0.020
N			
P	0.010	0.010	0.010
S	0.004	0.004	0.004
Thickness	25	50	50
Austenitizing T / ÌC	899ÌC	899ÌC	899ÌC
Temper T / ÌC	621ÌC	621ÌC	621ÌC

Chemistry for 690 MPa

Input	25 mm	50 mm
C	0.04	0.04
Mn	1.00	1.00
Si	0.30	0.30
Cr	0.65	0.55
Ni	1.75	2.50
Mo	0.45	0.50
Cu	1.20	1.20
Nb	0.030	0.030
Al	0.020	0.020
N		
P	0.010	0.010
S	0.004	0.004
Thickness	25	50
Austenitizing T / ÌC	899ÌC	899ÌC
Temper T / ÌC	593 – 649ÌC	593-649ÌC

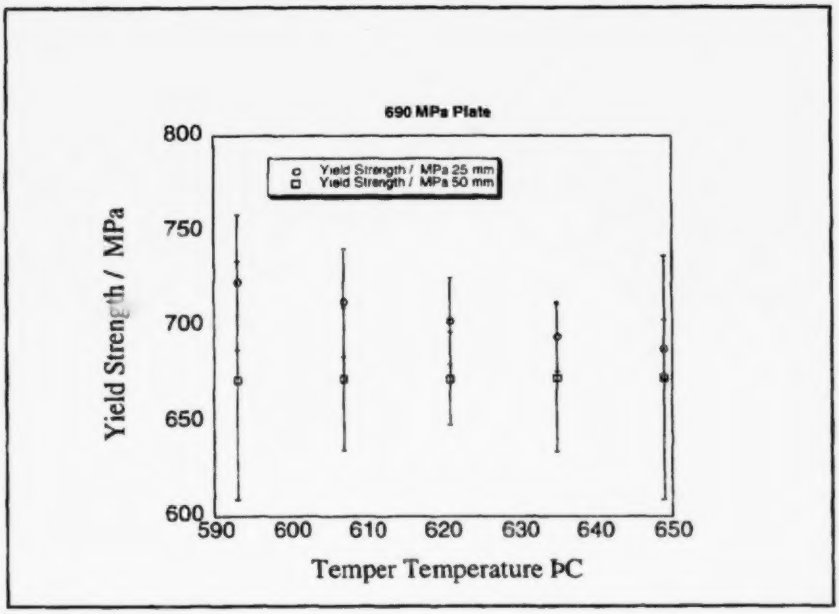
690 MPa Plate
Yield Strength / MPa 25 mm
Yield Strength / MPa 50 mm
Yield Strength / MPa
800
750
700
650
600
590
600
610
620
630
640
650
Temper Temperature ÞC

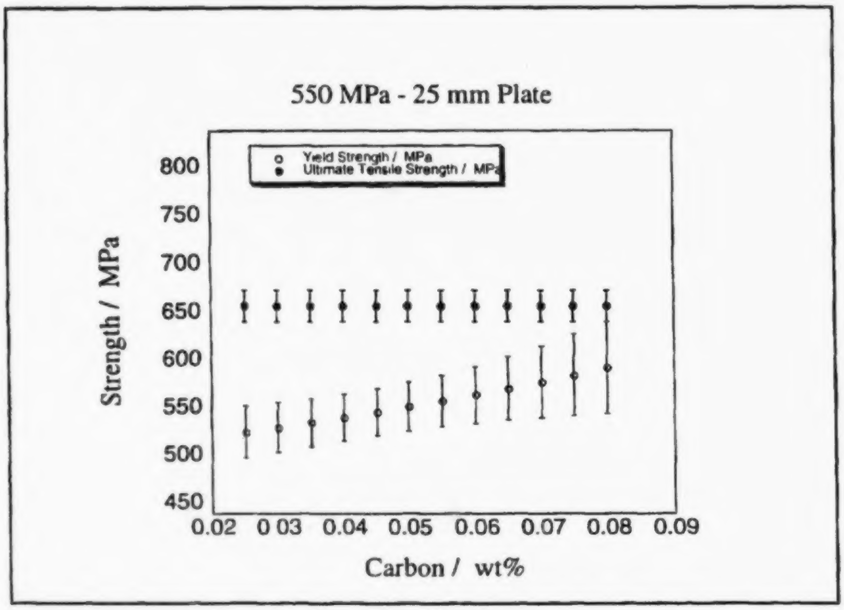
550 MPa - 25 mm Plate
Yield Strength / MPa
Ultimate Tensile Strength / MPa
Strength / MPa
800
750
700
650
600
550
500
450
0.02
0 03
0.04
0.05
0.06
0.07
0.08
0.09
Carbon / wt%

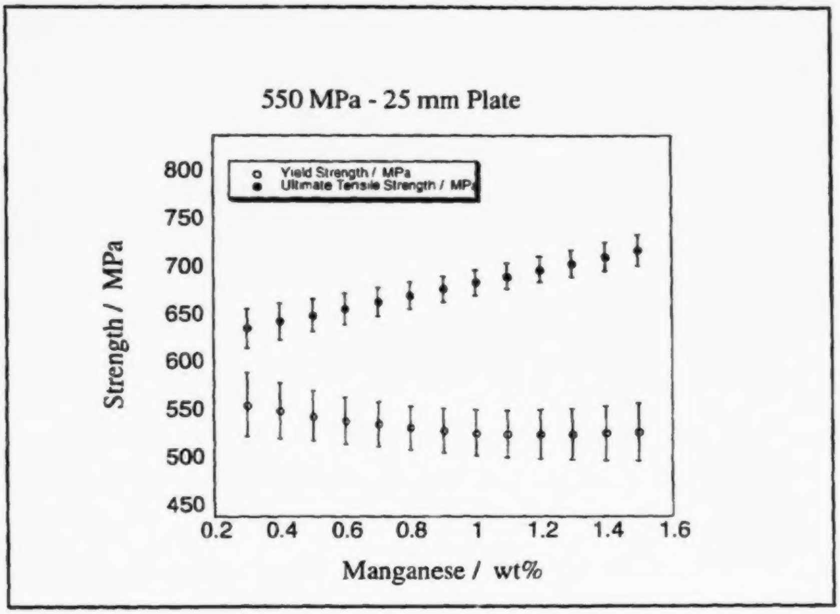
550 MPa - 25 mm Plate
Yield Strength / MPa
Ultimate Tensile Strength / MP
Strength / MPa
800
750
700
650
600
550
500
450
0.2
0.4
0.6
0.8
1
1.2
1.4
1.6
Manganese / wt%

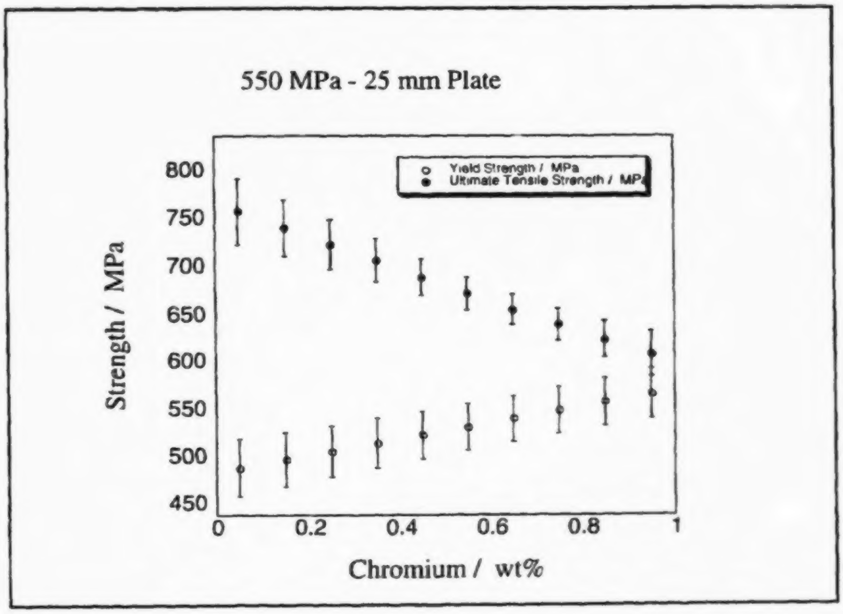
550 MPa - 25 mm Plate
Yield Strength / MPa
Ultimate Tensile Strength / MP
Strength / MPa
800
750
700
650
600
550
500
450
0
0.2
0.4
0.6
0.8
1
Chromium / wt%

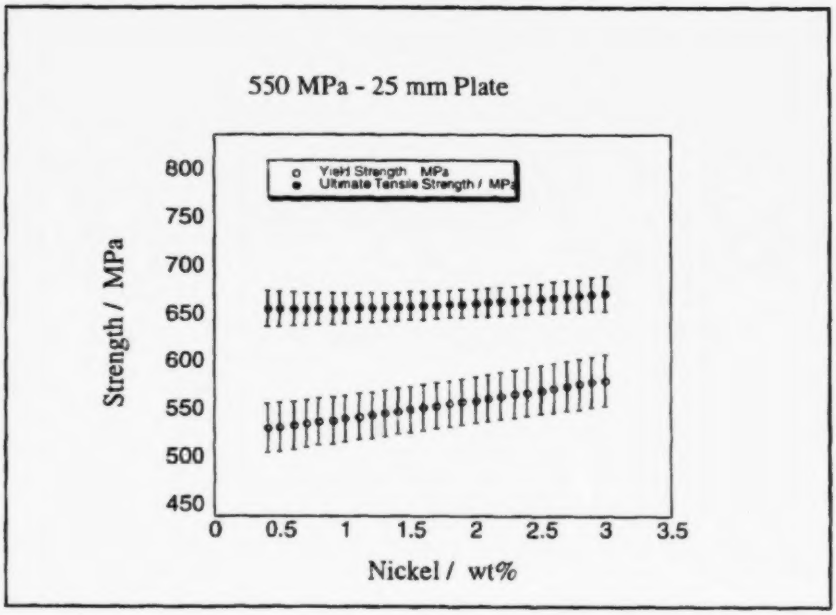
550 MPa - 25 mm Plate
Yield Strength MPa
Ultimate Tensile Strength / MP
Strength / MPa
800
750
700
650
600
550
500
450
0
0.5
1
1.5
2
2.5
3
3.5
Nickel / wt%

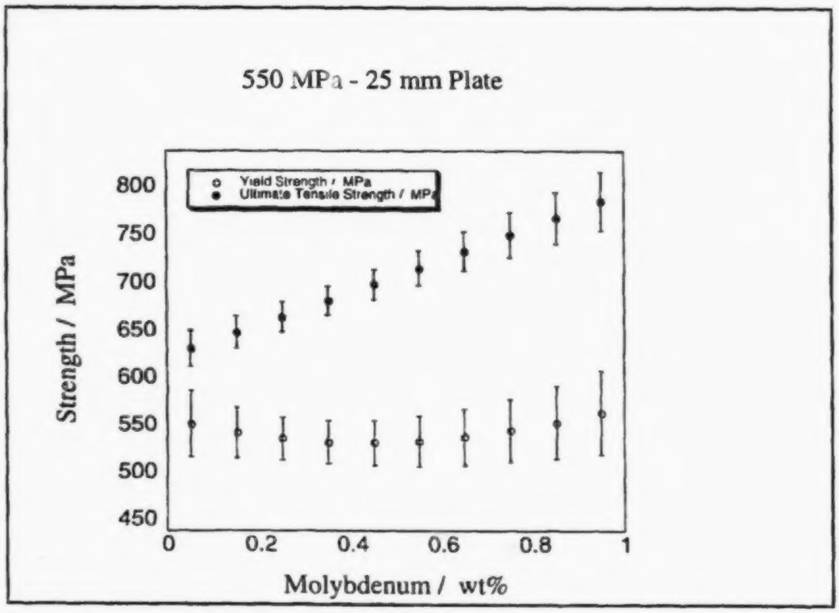
550 MPa - 25 mm Plate
Yield Strength / MPa
Ultimate Tensile Strength / MP
Strength / MPa
800
750
700
650
600
550
500
450
0
0.2
0.4
0.6
0.8
1
Molybdenum / wt%

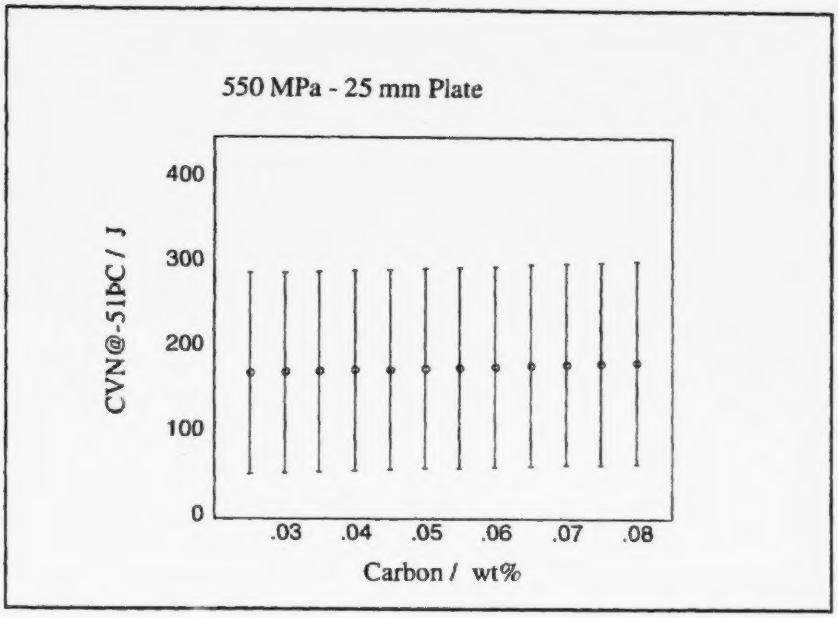
550 MPa - 25 mm Plate
CVN@-51ÞC / J
0
100
200
300
400
.03
.04
.05
.06
.07
.08
Carbon / wt%

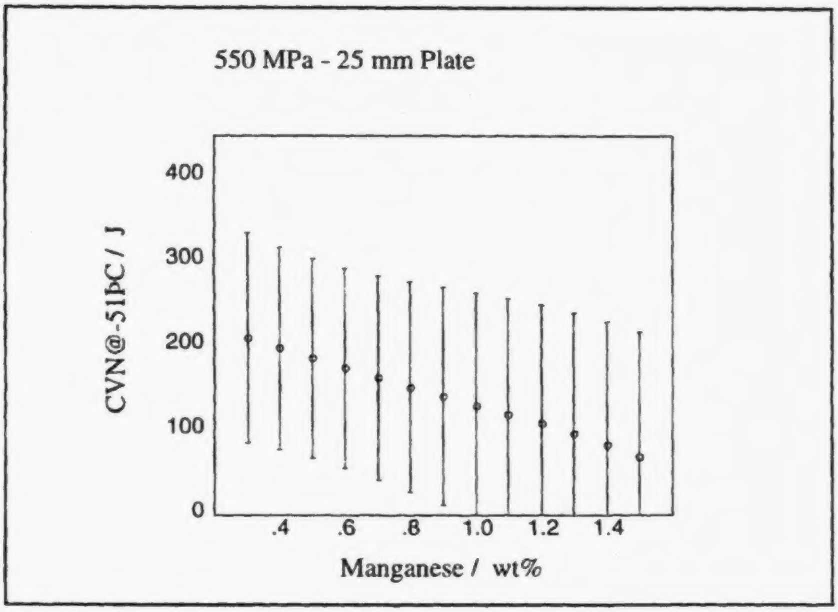
550 MPa - 25 mm Plate
CVN@-51ÞC / J
0
100
200
300
400
.4
.6
.8
1.0
1.2
1.4
Manganese / wt%

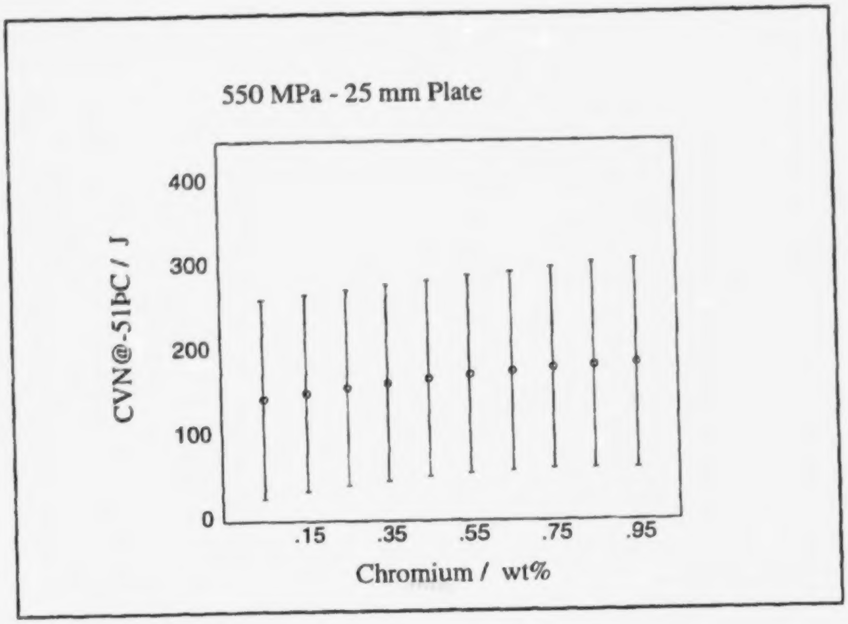
550 MPa - 25 mm Plate
CVN@-51ÞC / J
400
300
200
100
0
.15
.35
.55
.75
.95
Chromium / wt%

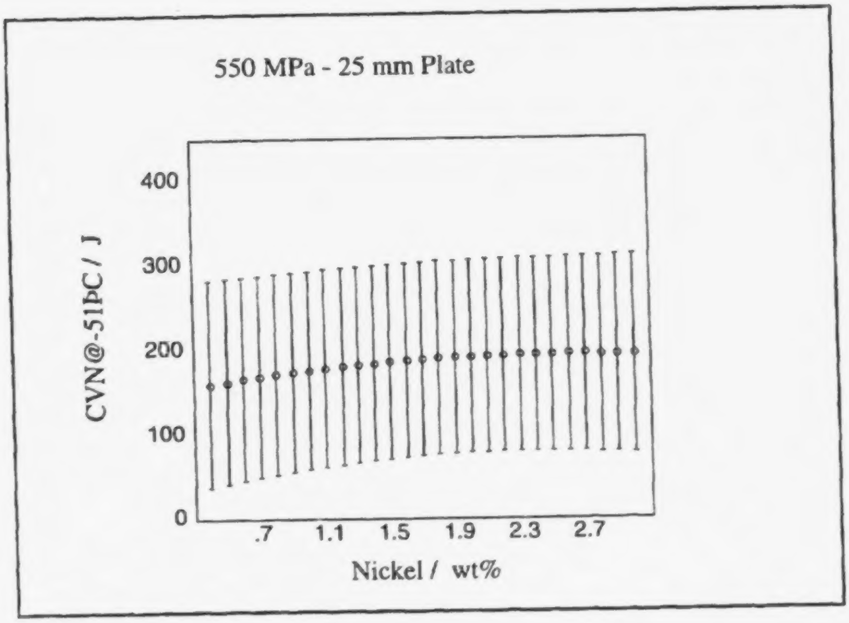
550 MPa - 25 mm Plate
CVN@-51ÞC / J
400
300
200
100
0
.7
1.1
1.5
1.9
2.3
2.7
Nickel / wt%

Conclusions

- 550 MPa - 25 mm Plate
  - Chemistry lean for YS
  - Meets CVN@-51°C
- 550 MPa - 50 mm Plate
  - Chemistry rich for YS
  - Meets CVN@-51°C
- A736 - 50 mm plate
  - Chemistry does not meet specifications

Conclusion

- A neural net analysis is a useful technique to determine chemistry modification in order to satisfy mechanical property requirements by analyzing the test data from a limited number of test and minimizes the need for many experimental heats.

#516465 (50)

Non-Magnetic Stainless Steel Hulls: Past, Present and Future*

by

A. John Sedriks and Philip J. Dudt*****

**Office of Naval Research, Materials Division, Arlington, VA 22217, USA

***Naval Surface Warfare Center, Carderock Division, West Bethesda, MD 20817, USA

ABSTRACT

Issues are discussed relating to (i) stress-corrosion cracking resistance, (ii) controlling weld corrosion and hot cracking of welded materials, (iii) coating technology requirements and (iv) magnetic properties of certain stainless steels being considered as candidate construction materials for the non-magnetic advanced double hulls of possible future U.S. Navy combatants. Among materials discussed are the domestically produced stainless steel grades S31600 (type 316), S20910 (Nitronic 50), N08367 (6XN) and the German stainless steel 1.3964.9 and it's weld filler material 1.3954.0. Past and present experience is discussed in relation to the reported operating experiences with post-World War II German submarines and mine countermeasure vessels constructed from the non-magnetic stainless steel 1.3964.9. Possible future developments are considered in terms of the non-magnetic requirement for the larger (e.g. 170 metre) hulls of U.S. Navy combatants and of metallic, as opposed to the currently used GRP, hulls of mine countermeasure vessels. The need for welding/joining procedures in which the generation of the hexavalent chromium ion is minimized or eliminated is emphasized. For underwater hull coatings the need is identified for an environmentally acceptable coating system which is capable of preventing crevice corrosion within the tight crevice formed between the stainless steel and the paint layer.

INTRODUCTION

The disturbance of the earth's magnetic field by a ferromagnetic warship can be used as a means of it's detection and/or incapacitation, particularly by magnetically triggered mines. Traditional means for reducing a warship's magnetic signature are deperming, wiping, and degaussing. However, it is sometimes considered preferable to reduce the magnetic signature by constructing the ship's hull from non-magnetic materials. While wood hulls were used for the earlier minesweepers, two of the more recent ways of accomplishing this for mine countermeasure vessels have involved using (i) glass-fiber reinforced plastic (GRP) and (ii) non-magnetic austenitic stainless steels. The stainless steel approach was adopted by the German Navy, whereas the GRP approach was adopted by the British Navy and the Italian Navy and more recently by the U.S. Navy and the Australian Navy.

There is now multi-year service experience with both GRP and stainless steel hulls for mine countermeasure vessels. In a recent article summarizing the performance of the German mine countermeasure vessels (1), it is claimed that the first German stainless steel vessel has fulfilled all expectations after eight years of service. The author also notes that the anticipated eddy current problem was easily managed by the vessel's degaussing system, and there had been no changes in the non-magnetic characteristics of the hull material during the eight year service period.

The possibility of building warships with non-magnetic advanced double hulls much larger in size (e.g. 170 metres in length) than mine countermeasure vessels (e.g. 50 metres in length) has generated further interest in the performance of austenitic stainless steels, since the limited stiffness (lower modulus) of GRP has traditionally restricted it's use to ship hulls 60 metres or less in length. To date the longest polymer-matrix composite hull has been that of the Swedish Navy corvette VISBY at 72.8 metres, where the additional length has been achieved in part by replacing the glass fibers in the GRP with carbon fibers (2). It is the purpose of this review to note past experience with austenitic stainless steel hulls, as reported in publications describing the German Navy's experience with such materials, and to discuss the possible use of non-magnetic austenitic stainless steels as hull materials for U.S. Navy vessels. The stainless steels considered in this paper are S31600 (AISI type 316), S20910 (Nitronic 50, 22-13-5, XM-19, Carpenter 22Cr-13Ni-5Mn, Aquamet 22), N08367 (AL 6XN), and those described by the German VDE Werkstoff Numbers 1.3964.9 and 1.3954.0. For brevity these steels will be referred to in this paper as type 316, Nitronic 50, 6XN, 1.3964.9, and 1.3954.0. The chemical compositions, mechanical properties, and pitting resistance equivalent numbers (PREN) calculated from the specified maximum alloying levels of chromium, molybdenum and nitrogen of these stainless steels, are shown in Figure 1. Increasing values of PREN are linked with increasing resistance to pitting and crevice corrosion. The chemical composition of 1.3954.0 is noted in the text.

STRESS-CORROSION CRACKING

Service Experience with Stress-Corrosion Failures

Since the German Navy has been, by far, the greatest user of metallic non-magnetic hulls, most of the knowledge about stress-corrosion cracking in service derives from publications describing their experience. Austenitic stainless steels were not initially selected as the non-magnetic hull materials for their first post-World War II classes of submarines. The non-magnetic hulls of the first submarines were in fact constructed from a chromium-modified Hadfields manganese steel with the approximate composition Fe-17.7%Mn-4.7%Cr-0.48%C-0.02%Ni (3). Unfortunately this steel exhibited stress-corrosion cracking of components in service and was discontinued as a material of construction for that reason. The German stainless steel 1.3964.9 (Figure 1) was selected as the non-magnetic hull material for the subsequent classes of submarines and the mine countermeasure vessels of the FRANKENTHAL and HAMELN classes, and is the likely material for the future 212 class of submarines to be introduced in 2003 (4). There have been no reports of stress-corrosion problems in service for the follow-on 206 or 206A classes of submarines or the mine countermeasure vessels. A German submarine and mine countermeasure vessel with hulls constructed from the non-magnetic austenitic stainless steel 1.3964.9 are shown in Figure 2.

Laboratory Stress-Corrosion Tests of Other Candidate Alloys

Over the last four decades there has been significant laboratory stress-corrosion testing of austenitic stainless steels (5). The three stress corrosion tests that are most widely used to test for resistance to chloride-induced stress-corrosion cracking are: (i) the boiling 42% magnesium chloride test (ASTM G36), (ii) the boiling acidified 25% sodium chloride test (ASTM G123), and (iii) the Wick test, in which a porous insulating material is used as a wick to draw salt solution to the heated surface of a stressed specimen. A summary of the stress-corrosion test data for 6XN, Nitronic 50, and type 316 stainless steel is summarized in Figure 3 where it is seen that 6XN fails the boiling magnesium chloride test but passes the boiling sodium chloride and the Wick tests, whereas type 316 fails all three tests (4). Nitronic 50 fails the boiling magnesium chloride test (6), and there is no data available for this material for the other two tests.

Ambient temperature seawater is generally not considered to cause stress corrosion cracking in austenitic stainless steels (7) or nickel-base alloys (8), and exposure of type 316 U-bend specimens even in boiling seawater for three months did not reveal any stress-corrosion cracking (9). However, it has been found that type 316 will exhibit stress corrosion cracking in vapor spaces above heated chloride solutions (10) and in the atmosphere above indoor swimming pools (11). The mechanisms of this type of cracking remain to be established and type 316 clearly should not be used in locations subject to condensation of chloride/chlorine bearing moisture. It is useful to note here that type 316LN is the main grade used in shipboard chemical tanker construction for which a minimum of 2.75% Mo is specified (12). (The suffix N in 316LN indicates a nitrogen alloying addition in the range 0.10

to 0.16% nitrogen for increased strength.) No stress corrosion problems have been reported to date for shipboard chemical tanker applications. However, more research is warranted to establish if this is likely to be a problem with combatants.

CONTROLING WELD CORROSION AND HOT CRACKING

Background

A detailed schematic of a solidified weldment in an austenitic stainless steel is illustrated in Figure 4 (13). The weld nugget (also known as the composite region) contains the bulk of the filler metal plus some material from the surrounding melted base metal. Adjacent to the nugget is a zone of base metal that melted and solidified without mixing with the filler metal, which is labeled as the unmixed zone. In these two regions there was complete melting resulting in a cast structure. The next zone is the partially melted zone with a gradation of the melted portion from 100% to 0% at the unmelted base metal boundary. The so-called heat-affected zone is the portion of the base metal within which all the microstructural changes occurred in the solid state. The zone labeled the weld decay zone is a region which is susceptible to intergranular corrosion due to the precipitation of chromium carbides at the grain boundaries and concurrent chromium depletion surrounding the precipitated carbides. The weld decay zone lies in the middle of the heat-affected zone, being bounded by portions of the heat-affected zone that saw time-temperature combinations above and below those required to precipitate chromium carbide surrounded by chromium depleted envelopes. The process by which the chromium depleted envelopes are formed is known as sensitization and the weld decay zone is often referred to as the sensitized region.

The metallurgical remedies used to reduce sensitization in austenitic stainless steels include (i) the use of low carbon (0.03% maximum) L-grades (e.g. type 316L instead of type 316), (ii) post-weld annealing treatment to rediffuse chromium back into the impoverished austenite, and (iii) the use of titanium or niobium plus tantalum alloying additions to precipitate the carbides at higher temperatures so that little carbon is left to precipitate as the chromium-rich grain-boundary carbide during cooling (5). The latter are known as stabilized grades. Of the three methods noted above, the use of the low carbon grades is the preferred method in ship construction. Low carbon grades are used in the construction of integral tanks in ships for ocean transport of chemicals.

Experience with German Stainless Steel 1.3964.9

The German stainless steel 1.3964.9, with 0.04%C (max) and 0.25%Nb (max) can be considered either as a niobium-stabilized grade or as a low carbon grade if the carbon content is less than 0.03%, with susceptibility to intergranular corrosion after welding being evaluated by the ASTM 262 test methodologies. The conventional method of welding austenitic stainless steels involves producing a final weld microstructure that is a mixture of the non-magnetic austenite and the magnetic delta ferrite formed at high temperatures (14). The presence of the delta ferrite significantly reduces the susceptibility of the weld to hot cracking. The optimum delta ferrite content for inhibition of hot cracking is 3% to 8% (14) and unfortunately this level of the magnetic delta ferrite produces a magnetic permeability that is not acceptable for mine countermeasure vessels. However, it has been possible to identify weld filler compositions that form delta ferrite during solidification and then fully transform to the non-magnetic austenite phase upon final cooling. With these fillers resistance to hot cracking is retained and the final weldment is non-magnetic. Studies in Australia (15,16) and Japan (17) have shown that filler composition ranges that exhibit this behavior include the German filler 1.3954.0 (Fe-22.0%Cr-17.5%Ni-7.5%Mn-3.5%Mo-0.7%Si-0.025%C-0.2%N) used for welding the hull steel 1.3964.9. It has been suggested that the PREN of the filler material should be one or two numbers higher than that of the base plate to ensure that if corrosion does initiate it will not be localized to the weldment (18).

Information on Other Candidate Alloys

Since 6XN is an L-grade containing less than 0.03%C problems due to chromium depletion at precipitated carbides are unlikely. However, 6XN can be sensitized by the formation of the sigma phase (19) at certain time-temperature combinations, though these would not normally be encountered in standard fabrication. The presence of sigma can be detected either metallographically or by corrosion testing according to ASTM G28, Practice A, or ASTM A262, Practices E or F (19). Alloys containing higher levels of molybdenum than 6XN, such as alloy 625 (9%Mo), alloy C-276 (16%Mo) and alloy C-22 (13%Mo) are used as weld filler materials for 6XN to eliminate any loss in localized corrosion resistance due to segregation of molybdenum by dendritic coring in the weld nugget which could result from the use of matching fillers or autogenous welding. Metallurgically acceptable arc-welding processes for 6XN are gas metal arc, gas tungsten arc, and shielded metal arc for thicknesses exceeding 3.2 mm (0.125 inches). Modifications to these and other welding processes aimed at meeting proposed lower levels for hexavalent chromium content in the welding fumes are being explored.

Nitronic 50, with 0.06%C (max) and 0.3%Nb (max), can be considered as a stabilized or partially stabilized grade, depending on exact heat chemistry, with the susceptibility to intergranular corrosion after welding being evaluated by the corrosion test described in ASTM A262, Practice C (Huey Test) (6) . The German Navy also uses the ASTM 262 methodology to test their hull steel which is similar to Nitronic 50. It is noted that Nitronic 50 can be supplied annealed at temperatures in the range 1066 C to 1121 C (1950 F to 2050 F) and that if it is to be used as thick sections in the as-welded condition, material annealed at 1121 C (2050 F) should be specified to minimize the possibility of intergranular attack (6). The matching filler, Nitronic 50 AWS E/ER 209, used with shielded metal arc, gas metal arc and gas tungsten arc welding processes results in a small quantity of ferrite in the weld which ensures sound weld deposits. This ferrite content produces a magnetic permeability value of approximately 1.2, which is not acceptable for many non-magnetic applications. Approaches for addressing this issue is covered in the section dealing with magnetic behavior.

As noted above, for applications requiring corrosion resistance, type 316L should be used for welded construction instead of type 316 to avoid intergranular corrosion due to sensitization. Type 316, given a heat treatment used to simulate sensitization during welding (1.5 hours at 650 C followed by furnace cooling), exhibited intergranular corrosion after a five year exposure to the marine atmosphere at Kure Beach, North Carolina (20).

The above discussion on the corrosion of welds has dealt with the avoidance of intergranular corrosion which can be caused by the welding processes. It is possible that in certain instances the weldment may also have a different pitting resistance, crevice corrosion resistance, and stress-corrosion cracking resistance in seawater from that of the base material. Such differences are currently unpredictable, and a simple comparison of these resistances using cast and wrought materials to simulate the weld and the base material, respectively, may not be useful because of the different alloy chemistries of the filler materials. If degradation in localized corrosion resistance is suspected as a result of a given welding process, corrosion testing in natural seawater should be carried out.

COATINGS FOR AUSTENITIC STAINLESS STEELS IN SEAWATER

Since austenitic stainless steels have to be painted to prevent fouling in seawater service, specialized multiple paint systems have to be used to prevent crevice corrosion in areas where the paint system is defective or damaged. The procedures described here derive from published sources (21) and discussions with researchers (22) and represent past practices and experience. These procedures are currently undergoing technological improvements as well as changes to bring them in line with proposed new European environmental regulations and therefore may not represent future practices (22).

The German Navy's underwater hull paint system has traditionally comprised four paint layers, namely a zinc-powder primer, coal tar epoxy, coal tar epoxy sealer, and anti-fouling paint, Figure 5. Zinc is known to cathodically protect austenitic stainless steels against crevice corrosion in seawater (5). The zinc-powder primer is applied in thicknesses between 20 and 40 micrometers (microns) to a surface prepared to a roughness of 40 micrometers, which has been identified by testing and past experience as the optimal surface for primer adhesion. The zinc primer is not a commercial off-the-shelf product, but is specially prepared from dry high-purity zinc powder and a water-free organic compound in a ratio of 90% zinc and 10% organic compound. This preparation is done on an as-required basis according to BWB (Bundesamt fuer Wehrtechnik und Beschaffung) specifications and quality control tests. The coal tar epoxy is placed on top of the zinc-powder primer in three applications of about 150 micrometers each to a total dry thickness of 450 micrometers. The function of the coal tar epoxy is to hold together and protect the zinc primer which has poor cohesion. A coating of coal tar epoxy sealer is then applied to produce a smooth and non-porous surface. Three layers of anti-fouling paint, usually of the self-polishing tri-butyl tin category of paints, is then applied on top of the coal tar epoxy sealer.

For above-waterline surfaces the zinc primer is overcoated by either a polyurethane CARC (Chemical Agent Resistant Coating) or a two-component organic epoxy paint. A schematic representation of traditional German Navy hull painting practices is illustrated in Figure 5.

Zinc or aluminum alloy sacrificial anodes are used in specific areas where additional protection against corrosion is needed (e. g. near electrical systems). The propeller and shaft are made of stainless steel similar to that of the hull to eliminate or minimize any galvanic corrosion.

The ongoing coatings research by the U.S. Navy in this area is stimulated by (i) the fact that the paint systems used on U.S. Navy ships have to be in compliance with the strict U.S. EPA regulations, (ii) concern about liquid metal embrittlement in situations where zinc in contact with stainless steel may inadvertently experience heating from welding, flame-cutting or flame straightening , and (iii) desire to have Navy-qualified off-the-shelf commercial paints as corrosion protection primers available from several suppliers.

Regarding environmental considerations, the U.S. Navy does not use self-polishing tributyl tin anti-fouling paints, coal tar epoxy, or high volatile organic content (VOC) solvents that may be required to carry a 90% zinc powder loading. An environmentally acceptable paint system is required and the ongoing research is aimed at identifying it. Among studies being carried out are seawater evaluations of solvent-borne inorganic zinc, water-borne inorganic zinc, zinc-rich epoxy, solvent-borne inorganic aluminum, water-borne inorganic aluminum, coal-tar epoxy, high solids epoxy, polyurethane, and silanes.

Regarding liquid metal embrittlement, probably the best known industrial failure caused by exposure of austenitic stainless steel to molten zinc is the Flixborough disaster of 1974 (5). At temperatures above the melting point of zinc (419C), zinc will diffuse into austenitic stainless steel, the depth of penetration increasing with time and temperature. At temperatures below 750C, a zinc alloy layer will be formed. However, at temperatures in excess of 750C and in the presence of tensile stresses, cracks will form and rapidly penetrate along grain boundaries leading to fracture (23,24). In the welding of stainless steel, cracking can occur if zinc is present in the region of the weld (25), and inorganic zinc primers and galvanized steel are the most likely sources of zinc (5). In view of this, it is hoped that a zinc-free primer will be identified as acceptable by the ongoing research.

MAGNETIC AND ELECTRIC FIELD ISSUES

For an austenitic stainless steel to be considered as a candidate material for non-magnetic ship hulls it must maintain it's non-magnetic behavior also after deformation and welding. Regarding deformation, it should be recognized that during fabrication the metal is bent to the design contours of the ship, which can require cold work from 1% to 3%. Also a surface combatant may be required to sustain rupture or high plastic whipping loads during an engagement. Accordingly, ship hull materials should have a deformation-modified martensite start temperature well below ambient, since the introduction of body-centred cubic martensitic phases could change the magnetic permeability of the material. For the German hull steel

1.3964.9, low magnetic permeability in the presence of high levels of deformation was demonstrated by extensive testing (26). Comparable testing of 6XN, Nitronic 50, and type 316 remains to be carried out.

Regarding welding, since 6XN is conventionally welded with non-magnetic nickel base alloy electrodes such as alloy 625, alloy C-276, and alloy C-22, the welds are expected to be fully non-magnetic. Some additional studies are warranted using new fluxes for deeper penetration and for minimizing weld fume generation (27). These welds are also expected to be non-magnetic.

As in the case of 1.3964 described in the previous section, Nitronic 50 welded using the 1.3954.0 filler has exhibited non-magnetic weldments. It remains to be established whether type 316 welded with the 1.3954.0 filler will exhibit non-magnetic weldments.

The German Navy uses sacrificial anodes for cathodic protection in areas of the 1.3964.9 stainless steel hulls where additional protection against corrosion is needed. Whether such additional cathodic protection would be needed for hulls made from the much more crevice corrosion resistant stainless steel 6XN remains to be established. However, this is a topic that deserves close examination since with conventional steel hulls cathodic protection is a major source of electric currents flowing around the hull (28-30). Other electromagnetic fields could arise from the galvanic currents generated if different materials are used for the hull on one hand and shafts and propellers on the other. It has been noted that no galvanic corrosion occurs when superaustenitic stainless steels such as 6XN are galvanically coupled to titanium alloys or nickel-chromium-molybdenum alloys such as alloy 625 or alloy C-276 (5). Weld-overlay or spray-formed coatings of these materials would be expected to exhibit similar behavior. Additional investigations are warranted in this area.

ADVANCED DOUBLE HULL CONCEPTS FOR FUTURE COMBATANTS

The U.S. Navy has been studying the advanced double hull (ADH) concept for many of it's surface warships since the early 1990s. In the ADH design the hull consists of an inner hull and an outer hull and the two hulls are connected at intervals by longitudinal members which form a cellular structure. In a conventional hull design there is a single hull plate which is stiffened on its interior surface by longitudinal and transverse members. The two types of hull design are illustrated in Figure 6.

The original studies were focussed on an ADH structure made from high-strength low alloy (HSLA) steel. The perceived advantages of the HSLA steel ADH were: (i) inherently greater strength due to the cellular structure, (ii) simplified fabrication due to the elimination of stiffening members and greater potential for automated welding, (iii) easier installation of the ships distributive systems, (iv) improved control of combat damage, and (v) reduced cost. Subsequent studies considering non-magnetic austenitic stainless steel as the hull material identified additional opportunities for (i) reduced magnetic signature, (ii) better fracture control by using a material which maintains its fracture toughness over the full range of temperatures encountered in service, and (iii) high resistance to shock, and (iv) reduced life-cycle costs through reduced maintenance and repair requirements.

The recognition of the combined benefits of the ADH design and the non-magnetic hull resulted in the authorization by United States Congress of further stainless steel ADH research (31). Current United States research activities in this area are summarized in Figure 7, which include identification of welding technologies aimed at reducing the generation of welding fume containing hexavalent chromium. The U. S. Occupational Safety and Health Administration (OSHA) is planning to reduce the Permissible Exposure Levels (PEL) for hexavalent chromium in welding fume from 100 micrograms per cubic metre to 0.5-5.0 micrograms per cubic metre time-weighted average over 8 hours (32,33). Various approaches in pursuit of the lower PEL for hexavalent chromium are shown in Figure 8 and approaches utilizing improved fume hoods are described in Reference 34.

Another hull design being reviewed is one utilizing GRP composites in the bow and stern sections in conjunction with a stainless steel midship section.

SUMMARY AND CONCLUSIONS

Type 316, which is less costly than 6XN and Nitronic 50, is a common commercially available stainless steel which may be useful for fabricating non-wetted internal ship structures such as internal decks and non-watertight bulkheads, which are a significant part of the total structure. For welded construction type 316L should be used to eliminate risk of intergranular corrosion which can occur in the marine atmosphere. Further research should be carried out to identify the processes that cause stress corrosion cracking of type 316 in vapor spaces above heated chloride solutions and above indoor swimming pools and to ensure that type 316 is not used in comparable locations in ship structures.

The possible use of Nitronic 50 is being considered primarily because it is most like the stainless steel used by the German Navy (1.3964.9) in terms of alloy chemistry and mechanical properties. However, it has a lower and variable molybdenum content than it's German counterpart (1.5-3.0% Mo for Nitronic 50 compared with 3.0-3.5% Mo for 1.3964.9), raising concerns about it's crevice corrosion resistance in seawater at the low end of the molybdenum specification (32). Specifying a 3.0% Mo minimum for Nitronic 50 for a ship construction grade could significantly change the situation. Consideration of the use of Nitronic 50 for the inner shell of the advanced double hull as a cost-saving measure would have to take into account the possibility of microbiologically influenced corrosion, if liquids are to be introduced in the space between the two hulls.

The superaustenitic stainless steel 6XN is the most highly alloyed of these three materials and exhibits the highest resistance to crevice corrosion of these three materials in seawater (32). While it is also the most costly of the three materials, the cost difference may represent a small percentage of the fabrication labor costs and other outfitting costs for a destroyer-sized hull. However, even with 6XN, an environmentally acceptable coating system capable of preventing crevice corrosion at the paint/metal interface would be needed.

REFERENCES

1. M. von Baur, "German Mine Countermeasure Vessels of Non-Magnetizable Steel", *Naval Forces*, 18, 6, (1997): p. 98

2. M. Valenti, "Stealth in the Water", *Mechanical Engineering, (January 2001), p.56*

3. E. H. Waas, "Setbacks in U-Boat Construction and Lessons Drawn from Them", *Jahrbuch der Schiffbautechnische Gesellschaft*, 61, (1967): p. 139 (see also printed discussion by Professor H.-J. Engell, Stuttgart, following the paper)

4. M. Borchert and J. Ritterhoff, "Class 212 Submarines," *Jahrbuch der Schiffbautechnische Gesellschaft*, 91, (1997): p. 499

5. A. J. Sedriks, *Corrosion of Stainless Steels: Second Edition*, Wiley-Interscience, John Wiley & Sons, New York, NY, pages 21, 218, 293, 347, and 418, 1996

6. "Nitronic 50," HPA Bulletin, Vol. 2, Issue 1, High Performance Alloys, Inc., Tipton, IN, March, 1997

7. B. F. Brown, "Stainless Steels in Marine Systems," *Handbook of Stainless Steels*, (editors D. Peckner and I. M. Bernstein), p. 37-1, McGraw-Hill, New York, NY, 1977

8. R. B. Niederberger, R. J. Ferrara, and F. A. Plummer, *Materials Performance*, 9, 8, (1970): p.18

9. A. J. Sedriks, "Corrosion Resistance of Austenitic Fe-Cr-Ni-Mo Alloys in Marine Environments," *International Metals Reviews*, 27, 6, (1982): p. 321

10. W. W. Kirk, F. H. Beck, and M. G. Fontana, in *Physical Metallurgy of Stress Corrosion Fracture*, p. 227, Interscience, New York, NY, 1959

11. J. W. Oldfield and B. Todd, "Ambient-Temperature Stress Corrosion Cracking of Austenitic Stainless Steels in Swimming Pools," *Materials Performance*, 29, 12, (1990): p.57

12. N. McPherson, "Shipbuilding with Stainless Steel", *Welding and Joining*, (September 1997): p.18

13. M. A. Streicher, "Theory and Application of Evaluation Tests for Detecting Susceptibility to Intergranular Attack in Stainless Steels and Related Alloys: Problems and Opportunities,"

Intergranular Corrosion of Stainless Alloys, ASTM STP 656, (editor R. F. Steigerwald), American Society for Testing and Materials, Philadelphia, PA, p. 3, 1978

14. R. Fenn, "The Welding Metallurgy of Stainless Steel", *Welding and Metal Fabrication,* (October 1987): p.360

15. B. Dixon, "Weld Metal Solidification Cracking in Austenitic Stainless Steels", *Australian Welding Research,* 16, 2, (1988): p. 2

16. B. Dixon, "Control of Magnetic Permeability and Solidification Cracking in Welded Non-Magnetic Steel", *Welding Journal, Welding Research Supplement,* (May, 1989): p.171s

17. Y. Araki et al, "Study of the Cr-Ni Austenitic Filler Metal Containing Mn", *Transactions of the Japan Welding Society,* 13, 2, (October 1982): p. 32

18. H. Schutz, "Aspects of Material Selection", *Proceedings of the International Symposium on Mine Warfare Vessels and Systems,* The Royal Institution of Naval Architects, London, England, 12-15 June, 1984, Paper No. 14

19. "AL-6XN Alloy", Allegheny Ludlum Corporation, Pittsburgh, PA, 1995

20. K. L. Money and W. W. Kirk, *Materials Performance,* 17, 7, (1978): p. 28

21. H.-J. Schroder and H. H. Schaedla, "Recent Experiences with Non-Magnetisable Steel as a Material for MCM Vessels" in *Proceedings of The Institute of Marine Engineers Conference on Cost Effective Maritime Defence,* RNEC, Manadon, Plymouth, U.K., August, 1994, p. 99.

22. H. Arendt, Wehrtechnische Dienststelle fur Schiffe und Marinewaffen, Germany, private communication, 17 August, 1998

23. "The Flixborough Disaster: Report of the Court of Inquiry," Department of Employment, H.M. Stationery Office, London, U.K., 1975

24. *Guide Notes on the Safe Use of Stainless Steel in Chemical Process Plant,* Institution of Chemical Engineers, Rugby, U.K., 1978

25. W. G. Ashbaugh, "Liquid Metal Embrittlement - Part 2," *Materials Performance,* 32, 2, (1993): p.88

26. H. Dietrich, W. Heimann, and F. Strom, "The Effects of Cold Forming on the Mechanical and Magnetic Properties of Stainless Steels", *TEW-Technische Berichte,* 2, 1, (1976): p. 61

27. T. Paskell, C. Lundin, and H. Castner, "GTAW Flux Increases Weld Joint Penetration", *Welding Journal,* (April 1997): p.57

28. "Mines and Mine Countermeasures," *The Naval Institute Guide in World Naval Weapons Systems 1997-1998,* Naval Institute Press, Annapolis, MD, p. 714, 1997

29. J. Fischerstrom, "Swedish Mine Countermeasures," *Naval Forces,* 19, 1, (1998): p. 40

30. "Countering ELFE and Other Electromagnetic Signatures,"*Maritime Defence,* 21, 5, (June 1996): p. 142

31. United States FY 99 National Defense Authorization Act (Strom Thurmond, 1998)

32. The National Shipbuilding Research Program: Impact of Recent and Anticipated Changes in Airborne Emission Exposure Limits on Shipyard Workers, Report No: NSRP 0463, March, 1996. Prepared by the Navy Joining Center and Navy/Industry Task Group for Ship Production, Committee 7 (SP-7)- Welding

33. The National Shipbuilding Research Program: Welding Fume Study - Final Report, Report No: NSRP 0525, N7-96-9, January, 1999. Report prepared by DynCorp BHS, Environmental Health and Safety Services, Reston, VA, for Ship Production Committee 7 (SP-7) - Welding

34. H.S. Caram and N. Turkmen, Development of a Fume Control System for Welding AL-6XN Superaustenitic Stainless Steel, Final Report, Office of Naval Research Grant No: N00014-99-0887, March 30, 2002, Lehigh University, Bethlehem, PA, USA

35. A. J. Sedriks and P. J. Dudt, "Corrosion Resistance, Coating, and Magnetic Property Issues of Non-Magnetic Austenitic Stainless Steels for Ship Hulls", *Corrosion,* 57, 1, (2001): p. 84

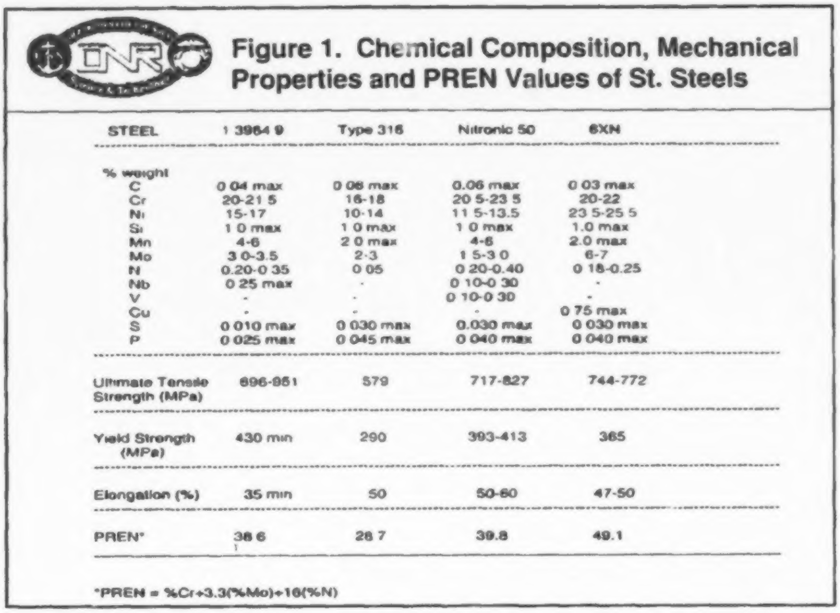

Figure 1. Chemical Composition, Mechanical Properties and PREN Values of St. Steels

STEEL	1.3964.9	Type 316	Nitronic 50	6XN
% weight				
C	0.04 max	0.06 max	0.06 max	0.03 max
Cr	20-21.5	16-18	20.5-23.5	20-22
Ni	15-17	10-14	11.5-13.5	23.5-25.5
Si	1.0 max	1.0 max	1.0 max	1.0 max
Mn	4-6	2.0 max	4-6	2.0 max
Mo	3.0-3.5	2-3	1.5-3.0	6-7
N	0.20-0.35	0.05	0.20-0.40	0.18-0.25
Nb	0.25 max	-	0.10-0.30	-
V	-	-	0.10-0.30	-
Cu	-	-	-	0.75 max
S	0.010 max	0.030 max	0.030 max	0.030 max
P	0.025 max	0.045 max	0.040 max	0.040 max
Ultimate Tensile Strength (MPa)	696-951	579	717-827	744-772
Yield Strength (MPa)	430 min	290	393-413	365
Elongation (%)	35 min	50	50-60	47-50
PREN*	38.6	28.7	39.8	49.1

*PREN = %Cr+3.3(%Mo)+16(%N)

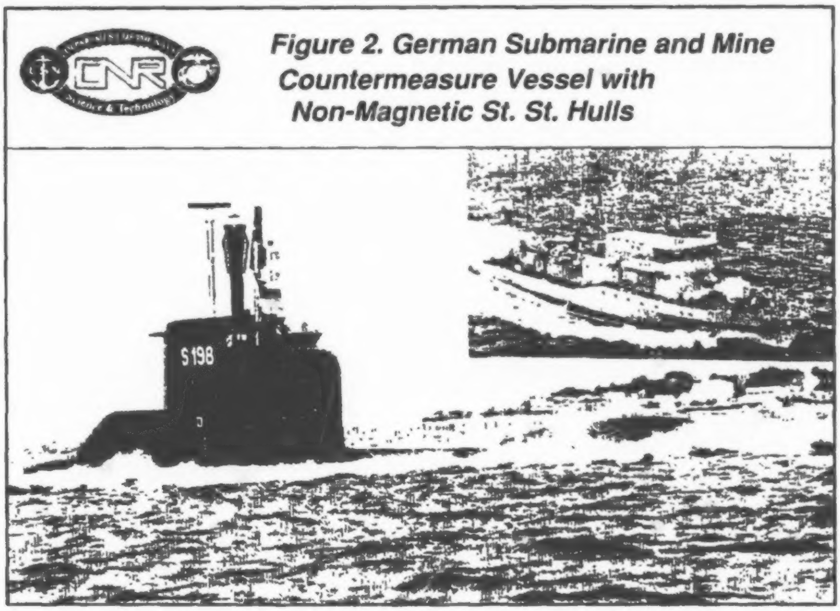

Figure 2. German Submarine and Mine Countermeasure Vessel with Non-Magnetic St. St. Hulls

Figure 3. Stress Corrosion Cracking (SCC) Resistance of Various Austenitic Stainless Steels**

	U-Bend SCC Test				
Stainless Steel	**Boiling 42% MgCl2**	**Wick Test**	**Boiling 25% NaCl**	**Boiling Seawater**	**Swimming Pool Atmosphere**
Type 316	F	F	F	P	F*
Nitronic 50	F	NT	NT	NT	NT
6XN	F	P	P	NT	NT

- F: Fails, cracking observed P: Passes, no cracking observed NT. Not tested
- F*: Failure of structural component. The Swedish Corrosion Institute recommends use of the highly alloyed stainless steels Sanicro 28, 254SMO, 654SMO and 1.4462W-Mo in swimming pool buildings (KI Bulletin No 106E, 1995)
- **Reference A John Sedriks, *Corrosion of Stainless Steels, 2nd Edition, John Wiley & Sons, New York, 1996*

Figure 4. Constituents of a Weld

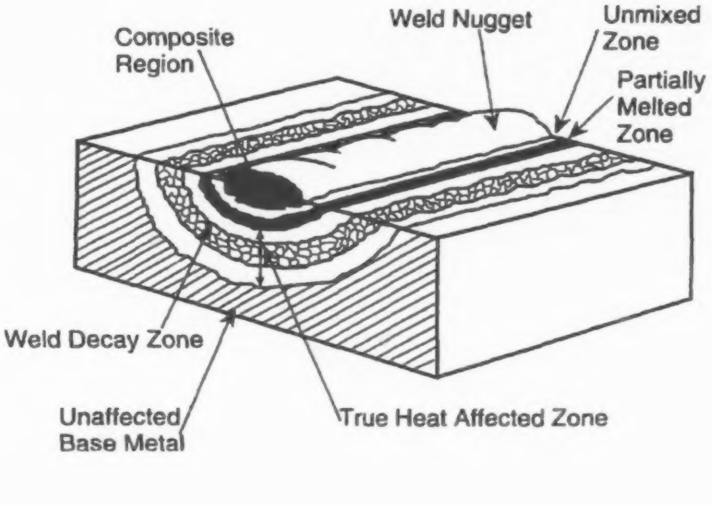
Composite Region
Weld Nugget
Unmixed Zone
Partially Melted Zone
Weld Decay Zone
Unaffected Base Metal
True Heat Affected Zone

Figure 5. Traditional German Navy Coating Technology for St. Steel Hulls

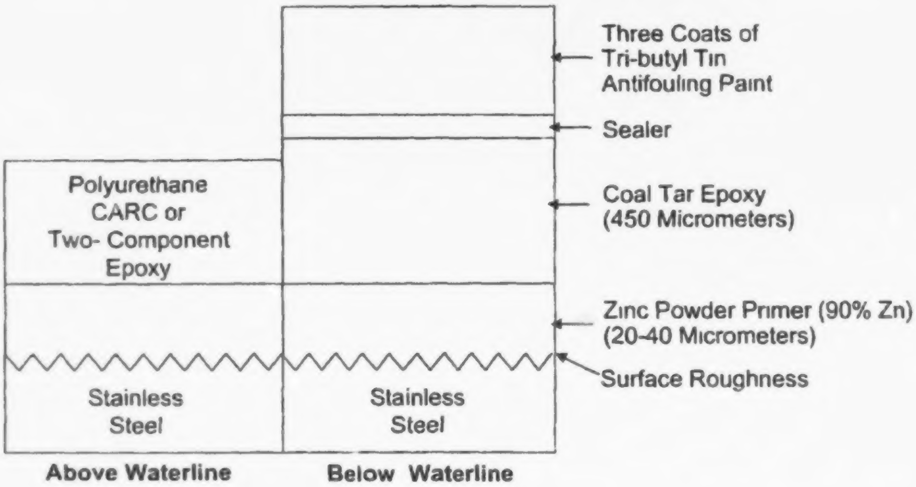
Three Coats of Tri-butyl Tin Antifouling Paint
Sealer
Polyurethane CARC or Two- Component Epoxy
Coal Tar Epoxy (450 Micrometers)
Zinc Powder Primer (90% Zn) (20-40 Micrometers)
Surface Roughness
Stainless Steel
Stainless Steel
Above Waterline
Below Waterline

DOUBLE HULL (ADH) (Fig.6)

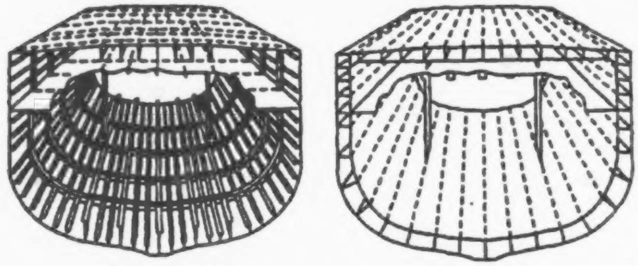

CONVENTIONAL HULL *ADVANCED DOUBLE HULL*

ADH advantages:

(I) Inherent strength of ADH cellular structure eliminates the need for transverse frames and most of the longitudinal stiffeners **(similar weight)**

(II) Cellular structure **reduces cost** by minimizing wiring, piping, and ducting distribution problems since there are no transverse frames in the way.

Figure 7. Current Programs in Support of Non-Magnetic Stainless Steel Advanced Double Hull Development

- **Naval Research Laboratory: Hull coating system development and MIC evaluation(ONR)**
- **Lehigh University ATLSS Engineering Research Center: Welding technology development (CDP)**
- **Metro-Machine of PA: Hull segment specimen construction and fatigue and stability tests (CDP)**
- **Naval Surface Warfare Center: Mechanical and explosion testing of weldments (CDP and ONR)**
- **---**
- ***CDP = Congressional Directed Program**

Figure 8. Joining Techniques for Minimizing or Eliminating Weld Fume Containing Hexavalent Chromium

- **Laser Welding**
- **Gas Tungsten Arc Welding with Penetrating Flux (FASTIG SS-7 Flux)***
- **Friction Stir Welding**
- **Improved Fume Extraction and Ventilation Equipment**
- **---**
- *** Reference: Welding Journal, August, 2000, p. 119**

#516466 (51)

An Evaluation of Microbiologically Influenced Corrosion in Double-Hull Ships

by

Brenda Little[1], Richard Ray[1] and Joanne Jones-Meehan[2]

[1]Naval Research Laboratory
Stennis Space Center, MS

[2]Naval Research Laboratory
Washington, D.C.

Abstract

Candidate materials for a double hull vessel, designed with permanent water ballast, were evaluated for potential microbiologically influenced corrosion in flowing and stagnant fresh and marine waters. Leaks were located at weld seams of Nitronic 50 and 316L stainless steel after six and eight weeks, respectively, exposure to stagnant seawater. In all cases, large numbers of bacteria are associated with the corrosion products. Residual material in pits was typical of removal of iron with preferential corrosion of delta ferrite. A scanning vibrating electrode technique was used to demonstrate that there were no persistent anodic sites in autogenous welds or heat-affected zones of these materials exposed in sterile seawater. In the presence of microorganisms anodic sites formed and persisted to initiate pitting. The spatial and causal relationship between bacteria and pitting in weldments in 300 series stainless steels is well documented. The mechanism for the preferential weld attack has never been satisfactorily explained. However, the mechanism may be an important consideration in the selection of a corrosion inhibitor.

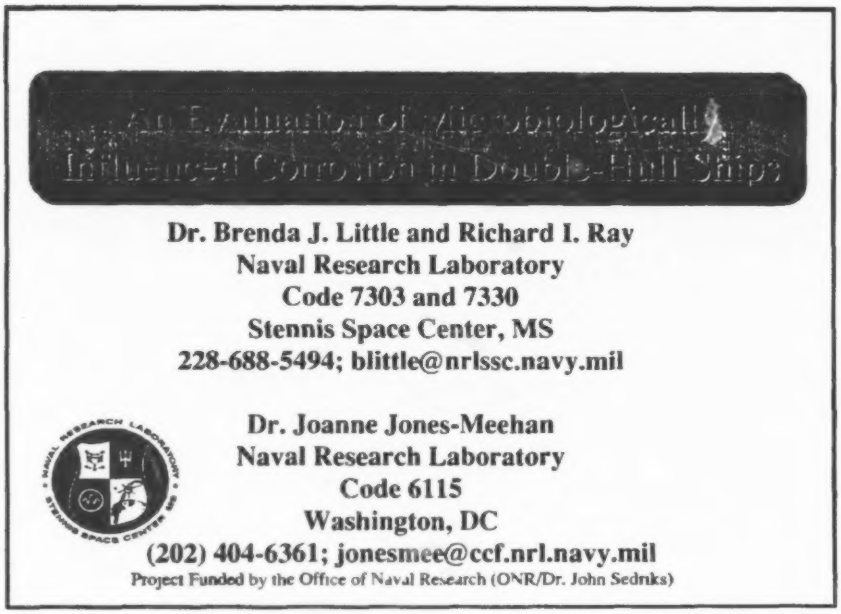

An Evaluation of Microbiologically Influenced Corrosion in Double-Hull Ships

Dr. Brenda J. Little and Richard I. Ray
Naval Research Laboratory
Code 7303 and 7330
Stennis Space Center, MS
228-688-5494; blittle@nrlssc.navy.mil

Dr. Joanne Jones-Meehan
Naval Research Laboratory
Code 6115
Washington, DC
(202) 404-6361; jonesmee@ccf.nrl.navy.mil

Project Funded by the Office of Naval Research (ONR/Dr. John Sedriks)

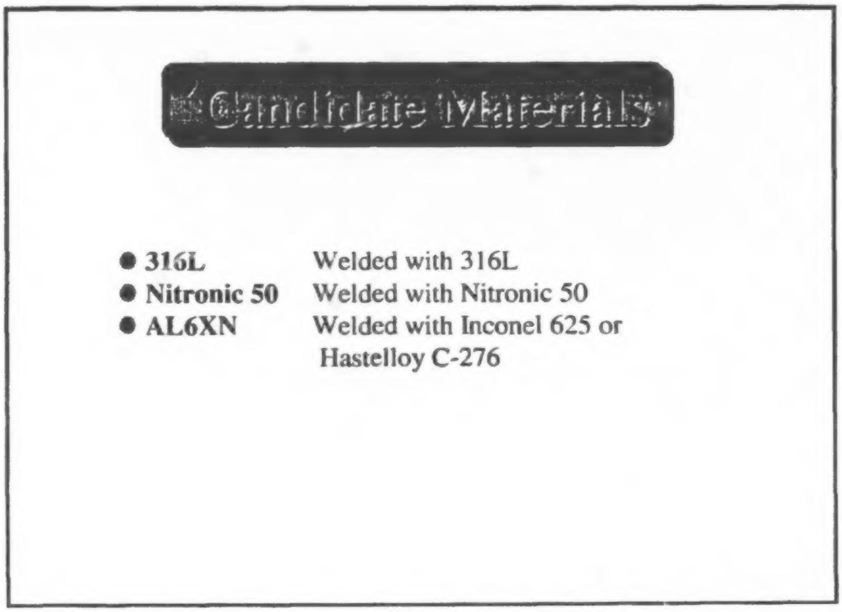

Candidate Materials

● **316L**	Welded with 316L
● **Nitronic 50**	Welded with Nitronic 50
● **AL6XN**	Welded with Inconel 625 or Hastelloy C-276

Chemical Analysis

	C	Cr	Cu	Fe	Mn	Mo	N	Nb	Ni	P	S	Si	Y
316L	.013	16.982	.393	Bal.	1.249	2.137	.043		10 255	.030	.002	.380	
Nitronic 50	.040	21.0		Bal.	5.14	2.20	.25	.18	12.3	.028	.004	.52	.15
AL6XN	017	20.45	.21	Bal	35	6.22	.21		23.9	.021	.0004	.390	

Boxes Before Exposure

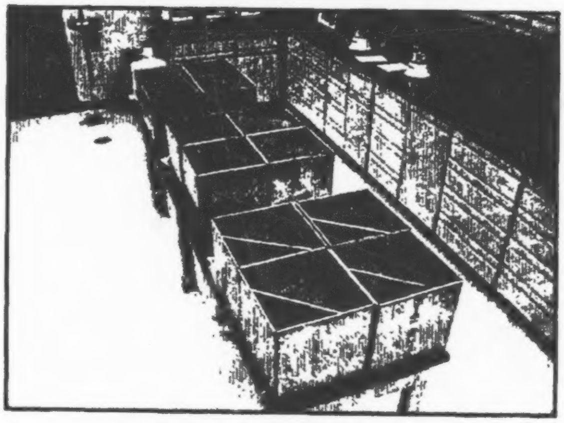

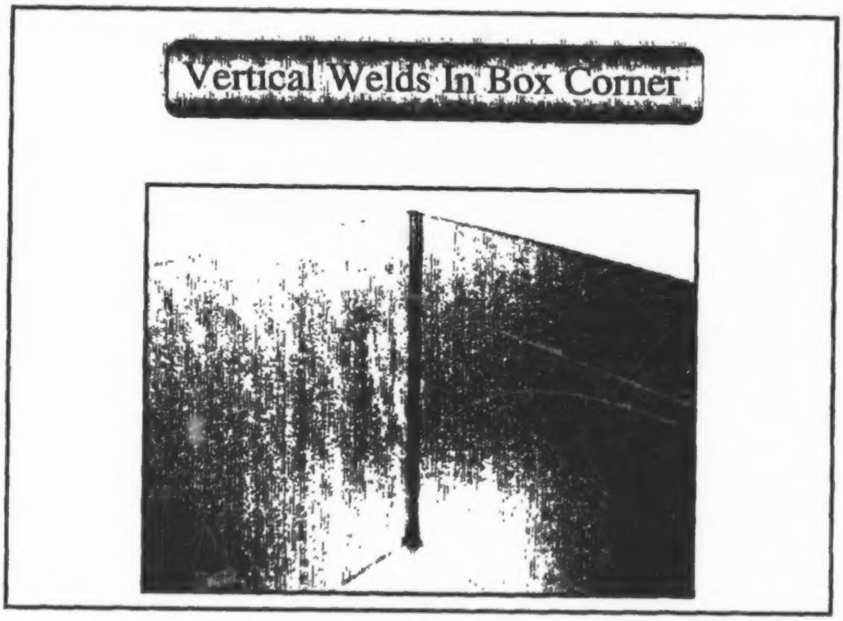

Vertical Welds In Box Corner

Exposure Conditions

1. **Flowing Tap Water**
   (pH 7.91, temp. 23.1°C, negative MICKIT results)
2. **Stagnant Tap Water**
   (pH 7.84, temp 24.6°C, negative MICKIT results)

- **Stagnant Seawater**
  (pH 7.85, temp 24.6°C, positive MICKIT results)
  (All above maintained at NRL/SSC)
- **Flowing Seawater**
  (pH 7.81, temp 19 – 26°C, positive MICKIT results)
  (maintained at NRL/Key West)

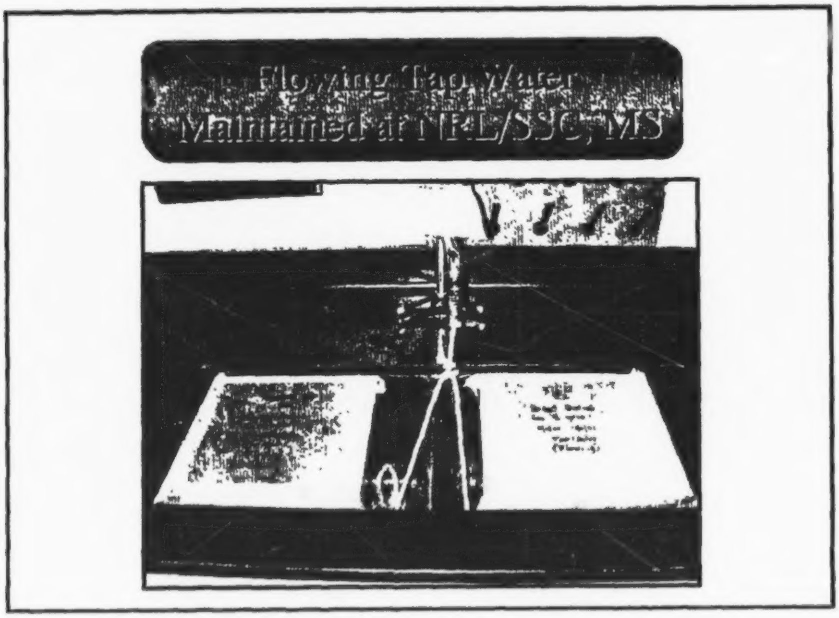

Flowing Tap Water Maintained at NRL/SSC, MS

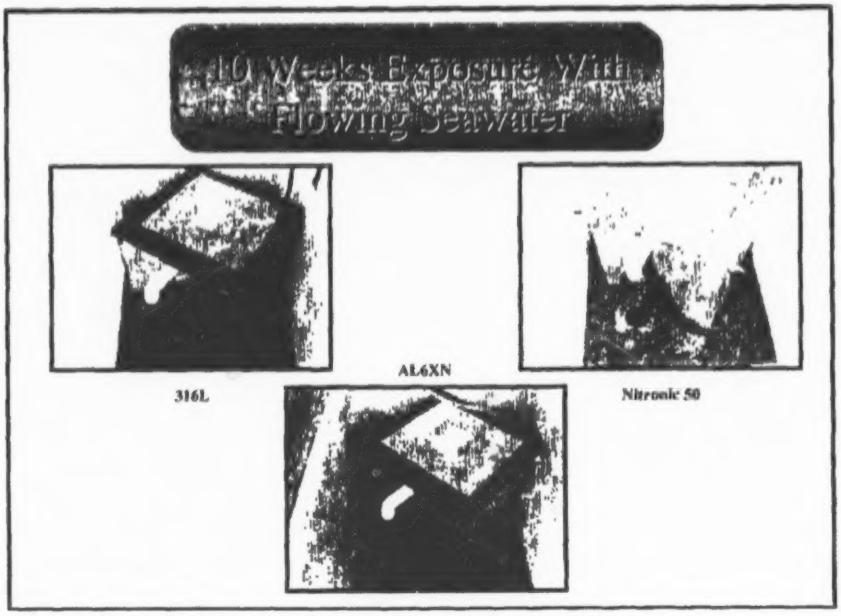

10 Weeks Exposure With Flowing Seawater

316L

AL6XN

Nitronic 50

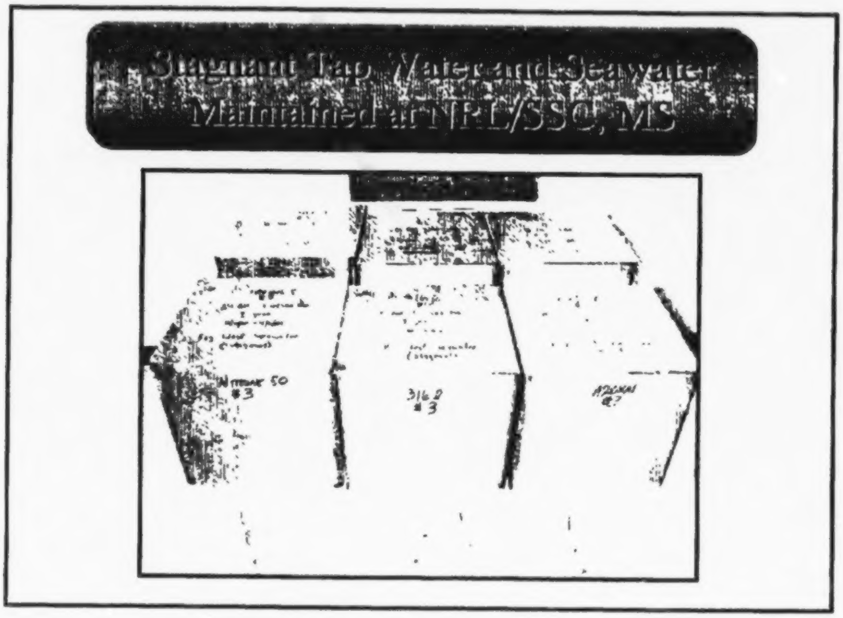

Stagnant Tap Water and Seawater Maintained at NRL/SSC, MS

Nitronic 50
#3
316L
#3

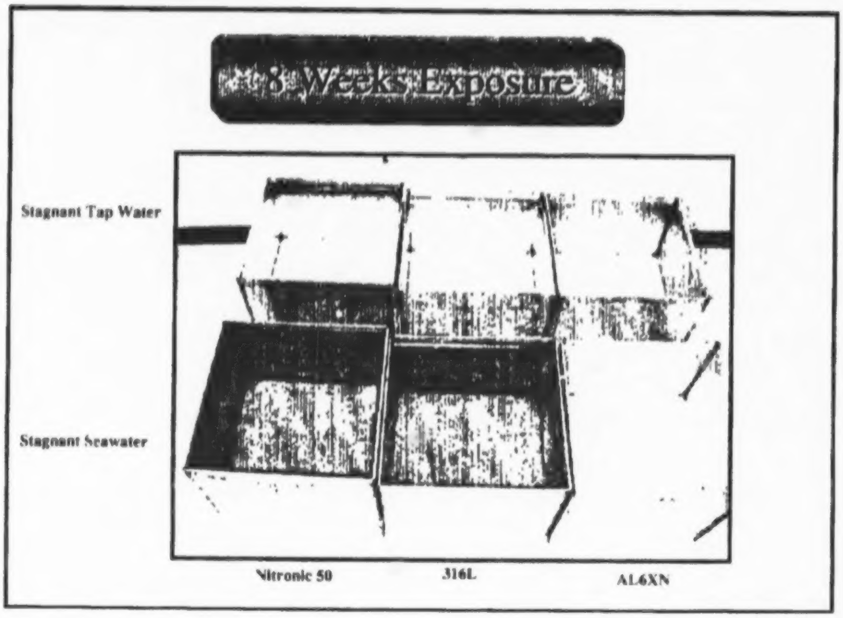

8 Weeks Exposure

Stagnant Tap Water
Stagnant Seawater
Nitronic 50
316L
AL6XN

No Corrosion Visible on AL6XN With Stagnant Tap Water at 10 Weeks

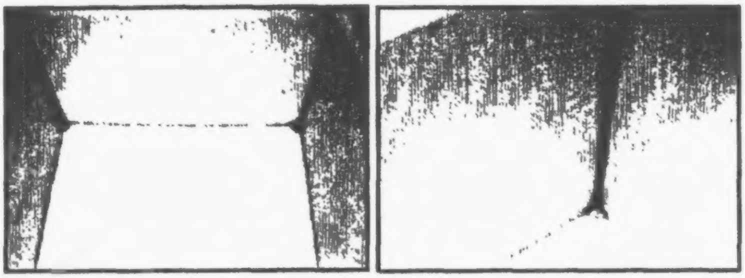

No Corrosion Visible in Flowing or Stagnant Tap Water at 26 Weeks

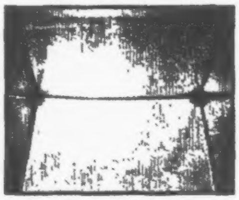

316L Inside Box

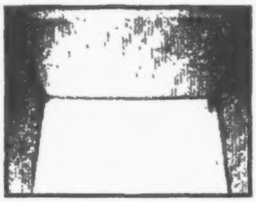

AL6XN Inside Box

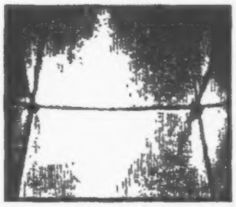

Nitronic 50 Inside Box

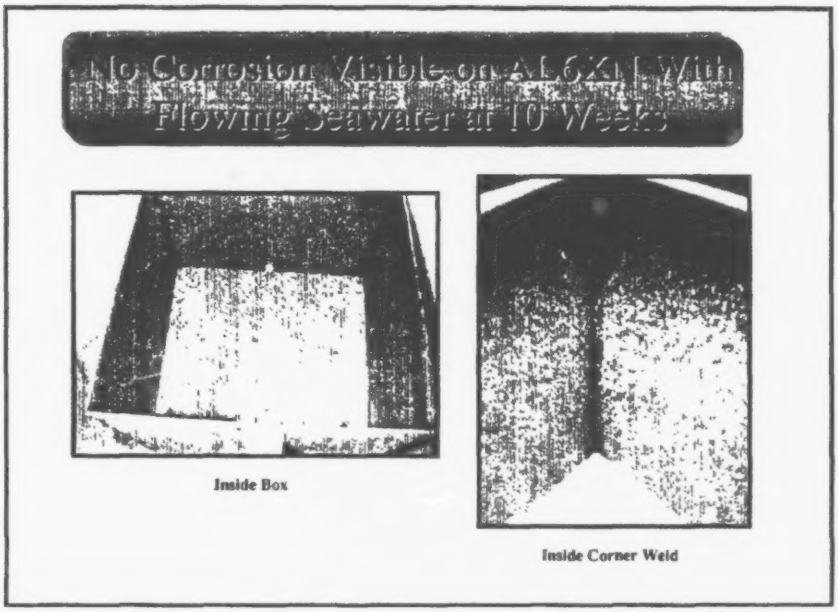

No Corrosion Visible on AL6XN With Flowing Seawater at 10 Weeks

Inside Box

Inside Corner Weld

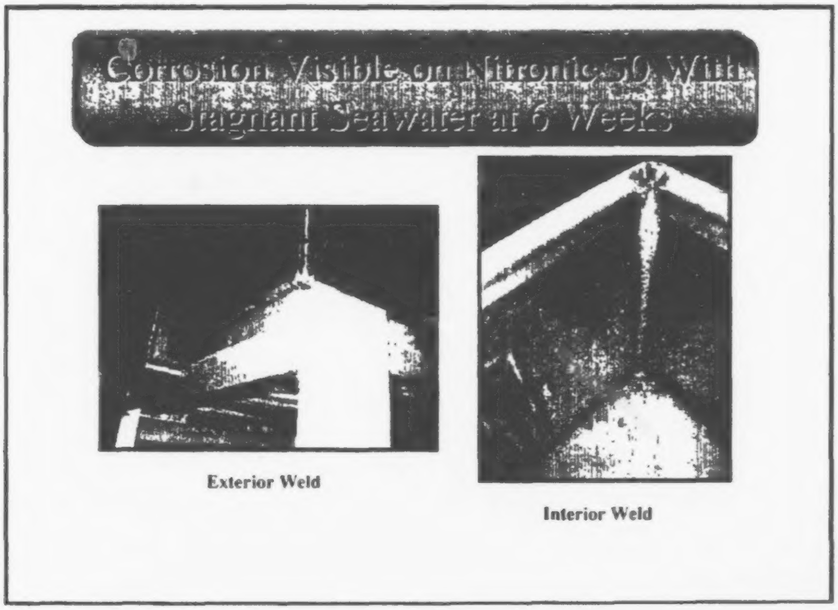

Corrosion Visible on Nitronic 50 With Stagnant Seawater at 6 Weeks

Exterior Weld

Interior Weld

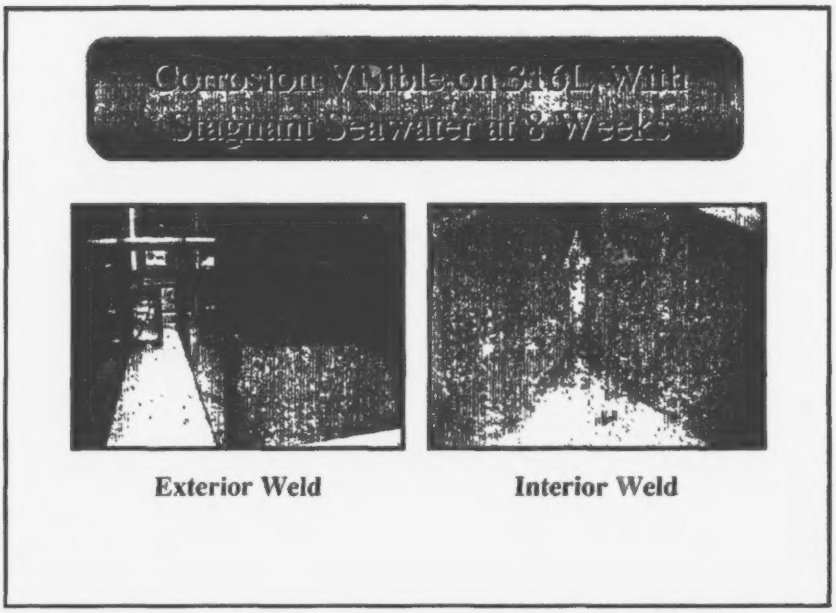

Corrosion Visible on 316L With Stagnant Seawater at 8 Weeks

Exterior Weld

Interior Weld

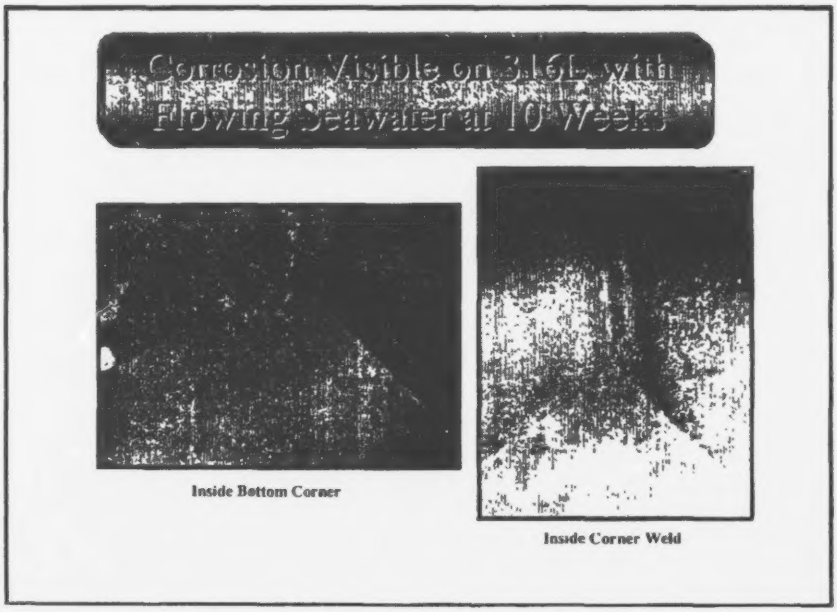

Corrosion Visible on 316L with Flowing Seawater at 10 Weeks

Inside Bottom Corner

Inside Corner Weld

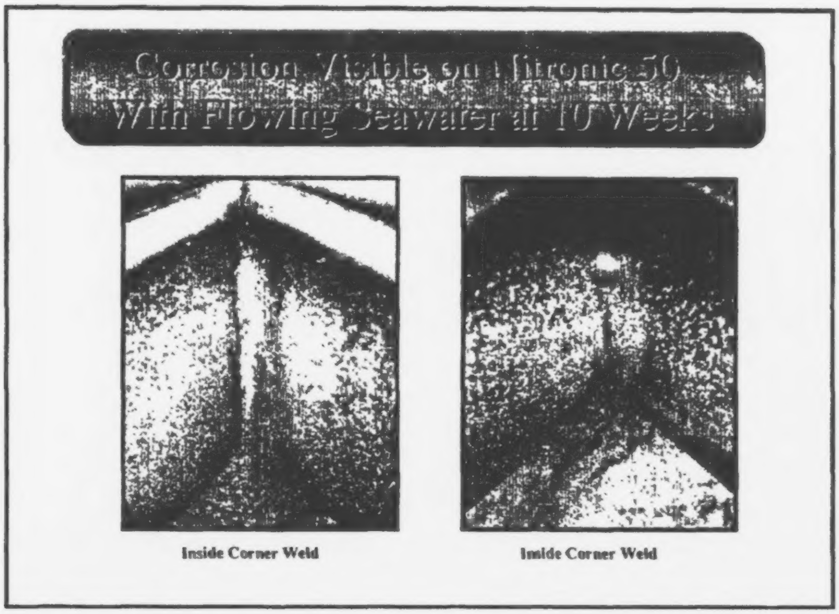

Corrosion Visible on Nitronic 50 With Flowing Seawater at 10 Weeks

Inside Corner Weld

Inside Corner Weld

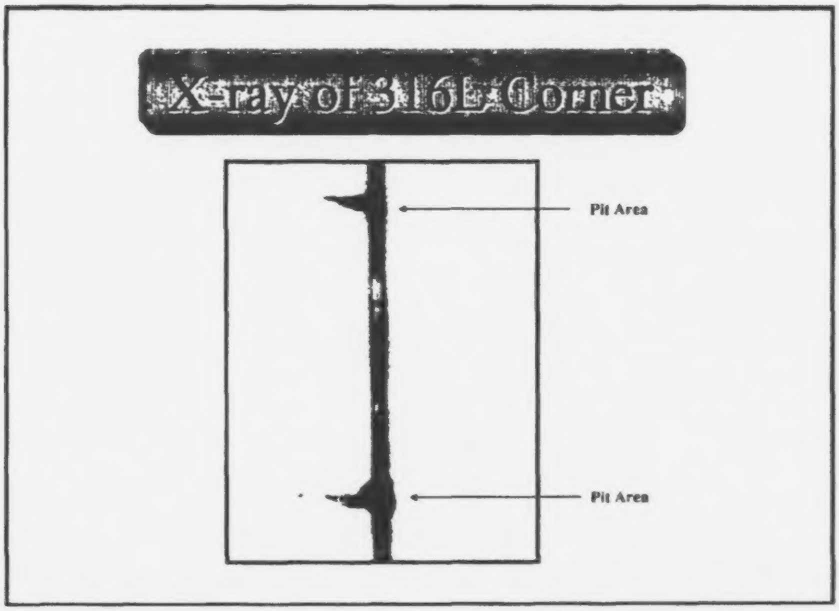

X-ray of 316L Corner

Pit Area

Pit Area

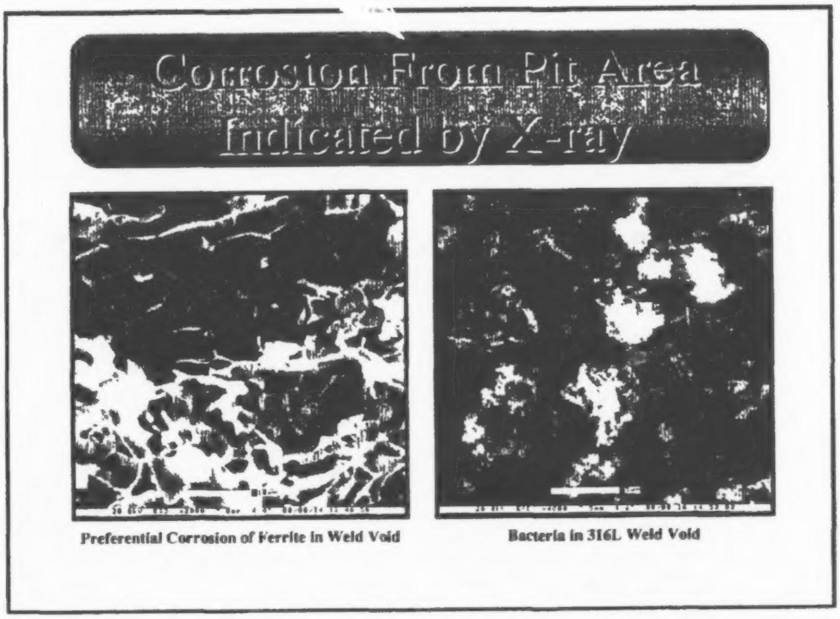

Corrosion From Pit Area Indicated by X-ray

Preferential Corrosion of Ferrite in Weld Void

Bacteria in 316L Weld Void

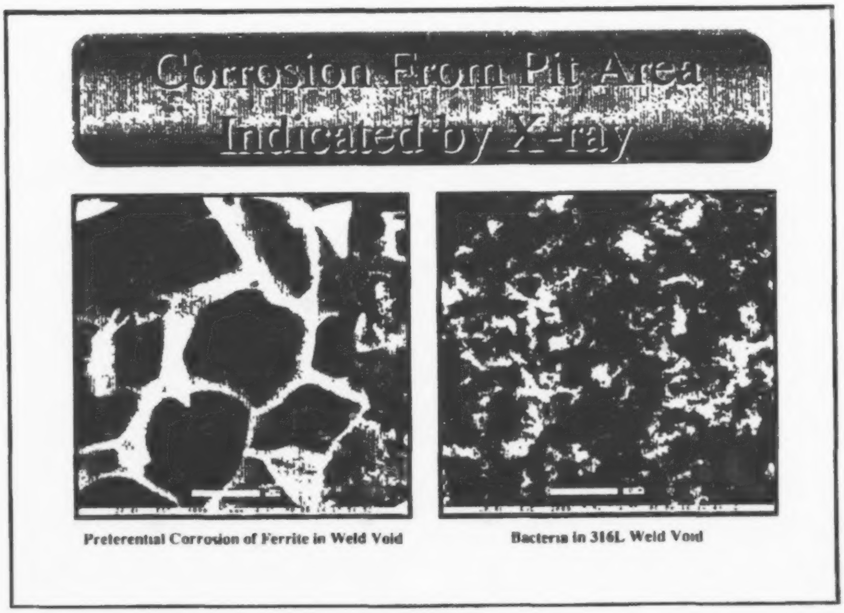

Corrosion From Pit Area Indicated by X-ray

Preferential Corrosion of Ferrite in Weld Void

Bacteria in 316L Weld Void

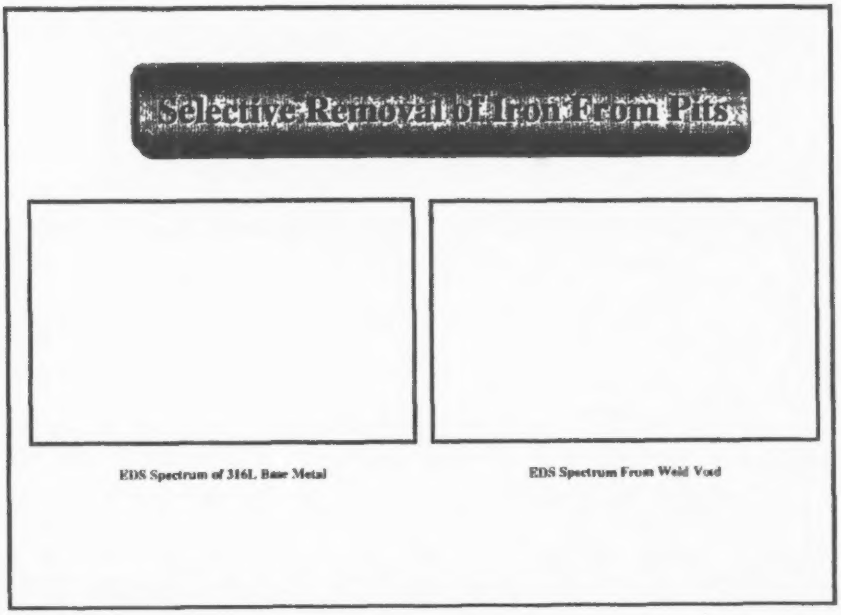

Selective Removal of Iron From Pits

EDS Spectrum of 316L Base Metal

EDS Spectrum From Weld Void

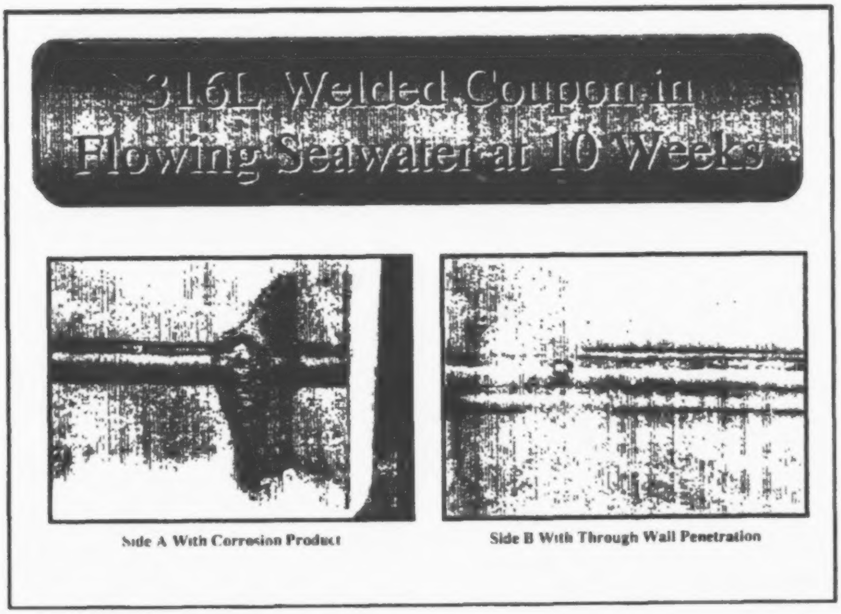

316L Welded Coupon in Flowing Seawater at 10 Weeks

Side A With Corrosion Product

Side B With Through Wall Penetration

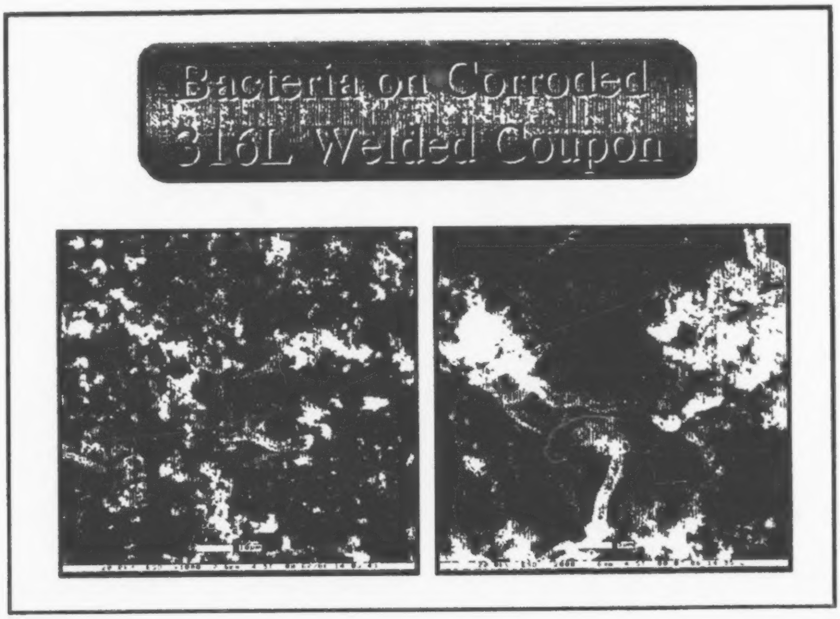

Bacteria on Corroded 316L Welded Coupon

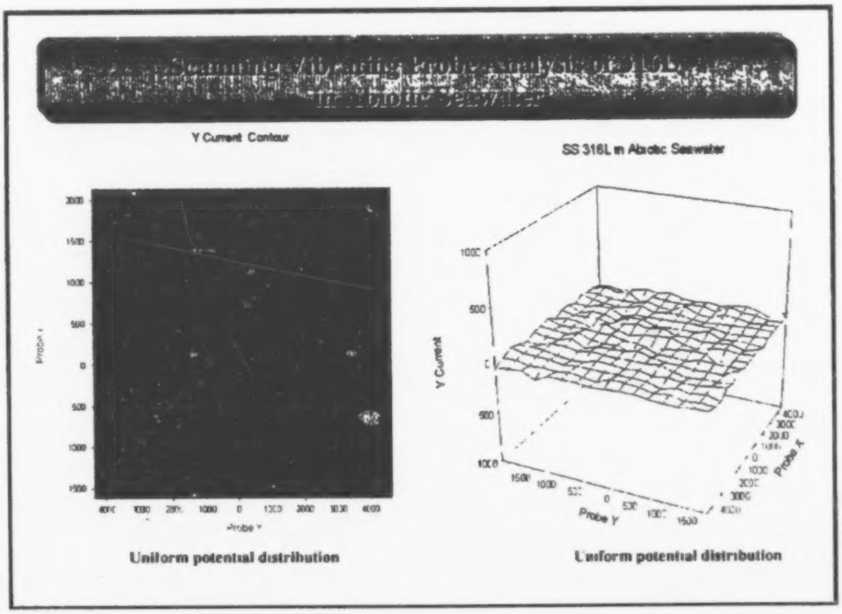

Scanning Vibrating Probe analysis of 316L in Abiotic Seawater

Y Current Contour

SS 316L in Abiotic Seawater

Uniform potential distribution

Uniform potential distribution

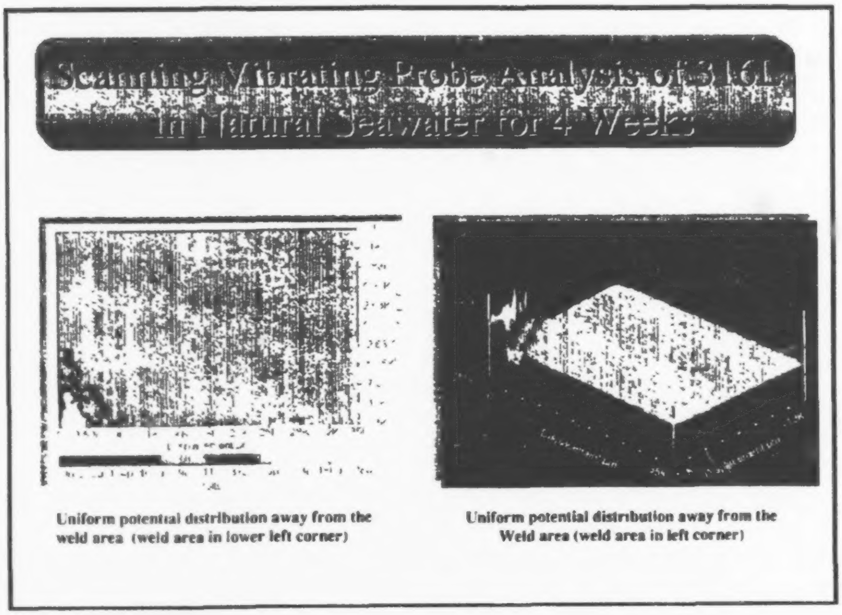

Scanning Vibrating Probe Analysis of 316L in Natural Seawater for 4 Weeks

Uniform potential distribution away from the weld area (weld area in lower left corner)

Uniform potential distribution away from the Weld area (weld area in left corner)

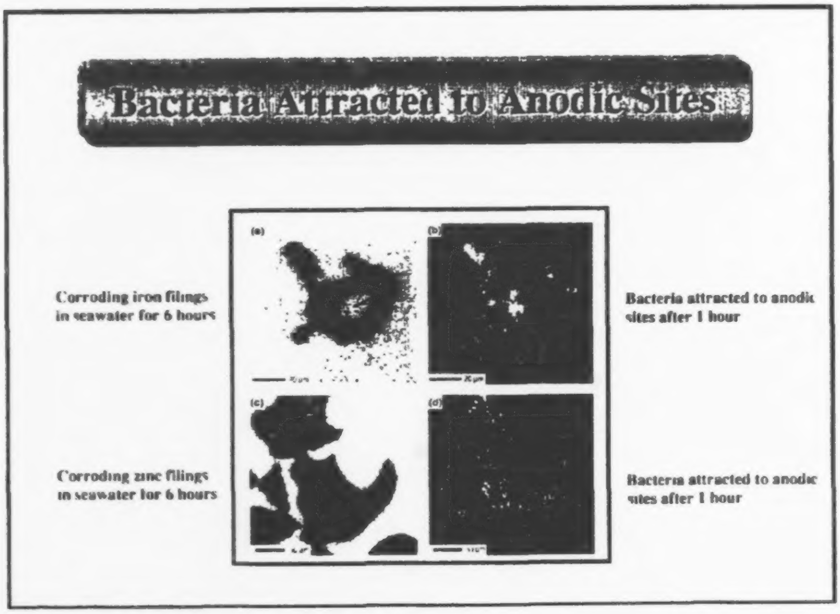

Bacteria Attracted to Anodic Sites

Corroding iron filings in seawater for 6 hours

Bacteria attracted to anodic sites after 1 hour

Corroding zinc filings in seawater for 6 hours

Bacteria attracted to anodic sites after 1 hour

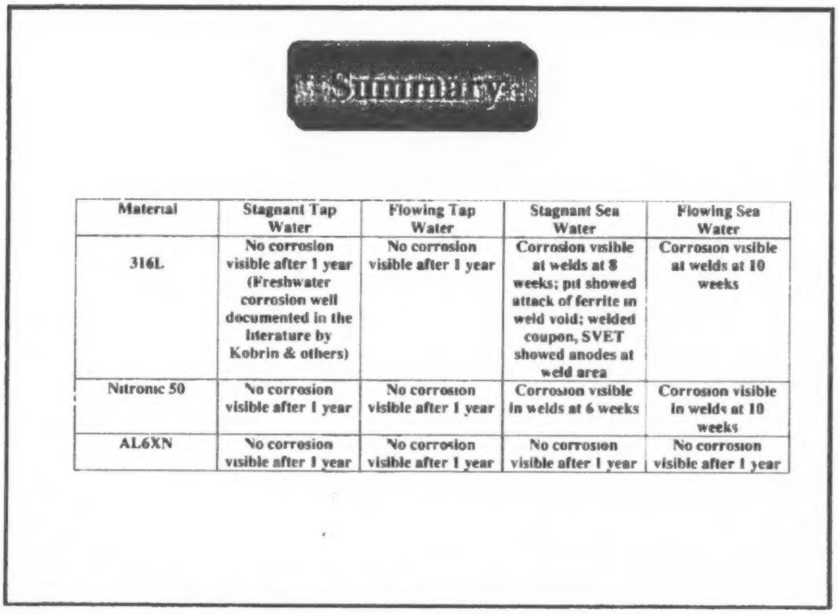

Summary

Material	Stagnant Tap Water	Flowing Tap Water	Stagnant Sea Water	Flowing Sea Water
316L	No corrosion visible after 1 year (Freshwater corrosion well documented in the literature by Kobrin & others)	No corrosion visible after 1 year	Corrosion visible at welds at 8 weeks; pit showed attack of ferrite in weld void; welded coupon, SVET showed anodes at weld area	Corrosion visible at welds at 10 weeks
Nitronic 50	No corrosion visible after 1 year	No corrosion visible after 1 year	Corrosion visible in welds at 6 weeks	Corrosion visible in welds at 10 weeks
AL6XN	No corrosion visible after 1 year	No corrosion visible after 1 year	No corrosion visible after 1 year	No corrosion visible after 1 year

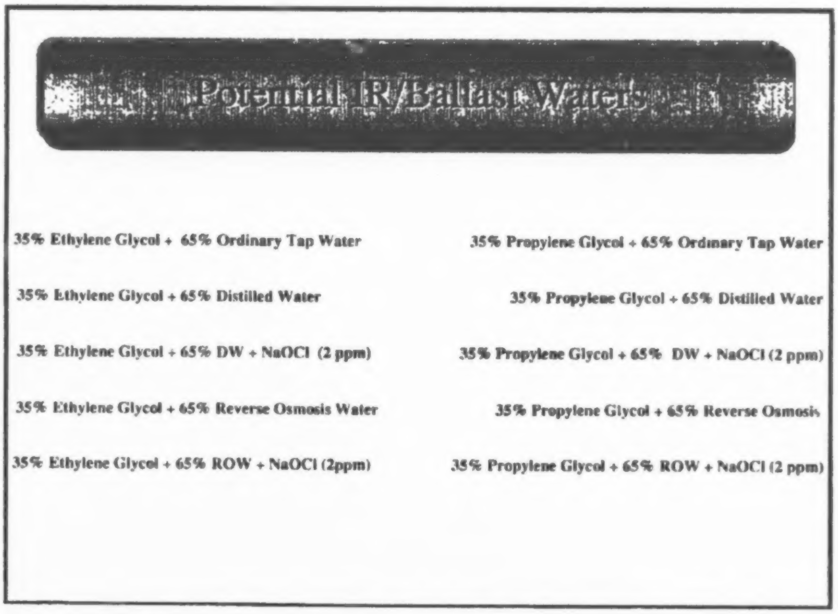

Potential IR/Ballast Waters

35% Ethylene Glycol + 65% Ordinary Tap Water

35% Ethylene Glycol + 65% Distilled Water

35% Ethylene Glycol + 65% DW + NaOCl (2 ppm)

35% Ethylene Glycol + 65% Reverse Osmosis Water

35% Ethylene Glycol + 65% ROW + NaOCl (2ppm)

35% Propylene Glycol + 65% Ordinary Tap Water

35% Propylene Glycol + 65% Distilled Water

35% Propylene Glycol + 65% DW + NaOCl (2 ppm)

35% Propylene Glycol + 65% Reverse Osmosis

35% Propylene Glycol + 65% ROW + NaOCl (2 ppm)

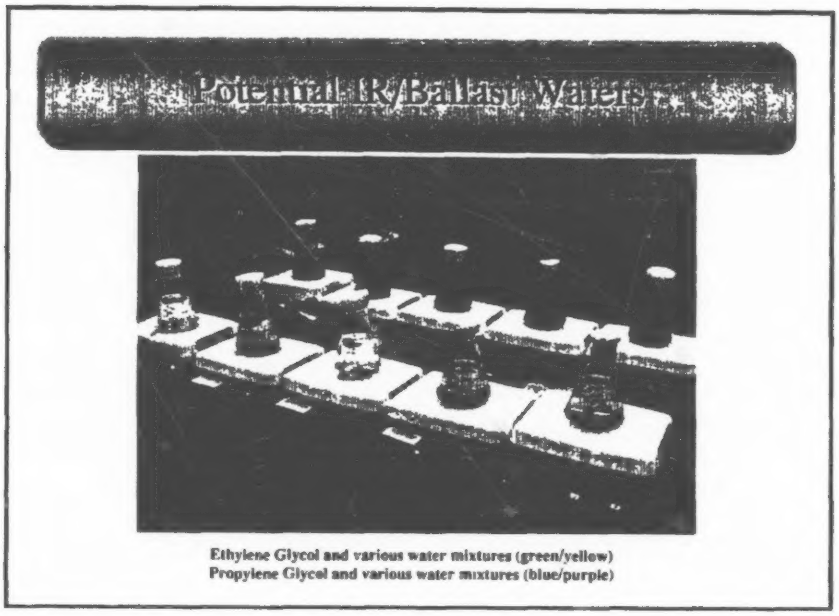

Potential IR/Ballast Waters

Ethylene Glycol and various water mixtures (green/yellow)
Propylene Glycol and various water mixtures (blue/purple)

#516467 (52)

An Efficient Fuzzy Finite Element Methodology for Structural Systems

by

U.O. Akpan, T. S. Koko and B. K. Gallant

Research and Emerging Technologies Department
Martec Limited, Suite 400, 1888 Brunswick Street, Halifax, N.S., Canada B3J 3J8.

Abstract

Many practical engineering systems are ill defined and imprecisely known to be modelled and analyzed by conventional deterministic procedures. Analysis of such systems requires the use of fuzzy information, that is, information that is vague, imprecise, qualitative, linguistic or incomplete. Aging marine, aerospace, nuclear, civil and military structures and machines, and space structures, are practical examples of fuzzy systems. In aging structures, the effects of loading and environmental conditions on the structural/material properties are not precisely known. In space structures, the impact of the extreme operating conditions of the space environment such as microgravity, extreme temperature and vacuum conditions on the structural system is not accurately known. Simple deterministic modelling of these systems will lead to results that are not accurate. To circumvent this problem, fuzzy modelling strategy, that recognizes the vague nature of the input parameters, has been developed.

An efficient approach for modelling the response of structures systems with fuzzy parameters is developed. The methodology involves integrated deterministic finite element, sensitivity, response surface and fuzzy analyses. The uncertainties in the mechanical, electrical, thermal and loading parameters of a structural system are represented using convex normal fuzzy sets. Vertex solution methodology that is based on α-cut representation is used for the fuzzy analysis. In order to facilitate efficient computation, sensitivity analysis is first used to streamline the number of input fuzzy variables. Response surface methodology is then employed to approximate the fuzzy finite element response quantity at the normal points and combinatorial optimization is then performed on the response surface approximate quantity to determine the binary combinations of the fuzzy variables that result in extreme responses at an α-level. The true values of the extreme responses at an α-level are obtained by applying the binary combinations of the fuzzy variables that result in extreme responses to the finite element model. The merit of the proposed methodology is computational efficiency without compromise on accuracy and this is demonstrated through some example problems.

AN EFFICIENT FUZZY FINITE ELEMENT METHODODLOGY FOR STRUCTURAL SYSTEMS

By

U. O. Akpan, T. S. Koko, B. K. Gallant and T. Dunbar

Research and Emerging Technology Department, Martec Limited, Suite 400, 1888
Brunswick Street, Halifax, N.S, Canada B3J 3J8

The 9th CF/DRDC MEETING on
NAVAL APPLICATIONS OF MATERIAL TECHNOLOGY
5-7 MAY 2001

OUTLINE

- INTRODUCTION
- FUZZY LOGIC FRAMEWORK FOR UNCERTAINTY ANALYSIS
- FUZZY FINITE ELEMENT METHODOLOGIES
- RESPONSE SURFACE SOLUTION STRATEGY
- EXAMPLES
- SUMMARY/CONCLUSION

Martec Limited
Advanced Engineering and
Research Consultants

INTRODUCTION (1)

BACKGROUND AND MOTIVATION

- ⇒ EXISTENCE OF SUBJECTIVE UNCERTAINTIES SUCH AS QUALITATIVE INFORMATION, EXPERT OPINION AND THE DESIRE TO INCOROPRATE THEM INTO ANALYSIS AND DESIGN OF.
  - ⇒ COMPLEX, AND ILL DEFINED STRUCTURAL SYSTEM (AGING AEROSPACE, CIVIL, NUCLEAR AND SPACE STRUCTURES)
  - ⇒ ADAPTIVE AND INTELLIGENT SMART STRUCTURES

Martec Limited
Advanced Engineering and
Research Consultants

INTRODUCTION (2)

- ♦ SUBJECTIVE UNCERTAINTIES COULD ARISE IN:
  - ⇒ APPLIED LOAD
  - ⇒ MATERIAL PROPERTIES-MECHANICAL, ELECTRO-MECHANICAL, THERMAL
  - ⇒ GEOMETRY/BOUNDARY CONDITIONS
  - ⇒ ENVIRONMENTAL CONDITIONS/ & THEIR EFFECT ON LOAD, PROPERTIES
- ♦ FUZZY LOGIC APPROACH OFFERS A REALISTIC FRAMEWORK FOR INCORPORATING THESE UNCERTAINTIES

Martec Limited
Advanced Engineering and
Research Consultants

INTRODUCTION (3)

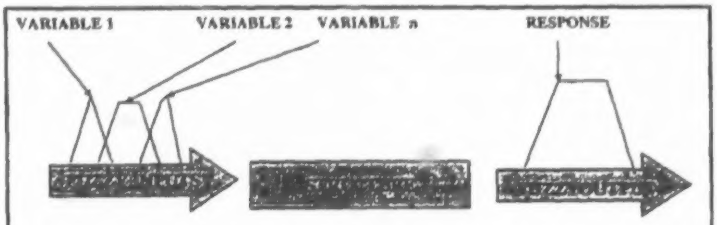

INTRODUCTION (4)

MERIT OF FUZZY APPROACH

- RATIONAL, SYSTEMATIC AND CONSISTENT FRAMEWORK FOR INCORPORATING SUBJECTIVE UNCERTAINTIES SUCH AS:
  - ⇒ EXPERT OPINION
  - ⇒ INCOMPLETE/IMPRECISE INFORMATION
- REALISTIC FRAMEWORK FOR COMPUTING RESPONSE BOUNDS
- REALISTIC FOR DECISION MAKING AND RISK QUANTIFICATION
- SENSITIVIVITY TO AVAILABLE INFORMATION

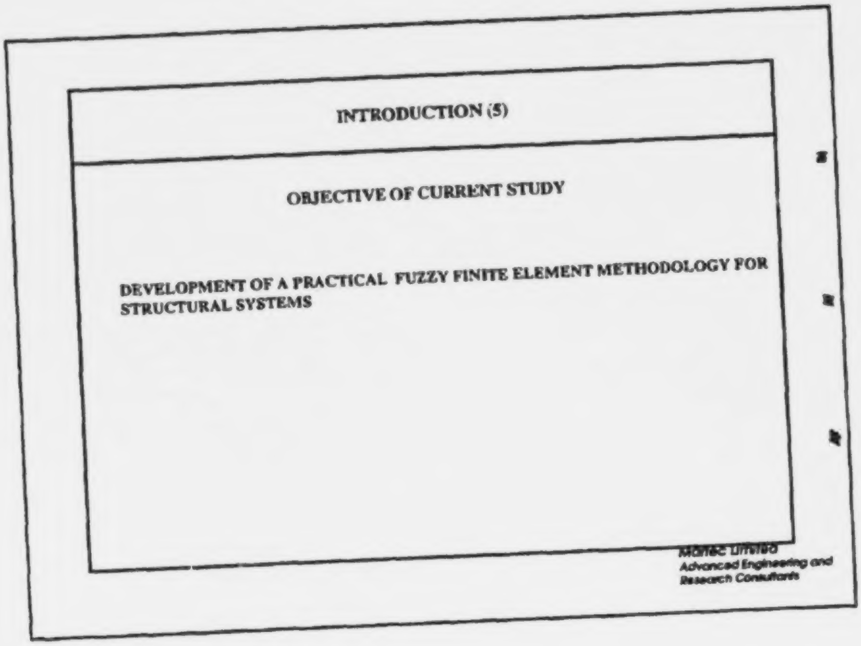

INTRODUCTION (5)

OBJECTIVE OF CURRENT STUDY

DEVELOPMENT OF A PRACTICAL FUZZY FINITE ELEMENT METHODOLOGY FOR STRUCTURAL SYSTEMS

Martec Limited
Advanced Engineering and
Research Consultants

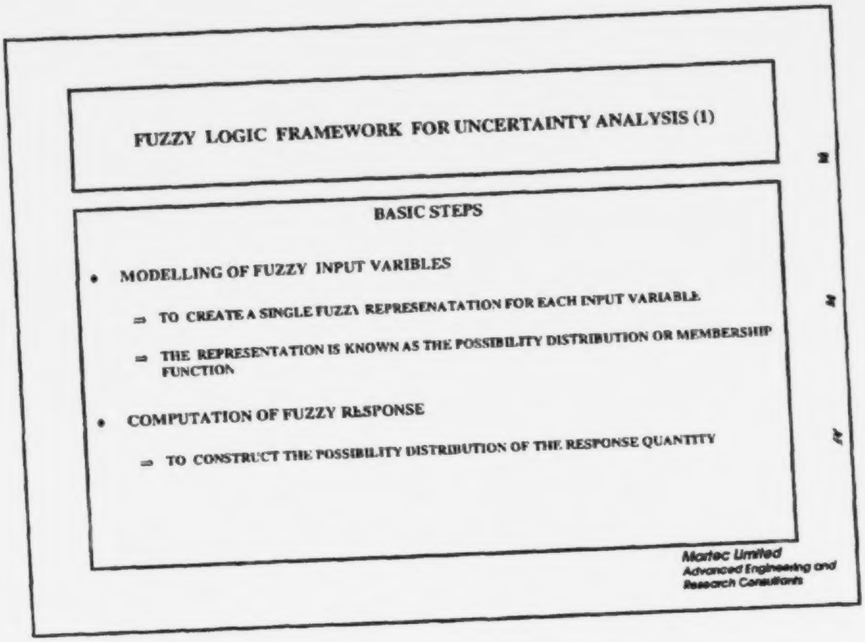

FUZZY LOGIC FRAMEWORK FOR UNCERTAINTY ANALYSIS (1)

BASIC STEPS

- MODELLING OF FUZZY INPUT VARIBLES
  - ⇒ TO CREATE A SINGLE FUZZY REPRESENATATION FOR EACH INPUT VARIABLE
  - ⇒ THE REPRESENTATION IS KNOWN AS THE POSSIBILITY DISTRIBUTION OR MEMBERSHIP FUNCTION
- COMPUTATION OF FUZZY RESPONSE
  - ⇒ TO CONSTRUCT THE POSSIBILITY DISTRIBUTION OF THE RESPONSE QUANTITY

Martec Limited
Advanced Engineering and
Research Consultants

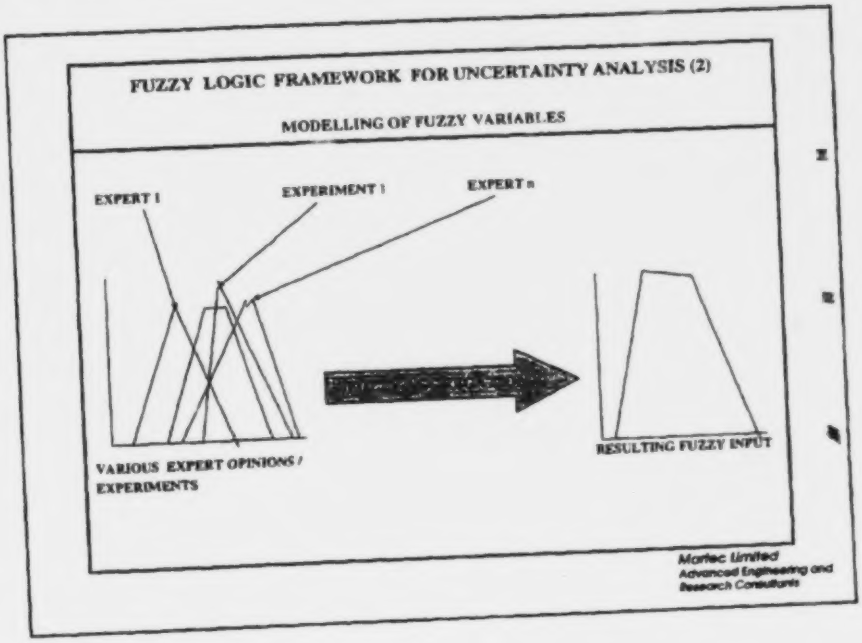

FUZZY LOGIC FRAMEWORK FOR UNCERTAINTY ANALYSIS (2)

MODELLING OF FUZZY VARIABLES

EXPERT 1
EXPERIMENT 1
EXPERT n
VARIOUS EXPERT OPINIONS / EXPERIMENTS
RESULTING FUZZY INPUT

Martec Limited
Advanced Engineering and Research Consultants

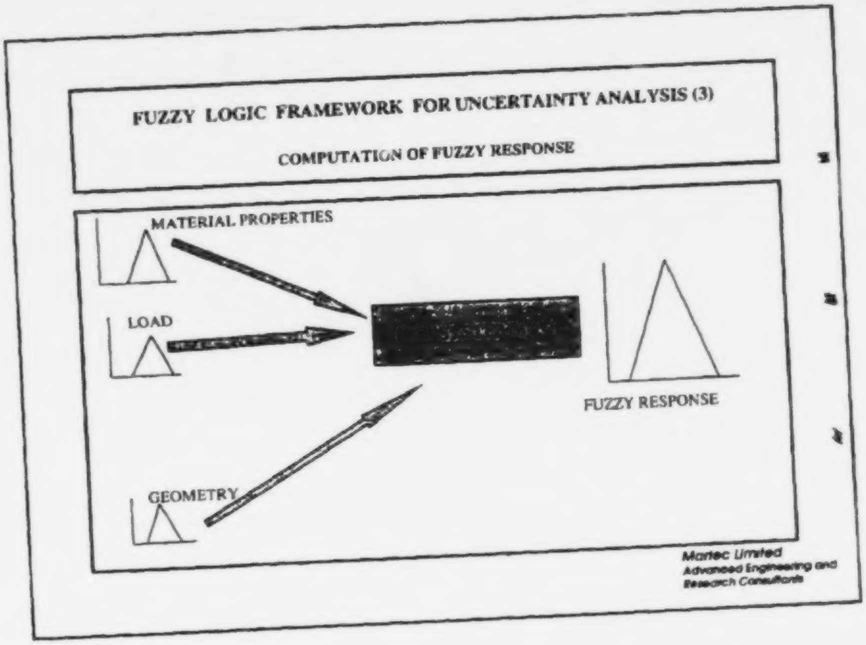

FUZZY LOGIC FRAMEWORK FOR UNCERTAINTY ANALYSIS (3)

COMPUTATION OF FUZZY RESPONSE

MATERIAL PROPERTIES
LOAD
GEOMETRY
FUZZY RESPONSE

Martec Limited
Advanced Engineering and Research Consultants

FUZZY FINITE ELEMNT METHODOLOGIES (1)

APPROACHES

- EXPLICIT FORMULATION
- DIRECT VERTEX METHOD

THE FIRST STEP REQUIRED IN BOTH APPROACHES IS α -LEVEL REPRESENTATION OF INPUT VARIABLES

Martec Limited
Advanced Engineering and
Research Consultants

FUZZY FINITE ELEMNT METHODOLOGIES (2)

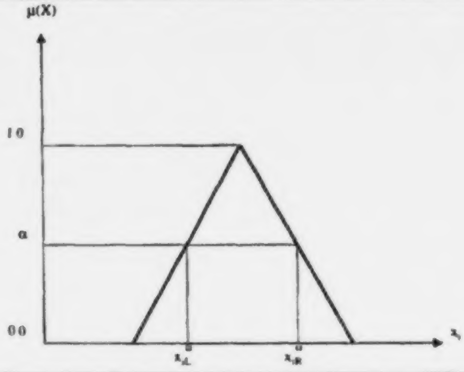

Martec Limited
Advanced Engineering and
Research Consultants

FUZZY FINITE ELEMNT METHODOLOGIES (3)

EXPLICIT METHOD

- **FUZZY MATHEMATICAL OPERATIONS SUCH AS:**
  - ⇒ FUZZY ARITHMETIC
  - ⇒ FUZZY CALCULUS
  - ⇒ ARE EXPLICITLY USED IN FORMULATING SYSTEM EQUATIONS

Martec Limited
Advanced Engineering and
Research Consultants

FUZZY FINITE ELEMNT METHODOLOGIES (4)

EXPLICIT METHOD

$$a^{\alpha} + b^{\alpha} = (a_L^{\alpha}, a_R^{\alpha}) + (b_L^{\alpha}, b_R^{\alpha}) = (a_L^{\alpha} + b_L^{\alpha}, a_R^{\alpha} + b_R^{\alpha})$$

$$a^{\alpha} - b^{\alpha} = (a_L^{\alpha}, a_R^{\alpha}) - (b_L^{\alpha}, b_R^{\alpha}) = (a_L^{\alpha} - b_R^{\alpha}, a_R^{\alpha} - b_L^{\alpha})$$

$$a^{\alpha} \mathrm{X}\, b^{\alpha} = (a_L^{\alpha}, a_R^{\alpha}) \,\mathrm{X}\, (b_L^{\alpha}, b_R^{\alpha}) = \begin{pmatrix} min(a_L^{\alpha} b_L^{\alpha}, a_L^{\alpha} b_R^{\alpha}, a_R^{\alpha} b_L^{\alpha}, a_R^{\alpha} b_R^{\alpha}, \\ max(a_L^{\alpha} b_L^{\alpha}, a_L^{\alpha} b_R^{\alpha}, a_R^{\alpha} b_L^{\alpha}, a_R^{\alpha} b_R^{\alpha} \end{pmatrix}$$

$$a^{\alpha} \mathrm{X}\, (b^{\alpha})^{-1} = (a_L^{\alpha}, a_R^{\alpha}) \div (b_L^{\alpha}, b_R^{\alpha}) = \begin{pmatrix} min(a_L^{\alpha}/b_L^{\alpha}, a_L^{\alpha}/b_R^{\alpha}, a_R^{\alpha}/b_L^{\alpha}, a_R^{\alpha}/b_R^{\alpha}, \\ max(a_L^{\alpha}/b_L^{\alpha}, a_L^{\alpha}/b_R^{\alpha}, a_R^{\alpha}/b_L^{\alpha}, a_R^{\alpha}/b_R^{\alpha} \end{pmatrix}$$

Martec Limited
Advanced Engineering and
Research Consultants

FUZZY FINITE ELEMNT METHODOLOGIES (5)

DIRECT VERTEX METHOD

- DETERMINISTIC FEA SYSTEM MODEL CAN BE USED
- SELECTION OF α-LEVELS
- COMPUTATION OF MAXIMUM/MINIMUM RESPONSES AT EACH α-LEVEL BY BINARY COMBINATION OF INPUT FUZZY VARIABLES
- REQUIRES 2^n COMPUTATION FOR EACH α-LEVEL
- THE HIGHER THE NUMBER OF α-LEVELS THE GREATER THE ACCURACY OF THE POSSIBILITY DISTRIBUTION OF RESPONSE

Martec Limited
Advanced Engineering and
Research Consultants

FUZZY FINITE ELEMENT METHODOLOGIES (6)

LIMITATIONS OF EXPLICIT FORMULATION

⇒ NOT FEASIBLE FOR COMPLICATED PROBLEMS

⇒ REQUIRES REWRITING OF EXISTING DETERMINISTIC STRUCTURAL FEA CODES

⇒ ALGORITHMS FOR DEVELOPMENT OF CONSTRAINED INTERVAL MATHEMATIC IS REQUIRED AND THIS IS NOT WELL DEVELOPED

⇒ EXISTING ALGORITHMS DO NOT CONSIDER CONSTRAINED INTERVAL MATHEMATICS AND THERFORE CAN GIVE UNBOUNDED SOLUTIONS

Martec Limited
Advanced Engineering and
Research Consultants

FUZZY FINITE ELEMENT METHODOLOGIES (7)

MERITS OF DIRECT VERTEX METHOD

- ⇒ FEASIBLE FOR COMPLICATED AND PRACTICAL PROBLEMS
- ⇒ EXISTING DETERMINISTIC STRUCTURAL FEM CODES CAN BE USED
- ⇒ THERFORE LOW DEVELOPMENTAL COST

LIMITATIONS OF DIRECT VERTEX METHOD

- ⇒ REQUIRES 2^N COMPUTATION FOR EACH α-LEVEL
- ⇒ THIS COULD BE VERY COMPUTATIONALLY EXPENSIVE AND THEREFORE NOT FEASIBLE FOR VERY LARGE AND COMPLICATED STRUCTURES

Martec Limited
Advanced Engineering and
Research Consultants

RESPONSE SURFACE BASED FUZZY FINITE ELEMENT

STEP 1
DEVELOP LINEAR OR QUADRATIC POLYNOMIAL RESPONSE SURFACE OF RESPONSE QUANTITY BASED ON NORMAL VALUES OF FUZZY INPUT VARIABLES

STEP 2
PERFORM OPTIMIZATION USING RESPONSE SURFACE TO DETERMINE BINARY COMBINATION OF FUZZY INPUT VARIABLES FOR MAXIMUM AND MINIMUM RESPONSES AT AN α-LEVEL

STEP 3
USE THE BINARY COMBINATIONS AND DETERMINSTIC FINITE ELEMENT MODEL TO COMPUTE ACTUAL BOUNDS OF RESPONSE AT AN α-LEVEL

STEP 4
REPEAT STEPS 1-3 FOR ALL α-LEVELS

Martec Limited
Advanced Engineering and
Research Consultants

RESPONSE SURFACE BASED FUZZY FINITE ELEMENT

STEP 1

DEVELOP LINEAR OR QUADRATIC RESPONSE SURFACE OF RESPONSE QUANTITY BASED ON NORMAL VALUES OF FUZZY INPUT VARIABLES

STEP 2

PERFORM COMBINATORIAL OPTIMIZATION USING RESPONSE SURFACE TO DETERMINE BINARY COMBINATION OF FUZZY INPUT VARIABLES FOR MAXIMUM AND MINIMUM RESPONSES AT AN α -LEVEL

STEP 3

USE THE BINARY COMBINATIONS AND DETERMINSTIC FINITE ELEMENT MODEL TO COMPUTE ACTUAL BOUNDS OF RESPONSE AT AN α -LEVEL

STEP 4

REPEAT STEPS 1-3 FOR ALL A-LEVELS

Martec Limited
Advanced Engineering and Research Consultants

FLOW CHART FOR RESPONSE SURFACE BASED FUZZY FINITE ELEMENT

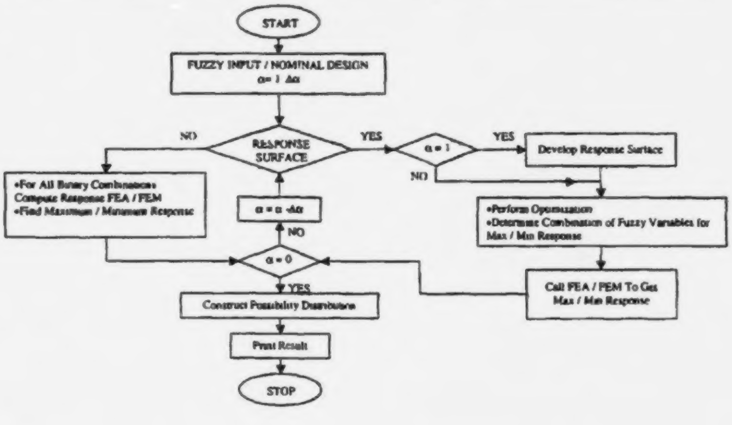
START
FUZZY INPUT / NOMINAL DESIGN
α= 1 Δα
NO
RESPONSE SURFACE
YES
α = 1
YES
Develop Response Surface
NO
•For All Binary Combinations•
Compute Response FEA / FEM
•Find Maximum / Minimum Response
α = α -Δα
NO
•Perform Optimization
•Determine Combination of Fuzzy Variables for Max / Min Response
α = 0
YES
Call FEA / FEM To Get Max / Min Response
Construct Possibility Distribution
Print Result
STOP

Martec Limited
Advanced Engineering and Research Consultants

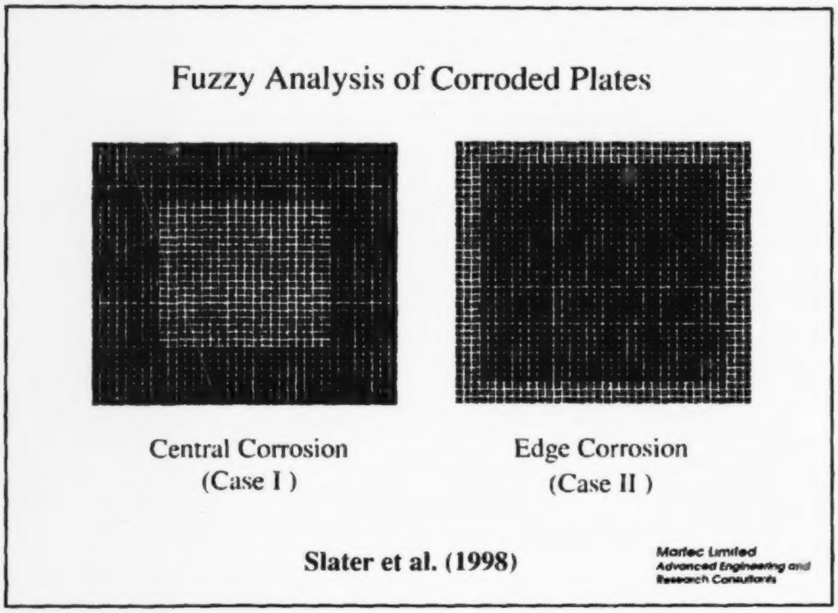

Fuzzy Analysis of Corroded Plates

Central Corrosion
(Case I)

Edge Corrosion
(Case II)

Slater et al. (1998)

Martec Limited
Advanced Engineering and
Research Consultants

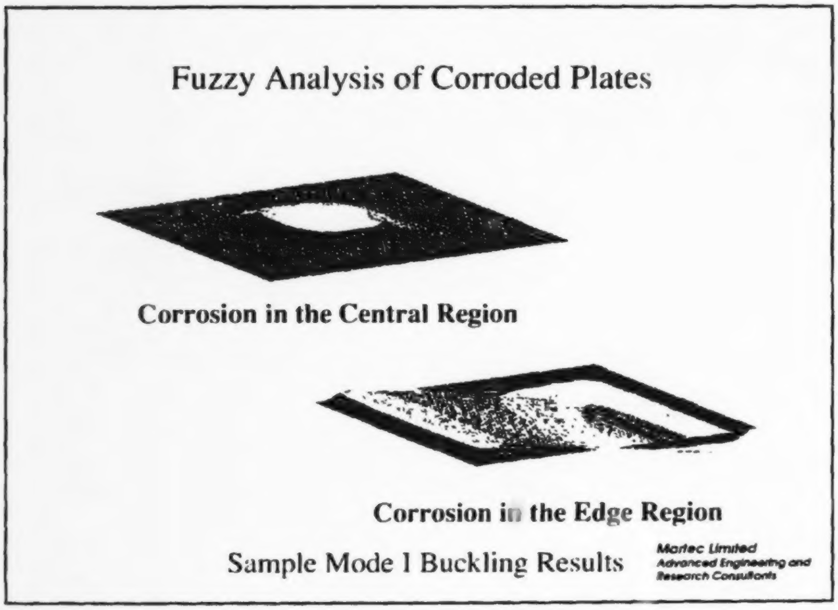

Fuzzy Analysis of Corroded Plates

Corrosion in the Central Region

Corrosion in the Edge Region

Sample Mode 1 Buckling Results

Martec Limited
Advanced Engineering and
Research Consultants

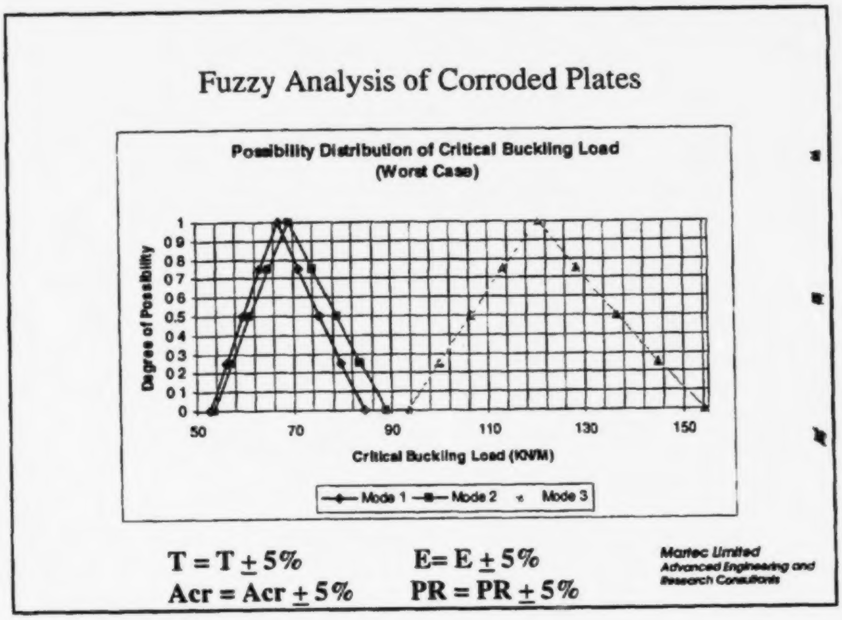

Fuzzy Analysis of Corroded Plates

T = T ± 5%   E= E ± 5%

Acr = Acr ± 5%   PR = PR ± 5%

Martec Limited
Advanced Engineering and Research Consultants

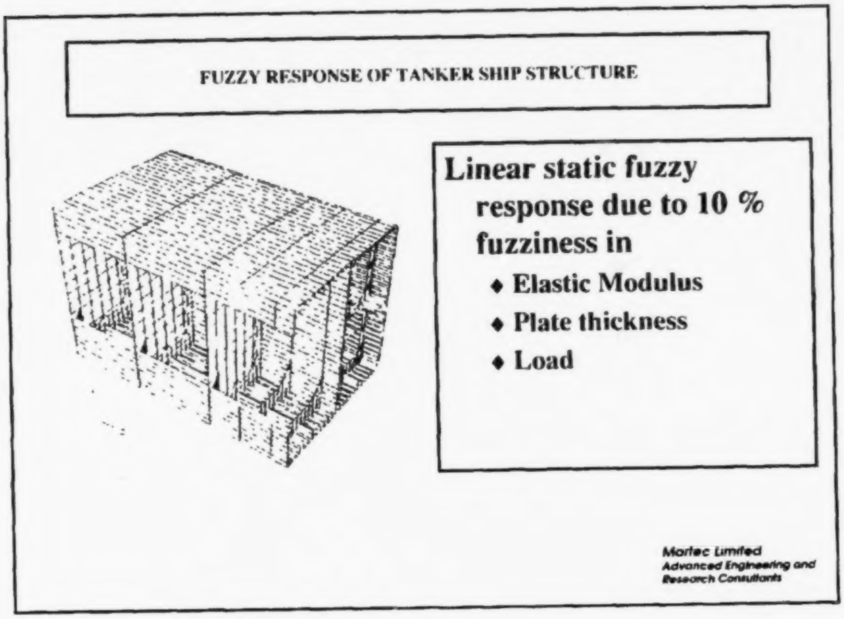

FUZZY RESPONSE OF TANKER SHIP STRUCTURE

Linear static fuzzy response due to 10 % fuzziness in

- **Elastic Modulus**
- **Plate thickness**
- **Load**

Martec Limited
Advanced Engineering and Research Consultants

FUZZY RESPONSE OF TANKER SHIP STRUCTURE

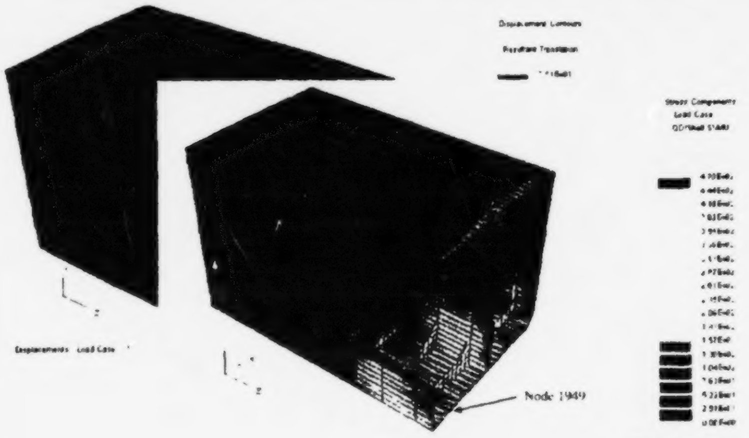
Displacement Contours
Resultant Translation
Stress Components
Load Case
Displacements Load Case
Node 1949

Martec Limited
Advanced Engineering and Research Consultants

FUZZY RESPONSE OF TANKER SHIP STRUCTURE

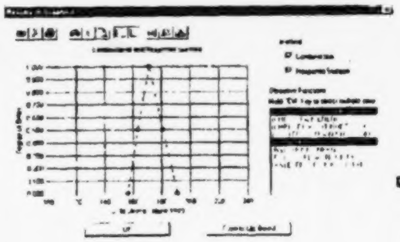

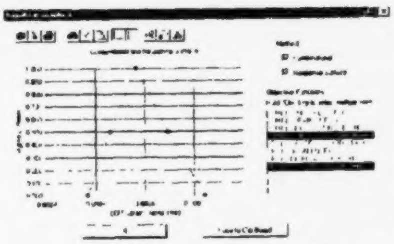

Martec Limited
Advanced Engineering and Research Consultants

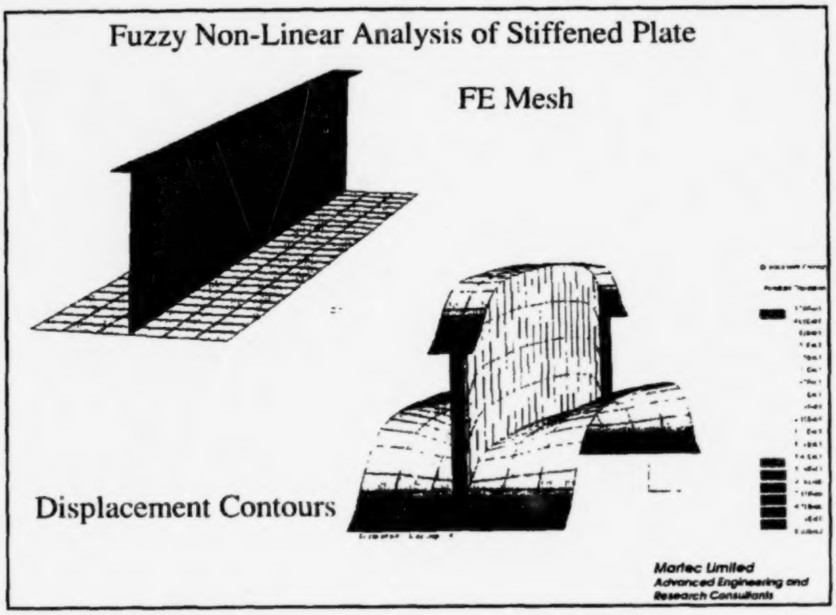

Fuzzy Non-Linear Analysis of Stiffened Plate

FE Mesh

Displacement Contours

Martec Limited
Advanced Engineering and Research Consultants

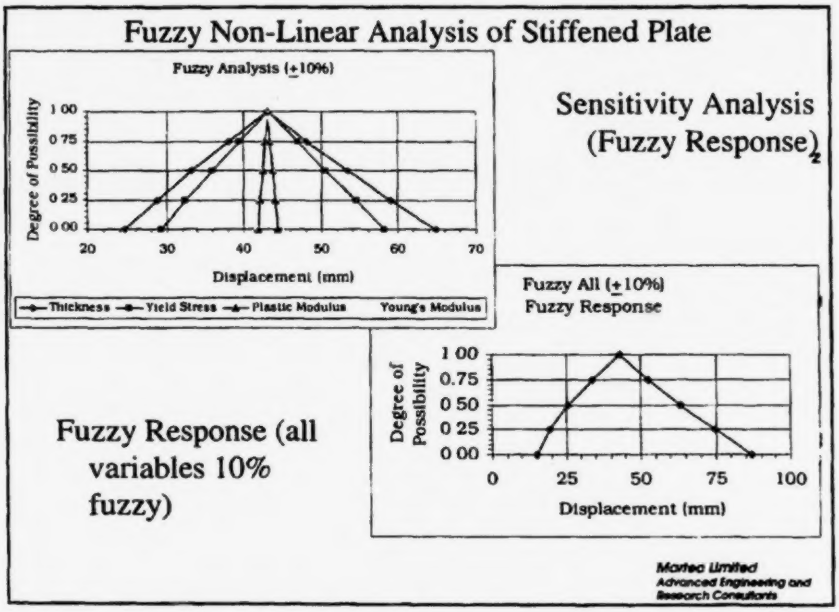

Fuzzy Non-Linear Analysis of Stiffened Plate

Sensitivity Analysis (Fuzzy Response)

Fuzzy All (±10%)
Fuzzy Response

Fuzzy Response (all variables 10% fuzzy)

Martec Limited
Advanced Engineering and Research Consultants

Fuzzy Non-Linear Analysis of Stiffened Plate (Corrosion with Aging)

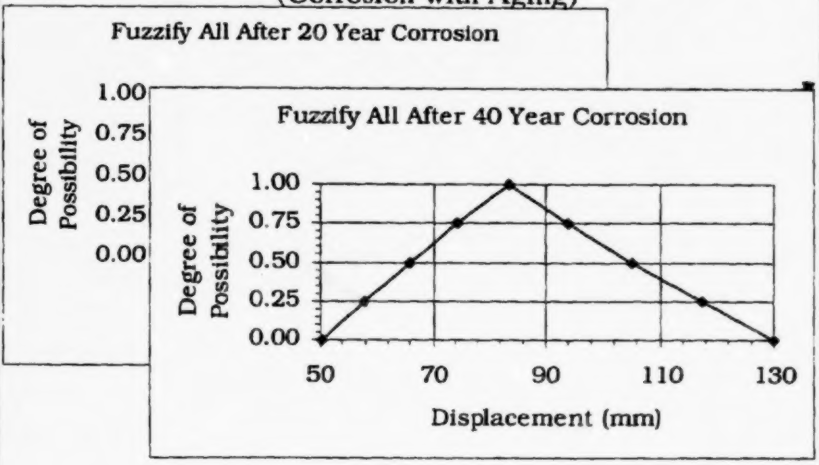

SUMMARY/CONCLUSIONS

- A PRACTICAL STRATEGY FOR FUZZY FINITE ELEMENT ANALYSIS OF STRUCTURAL SYSTEMS HAS BEEN FORMULATED AND IMPLEMENTED
- METHOD COMBINES POLYNOMIAL RESPONSE SURFACE WITH VERTEX FUZZY MODELLING
- EXAMPLE PROBLEMS THAT DEMONSTRATE THE MERITS OF THE METHOD HAVE BEEN PRESENTED
- MERITS INCLUDE
  - ⇒ COMPATIBILITY WITH EXISTING DETERMINISTIC FEA CODES
  - ⇒ ABILITY TO ACCUMODATE MORE FUZZY VARIABLES
  - ⇒ LOW COMPUTATIONAL COST

PUBLISHING WITH WEB TOOLS

P.R. Roberge
Department of Chemistry and Chemical Engineering,
Royal Military College of Canada, Kingston, Ontario, Canada, K7K 7B4
roberge-p@rmc.ca or http://corrosion-doctors.org

Abstract

Web based training (WBT) is fast becoming an accepted training method for industrial personnel too pressed for time. Advances in computer network technology and improvements in bandwidth have rendered the WBT option increasingly interesting and much of the same is predicted for the next decades. In order to introduce these technologies in the classroom, new paradigms have to be developed to satisfy requirements specific to training. However, technical changes usually impact educational methods very slowly. The introduction of the overhead projector in the classroom, for example, has yet to replace the use of chalk, a very small change indeed. This paper presents a relatively inexpensive and progressive approach to the introduction of WBT as a training aid by building-up adequate features into an existing information Web site.

Introduction

The exponential growth in Internet technologies has made Web-based training (WBT) a viable alternative for delivering training to individuals anywhere in the world at any time. This delocalization of supply and demand opens new challenges and opportunities that are quite exciting in specialized areas of expertise, for which experts often are unavailable for such mundane tasks as teaching and training. The possibilities to offer adequate training via the Internet or Intranet are probably the area of greatest predictable growth in the field of professional training. However, current Web-based pages are mostly the presentation of information that was never designed to fit into an intellectual schema for training.

In spite of the tremendous advantages offered by these new technologies, experience has shown that an enormous investment in professional time in planning and developing course material is required. Some of the advantages and disadvantages of WBT and more conventional education techniques are summarized in Table 1. Fortunately, some Web sites are readily designed to support WBT. The Corrosion Doctors site is an excellent example of such sites. It was recently decided at KTS, the developer and maintainer of the site, to reengineer the information spread out throughout the site and build multifunctional training features into many of the forty information modules present on the site. This paper presents an incremental approach to WBT development that will hopefully help avoid many of the pitfalls facing the introduction of a new technology in the classroom, while providing the means to test new concepts before the creation of full-scale training packages.

Designing a Computer Based Training Course

As a first step in organizing materials for on-line training, it is useful to cast discussions about what should be taught into a standardized pedagogical framework. The creation of on-line materials and the presentation of these materials should be driven from a mental model of what the target students should learn, a less than trivial question [1]. Engineers, for example, do need to learn on their own, deal with unexpected situations and solve problems. Following the example provided by Bourne, the types of things that engineering students should learn have been classified into two well-known taxonomies in education [1]. Barrett's taxonomy proposes that learning should be divided into four categories: literal recognition (recall), inferential comprehension, evaluation, and appreciation [2].

Table 1 - The advantages and disadvantages of CBT when compared to conventional education techniques.

Advantages	*Disadvantages*
Potential for achieving higher student cognition	Lack of human interaction and engagement
Direct linkages to Internet resources	Lack of teamwork
Rapid updating of information and course materials	Low inspiration factor, especially when working in isolation
Efficient retrieval of specific information using electronic text processing	Limited verbal communication skills development
Possible interactivity of course material	Requirement for expensive hardware
Tracking user interaction with the course material	Developers need of computing and software skills outside of own expertise
Access to a large student and professional "market"	Production of WBT material can be time consuming and costly
Cross platform and open systems delivery	Need of support staff
Opportunity for interactions among students	Bandwidth limitations
Reusability of training material across programs	Often too 'static'
Optimization of a steadily shrinking expert instructor pool	
Freedom to follow individual pace and learning styles for students	

Merrill's taxonomy uses a performance-context matrix that includes the actions of remember, use, or find(create) [3]. The content is classified as fact, concept (classification), procedure or principle. The taxonomies appear to be useful for classifying learning outcomes in engineering and in selecting the technology required for on-line implementation. Table 2 presents some typical learning outcomes that may serve as a basis for classification of how we should structure engineering learning scenarios (adapted from [1]). Examples are given in the right hand column of particular engineering problems in the area of corrosion engineering.

One of the most significant capabilities that can be supplied to users is interaction. Presentation of text and graphic materials in hypertext form is indeed useful; however, Web-based materials are significantly more interesting when they are interactive. For example, a common technique is to add forms to hypertext markup language (HTML) documents so that the user can interact with the Web page. In an on-line classroom setting, this type of capability can be useful for creating surveys, tests, and shared materials. Animation, tutorial systems, and access to bulletin boards, provide additional capabilities. With a Web browser, it is very simple to embed access to file transfer protocol (FTP). Thus, if there are files that students need to download, this capability can be embedded directly in the HTML document.

Table 2 - Examples of typical learning outcomes.

Typical Engineering Knowledge	Barrett	Merrill	Sample Problems
What is . . . (identification)	Literal	Remember fact	What are the units of corrosion penetration rates? Relate these to Faraday's law
Recall characteristics	Literal	Remember concept	State the characteristics of each type of corrosion testing studied.
Describe a process	Literal	Remember process	Describe how the linear polarization method can yield corrosion rates.
How to do something	Literal	Remember procedure	List the procedure to draw an Evans' diagram.
Set up a problem using guidelines	Literal	Remember principle	State the guidelines to design an anodic protection system.
Recognize types of corrosion inhibitors	Inferential	Use a concept (classify things into categories)	Given these five corrosion inhibitors, identify which are passivators.
What will happen if?	Inferential	Use principle	What will happen if the pH of a steel vessel was to drop below 6.2 from 10.2?
Apply a learned pattern or sequence	Appreciation	Use procedure	Using the information in the cathodic protection module, calculate the number of sacrificial anodes that would be required to form a calcareous deposit on a steel pile immersed in seawater.
Linkage between theory and practice	Appreciation	Use principles (laws and heuristics) to solve a problem	Use the Pourbaix diagram of Cr to determine the control current and potential for the anodic protection of a S43000 stainless steel vessel.
Linkage to real world complexity	Appreciation	Use principles	Using straight value depreciation, decide between two copper-nickel alloys for the design of a heat exchanger.
Creating specifications and implementing	Evaluation	Find principles	Evaluate the corrosion monitoring needs of this section of a chemical processing plant and design a cost effective strategy to generate reliable data.
Finding out (analyzing)	Evaluation	Find principles	Create a set of guidelines to determine the points of a plant susceptible to localized corrosion.

The following list displays the types of desired education outcomes and how these outcomes can be facilitated by different components of the training model [1]:

1. Easy access to knowledge: The Web greatly facilitates access to all kinds of knowledge stored on FTP sites, in libraries, and on HTTP servers that can greatly facilitate an engineering student's search for information.

2. Learning to work in a team: Working in teams has become the norm in the engineering industry. Further, teams are often constituted from individuals who are not in the same location. With excellent network capabilities, teams of individuals with specific expertise can be easily brought together electronically to rapidly accomplish a task. In engineering education, we need to emulate this environment so that students can have preparatory experiences that will mimic the real engineering environments that they will encounter after graduation.
3. Design discussions: Design can be facilitated using on-line discussions among teams of student designers at different institutions.
4. Immediate feedback: Providing immediate feedback to instructors and students alike is an essential component of the training model. The common gateway interface (CGI) of HTTP servers permits writing programs that can access and manipulate data supplied from Web clients.
5. Continual monitoring and self-evaluation: CGI permits doing such things as monitoring which students access materials, determining when and where students use materials, accessing the state of knowledge of a class continuously, providing homework grading, feedback and on-line testing.
6. Laboratory experiences: The lecture and laboratory can be more easily combined using on-line methods. Current courses that are on-line provide lecture materials and interactive questioning. Laboratories can be provided either via simulation programs or via demonstration. Combining lectures and laboratories can be quite useful for on-line education.

Reengineering an Existing Web Site

There are quite a few Web sites containing elements of corrosion information. A search of the generic term corrosion would typically find upwards of 600,000 Web pages with variable references to the subject. The following sections will discuss various aspects related to the creation, development, and operation of the Corrosion Doctors Web site. From its launching in mid August 1999, the site has reached an interesting level of Web traffic in its first eighteen months of existence, with positive indicators that the site is actually fulfilling its initial goal of bridging large distances across many disciplines.

Early Days (1997-1998)

Two information modules and one Aircraft Corrosion Newsletter had been developed in the early part of 1997, following the suggestion made by military personnel at one Canadian Forces Base. The main goal of these Web pages was to improve the communication of complex data and concepts between distant locations. The pages were created using a very efficient tool, Frontpage 97, requiring a minimum of programming skills. However, while these pages were developed in a relatively straightforward manner, they had to be transferred to a UNIX based Web server by a different team, with a few levels of bureaucratic annoyances. In practice this met that the pages turnover was very slow and absolutely limited to HTML code.

The Corrosion Doctors Site

The interest and need to interface to a largely distributed community were reexamined in a study carried out by an external advisor in the first part of 1999. One obvious conclusion of the study was to seek a Web service adapted to the development tools chosen and free of local politics. The reengineered site was launched in mid August 1999 as the ***Corrosion Doctors***. It was decided, early in the existence of the site, to build it on feedback and collaborations from the broadest community possible. Most of the first months of the Web site development were spent learning the rudiments of information for Web delivery while conducting surveys designed to reveal specific aspects of the corrosion engineering profession.

The Surveys

Six surveys were conducted by inviting the active participants of two well known Internet corrosion discussion groups [4;5], totaling approximately twelve hundred active members, to reach a specific page of the site and answer a set of both short and specific questions related to one of the following themes:

- 1st Survey: Human Errors in Corrosion, 50 participants
- 2nd Survey: Educating the Corrosion Engineers, 60 participants
- 3rd Survey: Information Sources, 52 participants
- 4th Survey: Facing Management, 42 participants
- 5th Survey: Working with Others, 31 participants
- 6th Survey: Computer Based Training, 94 participants

The first five surveys have been designed after a landmark paper by Francis LaQue originally published in 1978 and reprinted since then [6]. Typically, list members were notified of a survey or of its displayed results. As can be seen in the previous list, some of these surveys were more popular than others. The surveys were carried with dynamic HTML pages that permitted to collect the answers in a database for further analysis. In the survey designed to reveal the importance of different information sources used by corrosion engineers, the participants were asked to select among a series of optional answers the one that best fitted a specific question:

- Books
- Journals
- Conferences & their associated activities and publications
- Software systems (databases, CDs, etc.)
- Own network of friends and contacts
- Internet discussion groups such as UMIST, NACE and others
- Internet sources others than above, e.g. Web sites
- Other

The questions themselves were semi-repetitive, asking of the participants to identify which of the proposed information sources was either the most dependable or least dependable source. Figures 1 and 2 show respectively the breakdown of answers to the question "What is the most dependable information source you depend upon to carry your work?" and to the question "What is the least dependable information source you depend upon to carry your work?" The information explaining the surveys, the surveys themselves as well as their results have been edited and process into two information modules called the Portrait of a Corrosion Engineer and the Human Factor (Figure 3).

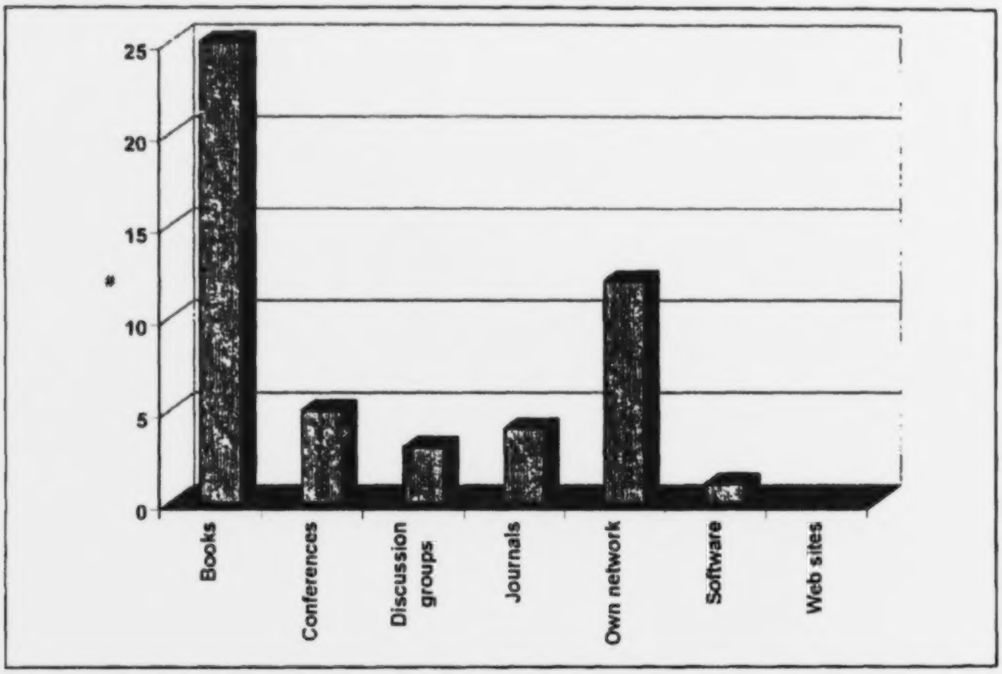

Figure 1: Compilation of the results to the question "What is the most dependable information source you depend upon to carry your work?"

The Corrosion Doctors site presently contains corrosion information from a multitude of sources. The backbone of the information assembled during the first year of operation was constructed in specific themes gathered in information modules. One of the main advantages of Web publishing is the flexibility permitted by inter-linkages. With some careful design considerations, it is possible to continuously and seamlessly develop sections of a Web site without the users or visitors of the site being inconvenienced or annoyed by these changes. The approach chosen for this maximum flexibility was to use frames for each module and an open architecture for the main pages of the site. Each module would thus have its own table of contents supporting an internal navigation scheme and a banner to identify its location in hyperspace. The Corrosion Doctors Web site presently contains forty information modules divided in the following categories:

- Corrosion Basics (17 Modules)
- Corrosion Prevention and Control (12 Modules)
- Corrosion Testing (4 Modules)
- Education vs. Corrosion (2 Modules)
- Electrochemical Power Sources (5 Modules)

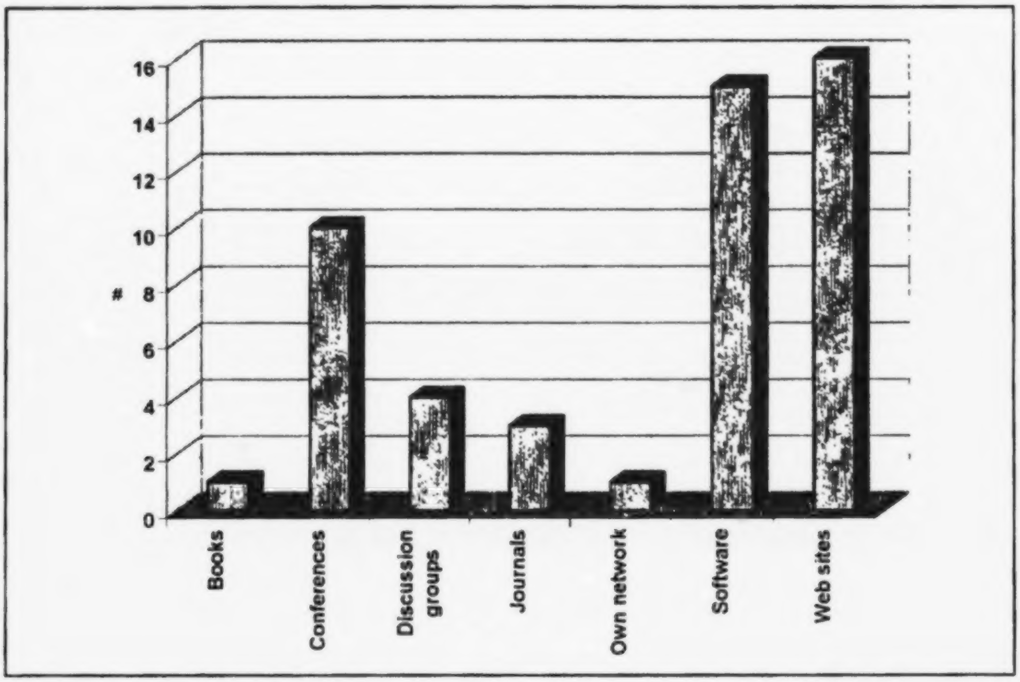

Figure 2: Compilation of the results to the question "What is the least dependable information source you depend upon to carry your work?"

Human Factor

brought to you by the Corrosion Doctors

[illegible]

[illegible]

Figure 3: Entry page of the information module summarizing the survey on the human factor in corrosion problems

News Bulletins

The News Bulletins were created to accelerate the diffusion of the site activities. People are busy and searching the Web for corrosion information is neither their main preoccupation nor even an accepted information gathering method. If one believes the results of the survey on the Information Sources used by modern corrosion engineers, the Web would be the least credible source of information one would consult (Figure 2). It is generally felt, at least in the corrosion community that is active in the Internet discussion groups that the quality of technical information is simply not there yet. Such a sentiment cannot be generalized to other professions and other disciplines such as environmental science and other scientific areas since excellent and informative sites have reached the top of visibility charts, achieving to attract record numbers of visitors.

In order to build up the interest for the information displayed on the site, it was decided to create the News Bulletins for direct Internet distribution. The first issue was sent to approximately three hundred recipients in March 2000. Subsequent Bulletins were sent at regular intervals to a growing list of recipients. The impact of these News Bulletins on site visits was immediate.

Site Index

One feature that was immediately accepted by both human and machine visitors was the site Index. The Index was created to overcome the partitioning caused by the use of frames initially for the construction of the information modules and subsequently for the pages of the Corrosion Doctors Journal. Navigating through the Web site had become increasingly complex as the number of information modules and the number of associated pages had grown into a real maze. The site Index lists, for each letter of the alphabet, hypertext references to most pages of the site that, in turn, have a return link to the Index.

The main difficulty was to decide how each page would be referenced for the site Index as well as for visiting spiders and crawlers. However, the effort was not done in vain since many of the keywords used in the indexing process have now reached the highest level of citation with most of the popular search engines. An additional feature was added for the human visitors, allowing them to search the site using their own words and Boolean logic to find citations directly related to their queries (Figure 4).

The Corrosion Doctors' Journal

Six papers have been published in Volume 2000 of the Corrosion Doctors' Journal. As with the information Modules, special care was given to the presentation of these papers in a fashion that permitted full integration of the Journal content into the site with an almost infinite level of possibilities of interlinks and hyper-referencing. A different navigational arrow has been used in the Journal pages to provide internal linkages while giving a sense of orientation to visitors coming to a specific page of the site from external referrals. There is presently no ambition to promote the Corrosion Doctors Journal out of the site context and compete with existing publications. The feature is experimental and wants to prove that high level corrosion information can be distributed through the Web. It is also a simple method for absorbing complete documents without the need to condense and digest the information unnecessarily.

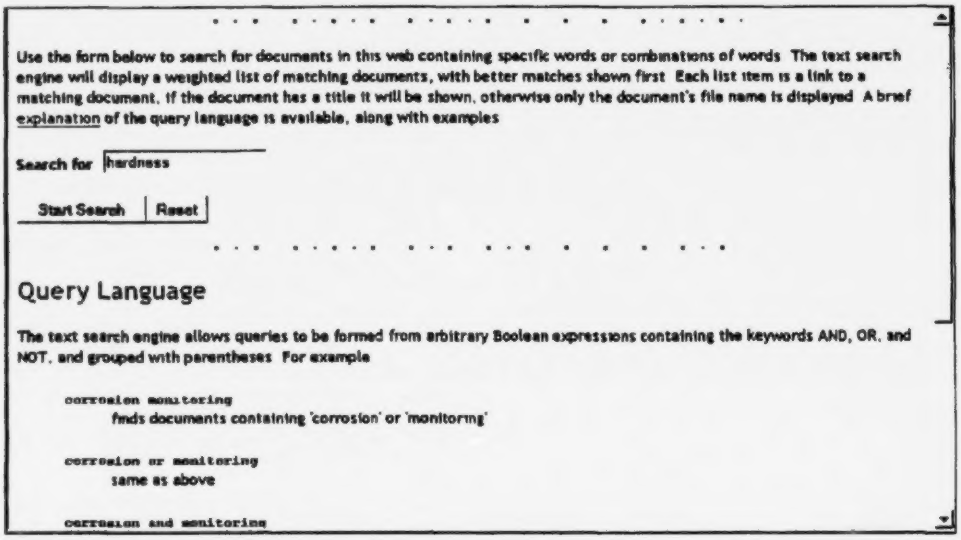

Use the form below to search for documents in this web containing specific words or combinations of words The text search engine will display a weighted list of matching documents, with better matches shown first Each list item is a link to a matching document, if the document has a title it will be shown, otherwise only the document's file name is displayed A brief explanation of the query language is available, along with examples

Search for hardness

Query Language

The text search engine allows queries to be formed from arbitrary Boolean expressions containing the keywords AND, OR, and NOT, and grouped with parentheses For example

`corrosion monitoring`
finds documents containing 'corrosion' or 'monitoring'

`corrosion or monitoring`
same as above

`corrosion and monitoring`

Figure 4: Customized search facility supported on the Corrosion Doctors site.

Building up the Training Center

After a little more than one year of development, the site contained close to one thousand pages of diverse and tested Web material. Two new features were then created to add depth to the site content, the Web Journal mentioned in the previous section and a Training Center. This Training Center was considered to be a prudent approach for testing some concepts of WBT before developing full scale training packages. These experiments were deemed necessary since development guidelines, market analyses, or accreditation requirements are greatly missing in this new promising field of communication and information processing.

Educators' list

A survey was designed to help define who could be interested to use the Corrosion Doctors site as a support medium for training in corrosion science and engineering. Filling up this survey was the first step in joining the Corrosion Doctors Educators' list. This survey, as with all the surveys carried so far on the site, was constructed in a manner that could be answered in a few mouse clicks. There was also room for more elaborate comments. The survey participants were asked to provide contact information and some details on their teaching experience and actual teaching involvement. Following this preamble, the participants were asked to select the most useful topics amongst a list of twenty-four titles corresponding to Modules of the site. Forty-four participants have answered this particular survey and the results obtained are summarized in Table 3.

Refocusing Web Development Efforts

One important exercise in reengineering the site towards a new role was to analyze its features in terms of development effort as a function of the dynamic potential of these features and interest shown by visitor frequency (Figure 5). The dynamic potential axis in this figure represents the easiness to change, add, or subtract from each page or feature. While both the Journal and the Training Center were designed to provide depth to the site, reengineering the site towards training made much more sense in terms of efficiently developing a Web site with limited resources and funding support. Following this analysis, it was decided to gradually dismantle the Journal and all its associated features and focus on furthering the Training Center.

Table 3 – Results of the survey on using information modules in support of training.

Corrosion Basics	Interested	% interest
Atmospheric Corrosion	22	50
Causes and Forms of Corrosion	35	**80**
Hot Corrosion	15	34
Kinetics	24	55
Elements of Risk	20	45
Microbiologically Influenced Corrosion	16	36
Natural Waters	17	39
Reference Electrodes	17	39
Reinforced Concrete	11	25
Seawater	27	**61**
Soil Corrosion	13	30
Thermodynamics	24	55
Corrosion Prevention and Control		
Anodic Protection	12	27
Cathodic Protection	23	52
Corrosion Inhibitors	23	52
Corrosion Monitoring – Basics	28	**64**
Inspection	21	48
Life Prediction	21	48
Materials Selection	26	59
Protective Metallic Coatings	31	**70**
Protective Organic Coatings	22	50
Corrosion Testing		
Corrosion Testing – Basics	35	**80**
Electrochemical Test Methods	33	**75**
Testing for Pitting and Crevice Susceptibility	18	41

Engineering Problems

Most learning outcomes presented in Table 2, with the exception of the Literal (Barrett) or Remember (Merrill) outcomes, can be advantageously supported in a Web format by numerical questions. Typical engineering tasks require that specific goals be reached using a diversity of mathematical tools varying with contexts and situations. The main virtue of regular assignments, when teaching an engineering topic, is to keep the students focused on reasons and methods to accomplish specific tasks. Teaching corrosion engineering means going through detours in various fields that do not necessarily seem to be related, at least to an average student. The breadth of information presently on the site can be used to build questions on specific themes. The level of difficulty of each problem is indicated in decreasing order, with 5 corresponding to the most difficult and 1 to the easiest.

1. Thickness of a galvanized coating: Knowledge of metallic coatings and atmospheric corrosion (level 2)
2. Corrosion inhibition in cleaning acids: Knowledge of electrochemical methods and corrosion inhibition (level 3)
3. Copper sulfate reference half cell potential: Knowledge of basic thermodynamics (level 3)
4. Choosing the material of construction of a heat exchanger: Knowledge of corrosion economics (level 2)
5. Galvanic coupling causing galvanic corrosion: Knowledge of corrosion kinetics (level 4)
6. Choosing a paint schedule: Knowledge of corrosion economics (level 2)
7. Anodic vs. cathodic corrosion inhibition: Knowledge of corrosion kinetics and corrosion inhibitors (level 4)
8. Cathodic protection and calcareous deposits: Knowledge of corrosion kinetics, seawater, cathodic protection and basic corrosion rates (level 5)

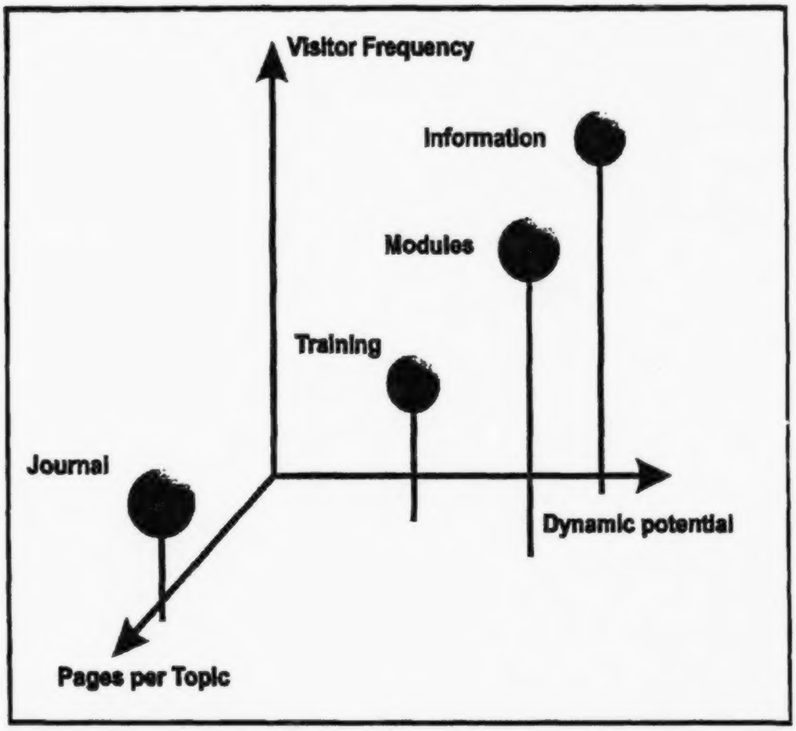

Figure 5: Schematic representation of four types of features supported on the Corrosion Doctors site as a function of visitor frequency, number of pages per topic, and dynamic potential.

A course program can be designed by threading the course content to meet the specific objectives required to complete this type of engineering problems. Once a structure is adopted the problems themselves can be reworked quite easily since they all require different sources of knowledge.

Summary

Advances in computer network technology and improvements in bandwidth will usher in capabilities for unlimited multimedia access. Web browsers that support 3-D virtual reality, animation, interactions, chat and conferencing, and real-time audio and video will offer unparalleled training opportunities. With the tools at hand today, it is possible to craft highly effective WBT to meet the training needs of a diverse population. However, these opportunities are presently perceived as any other research activities by training institutions. Most of the successes in WBT have so far been achieved for courses in software and computer engineering. In such cases the medium is also the training breadboard.

For hard courses in other disciplines progress will be much more difficult for two main reasons: the first and probably most obvious is the effort required to transform the training material into a computerized format. Such endeavor has been estimated to be of the order of one hundred hours of preparation for a typical university lecture. The second obstacle is subtler and maybe more challenging than the first since is psychological in nature. As much as software engineers understand the mechanics to produce and run a WBT course, the opposite is true of many specialists in other disciplines. This lack of familiarity can easily turn into an obstinate opposition to an estranging technology.

References

(1)Bourne JR, .Brodersen AJ, Campbell JO, Dawant MM, Shiavi RG. A Model for On-Line Learning Networks in Engineering Education. Journal of Engineering Education 1996; 85(3).

(2)Smith RJ, Barrett TC. Teaching Reading in the Middle Grades. Reading, MA: Addison-Wesley, 1974.

(3)Merrill MD. The Descriptive Component Display Theory. In: Merrill MD, Twitchell DG, editors. Instructional Design Theory. Englewood Cliffs, NJ: Educational Technology Publications, 1994: 111-157.

(4)CORROS-L: The corrosion discussion list. http://www.cp.umist.ac.uk/corros-l/Default.htm . 2000.

(5)NACE International List Servers. http://www.nace.org/naceframes/Discussion/ncnindex.htm . 2000.

(6)LaQue FL. What can management expect from a corrosion engineer? Materials Performance 1985; 25(8):82-84.

#516469 (54)

Lessons Learned From Operational CPF Trials

by

John F. Porter* and Colin Smith** and LCdr. Chris Hargreaves***

* Dockyard Laboratory, DREA, Halifax, N.S.
** NETE, LaSalle, Quebec
*** Directorate of Maritime Ship Support, Hull, Quebec

Abstract

Since shortly after the introduction of the Canadian Patrol Frigate to the Canadian Navy, the Dockyard Laboratory (Atlantic), the Naval Engineering and Test Establishment and the Directorate of Maritime Ship Support have collaborated to undertake numerous experimental trials onboard these platforms. These trials have predominately been in response to operational challenges such as structural and component cracking and have included a wide variety of experimental set-ups, monitoring operational conditions such as temperature, strain, motion, position and environment. While these trials have been instrumental in resolving numerous operational issues, a number of lessons have been learned. These lessons are being employed to conduct more effective experimental evaluations and in the development of advanced sensing systems for marine platforms.

This presentation will review the history of these collaborative trials and a summary of the lessons learned will be provided. A preview of forthcoming trial evaluations, employing recently developed advanced sensing systems will also be discussed.

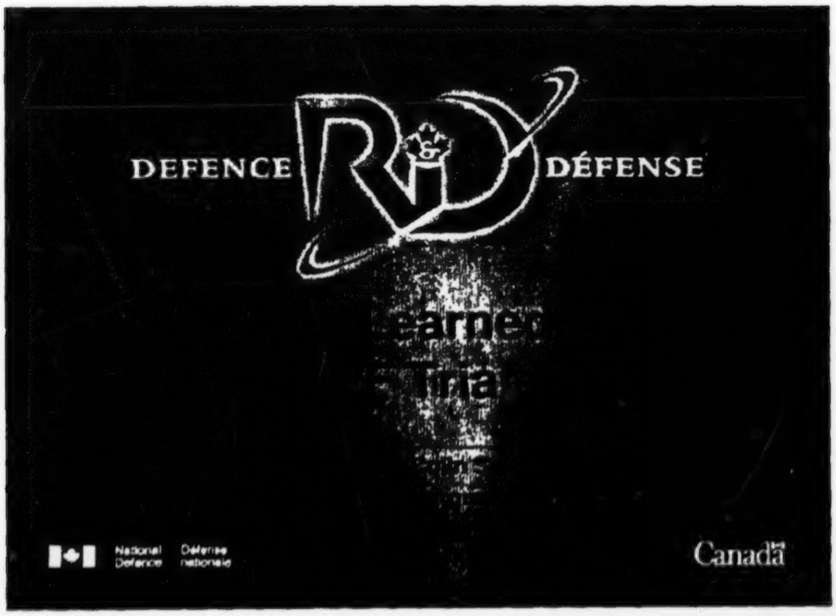

DEFENCE DÉFENSE

earned

ina

National Defence Défense nationale

Canadä

Canadian Patrol Frigate Sea Trials

Collaborations between DREA, DMSS, and NETE to:

- **Assist in platform investigations**
- **Enhance platform health monitoring capabilities**
- **Define mission and platform strain spectra**
- **Improve understanding of fatigue and fracture processes**

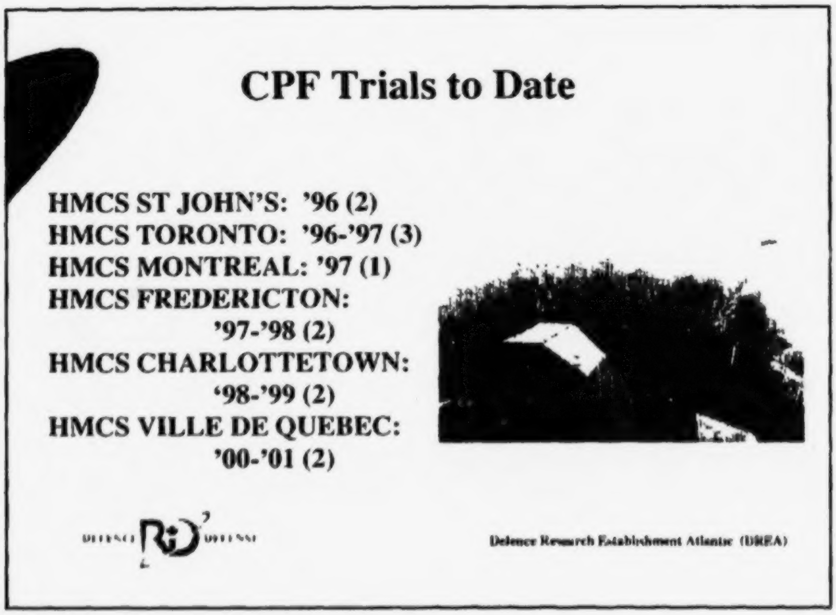

CPF Trials to Date

HMCS ST JOHN'S: '96 (2)
HMCS TORONTO: '96-'97 (3)
HMCS MONTREAL: '97 (1)
HMCS FREDERICTON:
'97-'98 (2)
HMCS CHARLOTTETOWN:
'98-'99 (2)
HMCS VILLE DE QUEBEC:
'00-'01 (2)

Defence Research Establishment Atlantic (DREA)

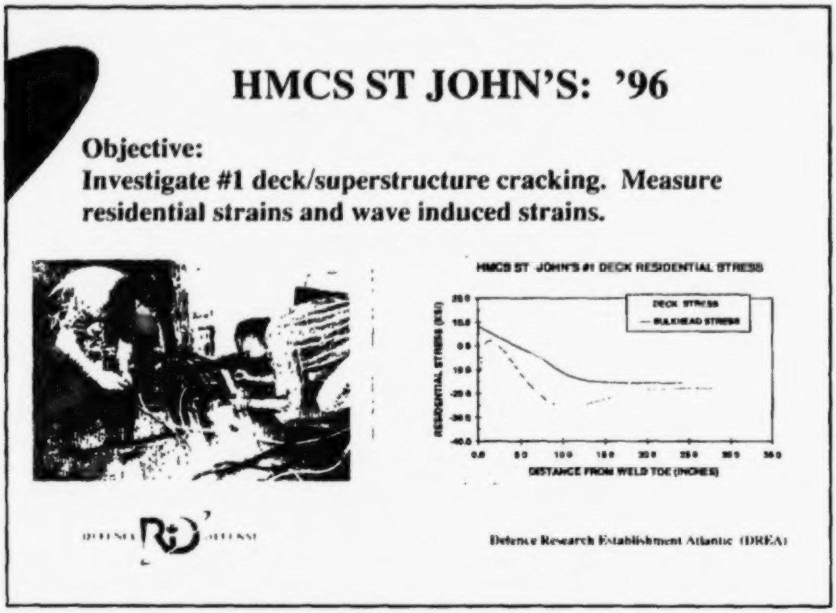

HMCS ST JOHN'S: '96

Objective:

Investigate #1 deck/superstructure cracking. Measure residential strains and wave induced strains.

HMCS ST JOHN'S #1 DECK RESIDENTIAL STRESS
DECK STRESS
BULKHEAD STRESS
RESIDENTIAL STRESS (KSI)
20.0
10.0
0.0
-10.0
-20.0
-30.0
-40.0
0.0
5.0
10.0
15.0
20.0
25.0
30.0
35.0
DISTANCE FROM WELD TOE (INCHES)

Defence Research Establishment Atlantic (DREA)

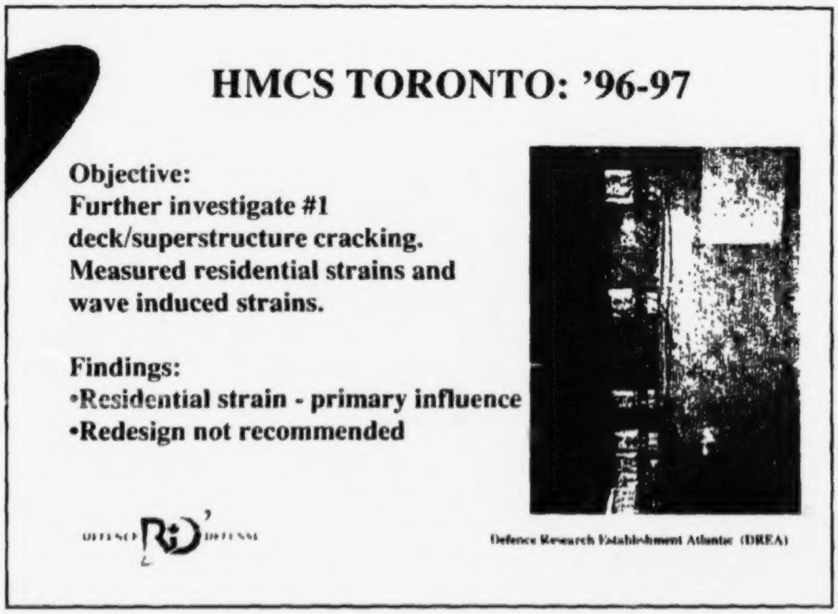

HMCS TORONTO: '96-97

Objective:
Further investigate #1 deck/superstructure cracking. Measured residential strains and wave induced strains.

Findings:
- **Residential strain - primary influence**
- **Redesign not recommended**

Defence Research Establishment Atlantic (DREA)

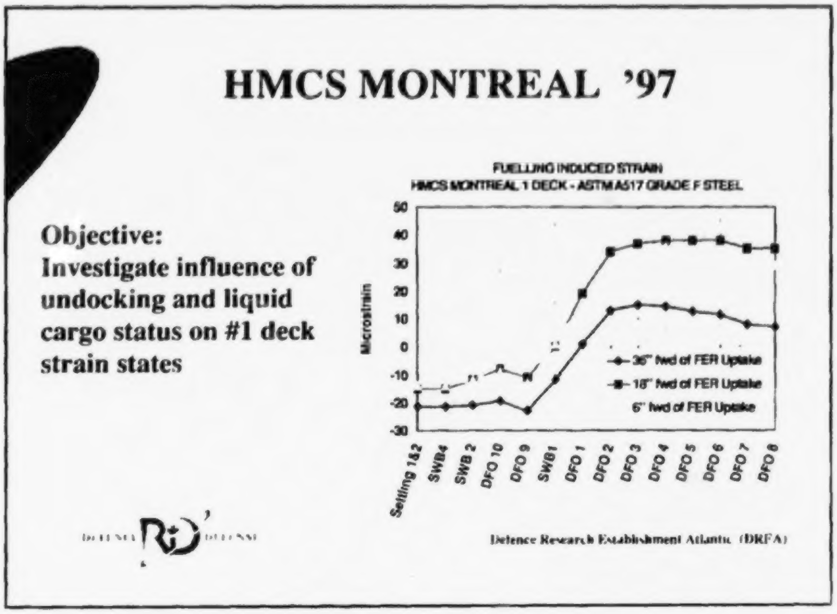

HMCS MONTREAL '97

Objective:
Investigate influence of undocking and liquid cargo status on #1 deck strain states

Defence Research Establishment Atlantic (DREA)

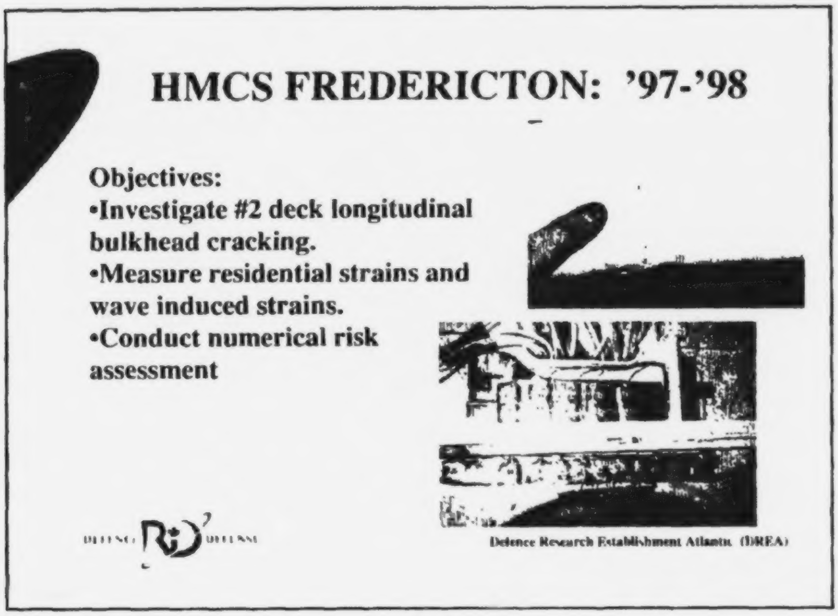

HMCS FREDERICTON: '97-'98

Objectives:

- **Investigate #2 deck longitudinal bulkhead cracking.**
- **Measure residential strains and wave induced strains.**
- **Conduct numerical risk assessment**

Defence Research Establishment Atlantic (DREA)

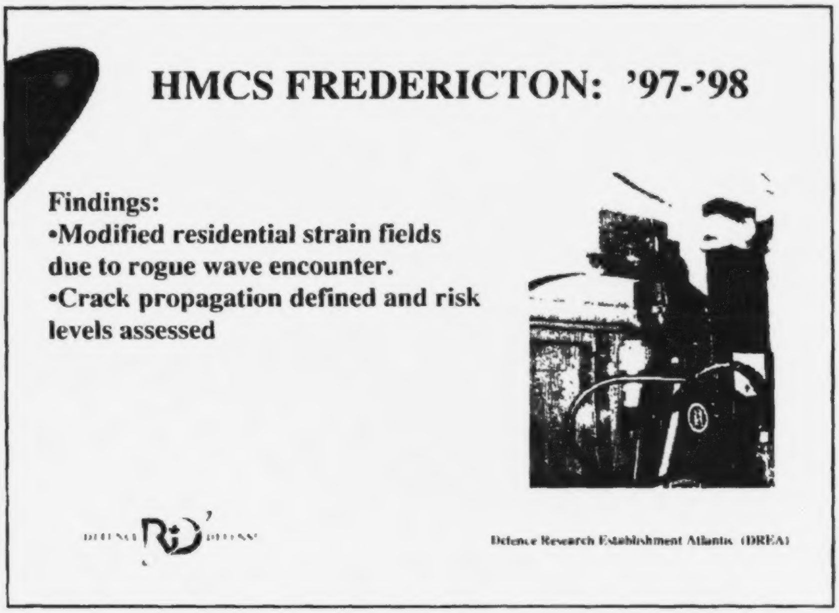

HMCS FREDERICTON: '97-'98

Findings:

- **Modified residential strain fields due to rogue wave encounter.**
- **Crack propagation defined and risk levels assessed**

Defence Research Establishment Atlantic (DREA)

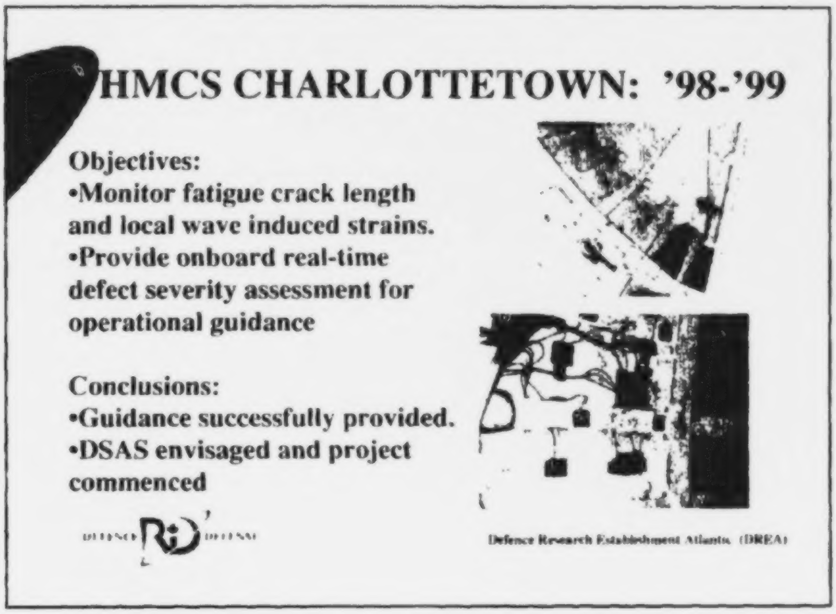

HMCS CHARLOTTETOWN: '98-'99

Objectives:
- Monitor fatigue crack length and local wave induced strains.
- Provide onboard real-time defect severity assessment for operational guidance

Conclusions:
- Guidance successfully provided.
- DSAS envisaged and project commenced

Defence Research Establishment Atlantic (DREA)

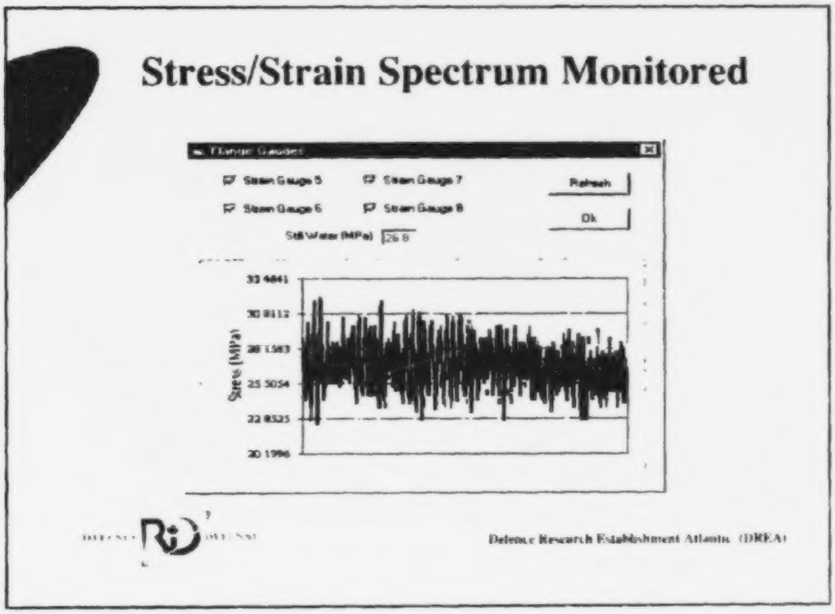

Stress/Strain Spectrum Monitored

☑ Strain Gauge 5
☑ Strain Gauge 7
☑ Strain Gauge 6
☑ Strain Gauge 8

Still Water (MPa) 26.6

Refresh
Ok
33 4841
30 8112
28 1583
25 5054
22 8525
20 1996
Stress (MPa)

Defence Research Establishment Atlantic (DREA)

Severity Factor Assessment

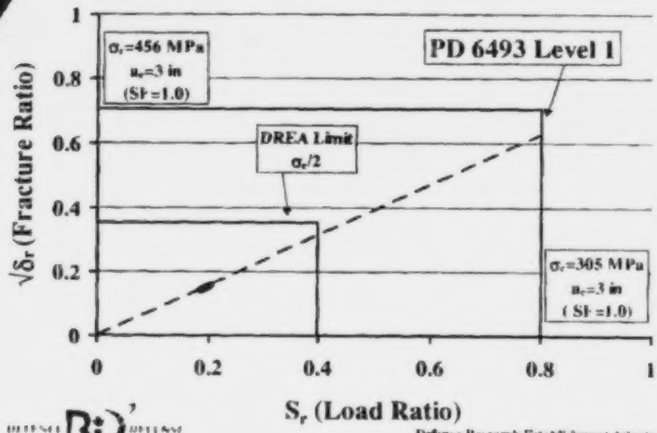

Defence Research Establishment Atlantic (DREA)

Operator Severity Assessment Display

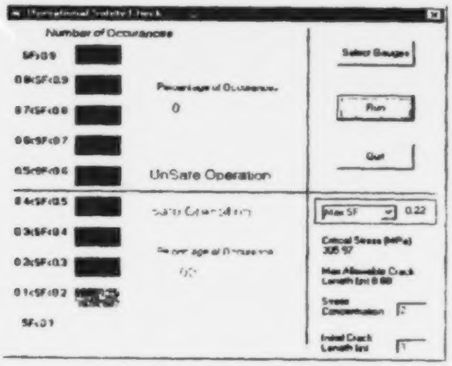
Operational Safety Check
Number of Occurances
SF>0.9
0.8<SF<0.9
0.7<SF<0.8
0.6<SF<0.7
0.5<SF<0.6
0.4<SF<0.5
0.3<SF<0.4
0.2<SF<0.3
0.1<SF<0.2
SF<0.1
Select Gauges
Run
Quit

Percentage of Occurances
0

UnSafe Operation

Safe Operation

Percentage of Occurances

Max SF 0.22

Critical Stress (MPa) 305.97

Max Allowable Crack Length (in) 0.80

Stress Concentration 2

Initial Crack Length (in) 1

Defence Research Establishment Atlantic (DREA)

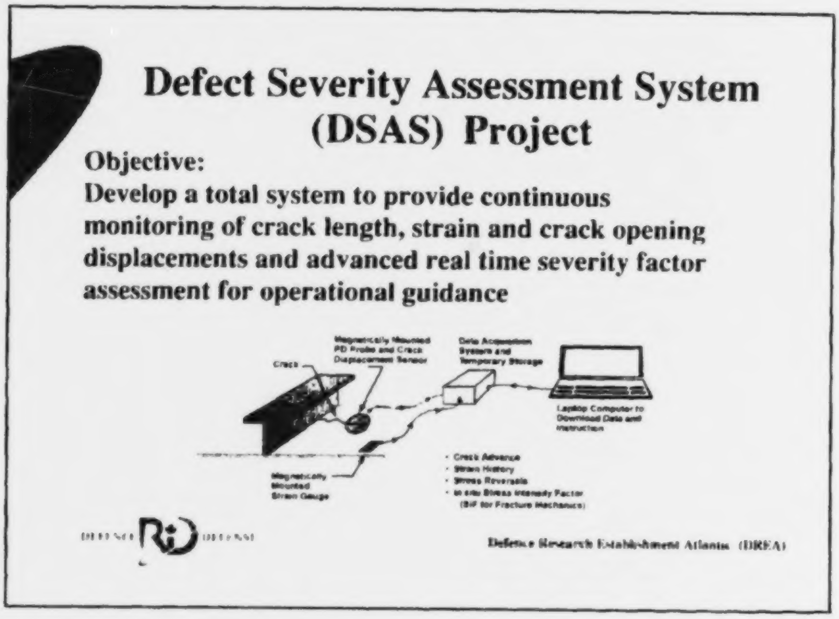

Defect Severity Assessment System (DSAS) Project

Objective:

Develop a total system to provide continuous monitoring of crack length, strain and crack opening displacements and advanced real time severity factor assessment for operational guidance

Magnetically Mounted PD Probe and Crack Displacement Sensor
Data Acquisition System and Temporary Storage
Crack
Laptop Computer to Download Data and Instruction
Magnetically Mounted Strain Gauge

- Crack Advance
- Strain History
- Stress Reversals
- in situ Stress Intensity Factor (SIF for Fracture Mechanics)

Defence Research Establishment Atlantic (DREA)

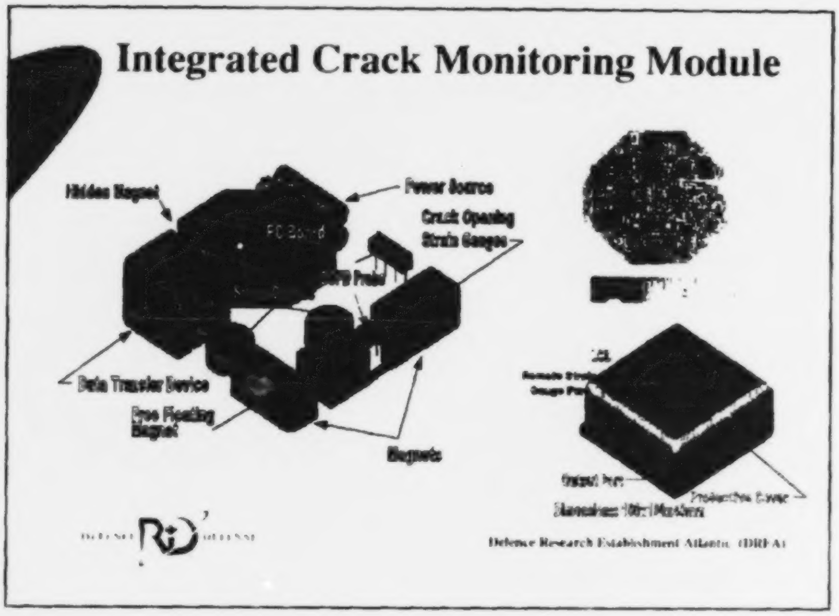

Integrated Crack Monitoring Module

Hidden Magnet
Power Source
Crack Opening Strain Gauges
PC Board
Probe
Data Transfer Device
Free Floating Magnet
Magnets
Output Port
Protective Cover

Defence Research Establishment Atlantic (DREA)

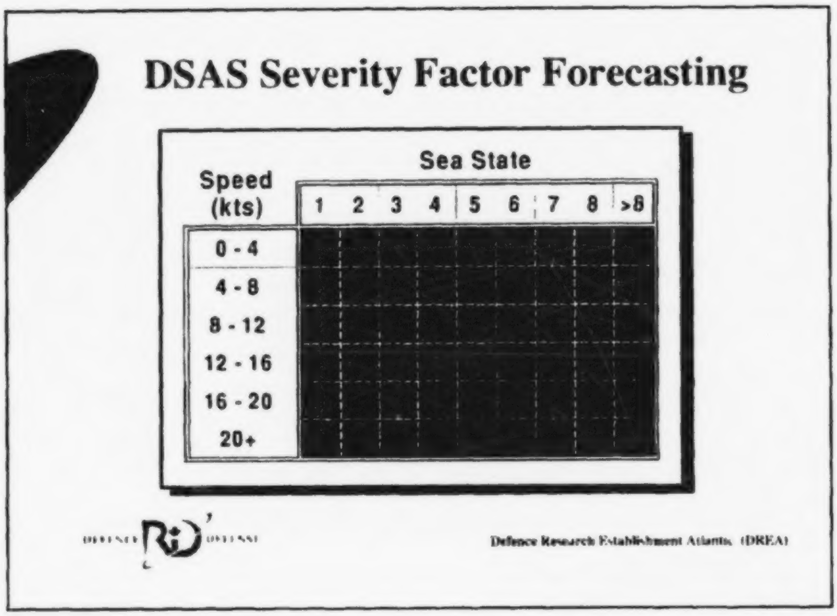

DSAS Severity Factor Forecasting

Speed (kts)	Sea State 1	2	3	4	5	6	7	8	>8
0 - 4									
4 - 8									
8 - 12									
12 - 16									
16 - 20									
20+									

Defence Research Establishment Atlantic (DREA)

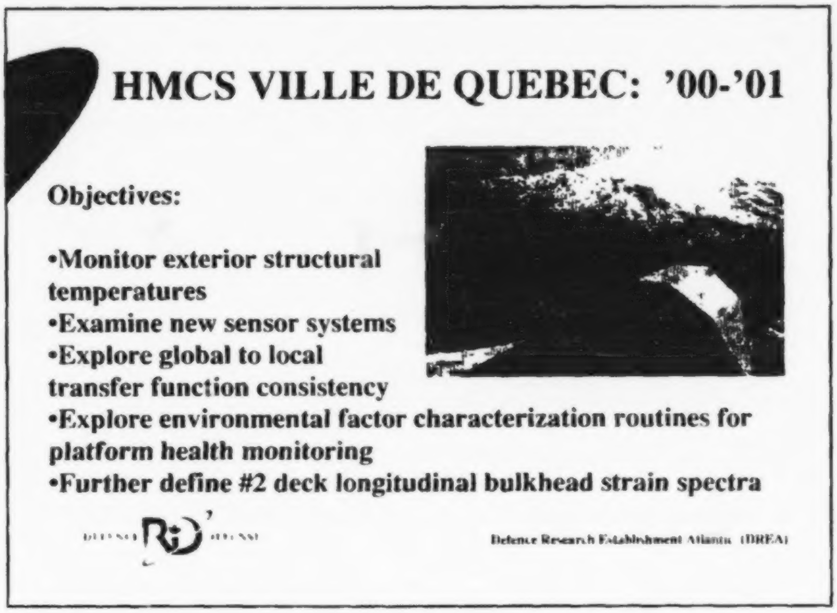

HMCS VILLE DE QUEBEC: '00-'01

Objectives:

- **Monitor exterior structural temperatures**
- **Examine new sensor systems**
- **Explore global to local transfer function consistency**
- **Explore environmental factor characterization routines for platform health monitoring**
- **Further define #2 deck longitudinal bulkhead strain spectra**

Defence Research Establishment Atlantic (DREA)

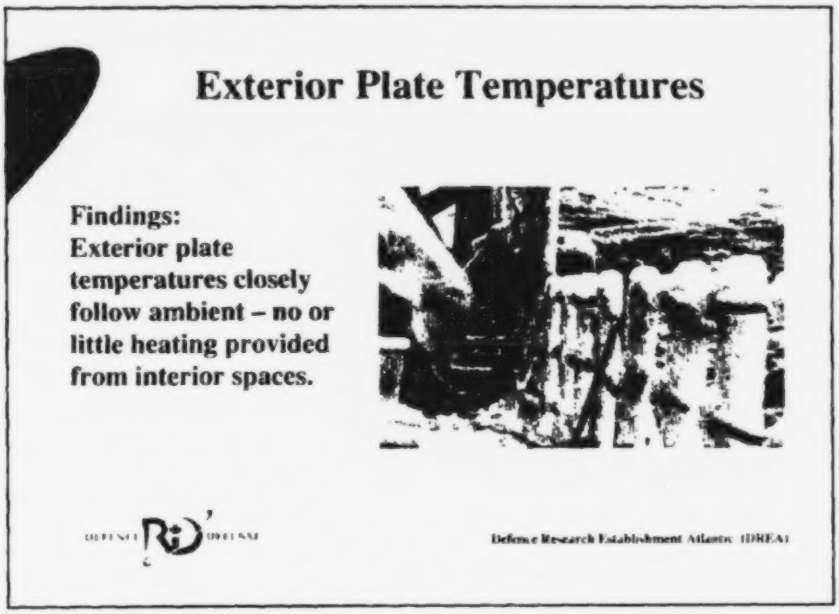

Exterior Plate Temperatures

Findings:
Exterior plate temperatures closely follow ambient – no or little heating provided from interior spaces.

Defence Research Establishment Atlantic (DREA)

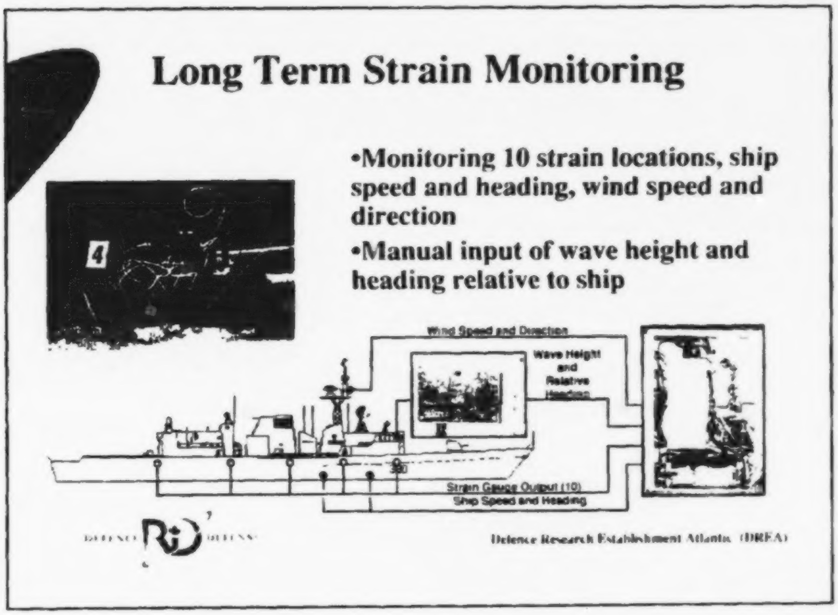

Long Term Strain Monitoring

- **Monitoring 10 strain locations, ship speed and heading, wind speed and direction**
- **Manual input of wave height and heading relative to ship**

4
Wind Speed and Direction
Wave Height and Relative Heading
Strain Gauge Output (10)
Ship Speed and Heading
330

Defence Research Establishment Atlantic (DREA)

Global and Local Strain Consistency

Findings to date: Apparent independence on environmental factors for transfer functions between local and global strains

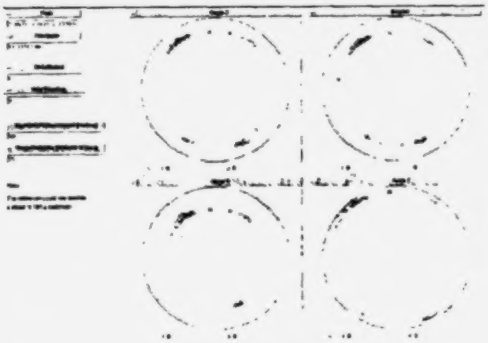

5-6 meter waves

Defence Research Establishment Atlantic (DREA)

Platform Health Monitoring (PHM) Development Project

Application of lessons learned and emerging technologies to create continuous monitoring system for naval platforms

PHM Project Activities

Emerging technology applications;
- Non-traditional sensors
- Large area sensors
- Rigid body dynamics derived stresses
- Differential GPS
- Wireless communications
- Integration of numerical and experimental capabilities
- Integration of remote sensor data
- Enhanced environment description

Some Lessons Learned

Technical Lessons:

- All ships crack, however not all cracks are of serious concern. The ability to distinguish between the serious and nuisance cracking is an essential capability
- Real-time defect risk assessment for the operator is a proven capability
- Weldable gages remain the most effective, reliable sensors available
- Data acquisition should be "stand-alone"
- Manual data input (Bridge log) is an invaluable backup to automated or semi-automated data collection systems

Some Lessons Learned (cont.)

Not-So Technical Lessons:

•Teamwork between DREA, DMSS, NETE and the Fleet has proven an extremely effective means of addressing short and long term operational issues.

•A half hour in the CO's cabin is worth more than 3 months of trial request paperwork.

•"Smith's Law" – The ideal gage location is always the most awkward.

•"Finagles Law" – The most obviously correct data, beyond all need of verification, is erroneous.

Defence Research Establishment Atlantic (DREA)

#516470 (55)

Application of Modern S690 Materials for the Hull of Minesweeping Drones

by

Cees van Sevenhoven
RNLN/DMKM/MARTECH
Royal Dutch Navy
C.Sevenhoven@MINDEF.NL

Abstract

An investigation has been carried out for the material selection of the hull structure of the Minesweeping Drone. The aim has been to determine the static and dynamic behaviour of Modern S690 [HY 100] materials and their weldments versus S355 material [grade 50] and the effect of hydrogen charging due to the imposed electric signature on the integrity of the hull structure.

Information will be given about: Cold cracking resistance; Hydrogen loading and resistance to cracking, Thermal elasticity, Dynamic properties etc.

1. Introduction

In order to counter the threat of mines in coastal area's the Royal Netherlands Navy [RNLNavy] is designing unmanned minesweeping vessels (drones). Four of these drones will be controlled by one adapted Alkmaar class minehunter. The challenge for the RNLNavy is to design an remotely controlled unmanned drone that is capable to remain in operation after surviving the effects of mine-explosions.

The design of the drone is based on a 'cylinder' that provides the vessel with buoyancy and the required resistance against the effects of mine explosions. It further serves as core for the magnetic minesweeping system. This system simulates the magnetic signature of merchant and navy ships. These signatures are produced by cables that are wound around the cylinder. The internal space of the cylinder is used to house the technical systems. In addition to the magnetic minesweeping system the drone is equipped with an electric as well as an acoustic minesweeping system. The combinations of the different signatures results in rather low potentials at the hull side which leads to the hydrolysis of water and subsequent possible hydrogen absorption by the steel.

A material investigation has been carried out for the material selection for the hull, with respect to shock loading as well as to the risk of hydrogen loading of the hull material during operational services. A short summary of this examination will be given.

2. Material investigation

The scope of the material investigation was to determine the static and dynamic material properties of S690 material versus the common structural steel S355 and the effect of hydrogen charging of both steels and their reactions under dynamic loading.

Although the Royal Netherlands Navy has quite some experience and knowledge concerning materials with a yield strength level of 690 MPa [this was the construction material for the Walrus class submarines] a number of uncertainties remain for the more modern type of S690 steels, which fulfil the requirements of EN 10137-2/3.

These uncertainties of S690 steels can be summarised as follows:

- Lower ductility than Submarine steel
- More uncertainty about the steel producer
- The cold cracking susceptibility
- Dynamic behaviour
- HAZ properties
- Thermal elasticity of the steel, weld joints and HAZ
- Weldability
- Weld joint behaviour between S355 and S690 material
- The effect of hydrogen loading of the steel hull

The following test procedures have been carried out:

- Three different steel suppliers have delivered commercial S690 according EN 10137 in material thicknesses of 10 and 25 mm.
- Static and dynamic behaviour for parent material and their weld joints.
- The welding processes SMAW and FCAW where used.
- Hydrogen requirement welding consumables $H_{DM} \leq 5$ ml/100gr; for tack welds $H_{DM} \leq 3$ ml/100gr.
- Heat input range from 1,0 to 2,5 kJ/mm.
- Tekken test to estimate the minimum preheat temperature.
- Dynamic tests: Dynamic Tear acc. ASTM E208 and Pellini tests acc. ASTM-E208.
- Charpy- V test measure the fracture appearance and lateral expansion .

The results showed:

The cold cracking, static and dynamic properties of the S690 steels vary depending on the production process and chemical composition of the base materials. The heat input during welding has to be restricted to fulfil the mechanical requirements in the final construction. A proper selection of welding consumables is of course required to be sure that the weld is not the weakest part of the joint.

The dynamic properties of the base materials fulfil the requirement at - 20°C. Commercial available S690 steels according to EN10137 with increased Charpy-V characteristics at - 40°C to a level of 120 Joule are of importance.

3. Hydrogen

The amount of diffusible hydrogen that can arise due to imposing a high potential at the drone hull has been simulated and measured on small pieces of S690 and S355 steels in natural seawater. The charging conditions comprises several charging times and different potentials like -1500mV, -2000mV and – 2500mV with charging times ranging from 1 – 9 days.

The diffusible hydrogen has been measures with a Yanaco gas chromatograph. The results show that with longer charging times and higher negative potentials a higher hydrogen content is reached.

The evolution of hydrogen is rather high in the first five hours, after one day more than 95 % of the hydrogen is released again. The behaviour for S690 and S355 are the same.

Charpy-V test specimens as well as Dynamic Tear specimens were tested with and without hydrogen load. No significant difference in performance has been noticed.

In order to determine whether charging with hydrogen leads to cracking in high restraint weld joints or areas with high stresses Tekken test and NACE-test, 4-points bending test, have been performed in natural seawater. In the Tekken test with fillet welds a little cracking was observed. Therefore full penetration welding is necessary.

After inspection it showed that none of the welds neither S355 nor S690 were cracked even after a mechanical stress near the yield point has been applied. The test program is still running with more different S690 steels and weld joints and a plastic deformation over the weld of 4 %.

The specimen were tested in natural seawater with a loading time of 9 days and a potential of -2000mV. The results showed no defects at all. Only 1 specimen failed at a potential of -2500mV.

In general it can be said that S690 steel is well suitable for the hull construction when applying the correct material and welding specification and manufacturing procedures.

Application of Modern S690 Materials for the Hull of Minesweeping Drones

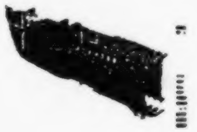

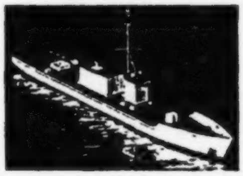

Cees van Sevenhoven
RNLNDMKMMARTECH

Subjects

- Application of Steel S690 [HY100]
-
- Steel S690 welded to S355
-
- Impact of Hydrogen

Trojka Signatures

- Magnetic signature
- Electric signature
- Acoustic signature

Drone Construction must be kept operational

RISKS ??

1. Plastic deformation in hull too high for steel S355 [Gr 50]
Solution: S690 ??[HY 100]

2. Integration electric mine sweeping system gives hydrolysis of water...

Conditions application S690

- Commercial available
- Production hull [specialized company?]
- No preheating at the shipyard
- All welding processes applicable?
- Miner cost price increase

S690 steel investigation

nmax 6
pralsim 6
Naxtra M7

Base material properties

- Static
- Dynamic
- Crack susceptibility
- HAZ properties

Specification Material S 690

- Rp0,2 690 - 810 MPa
- Re/Rm ≤ 0,96
- A5 ≥ 14 %
- KCV ≥ 80 Joule at T = - 40 °C
- Shear fracture ≥ 50 % at T = - 40 °C
- DT- Test : FATT ≥ 50 % at T = - 20 ° C
-
- ***2 Steels fulfilled these requirements!!!***

S690 Welding consumables

- Static
- Dynamic
- Crack susceptibility
- HAZ properties
- Hydrogen content

Application of Steel S690 Conclusion

Steel S690 is commercial available

- **Satisfies the RNLN requirements**
- **Additional specification necessary**

Construcion of the Drone

- **To be carried out by a specialised company**
- **Selection of welding consumables**

Application of S690 on the Shipyard Final conclusion

- Welding of components in the Cylinder S355 to S690:
- No preheating required
- Only thick butt welds need preheating
- Selection of welding consumables

Hydrogen Measurements

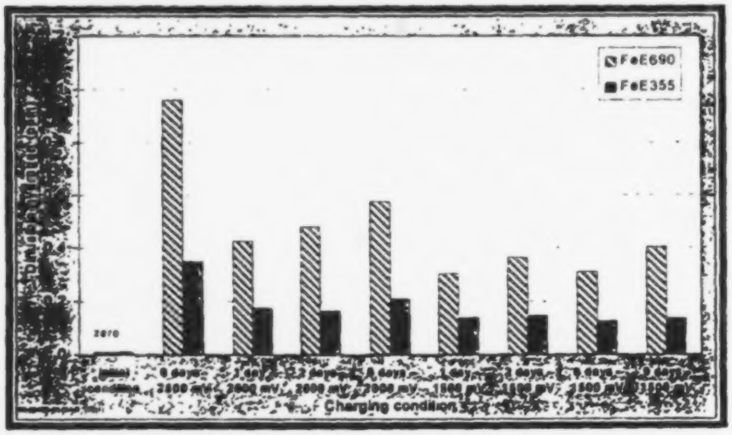

Effect of Hydrogen on Steel
S 690 en S 355

- Dynamic testing of S690 and S355 [illegible] no significant [illegible] hydrogen charging [illegible]

Fracture Apperance DT-test

- Influence test location
-
- Results different
-
- Notch performance

Effect Hydrogen on Steel S 690 en S 355

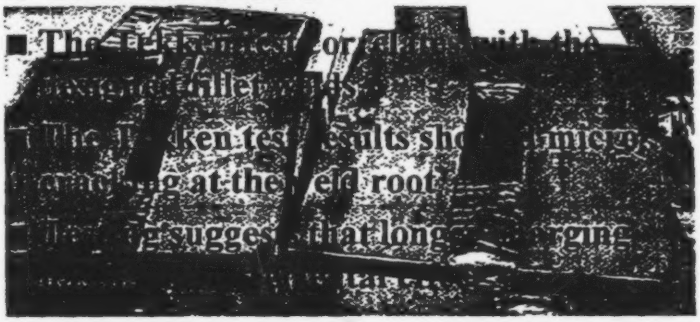

- The Tekken test correlates with the [illegible]esigned fillet welds.
- The Tekken test results show microcracking at the weld root.
- [illegible] suggests that longer [illegible]rging [illegible]

Tekken test H-loading

Conclusion Hydrogen susceptibility of Steel

- Hydrogen charging of the Trojka Drone has no negative influence on the steel properties
- Fillet welds must be replaced by Butt welds
- For both steels the influence is comparable

Drop weight test of fillet welds

- Evaluation of designed throat thickness
- All throat thicknesses under 6 mm failed regardless the strength level of the weld metal
- Throat thickness over 8 mm passed the test

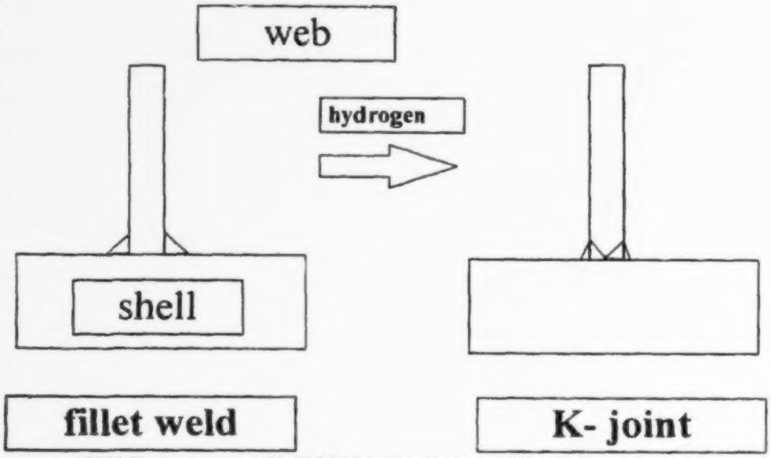

web

hydrogen

shell

fillet weld

K- joint

Final conclusion investigation

- S 690 applicable
-
- Adjust design due to hydrogen and shock
-
- Long term effects of hydrogen and K-butt weld are to be determined

Additional Hydrogen testing

- Tekken NACE

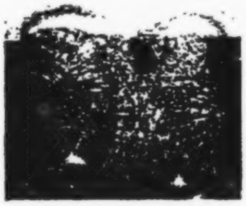

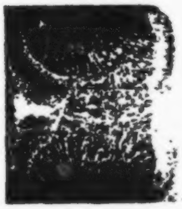

NACE test loaded at -2500 mV; 6 days

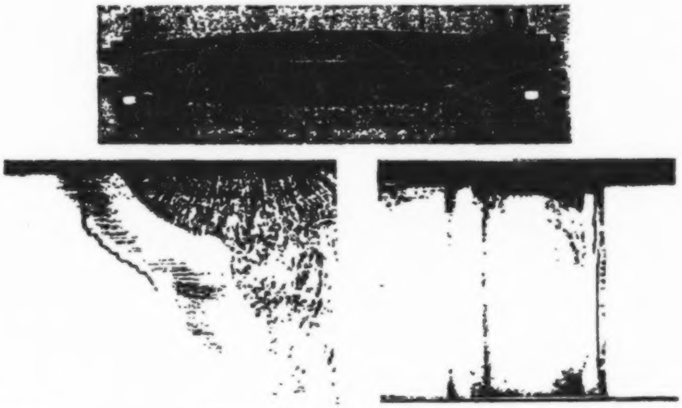

Final Conclusion

- **Full penetration welding not necessary.**
- **Deep penetration welding is allowable.**
- **Commercial available according EU-Standard not possible.**

Dr. Vinod S. Agarwala, Ph.D., P.E., FASM, FNACE
Senior Staff Scientist - Materials Engineering
Research & Engineering Group
Naval Air Systems Command
48110 Shaw Road Unit 5
Patuxent River, MD 20670-1906
agarwalavs@navair.navy.mil
(301) 342-8002;
fax (301) 757-1895

Alan Aitchison
Principal Welding Engineer
BAE SYSTEMS MARINE
Barrow in Furness
Cumbria
LA14 1AF
United Kingdom
FAX 01229 87 4294 - England internal code
TEL 01229 87 5579
alan.aitchison@baesystems.com

U.O. Akpan
Martec Ltd
1888 Brunswick Street, Suite 400
Halifax, N.S. B3J 3J8
902 425 5101
uakpan@martec.com

Lt J Allen
Fleet Maintenance Facility Cape Scott
FMO Halifax, N.S. B3K 2X0
fax 427-4527

Bob Armstrong
Dockyard Laboratory (A)
Defence Research Establishment Atlantic
P.O. Box 99000 Stn Forces
Halifax, Nova Scotia B3K 5X5
(902) 427-0550 Ext 3436

Mr Darren Begg
Fleet Technology Limited
311 Legget Drive
Kanata, Ontario K2K 1Z8
darren@fleetech.com
613 592 2830 x 229
fax 613 592 4950

Dr. Craig Bennett
Associate Professor and Acting Head
Department of Physics, Acadia University
and Director, Acadia Centre for Microstructural Analysis
Wolfville, Nova Scotia, Canada B0P 1X0
902-585-1150
fax 902-585-1816
craig.bennett@acadiau.ca

Mr. Jorgen Bernt
J O Bernt and Associates Limited
649 Welham Rd
Barrie ON L4N 6E7
jammbco@aol.com

Mr Orest Bluy DSTM 4
National Defence Headquarters DRDC
Constitution Building
305 Rideau Street, 8th Floor
Ottawa, Ontario K1A 0K2
613 996-3987
fax 990-1205
Orest.Bluy@drdc-rddc.dnd.ca

D.P. Brennan
Martec Ltd
1888 Brunswick Street, Suite 400
Halifax, N.S. B3J 3J8
902 425 5101
fax 4211923
brennan@martec.com

Mr Ron Chisholm HF31.3
Engr Dept/NAO/Senior Hull Inspector
Fleet Maintenance Facility Cape Scott
FMO Halifax, N.S. B3K 2X0
902 427 0550 3885
fax 427-4527

Mr. John Church
Weld Process International Suite 1206
2261 Lakeshore Blvd West
Etobicoke
Ontario M8V 3X1
416 253 6649
fax 416 253 9334

Pierre Cloutier
BOC Canada Ltd
5555 boul des Grandes Prairies
Montreal Quebec H1R 1B4
514 323 6410
pierreCloutier@BOCCanada.com

Cdr Peter Crosby
Director of Naval Construction
Royal New Zealand Navy
Naval Staff N44
HQ NZ Defence Force
Private Bag
Wellington, New Zealand
64 4 4960329
fax 64 4 4960390
peter.crosby@nzdf.mil.nz

Ernest J. Czyryca
Naval Surface Warfare Center
Carderock Division
Welding and NDE Branch, Code 614
9500 MacArthur Blvd
West Bethesda, MD 20817-5700
(301) 227-5073
fax 301-227-5576
CzyrycaEJ@nswccd.navy.mil

Mrs Jody Dalzel-Job
DERA Rosyth
South Arm
Rosyth Royal Dockyard
Dunfermline, Fife, KY11 2XR
Scotland
44 1383 435113
fax 44 1383 435167
jsdjob@mail.dera.gov.uk

Dr. S. DasGupta
Electrofuel Inc.
21 Hanna Avenue
Toronto, Ont., Canada
M6K 1W8
www.electrofuel.com
416 535 1114
fax 416 535 2361
sdasgupta@electrofuel.com

Gary Dease
Dockyard Laboratory (A)
Defence Research Establishment Atlantic
P.O. Box 99000 Stn Forces
Halifax, Nova Scotia B3K 5X5

Dr Virginia G. DeGiorgi
Code 6350
Multifunctional Materials Branch
Naval Research Laboratory
4555 Overlook Ave. SW
Washington, D.C.
USA 20375-5000
(202) 767-9027
fax 404-7176
virginia.degiorgi@nrl.navy.mil

A.S.(Vijay) Deshpande
Bodycote Materials Testing Canada Inc.
2395 Speakman Drive
Mississauga, Ontario L5K 1B3
905 822 4111
fax 905 822 0781

Sue Dickout DMSS 2-4
National Defence Headquarters
101 Colonel By Drive
Ottawa, Ontario K1A 0K2
819 994 8649
fax 819 997 7058
sdickout@dmcs.dnd.ca

Françoise Dubois-Artiga
DCN indret
CESMAN/RDMPC
44 620 LA MONTAGNE
France
Tel : 33 2 40 84 77 06
Fax :33 2 40 84 79 94
cesman.dcn-indret@wanadoo.fr

Darren P. Edwards
Aeronautical and Maritime Research Laboratory
P.O. Box 4331, Melbourne, Victoria 3001
Australia
+61 39626-7306
fax +61 39626-7087
Darren.Edwards@dsto.defence.gov.au

Marc Fontaine
BOC Canada Ltd
579 Godin
Ville Vanier Quebec G1M 3G7
418 688 0150
fax 418 688 3409
marcfontaine@BOCCanada.com

Dr. Terry Foster
Head/Dockyard Lab(P)
Esquimalt Defence Research Detachment
P.O. Box 17000 Stn Forces
Victoria, British Columbia V9A 7N2
250 363 2849
fax 363 2856
Terry.Foster@edrd.dnd.ca

John Galsworthy
Structural Materials Center
Room 2008 Building A7
DERA Farnborough
Hants, GU14 0LX
United Kingdom
01252 397294
fax 01252 397298
jcgalsworthy@dera.gov.uk

Michael Gharghouri
Assistant Professor
Dept. Of Mining and Metallurgical Engineering
Dal Tech, Dalhousie University
1360 Barrington St., Room G212
P.O.Box 1000
Halifax, Nova Scotia B3J 2X4
(902) 494-3297
(902) 425-1037
Michael.Gharghouri@Dal.Ca

Mr Jim Gianetto
Metals Technology Labs
Energy Mines and Resources Canada
555 Booth St.
Ottawa, Ontario K1A 0G1
(613) 992-4425
fax(613) 992-8735
jgianett@nrcan.gc.ca

Mr. Randy Haggett
Dockyard Laboratory (A)
Defence Research Establishment Atlantic
P.O. Box 99000 Stn Forces
Halifax, Nova Scotia B3K 5X5
(902) 427-0550 Ext 3443
fax (902) 427-3435
haggett@drea.dnd.ca

LCdr Chris Hargreaves DMSS 2-3
National Defence Headquarters
101 Colonel By Dr
Ottawa Ont K1A 0K2
chargrea@dmcs.dnd.ca

LCdr Peter Hartley
NDHQ DMSS 4-8
Louis St Laurent Bldg
Hull QC K1A 0K2

Dr John Hiltz
Dockyard Laboratory (A)
Defence Research Establishment Atlantic
P.O. Box 99000 Stn Forces
Halifax, Nova Scotia B3K 5X5
(902) 427-0550 Ext 3425
fax (902) 427-3435
hiltz@drea.dnd.ca

Roger Hollingshead
Business Development Officer
Defence Research Establishment Atlantic
P.O.Box 1012
Dartmouth, Nova Scotia B2Y 3Z7
426 3100 x166
hollingshead@drea.dnd.ca

Dr Calvin Hyatt
Dockyard Laboratory (A)
Defence Research Establishment Atlantic
P.O. Box 99000 Stn Forces
Halifax, Nova Scotia B3K 5X5
(902) 427-0550 Ext 3433
fax (902) 427-3435
hyatt@drea.dnd.ca

Moe Islam
Integrated Manufacturing Technologies Institute
National Research Council Canada
800 Collip Circle
London ON N6G 4X8
519 430 7059
fax 519 430 7064

Dr. R.L. Jones
Structural Materials Center
MSS, Room 1011, A7 Bldg
Defence Evaluation and Research Agency
Farnborough, Hants, GU14 OLX
United Kingdom
011 44 (0) 1252 392125
fax 44 (0) 1252 392149
rlJONES@DERA.GOV.UK

Mr Ken KarisAllen
Facts Engineering
P.O.Box 20039
Halifax, Nova Scotia B3R 2K9
Facts@fox.nstn.ca

Dennis Kazimer
Fleet Maintenance Facility Cape Scott
FMO Halifax, N.S. B3K 2X0
902 427 0550 ext
fax 427-4527

Steve Kavanaugh
Dockyard Laboratory (A)
Defence Research Establishment Atlantic
P.O. Box 99000 Stn Forces
Halifax, Nova Scotia B3K 5X5
(902) 427-0550 Ext 3186

Irv Keough
Dockyard Laboratory (A)
Defence Research Establishment Atlantic
P.O. Box 99000 Stn Forces
Halifax, Nova Scotia B3K 5X5
(902) 427-0550 Ext 3441

Donald Kerr
Halifax Shipyard
PO Box 9110
3099 Barrington St
Halifax NS B3K 5M7
902 492-5820
fax 902 422 5253
cell 222-4108
kerr.donald@halifaxshipyard.com

Bob Klassen
Dept. Chem./Chem. Eng.,
Royal Military College of Canada
PO Box 17000 Stn Forces
Kingston, Ontario K7K 7B4
613-541-6000 ext. 6086
fax 613-542-9489
Klassen@rmc.ca

Dr T.S. Koko
Martec Ltd
1888 Brunswick Street, Suite 400
Halifax, N.S. B3J 3J8
902 425 5101
fax 4211923
koko@martec.com

Danny Leblanc
BOC Canada Ltd
695 Babin
St. Dieppe Ind Park
Dieppe NB E1A 5M7

Derek Lenard
Dockyard Lab(E)
Esquimalt Defence Research Detachment
P.O. Box 17000 Stn Forces
Victoria, British Columbia V9A 7N2
250 363 2945
fax 250 363 2856
lenard@edrd.dnd.ca

Geoff Lewis
Manufacturing Industries Branch
Industry Canada
1505 Barrington Street, 16th Floor
Halifax, Nova Scotia B3J 2V9
902-426-9475
fax 902 426 6094
lewis.geoff@ic.gc.ca

Keith Lucas
Naval Research Laboratory
4555 Overlook Ave. SW
Washington, D.C.
USA 20375-5000
fax 404-7176
klucas@ccsalpha3.nrl.navy.mil

Mr Ken MacKay
Martec Ltd. Suite 400
1888 Brunswick St.
Halifax, Nova Scotia B3F 3F8
902 425 5101
Mackay@martec.com

Brian MacKeigan
Metallurgical Engineer
Praxair Distribution Inc
40 Gurholt Drive
Dartmouth NS B3B 1J9
468 0987
fax 468 5702

Dr. James R. Matthews
Dockyard Laboratory (A)
Defence Research Establishment Atlantic
P.O. Box 99000 Stn Forces
Halifax, Nova Scotia B3K 5X5
(902) 427-0550 Ext 3444
fax (902) 427-3435
jim.matthews@drea.dnd.ca

Dr. K. Jagath Mawella
STGMT, Ash 0a#95, DPA
MOD, Abbeywood, Bristol BS34 8JH
United Kingdom
+44 00 117 913 5050
fax +44 00 117 913 5943
STGMT@dpa.mod.uk

Ken I. McRae
Head Air Vehicles Research Section
National Defence Headquarters
DRDC /AVRS
Ottawa Ontario K1A 0K2
Ken.Mcrae@nrc.ca
613 991 6908

Dr. Joanne Jones-Meehan
Naval Research Laboratory/Code 6115
4555 Overlook Ave., SW
Washington, DC 20375-5320
202-404-6361
fax: 202-404-8515
jonesmee@ccsalpha3.nrl.navy.mil

Edward A. Metzbower
Head, Physical Metallurgy Branch
Naval Research Laboratory Code 6320
Washington DC 20375-5320
202 767 2396
fax 202 767 2623
metzbower@anvil.nrl.navy.mil

Dr. Richard Morchat
Head/ Dockyard Laboratory (A)
Defence Research Establishment Atlantic
P.O. Box 99000 Stn Forces
Halifax, Nova Scotia B3K 5X5
(902) 427-0550 Ext 3421
fax (902) 427-3435
morchat@drea.dnd.ca

Cheryl Munroe
Administrative Assistant
DREA/Dockyard Laboratory (A)
Halifax, Nova Scotia B3K 5X5
(902) 427-0550 Ext 3422

Kevin G. Morrison
Nu-Tech Precision Metals Inc.
460 McCartney Street
P.O. Box 7
Arnprior ON K7S 3H2
6132 623 6544
fax 613 623 8183
nutech@magma.ca

Dr Jack Morrison
Dockyard Lab(E)
Esquimalt Defence Research Detachment
P.O. Box 17000 Stn Forces
Victoria, British Columbia V9A 7N2

Warren C.E. Nethercotte, Deputy DG
Defence Research Establishment Atlantic
P.O.Box 1012
Dartmouth, Nova Scotia B2Y 3Z7

Dr. Sandra Nevill
Visiting Scientist Code 6401
Bldg 60, Rm 324
Naval Surface Warfare Center
Carderock Division Headquarters
9500 MacArthur Blvd
West Bethesda, MD
20817-5700
Phone: 301-227-4944 fax: 301-227-4814

Mr. Marco Nottegar
Marine Systems Section
Naval Engineering Test Establishment (NETE)
9401 Wanklyn
Lasalle QC H8R 1Z7
514 366 4310 (ext 418)
fax(514)365-0262
nottegam@nete.dnd.ca

Prof David L. Olson
Center for Welding and Joining
Colorado School of Mines
1500 Illinois Street Hill Hall
Golden CO USA 80401
dolson@mines.edu
303-273-3955

Vaughn Osborne
Lincoln Electric
177 Silistria Dr
Dartmouth NS B2W 6B1

Cdr Dan Parks CFLO
Defence Research Establishment Atlantic
P.O.Box 1012
Dartmouth, Nova Scotia B2Y 3Z7

Capt(N) JSR Payne
CO FMF Cape Scott
Building D200
P.O. Box 99000 Stn Forces Halifax
Halifax Nova Scotia B3K 5X5
902 427 0550 ext 2623
fax 902 427 0518

Steven Peabody
FMF CAPE BRETON
Engineering Division (NA)
P.O. Box 17000 Stn Forces
Victoria, British Columbia V9A 7N2
250 363 5872
fax 250 363 2941

Susan Pecman DMSS 2-4-2
National Defence Headquarters
101 Colonel By Drive
Ottawa, Ontario K1A 0K2
819 994 8648
fax 819 997 7058
s.pecman@dnd.ca

Gigi Pelletier
Pelletier and Zwicker Ltd.
6628 Highway #2
Enfield, NS
902 883 7628
gpelleti@is2.dal.ca

Lt(N) Russ Peters
FMF CAPE BRETON
Engineering Division (NA)
P.O. Box 17000 Stn Forces
Victoria, British Columbia V9A 7N2
250 363 5873
fax 250 363 2941
lt-n.rk.peters@dnd.ca

Mr. John Porter
Dockyard Laboratory (A)
Defence Research Establishment Atlantic
P.O. Box 99000 Stn Forces
Halifax, Nova Scotia B3K 5X5
(902) 427-0550 Ext 3423
fax (902) 427-3435
porter@drea.dnd.ca

John Power
Dockyard Laboratory (A)
Defence Research Establishment Atlantic
P.O. Box 99000 Stn Forces
Halifax, Nova Scotia B3K 5X5
(902) 427-0550 Ext 3438

Chris Punshon
Electron Beam Applications Section Manager,
TWI, United Kingdom
9 011 44 1223891162
chris.punshon@twi.co.uk

Christopher Purcell
Defence Research Establishment Atlantic
P.O.Box 1012
Dartmouth, Nova Scotia B2Y 3Z7

L.N. Pussegoda
Fleet Technology Ltd.
311 Legget Drive
Kanata, Ontario K2K 1Z8
(613) 592-2830 ext 205
fax 613 592 4950
nickp@fleetech.com

P.R. Roberge
Department of Chemistry and Chemical
Engineering
Royal Military College of Canada
Kingston, Ontario K7K 5L0
613 541 6000 ext 6485
fax 542 9489
roberge@rmc.ca

Etienne Robichaud
Dockyard Laboratory (A)
Defence Research Establishment Atlantic
P.O. Box 99000 Stn Forces
Halifax, Nova Scotia B3K 5X5
(902) 427-0550 Ext 3185

Philip A. Rushton, MASc., Research Engineer
Advanced Research & Emerging Technologies
Division
Martec Limited
1888 Brunswick Street, Suite 400
Halifax, NS B3J 3J8

Dr. Mahi Sahoo
Materials Technology Laboratory (CANMET)
568 Booth St.
Ottawa, Ontario K1A 0G1
613 992-5475
fax 613 992-8735
msahoo@nrcan.gc.ca

Kumar Sadayappan
Materials Technology Laboratory (CANMET)
568 Booth St.
Ottawa, Ontario K1A 0G1
613 992 0741
fax 613 992 8735
ksadayap@nrcan.gc.ca

Dr Paul Saville
Dockyard Laboratory Pacific
P.O. Box 17000 Stn Forces
Victoria, British Columbia V9A 7N2
250 363 2892
fax 363 2856
Paul.Saville@edrd.dnd.ca

Dr. John Sedriks
Offive of Naval Research
Materials Division
Code 332
800 N. Quincy St.
Arlington, VA 22217-5000
USA
(703) 696 4402
John_Sedriks@onr.navy.mil

Guowu Shen
NRCan
568 Booth St
Ottawa ON K1A 0G1
613 996 4367
fax 613 992 8735
Gshen@NRCan.gc.ca

Rene Sicard
Tektrend International Inc.
2001 St. Regis Boulevard
Dollard des Ormeaux QC H9B 2M9
(514) 421 1417

Dr Patricia Shaw
Defence Operational Technology Support Establishment
Private Bag 32901, Devonport
Auckland, New Zealand
64 9 445 5844
fax 64 9 445 5890
shaw@dse.govt.nz

Mike Sim
DNPS-MAT CP4-5-121
Department of Defence
Canberra ACT 2600 Australia
61 2 6266 2862
fax 61 2 6266 4580
mike.sim@cbr.defence.gov.au

Dr Jeff Szabo
Dockyard Laboratory (A)
Defence Research Establishment Atlantic
P.O. Box 99000 Stn Forces
Halifax, Nova Scotia B3K 5X5
(902) 427-0550 Ext 3427
fax (902) 427-3435
jeff.szabo@drea.dnd.ca

Don Tambling
Bodycote Materials Testing Canada Inc.
2395 Speakman Drive
Mississauga, Ontario L5K 1B3
905 822 4111
fax 905 822 0781

Hugh Templin
FMF Cape Scott
P.O. Box 99000 Stn Forces
Halifax, Nova Scotia B3K 5X5
427 0550 ext 4529

Dr. J.C. Thornley
Research and Productivity Council
921 College Hill Road
Fredericton N.B.
E3B 6Z9
506 452 1378
fax 506 452 1395
cthornle.rpc.unb.ca

Sanjay Tiku
Fleet Technology Limited
311 Legget Drive
Kanata, Ontario K2K 1Z8
sanjayt@fleetech.com
613 592 2830
fax 613 592 4950

Dr. Andre Y. Tremblay
University of Ottawa
Department of Chemical Engineering
161, rue Louis-Pasteur. C.P.450, Succ.A
Ottawa, ON
K7N 6N5
613 562 5800 ext 6094
fax 613 562 5172
ayt@eng.uottawa.ca

Mr Cees Van Sevenhoven
Ministry of Defence Royal
Netherlands Navy Directorate of Materiel
Naval Architecture and Marine Engineering
van der Burchlaan 31
Head of Section: Materials and Corrosion
Postbus 20702
2500 ES The Hague
The Netherlands
31 703162708/2728
mobile 31 620616077
fax 31 703163131

Mr. Dwight Veinot
Dockyard Laboratory (A)
Defence Research Establishment Atlantic
P.O. Box 99000 Stn Forces
Halifax, Nova Scotia B3K 5X5
(902) 427-0550 Ext 3428
fax (902) 427-3435
Dwight.veinot@drea.dnd.ca

M.M. Vijay
VLN Advanced Technologies Inc.
PO Box 27076
Gloucester Centre Postal Outlet
Gloucester, ON, Canada K1J 9L9
mohan.vijay@nrc.ca

Yueping Wang
Dockyard Laboratory (A)
Defence Research Establishment Atlantic
P.O. Box 99000 Stn Forces
Halifax, Nova Scotia B3K 5X5
(902) 427-0550 Ext 3035
fax (902) 427-3435
wang@drea.dnd.ca

Michael E Wells
Naval Surface Warfare Center
Carderock Division, Code 615
9500 MacArthur Blvd
West Bethesda, MD 20817-5700
(301) 227-5026
fax 301-227-5576
WellsME@nswccd.navy.mil

Dr Mary Anne White
Dalhousie University
Dept of Chemistry
Halifax NS B3H 4J3
mawhite@chem1.chem.dal.ca

Steven Xu
Civil Engineering Department
University of Manitoba
Winnipeg, Manitoba
Canada, R3T

Lijue Xue
Integrated Manufacturing Technologies Institute
National Research Council Canada
800 Collip Circle
London ON N6G 4X8
519 430 7059
fax 519 430 7064
lijue.xue@nrc.ca

Blaine Zwicker
Pelletier and Zwicker Ltd.
3655 Leaman St
Halifax NS B3K 4A2
455 5900
pellzwic@hfx.eastlink.ca

UNCLASSIFIED
SECURITY CLASSIFICATION OF FORM
(highest classification of Title, Abstract, Keywords)

DOCUMENT CONTROL DATA

(Security classification of title, body of abstract and indexing annotation must be entered when the overall document is classified)

1 **ORIGINATOR** (the name and address of the organization preparing the document. Organizations for whom the document was prepared, e g Establishment sponsoring a contractor's report, or tasking agency, are entered in section 8) Defence Research Establishment Atlantic PO Box 1012 Dartmouth N.S. B2Y 3Z7	2 **SECURITY CLASSIFICATION** (overall security classification of the document including special warning terms if applicable) Unclassified

3 **TITLE** (the complete document title as indicated on the title page Its classification should be indicated by the appropriate abbreviation (S,C,R or U) in parentheses after the title)

Abstracts and Summaries of 9th CF/DRDC Meeting on Naval Applications of Materials Technology

4 **AUTHORS** (Last name, first name, middle initial If military, show rank, e g Doe, Maj John E)

Matthews, James R. (editor)

5 **DATE OF PUBLICATION** (month and year of publication of in document) October 2001	6a **NO OF PAGES** (total containing information Include Annexes, Appendices, etc) 936	6b **NO OF REFS** (total cited document) more than 200

7 **DESCRIPTIVE NOTES** (the category of the document, e g technical report, technical note or memorandum. If appropriate, enter the type of report, e g interim, progress, summary, annual or final Give the inclusive dates when a specific reporting period is covered)

Conference Proceedings (Special Report)

8 **SPONSORING ACTIVITY** (the name of the department project office or laboratory sponsoring the research and development Include the address)

DREA

9a **PROJECT OR GRANT NO** (if appropriate, the applicable research and development project or grant number under which the document was written Please specify whether project or grant) 1gh	9b **CONTRACT NO** (if appropriate, the applicable number under which the document was written)
10a **ORIGINATOR'S DOCUMENT NUMBER** (the official document number by which the document is identified by the originating activity This number must be unique to this document) DREA SR 2001-094	10b **OTHER DOCUMENT NOS** (Any other numbers which may be assigned this document either by the originator or by the sponsor)

11 **DOCUMENT AVAILABILITY** (any limitations on further dissemination of the document, other than those imposed by security classification)

(X) Unlimited distribution
( ) Distribution limited to defence departments and defence contractors, further distribution only as approved
( ) Distribution limited to defence departments and Canadian defence contractors, further distribution only as approved
( ) Distribution limited to government departments and agencies, further distribution only as approved
( ) Distribution limited to defence departments, further distribution only as approved
( ) Other (please specify)

12 **DOCUMENT ANNOUNCEMENT** (any limitation to the bibliographic announcement of this document This will normally correspond to the Document Availability (11) However, where further distribution (beyond the audience specified in 11) is possible, a wider announcement audience may be selected)

UNCLASSIFIED
SECURITY CLASSIFICATION OF FORM

13 **ABSTRACT** (a brief and factual summary of the document It may also appear elsewhere in the body of the document itself It is highly desirable that the abstract of classified documents be unclassified Each paragraph of the abstract shall begin with an indication of the security classification of the information in the paragraph (unless the document itself is unclassified) represented as (S), (C), (R), or (U) It is not necessary to include here abstracts in both official languages unless the text is bilingual)

This was the ninth naval materials CF/DRDC (Canadian Forces/Defence Research and Development Canada) meeting. These meetings have been held every two years since 1985. The first four meetings were devoted to fabrication and inspection of submarine pressure hulls with sessions on welding, inspection and fracture. The last five have expanded to include all aspects of naval materials.

The purpose of these meetings has been to bring together industrial research contractors, university contractors, defence scientists, and NDHQ (National Defence Headquarters) design authorities from the naval materials technology area and invited scientists and engineers from other countries to share advances in naval materials technology in a conference like setting.

The program includes Welding and Laser Surface Modification, Environmental Research, Corrosion and Coatings, Vibroacoustic Materials, Ship Fracture, Fatigue, Firesafe Materials, Non-Destructive Evaluation, Metallurgy and Failure Analysis, Organic Materials (Polymers), Fuels and Lubricants and Naval Consulting.

14 **KEYWORDS, DESCRIPTORS or IDENTIFIERS** (technically meaningful terms or short phrases that characterize a document and could be helpful in cataloguing the document They should be selected so that no security classification is required Identifiers, such as equipment model designation, trade name, military project code name, geographic location may also be included If possible keywords should be selected from a published thesaurus e g Thesaurus of Engineering and Scientific Terms (TEST) and that thesaurus-identified If it not possible to select indexing terms which are Unclassified, the classification of each should be indicated as with the title)

naval materials
corrosion
coatings
welding
fracture
NDE
fatigue
laser surface modification
fire safe materials
organic materials
polymers
vibration materials
damping materials

Defence R&D Canada
is the national authority for providing
Science and Technology (S&T) leadership
in the advancement and maintenance
of Canada's defence capabilities.

R et D pour la défense Canada
est responsable, au niveau national, pour
les sciences et la technologie (S et T)
au service de l'avancement et du maintien des
capacités de défense du Canada.

516410

CA011837

DEFENCE DÉFENSE

www.drdc-rddc.dnd.ca